Handbook of Advanced Chromatography/ Mass Spectrometry Techniques

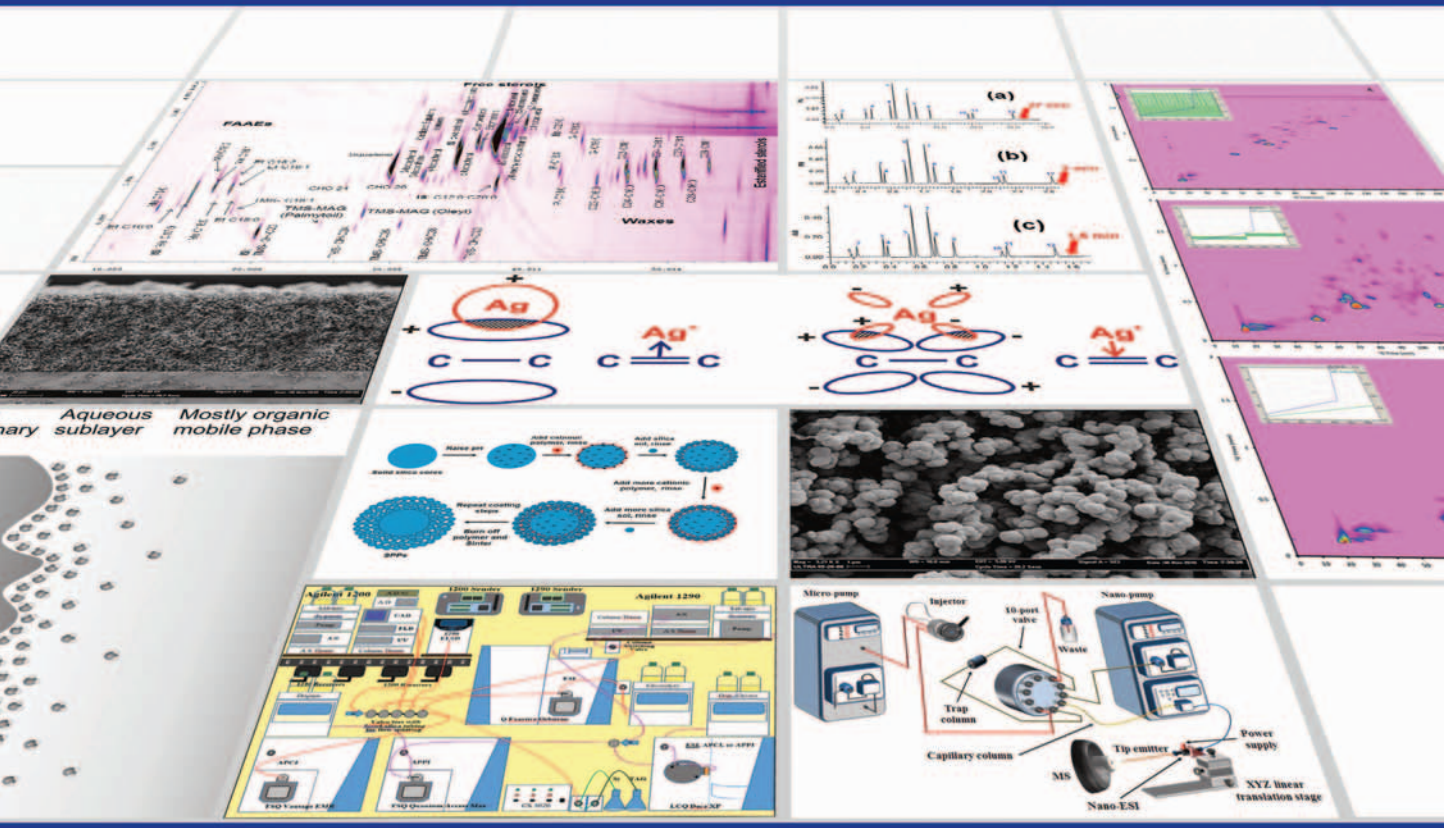

Edited by
Michal Holčapek
Wm. Craig Byrdwell

AOCS PRESS
AP

Handbook of Advanced Chromatography/Mass Spectrometry Techniques

To my wife Martina and sons Filip and
David for their patience and continuous support of my scientific work.
– Michal Holčapek

Handbook of Advanced Chromatography/Mass Spectrometry Techniques

Edited by

Michal Holčapek

University of Pardubice, Pardubice, Czech Republic

Wm. Craig Byrdwell

Food Composition and Methods Development Lab, USDA, ARS
Beltsville Human Nutrition Research Center, Beltsville, Maryland
United States

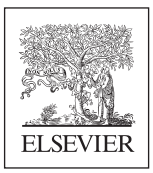

ACADEMIC PRESS
An imprint of Elsevier

Academic Press and AOCS Press
Academic Press is an imprint of Elsevier
125 London Wall, London EC2Y 5AS, United Kingdom
525 B Street, Suite 1800, San Diego, CA 92101-4495, United States
50 Hampshire Street, 5th Floor, Cambridge, MA 02139, United States
The Boulevard, Langford Lane, Kidlington, Oxford OX5 1GB, United Kingdom

Published in cooperation with American Oil Chemists' Society www.aocs.org
Director, Content Development: Janet Brown

Notices
Knowledge and best practice in this field are constantly changing. As new research and experience broaden our understanding, changes in research methods, professional practices, or medical treatment may become necessary.

Practitioners and researchers must always rely on their own experience and knowledge in evaluating and using any information, methods, compounds, or experiments described herein. In using such information or methods they should be mindful of their own safety and the safety of others, including parties for whom they have a professional responsibility.

To the fullest extent of the law, neither the Publisher nor the authors, contributors, or editors, assume any liability for any injury and/or damage to persons or property as a matter of products liability, negligence or otherwise, or from any use or operation of any methods, products, instructions, or ideas contained in the material herein.

Library of Congress Cataloging-in-Publication Data
A catalog record for this book is available from the Library of Congress

British Library Cataloguing-in-Publication Data
A catalogue record for this book is available from the British Library

ISBN: 978-0-12-811732-3

Publisher: Andre Gerhard Wolff
Acquisition Editor: Nancy Maragioglio
Editorial Project Manager: Billie Jean Fernandez
Production Project Manager: Poulouse Joseph
Designer: Victoria Pearson

Typeset by TNQ Books and Journals

Contents

List of Contributors

María Asensio-Ramos
Volcanologic Institute of the Canary Islands (INVOLCAN), Puerto de la Cruz, Spain

William C. Byrdwell
U.S. Department of Agriculture, Beltsville, MD, United States

Francesco Cacciola
University of Messina, Messina, Italy

Alberto Cavazzini
Università di Ferrara, Ferrara, Italy

Alessia Ciogli
Sapienza Università di Roma, Roma, Italy

Ilaria D'Acquarica
Sapienza Università di Roma, Roma, Italy

Giovanni D'Orazio
Universidad de la Laguna (ULL), La Laguna, Spain; Italian National Council of Research, Monterotondo, Italy

Monika M. Dittmann
Agilent Technologies GmbH, Waldbronn, Germany

Paola Donato
University of Messina, Messina, Italy

Paola Dugo
University of Messina, Messina, Italy; University Campus Bio-Medico of Rome, Rome, Italy; Chromaleont SrL, Messina, Italy

Chiara Fanali
University Campus-Biomedico, Rome, Italy

Salvatore Fanali
Italian National Council of Research, Monterotondo, Italy

Francesco Gasparrini
Sapienza Università di Roma, Roma, Italy

Davy Guillarme
University of Geneva, Geneva, Switzerland; University of Lausanne, Lausanne, Switzerland

Javier Hernández-Borges
Universidad de la Laguna (ULL), La Laguna, Spain

Michal Holčapek
University of Pardubice, Pardubice, Czech Republic

Omar H. Ismail
Sapienza Università di Roma, Roma, Italy

Pavel Jakubec
Charles University, Hradec Králové, Czech Republic

Pavel Jandera
University of Pardubice, Pardubice, Czech Republic

Miroslav Lísa
University of Pardubice, Pardubice, Czech Republic

Yongqin Lv
Beijing University of Chemical Technology, Beijing, China

Luigi Mondello
University of Messina, Messina, Italy; University Campus Bio-Medico of Rome, Rome, Italy; Chromaleont SrL, Messina, Italy

Lucie Nováková
Charles University, Hradec Králové, Czech Republic

Marco Pierini
Sapienza Università di Roma, Roma, Italy

Kateřina Plachká
Charles University, Hradec Králové, Czech Republic

Giorgia Purcaro
Chromaleont SrL, Messina, Italy

Anna Rocco
Italian National Council of Research, Monterotondo, Italy

Dwight R. Stoll
Gustavus Adolphus College, St. Peter, MN, United States

Frantisek Svec
Beijing University of Chemical Technology, Beijing, China

Peter Q. Tranchida
University of Messina, Messina, Italy

Jean-Luc Veuthey
University of Geneva, Geneva, Switzerland; University of Lausanne, Lausanne, Switzerland

Claudio Villani
Sapienza Università di Roma, Roma, Italy

Xiaoli Wang
Agilent Technologies GmbH, Waldbronn, Germany

Preface

Six years have already passed since the publication of our previous book Extreme Chromatography: Faster, Hotter, Smaller. New developments in the coupling of separation techniques with mass spectrometry (MS) have advanced quickly, therefore we have assembled this up-to-date compendium of new and advanced analytical techniques that have been developed in recent years for the analysis of various types of molecules in a variety of complex matrices. The major reason for this fast progress in our field is the instrumental advancements in both MS and chromatography. The liquid chromatography/mass spectrometry (LC/MS) market is extremely competitive, and multiple vendors are offering new or improved hardware and software solutions that are the basis for development of new analytical methods with better sensitivity, selectivity, high-throughput, and other important analytical characteristics. High-resolution mass spectrometers coupled to chromatographic systems were much less widespread a decade ago. Nowadays, it is a common standard for many analytical groups to have multiple LC/MS systems including high-resolution time-of-flight—based mass analyzers or ultrahigh-resolution Fourier transform analyzers, in the form of Orbitrap or ion cyclotron resonance mass spectrometers. High resolution is typically accompanied by high mass accuracy on the condition of proper calibration procedures. It is evident that such dramatic improvements in the quality of mass spectrometric data provide new possibilities for an analytical chemist in terms of qualitative and quantitative analysis, but on the other hand it requires a much higher level of expertise for an analytical chemist. Therefore, we have to put more emphasis on the education of analytical chemists to enable them to fully explore the complexity of studied samples.

Advancements in the field of chromatography have surely not lagged behind developments in the MS world. The transition from conventional high-performance liquid chromatography (HPLC) to ultrahigh-performance liquid chromatography (UHPLC) is continuing, and nowadays UHPLC systems are dominating the field because of clear advantages in terms of speed, chromatographic resolution, and overall performance of the system (Chapter 1). A very strong partner and competitor to liquid chromatography is supercritical fluid chromatography (SFC, Chapter 12). Theoretical advantages of this technique have been known for decades, but it has not been fully explored until recent years because of the limitations of lower reproducibility and insufficiently robust coupling with MS. Now these issues have been successfully solved, and reliable commercial systems are now available, so we can expect further increases in the number of applications of SFC, or more accurately stated, ultrahigh-performance supercritical chromatography. It has been generally realized that biological systems are more complex than initially anticipated, so researchers also need more dimensions in chromatography (i.e., multidimensional chromatography, Chapters 7, 8 and 11) and MS (i.e., multidimensional MS, Chapter 10) to describe such complex systems in more detail. Continuous progress has been observed in stationary phase design (Chapter 6) and also in the introduction of new separation modes, such as hydrophilic interaction liquid chromatography (Chapter 2). Biological complexity also includes various types of isomerism, which requires dedicated chromatographic systems for their resolution, such as chiral chromatography (Chapter 3) and silver-ion chromatography (Chapter 4). Another important trend of the last decade is miniaturization, which results in the use of capillary or chip-based separation systems (Chapter 9). Monolithic columns have proved to be very efficient for various applications, as summarized in Chapter 5.

This book includes 12 chapters prepared by scientific leaders in particular fields, who carefully prepared or updated their chapters. We believe that this collection of up-to-date LC/MS, gas chromatography/mass spectrometry, and supercritical fluid chromatography/mass spectrometry techniques should help both newcomers and advanced practitioners to improve their theoretical knowledge and also encourage them to implement new technologies in practice. Individual chapters show advantages and limitations of individual methodologies, illustrated by practical examples of where these methods can be useful. We believe that this book should be a practical guide for the laboratory rather than just another dust-covered item in the library.

Michal Holčapek and William Craig Byrdwell

CHAPTER

1 THEORY AND PRACTICE OF UHPLC AND UHPLC–MS

Davy Guillarme[1,2], **Jean-Luc Veuthey**[1,2]
University of Geneva, Geneva, Switzerland[1]; *University of Lausanne, Lausanne, Switzerland*[2]

1. INTRODUCTION

Reversed-phase liquid chromatography (RPLC) is currently one of the most widely used separation techniques. During the last few years, some substantial improvements, such as innovative supports and instrumentation, have been brought forth to perform high-throughput analyses and highly efficient separations in RPLC (Guillarme et al., 2007b; Novakova et al., 2006). Such advances were mainly driven by the need to handle either a growing number of analyses or more complex samples.

Regarding high-throughput separations, there is a growing demand in numerous fields, including toxicology, doping, forensics, clinical chemistry, and environmental analyses, where the delivery time response must be reduced as much as possible. The pharmaceutical field, with its need for enhanced productivity and reduced costs, is certainly the main driving force for faster separations (Wren and Tchelitcheff, 2006). Because of the high number of analyses required for common pharmaceutical applications, such as purity assays, pharmacokinetic studies, and quality control, rapid analytical procedures (less than 5 min including equilibration time) are often mandatory (Al-Sayah et al., 2008).

Highly efficient separations are also necessary for many applications, including proteomics, plant extract analysis, and metabolomics, which all deal with very complex samples, such as biological samples, tryptic digests, or natural plant extracts (Grata et al., 2008; Petricoin and Liotta, 2004). With such difficult samples, conventional high-pressure liquid chromatography (HPLC) systems present some obvious limitations.

Among the different strategies used to achieve fast and high-resolution separations, ultrahigh-pressure liquid chromatography (UHPLC) has been rapidly recognized as a powerful and robust analytical tool. As shown in Fig. 1.1, the number of articles published in the fields of UHPLC and UHPLC–mass spectrometry (MS) has risen very quickly since 2004. Thus, in this chapter, the possibility to speed up and/or attain highly efficient separations will be demonstrated, using the UHPLC strategy in combination with UV as well as MS detectors. This chapter will also discuss the advantages and drawbacks of this approach, in comparison with other existing techniques.

Handbook of Advanced Chromatography/Mass Spectrometry Techniques. http://dx.doi.org/10.1016/B978-0-12-811732-3.00001-7

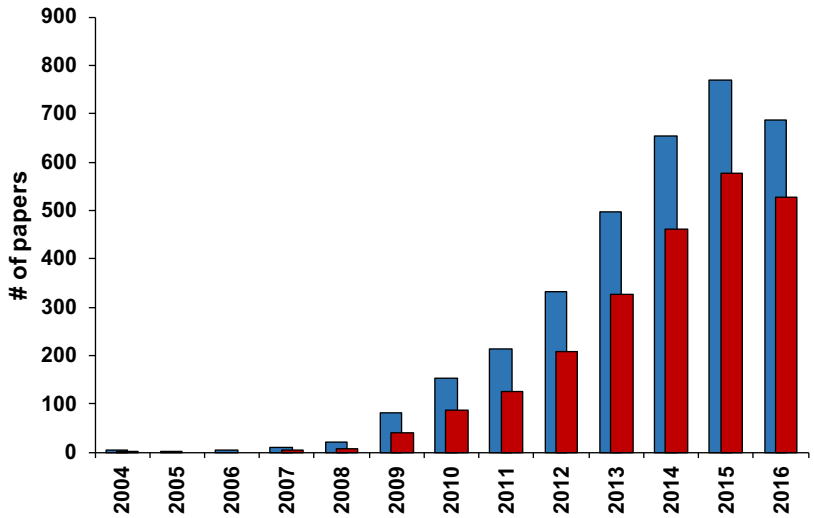

FIGURE 1.1

Number of papers published each year in the field of ultrahigh-pressure liquid chromatography (UHPLC) and UHPLC–mass spectrometry (MS), since 2004. Before this date, only few papers were published by Jorgenson's and Lee's groups. *Blue bars* (light gray in print versions) were obtained with keyword "UHPLC", whereas *red bars* (dark gray in print versions) were obtained with an additional filter (keyword "MS").

From Scifinder scholar 2016 search of the chemical abstracts database. Date of information gathering: August 2016.

2. BRIEF DESCRIPTION OF ULTRAHIGH-PRESSURE LIQUID CHROMATOGRAPHY AND HISTORICAL BACKGROUND

2.1 INTEREST IN SMALL PARTICLES IN LIQUID CHROMATOGRAPHY

In liquid chromatography (LC), it is well established that a reduction of particle size (d_p) provides an important gain in chromatographic performance (Knox, 1977; Knox and Saleeem, 1969; Poppe, 1997). Indeed, the reduction of d_p allows faster separations as well as higher plate counts. Since the beginning of LC, there has been a continuing progression in the reduction of particle size that has culminated in the commercialization of columns packed with sub-2 μm particles (Table 1.1). According to Eqs. (1.1) and (1.2), these small particles lead to significant improvements in terms of (1) efficiency because N (number of theoretical plates) is inversely proportional to d_p, and (2) time reduction because the optimal mobile phase linear velocity (u) is inversely proportional to particle diameter.

$$N = \frac{L}{h \cdot d_p} \tag{1.1}$$

where, L is the column length, h the reduced plate height (generally between 2 and 3), and d_p the particle size.

$$u = \frac{v \cdot D_m}{d_p} \tag{1.2}$$

Table 1.1 Evolution of Particles Size in Liquid Chromatography

Years	Particle Size (μm)	Plates/15 cm
1950s	100	200
1967	50	1000
1972	10	6000
1985	5	12,000
1992	3−3.5	22,000
1996[a]	1.5	30,000
2000	2.5	25,000
2004	1.7	30,000

[a]*Nonporous silica or resins.*
Adapted from Majors, R.E., 2003. HPLC column packing design. LC-GC Eur. 16, 8−13.

where, v is the reduced linear velocity and D_m the diffusion coefficient of the solute into the mobile phase.

At the end of the 1960s, Horváth et al. introduced columns packed with rigid pellicular particles (40−50 μm) compatible with high pressures (Horvath et al., 1967). The thin porous coating allowed a rapid solute mass transfer into and out of the packing, producing a significant improvement in terms of column efficiency compared with the large porous particles commonly employed at that time. Nevertheless, this pellicular packing had a too limited surface area and therefore low sample capacity.

The transition from large porous and pellicular particles to smaller particles (in the range of 10 μm) occurred in the 1970s (Majors, 2003). However, particles of silica smaller than 40 μm have demonstrated some difficulties with packing reproducibility, and irregular shapes of microporous particles were used (Kirkland, 1972; Majors, 1972; Snyder, 1969; Asshauer and Halasz, 1974), until spherical materials were developed and improved (Endele et al., 1974; Vivilecchia et al., 1974).

In 1977, Knox stated that ultrafast LC would require a new generation of particles and instrumentation. Particles of 1 or 2 μm should be used to obtain $t_0 \approx 10$ s at reasonable pressures, in combination with column lengths of 20−40 mm (Knox, 1977). However, due to the dramatic reduction of the column volume, and the use of elevated mobile phase flow rate, the instrumentation was critical, and contributed strongly to additional peak broadening. Specifically, the injector (e.g., precise injection of small amounts) and detector devices (e.g., reduction of cell volume and improvement of electronics, such as acquisition rate and time constant) were not initially adapted. For this reason, 20−30 years have been spent to develop instrumentation compatible with short columns packed with sub-2 μm particles.

In the 1980s, columns packed with 5 μm particles became the standard, and in the early 1990s, 3−3.5 μm particle diameters were commercially available. The latter demonstrated 30%−50% faster analysis times and higher efficiencies compared with 5 μm particles. An additional advantage is that methods developed on columns packed with 5 μm can be easily transferred to a similar 3 or 3.5 μm stationary phase. To further improve chromatographic performance, small nonporous supports of 1.5 μm were introduced in 1996 (Majors, 2003). These supports minimize the pore diffusion and mass transfer resistance effects. Therefore, nonporous silica columns can work in a much wider flow rate

range without any loss of chromatographic performance and provide high efficiency (equivalent to 200,000 plates/m). However, due to the reduction in surface area, nonporous supports exhibit lower retention times and too limited loading capacity in comparison with porous columns. Nowadays, such materials are only proposed for separating very large molecules that slowly diffuse in the mobile phase (Lommen and Snyder, 1993).

In 2004, the first available porous silica with sub-2 µm particle size was commercialized (1.7 µm), allowing a better resolution compared with the current 5 or 3.5 µm. As shown in Fig. 1.2, the kinetic performance can be drastically improved when decreasing the particle size from the conventional columns packed with 5 µm particles to the sub-2 µm particles. With the latter, it is possible to attain an H value of less than 5 µm, meaning that a column of only 50 mm packed with sub-2 µm particles can provide an efficiency of 10,000 plates (i.e., equivalent to a 150 mm column length packed with 5 µm particles). In addition, the mobile phase linear velocity should be increased with smaller particles (see Eq. 1.2), and thus it is possible to work three times faster when using sub-2 µm versus 5 µm particles. Finally, the mass transfer resistance (right hand side of the Van Deemter curve) is drastically reduced, allowing columns to work at a linear velocity higher than the optimal one, with only a limited impact on efficiency. Because of these kinetic characteristics, the

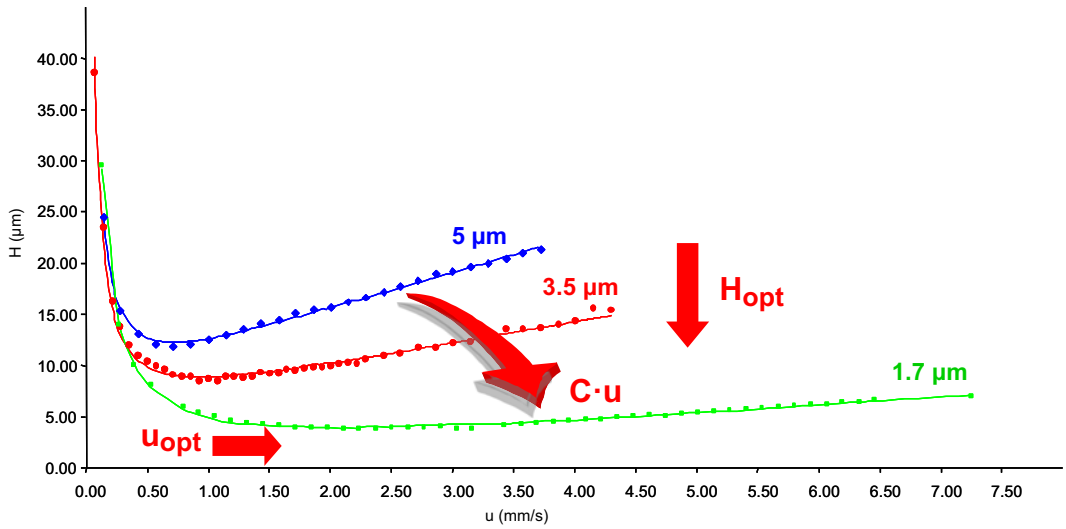

FIGURE 1.2

Impact of particle size reduction on the Van Deemter curves. These experimental curves were obtained with a mobile phase: H_2O/MeCN (60:40 v/v), with butylparaben 25 ppm in H_2O, UV detection: 254 nm, columns: XTerra RP18 4.6 × 150 mm, 5 µm; XTerra RP 18 4.6 × 50 mm, 3.5 µm; Acquity Shield bridged ethylsiloxane/silica hybrid C18 2.1 × 50 mm, 1.7 µm.

Adapted from Nguyen, D.T.T., Guillarme D., Rudaz, S., Veuthey, J.L., 2006a. Fast analysis in liquid chromatography using small particles size and ultra-high pressure. J. Sep. Sci. 29, 1836–1848; Nguyen, D.T.T., Guillarme, D., Rudaz, S., Veuthey, J.L., 2006b. Chromatographic behaviour and comparison of column packed with sub-2 µm stationary phases in liquid chromatography. J. Chromatogr. A 1128, 105–113, with permission.

analysis time can be reduced by a factor of 9, for a similar efficiency between HPLC (150 mm, 5 µm) and UHPLC (50 mm, 1.7 µm) at the optimal linear velocity. On the other hand, it is possible to increase the column length to have a better efficiency without increasing the analysis time in comparison with an HPLC procedure.

In gradient mode, several authors have demonstrated that decreasing particle size improves peak capacity and thus chromatographic resolution (Neue and Mazzeo, 2001; Gilar et al., 2004). Indeed, particle size reduction has more impact than reducing column length, gradient time or flow rate to improve peak capacity in gradient mode.

However, these columns packed with small particles generate an elevated backpressure (>400 bar) often incompatible with conventional instrumentation. Darcy's law (Eq. 1.3) shows the dependence of column inlet pressure on the particle diameter d_p.

$$\Delta P = \frac{u \cdot L \cdot \eta \cdot \phi}{d_p^2} \tag{1.3}$$

where, L is the column length, η the mobile phase viscosity, and ϕ the flow resistance.

At the optimal linear velocity (u_{opt}), the pressure drop is inversely proportional to the cube of particle diameter (according to Eqs. 1.2 and 1.3). Thus, under optimal flow-rate conditions, 1.7 µm particles generate a pressure 25 times higher than that of 5 µm particles for an identical column length. Then, the backpressure limitation of conventional HPLC at 400 bar can turn out to be an issue, and there is a need to employ dedicated LC systems that withstand ultrahigh pressures (up to 1500 bar nowadays).

2.2 INTEREST IN VERY HIGH PRESSURES IN LIQUID CHROMATOGRAPHY

As described by Eq. (1.3), reducing the particle size rapidly increases the backpressure (Fekete et al., 2014a). Early in the sixties, Knox showed that the speed limitation of chromatographic systems would be related to the maximum operating pressure. In addition, when there is a need to improve efficiency with long columns, an increase in pressure drop is mandatory to work within acceptable flow-rate conditions (Knox and Saleem, 1969; Giddings, 1965; Knox, 1961).

Desmet et al. described a useful approach illustrating the influence of maximal backpressure (ΔP_{max}) on achievable N and t_0, based on the Van Deemter data (u, H), column permeability ($K_{v,0}$) and mobile phase viscosity (η) with Eqs. (1.4) and (1.5) (Desmet et al., 2005a,b, 2006a,b; Billen et al., 2007; Desmet and Cabooter, 2009; Desmet, 2008).

$$N = \frac{\Delta P_{max}}{\eta}\left(\frac{K_{v,0}}{u_0 H}\right) \tag{1.4}$$

$$t_0 = \frac{\Delta P_{max}}{\eta}\left(\frac{K_{v,0}}{u_0^2}\right) \tag{1.5}$$

The kinetic plot representation (that corresponds to the kinetic performance of a chromatographic system, considering (1) mobile phase flow rate and column length, as variables and (2) mobile phase nature and composition as well as maximal pressure supported by the system, as constants) is advantageous because the performance of different LC supports can be directly compared whatever their lengths, particle sizes, and pressure drops. Fig. 1.3 shows kinetic plots representing the achievable

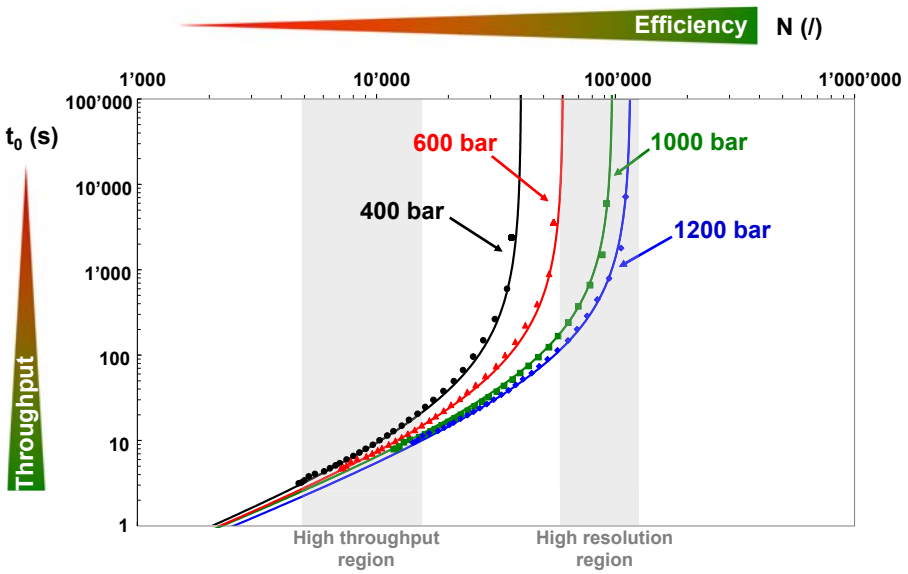

FIGURE 1.3

Representation illustrating the importance of increasing the maximum pressure of the system in ultrahigh-pressure liquid chromatography. Kinetic plots were constructed for a Waters Acquity bridged ethylsiloxane/silica hybrid C18, 1.7 μm column, considering a mobile phase viscosity of 0.85 cp (mobile phase ACN:H_2O 40:60 at 30°C).

efficiency on the X-axis as a function of the time required to attain a given efficiency on the Y-axis. The curves were constructed for a column packed with sub-2 μm particles and using different maximal operating pressures, namely 400, 600, 1000, and 1200 bar. This representation shows that, when dealing with high-throughput separations requiring short columns (N in the range 5000−15,000 plates), the corresponding analysis times were almost identical for systems with a maximal pressure drop of 600, 1000, or 1200 bar. However, the performance was reduced with a conventional HPLC system compatible with only 400 bar (logarithmic scale). These observations were related to the achievable mobile phase flow rate and that optimal linear velocity (u_{opt}) cannot always be reached, depending on the upper pressure limit.

On the other hand, when a very high efficiency is required (right side of the kinetic curves, N ranging between 50,000−100,000 plates), the maximal operating pressure of the system becomes a critical parameter. Indeed, for a system that withstands 400 bar, the maximal achievable efficiency would only be equal to 40,000 plates, because a compromise should be found between column length and mobile phase flow rate, to maintain reasonable backpressure. Then, the N value increases proportionally with the maximal pressure drop, up to 120,000 plates for a system compatible with a maximal pressure of 1200 bar. To attain such efficiency, a column of 45−60 cm packed with sub-2 μm particles could be employed, as reported in the literature (Cabooter et al., 2008). Thus, there is a need to work with a dedicated system compatible with ultrahigh pressure, when using columns packed with sub-2 μm particles.

2.3 PRELIMINARY WORKS OF J.W. JORGENSON AND M.L. LEE IN ULTRAHIGH-PRESSURE LIQUID CHROMATOGRAPHY

The first report on UHPLC was published in 1972 by Bidlingmeyer and Rogers who employed long, thick columns packed with sub-2 μm particles. However, irreproducible results were obtained because of the inherent difficulty in packing such columns at that time.

The first remarkable separation performed at a pressure up to 4100 bar in a fused-silica capillary column (52 cm length, 30 μm I.D., 1.5 μm nonporous particles) was described in 1997 by Jorgenson et al. For an analysis time of less than 10 min, a number of plates in the range of 140,000−190,000 were obtained with small molecules (MacNair et al., 1997). In 2003, the upper pressure limit of their system was extended and the particle size decreased to obtain outstanding chromatographic performance. As shown in Fig. 1.4A, a separation of four model compounds under isocratic conditions was obtained at a pressure of 7200 bar using a column of 43 cm length, 30 μm I.D., packed with 1.0 μm nonporous particles. For this separation, analysis time was reduced to less than 4 min for plate number values between 196,000 and 310,000 (Jerkovich et al., 2003).

Later, Lee et al. also investigated UHPLC with capillary columns but with the aim of reducing analysis times as much as possible. For this purpose, they developed a system able to work up to a pressure of 3600 bar, and a separation of benzodiazepines was performed in less than 60 s using a column of 125 mm length, 29 μm I.D., and packed with 1.5 μm nonporous particles (Fig. 1.4B) (Lippert et al., 1999). Their UHPLC setup was also successfully coupled to electrospray ionization−time of flight (ESI−TOF) via a sheath liquid interface to carry out high-speed and high-

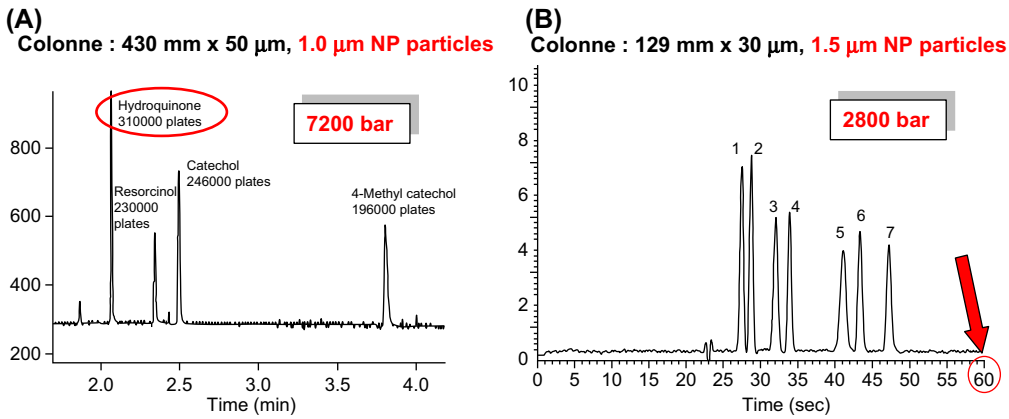

FIGURE 1.4

Illustration of the first ultrahigh-pressure liquid chromatography experiments made by the groups of Jorgenson et al. and Milton Lee et al. (A) Ultraefficient separation of small organic test compounds obtained; conditions: 7200 bar inlet pressure, capillary column (430 mm × 50 μm I.D., packed with 1.0 μm nonporous particles) (Jerkovich et al., 2003). (B) Ultrafast separation of a triazine herbicides mixture. Conditions: 2800 bar inlet pressure; capillary column (129 mm × 30 μm I.D. packed with 1.5 μm Kovasil mass spectrometry-H nonporous particles).

(B) Adapted from Lippert, J.A., Xin, B., Wu, N., Lee, M.L., 1999. Fast ultrahigh-pressure liquid chromatography: on-column UV and time-of-flight mass spectrometric detection. J. Microcolumn Sep. 11, 631−643, with permission.

resolution analyses of pharmaceutical compounds and herbicides. Columns of different geometries (29–100 μm I.D.) were used to obtain separations in less than 100 s with efficiencies ranging from 20,000 to 30,000 plates (Wu et al., 2001). Furthermore, elevated mobile phase temperature was employed to reduce the pressure drop and make the use of longer columns or smaller particles possible. Lee et al. (Xiang et al., 2003a,b) investigated this approach on a capillary column (145 mm length, 50 μm I.D., 1.0 μm nonporous particles) packed with zirconia material, due to its chemical stability at elevated temperature. A separation of various benzodiazepines was carried out in less than 1.2 min at 100°C using this column, at a pressure of 1480 bar. Five herbicides were also resolved with excellent efficiency in only 60 s at 90°C and 1800 bar.

As described, most of Jorgenson's publications in UHPLC were dedicated to complex mixtures requiring a high number of plates ($N > 100{,}000$), whereas Lee et al. mainly used UHPLC for performing high-throughput analysis of small molecules with a limited efficiency ($N < 30{,}000$).

3. KINETIC COMPARISON OF ULTRAHIGH-PRESSURE LIQUID CHROMATOGRAPHY WITH OTHER EXISTING TECHNOLOGIES FOR FAST AND HIGH-RESOLUTION LIQUID CHROMATOGRAPHY

3.1 BRIEF PRESENTATION OF THE ALTERNATIVE APPROACHES TO ULTRAHIGH-PRESSURE LIQUID CHROMATOGRAPHY

Table 1.2 summarizes the main characteristics (advantages and limitations) of alternative approaches to obtain fast and high-resolution separations.

Monolithic supports consist of a single rod of porous material that presents unique features in terms of permeability and efficiency. These materials were mainly developed by Hjerten et al. (1989), Svec and Frechet, (1992) and Tanaka et al. (Minakuchi et al., 1996). Silica-based monolithic supports are the most interesting ones for conventional RPLC and have been available from Merck and Phenomenex since 2000 and 2006, respectively. Their bimodal structure is characterized by 2-μm macropores and 13-nm mesopores, leading to efficiency equivalent to that of porous 3.5 μm silica particles (Cabrera, 2004). Tallarek et al. demonstrated that this material exhibits elevated permeability, equivalent to that of a column packed with 11 μm particles (Leinweber and Tallarek, 2003). The low generated backpressure and good mass transfer allow the application of elevated flow rates (3–10 times higher), thus enabling ultrafast separations, down to only a few seconds for the separation of several substrates and metabolites (Van Nederkassel et al., 2003). Alternatively, it is also possible to use very long monoliths at a reasonable flow rate to reach an elevated resolution in a practical analysis time. For example, Tanaka et al. (Miyamoto et al., 2008) constructed an 11.4 m column by coupling numerous monolith columns, which provide 1,000,000 theoretical plates for an analysis time around 16 h. In 2011, a second generation of monolith has been released. The latter possesses smaller macropores of 1.2 μm and larger mesopores of 15 nm. As recently reported (Hormann and Tallarek, 2014), because of a more dense packing, this second generation of silica monoliths provides kinetic performance close to that of columns packed with porous sub-2 μm particles. However, it possesses significantly lower permeability compared with the first-generation silica monoliths. Therefore, its use for high-resolution separations may be limited. Despite these exceptional properties, monoliths are not widely used and less than 1% of chromatographers routinely use silica-based monolithic columns (Majors, 2008). Several explanations for their limited

Table 1.2 Comparison of Selected Fast Chromatographic Approaches

Approaches	Advantages	Limitations
Monoliths	Very low backpressure due to the elevated permeability	Lack of chemistries (C18, C18 endcapped, C8) and providers
	Approach compatible with a conventional HPLC system	Direct method transfer impossible between conventional HPLC and monolithic supports
	Different geometries (e.g., 2.1 mm I.D.) are available	Limited resistance in terms of backpressure (<200 bar) and pH ($2 < pH < 8$)
High-temperature liquid chromatography (HTLC)	Green chemistry: decrease of the organic modifier amount at elevated temperature	Stability of the solutes and silica-based stationary phases can be critical at $T > 100^{\circ}C$
	Improvement of peak shape for basic drugs and large molecules (e.g., peptides and proteins)	Need to use dedicated instrumentation (preheating and cooling devices + backpressure regulator)
	Possible to use this strategy with UHPLC system to further improve performance	Method transfer difficult because of changes in selectivity with temperature
Ultrahigh-pressure liquid chromatography (UHPLC)	Easy method transfer between HPLC and UHPLC	Need to use dedicated instrumentation (low σ^2_{ext}, elevated acquisition rate, fast injection) and column compatible with ultrahigh pressures
	Important decrease in analysis time	Cost of instrumentation and consumables higher than conventional HPLC
	Large variety of columns packed with sub-2 μm particles (more than 10 providers)	Solvent compressibility and frictional heating are issues for ΔP close to 1000 bar
Superficially porous particles (SPP)	Interesting approach to limit diffusion of large molecules in pores	Limited number of chemistries (C18, C8, HILIC) and providers
	The quality of the packing is excellent ($h \approx 1.5$) compared to other materials ($h \approx 2-2.5$)	Retention and loading capacity slightly lower than conventional HPLC (particularly for sub-2 μm SPP)
	Approach potentially compatible with a conventional HPLC system	Lower resistance in terms of backpressure (<600 bar) and pH ($2 < pH < 9$) compared with fully porous particles

HPLC, *High-pressure liquid chromatography;* HILIC, *hydrophilic interaction liquid chromatography.*
Adapted from Guillarme, D., Ruta, J., Rudaz, S., Veuthey, J.-L., 2010a. New trends in fast and high-resolution liquid chromatography: a critical comparison of existing approaches. Anal. Bioanal. Chem. 397, 1069−1082; Guillarme, D., Schappler, J., Rudaz, S., Veuthey, J.L., 2010b. Coupling ultra-high pressure liquid chromatography with mass spectrometry. Trends Anal. Chem. 29, 15−27.

use include patent exclusivity (limited number of suppliers), low range of column chemistry and geometry (columns are available in 2, 3, and 4.6 mm I.D. but only with a maximal length of 100 mm), and the limited resistance of the support in terms of pH and, more importantly, backpressure ($\Delta P_{max} = 200$ bar) (Brice et al., 2009).

High-temperature liquid chromatography (HTLC) is a simple and elegant strategy to improve chromatographic performance. An elevated mobile phase temperature (beyond 60°C and up to 200°C) could be valuable for improving chromatographic performance. Indeed, a temperature increase results in a significant reduction of mobile phase viscosity, leading to higher diffusion coefficients and improved mass transfer, thereby increasing the optimal linear velocity toward higher values (u_{opt} proportional to the ratio T/η) (Heinisch and Rocca, 2009; Li et al., 1997; Guillarme et al., 2007c). Temperature, which directly impacts solvent viscosity, also causes a significant reduction in column backpressure at a constant flow rate. Because of these features, it is possible to maintain resolution and accelerate separations by a factor 3–5 (at 90°C) and up to a factor of 20 (at 200°C), with hydro-organic mixtures containing MeOH and water (Guillarme et al., 2004). Alternatively, longer columns with acceptable backpressures can be employed at elevated temperatures, although it becomes difficult to work under optimal flow rate conditions. In addition to its kinetic performance, HTLC has some additional benefits, summarized in Table 1.2. First, both the dielectric constant and surface tension of water decrease at elevated temperature, and thus water can replace a significant proportion of the organic solvent in the mobile phase (5%–10% less organic solvent for each 30°C) (Guillarme and Heinisch, 2005; Hartonen and Riekkola, 2008). Second, an improvement of the peak shape has been reported for basic compounds because of a decrease of their pK_a values and thus a reduction of secondary interactions with residual silanol groups (Heinisch et al., 2006; Albert et al., 2005). For large molecules, such as peptides, the peak shapes can also be improved because diffusion coefficients strongly increase with temperature. Finally, as temperature is a thermodynamic parameter, it can be used to tune selectivity during method development (McNeff et al., 2007). Although HTLC has been investigated in academic laboratories, it remains seldom used in an industrial environment. The major limitations of this approach are related to the limited number of stable stationary phases compatible with elevated temperature (Teutenberg et al., 2007), the required modification of LC equipment to adequately control the mobile phase temperature (Thompson et al., 2001), and most importantly, the putative thermal degradation of compounds (Thompson and Carr, 2002).

The most recently introduced strategy to improve chromatographic performance is the use of superficially porous particles (SPP), also named fused-core or core–shell, which became commercially available in 2007 under the trademark Halo from Advanced Materials Technology (Wilmington, DE, USA) (Fekete et al., 2014b). This technology was originally developed by J.J. Kirkland in the 1990s to limit diffusion of the macromolecules into the pores (Kirkland, 1992), but smaller particle sizes (1.3, 1.7, 2.5–2.7 μm) have now been incorporated. Nowadays, this approach consists of using sub-3 μm SPP composed of a solid inner core and a thin porous outer core. In comparison with totally porous particles of similar diameters, the diffusion path is much shorter because the inner core is solid-fused silica, which is impenetrable by analytes (thus decreasing the C-term of the Van Deemter curve, mass transfer resistance) (Salisbury, 2008; Cavazzini et al., 2007). This obviously minimizes peak broadening, especially at elevated linear velocities (Destefano et al., 2008). This characteristic is particularly important for the separation of large molecules (i.e., peptides or intact proteins) because slow mass transfer induces a loss of efficiency with rapid separations on porous particles (Gritti et al., 2007). Additionally, this material presents an extremely narrow particle size distribution and high packing density compared to porous particles, leading to a smaller A term in the Van Deemter curve (i.e., Eddy diffusion) (Gritti et al., 2007). Additionally, the presence of a solid core within an SPP has a direct impact on longitudinal diffusion (B term of the Van Deemter equation). It decreases the B term contribution to the plate height by about 20%. Indeed, various authors have determined h values down

to 1.5 (Gritti et al., 2007) or even 1 (Gritti et al., 2010) for such columns, in contrast to values of 2–3 for columns packed with porous particles. Thus, for an identical column length, the semiporous particles of 2.7 μm particles maintain around 80% of the efficiency of sub-2 μm particles but with a twofold lower backpressure (Cunliffe et al., 2007; Fekete et al., 2009). This promising approach has grown quickly in recent years, and today the number of suppliers for SPP particle columns is relatively large (Majors, 2008; Novakova and Vickova, 2009). However, even if the generated backpressure is two times lower than that of columns packed with sub-2 μm particles, the resistance of the support to pressure claimed by providers is also almost twice lower (600 vs. 1000 bar).

3.2 BEST LIQUID CHROMATOGRAPHY APPROACH IN ISOCRATIC MODE—THEORY AND APPLICATIONS

In isocratic mode, the throughput and resolving power of the different strategies were evaluated using a 2D map reported in Fig. 1.5. In this representation, two important parameters were selected. For the

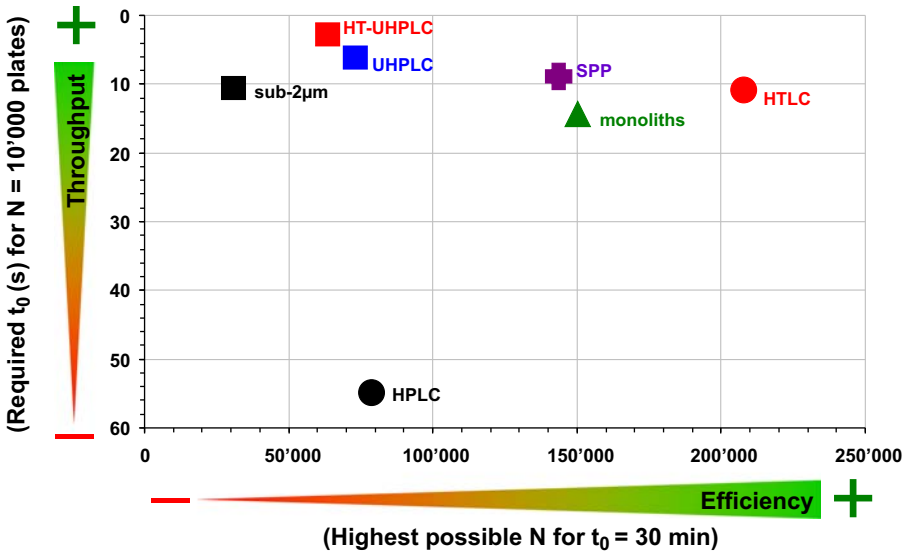

FIGURE 1.5

Performance comparison of liquid chromatography strategies in isocratic mode in terms of throughput (t_0 for $N = 10{,}000$ plates) and maximal resolution (N_{max} for $t_0 = 30$ min) for a model compound, butylparaben with MW of 200 g/mol. The data were gathered using the kinetic plot methodology, considering a maximal pressure of 200 bar for monoliths, 400 bar for high-pressure liquid chromatography (HPLC), high-temperature liquid chromatography (HTLC) and sub-2 μm, 600 bar for superficially porous particles (SPP) and 1000 bar for ultrahigh-pressure liquid chromatography (UHPLC) and HT-UHPLC.

Adapted from Guillarme, D., Ruta, J., Rudaz, S., Veuthey, J.-L., 2010a. New trends in fast and high-resolution liquid chromatography: a critical comparison of existing approaches. Anal. Bioanal. Chem. 397, 1069–1082; Guillarme, D., Schappler, J., Rudaz, S., Veuthey, J.L., 2010b. Coupling ultrahigh pressure liquid chromatography with mass spectrometry. Trends Anal. Chem. 29, 15–27, with permission.

separation speed, the column dead time ($t_{10,000}$) required to attain an efficiency of 10,000 plates was estimated. Such a plate number is generally sufficient for high-throughput separations of conventional samples that contain a limited number of compounds. For the resolving power, the maximal achievable efficiency $N_{30\ \mathrm{min}}$ was calculated for a column dead time of 30 min (equivalent to an analysis time of 3 h for $k = 5$). This analysis time is quite long but not prohibitive when dealing with very complex samples (e.g., proteomics, metabolomics, etc.). Basically, the values of $t_{10,000}$ and $N_{30\ \mathrm{min}}$ were calculated using the Van Deemter data (H, u) and permeability values $K_{v,0}$ experimentally determined for each analytical strategy. Then, the data were computed considering the maximal pressure drop of the system (ΔP_{max} of 200 bar for monoliths; 400 bar for HPLC, sub-2 μm, and HTLC; 600 bar for SPP; and 1000 bar for UHPLC and HT-UHPLC). The corresponding column lengths and mobile phase flow rates required were calculated. Thus, the column dead times and plate numbers presented in Fig. 1.5 always correspond to a pressure drop equal to ΔP_{max} with variable column lengths and mobile phase flow rates. For a better understanding of the employed procedure to construct this 2D map, readers can refer to a few didactic papers on kinetic plot methodology (Desmet et al., 2005a,b, 2006a,b; Billen et al., 2007; Desmet and Cabooter, 2009; Desmet, 2008; Fekete et al., 2015).

According to Fig. 1.5, in terms of throughput (Y-axis), conventional HPLC ($t_{10,000} = 55$ s for $N = 10{,}000$ plates) is clearly not competitive with the other strategies. As expected from theory, the analysis time can be significantly reduced with monoliths ($t_{10,000} = 15$ s) because of the very low generated backpressure, but this material suffers from a too limited upper pressure limit compared with SPP columns or those packed with sub-2 μm particles. HTLC appeared beneficial for reducing the analysis time ($t_{10,000} = 11$ s) because of the improvement of diffusion coefficients related to the mobile phase viscosity decrease with temperature. For example, Yang et al. (2000) showed that ultrafast separations could be achieved at very high temperatures. A separation of five alkylphenones was carried out with a conventional 50 × 4.6 mm column packed with 2.5-μm particles in only 20 s (ΔP of 360 bar), instead of 20 min at ambient temperature. The use of columns packed with sub-2 μm particles remains the most efficient strategy to improve throughput, particularly when small particles are combined with high pressure and elevated temperature, where a 20-fold increase of throughput compared to that of conventional HPLC ($t_{10,000} = 3$ s for $N = 10{,}000$ plates) is possible. As shown in Fig. 1.6A, a mixture of four preservatives was separated in less than 10 s by HT-UHPLC using a 50 × 2.1 mm column packed with 1.7 μm particles at 1.8 mL/min and 90°C (Nguyen et al., 2007).

The maximal efficiency that can be reached for a $t_0 = 30$ min (X-axis, $N_{30\ \mathrm{min}}$) is between 31,000 and 208,000 plates. Unfortunately, long columns operating in the B term–dominated region of the Van Deemter curve are required (low mobile phase flow rate zone) (Guillarme et al., 2009; Desmet et al., 2006a,b). To reach such elevated efficiencies, the required column was between 0.6 and 3.4 m in length, whereas the mobile phase flow rates ranged between 50 and 270 μL/min for a 2.1-mm I.D. column. Therefore, the strategies involving the use of small particles (i.e., sub-2 μm, UHPLC and HT-UHPLC) are less potent ($31{,}000 < N_{30\ \mathrm{min}} < 73{,}000$ plates) because of the elevated generated backpressure. This observation has been experimentally confirmed by Sandra et al. (De Villiers et al., 2006b) who demonstrated that an N_{max} of 74,000 plates was possible for a test mixture under isocratic conditions at 40°C, using a 450 mm column length packed with 1.7 μm particles at 1000 bar. In contrast, the maximal efficiency of columns packed with 5-μm particles reported in Fig. 1.5 was around 80,000 plates and can be increased by 2.6-fold at elevated temperatures. Because of their elevated permeability, monolithic supports also represent a valuable strategy for increasing the plate

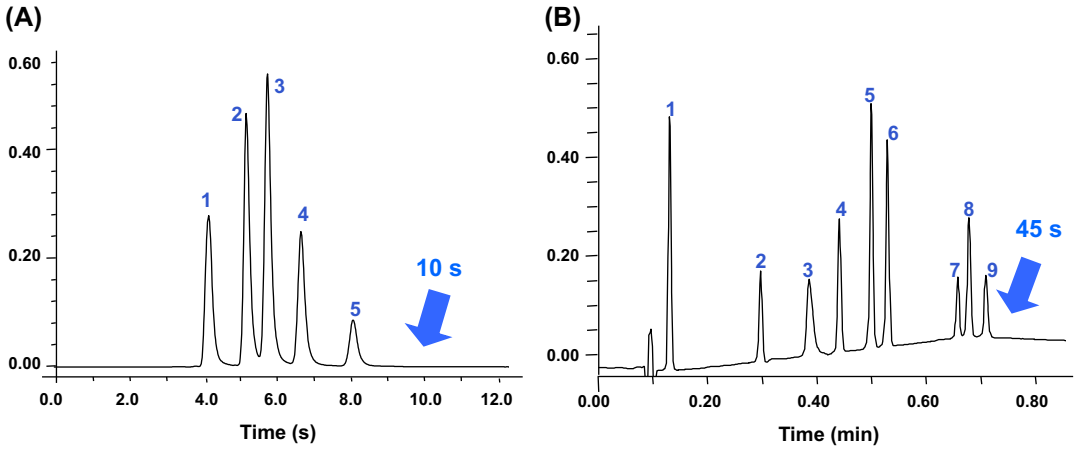

FIGURE 1.6

Ultrafast separations carried out in HT-ultrahigh-pressure liquid chromatography. (A) Isocratic separation of various preservatives and uracil. Column: Acquity bridged ethylsiloxane/silica hybrid (BEH) C18 (50 × 2.1 mm I.D., 1.7 μm); mobile phase: water−acetonitrile (50:50%, v/v); flow rate: 1800 μL/min; temperature: 90°C; (B) Gradient separation of several doping agents. Column: Acquity BEH Shield RP18 (50 × 2.1 mm I.D., 1.7 μm); mobile phase: 0.1% formic acid in water−0.1% formic acid in acetonitrile; flow rate: 1800 μL/min; temperature: 90°C.

Adapted from Nguyen, D.T.T., Guillarme, D., Heinisch, S., Barrioulet, M.P., Rocca, J.L., Rudaz, S., Veuthey J.L., 2007. High throughput liquid chromatography with sub-2 μm particles at very high pressure and high temperature. J. Chromatogr. A 1167, 76–84, with permission.

count compared to conventional HPLC ($N_{30\ \mathrm{min}}$ is twofold higher) (Tanaka et al., 2002). However, the column length needs to be around 1.7 m, so numerous commercially available 100 mm columns length need to be coupled in series. Although some authors have coupled up to 10 columns, the cost becomes rapidly prohibitive (Bones et al., 2008). Despite the elevated maximal efficiency observed with monoliths, this approach is not competitive with HTLC because the lower maximal pressure drop capability ($\Delta P_{\mathrm{max}} = 200$ bar) limits the length of monolith that can be employed. In HTLC, more than 200,000 plates for a $t_0 = 30$ min can be attained, but with a 3 m column, which can be very expensive (12 250-mm columns). Experimentally, Sandra et al. coupled in series eight 250-mm columns packed with 5-μm particles, corresponding to a total length of 2 m. With this configuration, efficiencies as high as 180,000 plates were attained at 80°C for a test mixture, with t_0 values of 20 min and analysis times around 100 min (Lestremau et al., 2006, 2007). Finally, SPP technology provides $N_{30\ \mathrm{min}}$ values similar to monoliths but with more acceptable column lengths and mobile phase flow rates, such as 1 m and 90 μL/min for a 2.1-mm I.D. column. These results can be attributed to the elevated plates/m values of the SPP column in conjunction with a backpressure around twofold lower than that of columns packed with sub-2 μm particles.

In conclusion, high-throughput separations require the use of columns packed with small particles (UHPLC) and should be carried out preferentially at increased temperatures (HT-UHPLC). It was also demonstrated that temperature and maximal system pressure drop should

be increased as much as possible because both parameters are beneficial for increasing the plate count as well as the throughput. Finally, the use of sub-3 μm SPP allows an additional gain in performance.

3.3 BEST LIQUID CHROMATOGRAPHY APPROACH IN GRADIENT MODE—THEORY AND APPLICATIONS

In the case of complex analyses, the separation is generally carried out in gradient mode, to handle compounds possessing very different physicochemical properties and/or improves the resolving power. In gradient mode, peak capacity must be calculated to estimate the performance (Neue, 2008). Peak capacity describes the number of peaks that can be separated with a resolution of 1 during the gradient duration and depends mainly on the isocratic efficiency, column dead time, and gradient time. Two parameters were selected to evaluate the throughput and resolving power in gradient mode, namely the gradient time required to attain a peak capacity of 100 (t_{100}) and the maximal peak capacity for a gradient time of 3 h ($P_{3\ h}$).

In recent papers (Guillarme et al., 2009, 2010a,b), the strategy developed by Schoenmakers et al. (Wang et al., 2006) was applied to construct kinetic plots in gradient mode. In the graphical representation proposed in Fig. 1.7, a similar approach was employed, using data previously obtained in isocratic mode (H, u, and $K_{v,0}$) for each analytical strategy. Both the lowest gradient times, t_{100} and highest peak capacities, $P_{3\ h}$, correspond to a pressure drop equal to ΔP_{max} and consequently to different column lengths and mobile phase flow rates.

According to Fig. 1.7, in terms of throughput, the ranking was similar for isocratic and gradient modes, and columns packed with small particles were clearly advantageous (i.e., sub-2 μm, UHPLC and HT-UHPLC). Indeed, it is theoretically possible to attain a $P = 100$ in only 30 s with HT-UHPLC, whereas 7 min are required in conventional HPLC at 400 bar. Columns packed with superficially porous sub-3 μm particles (SPP technology) performed almost equivalently to columns packed with porous sub-2 μm particles (t_{grad} of 1.4 min for $P = 100$), but monoliths and HTLC were less powerful (t_{grad} around 2.5 min for $P = 100$). These calculated values were in agreement with examples from the literature. For the separation of various pharmaceutical compounds, 50 mm columns packed with porous sub-2 μm or superficially porous sub-3 μm particles produce experimental P values higher than 70 in less than 2 min at ambient temperature (Zhang et al., 2009). Fig. 1.6B shows the potential of HT-UHPLC, with a gradient separation of various steroids in less than 45 s, at a temperature of 90°C. Heinisch et al. (Heinisch and Rocca, 2009; Barrioulet et al., 2007) also reported an impressive chromatogram of nine small aromatic compounds separated in less than 15 s by HT-UHPLC. This separation was performed with a 7.8 s gradient, time using a 50 × 2.1 mm, 1.7 μm column at 2 mL/min and 90°C.

In terms of resolving power, monoliths, SPP, UHPLC, HT-UHPLC, and HTLC offer almost the same peak capacities, ranging between 415 and 480 for a gradient time of 3 h. Compared with the isocratic mode, UHPLC and HT-UHPLC generate higher peak capacities in gradient mode. This is because peak capacity is strictly related not only to the chromatographic efficiency but also to the column dead time in gradient mode. Because the latter is strongly reduced in UHPLC and HT-UHPLC compared to the traditional approaches, the maximal peak capacity for a 3 h gradient is enhanced. Conventional HPLC at 400 bar offers around 30% less peak capacity compared to the other approaches, demonstrating that 5 μm particles do not present any practical benefit in gradient mode.

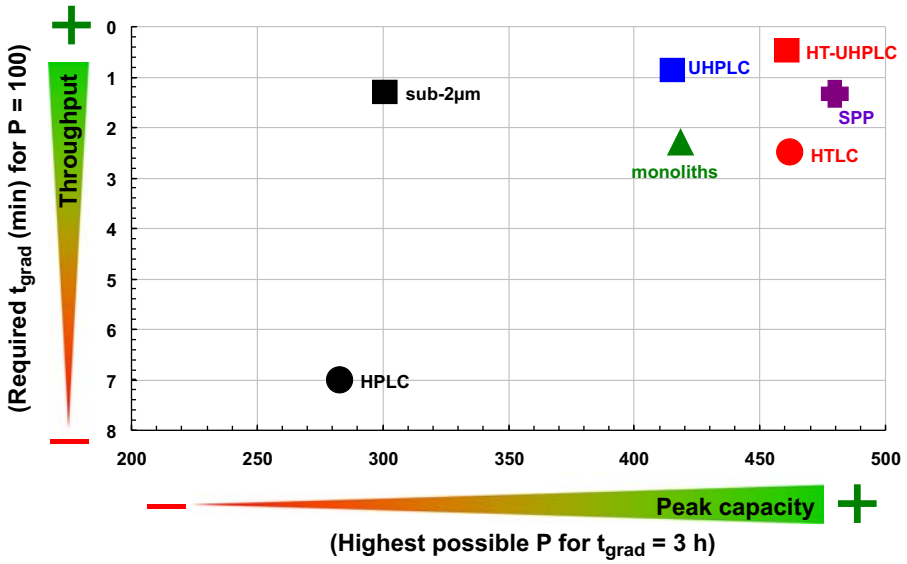

FIGURE 1.7

Performance comparison of liquid chromatography strategies in gradient mode in terms of throughput (t_{grad} for $P = 100$) and maximal resolution (P_{max} for $t_{grad} = 3$ h) for a model compound, butylparaben with MW of 200 g/mol. The data were gathered using the kinetic plot methodology applied to gradient elution and considering the same maximal pressure as for isocratic mode. *HTLC*, high-temperature liquid chromatography; *HT-UHPLC*, high-temperature ultrahigh-pressure liquid chromatography; *SPP*, superficially porous particles; *UHPLC*, ultrahigh-pressure liquid chromatography.

Adapted from Guillarme, D., Ruta, J., Rudaz, S., Veuthey, J.-L., 2010a. New trends in fast and high-resolution liquid chromatography: a critical comparison of existing approaches. Anal. Bioanal. Chem. 397, 1069–1082; Guillarme, D., Schappler, J., Rudaz, S., Veuthey, J.L., 2010b. Coupling ultra-high pressure liquid chromatography with mass spectrometry. Trends Anal. Chem. 29, 15–27, with permission.

Additionally, the sub-2 µm strategy, with a maximal pressure of only 400 bar, was also significantly less practical because of the low packing permeability and small backpressure limitation that reduces the column length and mobile phase flow rate that can be employed.

In conclusion, the SPP and UHPLC technologies are very attractive for maximizing both the throughput and resolution in gradient mode. Whatever the selected strategy, the use of elevated mobile phase temperature is an additional parameter to improve gradient performance.

4. PROBLEMS RELATED TO ULTRAHIGH-PRESSURE LIQUID CHROMATOGRAPHY

According to Table 1.2, the main drawbacks of UHPLC are (1) the need to acquire a dedicated system, optimized in terms of high backpressure pumps and injector, acquisition rate of the detector, injection

cycle time, dwell volume, and system dead volume (Fountain et al., 2009), (2) the need to work with a column that withstands ultrahigh pressures, (3) the elevated backpressure that can produce some important changes in solvent properties (frictional heating and solvent compressibility effects). All these limitations are discussed in detail below.

4.1 THE NEED TO WORK WITH A DEDICATED INSTRUMENTATION

Currently, there is a wide choice of instruments that withstand pressures above 400 bar, from various suppliers. Regarding the selection of a UHPLC system, the cost is certainly a decisive consideration, but it is also important to look at specifications of all available instruments on the market, which are not equivalent. The most important feature is certainly the upper pressure limit and corresponding flow rate, which mostly defines the price of a UHPLC system. For commercial systems, ΔP_{max} varies between 600 and 1500 bar. It has been demonstrated that for fast or ultrafast separations of simple mixtures, the use of small particles was obvious, but there was no need to work with very elevated pressures (Eugster et al., 2010; Grata et al., 2008). For high-throughput experiments, UHPLC instruments with pressure limits around 600–800 bar could provide a suitable solution at a reasonable price. On the other hand, for high-resolution separation, a system with an elevated maximal pressure is mandatory to work at acceptable flow rates (Eugster et al., 2010; Grata et al., 2008). Beside the pressure capability of the apparatus, it is also important that the instrument was adapted to operate in fast and ultrafast modes with reduced column volumes. Indeed, small diameter columns (1 and 2.1 mm I.D.) commonly employed in UHPLC require limited extra-column volumes of detection, tubing, and injection. The following criteria have to be fulfilled to perform suitable separations.

The volumes of the connecting tubes should be drastically reduced. For this reason, the tubing length should be as short as possible and its diameter selected as a compromise between an acceptable pressure drop and a low volume. Hence, a system plumbed with 0.003 or 0.005″ I.D. stainless steel tubing and zero-dead volume fittings should be preferred for UHPLC experiments.

The injection volume should be selected in agreement with column geometry. A rule of thumb is to maintain the injected volume between 1% and 5% of the column dead volume in isocratic mode. As most of the experiments carried out in UHPLC are performed with a 50×2.1 mm column ($V_0 = 120$ µL), the injected volume should be between 1 and 5 µL, to limit band broadening. In addition, a fast injection cycle time is mandatory for analysis times lower than 1 or 2 min.

Last but not least, the detector cell volume, time constant, and acquisition rate should be carefully selected. The detector used in UHPLC should ideally possess a low cell volume (<2 µL), while the sensitivity should not be lower compared to that of a conventional HPLC instrument (pathlength of 10 mm). The detector time constant has to be fast enough ($\tau \leq 100$ ms) because peak widths are very small in UHPLC (only a few seconds). Finally, the UV detector sampling rate must be sufficiently high to acquire a suitable amount of data points for each peak (>20 Hz).

Finally, to reduce the detrimental effect of extra-column volumes and avoid unacceptable loss in efficiency, chromatographic conditions leading to sufficient retention factors (k or k_e at least equal to 3) are recommended in UHPLC.

The last critical parameter to perform ultrafast separations in gradient mode is the system dwell volume, which corresponds to the time necessary for the mixed solvents to reach the column inlet. To work with ultrafast separations, a small gradient delay volume is obviously required. With a large

dwell volume, fast separations are compromised because an isocratic hold is generated at the beginning of the gradient, inducing potential changes in selectivity and longer analysis times.

To check the compatibility of a UHPLC instrument with a given column geometry, it is recommended to characterize the chromatographic system by determining the extra-column and dwell volumes. For optimal compatibility with ultrafast separations, the former should be lower than 20 μL, whereas the latter should be reduced to a few 100 μL. Finally, a comparative study made by a pharmaceutical company on various UHPLC systems can be found elsewhere, for additional information (Cunliffe et al., 2007).

4.2 THE NEED FOR SPECIFIC COLUMNS COMPATIBLE WITH ULTRAHIGH PRESSURES

An important aspect when selecting a UHPLC setup is the selection of a stationary phase that should provide sufficient selectivity as well as acceptable performance and lifetime. Before the commercialization of UHPLC technology, only nonporous particles were used. Jorgenson et al. were the first to compare 1.5 μm porous hybrid particles packed into a 30 μm I.D. fused silica capillary column supplied by Waters (Milford, USA) to 1.0 μm nonporous silica material (Mellors and Jorgenson, 2004). Chromatographic performance was evaluated at pressures up to 4500 bar, and hybrid particles were similar to 1.0 μm nonporous silica particles, in terms of pressure resistance.

In 2004, Waters launched a new generation of hybrid columns packed with 1.7 μm particles that were stable up to 1000 bar. A bridged ethylsiloxane/silica hybrid (BEH) particle provides mechanical and chemical resistance in extreme conditions of pH (1−12), pressure, and temperature (up to 180°C (Gika et al., 2008b)). Numerous other providers have also made available stationary phases packed with sub-2 μm particles, demonstrating the opportunity to transfer almost all existing methods from HPLC to UHPLC. Indeed, the variety of phase chemistries can resolve almost all analytical issues: C8 and C18 for compounds of average polarity; C4 and cyano for the most apolar analytes; diol, amino, silica, and hydrophilic interaction liquid chromatography (HILIC) for polar molecules and biphenyl; perfluorophenyl or zirconia for alternative selectivity. All these stationary phases are not only equivalent in terms of pressure tolerance (from 600 to 1500 bar) and particle size (from 1.5 to 2 μm) but also pH and temperature ranges. Some performance comparisons between the different phases can be found in the literature, and data for column lifetime have also been published.

One of the main criticisms made by early UHPLC users has been the reduced lifetime of columns packed with sub-2 μm particles, compared to conventional columns. It is true that UHPLC columns are systematically exposed to very high pressures, but the packing pressure has been increased in the meantime. In our laboratory, we observed that lifetimes of UHPLC and regular HPLC columns were comparable. However, column lifetime could be expressed as the number of injections, number of column volumes or period of time used. With the latest generation of columns packed with sub-2 μm particles commercialized by different suppliers, it is possible to perform between 500 and 2000 injections or even more on a single column (King et al., 2005; Grumbach et al., 2005). Such values correspond to about 5000−20,000 column volumes, which are fully comparable to those obtained on standard HPLC columns. However, when considering the corresponding period of time, it is significantly reduced compared to conventional HPLC because of the higher throughput of UHPLC. For example, in a routine laboratory that performs a UHPLC analysis in 1−5 min, several hundreds of injections can be performed within a day.

4.3 THE CHANGES IN SOLVENT PROPERTIES WITH PRESSURE

Martin and Guiochon (2005) demonstrated that beyond 100 bar, experimental parameters that are considered as constant by chromatographers (e.g., column porosity, mobile phase density and viscosity, diffusion coefficient, retention factors, and efficiency) could depend on pressure to some extent. Consequently, irreproducible retention factors or loss in efficiency can be observed.

Frictional heating of the mobile phase is certainly the most critical effect that can be observed in UHPLC conditions (Halasz et al., 1975) and has been largely investigated in recent years by Colon et al., Guiochon et al., Sandra et al., and Desmet et al. Columns packed with small particles present low permeability, and thus generate a considerable amount of frictional heating under high pressure drops and elevated flow rates. The heat generation, or power dissipation, is the product of pressure drop (ΔP) and flow rate (F) as reported in Eq. (1.6) (MacNair et al., 1997).

$$Power = F \cdot \Delta P \tag{1.6}$$

Frictional heating and poor heat dissipation cause significant radial and axial temperature gradients across the column. An irregular radial temperature profile produces solute retention alteration, unexpected changes in selectivity and additional band broadening (Jerkovich et al., 2003; Martin and Guiochon, 1983). Reducing the column diameter to capillary dimensions largely eliminates this effect (Jerkovich et al., 2003). Therefore, only capillary columns (e.g., 30–150 μm I.D.) were used before commercialization of UHPLC systems, but Jorgenson et al. (MacNair et al., 1997) recognized that columns of larger diameter could be used with a reasonable value of generated power (i.e., <1 W).

In 2004, Colón et al. investigated in detail the power dissipation of columns with diameters in the mm range, and confirmed that the latter, packed with small particles, would generate acceptable frictional heating. A column of 150 × 1 mm I.D. packed with 1.5 μm particles size with a flow rate of 85 μL/min generated about 1380 bar. Under these conditions, the power dissipation was 195 mW, which corresponded to values encountered in conventional HPLC. Similar results were obtained with a 2.1 mm I.D. column packed with 1.7 μm particles at a linear velocity of 2.5 mm/s (Colon et al., 2004). Thus, the frictional heating generated with the 1–2.1 mm I.D. UHPLC columns employed nowadays was not detrimental to the separation performance (Nguyen et al., 2006a,b).

Sandra et al. investigated the effects of the temperature gradient across the column length due to frictional heating. Experimental data obtained on a 2.1 mm I.D. column packed with 1.7 μm particles, at 1000 bar with a conventional still-air column heater showed no significant efficiency loss (De Villiers et al., 2006a,b).

On the other hand, Guiochon et al. demonstrated the importance of the column external environment on its performance and particularly that frictional heating effects could be detrimental with a 2.1 mm I.D. column. This is illustrated in Fig. 1.8 where an experimental setup allowed the measure of the temperature at the surface of the column and the temperature of the liquid at the column outlet. With this strategy, complete temperature profiles along and across various UHPLC columns under still air conditions at room temperature were constructed. For this purpose, four different column lengths were considered, namely 150, 100, 50, and 30 mm lengths, in 1 and 2.1 mm I.D. Only the results for 2.1 mm I.D. columns of 50, 100, and 150 mm are presented in Fig. 1.8. The authors concluded that, with columns of 2.1 mm I.D., the difference between the inlet and outlet temperature (longitudinal gradient) was between 10 and 20°C, whereas it varied between 3 and 16°C with 1 mm I.D. columns, depending on the considered column length (Gritti and Guiochon, 2008; Novakova et al., 2010).

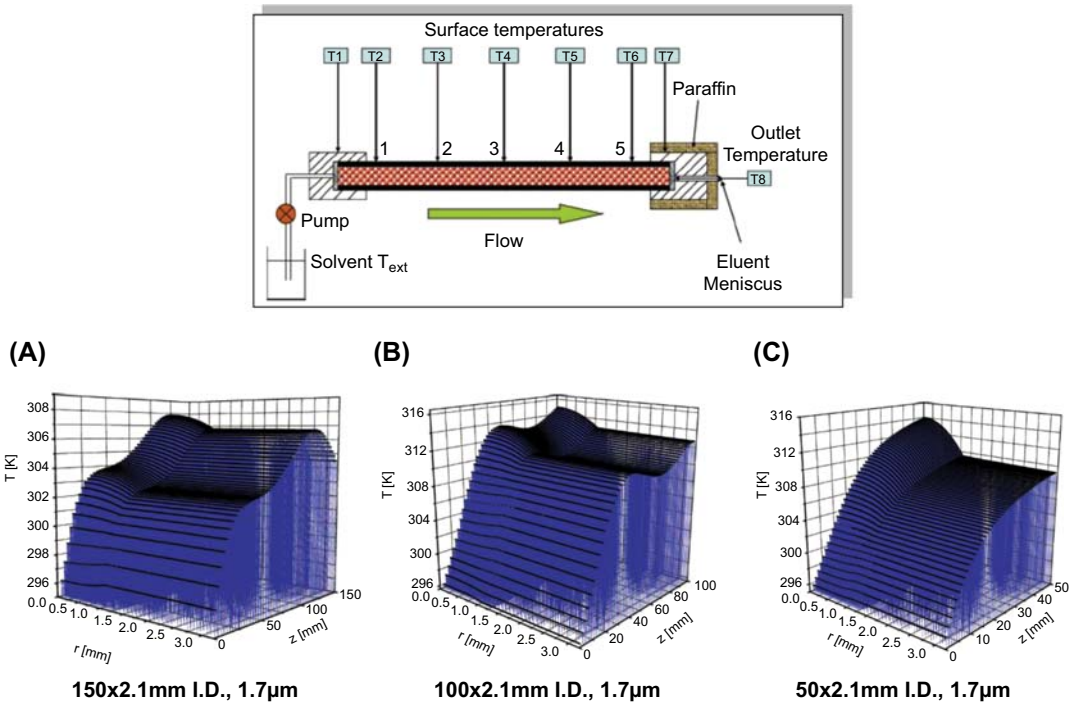

FIGURE 1.8

3D representation of the temperature profiles along and across various chromatographic columns (A) 150 mm × 2.1 mm (BEH) bridged ethylsiloxane/silica hybrid-C18 column, flow rate = 0.95 mL/min, P_{inlet} = 979 bar. (B) 100 mm × 2.1 mm BEH-C18 column, flow rate = 1.45 mL/min, P_{inlet} = 1005 bar. (C) 50 mm × 2.1 mm BEH-C18 column, flow rate = 2 mL/min, P_{inlet} = 775 bar. The experimental setup used to measure the temperature of the surface of the column and the temperature of the liquid exiting the column outlet is also shown.

Adapted from Gritti, F., Guiochon, G., 2008. Complete temperature profiles in ultra-high-pressure liquid chromatography columns. Anal. Chem. 80, 5009–5020, with permission.

To reduce the effect of thermal gradient, Desmet et al. split up a column with a given length L into n segments with length L/n, while providing an active cooling to the capillaries connecting the segments. In this way, the viscous heat was removed at a location where the radial heat removal does not lead to an efficiency loss (i.e., in the thin connection capillaries), while the column segments can be operated under near-adiabatic conditions without suffering from an unacceptable rise of the mobile phase temperature (Broeckhoven et al., 2010).

Besides frictional heating effects, mobile phase viscosity is also dependent on pressure, and organic solvents such as methanol and acetonitrile are more compressible than water (Foley et al., 1989). Jorgenson et al. investigated the solvent compressibility effects in gradient mode and not only noticed a reduction of reproducibility in peptide retention times from run to run in UHPLC conditions (for pressures up to 5000 bar) but also indicated that this problem could be resolved with a

second-generation system (MacNair et al., 1999). In another study performed in isocratic mode, the surge in linear velocity caused by mobile phase compression at the start of isocratic UHPLC runs (with pressures up to 6300 bar) was found to induce a 50% increase in the measured Knox C-term (Jerkovich et al., 2005). However, because the maximal pressure of commercial UHPLC instrument is limited to 1500 bar, the negative impacts of solvent compressibility (i.e., lack of reproducibility and increase of C-term) are less critical.

5. METHOD TRANSFER FROM HIGH-PRESSURE LIQUID CHROMATOGRAPHY TO ULTRAHIGH-PRESSURE LIQUID CHROMATOGRAPHY

In various fields of application (i.e., pharmaceutical, environment, food, etc.), it is essential to be able to transfer existing methods (performed in conventional HPLC conditions) to faster separations involving the use of columns packed with sub-2 µm particles. As most providers now offer equivalent stationary phases packed with 5, 3, and sub-2 µm particles, a geometrical transfer can be performed if the stationary phase chemistry remains identical between the original and final sets of conditions. For this purpose, some rules have to be strictly applied in both isocratic and gradient modes.

5.1 THE RULES FOR ISOCRATIC MODE—THEORY AND APPLICATIONS

For an isocratic transfer between conventional HPLC and UHPLC, two important parameters have to be adjusted, namely the injection volume and the mobile phase flow rate (Guillarme et al., 2007a,b,c).

To avoid a detrimental extra-column band broadening and maintain equivalent sensitivity, it is necessary to adapt the injection volume in agreement with the change of column dimensions. In LC, the injected volume should represent only 1%–5% of the column volume. The latter should be adjusted proportionally to the column internal diameter (d_c) and length (L). Therefore, the injection volume is independent of the particle size and only proportional to the column volume. The new injected volume $\left(V_{inj_2}\right)$ can be determined simply by maintaining the ratio of column dead volume and injected volume constant between regular HPLC and UHPLC.

$$V_{inj_2} = V_{inj_1} \cdot \frac{d_{c2}^2}{d_{c1}^2} \cdot \frac{L_2}{L_1} \tag{1.7}$$

In this equation, subscripts 1 and 2 are related to HPLC and UHPLC column dimensions, respectively. For example, from a conventional 150 × 4.6 mm, 5 µm column to a UHPLC 50 × 2.1 mm, 1.7 µm column, the injected volume should be decreased by 14-fold. To maximize sensitivity, it is possible to inject larger volume but in this case, the sample should be dissolved in a solvent of weaker eluent strength than the initial mobile phase composition (sample focusing).

Regarding mobile phase flow rate, this parameter should be adapted to remain close to maintaining a constant reduced mobile phase linear velocity (v). In HPLC, it is well known that the mobile phase linear velocity (u) is directly proportional to the square of column diameter and also depends on the particle size (d_p) of the support. It is however, completely independent of the column length. For a successful method transfer, it is mandatory to maintain the product $u \times d_p$ constant, to take into

account simultaneous changes in column diameter and particle size of the support. Therefore, for a geometrical transfer, the UHPLC flow rate (F_2) can be calculated with the following equation:

$$F_2 = F_1 \cdot \frac{d_{c_2}^2}{d_{c_1}^2} \cdot \frac{d_{p_1}}{d_{p_2}} \tag{1.8}$$

As an example, from a regular 150 × 4.6 mm, 5 µm column to a UHPLC 50 × 2.1 mm, 1.7 µm column, the mobile phase flow rate should be decreased by 1.6-fold.

The expected analysis time of the transferred method (t_{ana_2}) is directly proportional to the change in column dead time and can be estimated according to:

$$t_{ana_2} = t_{ana_1} \cdot \frac{d_{p_2}}{d_{p_1}} \cdot \frac{L_2}{L_1} \tag{1.9}$$

The expected backpressure (ΔP_2) can be calculated from Darcy's law, which shows that ΔP is inversely proportional to d_p^3 (at the optimal linear velocity) and is strictly related to the column length:

$$\Delta P_2 = \Delta P_1 \cdot \frac{L_2}{L_1} \cdot \frac{d_{p_1}^3}{d_{p_2}^3} \tag{1.10}$$

Finally, the expected solvent consumption of the transferred method (V_2) can be calculated by taking into account the change in internal diameter and column length.

$$V_2 = V_1 \cdot \frac{d_{c_2}^2}{d_{c_1}^2} \cdot \frac{L_2}{L_1} \tag{1.11}$$

Therefore, from a regular 150 × 4.6 mm, 5 µm column to a UHPLC 50 × 2.1 mm, 1.7 µm column, the analysis time is reduced by ninefold. For the abovementioned transfer, the efficiency would be identical, while the backpressure should be ninefold higher and the solvent consumption reduced by 14-fold. This shows the obvious benefits of the UHPLC strategy.

It is possible to find in the literature a large number of applications showing the possibility to transfer isocratic HPLC methods to columns packed with sub-2 µm particles, providing that the chemistry of the two analytical supports remains identical. One example is reported in Fig. 1.9 and presents a method transfer from a conventional 150 × 4.6 mm, 5 µm column to a UHPLC 50 × 2.1 mm, 1.9 µm column (Russo et al., 2008). Both columns provide an equivalent efficiency of around 10,000 plates (similar L/d_p ratio). As shown in the chromatograms, efficiency, selectivity, and resolution remain equivalent for the separation of seven common anxiolytic agents. After adjustment of mobile phase flow rate, the analysis time is decreased by a factor of 7 (22 vs. 3.2 min), as expected from theory for a transfer from 5 to 1.9 µm particles.

5.2 THE RULES FOR GRADIENT MODE—THEORY AND APPLICATIONS

The rules for gradient method transfer between conventional HPLC and UHPLC are not only more complex than isocratic ones but also based on the basic principles of chromatography. First, the injection volume and mobile phase flow rate should be adapted in a similar way as the isocratic mode (see Eqs. 1.7 and 1.8) (Guillarme et al., 2008).

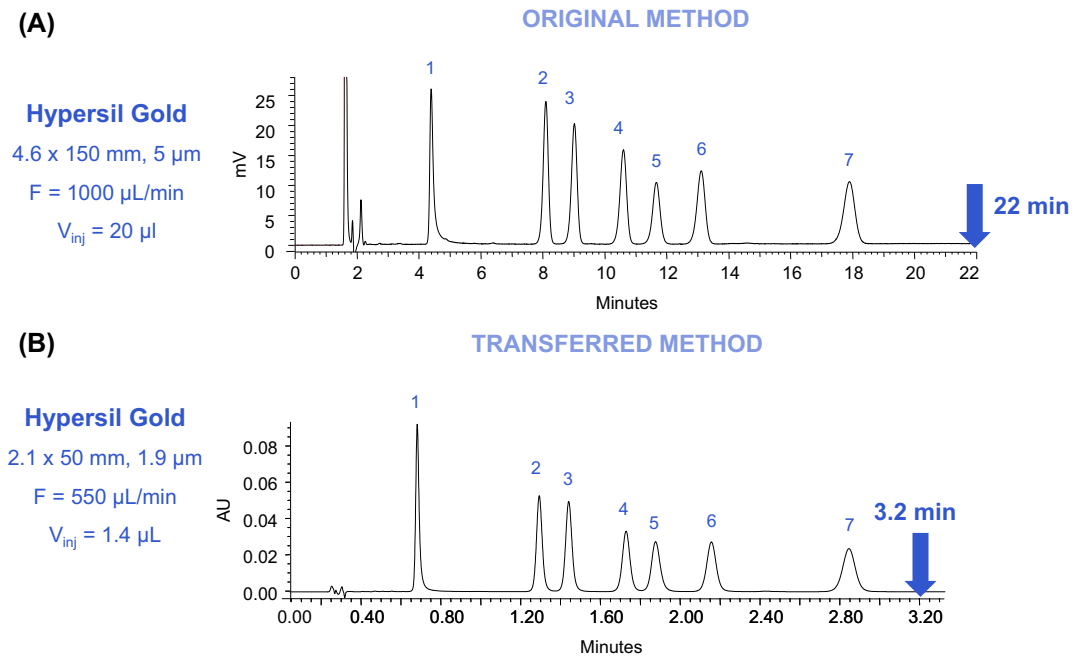

FIGURE 1.9

Isocratic method transfer from regular high-pressure liquid chromatography to ultrahigh-pressure liquid chromatography. Separation of a benzodiazepines mixture in isocratic mode with a mobile phase containing ACN–water (31:69, v/v) with 0.1% formic acid, T = 30°C and λ = 254 nm. (A) Hypersil GOLD 150 × 4.6 mm, 5 µm, F = 1000 µL/min, V_{inj} = 20 µL. (B) Hypersil GOLD 50 × 2.1 mm, 1.9 µm, F = 550 µL/min, V_{inj} = 1.4 µL.

In linear or multilinear gradient elution, the gradient profile can be decomposed as the combination of various isocratic and gradient segments. The rules for efficient gradient transfer originally established by Snyder and Dolan (1998) should be strictly followed. For both parts, it is important to scale the gradient volume in proportion to the number of column volumes to yield identical elution patterns, whereas the initial and final compositions should be constant. In fact, the number of column volumes percolated during the gradient in the regular HPLC system should be equivalent to that of the UHPLC setup.

For any isocratic step within the gradient (i.e., initial isocratic step, isocratic step during a multilinear gradient and also reequilibrating time), the ratio between the isocratic step time (t_{iso}) and the column dead time should be maintained equivalent between conventional HPLC and UHPLC conditions. Therefore, the UHPLC isocratic step (t_{iso_2}) can be determined using:

$$t_{iso_2} = t_{iso_1} \cdot \frac{d_{p_2}}{d_{p_1}} \cdot \frac{L_2}{L_1} \tag{1.12}$$

As an example, from a regular 150 × 4.6 mm, 5 µm column to a UHPLC 50 × 2.1 mm, 1.7 µm column, the isocratic steps which occurred during the gradient process should be reduced by ninefold.

For slope segments, it is mandatory to keep the initial and final gradient composition (*%B*) constant. The new gradient time (t_{grad_2}) can be expressed as:

$$t_{grad_2} = \frac{(\%B_{final_1} - \%B_{initial_1})}{slope_2} \tag{1.13}$$

The gradient slope ($slope_2$) should be calculated to maintain the product of gradient slope and column dead time constant. The new gradient slope ($slope_2$) can be expressed as:

$$slope_2 = slope_1 \cdot \frac{d_{c_1}^2}{d_{c_2}^2} \cdot \frac{L_1}{L_2} \cdot \frac{F_2}{F_1} \tag{1.14}$$

As an example, from a regular 150 × 4.6 mm, 5 µm column to a UHPLC 50 × 2.1 mm, 1.9 µm column, the gradient slope during the gradient process should be increased by ninefold.

When transferring a gradient method from regular HPLC to UHPLC, some changes in selectivity could occur during the gradient run because of differences in dwell volume between the original and the UHPLC configuration. The system dwell volume (V_d) refers to the volume between the mixing point of solvents and the head of the analytical column (Dolan, 2006). After starting the gradient, it will take time until the selected percentage of solvent reaches the column. Because the gradient dwell volume may differ from one system to another, this extra isocratic step would be different and could result in retention time variations affecting resolution for early eluting peaks when transferring a method. To overcome this problem, the ratio of system dwell time (t_d) and column dead time (t_0) must be held constant while changing column dimensions, particle size or mobile phase flow rate.

As the column dead time is reduced by around ninefold between a regular 150 × 4.6 mm, 5 µm column and a 50 × 2.1 mm, 1.7 µm column, the system dwell time should be reduced by the same factor. As mentioned previously, it is then mandatory to work with a UHPLC system possessing a low dwell volume (no more than a few 100 µL) to limit its influence.

Again, many applications of the above discussed approach can be found in the literature. One example has been selected, and it is presented in Fig. 1.10. The original separation of 12 pharmaceutical compounds was achieved using a 150 × 4.6 mm, 5 µm, C18 column and subsequently transferred to UHPLC with a 50 × 2.1 mm, 1.7 µm column possessing strictly similar chemistry (Guillarme et al., 2008). The original separation was performed in ~27 min and was efficiently transferred to UHPLC, giving a separation that was complete in less than 3 min (reduction by a factor of 9, as expected from theory). In addition, both separations were equivalent in terms of sensitivity, peak capacities, and resolution, mainly because of an adequate reduction of system dwell volume (from 1 mL to 100 µL for HPLC and UHPLC, respectively). Finally, the mobile phase flow rate can be increased up to the maximal operating pressure of instrumentation to further reduce analysis time. As illustrated in Fig. 1.10C, at 1000 µL/min the analysis time was cut to only 1.6 min but with a slight loss (about 10%) of chromatographic performance.

6. FIELDS OF APPLICATION FOR ULTRAHIGH-PRESSURE LIQUID CHROMATOGRAPHY—MASS SPECTROMETRY AND RELATED ISSUES

The coupling of UHPLC with MS appears as the ultimate approach in terms of sensitivity, selectivity, and peak assignment for the determination of analytes at low concentrations in complex matrices. Two

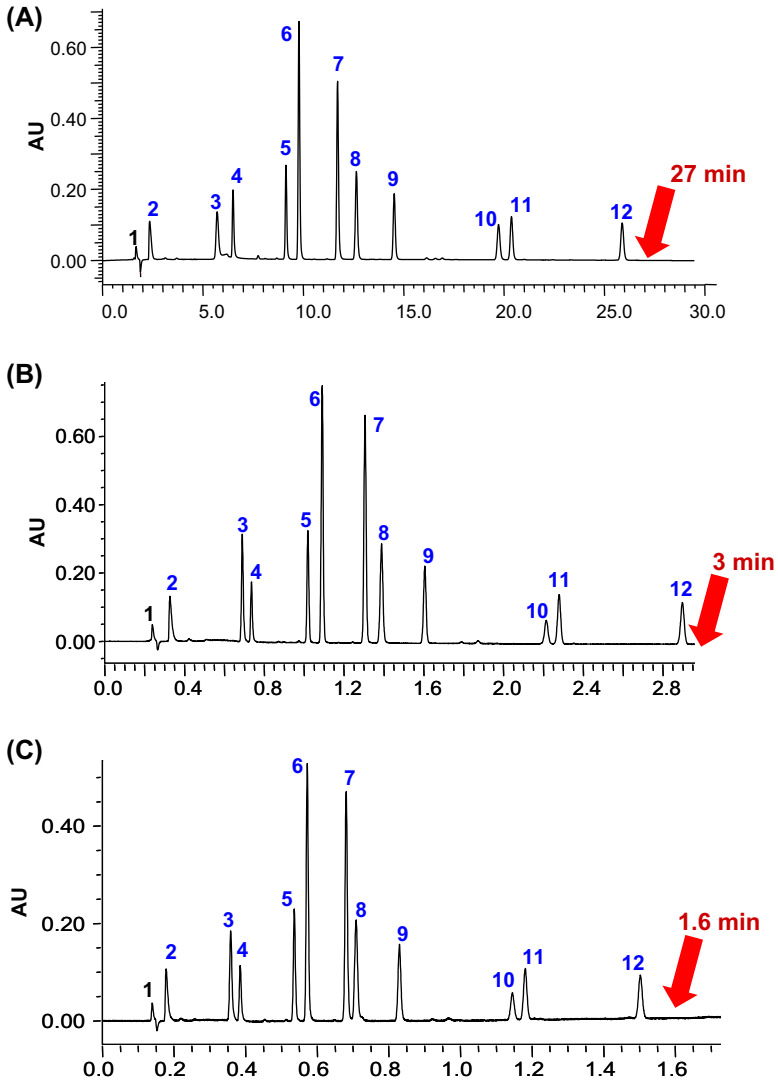

FIGURE 1.10

Gradient method transfer from regular high-pressure liquid chromatography (HPLC) to ultrahigh-pressure liquid chromatography (UHPLC). Separation of a pharmaceutical mixture containing the main product (6) and 11 impurities in gradient mode with HPLC and UHPLC systems: (A) original HPLC method: column: XBridge C18 150 × 4.6 mm, 5 μm; flow rate: 1000 μL/min; injected volume: 20 μL; total gradient time: 45 min. (B) Transferred UHPLC method: column: Acquity bridged ethylsiloxane/silica hybrid (BEH) C18 50 × 2.1 mm, 1.7 μm; flow rate: 610 μL/min; injected volume: 1.4 μL; total gradient time: 5.1 min. (C) Transferred and optimized UHPLC method: column: Acquity BEH C18 50 × 2.1 mm, 1.7 μm; flow rate: 1000 μL/min; injected volume: 1.4 μL; total gradient time: 3.1 min.

Adapted from Guillarme, D., Nguyen, D.T.T., Rudaz, S., Veuthey, J.L., 2008. Method transfer for fast liquid chromatography in pharmaceutical analysis: application to short columns packed with small particles – part II, gradient separation. Eur. J. Pharm. Biopharm. 68, 430–440.

main types of MS analyzers have been coupled with UHPLC, namely quadrupole-based and TOF-MS instruments. The first, operating in the selected ion monitoring (SIM) or selected reaction monitoring (SRM) modes, was preferentially selected for targeted analysis (e.g., bioanalysis, multiresidue screening), whereas the second was particularly useful for nontargeted analysis (e.g., drug metabolism studies, metabolomics).

Regarding quadrupole-based analyzers, the sampling rate can be an issue and modern instruments possessing improved acquisition rates should be selected for hyphenation with UHPLC. With the new generation of analyzers, dwell times have been reduced, down to less than 1 ms for some providers, in SIM as well as in SRM modes (Schappler et al., 2009; Guillarme et al., 2010b; Rodriguez-Aller et al., 2013). TOF instruments are also well adapted to record and store data over a broad mass range without compromising sensitivity. With the latest generation of TOF-MS, high mass resolution (e.g., up to 100,000 FWHM) can be attained at speeds of up to 100 full spectra per second (Rodriguez-Aller et al., 2013).

Aside from the acquisition rate, it has been demonstrated that MS instruments could represent a nonnegligible source of extra-column band broadening in UHPLC compared to a UV detector (Grata et al., 2009; Spaggiari et al., 2013). In addition, even if fast polarity switching (i.e., 15−20 ms) and/or fast ESI/atmospheric pressure chemial ionization mode switching (i.e., 20 ms) are available from several providers to increase productivity, it always compromised sensitivity, peak width, and sampling rate in UHPLC, and should then be used with caution (Schappler et al., 2009; Guillarme et al., 2010b; Grata et al., 2009).

Fig. 1.1 shows that UHPLC−MS(/MS) is the detector of choice for more than 70% of separations carried out by UHPLC. The current state of the art of UHPLC−MS(/MS) is reported in this chapter, with emphasis on the throughput increase and/or resolution improvement afforded by UHPLC technology, and its impact on MS detection capabilities. For this purpose, three promising application fields of the technique were considered: (1) bioanalysis and drug metabolism with tandem MS operating in the SRM mode on triple quadrupole mass spectrometer (QqQ) analyzers; (2) rapid multiresidue screening, using either quadrupole-based instruments in SRM mode or quadrupole time-of-flight mass spectrometer (QqTOF) analyzers; and (3) metabolomics, taking advantage of the very high chromatographic resolution of UHPLC in combination with the exact mass measurement of QqTOF/MS (Guillarme et al., 2010b; Rodriguez-Aller et al., 2013).

6.1 ULTRAHIGH-PRESSURE LIQUID CHROMATOGRAPHY−MASS SPECTROMETRY/MASS SPECTROMETRY FOR HIGH THROUGHPUT IN BIOANALYSIS

Challenges in bioanalytical laboratories include the development of fast LC−MS methods able to separate closely related compounds, such as analytes and metabolites, from endogenous components (Spaggiari et al., 2014).

Because UHPLC greatly enhances the separation throughput and resolution, peaks as narrow as (or less than) 1 s can be obtained. This induces practical issues for bioanalytical applications using MS because sufficient data points (e.g., >15 points per peak) are essential to ensure reliable quantitation. Several critical applications can be found in the literature. For example, Petsalo et al. (2008) published a UHPLC−tandem mass spectrometry (MS/MS) procedure for analyzing nine drugs and their respective metabolites in urine, using a 4 min gradient. An ESI source operating sequentially in positive and negative polarity modes was employed, and dwell times (DT) of 20−30 ms were applied

for each SRM transition. Because peak widths of 4 s were experimentally obtained, only six points were acquired to define peaks, which could limit performance, particularly at the lower limit of quantitation. To accommodate the small UHPLC peak widths, DT can be reduced when many SRM transitions have to be monitored (Schappler et al., 2009), but this can result in sensitivity loss. An alternative approach consists of using various time windows during the acquisition, as proposed by Berg et al. (2009). Finally, to circumvent DT reduction, Li et al. (2008) suggested a useful "peak parking" strategy, which consisted of reducing the flow rate during peak elution, and thus extending the MS acquisition window for quantitative bioanalytical assays. However, the latter strategy is only suitable when a limited number of targeted analytes are analyzed.

In addition, it has been demonstrated in various studies that a significant reduction of matrix effects was brought about by UHPLC technology, compared to regular HPLC. As an example, Chambers et al. (2007) proved that polymeric mixed-mode solid-phase extraction (SPE), combined with UHPLC technology and appropriate mobile phase pH, provided significant benefits for reducing matrix effects from plasma matrix components, and improving the ruggedness and sensitivity of bioanalytical methods.

Considering the analysis time reduction offered by UHPLC technology, the sample preparation procedure becomes the limiting step in terms of total analysis time. Numerous UHPLC bioanalytical applications still involve traditional sample preparation procedures, which drastically increase the total analysis time. A few authors have suggested solutions to this issue, while maintaining sufficient sample preparation selectivity. To date, solid–liquid extraction (SLE) and SPE based on a 96-well plate format were used prior to UHPLC–MS/MS bioanalysis, allowing for selective, sensitive, and, above all, high-throughput analyses (Licea-Perez et al., 2007; Yadav et al., 2008).

6.2 HIGH RESOLUTION DRUG METABOLISM BY ULTRAHIGH-PRESSURE LIQUID CHROMATOGRAPHY–MASS SPECTROMETRY USING QUADRUPOLE TIME-OF-FLIGHT MASS SPECTROMETER ANALYZERS

In drug metabolism experiments, there are also many challenges because of the complex nature of biological matrices and the large diversity of produced metabolites. To identify unknown metabolites, high chromatographic resolution and mass accuracy for fragmentation patterns are key requirements. UHPLC with high resolution analyzers such as QqTOF are particularly useful to fulfill both tasks in a high-throughput environment.

Castro-Perez et al. (2005) were the first to report the use of UHPLC technology with a QqTOF analyzer in the early drug discovery process. This study emphasized improved resolution, in terms of chromatographic and mass spectral quality, and the associated gain in sensitivity afforded by the UHPLC–QqTOF/MS system. These features were explained by the combination of reduced peak width and low ion suppression due to the enhanced resolution of metabolites and endogenous compounds.

Walles et al. have investigated the benefits and drawbacks of three UHPLC–QqTOF/MS methods for fast metabolite identification using alternative MS/MS experiments (MS^E) (Walles et al., 2007; Plumb et al., 2006; Crockford et al., 2008). The high efficiency attributable to UHPLC was the key to the successful identification of isobaric metabolites. In fact, they could not be distinguished with the accurate mass of QqTOF, as they had an identical elemental composition and often similar MS/MS fragmentation patterns. It can be noted that the time spent for structure elucidation created additional bottlenecks and becomes the limiting step when UHPLC–QqTOF experiments are performed.

6.3 ULTRAHIGH-PRESSURE LIQUID CHROMATOGRAPHY—MASS SPECTROMETRY FOR MULTIRESIDUE SCREENING

Multiresidue screening techniques are generally developed to quickly assess the presence of contaminants in a complex sample. Thus, the developed method should be able to detect as many components as possible in a single analytical run. In this context, UHPLC coupled with tandem MS or TOF/MS remains the gold standard. Multiresidue screening methods with UHPLC technology have been applied to a wide variety of analytes and matrices, including: (1) doping agents (Thorngren et al., 2008; Badoud et al., 2009, 2010; Nicoli et al., 2016) and veterinary drugs (Kaufmann et al., 2007) in biological matrices; (2) drugs (Kasprzyk-Hordern et al., 2008a,b), pesticides (Gervais et al., 2008), and herbicides (Pastor Montoro et al., 2007) in environmental matrices; and (3) veterinary drugs (Stolker et al., 2008), drugs (Cai et al., 2008), and pesticides (Romero-Gonzalez et al., 2008; Taylor et al., 2008; Garrido Frenich et al., 2008) in food samples.

Because of the high number of investigated compounds, conventional HPLC runs can be relatively long, particularly to avoid peak coelution leading to matrix effects. It is indeed important to attain sufficient chromatographic resolution, to minimize coelution of compounds with close *m/z* ratios and similar fragmentation pathways. As shown in Fig. 1.11, for the separation of 103 doping agents in a

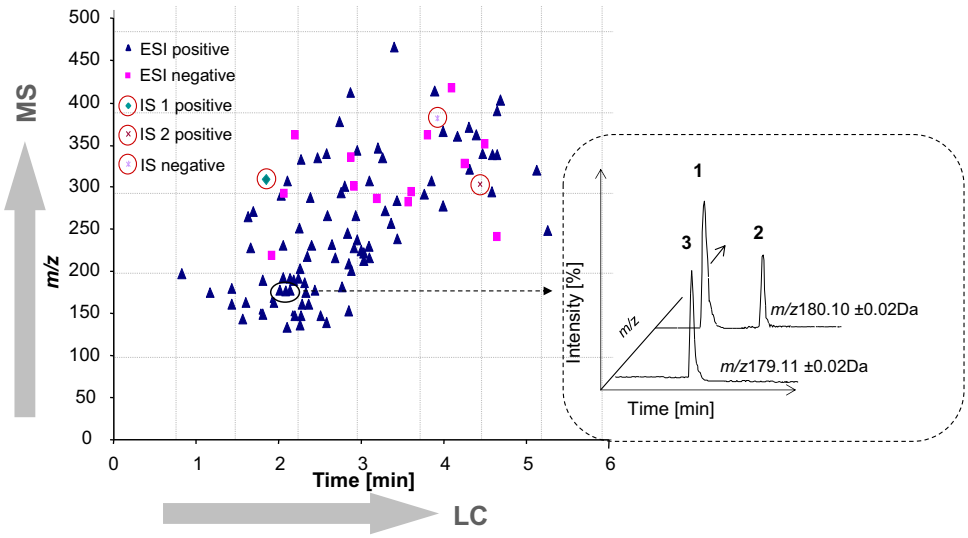

FIGURE 1.11

Separation of 103 doping agents in urine sample according to *m/z* and t_R values. Data from electrospray ionization (ESI) positive and negative mode are plotted together. The three I.S are *circled with a continuous line*. A zone (*dashed line*) is magnified to show the selectivity of coupling ultrahigh-pressure liquid chromatography to the quadrupole time-of-flight mass spectrometer. In the magnified zone, the compounds (1) methylephedrine, (2) 3,4-methylenedioxyamphetamine, and (3) nikethamide are separated as a function of time, intensity, and *m/z*.

Adapted from Badoud, F., Grata, E., Perrenoud, L., Avois, L., Saugy, M., Rudaz, S., Veuthey, J.L., 2009. Fast analysis of doping agents in urine by ultra-high-pressure liquid chromatography–quadrupole time-of-flight mass spectrometry: I. Screening analysis. J. Chromatogr. A 1216, 4423–4433, with permission.

urine sample, gradient conditions were selected to elute analytes presenting a wide polarity range, and formic acid is generally the preferred additive in the mobile phase. To screen compounds by UHPLC, 50–100 mm column lengths were used with gradient times ranging between 5 and 15 min, followed by a reequilibration time of 2–4 min. The column length should be selected in agreement with the gradient time because the longest column did not always provide the highest peak capacity in UHPLC. Indeed, a 50 mm column was found to be optimal for gradient times shorter than 7 min, whereas a 100 mm column was only beneficial for longer gradients. Finally, the 2.1 mm I.D. column was often preferred, to limit extra-column band broadening contributions. Only Kasprzyk-Hordern et al. (2008a,b) reported the successful screening of about 50 pharmaceuticals in wastewater using a 1 mm I.D. column. Even if the consumption of mobile phase and analyte was drastically reduced, peaks were notably broader and distorted with a 1 mm I.D. column, as expected from the influence of external volume contributions.

From the above papers, an approximate increase in throughput by three- to fivefold was observed in UHPLC compared to conventional HPLC methods. In addition to the analysis time decrease, an equivalent or higher chromatographic resolution was reported (Pastor Montoro et al., 2007; Petrovic et al., 2006; Farre et al., 2008). Such improvements were attributed not only to an increase in peak capacity but also to column selectivity changes. Because of different column chemistries, strict comparisons were not always possible.

6.4 ULTRAHIGH-PRESSURE LIQUID CHROMATOGRAPHY–MASS SPECTROMETRY IN METABOLOMICS

Due to the inherent complexity of biological samples and because metabolites can be found at low concentrations, there is a need for analytical systems providing high resolution and increased sensitivity. For this reason, the value of UHPLC–TOF/MS and QqTOF/MS platforms has been demonstrated in a number of studies. The strong reduction of analysis time provided by UHPLC versus HPLC opens up the possibility of high-throughput screening for metabolomic fingerprinting. On the other hand, a longer UHPLC run can be employed to increase the amount of information, essentially for metabolomic profiling. The UHPLC platform has been applied for the global metabolic profiling of (1) human and animal biological fluids, including rat urine (Gika et al., 2008b,c; Plumb et al., 2005), human urine (Gika et al., 2008a,b,c; Guy et al., 2008; Wong et al., 2008), and human serum (Dunn et al., 2008), as well as (2) plant extracts, such as *Arabidopsis thaliana* (Grata et al., 2008; Glauser et al., 2008) and *Panax* herbs (Xie et al., 2008a,b; Dan et al., 2008).

Wilson et al. have used UHPLC for the profiling of rat and mouse urine since 2005 (Gika et al., 2008a,b,c; Plumb et al., 2005). Initially, biological fluids were analyzed on a 50 mm column packed with 1.7 μm particles in combination with TOF/MS. In terms of chromatography, the average peak widths were around 1 s, thus generating a peak capacity of 60 for UHPLC runs of only 1 min. With the additional TOF/MS information, a total of 1000 features (i.e., signals observed with specific m/z and retention times that can be considered as a variable for data treatment) were determined in rat urine. This number was equivalent, or even better than, that achieved on conventional HPLC instrumentation, but with a 10-fold reduction in analysis time. The study performed by Nordstrom et al. (2006) on the quantitative analysis of endogenous and exogenous metabolites in human serum confirmed these results. Indeed, UHPLC provided 20% more detected components in comparison with HPLC. Finally, it was demonstrated that UHPLC displayed some additional advantages over HPLC, such as better

retention time repeatability and signal-to-noise ratios. Finally, two interesting approaches, namely, the application of elevated temperature in UHPLC (up to 180°C) and the use of HILIC columns packed with sub-2 μm particles, were proposed by Wilson et al. to further extend the applicability of UHPLC in metabolomics (Gika et al., 2008b,c).

Because of the complexity and chemical diversity of metabolites present in natural plant extracts, metabolomics is also gaining interest in the field of phytochemistry. The use of UHPLC−TOF/MS as well as QqTOF/MS for untargeted metabolic profiling has been reported by two research groups. Jia et al. reported the profiling of several medicinal *Panax* herbs (Xie et al., 2008a,b; Dan et al., 2008), while Wolfender et al. evaluated a UHPLC−TOF/MS platform for the analysis of a model plant, *A. thaliana* (Grata et al., 2008; Glauser et al., 2008). As shown in Fig. 1.12, they proposed a useful and sensitive multistep strategy for the detection, isolation, and identification of stress-induced metabolites

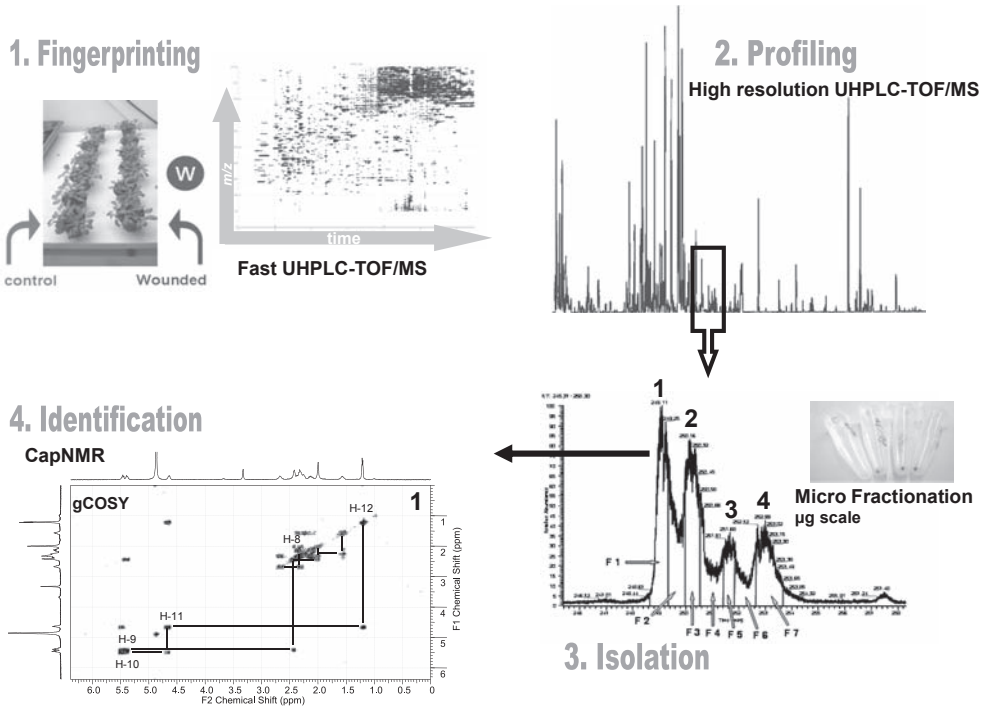

FIGURE 1.12

Plant metabolomics based on a four-step strategy: fingerprinting, profiling, isolation, and identification of stress biomarkers. *UHPLC−TOF/MS*, ultrahigh-pressure liquid chromatography−time-of-flight mass spectrometry; *cap NMR*, cap nuclear magnetic resonance spectroscopy.

Adapted from Guillarme, D., Ruta, J., Rudaz, S., Veuthey, J.-L., 2010a. New trends in fast and high-resolution liquid chromatography: a critical comparison of existing approaches. Anal. Bioanal. Chem. 397, 1069–1082; Guillarme, D., Schappler, J., Rudaz, S., Veuthey, J.L., 2010b. Coupling ultra-high pressure liquid chromatography with mass spectrometry. Trends Anal. Chem. 29, 15–27, with permission.

in *A. thaliana* after leaf wounding, which mimicked herbivore attack (Grata et al., 2008; Glauser et al., 2008). In the first step, a rapid screening gradient was carried out by UHPLC–TOF/MS using a short column of 50 mm. This metabolite fingerprinting was performed on numerous plant specimens to evaluate the intrasample variability and achieve adequate pool formation (Grata et al., 2008). The second step consisted of high resolution metabolite profiling of selected pool samples using a UHPLC column of 150 mm. Gradient conditions used in the metabolomic fingerprinting were adequately transferred to the new column geometry, and analysis times were increased up to 100 min. This profiling allowed confirmation of the presence of different stress-related compounds. The high peak capacity afforded by long columns packed with sub-2 μm was indeed essential to obtain a complete deconvolution of the biomarkers, and resolution of numerous closely related isomers (Grata et al., 2008). The last step of the process was the complete structural determination of minor biomarkers in plants using LC–MS triggered preparative isolation. For this purpose, the UHPLC separation obtained during the metabolic profiling was transferred to semipreparative conditions, using a 19 mm I.D. column packed with 5 μm particles of the same chemistry. Based on the use of a capillary-nuclear magnetic resonance probe, 1D and 2D spectra of good quality were obtained at the μg level, allowing unambiguous structural elucidation of the isolated wound-biomarkers (including known signaling molecules, as well as original oxylipins and jasmonates) (Glauser et al., 2008). This generic analytical platform can be used to screen various other plant extracts.

7. CONCLUSION/PERSPECTIVES

As shown in this chapter, UHPLC is a powerful technology, which is quite easy to implement. With this strategy, it is possible to increase drastically the throughput, while maintaining equivalent performance and/or to increase the resolution within an acceptable analysis time. However, to take full advantage of this platform, it is important to keep in mind that the performance of UHPLC is based not only on the column packing but also on the quality of the chromatographic system. For this reason, UHPLC experiments should be performed on a system compatible with ultrahigh pressure, which possesses reduced system and dwell volumes.

The coupling of UHPLC with MS appears to be the ultimate approach, in terms of sensitivity, selectivity, and peak assignment for the determination of analytes at low concentrations in complex matrices. This strategy has become very popular and has now been applied in numerous fields of application, such as bioanalysis, drug metabolism, multiresidue screening, and metabolomics. However, it is recommended to work with an MS device of the latest generation (quadrupole-based and TOF instruments are the most appropriate) that possesses a sufficient data acquisition rate.

In the future, if 2.1 mm I.D. column becomes the standard dimension for UHPLC, there is certainly not much interest in reducing even more the particle size of the support. Indeed, the backpressure generated by such packing would be detrimental for the chromatographic separation because of the axial and longitudinal temperature gradients within the column (frictional heating effects). To limit these negative effects, the solution would be to work with reduced I.D. (500 μm–1 mm) columns. But in this case, the current chromatographic system needs to be strongly improved in terms of extra-column and dwell volumes. From our point of view, the use of small particles, in conjunction with ultrahigh pressure and elevated temperature, up to 90°C (HT-UHPLC), is certainly more promising both not only for throughput and resolution but also for selectivity and peak shape.

Finally, monolithic columns as well as columns packed with sub-3 μm SPP should be neglected as they could represent some good alternatives to columns packed with fully porous sub-2 μm particles.

REFERENCES

Albert, M., Cretier, G., Guillarme, D., Heinisch, S., Rocca, J.L., 2005. Some advantages of high temperature for the separation of pharmaceutical compounds with mass spectrometry detection. J. Sep. Sci. 28, 1803−1811.

Al-Sayah, M.A., Rizos, P., Antonucci, V., Wu, N., 2008. High throughput screening of active pharmaceutical ingredients by UPLC. J. Sep. Sci. 31, 2167−2172.

Asshauer, J., Halasz, I., 1974. Reproducibility and efficiency of columns packed with 10 μm silica in liquid chromatography. J. Chromatogr. Sci. 12, 139−147.

Badoud, F., Grata, E., Perrenoud, L., Avois, L., Saugy, M., Rudaz, S., Veuthey, J.L., 2009. Fast analysis of doping agents in urine by ultra-high-pressure liquid chromatography−quadrupole time-of-flight mass spectrometry: I. Screening analysis. J. Chromatogr. A 1216, 4423−4433.

Badoud, F., Grata, E., Perrenoud, L., Saugy, M., Rudaz, S., Veuthey, J.L., 2010. Fast analysis of doping agents in urine by ultra-high-pressure liquid chromatography−quadrupole time-of-flight mass spectrometry. II: confirmatory analysis. J. Chromatogr. A 1217, 4109−4119.

Barrioulet, M.P., Heinisch, S., Rocca, J.L., 2007. L'intérêt de la haute température en chromatographie en phase liquide. Spectra Anal. 36, 38−44.

Berg, T., Lundanes, E., Christophersen, A.S., Strand, D.H., 2009. Determination of opiates and cocaine in urine by high pH mobile phase reversed phase UPLC−MS/MS. J. Chromatogr. B 877, 421−432.

Bidlingmeyer, B.A., Rogers, L.B., 1972. Investigation of pressure-induced changes in chromatographic selectivity of methyl and ethyl orange on silica-gel. J. Sep. Sci. 7, 131−158.

Billen, J., Guillarme, D., Rudaz, S., Veuthey, J.L., Ritchie, H., Grady, B., Desmet, G., 2007. Relation between the particle size distribution and the kinetic performance of packed columns: application to a commercial sub-2 μm particle material. J. Chromatogr. A 1161, 224−233.

Bones, J., Duffy, C., Macka, M., Paull, B., 2008. Using coupled monolithic rods for ultra-high peak capacity LC and LC-MS under normal LC operating pressures. Analyst 133, 180−183.

Brice, R.W., Zhang, X., Colon, L.A., 2009. Fused-core, sub-2 μm packings, and monolithic HPLC columns: a comparative evaluation. J. Sep. Sci. 32, 2723−2731.

Broeckhoven, K., Billen, J., Verstraeten, M., Choikhet, K., Dittman, M., Rozing, G., Desmet, G., 2010. Towards a solution for viscous heating in ultra-high pressure liquid chromatography using intermediate cooling. J. Chromatogr. A 1217, 2022−2031.

Cabooter, D., Lestremau, F., Lynen, F., Sandra, P., Desmet, G., 2008. Kinetic plot method as a tool to design coupled column systems producing 100,000 theoretical plates in the shortest possible time. J. Chromatogr. A 1212, 23−34.

Cabrera, K., 2004. Applications of silica-based monolithic HPLC columns. J. Sep. Sci. 27, 843−852.

Cai, Z., Zhang, Y., Pan, H., Tie, X., Ren, Y., 2008. Simultaneous determination of 24 sulfonamide residues in meat by ultra-performance liquid chromatography tandem mass spectrometry. J. Chromatogr. A 1200, 144−155.

Castro-Perez, J., Plumb, R.S., Granger, J.H., Beattie, I., Joncour, K., Wright, A., 2005. Increasing throughput and information content for in vitro drug metabolism experiments using ultra-performance liquid chromatography coupled to a quadrupole time-of-flight mass spectrometer. Rapid Commn. Mass Spectrom. 19, 843−848.

Cavazzini, A., Gritti, F., Kaczmarski, K., Marchetti, N., Guiochon, G., 2007. Mass-transfer kinetics in a shell packing material for chromatography. Anal. Chem. 79, 5972−5979.

Chambers, E., Wagrowski-Diehl, D.M., Lu, Z., Mazzeo, J.R., 2007. Systematic and comprehensive strategy for reducing matrix effects in LC-MS/MS analyses. J. Chromatogr. B 852, 22−29.

Colon, L.A., Cintron, J.M., Anspach, J.A., Fermier, A.M., Swinney, K.A., 2004. Very high pressure HPLC with 1 mm id columns. Analyst 129, 503–504.

Crockford, D.J., Maher, A.D., Ahmadi, K.R., Barrett, A., Plumb, R.S., Wilson, I.D., Nicholson, J.K., 2008. 1H NMR and UPLC-MSE statistical heterospectroscopy: characterization of drug metabolites (xenometabolome) in epidemiological studies. Anal. Chem. 80, 6835–6844.

Cunliffe, J.M., Adams-Hall, S.B., Maloney, T.D., 2007. Evaluation and comparison of very high pressure liquid chromatography systems for the separation and validation of pharmaceutical compounds. J. Sep. Sci. 30, 1214–1223.

Dan, M., Su, M., Gao, X., Zhao, T., Zhao, A., Xie, G.X., Qiu, Y., Zhou, M., Liu, Z., Jia, W., 2008. Metabolite profiling of *Panax notoginseng* using UPLC-ESI-MS. Phytochemistry 69, 2237–2244.

De Villiers, A., Lauer, H., Szucs, R., Goodall, S., Sandra, P., 2006a. Influence of frictional heating on temperature gradients in ultra-high-pressure liquid chromatography on 2.1 mm I.D. columns. J. Chromatogr. A 1113, 84–91.

De Villiers, A., Lestremau, F., Szucs, R., Gélébart, S., David, F., Sandra, P., 2006b. Evaluation of ultra performance liquid chromatography: part I. Possibilities and limitations. J. Chromatogr. A 1127, 60–69.

Desmet, G., Cabooter, D., 2009. Are short columns always the best option? LC-GC Eur. 22, 70–77.

Desmet, G., Clicq, D., Gzil, P., 2005a. Geometry-independent plate height representation methods for the direct comparison of the kinetic performance of LC supports with a different size or morphology. Anal. Chem. 77, 4058–4070.

Desmet, G., Gzil, P., Clicq, D., 2005b. Kinetic plots to directly compare the performance of LC supports. LC-GC Eur. 18, 403–409.

Desmet, G., Cabooter, D., Gzil, P., Verelst, H., Mangelings, D., Van der Heyden, Y., Clicq, D., 2006a. Future of high pressure liquid chromatography: do we need porosity or do we need pressure? J. Chromatogr. A 1130, 158–166.

Desmet, G., Clicq, D., Nguyen, D.T.T., Guillarme, D., Rudaz, S., Veuthey, J.L., Vervoort, N., Torok, G., Cabooter, D., Gzil, P., 2006b. Including practical constraints in the kinetic plot representation of chromatographic performance data: theory and application to experimental data. Anal. Chem. 78, 2150–2162.

Desmet, G., 2008. Comparison techniques for HPLC column performance. LC-GC Eur. 21, 310–320.

Destefano, J.J., Langlois, T.J., Kirkland, J.J., 2008. Characteristics of superficially-porous silica particles for fast HPLC: some performance comparisons with sub-2-μm particles. J. Chromatogr. Sci. 46, 254–260.

Dolan, J.W., Snyder, L.R., 1998. Maintaining fixed band spacing when changing column dimensions in gradient elution. J. Chromatogr. A 799, 21–34.

Dolan, J.W., 2006. Dwell volume revisited. LC-GC N. Am. 24, 458–466.

Dunn, W.B., Broadhurst, D., Brown, M., Baker, P.N., Redman, C.W.G., Kenny, L.C., Kell, D.B., 2008. Metabolic profiling of serum using ultra performance liquid chromatography and the LTQ-orbitrap mass spectrometry system. J. Chromatogr. B 871, 288–298.

Endele, R., Halasz, I., Unger, K., 1974. Influence of the particle size (5–35 μm) of spherical silica on column efficiencies in high-pressure liquid chromatography. J. Chromatogr. A 99, 377–393.

Eugster, P.J., Guillarme, D., Rudaz, S., Veuthey, J.L., Carrupt, P.A., Wolfender, J.L., 2010. Ultra-high pressure liquid chromatography for crude plant extracts profiling. J. AOAC Int. 94, 51–70.

Farre, M., Gros, M., Hernandez, B., Petrovic, M., Hancock, P., Barcelo, D., 2008. Analysis of biologically active compounds in water by ultra-performance liquid chromatography quadrupole time-of-flight mass spectrometry. Rapid Commn. Mass Spectrom. 22, 41–51.

Fekete, S., Fekete, J., Ganzler, K., 2009. Facts and myths about columns packed with sub-3 μm and sub-2 μm particles. J. Pharm. Biomed. Anal. 49, 56–64.

Fekete, S., Schappler, J., Veuthey, J.L., Guillarme, D., 2014a. Current and future trends in UHPLC. J. Chromatogr. A 63, 2–13.

Fekete, S., Dong, M.W., Guillarme, D., 2014b. Superficially porous particles: perspectives, practices and trends. LC-GC Eur. 27, 312−323.

Fekete, S., Veuthey, J.L., Guillarme, D., 2015. Comparison of the most recent chromatographic approaches applied for fast and high resolution separations: theory and practice. J. Chromatogr. A 1408, 1−14.

Foley, J.P., Crow, J.A., Thomas, B.A., Zamora, M., 1989. Unavoidable flow-rate errors in high-performance liquid chromatography. J. Chromatogr. A 478, 287−309.

Fountain, K.J., Neue, U.D., Grumbach, E.S., Diehl, D.M., 2009. Effects of extra-column band spreading, liquid chromatography system operating pressure, and column temperature on the performance of sub-2-μm porous particles. J. Chromatogr. A 1216, 5979−5988.

Garrido Frenich, A., Martinez Vidal, J., Pastor-Montoro, E., Romero-Gonzalez, R., 2008. High-throughput determination of pesticide residues in food commodities by use of ultra-performance liquid chromatography-tandem mass spectrometry. Anal. Bioanal. Chem. 390, 947−959.

Gervais, C., Brosillon, S., Laplanche, A., Helen, C., 2008. Ultra-pressure liquid chromatography−electrospray tandem mass spectrometry for multiresidue determination of pesticides in water. J. Chromatogr. A 1202, 163−172.

Giddings, J.C., 1965. Comparison of theoretical limit of separating speed in gas and liquid chromatography. Anal. Chem. 37, 60−63.

Gika, H.G., Macpherson, E., Theodoridis, G.A., Wilson, I.D., 2008a. Evaluation of the repeatability of ultra-performance liquid chromatography−TOF-MS for global metabolic profiling of human urine samples. J. Chromatogr. B 871, 299−305.

Gika, H.G., Theodoridis, G., Extance, J., Edge, A.M., Wilson, I.D., 2008b. High temperature-ultra performance liquid chromatography−mass spectrometry for the metabonomic analysis of Zucker rat urine. J. Chromatogr. B 871, 279−286.

Gika, H.G., Theodoridis, G.A., Wilson, I.D., 2008c. Hydrophilic interaction and reversed-phase ultra-performance liquid chromatography TOF-MS for metabonomic analysis of Zucker rat urine. J. Sep. Sci. 31, 1598−1608.

Gilar, M., Daly, A.E., Kele, M., Neue, U.D., Gebler, J.C., 2004. Implications of column peak capacity on the separation of complex peptide mixtures in single- and two-dimensional high-performance liquid chromatography. J. Chromatogr. A 1061, 183−192.

Glauser, G., Guillarme, D., Grata, E., Boccard, J., Thiocone, A., Carrupt, P.A., Veuthey, J.L., Rudaz, S., Wolfender, J.L., 2008. Optimized liquid chromatography-mass spectrometry approach for the isolation of minor stress biomarkers in plant extracts and their identification by capillary nuclear magnetic resonance at the microgram scale. J. Chromatogr. A 1180, 90−98.

Grata, E., Boccard, J., Guillarme, D., Glauser, G., Carrupt, P.A., Farmer, E.E., Wolfender, J.L., Rudaz, S., 2008. UPLC-TOF-MS for plant metabolomics: a sequential approach for wound markers analysis in *Arabidopsis thaliana*. J. Chromatogr. B 871, 261−270.

Grata, E., Guillarme, D., Glauser, G., Boccard, J., Carrupt, P.A., Veuthey, J.L., Rudaz, S., Wolfender, J.L., 2009. Metabolite profiling of plant extracts by high temperature UHPLC-TOF/MS. J. Chromatogr. A 1216, 5660−5668.

Gritti, F., Guiochon, G., 2008. Complete temperature profiles in ultra-high-pressure liquid chromatography columns. Anal. Chem. 80, 5009−5020.

Gritti, F., Cavazzini, A., Marchetti, N., Guiochon, G., 2007. Comparison between the efficiencies of columns packed with fully and partially porous C18-bonded silica materials. J. Chromatogr. A 1157, 289−303.

Gritti, F., Leonardis, I., Shock, D., Stevenson, P., Shalliker, A., Guiochon, G., 2010. Performance of columns packed with the new shell particles, Kinetex-C18. J. Chromatogr. A 1217, 1589−1603.

Grumbach, E.S., Wheat, T.E., Kele, M., Mazzeo, J.R., 2005. Developing columns for UPLC: design considerations and recent developments. LC-GC Eur. 12, 40−44.

Guillarme, D., Heinisch, S., Rocca, J.L., 2004. Effect of temperature in reversed phase liquid chromatography. J. Chromatogr. A 1052, 39–51.

Guillarme, D., Heinisch, S., 2005. Detection modes with high temperature liquid chromatography, a review. Sep. Purif. Rev. 34, 181–216.

Guillarme, D., Nguyen, D.T.T., Rudaz, S., Veuthey, J.L., 2007a. Method transfer for fast liquid chromatography in pharmaceutical analysis: application to short columns packed with small particles – part I, isocratic separation. Eur. J. Pharm. Biopharm. 66, 475–482.

Guillarme, D., Nguyen, D.T.T., Rudaz, S., Veuthey, J.L., 2007b. Recent developments in liquid chromatography – impact on qualitative and quantitative performance. J. Chromatogr. A 1149, 20–29.

Guillarme, D., Russo, R., Rudaz, S., Bicchi, C., Veuthey, J.L., 2007c. Chromatographic performance of silica-based stationary phases in high temperature liquid chromatography: pharmaceutical applications. Curr. Pharm. Anal. 4, 221–229.

Guillarme, D., Nguyen, D.T.T., Rudaz, S., Veuthey, J.L., 2008. Method transfer for fast liquid chromatography in pharmaceutical analysis: application to short columns packed with small particles – part II, gradient separation. Eur. J. Pharm. Biopharm. 68, 430–440.

Guillarme, D., Grata, E., Glauser, G., Wolfender, J.L., Veuthey, J.L., Rudaz, S., 2009. Some solutions to obtain very efficient separations in isocratic and gradient modes using small particles size and ultra-high pressure. J. Chromatogr. A 1216, 3232–3243.

Guillarme, D., Ruta, J., Rudaz, S., Veuthey, J.-L., 2010a. New trends in fast and high-resolution liquid chromatography: a critical comparison of existing approaches. Anal. Bioanal. Chem. 397, 1069–1082.

Guillarme, D., Schappler, J., Rudaz, S., Veuthey, J.L., 2010b. Coupling ultra-high pressure liquid chromatography with mass spectrometry. Trends Anal. Chem. 29, 15–27.

Guy, P.A., Tavazzi, I., Bruce, S.J., Ramadan, Z., Kochhar, S., 2008. Global metabolic profiling analysis on human urine by UPLC–TOFMS: issues and method validation in nutritional metabolomics. J. Chromatogr. B 871, 253–260.

Halasz, I., Endele, R., Asshauer, J., 1975. Ultimate limits in high-pressure liquid chromatography. J. Chromatogr. A 112, 37–60.

Hartonen, K., Riekkola, M.L., 2008. Liquid chromatography at elevated temperatures with pure water as the mobile phase. Trends Anal. Chem. 27, 1–14.

Heinisch, S., Rocca, J.L., 2009. Sense and nonsense of high-temperature liquid chromatography. J. Chromatogr. A 1216, 642–658.

Heinisch, S., Puy, G., Barrioulet, M.P., Rocca, J.L., 2006. Effect of temperature on the retention of ionizable compounds in reversed-phase liquid chromatography: application to method development. J. Chromatogr. A 1118, 234–243.

Hjerten, S., Liao, J.L., Zhang, R., 1989. High-performance liquid chromatography on continuous polymer beds. J. Chromatogr. A 473, 273–275.

Hormann, K., Tallarek, U., 2014. Mass transport properties of second-generation silica monoliths with mean mesopore size from 5 to 25 nm. J. Chromatogr. A 1365, 94–105.

Horvath, C.G., Preiss, B.A., Lipsky, S.R., 1967. Fast liquid chromatography. Investigation of operating parameters and the separation of nucleotides on pellicular ion exchangers. Anal. Chem. 39, 1422–1428.

Jerkovich, A.D., Mellors, J.S., Jorgenson, J.W., 2003. The use of micron-sized particles in ultrahigh-pressure liquid chromatography. LC-GC Eur. 16, 20–23.

Jerkovich, A.D., Mellors, J.S., Thompson, J.W., Jorgenson, J.W., 2005. Linear velocity surge caused by mobile-phase compression as a source of band broadening in isocratic ultrahigh-pressure liquid chromatography. Anal. Chem. 77, 6292–6299.

Kasprzyk-Hordern, B., Dinsdale, R.M., Guwy, A.J., 2008a. Multiresidue methods for the analysis of pharmaceuticals, personal care products and illicit drugs in surface water and wastewater by solid-phase extraction

and ultra performance liquid chromatography-electrospray tandem mass spectrometry. Anal. Bioanal. Chem. 391, 1293−1308.

Kasprzyk-Hordern, B., Dinsdale, R.M., Guwy, A.J., 2008b. The effect of signal suppression and mobile phase composition on the simultaneous analysis of multiple classes of acidic/neutral pharmaceuticals and personal care products in surface water by solid-phase extraction and ultra performance liquid chromatography-negative electrospray tandem mass spectrometry. Talanta 74, 1299−1312.

Kaufmann, A., Butcher, P., Maden, K., Widmer, M., 2007. Ultra-performance liquid chromatography coupled to time of flight mass spectrometry (UPLC-TOF): a novel tool for multiresidue screening of veterinary drugs in urine. Anal. Chim. Acta 586, 13−21.

King, S., Stoffolano, P.J., Robinson, E., Eichhold, T.E., Hoke, S.H., Baker, T.R., Richarson, E.C., Wehmeyer, K.R., 2005. The evaluation and application of UPLC for the rapid analysis of dose formulations. LC-GC Eur. 12, 36−39.

Kirkland, J.J., 1972. High performance liquid chromatography with porous silica microspheres. J. Chromatogr. Sci. 10, 593−599.

Kirkland, J.J., 1992. Superficially porous silica microspheres for the fast high-performance liquid chromatography of macromolecules. Anal. Chem. 64, 1239−1245.

Knox, J.H., Saleem, M., 1969. Kinetic conditions for optimum speed and resolution in column chromatography. J. Chromatogr. Sci. 7, 614−622.

Knox, J.H., 1961. Speed of analysis by gas chromatography. J. Chem. Soc. 1, 433−441.

Knox, J.H., 1977. Practical aspects of LC theory. J. Chromatogr. Sci. 15, 352−364.

Leinweber, F.C., Tallarek, U., 2003. Chromatographic performance of monolithic and particulate stationary phases: hydrodynamics and adsorption capacity. J. Chromatogr. A 1006, 207−228.

Lestremau, F., Cooper, A., Szucs, R., David, F., Sandra, P., 2006. High-efficiency liquid chromatography on conventional columns and instrumentation by using temperature as a variable: I. Experiments with 25 cm × 4.6 mm I.D., 5 μm ODS columns. J. Chromatogr. A 1109, 191−196.

Lestremau, F., De Villiers, A., Lynen, F., Cooper, A., Szucs, R., Sandra, P., 2007. High efficiency liquid chromatography on conventional columns and instrumentation by using temperature as a variable: kinetic plots and experimental verification. J. Chromatogr. A 1138, 120−131.

Li, J., Hu, Y., Carr, P.W., 1997. Fast separations at elevated temperatures on polybutadiene-coated zirconia reversed-phase material. Anal. Chem. 69, 3884−3888.

Li, F., Maguigad, J., Peizer, M., Jiang, X., Ji, Q.C., 2008. A novel "peak parking" strategy for ultra-performance liquid chromatography/tandem mass spectrometric detection for enhanced performance of bioanalytical assays. Rapid Commn. Mass Spectrom. 22, 486−494.

Licea-Perez, H., Wang, S., Bowen, C.L., Yang, E., 2007. A semi-automated 96-well plate method for the simultaneous determination of oral contraceptives concentrations in human plasma using ultra performance liquid chromatography coupled with tandem mass spectrometry. J. Chromatogr. B 852, 69−76.

Lippert, J.A., Xin, B., Wu, N., Lee, M.L., 1999. Fast ultrahigh-pressure liquid chromatography: on-column UV and time-of-flight mass spectrometric detection. J. Microcolumn Sep. 11, 631−643.

Lommen, D.C., Snyder, L.R., 1993. Fast HPLC separations with small non porous particles. LC-GC Eur. 11, 222−232.

MacNair, J.E., Lewis, K.C., Jorgenson, J.W., 1997. Ultrahigh-pressure reversed-phase liquid chromatography in packed capillary columns. Anal. Chem. 69, 983−989.

MacNair, J.E., Patel, K.D., Jorgenson, J.W., 1999. Ultrahigh-pressure reversed-phase capillary liquid chromatography − isocratic and gradient elution using columns packed with 1.0-μm particles. Anal. Chem. 71, 700−708.

Majors, R.E., 1972. High-performance liquid chromatography on small particle silica gel. Anal. Chem. 44, 1722−1726.

Majors, R.E., 2003. HPLC column packing design. LC-GC Eur. 16, 8−13.

Majors, R.E., 2008. Highlights of HPLC 2008: part I. LC-GC N. Am. 26, 676–691.
Martin, M., Guiochon, G., 1983. Pressure dependence of diffusion coefficient and effect on plate height in liquid chromatography. Anal. Chem. 55, 2302–2309.
Martin, M., Guiochon, G., 2005. Effects of high pressure in liquid chromatography. J. Chromatogr. A 1090, 16–38.
McNeff, C.V., Yan, B., Stoll, D.R., Henry, R.A., 2007. Practice and theory of high temperature liquid chromatography. J. Sep. Sci. 30, 1672–1685.
Mellors, J.S., Jorgenson, J.W., 2004. Use of 1.5-μm porous ethyl-bridged hybrid particles as a stationary-phase support for reversed-phase ultrahigh-pressure liquid chromatography. Anal. Chem. 76, 5441–5450.
Minakuchi, H., Nakanishi, K., Soga, N., Ishizuka, N., Tanaka, N., 1996. Octadecylsilylated porous silica rods as separation media for reversed-phase liquid chromatography. Anal. Chem. 68, 3498–3501.
Miyamoto, K., Hara, T., Kobayashi, H., Morisaka, H., Tokuda, D., Horie, K., Koduki, K., Makino, S., Nunez, O., Yang, C., 2008. High-efficiency liquid chromatographic separation utilizing long monolithic silica capillary columns. Anal. Chem. 80, 8741–8750.
Neue, U.D., Mazzeo, J.R., 2001. A theoretical study of the optimization of gradients at elevated temperature. J. Sep. Sci. 24, 921–929.
Neue, U.D., 2008. Peak capacity in unidimensional chromatography. J. Chromatogr. A 1184, 107–130.
Nguyen, D.T.T., Guillarme, D., Rudaz, S., Veuthey, J.L., 2006a. Fast analysis in liquid chromatography using small particles size and ultra-high pressure. J. Sep. Sci. 29, 1836–1848.
Nguyen, D.T.T., Guillarme, D., Rudaz, S., Veuthey, J.L., 2006b. Chromatographic behaviour and comparison of column packed with sub-2 μm stationary phases in liquid chromatography. J. Chromatogr. A 1128, 105–113.
Nguyen, D.T.T., Guillarme, D., Heinisch, S., Barrioulet, M.P., Rocca, J.L., Rudaz, S., Veuthey, J.L., 2007. High throughput liquid chromatography with sub-2 μm particles at very high pressure and high temperature. J. Chromatogr. A 1167, 76–84.
Nicoli, R., Guillarme, D., Leueuberger, N., Baume, N., Robinson, N., Saugy, M., Veuthey, J.L., 2016. Analytical strategies for doping control purposes: needs, challenges, and perspectives. Anal. Chem. 88, 508–523.
Nordstrom, A., O'Maille, G., Qin, C., Siuzdak, G., 2006. Nonlinear data alignment for UPLC–MS and HPLC–MS based metabolomics: quantitative analysis of endogenous and exogenous metabolites in human serum. Anal. Chem. 78, 3289–3295.
Novakova, L., Vickova, H., 2009. A review of current trends and advances in modern bio-analytical methods: chromatography and sample preparation. Anal. Chim. Acta 656, 8–35.
Novakova, L., Solichova, D., Solich, P., 2006. Advantages of ultra performance liquid chromatography over high-performance liquid chromatography: comparison of different analytical 2 approaches during analysis of diclofenac gel. J. Sep. Sci. 29, 2433–2443.
Novakova, L., Veuthey, J.L., Guillarme, D., 2010. Practical method transfer from HPLC to UHPLC: the importance of frictional heating. J. Chromatogr. A 1218, 7971–7981.
Pastor Montoro, E., Romero Gonzalez, R., Garrido Frenich, A., Hernandez Torres, M.E., Martinez Vidal, J.L., 2007. Fast determination of herbicides in waters by ultra-performance liquid chromatography/tandem mass spectrometry. Rapid Commn. Mass Spectrom. 21, 3585–3592.
Petricoin, E.F., Liotta, L.A., 2004. Proteomic approaches in cancer risk and response assessment. Trends Mol. Med. 10, 59–64.
Petrovic, M., Gros, M., Barcelo, D., 2006. Multi-residue analysis of pharmaceuticals in wastewater by ultra-performance liquid chromatography–quadrupole–time-of-flight mass spectrometry. J. Chromatogr. A 1124, 68–81.
Petsalo, A., Turpeinen, M., Pelkonen, O., Tolonen, A., 2008. Analysis of nine drugs and their cytochrome P450-specific probe metabolites from urine by liquid chromatography–tandem mass spectrometry utilizing sub 2 μm particle size column. J. Chromatogr. A 1215, 107–115.

Plumb, R.S., Granger, J.H., Stumpf, C.L., Johnson, K.A., Smith, B.W., Gaulitz, S., Wilson, I.D., Castro-Perez, J., 2005. A rapid screening approach to metabonomics using UPLC and oa-TOF mass spectrometry: application to age, gender and diurnal variation in normal/Zucker obese rats and black, white and nude mice. Analyst 130, 844–849.

Plumb, R.S., Johnson, K.A., Rainville, P., Smith, B.W., Wilson, I.D., Castro-Perez, J.M., Nicholson, J.K., 2006. UPLC/MSE: a new approach for generating molecular fragment information for biomarker structure elucidation. Rapid Commn. Mass Spectrom. 20, 1989–1994.

Poppe, H., 1997. Some reflections on speed and efficiency of modern chromatographic methods. J. Chromatogr. A 778, 3–21.

Rodriguez-Aller, M., Gurny, R., Veuthey, J.L., Guillarme, D., 2013. Coupling UHPLC with MS(/MS): constraints and possible applications. J. Chromatogr. A 1292, 2–18.

Romero-Gonzalez, R., Garrido Frenich, A., Martinez Vidal, J.L., 2008. Multiresidue method for fast determination of pesticides in fruit juices by ultra performance liquid chromatography coupled to tandem mass spectrometry. Talanta 76, 211–225.

Russo, R., Guillarme, D., Nguyen, D.T.T., Bicchi, C., Rudaz, S., Veuthey, J.L., 2008. Pharmaceutical applications on columns packed with sub-2 μm particles. J. Chromatogr. Sci. 46, 199–208.

Salisbury, J.J., 2008. Fused-core particles: a practical alternative to sub-2 micron particles. J. Chromatogr. Sci. 46, 883–886.

Schappler, J., Nicoli, R., Nguyen, D.T.T., Rudaz, S., Veuthey, J.L., Guillarme, D., 2009. Coupling ultra-high pressure liquid chromatography with single quadrupole mass spectrometry for the analysis of a complex drug mixture. Talanta 78, 377–387.

Snyder, L.R., 1969. Column efficiencies in liquid adsorption chromatography: past, present and future. J. Chromatogr. Sci. 7, 352–360.

Spaggiari, D., Fekete, S., Eugster, P.J., Veuthey, J.L., Geiser, L., Rudaz, S., Guillarme, D., 2013. Contribution of various types of liquid chromatography-mass spectrometry instruments to band broadening in fast analysis. J. Chromatogr. A 1310, 45–55.

Spaggiari, D., Geiser, L., Rudaz, S., 2014. Coupling ultra-high-pressure liquid chromatography with mass spectrometry for in-vitro drug-metabolism studies. Trends Anal. Chem. 63, 129–139.

Stolker, A.A.M., Rutgers, P., Oosterink, E., Lasaroms, J.J.P., Peters, R.J.B., Van Rhijn, J.A., Nielen, N.W.F., 2008. Comprehensive screening and quantification of veterinary drugs in milk using UPLC-ToF-MS. Anal. Bioanal. Chem. 391, 2309–2322.

Svec, F., Frechet, J.M.J., 1992. Continuous rods of macroporous polymer as high-performance liquid chromatography separation media. Anal. Chem. 64, 820–822.

Tanaka, N., Kobayashi, H., Ishizuka, N., Minakuchi, H., Nakanishi, K., Hosoya, K., Ikegami, T., 2002. Monolithic silica columns for high-efficiency chromatographic separations. J. Chromatogr. A 965, 35–49.

Taylor, M.J., Keenan, G.A., Reid, K.B., Uria Fernandez, D., 2008. The utility of ultra-performance liquid chromatography/electrospray ionisation time-of-flight mass spectrometry for multi-residue determination of pesticides in strawberry. Rapid Commn. Mass Spectrom. 22, 2731–2746.

Teutenberg, T., Tuerk, J., Holzhauser, M., Giegold, S., 2007. Temperature stability of reversed phase and normal phase stationary phases under aqueous conditions. J. Sep. Sci. 30, 1101–1114.

Thompson, J.D., Brown, J.S., Carr, P.W., 2001. Dependence of thermal mismatch broadening on column diameter in high-speed liquid chromatography at elevated temperatures. Anal. Chem. 73, 3340–3347.

Thompson, J.D., Carr, P.W., 2002. A study of the critical criteria for analyte stability in high-temperature liquid chromatography. Anal. Chem. 74, 1017–1023.

Thorngren, J.O., Ostervall, F., Garle, M., 2008. A high-throughput multicomponent screening method for diuretics, masking agents, central nervous system (CNS) stimulants and opiates in human urine by UPLC-MS/MS. J. Mass Spectrom. 43, 980–992.

Van Nederkassel, A.M., Aerts, A., Dierick, A., Massart, D.L., Van Der Heyden, Y., 2003. Fast separations on monolithic silica columns: method transfer, robustness and column ageing for some case studies. J. Pharm. Biomed. Anal. 32, 233–249.

Vivilecchia, R.V., Cotter, R.L., Limpert, R.J., Thimot, N.Z., Little, J.N., 1974. Considerations of small particles in different modes of liquid chromatography. J. Chromatogr. A 99, 407–424.

Walles, M., Gauvin, C., Morin, P.E., Panetta, R., Ducharme, J., 2007. Comparison of sub-2-μm particle columns for fast metabolite ID. J. Sep. Sci. 30, 1191–1199.

Wang, X., Stoll, D.R., Carr, P.W., Schoenmakers, P.J., 2006. A graphical method for understanding the kinetics of peak capacity production in gradient elution liquid chromatography. J. Chromatogr. A 1125, 177–181.

Wong, M.C.Y., Lee, W.T.K., Wong, J.S.Y., Frost, G., Lodge, J., 2008. An approach towards method development for untargeted urinary metabolite profiling in metabonomic research using UPLC/QToF MS. J. Chromatogr. B 871, 341–348.

Wren, S.A.C., Tchelitcheff, P., 2006. Use of ultra-performance liquid chromatography in pharmaceutical development. J. Chromatogr. A 1119, 140–146.

Wu, N., Lippert, J.A., Lee, M.L., 2001. Practical aspects of ultrahigh pressure capillary liquid chromatography. J. Chromatogr. A 911, 1–12.

Xiang, Y., Yan, B., McNeff, C.V., Carr, P.W., Lee, M.L., 2003a. Synthesis of micron diameter polybutadiene-encapsulated non-porous zirconia particles for ultrahigh pressure liquid chromatography. J. Chromatogr. A 1002, 71–78.

Xiang, Y., Yan, B., Yue, B., McNeff, C.V., Carr, P.W., Lee, M.L., 2003b. Elevated-temperature ultrahigh-pressure liquid chromatography using very small polybutadiene-coated nonporous zirconia particles. J. Chromatogr. A 983, 83–89.

Xie, G.X., Ni, Y., Su, M.M., Zhang, Y.Y., Zhao, A.H., Gao, X.F., Liu, Z., Xiao, P.G., Jia, W., 2008a. Application of ultra-performance LC-TOF MS metabolite profiling techniques to the analysis of medicinal *Panax* herbs. Metabolomics 4, 248–260.

Xie, G.X., Plumb, R.S., Su, M., Xu, Z., Zhao, A., Qiu, M., Long, X., Liu, Z., Jia, W., 2008b. Ultra-performance LC/TOF MS analysis of medicinal *Panax* herbs for metabolomic research. J. Sep. Sci. 31, 1015–1026.

Yadav, M., Contractor, P., Upadhyay, V., Gupta, A., Guttikar, S., Singhal, P., Goswami, S., Shrivastav, P.S., 2008. Automated liquid–liquid extraction based on 96-well plate format in conjunction with ultra-performance liquid chromatography tandem mass spectrometry (UPLC–MS/MS) for the quantitation of methoxsalen in human plasma. J. Chromatogr. B 872, 167–171.

Yang, B., Zhao, J., Brown, J.S., Blackwell, J., Carr, P.W., 2000. High-temperature ultrafast liquid chromatography. Anal. Chem. 72, 1253–1262.

Zhang, Y., Wang, X., Mukherjee, P., Petersson, P., 2009. Critical comparison of performances of superficially porous particles and sub-2 μm particles under optimized ultra-high pressure conditions. J. Chromatogr. A 1216, 4597–4605.

FURTHER READING

Cunliffe, J.M., Maloney, T.D., 2007. Fused-core particle technology as an alternative to sub-2-μm particles to achieve high separation efficiency with low backpressure. J. Sep. Sci. 30, 3104–3109.

Ruta, J., Guillarme, D., Rudaz, S., Veuthey, J.L., 2010. Comparison of columns packed with porous sub-2 μm and superficially porous sub-3 μm particles for peptides analysis at ambient and high temperature. J. Sep. Sci. 33, 2465–2477.

CHAPTER

ADVANCES IN HYDROPHILIC INTERACTION LIQUID CHROMATOGRAPHY

2

Pavel Jandera
University of Pardubice, Pardubice, Czech Republic

1. INTRODUCTION

In reversed-phase (RP) systems, most frequently used in contemporary high-performance liquid chromatography (HPLC) practice, the stationary phase is nonpolar, usually an alkyl-silica type bonded phase, whereas the mobile phase is a mixture of one or more organic solvents and water or an aqueous buffer. As a rule, sample retention increases for more lipophilic samples and stationary phases and in more polar mobile phases; polar solutes are less strongly retained than the nonpolar ones. Very hydrophilic samples such as carbohydrates or small strongly polar compounds are weakly retained in RP-LC systems and often elute close to the column hold-up volume, so that their separation from one another and from polar matrix interferences may be difficult to accomplish, even in highly aqueous mobile phases (Pereira et al., 2009). On the other hand, the stationary phase in normal-phase (NP) chromatography is more polar than the mobile phase, and—opposite to RP-HPLC—retention increases with increasing polarity of samples and of the stationary phase and also in less polar mobile phases. In nonaqueous mobile phases traditionally used in conventional NP (adsorption) chromatography, the retention mechanism is based on the competition between the sample and the mobile phase for localized polar adsorption centers on the adsorbent surface (Snyder et al., 2009). However, strongly polar compounds are often excessively retained in nonaqueous NP systems or are poorly soluble in nonpolar or in weakly polar organic solvents. Often, their separation on polar stationary phases can be improved by adding water to the mobile phase (Huber et al., 1984). Some water accumulates close to the polar surface, where it forms a diffuse layer more polar than the bulk aqueous–organic mobile phase, which is less rich in water (Fig. 2.1). This approach had been occasionally used a long time before Alpert introduced the name "hydrophilic interaction liquid chromatography" (HILIC) for this separation mode (Alpert, 1983, 1990). The term "hydrophilic" refers to affinity for water. Essentially, HILIC systems can be understood as a "normal-phase stationary phase" in combination with a "reversed-phase mobile phase," usually containing 50% or more of water. The HILIC technique provides appropriate retention and resolution for many polar compounds, often with better separation efficiency in comparison to the RP chromatography (Gritti et al., 2010). The diffusion coefficients of ionized basic compounds in less viscous organic-rich mobile phases under HILIC conditions are approximately twice those under RP conditions, leading to improved

Handbook of Advanced Chromatography/Mass Spectrometry Techniques. http://dx.doi.org/10.1016/B978-0-12-811732-3.00002-9

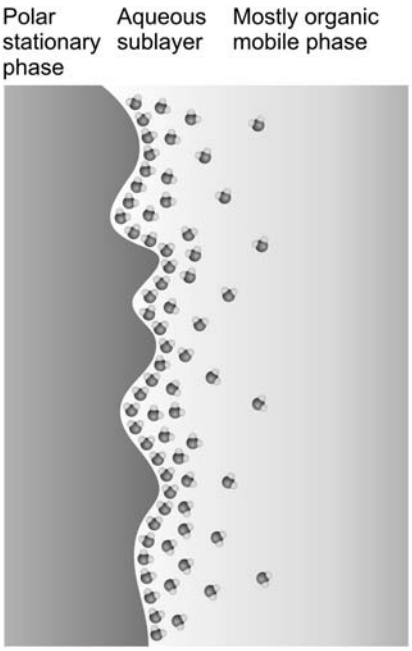

FIGURE 2.1

Schematic representation of a diffuse water layer at the surface of a polar stationary phase in a highly organic environment.

separation efficiency (lower height equivalent of a theoretical plate, HETP) (McCalley, 2007, 2008). Another reason for the increasing popularity of HILIC is its excellent suitability for coupling to mass spectrometry (LC/MS).

Originally, HILIC was applied to carbohydrate and peptide analysis in proteomics and glycomics (Zhu et al., 1991; Feste and Kahn, 1992; Churms, 1996; Lin and Lee, 1998; Strege, 1998). Later, HILIC has gradually been used for separations of drugs, toxins, plant extracts, and other small polar compounds in clinical, food, and pharmaceutical analysis (Tolstikov and Fiehn, 2002; Garbis et al., 2001). Growing interest in HILIC separations resulted in several recently published review articles. An excellent overview on recent progress in the development of polar stationary phases until 2006 was written by Hemström and Irgum (2006); more recent advances are included in reviews by Jandera (2011) and by Buszewski and Noga (2012). Other reviews have focused on the effects of the operating conditions on HILIC separations (Hao et al., 2008), separation efficiency (Ikagami et al., 2008), HILIC method development (Dejaegher et al., 2008), coupling HILIC systems with MS and MS/MS (Nguyen and Schug, 2008; Hsieh, 2008), implementation of HILIC systems in two-dimensional (2D) separation modes (Jandera, 2008), and on HILIC applications in biological (Yoshida, 2004; Jian et al., 2010), pharmaceutical (Dejaegher and Vander Heyden, 2010), and metabolite (Iwasaki et al., 2007; Spagou et al., 2010) analysis. An excellent book on HILIC has appeared recently, covering various aspects of the technique: separation mechanism, stationary phases, method development, and applications (Olsen and Pack, 2013).

2. COLUMNS FOR HYDROPHILIC INTERACTION LIQUID CHROMATOGRAPHY SEPARATIONS

Properties of HILIC separation systems strongly depend both on the stationary phase and composition of the mobile phase. Polar, hydrophobic, or ion-exchange interactions potentially contribute to sample retention, often giving rise to a mixed retention mechanism. In acetonitrile-rich mobile phases, hydrophilic interactions control the retention (HILIC systems), whereas in highly aqueous mobile phases the column may show essentially RP behavior with the major role being hydrophobic interactions. NP separations on bare silica and amino-silica columns in aqueous-organic mobile phases were reported as early as in 1970s (Linden and Lawhead, 1975); since then, a large variety of silica-based columns suitable for HILIC separations have been developed, providing excellent separations of peptides, proteins, oligosaccharides, drugs, metabolites, and various natural polar compounds. Bare silica gel, hydrosilated or hybrid silica, inorganic oxides, or organic polymers carrying various polar groups, but also ion exchangers and mixed-mode or zwitterionic-bonded ligands, have proved useful as HILIC materials.

2.1 SILICA GEL AND HYBRID INORGANIC SORBENTS

Highly purified "sil-gel" spherical silica particles (type B silica) formed by the aggregation of silica sols in the air, stable to at least pH 9, are still the most frequently used column materials in HILIC chromatography. *Bare silica gel* shows suitable separation of many types of polar compounds. The efficiency of silica particles improves with their decreasing size. Recently, fully porous sub-2 μm particles were introduced for UHPLC (ultra-high performance liquid chromatography) in the HILIC mode (Ahn et al., 2010; Lurie et al., 2011; Nováková et al., 2014). Better separation efficiency for polar and basic compounds on sub-2 μm core−shell silica particles was reported, in comparison to fully porous particles of the same size, because of a reduced diffusion path inside the particles and consequently reduced sample transfer resistance (van Deemter C-coefficients) under HILIC conditions (Heaton and McCalley, 2014). On bare silica columns, the retention mechanism in aqueous−organic mobile phases may be attributed to partitioning, adsorption, and ion exchange, depending on the nature of the analytes, the composition of the mobile phase, and the characteristics of the analytical support (Chauve et al., 2010). Separations of polar drugs can often be accomplished on bare silica gel columns in aqueous−organic mobile phases with acetonitrile concentrations ranging from 75% to 95%, usually containing 10−100 mmol/L ammonium acetate or formate buffers. HILIC applications of silica gel columns in pharmaceutical analysis have been reviewed in detail (Dejaeghar and Vander Heyden, 2010). At higher pH, ionization of the silanol groups on the silica gel surface increases, and cation exchange may play a significant role in retention, especially of positively charged basic compounds, which are generally strongly retained on silica gel by hydrogen bonding and ion-exchange interactions (Pack and Risley, 2005). The peak symmetry of basic compounds on "sil-gel" columns in HILIC mobile phases (acetonitrile−ammonium formate buffer) often improves in comparison to RP-HPLC (McCalley, 2007). Addition of trifluoroacetic acid to HILIC mobile phases generally suppresses ion-exchange interactions on the silica surface but may promote an ion-pairing mechanism.

Continuing efforts have been reported to develop new types of sorbents with improved thermal and pH stability, such as 1.7 μm bridged ethylene hybrid (BEH) organic−silica gel particles. BEH columns with bonded amide, diol, or cyanophenyl polar ligands differ from underivatized BEH hybrid particles

in separation selectivities for various polar test probes under HILIC conditions (Fountain et al., 2010). Silica gel supports coated with metal dioxides or graphene oxide (GO) also show improved stability in comparison to conventional silica-based HPLC materials (Janečková et al., 2010; Nawrocki et al., 2004; Jandera et al., 2006b; Randon et al., 2006). For improved stability, SiO_2 particles were wrapped by GO sheets (Yang et al., 2009). The GO surface is covered with a monolayer of oxidized carbon atoms containing polar hydroxy-, epoxy-, and carboxy groups (Booth et al., 2008; Dreyer et al., 2010).

Materials with ZrO_2 nanoparticle multilayers immobilized on a SiO_2 surface show the advantages of the high chemical and temperature stability of the ZrO_2 surface (up to 200°C and in the mobile phase range of pH 1−14), while preserving the inner pore structure of SiO_2 (Dun et al., 2004). Bare ZrO_2 and ZrO_2/SiO_2 monoliths provide separation of some compounds with different spatial configurations in the HILIC mode (da Silva et al., 2014; Randon et al., 2010).

A ZrO_2−SiO_2 stationary phase was prepared by coating silica particles with ZrO_2 "layer by layer," modified by surface bonding adenosine-5-monophosphate. The stationary phase with the bonded nucleotide is suitable for HILIC separations. By adjusting the pH of the mobile phase, the stationary phase can also show some ionic interactions resulting in changes in selectivity (Wang et al., 2015). Basic compounds showed a mixed HILIC/RP mechanism, whereas weak acids were retained only in the HILIC mode, most strongly in the pH range from 4 to 5. Above pH 5, electrostatic repulsion weakened the retention and improved the peak symmetry and resolution of nonsteroidal antiinflammatory drugs (florfenicol, flufenamic acid, mefenamic acid, ibuprofen, ketoprofen, sulindac, and indoprofen).

2.2 CHEMICALLY BONDED SILICA-BASED STATIONARY PHASES

Silica gel materials modified with various polar functionalities have been prepared for improved retention and separation selectivity of various sample types in HILIC. These mainly include diol, amino, amide, cyclodextrin (CD), ion exchange, zwitterionic, poly(2-hydroxyethyl aspartamide) or poly(succinimide), and other bonded phases prepared by chemical modification of the silica gel surface. The preparation and applications of some of these were covered in earlier reviews (Jandera, 2011; Buszewski and Noga, 2012). Structures of some bonded ligands frequently used as HILIC stationary phases are shown in Figs. 2.2−2.5: Fig. 2.2A presents simple bonded ligands, Fig. 2.2B amide and polysuccinimide phases, Fig. 2.3A cyclodextrine and sugar bonded ligands, Fig. 2.3B mixed-mode stationary phases providing HILIC and ion-exchange retention mechanisms, Fig. 2.4 some silica hydride bonded phases, and Fig. 2.5 zwitterionic ligands.

2.2.1 Amino, Amide Amino Acid, and Peptide Bonded Stationary Phases

Aminopropyl silica has been traditionally used for NP separations of sugars, amino acids, peptides, carboxylic acids, nucleosides, and some pharmaceuticals in aqueous−organic mobile phases (Olsen, 2001). Bonded amino stationary phases show increased affinities for acidic compounds, due to weak ion-exchange interactions. The contribution of the ion-exchange mechanism to the retention may cause weaker retention at increasing ionic strength of the mobile phase (Oyler et al., 1996). The primary amino group is relatively reactive, which may cause bleeding of the bonded phase by self-decomposition, or formation of Schiff bases with aldehydes, which may cause problems in HILIC separations of carbohydrates on amino-bonded silica (Ikegami et al., 2008). Aminopropyl-silica columns provide an increased rate of anomer mutarotation, eliminating the formation of doublet

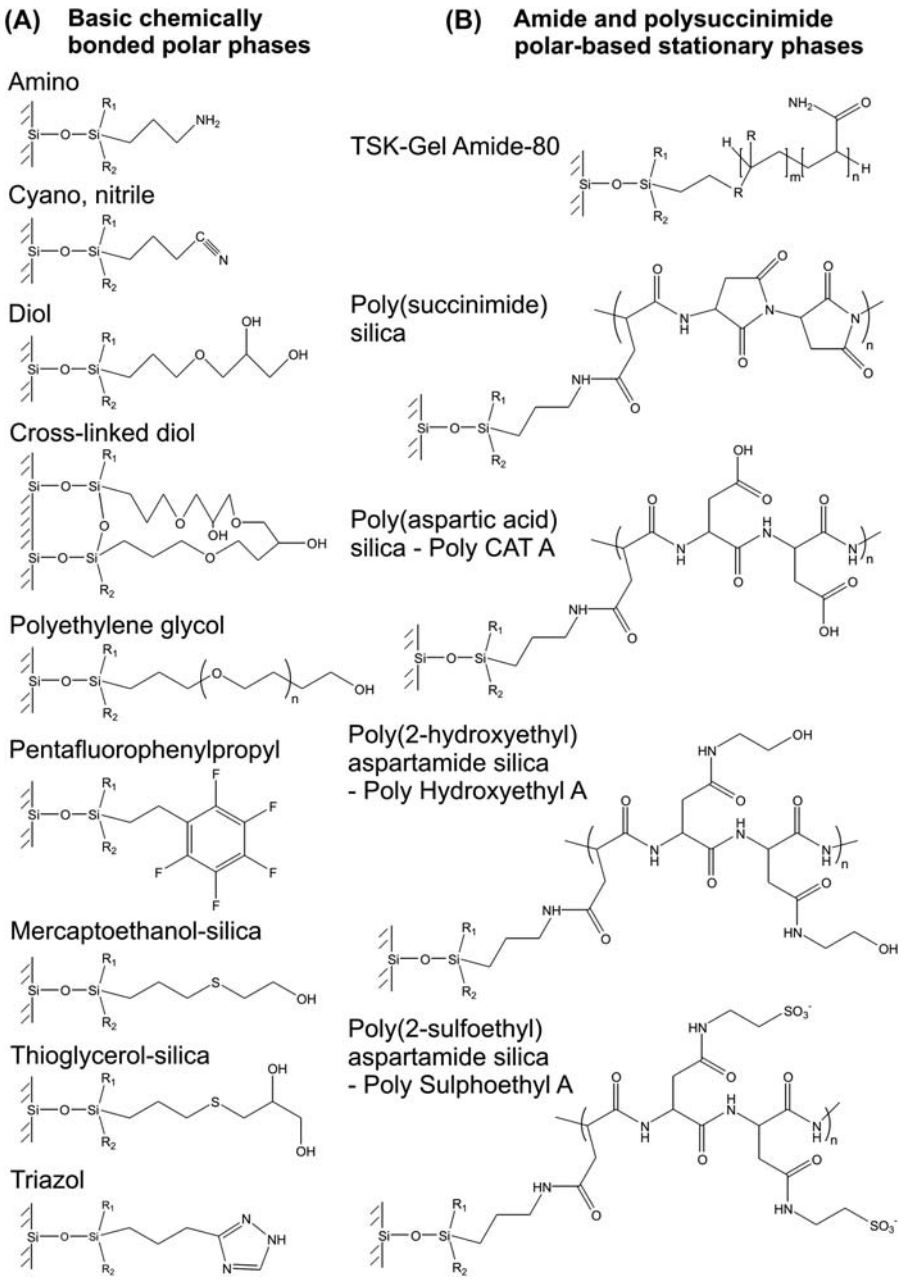

FIGURE 2.2

Structures of some simple polar (A), amide and polysuccinimide (B) HILIC stationary phases chemically bonded on a silica gel surface.

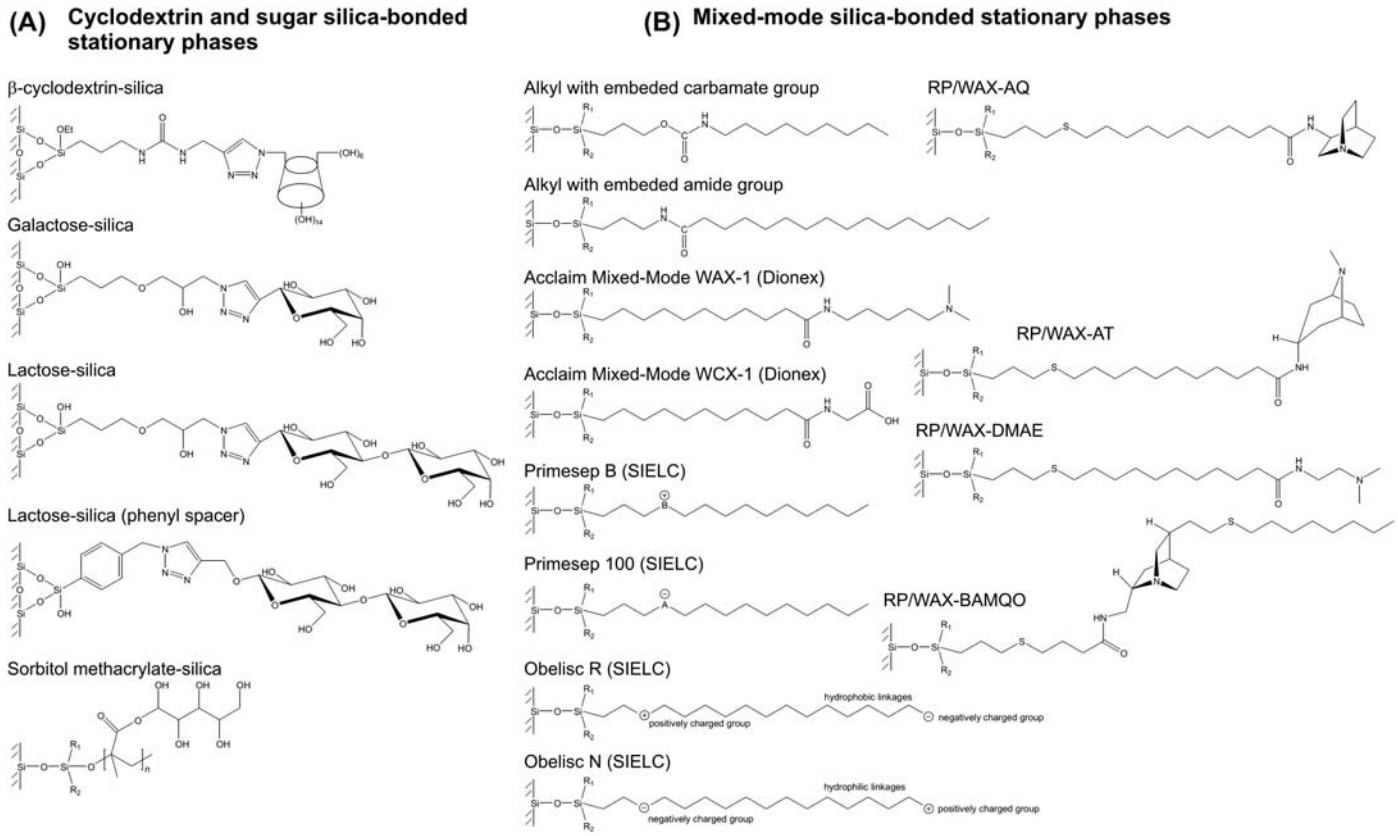

FIGURE 2.3

Structures of some cyclodextrin and sugar silica-bonded HILIC stationary phases (A) and mixed-mode HILIC/ion-exchange stationary silica-bonded phases (B).

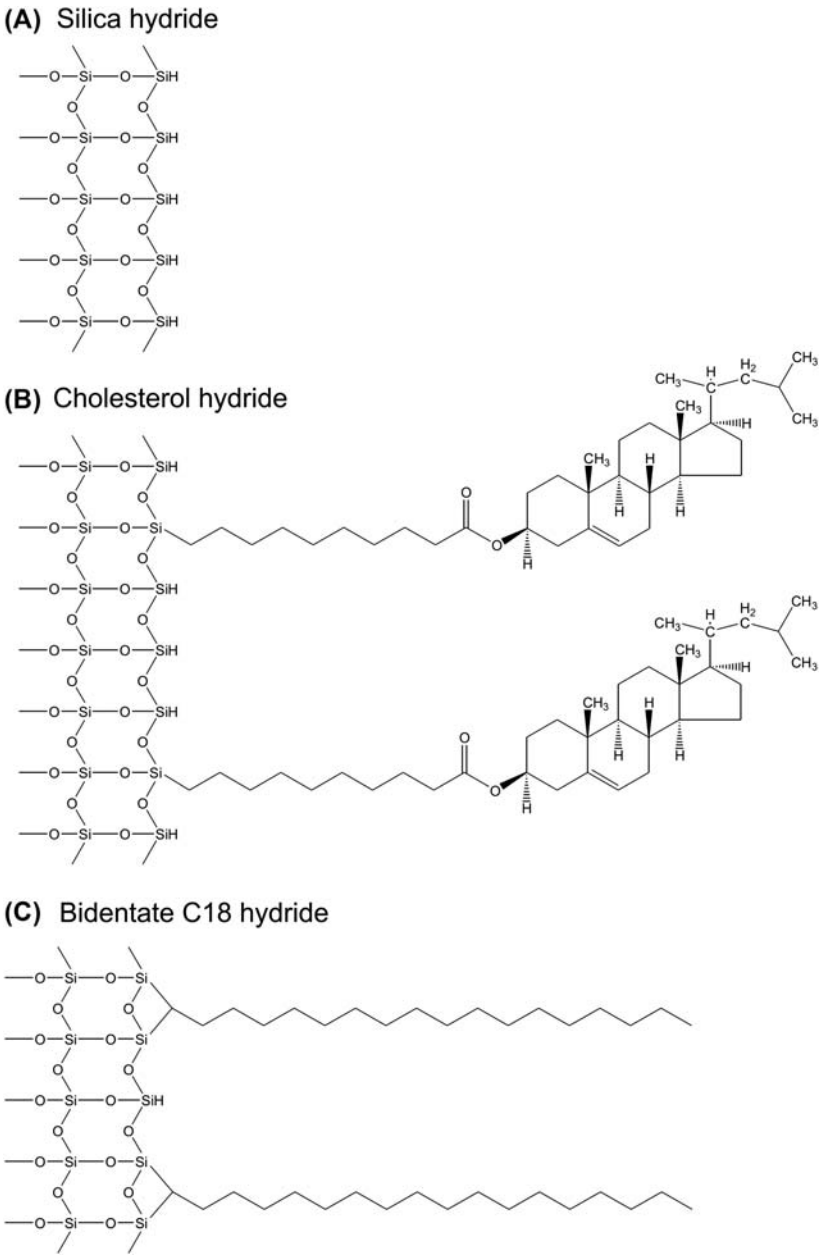

FIGURE 2.4

Structures of unmodified silica hydride (A) and hydrosilated silica modified with nonpolar cholesterol (B) and bidentate octadecyl (C) ligands.

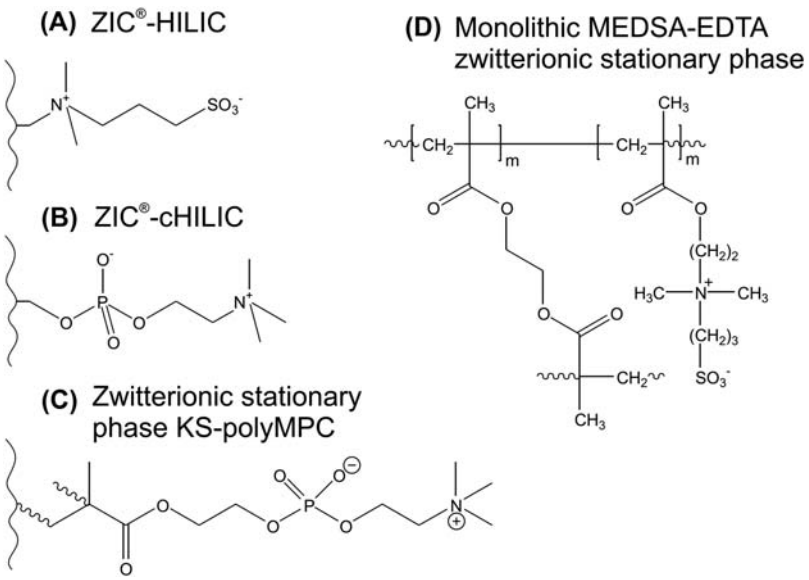

FIGURE 2.5

Structures of zwitterionic HILIC stationary phases: silica-bonded sulfobetaine ZIC-HILIC (A), phosphorylcholine ZIC-cHILIC (B), poly amino-phosphate (C), and organic polymer *N*,*N*-dimethyl-*N*-methacryloxyethyl-*N*-(3-sulfopropyl)ammonium−ethylene-dimethacrylate (D).

peaks of monosaccharide diastereomers and hence better peak shapes in the separation of sugars. Stationary phases containing secondary or tertiary amine groups, such as the YMC-Pack Polyamine II, cannot form Schiff bases with carbonyl compounds, which may improve the column stability and lifetime with respect to aminopropyl silica (Jandera, 2011).

Amide stationary phases contain a carbamoyl or an amide group bonded to the silica gel surface *via* a short alkyl spacer and are generally recommended for efficient and fast separations of highly polar samples (Fig. 2.2B). Amide-silica columns are often applied to the separation of peptides but are also suitable for HILIC separations of other hydrophilic or amphiphilic high-molecular weight samples, such as oligosaccharides, glycoproteins, or glycosides (Yoshida, 1997). In contrast to the amino−silica or poly(2-sulphoethyl aspartamide) columns, the retention of ionizable analytes is unaffected by ion-exchange interactions. Consequently, buffer additives to the mobile phases usually are not necessary for the separation, resulting in improved stability over a long period (Hemstrom and Irgum, 2006).

Some amide stationary phases have been specifically designed for HILIC applications; e.g., *carbamoyl-silica* HILIC TSKgel Amide-80, which shows stronger retention of many polar compounds in comparison to silica gel (Guo and Gaiki, 2005) and has been used for HILIC separations of mono- and oligosaccharides, sugar derivatives, peptides, and amino acids (Karlsson et al., 2005). 1.7 μm BEH amide columns strongly retain polar basic pteridines, for which they provided improved separation under HILIC−UHPLC conditions versus underivatized BEH silica, especially at a high pH (Nováková et al., 2010). Important contributions of ionic interactions and adsorption to retention are

generally reported for the amino acid bonded phases. "Thiol-ene" click reactions (see more on "click" reactions below) were employed for preparation of *amino acid bonded stationary phases*. By reactions between cysteine (Shen et al., 2012) or cystine (Xu et al., 2014) and the silica gel surface modified by horizontal polymerization of vinyl trichlorosilane, selective and efficient stationary phases were prepared for separations of nucleosides, sulfadiazine, sufisoxazole, and derivatives of benzoic acid in mobile phases containing salts.

Linear peptides immobilized on silica surfaces possess multiple amidic bonds and have traditionally been applied to LC of structurally similar compounds, such as for chiral separations, and for purification, fractionation, and isolation of peptides, proteins, etc., in HILIC systems (Kikta and Grushka, 1977; Shundo et al., 2009; Ohayama et al., 2008; Xue et al., 2009; Li et al., 2013). At a lower pH and higher ionic strength of the mobile phase, only the retention of acidic compounds decreased because of an ion-exchange mechanism; the retention of basic compounds was barely affected.

2.2.2 Diol, Polyethylene Glycol, Thioglycerol, Cyclodextrin, and Sugar Bonded Phases

Chemically bonded *diol phases* are prepared by bonding glycidoxypropyltrimethoxy silane to the silica gel surface and contain neutral hydrophilic 2,3-dihydroxypropyl ligands, which show high polarity and hydrogen bonding properties (Fig. 2.2A) and have been used for HILIC separations of proteins (Regnier and Noel, 1976) and low-molecular phenolic compounds in the HILIC mode (Jandera and Hájek, 2009). Diol columns may resolve anomers and different cyclic forms of monosaccharides, which allow monitoring the rate of the transition between the individual forms (mutarotation) (Pazourek, 2010).

The Luna HILIC 200 cross-linked diol stationary phase contains both oxyethylene and hydroxy bonded groups and combines to a certain extent the properties of the polyethylene glycol (PEG) and the diol columns (Fig. 2.2A). It shows improved stability against hydrolysis and better peak shape and resolution in comparison to the noncross-linked diol-silica phases (Jandera et al., 2010a; Jandera and Hájek, 2009). For example, nicotine and its principal metabolites cotinine, trans-3-hydroxycotinine, nicotine-*N*-oxide, and cotinine-*N*-oxide in urine were separated on a Luna HILIC 200 column using gradient elution from 98% to 35% acetonitrile at pH 3.0 with 10 mmol/L ammonium formate buffer (Marclay and Saugy, 2010). Six basic hydrophilic sympathomimetic drugs were separated by nano-LC under HILIC conditions on aminopropyl-silica and Luna HILIC 200 columns (Aturki et al., 2011). Hydrophobic interactions are more pronounced with less polar polyethylene glycol (PEG) bonded stationary phases than with diol columns (Blahová et al., 2006). The separations on diol and PEG stationary phases show highly different selectivities in comparison to bonded alkyl-silica columns, both in RP mode (Jandera et al., 2008) and under HILIC conditions (Wang et al., 2005; Jandera and Hájek, 2009).

CD stationary phases bonded on silica were prepared via click chemistry by immobilization of alkyne-modified β-cyclodextrin on the surface of azide-modified silica particles (Fig. 2.3A). Bonded CD stationary phases show chiral recognition properties under HILIC conditions (Liu et al., 2008), which have been used for chiral separations of sugar alcohols, monosaccharides, and oligosaccharides with 1−8 monosaccharide units (Armstrong and Jin, 1989). The retention increases with increasing number of monosaccharide units, which is attributed to interactions with the hydrophilic aqueous layer on the exterior of the CD molecules rather than to the penetration of sample molecules inside the cavity (Berthod et al., 1998). CD-bonded columns retain amino acids and some other polar samples more

strongly in comparison to the TSKgel Amide-80 phase and are more stable and reproducible than the aminopropyl silica stationary phases (Risley and Strege, 2000).

2-*mercaptoethanol* and oxidized 1-thioglycerol groups were attached onto vinylized silica, followed by oxidation with excess hydrogen peroxide in aqueous medium to yield stationary phases that can be used both in HILIC and in the RP mode (Fig. 2.2A). The separation selectivity and even the elution order of various sample types such as vitamins, nucleosides, and bases on these columns differ significantly from the behavior of polar compounds on diol bonded phases (Wu et al., 2008; Bicker et al., 2008).

A variety of *sugar stationary phases* were prepared using the "click" chemistry approach, in which sugar alkynes are covalently coupled to the azido-activated silica gel surface in the presence of a copper catalyst (Guo et al., 2007; Yu et al., 2009; Santoyo-Gonzalez and Hernandez-Mateo, 2009). The bonded carbohydrates retain their configurations, so that these highly polar stationary phases can be applied to stereoselective separations of monosaccharides and for HILIC separations of highly polar amino acids, glycopeptides, oligonucleotides, and natural products such as flavonoids (Moni et al., 2010). Separation selectivity differing from that of other polar-bonded columns and bare silica was also found for a hydrophilic stationary phase prepared by graft polymerization of sorbitol methacrylate on the surface of silica particles (Persson et al., 2008). Columns packed with carbohydrate-modified silica particles may show fair efficiencies for separation of oligosaccharides and chiral separations in the HILIC mode.

Several other polar stationary phases bonded on silica gel were used for separations under HILIC conditions, such as the Cosmosil HILIC column with 1,2,4-triazol groups bonded on silica, which has basic character and was reported to provide highly efficient separations of water-soluble vitamins, carboxylic acids, amino acids, peptides, and polar pharmaceuticals (Ikegami et al., 2008).

2.2.3 Polysuccinimide Bonded Stationary Phases

Alpert prepared a series of HILIC stationary phases by reaction of aminopropyl-silica with poly(-succinimide) followed by a second reaction step such as alkaline hydrolysis yielding poly(aspartic acid)-silica, reaction with 2-aminoethanol providing poly(2-hydroxyethyl)aspartamide-silica, which may be followed by further modification with 2-aminoethylsulfonic acid to poly(2-sulfoethyl) aspartamide-silica (Fig. 2.2B) (Alpert, 1983, 1990). A wide range of *poly(succinimide)-silica* bonded materials available commercially have been applied for separations of various highly polar compounds such as peptides, proteins, nucleic acid constituents, oligosaccharides, carbohydrates, etc., in buffered aqueous−organic mobile phases.

PolySulfoethyl A shows a mixed-mode HILIC/cation-exchange mechanism and was used for separations of hydrophilic peptides in aqueous−organic mobile phases containing 50% or more acetonitrile, with increasing salt gradients. The separations show complementary selectivity to RP systems (Alpert and Andrews, 1988). The separation efficiency may be poor in mobile phases containing less than 90% acetonitrile; hence the PolySulfoethyl A column is recommended for not too strongly retained samples (Hartmann et al., 2003).

PolyHydroxyethyl A can be applied for separations of phosphorylated and nonphosphorylated amino acids, peptides and glycopeptides, proteins, oligonucleotides, carbohydrates and glycosides, and small polar solutes. Plant metabolites elute in the order: polar lipids, flavonoids, glucosinolates, saccharides, and amino acids. Successful separations with symmetrical peaks require mobile phases containing at least 7−10 mM electrolyte (such as triethylammonium buffer), especially for ionized solutes (Oyler et al., 1996; Zhu et al., 1991; Tolstikov and Fiehn, 2002).

PolyGlycoplex columns are suitable for separations of monosaccharides, oligosaccharides, and sialyl sugars or their *p*-nitrobenzyloxy derivatives (Alpert et al., 1994).

2.2.4 Other Polymer Coated and Bonded Silica Stationary Phases

The popularity of polysaccharide bonded silica stationary phases (Fig. 2.3A) for HILIC separations has steadily increased. Commercially available native cyclofructan-6 chemically bonded to porous silica particles (FRULIC-N) (Qiu et al., 2011; Padivitage et al., 2013) or to superficially porous silica (core−shell) particles (Dolzan et al., 2014) has been employed for separations of nucleic bases, nucleosides, nucleotides, xanthines, β-blockers, phenolic acids, carbohydrates, and other compounds in HILIC and in purely organic NP modes.

The dextran-bonded stationary phase prepared by reacting dextran with carbonyldiimidazole (CDI)-activated silica (Sheng et al., 2014) was reported to preserve the hydrophilic interactions of dextran and the high mechanical strength of the silica better than earlier prepared dextran-bonded phases. The retention can be adjusted by varying the salt concentration in the mobile phase. Efficient separations of sugars, sugar alcohols, oligosaccharides, and glycosilated peptides were achieved, with promising application possibilities in glycobiology and proteomics.

A hydrophilic polymer layer improves the pH stability of the silica-based stationary phases in comparison to unmodified silica. A polyvinyl alcohol (PVA)−coated silica stationary phase (PVA-Sil) was prepared by dipping silica particles into a hot PVA solution and then settling the suspension, providing a thin layer of PVA, which shields silanol groups from interactions with basic organic compounds and suppresses unwanted electrostatic interactions (Ji et al., 2014). The method can be extended to prepare different stationary phases with additional functionalities by doping desired ingredients in a PVA solution. Stronger retention of some nucleosides and similar performance with an efficiency of ∼57,000 theoretical plates/m of PVA-Sil were observed relative to the commercial bare silica. Simultaneous separation of eight cephalosporins was achieved with a gradient of decreasing content of acetonitrile in buffered mobile phases. Recently, a highly stable stationary phase (up to pH 12) was prepared by coating porous graphitic carbon with PVA (Hou et al., 2016). The material shows characteristic HILIC properties, but the separation selectivity differs from other HILIC columns.

2.2.5 Zwitterionic and Mixed-Mode Silica Stationary Phases

Silica-bonded *zwitterionic* stationary phases containing both positively and negatively charged moieties (Fig. 2.5) are widely used in the practice of HILIC and often show a dual HILIC/RP retention mechanism, depending on the mobile phase composition (Jiang et al., 2006; Boersema et al., 2007; Zhang et al., 2012).

Mixed-mode anion−cation exchange/hydrophilic interaction liquid chromatography (ACE/HILIC materials, Fig. 2.5) shows improved separation selectivity for small molecule drugs by combining ionic interactions with polar hydrophilic interactions (Zhu et al., 1991; Strege et al., 2000).

Irgum's group introduced sulfoalkylbetaine stationary phases for HILIC separations (Jiang and Irgum, 1999; Viklund and Irgum, 2000; Wikberg et al., 2009). The active zwitterionic layer grafted on wide-pore silica gel or a polymer support contains both strongly acidic sulfonic acid groups and strongly basic quaternary ammonium groups, separated from each other by a short alkyl spacer. The two oppositely charged groups are present in a 1:1 M ratio, so that there is only a very low net negative surface charge of the bonded layer, attributed to the larger distance of the sulphonic groups from the silica gel surface (Guo and Gaiki, 2005).

Sulfobetaine-bonded ZIC−HILIC silica (Fig. 2.5A and D) is suitable for separation of a wide range of small polar compounds (Appelblad and Abrahamsson, 2005), metabolomes (Idborg et al., 2005a,b), glucosinolates (Wade et al., 2007), aminoglycosides (Oertel et al., 2004b), peptides (Boersema et al., 2007), or glycopeptides (Takegawa et al., 2006). Polar (hydrogen-bonding and dipole−dipole) interactions in the stationary phase are of primary importance, even though weak electrostatic interactions may affect the separation of partially ionized analytes. The HILIC separation of peptides on ZIC-HILIC columns strongly depends on pH. At pH = 3, it resembles separations on strong cation exchangers (SCX). At a higher pH (7−8), chromatographic resolution improves, especially for prevalent +2 and +3 charged peptides in comparison to SCX separations. The resolution was the best at pH 6.8, but the orthogonality against a C_{18} phase was better at pH = 3 (Boersema et al., 2007). HILIC on a capillary zwitterionic ZIC-cHILIC column in combination with electrospray ionization mass spectrometry has been applied to the detection and identification of more than 100 *N*-glycopeptides and *O*-glycopeptides in a single run (Takegawa et al., 2008). Glycopeptides could be distinguished by their glycan composition on a monolithic silica gel capillary surface modified with sulfobetaine stationary phase, in contrast to RP-HPLC (Wohlgemuth et al., 2010). Purine and pyrimidine bases and nucleosides can be separated using gradient elution with a decreasing concentration of acetonitrile in buffered aqueous−organic mobile phase on sulfobetaine ZIC-HILIC columns. The compounds elute in order of decreasing hydrophobicities, in agreement with generally observed HILIC behavior (Marrubini et al., 2010).

Phosphorylcholine stationary phases for HILIC separations (Fig. 2.5B and C) are prepared by graft polymerization of 2-methacryloyloxyethyl phosphorylcholine onto the surface of silica gel support (Jiang et al., 2006). They differ from the sulfobetaine ZIC-HILIC material not only by the nature of the negatively charged group but also by the charge arrangement, causing significant differences in the elution order and in the separation selectivity for peptides and other samples, e.g., free amino acid and carboxylic acid ligands and their metal complexes in plant samples (Weber et al., 2008).

Amino-phosphate zwitterionic stationary phases contain a negatively charged phosphate group bonded via an ester spacer and a positively charged quaternary amine group (Jiang et al., 2007). Successful separations of vitamins, nucleosides, deoxynucleosides, nucleobases, and aromatic acids were accomplished in aqueous acetonitrile containing ammonium formate. The retention of basic compounds increased at higher buffer pH, whereas the retention factors of uncharged analytes, such as nicotinamide, are almost independent of pH. Cheng et al. (2013) reported a novel amino-phosphate zwitterionic stationary phase with phospho amine and diamine groups for HILIC applications.

Mixed-mode HILIC/ion-exchange columns possessing a ligand with a long alkyl chain and a hydrophilic polar terminal group bonded on the silica gel support (such as the *Acclaim mixed-mode column*—Fig. 2.3B) have been introduced to enable separations of a wide range of strongly and weakly polar, or even nonpolar, compounds in organic-rich mobile phases (Wu et al., 2008). A weak anion exchanger, PolyWAX LP, prepared by modifying silica with a cross-linked coating of linear poly(ethyleneimine) can be also used for mixed-mechanism HILIC/ion-exchange separations in highly organic mobile phases.

A combined anion-exchange/cation-exchange/HILIC mechanism on silica-based weak ion exchangers was found useful for the analysis and purification of dipeptides and other compounds in biological samples, and of synthetic combinatorial chemistry products, using combined gradients of pH and increasing concentration of water (Strege et al., 2000).

A *trimodal stationary phase* prepared by coating porous spherical silica particles with charged organic polymer nanobeads (0.1 μm) has the inner pore area covalently modified with an organic ion-exchange layer. The outer surface is modified with strong cation-exchange groups; hence the spatial separation of the anion-exchange and cation-exchange regions in the stationary phase provides possibilities for simultaneous separations of acids, bases, and neutral compounds using a mixed HILIC/ion-exchange retention mechanism at high acetonitrile concentrations. The material was used for simultaneous separation of ionized hydrophilic drugs and their counterions such as penicillin G and its potassium salt (Liu and Pohl, 2010).

A mixed-mode glutamine silica-bonded stationary phase containing an amino alcohol group and two different amide groups, one being a polar head and the other embedded in an aromatic phenyl ring, retains polar, moderately polar, and nonpolar analytes (Aral et al., 2015). The column shows similar properties to zwitterionic stationary phases and provides a HILIC−ion exchange dual retention mechanism. Six nucleotides were resolved in 10 min in the HILIC mode with phosphate buffer (pH 3.25); phytohormones and phenolic compounds were separated under RP conditions.

A *mixed-mode glutathione HILIC*/cation-exchange stationary phase was used to analyze peptides varying both in hydrophobicity/hydrophilicity and charge. Neutral fructosan with a high degree of polymerization was separated from basic chitooligosaccharides. Strongly acidic carrageenan oligosaccharides could also be resolved (Shen et al., 2013). The retention mechanism was attributed to the ERLIC mode (HILIC combined with electrostatic repulsion interactions) in mobile phases containing low amounts of buffers (Alpert, 2008).

Neomycin is a hydrophilic aminoglycoside that contains six amino groups, seven hydroxyl groups, and six glycosidic oxygen functions, which has been grafted onto the surface of silica gel to act as a suitable stationary phase for HILIC separations of nucleosides, cytokinins, and sulfonamides in buffered aqueous acetonitrile. It offers additional selectivity for charged compounds, such as organic acids by mixed-mode hydrophilic/ion-exchange interactions (Oertel et al., 2004a; Peng et al., 2013a).

Thiol-ene click chemistry, based on the reaction between a thiol and an alkene (alkene hydrothiolation), was used for coupling thioglycolic acid onto vinyl-bonded silica to provide a *Thiol-Click-COOH* column with high reaction yields and stereoselectivity. The material, which is more hydrophilic than pure silica columns, was reported to provide selective separations of 13 nucleosides and bases, and four water soluble vitamins, because of a combined HILIC−ion exchange mechanism (Lowe, 2010; Peng et al., 2013b).

The steviol glycoside Rebaudioside A (RA) (Liang et al., 2015), an *ent*-kaurene-type diterpene glycoside, contains a hydrophobic aglycone and four hydrophilic sugar units. RA was immobilized on silica through the "thiol-ene" click chemistry reaction between the terminal alkene group in RA and thiol groups on the silica surface to provide a HILIC/RPLC mixed-mode stationary phase, which enables separation of several sugars whose retention decreases with increasing content of water in the mobile phase, in agreement with the HILIC mechanism. However, the RP mechanism could be applied for separation of glycosides in highly aqueous mobile phases, too.

2.3 AQUEOUS NORMAL-PHASE CHROMATOGRAPHY ON HYDROSILATED SILICA PHASES

Through the hydrosilation process, ordinary silica gel (B-type) can be transformed to C-type, "hydride silica," by transforming up to 95% of the original surface silanols (Si−O−H) to nonpolar silicon

hydride Si−H groups. The silica hydride material is less polar and shows less attraction for water (Pesek and Matyska, 2009) and improved pH stability in comparison to sil-gel columns; hence the authors suggested to denote the retention mechanism on hydrosilated silica as "aqueous normal-phase chromatography" rather than HILIC. However, HILIC separations are also essentially conducted in an NP system. Water adsorbed on hydrosilated materials at the point of column saturation fills only 2.6%−5.5% of the pore volume, which corresponds to approximately half a monomolecular adsorbed water layer (Soukup et al., 2013; Soukup and Jandera, 2014). According to recent studies, water uptake on the hydrosilated surface could probably be explained by the effects of the electrical interfacial double layer at the adsorbent surface, characterized by the zeta potential, rather than by adsorption on residual silanol groups (Kulsing et al., 2014, 2015).

Hydrosilated silica can be chemically modified by low-polarity bonded groups, such as alkyls or cholesterol, to provide a mixed-mode HILIC-RP retention mechanism and improved selectivities for separations of moderately polar compounds, using either the RP mode in highly aqueous mobile phases or the NP mode in buffered mobile phases containing more than 50%−70% acetonitrile (Soukup and Jandera, 2012a,b). The UDC cholesterol and C_{18} bidentate columns (Fig. 2.4) show significant mixed hydrophobic and NP retention mechanisms, whereas weak retention is observed on silica hydride and Diamond hydride columns (containing ∼2.5% carbon) in the RP mode (Soukup and Jandera, 2012a,b). Hence, a single column can be used with different selectivities and elution order in successive experiments in RP and NP modes, switching between different RP compatible water-rich and NP compatible highly organic mobile phases (Pesek et al., 2013). Strong retention of both hydrophobic and hydrophilic peptides in high-organic mobile phases was used for their simultaneous separations on a Diamond hydride column using a gradient of decreasing acetonitrile concentration in water (from 80%−90% to 30%−50%) with addition of 0.1% acetic or formic acid (Boysen et al., 2011). This column also provided better separation and suppressed peak tailing of acidic lipids such as (lyso-) phosphatidic acids with an acetonitrile concentration decreasing from 99.7% to 75% at pH 4, in comparison to bare or chemically modified silica columns (Cífková et al., 2016).

Matyska et al. (2010) modified the silica hydride surface with undecanoic acid (UDA silica). This stationary phase showed increased separation selectivity for mono-, di-, and triphosphate nucleotides because of enhanced ion-interaction (ion repulsion) properties with respect to the Diamond hydride column. The unmodified silica hydride provides similar elution order but stronger retention of more polar phenolic acids in comparison with hydrosilated silica modified by attaching cholesterol or bidentate C_{18} ligands under comparable HILIC conditions. The elution order of phenolic acids is identical on various hydrosilated columns and the retention increases with increasing polarity of the stationary phase surface: Bidentate C_{18} < cholesterol < Diamond hydride < silica hydride. The Diamond hydride column provides the best resolution and baseline separation of eight phenolic acids in a HILIC gradient with decreasing acetonitrile concentration (Soukup et al., 2013).

2.4 MONOLITHIC COLUMNS FOR HYDROPHILIC INTERACTION LIQUID CHROMATOGRAPHY SEPARATIONS

2.4.1 Silica Gel and Hybrid Monoliths

Bare silica monoliths generally show low HILIC retention. The domain size (i.e., the sum of the average sizes of the through-pores and skeleton) controls the efficiency of a silica gel monolithic

column (Vervoort et al., 2004). Coating the monolithic silica surface with cationic latex nanoparticles by electrostatic attachment provides separation media that retain the high efficiency and permeability of the native silica monolith, but show a significantly larger amount of adsorbed water, leading to stronger HILIC/ion-exchange retention (Ibrahim and Lucy, 2012). Fast separations of benzoates, nucleotides, and amino acids at high acetonitrile concentrations in the mobile phase were reported on latex-coated monoliths, based on mixed-mode electrostatic repulsion−hydrophilic liquid interactions (ERLIC) (Ibrahim et al., 2010).

Hybrid monolithic silica capillary columns for HILIC were prepared by on-column polymerization of acrylic acid on monolithic silica in a fused silica capillary modified with anchor groups. The products maintained their high permeability and provided a theoretical plate height (H) of 10−20 μm for polar solutes, including nucleosides and carbohydrates (Horie et al., 2007).

Zwitterionic silica-based monolithic capillary columns were prepared by grafting a layer of zwitterionic monomer ([2-(methacryloyloxy)ethyl]-dimethyl-(3-sulfopropyl)-ammonium hydroxide or 2-methacryloyloxyethyl phosphorylcholine) on the silica monolithic surface (Moravcová et al., 2014). Two types of efficient capillary zwitterionic organic-silica hybrid monolithic columns were synthesized in a single-step thermally induced polymerization, by using [2-(methacryloyloxy)-ethyl] dimethyl-(3-sulfopropyl)ammonium hydroxide or [2-(methacryloyloxy)-ethyl] phosphorylcholine as the organic monomers and [3-(methacryloxy)-propyl]trimethoxysilane. The columns were suitable for HILIC separations of various low-molecular-weight neutral, basic, and acidic analytes, as well as small peptides in tryptic digests (Lin et al., 2012).

2.4.2 Organic Polymer Hydrophilic Interaction Liquid Chromatography Columns

Monolithic (poly)methacrylate diol or (poly)hydroxymethacrylate columns were successfully employed for HILIC separations of oligonucleotides. Unfortunately, organic polymer monolithic columns traditionally have shown rather low separation efficiency for low-molecular-weight compounds (Nischang and Bruggemann, 2010). Organic polymer-based monoliths have a heterogeneous structure, which rather resembles a net of interconnected nonporous cauliflower-like microglobules with low surface area. This morphology is suitable for separation of polymers requiring large pores (15−100 nm) with relatively low specific surface area (10−150 m^2/g) (Svec, 2012). Large molecules of biopolymers cannot diffuse into the small pores in the microglobules of organic monoliths and can access only the large pores by convection; hence they provide narrow peaks. On the contrary, small molecules can penetrate into the narrow pores by slow diffusion, generally resulting in a poor separation efficiency (Svec and Lv, 2015). Essential improvement in the performance of monoliths was achieved by controlling the inner pore morphology of the monolithic bed structure. The proportion of mesopores should be increased while preserving a sufficient amount of through-pores (Nischang et al., 2010; Nischang and Clauson, 2016). Several strategies were followed to this end:

1. Chemistry and proportions of the functional monomers, cross-linkers, and porogen solvents have major impacts on the morphology of the final monolith (Arrua et al., 2012).
2. The initiation conditions and the temperature of polymerization should be carefully adjusted (Urban and Jandera, 2013).
3. Termination of the polymerization reaction at an early stage, in less than 1 h, provided incomplete polymerization, and consequently, less cross-links and larger porosity of the final monoliths

(Greiderer et al., 2009). However, nanostructural heterogeneity in the polymer network and a void volume can be formed during polymerization because of different local compositions of monomer and cross-linkers. This may cause poor reproducibility of monoliths prepared using this approach.

4. The chromatographic performance of the organic polymer monoliths could also be improved via adjustment of the pore morphology using postpolymerization modifications or two-step monolith fabrication (Currivan and Jandera, 2014), hypercrosslinking (Urban et al., 2010), or incorporation of additional structural elements into the monolithic skeleton, such as carbon nanotubes (Svec and Lv, 2015).

Organic polymer monoliths with zwitterionic groups incorporated into (poly)methacrylate monolithic structures are suitable for HILIC separations of neutral, basic, and acidic polar compounds in aqueous−organic mobile phases with 60% or more acetonitrile. Polymer monolithic columns containing sulfoalkylbetaine moieties were prepared by photo-induced (Viklund et al., 2001) or thermal (Jiang et al., 2007) copolymerization of ethylene dimethacrylate (EDMA) and *N*,*N*-dimethyl-*N*-methacryloxyethyl-*N*-(3-sulfopropyl)ammonium betaine (MEDSA) inside fused silica capillaries (Fig. 2.5). Capillary monolithic columns prepared by copolymerization of methacryloxyethyl-*N*-(3-sulfopropyl) ammonium betaine (MEDSA) with EDMA or with 1,2-bis(p-vinylphenyl) ethane (BVPE) were employed for separations of nucleic bases and other neutral, basic, and acidic polar analytes in aqueous−organic mobile phases with 60% or more acetonitrile (Jiang et al., 2007; Foo et al., 2012). Their performance compared favorably to particle-packed silica-based zwitterionic columns.

Porosity, permeability, selectivity, and retention characteristics of monolithic sulfobetaine columns improve when using water-containing porogen solvents in the polymerization process (Viklund et al., 2001; Jiang et al., 2007; Foo et al., 2012; Urban et al., 2009). Long-chain alkyl monomers and cross-linkers increased the proportion of the mesopores in polymethacrylate monolithic columns, resulting in improved separation efficiency up to 70,000−80,000 theoretical plates/m for small molecules. Monolithic stationary phases prepared by copolymerization of 3-chloro-2-hydroxypropyl methacrylate and ethylene dimethacrylate in a fused silica capillary could be further functionalized by reaction with triethanolamine ligands and used for separations of nucleobases and substituted benzoic acids (Qiao and Shi, 2015).

Dimethacrylate cross-linkers with relatively long polar (poly)oxyethylene chains generally improve the performance of polar monolithic columns for HILIC applications. By copolymerizing MEDSA with *N*,*N*′-methylenebisacrylamide (MBA) (Yuan et al., 2013), 1,4-bis(acryloyl)piperazine (PDA) (Liu et al., 2014), or bisphenol A glycerolate dimethacrylate (BIGDMA) (Staňková et al., 2013) cross-linkers, columns with significantly improved efficiency for small molecules were prepared. For the last type of monolithic column, excellent long-term stability, reproducibility of preparation within 1%−3% (relative), and efficiency up to 60,000 theoretical plates/m were reported at the optimum flow rate of 1−3 μL/min. After correction for extra-column contributions to band broadening, the efficiency increased to 120,000 theoretical plates/m (Jandera and Staňková, 2015).

Recently, Li et al. (2016) investigated the effect of three charged hydrophilic groups introduced into hydrophilic sulfobetaine stationary phases, namely *N*,*N*-dimethyl-*N*-acryloyloxyethyl-*N*-(3-sulfopropyl)ammonium betaine (SPDA), [2-(acryloyloxy)ethyl] trimethylammonium chloride (AETA), and 3-sulfopropyl acrylate potassium salt (SPA), on the chromatographic properties of

zwitterionic monolithic capillary columns. Depending on the combination of stationary phase−mobile phase−solute, hydrophilic interactions and electrostatic and hydrogen-bonding interactions, together with molecular shape, contribute to the retention and separation selectivity of analytes. Because of the weak anion exchange properties, the zwitterionic poly(SPDA-co-MBA) hydrophilic monoliths exhibit the best separations for phenols, β-blockers, and small peptides, in terms of selectivity, peak shape, and analysis time. On the other hand, the cationic poly(AETA-co-MBA) monolith provided the best separation for nucleobases and nucleosides.

A two-step surface modification of a poly(styrene-co-vinylbenzyl chloride-co-divinylbenzene) nonpolar monolithic layer, including hypercross-linking and thermally initiated surface grafting of [2-(methacryloyloxy)ethyl]dimethyl(3-sulfopropyl)ammonium hydroxide, has been used to form a second zwitterionic layer for efficient separation of small polar compounds (Škeříková and Urban, 2013). A primary monolithic poly(lauryl methacrylate-co-tetraethyleneglycol dimethacrylate) layer could be used as a stable scaffold for a second, polar monolithic layer with zwitterionic functionality by in situ copolymerization of poly(*N*,*N*-dimethyl-*N*-methacryloxyethyl-*N*-(3-sulfopropyl)ammonium betaine-co-bisphenol A glycerolate dimethacrylate) on the primary monolith; Friedel−Crafts grafting onto the scaffold layer was not necessary. The column was suitable for HILIC separations of phenolic acids, flavones, nucleosides, and bases of nucleic acids, with similar efficiencies, but with selectivities differing from zwitterionic methacrylate monolithic columns prepared by a single step polymerization (Currivan et al., 2015).

2.5 HYDROPHILIC INTERACTION LIQUID CHROMATOGRAPHY COLUMN SURVEY

Usually, 100−150 mm long, 4.6 mm I.D. columns packed with 3−5 μm particles are used for standard HILIC separations; smaller diameter columns are preferred for HILIC coupled online with MS detection. The column length and flow rate can be changed for increasing resolution or decreasing run time, with pressure as the limiting factor. Working at very high pressures considerably increases the speed of separation; however, secondary impacts on HILIC separations were observed. The retention of sugars in hydrophilic interaction chromatography decreases at high pressures, probably because of changes in the hydration of strongly polar analytes as they move from the bulk highly organic mobile phase into the water-rich layer at the surface of the polar adsorbent (Neue et al., 2010).

The retention of selected probes was used as an indicator of specific interactions: the relative retention of cytosine versus uracil as the probe of the "hydrophilicity" of the HILIC phases; the relative retention of adenosine versus adenine as a probe of the hydrogen bonding activity of the stationary phase; and the relative retention of benzyltrimethylammonium versus cytosine as the probe of the cation-exchange/anion-exchange character of the column (Ibrahim and Lucy, 2012; Neue et al., 2006).

HILIC stationary phases with various chemistries provide different retention times and selectivities for individual analytes. Very similar selectivities were found for neutral, acidic, and basic analytes on bare silica and on diol stationary phases. Cyanopropyl columns provide different selectivity for basic compounds, whereas aminopropyl stationary phases show a strong retention preference for acidic compounds, due to the ion-exchange effect, whereas bare silica stationary phases show a strong preference for basic compounds attributed to interactions between the surface silanols and ionized analytes (Vlčková et al., 2014).

Ikegami et al. (2008) compared the separation properties of some types of particle-packed and monolithic polar columns (bare silica, amino−silica, amide−silica, diol−silica, cyano−silica,

polysuccinimide−silica, sulfobetaine−silica, triazol−silica, and CD−silica) frequently used for HILIC separations of carboxylic- and amino-acids, peptides, amines, amides and substituted urea derivatives, nucleic bases and nucleosides, poly-alcohols, and oligosaccharides and carbohydrates. Some HILIC columns may require lower flow rates for optimum performance. Similar to RP-HPLC, the efficiency and column back-pressure increase with decreasing particle size; organic polymer columns usually show higher heights equivalent to theoretical plate (HETP) in comparison to silica-based columns (Gritti et al., 2010).

Guo and Gaiki (2005) compared the retention of representative carboxylic acids, nucleosides, and nucleotides on bare silica and polar silica-bonded amide, amino, aspartamide, and sulfobetaine stationary phases commonly used in the HILIC mode. Silica gel showed the least retention but the highest selectivity differences with respect to other polar bonded stationary phases. In another study, the chromatographic behavior of 10 model peptides on bare silica, amide, poly-hydroxyethyl aspartamide, diol, and zwitterionic HILIC columns was investigated. The Alltima−Alltech silica column showed the best performance for the selected peptide set, followed by the zwitterionic ZIC-HILIC column (Van Dorpe et al., 2010). A generic screening protocol was suggested for the selection of the best column packed with BEH organic silica gel 1.7 μm particles, suitable for fast HILIC separations. The selection from among three stationary phases, namely bonded amide, diol, and cyanophenyl polar ligands, which differ from one another and from underivatized BEH HILIC, is based on the selectivity correlations obtained in experiments with 28 polar test probes in weakly acidic (pH = 3) and weakly basic (pH = 9) mobile phases (Fountain et al., 2010).

Schuster and Lindner (2013) applied the linear solvation energy relationship (LSER) model using 68 test compounds comprising small neutral, basic, acidic, zwitterionic, and amphoteric molecules with a broad range of solvatochromic parameters to characterize 22 silica-based polar stationary phases into basic, neutral, or acidic classes at pH = 3. The "acidic" modified columns exhibit only weak hydrogen bond acceptor properties and are less capable of achieving an even distribution of diverse analytes along the available retention window, in contrast to "basic" (bonded amino) and "neutral" columns. Of the "neutral" columns, amide and zwitterionic columns show a broader retention window for a wide range of analytes in comparison to diol columns (Kawachi et al., 2011) and therefore are preferred as the first choice for HILIC separations (Dinh et al., 2011). The results of these studies confirmed major effects of hydrogen bonding and ionic interactions on the retention.

3. SEPARATION MECHANISM AND EFFECTS OF THE ADSORBED WATER AND MOBILE PHASE

3.1 ADSORPTION OF WATER ON POLAR COLUMNS

The mechanism of separation on polar columns in aqueous−organic mobile phases is complicated. HILIC is traditionally understood as the partition process between the aqueous layer accumulated close to the solid surface and a bulk mobile phase containing high concentrations (usually more than 60%) of a polar organic solvent in water (Alpert, 1990). However, the actual separation mechanism is obviously more complex, and differences in the chromatographic selectivities of various polar compounds indicate that adsorption on polar functionalities on the solid phase surface may also play an important role in the retention (Jandera, 2011). Both polar and hydrophobic groups on the structure of adsorbents may cause excess adsorption of either acetonitrile or water, depending on the mobile

phase composition (Noga et al., 2013). In organic solvent normal-phase adsorption chromatography, the retention is primarily based on competition between the solute and the polar solvent for the localized adsorption sites on the surface of a polar adsorbent, usually bare silica gel. Polar solvents, especially water, are strongly adsorbed on polar adsorbents from mixed aqueous–organic mobile phases. In the original HILIC model, Alpert (1990) considered a partition-driven retention mechanism in which the analytes distribute between the stagnant water-rich layer adsorbed onto the polar sorbent on one hand and the water-poor bulk mobile phase on the other, without contribution of the sorbent backbone.

However, the solid adsorbent cannot be considered as an inert support for the adsorbed "pseudo-stationary" aqueous phase in mobile phases containing 2%–40% water in organic solvent (usually acetonitrile). Although the water uptake is often characterized in terms of "adsorbed water layers," there is an essential difference between the water retained in HILIC and that in classical adsorption organic solvent normal-phase chromatography. A compact water layer can be accumulated on the adsorbent surface from traces of water present in nonpolar or weakly polar organic solvents. On the other hand, water is miscible at any proportion with acetonitrile, acetone, methanol, or other polar organic solvents. Hence, an adsorbed "water layer" is rather diffuse, without sharp boundaries, and the concentration of water progressively decreases from the solid surface toward the bulk organic-rich mobile phase outside (and, possibly even partly inside) the pores of the stationary phase (Fig. 2.1). Specific solid phase effects such as hydrogen-bonding and ionic interactions with polar functional groups such as ionized silanol groups on bare silica, or residual silanols on silica-bonded phases, may contribute to the sample retention and also affect the amount of water adsorbed on the solid support; even nonpolar siloxane groups may adsorb some water at very low organic solvent concentrations (McCalley, 2010).

The plethora of polar stationary phases used in the contemporary practice of HILIC separations show large variability in the amount of adsorbed water in aqueous–organic mobile phases, depending on the column type. Computer molecular dynamics simulation studies indicate that the relative proportion of the amount of water contained in the pores of silica-based phases to the water concentration in the bulk mobile phase increases at low total water concentrations in the column (Melnikov et al., 2011). The water molecules close to the silica surface are almost immobilized by the hydrogen bonds to the silanol groups. NMR studies of bare silica and silica with bonded zwitterionic sulfobetaine groups suggested that three types of water can be distinguished inside the 6–10 nm pores: (1) free water molecules, (2) "freezable" bound water, and (3) water bound within the polymeric stationary phase network that does not freeze at the regular water freezing temperature (Wikberg et al., 2011). This may be the reason why separations are often irreproducible or fail in mobile phases containing less than 2% water in acetonitrile. Water adsorption can often be described by the Langmuir model, Eq. (2.1), which enables measuring the adsorbed amount of water over a varying composition of the bulk mobile phase (Langmuir, 1916):

$$q_i = \frac{ac_m}{1 + \frac{c_m a}{q_s}} \tag{2.1}$$

where q_i is the adsorbed water concentration, c_m is the water concentration in the bulk mobile phase, and a is the distribution constant of water in the pores of the stationary phase, forming a layer between the column and acetonitrile at very low c_m. The plateaus of the isotherms characterized by q_s in Eq. (2.1) give the saturation capacities for water adsorption, which can be calculated from the

experimental parameters of the Langmuir equation determined by the frontal analysis technique, where a sample solution is pumped through the column and the breakthrough volume of the sample from the column is usually monitored online in the column effluent using a nonspecific (refractive index or low-wavelength UV) detector (Vajda et al., 2013). As the boundaries of the adsorbed water diffusion layer are difficult to determine and depend on the composition of the bulk mobile phase, the adsorbed water amount may be characterized in terms of the percentage of the water-occupied pore volume.

The water breakthrough volumes, V_B, at varying concentrations of water in the column feed (from 0% to column saturation) could be measured using off-line coulometric Karl Fischer titration of small collected column effluent fractions. This method does not rely on the online nonspecific detection, which may be affected by interfering compounds. The amount of the water retained in the stationary phase can be conveniently expressed in terms of the volume fraction of the excess water contained in the inner pore volume, q_{ex}, (over the bulk mobile phase water concentration, c_m) and was calculated from Eq. (2.2) (Soukup and Jandera, 2013):

$$q_{ex} = \frac{(V_B - V_M) \cdot c_m}{V_i} \tag{2.2}$$

V_M is the total column hold-up volume, including the inner pore volume, $V_i = \varepsilon_i V_M$, and the outer (interparticle) volume, $V_0 = \varepsilon_0 V_M$; ε_i and ε_0 are the inner pore and the inter-particle porosities, respectively. Uracil or thiourea are often used as column hold-up volume, V_M, markers in RPLC, which are quite strongly retained on polar columns under HILIC (NP) conditions (Urban et al., 2009). Benzene and toluene are more suitable nonretained markers of column hold-up volume in acetonitrile-rich mobile phases (Urban and Jandera, 2013). Their elution times on silica columns slightly increase as the water content in the mobile phase grows from 0% to 30%, which means that the water amount adsorbed close to the polar adsorbent surface depends on the water concentration in the bulk mobile phase (McCalley and Neue, 2008). Water adsorption isotherms on nonmodified and monomeric functionalized silica phases show monolayer formation followed by multilayer adsorption, whereas water uptake on polymeric functionalized silica stationary phases may lead to the formation of hydrogels (Vajda et al., 2013). The water uptake correlates with the retention factors of neutral analytes, supporting the idea of the coexistence of adsorption and partitioning of neutral solutes in the water concentration regime normally encountered in HILIC (Dinh et al., 2013).

Frontal analysis with Karl Fischer titration was used for the determination of water uptake on 19 stationary phases, including fully porous and core−shell silica gel and silica-bonded phases with different polarities: octadecyl and cholesterol, phenyl, nitrile, pentafluorophenylpropyl, diol, zwitterionic sulfobetaine and phosphorylcholine ligands bonded on silica, hybrid organic-silica, and hydrosilated silica stationary phases, together with a few nonpolar alkyl-bonded phases (Soukup and Jandera, 2014). All columns adsorb water from acetonitrile, and even though there are large differences between the individual stationary phases, the adsorption can be described by Langmuir isotherms, Eq. (2.1). Six isotherm examples are shown in Fig. 2.6. Nonpolar long alkyl chain (YMC Carotenoid) and hydrosilated (Cogent Silica C, Cogent C18 Bidentate) columns show steep isotherms with low plateau water concentrations (low water uptake), whereas the water adsorption isotherms on polar columns (YMC Triart Diol HILIC, ZIC HILIC, and TSKgel Amide-80) have a much less steep slope and at least one order of magnitude higher water saturation concentrations, which is often not achieved even in mobile phases containing 20% water in acetonitrile (Soukup and Jandera, 2014).

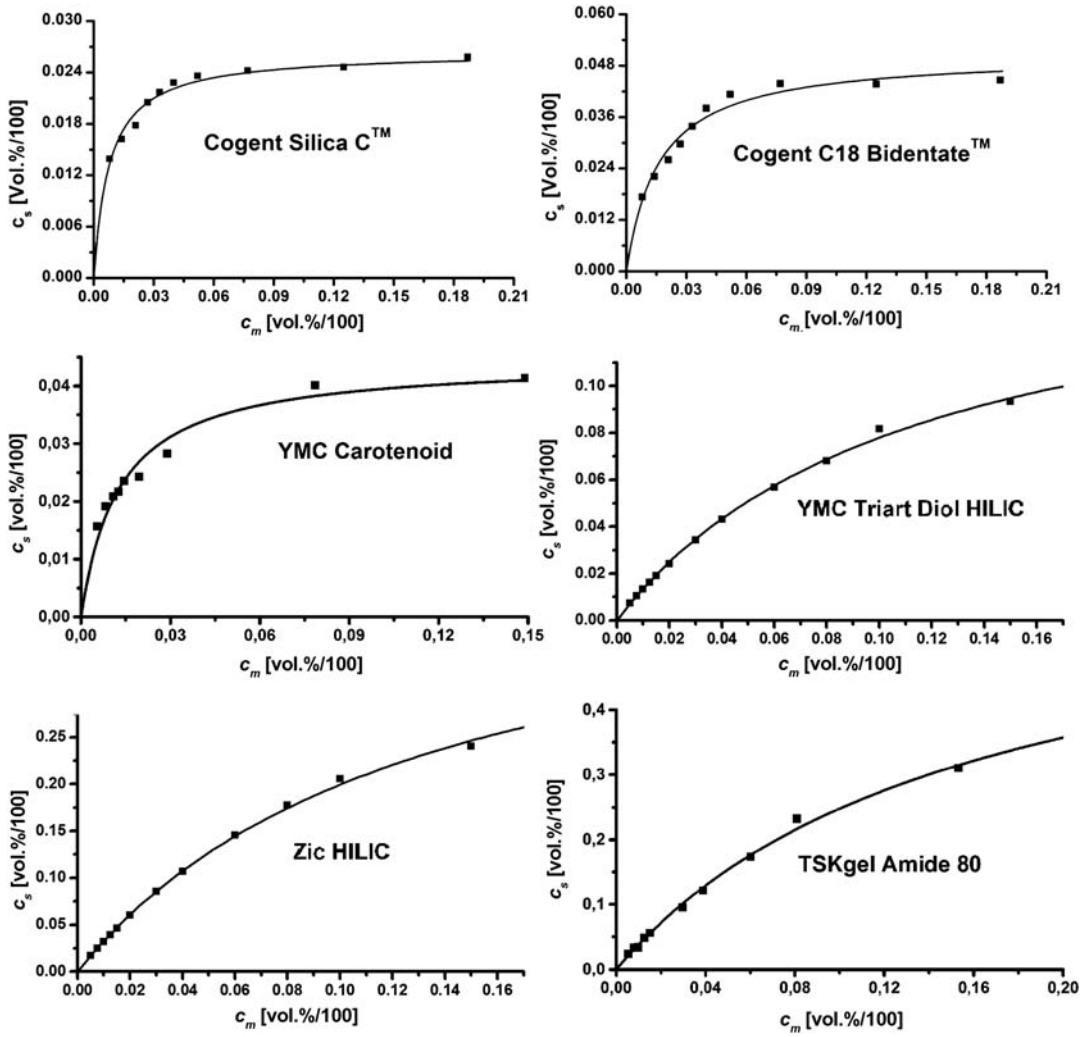

FIGURE 2.6

Langmuir isotherms of water adsorbed on two hydrosilated (Cogent Silica, Cogent Bidentate) and four silica gel (C-30 YMC carotenoid, YMC Triart Diol HILIC, zwitterionic sulfobetaine ZIC-HILIC, and TSkgel Amide-80) bonded stationary phases. *cm*, volume fraction of water in the mobile phase in equilibrium with the stationary phase; *cs*, volume fraction of excess water contained in the pores of the stationary phase.

Based on unpublished data from J. Soukup, P. Jandera, P. Janás.

Fig. 2.7 compares the column saturation capacities, q_s, calculated from the Langmuir isotherms. The TSKgel amide, ZIC-HILIC and ZIC-cHILIC, and TSKgel NH_2 columns have high saturation capacities, corresponding to ~45% (vol/vol) water in the bulk mobile phase, which is consistent with their high affinity to water reported elsewhere (Dinh et al., 2013). A relatively high saturation capacity,

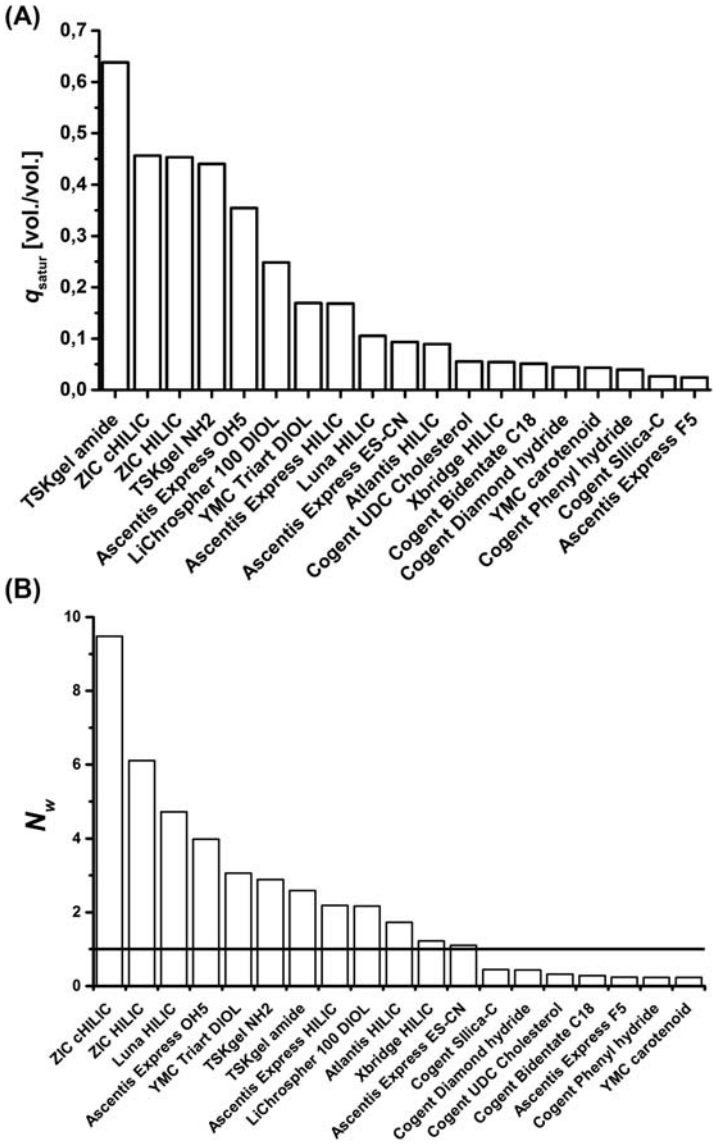

FIGURE 2.7

Water adsorption on high-performance liquid chromatography columns: (A) excess water saturation capacities, q_{satur}, calculated from Eq. (2.1) and (B) the equivalent number of adsorbed monomolecular water layers, N_w, inside the pores at full saturation capacity of the columns.

Based on the data from Soukup, J., Jandera, P., 2014. J. Chromatogr. A 1374, 102–111.

35.4% (v/v) water, was observed for the Ascentis Express OH column, whereas the Xbridge HILIC, Atlantis HILIC, Ascentis Express ES-CN, and Ascentis Express F5 columns have lower saturation capacities, less than 9% v/v. At full column saturation, the excess adsorbed water, V_{ex}, fills up to 45.3% of the pore volume of normal silica-based columns but only 2.6%−5.5% of the pore volume of hydrosilated silica columns. Because of the low affinity of the hydrosilated silica material to water, saturation capacities are as low as 0.2%−0.4% water in the inner pore volume, which are achieved in mobile phases containing 3%−6% v/v water (for the hydrosilated bare silica or bonded C18 Bidentate columns), in agreement with the Pesek ANP model (Pesek and Matyska, 2009). This low water saturation capacity is similar to the long nonpolar alkyl chain (C30) columns. On the other hand, polar columns used frequently in HILIC show much less steep water isotherms and relatively high saturation capacities, which are not approached even in mobile phases containing 20% v/v water in acetonitrile (Soukup and Jandera, 2014).

Fig. 2.7(B) shows the water uptake in terms of the number of "hypothetical" monomolecular water layer equivalents, N_w, at full saturation capacity of the 19 columns tested (Soukup and Jandera, 2014). The number of adsorbed water layer equivalents generally agrees with the order of column sorption capacities in Fig. 2.7(A) but with some exceptions from the rule. Less than one monomolecular water layer equivalent (full horizontal line) was adsorbed on the silica hydride-based stationary phases and on moderately polar core−shell columns (Ascentis Express F5 and Ascentis Express CN) at the column saturation capacity. On strongly polar stationary phases, several water layer equivalents are captured from the mobile phase. The sample partition between the bulk mobile phase and a submonomolecular layer of adsorbed water lacks a physical meaning. Rather, competition between the adsorbed water and polar solutes based on a NP adsorption mechanism (Pesek and Matyska, 2009) is more realistic. Hence, a low number of the adsorbed monomolecular equivalents, $N_w < 1$, may be used to distinguish between aqueous normal phase (ANP) and traditional HILIC (Soukup and Jandera, 2014). The strongest affinity to water was observed on the ZIC-cHILIC stationary phase, where more than nine water layer equivalents were adsorbed at the saturation capacity. Columns with bonded hydroxyl and diol ligands show stronger water adsorption in comparison to bare silica.

3.2 MOBILE PHASE IN HYDROPHILIC INTERACTION LIQUID CHROMATOGRAPHY SEPARATIONS

HILIC of polar compounds on polar stationary phases employs aqueous−organic mobile phases, usually containing 60%−95% organic solvent (acetonitrile) in water or an aqueous buffer (often volatile ammonium formate or ammonium acetate, compatible with MS detection and online identification). It is recommended to perform initial experiments at a relatively high concentration (e.g., 40%) of aqueous buffer and then increase the concentration of acetonitrile until acceptable sample retention and resolution are achieved. A scouting gradient of decreasing acetonitrile concentration starting from 95% acetonitrile can be helpful for this purpose.

Selection of the organic solvent has a strong effect on the retention and overall separation performance in HILIC mode. Increasing polarity and the ability to participate in proton−donor/proton−acceptor interactions enhance the solvent strength, which generally decreases in the order: water > methanol > ethanol > 2-propanol > tetrahydrofuran > acetonitrile (Fountain et al., 2010). Acetonitrile, an aprotic solvent, which does not show proton−donor interactions, shows the best

retention and separation selectivity among all water-miscible organic solvents in HILIC (or in ANP) chromatography. Methanol and other lower alcohols are protic solvents that provide significant hydrogen bonding interactions and compete with water for solvation of the polar adsorbent surface, decreasing the amount of adsorbed water layer on polar stationary phases (Quiming et al., 2007b). Theoretically, it is possible to substitute water by an organic solvent and to employ, e.g., a methanol−acetonitrile mobile phase in "nonaqueous HILIC chromatography," but usually the retention is weaker than that in conventional HILIC separations (Bicker et al., 2008; Soukup and Jandera, 2013).

Mobile phases containing methanol (and to lesser extent ethanol, 2-propanol, or other protic solvents) often provide insufficient sample retention and broad or nonsymmetric peak shapes. The poor performance of alcohols as organic components of HILIC mobile phases is attributed to their similarity to water in providing strong hydrogen-bonding interactions. The retention is obviously promoted by increasing differences in selective polar interactions between the highly aqueous liquid layer occluded on the surface of polar adsorbents and the bulk organic-rich mobile phase. These differences are higher with acetonitrile-rich mobile phases in comparison to the mobile phases containing protic organic solvents.

The attempts to replace acetonitrile with a less toxic solvent have not been very successful so far. Acetone has similar polarity as acetonitrile but shows lower sample retention under HILIC conditions. Moreover, it cannot be used with UV detection and provides lower intensity MS signals (Fountain et al., 2010). At high concentrations of carbon dioxide added to ethanol-water mobile phases, HILIC separations of nucleic bases and other simple polar compounds on bare silica were reported to resemble those in acetonitrile-water mobile phases (Pereira et al., 2010). However, the routine use of such mobile phases can be subject to serious practical problems.

HILIC mobile phases usually contain a buffer, whose pH and ionic strength are usually selected to enhance the sample ionization, retention, and separation selectivity, i.e., pH $>$ 7 for acids and pH $<$ 7 for bases (Jandera, 2008; Hao et al., 2008). The retention in HILIC systems with uncharged stationary phases usually increases with increased salt (buffer) concentrations, probably because of enhanced hydrogen-bonding interactions between the analyte and the stationary phase. On the other hand, the retention of ionic samples on a stationary phase with ionic or ionizable functionalities may decrease with increasing ionic strength because the salt counterions displace the retained ionized sample molecules by ion-exchange interactions. That is why the retention of acidic compounds on bonded amino phases decreases at higher salt concentrations, in contrast to other simple polar bonded silica-based stationary phases (Nguyen et al., 2010).

High ionic strengths often reduce peak tailing in HILIC systems. Some samples may require a buffer concentration of 100 mmol/L or higher for acceptable peak shapes. The addition of trifluoroacetic acid (TFA) to the mobile phase may also improve peak shapes of basic compounds by formation of ion associates. However, high ionic strengths or TFA additives are not recommended in HILIC/MS applications because they may suppress sample ionization in the mass spectrometer.

In some applications, water was partly replaced by a weaker polar protic solvent. For example, the retention of methacrylic acid, cytosine, nortriptyline, and nicotinic acid on a BEH-HILIC column increased considerably and the separation improved when substituting 5% of water with a second organic solvent (methanol, ethanol, or 2-propanol) in the original buffered mobile phase containing 90% acetontrile (Grumbach et al., 2008). Water can even be fully replaced by a polar organic solvent in so-called "nonaqueous HILIC chromatography" (NA-HILIC), employing mixed

polar organic mobile phases. There is no water in the mobile phase; instead, the liquid diffuse layer adsorbed on the stationary phase contains an increased concentration of an organic "protic modifier." NA-HILIC may fill the gap between traditional nonaqueous NP (employing a nonpolar and one or more polar organic solvents) and aqueous–organic HILIC systems. It can potentially be useful in the analysis of some poorly soluble oligomers or weakly polar compounds, which may precipitate in water-containing HILIC mobile phases. Selecting the type of protic solvent added to acetonitrile—ethylene diol, methanol, or ethanol—(with elution strength decreasing in that order), the retention and separation selectivity of nucleobases, nucleosides, and deoxynucleosides could be adjusted in HILIC on bare silica, diol (Luna HILIC), bonded thioglycerol, and oxidized thioglycerol polar bonded phases.

In HILIC mode, the retention on polar columns increases with decreasing concentration of water in a water/organic mobile phase. The effect of water in the mobile phase on the sample retention factor, $k = t_R/t_M$, can sometimes be described by Eq. (2.3), or by Eq. (2.4) (Jandera and Churáček, 1974), in the limited range of high water concentrations:

$$\log k = a_1 - m_{\mathrm{HILIC}} \cdot \log \varphi_{\mathrm{H_2O}} \tag{2.3}$$

$$\log k = a' - m_{\mathrm{HILIC}} \cdot \varphi_{\mathrm{H_2O}} \tag{2.4}$$

where $\varphi_{\mathrm{H_2O}}$ is the volume fraction of water, "a_1" is the (extrapolated) logarithm of the retention factor in pure water, and "a'" is the logarithm of the retention factor in pure organic solvent. (t_R is the sample retention time and t_M is the elution time of a nonretained standard, i.e., the column hold-up time.) The parameter "m_{HILIC}" characterizes the rate of decreasing retention with increasing content of water in the highly aqueous mobile phases. Traditionally, it has been believed that Eq. (2.3) characterizes the retention in adsorption systems and Eq. (2.4) in partition systems (Snyder and Poppe, 1980). In fact, various experimental HILIC systems show better data fit for either of the two equations (Jandera, 2011). However, a good fit of any model equation to the experimental data does not guarantee the correctness of the model. Furthermore, the original idea of the validity of Eq. (2.4) was applied to immiscible stationary and mobile phases, such as RP-LC with long-chain chemically bonded alkyl-silica materials, or organic NP-LC (Snyder, 1974). The correct application of theoretical models relies on knowledge of the exact volumes of both the stationary and mobile phases in the column, which can hardly be guaranteed in HILIC systems, where the amount of adsorbed water changes with the composition of the bulk aqueous–organic mobile phase.

In many cases, neither Eq. (2.3) nor Eq. (2.4) fits the HILIC experimental data satisfactorily. For example, this was the case with 35 acidic, basic, and neutral polar compounds on bare silica and bonded aminopropyl, amide, diol and cyanopropyl columns, including fully porous, hybrid, and core–shell types of particles (Vlčková et al., 2014). Combining Eq. (2.3) and Eq. (2.4), we obtain Eq. (2.5), which takes into account a dual HILIC-RP retention mechanism and provides improved fit to the retention data over a broader range of aqueous–organic mobile phase compositions, in comparison to polynomial empirical equations (Jin et al., 2008; Jandera and Hájek, 2009):

$$\ln k = a + b \ln \varphi_{\mathrm{H_2O}} - c\varphi_{\mathrm{H_2O}} \tag{2.5}$$

The ratio of terms b and c of Eq. (2.5) was tentatively employed to estimate the importance of the relative contributions of partitioning and the surface adsorption mechanism (Karatapanis et al., 2011). Based on the results of application of Eq. (2.5) to the retention of water-soluble vitamins, it was

concluded that the transition from a partitioning to a surface adsorption mechanism for neutral compounds occurs at more than 75%−80% acetonitrile on diol, silica, and amino columns, depending on the different degree of hydration of the stationary phases. For electrostatically attracted compounds, surface adsorption remains the dominant retention mechanism even at lower acetonitrile concentrations.

In spite of differences in the conclusions of some studies of HILIC mechanisms, the adsorption and the partition retention mechanisms most probably actually coexist in many HILIC systems, depending on the solute, the stationary phase polar functional groups, and the eluting conditions (Dinh et al., 2013; Soukup and Jandera, 2014). For example, less hydrophilic nortriptyline was reported to be retained by a partition-like mechanism and cytosine by a more hydrophilic mechanism, rather than by an adsorption-like mechanism, which was attributed to slower diffusion of the more retained polar species in the viscous diffuse water layer, even though diffusion is not a thermodynamic phenomenon (Karatapanis et al., 2011; Heaton and McCalley, 2014).

Many ionized compounds can be separated in HILIC systems. Very often, either attractive (ion exchange) or repulsive (ion exclusion or ion repulsion) electrostatic interactions participate in the retention mechanism, especially on strong (SAX) or weak (WAX) anion-exchange columns. The addition of salts, weak acids, bases, or ion-pairing reagents as mobile phase additives usually significantly improves the separation in the mixed HILIC/ion-exchange mode (Mant and Hodges, 2008). Adjusting the pH and salt (buffer) concentrations may significantly improve the retention selectivity, peak profile, and separation, however, with very different selectivity effects for acids and bases (Heaton et al., 2014). On bare silica columns, acids show much stronger retention in mobile phases containing trifluoroacetic acid than that in ammonium formate buffers, where—on the contrary—bases are better retained (McCalley, 2015).

Some mixed-mode silica-based HILIC/IEX stationary phases can be used for separations of polar and ionic solutes under HILIC conditions in organic solvent-rich mobile phases and for separations of less-polar compounds under RP conditions in more aqueous mobile phases. The RP/WAX phases differ from the typical HILIC stationary phases, TSKGel Amide-80, ZIC-HILIC, or polysulfoethyl A, to which they provide a certain degree of complementary application possibilities (Lammerhofer et al., 2008).

At increased concentration of acetonitrile, adequate retention and satisfactory resolution of both basic and acidic peptides can be achieved in a single run, on either SAX or WAX columns at low pH, where HILIC and electrostatic repulsion retention mechanisms superimpose to produce the ERLIC mode, which offers possibilities for independently adjusting the HILIC and the ion-exchange selectivities in highly organic mobile phases (Alpert, 2008; Alpert et al., 2015).

3.3 DUAL HYDROPHILIC INTERACTION LIQUID CHROMATOGRAPHY/REVERSED-PHASE RETENTION MECHANISM

Increasing the water concentration in a mobile phase is connected with a decrease in sample retention over a more or less limited range of high organic solvent concentration in the mobile phase, where the retention is controlled essentially by the sample's polar interactions in the HILIC mode. When a certain concentration of water in the bulk mobile phase is exceeded, the sample is not retained and elutes close to the column hold-up (dead) volume. However, by further increasing the concentration of water in the mobile phase, some compounds may become retained again because of the solvophobic interactions with nonpolar moieties contained in the stationary phase, which is typical for RP behavior.

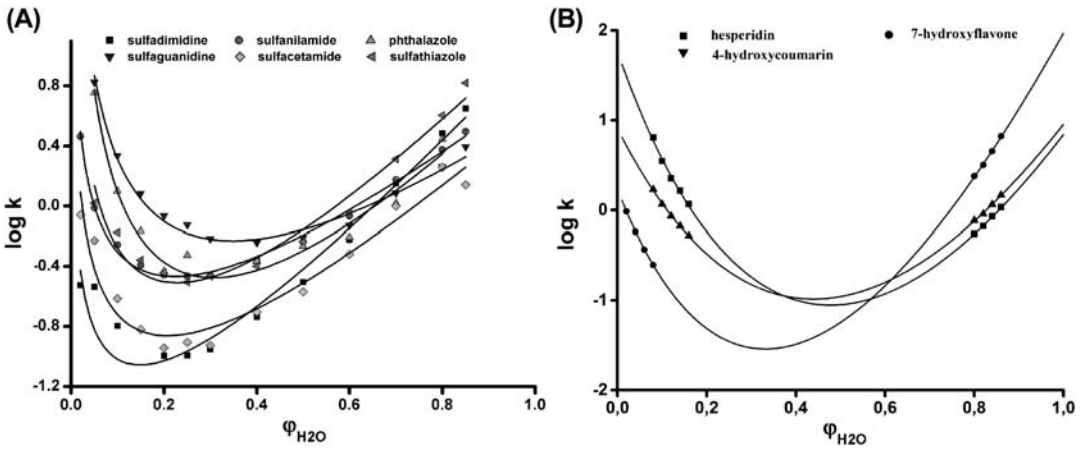

FIGURE 2.8

Effect of the volume fraction of aqueous buffer, φ_{H_2O}, in aqueous-acetonitrile mobile phase on the retention factor, k, of sulfonamides on monolithic column BIGDMA-MEDSA (A) and flavonoids on carbamoyl bonded silica column TSKgel Amide-80 (B). Points are the experimental data and lines the best fit plots of Eq. (2.5).

Based on unpublished results from P. Jandera, M. Staňková, P. Janás.

Hence, many polar columns show a dual HILIC-RP retention mechanism: nonpolar (RP) at high water concentrations and polar (HILIC) in mobile phases with high concentrations of organic solvents. In this case, the graphs of the sample retention factors, k, versus the volume fraction of water, $\varphi_{(H_2O)}$, show characteristic U-profiles over a broad range of binary aqueous–organic mobile phases (see examples in Fig. 2.8). The dual HILIC-RP behavior depends both on the column and sample, and it probably increases for polar stationary phases containing significant nonpolar moieties in the structure.

In the presence of a dual HILIC-RP mechanism, the effects of the volume fraction of the more polar solvent, water, $\varphi_{(H_2O)}$, on the retention factor, k, can often be described by Eq. (2.6) over a broad range of compositions of aqueous–organic mobile phases $\left(\text{at } \varphi_{(H_2O)} > 0.02\right)$:

$$\log k = a + m_{RP} \cdot \varphi_{H_2O} - m_{HILIC} \cdot \log\left(1 + b \cdot \varphi_{H_2O}\right) \tag{2.6}$$

The parameter m_{RP} characterizes the effect of the increasing concentration of water in the mobile phase on the retention because of the RP mechanism in water-rich mobile phases, whereas the parameter m_{HILIC} is a measure of the water contribution to the decrease of retention in highly organic mobile phases (i.e., the HILIC range). The system constant, a, depends on the solute and type of organic solvent. The empirical term, b, improves the description of the retention at low water concentrations (Jandera and Hájek, 2009).

Eq. (2.6) describes the U-shaped experimental graphs, where the "U-turn" transition from the HILIC to the RP mode can be localized at the minimum retention corresponding to the φ_{min} concentration of water in the mobile phase:

$$\varphi_{min} = 0.434 m_{HILIC}/m_{RP} \tag{2.7}$$

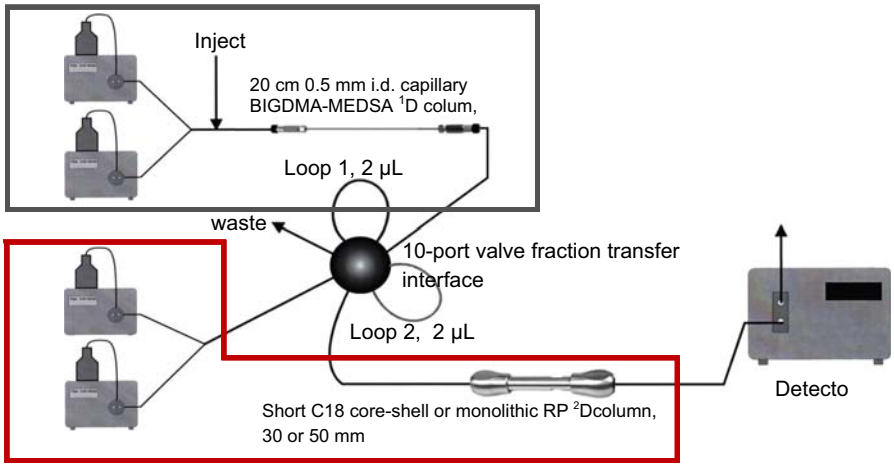

FIGURE 2.9

Instrumental two-dimensional comprehensive HILIC × RP HPLC setup with a zwitterionic polymethacrylate capillary column in the first dimension and a short efficient C18 column in the second dimension.

The "U-turn" mobile phase composition generally depends on the polarity of sample and on the type of stationary phase. The transition between the HILIC and the RP behavior is observed at a lower volume fraction of the aqueous buffer on less PEG columns (such as bonded polyethylene glycol in 70%−90% acetonitrile), in comparison to more polar columns, e.g., diol, zwitterionic, etc., in 40%−70% acetonitrile (Jandera and Hájek, 2009).

Zwitterionic polymethacrylate monolithic columns show dual HILIC and RP mechanisms. Orthogonal selectivity in the HILIC and the RP ranges may provide excellent separations of flavonoids and phenolic acids (as well as others) on a single column in both retention modes. Silica hydride columns with bidentate or cholesterol nonpolar ligands bonded on the surface also show dual retention mechanisms, despite very low affinity to water (Soukup and Jandera, 2012a,b).

Some columns may provide practically useful separations only either at high organic solvent concentrations (HILIC) or in highly aqueous mobile phases (RP), ruling out from practical use the major part of the medium mobile phase composition range, where the retention is too low. The useful mobile phase range depends both on the stationary phase and on the analyte. For example, organic polymer zwitterionic columns provide relatively broad mobile phase ranges both for HILIC and RP separation modes. Fig. 2.8A shows examples of U-turn retention plots of sulfonamides on a home-made capillary zwitterionic column (Staňková and Jandera, 2016) and Fig. 2.8B the U-turn retention plots of flavonoids on a commercial bonded amide column.

In a recent study, the retention of 35 small polar compounds was compared among aminopropyl, amide, diol, and cyanopropyl columns with silica-based, hybrid, and fused-core particles (Vlčková, et al., 2014). Most acidic and neutral compounds experienced greater retention under RP conditions than that under HILIC conditions. Only with the beta-blockers atenolol and propranolol were typical U-profile retention−mobile phase graphs observed. The aminopropyl stationary phase strongly retains

acids because of electrostatic interactions, even under RP conditions. Bare silica exhibits a preference for basic compounds by interactions with the acidic surface of silanols.

Because the separation selectivities on a dual-mechanism column are highly complementary (orthogonal), a single column can be used to obtain useful information on the sample injected subsequently in acetonitrile-rich (HILIC) and highly aqueous (RP) mobile phases (Jandera et al., 2010a,b). The dual mechanism is best used with alternating increasing (HILIC) and decreasing (RP) concentration gradients of water in buffered mobile phase at pH = 3.1, both in unidimensional and 2D HPLC separations (Jandera et al., 2013).

3.4 SAMPLE STRUCTURE AND SELECTIVITY IN HYDROPHILIC INTERACTION LIQUID CHROMATOGRAPHY

Correlations between the retention factor, k, and sample hydrophobicity are often used in RP chromatography to predict the effect of sample polarity on retention. The original approach was based on simple correlation of log k with the logarithm of the sample partition coefficient between octanol and water, log P. This correlation may give a useful first indication of the effect of polarity on the retention of neutral compounds; for ionizable compounds, the partition coefficient P should be substituted by the distribution ratio, D, taking into account the retention of both the nonionized and ionized solute forms, which of course depends on pH (Kumar et al., 2013).

Combined effects of the solute structure and the mobile phase composition on the HILIC retention were employed in a model based on five predictors, including the %ACN in the mobile phase, the log D, the number of hydrogen bond donors, the desolvation energy in octanol, and the total absolute atomic charge structural descriptors. The model was applied to predict the retention of adrenoreceptor agonists and antagonists on a PVA-bonded stationary phase under HILIC conditions (Quiming et al., 2008a). Also, a two-parameter model employing the %ACN and the solute local dipole index was used to predict the HILIC retention of seven ginsenosides on a polyamine-bonded stationary phase (Quiming et al., 2008b).

The effects of the sample structural contributions in RP-LC are described in detail by the LSER model, which employs multiple correlations between the retention (log k) and so-called solvatochromic parameters (molecular structural descriptors), characterizing the solubility and solvation of the solute and the stationary phase (Tan et al., 1996).

$$\log k = c + v \cdot V + s \cdot S + a \cdot A + b \cdot B + d^{-}D^{-} + d^{+}D^{+} \tag{2.8}$$

The structural descriptors in Eq. (2.8) characterize the properties of the sample: the volume of the solvated solute molecule, V, is called the McGowan characteristic volume, which is proportional to the size of sample molecule (in cm^3/mol/100) and the energy necessary to disrupt solvent−solvent bonds to form a cavity accommodating a sample molecule (Abraham et al., 2004); S characterizes the sample polarity and polarizability; B and A represent the hydrogen-bonding basicity and the hydrogen-bonding acidity, respectively. Ionic molecular descriptors D^{-} and D^{+} were later added by Chirita et al. (2011) to the LSER model, to take into account the degree of dissociation of weak acids and weak bases, depending on pH. For neutral species, the D parameters are zero; fully dissociated acids or bases have D values close to 1.

The parameters v, s, a, b, d^{-}, and d^{+} of Eq. (2.8) characterize the response of the separation system (the specific combination of the stationary and the mobile phases) to the solute structural parameters.

The system response coefficients are determined by multiple linear regression applying Eq. (2.8) to a representative group of sample compounds.

The original LSER model was also later applied in HILIC chromatography. Relatively good fit of the LSER model was found for the silica hydride, bonded polyethylene glycol, diol, and zwitterionic sulfobetaine columns in the HILIC range up to 95% acetonitrile (Jandera et al., 2010b). The LSER model does not allow direct comparison of column selectivity, but it is a useful tool in column design, which helps to verify the expected effects on retention of various ligands immobilized on the silica surface (Bicker et al., 2008).

3.5 TEMPERATURE EFFECTS

Elevated temperature often improves the HILIC bandwidths, and consequently the efficiency of separation, by decreasing the mobile phase viscosity and accelerating the diffusion. Furthermore, temperature affects the Gibbs molar free energy of retention, ΔG^0, and consequently the distribution constant, K, and the retention factor, k, in chromatography. The temperature effects in chromatography can often be described by the Van't Hoff equation (Melander and Horvath, 1980):

$$\ln k = \ln K + \ln \frac{V_S}{V_M} = -\frac{\Delta G^0}{RT} = \frac{\Delta S^0}{R} + \ln \frac{V_S}{V_M} - \frac{\Delta H^0}{RT} = A_i + \left(\frac{B_i}{T}\right) \tag{2.9}$$

ΔH^0 is the standard partial molar free enthalpy of retention and ΔS^0 is the corresponding standard partial molar free entropy; T is thermodynamic temperature (in Kelvins); V_S and V_M are the volumes of the stationary phase and mobile phases in the column, respectively. Hence, temperature usually affects the retention and selectivity of a separation through the decrease in enthalpy. Good fit of Eq. (2.9) to the experimental data is considered as proof of an enthalpy-controlled exothermic process within the experimental temperature range (Melander and Horvath, 1980). In addition to changing enthalpy, the retention can be connected with entropic changes, namely conversion between different sample configurations (Hao et al., 2008). For example, an enthalpy-controlled retention process (positive B_i terms in Eq. 2.9) and improved separations at elevated temperature were found in HILIC separations of polar compounds on mercapto-ethanol and 1-thioglycerol columns (ΔH^0 from 4.5 to 19.5 kJ/mol) (Wu et al., 2008). Phenolic acids and flavonoids show linear Van't Hoff log k versus $1/T$ plots both on silica hydride and UDC cholesterol silica hydride columns, both in the highly organic (HILIC) and highly aqueous (RP) mobile phase ranges. Hence, enthalpic effects control the retention in both retention modes, but the energy of interactions with the stationary phase is 3−5 times stronger in the HILIC range, which suggests a stronger effect of adsorption with respect to partition distribution in the HILIC (NP) mode. Optimum HILIC mode separations on hydrosilated silica and UDC cholesterol silica hydride columns have been achieved at ambient temperature (Soukup and Jandera, 2012b).

Most silica-based and organic polymer monolithic zwitterionic columns yielded Van't Hoff B_i parameters close to zero, indicating low or negligible enthalpic effects on retention. The retention of acids on dual-mechanism zwitterionic columns in acetonitrile-rich mobile phases (HILIC mode) may show significant entropic effects, whereas the same column is subject to a "regular" enthalpy-controlled exothermic retention mechanism in more aqueous mobile phases (in the RP mode) (Škeříková and Jandera, 2010).

4. HYDROPHILIC INTERACTION LIQUID CHROMATOGRAPHY MODE IN TWO-DIMENSIONAL LIQUID CHROMATOGRAPHY SEPARATION SYSTEMS

The number of peaks that can be separated in a single HPLC run can hardly exceed 100. However, in clinical, pharmaceutical, food, natural and environmental analysis, molecular biology, and elsewhere, we encounter samples that may contain even millions of compounds, in concentrations possibly spanning over 10 orders of magnitude. The peak capacity, i.e., the maximum number of peaks that can be separated in a sample, can be significantly increased by combining two or more different separation mechanisms in multidimensional separation systems (Stoll et al., 2007; Guiochon et al., 2008; Fairchild et al., 2009; Grosskreutz et al., 2012; Jandera, 2012b).

To quantify the differences in selectivity of the individual HILIC columns, the correlation coefficient, r^2, between the retention factors, k, of a suitably selected group of test compounds, or of their logarithms, on various polar columns and a reference column (such as bare silica) may be measured to calculate the coefficients s^2, characterizing the relative separation selectivities of the individual polar columns (Neue et al., 2006):

$$s^2 = 1 - r^2 \tag{2.10}$$

$s^2 = 1$ for fully noncorrelated (orthogonal) systems ($r^2 = 0$), whereas $s^2 = 0$ for equivalent separation systems. The 2D peak capacity can theoretically reach the product of the peak capacities of the individual systems in orthogonal 2D separation systems, where the retention in the first dimension is not correlated with the retention in the second dimension. In practice, most 2D systems show a lower number of resolved peaks because of more or less significant retention correlation in the two dimensions (Gilar et al., 2005). Coupled HILIC and RP separation systems offer two completely different retention mechanisms and a very high degree of orthogonality in comparison to other 2D LC systems (Jandera, 2008). Hence, 2D separation systems combining HILIC and RP modes allow the number of compounds resolved in complex samples to be significantly increased (Guiochon et al., 2008).

The expected increase in the number of really separated compounds (the practical peak capacity) that can be achieved in various off-line and online multidimensional setups and the price to be paid for it in terms of the analysis time and sample dilution (i.e., decreased sensitivity) have been reviewed in detail (Guiochon et al., 2008). Later, the performance of off-line, online stop-flow, and comprehensive HILIC chromatography combined with RPLC was compared in terms of peak capacities, analysis times, and peak production rates (Kalili and de Villiers, 2013). An online comprehensive LC × LC system is best for samples requiring peak capacities up to 600. The off-line or stop-flow systems provide higher peak capacities, at the cost of long separation times. The contribution of the stop-flow to band broadening was found negligible.

Generally, the peak capacity is higher in gradient mode than that under isocratic conditions. Hence, the number of resolved peaks increases when simultaneous gradients are used in the first dimension and in the second dimension of a comprehensive online 2D setup (Jandera, 2012a). Optimization of the gradient range and gradient profile, especially in the second dimension, can significantly increase the practical 2D peak capacity (Cacciola et al., 2007; Jandera et al., 2011).

The off-line approach using two (or more) separate columns is very simple, does not necessitate any special instrumentation, and has been practiced for many years. It allows independent optimization

of the two separation systems; the fractions collected from the first column can be pretreated before injection onto the second column, such as using evaporation to dryness of manually collected HILIC fractions before introduction to a C_{18} column in the second dimension (Liang et al., 2012). Off-line coupling of HILIC and RP-LC was shown to provide a powerful separation system for procyanidins (Kalili and de Villiers, 2010) and flavonoids (Beelders et al., 2012). Another recent example reports an off-line RP-HILIC method coupled with MS for impurity profiling of infusion solutions (Schiesel et al., 2012). Unfortunately, off-line procedures are labor demanding and time demanding.

Online combinations of HILIC and RP-HPLC (Fig. 2.9) are subject to compatibility problems originating from the differences in the mobile phase elution strengths in the HILIC and RP modes. High concentrations of the organic solvents used for HILIC separations usually provide weak retention in the RP systems, whereas the mobile phases rich in water used in RP-HPLC are usually too strong as HILIC eluents. If the mobile phase from the first (HILIC) dimension is used for the fraction transfer to the second dimension, a significant decrease in retention and unsymmetric or even split peaks may appear, with detrimental effects on the separation (Jandera et al., 2012).

The compatibility of the mobile phases used in 2D HILIC-RP systems can be improved in several ways (Kalili and de Villiers, 2013):

1. Transferring only small volume fractions online from the first dimension to the second dimension column (for example, 2 μL onto a 50 × 3 mm I.D. C18 column) often minimizes the sample solvent effects in the second dimension, however, sometimes with possible negative impacts on the sensitivity of 2D separations (Guiochon et al., 2008).
2. The mobile phase strength in the acetonitrile-rich fractions transferred from the HILIC column can be modulated by diluting with water before introducing the fractions onto an RP column in the second dimension using a make-up flow mediated by an additional auxiliary pump (Wang et al., 2008c).
3. Fractions from the first column can be trapped on a small column and another solvent can be used for the transfer to the second dimension (Wilson et al., 2007).

Approaches 1 and 2 can be combined. For example, 2D HILIC × RP separation of phenolic compounds in green tea was reported using a diol HILIC column in the first dimension and a gradient of water and methanol in acetonitrile with acetic acid additive. 50 μL fractions were collected with 1 min frequency and evaporated under nitrogen to 2 μL before introduction onto a C18 column in the second dimension (Kalili and de Villiers, 2013).

Online 2D separations can employ either serial or parallel column setups. Serial column coupling does not require complex instrumentation, and allows only a moderate increase in peak capacity, because of the additivity of the contributions of the individual columns, in contrast to comprehensive online 2D LC × LC providing multiplicative effects on peak capacity and considerably higher peak production rate (i.e., the number of resolved compounds in a preset separation time). A set of serially coupled columns containing different stationary phases behaves like a new column with modified selectivity, which may enable separations of samples with widely differing properties (Alvarez Segura et al., 2016). An octadecylsilica column in the first dimension serially coupled with a HILIC column in the second dimension, to which a gradient of acetonitrile in water up to the end concentration of 80% or more was applied, allowed separation of a broad range of pharmaceuticals in a single run (Louw et al., 2008). A serial combination of a ZIC-HILIC sulfobetaine column and an amide column with a HILIC gradient run from 95% to 35% aqueous buffer in acetonitrile allowed simultaneous separations

of polar and nonpolar metabolites in a mouse serum sample (Chalcraft and McCarry, 2013). Tandem coupling of a C_{18} column with a zwitterionic column was employed for separation of polar and nonpolar phenolic compounds in wine, with a single gradient of simultaneously increasing concentration of acetonitrile and decreasing salt concentration (Greco et al., 2013).

A 2D capillary liquid chromatography−Fourier transform mass spectrometry method, employing a 100 mm × 150 μm I.D. C_{18} RP column serially coupled with a 250 mm × 200 μm I.D. (polyhydroxyethyl aspartamide) HILIC column, was used for the analysis of 11 quaternary ammonium compounds in brain extracts, including acylcarnitines of low polarity. To overcome the mobile phase compatibility problem on the two columns, they were connected via a T-piece allowing addition of a make-up flow of 95% acetonitrile to the effluent from the RP column before transfer to the HILIC column (Falasca et al., 2012).

An interesting solution to the problem of different elution strengths required to elute polar and nonpolar compounds employed a column-switching setup, where the sample was first injected onto two serially coupled 100 mm × 2.1 mm BEH columns. A plug of early eluting weakly polar compounds was directed onto a trapping RP column, where the analytes were stored until the separation of polar compounds on the HILIC columns had been finished. Then the configuration of switching valves was changed to redirect the weakly polar compounds onto a Phenyl Hexyl RP column, where they were separated using a gradient of increasing acetonitrile concentration in 0.02% aqueous formic acid (Cabooter et al., 2014).

A crucial point affecting the separation time in comprehensive 2D liquid chromatography is the performance of the column used in the second dimension, which should allow highly efficient fast chromatographic separations. For this purpose, UHPLC with a short column packed with sub-2 μm particles can be used at a very high operating pressure (Cacciola et al., 2011). A core−shell column represents another possibility that can be used with conventional liquid chromatographic instrumentation (Jandera et al., 2015). Online connection of a capillary HILIC column in the first dimension and an ultra-high performance RP-LC in the second dimension, coupled with MS, was used for high-resolution separation and detailed characterization of anthocyanins and related pigments in berries and aged red wine (Willemse et al., 2014, 2015). Because of lower flow resistance, monolithic columns can be used in the second dimension at higher flow rates in comparison to particle-packed columns operated at the same operating pressure. Very fast second-dimension gradient separations on core−shell columns were achieved at ambient temperature without excessive backpressure and without compromising optimal first dimension sampling rates. Very good band symmetry and retention time repeatability in gradient separations of phenolic compounds and flavonoids could be achieved in optimized comprehensive HILIC × RP on a 0.5 mm I.D. monolithic sulfobetaine HILIC capillary column coupled with various 2.5−5 cm long, 3 mm I.D. monolithic and core−shell C_{18} columns. A flow rate of a few microliters per min was used on the capillary column in the first dimension; the short C_{18} columns were operated at flow rates of 3−5 mL/min in the second dimension (Jandera et al., 2012).

Polar columns showing a dual RP-HILIC mechanism allow a combined 2D RP × RP and HILIC × RP setup to be used. In the first dimension, the RP mode in a highly aqueous mobile phase alternates with the HILIC mode in a mobile phase with a high acetonitrile concentration. In the second dimension, the RP mode can be used. A recently introduced zwitterionic polymethacrylate sulfobetaine BIGDMA-MEDSA capillary column shows a dual HILIC/RP mechanism at high concentrations of acetonitrile and RP behavior in water-rich mobile phases (Staňková and Jandera, 2016).

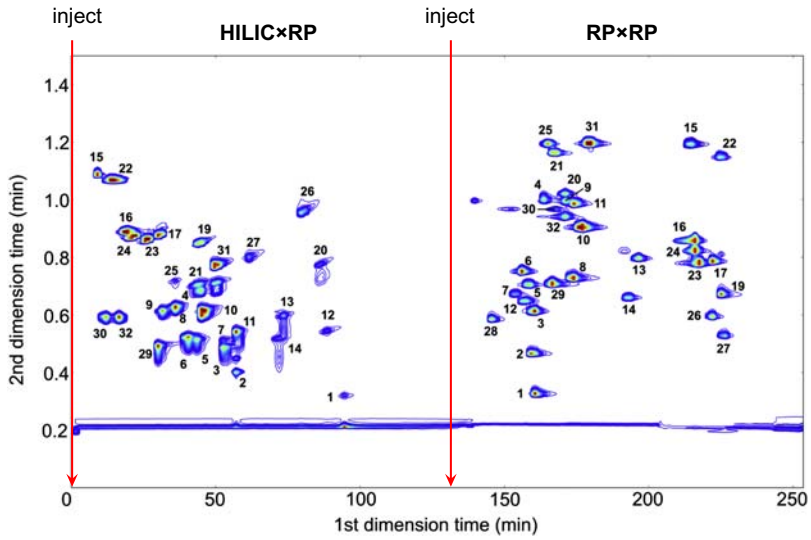

FIGURE 2.10

Dual comprehensive two-dimensional chromatogram of polyphenolic and flavonoid compounds recorded in subsequent HILIC mode (left, gradient of decreasing acetonitrile concentration) and reversed-phase mode (right, gradient of increasing acetonitrile concentration) on a single monolithic capillary zwitterionic polymethacrylate BIGMA-MEDSA column in the first dimension coupled online with a Kinetex XB-C_{18}, 50 × 3.1 mm I.D., core–shell column in the second dimension.

Based on the data from Hájek, T., Jandera, P., Staňková, M., Česla, P., 2016. J. Chromatogr. A 1446, 91–102.

The BIGDMA-MEDSA column in the first dimension coupled online with a short monolithic or core–shell C_{18} column was used for combined alternating HILIC × RP and RP × RP comprehensive 2D separations of polyphenolic compounds. During the HILIC × RP period, a gradient of decreasing acetonitrile gradient was used for the separation in the first dimension. At the end of the gradient, the polymeric monolithic microcolumn was equilibrated with a highly aqueous mobile phase and was ready for the second sample injection in the RP × RP period. This time a gradient of increasing concentration of acetonitrile was used in the first dimension. Fig. 2.10 presents 2D chromatograms of flavones and related polyphenolic compounds, acquired with a single first-dimension BIGDMA-MEDSA capillary column in two experiments with consecutive injections of the sample, the first one into a decreasing and the second into an increasing acetonitrile gradient (Hájek et al., 2016). The automated dual LC × LC approach allows obtaining three-dimensional data in a relatively short time.

5. SUMMARY AND PERSPECTIVES FOR FURTHER DEVELOPMENT

A number of new types of polar stationary phases have been reported during the past years, based either on silica gel, other inorganic supports, or on organic polymers. Many column types have been successfully used for separations of various classes of strongly and moderately polar, or even ionic,

compounds. Large differences in retention and separation selectivity, depending on the chemistry of stationary phases, indicate that the retention mechanism is more complex than the originally suggested partition between the water layer adsorbed on a solid support and the bulk mobile phase. Probably, a sample-dependent mix of nonpolar and selective polar [hydrogen bonding, dipole−dipole, ion-exchange, and ion-repulsion (ERLIC)] interactions participates in separation.

The column types used in HILIC strongly differ in the adsorption capacity for water. The columns based on hydrosilated silica show less than a monomolecular water layer capacity, which suggests that the adsorption process (i.e., NP-LC) characterizes the retention more appropriately than the partition process.

We can expect future development of tailor-made HILIC stationary phases intended for specific types of samples. Another almost unexplored promising field is better utilization of mobile phases for adjusting the retention mechanism (HILIC-RP) on a single column to extend separation selectivity by alternating use of different separation conditions. These possibilities can probably be used in future 2D combinations implementing the HILIC mode in off-line, serial, stop-and-go, and comprehensive setups, and their combinations, to improve peak capacities for complex samples containing hundreds of compounds.

REFERENCES

Abraham, M.H., Ibrahim, A., Zissimos, A.M., 2004. Determination of sets of solute descriptors from chromatographic measurements. J. Chromatogr. A 1037, 29−47.

Ahn, J., Bones, J., Yu, Y.Q., Rudd, P.M., Gilar, M., 2010. Separation of 2-aminobenzamide labeled glycans using hydrophilic interaction chromatography columns packed with 1.7 μm sorbent. J. Chromatogr. B 2010 (878), 403−408.

Alpert, A.J., 1983. Cation-exchange high-performance liquid chromatography of proteins on poly(aspartic acid)-silica. J. Chromatogr. A 266, 23−37.

Alpert, A.J., 1990. Hydrophilic-interaction chromatography for the separation of peptides, nucleic acids and other polar compounds. J. Chromatogr. 449, 177−196.

Alpert, A.J., 2008. Electrostatic repulsion hydrophilic interaction chromatography for isocratic separation of charged solutes and selective isolation of phosphopeptides. Anal. Chem. 80, 62−76.

Alpert, A.J., Andrews, P.C., 1988. Cation-exchange chromatography of peptides on poly(2-sulfoethyl aspartamide)-silica. J. Chromatogr. 443, 85−96.

Alpert, A.J., Shukla, M., Shukla, A.K., Zieske, L.R., Yuen, S.W., Ferguson, M.A.J., Mehlert, A., Pauly, M., Orlando, R., 1994. Hydrophilic-interaction chromatography of complex carbohydrates. J. Chromatogr. A 676, 191−202.

Alpert, A.J., Hudecz, O., Mechtler, K., 2015. Anion-exchange chromatography of phosphopeptides: weak anion exchange versus strong anion exchange and anion-exchange chromatography versus electrostatic repulsion-hydrophilic interaction chromatography. Anal. Chem. 87, 4704−4711.

Alvarez-Segura, T., Torres-Lapasio, J.R., Ortiz-Bolsico, C., Garcia-Alvarez-Coque, M.C., 2016. Stationary phase modulation in liquid chromatography through the serial coupling of columns: a review. Anal. Chim. Acta 923, 1−23.

Appelblad, P., Abrahamsson, P., September, 2005. MS detection of homocysteine, methyl-malonic acid, and succinic acid using HILIC separation on a covalently bonded zwitterionic stationary phase. LCGC N. Am. (Suppl.), 24−25.

Aral, T., Aral, H., Zizadanogullari, B., Zizadanogullari, R., 2015. Synthesis of a mixed-model stationary phase derived from glutamine for HPLC separation of structurally different biologically active compounds: HILIC and reversed-phase applications. Talanta 131, 64−73.

Armstrong, D.W., Jin, H.L., 1989. Evaluation of the liquid chromatographic separation of monosaccharides, disaccharides, trisaccharides, tetrasaccharides, deoxysaccharides and sugar alcohols with stable cyclodextrin bonded phase columns. J. Chromatogr. 462, 219–232.

Arrua, R.D., Causon, T.J., Hilder, E.F., 2012. Recent developments and future possibilities for polymer monoliths in separation science. Analyst 137, 5179–5189.

Aturki, Z., D'Orazio, G., Rocco, A., Si-Ahmed, K., Fanali, S., 2011. Investigation of polar stationary phases for the separation of sympathomimetic drugs with nano-liquid chromatography in hydrophilic interaction liquid chromatography mode. Anal. Chim. Acta 685, 103–110.

Beelders, T., Kalili, K.M., Joubert, E., de Beer, E., de Villiers, A., 2012. Comprehensive two-dimensional liquid chromatographic analysis of rooibos (*Aspalathus linearis*) phenolics. J. Sep. Sci. 35, 1808–1829.

Berthod, A., Chang, S.S.C., Kullman, J.P.S., Armstrong, D.W., 1998. Practice and mechanism of HPLC oligosaccharide separation with a cyclodextrin bonded phase. Talanta 47, 1001–1012.

Bicker, W., Wu, J.Y., Lammerhofer, M., Lindner, W., 2008. Hydrophilic interaction chromatography in nonaqueous elution mode for separation of hydrophilic analytes on silica-based packings with noncharged polar bondings. J. Sep. Sci. 31, 2971–2987.

Blahová, E., Jandera, P., Cacciola, F., Mondello, L., 2006. Two-dimensional and serial column reversed-phase separation of phenolic antioxidants on octadecyl-, polyethyleneglycol-, and pentafluorophenylpropyl-silica columns. J. Sep. Sci. 29, 555–566.

Boersema, P.J., Divecha, N., Heck, A.J.R., Mohammed, S., 2007. Evaluation and optimization of ZIC-HILIC-RP as an alternative MudPIT strategy. J. Proteome Res. 6, 937–946.

Booth, T.J., Blake, P., Nair, R.R., Jiang, D., Hill, E.W., Bangert, U., Bleloch, A., Gass, M., Novoselov, K.S., Katsnelson, M.I., 2008. Macroscopic graphene membranes and their extraordinary stiffness. Nano Lett. 8, 2442–2446.

Boysen, R.A., Yang, Y., Chowdhury, J., Matyska, M.T., Pesek, J.J., Hearn, M.T.W., 2011. Simultaneous separation of hydrophobic and hydrophilic peptides with a silica hydride stationary phase using aqueous normal phase conditions. J. Chromatogr. A 1218, 8021–8026.

Buszewski, B., Noga, S., 2012. Hydrophilic interaction liquid chromatography (HILIC)—a powerful separation technique. Anal. Bioanal. Chem. 402, 231–247.

Cabooter, D., Choikhet, K., Lestreau, F., Dittman, M., Desmet, G., 2014. Towards a generic variable column length method development strategy for samples with a large variety in polarity. J. Chromatogr. A 1372, 174–186.

Cacciola, F., Jandera, P., Hajdú, Z., Česla, P., Mondello, L., 2007. Comprehensive two-dimensional LC × LC with parallel gradients for separation of phenolic and flavone antioxidants. J. Chromatogr. A 1149, 73–87.

Cacciola, F., Delmonte, P., Jaworska, K., Dugo, P., Mondello, L., Rader, J.I., 2011. Employing ultra high pressure liquid chromatography as the second dimension in a comprehensive two-dimensional system for analysis of *Stevia rebaudiana* extracts. J. Chromatogr. A 1218, 2012–2018.

Chalcraft, K.R., McCarry, B.E., 2013. Tandem LC columns for the simultaneous retention of polar and nonpolar molecules in comprehensive metabolomics analysis. J. Sep. Sci.

Chauve, B., Guillarme, D., Cléon, P., Veuthey, J.-L., 2010. Evaluation of various HILIC materials for the fast separation of polar compounds. J. Sep. Sci. 33, 752–764.

Cheng, X.D., Peng, X.T., Yu, Q.W., Yuan, B.F., Feng, Y.Q., 2013. Preparation of a novel amino-phosphate zwitterionic stationary phase for hydrophilic interaction chromatography. Chromatographia 76, 1569–1576.

Chirita, R.-I., West, C., Zubrzycki, S., Finaru, A.L., Elfakir, C., 2011. Investigations on the chromatographic behaviour of zwitterionic stationary phases used in hydrophilic interaction chromatography. J. Chromatogr. A 1218, 5939–5963.

Churms, S.C., 1996. Recent progress in carbohydrate separation by high-performance liquid chromatography based on hydrophilic interaction. J. Chromatogr. A 720, 75–91.

Cífková, E., Hájek, R., Lísa, M., Holčapek, M., 2016. Hydrophilic interaction liquid chromatography-mass spectrometry of (lyso)phosphatidyl acids, (lyso)phosphatidylserines and other lipid classes. J. Chromatogr. A 1439, 65–73.

Currivan, S., Jandera, P., 2014. Modification reactions applicable to polymeric monolithic columns. A review. Chromatography 1, 24−53.

Currivan, S., Macák, J.M., Jandera, P., 2015. Polymethacrylate monolithic columns for hydrophilic interaction liquid chromatography prepared using a secondary surface polymerization. J. Chromatogr. A 1402, 82−93.

da Silva, C.G.A., Collins, C.H., Bottoli, C.B.G., 2014. Monolithic capillary columns based on silica and zirconium oxides for use in hydrophilic interaction liquid chromatography. Microchem. J. 116, 249−254.

Dejaegher, B., Vander Heyden, Y., 2010. HILIC methods in pharmaceutical analysis. J. Sep. Sci. 33, 698−715.

Dejaegher, B., Mangelins, D., Vander Heyden, Y., 2008. Method development for HILIC assays. J. Sep. Sci. 31, 1438−1448.

Dinh, N.P., Jonsson, T., Irgum, K., 2011. Probing the interaction mode in hydrophilic interaction chromatography. J. Chromatogr. A 1218, 5880−5891.

Dinh, N.P., Jonsson, T., Irgum, K., 2013. Water uptake on polar stationary phases under conditions for hydrophilic interaction chromatography and its relation to solute retention. J. Chromatogr. A 1320, 33−47.

Dolzan, M.D., Spudeit, D.A., Breitbach, Z.S., Barber, W.E., Micke, G.A., Armstrong, D.W., 2014. Comparison of superficially porous and fully porous silica supports used for a cyclofructan 6 hydrophilic interaction liquid chromatographic stationary phase. J. Chromatogr. A 1365, 124−130.

Dreyer, D.R., Park, S., Bielawski, C.W., Ruoff, R.S., 2010. The chemistry of graphene oxide. Chem. Soc. Rev. 39, 228−240.

Dun, H., Zhang, W., Wei, Y., Song, X., Li, Y., Chen, L., 2004. Layer-by-layer self-assembly of multilayer zirconia nanoparticles on silica spheres for HPLC packings. Anal. Chem. 76, 5016−5023.

Fairchild, J.N., Horváth, K., Guiochon, G., 2009. Approaches to comprehensive multidimensional liquid chromatography systems. J. Chromatogr. A 1216, 1363−1371.

Falasca, S., Petruzziello, F., Kretz, R., Rainer, G., Zhang, X.Z., 2012. Analysis of multiple quaternary ammonium compounds in the brain using tandem capillary column separation and high resolution mass spectrometric detection. J. Chromatogr. A 1241, 46−51.

Feste, A.S., Khan, I., 1992. Separation of glucooligosaccharides and polysaccharide hydrolysates by gradient elution hydrophilic interaction chromatography with pulsed amperometric detection. J. Chromatogr. 630, 129−139.

Foo, H.C., Heaton, J., Smith, N.W., Stanley, S., 2012. Monolithic poly (SPE-co-BVPE) capillary columns as a novel hydrophilic interaction liquid chromatography stationary phase for the separation of polar analytes. Talanta 100, 344−348.

Fountain, K.J., Xu, J., Diehl, D.M., Morrison, D., 2010. Influence of stationary phase chemistry and mobile-phase composition on retention, selectivity, and MS response in hydrophilic interaction chromatography. J. Sep. Sci. 33, 740−751.

Garbis, S.D., Melse-Boonstra, A., West, C.E., van Breemen, R.B., 2001. Determination of folates in human plasma using hydrophilic interaction chromatography − tandem mass spectrometry. Anal. Chem. 73, 5358−5364.

Gilar, M., Olivova, P., Daly, A.E., Gebler, J.C., 2005. Orthogonality of separation in two-dimensional liquid chromatography. Anal. Chem. 77, 6426−6434.

Greco, G., Grosse, S., Letzel, T., 2013. Serial coupling of reversed-phase and zwitterionic hydrophilic interaction LC/MS for the analysis of polar and nonpolar phenols in wine. J. Sep. Sci. 36, 1379−1388.

Greiderer, A., Trojer, L., Huck, C.W., Bonn, G.K., 2009. Influence of the polymerisation time on the porous and chromatographic properties of monolithic poly(1,2-bis(p-vinylphenyl))ethane capillary columns. J. Chromatogr. A 1216, 7747−7754.

Gritti, F., dos Santos Pereira, A., Sandra, P., Guiochon, G., 2010. Efficiency of the same neat silica column in hydrophilic interaction chromatography and per aqueous liquid chromatography. J. Chromatogr. A 1217, 683−688.

Grosskreutz, S.R., Secor, M.H., Stoll, D.R., 2012. Selective comprehensive multidimensional separation for resolution enhancement in HPLC. Part I: principles and instrumentation. J. Chromatogr. A 1228, 31−40.

Grumbach, E.S., Diehl, D.M., Neue, U.D., 2008. The application of novel 1.7 μm ethylene bridged hybrid particles for hydrophilic interaction chromatography. J. Sep. Sci. 31, 1511−1518.

Guiochon, G., Marchetti, N., Mriziq, K., Shaliker, R.A., 2008. Implementation of two-dimensional liquid chromatography. J. Chromatogr. A 1189, 109−168.

Guo, Y., Gaiki, S., 2005. Retention behavior of small polar compounds on polar stationary phases in hydrophilic interaction chromatography. J. Chromatogr. A 1074, 71−90.

Guo, Y., Srinivasan, S., Gaiki, S., 2007. Investigating the effect of chromatographic conditions on retention of organic acids in hydrophilic interaction chromatography using a design of experiment. Chromatographia 66, 223−229.

Hájek, T., Jandera, P., Staňková, M., Česla, P., 2016. Automated dual two-dimensional liquid chromatography approach for fast acquisition of three-dimensional data using combinations of zwitterionic polymethacrylate and silica-based monolithic columns. J. Chromatogr. A 1446, 91−102.

Hao, Z., Xiao, B., Weng, N., 2008. Impact of column temperature and mobile phase composition on selectivity of hydrophilic interaction chromatography (HILIC). J. Sep. Sci. 31, 1449−1464.

Hartmann, E., Chen, Y., Mant, C.T., Jungbauer, A., Hodges, R.S., 2003. Comparison of reversed-phase liquid chromatography and hydrophilic interaction/cation-exchange chromatography for the separation of amphipathic α-helical peptides with L- and D-amino acid substitutions in the hydrophilic face. J. Chromatogr. A 1009, 61−71.

Heaton, J.C., McCalley, D.V., 2014. Comparison of the kinetic performance and retentivity of sub-2 μm core-shell, hybrid and conventional bare silica phases in hydrophilic interaction chromatography. J. Chromatogr. A 1371, 106−116.

Heaton, J.C., Russell, J.J., Underwood, T., Boughtflower, R., McCalley, D.V., 2014. Comparison of peak shape in hydrophilic interaction chromatography using acidic salt buffers and simple acid solutions. J. Chromatogr. A 1347, 39−48.

Hemström, P., Irgum, K., 2006. Hydrophilic interaction chromatography. J. Sep. Sci. 29, 1784−1821.

Horie, K., Ikegami, T., Hosoya, K., Saad, N., Fiehn, O., Tanaka, N., 2007. Highly efficient monolithic silica capillary columns modified with poly(acrylic acid) for hydrophilic interaction chromatography. J. Chromatogr. A 1164, 198−205.

Hou, Y., Zhang, F., Liang, X., Yang, B., Liu, X., Dasgupta, P.K., 2016. Poly (vinyl) alcohol modified porous graphitic carbon stationary phase for hydrophilic interaction chromatography. Anal. Chem. 88, 4676−4681.

Hsieh, Y., 2008. Potential of HILIC-MS in quantitative bioanalysis of drugs and drug metabolites. J. Sep. Sci. 31, 1481−1491.

Huber, J.F.K., Pawlowska, M., Markl, P., 1984. Solvent-generated liquid-liquid chromatography with aqueous ternary systems. Chromatographia 19, 19−28.

Ibrahim, M.E.A., Lucy, C.A., 2012. Mixed mode HILIC/anion exchange separations on latex coated silica monolith. Talanta 100, 313−339.

Ibrahim, M.E.A., Zhou, T., Lucy, C.A., 2010. Agglomerated silica monolithic column for hydrophilic interaction LC. J. Sep. Sci. 33, 773−778.

Idborg, H., Zamani, L., Edlund, P.-O., Schuppe-Koistinen, I., Jacobsson, S.P., 2005a. Metabolic fingerprinting of rat urine by LC/MS: part 1. Analysis by hydrophilic interaction liquid chromatography-electrospray ionization mass spectrometry. J. Chromatogr. B 828, 9−13.

Idborg, H., Zamani, L., Edlund, P.-O., Schuppe-Koistinen, I., Jacobsson, S.P., 2005b. Metabolic fingerprinting of rat urine by LC/MS: part 2. Data pretreatment methods for handling of complex data. J. Chromatogr. B 828, 14−20.

Ikegami, T., Tomomatsu, K., Takubo, H., Horie, K., Tanaka, N., 2008. Separation efficiencies in hydrophilic interaction chromatography. J. Chromatogr. A 1184, 474−503.

Iwasaki, Y., Ishii, Y., Ito, R., Saito, K., Nakazawa, H., 2007. New approaches for analysis of metabolism compounds in hydrophilic interaction chromatography. J. Liq. Chromatogr. Rel. Technol. 30, 2117−2126.

Jandera, P., 2008. Stationary phases for hydrophilic interaction chromatography, their characterization and implementation into multidimensional chromatography concepts. J. Sep. Sci. 31, 1421−1437.

Jandera, P., 2011. Stationary and mobile phases in hydrophilic interaction chromatography. Anal. Chim. Acta 692, 1−25.

Jandera, P., 2012a. Programmed elution in comprehensive two-dimensional liquid chromatography − a review. J. Chromatogr. A 1255, 112−129.

Jandera, P., 2012b. Comprehensive two-dimensional liquid chromatography − theoretical considerations, a review. Cent. Eur. J. Chem. 10, 844−875.

Jandera, P., Churáček, J., 1974. Gradient elution in liquid chromatography. I. The influence of the composition of the mobile phase on the capacity ratio (retention volume, band width, and resolution) in isocratic elution − theoretical considerations. J. Chromatogr. 91, 207−221.

Jandera, P., Hájek, T., 2009. Utilization of dual retention mechanism on columns with bonded PEG and diol stationary phases for adjusting the separation selectivity of phenolic and flavone natural antioxidants. J. Sep. Sci. 32, 3603−3619.

Jandera, P., Staňková, M., 2015. The effects of the column length on the efficiency of capillary zwitterionic organic polymer monolithic columns in HILIC chromatography. Chromatographia 79, 853−859.

Jandera, P., Novotná, K., Beldean-Galea, M.S., Jíša, K., 2006. Retention and selectivity tests of silica-based and metal-oxide bonded stationary phases for RP-HPLC. J. Sep. Sci. 29, 856−871.

Jandera, P., Vyňuchalová, K., Hájek, T., Česla, P., Vohralík, G., 2008. Characterization of HPLC columns for two-dimensional LC × LC separations of phenolic acids and flavonoids. J. Chemom. 22, 203−217.

Jandera, P., Hájek, T., Škeříková, V., Soukup, J., 2010a. Dual hydrophilic interaction-reversed phase retention mechanism on polar columns: structural correlations and implementation for 2D separations on a single column. J. Sep. Sci. 33, 841−852.

Jandera, P., Urban, J., Škeříková, V., Langmaier, P., Kubíčková, R., Planeta, J., 2010b. Polymethacrylate monolithic and hybrid particle-monolithic columns for reversed-phase and hydrophilic interaction capillary liquid chromatography. J. Chromatogr. A 1217, 22−33.

Jandera, P., Hájek, T., Česla, P., 2011. Effects of the gradient profile, sample volume and solvent on the separation in very fast gradients, with special attention to the second-dimension gradient in comprehensive two-dimensional liquid chromatography. J. Chromatogr. A 1218, 1995−2006.

Jandera, P., Hájek, T., Staňková, M., Vyňuchalová, K., Česla, P., 2012. Optimization of comprehensive two-dimensional gradient chromatography coupling in-line hydrophilic interaction and reversed phase liquid chromatography. J. Chromatogr. A 1268, 91−101.

Jandera, P., Staňková, M., Hájek, T., 2013. New zwitterionic polymethacrylate monolithic columns for uni-dimensional and two-dimensional micro liquid chromatography. J. Sep. Sci. 36, 2430−2440.

Jandera, P., Hájek, T., Staňková, M., 2015. Monolithic and core-shell columns in comprehensive two-dimensional liquid chromatography − review. Anal. Bioanal. Chem. 407, 139−151.

Janečková, L., Kalíková, K., Bosáková, Z., Tesařová, E., 2010. Study of interaction mechanisms on zirconia-based polystyrene HPLC column. J. Sep. Sci. 33, 3043−3051.

Ji, S.L., Zhang, F.F., Wu, S.J., Yang, B.C., Liang, X.M., 2014. Facile preparation of polyvinyl alcohol coated SiO_2 stationary phases for high performance liquid chromatography. Analyst 139, 5594−5599.

Jian, W., Edom, R.W., Xu, Y., Weng, N., 2010. Recent advances in application of hydrophilic interaction chromatography for quantitative bioanalysis. J. Sep. Sci. 33, 681−697.

Jiang, W., Irgum, K., 1999. Covalently bonded polymeric zwitterionic stationary phase for simultaneous separation of inorganic cations and anions. Anal. Chem. 71, 333−344.

Jiang, W., Fischer, G., Girmay, Y., Irgum, K., 2006. Zwitterionic stationary phase with covalently bonded phosphorylcholine type polymer grafts and its applicability to separation of peptides in the hydrophilic interaction liquid chromatography mode. J. Chromatogr. A 1127, 82−91.

Jiang, Z., Smith, N.W., Ferguson, P.D., Taylor, M.R., 2007. Hydrophilic interaction chromatography using methacrylate-based monolithic capillary column for the separation of polar analytes. Anal. Chem. 79, 1243−1250.

Jin, G., Guo, Z., Zhang, F., Xue, X., Jin, Y., Liang, X., 2008. Study on the retention equation in hydrophilic interaction liquid chromatography. Talanta 76, 522−527.

Kalili, K.M., de Villiers, A., 2013. Systematic optimisation and evaluation of on-line, off-line and stop-flow comprehensive hydrophilic interaction chromatography × reversed phase liquid chromatographic analysis of procyanidins, Part I: theoretical considerations. J. Chromatogr. A 1289, 58−68.

Kallili, K.M., de Villiers, A., 2010. Off-line comprehensive two-dimensional hydrophilic interaction × reversed phase liquid chromatographic analysis of green tea phenolics. J. Sep. Sci. 33, 853−863.

Karatapanis, A.E., Fiamegos, Y.C., Stalikas, C.D., 2011. A revisit to the retention mechanism of hydrophilic interaction liquid chromatography using model organic compounds. J. Chromatogr. A 1218, 2871−2879.

Karlsson, G., Winge, S., Sandberg, H., 2005. Separation of monosaccharides by hydrophilic interaction chromatography with evaporative light scattering detection. J. Chromatogr. A 1092, 246−249.

Kawachi, Y., Ikegami, T., Takubo, H., Ikegami, Y., Miyamoto, M., Tanaka, N., 2011. Chromatographic characterization of hydrophilic interaction liquid chromatography stationary phases: hydrophilicity, charge effects, structural selectivity, and separation efficiency. J. Chromatogr. A 1218, 5903−5919.

Kikta, E.J., Grushka, E., 1977. Bonded peptide stationary phases for separation of amino-acids and peptides using liquid-chromatography. J. Chromatogr. 135, 367−376.

Kulsing, C., Yang, Y., Munerab, C., Tseb, C., Matyska, M.T., Pesek, J.J., Boysen, R.L., Hearn, M.T.W., 2014. Correlations between the zeta potentials of silica hydride-based stationary phases, analyte retention behaviour and their ionic interaction descriptors. Anal. Chim. Acta 817, 48−60.

Kulsing, C., Nolvachai, Y., Marriott, P.J., Boysen, R.L., Matyska, M.T., Pesek, J.J., Hearn, M.T.W., 2015. Insights into the origin of the separation selectivity with silica hydride adsorbents. J. Phys. Chem. B 119, 3063−3069.

Kumar, A., Heaton, J.C., McCalley, D.V., 2013. Practical investigation of the factors that affect the selectivity in hydrophilic interaction chromatography. J. Chromatogr. A 1276, 33−46.

Lammerhofer, M., Richter, M., Wu, J., Nogueira, R., Bicker, W., Lindner, W., 2008. Mixed-mode ion-exchangers and their comparative chromatographic characterization in reversed-phase and hydrophilic interaction chromatography elution modes. J. Sep. Sci. 31, 2572−2588.

Langmuir, I., 1916. The constitution and fundamental properties of solids and liquids. Part I. Solids. J. Am. Chem. Soc. 38, 2221−2295.

Li, J., Li, Y., Chen, T., Xu, L., Liu, X., Zhang, X., Zhang, H., 2013. Preparation, chromatographic evaluation and comparison between linear peptide- and cyclopeptide-bonded stationary phases. Talanta 109, 152−159.

Li, H., Liu, C., Wang, Q., Zhou, H., Jiang, Z., 2016. The effect of charged groups on hydrophilic monolithic stationary phases on their chromatographic properties. J. Chromatogr. A 1469, 77−87.

Liang, Z., Li, K., Wang, X., Ke, Y., Liang, X., 2012. Combination of off-line two-dimensional hydrophilic interaction liquid chromatography for polar fraction and two-dimensional hydrophilic interaction liquid chromatography − reversed-phase liquid chromatography for medium-polar fraction in a traditional Chinese medicine. J. Chromatogr. A 1224, 61−69.

Liang, T., Fu, Q., Shen, A.J., Wang, H., Jin, Y., Xin, H.X., Ke, Y.X., Guo, Z.M., Liang, X.M., 2015. Preparation and chromatographic evaluation of a newly designed steviol glycoside modified-silica stationary phase in hydrophilic interaction liquid chromatography and reversed phase liquid chromatography. J. Chromatogr. A 1388, 110−118.

Lin, S.C., Lee, W.C., 1998. Separation of a fructo-oligosaccharide mixture by hydrophilic interaction chromatography using silica-based micropellicular sorbents. J. Chromatogr. A 803, 302−306.

Lin, H., Ou, J., Zhang, Z., Dong, J., Wu, M., Zou, H., 2012. Facile preparation of zwitterionic organic-silica hybrid monolithic capillary column with an improved "one-pot" approach for hydrophilic-interaction liquid chromatography (HILIC). Anal. Chem. 84, 2721−2728.

Linden, J.C., Lawhead, C.L., 1975. Liquid chromatography of saccharides. J. Chromatogr. 105, 125−133.

Liu, X., Pohl, C.A., 2010. HILIC behavior of a reversed-phase/cationexchange/anion-exchange trimode column. J. Sep. Sci. 33, 779−786.

Liu, Y., Xue, X., Guo, Z., Xu, Q., Zhang, F., Liang, X., 2008. Novel two-dimensional reversed-phase liquid chromatography/hydrophilic interaction chromatography, an excellent orthogonal system for practical analysis. J. Chromatogr. A 1208, 133−140.

Liu, C., Chen, W., Yuan, G., Xiao, Y., Crommen, J., Xu, S., Jiang, Z., 2014. Influence of the cross-linker type on the chromatographic properties of hydrophilic sulfoalkylbetaine-type monolithic columns. J. Chromatogr. A 1373, 73−80.

Louw, S., Pereira, A.S., Lynen, F., Hanna-Brown, M., Sandra, P., 2008. Serial coupling of reversed-phase and hydrophilic interaction liquid chromatography to broaden the elution window for the analysis of pharmaceutical compounds. J. Chromatogr. A 1208, 90−94.

Lowe, A.B., 2010. Thiol-ene "click" reactions and recent applications in polymer and materials synthesis. Polym. Chem. 1, 17−36.

Lurie, I.S., Li, L., Toske, S.G., 2011. Hydrophilic interaction chromatography of seized drugs and related compounds with sub 2 μm particle columns. J. Chromatogr. A 1218, 9336−9344.

Mant, C.T., Hodges, R.S., 2008. Mixed-mode hydrophilic interaction/cation-exchange chromatography: separation of complex mixtures of peptides of varying charge and hydrophobicity. J. Sep. Sci. 31, 1573−1584.

Marclay, F., Saugy, M., 2010. Determination of nicotine and nicotine metabolites in urine by hydrophilic interaction chromatography-tandem mass spectrometry: potential use of smokeless tobacco products by ice hockey players. J. Chromatogr. A 1217, 7528−7538.

Marrubini, G., Castillo-Mendoza, B.E., Massolini, G., 2010. Separation of purine and pyrimidine bases and nucleosides by hydrophilic interaction chromatography. J. Sep. Sci. 33, 803−816.

Matyska, M.T., Pesek, J.J., Duley, J., Zamzami, M., Fischer, S.M., 2010. Aqueous normal phase retention of nucleotides on silica hydride-based columns: method development strategies for analytes relevant in clinical analysis. J. Sep. Sci. 33, 930−938.

McCalley, D.V., 2007. Is hydrophilic interaction chromatography with silica columns a viable alternative to reversed-phase liquid chromatography for the analysis of ionisable compounds? J. Chromatogr. A 1171, 46−55.

McCalley, D.V., 2008. Evaluation of the properties of a superficially porous silica stationary phase in hydrophilic interaction chromatography. J. Chromatogr. A 1193, 85−91.

McCalley, D.V., 2010. Study of the selectivity, retention mechanisms and performance of alternative silica-based stationary phases for separation of ionised solutes in hydrophilic interaction chromatography. J. Chromatogr. A 1217, 3408−3417.

McCalley, D.V., 2015. Study of retention and peak shape in hydrophilic interaction chromatography over a wide pH range. J. Chromatogr. A 1411, 41−49.

McCalley, D.V., Neue, U.D., 2008. Estimation of the extent of the water-rich layer associated with the silica surface in hydrophilic interaction chromatography. J. Chromatogr. A 1192, 225−229.

Melander, W., Horvath, C., 1980. Reversed-phase chromatography. In: Horvath, C. (Ed.), High-performance Liquid Chromatography, vol. 2. Academic Press, New York, pp. 114−320.

Melnikov, S.M., Hoeltzel, A., Seidel-Morgenstern, A., Tallarek, U., 2011. Composition, structure and mobility of water-acetonitrile mixtures in a silica nanopore studied by molecular dynamics simulations. Anal. Chem. 83, 2569−2577.

Moni, L., Ciogli, A., Acquarica, I.D., Dondoni, A., Gasparrini, F., Marra, A., 2010. Synthesis of sugar-based silica gels by copper-catalysed azide-alkyne cycloaddition via a single-step azido-activated silica intermediate and the use of the gels in hydrophilic interaction chromatography. Chem. Eur. J. 16, 5712−5722.

Moravcová, D., Haapala, M., Planeta, J., Hyotylainen, T., Kostiainen, R., Wiedmer, S.K., 2014. Separation of nucleobases, nucleosides, and nucleotides using two zwitterionic silica-based monolithic capillary columns coupled with tandem mass spectrometry. J. Chromatogr. A 1373, 90−96.

Nawrocki, J., Dunlap, C., Mc Cormick, A., Carr, P.W., 2004. Part I. Chromatography using ultra-stable metal oxide-based stationary phases for HPLC. J. Chromatogr. A 1028, 1−30.

Neue, U.D., O'Gara, J.E., Mendez, A., 2006. Selectivity in reversed-phase separations − influence of the stationary phase. J. Chromatogr. A 1127, 161−174.

Neue, U.D., Hudalla, C.J., Iraneta, P.C., 2010. Influence of pressure on the retention of sugars in hydrophilic interaction chromatography. J. Sep. Sci. 33, 838−840.

Nguyen, H.P., Schug, K.A., 2008. The advantages of ESI-MS detection in conjunction with HILIC mode separations: fundamentals and applications. J. Sep. Sci. 31, 1465−1480.

Nguyen, H.P., Yang, S.H., Wigginton, J.G., Simpkins, J.W., Schug, K.A., 2010. Retention behavior of estrogen metabolites on hydrophilic interaction chromatography stationary phases. J. Sep. Sci. 33, 793−802.

Nischang, I., Bruggemann, O., 2010. On the separation of small molecules by means of nano-liquid chromatography with methacrylate-based macroporous polymer monoliths. J. Chromatogr. A 1217, 5389−5397.

Nischang, I., Clauson, T.J., 2016. Porous polymer monoliths: from their fundamental structure to analytical engineering applications. Trends Anal. Chem. 75, 108−117.

Nischang, I., Teasdale, I., Bruggemann, O., 2010. Towards porous polymer monoliths for the efficient, retention-independent performance in the isocratic separation of small molecules by means of nano-liquid chromatography. J. Chromatogr. A 1217, 7514−7522.

Noga, S., Bocian, S., Buszewski, B., 2013. Hydrophilic interaction liquid chromatography columns classification by effect of solvation and chemometric methods. J. Chromatogr. A 1278, 89−97.

Nováková, L., Kaufmannová, I., Jánská, R., 2010. Evaluation of hybrid hydrophilic interaction chromatography stationary phases for ultra-HPLC in analysis of polar pteridines. J. Sep. Sci. 33, 765−772.

Nováková, L., Havlíková, L., Vlčková, H., 2014. Hydrophilic interaction chromatography of polar and ionizable compounds by UHPLC. Trends Anal. Chem. 63, 55−64.

Oertel, R., Neumeister, V., Kirch, W., 2004a. Hydrophilic interaction chromatography combined with tandem-mass spectrometry to determine six aminoglycosides in serum. J. Chromatogr. 1058, 197−201.

Oertel, R., Renner, U., Kirch, W., 2004b. Determination of neomycin by LC-tandem mass spectrometry using hydrophilic interaction chromatography. J. Pharm. Biomed. Anal. 35, 633−638.

Ohyama, K., Oyamada, K., Kishikawa, N., Ohba, Y., Wada, M., Maki, T., Nakashima, K., Kuroda, N., 2008. Preparation and characterization of poly(L-phenylalanine) chiral stationary phases with varying peptide length. J. Chromatogr. A 1208, 242−245.

Olsen, B.A., 2001. Hydrophilic interaction chromatography using amino and silica columns for the determination of polar pharmaceuticals and impurities. J. Chromatogr. A 913, 112−122.

Olsen, B.A., Pack, B.W. (Eds.), 2013. Hydrophilic Interaction Chromatography. Wiley, Hoboken, NJ.

Oyler, A.R., Armstrong, B.L., Cha, J.Y., Zhou, M.X., Yang, Q., Robinson, R.I., Dunphy, R., Burinsky, D.J., 1996. Hydrophilic interaction chromatography on amino-silica phases complements reversed-phase high-performance liquid chromatography and capillary electrophoresis for peptide analysis. J. Chromatogr. A 724, 378−383.

Pack, B.W., Risley, D.S., 2005. Evaluation of a monolithic silica column operated in the hydrophilic interaction chromatography mode with evaporative light scattering detection for the separation and detection of counter-ions. J. Chromatogr. A 1073, 269−275.

Padivitage, N.L.T., Dissanayake, M.K., Armstrong, D.W., 2013. Separation of nucleotides by hydrophilic interaction chromatography using the FRULIC-N column. Anal. Bioanal. Chem. 405, 8837−8848.

Pazourek, J., 2010. Monitoring of mutarotation of monosaccharides by hydrophilic interaction chromatography. J. Sep. Sci. 33, 974−981.

Peng, X., Feng, Y., Hu, X., 2013a. Preparation and characterization of the neomycin-bonded silica stationary phase for hydrophilic-interaction chromatography. Chromatographia 76, 459−465.

Peng, X., Liu, T., Ji, S., Feng, Y., 2013b. Preparation of a novel carboxyl stationary phase by "thiol-ene" click chemistry for hydrophilic interaction chromatography. J. Sep. Sci. 36, 2571−2577.

Pereira, A.D., David, F., Vanhoenacker, G., Sandra, P., 2009. The acetonitrile shortage: is reversed HILIC with water an alternative for the analysis of highly polar ionizable solutes? J. Sep. Sci. 32, 2001−2007.

Pereira, A.D., Jiménez Girón, A., Admasu, E., Sandra, P., 2010. Green hydrophilic interaction chromatography using ethanol-water-carbon dioxide mixtures. J. Sep. Sci. 33, 834−837.

Persson, J., Hemström, P., Irgum, K., 2008. Preparation of a sorbitol methacrylate grafted silica as stationary phase for hydrophilic interaction chromatography. J. Sep. Sci. 31, 1504−1510.

Pesek, J.J., Matyska, M.T., 2009. Our favorite materials: silica hydride stationary phases. J. Sep. Sci. 32, 3999−4011.

Pesek, J.J., Matyska, M.T., Boysen, R.L., Yang, Y., Hearn, M.T.W., 2013. Aqueous normal-phase chromatography using silica-hydride-based stationary phases. Trends Anal. Chem. 42, 64−73.

Qiao, L.Y., Shi, X., 2015. Preparation and evaluation of surface-bonded tricationic ionic liquid silica as stationary phases for high-performance liquid chromatography. J. Chromatogr. A 1396, 62−71.

Qiu, H.X., Loukotková, L., Sun, P., Tesařová, E., Bosáková, Z., Armstrong, D.W., 2011. Cyclofructan 6 based stationary phases for hydrophilic interaction liquid chromatography. J. Chromatogr. A 1218, 270−279.

Quiming, N.S., Denola, N.L., Soliev, A.B., Saito, Y., Jinno, K., 2007b. Retention behavior of ginsenosides on a poly(vinyl alcohol)-bonded stationary phase in hydrophilic interaction chromatography. Anal. Bioanal. Chem. 389, 1477−1488.

Quiming, N.S., Denola, N.L., Bin Samsuri, S.R., Saito, Y., Jinno, K., 2008a. Development of retention prediction models for adrenoreceptor agonists and antagonists on a polyvinyl alcohol-bonded stationary phase in hydrophilic interaction chromatography. J. Sep. Sci. 31, 1537−1549.

Quiming, N.S., Denola, N.L., Saito, Y., Jinno, K., 2008b. Multiple linear regression and artificial neural network retention prediction models for ginsenosides on a polyamine-bonded stationary phase in hydrophilic interaction chromatography. J. Sep. Sci. 31, 1550−1563.

Randon, J., Huguet, S., Piram, S., Puy, G., Demesmay, C., Rocca, J.L., 2006. Synthesis of zirconia monoliths for chromatographic separations. J. Chromatogr. A 1109, 19−25.

Randon, J., Huguet, S., Demesmay, C., Berthod, A., 2010. Zirconia based monoliths used in hydrophilic-interaction chromatography for original selectivity of xanthines. J. Chromatogr. A 1217, 1496−1500.

Regnier, F.E., Noel, R., 1976. Glycerolpropylsilane bonded phases in the steric exclusion chromatography of biological macromolecules. J. Chromatogr. Sci. 14, 316−320.

Risley, D.S., Strege, M.A., 2000. Chiral separations of polar compounds by hydrophilic interaction chromatography with evaporative light scattering detection. Anal. Chem. 72, 1736−1739.

Santoyo-Gonzalez, F., Hernandez-Mateo, F., 2009. Silica-based clicked hybrid glyco materials. Chem. Soc. Rev. 38, 3449−3462.

Schiesel, S., Laemmerhofer, M., Lindner, W., 2012. Comprehensive impurity profiling of nutritional infusion solutions by multidimensional off-line reversed-phase liquid chromatography × hydrophilic interaction chromatography-ion trap mass-spectrometry and charged aerosol detection with universal calibration. J. Chromatogr. A 1259, 100−110.

Schuster, G., Lindner, W., 2013. Comparative characterization of hydrophilic interaction liquid chromatography columns by linear solvation energy relationships. J. Chromatogr. A 1273, 73−94.

Shen, A.J., Guo, Z.M., Cai, X.M., Xue, X.Y., Liang, X.M., 2012. Preparation and chromatographic evaluation of a cysteine-bonded zwitterionic hydrophilic interaction liquid chromatography stationary phase. J. Chromatogr. A 1228, 175−182.

Shen, A.J., Li, X.L., Dong, X.F., Wei, J., Guo, Z.M., Liang, X.M., 2013. Glutathione-based zwitterionic stationary phase for hydrophilic interaction/cation-exchange mixed-mode chromatography. J. Chromatogr. A 1314, 63−69.

Sheng, Q.Y., Su, X.D., Li, X.L., Ke, Y.K., Liang, X.M., 2014. A dextran-bonded stationary phase for saccharide separation. J. Chromatogr. A 1345, 57−67.

Shundo, A., Mallik, A.K., Sakurai, T., Takafuji, M., Nagaoka, S., Ihara, H., 2009. Controllable shape selectivity based on highly ordered carbonyl and methyl groups in simple beta-structural polypeptide on silica. J. Chromatogr. A 1216, 6170−6176.

Škeříková, V., Jandera, P., 2010. Effects of the operation parameters on HILIC separations of phenolic acids on zwitterionic monolithic capillary columns. J. Chromatogr. A 1217, 7981−7989.

Škeříková, V., Urban, J., 2013. Highly stable surface modification of hypercrosslinked monolithic capillary columns and their application in hydrophilic interaction chromatography. J. Sep. Sci. 36, 2806−2812.

Snyder, L.R., 1974. Role of the solvent in liquid-solid chromatography. Rev. Anal. Chem. 46, 1384−1393.

Snyder, L.R., Poppe, H., 1980. Mechanism of solute retention in liquid-solid chromatography and the role of the mobile phase in affecting separation: competition versus "sorption". J. Chromatogr. 184, 363−413.

Snyder, L.R., Kirkland, J.R., Dolan, J.W., 2009. Introduction to Modern Liquid Chromatography, third ed. Wiley, Hoboken, NJ.

Soukup, J., Jandera, P., 2012a. Hydrosilated silica-based columns: the effects of mobile phase and temperature on dual HILIC-RP separation mechanism of phenolic acids. J. Chromatogr. A 1228, 125−134.

Soukup, J., Jandera, P., 2012b. The effect of temperature and mobile phase composition on separation mechanism of flavonoid compounds on hydrosilated silica-based columns. J. Chromatogr. A 1245, 98−108.

Soukup, J., Jandera, P., 2013. Comparison of non-aqueous hydrophilic interaction chromatography with aqueous normal-phase chromatography on hydrosilated silica-based stationary phases. J. Sep. Sci. 36, 2753−2759.

Soukup, J., Jandera, P., 2014. Adsorption of water from aqueous acetonitrile on silica-based stationary phases in HILIC (aqueous normal-phase) liquid chromatography. J. Chromatogr. A 1374, 102−111.

Soukup, J., Janás, P., Jandera, P., 2013. Gradient elution in aqueous normal-phase liquid chromatography on hydrosilated silica-based stationary phases. J. Chromatogr. A 1286, 111−118.

Spagou, K., Tsoukali, H., Raikos, N., Gika, H., Wilson, I.D., Theodoridis, G., 2010. Hydrophilic interaction chromatography coupled to MS for metabonomic/metabolomic studies. J. Sep. Sci. 33, 716−727.

Staňková, M., Jandera, P., 2016. Dual retention mechanism in two-dimensional LC separations of barbiturates, sulfonamides, nucleic bases and nucleosides on polymethacrylate zwitterionic monolithic micro-columns. Chromatographia 79, 657−666.

Staňková, M., Jandera, P., Urban, J., Škeříková, V., 2013. Cross-linker effects on the separation efficiency on (poly)methacrylate capillary monolithic columns. Part II. Aqueous normal-phase liquid chromatography. J. Chromatogr. A 1289, 47−57.

Stoll, D.R., Li, X., Wang, X., Carr, P.W., Porter, S.E.G., Rutan, G.C., 2007. Fast, comprehensive two-dimensional liquid chromatography. J. Chromatogr. A 1168, 3−43.

Strege, M.A., 1998. Hydrophilic interaction chromatography-electrospray mass spectrometry analysis of polar compounds for natural product drug discovery. Anal. Chem. 70, 2439−2445.

Strege, M.A., Stevenson, S., Lawrence, S.M., 2000. Mixed mode anion-cation exchange/hydrophilic interaction liquid chromatography-electrospray mass spectrometry as an alternative to reversed phase for small molecule drug discovery. Anal. Chem. 72, 4629−4633.

Svec, F., 2012. Quest for organic polymer-based monolithic columns affording enhanced efficiency in high performance liquid chromatography separations of small molecules in isocratic mode. J. Chromatogr. A 1228, 250−262.

Svec, F., Lv, Y., 2015. Advances and recent trends in the field of monolithic columns for chromatography. Anal. Chem. 87, 250−275.

Takegawa, Y., Deguchi, K., Keira, T., Ito, H., Nakagawa, H., Nishimura, S., 2006. Separation of isomeric 2-aminopyridine derivatized *N*-glycans and *N*-glycopeptides of human serum immunoglobulin G by using a zwitterionic type of hydrophilic-interaction chromatography. J. Chromatogr. A 1113, 177−181.

Takegawa, Y., Ito, H., Keira, T., Deguchi, K., Nakagawa, H., Nishimura, S.-I., 2008. Profiling of *N*- and *O*-glycopeptides of erythropoietin by capillary zwitterionic type of hydrophilic interaction chromatography/electrospray ionization mass spectrometry. J. Sep. Sci. 31, 1585−1593.

Tan, L.C., Carr, P.W., Abraham, M.H., 1996. Study of retention in reversed-phase liquid chromatography using linear solvation energy relationships. 1. The stationary phase. J. Chromatogr. A 752, 1−18.

Tolstikov, V.V., Fiehn, O., 2002. Analysis of highly polar compounds of plant origin: combination of hydrophilic interaction chromatography and electrospray ion trap mass spectrometry. Anal. Biochem. 301, 298−307.

Urban, J., Jandera, P., 2013. Recent advances in the design of organic polymer monoliths for reversed-phase and hydrophilic interaction chromatography separations of small molecules. Anal. Bioanal. Chem. 405, 2123−2131.

Urban, J., Škeříková, V., Jandera, P., Kubíčková, R., Pospíšilová, M., 2009. Preparation and characterization of polymethacrylate monolithic capillary columns with dual hydrophilic interaction reversed-phase retention mechanism for polar compounds. J. Sep. Sci. 32, 2530−2543.

Urban, J., Svec, F., Fréchet, J.M.J., 2010. Hypercrosslinking: new approach to porous polymer monolithic capillary columns with large surface area for the highly efficient separation of small molecules. J. Chromatogr. A 1217, 8212−8221.

Vajda, P., Felinger, A., Guiochon, G., 2013. Evaluation of surface excess isotherms in liquid chromatography. J. Chromatogr. A 1291, 41−47.

Van Dorpe, S., Vergote, V., Pezeshki, A., Burvenich, C., Peremans, K., De Spiegeleer, B., 2010. Hydrophilic interaction LC of peptides: columns comparison and clustering. J. Sep. Sci. 33, 728−739.

Vervoort, N., Gzil, P., Baron, G.V., Desmet, G., 2004. Model column structure for the analysis of the flow and band-broadening characteristics of silica monoliths. J. Chromatogr. A 1030, 177−186.

Viklund, C., Irgum, K., 2000. Synthesis of porous zwitterionic sulfobetaine monoliths and characterization of their interaction with proteins. Macromolecules 33, 2539−2544.

Viklund, C., Sjorgen, A., Irgum, K., Nes, I., 2001. Chromatographic interactions between proteins and sulfoalkylbetaine-based zwitterionic copolymers in fully aqueous low-salt buffers. Anal. Chem. 73, 444−452.

Vlčková, H., Ježková, K., Štětková, K., Tomšíková, H., Solich, P., Nováková, L., 2014. Study of the retention behavior of small polar molecules on different types of stationary phases used in hydrophilic interaction liquid chromatography. J. Sep. Sci. 37, 1297−1307.

Wade, K.L., Garard, I.J., Fahey, J.W., 2007. Improved hydrophilic interaction chromatography method for the identification and quantification of glucosinolates. J. Chromatogr. A 1154, 469−472.

Wang, X., Li, W., Rasmussen, H.T., 2005. Orthogonal method development using hydrophilic interaction chromatography and reversed-phase high-performance liquid chromatography for the determination of pharmaceuticals and impurities. J. Chromatogr. A 1083, 58−62.

Wang, Y., Lu, X., Xu, G., 2008c. Simultaneous separation of hydrophilic and hydrophobic compounds by using an on-line HILIC − RPLC system with two detectors. J. Sep. Sci. 31, 1564−1572.

Wang, Q., Luo, Z., Ye, M., Wang, Y., Xu, L., Shi, Z., Xu, L., 2015. Preparation, chromatographic evaluation and application of adenosine 5′-monophosphate modified ZrO_2/SiO_2 stationary phase in hydrophilic interaction chromatography. J. Chromatogr. A 1383, 58−69.

Weber, G., von Wiren, N., Hayen, H., 2008. Hydrophilic interaction chromatography of small metal species in plants using sulfobetaine- and phosphorylcholine-type zwitterionic stationary phases. J. Sep. Sci. 31, 1615−1622.

Wikberg, E., Verhage, J.J., Viklund, C., Irgum, K., 2009. Grafting of silica with sulfobetaine polymers via aqueous reversible addition fragmentation chain transfer polymerization and its use as a stationary phase in HILIC. J. Sep. Sci. 32, 2008−2016.

Wikberg, E., Sparrman, T., Wiklund, C., Johnsson, T., Irgum, K.A., 2011. A ^2H nuclear magnetic resonance study of the state of water in neat silica and zwitterionic stationary phases and its influence on the chromatographic

retention characteristics in hydrophilic interaction high performance liquid chromatography. J. Chromatogr. A 1218, 6630−6638.
Willemse, C.M., Stander, M.A., Vestner, J., Tredoux, A.G.J., de Villiers, A., 2014. Comprehensive two-dimensional liquid chromatographic analysis of anthocyanins. J. Chromatogr. A 1359, 189−201.
Willemse, C.M., Stander, M.A., Vestner, J., Tredoux, A.G.J., de Villiers, A., 2015. Comprehensive two-dimensional hydrophilic interaction chromatography (HILIC) × reversed-phase liquid chromatography coupled to high-resolution mass spectrometry (RP-LC-UV-MS) analysis of anthocyanins and derived pigments in red wine. Anal. Chem. 87, 12006−12015.
Wilson, S.R., Jankowski, M., Pepaj, M., Mihailova, A., Boix, F., Truyols, G.V., Lundanes, E., Greibrokk, T., 2007. 2D LC separation and determination of bradykinin in rat muscle tissue dialysate with on-line SPE-HILIC-SPE-RP-MS. Chromatographia 66, 469−474.
Wohlgemuth, J., Karas, M., Jiang, W., Hendriks, R., Andrecht, S., 2010. Enhanced glyco-profiling by specific glycopeptide enrichment and complementary monolithic nano-LC (ZIC-HILIC/RP18e)/ESI-MS analysis. J. Sep. Sci. 33, 880−890.
Wu, J.Y., Bicker, W., Lindner, W., 2008. Separation properties of novel and commercial polar stationary phases in hydrophilic interaction and reversed-phase liquid chromatography mode. J. Sep. Sci. 31, 1492−1503.
Xu, L., Zhao, T., Guan, X.M., Tang, W.J., Liu, X.Y., Zhang, H.X., 2014. Preparation, chromatographic evaluation and comparison of cystine- and cysteine-bonded stationary phases. Anal. Methods 6, 2205−2214.
Xue, M.Z., Huang, H.X., Ke, Y.X., Chu, C.H., 2009. "Click dipeptide": a novel stationary phase applied in two-dimensional liquid chromatography. J. Chromatogr. A 1216, 8623−8629.
Yang, H., Shan, C., Li, F., Han, D., Zhang, Q., Niu, L., 2009. Covalent functionalization of polydisperse chemically-converted graphene sheets with amine-terminated ionic liquid. Chem. Commun. 26, 3880−3882.
Yoshida, T., 1997. Peptide separation in normal phase liquid chromatography. Anal. Chem. 69, 3038−3043.
Yoshida, T., 2004. Peptide separation by hydrophilic-interaction chromatography: a review. J. Biochem. Biophys. Methods 60, 265−280.
Yu, L., Li, X., Guo, Z., Zhang, X., Liang, X., 2009. Hydrophilic interaction chromatography based enrichment of glycopeptides by using click maltose: a matrix with high selectivity and glycosylation heterogeneity coverage. Chem. Eur. J. 15, 12618−12626.
Yuan, G.X., Peng, Y.B., Liu, Z.H., Hong, J.Y., Xiao, Y., Guo, J.L., Smith, N.W., Crommen, J., Jiang, Z.J., 2013. A facile and efficient strategy to enhance hydrophilicity of zwitterionic sulfoalkylbetaine type monoliths. J. Chromatogr. A 1301, 88−97.
Zhang, T., Creek, D.J., Barrett, M.P., Blackburn, B., Watson, D.G., 2012. Evaluation of coupling reversed phase, aqueous normal phase, and hydrophilic interaction liquid chromatography with orbitrap mass spectrometry for metabolomic studies of human urine. Anal. Chem. 84, 1994−2001.
Zhu, B.Y., Mant, C.T., Hodges, R.S., 1991. Hydrophilic-interaction chromatography of peptides on hydrophilic and strong cation-exchange columns. J. Chromatogr. 548, 13−24.

FURTHER READING

Abraham, M.H., Rosés, M., 1994. Hydrogen bonding. 38. Effect of solute structure and mobile phase composition on reversed-phase high-performance liquid chromatographic capacity factors. J. Phys. Org. Chem. 7, 672−684.
Abraham, M.H., Rosés, M., Poole, C.F., Poole, S.K., 1997. Hydrogen bonding. 42. Characterization of reversed-phase high-performance liquid chromatographic C18 stationary phases. J. Phys. Org. Chem. 10, 358−368.
Aggarwal, P., Tolley, H.D., Lee, M.L., 2012. Monolithic bed structure for capillary liquid chromatography. J. Chromatogr. A 1219, 1−14.

Ali, M.S., Rafiuddin, S., Al-Jawi, D.A., Al-Hetari, Y., Ghori, U.M.H., Khatri, A.J., 2008. Stability-indicating assay of sodium cromoglicate in ophthalmic solution using mixed-mode hydrophilic interaction chromatography. J. Sep. Sci. 31, 1645−1650.

Appelblad, P., Jonsson, T., Jiang, W., Irgum, K., 2008. Fast hydrophilic interaction liquid chromatographic separations on bonded zwitterionic stationary phase. J. Sep. Sci. 31, 1529−1536.

Baba, Y., 1989. Computer-assisted retention prediction for high-performance liquid chromatography in the ion-exchange mode. J. Chromatogr. 485, 143−168.

Brown, S.D., White, C.A., Bartlett, M.G., 2002. Hydrophilic interaction liquid chromatography/electrospray mass spectrometry determination of acyclovir in pregnant rat plasma and tissues. Rapid Commun. Mass Spectrom. 16, 1871−1876.

Cai, X., Zou, L., Dong, J., Zhao, L., Wang, Y., Xu, Q., Xue, X., Zhang, X., Liang, X., 2009. Analysis of highly polar metabolites in human plasma by ultra-performance hydrophilic interaction liquid chromatography coupled with quadrupole-time of flight mass spectrometry. Anal. Chim. Acta 650, 10−15.

Callahan, D.L., Souza, D., Bacic, A., Rossner, U., 2009. Profiling of polar metabolites in biological extracts using diamond hydride-based aqueous normal phase chromatography. J. Sep. Sci. 32, 2273−2280.

Chambers, T.K., Fritz, J.S., 1998. Effect of polystyrene-divinylbenzene resin sulfonation on solute retention in high-performance liquid chromatography. J. Chromatogr. A 797, 139−147.

Courtois, J., Byström, E., Irgum, K., 2006. Novel monolithic materials using poly(ethylene glycol) as porogen for protein separation. Polymer 47, 2603−2611.

Daunoravicius, Z., Juknaite, I., Naujalis, E., Padarauskas, A., 2006. Simple and rapid determination of denaturants in alcohol formulations by hydrophilic interaction chromatography. Chromatographia 63, 373−377.

de Person, M., Hazotte, A., Elfakir, C., Lafosse, M., 2005. Development and validation of a hydrophilic interaction chromatography-mass spectrometry assay for taurine and methionine in matrices rich in carbohydrates. J. Chromatogr. A 1081, 174−181.

Deguchi, K., Keira, T., Yamada, K., Ito, H., Takegawa, Y., Nakagawa, H., Nishimura, S.I., 2008. Two-dimensional hydrophilic interaction chromatography coupling anion-exchange and hydrophilic interaction columns for separation of 2-pyridylamino derivatives of neutral and sialylated *N*-glycans. J. Chromatogr. A 1189, 169−174.

Du, C.M., Valko, K., Bevan, C., Reynolds, D., Abraham, M.H., 2000. Characterizing the selectivity of stationary phases and organic modifiers in reversed-phase high-performance liquid chromatographic systems by a general solvation equation using gradient elution. J. Chromatogr. Sci. 38, 503−511.

Dunkel, A., Köster, J., Hofmann, T., 2007. Molecular and sensory characterization of γ-glutamyl peptides as key contributors to the kokumi taste of edible beans (*Phaseolus vulgaris* L.). J. Agric. Food Chem. 55, 6712−6719.

Gika, H.G., Theodoridis, G.A., Wilson, I.D., 2008. Hydrophilic interaction and reversed-phase ultra-performance liquid chromatography TOF-MS for metabonomic analysis of Zucker rat urine. J. Sep. Sci. 31, 1598−1608.

Godejohann, M., 2007. Hydrophilic interaction chromatography coupled to nuclear magnetic resonance spectroscopy and mass spectroscopy − a new approach for the separation and identification of extremely polar analytes in bodyfluids. J. Chromatogr. A 1156, 87−93.

Gremilogianni, A.M., Megoulas, N.C., Koupparis, M.A., 2010. Hydrophilic interaction vs ion pair liquid chromatography for the determination of streptomycin and dihydrostreptomycin residues in milk based on mass spectrometric detection. J. Chromatogr. A 1217, 6646−6651.

Grumbach, E.S., Wagrowski-Diehl, D.M., Mazzeo, J.R., Alden, B., Iraneta, P.C., 2004. Hydrophilic interaction chromatography using silica columns for the retention of polar analytes and enhanced ESI-MS sensitivity. LCGC 22, 10101023.

Guerrouache, M., Pantazaki, A., Millot, M.-C., Carbonnier, B., 2010. Zwitterionic polymeric monoliths for HILIC/RP mixed mode for CEC separation applications. J. Sep. Sci. 33, 787−792.

Guinebault, P., Broquaire, M., 1981. Large-volume injection of samples dissolved in a noneluting solvent. Application to the determination of antipyrine using normal-phase high-performance liquid chromatography. J. Chromatogr. 217, 509−522.

Guo, Z., Lei, A., Zhang, Y., Xu, Q., Xue, X., Zhang, F., Liang, X., 2007. "Click saccharides": novel separation materials for hydrophilic interaction liquid chromatography. Chem. Commun. 2491−2493.

Hodges, R.S., Chen, Y., Kopecky, E., Mant, C.T., 2004. Monitoring the hydrophilicity/hydrophobicity of amino acid side-chains in the non-polar and polar faces of amphipathic α-helices by reversed-phase and hydrophilic interaction/cation-exchange chromatography. J. Chromatogr. A 1053, 161−172.

Holdšvendová, P., Suchánková, J., Bunček, M., Bačkovská, V., 2007. Hydroxymethyl methacrylate-based monolithic columns designed for separation of oligonucleotides in hydrophilic-interaction capillary liquid chromatography. J. Biochem. Biophys. Methods 70, 23−29.

Hosoya, K., Hira, N., Yamamoto, K., Nishimura, M., Tanaka, N., 2006. High-performance polymer-based monolithic capillary column. Anal. Chem. 78, 5729−5735.

Hsieh, Y., Galviz, G., Long, B., 2009. Ultra-performance hydrophilic interaction liquid chromatography/tandem mass spectrometry for the determination of everolimus in mouse plasma. Rapid Commun. Mass Spectrom. 23, 1461−1466.

Ibrahim, M.E.A., Liu, Y., Lucy, C.A., 2012. A simple graphical representation of selectivity in hydrophilic interaction liquid chromatography. J. Chromatogr. A 1260, 126−131.

Ikegami, T., Fujita, H., Horie, K., Hosoya, K., Tanaka, N., 2006. HILIC mode separation of polar compounds by monolithic silica capillary columns coated with polyacrylamide. Anal. Bioanal. Chem. 386, 578−585.

Ikegami, T., Horie, K., Jaafar, J., Hosoya, K., Tanaka, N., 2007a. Preparation of highly efficient monolithic silica capillary columns for the separations in weak cation-exchange and HILIC modes. J. Biochem. Biophys. Methods 70, 31−37.

Ikegami, T., Ichimaru, J., Kajiwara, W., Nagasawa, N., Hosoya, K., Tanaka, N., 2007b. Anion-and cation-exchange microHPLC utilizing poly(methacrylates)-coated monolithic silica capillary columns. Anal. Sci. 23, 109−113.

Ji, H.Y., Park, E.J., Lee, K.C., Lee, H.S., 2008. Quantification of doxazosin in human plasma using hydrophilic interaction liquid chromatography with tandem mass spectrometry. J. Sep. Sci. 31, 1628−1633.

Jiang, W., Irgum, K., 2002. Tentacle-type zwitterionic stationary phase prepared by surface-initiated graft polymerization of 3-[*N*,*N*-dimethyl-*N*-(methacryloyloxyethyl)-ammonium] propanesulfonate through peroxide groups tethered on porous silica. Anal. Chem. 74, 1993−2003.

Li, R., Huang, J.X., 2004. Chromatographic behavior of epirubicin and its analogues on high-purity silica in hydrophilic interaction chromatography. J. Chromatogr. A 1041, 163−169.

Liu, X.D., Pohl, C., 2008. New hydrophilic interaction/reversed-phase mixed-mode stationary phase and its application for analysis of nonionic ethoxylated surfactants. J. Chromatogr. A 1191, 83−89.

Naidong, W., Zhou, W., Song, Q., Zhou, S., 2004. Direct injection of 96-well organic extracts onto a hydrophilic interaction chromatography/tandem mass spectrometry system using a silica stationary phase and an aqueous/organic mobile phase. Rapid Commun. Mass Spectrom. 18, 2963−2968.

Park, J.H., Carr, P.W., Abraham, M.H., Taft, R.W., Doherty, R.M., Kamlet, M.J., 1988. Some observations regarding different retention properties of HPLC stationary phases. Chromatographia 25, 373−381.

Pesek, J.J., Matyska, M.T., Larrabee, S., 2007. HPLC retention behavior on hydride-based stationary phases. J. Sep. Sci. 30, 637−647.

Pisano, R., Breda, M., Grassi, S., James, C.A., 2005. Hydrophilic interaction liquid chromatography-APCI-mass spectrometry determination of 5-fluorouracil in plasma and tissues. J. Pharm. Biomed. Anal. 38, 738−745.

Puy, G., Demesmay, C., Rocca, J.L., Iapichella, J., Galarneau, A., Brunel, D., 2006. Electrochromatographic behavior of silica monolithic capillaries of different skeleton sizes synthesized with a simplified and shortened sol-gel procedure. Electrophoresis 27, 3971−3980.

Quiming, N.S., Denola, N.L., Saito, Y., Jinno, K., 2007a. Retention prediction of adrenoreceptor agonists and antagonists on unmodified silica phase in hydrophilic interaction chromatography. Anal. Bioanal. Chem. 388, 1693−1706.

Quiming, N.S., Denola, N.L., Ueta, I., Saito, Y., Tatematsu, S., Jinno, K., 2007c. Retention prediction of adrenoreceptor agonists and antagonists on a diol column in hydrophilic interaction chromatography. Anal. Chim. Acta 598, 41−50.

Snyder, L.R., 1968. Principles of Adsorption Chromatography. Marcel Dekker, New York.

Snyder, L.R., Dolan, J.W., Gant, J.R., 1979. Gradient elution in high-performance liquid chromatography: I. Theoretical basis for reversed-phase systems. J. Chromatogr. 165, 3−30.

Wang, Y., Lehmann, R., Lu, X., Zhao, X., Xu, G., 2008a. Novel, fully automatic hydrophilic interaction/reversed-phase column-switching high-performance liquid chromatographic system for the complementary analysis of polar and apolar compounds in complex samples. J. Chromatogr. A 1204, 28−34.

Wang, Y., Lu, X., Xu, G., 2008b. Development of a comprehensive two-dimensional hydrophilic interaction chromatography/quadrupole time-of-flight mass spectrometry system and its application in separation and identification of saponins from *Quillaja saponaria*. J. Chromatogr. A 1181, 51−59.

Xu, M.C., Peterson, D.S., Rohr, T., Švec, F., Frechet, J.M.J., 2003. Polar polymeric stationary phases for normal-phase HPLC based on monodisperse macroporous poly(2,3-dihydroxypropyl methacrylate-co-ethylene dimethacrylate) beads. Anal. Chem. 75, 1011−1021.

Xue, Y., Liu, J., Unger, S., 2006. A 96-well single-pot liquid-liquid extraction, hydrophilic interaction liquid chromatography-mass spectrometry method for the determination of muraglitazar in human plasma. J. Pharm. Biomed. Anal. 41, 979−988.

Yanagida, A., Murao, H., Ohnishi-Kameyama, M., Yamakawa, Y., Shoji, A., Tagashira, M., Kanda, T., Shindo, H., Shibusawa, Y., 2007. Retention behavior of oligomeric proanthocyanidins in hydrophilic interaction chromatography. J. Chromatogr. A 1143, 153−161.

Yoshida, T., Okada, T., 1999. Peptide separation in normal-phase liquid chromatography. Study of selectivity and mobile phase effects on various columns. J. Chromatogr. A 840, 1−9.

Zhang, H., Guo, Z., Zhang, F., Xu, Q., Liang, X., 2008. HILIC for separation of co-eluted flavonoids under RP-HPLC mode. J. Sep. Sci. 31, 1623−1627.

This page intentionally left blank

CHAPTER

3 CHIRAL SEPARATIONS. CHIRAL DYNAMIC CHROMATOGRAPHY IN THE STUDY OF STEREOLABILE COMPOUNDS

Francesco Gasparrini[1], Ilaria D'Acquarica[1], Marco Pierini[1], Claudio Villani[1], Omar H. Ismail[1], Alessia Ciogli[1], Alberto Cavazzini[2]

Sapienza Università di Roma, Roma, Italy[1]; Università di Ferrara, Ferrara, Italy[2]

1. INTRODUCTION

The wide variety of chromatographic techniques developed and improved over the past three decades (Ward and Ward, 2010) allows researchers at the moment to address and resolve most of the problems related to the separation of molecular or ionic species, from both preparative and analytical points of view. Examples of preparative separations have been performed for synthetic products, bioactive molecules extracted from biological sources, and for racemates of chiral drugs (Francotte, 2009; Sticher, 2008; Bucar et al., 2013). Typical analytical separations have been applied for the quantification of compounds in complex mixtures, the determination of enantiomeric excess of scalemic mixtures, and the identification of organic compounds by hyphenated chromatographic techniques (Wilkins, 1983; Holt et al., 1997; Ellis and Roberts, 1997; Guetens et al., 2002a,b). A peculiar and elegant application of chromatography has also been devoted to supramolecular chemistry, where it allows calculation of the thermodynamic stability of supramolecular adducts and the association constants of host–guest complexes (Ciogli et al., 2013; Gasparrini et al., 1997b, 2002b). Moreover, chromatography has recently been used for the study of internal molecular dynamics of a range of stereochemically labile organic compounds and for the determination of kinetic parameters of the pertinent equilibrium (i.e., the reversible isomerization of one enantiomer into the other) (Ceccacci et al., 2003; D'Acquarica et al., 2006).

In this context, the implementation of highly efficient chromatographic techniques pushed to their extreme limits may represent a very effective tool to achieve thermodynamic and kinetic data (Krupcik et al., 2003; Katsanos et al., 1998; Wolf, 2005, 2008), when experimental conditions make the use of alternative methods difficult or impossible, such as dynamic nuclear magnetic resonance (DNMR) spectroscopy and batchwise classical approaches.

This chapter provides a basic overview of the concepts behind the determination of reaction rate constants and activation barriers by dynamic chromatography (DC). Several examples of the application of such technique in the study of model stereochemically labile compounds have been provided as well.

Handbook of Advanced Chromatography/Mass Spectrometry Techniques. http://dx.doi.org/10.1016/B978-0-12-811732-3.00003-0

2. DYNAMIC CHROMATOGRAPHY: GENERAL PRINCIPLES

Typically, efficient chromatographic separation of complex mixtures results in a series of baseline well-resolved peaks. However, if some of the species involved are subjected to a secondary dynamic equilibrium concomitant with the chromatographic distribution equilibria, band spreading and peak distortion may be observed, and the peaks may be joined by an elevated baseline, commonly referred as a plateau. Such a type of dynamic profile (also called *dynamic chromatogram*) is depicted in Fig. 3.1, for the simple instance of a couple of isomers I_A and I_B, which may interconvert one to each other according to the chemical equilibrium (Eq. 3.1).

$$I_A \underset{kv_{-1}}{\overset{kv_1}{\rightleftarrows}} I_B \quad \boldsymbol{K}_{eq} = \frac{kv_1}{kv_{-1}} = \frac{I_B}{I_A} \tag{3.1}$$

As a function of the time spent by the two isomers inside the chromatographic column and of the operating temperature set during separation, three line-shapes (*a*, *b*, and *c*) may, in principle, be registered in the final chromatograms, and they are shown in Fig. 3.1.

Line-shape (*a*) refers to a situation where no appreciable interconversion occurred between I_A and I_B during the chromatographic run, and two baseline-resolved peaks are observed. Line-shape (*b*) refers to an active interconversion between I_A and I_B species, which happened faster than the separation of the single species during their elution through the chromatographic column. In other words, all molecules of I_A and I_B have undergone at least one interconversion cycle during elution. As a result, the peaks relevant to I_A and I_B coalesced to a single one, having an intermediate retention time (tr) between those of the single species (i.e., trI_A and trI_B). Such a dynamic profile is not suited to obtain kinetic information about the occurred isomerization process. Finally, line-shape (*c*) refers to an intermediate situation between (*a*) and (*b*), as pointed out by an elevated baseline between the two well-resolved I_A and I_B peaks (plateau zone). This is diagnostic for an active, but only partial, interconversion occurred between I_A and I_B on the time scale of the chromatographic separation. In other words, in the scenario depicted in line-shape (*c*), only a fraction of I_A and I_B molecules underwent isomerization during the separation process, giving rise to the interference region lying between the couple of classical peaks, which, in turn, are generated by the other fraction of molecules never involved in the dynamic process.

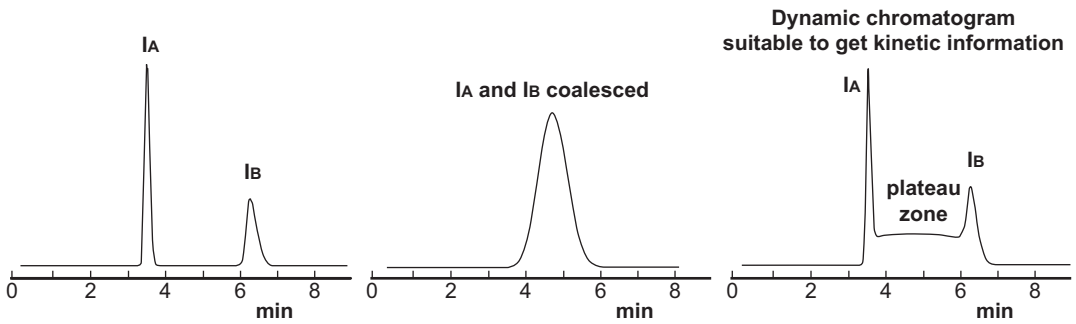

FIGURE 3.1

Line-shape of chromatograms showed by isomeric I_A and I_B species that undergo interconversion during elution through the chromatographic column.

Both shape and height of such a plateau inside a dynamic chromatogram contain all the kinetic information useful to describe the secondary equilibrium (an isomerization process in the proposed example) that occurred during separation. Thus, rate constants of chemical processes can be investigated by suitable line-shape analysis of the dynamic profiles, that is to say, by simulating/analyzing dynamic chromatograms according to one of the several mathematical models available in the literature (see Section 3). In the most frequently employed approach, the iterative comparison of simulated and experimental chromatograms until reaching of a good similarity affords the desired kinetic data. The implementation of such an experimental approach is commonly known as DC. A suitable choice of the operating conditions to set in the DC analysis may yield appropriate dynamic chromatograms. Effective modulation of the plateau height can be tuned by both the temperature and the residence time of the interconverting species inside the column, which can be optimized through a judicious selection of mobile phase (MP) and flow rate. In such a way, errors associated with the determination of rate constants can be minimized. However, a likely drawback of the method is that the stationary phase (SP) may have a perturbing effect on the kinetics of the dynamic process. In fact, the forward and backward rate constants determined experimentally by the interconverting I_A and I_B species during a DC experiment are expressed by apparent rate constants $\left(kv_1^{app} \text{ and } kv_{-1}^{app}\right)$ that result from a double-weighed contribution coming from the same process occurring in both mobile $\left(kv_1^{m} \text{ and } kv_{-1}^{m}\right)$ and stationary $\left(kv_1^{s} \text{ and } kv_{-1}^{s}\right)$ phases, according to the thermodynamic cycle and equations reported in Fig. 3.2.

In a typical DC experiment, the forward rate constant kv_1 matches that in the MP, kv_1^{m}, and is approximated by the apparent rate constant kv_1^{app}; the backward rate constant kv_{-1} matches kv_{-1}^{m} and is approximated by the kv_{-1}^{app}. The factors employed to modulate the kinetic contributions from the mobile (coefficients XI_A^m and XI_B^m) and stationary (coefficients XI_A^s and XI_B^s) phases are represented by the molar fractions that I_A and I_B assume in the two chromatographic phases (Fig. 3.2). In turn, these latter can be directly calculated from the capacity factors $k'I_{A/B}$ of compounds I_A and I_B (see the relevant equations in Fig. 3.2).

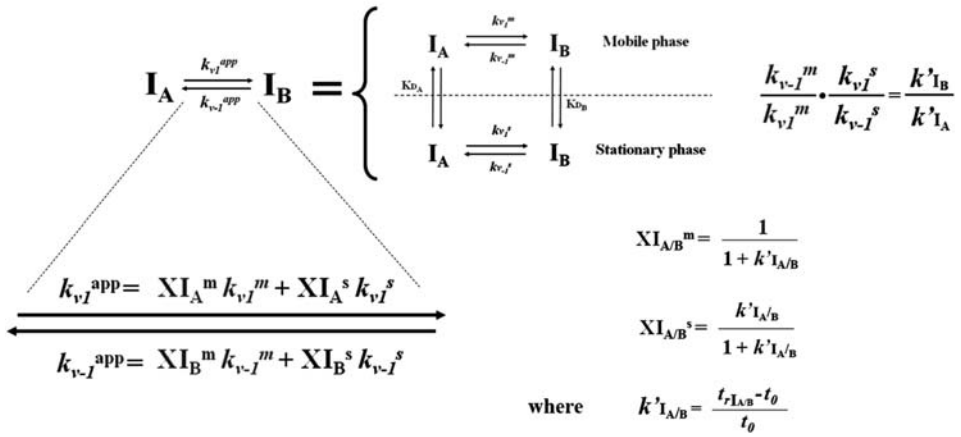

FIGURE 3.2

Thermodynamic cycle involved during dynamic chromatography experiments (for the meaning of symbols, see text).

3. MODELS AVAILABLE TO SIMULATE/ANALYZE DYNAMIC CHROMATOGRAMS

Several mathematical models have been developed in the last three decades to extract kinetic data from dynamic chromatograms. The *continuous flow model* is the oldest model, developed by Horváth et al. in 1984 (Melander et al., 1984; Jacobson et al., 1984). Because of its limited flexibility to the development of the required iterative procedures it is currently out-of-date. In fact, rather complex mathematics is involved, i.e., the coupled chromatographic and secondary chemical equilibria are described by suitable differential equations that have to be resolved by nontrivial numerical solutions.

Much more important, from an operative point of view, is the approach known as the *theoretical plates model* (TPM) (Bürkle et al., 1984). It portrays the chromatographic column as a discontinuous entity constituted by a defined number, N_{th}, of elementary chemical reactors (called *theoretical plates*) and approximates the concurrent chromatographic and secondary chemical equilibria as occurring inside each theoretical plate in three successive steps: (1) equilibration between the MP and SP of the species involved in the secondary chemical process; (2) chemical evolution of each species according to the involved kinetic law (frequently, but not necessarily, irreversible first-order kinetics) for a time Δt corresponding to that of the residence of the MP inside each theoretical plate ($\Delta t = t_0/N_{th}$, with t_0 being the dead time); and (3) shifting of the MP from the actual plate to the next one, according to the flow direction imposed on the MP through the column. The whole of these three steps have to be repeated a number of times (*n_shift*) sufficient to elute all the injected species from the column [in its practical use, this number is calculated by the following equation: $n\_shif\ t = (\mathrm{tr}_{\max} + 3\mathrm{W}_{0.5})/\Delta t$, where $\mathrm{tr}_{\max}$ is the retention time of the last eluted species and $3\mathrm{W}_{0.5}$ is three times the width at half-height of the last eluted peak]. On the whole, the TPM model proved to be very effective and relatively easy to be implemented into computer programs that automatically iterate the simulation of experimental dynamic chromatograms until achieving good agreement. However, because the time of simulation is exponentially related to N_{th}, only separations with not too many marked efficiencies (smaller than about 10,000 theoretical plates) can be treated in an iterative way yielding reasonable simulation times. Examples of widely employed computer programs implementing the TPM model are SIMUL (Jung, 1992), ChromWin (Trapp and Schurig, 2001b), Auto DHPLC y2k (Gasparrini et al., 2002a; Cabri et al., 2008; Cirilli et al., 2009b), and ChromWin_2D (Trapp et al., 2003; Trapp, 2004).

The *classical stochastic model* (CSM) or simply the *stochastic model*, which was developed in its current formulation by the joint contributions from Keller and Giddings (1960) and Kramer (1975), has also proved to be very useful. An additional contribution to the approach, called the *improved stochastic model*, was more recently reported (Trapp and Schurig, 2001b). The CSM model exclusively refers to the instance of monoequilibrium processes featuring first-order kinetics, occurring during a chromatographic separation. In this case, the concurrent chromatographic and secondary chemical equilibria are indirectly taken into account by expressing the profiles of the dynamic chromatograms by means of two typologies of time-dependent distribution functions: the first one, $\phi(t)$, related to the fraction of molecules of $\mathrm{I_A}$ and $\mathrm{I_B}$ never involved in the secondary chemical equilibrium [$\phi(t) = \phi\mathrm{I_A}(t) + \phi\mathrm{I_B}(t)$], and the other one, $\varphi(t)$, expressing the plateau zone due to the fraction of $\mathrm{I_A}$ and $\mathrm{I_B}$ molecules that underwent the transformation at least once during the chromatographic separation [$\varphi(t) = \varphi\mathrm{I_A}(t) + \varphi\mathrm{I_B}(t)$]. Although $\phi(t)$ [and then also its parent components $\phi\mathrm{I_A}(t)$ and $\phi\mathrm{I_B}(t)$] is not related to the rate constants of the secondary process and may be successfully

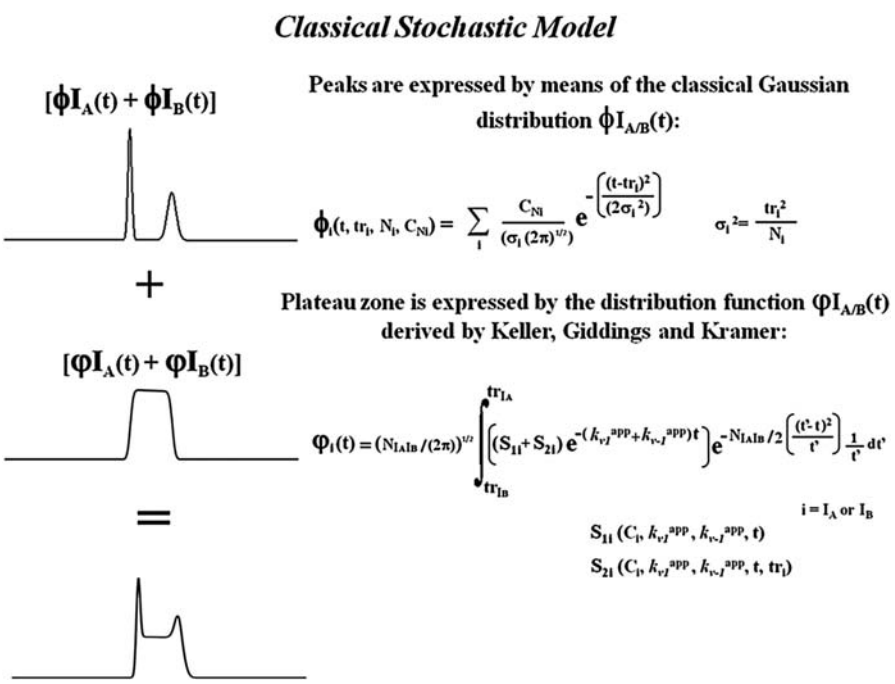

FIGURE 3.3

Classical stochastic model.

described by a classical Gaussian distribution, the function $\varphi(t)$ is exponentially related to both kv_1^{app} and kv_{-1}^{app} because it may be evinced by its mathematical expression derived by Keller, Giddings, and Kramer as shown in Fig. 3.3.

The primary advantage of the CSM model is the very short time of simulation, which results from the fact that it is significantly independent of N_{th}. This allows a quick treatment of dynamic chromatograms obtained by employing very efficient techniques, such as high-resolution gas chromatography (HRGC) and ultra-high performance liquid chromatography (UHPLC). An example of the relationships between time of simulation (seconds) of dynamic chromatograms and chromatographic efficiency (number of theoretical plates) involved in the TPM and CSM models is given in Fig. 3.4.

Computer programs implementing the CSM model, and widely tested on a large variety of first-order processes, involving both constitutional and conformational isomerizations (i.e., enantiomerizations, diastereomerizations, tautomerizations, etc.) are ChromWin (Trapp and Schurig, 2001b) and Auto DHPLC y2k (Gasparrini et al., 2002a; Cabri et al., 2008; Cirilli et al., 2009b). To strongly reduce the computational time, which in the aforementioned iterative procedure of comparison between simulated and experimental chromatograms is not negligible, the modification of kinetic and, if desired, chromatographic parameters is automated in the Auto DHPLC y2k program by the use of an algorithm driven by a simplex procedure. In this way, the user is not busy in this tedious step. Moreover, the same program also implements the possibility of taking tailing effects into account, thus extending the

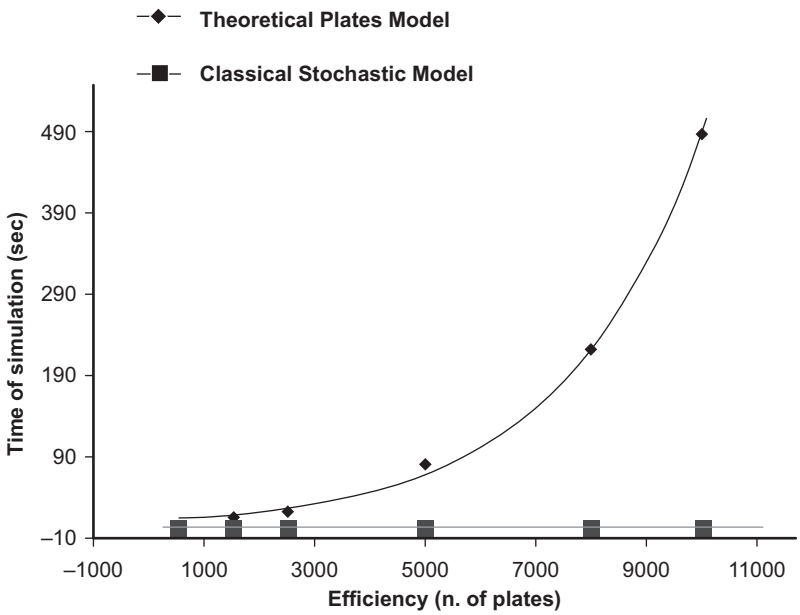

FIGURE 3.4

Relationships between time of simulation (seconds) of dynamic chromatograms and chromatographic efficiency (number of theoretical plates) involved in the theoretical plates model and classical stochastic model.

applicability of the procedure (for both TPM and CSM methods) to the frequent occurrence of nonlinear sample repartition between MP and SP.

Even faster than the just-described model is that based on the derivation of the so-called *unified equation of chromatography* (UEC) (Trapp, 2006), which overcomes an earlier approximate version (Trapp and Schurig, 2001a) that only worked in the simplified case of enantiomerization processes. The UEC allows direct calculation of rate constants of secondary chemical first-order reactions by a few iterative steps, without the need of performing a computationally extensive simulation of elution profiles. The only parameters required to perform the calculus are: (1) the retention times of the reacting species, trI_A and trI_B; (2) the peak widths at half-height, $W_{0.5}I_A$ and $W_{0.5}I_B$; (3) the relative height of the plateau, h_p; (4) the initial amounts of the reacting species, I_{A0} and I_{B0}; and (5) the equilibrium constant, $\boldsymbol{K}_{eq} = I_B/I_A$. However, although very fast, this approach does not assure estimations with acceptable accuracy when the plateau height approaches that of the residual adjacent peaks (Cirilli et al., 2009b) or when the dynamic chromatograms are affected by marked asymmetry (Uray et al., 2010). Furthermore, because no simulation of the experimental dynamic chromatograms is performed by this model, it is not possible to directly check the reliability of the estimated rate constants by superimposition of simulated and experimental profiles.

A further commonly employed mathematical approach is that often labeled with the generic term of the *deconvolution method*, although there are at least three different ways in which this method may practically be addressed. Such an approach, in fact, requires that the dynamic chromatogram is resolved into the components related to the fractions of molecules reacted (area of the plateau zone)

and not reacted (area of the residual peaks on either side of the dynamic profile) during the separation. Thus, deconvolution can be performed by: (1) the combined use of two or more tools of separation, which give rise to multidimensional hardware systems (Trapp, 2004; Marriott et al., 2001); (2) the Gaussian or exponentially modified Gaussian functions (Krupcik et al., 2000a,b; Oswald et al., 2002a,b); or (3) the combined use of two or more detectors (one of which must be chiro-optical) as monitoring tools of monodimensional chromatographic separations (Mannschreck et al., 1988; Mannschreck and Kiessl, 1989; Wolf et al., 1995; Allenmark and Oxelbark, 1998; Nishikawa et al., 1997; Kusano et al., 1999).

Finally, a novel stochastic approach to the DC has just been proposed in 2010 (Pasti et al., 2010). The novelty of the model is a microscopic point of view of the interconnections existing between repartition and secondary chemical equilibria, so that it might be suitably referred to as the *microscopic stochastic model* (MSM). In its formalism, the shape of a dynamic chromatogram is calculated in the frequency domain when the reaction follows a simple reversible first-order scheme. Then, the derived solutions are expressed in closed form in the Fourier domain. However, at the moment, the model is not implemented in any dedicated standalone software, and because of the quite complex mathematics involved, it is unlikely that such an approach may routinely be used in DC experiments. Nevertheless, the MSM model could attract specific interest on the basis of its ability to correlate macroscopic classical chromatographic parameters with the behavior properties of individual molecules (Pasti et al., 2005, 2016; Felinger et al., 2005).

4. CALCULATION OF FREE ENERGY ACTIVATION BARRIERS AND THEIR ENTHALPIC AND ENTROPIC CONTRIBUTIONS

The stereochemical or constitutional lability of some organic compounds plays a major role in all aspects of chemistry, spanning a wide bridge from drug development to supramolecular chemistry. A proper evaluation of the propensity of such compounds to undergo isomerization is commonly given by the associated free energy activation barrier $\Delta G^{\neq}$. This latter is logarithmically correlated to the rate constant of the above-mentioned process and promptly calculated by resorting to the Eyring equation:

$$-\Delta G^{\neq} = RT \ln\left(\frac{hk_v}{\kappa K_B T}\right)$$

where R is the universal gas constant, T is the absolute temperature, h is Planck's constant, κ is a transmission coefficient, and K_B is the Boltzmann constant. Moreover, it is possible to split out from a set of $\Delta G^{\neq}$ values the relevant enthalpic ($\Delta H^{\neq}$) and entropic ($\Delta S^{\neq}$) contributions by performing a number of kinetic determinations at different temperatures and carrying out a relevant van't Hoff analysis. In fact, enthalpic and entropic activation quantities may be assessed as the slope and intercept of van't Hoff plots of $\Delta G^{\neq}/T$ versus T^{-1}, respectively (see Fig. 3.5), which are based on the Gibbs equation rewritten in the following form:

$$\frac{\Delta G^{\neq}}{T} = \frac{\Delta H^{\neq}}{T} - \Delta S^{\neq}$$

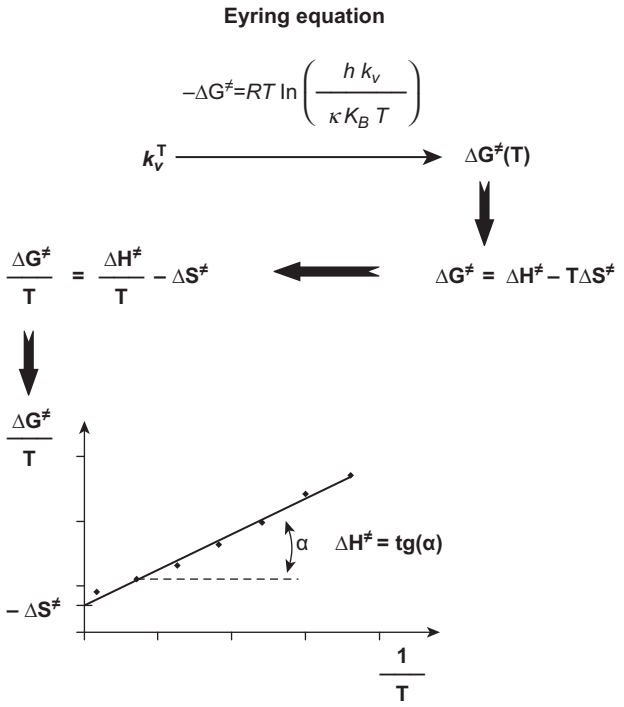

FIGURE 3.5

Calculation of free energy activation barriers and their enthalpic and entropic contributions.

Interesting information achievable from such a kind of investigation concerns the evaluation of the influence of temperature on a given chemical equilibrium. In fact, appreciable entropic contributions are responsible for marked variations of $\Delta G^{\neq}$ values in response to modest temperature variations. In turn, $\Delta S^{\neq}$ values of nonnegligible extent are diagnostic for the occurrence of nonmonomolecular transformations (i.e., reaching of the transition state that does not match a first-order process). It is widely known that isomerizations are first-order reactions, but they can be based either on monomolecular or bimolecular mechanisms. Conformational changes are normally based on monomolecular mechanisms and, as such, do not require the assistance of a secondary molecular partner. Atropoisomerism is an intramolecular event that falls into this class of reactions, featuring pure first-order kinetics (Gasparrini et al., 1997a, 2000, 2001, 2002a; Dell'Erba et al., 2002; Andreani et al., 2004; Borsato et al., 2004; Dalla Cort et al., 2005; Lunazzi et al., 2010; Levi Mortera et al., 2012; Rizzo et al., 2013, 2014, 2015; Chiarucci et al., 2014; Sabia et al., 2014, 2016; Menta et al., 2015). On the other hand, configurational isomerizations (i.e., processes involving rupture and reformation of chemical bonds) are commonly promoted by species that act as catalysts and that therefore do not modify their concentration during the interconversion (a bimolecular mechanism). Tautomeric equilibria (Ballini et al., 2000; Fontana et al., 2002; Angelini et al., 2007; Siani et al., 2008), enantiomerizations (Gasparrini et al., 2003; Cirilli et al., 2007, 2009a; Trapp et al., 2002), and diastereomerizations driven by reversible proton abstraction from

stereogenic atoms (Cabri et al., 2008, 2011; D'Acquarica et al., 2010; Carradori et al., 2012; Kotoni et al., 2014) are important examples of configurational isomerizations featuring pseudo first-order kinetics. Thus, it is expected that conformational isomerizations are barely affected by temperature, whereas the opposite trend should be predicted for configurational interconversions. For the latter reactions, they could be theoretically predicted to have activation entropies roughly up to about −40 to −30 entropic units (e.u.) because the loss of translational and rotational degrees of freedom, having values of approximately −50 e.u., should be partially compensated by new low-frequency motions arising in the transition state and quantifiable at about 10−20 e.u. (Page and Jencks, 1971). The case of rather negative activation entropies related to enantiomerization processes of the configurational type is also well known, involving the formation of zwitterionic species by heterolytic bond cleavage, as reported for the enantiomerization of aziridines and diaziridines (Trapp and Schurig, 2000; Shustov et al., 1988, 1989). According to such considerations, $|\Delta S^{\neq}|$ values always smaller than 17 e.u. have indeed been detected by DC experiments in quite a wide range of conformational stereochemical isomerizations (prevalently enantiomerizations and epimerizations) (see Fig. 3.6). In contrast, configurational isomerizations, again studied by DC methods and including enantiomerizations, epimerizations, and geometrical diastereomerizations, afforded $-\Delta S^{\neq}$ values always larger than 19 e.u. (Fig. 3.6).

5. APPLICATION OF DYNAMIC CHROMATOGRAPHY METHODS WITHIN EXTREME OPERATING CONDITIONS

The great advantage in using DC techniques is promptly highlighted when they are compared with classical kinetic determinations based on batchwise procedures. Typically, in the latter case, isomerization rate constants are obtained by monitoring the amount variations of one of the reacting species as a function of time. Frequently, a chromatographic technique is employed as the monitoring tool, so that the progressive residual amount of a reacting species or the increasing amount of the formed product is evaluated by the areas underlying the registered chromatographic peaks. When the studied isomerization involves chiral molecules, as necessarily occurs in enantiomerizations, the variation of enantiomeric excess is monitored as a function of time by off-line enantioselective chromatography. In a typical experiment, pure or enriched samples are allowed to equilibrate into an isolated and thermostatted system in the presence of reaction solvent, and the progression of the isomerization is monitored by chromatography under conditions of suppressed interconversion. Although rigorous and of general applicability, batchwise approaches are usually laborious, time-consuming, and expensive in terms of the amount of product to process. Moreover, a preliminary collection of pure or highly enriched reactants at preparative or semipreparative scale must be accomplished, starting from the equilibrated mixture of the couple of interconverting species to be analyzed (a racemic mixture, for the case of enantiomerizations). All these drawbacks are completely overcome by using the DC approach. However, two main limitations should also be taken into account in this case: (1) the limited range of solvents that can be used and (2) the perturbing effect of the SP (see Section 7).

A quite great number of enantiomerizations/diastereomerizations of chiral species have been studied by DC approaches in the past two decades. In several cases, the chromatographic results were supported and/or compared to alternative kinetic methods, such as DNMR spectroscopy (Gasparrini et al., 1995, 2002a; Dell'Erba et al., 2002; Dalla Cort et al., 2005) and stopped-flow gas

Conformational isomerizations			Configurational isomerizations		
Compound	$\Delta S^{\neq}$ **(e.u.)**	$\Delta G^{\neq}$ **(kcal mol^{-1})**	**Compound**	$\Delta S^{\neq}$ **(e.u.)**	$\Delta G^{\neq}$ **(kcal mol^{-1})**
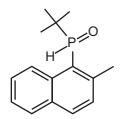	(diastereomerization) DHPLC		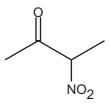	(enantiomerization) DHRGC	
	0.5	14.8 (–68 °C)		–19	29.8 (160 °C)
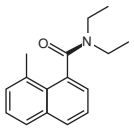	(enantiomerization) DHPLC		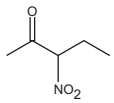	(enantiomerization) DHRGC	
	–9.9	22.7 (50 °C)		–35	29.8 (160 °C)
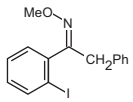	(enantiomerization) DHPLC		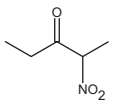	(enantiomerization) DHRGC	
	2.0	15.0 (–70 °C)		–37	29.3 (160 °C)
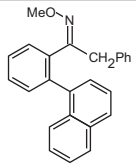	(enantiomerization) DHPLC		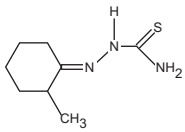	(enantiomerization) DHPLC Second-order process	
	–3.0	19.8 (–10 °C)		–40	22.0 (50 °C)
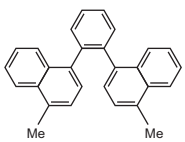	(diastereomerization) DHPLC		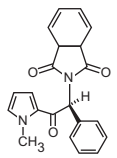	(enantiomerization) DHPLC First-order process	
	–4.0	19.5 (–5 °C)		–44	24.0 (45 °C)
				Second-order process	
				–40	18.5 (–5 °C)
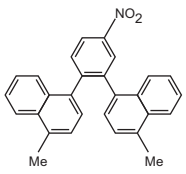	(diastereomerization) DHPLC		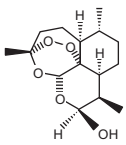	(epimerization) DHPLC First-order process (different pHs)	
	5.0	19.0 (–5 °C)		–31 ÷ –20	22.1 (25 °C)

FIGURE 3.6

Activation entropies ($\Delta S^{\neq}$, e.u.) and free energies ($\Delta G^{\neq}$, kcal/mol) of conformational and configurational isomerizations calculated by DHPLC and DHRGC.

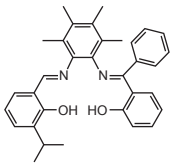	(enantiomerization) DHPLC		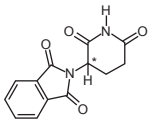	(enantiomerization) DHRGC	
	–9.2	21.8 (30 °C)		–59	38.0 (220 °C)
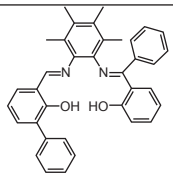	(enantiomerization) DHPLC		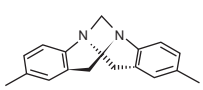	(enantiomerization) DHRGC	
	–16.9	21.9 (30 °C)		–55	33.6 (190 °C)
Conformational isomerizations			Conformational isomerizations		
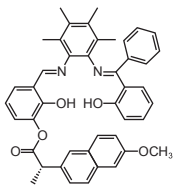	(diastereomerization) DHPLC		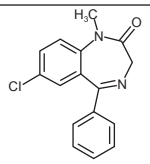 diazepam	(enantiomerization) DHPLC	
	–2.9	21.9 (30 °C)		–	17.7 (– 20 °C)
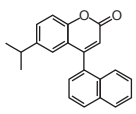	(enantiomerization) DHPLC		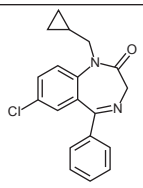 prazepam	(enantiomerization) DHPLC	
	–2.0	21.7 (30 °C)		–	18.7 (– 20 °C)
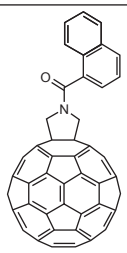	(enantiomerization) DHPLC		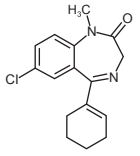 tetrazepam	(enantiomerization) DHPLC	
	–	14.3 (–70 °C)		–	18.1 (– 20 °C)
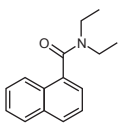	(enantiomerization) DHPLC		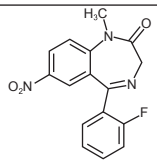 flunitrazepam	(enantiomerization) DHPLC	
	–	14.9 (–60 °C)		–	15.7 (– 55 °C)

FIGURE 3.6 Cont'd

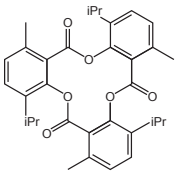	(diastereomerization) DHPLC		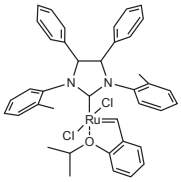	(diastereomerization) DHPLC	
	–	19.9 (15 °C)		–18.5	16.3 (–50 °C)
				–12.0	16.8 (–50 °C)
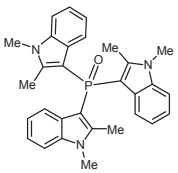	(enantiomerization) DHPLC		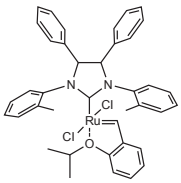	(enantiomerization) DHPLC	
	–15	20.3 (–10 °C)		–21.5	17.2 (–25 °C)
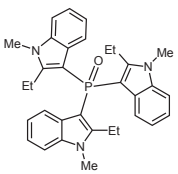	(enantiomerization) DHPLC		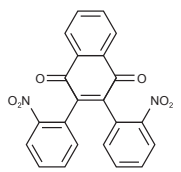	(enantiomerization) DHPLC	
	–12	23.7 (30 °C)		–	20.5 (15 °C)
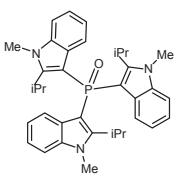	(enantiomerization) DHPLC		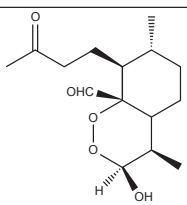	(epimerization) DHPLC	
	–12	24.8 (35 °C)		–	23.7 (50 °C)
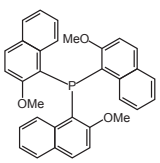	(enantiomerization) DHPLC		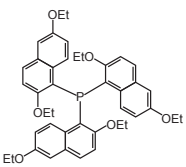	(enantiomerization) DHPLC	
	–	18.7 (–10 °C)		–	17.9 (–10 °C)
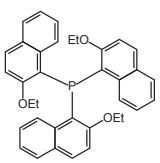	(enantiomerization) DHPLC		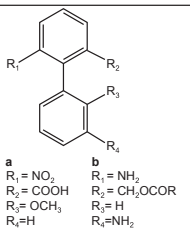	(enantiomerization) DHPLC	
	–	17.9 (–10 °C)		–	**a** 21.9 (24 °C)
				–	**b** 19.7 (–5 °C)

FIGURE 3.6 Cont'd

chromatography (Wolf, 2005; Trapp and Schurig, 2000). It was therefore found out that the DC methods, in the whole of their different forms, can ensure the coverage of a very wide range of activation energies, from the very small value of about 15 kcal/mol (Gasparrini et al., 2000) to the much greater value of 38 kcal/mol (Trapp et al., 2002). A schematic representation of the optimal range of applicability of DC [including gas chromatography, high-performance liquid chromatography (HPLC), and UHPLC] and DNMR techniques in the determination of activation barriers for isomerization processes is given in Fig. 3.7.

In Fig. 3.6 some representative examples of isomerizations are collected whose activation barriers determined by DC methods range between the extreme values of 14.7 and 38.0 kcal/mol. Both temperature and residence time of the interconverting species inside the column are parameters that can be tuned to approach the upper or lower limits of the above range. The residence time may be effectively modulated by changing the flow rate, but also by drastically improving the chromatographic efficiency. Very high efficiencies, in fact, allow better resolutions in shorter times, and this strongly reduces the residence time of stereolabile species having extremely low activation barriers to interconversion. A second strategy is to reduce the column temperature, and several examples of cryochromatography on chiral stationary phases (CSPs) at temperatures ranging from −50°C down to −80°C are listed in Fig. 3.6. The chemical and stereochemical diversity of the solutes investigated, together with the values of energy barriers spanning from 14.8 to 24.8 kcal/mol, indicate that the DC approach is well suited to study a broad range of intriguing chiral molecules with labile stereogenic elements. The implementation of novel and more efficient chromatographic materials, columns, and improved hardware, such as in the UHPLC approach, may introduce additional resolving power and speed of analysis, thus extending the application range of the dynamic technique.

6. ULTRA-HIGH PERFORMANCE LIQUID CHROMATOGRAPHY

Analytical liquid chromatography (LC) separations in the field of modern life sciences must address formidable challenges, linked to the requirement of a sharp reduction in the overall analysis time and

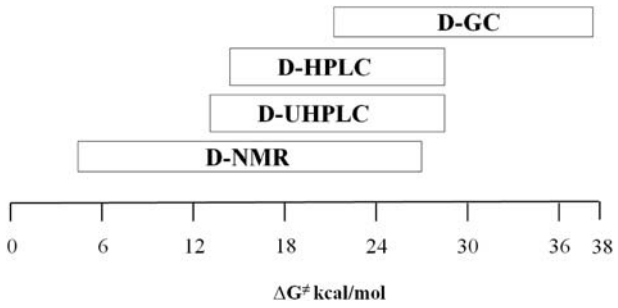

FIGURE 3.7

Optimal range of applicability of dynamic chromatography [including gas chromatography (GC), high-performance liquid chromatography (HPLC), and ultra-high performance liquid chromatography (UHPLC)] and dynamic nuclear magnetic resonance (DNMR) techniques in the determination of activation barriers for isomerization processes.

to the ever-increasing complexity of samples that must be analyzed. To perform fast separations while maintaining acceptable efficiency, resolution, and overall chromatographic performance, a compromise is necessary between eluent flow rate, column length, and back pressure.

According to theoretical treatments of the LC chromatographic process, one potential approach to increase column efficiency is to decrease the average size, d_p, of the packing particles in the column (Giddings, 1965; Knox, 1977; Poppe, 1997). Thus, during the last three decades, HPLC has witnessed a smooth evolution of the packing material size from the original 10 to 5 μm, and later to 3 μm. A parallel shortening of the standard column length has been observed, moving from the classical 30 or 25 cm to the 10 or 5 cm format, or even to very short 2−3 cm column lengths for fast (but lower efficiency) separations in the subminute range. To retain high efficiency together with reduced analysis time, sub-2 μm spherical porous particles have been proposed as new packing materials in the last years (Wu et al., 2001; Jerkovich et al., 2003). Columns packed with sub-2 μm particles have very low permeabilities (permeability is proportional to d_p^2), whereas their optimum flow velocity for maximum efficiency is higher compared to columns packed with larger particles. The combination of reduced particle size with high eluent flow rates results in a drastic increase in the column inlet pressure, which is proportional to the inverse of d_p^2 (Desmet et al., 2006; Neue and Kele, 2007; Gritti and Guiochon, 2008).

Columns packed with sub-2 μm particles very quickly move outside the pressure range of classical HPLC (roughly up to 40 MPa) when they are operated at their optimum flow rates or above, and this poses two problems in terms of mechanical stability of the SP particles and in terms of dedicated instruments, both of which are required to function under operating pressures reaching 100 MPa or higher.

Today, several manufacturers produce analytical LC instruments that are able to deal with pressures higher than 40 MPa, such as UPLC for ultra performance liquid chromatography or other variants of the technique (RRLC for rapid resolution liquid chromatography, UHPLC, VHPLC for very high-pressure liquid chromatography). Columns and SPs compatible with extreme pressures are available as well. However, the large repertoire of SP chemistries presented by HPLC columns is not found for the UHPLC counterpart (Guillarme et al., 2007; Wales et al., 2008; Carr et al., 2009).

Enantioselective LC systems can, in principle, benefit from a substantial increase in sample throughput by employing smaller particles packed in short columns and using high linear velocities of the eluent. Unfortunately, if the number and types of achiral conventional SPs for UHPLC applications are scarce compared to HPLC, the situation is even worse in chiral LC, where no UHPLC-dedicated CSP is commercially available so far.

Recently, brush-type CSPs for UHPLC applications have been developed as the result of transition from the 5 μm to the sub-2 μm format of the underlying silica particles (Cancelliere et al., 2010; Kotoni et al., 2012b; D'Acquarica et al., 2014; Cavazzini et al., 2014). These UHPLC brush-type CSPs combine the use of reduced particle size with established chiral selectors for the generation of advanced materials with high throughput and/or high resolution capabilities. Two well-known selectors have been selected for this transition.

The first one is the DACH-DNB CSP (Cancelliere et al., 2006). It was prepared starting from 1.9 μm spherical silica particles using a synthetic strategy that generates the intermediate DACH-CSP in a single step, starting from a slurry of bare silica, the chiral 1,2-diamine, and glycidoxypropyltrimethoxysilane. Subsequent treatment of the intermediate silica with dinitrobenzoyl chloride gave the final CSP where π-acidic aromatic fragments are fixed on the diamine framework through amide linkages (Fig. 3.8).

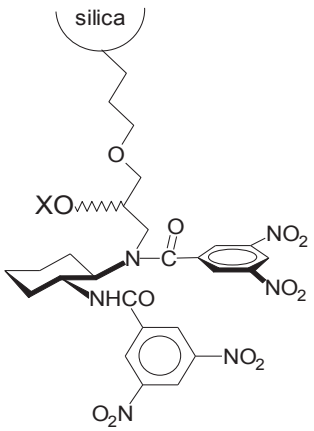

FIGURE 3.8

Chemical structure of the DACH-DNB CSP.

When the efficiency of a stainless-steel (100 × 4.1 mm I.D.) column packed with 1.9 μm DACH-DNB CSP was monitored as a function of the eluent flow rate (van Deemter analysis), a value of $H_{min} = 5.2$ μm was found at the optimum linear velocity, $\mu_{opt} = 4.00$ mm/s, using methyl benzoate as a test solute and 10% chloroform in *n*-hexane as the eluent. The van Deemter plot of the column packed with 1.9 μm DACH-DNB CSP showed a flat portion at high linear velocities of the eluent, suggesting a potential high efficiency use of the column in the subminute separation regime (Fig. 3.9).

Indeed, several very fast chiral separations on the 1.9 μm DACH-DNB CSP have been reported for a range of compounds including alkyl−aryl sulfoxides, secondary phosphine oxides, and acylated amines. The combination of high flow rates, short column length (50 × 4.1 mm I.D.), and large enantioselectivity ($\alpha = 1.87$) resulted in a complete separation of the enantiomers of a chiral 1-naphthamide in less than 15 s (Fig. 3.10).

The second selector used for the transition from the 5 μm to a sub-2 μm format is the Whelk-O1 (Kotoni et al., 2012a,b; Cavazzini et al., 2014). The Whelk-O1 selector was successfully covalently immobilized onto 1.7 μm large surface area totally porous spherical silica particles. Columns packed with the 1.7 μm Whelk-O1 CSP showed excellent kinetic performance that was then fully exploited to reduce analysis time to 10−45 s for a number of racemates and/or to enhance resolution of more difficult enantiomeric pairs. The resolution of a broad set of compounds, including alcohols, polar sulfoxides and phosphine oxides, and acidic drugs, was achieved on these columns. Comparison with commercial columns packed with 5 μm particles clearly illustrated the advantages in terms of speed gain, peak shape, resolution, and solvent consumption (see Fig. 3.11).

The chromatographic separation of stereolabile chiral compounds is one particular case in which enantioselective UHPLC columns and hardware find immediate practical applications. Two extreme scenarios can be envisaged when stereolabile chiral compounds, featuring energy barriers to enantiomer interconversion lower than 18 kcal/mol, must be resolved by chromatography. In one situation, the column temperature can be lowered down to cryogenic temperatures to a point where the half-life times of the interconverting enantiomers are commensurate with the analysis time. With high-viscosity eluents, the column inlet pressure rises rapidly with decreasing temperature, and only UHPLC systems

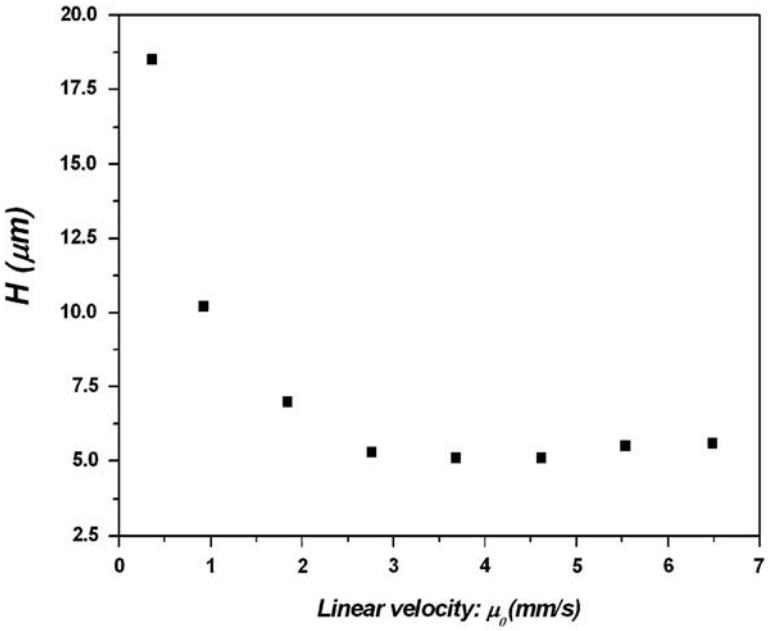

FIGURE 3.9

Representation of the van Deemter plot of the column packed with 1.9 μm DACH-DNB CSP.

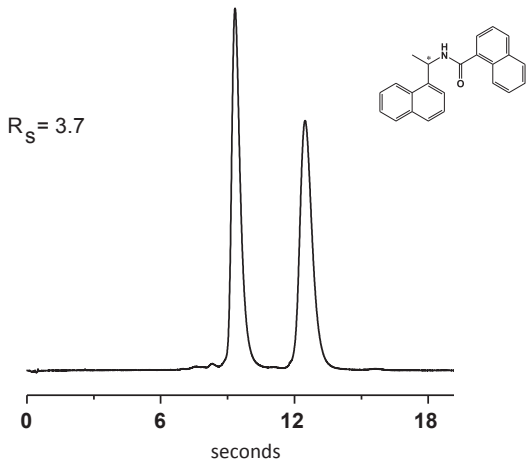

FIGURE 3.10

Ultra-fast enantioresolution of *N*-(1-(naphthalen-5-yl)ethyl)-1-naphthamide on the 1.9 mm DACH-DNB CSP packed into a stainless-steel (50 × 4.1 mm I.D.) column.

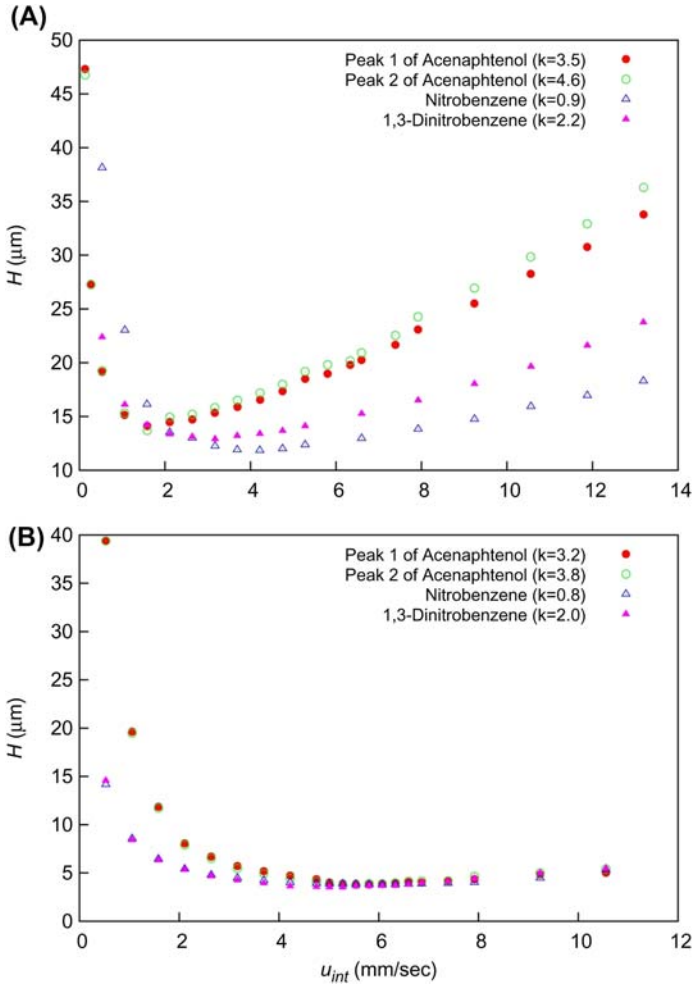

FIGURE 3.11

Van Deemter plot for chiral and achiral compounds on Whelk-O1 chiral stationary phases. (A) 250 × 4.6 mm I.D. column packed with fully-porous particles of 5-µm average size. (B) 100 × 4.6 mm I.D. column packed with fully-porous particles of 1.7-µm average size. Eluent: hexane/dichloromethane 8:2 (v/v) + 3% methanol.

can be used under these extreme experimental conditions. In the other situation, the chromatographic time scale is shifted into the seconds regime by the combined use of short columns packed with sub 2-µm particles and high eluent flow rates. Under these conditions, the overall analysis time can be cut by a factor of 10, compared to a conventional column, and the time scale of the separation can approach the time scale of the enantiomer interconversion at a given temperature.

With the aim of comparing the UHPLC technique advantages with the well-consolidated HPLC, atropoisomeric chiral species have been resolved on a chiral column based on the DACH-DNB selector, and the chromatographic time scale was shifted from the minutes into the seconds range. This is the case

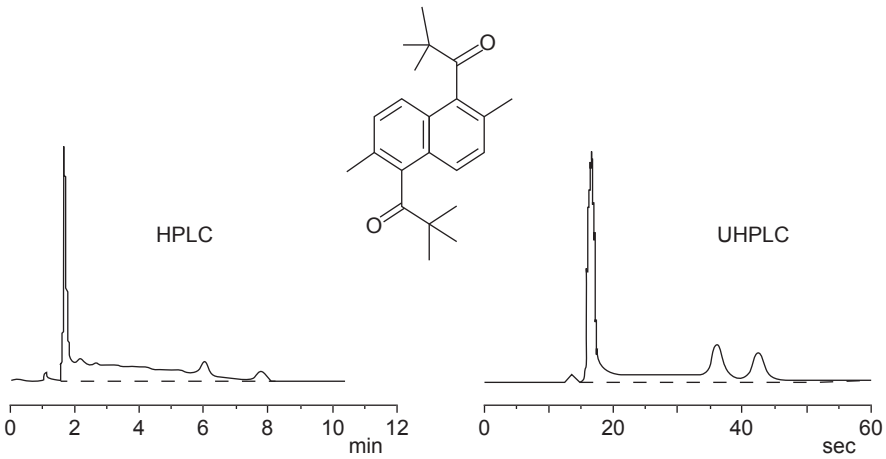

FIGURE 3.12

Comparison of the ultra-high performance liquid chromatography (UHPLC) technique advantages with the well-consolidated high-performance liquid chromatography (HPLC).

of a chiral bis-ketone with two stereogenic axes (Fig. 3.12), which was effectively resolved into its three stereoisomers (a couple of conformational enantiomers and an achiral *meso*-form). In chromatographic runs performed at 10°C by resorting to both HPLC (Gasparrini et al., 1995) and UHPLC methods (Cancelliere et al., 2010), the very different residence times that the stereoisomers spent inside the column appeared evident. Accordingly, a marked difference in the extent of isomerization is clearly visible in the resulting dynamic chromatograms, the plateau almost lacking in the case of UHPLC (Fig. 3.12). Schematically, if we state that the residence time decreases by a factor of 10 when changing from HPLC to UHPLC (a quite low value, relative to optimized conditions), it may be generalized that, to assure the same half-life time ($t_{1/2}$) of the process, the operating temperature has to be increased by a ΔT amount predictable by the following linear equation: $\Delta T = 0.8611 \times \Delta G^{\neq} + 1.0676$.

This means that to measure an activation energy of 15 kcal/mol, an operating temperature of −49°C will be required by UHPLC, for a run time of about 1 min, whereas HPLC will require −63°C for a run time of about 10 min. From a different point of view, the same transition of technique (i.e., from UHPLC to HPLC) would allow one to measure $\Delta G^{\neq}$ values lower than about 1 kcal/mol at any established temperature in the range −100 to +30°C, under the same conditions (Fig. 3.7). In general, a much more marked modulation of plateau zones may be obtained by suitable modest column temperature changes, compared to huge changes of the eluent flow rate (Cancelliere et al., 2010). Thus, very high activation barriers, not far from 40 kcal/mol, can be estimated by heating the column up to 200°C, for a $t_{1/2}$ of about 30 min. Such temperature values are typical of HRGC, which is suitable only for thermally stable and volatile compounds. A quite great number of stereoisomerizations (commonly enantiomerizations) have been studied by dynamic HRGC (DHRGC), featuring $\Delta G^{\neq}$ values almost close to 30 kcal/mol. Selected examples from the literature are collected in Fig. 3.6. In the case of thalidomide, an extreme enantiomerization barrier of 38.0 kcal/mol at 220°C was reported (Trapp et al., 2002).

7. PERTURBING EFFECTS OF STATIONARY PHASES ON $\Delta G^{\neq}$ VALUES MEASURED BY DYNAMIC CHROMATOGRAPHY METHODS

Calculation of activation barriers by DC is affected by additive contributions arising from the particular type of SP used. Such perturbing effects may be either inhibitory or promotional, so that the measured apparent rate constants kv_1^{app} and kv_{-1}^{app} may be under- or overestimated with respect to the related values found in the MP. Such deviations are more marked as the species involved in the interconversion process are more retained. Therefore, when the species under investigation are enantiomers, the forward and backward rate constants found are necessarily different one from each other because the transient adducts formed by interaction with the chiral selector on the SP are diastereoisomers. Thus, apparent enantiomerization rate constants determined by DC techniques $\left(kv_{en}^{app}\right)$ are generally expressed as the arithmetic mean of the apparent rate constants for the forward and backward processes (i.e., $kv_{en}^{app} = \left(kv_1^{app} + kv_{-1}^{app}\right)/2$). Comparisons of rate constants measured by both DC and DNMR or classic batchwise approaches stressed again the importance to distinguish among conformational and configurational isomerizations. Generally, in the first case, rate constants are underestimated, and quite moderate SP perturbations are observed (Gasparrini et al., 1997a, 2000, 2001, 2002a; Dell'Erba et al., 2002; Borsato et al., 2004; Dalla Cort et al., 2005; Lunazzi et al., 2010). A logical explanation may be that, after complexation of the labile species on the SP, the hindered bond rotation relevant to the studied conformational stereomutation may easily find an additional physical opposition by the phase, with consequent increasing of the related activation barrier. Such an effect, defined as the indirect perturbing contribution of the SP (SP_{IPC}) (Cirilli et al., 2009b), can be reduced, but never suppressed, by minimizing the residence time of the species inside the column. An illustrative example of such evidence is shown in Fig. 3.13, where both classic and dynamic chromatograms are reported for the two couples of residual enantiomers of a hindered secondary aryl phosphine oxide, which is endowed with two asymmetry elements, the phosphorous atom (P) and the axis colinear with the P−Csp^2 bond (Gasparrini et al., 2000).

Although the *R*/*S* inversion of the phosphorous is a strongly disfavored configurational process, not observed at temperatures below 25°C, rotational motion around the stereogenic axis is a conformational modification that readily occurs. At −65°C, the ^{31}P-DNMR technique afforded an activation barrier of 14.8 kcal/mol for the interconversion of the more stable (the *R* or *S* synclinal conformer, *sc*) into the less stable species (the *R* or *S* anticlinal conformer, *ac*). The equivalent measure performed by DHPLC (simulation based on TPM) at the same temperature on the separated residual enantiomers [i.e., by DHPLC on the split couples of equilibria $R(+sc) \leftrightarrows R(-ac)$ and $S(-sc) \leftrightarrows S(+ac)$] afforded the same value for the couple of diastereomers less retained [from $R(+sc)$ to $R(-ac)$], whereas a bit greater barrier (+0.3 kcal/mol) for the most retained [from $S(-sc)$ to $S(+ac)$]. Thus, it may be generalized that to obtain kinetic data as close as those achieved by classical batchwise or DNMR approaches, one should choose operating conditions that allow, at the same time, a suitable good chromatographic resolution, a considerable plateau height, and the shortest residence time of the interconverting species inside the column.

In the case of configurational isomerizations (enantiomerizations as well as tautomerizations or acid-catalyzed geometrical isomerizations), the SP may affect much more strongly the corresponding apparent pseudo first-order rate constants. This is because both the chiral selector and the chromatographic matrix might not be kinetically inert in principle. The SP can, in fact, act as a promoting

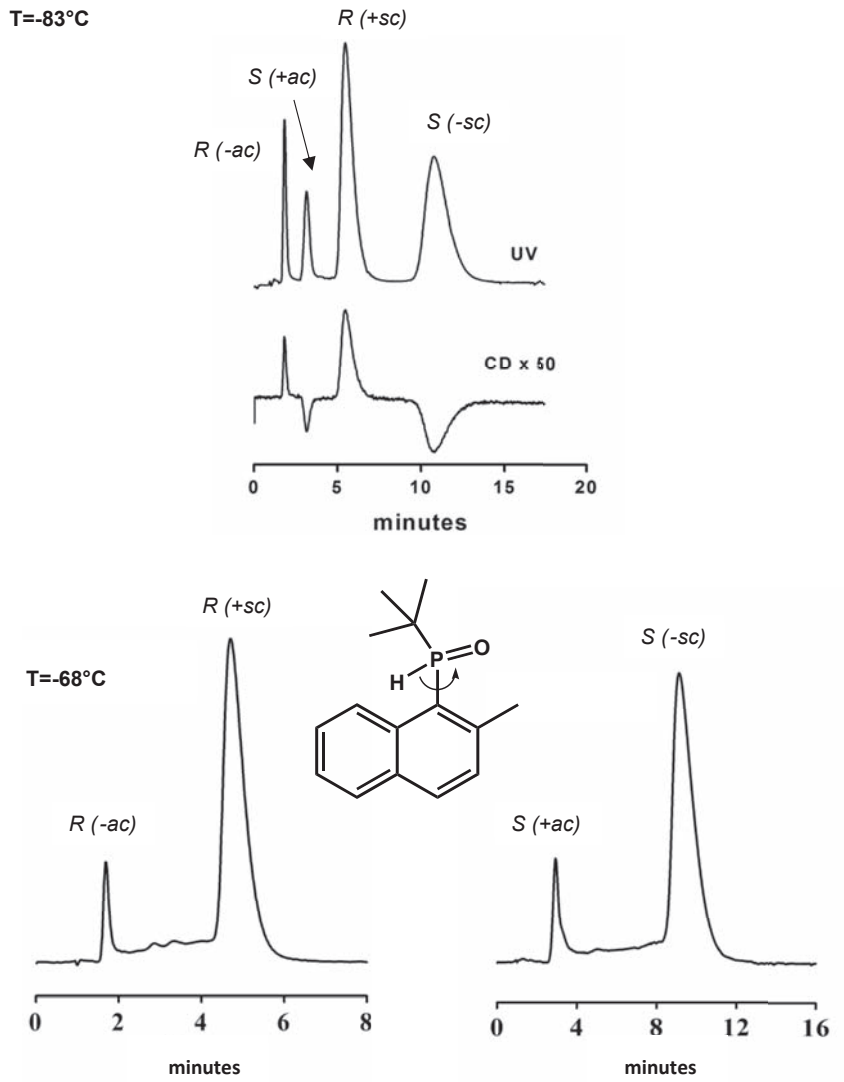

FIGURE 3.13

Evidence of indirect perturbing SP_{IPC} effect displayed by the racemic version of the DACH-DNB stationary phase on the diastereomerization rate constants of a hindered secondary aryl phosphine oxide.

or an inhibiting agent, increasing or decreasing the enantiomerization barrier of the studied chiral samples. This second type of SP effect was referred as a direct perturbing contribution (SP_{DPC}) (Cirilli et al., 2009b). Thus, while SP_{IPC} arises from a modification of the species involved in the isomerization, which changes its structure to form the proper *SP:substrate* adduct, the SP_{DPC} effect comes as

an additive term governed by independent catalytic sites bonded to the SP, which, in most cases, are represented by acid or basic groups acting as promoters. Therefore, from a mathematical point of view, the forward and backward rates of bimolecular processes leading to configurational isomerizations inside a chromatographic tool can be described by the two following general types of kinetic equations (Cirilli et al., 2009b):

$$ {}^{1}kv^{s} = {}^{2}kv^{s}_{IPCBase} \times [Base] + {}^{2}kv^{s}_{IPCAcid} \times [Acid] + {}^{2}kv^{s}_{DPC} \times [S_{SP}] + {}^{1}k_{0} \tag{3.2} $$

$$ {}^{1}kv^{m} = {}^{2}kv^{m}_{Base} \times [Base] + {}^{2}kv^{m}_{Acid} \times [Acid] + {}^{1}k_{0} \tag{3.3} $$

and by Eq. (3.4) the related apparent one

$$ {}^{1}kv^{app} = {}^{2}kv^{app}_{IPCBase} \times [Base] + {}^{2}kv^{app}_{IPCAcid} \times [Acid] + {}^{2}kv^{app}_{DPC} \times [S_{SP}] + {}^{1}k_{0} \tag{3.4} $$

The superscript 1 or 2 at the left sides of the rate constants refers to the kinetic order; the superscript s (*stationary*) or m (*mobile*) at the right sides of the rate constants refers to the chromatographic phase in which each constant is considered; Base and Acid represent the catalytic species potentially acting in the MP and SP; the term S_{SP} refers to the sites of the SP that can display catalytic effects; finally, ${}^{1}k_{0}$ expresses a first-order rate constant that accounts for any generic contribution not coming from either the SP or an explicit catalytic species. According to Eq. (3.2), any kind of SP_{DPC} contribution can be potentially and easily removed by ad hoc experiments. Indeed, this was performed for the specific case of a chiral ketone displaying anti-MAO activity, which enantiomerizes by a keto-enolate equilibrium (Cirilli et al., 2009). The pseudo first-order enantiomerization rate constants for the process catalyzed by diethylamine (DEA) were measured by both a batchwise and the DHPLC approach at different DEA concentrations and temperatures. The results showed a negligible ${}^{1}k_{0}$ term, so that Eqs. (3.2) and (3.3) may be rewritten in the simplified Eqs. (3.5) and (3.6), respectively, which, in turn, afford Eq. (3.7), expressing the related apparent pseudo first-order enantiomerization rate constant ${}^{1}kv^{app}$:

$$ {}^{1}kv^{s} = {}^{2}kv^{s}_{IPC} \times [DEA] + {}^{2}kv^{s}_{DPC} \times [S_{SP}] \tag{3.5} $$

$$ {}^{1}kv^{m} = {}^{2}kv^{m} \times [DEA] \tag{3.6} $$

$$ {}^{1}kv^{app} = {}^{2}kv^{app}_{IPC} \times [DEA] + {}^{2}kv^{app}_{DPC} \times [S_{SP}] \tag{3.7} $$

According to Eq. (3.7), at each temperature the SP_{DPC} contribution expressed by the term ${}^{2}kv^{app}_{DPC} \times [S_{SP}]$ was split out as the intercept in plots of ${}^{1}kv^{app}$ versus DEA concentration, while, from the same relationships, the slope afforded the apparent second-order enantiomerization rate constant ${}^{2}kv^{app}_{IPC}$. By comparison of these latter ones with the equivalent data coming from the batchwise determination, a SP_{IPC} effect of +27% and +20% was quantified on the second-order rate constants at the temperatures of 35 and 45°C, respectively (i.e., a reduction of the correspondent $\Delta G^{\neq}$ values of only 0.15 and 0.12 kcal/mol). Interestingly, in this case, the SP showed a promotion effect, which is normally not found in monomolecular isomerizations (vide supra). Presumably, the SP can slightly increase the formal DEA concentration on its surface, and DEA absorption may achieve a saturation level only over a critical catalyst concentration, estimated as 2×10^{-2} M for the specific studied case. Therefore, even minor SP_{IPC} effects could be expected for catalyst concentrations smaller than the critic limit.

8. DYNAMIC CHROMATOGRAPHY AS A TOOL TO QUANTIFY CATALYTIC SITES BONDED ON CHROMATOGRAPHIC SUPPORTS

A severe problem in chromatographic analyses requiring rigorous quantification of chiral drugs is when the species to resolve may be involved into secondary equilibria during their separation. In fact, both the selector and matrix of the SP may be endowed on their surfaces with chemical groups responsible for possible catalytic effects. Such an event was quite recently specifically addressed in a study showing that even international pharmacopoeias can contain shortcomings arising from the aforementioned chemical lability (Cabri et al., 2008; D'Acquarica et al., 2010). Dihydroartemisinin is a powerful antimalarial drug that may easily interconvert between its two epimeric forms, α and β. It was proposed as an effective strategy to set optimized operating conditions (suitable choice of column length, MP flow rate, and temperature) aimed to slow down the secondary equilibrium. It was also stressed that commercial columns containing the same SP as the discriminating tool (all RP-C18 columns, in the specific case) can have a marked differential SP_{DPC} effect in promoting the $\beta \leftrightarrows \alpha$ epimerization. In other words, the concentration of catalytic sites present on the SP surfaces not prepared according to standardized and uniform procedures may significantly differ from each other. However, the experimental determination of the ${}^{2}k\nu_{DPC}^{app} \times [S_{SP}]$ term present in Eq. (3.7) of Section 7 may represent a valuable tool to gain quantitative information on the abundance of S_{SP} sites. The results obtained could have direct implications in any analytical investigation aimed at quantitating this family of drugs.

In parallel studies performed on an anti-MAO drug (Cirilli et al., 2009b), within the limit of the adopted approximations (which include the assumption of amino groups as basic S_{SP} sites bonded to the silica matrix, uncovered by the deposed chiral selector), the $[S_{SP}]$ concentration was estimated as 4.5×10^{-3} M. This, in turn, was assessed to correspond to uncovered amino groups included in a range from 3% to 5% of the whole parent amino groups originally bonded to the matrix. Therefore, such an approach discloses wide perspectives for studies aimed to give accurate characterization of the surface of chromatographic supports. Nevertheless, for a rigorous application of DC methods to these kinds of determinations, further dedicated studies have to be envisaged.

REFERENCES

Allenmark, S., Oxelbark, J., 1998. Inversion barriers in sulfoxide functions studied by enantioselective liquid chromatography and chiroptical methods. Chirality 9, 638–642.

Andreani, R., Bombelli, C., Borocci, S., Lah, J., Mancini, G., Mencarelli, P., Vesnaver, G., Villani, C., 2004. New biphenylic derivatives: synthesis, characterisation and enantiodiscrimination in chiral aggregates. Tetrahedron: Asymmetry 15, 987–994.

Angelini, G., De Maria, P., Fontana, A., Pierini, M., Siani, G., 2007. Ionization and tautomerization of 2-nitrocyclohexanone in aqueous solution. J. Org. Chem. 72, 4039–4047.

Ballini, R., Cerritelli, S., Fontana, A., De Maria, P., Pierini, M., Siani, G., 2000. Equilibrium constants for ionisation and enolisation of 3-nitrobutan-2-one. Eur. J. Org. Chem. 8, 1641–1646.

Borsato, G., Della Negra, F., Gasparrini, F., Misiti, D., Lucchini, V., Possamai, G., Villani, C., Zambon, A., 2004. Internal motions in a fulleropyrrolidine tertiary amide with axial chirality. J. Org. Chem. 69, 5785–5788.

Bucar, F., Wube, A., Schmid, M., 2013. Natural product isolation-how to get from biological material to pure compounds. Nat. Prod. Rep. 30, 525–545.

Bürkle, W., Karfunkel, H., Schurig, V., 1984. Dynamic phenomena during enantiomer resolution by complexation gas chromatography. A kinetic study of enantiomerization. J. Chromatogr. A 288, 1–14.

Cabri, W., Ciogli, A., D'Acquarica, I., Di Mattia, M., Galletti, B., Gasparrini, F., Giorgi, F., Lalli, S., Pierini, M., Simone, P., 2008. On-column epimerization of dihydroartemisinin: an effective analytical approach to overcome the shortcomings of the international pharmacopoeia monograph. J. Chromatogr. B 875, 180–191.

Cabri, W., D'Acquarica, I., Simone, P., Di Iorio, M., Di Mattia, M., Gasparrini, F., Giorgi, F., Mazzanti, A., Pierini, M., Quaglia, M., Villani, C., 2011. Stereolability of dihydroartemisinin, an antimalarial drug: a comprehensive thermodynamic investigation − Part I. J. Org. Chem. 76, 1751−1758.

Cancelliere, G., D'Acquarica, I., Gasparrini, F., Maggini, M., Misiti, D., Villani, C., 2006. Twenty years of research on silica-based chiral stationary phases. J. Sep. Sci. 29, 770−781.

Cancelliere, G., Ciogli, A., D'Acquarica, I., Gasparrini, F., Kocergin, J., Misiti, D., Pierini, M., Ritchie, H., Simone, P., Villani, C., 2010. Transition from enantioselective high performance to ultra-high performance liquid chromatography: a case study of a brush-type chiral stationary phase based on sub 5-micron to sub 2-micron silica particles. J. Chromatogr. A 1217, 990−999.

Carr, P.W., Wang, X., Stoll, D.R., 2009. Effect of pressure, particle size, and time on optimizing performance in liquid chromatography. Anal. Chem. 81, 5342−5353.

Carradori, S., Cirilli, R., Dei Cicchi, S., Ferretti, R., Menta, S., Pierini, M., Secci, D., 2012. 3-Methylcyclohexanone thiosemicarbazone: determination of E/Z isomerization barrier by dynamic high-performance liquid chromatography, configuration assignment and theoretical study of the mechanisms involved by the spontaneous, acid and base catalyzed processes. J. Chromatogr. A 1269, 168−177.

Cavazzini, A., Marchetti, N., Guzzinati, R., Pierini, M., Ciogli, A., Kotoni, D., D'Acquarica, I., Villani, C., Gasparrini, F., 2014. Enantioseparation by ultra-high-performance liquid chromatography. TrAC Trends Anal. Chem. 63, 95−103.

Ceccacci, F., Mancini, G., Mencarelli, P., Villani, C., 2003. Determination of the rotational barrier of a chiral biphenyl: comparison of theoretical and experimental data. Tetrahedron: Asymmetry 14, 3117−3122.

Chiarucci, M., Ciogli, A., Mancinelli, M., Ranieri, S., Mazzanti, A., 2014. The experimental observation of the intramolecular NO_2/CO interaction in solution. Angew. Chem. Int. Ed. Engl. 53, 5405−5409.

Ciogli, A., Kotoni, D., Gasparrini, F., Pierini, M., Villani, C., 2013. Chiral supramolecular selectors for enantiomer differentiation in liquid chromatography. Top. Curr. Chem. 340, 73−105.

Cirilli, R., Ferretti, R., La Torre, F., Secci, D., Bolasco, A., Carradori, S., Pierini, M., 2007. High-performance liquid chromatographic separation of enantiomers and diastereomers of 2-methylcyclohexanone thiosemicarbazone, and determination of absolute configuration and configurational stability. J. Chromatogr. A 1172, 160−169.

Cirilli, R., Costi, R., Di Santo, R., Gasparrini, F., La Torre, F., Pierini, M., Siani, G., 2009a. A rational approach to predict and modulate stereolability of chiral alpha substituted ketones. Chirality 21, 24−34.

Cirilli, R., Costi, R., Di Santo, R., La Torre, F., Pierini, M., Siani, G., 2009b. Perturbing effects of chiral stationary phase on enantiomerization second-order rate constants determined by enantioselective dynamic high-performance liquid chromatography: a practical tool to quantify the accessible acid and basic catalytic sites bonded on chromatographic supports. Anal. Chem. 81, 3560−3570.

D'Acquarica, I., Gasparrini, F., Pierini, M., Villani, C., Zappia, G., 2006. Dynamic HPLC on chiral stationary phases: a powerful tool for the investigation of stereomutation processes. J. Sep. Sci. 29, 1508−1516.

D'Acquarica, I., Gasparrini, F., Kotoni, D., Pierini, M., Villani, C., Cabri, W., Di Mattia, M., Giorgi, F., 2010. Stereodynamic investigation of labile stereogenic centres in dihydroartemisinin. Molecules 15, 1309−1323.

D'Acquarica, I., Kotoni, D., Ciogli, A., Pierini, M., Kocergin, J., Ritchie, H., Villani, C., Gasparrini, F., 2014. The evolution of chiral stationary phases from HPLC to UHPLC. LC−GC Eur. 27, 128−137.

Dalla Cort, A., Gasparrini, F., Lunazzi, L., Mandolini, L., Mazzanti, A., Pasquini, C., Pierini, M., Rompietti, R., Schiaffino, L., 2005. Stereomutations of atropisomers of sterically hindered salophen ligands. J. Org. Chem. 70, 8877−8883.

Dell'Erba, C., Gasparrini, F., Grilli, S., Lunazzi, L., Mazzanti, A., Novi, M., Pierini, M., Tavani, C., Villani, C., 2002. Conformational studies by dynamic NMR. 86. Structure, stereodynamics, and cryogenic enantioseparation of the stereolabile isomers of o-dinaphthylphenyl derivatives. J. Org. Chem. 67, 1663−1668.

Desmet, G., Clicq, D., Nguyen, D.T.-T., Guillarme, D., Rudaz, S., Veuthey, J.-L., Vervoort, N., Torok, G., Cabooter, D., Gzil, P., 2006. Practical constraints in the kinetic plot representation of chromatographic performance data: theory and application to experimental data. Anal. Chem. 78, 2150−2162.

Ellis, L.A., Roberts, D.J., 1997. Chromatographic and hyphenated methods for elemental speciation analysis in environmental media. J. Chromatogr. A 774, 3−19.

Felinger, A., Pasti, L., Dondi, F., van Hulst, M., Schoenmakers, P.J., Martin, M., 2005. Stochastic theory of size exclusion chromatography: peak shape analysis on single columns. Anal. Chem. 77, 3138−3148.

Fontana, A., De Maria, P., Pierini, M., Siani, G., Cerritelli, S., Macaluso, G., 2002. Ab initio analysis on metal ion catalysis in the enolization reactions of some acetylheterocycles: kinetics of the enolization reactions of 3-acetyl-5-methylisoxazole, 5-acetyl-3-methylisoxazole and 3(5)-acetylpyrazole. J. Phys. Org. Chem. 15, 247−257.

Francotte, E.R., 2009. Enantioselective chromatography: from its emergence to its successful implementation in the pharmaceutical environment. Chimia 63, 867−871.

Gasparrini, F., Lunazzi, L., Misiti, D., Villani, C., 1995. Organic stereochemistry and conformational analysis from enantioselective chromatography and dynamic nuclear magnetic resonance measurements. Acc. Chem. Res. 28, 163−170.

Gasparrini, F., Misiti, D., Pierini, M., Villani, C., 1997a. Enantiomerization barriers by dynamic HPLC. Stationary phase effect. Tetrahedron: Asymmetry 8, 2069−2073.

Gasparrini, F., Misiti, D., Villani, C., Wennemers, H., Still, W.C., 1997b. Enantioselective and diastereoselective binding study of silica bound macrobicyclic receptors by HPLC. J. Org. Chem. 62, 8221−8224.

Gasparrini, F., Lunazzi, L., Mazzanti, A., Pierini, M., Pietrusiewicz, K.M., Villani, C., 2000. Comparison of dynamic HPLC and dynamic NMR in the study of conformational stereodynamics: case of the enantiomers of a hindered secondary phosphine oxide. J. Am. Chem. Soc. 122, 4776−4780.

Gasparrini, F., D'Acquarica, I., Pierini, M., Villani, C., 2001. Chromatographic resolution and enantiomerization barriers of axially chiral 1-naphthamides. J. Sep. Sci. 24, 941−946.

Gasparrini, F., Grilli, R., Leardini, L., Lunazzi, L., Mazzanti, A., Nanni, D., Pierini, M., Pinamonti, M., 2002a. Conformational studies by dynamic NMR. 89. Stereomutation and cryogenic enantioseparation of conformational antipodes of hindered aryl oximes. J. Org. Chem. 67, 3089−3095.

Gasparrini, F., Misiti, D., Pierini, M., Villani, C., 2002b. A chiral A2B2 macrocyclic minireceptor with extreme enantioselectivity. Org. Lett. 4, 3993−3996.

Gasparrini, F., Pierini, M., Villani, C., De Maria, P., Fontana, A., Ballini, R., 2003. Enantiomerization study of some α-nitroketones by dynamic high-resolution gas chromatography. J. Org. Chem. 68, 3173−3177.

Giddings, J.C., 1965. Comparison of theoretical limit of separating speed in gas and liquid chromatography. Anal. Chem. 37, 60−63.

Gritti, F., Guiochon, G., 2008. Heat exchanges in fast, high-performance liquid chromatography. A complete thermodynamic study. Anal. Chem. 80, 6488−6499.

Guetens, G., De Boeck, G., Highley, M.S., Wood, M., Maes, R.A., Eggermont, A.A., Hanauske, A., de Bruijn, E.A., Tjaden, U.R., 2002a. Hyphenated techniques in anticancer drug monitoring. II. Liquid chromatography-mass spectrometry and capillary electrophoresis-mass spectrometry. J. Chromatogr. A 976, 239−247.

Guetens, G., De Boeck, G., Wood, M., Maes, R.A., Eggermont, A.A., Highley, M.S., van Oosterom, A.T., de Bruijn, E.A., Tjaden, U.R., 2002b. Hyphenated techniques in anticancer drug monitoring. I. Capillary gas chromatography-mass spectrometry. J. Chromatogr. A 976, 229−238.

Guillarme, D., Nguyen, D.T.-T., Rudaz, S., Veuthey, J.-L., 2007. Recent developments in liquid chromatography-impact on qualitative and quantitative performance. J. Chromatogr. A 1149, 20−29.

Holt, R.M., Newman, M.J., Pullen, F.S., Richards, D.S., Swanson, A.G., 1997. High-performance liquid chromatography/NMR spectrometry/mass spectrometry: further advances in hyphenated technology. J. Mass Spectrom. 32, 64−70.

Jacobson, J., Melander, W.R., Vaisnys, G., Horváth, C., 1984. Kinetic study on cis-trans proline isomerization by high-performance liquid chromatography. J. Phys. Chem. 88, 4536−4542.

Jerkovich, A.D., Mellors, J.S., Jorgenson, J.W., 2003. The use of micrometer-sized particles in ultra high pressure liquid chromatography. LC−GC Eur. 16, 20−23.

Jung, M., 1992. Program simul, no. 620. Quantum chemistry program exchange. QCPE Bull. 3, 12.

Katsanos, N.A., Thede, R., Roubani-Kalantzopoulou, F., 1998. Diffusion, adsorption and catalytic studies by gas chromatography. J. Chromatogr. A 795, 133−184.

Keller, R.A., Giddings, J.C., 1960. Multiple zones and spots in chromatography. J. Chromatogr. A 3, 205−220.

Knox, J.H., 1977. Practical aspects of LC theory. J. Chromatogr. Sci. 15, 352−364.

Kotoni, D., Ciogli, A., D'Acquarica, I., Kocergin, J., Szczerba, T., Ritchie, H., Villani, C., Gasparrini, F., 2012a. Enantioselective ultra-high and high performance liquid chromatography: a comparative study of columns based on the Whelk-O1 selector. J. Chromatogr. A 1269, 226−241.

Kotoni, D., Ciogli, A., Molinaro, C., D'Acquarica, I., Kocergin, J., Szczerba, T., Ritchie, H., Villani, C., Gasparrini, F., 2012b. Introducing enantioselective ultrahigh-pressure liquid chromatography (eUHPLC): theoretical inspections and ultrafast separations on a new sub-2-μm Whelk-O1 stationary phase. Anal. Chem. 84, 6805−6813.

Kotoni, D., Piras, M., Cabri, W., Giorgi, F., Mazzanti, A., Pierini, M., Quaglia, M., Villani, C., Gasparrini, F., 2014. Thermodynamic and kinetic investigation of monoketo-aldehyde-peroxyhemiacetal-(mka), a stereolabile degradation product of dihydroartemisinin. RSC Adv. 4, 32847−32857.

Kramer, R., 1975. Simultan-reaktionsgaschromatographie mit reversibler reaktion erster ordnung. I. J. Chromatogr. A 107, 241–252.

Krupcik, J., Oswald, P., Spanik, I., Majek, P., Bajdichova, M., Sandra, P., Armstrong, D.W., 2000a. The use of computerized peak deconvolution for determination of energy barrier to enantiomerization in dynamic gas chromatography. J. Microcolumn Sep. 12, 630–636.

Krupcik, J., Oswald, P., Spanik, I., Majek, P., Bajdichova, M., Sandra, P., Armstrong, D.W., 2000b. On the use of a peak deconvolution procedure for the determination of energy barrier to enantiomerization in dynamic chromatography. Analusis 28, 859–863.

Krupcik, J., Oswald, P., Majek, P., Sandra, P., Armstrong, D.W., 2003. Determination of the interconversion energy barrier of enantiomers by separation methods. J. Chromatogr. A 1000, 779–800.

Kusano, T., Tabatabai, M., Okamoto, Y., Boehmer, V., 1999. The cone-to-cone interconversion of partially o-methylated calix[4]arenes: first experimental values for the energy barriers. J. Am. Chem. Soc. 121, 3789–3790.

Levi Mortera, S., Sabia, R., Pierini, M., Gasparrini, F., Villani, C., 2012. The dynamic chromatographic behavior of tri-o-thymotide on HPLC chiral stationary phases. Chem. Commun. 48, 3167–3169.

Lunazzi, L., Mancinelli, M., Mazzanti, A., Pierini, M., 2010. Stereomutation of axially chiral aryl coumarins. J. Org. Chem. 75, 5927–5933.

Mannschreck, A., Andert, D., Eiglsperger, E., Gmahl, E., Buchner, H., 1988. Chiroptical detection. Novel possibilities of its application to enantiomers. Chromatographia 25, 182–188.

Mannschreck, A., Kiessl, L., 1989. Enantiomerization during HPLC on an optically active sorbent. Deconvolution of experimental chromatograms. Chromatographia 28, 263–266.

Marriott, P., Trapp, O., Shellie, R., Schurig, V., 2001. Time-resolved cryogenic modulation reveals isomer interconversion profiles in dynamic chromatography. J. Chromatogr. A 919, 115–126.

Melander, W.R., Lin, H.-J., Jacobson, J., Horváth, C., 1984. Dynamic effect of secondary equilibria in reversed-phase chromatography. J. Phys. Chem. 88, 4527–4535.

Menta, S., Pierini, M., Cirilli, R., Grisi, F., Perfetto, A., Ciogli, A., 2015. Stereolability of chiral ruthenium catalysts with frozen NHC ligand conformations investigated by dynamic-HPLC. Chirality 27, 685–692.

Neue, U.D., Kele, M., 2007. Performance of idealized column structures under high pressure. J. Chromatogr. A 1149, 236–244.

Nishikawa, T., Hayashi, Y., Suzuki, S., Kubo, H., Ohtani, H., 1997. On-column enantiomerization of 3-hydroxybenzodiazepines during chiral liquid chromatography with optical rotation detection. J. Chromatogr. A 767, 93–100.

Oswald, P., Desmet, K., Sandra, P., Krupcik, J., Armstrong, D.W., 2002a. Determination of the enantiomerization energy barrier of some 3-hydroxy-1,4-benzodiazepine drugs by supercritical fluid chromatography. J. Chromatogr. B 779, 283–295.

Oswald, P., Desmet, K., Sandra, P., Krupcik, J., Armstrong, D.W., 2002b. Evaluation of reversible and irreversible models for the determination of the enantiomerization energy barrier for n-(*p*-methoxybenzyl)-1,3,2-benzodithiazol-1-oxide by supercritical fluid chromatography. Chirality 14, 334–339.

Page, M.I., Jencks, W.P., 1971. Entropic contributions to rate accelerations in enzymic and intramolecular reactions and the chelate effect. Proc. Natl. Acad. Sci. U.S.A. 68, 1678–1683.

Pasti, L., Cavazzini, A., Felinger, A., Martin, M., Dondi, F., 2005. Single-molecule observation and chromatography unified by Lévy process representation. Anal. Chem. 77, 2524–2535.

Pasti, L., Cavazzini, A., Nassi, M., Dondi, F., 2010. Dynamic chromatography: a stochastic approach. J. Chromatogr. A 1217, 1000–1009.

Pasti, L., Marchetti, N., Guzzinati, R., Catani, M., Bosi, V., Dondi, F., Sepsey, A., Felinger, A., Cavazzini, A., 2016. Microscopic models of liquid chromatography: from ensemble averaged information to resolution of fundamental viewpoint at single-molecule level. TrAC Trends Anal. Chem. 81, 63–68.

Poppe, H., 1997. Some reflections on speed and efficiency of modern chromatographic methods. J. Chromatogr. A 778, 3–21.

Rizzo, S., Benincori, T., Bonometti, V., Cirilli, R., Mussini, P.R., Pierini, M., Pilati, T., Sannicolò, F., 2013. Steric and electronic effects on the configurational stability of residual chiral phosphorus-centered three-bladed propellers: tris-aryl phosphanes. Chem. A Eur. J. 19, 182–194.

Rizzo, S., Cirilli, R., Pierini, M., 2014. Chirality in the absence of rigid stereogenic elements: steric and electronic effects on the configurational stability of C-3 symmetric residual tris-aryl phosphanes. Chirality 26, 601–606.

Rizzo, S., Menta, S., Benincori, T., Ferretti, R., Pierini, M., Cirilli, R., Sannicolò, F., 2015. Determination of the enantiomerization barrier of the residual enantiomers of C3-symmetric tris[3-(1-methyl-2-alkyl)indolyl]phosphane oxides: case study of a multitasking HPLC investigation based on an immobilized polysaccharide stationary phase. Chirality 27, 888−899.

Sabia, R., Ciogli, A., Pierini, M., Gasparrini, F., Villani, C., 2014. Dynamic high performance liquid chromatography on chiral stationary phases. Low temperature separation of the conformational enantiomers of diazepam, flunitrazepam, prazepam and tetrazepam. J. Chromatogr. A 1363, 144−149.

Sabia, R., De Martino, M., Cavazzini, A., Villani, C., 2016. The dynamic behavior of clobazam on high performance liquid chromatography chiral stationary phases. Chirality 28, 17−21.

Shustov, G.V., Kadorkina, G.K., Kostyanovsky, R.G., Rauk, A., 1988. Asymmetric nitrogen. 67. Geminal systems. 41. Chiroptical properties of N-chloro and N-bromo derivatives of three-membered nitrogen heterocycles: aziridines and diaziridines. J. Am. Chem. Soc. 110, 1719−1726.

Shustov, G.V., Varlamov, S.V., Chervin, I.I., Aliev, A.E., Kostyanovsky, R.G., Kim, D., Rauk, A., 1989. Asymmetric nitrogen. 72. Geminal systems. 46. N-chlorooxaziridines: optical activation, absolute configuration, and chiroptical properties. J. Am. Chem. Soc. 111, 4210−4215.

Siani, G., Angelini, G., De Maria, P., Fontana, A., Pierini, M., 2008. Solvent effects on the rate of the keto−enol interconversion of 2-nitrocyclohexanone. Org. Biomol. Chem. 6, 4236−4241.

Sticher, O., 2008. Natural product isolation. Nat. Prod. Rep. 25, 517−554.

Trapp, O., Schurig, V., 2000. Stereointegrity of Tröger's base: gas-chromatographic determination of the enantiomerization barrier. J. Am. Chem. Soc. 122, 1424−1430.

Trapp, O., Schurig, V., 2001a. Approximation function for the direct calculation of rate constants and Gibbs activation energies of enantiomerization of racemic mixtures from chromatographic parameters in dynamic chromatography. J. Chromatogr. A 911, 167−175.

Trapp, O., Schurig, V., 2001b. ChromWin − a computer program for the determination of enantiomerization barriers in dynamic chromatography. Comput. Chem. 25, 187−195.

Trapp, O., Schoetz, G., Schurig, V., 2002. Stereointegrity of thalidomide: gas-chromatographic determination of the enantiomerization barrier. J. Pharm. Biomed. Anal. 27, 497−505.

Trapp, O., Shellie, R., Marriott, P., Schurig, V., 2003. Simulation of elution profiles for two-dimensional dynamic gas chromatographic experiments. Anal. Chem. 75, 4452−4461.

Trapp, O., 2004. Evaluation and prediction of stereoisomerizations in comprehensive two-dimensional chromatography. J. Chem. Inf. Comput. Sci. 44, 1671−1679.

Trapp, O., 2006. Unified equation for access to rate constants of first-order reactions in dynamic and on-column reaction chromatography. Anal. Chem. 78, 189−198.

Uray, G., Jahangir, S., Fabian, W.M., 2010. On- and off-column enantiomerization of 4,4′-bisquinolin-2-ones: a comparison of auto DHPLC y2k and DCXplorer calculated thermodynamic data generated by dynamic high performance liquid chromatography with theoretically calculated data. J. Chromatogr. A 1217, 1017−1023.

Wales, T.E., Fadgen, K.E., Gerhardt, G.C., Engen, J.R., 2008. High-speed and high-resolution UPLC separation at zero degrees celsius. Anal. Chem. 80, 6815−6820.

Ward, T.J., Ward, K.D., 2010. Chiral separations: fundamental review. Anal. Chem. 82, 4712−4722.

Wilkins, C.L., 1983. Hyphenated techniques for analysis of complex organic mixtures. Science 222, 291−296.

Wolf, C., König, W.A., Roussel, C., 1995. Influence of substituents on the rotational energy barrier of atropisomeric biphenyls − studies by polarimetry and dynamic gas chromatography. Liebigs Ann. 781−786.

Wolf, C., 2005. Stereolabile chiral compounds: analysis by dynamic chromatography and stopped-flow methods. Chem. Soc. Rev. 34, 595−608.

Wolf, C., 2008. Dynamic Stereochemistry of Chiral Compounds. The Royal Society of Chemistry, Cambridge, United Kingdom.

Wu, N., Lippert, J.A., Lee, M.L., 2001. Practical aspects of ultrahigh pressure capillary liquid chromatography. J. Chromatogr. A 911, 1−12.

FURTHER READING

Giddings, J.C., 1960. Kinetic processes and zone diffusion in chromatography. J. Chromatogr. A 3, 443−453.

CHAPTER

SILVER-ION LIQUID CHROMATOGRAPHY—MASS SPECTROMETRY

4

Michal Holčapek, Miroslav Lísa
University of Pardubice, Pardubice, Czech Republic

1. INTRODUCTION

The ability of silver ion and some other metal ions to interact with double bonds (DBs) has been well known for a long time (Dobson et al., 1995; Guha and Janak, 1972; Devries, 1962; Morris, 1962). Silver-ion chromatography, sometimes called argentation chromatography, is a separation technique based on the formation of weak reversible charge-transfer complexes between silver ions and DBs of unsaturated organic molecules. Silver-ion chromatography can be performed either in a planar arrangement (silver-ion thin layer chromatography, Ag-TLC) or on a column, which is often used for preparative purposes or silver-ion high-performance liquid chromatography (Ag-HPLC) used for high-resolution separations. Ag-TLC is a well-established technique in the analysis of lipids and other organic molecules containing DBs because it is cheap, simple to use, and applicable both on analytical and preparative scales. Ag-TLC has been reviewed in several works (Dobson et al., 1995; Momchilova and Nikolova-Damyanova, 2003); therefore it is not discussed in this chapter.

The retention in Ag-HPLC is governed by the DB number. More DBs mean stronger interactions and therefore higher retention times. In practice, the situation is not as simple because other factors have to be taken into account, such as the DB geometry (*cis* vs. *trans*), distances among individual DB (from the conjugation to remote DB), overall molecular structures, the type of stationary phase, the composition of mobile phase, the gradient steepness, separation temperature, etc. The majority of Ag-HPLC applications are in the area of lipids, but this technique has a great potential also for other compounds containing DBs (Guha and Janak, 1972; Williams and Mander, 2001; Mander and Williams, 2016). This chapter focuses mainly on lipids, such as triacylglycerols (TGs), fatty acids (FAs), and fatty acid methyl esters (FAMEs), but other nonpolar lipids (e.g., sterols, wax esters, cholesterol esters, vitamins, carotenoids) can be analyzed as well (Vrkoslav et al., 2013; Joh et al., 1995; Kakela et al., 2002; Shan and Wilson, 2002).

2. MECHANISM OF SILVER-ION INTERACTION WITH DOUBLE BONDS

Zeise prepared the first organometallic complex in the 1820s (i.e., Zeise's salt $K[PtCl_3(C_2H_4)]\cdot H_2O$ (Zeise, 1831)), which stimulated more scientific research in the field of organometallic chemistry.

Handbook of Advanced Chromatography/Mass Spectrometry Techniques. http://dx.doi.org/10.1016/B978-0-12-811732-3.00004-2

Today, organometallic complexes are of great interest because of their applications in bond activation processes and catalysis. In the field of chromatography, organometallic complexes are used for the separation of unsaturated organic compounds based on their interactions with metals immobilized in the stationary phase (Guha and Janak, 1972), especially silver-ion chromatography uses the capability of unsaturated compounds to form organometallic complexes containing silver(I) ions (Mander and Williams, 2016; Williams and Mander, 2001). Unsaturated compounds form weak reversible complexes of different strengths with silver ions immobilized in the stationary phase, during their elution through the chromatographic column. It is a dynamic system with continuous establishment of equilibrium among complexed and free components with a high equilibrium constant. Complexes are of the charge-transfer type, where unsaturated compounds donate electrons to the silver ion (acceptor). The description of complexation bonding between DB and silver(I) ion by the Dewar—Chatt—Duncanson model (Dewar, 1951; Chatt and Duncanson, 1953) is now widely accepted. This model describes the stabilization of complexes as a combination of σ-donation and π-back-bonding interactions between DB and the metal, i.e., donation of π-electrons from the occupied 2*p* bonding orbital of the olefinic DB into vacant 5*s* and 5*p* orbitals of the silver ion (σ-type bond, Fig. 4.1A), and the back-donation of *d*-electrons from occupied *4d* orbitals of the silver ion into unoccupied π^*-2*p* antibonding orbitals of the olefinic DB (π-type bond, Fig. 4.1B). This model describes only bonding between DBs and silver ions, but the stability constant of the complex also depends on steric and polar effects. A number of experimental and theoretical studies have been done for complexes of the silver ion with short olefins because these complexes are important in organometallic chemistry. Early studies of stability constants of organosilver complexes used distribution methods based on the distribution of organic compounds between an organic phase and silver nitrate aqueous solution (Lucas et al., 1943; Winstein and Lucas, 1938). These results have been confirmed later by various analytical techniques, i.e., UV, infrared, and Raman spectroscopy, based on shifts in absorption maxima between complexed and free unsaturated compounds (Hosoya and Nagakura, 1964), X-ray studies of organosilver monocrystals (Gmelin, 1975; Bressan et al., 1967), electron spin resonance (Kasai et al., 1980), etc. General conclusions of complex stability affected by structural factors are as follows: The stability of complexes containing *cis*-DB is higher than with *trans*-DB (Lucas et al., 1943; Morris, 1966); complexes of methylene-interrupted DB are stronger than conjugated ones; the stability of

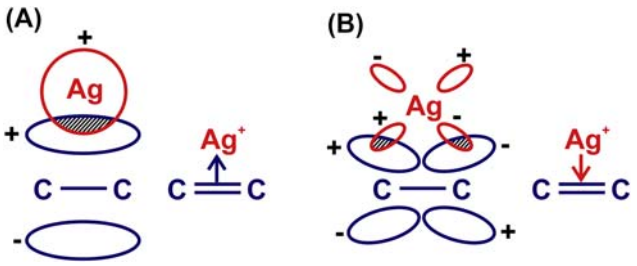

FIGURE 4.1

Description of complex bonding between silver ions and double bonds (DBs) by the Dewar—Chatt—Duncanson model: (A) σ-donation and (B) π-back-bonding interactions between the metal and DB. *Ag*, silver ion.

Redrawn with permission from Dewar, J.S., 1951. A review of the pi-complex theory. Bulletin De La Societe Chimique De France 18, C71—C79.

complexes increases with increasing distance of DB (Winstein and Lucas, 1938); the stability of complexes decreases with increasing chain length (Conacher, 1976); and the stability of complexes increases by substitution of hydrogen with deuterium atoms (Cvetanović et al., 1965).

In the silver-ion chromatographic process, interactions between DBs of unsaturated compounds and silver ions are rather complex. Electron spin resonance shows the interaction of a silver ion with two molecules (Kasai et al., 1980), and X-ray diffraction of a monocrystal shows the coordination of one silver ion with two DBs from different molecules (Gmelin, 1975; Bressan et al., 1967). The interaction of a silver ion with the carboxylic oxygen of unsaturated compounds has also been shown (Winstein and Lucas, 1938). In addition to many interactions of silver ions and unsaturated compounds, the retention is also influenced by the quality of column packing, i.e., the density and accessibility of silver ions on the surface of the stationary phase. Nowadays, most Ag-HPLC columns are based on the silica matrix chemically modified with an alkylphenylsulfonic moiety, with bonding of silver ions by ionic bonds. Free silanol groups may interact with unsaturated molecules during the chromatographic process, and molecules are separated based on mixed retention mechanisms. The separation of lipids is more complex because of a number of combinations of interactions among silver ions, DBs, and carboxyl oxygen atoms. Electrostatic forces within and between fatty acyl chains could also influence their retention behavior, but little is known about these forces so far.

3. PARAMETERS AFFECTING SILVER-ION HIGH-PERFORMANCE LIQUID CHROMATOGRAPHY

3.1 TYPES OF SILVER-ION SYSTEMS

Three potential ways for embedding silver ions in the HPLC system have been described so far (Momchilova and Nikolova-Damyanova, 2003; Nikolova-Damyanova, 2005, 2009): (1) adsorption of silver ions on the stationary phase, (2) silver ions embedded in the stationary phase via ionic bonds, and (3) addition of silver ions into the mobile phase.

1. Silver complexation column (Jeffrey, 1991; Schuyl et al., 1998)—in the past, silver-ion columns for HPLC were prepared by the adsorption of silver ions (typically in the form of silver nitrate) on silica columns and then washed carefully with different solvents and the final washing with the mobile phase. A certain part of silver ions is adsorbed on the silica gel. Some papers present good separations with this type of column, but at present they have almost disappeared because of serious drawbacks, such as the leakage of silver ions into the mobile phase [critical for mass spectrometry (MS) coupling], poor reproducibility, and also technical skills required for the reproducible preparation of columns.
2. Strong cation exchanger modified with silver ions (Emken et al., 1964; Christie, 1987; Toschi et al., 1993)—silver ions replace initial protons in the $-SO_3H$ functional groups (estimated silver content is 50–80 mg) and then $-SO_3Ag$ interacts with DB during the chromatographic process. This ionic bond is rather stable and no leakage of silver ions is detected even for long-time use in high-performance liquid chromatography–mass spectrometry (HPLC/MS) experiments. Nowadays, practically all Ag-HPLC/MS papers are based on the ion-exchanger type of silver-ion columns. The commercial silver-ion columns, Chromspher Lipids, can be now purchased from Agilent Technologies. Some researchers rely on their laboratory-made silver-ion columns with

comparable performance according to the procedure published by Christie (1987). Recommended eluents for silver-ion columns are dichloromethane, dichloroethane, acetone, acetonitrile, toluene, and ethylacetate. Aqueous solvents are discouraged because they permanently alter column properties, especially small anions can cause silver precipitation. Solvents should be free of peroxides or any reducing agents that can cause the reduction of silver(I) to the metal state. No acids should be used because of the back replacement of silver ions to protons.

3. The addition of silver ions into the mobile phase using C18 column (Correa et al., 1999; Nikolova-Damyanova et al., 1993). This approach is not compatible with MS detection because nonvolatile inorganic salts cause contamination of the ion source and because of ion suppression effects. The retention mechanism in this arrangement is a combination of silver ion and reversed-phase (RP) modes.

3.2 MOBILE-PHASE COMPOSITION

Optimization of the mobile phase is a crucial step in Ag-HPLC because the proper optimization of solvent composition and gradient steepness can significantly improve the separation, including the regioisomeric resolution. Two types of mobile phases are most frequently used in Ag-HPLC. The first type is based on chlorinated solvents, such as dichloromethane or dichloroethane with the addition of other polar modifiers at low concentration, typically acetonitrile, acetone, or methanol (Christie, 1988; Juaneda et al., 1994; Laakso and Voutilainen, 1996; Nikolova-Damyanova et al., 1992, 1995a,b; Lísa et al., 2013). The second type is hexane-based mobile phases with the addition of acetonitrile as the polar modifier (Adlof and List, 2004; Adlof, 1994, 1995; Dugo et al., 2004, 2006a,b,c; Mondello et al., 2005; Lísa et al., 2013). In addition to these two main types, some other solvent combinations have been also reported as well, such as toluene, hexane and ethylacetate (Schuyl et al., 1998), methanol and acetonitrile (van der Klift et al., 2008), and 13 different eluent systems containing hexane, heptane, or isooctane with the addition of acetonitrile, propionitrile or butyronitrile (Muller et al., 2006), heptane with acetonitrile or acetone (Macher and Holmqvist, 2001), or acetone with acetonitrile (Nikolova-Damyanova et al., 1995a,b).

Hexane—acetonitrile mobile phases have a unique property of possible regioisomeric resolution of unsaturated TG, which has not been reported for chlorinated mobile phases. The disadvantage of a hexane—acetonitrile system is the low solubility of acetonitrile in hexane, which is only about 1%—1.5% at ambient temperature (Adlof and List, 2004). The miscibility problem strongly limits the range of applicable chromatographic conditions and significantly contributes to the reproducibility problem, which can be partly solved by using continuous magnetic stirring. Two alternative approaches have been tested regarding how to solve the miscibility limitation, while maintaining excellent chromatographic resolution, including the resolution of positional isomers. When acetonitrile is replaced by propionitrile, the miscibility is much better and the regioisomeric resolution is almost the same (Muller et al., 2006; Lísa et al., 2009a,b), but a serious health hazard arises because of the toxicity of propionitrile. The second approach relies on the addition of a third solvent with good mutual miscibility with both acetonitrile and hexane. The ideal combination is hexane—2-propanol—acetonitrile (Lísa et al., 2009a,b; Cvačka et al., 2006; Han et al., 1999; Holčapek et al., 2009, 2010; Vrkoslav et al., 2013), where remarkable improvements in the reproducibility of retention times are observed in comparison with traditional hexane—acetonitrile binary mixtures (Muller et al.,

2006; Lísa et al., 2009a,b). Standard deviations of retention times for three selected peaks (PLP, PLL, and LLL) in hexane−2-propanol−acetonitrile are 0.4%, 1.0%, and 0.7% for one-day measurements compared to 7.4%, 6.8%, and 5.2% for a hexane−acetonitrile mobile phase (Lísa et al., 2009a,b). Some shifts in retention times can occur on a longer time scale, but they can be efficiently eliminated by the use of the relative retention factor, $r = (t_{R,TG} - t_M)/(t_{R,std} - t_M)$. There are some important issues concerning mobile-phase preparation, which should be followed to obtain good reproducibility. Mobile phases should be prepared fresh every day using solvents dried with molecular sieves and kept in tightly closed containers to avoid evaporation. A low percentage of additives in hexane should be premixed in solvent containers (Dugo et al., 2006a,b,c; Lísa et al., 2009a,b). The degassing of mobile phase by an automatic degasser is preferred over continuous stripping with a stream of helium or sonication. Columns are conditioned using a low flow rate of the initial gradient composition (50 μL/min) overnight and the standard flow rate for 1 h before the analysis (Lísa et al., 2009a,b).

If the resolution is not sufficient on one silver-ion column, then more columns can be coupled in series, as demonstrated in several works (Adlof and List, 2004; Adlof, 1994, 1995; Lísa et al., 2009a,b; Holčapek et al., 2009, 2010). An increased length of chromatographic column improves the resolution of critical pairs, for example regioisomeric doublets (Lísa et al., 2009a,b; Holčapek et al., 2009, 2010) or DB positional isomers of FA derivatives (Juaneda et al., 1994). Unlike in nonaqueous reversed-phase (NARP) systems, the back pressure is not a limiting factor here because mobile phases typically consist of low-viscosity organic solvents (e.g., hexane, dichloromethane, dichloroethane) with a low percentage of polar modifier. Limiting factors are mainly long retention times associated with the extended column length and peak broadening effects for the multiple column coupling.

3.3 TEMPERATURE

Temperature plays an important role in the optimization of the chromatographic separation of lipids, which is not limited to Ag-HPLC, but is valid for other separation modes as well, such as NARP (Holčapek et al., 1999, 2003, 2005; Lísa and Holčapek, 2008). Increased temperature can result in the loss of resolution for critical TG pairs in NARP mode, where the retention time depends inversely on the temperature. In the case of Ag-HPLC, the correlation among retention times, temperature, and chromatographic resolution is more complex. The basic rule for the temperature dependence in Ag-HPLC mode is that higher temperature means higher retention times (Adlof and List, 2004; Lísa et al., 2009a,b, 2013; Adlof, 2007), which is rather an unusual behavior not known for other HPLC modes, where just the opposite behavior is common. The magnitude of this effect is directly related to the DB number and is more evident with *cis*-DB (Adlof and List, 2004). A possible explanation for this strange behavior has been proposed by Adlof (Adlof and List, 2004) based on the different stability of the acetonitrile complex with silver ions, which is probably exothermic and thereby less stable at higher temperatures, which allows an increased number of interactions for the analyte with silver ions at higher separation temperatures, resulting in higher retention.

Within a certain range, a temperature decrease causes lower retention in hexane−acetonitrile mobile phases, as demonstrated for FAME (Adlof, 2007) and TG (Adlof and List, 2004; Adlof, 2007). The retention of FAME standards decreases with decreasing temperature from 20 to −10°C; however, it significantly rises with a further temperature decrease (−20°C). A similar trend is observed for TG, but the retention behavior changes at 0°C. This behavior is not observed in chlorinated solvent systems (Adlof and List, 2004). The sudden increase in retention times at very low temperature can be

explained by several temperature-related factors (Adlof, 2007): (1) solubility of the sample in the mobile phase, (2) solubility of acetonitrile in hexane, (3) changes in the flexibility/3D configuration of the analyte or stationary phase. Another possible explanation is that the number of unsaturated molecules coordinated in the complex with the silver ion depends on the temperature, whereas only one unsaturated molecule forms the complex at 25°C in comparison to two coordinated molecules at 0°C (Winstein and Lucas, 1938). Temperature gradients (Adlof, 2007) could be used for the optimization of chromatographic resolution of complex FAME or TG, instead of the more common solvent composition gradient, but in our best knowledge this idea has not yet been used in any published paper.

4. SILVER-ION HIGH-PERFORMANCE LIQUID CHROMATOGRAPHY IN TWO-DIMENSIONAL HIGH-PERFORMANCE LIQUID CHROMATOGRAPHY—MASS SPECTROMETRY

The typical approach for increasing peak capacity is the use of two-dimensional (2D) HPLC, where the arrangement may be either off-line (Dugo et al., 2004, 2005, 2006a,b,c; Holčapek et al., 2009; Laakso and Christie, 1991) or online (Dugo et al., 2006a,b,c; Mondello et al., 2005; van der Klift et al., 2008; Wei et al., 2013). NARP is mostly used in the first dimension for off-line coupling (Dugo et al., 2004, 2005, 2006a,b,c; Holčapek et al., 2009), whereas the reversed arrangement is more typical for online comprehensive 2D (Dugo et al., 2006a,b,c; Mondello et al., 2005; van der Klift et al., 2008). The absence of any paper with Ag-HPLC mode used in the second dimension for online separation indicates that Ag-HPLC is not convenient for fast 1 min analysis required in such a setup. van der Klift et al. (2008) have reported a focusing effect in the second dimension because the second dimension solvent mixture (methanol—methyl-*tert*-butyl ether, 70:30) has a higher elution strength than the first dimension solvent mixture (acetonitrile—methanol). Online separation enables the fast separation of TGs in two chromatographic modes without the intervention of the operator and allows possible automation, whereas an off-line setup requires fraction collection in the first dimension with their subsequent analysis in the second dimension. The off-line approach is more laborious, but the resolution in both modes can be fully optimized without the limitation in 2D dictated by the modulation time (Fig. 4.2). By the way, regioisomeric separations have been reported only in the off-line arrangement (Dugo et al., 2004, 2006a,b,c; Holčapek et al., 2009).

Online and off-line Ag-SFC and NARP—HPLC coupling have been applied for the analysis of TG in fish oil, where off-line mode gives much better performance for complex samples (Francois et al., 2010). Another impressive example of comprehensive stop-flow and off-line multidimensional LC/MS with Ag and RP separation modes is the identification of 250 TGs in menhaden fish oil (Beccaria et al., 2015).

5. RETENTION BEHAVIOR

5.1 FATTY ACIDS AND THEIR DERIVATIVES

FAs are an important lipid class because of their functions in a human body. They are the main constituents of complex lipids, governing their retention behavior in Ag-HPLC because their DBs form complexes with silver ions. The separation of FAs in their free form using Ag-HPLC is feasible, but in

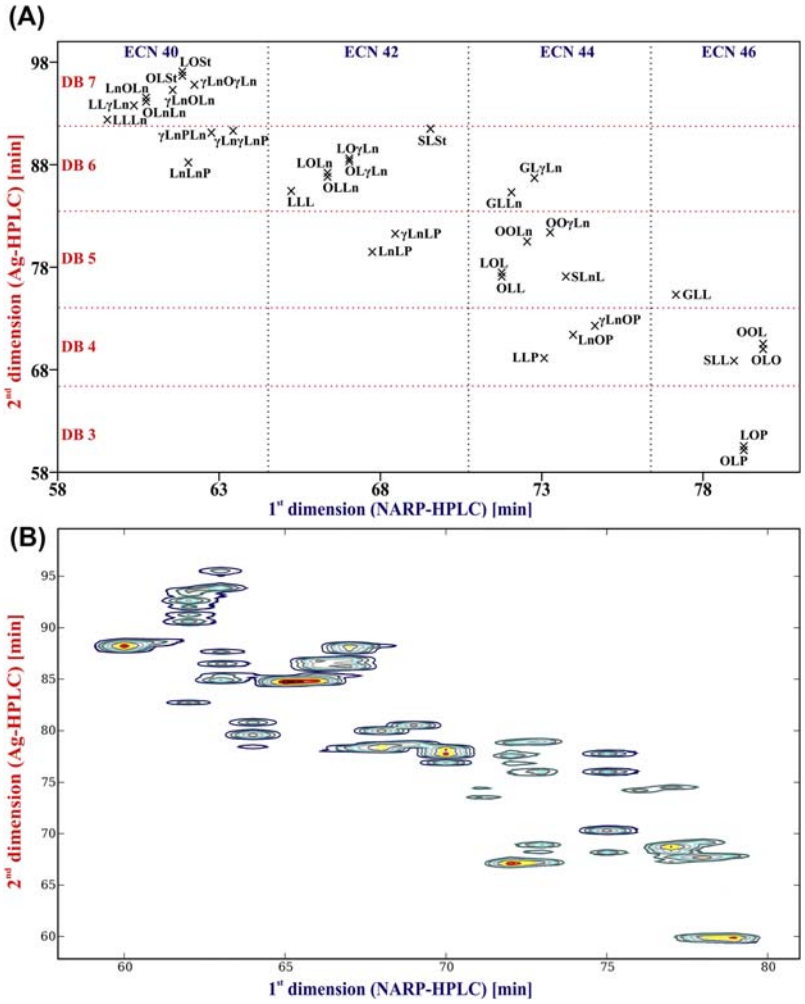

FIGURE 4.2

Off-line two-dimensional chromatograms of blackcurrant oil using nonaqueous reversed-phase (NARP) in the first dimension and silver-ion mode in the second dimension after fraction collection each minute: (A) dot plot with the peak identification, double bond (DB), and equivalent carbon number (ECN) labeling, (B) contour plot showing peak intensities. *Ag-HPLC*, silver-ion high-performance liquid chromatography.

Reprinted with permission from Holčapek, M., Velínská, H., Lísa, M., Česla, P., 2009. Orthogonality of silver-ion and non-aqueous reversed-phase HPLC/MS in the analysis of complex natural mixtures of triacylglycerols. J. Sep. Sci. 32, 3672–3680.

most cases they are separated as FAME or other derivatives (Nikolova-Damyanova, 2009). In general, retention times of FAs in Ag-HPLC are determined by the DB number, their *cis*/*trans* configuration, and the positions of DB in fatty acyl chains. There is no direct proportionality between retention times of FA and DB number, but in general, retention times of FAs increase with the increasing number of DB. For

example, Δ9,12−18:2 is retained about 3 times longer than a corresponding Δ9−18:1 homolog, Δ9,12,15−18:3 is retained 2.5 times more than Δ9,12−18:1, and Δ5,8,11,14,17−20:5 is retained 1.5 times more than Δ5,8,11,14−20:4 (Nikolova-Damyanova et al., 1992).

The complex of silver ions with *cis*-DB is stronger than with *trans*-isomers, and therefore *cis*-FA isomers are retained more strongly than *trans*-isomers. The retention behavior of polyunsaturated FAs containing *trans*-DB is given by the number and positions of *trans*-DB in the fatty acyl chain. Retention times of FAs decrease with the increasing number of *trans*-DB (Toschi et al., 1993; Adlof, 1994; Adlof and Lamm, 1998; Christie and Breckenridge, 1989; Phillips et al., 1997). The retention order of 18:3 FA isomers as methyl (Adlof, 1994) and phenacyl esters (Juaneda et al., 1994) is the following (Fig. 4.3):

$$\Delta 9t,12t,15t << \Delta 9t,12c,15t < \Delta 9c,12t,15t < \Delta 9t,12t,15c << \Delta 9c,12t,15c < \Delta 9t,12c,15c < \Delta 9c,12c,15t << \Delta 9c,12c,15c.$$

The stability of FA complexes with silver ions during the chromatographic process is also influenced by their position(s) in the fatty acyl chain and the number of methylene units between two DB. Conjugated dienes with various configurations and positions of DB in the fatty acyl chain are always eluted prior to *cis*-monoenes (Adlof and Lamm, 1998; Momchilova and Nikolova-Damyanova, 2000a,b,c). FAs with isolated DB are retained more strongly than FAs with methylene-interrupted DB

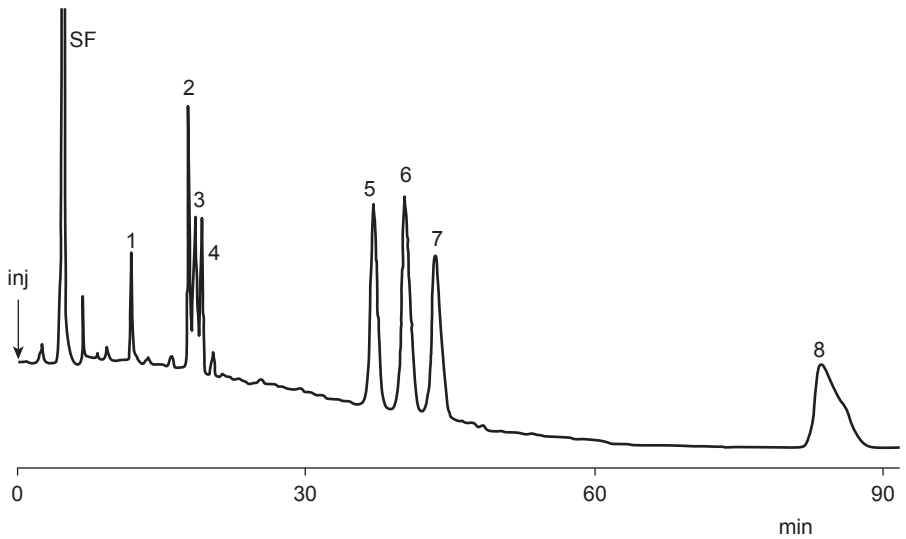

FIGURE 4.3

Separation of fatty acids phenacyl esters of C18:3 *cis*/*trans* geometrical isomers by silver-ion high-performance liquid chromatography. Peak annotation: SF—solvent front, 1—Δ9*t*,12*t*,15*t*, 2—Δ9*t*,12*c*,15*t*, 3—Δ9*c*,12*t*,15*t*, 4—Δ9*t*,12*t*,15*c*, 5—Δ9*c*,12*t*,15*c*, 6—Δ9*t*,12*c*,15*c*, 7—Δ9*c*,12*c*,15*t*, 8—Δ9*c*,12*c*,15*c*.

Reprinted with permission from Juaneda, P., Sebedio, J.L., Christie, W.W., 1994. Complete separation of the geometrical-isomers of linolenic acid by high-performance liquid – chromatography with a silver ion column. HRC – J. High Res. Chromatog. 17, 321–324.

(Nikolova-Damyanova et al., 1992). The series of positional isomers of C18:1 and C18:2 (Nikolova-Damyanova et al., 1992) or conjugated C18:2 (Delmonte et al., 2005) has been studied and their relative retention factors (k) were plotted against DB positions. The retention behavior of all series of isomers is similar, giving sinusoidal curves of k values of individual isomers. In general, FAs with the first DB at C_5—C_7 are the most strongly retained.

Although the fatty acyl chain length is supposed to have no effect in Ag-HPLC, FAs with longer chains are eluted slightly earlier than FAs with short chains (Juaneda et al., 1994). This phenomenon can be ascribed either to the normal-phase effect occurring in silica-based silver-loaded columns (Adlof, 1997) or to the lower complex stability for longer alkyl chains (Lucas et al., 1943; Winstein and Lucas, 1938). Similar behavior is reported for TG (Lísa et al., 2009a,b; Holčapek et al., 2010). The retention of various FA derivatives has been tested, i.e., short chain alkenyl esters (Nikolova-Damyanova et al., 1995a,b), benzyl and phenacyl esters (Nikolova-Damyanova et al., 1996), phenethyl, phenacyl and *p*-methoxyphenacyl esters (Momchilova et al., 1998), and 2-naphthacyl, 9-anthrylmethyl and 2-naphthylmethyl esters (Momchilova and Nikolova-Damyanova, 2000a,b,c). The elution order is the same for all derivatives, but the type of derivative affects the selectivity, mainly for positional isomers of FAs. *p*-Methoxyphenacyl esters provide the best selectivity for positional isomers of FAs, enabling separation according to the position of DB and the chain length. Changing the composition of the mobile phase can reverse the retention order, as demonstrated by the example of *p*-methoxyphenacyl esters, when 2-propanol was replaced by acetonitrile in dichloromethane-based mobile phases (Momchilova and Nikolova-Damyanova, 2000a,b,c). Conjugated linoleic acid isomers have been separated by Ag-HPLC and further structurally characterized by the inline combination of ozonolysis reaction and MS study of their fragmentation behavior (Sun et al., 2013).

5.2 TRIACYLGLYCEROLS

When retention rules described for FAs and their simple derivatives are compared with TGs, the complexity significantly increases because three FAs are present in the TG molecule, and they may occupy three different stereochemical positions, which results in an enormous number of combinations described by an equation $N = 1/2\ (n^3 + n^2)$, counting all isomers except for enantiomers. In case of a relatively simple natural lipidome, we can find at least 10 different FAs, which result in 550 combinations for TGs. Of course, not all combinations are present because only certain routes are preferred in the biosynthesis, but nevertheless it is a challenging task for an analytical chemist. The retention in Ag-HPLC is governed dominantly by a single molecular property, the nature of its unsaturation, i.e., the number, geometry (*cis* vs. *trans*) (Adlof and List, 2004; Holčapek et al., 2009, 2010; Adlof et al., 2002), and positions of DB (Laakso and Voutilainen, 1996; Lísa et al., 2009a,b; Holčapek et al., 2009, 2010). The steric availability (i.e., positional isomerism) of DBs (Schuyl et al., 1998; Adlof and List, 2004; Adlof, 1995; Lísa et al., 2009a,b; Holčapek et al., 2009, 2010) and the lengths of fatty acyl chains (Lísa et al., 2009a,b) are minor factors affecting the retention as well. The retention order of TG has been summarized for chlorinated mobile phases (Nikolova-Damyanova, 2009; Christie, 1988; Nikolova-Damyanova et al., 1995a,b) as follows:

$$\begin{aligned}\text{SaSaSa (DB} = 0) < \text{SaSaMo (1)} < \text{SaMoMo (2)} < \text{SaSaD (2)} < \text{MoMoMo (3)} < \text{SaMoD (3)} < \\ \text{MoMoD (4)} < \text{SaDD (4)} \leq \text{SaSaT (3)} < \text{SaMoT (4)} \leq \text{MoDD (5)} < \text{MoMoT (5)} < \text{SaDT (5)} \leq \\ \text{DDD (6)} < \text{MoDT (6)} \leq \text{SaTT (6)} < \text{DDT (7)} < \text{MoTT (7)} < \text{DTT (8)} < \text{TTT (9)},\end{aligned}$$

where symbols are defined as Sa for saturated, Mo for monounsaturated, D for diunsaturated, and T for triunsaturated FAs. Positional isomers are not distinguished. To avoid the confusion of using the same symbol in two meanings (i.e., S for both stearic acid and saturated, M for both myristic and monounsaturated), we use the symbol Sa for saturated and Mo for monounsaturated unlike the annotation used in most previous works. The retention behavior observed in our experiments in hexane–2-propanol–acetonitrile mobile phases (Lísa et al., 2009a,b; Holčapek et al., 2009, 2010) is mostly in a good agreement with published data with few exceptions. In mobile phases consisting of hexane–acetonitrile (Adlof, 1995; Dugo et al., 2004), heptane–acetonitrile (Macher and Holmqvist, 2001), or hexane–2-propanol–acetonitrile (Lísa et al., 2009a,b; Holčapek et al., 2009, 2010), the retention order of all TG follows the rule that an increasing number of DB means longer retention, while one exception is reported above for DMoMo (4) < DDSa (4) ≤ SaSaT (3). The explanation of changed retention patterns probably lies in the different mobile-phase composition, which affects the retention mechanism. The alkyl chain length has a small effect on the retention, but it does not change the retention order. Fig. 4.4 highlights this effect for TG with saturated FAs from C7:0 to C22:0, where TG with longer chains elute earlier (Holčapek et al., 2010). For TG of the LLSa type found in sunflower oil, the retention decrease in the LLSa series is ~0.4 min per two methylene units (Lísa et al., 2009a,b). The analysis of a randomized mixture containing six different TGs (PPP, SSS, OOO, LLL, LnLnLn, and AAA) and of numerous plant oils (Lísa et al., 2009a,b; Holčapek et al., 2009, 2010)

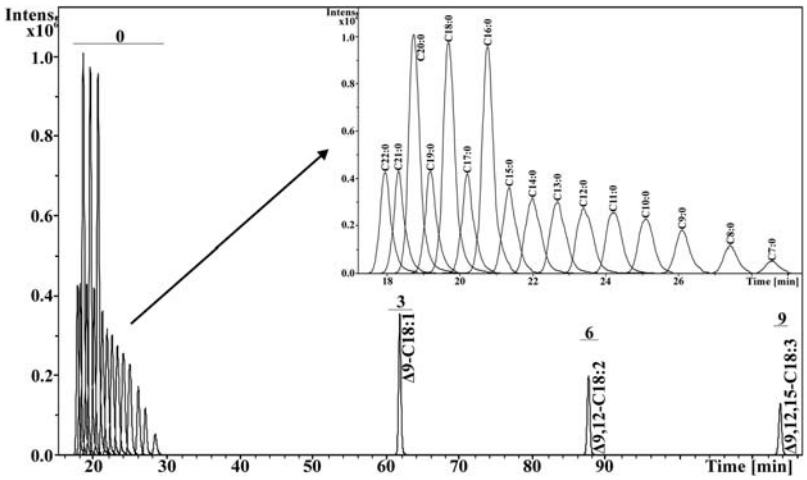

FIGURE 4.4

Ag-HPLC/APCI-MS chromatogram of monoacid triacylglycerols standards. Numbers correspond to the double bonds number. Inset zoom shows the resolution of saturated TG from C7:0 to C22:0. Concentrations of all standards are identical except for C16:0, C18:0, and C20:0 with doubled concentrations. *Ag-HPLC*, silver-ion high-performance liquid chromatography; *APCI*, atmospheric pressure chemical ionization; *MS*, mass spectrometry.

Reprinted with permission from Holčapek, M., Dvořáková, H., Lísa, M., Girón, A.J., Sandra, P., Cvačka, J., 2010. Regioisomeric analysis of triacylglycerols using silver-ion liquid chromatography-atmospheric pressure chemical ionization mass spectrometry: comparison of five different mass analyzers. J. Chromatogr. A 1217, 8186–8194.

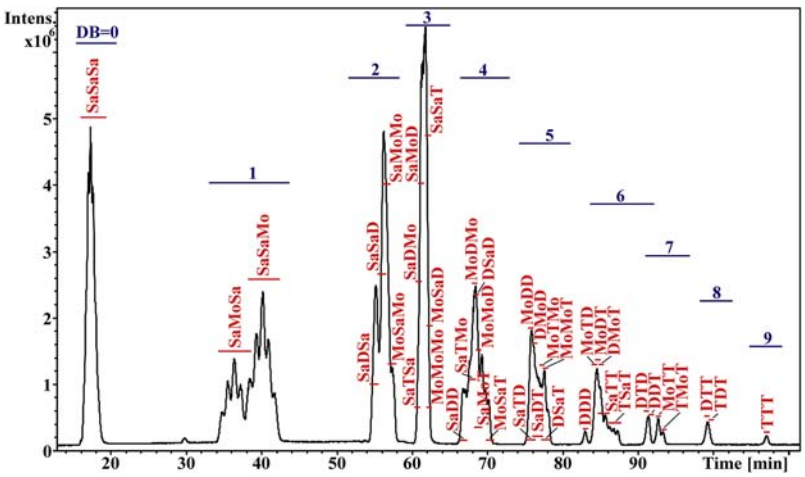

FIGURE 4.5

Ag-HPLC/APCI-MS chromatogram of the randomized mixture of PPP, SSS, OOO, LLL, LnLnLn, and AAA. Peak annotation: *D*, diunsaturated; *DB*, double bond number; *Mo*, monounsaturated; *Sa*, saturated; *T*, triunsaturated. *Ag-HPLC*, silver-ion high-performance liquid chromatography; *APCI*, atmospheric pressure chemical ionization; *MS*, mass spectrometry.

Redrawn with permission from Holčapek, M., Velínská, H., Lísa, M., Česla, P., 2009. Orthogonality of silver-ion and non-aqueous reversed-phase HPLC/MS in the analysis of complex natural mixtures of triacylglycerols. J. Sep. Sci. 32, 3672–3680.

enabled generalization of the retention order of TG, including positional isomers, valid in hexane−2-propanol−acetonitrile mobile phases (Fig. 4.5):

$$\text{SaSaSa (DB} = 0) << \text{SaMoSa (1)} < \text{SaSaMo (1)} << \text{SaDSa (2)} < \text{SaSaD (2)} \leq \text{SaMoMo (2)} < \text{MoSaMo (2)} << \text{SaTSa (3)} \leq \text{SaDMo (3)} \leq \text{SaMoD (3)} < \text{SaSaT (3)} \leq \text{MoSaD (3)} \leq \text{MoMoMo (3)} << \text{SaDD (4)} < \text{SaTMo (4)} \leq \text{MoDMo (4)} \leq \text{DSaD (4)} \leq \text{MoMoD (4)} \leq \text{SaMoT (4)} < \text{MoSaT (4)} << \text{SaTD (5)} \leq \text{MoDD (5)} \leq \text{DMoD (5)} \leq \text{SaDT (5)} \leq \text{MoTMo (5)} \leq \text{MoMoT (5)} \leq \text{DSaT (5)} << \text{DDD (6)} < \text{MoTD (6)} \leq \text{MoDT (6)} \leq \text{DMoT (6)} \leq \text{SaTT (6)} < \text{TSaT (6)} << \text{DTD (7)} \leq \text{DDT (7)} < \text{MoTT (7)} < \text{TMoT (7)} << \text{DTT (8)} \leq \text{TDT (8)} << \text{TTT (9)}.$$

We believe that this order is fully applicable for similar mobile phases containing acetonitrile (or propionitrile) in hexane (or heptane) with or without the addition of 2-propanol.

The randomized mixture containing monoacid TG differing only in the geometry of their DB (oleic acid, Δ9*c*-C18:1, O vs. elaidic acid, Δ9*t*-C18:1, E) shows (Holčapek et al., 2009) that these *cis*/*trans* regioisomers cannot be separated in NARP mode, but the partial separation of regioisomers and the full separation of other isobaric TG is achieved with Ag-HPLC/MS (Fig. 4.6) with the following retention order:

$$\text{EEE} << \text{EOE} < \text{OEE} << \text{OOE} < \text{OEO} << \text{OOO}.$$

This retention order is identical to that already published (Dobson et al., 1995), but additionally with the partial resolution of regioisomers. Physicochemical properties of *trans*-FAs are closer to

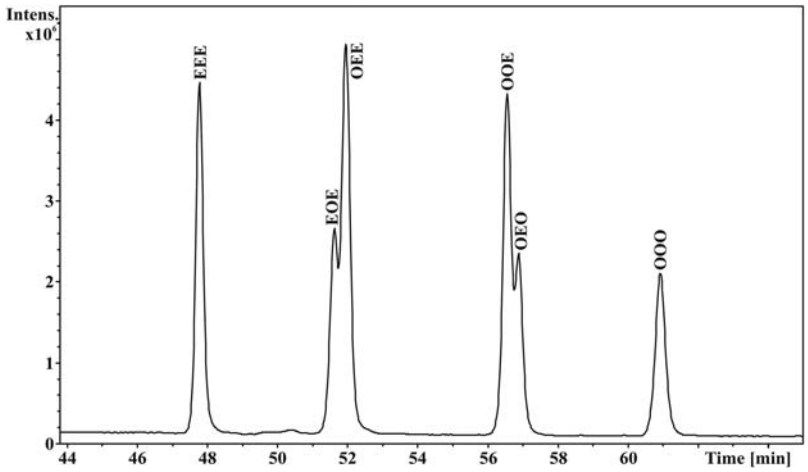

FIGURE 4.6

HPLC/APCI-MS chromatogram of the randomized mixture of OOO (Δ9-C18:1) and EEE (Δ9*t*-C18:1) using Ag-HPLC with three ChromSpher Lipids columns with a total length of 75 cm, flow rate 1 mL/min, column temperature 25°C, gradient of hexane—2-propanol—acetonitrile. *Ag-HPLC*, silver-ion high-performance liquid chromatography; *APCI*, atmospheric pressure chemical ionization; *MS*, mass spectrometry.

Reprinted with permission from Holčapek, M., Velínská, H., Lísa, M., Česla, P., 2009. Orthogonality of silver-ion and non-aqueous reversed-phase HPLC/MS in the analysis of complex natural mixtures of triacylglycerols. J. Sep. Sci. 32, 3672—3680.

saturated FAs because of the linear arrangement of alkyl chains containing *trans*-DB. Therefore, the retention of TG containing *trans*-FAs is slightly higher in NARP mode, but significantly lower in Ag-HPLC, compared to *cis*-FAs. This effect is more pronounced for outer *sn*-1/3 positions, because of better steric availability.

The effect of DB position in TG can be illustrated by the example of linolenic (Ln, Δ9,12,15-C18:3) versus gamma-linolenic (γLn, Δ6,9,12-C18:3) acids. LnLnLn has higher retention than γLnγLnγLn in most mobile phases [acetone—acetonitrile (Leskinen et al., 2008), chlorinated solvents (Laakso and Voutilainen, 1996)], whereas the reverse order is reported for the hexane—2-propanol—acetonitrile mobile phase (Holčapek et al., 2010). This example shows that the retention mechanism in Ag-HPLC is rather complex and not fully understood so far. If only one FA in a TG molecule differs in the DB position, then only peak broadening is observed because of small differences in retention times of isomers differing in the DB position only. Unlike FAs and their derivatives, the systematic study of the retention behavior of TG containing unusual DB positions is still missing. Neff et al. (1994) have shown that TG containing a triple bond (crepenynic, Δ9,12triple-C18:2) elute later in comparison to analogous TG containing DB at the same position (linoleic, Δ9,12-C18:2).

6. REGIOISOMERIC DETERMINATION OF TRIACYLGLYCEROLS

The position of FAs on the glycerol skeleton is very important from a nutritional point of view because enzymes in the human or animal body selectively hydrolyze preferred positions, which may result in

different biological availability of FAs depending on their stereochemical positions. This differentiation may be especially important in the case of essential FAs, which cannot be synthesized in the organism. The analysis of TG regioisomers is quite challenging because regioisomers have the identical elemental composition, identical ions in mass spectra, and in general very similar physicochemical properties. Ag-HPLC has the ability to resolve TG regioisomers. At present, the following techniques are the most convenient for the regioisomeric analysis: (1) Ag-HPLC (Schuyl et al., 1998; Adlof and List, 2004; Adlof, 1995, 2007; Dugo et al., 2004, 2006a,b,c; Lísa et al., 2009a,b; Holčapek et al., 2009, 2010), (2) MS (Holčapek et al., 2003, 2005, 2009; Lísa and Holčapek, 2008; Leskinen et al., 2008; Byrdwell, 2001, 2005; Byrdwell et al., 1996; Fauconnot et al., 2004; Jakab et al., 2003; Lísa et al., 2009a,b; Mottram et al., 1997, 2001; Mottram and Evershed, 1996), (3) enzymatic reactions (e.g., pancreatic lipase, phospholipase A_2) (Janssen et al., 2006) followed by some analytical technique (e.g., Ag-HPLC), and (4) nuclear magnetic resonance (NMR) spectroscopy (Standal et al., 2009). Each technique has certain limitations. NMR provides an absolute answer based on small differences in chemical shifts, but the practical applicability is severely limited by the need of pure compounds in milligram amounts, which is hard to achieve in most cases. Enzyme lipases with various levels of selectivity toward stereochemical positions of particular FAs are known, but their application in a quantitative manner is not straightforward because exact values of enzymatic stereoselectivity may not be known and they may also depend on experimental conditions, alkyl chain length, and DB number and positions. Furthermore, another analytical technique (e.g., HPLC) is required to detect the products of enzymatic hydrolysis. In mass spectra of regioisomers, different ratios of $[M + H{-}R_iCOOH]^+$ ions are observed for *sn*-1/3 versus *sn*-2 positions, but regioisomeric standards should be measured first for reliable quantitation. Chromatographic peak areas can be directly used for the quantitation because peak areas of regioisomers directly correspond to regioisomeric ratios (Lísa et al., 2009a,b; Holčapek et al., 2009). The regioisomeric separation is also feasible in NARP mode using the multiple column coupling and very long retention times about 100–300 min, depending on the DB number (Momchilova et al., 2004, 2006). Of course, this approach is not yet applicable for routine use, but new developments in RP column technology (for example sub-2 μm or porous shell particles) could enable such analysis within an acceptable retention window.

6.1 STANDARDS OF REGIOISOMERS

The severe problem in the regioisomeric analysis of TG is the lack of standards. A limited range of standards is commercially available mainly from Larodan (Malmö, Sweden) and some other suppliers. Their range is limited and prices are rather high for small amounts probably because of difficult preparative isolation. For this reason, Evans et al. (Li and Evans, 2005) have developed a synthetic procedure for regioisomeric TG starting from regioisomerically pure 1,3-diacylglycerols or 2-monoacylglycerols dissolved in chloroform, then 4-dimethylaminopyridine and selected FA chlorides are added dropwise with continuous stirring for 30 min, which yields pure TG regioisomers. This procedure has been used for synthesis of a wide range of regioisomeric series OXO/YOY (Li and Evans, 2005), PXP/YPY (Li et al., 2006), LXL/YLY, and AXA/YAY (Gakwaya et al., 2007), where X and Y are saturated FAs from C4:0 to C24:0 and unsaturated FAs containing one to six DBs. They report trends in ratios of fragment ions of regioisomers depending on the alkyl chain length and the DB number. The disadvantage of this approach is that the preparation of a wider series of regioisomers is laborious.

Randomization (i.e., chemical interesterification) is a common industrial process used for the modification of physicochemical properties of TG mixtures in food and cosmetic products (Akoh and Min, 2002). In our previous work (Lísa et al., 2009a,b), we have modified this procedure for the microscale range (low milligram amounts), which overcomes the lack of pure regioisomeric standards by the synthesis of regioisomeric mixtures having a well-defined composition. Theoretically, the randomization of binary mixtures of equal amounts of monoacid TG $R_1R_1R_1$ and $R_2R_2R_2$ should provide eight combinations of TGs at identical concentrations: $R_1R_1R_1$, $R_1R_2R_1$, $R_1R_1R_2$, $R_2R_1R_1$, $R_1R_2R_2$, $R_2R_2R_1$, $R_2R_1R_2$, and $R_2R_2R_2$. In practice, enantiomers $R_1R_1R_2$ versus $R_2R_1R_1$ and $R_1R_2R_2$ versus $R_2R_2R_1$ cannot be resolved in a nonchiral environment, therefore we obtain the following concentration ratios (in parenthesis) for initial TG and two regioisomeric pairs: $R_1R_1R_1$ (1), $R_1R_2R_1$ (1), $R_1R_1R_2 + R_2R_1R_1$ (2), $R_1R_2R_2 + R_2R_2R_1$ (2), $R_2R_1R_2$ (1), $R_2R_2R_2$ (1). Data obtained for a range of randomization reactions have proven that the reaction provides really a random distribution of statistically expected regioisomers (Lísa et al., 2009a,b; Holčapek et al., 2009, 2010). Fig. 4.7 shows the chromatogram of a ternary randomization mixture of OOO, LnLnLn, and PPP providing six regioisomeric doublets at concentration ratios 2:1 and one triplet OLnP/LnOP/OPLn with identical concentrations. Standards of all common and relatively rare monoacid TG are commercially available, and therefore tailored randomization can produce desired regioisomeric combinations. The randomization reaction can be performed also with FAs, if the TG standard is not available.

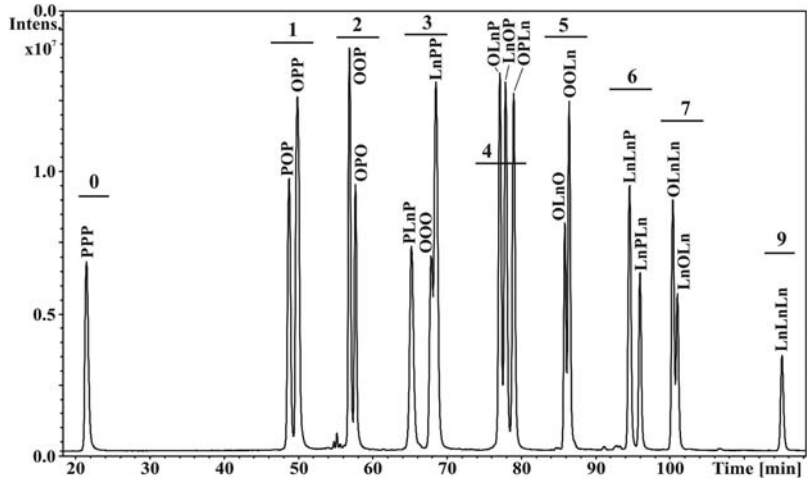

FIGURE 4.7

Ag-HPLC/APCI-MS analysis of randomized mixture of PPP/OOO/LnLnLn. *Ag-HPLC*, silver-ion high-performance liquid chromatography; *APCI*, atmospheric pressure chemical ionization; *MS*, mass spectrometry.

Reprinted with permission from Lísa, M., Holčapek, M., Boháč, M., 2009a. Statistical evaluation of triacylglycerol composition in plant oils based on high-performance liquid chromatography – atmospheric pressure chemical ionization mass spectrometry data. J. Agr. Food Chem. 57, 6888–6898; Lísa, M., Velínská, H., Holčapek, M., 2009b. Regioisomeric characterization of triacylglycerols using silver-ion HPLC/MS and randomization synthesis of standards. Anal. Chem. 81, 3903–3910.

6.2 SILVER-ION HIGH-PERFORMANCE LIQUID CHROMATOGRAPHY/MASS SPECTROMETRY OF TRIACYLGLYCEROLS REGIOISOMERS

The strength of interaction between silver ions and DBs also depends on the spatial availability or hindrance of DB on the molecular skeleton, which can result in the separation of regioisomers with Ag-HPLC. The effect of a polar organic modifier in hexane on the regioisomeric resolution is absolutely critical. Based on our study of effects of different solvents (Lísa et al., 2009a,b) on the regioisomeric resolution and also a comprehensive literature search, the following statements can be made. Chlorinated solvents have been used in numerous works reporting excellent overall separation, but we have not found any papers reporting the regioisomeric resolution. Almost all papers (Adlof and List, 2004; Adlof, 1995; Dugo et al., 2004, 2006a,b,c; Macher and Holmqvist, 2001; Lísa et al., 2009a,b; Holčapek et al., 2009, 2010; Adlof, 2007; Smith et al., 1981) published on the regioisomeric resolution of TG are based on mobile phases containing acetonitrile in hexane (or heptane), except for one work measured on a silver complexation column in toluene, hexane, and ethylacetate (Schuyl et al., 1998). When acetonitrile is replaced by other solvents (e.g., 2-propanol, ethanol, and ethylacetate) (Muller et al., 2006; Lísa et al., 2009a,b), peak shapes and the theoretical number of plates may even be increased for certain compositions, but the regioisomeric resolution is lost or at least dramatically reduced. We believe that acetonitrile plays an essential role in the formation of the complex with silver ions. This hypothesis is supported by experiments with propionitrile (Muller et al., 2006; Lísa et al., 2009a,b), where similar complex formation can be expected as well. No regioisomeric resolution is achieved for fully saturated TG (Lísa et al., 2009a,b; Holčapek et al., 2009).

For our studies of retention behavior of regioisomeric TG, randomized mixtures of monoacid TG have been used. The baseline separation for regioisomers containing up to three DBs and at least partial separation for TG with four to eight DBs can be achieved (Adlof, 1995; Lísa et al., 2009a,b; Holčapek et al., 2010). As a rule, the bigger the difference in the DB number of FAs means better separation of corresponding TG regioisomers, e.g., the baseline separation of P/L and P/Ln regioisomers is easily achieved (Lísa et al., 2009a,b). The example of partial resolution of LnOLn/OLnLn regioisomers (Fig. 4.7) containing seven DBs shows that the number of DB is probably not a limiting factor, but the critical requirement for the successful separation of highly polyunsaturated regioisomeric TG is the difference in the DB number between two FAs. Polyunsaturated TG containing FAs differing only by one DB are so-called critical pairs, e.g., O/L (peak splitting) and L/Ln (only peak shoulder). FAs differing by two and more DBs are well separated for TG containing up to four DBs and partially for five and more DBs. Some improvement may be expected with further extension of column length or temperature increase, at the expense of longer retention times and also higher costs of multiple columns.

The retention order of regioisomers follows the rule that more DBs in the *sn*-1/3 positions mean a stronger interaction with silver ions embedded in the stationary phase, which results in higher retention compared with regioisomers having the same DB number in the middle *sn*-2 position. Regioisomers of XYO/YXO and XYL/YXL types (X and Y are saturated FAs) are not resolved. A highly complex retention pattern is observed in the case of TG containing DB positional isomers, such as linolenic (Δ9,12,15-C18:3) and γ-linolenic (Δ6,9,12-C18:3) acids. When the only difference between two TGs is in DB positions for *sn*-2 FA (OLnO vs. OγLnO), then no visible chromatographic separation is observed (Holčapek et al., 2010). On the other hand, the same difference occurring in *sn*-1/3 positions (OOLn vs. OOγLn) leads to very good resolution, with the difference of retention times about 1.6 min.

The generally accepted opinion is that unsaturated FAs (mainly linoleic) preferentially occupy the *sn*-2 position in plant oils, whereas it is just the opposite for animal fats, where unsaturated FAs are found mainly in *sn*-1/3 positions. We have applied (Lísa et al., 2009a,b) our method for the quantitation of *sn*-2 occupation of representative plant oil (sunflower) and animal fat (lard) samples, as compared in Table 4.1, with other literature data for TG composed of palmitic, oleic, and linoleic acids. The positional preference is very strong because ratios of regioisomeric doublets are close to 100% in accordance with other papers (Leskinen et al., 2007; Leskinen, 2010; Herrera et al., 2010). An interesting example is TG composed of P, O, and L, where the *sn*-2 occupation preference for sunflower oil is in the order of increasing DB number (OLP/LOP/OPL = 63/36/1) in contrast to just the opposite preference of the lard sample (OLP/LOP/OPL = 3/12/85). This clearly shows the potential of regioisomeric analysis in the determination of food authenticity (plant vs. animal sources).

6.3 MASS SPECTROMETRIC IDENTIFICATION AND QUANTITATION OF TRIACYLGLYCEROLS REGIOISOMERS

Mass spectra of TG provide two basic types of ions sufficient for the structural assignment (Byrdwell et al., 1996; Mottram et al., 1997; Byrdwell and Emken, 1995): (1) molecular adducts with protons $[M + H]^+$ or other small cations depending on the mobile-phase composition, typically $[M + Na]^+$ or $[M + NH_4]^+$ and (2) fragment ions formed by the neutral loss (NL) of FAs $[M + H{-}R_iCOOH]^+$. In the case of conventional electron ionization (EI), the molecular radical cation $M^{+\bullet}$ provides fragment ions $[M{-}R_iCOO]^+$ by NL from all three stereochemical positions, but the NL from *sn*-2 is less preferred, as shown for the first time in the pioneering work published in 1964 (Barber and Merren, 1964). By the way, ion annotations $[M + H{-}R_iCOOH]^+$ and $[M{-}R_iCOO]^+$ are numerically identical, but these annotations show a different way of fragment ion formation. The same behavior has been reported later for soft ionization techniques, such as atmospheric pressure chemical ionization (APCI) (Mottram and Evershed, 1996; Mottram et al., 1997, 2001; Holčapek et al., 2003; Fauconnot et al., 2004), electrospray ionization (Malone and Evans, 2004; Li and Evans, 2005; Li et al., 2006; Gakwaya et al., 2007; Herrera et al., 2010; Leveque et al., 2010), and matrix-assisted laser desorption/ionization (Pittenauer and Allmaier, 2009). The relative ratio of fragment ions $[M + H{-}R_iCOOH]^+$ enables one to differentiate FAs in the side *sn*-1/3 positions versus the middle *sn*-2 position because the NL from the *sn*-2 position, providing an $[M + H{-}R_2COOH]^+$ ion, has a lower relative abundance in comparison to $[M + H{-}R_1COOH]^+$ and $[M + H{-}R_3COOH]^+$ fragment ions (Mottram and Evershed, 1996; Mottram et al., 1997, 2001; Schuyl et al., 1998; Byrdwell, 2001; Holčapek et al., 2003, 2005; Jakab et al., 2003; Cvačka et al., 2006; Lísa et al., 2007a,b, 2009a,b; Leskinen et al., 2008), as illustrated in the example of regioisomers SLnO/SOLn/OSLn in Fig. 4.8. The simple approach just determines the prevailing FAs in the middle *sn*-2 position based on the lower relative abundance of the corresponding $[M + H{-}R_iCOOH]^+$ fragment ion (Mottram and Evershed, 1996; Mottram et al., 1997, 2001; Holčapek et al., 2003; Dugo et al., 2004; Lísa and Holčapek, 2008), but the type of FAs (mainly DB number and positions) (Holčapek et al., 2005; Li and Evans, 2005; Li et al., 2006; Gakwaya et al., 2007) also affects relative abundances of corresponding $[M + H{-}R_iCOOH]^+$ fragment ions. An interesting example of the strong effect of DB position is the ratio of $[R_1R_1]^+/[R_1R_2]^+$ fragment ions, which is completely reversed in the case of OOγLn unlike all other regioisomers (Holčapek et al., 2010). A more exact approach is based on the construction of calibration curves using identical standards of regioisomeric pairs mixed at different ratios (Holčapek et al., 2003; Jakab et al., 2003;

Table 4.1 Regioisomeric Occupation of *sn*-2 Position for Saturated (Palmitic), Monounsaturated (Oleic), and Diunsaturated (Linoleic) Fatty Acids in Triacylglycerols of Plant (Sunflower, Olive, and Palm) Oils and Animal Fat (Lard)

	Sunflower Oil			Olive Oil	Palm Oil	Lard	
Regioisomers	**Lísa et al. (2009a,b)**	**Leskinen (2010)**	**Herrera et al. (2010)**	**Herrera et al. (2010)**	**Leskinen (2010)**	**Lísa et al. (2009a,b)**	**Leskinen et al. (2007)**
POP/OPP	100/0	–	99/1	97/3	86/14	8/92	0/100
OOP/OPO	98/2	91/9	100/0	98/2	95/5	12/88	4/96
PLP/LPP	100/0	–	–	–	–	1/99	–
LLP/LPL	97/3	–	–	–	–	9/91	–
OLP/LOP/OPL	63/36/1	–	–	–	–	3/12/85	–

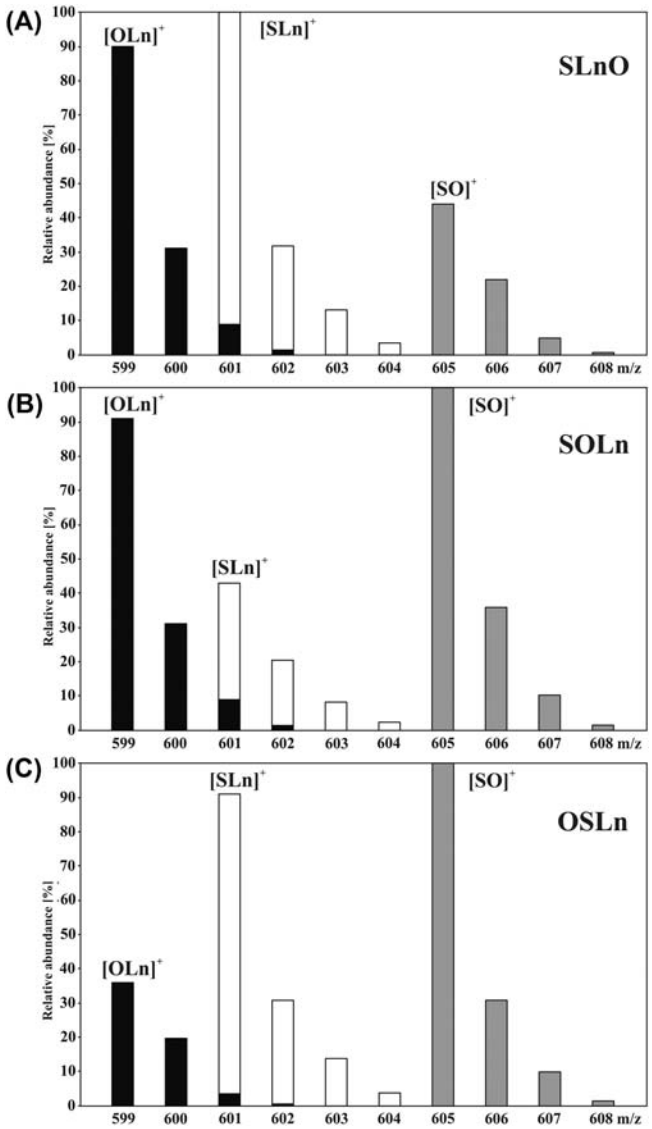

FIGURE 4.8

Normalized relative abundances of $[M + H{-}R_iCOOH]^+$ fragment ions in atmospheric pressure chemical ionization mass spectra of the regioisomeric triplet SLnO (A), SOLn (B), and OSLn (C).

Reprinted with permission from Holčapek, M., Dvořáková, H., Lísa, M., Girón, A.J., Sandra, P., Cvačka, J., 2010. Regioisomeric analysis of triacylglycerols using silver-ion liquid chromatography-atmospheric pressure chemical ionization mass spectrometry: comparison of five different mass analyzers. J. Chromatogr. A 1217, 8186–8194.

Fauconnot et al., 2004; Leskinen et al., 2007, 2008, 2010; Leskinen, 2010; Malone and Evans, 2004). In practice, this approach is time-consuming and also expensive because of prices of regioisomers and their limited availability. The literature data (Holčapek et al., 2010) measured on five different instruments can be used for the determination of the prevailing FAs in *sn*-2 position because the type of mass spectrometer has a relatively small effect on $[M + H{-}R_iCOOH]^+$ relative ratios for all tested instruments. The distribution of DB in individual FA chains is the governing factor for $[M + H{-}R_iCOOH]^+$ ratios. The main goal of our interinstrument comparison of APCI mass spectra of TG regioisomers has been to study to what extent are published ratios of $[M + H{-}R_iCOOH]^+$ ions applicable for different instruments and laboratories. Ratios of $[M + H{-}R_iCOOH]^+$ fragment ions strongly depend on the DB number and position in individual FAs, whereas the DB geometry and FA length have only minor influences. The data grouped according to the unsaturation level of individual FAs show a good correlation among values inside individual groups (Holčapek et al., 2010), especially considering the fact that differences in *cis*/*trans* isomerism (e.g., PEP vs. POP, EPP vs. OPP) or high differences in alkyl chain lengths (e.g., AOA vs. POP differs by eight carbon atoms) are negligible. On the other hand, positions of DB have a much stronger effect on $[M + H{-}R_iCOOH]^+$ ratios (Holčapek et al., 2010; Leskinen et al., 2008; Lísa et al., 2007a,b). The data for TG with a given unsaturation pattern can be generalized for other TG with the same unsaturation pattern, which can solve the lack of unusual standards but still provide accurate regioisomeric determination.

7. OTHER SILVER-ION HIGH-PERFORMANCE LIQUID CHROMATOGRAPHY/MASS SPECTROMETRY APPLICATIONS

Applications of Ag-HPLC/MS for TG, FAME, and other simple FA derivatives are well documented, but this technique is also applicable for unsaturated organic compounds, for example the analysis of underivatized sterols using ternary gradient elution with acetone, hexane, and acetonitrile (Shan and Wilson, 2002), vitamins in tissues of freshwater fish-feeding mammals (Kakela et al., 2002), wax esters in fish oils (Joh et al., 1995), and in jojoba oil and human hair extracts (Vrkoslav et al., 2013). Vrkoslav et al. (2013) reported the characterization of wax esters by Ag-HPLC/MS using hexane–acetonitrile–2-propanol mobile phases. The same trends in the retention behavior as for TG are recognized for the DB number, positions, and geometry. The analysis of phospholipids by Ag-HPLC would be highly desirable, but no acceptable compromise has been found so far between the mobile-phase composition and the efficient separation of intact phospholipids, unlike Ag-TLC (Stoll, 1996). Ag-HPLC has been used only for phospholipids after derivation, when the polar functional group is masked, as applied for sphingomyelins (Smith et al., 1981), phosphatidylethanolamines (Yeung et al., 1977), phosphatidylserines (Yeung et al., 1977), and phosphatidylinositols (Holub and Kuksis, 1971). The other possibility is the hydrolysis of phospholipids followed by esterification and then the analysis of FA derivatives, but no real Ag-HPLC application for intact phospholipids has been reported so far. Additional problems can arise from the presence of oxidized phospholipids in samples because functional groups formed during the oxidation of lipids can lead to irreversible retention on the silver-ion column, which can alter the retention characteristics of this column and reduce the column lifetime.

Applications in the area of organic chemistry have been reviewed recently by Mander and Williams (2016). Ag-HPLC has been used for the analysis of monounsaturated polyolefin oligomers in packaging materials and foods, followed by detailed characterization by multidimensional chromatography

(Lommatzsch et al., 2015). Guricza and Schrader (2015) applied Ag-HPLC coupled to ultrahigh-resolution MS for the analysis of complex asphaltene samples, which clearly confirms the potential of Ag-HPLC/MS even for the most complex analysis of unsaturated organic compounds.

8. CONCLUSIONS AND PERSPECTIVES

Ag-HPLC is a powerful liquid-phase separation technique for the characterization of TG, FAME, and other low to medium polar molecules differing in the number, geometry, and positions of DB. The introduction of hexane—acetonitrile mobile phases brings additional dimension in terms of the regioisomeric separation of glycerolipids. Ag-HPLC is the most reliable technique for regioisomeric quantitation. Reproducibility problems can be overcome by the addition of a third solvent miscible with both hexane and acetonitrile, for example 2-propanol. Possible introduction of silver-ion columns applicable for ultra-high performance liquid chromatography is highly desirable because of the relatively long retention times of the most demanding regioisomeric separations. A highly promising trend is the use of various configurations of 2D-HPLC, where Ag-HPLC can provide a high orthogonality to RP-HPLC, therefore 2D coupling Ag × RP is a natural choice for the comprehensive analysis of TG and other lipids. We believe that there is also a great potential of Ag-HPLC for the separation of other unsaturated molecules in addition to lipids, but this is still not fully explored.

The governing factor for the retention order in Ag-HPLC is the total number of DB, which causes the separation of complex samples into distinct groups differing in the DB number. The second parameter with comparable importance is the DB geometry, where the retention is significantly lower for *trans*-isomers because their conformation is closer to saturated chains in comparison to *cis*isomers. The positions of DB have a smaller effect on the retention and the smallest difference is observed for regioisomers, where DB in outer *sn*-1/3 positions cause slightly stronger retention compared to *sn*-2 regioisomers. The role of the mobile phase in Ag-HPLC is substantial, but complete understanding of the retention mechanism needs further experimental and computational studies. Moreover, separation temperature also shows unusual effects. In our opinion, these effects can be attributed, at least in part, to different lipid conformations, depending on the solvent composition and temperature, and subsequently the various extent of weak London forces among individual FA chains.

ACKNOWLEDGMENTS

This work was supported by the ERC CZ project No. LL1302 sponsored by the Ministry of Education, Youth and Sports of the Czech Republic.

REFERENCES

Adlof, R.O., 1994. Separation of cis and trans unsaturated fatty acid methyl-esters by silver ion high-performance liquid chromatography. J. Chromatogr. A 659, 95—99.

Adlof, R.O., 1995. Analysis of triacylglycerol positional isomers by silver ion high-performance liquid-chromatography. HRC — J. High Res. Chromatogr. 18, 105—107.

Adlof, R.O., 1997. Normal-phase separation effects with lipids on a silver ion high-performance liquid chromatography column. J. Chromatogr. A 764, 337−340.

Adlof, R., 2007. Analysis of triacylglycerol and fatty acid isomers by low-temperature silver-ion high performance liquid chromatography with acetonitrile in hexane as solvent: limitations of the methodology. J. Chromatogr. A 1148, 256−259.

Adlof, R., Lamm, T., 1998. Fractionation of cis- and trans-oleic, linoleic, and conjugated linoleic fatty acid methyl esters by silver ion high-performance liquid chromatography. J. Chromatogr. A 799, 329−332.

Adlof, R., List, G., 2004. Analysis of triglyceride isomers by silver-ion high-performance liquid chromatography − effect of column temperature on retention times. J. Chromatogr. A 1046, 109−113.

Adlof, R.O., Menzel, A., Dorovska-Taran, V., 2002. Analysis of conjugated linoleic acid-enriched triacylglycerol mixtures by isocratic silver-ion high-performance liquid chromatography. J. Chromatogr. A 953, 293−297.

Akoh, C.C., Min, D.B., 2002. Food Lipids: Chemistry, Nutrition, and Biotechnology. Marcel Dekker, New York.

Barber, M., Merren, T.O., 1964. The mass spectrometry of large molecules. 1. The triglycerides of straight chain fatty acids. Tetrahedron Lett. 5, 1063−1067.

Beccaria, M., Costa, R., Sullini, G., Grasso, E., Cacciola, F., Dugo, P., Mondello, L., 2015. Determination of the triacylglycerol fraction in fish oil by comprehensive liquid chromatography techniques with the support of gas chromatography and mass spectrometry data. Anal. Bioanal. Chem. 407, 5211−5225.

Bressan, G., Broggi, R., Lachi, M.P., Segre, A.L., 1967. Complexes of silver perchlorate with alpha omega-diolefins. J. Organomet. Chem. 9, 355−360.

Byrdwell, W.C., 2001. Atmospheric pressure chemical ionization mass spectrometry for analysis of lipids. Lipids 36, 327−346.

Byrdwell, W.C., 2005. The bottom-up solution to the triacylglycerol lipidome using atmospheric pressure chemical ionization mass spectrometry. Lipids 40, 383−417.

Byrdwell, W.C., Emken, E.A., 1995. Analysis of triglycerides using atmospheric-pressure chemical ionization mass-spectrometry. Lipids 30, 173−175.

Byrdwell, W.C., Emken, E.A., Neff, W.E., Adlof, R.O., 1996. Quantitative analysis of triglycerides using atmospheric pressure chemical ionization mass spectrometry. Lipids 31, 919−935.

Chatt, J., Duncanson, L.A., 1953. Olefin co-ordination compounds. 3. Infra-red spectra and structure − attempted preparation of acetylene complexes. J. Chem. Soc. 2939−2947.

Christie, W.W., 1987. A stable silver-loaded column for the separation of lipids by high-performance liquid-chromatography. J. High Res. Chromatog. 10, 148−150.

Christie, W.W., 1988. Separation of molecular-species of triacylglycerols by high-performance liquid- with a silver ion column. J. Chromatogr. 454, 273−284.

Christie, W.W., Breckenridge, G.H.M., 1989. Separation of cis-isomers and trans-isomers of unsaturated fatty acids by high-performance liquid-chromatography in the silver ion mode. J. Chromatogr. 469, 261−269.

Conacher, H.B.S., 1976. Chromatographic determination of cis-trans monoethylenic unsaturation in fats and oils − review. J. Chromatogr. Sci. 14, 405−411.

Correa, R.A., Ferraz, V., Medvedovici, A., Sandra, P., Cerne, K., David, F., 1999. Positional and configurational separation of fatty acid isomers by micro reversed-phase liquid chromatography with an Ag^{+}-containing mobile phase. J. Chromatogr. A 848, 83−93.

Cvačka, J., Hovorka, O., Jiroš, P., Kindl, J., Stranský, K., Valterová, I., 2006. Analysis of triacylglycerols in fat body of bumblebees by chromatographic methods. J. Chromatogr. A 1101, 226−237.

Cvetanović, R.J., Duncan, F.J., Falconer, W.E., Irwin, R.S., 1965. Secondary deuterium isotope effects on stability of silver ion-olefin complexes. J. Am. Chem. Soc. 87, 1827−1832.

Delmonte, P., Kataoka, A., Corl, B.A., Bauman, D.E., Yurawecz, M.P., 2005. Relative retention order of all isomers of cis/trans conjugated linoleic acid FAME from the 6,8- to 13,15-positions using silver ion HPLC with two elution systems. Lipids 40, 509−514.

Devries, B., 1962. Quantitative separations of lipid materials by column chromatography on silica impregnated with silver nitrate. Chem. Ind. 1049−1050.

Dewar, J.S., 1951. A review of the pi-complex theory. Bulletin De La Societe Chimique De France 18, C71−C79.

Dobson, G., Christie, W.W., Nikolova-Damyanova, B., 1995. Silver ion chromatography of lipids and fatty acids. J. Chromatogr. B 671, 197−222.

Dugo, P., Favoino, O., Tranchida, P.Q., Dugo, G., Mondello, L., 2004. Off-line coupling of non-aqueous reversed-phase and silver ion high-performance liquid chromatography-mass spectrometry for the characterization of rice oil triacylglycerol positional isomers. J. Chromatogr. A 1041, 135−142.

Dugo, P., Kumm, T., Lo Presti, M., Chiofalo, B., Salimei, E., Fazio, A., Cotroneo, A., Mondello, L., 2005. Determination of triacylglycerols in donkey milk by using high performance liquid chromatography coupled with atmospheric pressure chemical ionization mass spectrometry. J. Sep. Sci. 28, 1023−1030.

Dugo, P., Kumm, T., Chiofalo, B., Cotroneo, A., Mondello, L., 2006a. Separation of triacylglycerols in a complex lipidic matrix by using comprehensive two-dimensional liquid chromatography coupled with atmospheric pressure chemical ionization mass spectrometric detection. J. Sep. Sci. 29, 1146−1154.

Dugo, P., Kumm, T., Crupi, M.L., Cotroneo, A., Mondello, L., 2006b. Comprehensive two-dimensional liquid chromatography combined with mass spectrometric detection in the analyses of triacylglycerols in natural lipidic matrixes. J. Chromatogr. A 1112, 269−275.

Dugo, P., Kumm, T., Fazio, A., Dugo, G., Mondello, L., 2006c. Determination of beef tallow in lard through a multidimensional off-line non-aqueous reversed phase-argentation LC method coupled to mass spectrometry. J. Sep. Sci. 29, 567−575.

Emken, E.A., Dutton, H.J., Scholfield, C.R., 1964. Chromatographic separation of cis and trans fatty esters by argentation with macroreticular exchange resin. J. Amer. Oil Chem. Soc. 41, 388−390.

Fauconnot, L., Hau, J., Aeschlimann, J.M., Fay, L.B., Dionisi, F., 2004. Quantitative analysis of triacylglycerol regioisomers in fats and oils using reversed-phase high-performance liquid chromatography and atmospheric pressure chemical ionization mass spectrometry. Rapid Commun. Mass Spectrom. 18, 218−224.

Francois, I., Pereira, A.D., Sandra, P., 2010. Considerations on comprehensive and off-line supercritical fluid chromatography × reversed-phase liquid chromatography for the analysis of triacylglycerols in fish oil. J. Sep. Sci. 33, 1504−1512.

Gakwaya, R., Li, X.W., Wong, Y.L., Chivukula, S., Collins, E.J., Evans, J.J., 2007. Examining the collision-induced decomposition spectra of ammoniated triglycerides. III. The linoleate and arachidonate series. Rapid Commun. Mass Spectrom. 21, 3262−3268.

Gmelin, L., 1975. Gmelin Handbuch der Anorganischen Chemie. Springer, Berlin.

Guha, O.K., Janak, J., 1972. Charge-transfer complexes of metals in chromatographic separation of organic compounds. J. Chromatogr. 68, 325−343.

Guricza, L.M., Schrader, W., 2015. New Separation approach for asphaltene investigation: argentation chromatography coupled with ultrahigh-resolution mass spectrometry. Energy Fuels 29, 6224−6230.

Han, J.J., Iwasaki, Y., Yamane, T., 1999. Use of isopropanol as a modifier in a hexane-acetonitrile based mobile phase for the silver ion HPLC separation of positional isomers of triacylglycerols containing long chain polyunsaturated fatty acids. HRC − J. High Res. Chromatog. 22, 357−361.

Herrera, L.C., Potvin, M.A., Melanson, J.E., 2010. Quantitative analysis of positional isomers of triacylglycerols via electrospray ionization tandem mass spectrometry of sodiated adducts. Rapid Commun. Mass Spectrom. 24, 2745−2752.

Holčapek, M., Jandera, P., Fischer, J., Prokeš, B., 1999. Analytical monitoring of the production of biodiesel by high-performance liquid chromatography with various detection methods. J. Chromatogr. A 858, 13−31.

Holčapek, M., Jandera, P., Zderadička, P., Hrubá, L., 2003. Characterization of triacylglycerol and diacylglycerol composition of plant oils using high-performance liquid chromatography-atmospheric pressure chemical ionization mass spectrometry. J. Chromatogr. A 1010, 195−215.

Holčapek, M., Lísa, M., Jandera, P., Kabátová, N., 2005. Quantitation of triacylglycerols in plant oils using HPLC with APCI-MS, evaporative light-scattering, and UV detection. J. Sep. Sci. 28, 1315−1333.

Holčapek, M., Velínská, H., Lísa, M., Česla, P., 2009. Orthogonality of silver-ion and non-aqueous reversed-phase HPLC/MS in the analysis of complex natural mixtures of triacylglycerols. J. Sep. Sci. 32, 3672−3680.

Holčapek, M., Dvořáková, H., Lísa, M., Girón, A.J., Sandra, P., Cvačka, J., 2010. Regioisomeric analysis of triacylglycerols using silver-ion liquid chromatography-atmospheric pressure chemical ionization mass spectrometry: comparison of five different mass analyzers. J. Chromatogr. A 1217, 8186−8194.

Holub, B.J., Kuksis, A., 1971. Resolution of intact phosphatidylinositols by argentation thin-layer chromatography. J. Lipid Res. 12, 510−512.

Hosoya, H., Nagakura, S., 1964. Spectroscopic and theoretical studies of charge-transfer type molecular complexes are complexes between monoolefins and metal ions − selective complex formation abilities of copper (I), silver (I) and mercury (II) ions. Bull. Chem. Soc. Jpn. 37, 249−265.

Jakab, A., Jablonkai, I., Forgacs, E., 2003. Quantification of the ratio of positional isomer dilinoleoyl-oleoyl glycerols in vegetable oils. Rapid Commun. Mass Spectrom. 17, 2295−2302.

Janssen, H.G., Hrncirik, K., Szoradi, A., Leijten, M., 2006. An improved method for sn-2 position analysis of triacylglycerols in edible oils and fats based on immobilised lipase D (*Rhizopus delemar*). J. Chromatogr. A 1112, 141−147.

Jeffrey, B.S.J., 1991. Silver-complexation liquid chromatography for fast, high-resolution separations of triacylglycerols. J. Am. Oil Chem. Soc. 68, 289−293.

Joh, Y.G., Brechany, E.Y., Christie, W.W., 1995. Characterization of wax esters in the roe oil of amber fish, *Seriola aureovittata*. J. Am. Oil Chem. Soc. 72, 707−713.

Juaneda, P., Sebedio, J.L., Christie, W.W., 1994. Complete separation of the geometrical-isomers of linolenic acid by high-performance liquid − chromatography with a silver ion column. HRC − J. High Res. Chromatog. 17, 321−324.

Kakela, A., Kakela, R., Hyvarinen, H., 2002. Analysis of hepatic vitamins A(1), A(2), their fatty acyl esters, and vitamin E for biomonitoring mammals feeding on freshwater fish. Envir. Tox. Chem. 21, 390−396.

Kasai, P.H., Mcleod, D., Watanabe, T., 1980. Acetylene and ethylene complexes of copper and silver atoms-matrix-isolation electron-spin-resonance study. J. Amer. Chem. Soc. 102, 179−190.

Laakso, P., Christie, W.W., 1991. Combination of silver ion and reversed-phase high-performance liquid-chromatography in the fractionation of herring oil triacylglycerols. J. Am. Oil Chem. Soc. 68, 213−223.

Laakso, P., Voutilainen, P., 1996. Analysis of triacylglycerols by silver-ion high-performance liquid chromatography- atmospheric pressure chemical ionization mass spectrometry. Lipids 31, 1311−1322.

Leskinen, H.M., 2010. Quantification of triacylglycerol regioisomers by ultra-high-performance liquid chromatography and ammonia negative ion atmospheric pressure chemical ionization tandem mass spectrometry. Rapid Commun. Mass Spectrom. 24, 1−5.

Leskinen, H., Suomela, J.P., Kallio, H., 2007. Quantification of triacylglycerol regioisomers in oils and fat using different mass spectrometric and liquid chromatographic methods. Rapid Commun. Mass Spectrom. 21, 2361−2373.

Leskinen, H., Suomela, J.P., Pinta, J., Kallio, H., 2008. Regioisomeric structure determination of alpha- and beta-linolenoyldilinoleoylglycerol in blackcurrant seed oil by silver ion high-performance liquid chromatography and mass spectrometry. Anal. Chem. 80, 5788−5793.

Leskinen, H.M., Suomela, J.P., Yang, B., Kallio, H.P., 2010. Regioisomer compositions of vaccenic and oleic acid containing triacylglycerols in sea buckthorn (*Hippophae Rhamnoides*) pulp oils: influence of origin and weather conditions. J. Agr. Food Chem. 58, 537−545.

Leveque, N.L., Heron, S., Tchapla, A., 2010. Regioisomer characterization of triacylglycerols by non-aqueous reversed-phase liquid chromatography/electrospray ionization mass spectrometry using silver nitrate as a postcolumn reagent. J. Mass Spectrom. 45, 284−296.

Li, X.W., Evans, J.J., 2005. Examining the collision-induced decomposition spectra of ammoniated triglycerides as a function of fatty acid chain length and degree of unsaturation. I. The OXO/YOY series. Rapid Commun. Mass Spectrom. 19, 2528−2538.

Li, X.W., Collins, E.J., Evans, J.J., 2006. Examining the collision-induced decomposition spectra of ammoniated triglycerides as a function of fatty acid chain length and degree of unsaturation. II. The PXP/YPY series. Rapid Commun. Mass Spectrom. 20, 171−177.

Lísa, M., Holčapek, M., 2008. Triacylglycerols profiling in plant oils important in food industry, dietetics and cosmetics using high-performance liquid chromatography-atmospheric pressure chemical ionization mass spectrometry. J. Chromatogr. A 1198, 115−130.

Lísa, M., Holčapek, M., Řezanka, T., Kabátová, N., 2007a. High-performance liquid chromatography-atmospheric pressure chemical ionization mass spectrometry and gas chromatography-flame ionization detection characterization of Δ5-polyenoic fatty acids in triacylglycerols from conifer seed oils. J. Chromatogr. A 1146, 67−77.

Lísa, M., Lynen, F., Holčapek, M., Sandra, P., 2007b. Quantitation of triacylglycerols from plant oils using charged aerosol detection with gradient compensation. J. Chromatogr. A 1176, 135−142.

Lísa, M., Holčapek, M., Boháč, M., 2009a. Statistical evaluation of triacylglycerol composition in plant oils based on high-performance liquid chromatography − atmospheric pressure chemical ionization mass spectrometry data. J. Agr. Food Chem. 57, 6888−6898.

Lísa, M., Velínská, H., Holčapek, M., 2009b. Regioisomeric characterization of triacylglycerols using silver-ion HPLC/MS and randomization synthesis of standards. Anal. Chem. 81, 3903−3910.

Lísa, M., Denev, R., Holčapek, M., 2013. Retention behavior of isomeric triacylglycerols in silver-ion HPLC: effects of mobile phase composition and separation temperature. J. Sep. Sci. 36, 2888−2900.

Lommatzsch, M., Biedermann, M., Simat, T.J., Grobb, K., 2015. Argentation high performance liquid chromatography on-line coupled to gas chromatography for the analysis of monounsaturated polyolefin oligomers in packaging materials and foods. J. Chromatogr. A 1402, 94−101.

Lucas, H.J., Moore, R.S., Pressman, D., 1943. The coordination of silver ion with unsaturated compounds II cis- and trans-2-pentene. J. Am. Chem. Soc. 65, 227−229.

Macher, M.B., Holmqvist, A., 2001. Triacylglycerol analysis of partially hydrogenated vegetable oils by silver ion HPLC. J. Sep. Sci. 24, 179−185.

Malone, M., Evans, J.J., 2004. Determining the relative amounts of positional isomers in complex mixtures of triglycerides using reversed-phase high-performance liquid chromatography-tandem mass spectrometry. Lipids 39, 273−284.

Mander, L.N., Williams, C.M., 2016. Chromatography with silver nitrate: part 2. Tetrahedron 72, 1133−1150.

Momchilova, S., Nikolova-Damyanova, B., 2000a. Silver ion HPLC of *p*-methoxyphenacyl derivatives of unsaturated fatty acids. II. Chain length vs. double bond position. J. Liq. Chromatogr. R. T. 23, 2317−2325.

Momchilova, S., Nikolova-Damyanova, B., 2000b. Silver ion high performance liquid chromatography of polynuclear aromatic derivatives of positionally isomeric octadecenoic fatty acids. J. Liq. Chromatogr. R. T. 23, 1319−1330.

Momchilova, S., Nikolova-Damyanova, B., 2000c. Silver ion HPLC of *p*-methoxyphenacyl derivatives of unsaturated fatty acids. I. Mobile phase effects. J. Liq. Chromatogr. R. T. 23, 2303−2316.

Momchilova, S., Nikolova-Damyanova, B., 2003. Stationary phases for silver ion chromatography of lipids: preparation and properties. J. Sep. Sci. 26, 261−270.

Momchilova, S., Nikolova-Damyanova, B., Christie, W.W., 1998. Silver ion high-performance liquid chromatography of isomeric cis- and trans-octadecenoic acids - effect of the ester moiety and mobile phase composition. J. Chromatogr. A 793, 275−282.

Momchilova, S., Tsuji, K., Itabashi, Y., Nikolova-Damyanova, B., Kuksis, A., 2004. Resolution of triacylglycerol positional isomers by reversed-phase high-performance liquid chromatography. J. Sep. Sci. 27, 1033−1036.

Momchilova, S., Itabashi, Y., Nikolova-Damyanova, B., Kuksis, A., 2006. Regioselective separation of isomeric triacylglycerols by reversed-phase high-performance liquid chromatography: stationary phase and mobile phase effects. J. Sep. Sci. 29, 2578−2583.

Mondello, L., Tranchida, P.Q., Stanek, V., Jandera, P., Dugo, G., Dugo, P., 2005. Silver-ion reversed-phase comprehensive two-dimensional liquid chromatography combined with mass spectrometric detection in lipidic food analysis. J. Chromatogr. A 1086, 91−98.

Morris, L.J., 1962. Separation of higher fatty acid isomers and vinylogues by thin-layer chromatography. Chem. Ind. 1238−1240.

Morris, L.J., 1966. Separations of lipids by silver ion chromatography. J. Lipid Res. 7, 717−732.

Mottram, H.R., Evershed, R.P., 1996. Structure analysis of triacylglycerol positional isomers using atmospheric pressure chemical ionisation mass spectrometry. Tetrahedron Lett. 37, 8593−8596.

Mottram, H.R., Woodbury, S.E., Evershed, R.P., 1997. Identification of triacylglycerol positional isomers present in vegetable oils by high performance liquid chromatography atmospheric pressure chemical ionization mass spectrometry. Rapid Commun. Mass Spectrom. 11, 1240−1252.

Mottram, H.R., Crossman, Z.M., Evershed, R.P., 2001. Regiospecific characterisation of the triacylglycerols in animal fats using high performance liquid chromatography-atmospheric pressure chemical ionisation mass spectrometry. Analyst 126, 1018−1024.

Muller, A., Dusterloh, K., Ringseis, R., Eder, K., Steinhart, H., 2006. Development of an alternative eluent system for Ag+-HPLC analysis of conjugated linoleic acid isomers. J. Sep. Sci. 29, 358−365.

Neff, W.E., Adlof, R.O., Elagaimy, M., 1994. Silver ion high-performance liquid chromatography of the triacylglycerols of crepis-alpina seed oil. J. Am. Oil Chem. Soc. 71, 853−855.

Nikolova-Damyanova, B., 2005. Silver-ion HPLC of fatty acids and triacylglycerols. In: Lin, J.-T., McKeon, T.A. (Eds.), HPLC of Acyl Lipids. HNB Publishing, New York, pp. 221−268.

Nikolova-Damyanova, B., 2009. Retention of lipids in silver ion high-performance liquid chromatography: facts and assumptions. J. Chromatogr. A 1216, 1815−1824.

Nikolova-Damyanova, B., Herslof, B.G., Christie, W.W., 1992. Silver ion high-performance liquid chromatography of derivatives of isomeric fatty acids. J. Chromatogr. 609, 133−140.

Nikolova-Damyanova, B., Christie, W.W., Herslof, B.G., 1993. High-performance liquid chromatography for fatty acid derivatives in the combined silver ion and reversed-phase modes. J. Chromatogr. A 653, 15−23.

Nikolova-Damyanova, B., Christie, W.W., Herslof, B.G., 1995a. Retention properties of triacylglycerols on silver ion high-performance liquid-chromatography. J. Chromatogr. A 694, 375−380.

Nikolova-Damyanova, B., Christie, W.W., Herslof, B., 1995b. Silver ion high-performance liquid-chromatography of esters of isomeric octadecenoic fatty acids with short-chain monounsaturated alcohols. J. Chromatogr. A 693, 235−239.

Nikolova-Damyanova, B., Christie, W.W., Herslof, B., 1996. Mechanistic aspects of fatty acid retention in silver ion chromatography. J. Chromatogr. A 749, 47−54.

Phillips, K.M., Lugogo, R.D., Harris, R.F., Tarragotrani, M.T., Bailey, J.A., Stewart, K.K., 1997. Direct determination of trans-octadecenoic acid in diet composites using a combination of silver ion high performance liquid chromatography and capillary gas chromatography. J. Food Lipids 4, 173−188.

Pittenauer, E., Allmaier, G., 2009. The renaissance of high-energy CID for structural elucidation of complex lipids: MALDI-TOF/RTOF-MS of alkali cationized triacylglycerols. J. Am. Soc. Mass Spectrom. 20, 1037−1047.

Schuyl, P.J.W., De Joode, T., Vasconcellos, M.A., Duchateau, G., 1998. Silver-phase high-performance liquid chromatography electrospray mass spectrometry of triacylglycerols. J. Chromatogr. A 810, 53−61.

Shan, H., Wilson, W.K., 2002. Ternary gradient elution markedly improves silver-ion high performance liquid chromatography of unsaturated sterols. Steroid 67, 917−923.

Smith, M., Monchamp, P., Jungalwala, F.B., 1981. Separation of molecular-species of sphingomyelin and ceramide by argentation and reversed-phase HPLC. J. Lipid Res. 22, 714−719.

Standal, I.B., Axelson, D.E., Aursand, M., 2009. Differentiation of fish oils according to species by C-13-NMR regiospecific analyses of triacyglycerols. J. Am. Oil Chem. Soc. 86, 401—407.

Stoll, U., 1996. Identification of molecular species of phospholipids from pig heart by combining chromatographic techniques. Fett-Lipid 98, 178—182.

Sun, C., Black, B.A., Zhao, Y.Y., Gaänzle, M.G., Curtis, J.M., 2013. Identification of conjugated linoleic acid (CLA) isomers by silver ion-liquid chromatography/in-line ozonolysis/mass spectrometry. Anal. Chem. 85, 7345—7352.

Toschi, T.G., Capella, P., Holt, C., Christie, W.W., 1993. A comparison of silver ion HPLC plus GC with Fourier-transform IR spectroscopy for the determination of trans-double bonds in unsaturated fatty acids. J. Sci. Food Agr. 61, 261—266.

van der Klift, E.J.C., Vivó-Truyols, G., Claassen, F.W., Van Holthoon, F.L., Van Beek, T.A., 2008. Comprehensive two-dimensional liquid chromatography with ultraviolet, evaporative light scattering and mass spectrometric detection of triacylglycerols in corn oil. J. Chromatogr. A 1178, 43—55.

Vrkoslav, V., Urbanová, K., Háková, M., Cvačka, J., 2013. Analysis of wax esters by silver-ion high-performance liquid chromatography—tandem mass spectrometry. J. Chromatogr. A 1302, 105—110.

Wei, F., Ji, S.X., Hu, N., Lv, X., Dong, X.Y., Feng, Y.Q., Chen, H., 2013. Online profiling of triacylglycerols in plant oils by two-dimensional liquid chromatography using a single column coupled with atmospheric pressure chemical ionization mass spectrometry. J. Chromatogr. A 1312, 69—79.

Williams, C.M., Mander, L.N., 2001. Chromatography with silver nitrate. Tetrahedron 57, 425—447.

Winstein, S., Lucas, H.J., 1938. The coordination of silver ion with unsaturated compounds. J. Am. Chem. Soc. 60, 836—847.

Yeung, S.K.F., Kuksis, A., Marai, L., Myher, J.J., 1977. Resolution of molecular-species on intact serine and ethanolamine phosphatides by argentation chromatography of their trifluoroacetamides. Lipids 12, 529—537.

Zeise, W.C., 1831. Von der Wirkung zwischen Platinchlorid und Alkohol, und von den dabei entstehenden neuen Substanzen. Annalen der Physik 97, 497—541.

CHAPTER

POROUS MONOLITHIC LAYERS AND MASS SPECTROMETRY

5

Frantisek Svec, Yongqin Lv
Beijing University of Chemical Technology, Beijing, China

1. MASS TRANSPORT IN CHROMATOGRAPHY

Ever since the beginning of the 20th century, when Tswett first described the separation of chlorophylls in a liquid phase using a device filled with porous inorganic particles, and named the method chromatography (Tswett, 1906), chromatographers have been using columns packed with stationary phases in the shape of particles. Obviously, the column technology has been perfected during the following more than 110 years, and columns packed with particles are the "workhorse" of current liquid chromatography. The concept is simple: The mobile phase is pumped through the packed column and flows through the interstitial spaces that are, by default, always present between the particles. The vast majority of chromatographic packings are porous, with most of the interactive sites being presented on the pore surface, not at the external surface of the particles. The interactive sites are instrumental for attaining the separation, and the separated compounds have to reach them to achieve the separation. The pores inside the particle are filled with the mobile phase, which does not move and is stagnant. After injection of the sample in the stream of the mobile phase that is pushed through the voids between the packed particles, the difference between concentration of the separated compounds in the mobile phase and in the stagnant liquid in the pores is the driving force for transport of these compounds in the pores. Once the compound interacts with the interactive sites, its concentration in the stagnant liquid decreases and the concentration gradient drives more compounds to enter the pores. The mechanism of this transport is diffusion, which is described by Fick's second law:

$$\frac{\partial \varphi}{\partial t} = D \frac{\partial^2 \varphi}{\partial x^2} \tag{5.1}$$

where φ is the concentration of the substance, t is the time, x is the position, and D is the diffusion coefficient defined by the Stokes–Einstein equation:

$$D = \frac{k_B T}{6\pi\eta r} \tag{5.2}$$

where k_B is the Boltzmann constant, T is the temperature, η is the viscosity, and r is the radius of the diffusing entity. Eq. (5.1) indicates that the rate of diffusion depends on the diffusion coefficient D, which, according to Eq. (5.2), is specific for each compound and can only be enhanced by an increase

Handbook of Advanced Chromatography/Mass Spectrometry Techniques. http://dx.doi.org/10.1016/B978-0-12-811732-3.00005-4

in temperature or a decrease in viscosity of the mobile phase. These two effects are often interrelated because the viscosity of many liquids decreases with an increase in temperature. The size of the separated compound is given. The larger the molecule, the smaller the diffusion constant and the lower the overall diffusion rate. Hence, the diffusion of large molecules, such as proteins, nucleic acids, viruses, and synthetic polymers, is significantly slower than that observed for much smaller molecules including gases, ions, and small organic compounds. For years, this effect appeared to be a serious problem in efforts to accelerate chromatographic separation of large molecules. However, acceleration of separations of small molecules was an interesting target as well. Obviously, to reach the pore the compound also must diffuse within the mobile phase moving through the interparticular voids. This diffusion is again described by Eq. (5.1), including the diffusion constant. However, the contribution of mass transfer is less significant because the distance is always much shorter. The rule of thumb is that the size of the interstitial void is about one-fifth of the size of the packed spherical particles.

2. ACCELERATION OF SEPARATIONS

2.1 NONPOROUS PARTICLES

A closer view at Eq. (5.1) points at the significant effect of the distance x. The shorter the distance, the earlier the compound reaches it. The shortest distance we can imagine is just to the surface of packed particles that do not contain any pores. Indeed, columns for reversed phase separations packed with 1.5 μm silica-based nonporous particles have been commercially available in the United States since the mid-1990s, from Eichrom Technologies under the trade name Micra NPS. Although the catalog of this company demonstrates a number of interesting separations, these columns certainly do not represent the mainstream in column technologies. One of their problems is the small surface area of 1.9 m^2/g characterizing these nonporous particles, which embodies only the external surface of the individual beads. This is significantly less than a few 100 m^2/g typical of standard porous counterparts. As a result, these columns exhibit very low loading capacity, thus requiring high-sensitivity detection. The real killer for these columns was the high back pressure, for which chromatographic hardware was not available at that time.

2.2 SMALL POROUS PARTICLES

Fick's Law applies independent of the size of the column packing. Although the rate of diffusion does not change, decreasing the size of the particle enables reaching the most distant center of the bead in a shorter time. Consequently, separations can be achieved in a shorter period of time. This idea is not new, and the desirable decrease in size of packings was predicted by Martin and Synge (both were 1952 Nobel Prize winners for chromatography) as early as 1941, a long time before high-pressure liquid chromatography (HPLC) emerged. Majors published a description of early work in this area in his excellent overview table that demonstrated the timeline of efforts to minimize the effect of diffusion via decreasing the size of packings (Majors, 2015). For example, the industry standard was about 10 μm around 1972, and decreased to 5 μm in 1985, and to 3 μm in 1992. Current particle size standards lay close under 2 μm and were introduced in 2003. Currently, the high popularity of columns packed with sub-2 μm particles has been enabled by development and commercialization of advanced hardware that permits application of pressures exceeding 100 MPa.

Several groups have reported use of even smaller particles. However, some other challenges have emerged, such as evolution of the Joule heat caused by pumping the mobile phase under the significantly higher pressures. A noteworthy novel method pioneered by Wirth includes use of sub-500 nm silica particles and slip flow to achieve exceptional efficiencies (Wei et al., 2012). Despite these positives, the feasibility of this method in the real-life applications is yet to be demonstrated. The current general notion is that a significant further decrease in the packing size is unlikely in the near future.

2.3 CORE–SHELL PARTICLES

Another approach leading to a reduction in the length of diffusional path within the particles includes a change in the internal structure of the separation media. The original superficially porous particles, first introduced by Kirkland (1992), consisted of a nonporous 5 μm core embedded in a 1 μm thin porous shell. The diffusional path in the shell was short and enabled rapid separations of even large molecules such as peptides and proteins. Recently, columns have been launched that are packed with core–shell particles in the size range of sub-3 μm that enable separations equivalent to those achieved using columns packed with sub-2 μm beads, while requiring only half of the pressure. The enhanced performance appears to also result from a narrow particle size distribution that facilitates configuration of a more efficient packing structure, and reduces the eddy dispersion contribution to peak broadening. In contrast to fully porous particles prepared in a single step, their nonporous counterparts used as the core can be obtained almost monodisperse in size, and their dispersity does not change during the formation of the shell.

2.4 CONVECTIVE MASS TRANSPORT

As presented in the previous section, the rate of diffusional mass transport of a specific compound cannot be changed easily. The only variable to work with while trying to accelerate chromatographic separations is the distance along which the diffusion occurs. However, diffusion is not the only mechanism enabling mass transport. This is why several groups have explored the mechanism called convection. This different mechanism involves the transport of material between a boundary surface, such as solid surface, and a moving liquid.

The early 1990s represent era of boosted interest in highly permeable large-pore separation media called perfusive packings. The first commercial example of those beads developed by Regnier's group was called Poros (Afeyan et al., 1990). These beads featured 700 nm large transport pores to enhance mass transport and simultaneously contained 50 nm diffusive pores needed to achieve sufficient adsorption capacity. This combination of pores was not completely new, because the significant effect of similar morphologies has long been recognized in studies concerning heterogeneous catalysts. Nir and Pismen (1977) were probably the first who discovered the enhancement of catalyst effectiveness by convection. Rodrigues et al. (1992, 1993) quantified the concept of augmented diffusivity by forced convective flow due to a pressure gradient, and their studies became the key to understanding perfusion chromatography. They also challenged the overly optimistic views of Afeyan et al., who claimed that a large fraction of the mobile phase is permeating through the particles, and argued that only a very small fraction, typically less than 1% of the flow, can percolate through the particulate porous packing material (Rodrigues et al., 2003). The theoretical treatment of convective flow was further developed by Liapis et al. (Liapis et al., 1999; Meyers and Liapis, 1999).

The close to negligible fraction of the mobile phase that flows through even the large pore particles is the result of the very small pressure difference between the "top" and "bottom" of the relatively small size particle. A more significant pressure difference would be needed to push the liquid through the pores. However, this pressure is not accessible because the mobile phase chooses to flow through the areas with the highest permeability to flow, i.e., through the interstitial voids between the particles, and creation of a high pressure drop across a single particle is impossible. Because use of packed columns did not allow an increase in flow through the pores to enable convective mass transport, a completely different format of separation media was needed. And this is where the monolithic structures stepped in. One of the early papers claimed: "Instead of relying only on diffusion for intraparticular mass transfer, or on a combination of diffusion and convection as in perfusion media, we have introduced a new HPLC medium consisting of a continuous rod of rigid macroporous polymer, which does not have interstitial volume but only internal porosity. The resulting packing is essentially a single particle of a cylindrical shape" (Wang et al., 1993). One has to keep in mind that the monolithic structure fills completely the column tube with no interparticulate voids present, and therefore, all the mobile phase must flow through the pores of the stationary phase. As a result "… this made also possible that the mass transport was enhanced by convection" (Wang et al., 1993).

3. HISTORY OF MONOLITHS

3.1 EARLY ATTEMPTS

It might appear that materials and structures we call today monoliths emerged around the 1990s. Indeed, the monolithic columns applicable for efficient separations were first described at that time; and their advent represented the initial step in their widespread appearance, first in academic studies and later on also as commercial products. However, this does not mean that other people did not consider similar structures before.

For example, Mould and Synge wrote in 1952, in their paper concerning electrokinetic ultrafiltration analysis of polysaccharides: "An alternative possibility, suggested in discussions between Dr. A. J. P. Martin, Prof. A. Tiselius, and one of us (i.e. Robert Synge), is to use electro-endosmosis to move a solution through a continuous block of porous gel structure. In this way the equivalent of movement of liquid through a very thick ultrafiltration membrane is attained without the necessity of great hydrostatic pressures, which would destroy the membrane structure." (Mould and Synge, 1952). At the first look, this description sounds like suggesting the application of a monolith. However, these authors realized soon after that their idea was not feasible: "For porous materials at present available, however, the high hydrostatic pressures required to produce reasonable flow through a thick block would cause stresses, which would collapse the pore structure." (Mould and Synge, 1954). This problem was confirmed experimentally by Kubín et al. (1967) 13 years later. They tried desalination of polyvinylpyrrolidone in a hydrogel "monolith" prepared from 2-hydroxyethyl methacrylate cross-linked with 2% ethylene dimethacrylate placed in a glass tube. They found that permeability of the hydrogel was very poor and did not allow any appreciable flow rate.

Another approach to columns prepared within the confines of a chromatographic column included the preparation of open pore polyurethane foams (Hileman et al., 1973; Ross and Jefferson, 1970; Schnecko and Bieber, 1971). Although reasonable separations could be achieved both in gas and liquid chromatography, this technology did not thrive for several reasons, including poorer separation

performance compared with, at that time, young and more efficient HPLC columns, and inappropriate polyurethane chemistry that was not best suited for chromatography.

The brief history of the premonolithic era presented in the previous few paragraphs, which ended in the early 1970s, did not result in any useful product. Nothing then happened in the monolithic field for the next about 20 years, until the late 1980s and early 1990s. Thus, the truly successful monolithic columns and other monolithic structures are currently only about 25 years old.

3.2 MODERN HISTORY

The age of porous polymer monoliths actually started with a curiosity. Belenkii in the mid-1980s modeled chromatography of proteins in gradient elution mode using different stationary phases and column shapes. They found that often only a very short distance was required to achieve the desired separation, and postulated the concept of short separation beds that they published much later (Belenkii et al., 1993). However, this concept had one serious weakness. It did not consider the effect of slow mass transport controlled by diffusion in pores of relatively large particles available at that time that would affect the performance as detailed above. In addition, it was very difficult to pack particles in a homogeneously dense short bed without formation of unwanted channels. Therefore, the concept could not be validated and its potential was not demonstrated experimentally. Interestingly, the concept of short packed beds emerged recently again with the 5 mm long columns packed with sub-3 μm superficially porous particles. These columns enabled subsecond separations of small molecules (Wahab et al., 2016). In the late 1980s, Belenkii approached one of the authors of this chapter who, at that time, was preparing sheets of porous polymers via copolymerization of monovinyl and divinyl methacrylate monomers in the presence of a free radical initiator and a porogenic solvent for an unrelated project. Belenkii asked for a sample that might enable testing of his theory. Indeed, this continuous ~2 mm thin layer of porous polymer worked well, and the theory was validated experimentally thanks to the new format of the separation medium. The following work with discs made of the porous polymer and placed in a simple cartridge then demonstrated the ability of this novel shape to separate large molecules using a variety of chromatographic mechanisms, including reversed phase, ion exchange, and hydrophobic interaction (Svec and Tennikova, 1991; Tennikova et al., 1990, 1991). The method was first called "membrane chromatography" and the material was a "macroporous polymer membrane." However, the early separations were not very fast, with often several tens of minutes needed to separate a few proteins. The theoretical aspects of separations of proteins using short monolithic beds were then developed by Tennikova and Svec (2003).

At the same time, Hjertén strongly compressed pieces of polyacrylamide copolymer gels in a tube to obtain what he called a "continuous polymer bed," and demonstrated rapid separations of proteins using this novel separation medium (Hjertén et al., 1989; Liao et al., 1991). Although these columns were not genuine monoliths because they consisted of irregular gel particles and did not exhibit any permanent porous structure, their format was more "continuous" than that of typical packed columns. Most importantly, these compressed gels were counterintuitively permeable, and the separations were largely independent of the flow rate (Svec, 2008).

Another novel format of separation media emerged in 1992 and was first called a "continuous polymer rod" (Svec and Fréchet, 1992). This material was prepared in situ within the confines of a chromatographic column using copolymerization of methacrylate monomers in the presence of

porogenic solvents. The original conditions were a clone of the approach used for the preparation of macroporous beads two decades earlier (Svec et al., 1975). Surprisingly, the porous structure of this polymer was significantly different from that observed previously for the beads, as shown in Fig. 5.1.

This difference was assigned to the fact that the mechanism of pore formation during the polymerization in bulk within the tube was affected by the absence of both the interfacial tension and the dynamic forces that are typical of the suspension polymerization process (Svec and Fréchet, 1995).

The last contribution to the family of continuous porous structures was introduced by Tanaka in 1996 and the authors called their material a "porous silica rod" (Minakuchi et al., 1996).

The text above indicates that a number of various expressions were used for the materials prepared in different labs. The term "monolith" appeared for the first time in the paper published in 1996 (Viklund et al., 1996) and soon after became a standard. Today, this term is widely used by all researchers working with continuous porous materials.

Early studies with porous polymer-based monolithic columns clearly demonstrated that these columns enabled extremely fast separations of large molecules at high flow rates, yet at easily tolerable back pressures. These features made monolithic columns particularly suitable for high-throughput applications. For example, Fig. 5.2 shows the separation of five proteins achieved in less than 20 s (Xie et al., 1999).

Interestingly, it has been confirmed over and over again that the organic polymer–based monoliths have always been well suited for separation of large molecules such as proteins (Hjertén et al., 1989; Wang et al., 1993), nucleic acids (Sýkora et al., 1999), and synthetic polymers (Petro et al., 1996) but

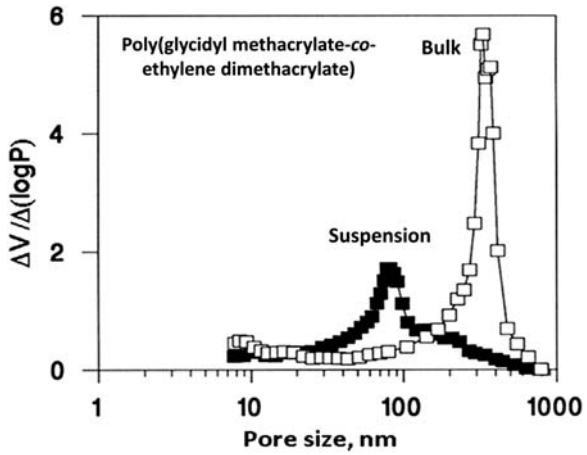

FIGURE 5.1

Differential pore size distribution plots of the poly(glycidyl methacrylate-*co*-ethylene dimethacrylate) beads and monolith prepared from the same polymerization mixture consisting of glycidyl methacrylate (24%), ethylene dimethacrylate (15%), cyclohexanol (48%), dodecanol (12%), and azobisisobutyronitrile (1% with respect to monomers) at a temperature of 70°C.

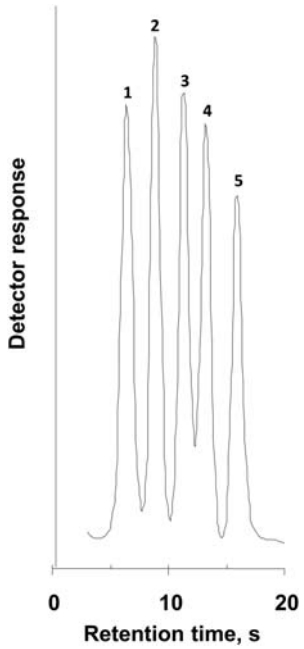

FIGURE 5.2

Fast reversed-phase separation of proteins. Conditions: Poly(styrene-*co*-divinylbenzene) monolithic column 50 × 4.6 mm I.D., mobile phase gradient 42%−90% acetonitrile in 0.15% aqueous trifluoroacetic acid in 0.35 min, flow rate 10 mL/min, UV detection at 280 nm. Peaks: ribonuclease (1), cytochrome c (2), bovine serum albumin (3), carbonic anhydrase (4), and ovalbumin (5).

not for small molecules (Wang et al., 1994). In contrast, silica-based monolithic columns enabled fast separations mostly for smaller molecules (Minakuchi et al., 1996), thus making these two column technologies complementary.

4. SPECIFIC FEATURES OF POROUS POLYMER MONOLITHS

Monolithic columns are rather different from their counterparts packed with particles. Because all the mobile phase is pumped through the monolith that fills the entire volume of the separation device, the first concern was their permeability to liquids, which is a function of the size of the pores they contain. Flow through a monolith containing only nanometer-sized pores typical of particulate chromatographic packings would require extremely high pressures that were likely to crush the structure. Hence, an ideal monolithic structure must contain pores large enough to enable flow through at a tolerable back pressure. Therefore, the preparation conditions had to be optimized to afford highly porous materials containing a network of interconnected pores having sizes in the low micrometer range. Accordingly, the back pressure typical of polymer-based monolithic columns

remained small even when liquids were pumped through the monoliths at very high rates (Viklund et al., 1996).

Another remarkable feature of monolithic columns is their high porosity, reaching 60%−80%, or in other words, the monolithic column may contain as little as about 20% of the solid. This appears to be much less than 60% of the column volume typically filled with particulate packings. Such a number might indicate that the space in a column is better used when it is packed with particles. However, this is not the case. Although the packed column contains about 40% of interparticulate voids through which the mobile phase must flow, it also includes the diffusional porosity within the packing that accounts for 40%−60% of the stationary phase. As a result, the dead volume of the column packed with porous particles is likely to be larger than that of the apparently highly porous monolith. However, in the case of monolithic materials, all mobile phase flows through the pores of the monolith, which volume is larger compared to that of flow through voids in a packed column. Thanks to the specific morphology of the monoliths, the resistance to flow is smaller, and the slow diffusion within the pores typical of particulate packings used in standard columns is replaced with much faster convection. In a slightly simplified view, the analytes are delivered to the point of interaction by flow not by diffusion. Liapis et al. (1999) developed a mathematical model that enabled prediction of the dynamic behavior, scale-up, and design of monoliths. Interestingly, their theoretical calculations largely confirmed that the monolithic structures prepared previously had porous properties very close to optimal.

5. SEPARATIONS USING MONOLITHIC COLUMNS AND MASS SPECTROMETRIC DETECTION

Once the monolithic columns were available, it did not take long to connect them to a mass spectrometer. Obviously, they were just another type of column that enabled separations at speeds that were difficult to achieve using packed columns at that time. In fact, most of the current applications of monolithic columns in conjunction with mass spectrometry (MS) still rely on this advantage. Although analytical size monolithic columns were used at the beginning of the monolithic era, the real boom occurred in late 1990s with the advent of microcolumn methods, first used in capillary electrochromatography (CEC) and then also in capillary liquid chromatography (cLC). The reason is that in situ preparation of monolithic capillaries is significantly easier than packing capillaries with particles. The summary of state-of-the-art concerning use of monoliths in both CEC and cLC was presented in an excellent recent review by Moravcová et al. (2016). Their paper describes many applications in which monolithic columns, both silica- and organic polymer-based, are used with MS detection. They also discuss that the invention of the nanoelectrospray interface was instrumental for an increased interest in combinations of CEC and cLC with MS. Another reason that we can add might be better accessibility of mass spectrometers that became a more common tool in analytical laboratories rather than a voluminous and very expensive curiosity. The authors of the review also presented pie-charts showing the percentages of individual interfaces and analyzers used in the works including monolithic columns that clearly demonstrated that electrospray represents the vast majority of interfaces and ion trap instruments prevail in analyzers. Their statistics also reveal that matrix-assisted laser desorption/ionization (MALDI) was used in only a very small percentage of

papers and argue that this is likely due to technically more complex off-line assembly needed. Although combinations of monolithic columns with MS detection are very well described in the above discussed review article (Moravcová et al., 2016), much less is known about combinations of monolithic layers and MS.

6. MONOLITHS IN LAYER FORMAT

One of the significant advantages of monoliths is their ability to be prepared using different methods and in a variety of shapes (Svec, 2010). Although columnar shapes remain most common, monoliths in the shape of flat layers are also finding their applications in connection with MS. The monolith alone can serve as a porous surface enhancing the ionization or combine two functions, i.e., chromatographic separation with MS detection of compounds in the separated spots. Combination of thin-layer chromatography (TLC) and mass spectroscopy is not new because it has been demonstrated by numerous groups. Based on prevailing applications of "classical" thin layers, most often formed from silica particles dispersed in a binder layer, the majority of studies have focused on application of this type of device. A detailed description of the current status quo can be found in a comprehensive review article that also presents a variety of typically used sampling methods (Cheng et al., 2011).

7. SILICA-BASED LAYERS

Thin monolithic layers based on silica emerged first as a commercial product distributed by Merck KGaA (Darmstadt, Germany) in the early 2000s (Hauck et al., 2001). The method of their production has never been revealed. These relatively small plates (6 × 3.6 cm) carried 10-μm-thick monolithic layers that gave the name to the technique: ultrathin-layer chromatography or UTLC. The separations using this technique were demonstrated with small drugs (Hauck and Schulz, 2003). These thin layers were also used in combination with time-of-flight secondary ion mass spectrometry detection (Orinak et al., 2005) and MALDI, both in a vacuum and at atmospheric pressure (Salo et al., 2005). Fig. 5.3 illustrates the performance of the monolithic silica layer and MALDI spectra of separated peaks "from-layer" obtained after application of a matrix α-cyano-4-hydroxycinnamic acid (CHCA).

However, production of these monolithic plates has recently been discontinued. The reasons that might underlie this decision are indicated by Poole and Poole (2011), based on analysis of the limited number of published studies: "Compared with stabilized particle layers they provide faster separations, improved mass detection limits, and lower solvent consumption at the expense of lower resolution and increased handling complexity. Sample application is problematic due to the low sample volumes and small application zones needed for optimized separations, a direct result of the thin film and short migration distances. The significant transmission of light by monolithic films together with the small zone dimensions and short migration distances adds to the problems of quantitative measurements by scanning densitometry. Samples applied using standard laboratory equipment for high performance thin-layer chromatography indicate rather poor performance. A zone capacity of only 5−6 with plate heights of 80−100 μm for low molecular weight compounds with RF values between 0.1 and 0.5 were obtained."

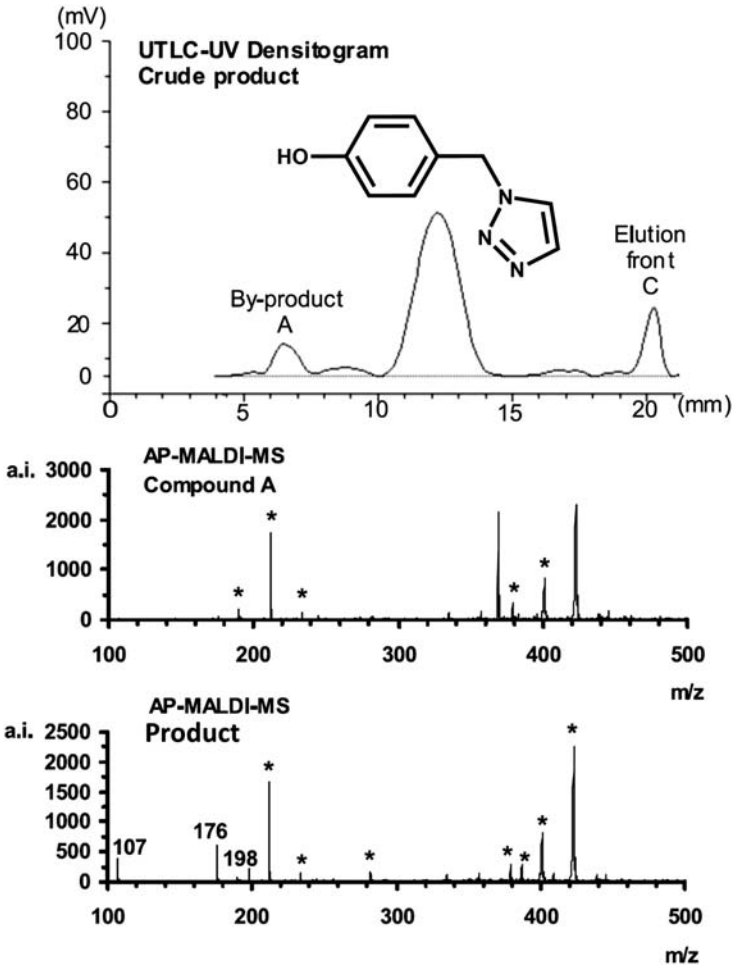

FIGURE 5.3

The separation of crude products from synthesis of triazole (*m/z* 176) using the mobile phase ethyl acetate-n-hexane (1:2 v/v) with 2% acetic acid and presented as ultrathin-layer chromatography (UTLC)-UV densitogram of the synthesis sample (top). Identification of peaks was achieved using atmospheric pressure matrix-assisted laser desorption/ionization (MALDI)-mass spectrometry (MS) spectra of the by-product A (*m/z* 369) (center) and the product (*m/z* 198 $[M+Na]^+$and *m/z* 107) (bottom). The main matrix ions are marked with *asterisks*.

Adapted from Salo, P.K., Salomies, H., Harju, K., Ketola, R.A., Kotiaho, T., Yli-Kauhaluoma, J., Kostiainen, R., 2005. Analysis of small molecules by ultra thin-layer chromatography-atmospheric pressure matrix-assisted laser desorption/ionization mass spectrometry. J. Am. Soc. Mass Spectrom. 16, 906–915. Copyright American Society for Mass Spectrometry, 2005.

8. ELECTROSPUN POLYMER LAYERS

Olesik's et al. pioneered a completely different approach to ultrathin layers with a monolithic-like structure. They first deposited electrospun polyacrylonitrile nanofibers on aluminum foil and also prepared glassy carbon fibers via in situ pyrolysis of the polyacrylonitrile (Clark and Olesik, 2009, 2010). The structure of these layers is shown in Fig. 5.4A. Poole and Poole (2011) commented on this approach: "The layers are sufficiently stable for general use without the need for a binder and were prepared in sizes from 2 to 3 cm wide and 6 cm long for separations. The poly(acrylonitrile) layers were made from fibers with 400 nm diameters and are 25 μm thick. The glassy carbon layers consist of fibers of 200−350 nm diameter and a thicknesses of 13−16 μm. Sample solutions of 50 nL were spotted by syringe to give starting zones of about 0.25−0.50 mm, and after development by capillary flow, separated zones <2.5 mm in diameter. Mobile phase velocity constants were generally higher than observed for high performance thin-layer plates. A remarkable feature of these layers is that for many compounds band broadening is minimal and constant plate height values <10 μm over development distances of 1−6 cm were observed. This performance is much higher than for stabilized particle layers using capillary flow."

The group then extended their technology and prepared electrospun layers with *aligned* polyacrylonitrile nanofibers shown in Fig. 5.4B (Beilke et al., 2013), which performance was demonstrated with the separations of pharmaceuticals. The aligned layers provided separations in a shorter time and with improved reproducibility.

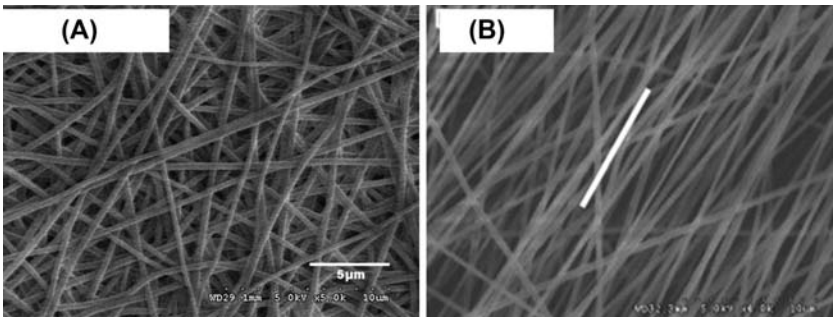

FIGURE 5.4

Scanning electron microcope images illustrating polyacrylonitrile layer prepared "conventional" electrospinning (A) and aligned electrospun polyacrylonitrile nanofibers generated on the rotating collector at rotational speeds of 1250 rpm (B).

Adapted with permission from Clark, J.E., Olesik, S.V., 2009. Technique for ultrathin layer chromatography using an electrospun, nanofibrous stationary phase. Anal. Chem. 81, 4121−4129. Copyright American Chemical Society, 2009 and from Beilke, M.C., Zewe, J.W., Clark, J.E., Olesik, S.V., 2013. Aligned electrospun nanofibers for ultra-thin layer chromatography. Anal. Chim. Acta. 761, 201−208. Copyright Elsevier, 2013.

They also prepared nanofiber layers from polyacrylonitrile solution in which carbon nanotubes or edge-plane carbon nanorods were dispersed (Fang and Olesik, 2014). The carbon nanoparticles in the layer contributed to the selectivity of separations due to strong π−π interactions. The enhanced resolution and efficiency were demonstrated with the separation of polycyclic aromatic hydrocarbons shown in Fig. 5.5.

The arsenal of chemistries of the electrospun layers was enlarged by using poly(vinyl alcohol) (Lu and Olesik, 2013b) and cellulose acetate (Rojanarata et al., 2013). The former separated neat or fluorescently labeled amino acids in methanol−butanol−water as the mobile phase. The latter were then used for screening of steroids adulterated in traditional medicines.

The Olesik's electrospun polyacrylonitrile and poly(vinyl alcohol) nanofibers have also proven to be excellent substrates for surface-assisted laser desorption/ionization (SALDI) and matrix enhanced SALDI MS of both small and large molecules (Lu and Olesik, 2013a). For example, poly(ethylene glycols) with a molecular mass of up to 900,000 could be detected in mass spectra with a reasonable signal-to-noise ratio. Also, ionization of polystyrene with a molecular mass of 4000 was achieved in SALDI mode without addition of any matrix. However, no signal was observed for the peptide angiotensin I in this mode. In contrast, a good signal with little background, shown in

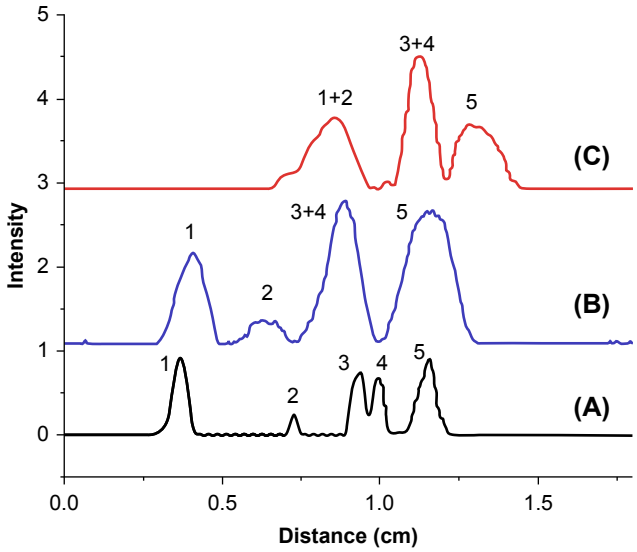

FIGURE 5.5

Comparison of chromatograms showing the separation of (1) benzo[a]pyrene, (2) chrysene, (3) pyrene, (4) fluoranthene, and (5) phenanthrene using 0.5% multiwall carbon nanotubes−polyacrylonitrile plates, (A) 0.5% edge-plane carbon−polyacrylonitrile plates (B) using mobile phase 60:40 acetonitrile−water, and pure polyacrylonitrile plates (C) using mobile phase 70:30 acetonitrile−water mobile phase.

Reproduced from Fang, X., Olesik, S.V., 2014. Carbon nanotube and carbon nanorod-filled polyacrylonitrile electrospun stationary phase for ultra-thin layer chromatography. Anal. Chim. Acta 830, 1−10. Copyright Elsevier, 2014.

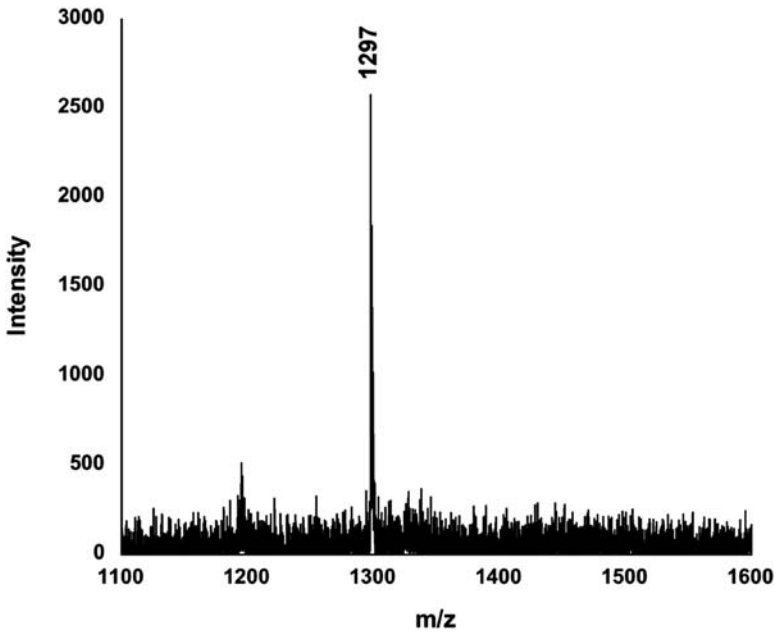

FIGURE 5.6

Matrix enhanced surface-assisted laser desorption/ionization time-of-flight mass spectrum of angiotensin I using the poly(vinyl alcohol) substrate. An amount of 800 amol of angiotensin I was applied, and the CHCA matrix concentration was 0.1 mg/mL. The spectrum is the sum of 100 laser shots.

Adapted with permission from Lu, T., Olesik, S.V., 2013a. Electrospun nanofibers as substrates for surface-assisted laser desorption/ionization and matrix-enhanced surface-assisted laser desorption/ionization mass spectrometry. Anal. Chem. 85, 4384–4391. Copyright American Chemical Society, 2013.

Fig. 5.6, was found while using a poly(vinyl alcohol) nanofiber substrate, after sampling a mixed solution of the peptide and matrix (CHCA). The signal strength exceeded that obtained after sampling directly at the stainless steel MALDI plate.

9. ORGANIC POLYMER–BASED LAYERS

It should be taken into consideration that monoliths in layer format were the initial shape when the organic polymer–based monoliths emerged (vide supra). The advantage brought to the field of MS through the use of organic polymer–based monolithic structures lies, among some other positive features, in the ease of the layer preparation and its availability in a variety of chemistries attained via selection of monomers used for their preparation. Also, the actual formation of these layers is simple. Once prepared, these layers can be applied just to simply enhance desorption and ionization prior to mass spectrometric detection; they can be used for separation using one dimensional thin-layer chromatography (1D TLC) followed by MALDI MS, and also for two-dimensional thin-layer chromatography (2D TLC) separation and MALDI MS.

9.1 PREPARATION OF MONOLITHIC LAYERS

9.1.1 Monolithic Spots

The first paper concerning preparation of a monolithic thin layer for surface enhanced laser desorption-ionization (SELDI) TOF MS of small molecules was published in the early 2000s (Peterson et al., 2004). The 10 μm "tall" monolithic cylinders were prepared from butyl methacrylate or benzyl methacrylate cross-linked with ethylene dimethacrylate in the presence of porogenic solvents, 1-dodecanol and cyclohexanol, and a photoinitiator, 2,2-dimethoxy-2-phenylacetophenone, using UV initiated polymerization. The mask shown in Fig. 5.7, featuring 100 circular spots with a diameter of 3 mm, was designed using Corel Draw software and printed on a transparency film using a standard office laser printer. This mask was attached on top of a glass wafer. A small volume of the polymerization mixture was placed on the top of a MALDI stainless steel plate, covered with the wafer-mask assembly, and polymerization carried out under UV lamp irradiation. The mask assembly was then carefully removed from the plate and the plate surface, with the attached monolithic spots shown in Fig. 5.7, was rinsed with methanol. An alternative procedure had to be used for polymerizations of mixtures containing styrene and divinylbenzene monomers that are not UV transparent. The monolithic spots were prepared via thermally initiated polymerization using 2,2′-azobisisobutyronitrile as the initiator. This polymerization mixture was spotted on a MALDI plate covered with a 10-μm-thick polyethylene film perforated with 3 mm holes that also acted as a sealing gasket on the top of which an

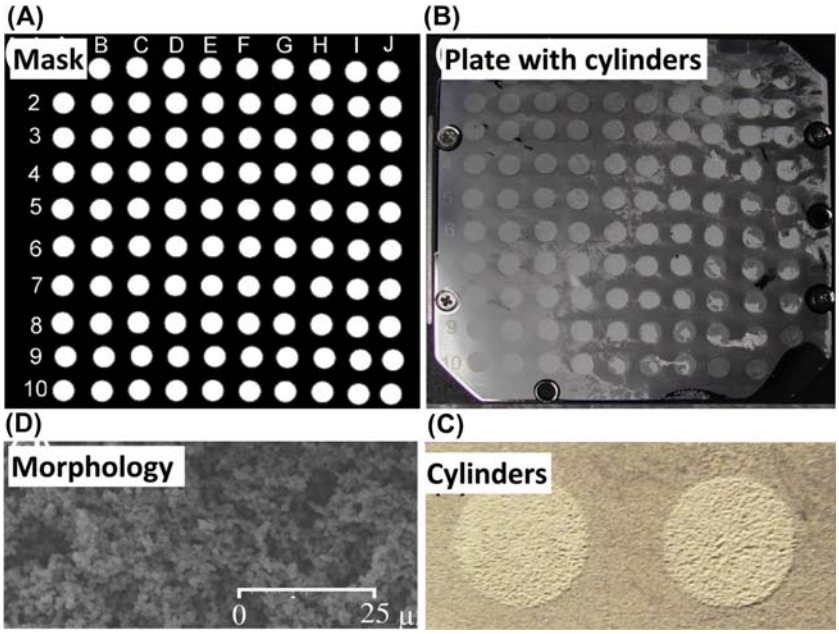

FIGURE 5.7

Mask used to prepare monoliths with a circular shape via photopolymerization of butyl methacrylate and ethylene dimethacrylate on the top face of a matrix-assisted laser desorption/ionization (MALDI) plate (A), top view of the MALDI plate with monoliths (B), optical micrograph of two adjacent monolithic spots (C), and scanning electron microscope micrograph of macroporous structure of monolith C (D).

aluminum plate was placed. The polymerization reaction was allowed to proceed at 80°C for 24 h. After the preparations and washing, the plates were dried and ready for use. Fig. 5.7 also shows the respective optical and scanning electron microscope (SEM) images of the monolithic spots and their morphology.

9.1.2 Continuous Monolithic Layers

Continuous layers were most often prepared as attached to a glass plate. Fig. 5.8 presents one of the implementations using a mold assembled from two glass plates separated by two Teflon strips placed along the longer sides of the plates, which define the thickness of the layer, and are held together with spring clamps. The bottom part of the figure then shows the morphology of the polymerized monolithic layer. In the typical preparation, the mold is filled with a polymerization mixture using capillary force, followed by photoinitiated or thermally initiated polymerization. The setup used for the preparation of monolithic layers is obviously very simple. However, some potential problems with the layer have to be taken into consideration.

Use of native glass for assembly of the mold might be the first choice. For example, Wouters et al. (2013) prepared a porous poly(butyl methacrylate-ethylene dimethacrylate) monolithic layer using photoinitiated polymerization of the monomer mixture placed between two untreated commercial microscopic glass slides. The problem was that the layer produced by

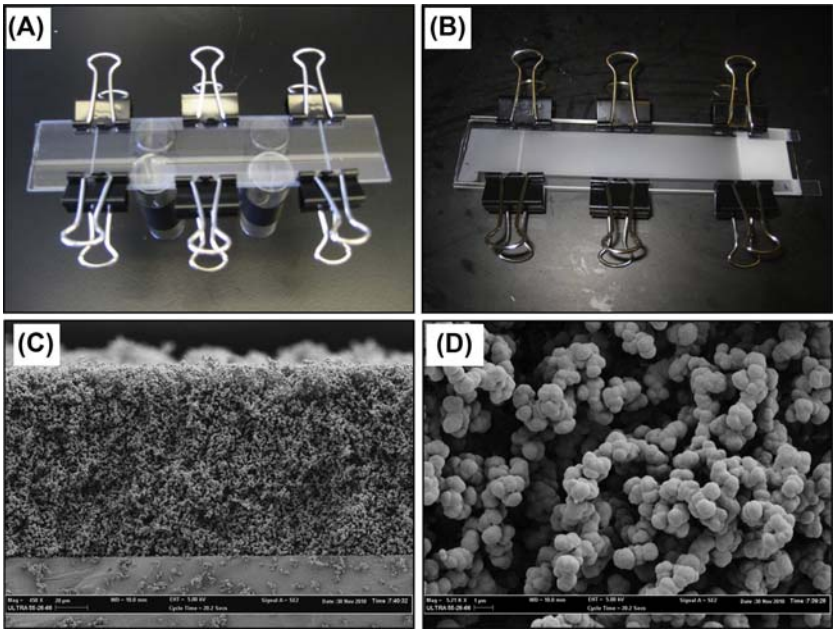

FIGURE 5.8

Mold consisting of two glass plates separated by Teflon strips located along the long side used for the preparation of monolithic layer (A), the mold containing the white monolithic layer (B), scanning electron microscope image of the cross section of the monolith (C), and detailed view of the morphology of the monolithic layer (D).

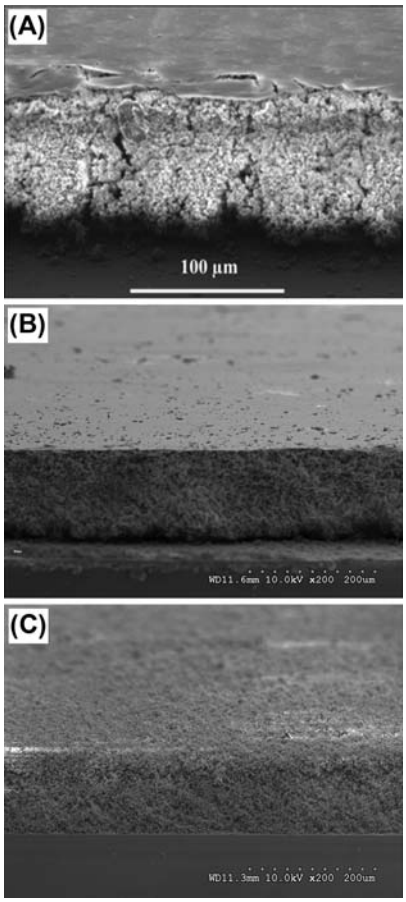

FIGURE 5.9

Scanning electron micrographs of poly(butyl methacrylate-*co*-ethylene dimethacrylate) monolithic layer prepared between two native glass plates (A) and a layer prepared using one plate (B), and both plates (C) functionalized with 3-(trimethoxysilyl)propyl methacrylate.

Adapted with permission from Wouters, B., Vanhoutte, D.J.D., Aarnoutse, P., Visser, A., Stassen, C., Devreese, B., Kok, W.T., Schoenmakers, P.J., Eeltink, S., 2013. Visualization procedures for proteins and peptides on flat-bed monoliths and their effects on matrix-assisted laser-desorption/ionization time-of-flight mass spectrometric detection. J. Chromatogr. A 1286, 222–228. Copyright Elsevier, 2013 and Han, Y., Levkin, P.A., Abarientos, I., Liu, H., Svec, F., Fréchet, J.M.J., 2010. Monolithic superhydrophobic layer with photopatterned virtual channel for the separation of peptides using two-dimensional thin layer chromatography – desorption electrospray ionization mass spectrometry. Anal. Chem. 82, 2520–2528. Copyright American Chemical Society, 2010.

polymerization had a smooth surface "skin" with occasional cracks. So, properties of the skin differed from those of the bulk. This is well demonstrated with the SEM image in Fig. 5.9A. The explanation for this has to be searched for in the basics of polymerization reactions. During the reaction, the monomer units are combined in a chain in which they are closer to each other compared

with the distance between them in monomer solution. As a result, shrinkage in the volume occurs during polymerization. The UV light, which penetrates through the top plate, has the highest intensity closest to the underside of the top plate. The intensity of the UV light then gradually attenuates because of the self-screening action of the polymerization mixture. Thus, the initiation rate in the vicinity of the bottom plate is the slowest. As a result, the monolith adheres to the top slide while it is released from the bottom slide already during the preparation process. The space between the released monolith and the bottom glass plate is then filled with the air, the polymerization conditions are different from those in the bulk of the layer, and the nonpermeable thin "skin" is formed.

Although not explicitly mentioned in the paper (Wouters et al., 2013), it is likely that the adhesion of the monolith to the native glass surface may not be too strong, and the monolith may peel off. This is why it appeared useful to functionalize the top glass plate, targeted for support of the thin layer, with 3-(trimethoxysilyl)propyl methacrylate, whereas the bottom plate was not. The reason why the bottom glass plate should not be functionalized was to avoid adhesion of the layer to that plate and to facilitate disassembly of the mold. The polymer layer prepared under these conditions is shown in Fig. 5.9B. Not surprisingly, it exhibited a smooth surface "skin" assembled at the polymer-glass interface (Han et al., 2010).

The situation changed when the bottom plate was also silylated. As noted previously, the polymerization rate is slower in the vicinity of the bottom plate leading to less firm attachment to that plate. On disassembling the mold, most of the polymer then adhered to the top plate, whereas only a light coating of polymer remained attached to the bottom plate. As a result, the desired internal structure of the monolithic layer was revealed at the surface (Fig. 5.9C). The morphology of the surface was also reflected in its apparent hydrophobicity. Although for the smooth surface the water contact angle was only 77 degrees, as it lacked topographical features, the "open" surface then featured a dual scale roughness and the water contact angle increased to a superhydrophobic value of 154 degrees (Han et al., 2010).

So far, we have discussed situations occurring during photoinitiated polymerization, which is well suited for monomers that are UV transparent such as methacrylates. Switching to non-UV transparent monomers, such as styrene and its derivatives, and divinylbenzene as the cross-linker, requires use of thermal initiation (Lv et al., 2013). In contrast to photopolymerization with the gradient of UV light intensity across the polymerizing layer, thermally initiated polymerization occurs in all the bulk mixture homogeneously, and adhesion of the monolith to both functionalized glass plates is equal. When the mold was disassembled, the polymer was torn into two parts with no priority for either of the glass plates. This resulted in a poorly defined thickness and a rough surface, as shown in Fig. 5.10A. The single glass plate vinylized approach did not work either. Certainly, the monolithic polymer layer did not adhere to the plain nonvinylized plate, whereas the entire monolith adhered to the vinylized plate. However once again, a smooth surface "skin" on the monolith was formed for the reason presented above (Fig. 5.10B). This problem was eventually solved using a simple trick. A strip of a commercial Scotch tape was attached to the smooth surface, and on removal of the tape, the top polymer "skin" adhered to the tape and was homogeneously removed from the entire plate, whereas the desired well-developed globular structure from beneath attached to the glass slip was revealed as shown in Fig. 5.10C. The change in surface morphology is again reflected in the increase in the water contact angle from 122 degrees for the smooth surface to 157 degrees observed for the globular counterpart (Lv et al., 2013).

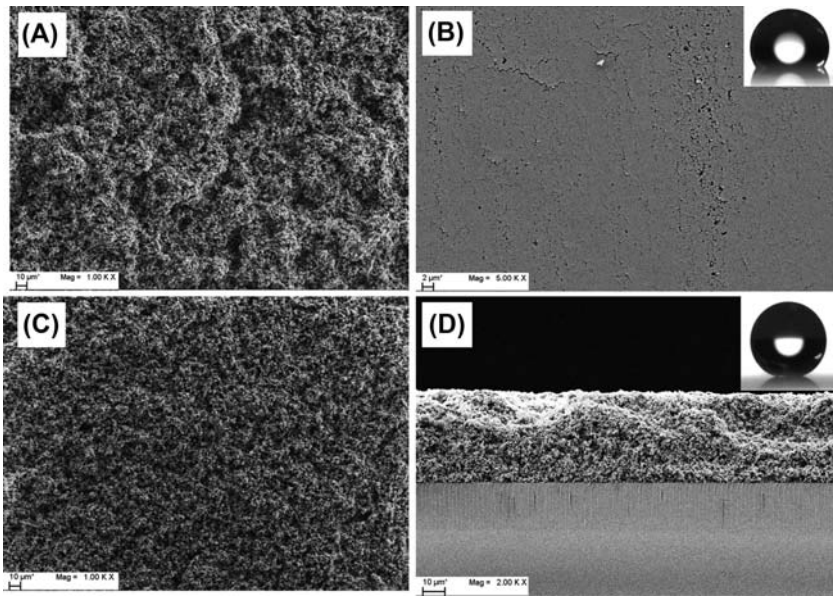

FIGURE 5.10

Scanning electron micrographs of monolithic poly(4-methylstyrene-*co*-chloro-methylstyrene-*co*-divinylbenzene) layers. (A) Layer with rough surface prepared using two vinylized glass plates; (B) layer with smooth surface prepared using one vinylized glass plate; (C) monolithic thin layer with surface opened using Scotch tape; and (D) cross section of the 50-μm-thick layer attached to glass plate support.

10. MONOLITHIC LAYERS ENHANCING DESORPTION/IONIZATION

Plates with poly(butyl methacrylate−ethylene dimethacrylate) monolithic cylinders were the first to be used for laser desorption/ionization MS. The hydrophobic porous surface of these monoliths enabled the transfer of sufficient energy to the analyte to induce desorption and ionization prior to time of flight mass spectrometric analysis (Peterson et al., 2004).

The desorption/ionization ability of the monolithic materials depends on several factors. For example, the applied laser power is an important variable. The left panel of Fig. 5.11 shows the mass spectrum obtained by irradiating a methacrylate-based monolith at a laser power slightly higher than that typically used for traditional matrices. Any higher laser power then leads to degradation of the polymer, and peaks typical of decomposition products of methacrylate polymers were observed. For comparison, the right panel presents the low-energy mass spectrum of a typical MALDI matrix, 2,5-dihydroxybenzoic acid (DHB), obtained at a typical laser power using a standard stainless steel plate. This matrix produces a large number of peaks, particularly in the area corresponding to m/z values below 600. With the DHB matrix, both the number and intensities of the undesired peaks exceeded those observed for the relatively featureless spectra of the monolithic matrix obtained at any laser power. This problem is still making use of the matrix that was less useful for detection of small molecules. Needless to say, the scale of the peak intensity axes in both panels are different by two

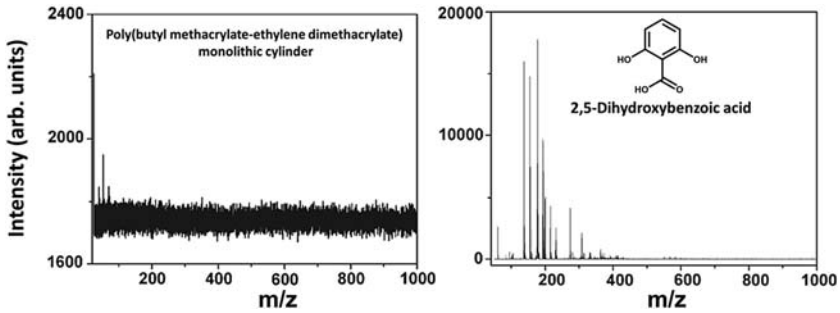

FIGURE 5.11

Laser desorption/ionization mass spectra of blank spot of porous butyl methacrylate—based monolith and of 2,5-dihydroxybenzoic acid matrix.

orders of magnitude, implying that no significant interferences are to be observed under normal use of the monolithic porous polymer matrix.

The pore size of the monoliths also plays a role in desorption and ionization. Fortunately, the easy control of porous properties via variation of the composition of the polymerization mixture is another advantage of the porous polymer monoliths, and enables a facile optimization of the pore size for the desired application. An effect of the solvent used for sample preparation was also observed. This is likely due to the differences in the wetting of the monolithic surface.

In contrast to many desorption/ionization matrices, exposure of the porous polymer monolith to air is not a problem because it does not contain any oxygen sensitive functionalities at the surface that would cause a loss of performance. Fig. 5.12 compares the mass spectrum of caffeine recorded immediately after spotting the monolithic layer to that obtained using the same sample on the same spots on a plate that had been left unprotected in the laboratory for 3 weeks. The spectra are practically identical. This demonstrates that both the monolithic matrix and the sample contained in the plate did not change even after a long period of time, and no specific precautions have to be applied to avoid contact with the environment. This finding also suggests that the monolithic spots can be used for the storage and archiving of at least nonvolatile samples.

One more advantage of the monolithic plates lies in their neutral chemistry. It is well known that many conventional low-molecular weight-matrices used in MALDI have an acidic character. This makes the use of MALDI difficult for the analysis of acid-labile compounds because they may decompose before being desorbed and ionized. For example, a complex, acid sensitive *N*,*N*′-bistrifluoroacetyl-di-(2-aminoethoxy)-[4-(1,4,7,10-tetraoxaundecyl) phenyl] methane with a molecular mass of 564 did not afford a useful MALDI-TOF MS mass spectrum using any common low molecular weight matrices. In contrast, ionization from the monolithic layer afforded a good spectrum that included peaks for the molecular ion and the sodium and potassium adducts (Peterson et al., 2004). This result clearly demonstrated that monolithic plates and spots can facilitate the ionization of numerous compounds that would be very difficult or impossible to analyze using more conventional MALDI techniques and matrices.

Instead of monolithic cylinders, Wouters et al. used photopolymerized 100 μm thick continuous monolithic poly(butyl methacrylate—ethylene dimethacrylate) layers. The only difference consisted in

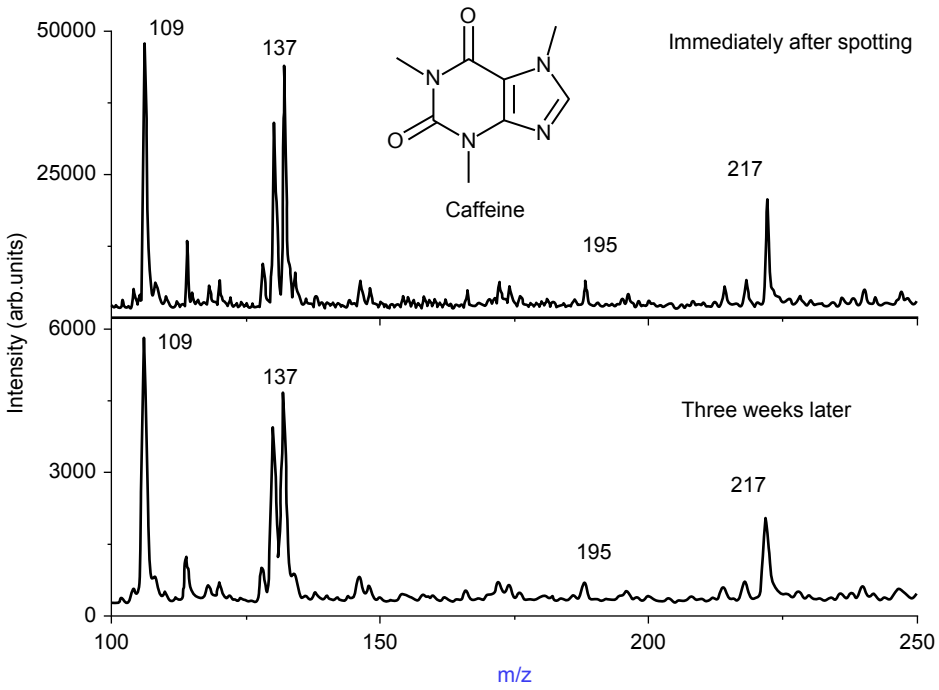

FIGURE 5.12

Mass spectrum of caffeine desorbed/ionized from surface of porous butyl methacrylate—based monolith obtained immediately after preparation of the spot and spectrum of the same spot recorded 3 weeks after the previous one.

application of a different porogenic system comprising 1,4-butanediol and 1-propanol. Motivation for their study was testing the potential of the monolith as a replacement for the labor-intensive and slow 2D polyacrylamide gel electrophoresis (PAGE) technique typically used in proteomics. They spotted solutions of the peptide angiotensin and protein cytochrome c on the monolithic layer while applying the same visualization methods as in PAGE, i.e., silver nitrate and Coomassie brilliant blue R to visualize and quantify. The detection limits were found comparable to those found for PAGE; however, the staining was achieved in a mere 10—15 min. In addition, fluorescamine-labeled angiotensin and cytochrome c were also spotted and amounts down to at least 6 ng could be detected. Complaints of the authors related to the poor spot-to-spot repeatability are likely the result of the heterogeneity of the surface "skin" discussed above.

The peptide and protein spots at the monolithic layer were covered with a solution of MALDI matrix CHCA, and mass accuracy, mass precision, and signal intensity were determined. Both angiotensin and cytochrome c were also spotted together with CHCA on the standard stainless steel MALDI plate. Based on results of the measurements, the authors concluded that the monolithic layers are unsuitable for the top-down identification of proteins, based on comparison with the direct spotting on the plate. However, there might be several reasons for the unsatisfactory results, with some of them mentioned by the authors themselves. Certainly, a thickness of 100 μm is too large, taking into account

that desorption/ionization in MALDI occurs only on the surface, not deeper than a couple of hundreds of nanometer. Because the compound is distributed throughout the entire thickness of the layer, its amount in the thin surface film is small. The presence of the less permeable "skin" at the top of the layer, which is permeable only through the cracks, also contributes to the loss of both sensitivity and repeatability. Although the use of a monolithic layer in 2D separations of proteins remains vital, similar studies should be repeated with a more precise porous polymer substrate to avoid the undesired interferences of thickness and the "skin."

11. MONOLITHIC LAYERS FOR THIN-LAYER CHROMATOGRAPHY–MASS SPECTROMETRY

TLC, one of the oldest chromatographic techniques (Izmailov and Shraiber, 1938), is mostly used to monitor the progress of organic reactions, to identify compounds present in a product mixture, and to determine product purity. The mobile phase advances vertically, driven by capillary forces, and the compounds are separated according to their differential in partitioning between the mobile phase and solid phase of the layer. Major benefits of this separation method are parallel separations of multiple samples, simple hardware, disposable "stationary phase," static detection, and easy archiving of separations. TLC may also be used for 2D separations, during which the separation and detection processes can be carried out independently, and at different times and locations (Poole, 2003a,b). Typical TLC plates are fabricated by attaching a layer of a sorbent such as silica, aluminum oxide, or cellulose to a flat support using a binder.

11.1 THIN-LAYER CHROMATOGRAPHY SEPARATION AND MASS SPECTROMETRIC DETECTION OF BIOMOLECULES

The TLC separation produces spots located along the development line, and their locations are characterized by their retardation factors (R_f value). However, this factor says nothing in relation to the structure of the compound residing in the spot. One solution to this problem is excision of the spot, extraction of the compound, and its reanalysis, typically using liquid chromatography and MS. Clearly, this procedure is tedious. This is why significant efforts have been invested in the development of mass spectrometric techniques enabling from-layer MS detection to obtain the desired molar mass information without further handling the sample. Because both TLC and MALDI MS operate with 2D devices/plates, MALDI MS prevailed in direct coupling with TLC.

In the mid-1990s, Gusev et al. published first demonstration of separations of proteins and peptides using TLC on plain silica layers with MALDI MS detection followed by a series of more specific papers (Gusev et al., 2000, 1995a,b; Mehl et al., 1997; Nicola et al., 1996; Vermillion-Salsbury et al., 1999). In addition to successful separation and detection, they also found that the detection limit was several orders of magnitude lower than that typical of conventional MALDI and even lower than "classical" UV detection (Gusev et al., 2000). They understood that most of the sample was not localized at the surface that was hit by the laser light but in the 100–250 μm thick bulk. To solve this problem, they concentrated the analyte on the surface of the layer using extraction with methanol followed by addition of a conventional MALDI matrix. It is likely that use of unsuitable commercial plain silica plates contributed to the poor separation performance. Therefore, development of novel

types of layers was desirable. The launch of monolithic plain silica-based ultrathin layers was one of the answers to this challenge. However, production of these layers was short-lived (vide supra).

We showed earlier in this chapter that preparation of thin layers supported by glass slides is simple. Thus, a 50-μm-thick monolithic poly(butyl methacrylate−ethylene dimethacrylate) layer was prepared and used for separation of fluorescamine-labeled peptides and proteins (Bakry et al., 2007). The labeling was required to observe the separated spots. Because the direct ionization of peptides from the monolithic layer was poor, CHCA was applied to amplify ionization, leading to a significant enhancement in ionization efficiency. Both spraying and spotting protocols were tested for matrix application. On spotting, undesired lateral migration of compounds in the thin layer was observed after the droplet of matrix solution was applied. This migration then moved the spot away from the original location and led to a decrease in resolution. Therefore, spraying was applied throughout the entire study. The enhancement in ionization efficiency likely resulted from the extraction function of the matrix solution, which increased the concentration of the peptide at the top of the monolithic layer, as suggested by Gusev et al. (1995b).

Fig. 5.13 shows the separation of three peptides and their characterization in spots using MALDI MS. Migration to the distance of 6 cm was rather fast and required only 5−6 min using 0.1 vol% trifluoroacetic acid in 40 vol% aqueous acetonitrile as the mobile phase. Spectra of [Sar^1,Ile^8]-angiotensin II, angiotensin II, and neurotensin feature two peaks, indicating that the spots contained both the original peptides and their fluorescamine-labeled counterparts (Bakry et al., 2007).

Similarly, proteins were also separated. A short optimization revealed that 0.1 vol% trifluoroacetic acid in 55−60 vol% aqueous acetonitrile was the most efficient mobile phase for that separation. Fluorescent labeling of the proteins enabled scanning of the plate using a fluorodensitometer, after separation of the spotted solution containing 1 pmol/μL of each compound. However, the labeling produced a host of biomolecules varying in the number of attached fluorescamines, which complicated quantification. To avoid this problem, nonlabeled proteins were detected. The sampling point was marked at the plate and scanning proceeded along the developed line. Fig. 5.14 shows the MALDI spectra of each separated protein acquired using sinapinic acid as the matrix because this compound was considered to be the matrix of choice for proteins over a wide mass range.

The previous study also included the preparation of a monolithic layer from a mixture consisting of styrene, divinylbenzene, 1-decanol, and tetrahydrofuran, with azobisisobutyronitrile as an initiator. Motivation for the use of this polymer was the assumption that the aromatic character of the layer might affect hydrophobicity and also contributes to the selectivity through the π−π interactions. Because these monomers are UV absorbing, the UV light is absorbed by the monomers and does not reach the initiator to achieve its decomposition to free radicals. Therefore, polymerization required thermal initiation. The poly(styrene-*co*-divinylbenzene) layers prepared this way were poor in quality and several defects such as cracks and nonuniform thickness could be observed. Therefore, this polymer layer was not used in the above project and more experiments were needed to obtain a useful thin layer.

The following experiments revealed that the major problem was the "skin" containing cracks and pinholes located at the external surface of the layer, such as those that were shown in Fig. 5.10. Removal of this "skin," as described above, and optimization of the composition of the polymerization mixture solved the problem (Lv et al., 2013).

The polymerization mixture used for the preparation of the layer was comprised of the monomers 4-methylstyrene, chloromethylstyrene, and divinylbenzene, porogens toluene and 1-dodecanol, and

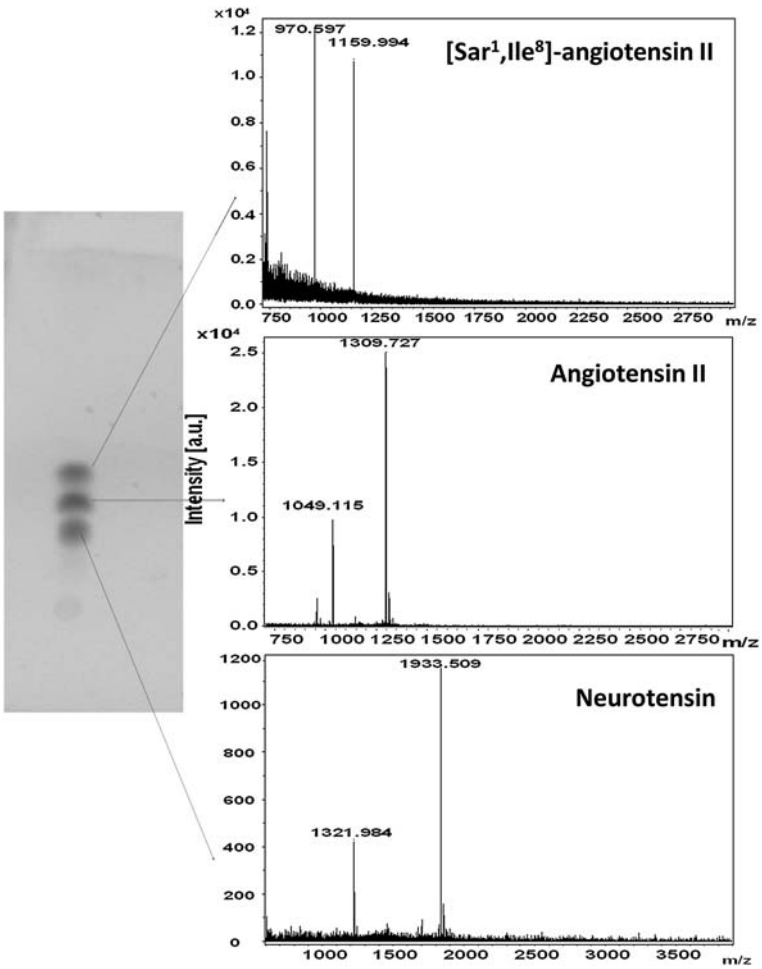

FIGURE 5.13

Thin-layer chromatography separation of mixture of peptides labeled with fluorescamine using poly(butyl acrylate-*co*-ethylene dimethacrylate) monolithic layer attached to a glass plate using 0.1 vol% trifluoroacetic acid in 45 vol% aqueous acetonitrile as the mobile phase (left) and matrix-assisted laser desorption/ionization time-of-flight mass spectrometryspectra of fluorescently labeled [Sar^1,Ile^8]-angiotensin II, angiotensin II, and neurotensin obtained "from-plate" using α-cyano-4-hydroxycinnamic acid as matrix.

azobisisobutyronitrile initiator. An SEM image of the layer is presented in Fig. 5.10. Compared with the previous monolithic poly(butyl methacrylate-*co*-ethylene dimethacrylate) plates presented by Bakry et al., the styrenics-based monolithic layers exhibited higher hydrophobicity, which was confirmed by better separation and slower migration of peptides, even in the mobile phase containing a higher percentage of acetonitrile. It is worth noting that the preparation is highly reproducible.

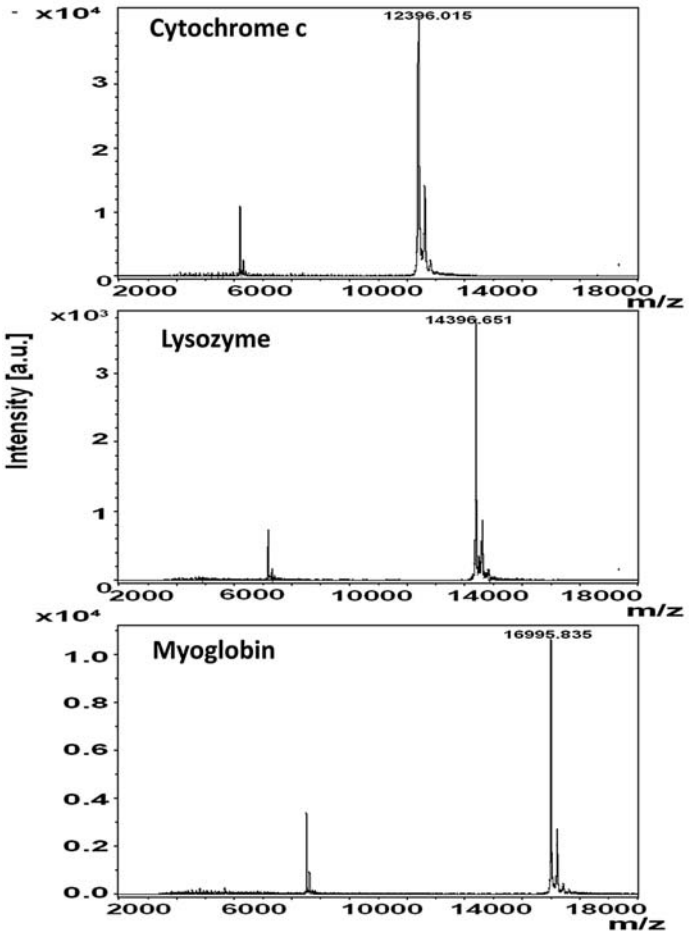

FIGURE 5.14

Matrix assisted laser desorption/ionization spectra of nonlabeled cytochrome c (1), lysozyme (2), and myoglobin (3) separated on 50-μm-thick poly(butyl acrylate-*co*-ethylene dimethacrylate) monolithic layer attached to a glass plate using 0.1 vol% trifluoroacetic acid in 60 vol% aqueous acetonitrile as the mobile phase obtained "from-plate" using sinapic acid as matrix.

Experiments with eight different plates and double spotting of peptide mixtures demonstrated excellent repeatability with an RSD for R_f of less than 2.5%.

This layer was also used for the separation of three fluorescamine-labeled proteins. Ribonuclease A, lysozyme, and myoglobin were separated in 15 min to distinct spots shown in Fig. 5.15. The elution order followed the hydrophobicity of the individual proteins, and MALDI mass spectra confirmed the

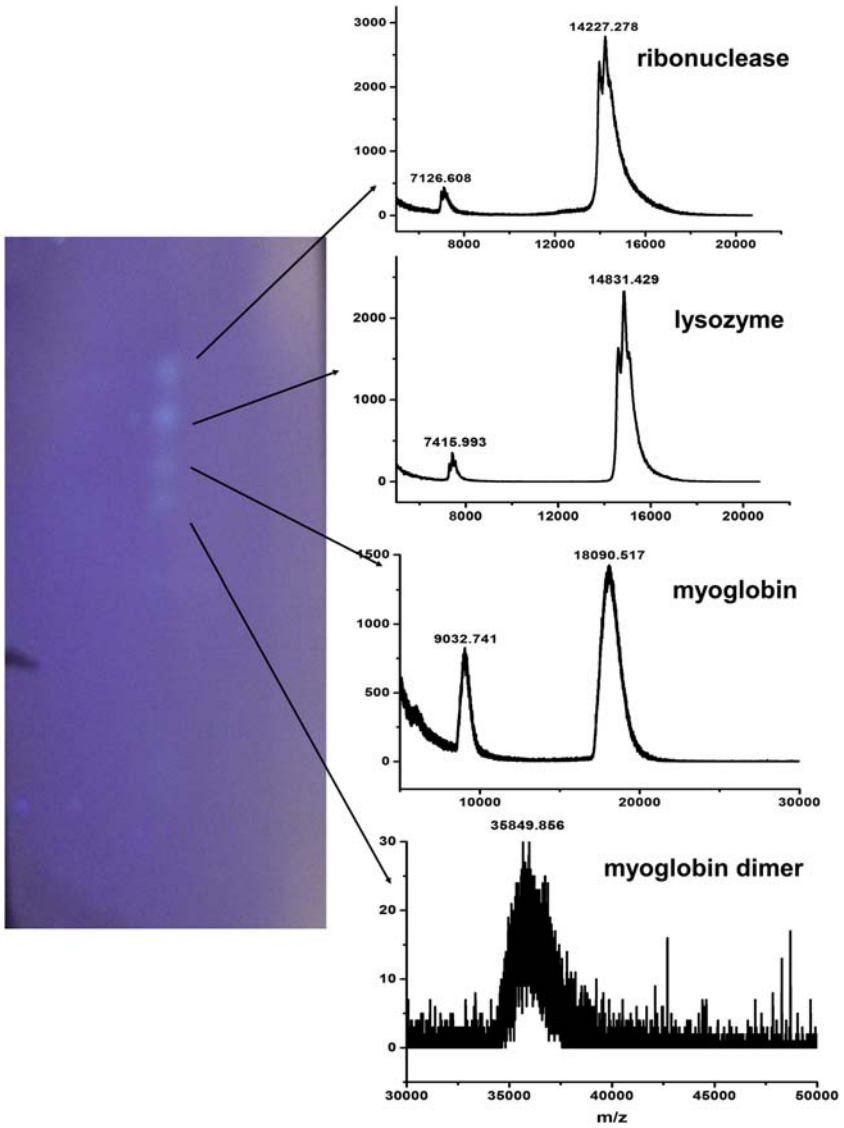

FIGURE 5.15

Thin-layer chromatography separation of a mixture of proteins ribonuclease A, lysozyme, myoglobin, and myoglobin dimer labeled with fluorescamine using 50-μm-thick poly(4-methylstyrene-*co*-chloromethylstyrene-*co*-divinylbenzene) monolithic layer developed by 65% acetonitrile in 0.1% aqueous trifluoroacetic acid solution and matrix-assisted laser desorption/ionization time-of flight mass spectrometry spectra obtained from the spots using sinapic acid matrix.

identity of the labeled proteins. The fourth spot with an $m/z = 34841.579$, which had the smallest R_f, was assigned to a myoglobin dimer, which is a known impurity in the commercial protein. Although the MS signal of this peak was weak because of the low concentration of the dimer in the sample, it contained two fluorescamine labels that enhanced the fluorescence and enabled visualization of its spot. The repeatability of R_f was again excellent with an RSD of less than 2.4%.

An additional benefit of the chemistry of these thin layers lies in their ability to get hypercrosslinked. The Friedel–Crafts alkylation reaction catalyzed by ferric chloride is known to form a large number of mesopores and leads to a significant increase in the surface area. Hypercrosslinking of the monoliths containing chloromethylstyrene units was introduced for monolithic capillary columns only recently (Maya and Svec, 2014; Skeříková and Urban, 2013; Urban et al., 2010a,b; Urban and Skeříková, 2014) and so has not been used previously for thin layers. In contrast to the original plate, a hypercrosslinked layer was able to separate even small molecules such as dyes (Lv et al., 2013).

11.2 TWO-DIMENSIONAL THIN-LAYER CHROMATOGRAPHY SEPARATION AND MASS SPECTROMETRIC DETECTION OF BIOMOLECULES

Because of its planar character, TLC is easily amenable to 2D separations that significantly increase the zone capacity. The simplest 2D implementation includes spotting the sample near a corner of the layer, developing the layer in one direction using the first mobile phase, drying the layer, and developing it with the second mobile phase after rotating it 90 degrees. Poole (2003a,b) outlined several techniques to generate orthogonality in 2D TLC. The simplest approach uses two different eluents with complementary selectivity. However, finding a system of two truly orthogonal solvents may be a challenging task (Ciesla and Waksmundzka-Hajnos, 2009; Poole and Poole, 1995).

Detection to visualize the results of the separation in 2D TLC is also important. Although the "classical" detection methods such as staining or labeling provide information related to the position of the spot and retardation factor, MS adds another dimension to the separation by identifying the isotopic mass of the separated compounds (Nurok et al., 1987). A desired sensitivity boost was ascribed to the introduction of the desorption electrospray ionization (DESI) interface (Cooks et al., 2006; Takats et al., 2004, 2005) that can be operated in scanning mode (Ifa et al., 2007; Wiseman et al., 2006). DESI has also been used for the direct detection of compounds from commercial TLC plates (Kertesz et al., 2008; Pasilis et al., 2007; Van Berkel et al., 2005).

While preparing plates for 2D TLC, several factors such as hydrophobicity, porous properties, separation performance, and mechanical strength must be considered to match the requirements of the intended chromatographic application. The hydrophobicity, which is, for example, required for the separation of peptides in reversed phase mode, was defined by the selection of chemistry of the monolithic poly(butyl methacrylate-*co*-ethylene dimethacrylate) layer and the adjustment of porous properties by variation in the proportion of porogenic solvents in the polymerization mixture (Han et al., 2010).

To develop a 2D TLC plate format enabling separation using two different mechanisms, a virtual hydrophilic channel with ionizable chemistry was photopatterned on one side of a superhydrophobic thin layer attached to a glass support. Separation in the first dimension then proceeded via ion exchange within the hydrophilic channel, whereas the remainder of the plate was used for the reversed phase separation in the second dimension.

Photografting was used for creation of the ion exchange channel. To do so, the pores of the entire superhydrophobic layer were filled with a mixture of 2-acrylamido-2-methyl-1-propanesulfonic acid, 2-hydroxyethyl methacrylate, and benzophenone dissolved in *tert*-butanol–water. UV-initiated photografting was then carried out through a simple home-made mask to produce a 0.6 mm wide channel across one side of the plate. Fig. 5.16A shows the optical microscopy image of the cross section of the patterned hydrophilic virtual channel filled with an aqueous solution of red dye. The aqueous phase is retained within the three dimensional channel by surface tension at the interface, which prevents it from entering the adjacent superhydrophobic areas of the monolithic thin layer.

The prepared 2D plates were then used for the separation of fluorescamine-labeled peptides: leucine enkephalin, bradykinin, angiotensin II, and val–tyr–val. An aqueous solution of the mixture of UV-labeled peptides was spotted close to the beginning of the grafted hydrophilic channel. The separation in the first dimension was then carried out using a mobile phase consisting of 30 vol% acetonitrile in 0.2 mol/L aqueous ammonium acetate at pH 7. To avoid the mobile phase running over the plate instead of through the channel, a paper tissue wick saturated with the mobile phase was placed at the sampling end of the ion exchange channel. The hydrophilic channel then pulled the aqueous mobile phase from the wick through the channel. For the separation in the second dimension orthogonal to the development in the first dimension, a standard chamber containing 0.1 vol%

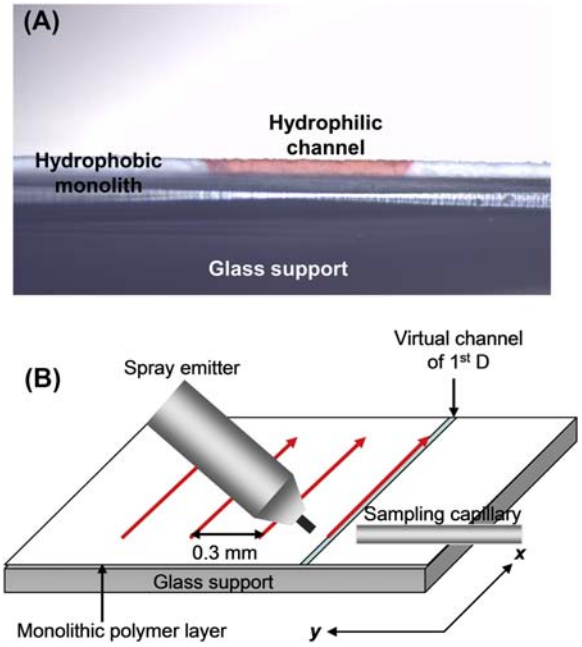

FIGURE 5.16

Optical microscopic image of cross section of the superhydrophilic channel filled with aqueous solution of red dye (A) and schematic illustration of desorption electrospray ionization scanning of surface of poly(butyl acrylate-*co*-ethylene dimethacrylate) monolithic layer to visualize the 2D separation (B).

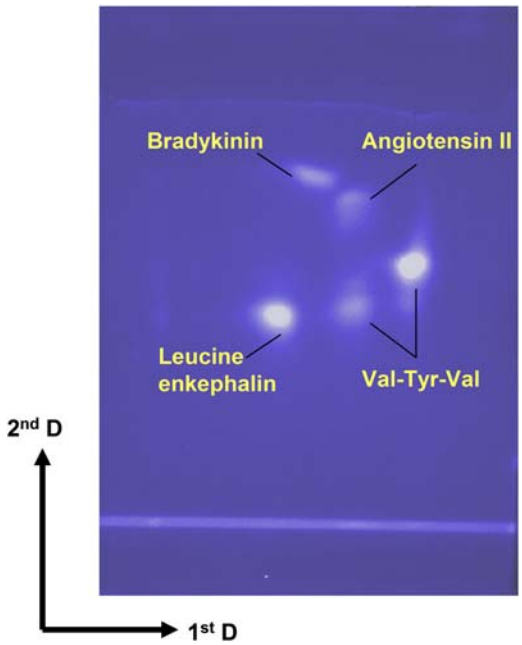

FIGURE 5.17

Two-dimensional Thin-layer chromatograohy separation of a mixture of labeled peptides including leucine enkephalin, bradykinin, angiotensin II, and val—tyr—val on monolithic polymer layer with dual chemistry detected using UV detection.

trifluoroacetic acid in 40 vol% aqueous acetonitrile was used. After completion of the 2D separation, the plate was air-dried and peptide spots were detected by illumination with UV light as shown in Fig. 5.17. Interestingly, val—tyr—val separated in two spots. Mass spectral analysis of the commercial tripeptide revealed that this tripeptide contained molecules with the expected molecular mass of 380 and a dimer with a mass of 760, thus explaining the origin of the two spots.

The unidirectional scanning described in the literature (Kertesz and Van Berkel, 2008) was then used for MS detection of nonlabeled peptides. Each selected lane on the surface of the plate was scanned in the same direction. The plate was placed on an insulated sample holder mounted on a *x*/*y*/*z* stage. Fig. 5.16B shows that the first lane was scanned by moving the plate in a direction parallel to the *x*-axis, which represents the direction of the separation in the first dimension, i.e., in the grafted channel, from low to high R_f. At the end of the first lane, the surface was moved back to the beginning of the lane. Then the surface was moved parallel to the *y*-axis and scanning of the next lane was carried out. The *y*-axis represents the direction of the separation in second dimension. This process was repeated until the entire plate was scanned.

Fig. 5.18 presents results of the separation of nonlabeled peptides in the first dimension. Their positions along the virtual channel were constructed from extracted ion profiles using DESI-MS. The separation profile also indicated a certain overlap of spots of the separated peptides and the mass spectra of the individual spots were not very clean.

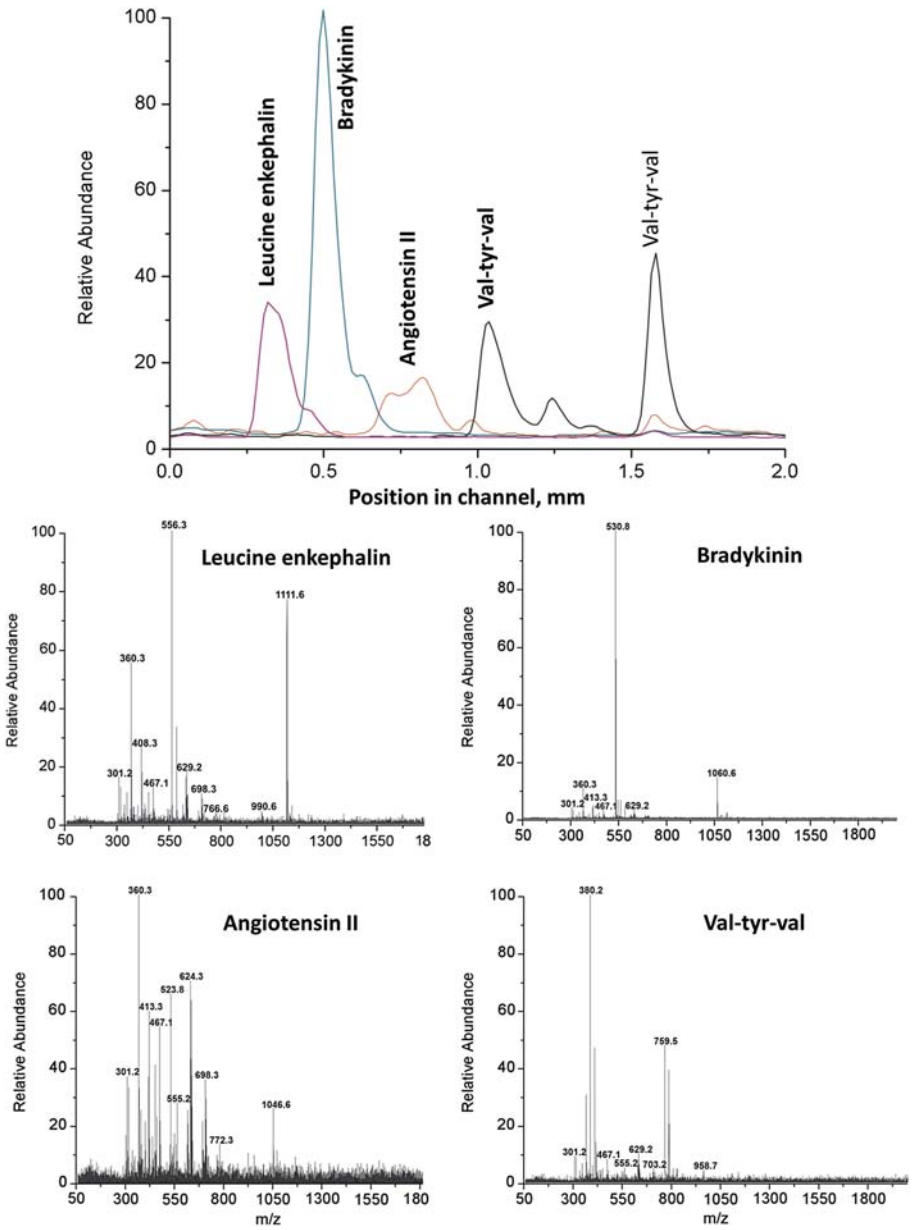

FIGURE 5.18

Desorption electrospray ionization (DESI) mass spectrometry (MS) scan of the first dimension separation of peptides leucine enkephalin, bradykinin, angiotensin II, and val–tyr–val achieved in the 30 mm long virtual channel grafted with the 2-acrylamido-2-methyl-1-propanesulfonic acid–2-hydroxyethyl methacrylate mixture (top spectrum) and DESI-MS spectra of individual peptides.

Fig. 5.19 then shows mass spectra corresponding to individual peptides found during the scanning of the plate after 2D separation. The spectra are significantly cleaner, thus demonstrating that the resolution improved after separation in the second dimension. Also, the order of the monitored peptides changed to leucine enkephalin, val−tyr−val, angiotensin II, and bradykinin, and it was different from that observed in the first dimension.

Although in the previous study photografting was used to create the virtual channel, this technique can also be used for the preparation of plates with a gradient of hydrophobicity designed for 2D separations. The parent monolithic porous layer supported at a glass plate was prepared from glycidyl methacrylate and ethylene dimethacrylate and then hydrolyzed using dilute sulfuric acid to produce a poly(glycerol methacrylate-*co*-ethylene dimethacrylate) thin layer. Although this reaction increased the hydrophilicity of the layer, it remained insufficient to completely avoid adsorption of some more hydrophobic compounds. Therefore, all the pores were first photografted with poly(ethylene glycol) methacrylate, thus producing a surface that exhibited a water contact angle close to 0 degrees, rendering the entire layer superhydrophilic. This hydrophilized monolithic layer was then wetted with a solution of benzophenone in lauryl methacrylate−ethanol mixture. The wetted layer was covered with the quartz plate, and the top of this plate with a mask nontransparent to the UV light. Creation of the diagonal gradient was very simple. The mask was attached with a string to a syringe pump set to a constant speed and moved diagonally across the mold over the course of 5 min. The ideal situation is modeled in Fig. 5.20A. The actual gradient was confirmed by measuring the water contact angle at different surface locations. The bottom left corner was the most hydrophilic part, with a contact angle of 0 degrees, whereas the most hydrophobic part at the top right corner exhibited a contact angle of 135 degrees. The gradient profile was also visualized in UV light after labeling the plate with 1-anilinonaphthalene-8-sulfonic acid solution (Fig. 5.20B).

The positive effect of TLC with the gradient of lauryl methacrylate is demonstrated with separations shown in Fig. 5.21 using four different plates. Clearly, the initial poly(glycidyl methacrylate-*co*-ethylene dimethacrylate) layer did not produce any good 2D separation (Fig. 5.21A). All peptides are retained close to the sampling corner and their spots after 2D development were smeared. Similarly, a plate with all epoxide groups hydrolyzed to reduce interactions with peptides did not provide a good result. The peptides migrated quickly through the plate without being adequately separated, and the spot shapes were poor (Fig. 5.21B). A slightly better separation was achieved using a monolithic TLC plate with a homogeneously grafted layer of poly(lauryl methacrylate). Fig. 5.21C shows that the peptides are separated with leucine enkephaline and oxytocin producing the smallest and the largest retardation factor, R_f. However, val−tyr−val and gly−tyr coeluted and their spot was located between the other two peptides.

Fig. 5.21D then represents the best separation using a plate with diagonally grafted hydrophobicity. The peptide mixture was spotted at the most hydrophilic part of the plate and the first dimension separation was carried out using acidic aqueous acetonitrile. This separation was very fast and accomplished in less than 1 min. At that time, the front of the mobile phase almost reached the end of the layer. This separation afforded three distinct spots of leucine enkephalin, coeluted val−tyr−val with gly−tyr, and oxytocin. This result was almost identical with that achieved with the homogeneously grafted hydrophobic plate. However, after turning the plate perpendicularly and developing it in the second dimension with acidic aqueous methanol, val−tyr−val and gly−tyr were clearly separated from each other with val−tyr−val having the larger R_f value.

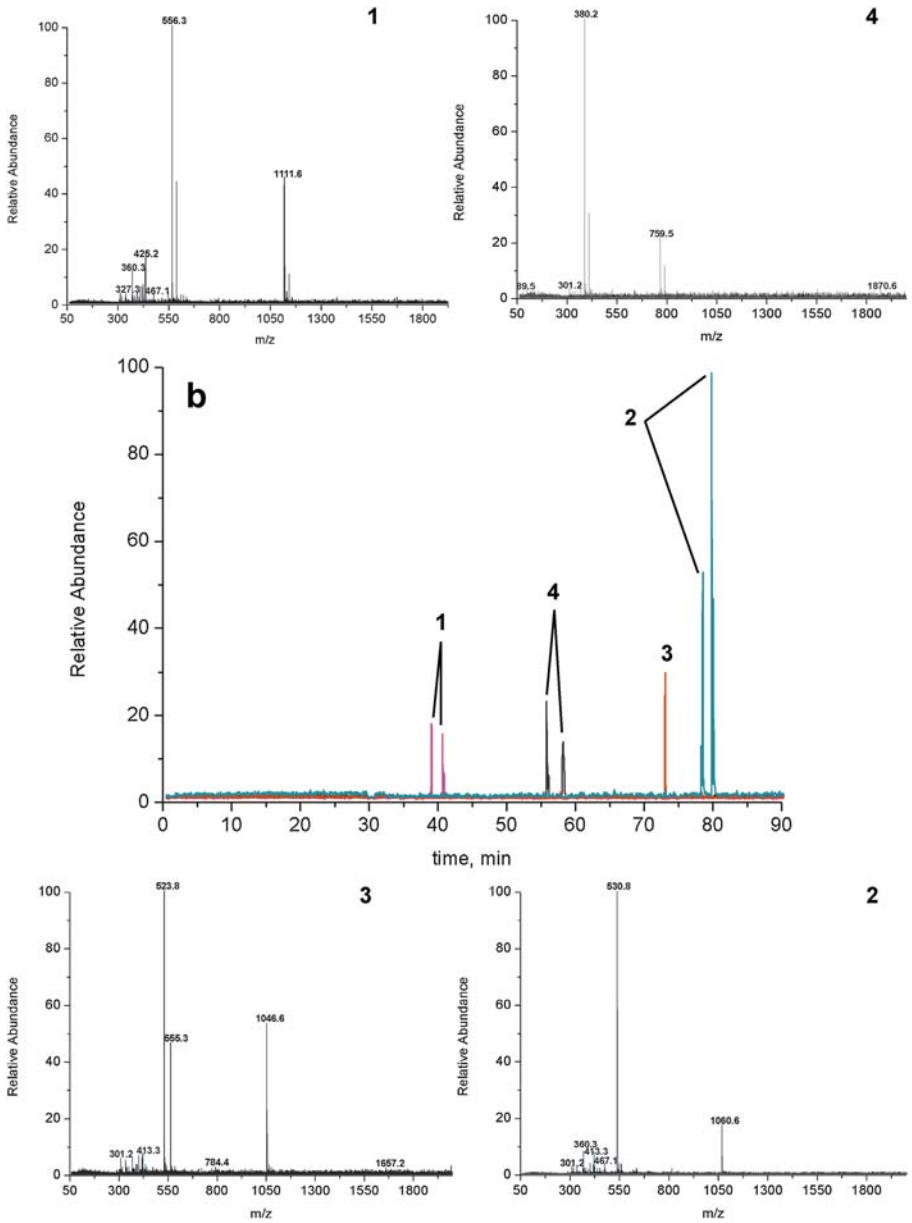

FIGURE 5.19

Desorption electrospray ionization (DESI) mass spectrometry (MS) spectra of leucine enkephalin, bradykinin, angiotensin II, and val–tyr–val observed during scan of the entire plate after two dimensional separation using monolithic polymer layer with dual chemistry.

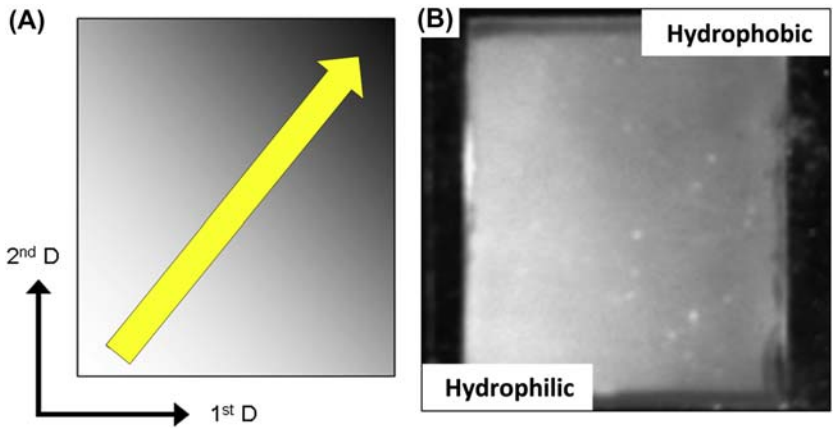

FIGURE 5.20

Artistic rendition of the gradient of hydrophobicity at a monolithic thin-layer chromatography plate increasing in the direction of the *arrow* together with suggested directions of the separations in first (1st D) and second dimension (2nd D) (A), and visualization of the gradient of hydrophobicity using fluorescent labeling with 1-anilinonaphthalene-8-sulfonic acid (B). The bright area at the left down corner represents the most hydrophilic part and the dark at top right most hydrophobic part.

The reason for the better separations on the diagonally grafted layer was considered to be the following. On the plate grafted in the "linear" manner, the peptides come into contact with the same hydrophobicity in both the first and the second dimensions. Therefore, all the spots are lined up along the diagonal. In contrast, the diagonally grafted layer provides a gradient of hydrophobicity during development in both dimensions and enables fine tuning of the separation. The oxytocin separated into two spots. The mass spectral analysis of the commercial nonapeptide indicated that it contained molecules with the expected molecular mass and that of a dimer, thus explaining the origin of the two spots. It is worth noting that the separation in the second dimension was completed in less than 3 min.

The feasibility of mass spectrometric detection was then demonstrated with leucine enkephalin and oxytocin. These two unlabeled larger peptides were mixed in equivalent quantities, and their separation carried out using conditions applied to the labeled peptides. After the separation in both dimensions was completed, the monolith was sprayed with the matrix solution and dried. Fig. 5.22 shows the mass spectra of leucine enkephalin and oxytocin, after the separation in the first and second dimensions, respectively. The signal-to-noise ratio is good even after separation in the first dimension, with no signal of the other peptide observed. However, the spectra of both peptides obtained after the 2D separation are cleaner because impurities typically contained in man-made peptides are separated away from the major spot. This "cleanup" advantage of the 2D TLC separations is similar to that observed above and presented in Figs. 5.18 and 5.19.

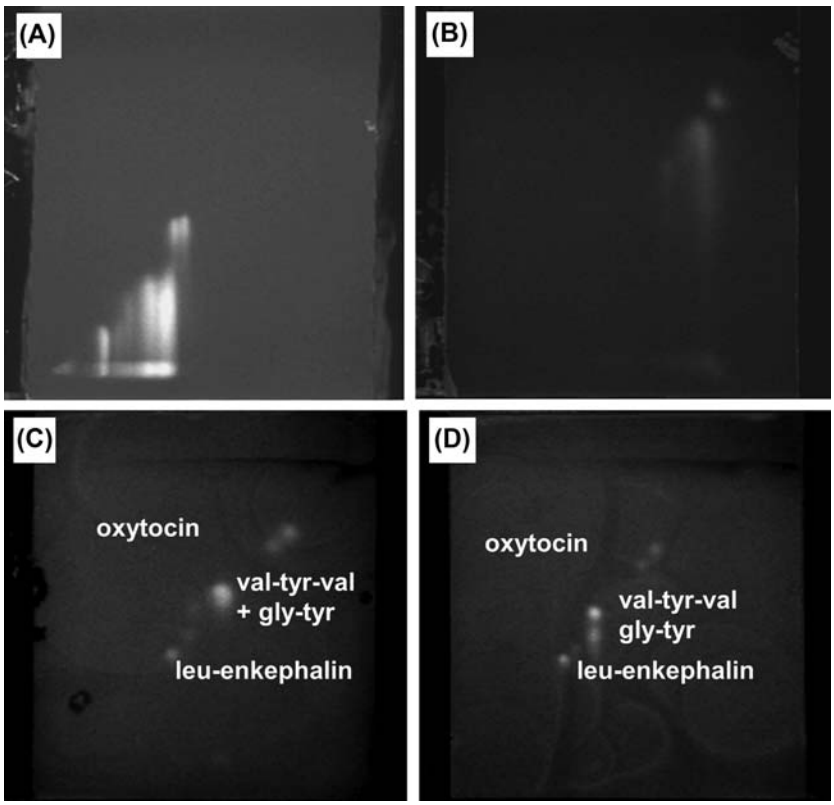

FIGURE 5.21

Separation of leucine enkephalin, gly−tyr, val−tyr−val, and oxytocin on plates consisting of poly(glycidyl methacrylate-ethylene dimethacrylate) monolith (A), poly(glycidyl methacrylate-ethylene dimethacrylate) monolith with hydrolyzed epoxy groups (B), monolithic layer with poly(lauryl methacrylate) homogeneously photografted on the entire surface (C), and monolithic layer with hydrophilized surface photografted with a diagonal gradient of poly(lauryl methacrylate) (D) using mobile phase 0.1% trifluoroacetic acid in 30% acetonitrile−water in the first dimension and 0.1% trifluoroacetic acid in 50% methanol−water in the second dimension.

12. CONCLUDING REMARKS

Monolithic thin layers represent an interesting format of materials that are most often used in columns. However, this chapter demonstrates that these layers are a very powerful tool enabling not only separations of small molecules, i.e., the typical domain of TLC, but also separations of biopolymers. Combination with MS makes this approach even more suitable, at least for rapid and easy screening of

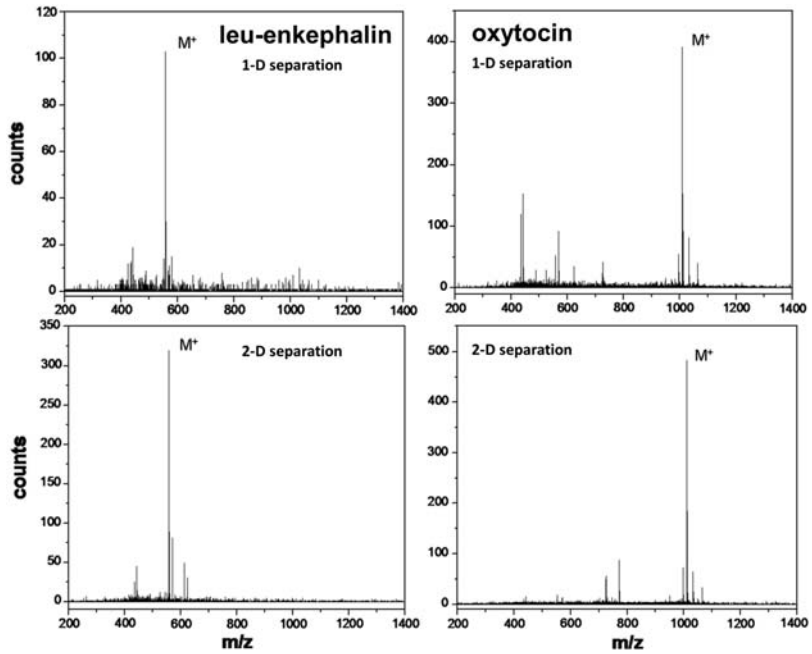

FIGURE 5.22

Matrix assisted laser desorption/ionization-mass spectrometry spectra of leucine enkephalin and oxytocin obtained after ionization from the plate after separation in first (left panels) and second dimension (right panels) α-cyano-4-hydroxycinnamic acid as matrix.

mixtures of interest before they are rigorously characterized using more sophisticated techniques. The specific advantages of separations using monolithic thin layers are possibility of parallel separation of multiple samples, very much welcome in high-throughput techniques, easy implementation of 2D separations, simple hardware, disposable "stationary phase," static detection, separation and detection that can be separated in time and location, archiving of separated compounds at the layer, and sample integrity. It is possible that in the future, TLC techniques may compete with the current gold standard of 2D gels widely used in proteomics. Further developments of MS techniques enabling ionization "from-layer," including DESI and laser ablation electrospray ionization will help to make TLC more attractive, not only in proteomics, and that new horizons will open for this analytical method.

REFERENCES

Afeyan, N.B., Gordon, N.F., Mazsaroff, I., Varady, L., Fulton, S.P., Yang, Y.B., Regnier, F.E., 1990. Flow-through particles for the high-performance liquid chromatographic separation of biomolecules: perfusion chromatography. J. Chromatogr. A 519, 1−29.

Bakry, R., Bonn, G.K., Mair, D., Svec, F., 2007. Monolithic porous polymer layer for the separation of peptides and proteins using thin-layer chromatography coupled with MALDI-TOF-MS. Anal. Chem. 79, 486−493.

Beilke, M.C., Zewe, J.W., Clark, J.E., Olesik, S.V., 2013. Aligned electrospun nanofibers for ultra-thin layer chromatography. Anal. Chim. Acta 761, 201−208.

Belenkii, B.G., Podkladenko, A.M., Kurenbin, O.I., Mal'tsev, V.G., Nasledov, D.G., Trushin, S.A., 1993. Peculiarities of zone migration and band broadening in gradient reversed-phase high-performance liquid chromatography of proteins with respect to membrane chromatography. J. Chromatogr. 645, 1−15.

Cheng, S.C., Huang, M.Z., Shiea, J., 2011. Thin layer chromatography/mass spectrometry. J. Chromatogr. A 1218, 2700−2711.

Ciesla, L., Waksmundzka-Hajnos, M., 2009. Two-dimensional thin-layer chromatography in the analysis of secondary plant metabolites. J. Chromatogr. A 1216, 1035−1052.

Clark, J.E., Olesik, S.V., 2009. Technique for ultrathin layer chromatography using an electrospun, nanofibrous stationary phase. Anal. Chem. 81, 4121−4129.

Clark, J.E., Olesik, S.V., 2010. Electrospun glassy carbon ultra-thin layer chromatography devices. J. Chromatogr. A 1217, 4655−4662.

Cooks, R.G., Ouyang, Z., Takats, Z., Wiseman, J.M., 2006. Ambient mass spectrometry. Science 311, 1566−1570.

Fang, X., Olesik, S.V., 2014. Carbon nanotube and carbon nanorod-filled polyacrylonitrile electrospun stationary phase for ultra-thin layer chromatography. Anal. Chim. Acta 830, 1−10.

Gusev, A.I., Proctor, A., Rabinovich, Y.I., Hercules, D.M., 2000. Interfacing matrix-assisted laser desorption/ionization mass spectrometry with column and planar separations. Fresenius' J. Anal. Chem. 366, 691−700.

Gusev, A.I., Proctor, A., Rabinovich, Y.I., Hercules, D.M., 1995a. Thin-layer chromatography combined with matrix-assisted laser desorption/ionization mass spectrometry. Anal. Chem. 67, 1805−1814.

Gusev, A.I., Vasseur, O.J., Proctor, A., Sharkey, A.G., Hercules, D.M., 1995b. Imaging of thin-layer chromatograms using matrix-assisted laser desorption/ionization mass spectrometry. Anal. Chem. 67, 4565−4570.

Han, Y., Levkin, P.A., Abarientos, I., Liu, H., Svec, F., Fréchet, J.M.J., 2010. Monolithic superhydrophobic layer with photopatterned virtual channel for the separation of peptides using two-dimensional thin layer chromatography − desorption electrospray ionization mass spectrometry. Anal. Chem. 82, 2520−2528.

Hauck, H.E., Bund, O., Fischer, W., Schulz, M., 2001. Ultra-thin layer chromatography (UTLC) − a new dimension in thin-layer chromatography. J. Planar Chromatogr. Modern TLC 14, 234−236.

Hauck, H.E., Schulz, M., 2003. Ultra thin-layer chromatography. Chromatographia 57, S/313−S/315.

Hileman, F.D., Sievers, R.E., Hess, G.G., Ross, W.D., 1973. In situ preparation of open pore polyurethane chromatographic columns. Anal. Chem. 45, 1126.

Hjertén, S., Liao, J.L., Zhang, R., 1989. High-performance liquid chromatography on continuous beds. J. Chromatogr. A 473, 273−275.

Ifa, D.R., Wiseman, J.M., Song, Q.Y., Cooks, R.G., 2007. Development of capabilities for imaging mass spectrometry under ambient conditions with desorption electrospray ionization (DESI). Int. J. Mass Spectrom. 259, 8−15.

Izmailov, N.A., Shraiber, M.S., 1938. A drop-chromatographic method of analysis and its utilization in pharmacy. Farmatsiya (Mosc. 1938−47) 1−7.

Kertesz, V., Van Berkel, G.J., 2008. Scanning and surface alignment considerations in chemical imaging with desorption electrospray mass spectrometry. Anal. Chem. 80, 1027−1032.

Kertesz, V., Van Berkel, G.J., Vavrek, M., Koeplinger, K.A., Schneider, B.B., Covey, T.R., 2008. Comparison of drug distribution images from whole-body thin tissue sections obtained using desorption electrospray ionization tandem mass spectrometry and autoradiography. Anal. Chem. 80, 5168−5177.

Kirkland, J.J., 1992. Superficially porous silica microspheres for the fast high-performance liquid chromatography of macromolecules. Anal. Chem. 64, 1239−1245.

Kubín, M., Špaček, P., Chromeček, R., 1967. Gel permeation chromatography on porous poly(ethylene glycol methacrylate). Collect. Czechoslov. Chem. Commun. 32, 3881−3887.

Liao, J.L., Zhang, R., Hjertén, S., 1991. Continuous beds for standard and micro high-performance liquid chromatography. J. Chromatogr. A 586, 21−26.

Liapis, A.I., Meyers, J.J., Crosser, O.K., 1999. Modeling and simulation of the dynamic behavior of monoliths. Effects of pore structure from pore network model analysis and comparison with columns packed with porous spherical particles. J. Chromatogr. A 865, 13−25.

Lu, T., Olesik, S.V., 2013a. Electrospun nanofibers as substrates for surface-assisted laser desorption/ionization and matrix-enhanced surface-assisted laser desorption/ionization mass spectrometry. Anal. Chem. 85, 4384−4391.

Lu, T., Olesik, S.V., 2013b. Electrospun polyvinyl alcohol ultra-thin layer chromatography of amino acids. J. Chromatogr. B 912, 98−104.

Lv, Y., Lin, Z., Tan, T., Svec, F., 2013. Preparation of porous styrenics-based monolithic layers for thin layer chromatography coupled with matrix-assisted laser-desorption/ionization time-of-flight mass spectrometric detection. J. Chromatogr. A 1316, 154−159.

Majors, R.E., 2015. Historical developments in HPLC and UHPLC column technology: the past 25 years. LC-GC N. Am. 33, 818−840.

Martin, A.J.P., Synge, R.L.M., 1941. A new form of chromatogram employing two liquid phases. Biochem. J. 35, 1358−1368.

Maya, A., Svec, F., 2014. A new approach to the preparation of large surface area poly(styrene-co-divinylbenzene) monoliths via knitting of loose chains using external crosslinkers and application of these monolithic columns for separation of small molecules. Polymer 55, 340−346.

Mehl, J.T., Gusev, A.I., Hercules, D.M., 1997. Coupling protocol for thin layer chromatography/matrix-assisted laser desorption ionization. Chromatographia 46, 358−364.

Meyers, J.J., Liapis, A.I., 1999. Network modeling of the convective flow and diffusion of molecules adsorbing in monoliths and in porous particles packed in a chromatographic column. J. Chromatogr. A 852, 3−23.

Minakuchi, H., Nakanishi, K., Soga, N., Ishizuka, N., Tanaka, N., 1996. Octadecylsilylated porous silica rods as separation media for reversed-phase liquid chromatography. Anal. Chem. 68, 3498−3501.

Moravcová, D., Rantamaki, A.H., Duša, F., Wiedmer, S.K., 2016. Monoliths in capillary electrochromatography and capillary liquid chromatography in conjunction with mass spectrometry. Electrophoresis 37, 880−912.

Mould, D.L., Synge, R.L.M., 1952. Electrokinetic ultrafiltration analysis of polysaccharides. A new approach to the chromatography of large molecules. Analyst 77, 964−970.

Mould, D.L., Synge, R.L.M., 1954. Separations of polysaccharides related to starch by electrokinetic ultrafiltration in collodion membranes. Biochem. J. 58, 571−585.

Nicola, A.J., Gusev, A.I., Hercules, D.M., 1996. Direct quantitative analysis from thin-layer chromatography plates using matrix-assisted laser desorption/ionization mass spectrometry. Appl. Spectrosc. 50, 1479−1482.

Nir, A., Pismen, L.M., 1977. Simultaneous intraparticle forced convection, diffusion and reaction in a porous catalyst. Chem. Eng. Sci. 32, 35−41.

Nurok, D., Habibi-Goudarzi, S., Kleyle, R., 1987. Statistical approach to solvent selection as applied to two-dimensional thin-layer chromatography. Anal. Chem. 59, 2424−2428.

Orinak, A., Arlinghaus, H.F., Vering, G., Orinakova, R., Hellweg, S., 2005. Introduction to time-of-flight secondary ion mass spectrometry application in chromatographic analysis. J. Chromatogr. A 1084, 113−118.

Pasilis, S.P., Kertesz, V., Van Berkel, G.J., 2007. Surface scanning analysis of planar arrays of analytes with desorption electrospray ionization-mass spectrometry. Anal. Chem. 79, 5956−5962.

Peterson, D.S., Hilder, E.F., Luo, Q., Svec, F., Fréchet, J.M.J., 2004. Porous polymer monolith for matrix-free laser desorption ionization time of flight mass spectrometry of small molecules. Rapid Commun. Mass Spectrom. 18, 1504−1512.

Petro, M., Svec, F., Gitsov, I., Fréchet, J.M.J., 1996. Molded monolithic rod of macroporus poly(styrene-co-divinylbenzene) as a novel separation medium for HPLC of synthetic polymers. "On column" precipitation and redissolution chromatography as an alternative to size exclusion chromatography. Anal. Chem. 68, 315−321.

Poole, C.F., 2003a. The Essence of Chromatography. Elsevier, Amsterdam.
Poole, C.F., 2003. Thin-layer chromatography: challenges and opportunities. J. Chromatogr. A 1000, 963–984.
Poole, C.F., Poole, S.K., 1995. Multidimensionality in planar chromatography. J. Chromatogr. A 703, 573–612.
Poole, S.K., Poole, C.F., 2011. High performance stationary phases for planar chromatography. J. Chromatogr. A 1218, 2648–2660.
Rodrigues, A.E., Lopes, J.C., Lu, Z.P., Loureiro, J.M., Dias, M.M., 1992. Importance of intraparticle convection in the performance of chromatographic processes. J. Chromatogr. A 590, 93–100.
Rodrigues, A.E., Lu, Z.P., Loureiro, J.M., Carta, G., 1993. Peak resolution in linear chromatography – effects of intraparticle convection. J. Chromatogr. A 653, 189–198.
Rodrigues, A.E., Mata, V.G., Zabka, M., Pais, L., 2003. Flow and mass transfer. In: Svec, F., Tennikova, T.B., Deyl, Z. (Eds.), Monolithic Materials: Preparation, Properties and Applications, pp. 325–350.
Rojanarata, T., Plianwong, S., Su-uta, K., Opanasopit, P., Ngawhirunpat, T., 2013. Electrospun cellulose acetate nanofibers as thin layer chromatographic media for eco-friendly screening of steroids adulterated in traditional medicine and nutraceutical products. Talanta 115, 208–213.
Ross, W.D., Jefferson, R.T., 1970. In situ formed open pore polyurethane as chromatography support. J. Chromatogr. Sci. 8, 386–389.
Salo, P.K., Salomies, H., Harju, K., Ketola, R.A., Kotiaho, T., Yli-Kauhaluoma, J., Kostiainen, R., 2005. Analysis of small molecules by ultra thin-layer chromatography-atmospheric pressure matrix-assisted laser desorption/ionization mass spectrometry. J. Am. Soc. Mass Spectrom. 16, 906–915.
Schnecko, H., Bieber, O., 1971. Foam filled columns in gas chromatography. Chromatographia 4, 109–112.
Skeříková, V., Urban, J., 2013. Highly stable surface modification of hypercrosslinked monolithic capillary columns and their application in hydrophilic interaction chromatography. J. Sep. Sci. 36, 2806–2812.
Svec, F., 2008. Stellan Hjertén's contribution to the development of monolithic stationary phases. Electrophoresis 29, 1593–1603.
Svec, F., 2010. Porous polymer monoliths: amazingly wide variety of techniques enabling their preparation. J. Chromatogr. A 1217, 902–924.
Svec, F., Fréchet, J.M.J., 1992. Continuous rods of macroporous polymer as high performance liquid separation media. Anal. Chem. 64, 820–822.
Svec, F., Fréchet, J.M.J., 1995. Kinetic control of of pore formation in macroporous polymers. The formation of "molded" porous materials with high flow characteristics for separation and catalysis. Chem. Mater. 7, 707–715.
Svec, F., Hradil, J., Čoupek, J., Kálal, J., 1975. Reactive polymers 1. Macroporous methacrylate copolymer containing epoxy groups. Angew. Macromol. Chem. 48, 135–143.
Svec, F., Tennikova, T.B., 1991. Polymeric separation media for chromatography of biopolymers in a novel shape. J. Bioact. Biocompat. Polym. 6, 393–405.
Sýkora, D., Svec, F., Fréchet, J.M.J., 1999. Separation of oligonucleotides on novel monolithic columns with ion-exchange functional surfaces. J. Chromatogr. A 852, 297–304.
Takats, Z., Wiseman, J.M., Gologan, B., Cooks, R.G., 2004. Mass spectrometry sampling under ambient conditions with desorption electrospray ionization. Science 306, 471–473.
Takats, Z., Wiseman, J.M., Cooks, R.G., 2005. Ambient mass spectrometry using desorption electrospray ionization (DESI): instrumentation, mechanisms and applications in forensics, chemistry, and biology. J. Mass Spectrom. 40, 1261–1275.
Tennikova, T.B., Svec, F., Belenkii, B.G., 1990. High performance membrane chromatography. A novel method of protein separation. J. Liq. Chromatogr. 13, 63–70.
Tennikova, T.B., Bleha, M., Svec, F., Almazova, T.V., Belenkii, B.G., 1991. High performance membrane chromatography of proteins. A novel method of protein separation. J. Chromatogr. A 555, 97–107.

Tennikova, T.B., Svec, F., 2003. Theoretical aspects of separation using short monolithic beds. In: Svec, F., Tennikova, T.B., Deyl, Z. (Eds.), In Monolithic Materials: Preparation, Properties and Applications, pp. 351−372.

Tswett, M.S., 1906. Adsorptionsanalyse und chromatographische Methode. Anwendung auf die Chemie des Chlorophylls. Ber. Dtsch. Bot. Ges. 24, 384−393.

Urban, J., Skeříková, V., 2014. Effect of hypercrosslinking conditions on pore size distribution and efficiency of monolithic stationary phases. J. Sep. Sci. 37, 3082−3089.

Urban, J., Svec, F., Fréchet, J.M.J., 2010a. Efficient separation of small molecules using a large surface area hypercrosslinked monolithic polymer capillary column. Anal. Chem. 82, 1621−1623.

Urban, J., Svec, F., Fréchet, J.M.J., 2010b. Hypercrosslinking: new approach to porous polymer monolithic capillary columns with large surface area for the highly efficient separation of small molecules. J. Chromatogr. A 1217, 8212−8221.

Van Berkel, G.J., Ford, M.J., Deibel, M.A., 2005. Thin-layer chromatography and mass spectrometry coupled using desorption electrospray ionization. Anal. Chem. 77, 1207−1215.

Vermillion-Salsbury, R.L., Hoops, A.A., Gusev, A.I., Hercules, D.M., 1999. Analysis of cationic pesticides by thin layer chromatography/matrix-assisted laser desorption ionization mass spectrometry. Int. J. Environ. Anal. Chem. 73, 179−190.

Viklund, C., Svec, F., Fréchet, J.M.J., Irgum, K., 1996. Monolithic molded porous materials with high flow characteristics for separation, catalysis, or solid phase chemistry: control of porous properties during polymerization. Chem. Mater. 8, 744−750.

Wahab, M.F., Wimalasinghe, R.M., Wang, Y., Barhate, C.L., Patel, D.C., Armstrong, D.W., 2016. Salient sub-second separations. Anal. Chem. 88, 8821−8826.

Wang, Q., Svec, F., Fréchet, J.M.J., 1993. Macroporous polymeric stationary phase rod as continuous separation medium for reversed phase chromatography. Anal. Chem. 65, 2243−2248.

Wang, Q., Svec, F., Fréchet, J.M.J., 1994. Reversed phase chromatography of small molecules and peptides on a continuous rod of macroporous styrene − divinylbenzene. J. Chromatogr. A 669, 230−235.

Wei, B., Rogers, B.J., Wirth, M.J., 2012. Slip flow in colloidal crystals for ultraefficient chromatography. J. Am. Chem. Soc. 134, 10780−10782.

Wiseman, J.M., Ifa, D.R., Song, Q.Y., Cooks, R.G., 2006. Tissue imaging at atmospheric pressure using desorption electrospray ionization (DESI) mass spectrometry. Angew. Chem. Int. Ed. 45, 7188−7192.

Wouters, B., Vanhoutte, D.J.D., Aarnoutse, P., Visser, A., Stassen, C., Devreese, B., Kok, W.T., Schoenmakers, P.J., Eeltink, S., 2013. Visualization procedures for proteins and peptides on flat-bed monoliths and their effects on matrix-assisted laser-desorption/ionization time-of-flight mass spectrometric detection. J. Chromatogr. A 1286, 222−228.

Xie, S., Allington, R.W., Svec, F., Fréchet, J.M.J., 1999. Rapid reversed phase separation of proteins and peptides using optimized “molded” monolithic poly(styrene-co-divinylbenzene) columns. J. Chromatogr. A 865, 169−174.

FURTHER READING

Svec, F., Tennikova, T.B., Deyl, Z., 2003. Monolithic Materials: Preparation, Properties, and Applications. Elsevier, Amsterdam.

CHAPTER

6

NEW MATERIALS FOR STATIONARY PHASES IN LIQUID CHROMATOGRAPHY/MASS SPECTROMETRY

Monika M. Dittmann, Xiaoli Wang
Agilent Technologies GmbH, Waldbronn, Germany

SYMBOLS

$d_{\mathbf{core}}$	particle core diameter
$D_{\mathbf{eff}}$	effective diffusion coefficient in a packed bed
D_m	diffusion coefficient in mobile phase
d_p	particle diameter
$D_{\mathbf{part}}$	diffusion coefficient in particle
D_{pz}	diffusion coefficient in porous zone
h	reduced plate height
H	plate height
k	retention factor
k''	zone retention factor
k_0	retention factor for unretained compound
K_0	permeability based on chromatographic velocity u_0
k_c	Kozeny−Carman constant
L	column length
P	pressure
u_0	chromatographic velocity
u_e	interstitial velocity

GREEK SYMBOLS

ε_e	interstitial porosity
ε_{pz}	porous zone porosity
ε_T	total porosity
η	viscosity
ν_e	reduced velocity
Φ_0	column resistance factor based on u_0
ρ	d_{core}/d_p

Handbook of Advanced Chromatography/Mass Spectrometry Techniques. http://dx.doi.org/10.1016/B978-0-12-811732-3.00006-6

1. INTRODUCTION

Although the benefit of using small particle sizes in combination with higher operating pressures in high-performance liquid chromatography (HPLC) was already predicted in the 1960s by Giddings (1964, 1965a) and Knox and Saleem (1969), the standard format for HPLC columns from the early 1980s were 4.6 mm × 250 mm columns packed with spherical particles of 5−10 μm diameter. These columns were operated with HPLC instruments with an upper pressure limit of 400 bar and produced plate numbers of c. 25000 with a column dead time of 2−5 min.

In the late 1990s, studies were reported from the groups of Jorgenson (MacNair et al., 1997; MacNair et al., 1999) and Lee (Wu et al., 2001) that made use of ultrasmall particles and high operating pressures. The first sub-2-micron particles were introduced by Agilent (Barber and Joseph, 2004) and Waters in 2004; at this time also the first commercial instrument with an operating pressure up to 1000 bar was introduced by Waters (Swartz and Murphy, 2005). Since then, a wide range of ultra-high performance LC (UHPLC) instruments have become commercially available from almost every major instrument vendor, and a new term—UHPLC—was coined for HPLC instruments and columns capable of operation above 400 bar.

In parallel to the progress in instrument development, new stationary phase morphologies were developed, with the promise of producing higher efficiencies with similar particle sizes compared to conventional particles. In particular, core−shell particles have become very successful and are now available in various particle sizes (between 1.3 and 5 μm) and chemistries (González-ruiz et al., 2015; Guiochon and Gritti, 2011; Hayes et al., 2014; Tanaka and McCalley, 2016). Certain core−shell materials are also available with larger pore sizes for the separation of biomolecules (Chen et al., 2015; Fekete et al., 2012a, 2013; Wagner et al., 2012).

Simultaneously, the development of stationary phase chemistries has made huge progress. More and more phases are being developed for specific separation tasks: hydrophilic interaction liquid chromatography (HILIC) phases for the separation of polar compounds, pH stable and temperature stable phases, low bleed phases for use specifically with mass spectrometry (MS), and phases suitable for supercritical fluid chromatography (SFC).

Although many columns are offered in different length and diameters, HPLC users are faced with a choice of hundreds of columns to select from for a specific separation problem.

The requirements for separation speed and resolution range from ultrafast separations of only a few compounds, as used in the second dimension of two-dimensional LC, to ultrahigh resolution of complex mixtures, such as in proteomics or metabolomics. As the use of MS coupled to LC for complex separation problems has dramatically increased over the past decade, the properties of stationary phase materials with respect to compatibility with MS detection have also become an important point of interest.

In this chapter we will discuss the latest developments in stationary phase technology with respect to particle morphology, as well as particle and phase chemistries.

The first part of this chapter will focus on mass transfer properties of core−shell particles compared to fully porous particles, covering the fundamental aspects of column performance as a function of morphology and particle size. The second part of the chapter will discuss new developments in stationary phase chemistry that are particularly important with respect to LC/MS analysis.

2. CORE–SHELL PARTICLES

One of the most important trends over the past 10 years was the development of high efficiency core–shell or superficially porous particles. This type of particle holds the promise to deliver higher efficiency compared to a fully porous particle of the same size. The concept of using a solid core covered by a thin porous layer to enhance mass transfer was initially introduced by Horvath and Lipsky in the late 60s (Horvath and Lipsky, 1969a,b; Horvath, 1967) followed by various approaches in the 1970s to create pellicular particles such as Zipax, Corasil, or Pellicosil (Done and Knox, 1972; Kennedy and Knox, 1972; Kirkland, 1972). The porous layer was impregnated with a liquid serving as the stationary phase, and the porous shell comprised only 5%–10% of the particle volume. Because of the limited particle porosity, the loading capacity of these particles was very low. The large size of these particles (c. 50 μm) and the insufficient stability of liquid stationary phase limited the use of this type of particles.

A second generation of core–shell particles was introduced in 1992 by Jack Kirkland and later commercialized by Agilent Technologies. These particles had an average size of 5 μm, with a shell thickness of 0.25 μm, and an average pore size of 300 Å. The general approach to produce these particles involved co-spray-drying an aqueous silica sol mixture and dense silica beads, so that a uniform porous shell formed around the solid core. The particle with the porous shell was sintered to give it strength and then rehydroxylated for subsequent surface chemical modification. These particles were mainly suited for the separation of large molecules such as proteins and peptides (Kirkland et al., 2000; Wang et al., 2006a,b).

The real breakthrough of core–shell particles for high efficiency separations of small molecules started in 2007 with the introduction of the HALO particles (2.7 μm with a shell thickness of 0.5 μm) by Advanced Materials Technology (Destefano et al., 2008; Kirkland et al., 2007). To date, many column vendors have introduced core–shell particles in sizes ranging from 1.3 to 5 μm.

2.1 PRODUCTION OF CORE–SHELL PARTICLES

The production of modern core–shell particles usually starts with producing a nonporous core using the Stöber process (Stöber et al., 1968). This process yields nonporous silica particles with a tightly controllable size distribution. Subsequently, a porous shell is added by either a layer-by-layer approach (Kirkland and Langlois, 2007) or by a one-step coacervation process (Chen et al., 2015; Chen and Wei, 2010).

2.1.1 Layer-By-Layer Process

In this method (Kirkland, 1970; Kirkland et al., 2000), large sol particles in ~50–100 nm size range are used for coating. Only one layer of sol particles is coated at a time. To get a 0.25 μm thick shell, five to six coatings must be applied. Between each coating, the excess polymer and sol particles must be washed out by filtration or centrifugation. This method is good for coating the large size sol and thin shell particles used for large molecule separations. Using this process to coat small sol particles of 10–16 nm would take 40–50 coats to get a 0.5 μm thick shell. This would not be efficient or practical. To overcome this issue, a multi-multilayer method was developed (Kirkland and Langlois, 2007). One layer of polymer, usually poly (diallyldimethylammonium chloride), is applied on the cores. This polymer, depending on molecular weight, can absorb several layers of sol particles, and

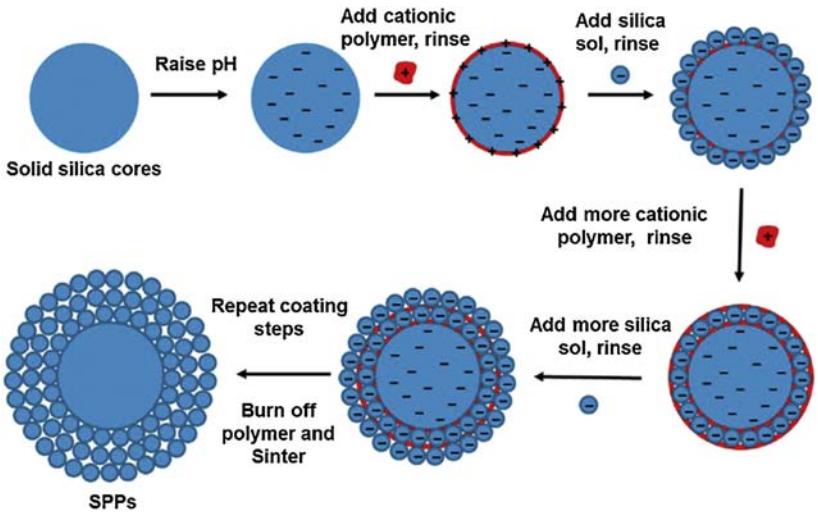

FIGURE 6.1

Schematic representation of layer-by-layer process for synthesis of core–shell particles.

Reprinted with permission from Chen, W., Jiang, K., Mack, A., Sachok, B., Zhu, X., Barber, W.E., Wang, X., 2015. Synthesis and optimization of wide pore superficially porous particles by a one-step coating process for separation of proteins and monoclonal antibodies. J. Chromatogr. A 1414, 147–157.

the porous shell grows 5–10 layers at a time, and so the shell grows much faster. It takes fewer coating steps but still needs more than 10 coating steps to get a 0.5 μm thick shell. It is still a labor intensive and time-consuming approach because of the numerous centrifugation steps that are needed to remove the extra material and loosely bound species in each coating cycle. Details of this process are shown in Fig. 6.1.

2.1.2 Coacervation Process

In this method, the surface-modified solid silica cores are suspended in coacervation reaction mixtures of urea, formaldehyde, and colloidal silica sol under acidic conditions. A coacervate of urea–formaldehyde polymer and the ultrapure silica sol particles is formed and is then coated on the solid cores. The urea–formaldehyde polymer is removed by burning in an oven, and the particles are then strengthened by sintering at higher temperatures. This process is shown in Fig. 6.2 and is described as follows:

1. Modifying the solid core surface with a proper functionality, such as urea–formaldehyde polymer.
2. Coating the dense silica cores with a urea–formaldehyde/silica sol coacervate film.
3. Eliminating the urea–formaldehyde polymer from the outer coating by heating.
4. Sintering to increase particle strength and eliminating undesirable micropores.
5. Rehydroxylating the surface of the core–shell particles.
6. Size classification to remove fines and aggregates.

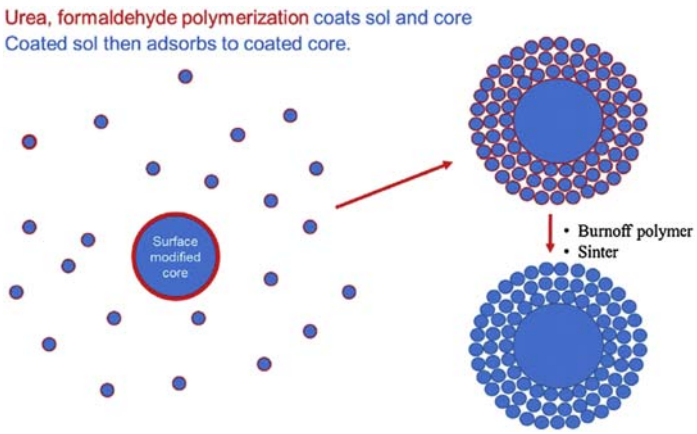

FIGURE 6.2

Schematic representation of coacervation method for synthesis of core–shell particles.

Reprinted with permission from Chen, W., Jiang, K., Mack, A., Sachok, B., Zhu, X., Barber, W.E., Wang, X., 2015. Synthesis and optimization of wide pore superficially porous particles by a one-step coating process for separation of proteins and monoclonal antibodies. J. Chromatogr. A 1414, 147–157.

2.1.3 Micelle Templating

A third method to generate core–shell particles is micelle templating (Langsi et al., 2015; Omamogho and Glennon, 2011; Omamogho et al., 2011) or pseudomorphic transformation (PMT) (Wei et al., 2016). In the PMT process, nonporous silica particles are dispersed in an alkaline solution with the presence of surfactant. When the temperature increases, the silica on the particle surface first dissolves and the silicic acid subsequently precipitates around ordered, positively charged micelles on the silica particles without changing the overall particle morphology. This process results in radially oriented pores with very little pore connectivity. Desmet et al. (Deridder et al., 2016) have shown in a theoretical investigation that this pore structure can lead to a significantly reduced B-term.

2.1.4 Other Core–Shell Particles

The preparation and evaluation of core–shell material possessing a carbon core and nanodiamond–polymer shell have been reported (Bobály et al., 2015; Wiest et al., 2011). These types of particles, however, show relatively low efficiencies and have not yet been extensively studied.

An overview of commercially available core–shell particles is given in González-ruiz et al. (2015).

Besides the benefit of higher efficiency, improved heat dissipation has been reported for core–shell particles (Grinias et al., 2014; Kostka et al., 2011). This property could potentially relieve some of the negative effects of heat friction, e.g., radial temperature gradients and transverse differential migration velocity (Gritti and Guiochon, 2010a).

2.2 MORPHOLOGY OF CORE–SHELL PARTICLES

A stationary phase (packed bed or monolithic) is characterized by the porosity of the interstitial space (surrounding the particles or monolithic skeleton) ε_e, the total porosity ε_T, and the porosity of the

porous zone ε_{pz}. The intraparticle porosity ε_{part} is the volume fraction of pores with respect to the total particle volume (Unger, 1979). For fully porous particles, ε_{pz} *is* equal to ε_{part}.

It is important to distinguish between external and internal porosity as both have different effects on separations. The external porosity determines the permeability of the column, whereas the internal porosity plays a role in retention and intraparticle diffusion.

Total porosity

$$\varepsilon_T = \frac{V_e + V_{\text{pore}}}{V} = \frac{V_0}{V} \tag{6.1}$$

External (interstitial) porosity

$$\varepsilon_e = \frac{V_e}{V} \tag{6.2}$$

Porous zone porosity

$$\varepsilon_{pz} = \frac{\varepsilon_T - \varepsilon_e}{(1-\varepsilon_e)\cdot(1-\rho^3)} \tag{6.3a}$$

with

$$\rho = \frac{d_{\text{core}}}{d_p} \tag{6.3b}$$

where V is the empty column volume, V_0 is the column dead volume or total volume occupied by mobile phase, V_e is the external or interstitial volume occupied by the flowing mobile phase, V_{pore} is the pore volume occupied by the stagnant mobile phase, d_p is the particle diameter, and d_{core} is the core diameter.

The different porosities play important roles in mass transfer and transport of the mobile phase.

For columns packed with spherical particles, the external porosity is determined by the quality and density of the packing and usually lies between 0.35 and 0.45; a well-packed column will have values around 0.4 (Giddings, 1965b).

External and porous zone porosities for different core–shell columns have been reported by Gritti and Guiochon [HALO columns (Gritti and Guiochon, 2012e), Kinetex columns (Gritti and Guiochon, 2012d), Poroshell columns (Gritti and Guiochon, 2012f)] and Cortecs columns (Gritti et al., 2014), where the values for ε_{pz} range between 0.33 and 0.37.

The permeability of a column is an important factor because it determines the pressure that is required to operate a column. For laminar flow, Darcy's law relates permeability to linear velocity (u):

$$K = \frac{u\cdot\eta\cdot L}{\Delta P} \tag{6.4}$$

where η is the eluent viscosity, L is the column length, and ΔP is the pressure drop.

For packed columns—with u being the linear velocity of a nonretained solute u_0—the permeability is related to particle size and porosity by

$$K_0 = d_p^2 \cdot \left[\frac{1}{36\cdot k_c}\cdot\frac{\varepsilon_e^3}{(1-\varepsilon_e)^2\cdot\varepsilon_T}\right] = \frac{d_p^2}{\Phi_0} \tag{6.5}$$

where k_c is the Kozeny–Carman constant ($k_c = 5$ for spherical particles), and Φ_0 is the column resistance factor (c. 500 for well-packed columns).

The average pore size of a particle is relevant to the size range of molecules to be separated. While core–shell particles with pore sizes ranging from 90 to 120 Å have been a great success for the fast separation of small molecules, separations of large biomolecules, such as proteins, require particles with larger pore sizes (≥300 Å) to allow unrestricted diffusion inside the pores. One early example is the commercial wide pore (300 Å) core–shell particle in 5 μm size introduced in 2001 (Kirkland et al., 2000).

More recently, wide pore (200–450 Å) core–shell particles in smaller particle sizes (3.5–3.6 μm) have been developed to meet the requirements for faster separations of larger molecules, such as monoclonal antibodies (Chen et al., 2015; Fekete et al., 2012a; Schuster et al., 2013). These wide-pore particles typically have a much thinner shell (~0.2 μm) in relation to the particle size; the core-to-diameter ratio ρ is typically 0.85 compared to a core–shell particle for small molecules ($\rho \sim 0.63$). Fekete et al. (2012b) have compared wide-pore core–shell particles ($d_p = 3.6$, $d_{\text{core}} = 3.2$, pore size ~ 200 Å) with fully porous particles ($d_p = 1.7$, pore size ~ 300 Å). They demonstrated similar separation efficiency for both particle types but a 2–4 times reduced loading capacity for the core–shell columns, mostly due to the low porous volume fraction of only ~0.4.

2.3 MASS TRANSFER IN FULLY POROUS AND CORE–SHELL PARTICLES

2.3.1 Theoretical Background

The concept of theoretical plates in chromatography was introduced by Martin and Synge (1941). They described a chromatographic column as consisting of a number of layers, in each of which equilibrium between the mobile and stationary phases is established: "The height equivalent of a theoretical plate (HETP) is defined as the thickness of the layer such that the solution issuing from it is in equilibrium with the mean concentration of solute in the non-mobile phase throughout the layer."

The HETP or H is defined as the thickness of that layer. The number of theoretical plates of a column is given by the ratio of the column length to the H value:

$$N = L/H \tag{6.6}$$

The value of H depends on a large number of parameters such as flow rate, diffusion coefficient, and retention factor of analyte, particle size, and morphology.

Based on the work of Martin and Synge, Van Deemter, Klinkenberg, and Zuiderweg in 1956 used chemical engineering principles to develop an expression for the variation of the HETP value with linear solvent velocity, now commonly known as the "Van Deemter equation," which is still widely used in the empirical form to fit experimental H–u data:

$$H = A + \frac{B}{u} + C \cdot u \tag{6.7}$$

u = linear velocity of mobile phase.

The parameter A is related to the eddy dispersion, i.e., the long-range and short-range dispersion effects resulting from packing inhomogeneity within a column.

The parameter B is related to longitudinal diffusion in the packing; it is inversely proportional to the mobile phase velocity because the lesser time the band spends in the column, the lesser time it has to diffuse.

The parameter C is related to mass transfer resistance in the stationary phase, i.e., to the time that molecules need to diffuse in and out of the particles and through their pores.

These three contributions account for all the band broadening because of the mass transfer processes in any type of chromatographic column (open tubular, packed bed, or monolithic columns), independent of the physical state of the mobile phase (gas, liquid, or supercritical fluid), the flow regime (laminar to turbulent), or the nature of the stationary phase.

A very good review that covers the early years of mass transfer theory is given by Knox (1998).

Giddings (1965b) suggested to reduce the HETP and the linear velocity to the dimensionless parameters h and ν to allow the direct comparison of data obtained with different particle sizes, eluents, or analytes. It also enables an extrapolation of plate heights from a set of experimental data to other conditions (analytes, particle sizes, solvents, temperatures, etc.). The reduced form of Eq. (6.7) is written as

$$h = a + \frac{b}{\nu} + c \cdot \nu \tag{6.8}$$

with the reduced plate height given by

$$h = H/d_p \tag{6.9}$$

and the reduced velocity by

$$\nu = \frac{u \cdot d_p}{D_m} \tag{6.10}$$

where D_m is the diffusion coefficient of analyte in the mobile phase.

Although the Van Deemter equation can be used to fit experimental data, the assumption that the eddy dispersion is independent of velocity is physically not sound. In 1965 Giddings (1965b) suggested the coupling between flow-induced and diffusion-induced transport of analytes within the interparticle space, which was later confirmed experimentally by Knox (1966).

Recently, the following form of the reduced plate height equation has been used (Catani et al., 2016; Daneyko et al., 2015; Gritti and Guiochon, 2015b):

$$h = h_a + h_b + h_{c_s} = a(\nu) + \frac{b}{\nu} + c_s\nu \tag{6.11}$$

In Eq. (6.11), h_a accounts for the coupling between flow-induced and diffusion-induced transport (eddy dispersion), h_b accounts for the longitudinal diffusion, and h_{c_s} accounts for the mass transfer resistance across the stationary phase. The terms in this form of the $h-\nu$ equation are independent, and the terms h_b and h_{c_s} can be determined directly from peak-parking experiments (Broeckhoven et al., 2008; Gritti and Guiochon, 2010b; Liekens et al., 2011; Miyabe et al., 2009a,b). The term $a(\nu)$ cannot be determined independently from the other contributions to h and has to be derived from subtracting the b/ν and the $c_s\nu$ contributions from experimental $h-\nu$ data (Catani et al., 2016; Gritti and Guiochon, 2012b,c, 2013b,d, 2014a, 2015b; Hormann and Tallarek, 2014).

2.3.1.1 Eddy Diffusion

Giddings (1965b) suggested the coupling of five different types of velocity inequalities in a chromatographic bed (transchannel, transparticle, short-range interchannel, long-range interchannel, and transcolumn).

$$h_a = \sum_{i}^{i=5} \frac{1}{1/2\lambda_i + \omega_i \cdot \nu} \tag{6.12}$$

Done and Knox (1972) later proposed an empirical expression for h_a that gives a good fit for individual h–ν curves, and it is still widely accepted because of its simplicity.

$$h_a = a\nu^{0.33} \tag{6.13}$$

With the introduction of a large variety of stationary phases with different properties, such as particle size, morphology, or pore structure, etc., it is very important to understand the contributions to band broadening from the different terms because they result from different properties of the packing and can be influenced by changing, e.g., the particle structure or the packing process. The introduction of new types of stationary phases, in combination with advances in computing power, has renewed the interest in studying the true nature of the h_a term.

Recent experimental (Catani et al., 2016; Gritti and Guiochon, 2012b,c, 2013b,d, 2014a, 2015b; Hormann and Tallarek, 2014) and computational (Daneyko et al., 2015; Desmet, 2013) studies have been devoted to studying the h_a contributions, and a strong coupling between the classical A-term and the portion of the C-term, which results from diffusion in the stagnant mobile phase surrounding the particles, could be demonstrated.

Desmet (2013) has proposed a finite length parallel zone model as an alternative model for the axial or eddy dispersion caused by the occurrence of local velocity biases or flow heterogeneities in porous media, such as those used in liquid chromatography columns. The mathematical plate height expression evolving from the model shows that the A- and C-term band-broadening effects that can originate from a given velocity bias should be coupled in an exponentially decaying way, instead of harmonically as proposed in Giddings' coupling theory. The resulting plate height equation is, however, very complex and requires fitting many unknown parameters, which makes it difficult to use in practice.

Daneyko et al. (2015) have presented an extension of Giddings' theory of coupled eddy dispersion to account for retention of analyte molecules due to stagnant regions in porous shells with zero mobile phase flow velocity. The plate height equation involved a modified eddy dispersion term and was tested against simulated data obtained for particle-packings with varied shell thicknesses and shell diffusion coefficients.

2.3.1.2 Longitudinal Diffusion

In the early days of liquid chromatography, the large particle sizes $\geq$5 μm resulted in such large contributions from the h_a- and the h_{c_s}-terms that the contributions from longitudinal diffusion could largely be neglected. With particle diameters approaching 1 μm, and the fact that columns packed with such particles are often operated close to the B-term regime, longitudinal diffusion is becoming a dominant factor in band broadening. Understanding the underlying mass transfer processes is therefore mandatory for proper modeling and successful design of chromatographic supports.

In general, the b-term plate height contribution (h_b) is linked to the effective longitudinal diffusion coefficient (D_{eff}) by Giddings (1965b) and Knox and Scott (1983):

$$h_b = \frac{2\gamma_{\text{eff}}}{\nu_e}\left(1 + k''\right) \tag{6.14a}$$

with

$$\gamma_{\text{eff}} = \frac{D_{\text{eff}}}{D_m} \tag{6.14b}$$

where ν_e is the reduced interstitial linear velocity.

The zone retention coefficient k'' is given by

$$k'' = k + k \cdot k_0 + k_0 \tag{6.15}$$

with

$$k_0 = \frac{V_i}{V_e} = \frac{\varepsilon_T}{\varepsilon_e} - 1 \tag{6.16}$$

where the value of k_0 for a packed bed is typically 0.25.

The effective diffusion coefficient D_{eff} is related to the diffusion in the mobile phase, D_m, and the diffusion inside the particle, D_{part} (or in the porous zone, D_{pz}). Based on Giddings' (1965b) work, Knox and Scott (1983) had proposed a residence time weighted (RTW) model to describe the combined diffusion in both phases, which has been in use until recently.

Desmet et al. (Broeckhoven et al., 2008; Desmet et al., 2008), however, demonstrated that the RTW model was not able to represent simulated and experimental D_{eff}/D_m values across a large range of retention factors. While the Knox model predicts a straight line for the dependency of $[D_{\text{eff}}/D_m \cdot (1 + k)]$ versus k, this relationship shows in fact a strong curvature—in particular in the range of low k values.

In 2011 Deridder and Desmet (2012; Desmet and Deridder, 2011) derived expressions for the h_b based on effective medium theory (EMT) and compared the results to the Knox model. They demonstrated the failure of the RTW model and could show that even the simplest version of the EMT equations (Maxwell-based expression) gives an excellent representation of simulated and experimental data. The Maxwell-based expression for the h_b-term is given by

$$h_b = \frac{2\gamma_{\text{eff}}\left(1 + k''\right)}{\nu_e} = \frac{2\varepsilon_e}{\varepsilon_T^2}\frac{1 + 2\beta_1(1 - \varepsilon_e)}{1 - \beta_1(1 - \varepsilon_e)}\Big/\nu_e \tag{6.17}$$

where β_1 is the particle polarizability constant (Desmet and Deridder, 2011).

$$\beta_1 = \frac{\alpha_{\text{part}} - 1}{\alpha_{\text{part}} + 2} \tag{6.18}$$

with

$$\alpha_{\text{part}} = \frac{\varepsilon_e \cdot k''}{1 - \varepsilon_e} \cdot \frac{D_{\text{part}}}{D_m} \tag{6.19}$$

The authors could show that the use of the EMT model provides a simple but exact expression to represent the way in which the solid core obstructs the effective intraparticle diffusion, in the case of core–shell particles.

The validity of these expressions was demonstrated experimentally (Deridder and Desmet, 2011) as well as numerically (Deridder and Desmet, 2011, 2012), showing that the complex dependency of the effective longitudinal diffusion coefficient (D_{eff}) on the intraparticle diffusion coefficient, the retention factor, and the packing density can be very accurately represented (Deridder and Desmet, 2012; Desmet and Deridder, 2011).

When considering particles with a solid core, one has to distinguish between D_{pz} (the diffusion coefficient experienced by the analytes once they enter the mesoporous zone) and D_{part} (the externally observed intraparticle diffusion coefficient). They are related by

$$D_{pz} = \frac{2+\rho^3}{2} \cdot D_{\text{part}} \tag{6.20}$$

As we will see in the next section, the porous zone diffusion coefficient D_{pz} will be used to calculate the h_{c_s}-term.

2.3.1.3 Intraparticle Diffusion

The contribution of intraparticle diffusion to the plated height is represented by the h_{c_s} term. Based on the work of Giddings, it can be written as (Desmet et al., 2015)

$$h_{c_s} = \frac{2}{\alpha} \cdot \frac{1}{Sh_{sz}} \cdot \frac{k''}{(1+k'')^2} \cdot \frac{D_m}{D_{pz}} \cdot \nu_e \tag{6.21}$$

with $\alpha = 6$ for spherical particles.

There exist formally different versions of Eq. (6.21) in the literature, which can all be converted into one another (Desmet and Broeckhoven, 2008).

The Sherwood number for the stationary zone Sh_{sz} for fully porous particles is equal to 10 for spherical particles and equal to 8 for cylinders. For particles possessing an impervious core, a shape factor f_s has to be applied as introduced by Horvath and Lipsky in 1969 (Horvath and Lipsky, 1969a):

$$Sh_{sz} = Sh_{sz,\text{fully porous}} \cdot f_s \tag{6.22}$$

$$f_s = \frac{1 - 5\rho^3 + 9\rho^5 - 5\rho^6}{1-\rho^3} \tag{6.23}$$

f_s is equal to unity for fully porous particles.

For spherical particles, Eq. (6.21) then takes the form

$$h_{c_s} = \frac{1}{30} \cdot f_s \cdot \frac{k''}{(1+k'')^2} \cdot \frac{D_m}{D_{pz}} \cdot \nu_e \tag{6.24}$$

For fully porous particles, $f_s = 1$ and $D_{pz} = D_{\text{part}}$.

2.3.2 Experimental Determination of h−ν Curves for Core−Shell and Fully Porous Particles

Several studies have been devoted to the mass transfer properties of core−shell particles, and it could be demonstrated that the efficiency of these particles is considerably higher than that of fully porous particles of the same size (Daneyko et al., 2015; Deridder and Desmet, 2012; Fekete et al., 2009; Gritti and Guiochon, 2013c; Guiochon and Gritti, 2011; Lambert et al., 2014; Liekens et al., 2011).

We have compared column performance for three fully porous (Zorbax C18) and two core−shell (Poroshell 120 C18) columns, where each particle type is made by a similar manufacturing process in different particle sizes. Column properties are given in Table 6.1. To minimize the impact of extra-column performance, columns with a diameter of 4.6 mm were used and the system variance was reduced to $<1\ \mu L^2$. This was achieved by modifying a standard UHPLC system (Agilent 1290 Infinity) with a fixed loop injection valve with an internal loop of 160 nL, 75 μm I.D. connection capillaries, and a 250 nL prototype detection cell.

$H-u$ curves were acquired at 30°C with butyrophenone as analyte in different mobile phase compositions (40%, 45%, 50%, 60%, 70%, and 80% acetonitrile in water) to study the impact of retention on column efficiency. The diffusion coefficients D_m of butyrophenone under these conditions were taken from Song et al. (2016).

Fig. 6.3 shows $H-u$ curves (upper panel) and the corresponding reduced ($h-\nu$) curves (lower panel) in 40%, 50%, 60%, and 70% acetonitrile/water. Open symbols correspond to core−shell particles and filled symbols to fully porous particles. As can be seen in the upper panel of Fig. 6.3, the columns packed with 2.7 μm core−shell particles show similar H values compared to the 1.8 μm fully porous particles, and the 4 μm core−shell particles outperform the 3.5 μm fully porous particles. The difference between the two particle types becomes clear when we plot the reduced plate height h versus reduced velocity ν (see lower panel of Fig. 6.3). The $h-\nu$ curves for the core−shell particles coincide with a minimum reduced plate height h of 1.4 at 70% ACN and 1.8 at 40% ACN. The h values for the 3.5 and 5.0 μm particles are 1.8 and 2.1, respectively. As we can see from the lower panel of Fig. 6.3, the minimum reduced plate heights and the optimum reduced velocities depend on the retention factor k. This has to be considered when comparing h values from sets of experiments that have been performed under different mobile phases or with different analytes.

The effective diffusion coefficient in a packed or monolithic column D_{eff} can be derived from peak-parking experiments (Broeckhoven et al., 2008; Gritti and Guiochon, 2010b; Liekens et al., 2011; Miyabe et al., 2009a,b) by determining the slope of the variance of a parked peak plotted versus the parking time.

To determine the intraparticle diffusion coefficients D_{part} and the porous-zone diffusion coefficients D_{pz}, peak-parking experiments were performed at 30°C in different mobile phases (40%, 45%, 50%, 60%, 70%, and 80% acetonitrile/water) on columns 2, 4, and 5 (see Table 6.1), according to the protocol described by Liekens et al. (2011). D_{eff} values were determined according to Eq. (6.25) and D_{eff}/D_m values were calculated using mobile phase diffusion coefficients, D_m, for butyrophenone in the different mobile phases at 30°C measured by Song et al. (2016). D_{eff}/D_m values for the other two columns were determined from the experimental h value at 0.2 mL/min (see Eq. 6.14a).

$$\Delta\sigma_x^2 = 2D_{\text{eff}} \cdot t_{\text{park}} \tag{6.25}$$

Table 6.1 Column Properties and $h-v$ Parameters for Three Fully Porous and Two Core−Shell Columns

Column #	Particle Type	d_p (μm)	d_{core} (μm)	ε_T	ε_e	ε_{pz}	Φ_0	max. P (bar)	% ACN	k	$a1$	$a2$	b	c_s
1	Zorbax	1.8	0	0.396	0.565	0.280	597	600	50	2.78	0.774	0.303	6.54	0.0136
									60	1.56	0.775	0.339	4.78	0.0180
2	Zorbax	3.5	0	0.398	0.553	0.257	573	400	45	7.00	0.291	0.567	9.86	0.0084
									50	4.81	0.436	0.451	7.58	0.0121
									60	2.50	0.367	0.542	5.14	0.0186
									70	1.39	0.488	0.470	3.71	0.0255
3	Zorbax	5	0	0.398	0.553	0.257	573	400	45	6.91	0.235	0.658	9.21	0.0094
									50	4.69	0.234	0.677	7.47	0.0123
									60	2.39	0.259	0.678	5.00	0.0191
									70	1.33	0.283	0.682	3.72	0.0247
4	Poroshell	2.7	1.7	0.395	0.563	0.370	602	600	45	5.91	0.326	0.457	9.04	0.0038
									50	4.10	0.341	0.435	6.89	0.0055
									60	2.16	0.268	0.557	4.72	0.0083
									70	1.24	0.286	0.548	3.53	0.0108
5	Poroshell	4	2.5	0.395	0.563	0.367	602	600	45	5.58	0.272	0.532	8.32	0.0044
									50	3.86	0.251	0.566	6.51	0.0061
									60	2.00	0.275	0.546	4.33	0.0095
									70	1.13	0.328	0.498	3.21	0.0127

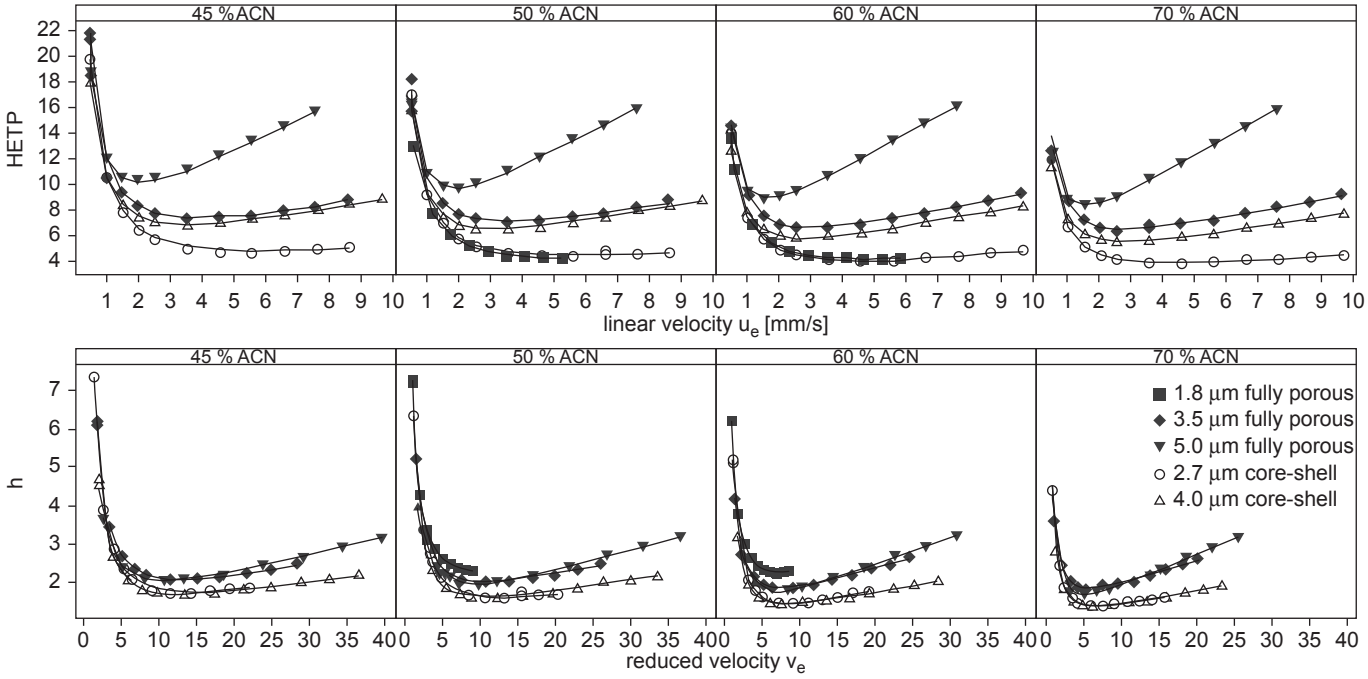

FIGURE 6.3

Curves of height equivalent of a theoretical plate versus interstitial velocity (upper panel) and h versus ν (lower panel) for three columns packed with fully porous and two columns packed with core−shell particles in different mobile phases. For column details, see Table 6.1.

Rearranging Eq. (6.17), the polarizability term β_1 can be written as (Liekens et al., 2011)

$$\beta_1 = \frac{1}{1-\varepsilon_e} \cdot \frac{b \cdot \left(\varepsilon_T^2/\varepsilon_e\right) - 2}{b \cdot \left(\varepsilon_T^2/\varepsilon_e\right) + 4} \tag{6.26}$$

with

$$b = 2 \cdot \frac{D_{\text{eff}}}{D_m} \cdot \left(1 + k''\right) \tag{6.27}$$

Rearranging Eq. (6.18) we obtain

$$\alpha_{\text{part}} = \frac{1 + 2\beta_1}{1 - \beta_1} \tag{6.28}$$

and D_{part}/D_m is then given by

$$\frac{D_{\text{part}}}{D_m} = \alpha_{\text{part}} \cdot \frac{1-\varepsilon_e}{\varepsilon_e \cdot k''} \tag{6.29}$$

where the corresponding diffusion coefficient in the porous zone, D_{pz}, is given by Eq. (6.20).

Fig. 6.4 shows the D_{eff}/D_m (Fig. 6.4A), D_{part}/D_m (Fig. 6.4B), and D_{pz}/D_m (Fig. 6.4C) as a function of the retention factor k. For all columns, similar D_{part}/D_m values were observed, which is in line with results from Liekens et al. (2011), where also similar D_{part}/D_m values for Zorbax and Poroshell columns were shown.

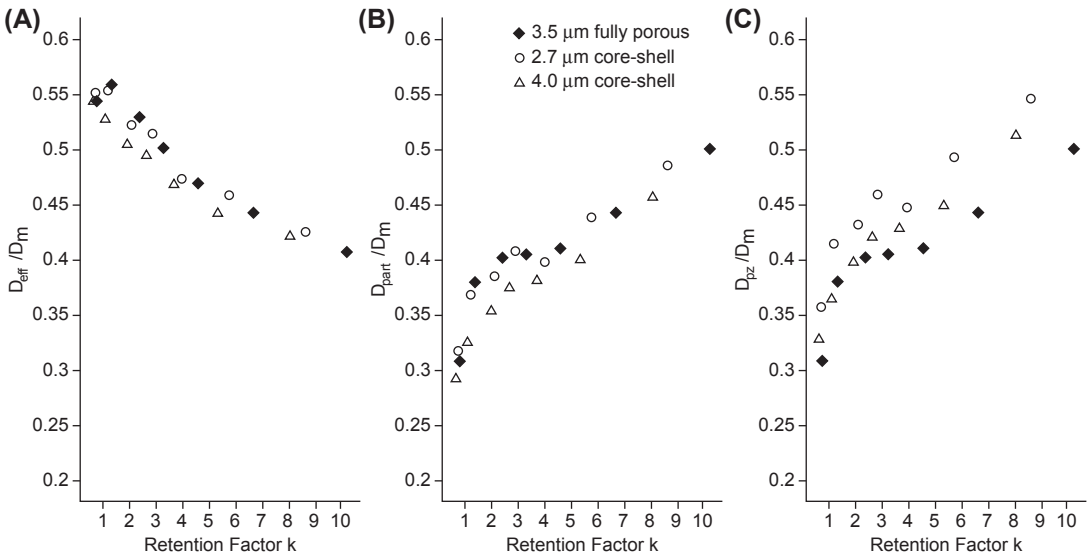

FIGURE 6.4

Plots of D_{eff}/D_m (A), D_{part}/D_m (B), and D_{pz}/D_m (C) versus retention factor for columns 2, 4, and 5 (Table 6.1).

For other core–shell particles, such as HALO or Kinetex, some authors (Gritti and Guiochon, 2012a; Liekens et al., 2011) have reported reduced D_{part}/D_m values compared to fully porous particles. In a theoretical study, Deridder et al. (2016) have shown that core–shell particles (in particular those with radially oriented pores such as micelle templated particles) can exhibit significantly reduced intraparticle diffusion, leading to lower h_b-term contributions.

Fig. 6.5 shows the h_a (upper panel), h_b (middle panel), and h_{c_s} (lower panel) contributions for three fully porous and two core–shell columns (see Table 6.1). The term h_b was calculated using the D_{eff}/D_m values derived from the peak-parking experiments or the experimental h values at low velocity (columns 1 and 3 in Table 6.1). The values for h_{c_s} were calculated according to Eq. (6.24) using the D_{pz} values derived from the D_{eff}/D_m values.

The values for h_a were determined by subtracting the h_b and h_{c_s} contributions from the experimental h values. The dependence of h_a on ν could be empirically fitted to a power function, such that Eq. (6.11) can be written as

$$h = a1 \cdot \nu^{a2} + \frac{b}{\nu} + c_s\nu \tag{6.30}$$

The parameters $a1$, $a2$, b, and c_s for all columns and conditions shown are listed in Table 6.1. For most columns, the parameter $a2$ is much larger compared to the value of 0.33 suggested by Done and Knox (1972).

Although the h_b values are almost identical for all columns, there is a clear difference between the h_a- and h_{c_s} -terms for the core–shell and the fully porous columns. The difference in h_{c_s} is on the one hand due to the higher D_{pz}/D_m values and on the other hand to the reduced shape factor for the core–shell particles. The differences in the h_a-term for core–shell particles have been frequently observed by other authors (Guiochon and Gritti, 2011) and are commonly attributed to a better column packing quality. There is an ongoing debate whether the improved column packing is related to a narrower particle size distribution (Destefano et al., 2008) or to higher surface roughness (Gritti and Guiochon, 2007; Gritti et al., 2010) of the particles. Recently Desmet (Catani et al., 2016; Ismail et al., 2016b) and Gritti and Guiochon (2015a,b) have reported on fully porous particles with a very narrow particle size distribution (Titan-C18) that also shows reduced plate heights well below 2.

The reduced plate height values for core–shell particles are similar to those reported from various authors. Gritti and Guiochon analyzed in detail the different contributions to h for 2.1 and 4.6 mm columns packed with different batches of Poroshell 120 (Gritti and Guiochon, 2012f), HALO (Gritti and Guiochon, 2012e), Kinetex (Gritti and Guiochon, 2012d, 2013c, 2014b), and Cortecs particles (Gritti et al., 2014). They generated h–ν curves and performed peak-parking experiments to determine the b-term and c_s-term. They used the RTW model to determine the D_{part}/D_m values, which results in very large values for D_{part}/D_m, in particular for the retained compound.

For a column I.D. of 4.6 mm, they reported reduced plate heights of 1.4–1.6 for most core–shell columns. For particles packed in 2.1 mm I.D. columns, they demonstrated overall higher h_{min} values, resulting mostly from a larger h_a contribution. Overall, their results showed a good reproducibility of the h_b- and h_{c_s}-terms, but (in particular for the 2.1 mm columns) a relatively large variation of the h_a-term. In addition, a strong impact of instrument configuration on the experimental h–ν curves was observed (Gritti et al., 2014) for narrow bore columns.

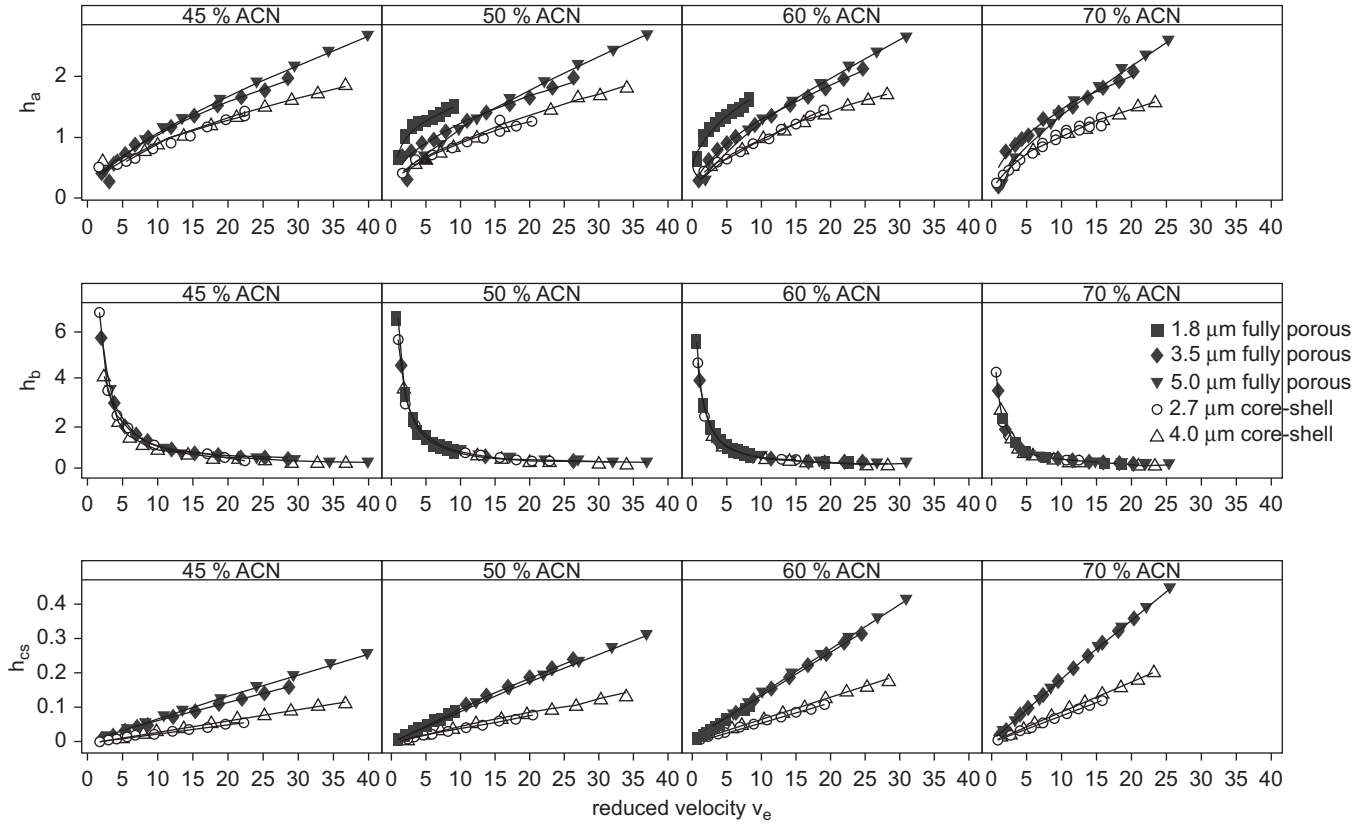

FIGURE 6.5

Plots of the individual contributions to the reduced plate height curves in different mobile phases. Upper panel h_a, medium panel h_b, and lower panel h_{c_s}.

In a review by Fekete et al. (2012), h_{min} values for various core–shell and fully porous particle have been summarized. Packed in 4.6 mm I.D. columns, the h_{min} values of core–shell particles are consistently lower by 0.4–0.6 compared to those of fully porous particles.

2.4 KINETIC COLUMN PERFORMANCE

The concept of kinetic column performance was introduced by Giddings (1964, 1965a) and was later revisited by Knox and Saleem (1969), Poppe (1997), Desmet et al. (2005), and Desmet et al. (2006). Compared to traditional H–u_0 curves, the kinetic plot representation delivers a highly relevant performance measure: the analysis time required to produce a desired number of plates. Kinetic plots can be used to directly compare supports with a different morphology and/or size, as well as different operating conditions, such as mobile phases with different physicochemical properties. They can also be used to predict optimum separation parameters such as flow rate, column length, or particle size for a given analytical problem. An excellent overview of the different types of kinetic plots is given in Desmet et al. (2015).

The kinetic plot approach combines information on column efficiency (H vs. u) with the permeability data of a specific column or support type. As a result, one can obtain the maximum plate number that can be achieved in a given separation time under given conditions. This is particularly useful when comparing columns with different particle sizes, particle size distributions, or particle morphologies (Billen and Desmet, 2007).

For a fixed column length, the H–u curve can be converted into a plot of t_0 versus N (fixed length kinetic plot) with

$$t_0 = \frac{L}{u_0} \tag{6.31}$$

and N derived from Eq. (6.6).

Fig. 6.6 shows kinetic plots for columns of fixed length L and different particles sizes (dashed lines). For each column length, the highest plate number is achieved at the optimum velocity, and higher plate numbers can only be obtained by using a longer column or smaller particle size. If there were no constraints, one could use infinitely long columns with very fine particles and (at the expense of separation time) achieve infinite plate counts. However, the maximum length of column that can be operated under a given set of conditions is limited by a set of experimental boundaries, namely maximum system operating pressure or flow rate, maximum allowed pressure drop for the column, column permeability, and eluent viscosity.

The pressure drop along a packed column can be derived from Darcy's law (Eq. 6.4)

$$\Delta P = u_0 \eta L \cdot \frac{\Phi_0}{d_p^2} \tag{6.32}$$

When combining Eqs. (6.31) and (6.32), the maximum length L^* for a column is given by

$$L^* = \sqrt{\frac{\Delta P_{max} \cdot t_0}{\eta} \cdot \frac{d_p^2}{\Phi_0}} \tag{6.33}$$

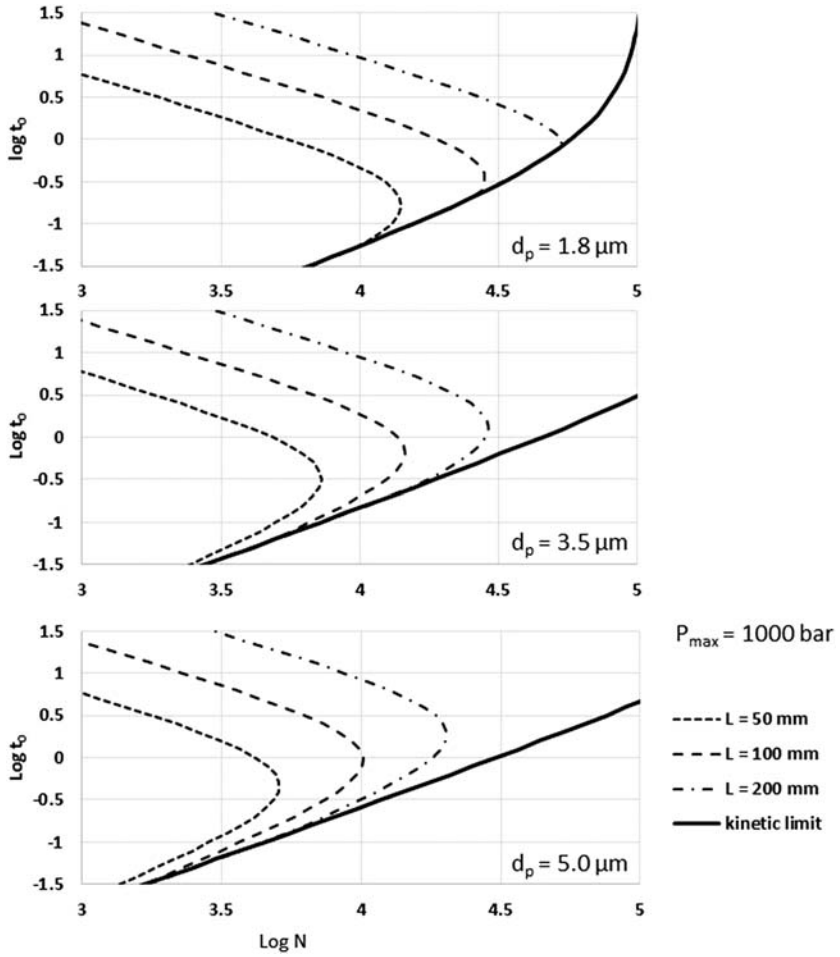

FIGURE 6.6

Fixed length (*dashed lines*) and fixed particle size (*solid lines*) kinetic plots for different particle sizes and a maximum pressure of 1000 bar, viscosity 0.8 cp, and column resistance factor 573.

and the corresponding maximum velocity by

$$u_0^* = \sqrt{\frac{\Delta P_{\max}}{\eta \cdot t_0} \cdot \frac{d_p^2}{\Phi_0}} \tag{6.34}$$

The resulting maximum plate number can then be derived from

$$N^* = \frac{L^*}{H\left(u_0^*\right)} \tag{6.35}$$

$H(u_0^*)$ can be derived from experimental data or from a predicted $H-u$ curve.

The plots of t_0 versus N^* for the different particle sizes are included in Fig. 6.6 as solid lines and represent the kinetic limit that cannot be exceeded under a given set of conditions. This kinetic limit can only be shifted to higher plate numbers by increasing the pressure limit or column permeability and by decreasing viscosity or the plate height H.

Experimental $H-u$ and permeability data can be directly converted to a kinetic plot through (Desmet et al., 2005)

$$t_0 = \left(\frac{\Delta P_{\max}}{\eta}\right) \cdot \left[\frac{K_{t_0}}{u_0^2}\right] \tag{6.36}$$

and

$$N^* = \left(\frac{\Delta P_{\max}}{\eta}\right) \cdot \left[\frac{K_{t_0}}{u_0 \cdot H}\right] \tag{6.37}$$

Fig. 6.7 shows the three different types of kinetic plots that are frequently used in the literature for the columns in Table 6.1, taking the pressure rating for the individual columns into consideration. Usually log N is plotted on the x-axis, and on the y-axis one can plot either log t_0 (separation time; see Fig. 6.7A), log(t_0/N^*) (plate production rate; see Fig. 6.7B), or log(t_0/N^{*2}) (proportional to the separation impedance E; see Fig. 6.7C) (Desmet et al., 2015; Vanderheyden et al., 2013). The first version allows a direct readout of the maximum number of plates that can be achieved in a certain separation time, whereas the other two plot types enhance the differences between different stationary phases.

The kinetic plots in Fig. 6.7 demonstrate a clear benefit for the core–shell particles because they generate higher plate numbers in the same time, compared to fully porous particles. In particular, they

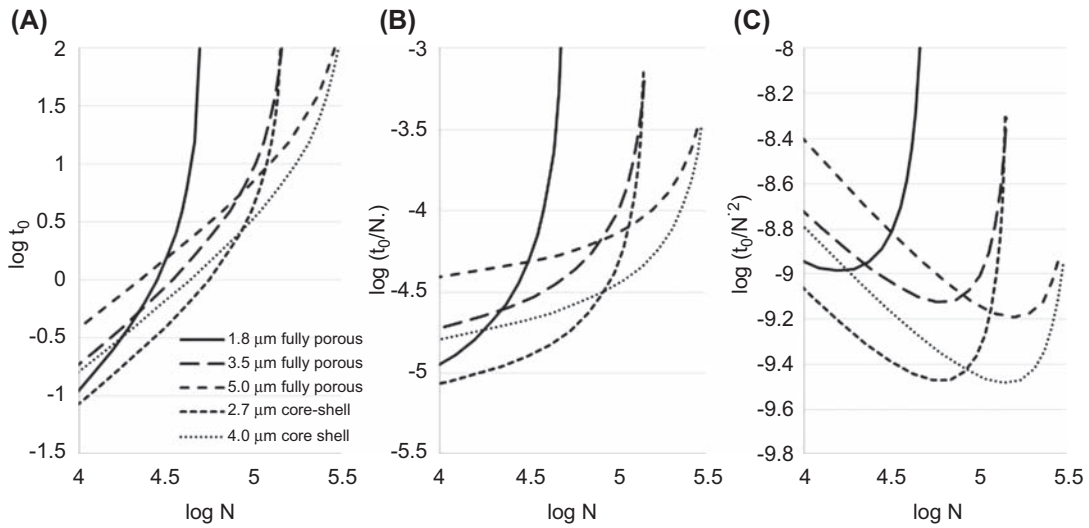

FIGURE 6.7

Different representations of experimental kinetic plots for the columns listed in Table 6.1 in 50% acetonitrile using the recommended pressure limits for each column. (A) log t_0 versus log N, (B) log (t_0/N) versus log N, and (C) log (t_0/N^2) versus log N.

show a markedly reduced separation impedance in Fig. 6.7C. This finding has been shown by many authors who have investigated the kinetic plot performance of core–shell versus fully porous particles (Bobály et al., 2014; Fekete et al., 2009; Fekete and Guillarme, 2013; Grand-Guillaume Perrenoud et al., 2014a; Kahsay et al., 2014; Vaast et al., 2012; Vanderheyden et al., 2013; Wang et al., 2012).

So far, we have considered columns packed with particles of fixed size. For a full optimization of kinetic performance, however, the particle size also has to be optimized along with column length. For each particle size, there is only one t_0/N pair that corresponds to an overall optimum. If the separation time is shorter or longer, a different particle size would give a better result. The pareto-optimal front that connects the overall optima for all particle sizes under given conditions is known as the Knox–Saleem limit (Knox and Saleem, 1969).

Carr et al. (2009) have developed a set of equations that allows the calculation of the kinetic limit under full optimization of linear velocity, column length, and particle size.

The fully optimized maximum plate number is given by

$$N^{**} = \left(\frac{\Delta P_{\max} \cdot t_0^{**}}{\Phi_0 \cdot \eta}\right)^{0.5} \cdot \frac{1}{h_{\min}} \tag{6.38}$$

with the associated optimized column length

$$L^{**} = \left[\frac{\Delta P_{\max} \cdot \nu_{\text{opt}}^2}{\Phi_0 \cdot \eta}\right]^{1/4} \cdot t_0^{3/4} \cdot D_m^{1/2} \tag{6.39}$$

optimized linear velocity,

$$u_0^{**} = \left[\frac{\Delta P_{\max} \cdot \nu_{\text{opt}}^2}{\Phi_0 \cdot \eta}\right]^{1/4} \cdot t_0^{-1/4} \cdot D_m^{1/2} \tag{6.40}$$

and optimal particle size

$$d_p^{**} = \left[\frac{\Phi \cdot \eta \cdot \nu_{\text{opt}}^2}{\Delta P_{\max}}\right]^{1/4} \cdot t_0^{1/4} \cdot D_m^{1/2} \tag{6.41}$$

For a better comparison of the kinetic properties of fully porous and core–shell particles, we have compared the kinetic plots for the 3.5 µm fully porous and the 4 µm core–shell particles in 50% acetonitrile in Fig. 6.8. Fig. 6.8 shows the fixed particle size kinetic plots and the associated Knox–Saleem limits calculated from Eq. (6.38). The Knox–Saleem limit for the core–shell particles is shifted to higher N, which is mainly because of the lower minimum plate height as the column resistance factors are quite similar.

From Eq. (6.41) we see that, for a set of fixed conditions (ΔP, η, Φ, D_m), the optimal particle size d_p^{**} depends on the separation time. Fig. 6.9 shows plots of d_p^{**} versus t_0 (upper panel) and plots of the maximum achievable plate number N versus t_0 (lower panel) for an operating pressure of 1000 bar [porosities, column resistance factors, and h–ν parameters are taken from column 2 (fully porous at 50% ACN, see Table 6.1) and column 5 (core–shell at 50% ACN, see Table 6.1)]. Fig. 6.9 shows that under the conditions selected, there is no large difference in optimum particle size between core–shell

FIGURE 6.8

Kinetic plots and Knox−Saleem limits for 3.5 μm fully porous and 4 μm core−shell particles in 50% acetonitrile, assuming a maximum pressure of 600 bar for both columns [$P_{max}=600$ bar, $\eta=0.8$ cp, $D_m=1.14\cdot10^{-9}$, $\Phi=573$ (fully porous), 602 (core−shell)].

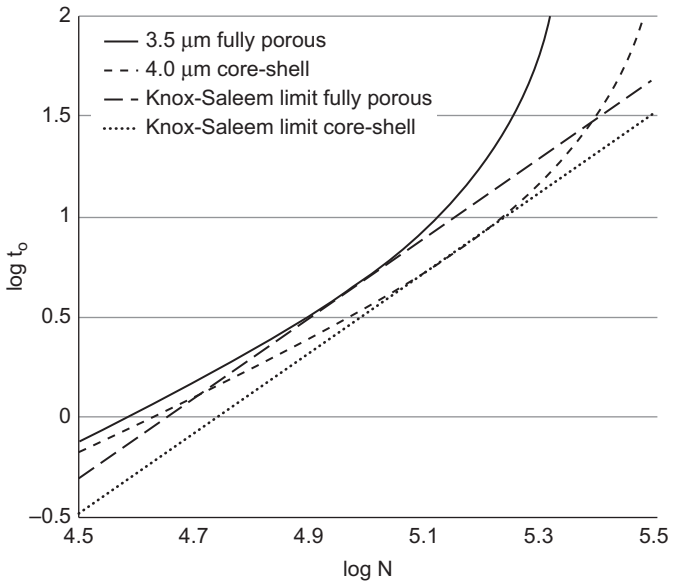

FIGURE 6.9

Optimum particle size and maximum achievable plate numbers for fully porous and core−shell particles [$P_{max}=1000$ bar, $\eta=0.8$ cp, $D_m=1.14\cdot10^{-9}$, $\Phi=573$ (fully porous), 602 (core−shell)].

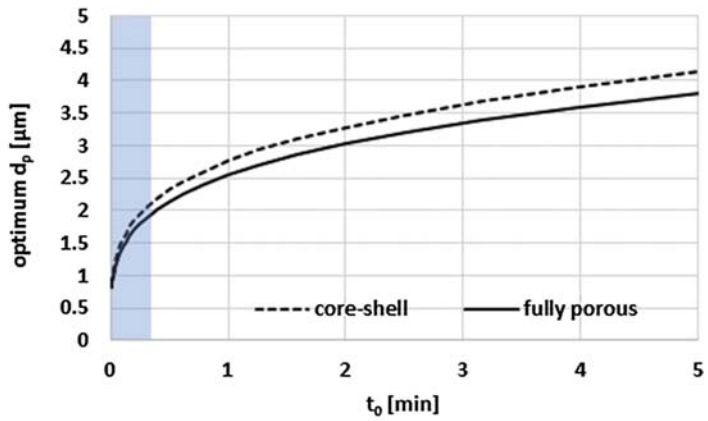

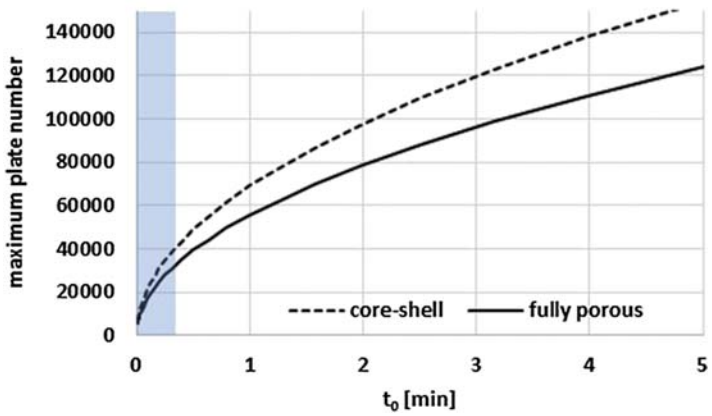

and fully porous particles. In the case shown here, this difference is mainly due to the difference in column resistance factors. The plate number that can be generated in a given time is, however, c. 20% higher compared to a fully porous particle. When selecting the optimum particle size, Fig. 6.9 shows that particles with a size below 2 μm are best suited only for very fast separations. High-resolution separations can be obtained with particle sizes between 2 and 4 μm particles, provided the column can be operated at high pressures. An impressive example of the resolution (peak capacity of ~1400) that can be obtained with coupled columns ($L = 900$ mm) packed with core–shell particles has been shown by De Vos et al. (2012).

3. PARTICLE CHEMISTRIES AND PHASE CHEMISTRIES

Once the desired column technology (particle or monolith) is selected, as described in the previous section, one has to choose the best particle chemistry and phase chemistry to achieve the desired selectivity to separate the compounds of interest. Different particle and phase chemistries require different mobile phase conditions, and as a result, it may or may not be compatible with MS detection.

The different HPLC modes and their stationary phase usage are well summarized in a 2012 HPLC column usage survey conducted by Majors (2012) (Table 6.2). Clearly, reversed-phase liquid

Table 6.2 Analytical High-Performance Liquid Chromatography Mode and Stationary Phase Usage

Chromatographic Mode	% Respondents Using Mode (Normalized) 1997	% Respondents Using Mode (Normalized) 2007	% Respondents Using Mode (Normalized) 2009	% Respondents Using Mode (Normalized) 2011
Reversed-phase (total)	46	38	35	35
Ion exchange (total)	17	18	15	18
Cation	(8.2)	(9.0)	(7.6)	(8.7)
Anion	(9.0)	(9.0)	(7.6)	(9.5)
Size exclusion	9.8	9.4	10	10
Normal-bonded phase (such as amino, diol)	16	14	11	9.6
Hydrophilic interaction liquid chromatography	–	4.2	7.6	8.2
Chiral	5.5	8.7	8.1	6.8
Adsorption	1.7	1.2	6.4	5.4
Affinity	1.7	2.8	2.8	2.4
Hydrophobic interaction chromatography	2.0	2.6	3.0	2.3
Other	0.6	1.2	0.7	2.3

Adapted from Majors, R.E., 2012. Current trends in HPLC column usage. LCGC Eur. 25, 1–7.

chromatography (RPLC) is the most dominant mode. RPLC is also naturally compatible with LC−MS by electrospray ionization because of the good solvent volatility and compatibility with volatile buffers. As a result, reversed-phase (RP) is often the first mode of choice in LC−MS and covers a very wide range of applications. In the last decade, the use of HILIC and SFC with MS coupling has dramatically increased. These separation modes offer complementary selectivity to RPLC and can provide excellent separation of polar analytes. In addition, HILIC and SFC can be easily coupled to MS (Grand-Guillaume Perrenoud et al., 2014b; Tang et al., 2016). Note that SFC is not listed in Table 6.2, but many different phases can be used in SFC, including RP columns, HILIC columns, normal phase columns, and chiral columns.

However, some separation modes are traditionally considered not MS compatible or not MS friendly. These include ionic exchange chromatography (IEX), hydrophobic interaction chromatography (HIC), and size exclusion chromatography (SEC). Both IEX and HIC use high salt concentrations in the mobile phase. In aqueous SEC (polymers and biomolecules), buffer is often used, and this limits the MS compatibility. In organic SEC (polymers), tetrahydrofuran is often used, and it tends to build carbon on the ion source and also has very limited buffer compatibility. As a result, MS detection is not commonly used in SEC. However, multidimensional LC can be used to desalt the eluent from these separation modes, and a second dimension separation (e.g., RPLC) can be easily coupled to MS detection. This is a powerful technique, especially in the biopharmaceutical analysis. Readers are referred to the recent publications on this topic (Largy et al., 2016; Stoll et al., 2016).

It is often realized that samples may have multiple dimensionalities; thus, more than one separation mechanism is needed to separate closely related compounds (Giddings, 1995). This has stimulated many efforts to develop "mixed-mode" stationary phases in recent years to achieve alternative selectivities. Depending on the relative strength of the modes and how the column is operated, these phases can be classified into different modes. For example, a C18 phase with added polar functional group is often treated as an RP column. On the other hand, a polar phase with added IEX sites is often considered as a HILIC column.

The most popular mixed-mode combinations include RP-IEX and HILIC-IEX. In these cases, the amount of charged sites on the surface is much less compared to traditional pure IEX phases. As a result, much less salt is needed in the mobile phase, and this makes them much more MS compatible. Even better, the separation of ionizable compounds in RPLC often requires ion-pairing reagents to increase retention and improve peak shape. But on the mixed-mode phases containing IEX, ion-pairing reagents are often not needed, making the analysis simpler.

Before discussing the particle and phase chemistries, it is important to understand the buffers that are volatile and compatible with MS. Table 6.3 lists the most commonly used LC−MS buffers and their buffer ranges. These buffers are very often used at a pH outside of their buffer range, and thus provide little or no buffer capacity. This can cause serious method-reproducibility problem. In addition, the addition of organic solvent can have a big impact on the pH, e.g., up to a 1.5 pH unit shift with acetate or formate when 60% acetonitrile is added (Subirats et al., 2009).

As an overview, the general MS compatibility and available stationary phases in the modes discussed above are listed in Table 6.4. Each type of stationary phase will be discussed in detail in the following sections. When selecting a stationary phase for LC−MS applications, one needs to consider several characteristics of the column. Table 6.5 serves as a good general guideline for this purpose. More discussion will be given in the next sections when discussing specific columns.

Table 6.3 Liquid Chromatography/Mass Spectrometry Volatile Buffers

Volatile Buffer	pK_a	Buffer Range
Trifluoroacetic acid	0.5	3.8−5.8
Formic acid	3.8	−
Ammonium formate	3.8	2.8−4.8
Acetic acid	4.8	−
Ammonium acetate	4.8	3.8−5.8
4-Methylmorpholine	8.4	7.4−9.4
Ammonium bicarbonate	6.3/9.2/10.3	6.8−11.3
Ammonium acetate	9.2	8.2−10.2
Ammonium formate	9.2	8.2−10.2
1-Methylpiperidine	10.1	10.0−12.0
Triethylammonium acetate	11.0	10.0−12.0
Pyrrolidine	11.3	10.3−12.3

Adapted from McMaster, M.C., 2005. LC/MS: A Practical User's Guide. John Wiley and Sons.

Table 6.4 Separation Modes, Their Mass Spectrometry Compatibility, and Stationary Phase Availability

Mode of Separation	Mass Spectrometry Compatibility	Available Stationary Phases
RPLC	Good	Numerous
HILIC	Good	Many
SFC	Good	Many
SEC	In general poor	Fair amount
Ionic exchange chromatography	No (due to high salt)	N/A
Hydrophobic interaction chromatography	No (due to high salt)	N/A

HILIC, *hydrophilic interaction liquid chromatography;* RPLC, *reversed-phase liquid chromatography;* SEC, *size exclusion chromatography;* SFC, *supercritical fluid chromatography.*

Table 6.5 Desired Characteristics for Liquid Chromatography−Mass Spectrometry Columns

Stationary phase	Good stability, no or low mass spectrometry bleed
Mobile phase	Requires no buffer, or compatible with low ionic strength buffer
Column hardware	Stainless steel or PEEK
Column dimension	Available in small I.D., e.g., $\leq$2.1 mm I.D.
Supply	Good batch-to-batch and column-to-column reproducibility
Method	Fast reequilibration
Scale-up	Same material is available in large I.D. column for sample enrichment purposes after peak identification on small I.D. column

3.1 PARTICLE CHEMISTRIES

Before discussing the phase chemistries, it is important to understand the chemistry for base particles. The major types of particle chemistries include silica, organic hybrid silica, silica hydride, and polymer. Each type of particle chemistry has its advantages and disadvantages, which are listed in Table 6.6.

Silica-based particles are by far the most popular ones used in LC and LC−MS with its long development history. A wide range of particle sizes and pore sizes is available for different applications. The bonding chemistry on silica particles is also well developed and very versatile. Its main disadvantages are the silanol activity and the poor stability in high-pH mobile phases. The silanol activity has been substantially reduced in the modern Type-B ultrapure silica compared to the Type-A silica but still exists. Silanol activity is further improved by organic hybrid silica chemistry, where organosilane is added to the silica skeleton. This greatly reduces the amount of active silanols on the particle surface and thus improves the peak shape of especially basic compounds. The high-pH stability is also greatly improved. As a result, an organic hybrid silica column can be used in low, medium, and high-pH mobile phases to tune selectivity during method development for ionizable compounds. Recently, organic hybrid silica also became available on core−shell particles. This enables fast and efficient method development based on the core−shell particle technology. Fig. 6.10 shows an example where pH is used to tune selectivity for fast separation of a mixture of acids, bases, and neutrals on a 2.7 μm high-pH stable core−shell particle column (Long et al., 2015).

Silica hydride is a relatively new way to reduce silanol activity of the silica surface, developed by Pesek et al. (2002) and has been marketed as Type-C silica. The silanols on the silica surface are initially converted to silica hydride, before different phases are put on the surface. This surface

Table 6.6 Properties of Various Particle Chemistries

Particle Chemistry	No. of Vendors	Available Particle Structure	Advantages	Disadvantages
Silica (Type-A and Type-B)	Numerous	Fully porous Core−shell	Good mechanical strength	Unstable in high pH
		Nonporous	Wide range of particle sizes and pore sizes	Silanol activity can cause bad peak shape
Organic hybrid silica	Many	Fully porous	Better high-pH stability	Availability from fewer vendors
		Core−shell	Less silanol activity	
Silica hydride (Type-C)	Limited	Fully porous	Much reduced silanol activity Chemical stability	Limited availability (hard to find equivalent columns)
Polymer	Many	Fully porous	Best chemical stability	Often lower efficiency than silica
		Nonporous	No silanol activity	Lower pressure capability due to lower mechanical strength

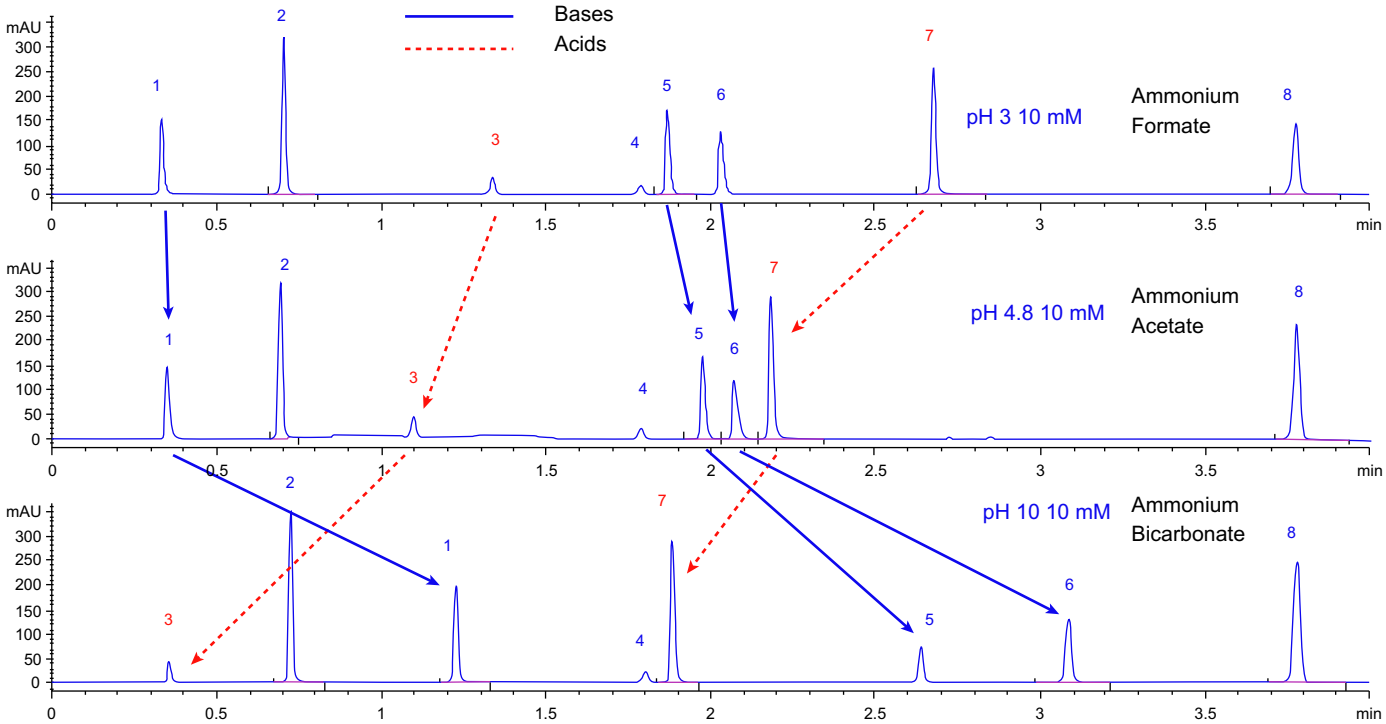

FIGURE 6.10

Selectivity control by altering pH. Column: 50 mm × 4.6 mm, 2.7 µm HPH Poroshell-C18; mobile phase A: 10 mM ammonium formate (pH 3), ammonium acetate (pH 4.8), or ammonium bicarbonate (pH 10) in water; mobile phase B: acetonitrile, gradient: 10%−90% B in 5 min, hold 2 min at 90%; flow rate: 2 mL/min; detection UV absorbance at 254 nm; temperature 30°C. Peaks: 1 = procainamide, 2 = caffeine, 3 = acetyl salicylic acid, 4 = hexanophenone degradant, 5 = dipyrimadole, 6 = diltiazem, 7 = diflunisal, and 8 = hexanophenone.

modification can also lead to better chemical stability. This material can be used in HILIC mode for efficient separation of hydrophilic metabolites in LC−MS (Pesek et al., 2008).

A polymeric particle is certainly the most chemically inert material and can be used in the widest pH range from 1 to 14. Due to the absence of silanols, it is also considered as an inert material. As a result, polymer particles are commonly used in bioseparations, whereas not so much in small molecule separations. A wide range of pore sizes is also available for different sizes of molecules. The biggest disadvantages compared to silica-based materials are its lower efficiency, lower mechanical strength, and incompatibility with certain organic solvents due to swelling. On the other hand, chemical modification on polymer beads is very versatile, and many different functional groups can be added to tune the selectivity.

3.2 PHASE CHEMISTRIES

There are numerous phase chemistries that can be put on the particle surface to generate different selectivities. It is important to note that the boundary between different classes of phases is becoming more and more vague. For example, the same polar phase can be used in HILIC and SFC. In this section, we discuss the different phase chemistries used in LC (RP, HILIC, mixed-mode phases) and SFC (chiral and achiral phases).

3.2.1 Liquid Chromatography Phases

3.2.1.1 Reversed Phase

RPLC is without a doubt the most widely used separation mode because of its wide applicability, ruggedness, and ease of use. Because of the long history of development, there are hundreds of different RPLC phases that exist today and cover a wide spectrum of hydrophobicity. In the early days, phosphate buffers were commonly used in LC-UV because of their wide pH range and UV transparency. But phosphate can be easily replaced by volatile buffers such as ammonium formate, ammonium acetate, and ammonium bicarbonate for LC−MS, without compromising the chromatography.

The retention mechanism of RPLC is relatively well understood, and this has led to several stationary phase classification methods (Euerby and Petersson, 2003; Kimita et al., 1989). One of the most comprehensive approaches is the hydrophobic-subtraction model (HSM) developed by Snyder et al. (2007). Each stationary phase is characterized by five parameters: hydrophobicity (H), steric hindrance (S), H-bond acidity (A), H-bond basicity (B), and cation exchange activity (C). Based on these parameters, the commercial phases can be classified into different groups as shown in Table 6.7. The columns in each group have relatively similar HSM parameters. The readers are referred to the review article by Snyder et al. (2004) for more details.

The HSM method is particularly useful in finding equivalent or orthogonal columns, depending on the need of a separation problem. An F value can be calculated by the HSM parameters between two columns, as given by Eq. (6.42):

$$F_s = \left[(H_2 - H_1)^2 + \left(S_2^* - S_1^*\right)^2 + (A_2 - A_1)^2 + (B_2 - B_1)^2 + (C_2 - C_1)^2\right]^{1/2} \tag{6.42}$$

If F is small (e.g., $\leq$3), two columns can be considered equivalent. If F is large, two columns will likely produce a different selectivity.

Table 6.7 Average Variation in Column Selectivity Parameters as a Function of Column Properties and Column Type

	Average Column Parameter				
Column Property or Type	***H***	***S****	***A***	***B***	***C* (pH 2.8)**
Type-B C18 (endcapped)	1	0.01	−0.07	−0.01	0.05
Change in Type-B C18 Column Parameters for a Change in Column Properties					
1. C3 to C18	0.4	−0.09	0.27	−0.02	0.18
2. Nonendcapped to endcapped	0.02	0.03	−0.38	0.02	−0.22
3. 6−30 nm pore	−0.20	−0.05	−0.16	0.09	0.14
4. 0.9−2.9 μmol/m^2	0.37	0.1	0.19	−0.07	0.16
Average Values of Column Parameters for Each Column Type					
5. Type-B C18	1	0.01	−0.07	−0.01	0.05
6. Type-B C8	0.83	0	−0.11	0.02	−0.02
7. Type-A C18	0.84		0.12	0.05	0.78
8. Embedded polar group	0.68	0	−0.54	−0.17	−0.65
9. Polar-group endcapped	0.94	−0.02	−0.01	0.01	−0.14
10. Polymeric alkylsilica (type-A)	0.94	0.04	0.42	−0.02	0.69
11. Cyanopropyl	0.41	−0.11	−0.58	−0.01	0.07
12. Phenylpropyl	0.6	−0.16	−0.23	0.02	0.16
13. Bonded zirconia	1.03	−0.01	−0.43	0.05	2.08
14. Fluoroalkyl	0.7	−0.03	0.1	0.04	1.03
15. Fluorophenyl	0.63	0.14	−0.26	0.01	0.55

Reprinted with permission from Snyder, L.R., Dolan, J.W., Carr, P.W., 2007. A new look at the selectivity of RPC columns. Anal. Chem. 79, 3255−3262.

Table 6.7 lists the most common RP phases covering a wide range of hydrophobicity, specifically they include the following:

1. Hydrophobic phases (C4 to C18). As shown by Majors (2012), these phases account for more than 60% of all RPLC phases. These phases are often the first choice when developing a method. The choice of the hydrocarbon chain length is dependent on the hydrophobicity of the analytes. In the protein analysis world, C4 or C8 is more frequently used because of the belief that C18 provides too strong of a binding to some proteins and thus may cause sample loss. In addition, large pore size particles or monoliths are used to accommodate the size of proteins. These phases are particularly dominant in protein and peptide analysis, as shown in Rauh's review article on LC−MS/MS for protein and peptide quantification in clinical chemistry (Rauh, 2012). All examples shown in this article used C18 phases for a wide variety of proteins.
2. Embedded polar group (EPG) phases. These phases were initially developed to address the dewetting problem of purely hydrophobic phases in highly aqueous mobile phase, to improve the

peak shape of some basic compounds, and to obtain different chromatographic selectivity. In a way, EPG phases can be considered "mixed-mode" phases because they provide both hydrophobic and polar interactions. The most common polar groups include amide, carbamate, ether, and urea. These groups provide hydrogen bonding interaction and thus can alter the selectivity for polar analytes, compared to pure hydrocarbon phases. More details about EPG phases can be found in the papers by Euerby and Petersson (2005) and Wilson et al. (2004).

3. Phenylalkyl phases. These phases provide another key interaction ($\pi-\pi$) to allow different selectivity. This is important to pharmaceutical analysis because most drugs contain phenyl groups. The most common phenyl phase is phenyl-hexyl, which has a six-carbon spacer between the phenyl ring and the silica surface. Some vendors offer phenyl phases with a longer carbon spacer. However, in general, the phenyl retention and selectivity characteristics decrease as the carbon spacer length increases. It is also important to note that the phenyl retention characteristics are strongly influenced by the organic modifier. The $\pi-\pi$ interaction is significantly stronger in methanol compared to that in acetonitrile. For example, the use of methanol on a phenyl-hexyl phase gives stronger retention and better selectivity of closely related steroids (Long, 2012).
4. Fluorinated phases. These phases can either be a fluorinated alkyl phase or a perfluorinated phenyl (PFP) phase, with the latter being a more popular one in practice (Przybyciel, 2005). These fluorinated phases provide strong dipole−dipole interactions and have excellent shape selectivity. In a recent study at Merck, the PFP phase was found to be the most effective in separating halogenated pharmaceutical isomers and their dehalogenated impurities (Regalado et al., 2014). Most PFP phases have a short fluorinated alkyl spacer chain such as propyl. However, such phases often suffer from poor chemical stability, and this can lead to strong background bleed in LC−MS. Some vendors use a longer alkyl spacer chain to stabilize the phase, but this comes at the cost of making the phase more C18-like and less PFP-like. More details about fluorinated phases can be found in the papers by Euerby et al. (2003) and Marchand et al. (2005b).
5. Cyano phases. These phases are one of the most polar RPLC phases. It can be easily seen from Table 6.7 that cyano phases have the lowest H (hydrophobicity) term in the HSM model. In addition, they have very strong hydrogen bonding acidity. As a result, cyano phases can be used in highly aqueous mobile phase conditions and can retain and separate very polar compounds. More details can be found in Marchand et al. (2005a).
6. Other phases. There are a number of unique phases that have been commercialized to address specific applications. For alkyl phases, C30 is available and has been shown to have good shape selectivity, e.g., for cis−trans carotenoid isomers (Emenhiser et al., 1996). For aromatic-based phases, some unique phases include naphthyl, pyrenyl, diphenyl and biphenyl phases. All these phases have stronger $\pi-\pi$ interaction characteristics than phenyl phases and can provide better selectivity for structural isomers including PAHs and steroids. Perhaps the most hydrophobic phase available is the graphitized carbon phase, which has both strong hydrophobicity and aromaticity (Hanai, 2003). The main challenge of this phase is its unpredictable retention behavior. It is not uncommon that some compounds may be irreversibly adsorbed onto the phase and not being eluted.

3.2.1.2 Hydrophilic Interaction Liquid Chromatography Phases

In contrast to RPLC, where the stationary phase is hydrophobic and the strong mobile phase is organic, HILIC uses hydrophilic stationary phases and highly organic mobile phases. As a result, one can

expect complimentary selectivity in HILIC versus RPLC. Very hydrophilic compounds can be well retained and separated in HILIC, whereas they are poorly retained in RPLC. The term HILIC was coined by Alpert in 1990, and since then we have seen a steady increase in interest in HILIC and many commercial efforts in developing new HILIC phases. In HILIC, highly organic mobile phases are used (normally >60% acetonitrile) and volatile buffers are also often used (e.g., ammonium formate). This makes HILIC easily compatible with MS. A very good review on HILIC has been written by Hemstrom and Irgum (2006).

To date, there are many different HILIC phases commercially available; the most commonly used ones are summarized in Table 6.8. These include bare silica, amine-based phases, amide phases, hydroxylated phases, and mixed-mode phases. The mixed-mode HILIC phases will be discussed in more detail in the next section.

The retention mechanism in HILIC is generally not as well understood as RPLC. However, there have been several attempts to classify different HILIC phases for selectivity. In general, it is believed that a surface layer of absorbed water is critical to the partition of analytes between the organic-rich mobile phase and the surface water layer (McCalley and Neue, 2008). For ionizable compounds, an ionic exchange mechanism with any stationary phase charged sites is also important to the overall retention (McCalley, 2010b). Rather comprehensive approaches have been developed by Dinh et al. (2011) and Kawachi et al. (2011). For example, the method by Kawachi uses nine parameters to describe each HILIC phase. However, a rather simple but not so comprehensive model developed by Ibrahim et al. (2012) is very useful to visualize the different selectivities between different phases.

Fig. 6.11 shows such a selectivity plot with two axes. The *x*-axis is the selectivity between cytosine and uracil, and this measures the phase hydrophilicity. The *y*-axis is the selectivity between benzyltrimethylammonium and cysotine, and this is to probe the ionic exchange characteristics of the phase. In such plots, different types of HILIC phases are clustered in groups and are far away from the RPLC phases. The silica phases show good hydrophilicity, but also strong cationic exchange properties, because of the deprotonated silanols in pH 6.8 buffer. If low-pH buffer is used, this value would decrease dramatically. In contrast, the amine phases show strong anionic exchange properties, obviously because of the amine groups. The zwitterionic phases, on the other hand, have rather intermediate hydrophilicity and ionic exchange properties.

Table 6.8 Hydrophilic Interaction Liquid Chromatography Phases

Phase Chemistry	Examples
Bare silica	Many silica
Amine	Aminoalkyl
	Triazole
Amide	Amide (monomeric or polymeric)
Hydroxylated	Hydroxyl (diol, penta-ol)
	Cyclodextrin
	Cyclofructan
Mixed-mode	Zwitterionic (single ligand)
	Hydrophilic interaction liquid chromatography/IEX

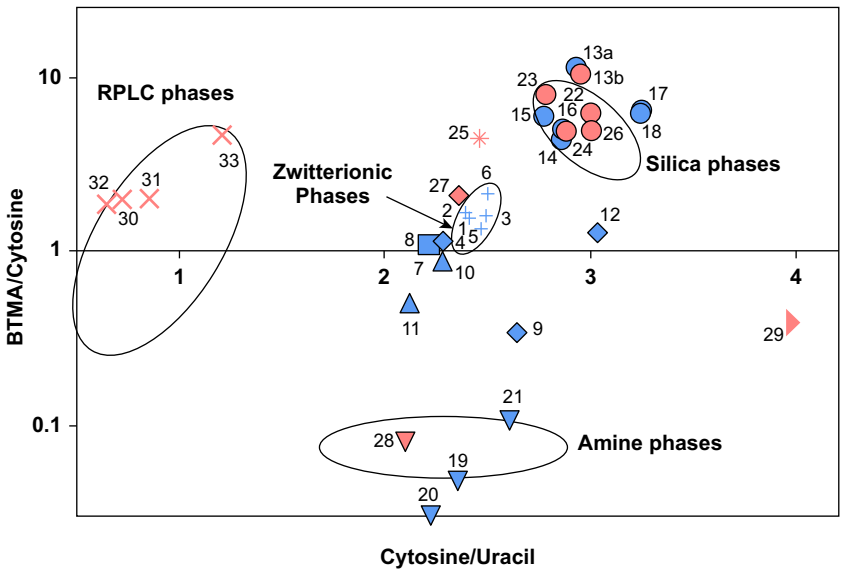

FIGURE 6.11

Hydrophilicity versus ion-exchange selectivity plot of hydrophilic interaction liquid chromatography phases; bare silica (•), amide (■), diol (▲), amine and/or triazole (▼), polymer substrate and/or polymer-coated silica (◆), zwitterionic (+), RPLC (×), latex-coated silica (∗), proprietary polar phase (►).

Reprinted with permission from Ibrahim, M.E.A., Liu, Y., Lucy, C.A., 2012. A simple graphical representation of selectivity in hydrophilic interaction liquid chromatography. J. Chromatogr. A 1260, 126–131.

3.2.1.3 Mixed-Mode Phases

A sample may contain both neutral and ionic compounds. In Giddings' term, the sample may have multiple sample dimensions (Giddings, 1995). In this case, a unimodal stationary phase may not be able to resolve all the compounds in the sample. This is the main motivation for developing mixed-mode phases. Ionic exchange functionality is the most common mechanism to be added to RP or HILIC because it can introduce the maximal change in selectivity. There are different ways to achieve mixed-mode columns as shown in Fig. 6.12.

1. Mixed beads. In this case, different beads with different functionalities are made separately. For example, one type of bead can be purely RP and the other can be ionic exchange. The two beads are then mixed together in a certain ratio before being packed into columns. A potential issue of this approach is that the synthesis of each bead has its own batch-to-batch variability, and combining two beads together will amplify the variation. As a result, this approach has not gained much popularity.
2. Mixed ligands. The main difference in the mixed ligands case versus the mixed beads case is that the two functionalities (e.g., RP and IEX) are bonded to the same particle. Typically, one ligand is bonded to the particle before the other ligand. So the amount of each ligand can be controlled in two separate steps. The synthesis reproducibility is improved from the mixed beads case, but the variation still adds up in a multistep synthesis.

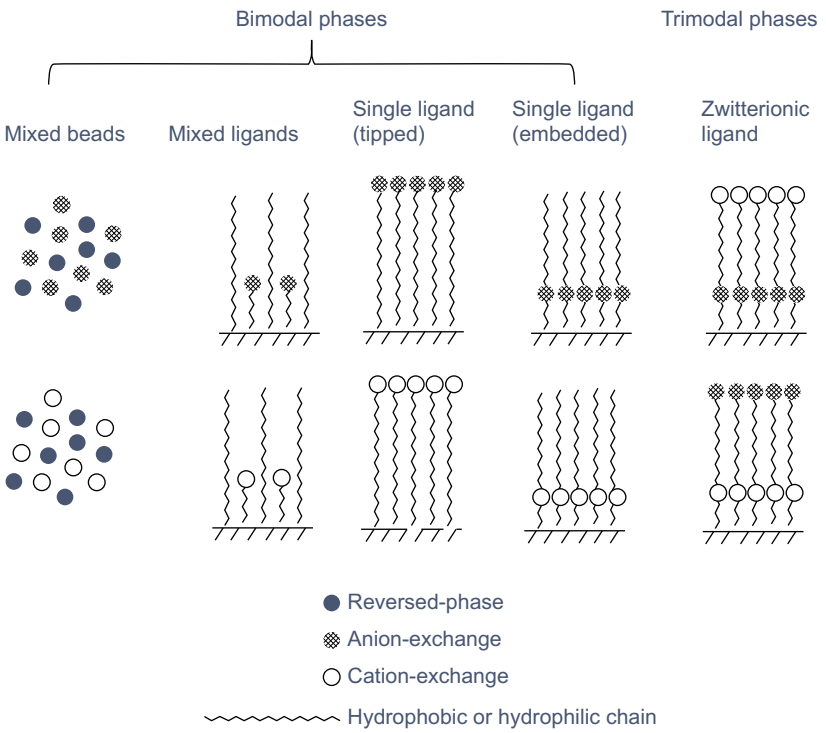

FIGURE 6.12

Different methods to produce mixed-mode columns.

3. Single ligand. In this case, one ligand with multiple functionalities is presynthesized and then put on the particle surface in a one-step reaction. The ligand can be bimodal, with either a negatively or a positively charged group and either on the tip of the ligand or embedded close to the particle surface. The ligand can also be trimodal with both negatively and positively charged groups on the same ligand. This type is often referred as a zwitterionic phase. In addition, the spacer group can be either hydrophobic or hydrophilic, and the position of the charged group can be tuned to offer different selectivity. However, the ratio of the RP/HILIC characteristics and the IEX characteristics is predetermined by the structure of the ligand. Because of the one-step synthesis, the batch-to-batch reproducibility is the best compared to mixed beads and mixed ligands approaches.
4. Single ligand with adsorbed nanoparticles. In this case, a mixed-mode particle with a bimodal single ligand is first synthesized. On the tip of the ligand, there is certain type of charge. Then, nanoparticles with the opposite charge are added to the single ligand particles, and they are adsorbed onto the particle's external surface via Coulombic attractions. The net result is that the final particle is trimodal, with RP, CEX, and AEX functionalities. Because of its complexity, it is not shown in Fig. 6.12.

There are many possible combinations of the approaches mentioned above to make unique stationary phases. Bimodal phases have two retention mechanisms, whereas trimodal phases have three

retention mechanisms. A number of mixed-mode phases are already commercially available and has been shown to provide unique selectivity and used in LC−MS applications. We will discuss some important ones next.

3.2.1.3.1 Reversed-Phase/Ionic Exchange Chromatography Mixed-Mode Phases. When silica is used as the base particle, there are always residual silanols left after the bonding step. When the pH of the mobile phase is medium or high, these silanols are deprotonated. This causes strong retention and bad peak tailing for basic compounds. This is a serious problem for the pharmaceutical industry because most of the drugs are basic molecules. To mitigate this problem, a low pH mobile phase is often used to protonate the silanols and improves the peak shape. In this case, trifluoroacetic acid (TFA) can give better peak shape than formic acid because of its stronger ion pairing ability. However, TFA causes serious ionization suppression in MS, so formic acid is preferred for MS sensitivity. As a result, LC−MS practitioners often use formic acid and accept a compromise in the peak shape.

Another problem of analyzing basic compounds is sample overload. While injection amount increases, peak shape quickly deteriorates (McCalley, 2010a). Different hypotheses have been proposed, and one of them by McCalley attributes sample overloading to the mutual repulsion between analytes on the particle surface. Using stronger ion pairing agent or higher ionic strength buffer mitigates the problem, but again, this causes MS signal suppression.

In 2010, scientists at Waters reported that adding a small amount of positive charge to a particle surface can significantly improve the peak shape and sample overloading capacity of basic compounds in low ionic strength buffers such as formic acid (Iraneta et al., 2010). They used the mixed ligands approach, where a small and controlled amount of positive charge is added to the bridged ethyl hybrid (BEH) particles before the C18 bonding. The phase is called charged surface hybrid (CSH), and it gives much improved peak shapes for basic drugs over BEH (Neue et al., 2013). The mixed-mode nature of the CSH phase also leads to different selectivities than the BEH phase (Iraneta et al., 2010). This is beneficial during method development.

Perhaps the most impactful application of the CSH material is its use for peptide mapping in a formic acid mobile phase. Peptide mapping in proteomics and the biopharmaceutical industry is most often done by LC−MS, and formic acid is the preferred mobile phase, in spite of the compromise in peak shape and sample overloading capacity. Fig. 6.13 shows the comparison of a Lys-C peptide mapping on CSH and BEH. The retention time is shorter on the CSH phase because of the repulsion between the surface positive charge and the basic peptides. However, peak shape was substantially better, and this led to an almost two times higher peak capacity on the CSH column. The elution order of some peptides was also changed because of the different selectivity.

As discussed above, mixed-mode phases can also be made with the single ligand approach. Different IEX functionalities (i.e., strong or weak, cation or anion exchange) can be built into the ligand at different positions in the ligand. Examples of such phases include the Thermo Scientific Mixed-Mode WCX-1 and WAX-1, and the Sielc Primesep acidic, basic and phenyl phases. Because the IEX and RP moieties are on the same ligand, their ratio is fixed. This is different than the mixed ligand phases, where the ratio of the two groups can be independently adjusted. As a result, the amount of surface charge of the single ligand mixed-mode phases is likely much higher than that of the mixed ligand phases. This may require high buffer concentration to elute ionic analytes and may limit the LC−MS applications. However, the main benefit of such phases is that it is possible to separate a mixture of neutrals, acids, and bases on one column in a single method.

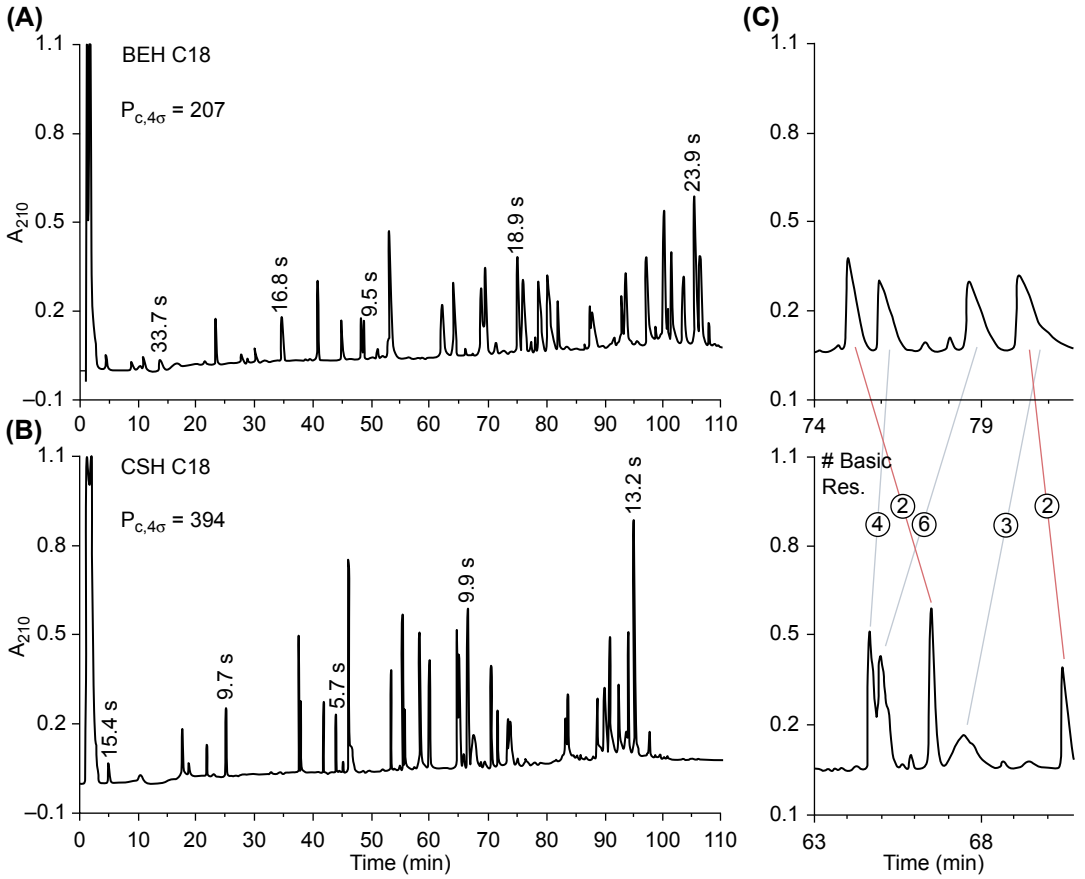

FIGURE 6.13

Lys-C peptide maps of trastuzumab obtained with (A) BEH C18 and (B) CSH C18. Peak widths at half height ($w_{0.5}$) are shown for five peptides spread across the separations. Peak capacities (4σ) were calculated from the averages of these values. (C) Corresponding retention windows from each peptide map. *Colored lines* indicate the change in elution order of the different peptide species, (peptides marked with *blue lines* (light gray in print versions) elute relatively earlier, peptides marked with *red lines* (gray in print versions) elute relatively later) as detected by electrospray ionization-mass spectrometry. The number of basic residues for each identified species is provided.

Reprinted with permission from Lauber, M.A., Koza, S.M., McCall, S.A., Alden, B.A., Iraneta, P.C., Fountain, K.J., 2013. High-resolution peptide mapping separations with MS-friendly mobile phases and charge-surface-modified C18. Anal. Chem. 85, 6936–6944.

More complicated trimodal mixed-mode phases have also been developed, typically including RP, cationic exchange, and anion exchange functionalities. Examples of such phases include the Thermo Scientific Acclaim Trinity P1, Imtakt Scherzo, and Sielc Obelisc R phases. Interestingly, these phases are made in three different ways. The Imtakt Scherzo phase is made by mixing two different beads, and each bead is a bimodal phase made by the mixed-ligand approach. The two beads, one is RP/SAX and

the other is RP/SCX, are mixed and then packed into columns. The Acclaim Trinity P1, on the other hand, is made by the single ligand with adsorbed nanoparticles approach. A single ligand RP/WAX phase was first made with the weak anion exchange group at the tip of the phase. Then nanopolymers with surface negative charges are adsorbed to the particle external surface by electrostatic interactions. The negatively charged nanopolymers provide the third functionality of strong cationic exchange sites. Perhaps a simpler way to make trimodal phases is the approach used in the Sielc Obelisc R phase. In such case, a zwitterionic ligand is made with (1) a positively charged group close to the particle surface, (2) a hydrophobic hydrocarbon chain as the linker, and (3) a negatively charged group at the tip of the ligand. Such phase is also often referred as a zwitterionic phase.

Lämmerhofer et al. compared the performance of several bimodal and trimodal RP/IEX phases, as well as several research mixed-mode phases made in their laboratory (Lämmerhofer et al., 2008). Fig. 6.14 shows the chromatograms in 40/60 acetonitrile/water with pH 6 ammonium acetate buffer. The two acidic solutes in the sample cannot be sufficiently retained on typical C18 phases. However, on almost all mixed-mode phases, they are well retained and separated. The selectivity of the sample can also be rationalized by the phase chemistries. For example, the Acclaim WAX-1 phase has the anion exchange site on the tip of the single ligand, which is very accessible for the acids in the sample. Therefore, the two acidic solutes were strongly retained. On the other hand, the Primesep B2 phase has the anion exchange site buried in the ligand, with less accessibility, and this led to the much shorter retention.

We can use the selectivity triangle, which is a graphical method to represent the HSM selectivity model developed by Zhang et al., to demonstrate the unique selectivity of mixed-mode RP/IEX phases. Fig. 6.15 shows the selectivity triangle based on the S, B, and C parameters in the HSM model. The farther the distance between two points, the more different the two phases are. Most RP phases are clustered in the center. Phases with the most different selectivities are labeled and listed in the figure. The three most different ones include (1) Inertsil CN-3, a cyano phase, (2) Vydac 218MS, a phase based on type-A silica, and (3) -SO3-HC-C8, a research mixed RP/SCX phase.

3.2.1.3.2 Hydrophilic Interaction Liquid Chromatography/Ionic Exchange Chromatography Mixed-Mode Phases. Similarly, IEX functionality can be added to HILIC phases to create bimodal or trimodal phases. In RPLC, the addition of charged groups dramatically decreases the phase hydrophobicity. As a result, to maintain some level of RP retention characteristics, a long alkyl chain is needed for RP/IEX mixed-mode phases. However, in HILIC, the phases need to be very hydrophilic, and addition of charges increases the phase hydrophilicity. This gives many possibilities of HILIC/IEX chemistry.

Examples of HILIC/IEX mixed-mode phases include the Thermo Scientific Acclaim Trinity P2 and GlycanPac AXH-1 phases, PolyLC PolySulfoethyl A, Sielc Obelisc N, and Merck Zic-HILIC phases. A zwitterionic ligand is an important way to make a trimodal phase and achieve unique selectivity, as already discussed in the HILIC section. On the other hand, there are some bimodal HILIC/IEX phases, such as the PolySulfoethyl A and GlycanPac AXH-1, which have been shown to be very useful for biomolecule separations. For example, the GlycanPac AXH-1 is a HILIC/WAX phase with proprietary chemistry. But it can be used in HILIC mode to effectively separate N-glycans, as shown in Fig. 6.16. Glycans can be separated into groups with different levels of sialylation, and within each group glycans are separated based on hydrophilicity.

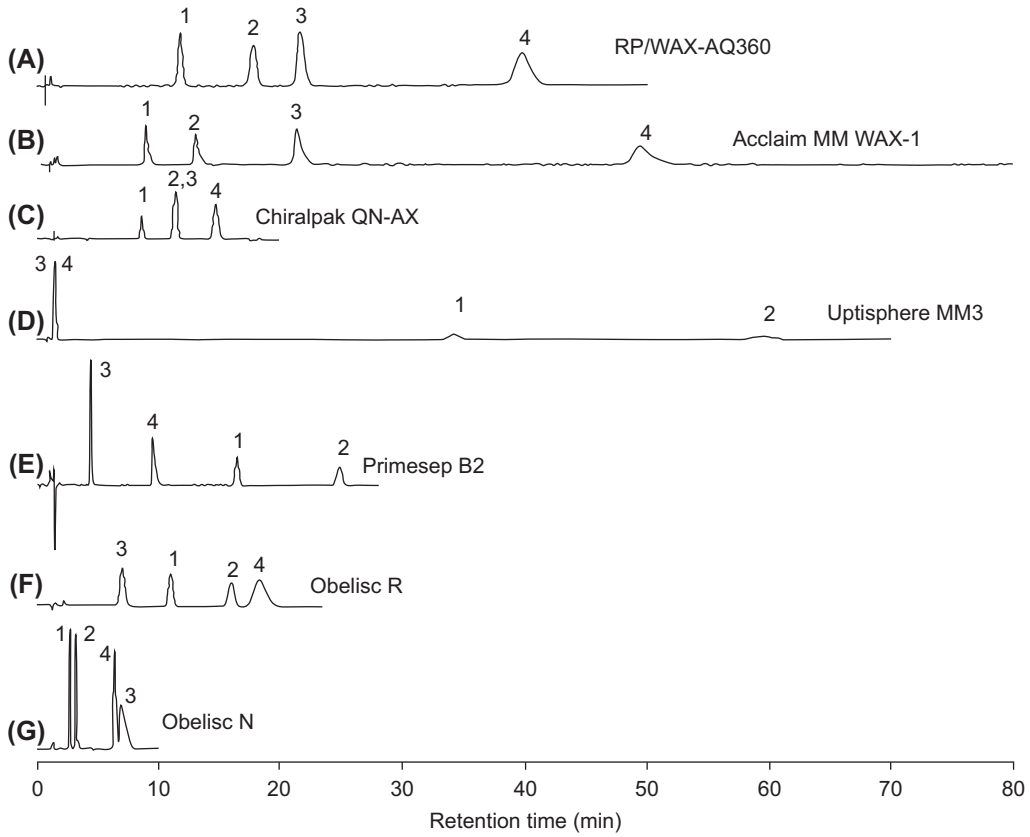

FIGURE 6.14

Comparison of the separation of the reversed-phase (RP) test mixture on an in-house developed RP/WAX-AQ360 phase with those obtained on commercially available mixed-mode phases employing RP-elution mode. Solutes: (1) butylbenzene; (2) pentylbenzene; (3) DETP (O,O-Diethyl thiophosphate); and (4) Boc-Pro-Phe.

Reprinted with permission from Lämmerhofer, M., Richter, M., Wu, J., Nogueira, R., Bicker, W., Lindner, W., 2008. Mixed-mode ion-exchangers and their comparative chromatographic characterization in reversed-phase and hydrophilic interaction chromatography elution modes. J. Sep. Sci. 31, 2572–2588.

3.2.2 Phases for Supercritical Fluid Chromatography

SFC has been investigated for a long time. There were several attempts in its history to make SFC into a mainstream separation technique, but this has not been very successful. In the last 5 years, there has been another round of renewed interest in SFC because of the efforts by the instrument companies to improve instrument ruggedness and performance. This also means that new columns are being developed for SFC. We will discuss chiral SFC columns and achiral SFC columns separately.

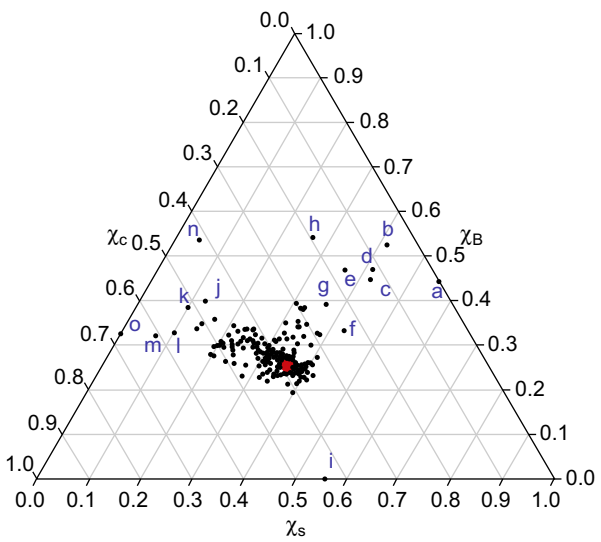

Labels	Stationary phases	Types
a	Inertsil CN-3	Cyano
b	EC Nucleosil 100-5 Protect	EPG
c	Hypersil Prism C18 RP	EPG
d	Bonus RP	EPG
e	BetaMax Acid	EPG
f	Purospher RP-18	B-C18
g	Discovery HS PEG	EPG
h	Hypurity Advance	EPG
i	Vydac 218MS	Type-A
j	HC-OH	Special
k	HC-C8	Special
l	ZirChrom-PS	Special
m	Nova-Pak CN HP 60A	Cyano
n	BioBasic Phenyl	Phenyl
o	–SO3-HC-C8	Special

FIGURE 6.15

Positions of the extreme phases based on the S^*-*B*-*C* triangle and the list of extreme phases.

Reprinted with permission from Zhang, Y., Carr, P.W., 2009. A visual approach to stationary phase selectivity classification based on the Snyder-Dolan Hydrophobic-Subtraction Model. J. Chromatogr. A 1216, 6685–6694.

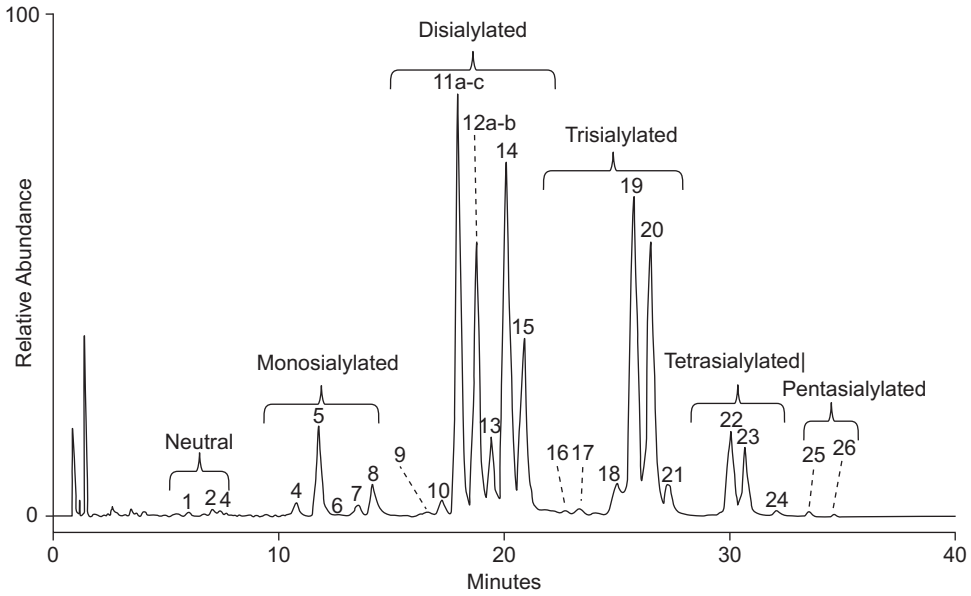

FIGURE 6.16

Liquid chromatography/mass spectrometry analysis of 2AB labeled *N*-glycans from bovine fetuin using the GlycanPac AXH-1 column.

Reprinted with permission from ThermoFisher Product Specification PS20695_E 05/14S.

3.2.2.1 Chiral

The advantages of SFC for chiral separations were recognized early on. Chiral separations in LC are typically done in normal phase, polar organic, or RP modes. In all cases, mass transfer in LC is substantially slower than that in SFC. More importantly, SFC is ideally suited for preparative chiral separation because of the much lower solvent consumption. Because of the need to transfer methods from analytical to preparative scales, analytical chiral separations are frequently done by SFC. In fact, chiral method screening is also commonly done in SFC mode to select the best column because of the faster run time. Almost all chiral columns used in LC can be used in SFC, with the exception of protein-based chiral phases (West, 2014).

The existing chiral stationary phases seem to be adequate for solving chiral separation problems. Therefore, there have not been many new chiral selectors developed in recent years. One new phase that is worth mentioning is the cyclofructan-based chiral phases developed by Armstrong (Sun and Armstrong, 2010; Sun et al., 2009). Cyclofructans are cyclic oligosaccharides, and they can be used as chiral selectors in their native form or derivatized forms (e.g., naphthylethyl or 3,5-dimenthylphenyl). These phases are particularly effective in separating primary, secondary, and tertiary amines and alcohols.

Most recently chiral selectors are being bonded to modern silica to further improve the speed of separation. For example, cyclofructans were bonded to 2.7 μm core−shell particles by Armstrong (Patel et al., 2015). Other chiral selectors such as macrocyclic glycopeptide and Pirkle type selector are also bonded to sub-2 μm fully porous particles with very narrow particle size distributions (Berger, 2016; Ismail et al., 2016a). In all these cases, ultrafast chiral separations of less than 1 min can be routinely achieved, and this can enable very fast method development with multiple column screening.

3.2.2.2 Achiral

For achiral separation, LC is still much more popular than SFC. However, the situation is changing because recent studies are showing that SFC can give three times shorter analysis time than LC at the same efficiency (Gritti and Guiochon, 2013a). The work by Lesellier and West has also shown that a wide spectrum of stationary phases can be used in SFC to separate different classes of compounds (Lesellier and West, 2015). Essentially almost all HPLC phases can be used in SFC. A selectivity classification method was developed for SFC similar to the hydrophobic subtraction model in RPLC. Fig. 6.17 shows the spider diagram based on the five column parameters that characterize the selectivity. The traditional RPs (e.g., C18, C8) and the traditional polar phases (e.g., silica, NH_2) are at the opposite positions of the space. The space between is filled with various phases with different degrees of hydrophobicity.

Similar to LC, smaller particles are being used more frequently in SFC. However, the absolute performance improvement of separation performance by decreasing particle size in SFC is not as big as that in LC, primarily because of the already faster diffusion coefficient in SFC. In addition, the higher backpressure when using really small particles will increase the SFC mobile phase density and this will decrease the sample diffusion coefficient. Therefore, SFC will become more "LC-like" when pressure increases; thus the performance improvement from LC to SFC is expected to be smaller at higher system pressure. As a result, the benefit of doing ultrahigh pressure SFC with really small particles is yet to be demonstrated.

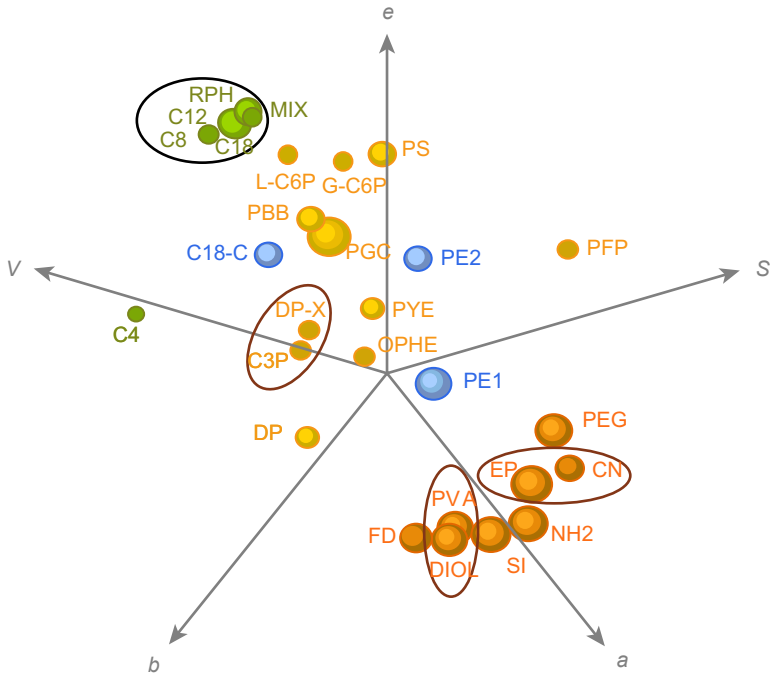

FIGURE 6.17

Spider diagram for a five-dimensional selectivity model for supercritical fluid chromatography columns.

Reprinted from with permission from West, C., Lesellier, E., 2008. A unified classification of stationary phases for packed column supercritical fluid chromatography. J. Chromatogr. A 1191, 21–39.

REFERENCES

Alpert, A.J., 1990. Hydrophilic-interaction chromatography for the separation of peptides, nucleic acids and other polar compounds. J. Chromatogr. A 499, 177–196.

Barber, W.E., Joseph, M., 2004. ZORBAX Rapid Resolution HT Columns – A Breakthrough in High-throughput HPLC Column Technology. Agilent Technologies. Application Note 5989–0599EN.

Berger, T.A., 2016. Kinetic performance of a 50 mm long 1.8 μm chiral column in supercritical fluid chromatography. J. Chromatogr. A 1459, 136–144.

Billen, J., Desmet, G., 2007. Understanding and design of existing and future chromatographic support formats. J. Chromatogr. A 1168, 73–99.

Bobály, B., Guillarme, D., Fekete, S., 2014. Systematic comparison of a new generation of columns packed with sub-2 μm superficially porous particles. J. Sep. Sci. 37, 189–197.

Bobály, B., Guillarme, D., Fekete, S., 2015. Evaluation of new superficially porous particles with carbon core and nanodiamond–polymer shell for protein characterization. J. Pharm. Biomed. Anal. 104, 130–136.

Broeckhoven, K., Cabooter, D., Lynen, F., Sandra, P., Desmet, G., 2008. Errors involved in the existing B-term expressions for the longitudinal diffusion in fully porous chromatographic media Part II: experimental data in packed columns and surface diffusion measurements. J. Chromatogr. A 1188, 189–198.

Carr, P.W., Wang, X., Stoll, D.R., 2009. Effect of pressure, particle size, and time on optimizing performance in liquid chromatography. Anal. Chem. 81, 5342−5353.

Catani, M., Ismail, O.H., Cavazzini, A., Ciogli, A., Villani, C., Pasti, L., Bergantin, C., Cabooter, D., Desmet, G., Gasparrini, F., Bell, D.S., 2016. Rationale behind the optimum efficiency of columns packed with new 1.9 μm fully porous particles of narrow particle size distribution. J. Chromatogr. A 1454, 78−85.

Chen, W., Jiang, K., Mack, A., Sachok, B., Zhu, X., Barber, W.E., Wang, X., 2015. Synthesis and optimization of wide pore superficially porous particles by a one-step coating process for separation of proteins and monoclonal antibodies. J. Chromatogr. A 1414, 147−157.

Chen, W., Wei, T.C., 2010. Superficially Porous Particles and Methods of Making and Using Same. US patent US7846337 B2. Agilent Technologies, Inc.

Daneyko, A., Hlushkou, D., Baranau, V., Khirevich, S., Seidel-Morgenstern, A., Tallarek, U., 2015. Computational investigation of longitudinal diffusion, eddy dispersion, and trans-particle mass transfer in bulk, random packings of core-shell particles with varied shell thickness and shell diffusion coefficient. J. Chromatogr. A 1407, 139−156.

De Vos, J., Stassen, C., Vaast, A., Desmet, G., Eeltink, S., 2012. High-resolution separations of tryptic digest mixtures using core-shell particulate columns operated at 1,200 bar. J. Chromatogr. A 1264, 57−62.

Deridder, S., Catani, M., Cavazzini, A., Desmet, G., 2016. A theoretical study on the advantage of core-shell particles with radially-oriented mesopores. J. Chromatogr. A 1456, 137−144.

Deridder, S., Desmet, G., 2011. Effective medium theory expressions for the effective diffusion in chromatographic beds filled with porous, non-porous and porous-shell particles and cylinders. Part II: numerical verification and quantitative effect of solid core on expected B-term band broadening. J. Chromatogr. A 1218, 46−56.

Deridder, S., Desmet, G., 2012. Calculation of the geometrical three-point parameter constant appearing in the second order accurate effective medium theory expression for the B-term diffusion coefficient in fully porous and porous-shell random sphere packings. J. Chromatogr. A 1223, 35−40.

Desmet, G., 2013. A finite parallel zone model to interpret and extend Giddings' coupling theory for the eddy-dispersion in porous chromatographic media. J. Chromatogr. A 1314, 124−137.

Desmet, G., Broeckhoven, K., 2008. Equivalence of the different Cm - and Cs -term expressions used in liquid chromatography and a geometrical model uniting them. Anal. Chem. 80, 8076−8088.

Desmet, G., Broeckhoven, K., De Smet, J., Deridder, S., Baron, G.V., Gzil, P., 2008. Errors involved in the existing B-term expressions for the longitudinal diffusion in fully porous chromatographic media Part I: computational data in ordered pillar arrays and effective medium theory. J. Chromatogr. A 1188, 171−188.

Desmet, G., Cabooter, D., Broeckhoven, K., 2015. Graphical data representation methods to assess the quality of LC columns. Anal. Chem. 87, 8593−8602.

Desmet, G., Cabooter, D., Gzil, P., Verelst, H., Mangelings, D., Heyden, Y.V., Clicq, D., 2006. Future of high pressure liquid chromatography: do we need porosity or do we need pressure? J. Chromatogr. A 1130, 158−166.

Desmet, G., Clicq, D., Gzil, P., 2005. Geometry-independent plate height representation methods for the direct comparison of the kinetic performance of LC supports with a different size or morphology. Anal. Chem. 77, 4058−4070.

Desmet, G., Deridder, S., 2011. Effective medium theory expressions for the effective diffusion in chromatographic beds filled with porous, non-porous and porous-shell particles and cylinders. Part I: theory. J. Chromatogr. A 1218, 32−45.

Destefano, J.J., Langlois, T.J., Kirkland, J.J., 2008. Characteristics of superficially-porous silica particles for fast HPLC: some performance comparisons with sub-2-μm particles. J. Chromatogr. Sci. 46, 254−260.

Dinh, N.G., Jonsson, T., Irgum, K., 2011. Probing the interaction mode in hydrophilic interaction chromatography. J. Chromatogr. A 1218, 5880−5891.

Done, J.N., Knox, J.H., 1972. The performance of packings in high speed liquid chromatography II. ZIPAX® the effect of particle size. J. Chromatogr. Sci. 10, 606−612.

Emenhiser, C., Englert, G., Sander, L.C., Ludwig, B., Schwartz, S.J., 1996. Isolation and structural elucidation of the predominant geometrical isomer of alpha-carotene. J. Chromatogr. A 719, 333−343.

Euerby, M.R., McKeown, A.P., Petersson, P., 2003. Chromatographic classification and comparison of commercially available perfluorinated stationary phases for reversed-phase liquid chromatography using principal component analysis. J. Sep. Sci. 26, 295−306.

Euerby, M.R., Petersson, P., 2003. Chromatographic classification and comparison of commercially available reversed-phase liquid chromatographic columns using principal component analysis. J. Chromatogr. A 994, 13−36.

Euerby, M.R., Petersson, P., 2005. Chromatographic classification and comparison of commercially available reversed-phase liquid chromatographic columns containing polar embedded groups/amino endcappings using principal component analysis. J. Chromatogr. A 1088, 1−15.

Fekete, S., Berky, R., Fekete, J., Veuthey, J.-L., Guillarme, D., 2012a. Evaluation of a new wide pore core-shell material (Aeris WIDEPORE) and comparison with other existing stationary phases for the analysis of intact proteins. J. Chromatogr. A 1236, 177−188.

Fekete, S., Berky, R., Fekete, J., Veuthey, J.-L., Guillarme, D., 2012b. Evaluation of recent very efficient wide-pore stationary phases for the reversed-phase separation of proteins. J. Chromatogr. A 1252, 90−103.

Fekete, S., Fekete, J., Ganzler, K., 2009. Shell and small particles; evaluation of new column technology. J. Pharm. Biomed. Anal. 49, 64−71.

Fekete, S., Guillarme, D., 2013. Kinetic evaluation of new generation of column packed with 1.3 μm core-shell particles. J. Chromatogr. A 1308, 104−113.

Fekete, S., Oláh, E., Fekete, J., 2012. Fast liquid chromatography: the domination of core-shell and very fine particles. J. Chromatogr. A 1228, 57−71.

Fekete, S., Veuthey, J.L., Eeltink, S., Guillarme, D., 2013. Comparative study of recent wide-pore materials of different stationary phase morphology, applied for the reversed-phase analysis of recombinant monoclonal antibodies. Anal. Bioanal. Chem. 405, 3137−3151.

Giddings, J.C., 1964. Comparison of the theoretical limit of separating ability in gas and liquid chromatography. Anal. Chem. 36, 1890−1892.

Giddings, J.C., 1965a. Comparison of theoretical limit of separating speed in gas and liquid chromatography. Anal. Chem. 37, 60−63.

Giddings, J.C., 1965b. Dynamics of Chromatography, Part I. Marcel Dekker, Inc., New York.

Giddings, J.C., 1995. Sample dimensionality: a predictor of order-disorder in component peak distribution in multidimensional separation. J. Chromatogr. A 703, 3−15.

González-ruiz, V., Olives, A.I., Martín, M.A., 2015. Core-shell particles lead the way to renewing high-performance liquid chromatography. TrAC Trends Anal. Chem. 64, 17−28.

Grand-Guillaume Perrenoud, A., Farrell, W.P., Aurigemma, C.M., Aurigemma, N.C., Fekete, S., Guillarme, D., 2014a. Evaluation of stationary phases packed with superficially porous particles for the analysis of pharmaceutical compounds using supercritical fluid chromatography. J. Chromatogr. A 1360, 275−287.

Grand-Guillaume Perrenoud, A., Veuthey, J.L., Guillarme, D., 2014b. Coupling state-of-the-art supercritical fluid chromatography and mass spectrometry: from hyphenation interface optimization to high-sensitivity analysis of pharmaceutical compounds. J. Chromatogr. A 1339, 174−184.

Grinias, J.P., Keil, D.S., Jorgenson, J.W., 2014. Observation of enhanced heat dissipation in columns packed with superficially porous particles. J. Chromatogr. A 1371, 261−264.

Gritti, F., Guiochon, G., 2007. Comparative study of the performance of columns packed with several new fine silica particles. Would the external roughness of the particles affect column properties? J. Chromatogr. A 1166, 30−46.

Gritti, F., Guiochon, G., 2010a. Comparison of heat friction effects in narrow-bore columns packed with core−shell and totally porous particles. Chem. Eng. Sci. 65, 6310−6319.
Gritti, F., Guiochon, G., 2010b. A protocol for the measurement of all the parameters of the mass transfer kinetics in columns used in liquid chromatography. J. Chromatogr. A 1217, 5137−5151.
Gritti, F., Guiochon, G., 2012a. Facts and legends on columns packed with sub-3 μm core-shell particles. LCGC N. Am. 30, 586−595.
Gritti, F., Guiochon, G., 2012b. Measurement of the eddy dispersion term in chromatographic columns. II. Application to new prototypes of 2.3 and 3.2 mm I.D. monolithic silica columns. J. Chromatogr. A 1227, 82−95.
Gritti, F., Guiochon, G., 2012c. Measurement of the eddy dispersion term in chromatographic columns: III. Application to new prototypes of 4.6 mm I.D. monolithic columns. J. Chromatogr. A 1225, 79−90.
Gritti, F., Guiochon, G., 2012d. Repeatability of the efficiency of columns packed with sub-3 μm core-shell particles: Part I. 2.6 μm Kinetex-C(18) particles in 4.6 mm and 2.1 mm × 100 mm column formats. J. Chromatogr. A 1252, 31−44.
Gritti, F., Guiochon, G., 2012e. Repeatability of the efficiency of columns packed with sub-3 μm core-shell particles: Part II. 2.7 μm Halo-ES-Peptide-C18 particles in 4.6 mm and 2.1 mm × 100 mm column formats. J. Chromatogr. A 1252, 45−55.
Gritti, F., Guiochon, G., 2012f. Repeatability of the efficiency of columns packed with sub-3 μm core-shell particles: Part III. 2.7 μm Poroshell 120 EC-C18 particles in 4.6 mm and 2.1 mm × 100 mm column formats. J. Chromatogr. A 1252, 56−66.
Gritti, F., Guiochon, G., 2013a. Limit of the speed-resolution properties in adiabatic supercritical fluid chromatography. J. Chromatogr. A 1295, 114−127.
Gritti, F., Guiochon, G., 2013b. Perspectives on the evolution of the column efficiency in liquid chromatography. Anal. Chem. 85, 3017−3035.
Gritti, F., Guiochon, G., 2013c. Speed-resolution properties of columns packed with new 4.6 μm Kinetex-C(18) core-shell particles. J. Chromatogr. A 1280, 35−50.
Gritti, F., Guiochon, G., 2013d. The van Deemter equation: assumptions, limits, and adjustment to modern high performance liquid chromatography. J. Chromatogr. A 1302, 1−13.
Gritti, F., Guiochon, G., 2014a. Mass transport of small retained molecules in polymer-based monolithic columns. J. Chromatogr. A 1362, 49−61.
Gritti, F., Guiochon, G., 2014b. Rapid development of core−shell column technology: accurate measurements of the intrinsic column efficiency of narrow-bore columns packed with 4.6 down to 1.3 μm superficially porous particles. J. Chromatogr. A 1333, 60−69.
Gritti, F., Guiochon, G., 2015a. The quantitative impact of the mesopore size on the mass transfer mechanism of the new 1.9 μm fully porous Titan-C18 particles II − analysis of biomolecules. J. Chromatogr. A 1392, 10−19.
Gritti, F., Guiochon, G., 2015b. The quantitative impact of the mesopore size on the mass transfer mechanism of the new 1.9 μm fully porous Titan-C18 particles. I: analysis of small molecules. J. Chromatogr. A 1384, 76−87.
Gritti, F., Leonardis, I., Abia, J.A., Guiochon, G., 2010. Physical properties and structure of fine core-shell particles used as packing materials for chromatography. Relationships between particle characteristics and column performance. J. Chromatogr. A 1217, 3819−3843.
Gritti, F., Shiner, S.J., Fairchild, J.N., Guiochon, G., 2014. Evaluation of the kinetic performance of new prototype 2.1 × 100 mm narrow-bore columns packed with 1.6 μm superficially porous particles. J. Chromatogr. A 1334, 30−43.
Guiochon, G., Gritti, F., 2011. Shell particles, trials, tribulations and triumphs. J. Chromatogr. A 1218, 1915−1938.
Hanai, T., 2003. Separation of polar compounds using carbon columns. J. Chromatogr. A 989, 183−196.

Hayes, R., Ahmed, A., Edge, T., Zhang, H., 2014. Core-shell particles: preparation, fundamentals and applications in high performance liquid chromatography. J. Chromatogr. A 1357, 36−52.

Hemstrom, P., Irgum, K., 2006. Hydrophilic interaction chromatography. J. Sep. Sci. 29, 1784−1821.

Hormann, K., Tallarek, U., 2014. Mass transport properties of second-generation silica monoliths with mean mesopore size from 5 to 25 nm. J. Chromatogr. A 1365, 94−105.

Horvath, C., Lipsky, S.R., 1969a. Column design in high pressure liquid chromatography. J. Chromatogr. Sci. 7, 109−116.

Horvath, C., Lipsky, S.R., 1969b. Rapid analysis of ribonucleosides and bases at the picomole level using pellicular cation exchange resin in narrow bore columns. Anal. Chem. 41, 1227−1234.

Horvath, C.G., 1967. Fast liquid chromatography: an investigation of operating parameters and the separation of nucleotides on pellicular ion exchangers. Anal. Chem. 39, 1422−1428.

Ibrahim, M.E.A., Liu, Y., Lucy, C.A., 2012. A simple graphical representation of selectivity in hydrophilic interaction liquid chromatography. J. Chromatogr. A 1260, 126−131.

Iraneta, P., Wyndham, K.D., McCabe, D.R., Walter, T.H., 2010. A Review of Waters Hybrid Particle Technology. Part 3. Charged Surface Hybrid (CSH) Technology and Its Use in Liquid Chromatography. Waters White Paper 720003469EN.

Ismail, O., Ciogli, A., Villani, C., De Martino, M., Pierini, M., Cavazzini, A., Bell, D.S., Gasparrini, F., 2016a. Ultra-fast high-efficiency enantioseparations by means of a teicoplanin-based chiral stationary phase made on sub-2 μm totally porous silica particles of narrow size distribution. J. Chromatogr. A 1427, 55−68.

Ismail, O.H., Catani, M., Pasti, L., Cavazzini, A., Ciogli, A., Villani, C., Kotoni, D., Gasparrini, F., Bell, D.S., 2016b. Experimental evidence of the kinetic performance achievable with columns packed with new 1.9 μm fully porous particles of narrow particle size distribution. J. Chromatogr. A 1454, 86−92.

Kahsay, G., Broeckhoven, K., Adams, E., Desmet, G., Cabooter, D., 2014. Kinetic performance comparison of fully and superficially porous particles with a particle size of 5 μm: intrinsic evaluation and application to the impurity analysis of griseofulvin. Talanta 122, 122−129.

Kawachi, Y., Ikegami, T., Takubo, K., KIkegami, Y., Miyamoto, M., Tanaka, N., 2011. Chromatographic characterization of hydrophilic interaction liquid chromatography stationary phases: hydrophilicity, charge effects, structural selectivity, and separation efficiency. J. Chromatogr. A 1218, 5903−5919.

Kennedy, G.J., Knox, J.H., 1972. The performance of packings in high performance liquid chromatography (HPLC) I. Porous and surface layered supports. J. Chromatogr. Sci. 10, 549−556.

Kimita, K., Iwaguchi, S., Jinno, O.K., Eksteen, R., Hosoya, K., Araki, M., Tanaka, N., 1989. Chromatographic characterization of silica C18 packing materials. Correlation between a preparation method and retention behavior of stationary phase. J. Chromatogr. Sci. 27, 721−728.

Kirkland, J.J., 1970. Superficially Porous Supports for Chromatography. US Patent US 3 505 735. E.I. DuPont et Nemours and Company, Wilmington, DE, USA.

Kirkland, J.J., 1972. Performance of Zipax® controlled surface porosity support in high-speed liquid chromatography. J. Chromatogr. Sci. 10, 129−137.

Kirkland, J.J., 1992. Superficially porous silica microspheres for fast high-performance liquid chromatography of macromolecules. Anal. Chem. 64, 1239−1245.

Kirkland, J.J., Langlois, T.J., 2007. Porous Microparticles Solid Cores. US Patent US 2007/0189944 A1. Advanced Materials Technology, Inc.

Kirkland, J.J., Langlois, T.J., DeStefano, J.J., 2007. Fused core particles for HPLC columns. Am. Lab. 39, 18−21.

Kirkland, J.J., Truszkowski, F.A., Dilks, C.H., Engel, G.S., 2000. Superficially porous silica microspheres for fast high-performance liquid chromatography of macromolecules. J. Chromatogr. A 890, 3−13.

Knox, J.H., 1966. Evidence for turbulence and coupling in chromatographic columns. Anal. Chem. 38, 253−261.

Knox, J.H., 1998. Band spreading in chromatography: a personal view. In: Brown, P. (Ed.), Advances in Chromatography, vol. 38. Taylor & Francis, pp. 1−49.

Knox, J.H., Saleem, M., 1969. Kinetic conditions for optimum speed and resolution in column chromatography. J. Chromatogr. Sci. 7, 614−622.

Knox, J.H., Scott, H.P., 1983. B and C terms in the van Deemter equation for liquid chromatography. J. Chromatogr. A 282, 297−313.

Kostka, J., Gritti, F., Kaczmarski, K., Guiochon, G., 2011. Modified Equilibrium-Dispersive Model for the interpretation of the efficiency of columns packed with core-shell particle. J. Chromatogr. A 1218, 5449−5455.

Lambert, N., Kiss, I., Felinger, A., 2014. Mass-transfer properties of insulin on core-shell and fully porous stationary phases. J. Chromatogr. A 1366, 84−91.

Lämmerhofer, M., Richter, M., Wu, J., Nogueira, R., Bicker, W., Lindner, W., 2008. Mixed-mode ion-exchangers and their comparative chromatographic characterization in reversed-phase and hydrophilic interaction chromatography elution modes. J. Sep. Sci. 31, 2572−2588.

Langsi, V.K., Ashu-Arrah, B.A., Glennon, J.D., 2015. Sub-2 μm seeded growth mesoporous thin shell particles for high-performance liquid chromatography: synthesis, functionalisation and characterisation. J. Chromatogr. A 1402, 17−26.

Largy, E., Catrain, A., Van Vyncht, G., Delobel, A., 2016. 2D-LC−MS for the analysis of monoclonal antibodies and antibody−drug conjugates in a regulated environment. Curr. Trends Mass Spectrom. 14, 29−35.

Lauber, M.A., Koza, S.M., McCall, S.A., Alden, B.A., Iraneta, P.C., Fountain, K.J., 2013. High-resolution peptide mapping separations with MS-friendly mobile phases and charge-surface-modified C18. Anal. Chem. 85, 6936−6944.

Lesellier, E., West, C., 2015. The many faces of packed column supercritical fluid chromatography − a critical review. J. Chromatogr. A 1382, 2−46.

Liekens, A., Denayer, J., Desmet, G., 2011. Experimental investigation of the difference in B-term dominated band broadening between fully porous and porous-shell particles for liquid chromatography using the Effective Medium Theory. J. Chromatogr. A 1218, 4406−4416.

Long, W.J., 2012. Fast Screening Methods for Steroids by HPLC with Agilent Poroshell 120 Columns. Agilent. Application Note 5991−0451EN.

Long, W.J., Mack, A., Wang, X., Barber, W.E., 2015. Selectivity and sensitivity improvements for ionizable analytes using high-pH stable superficially porous particles. LCGC N. Am. 33, 31−39.

MacNair, J.E., Lewis, K.C., Jorgenson, J.W., 1997. Ultrahigh-pressure reversed-phase liquid chromatography in packed capillary columns. Anal. Chem. 69, 983−989.

MacNair, J.E., Patel, K.D., Jorgenson, J.W., 1999. Ultrahigh-pressure reversed-phase capillary liquid chromatography: isocratic and gradient elution using columns packed with 1.0-micron particles. Anal. Chem. 71, 700−708.

Majors, R.E., 2012. Current trends in HPLC column usage. LCGC Eur. 25, 1−7.

Marchand, D.H., Croes, K., Dolan, J.W., Snyder, L.R., 2005a. Column selectivity in reversed-phase liquid chromatography VII. Cyanopropyl columns. J. Chromatogr. A 1062, 57−64.

Marchand, D.H., Croes, K., Dolan, J.W., Snyder, L.R., Henry, R.A., Kallury, K.M.R., Waite, S., Carr, P.W., 2005b. Column selectivity in reversed-phase liquid chromatography VIII. Phenylalkyl and fluoro-substituted columns. J. Chromatogr. A 1062, 65−78.

Martin, A.J.P., Synge, R.L.M., 1941. A new form of chromatogram employing two liquid phases. Biochem. J. 1358−1368.

McCalley, D.V., 2010a. The challenges of the analysis of basic compounds by high performance liquid chromatography: some possible approaches for improved separations. J. Chromatogr. A 1217, 858−880.

McCalley, D.V., 2010b. Study of the selectivity, retention mechanisms and performance of alternative silica-based stationary phases for separation of ionised solutes in hydrophilic interaction chromatography. J. Chromatogr. A 1217, 3408−3417.

McCalley, D.V., Neue, U.D., 2008. Estimation of the extent of the water-rich layer associated with the silica surface in hydrophilic interaction chromatography. J. Chromatogr. A 1192, 225−229.

McMaster, M.C., 2005. LC/MS: A Practical User's Guide. John Wiley and Sons.
Miyabe, K., Ando, N., Guiochon, G., 2009a. Peak parking method for measurement of molecular diffusivity in liquid phase systems. J. Chromatogr. A 1216, 4377−4382.
Miyabe, K., Matsumoto, Y., Ando, N., 2009b. Peak parking-moment analysis method for the measurement of surface diffusion coefficients. Anal. Chem. 25, 211−218.
Neue, U.D., Iraneta, P., Gritti, F., Guiochon, G., 2013. Adsorption of cations onto positively charged surface mesopores. J. Chromatogr. A 1318, 72−83.
Omamogho, J., Glennon, J.D., 2011. Process for Preparing Silica Microparticles. Patent US 2011/0226990 A1.
Omamogho, J.O., Hanrahan, J.P., Tobin, J., Glennon, J.D., 2011. Structural variation of solid core and thickness of porous shell of 1.7 μm core-shell silica particles on chromatographic performance: narrow bore columns. J. Chromatogr. A 1218, 1942−1953.
Patel, D.C., Breitbach, Z.S., Wahab, M.F., Barhate, C.L., Armstrong, D.W., 2015. Gone in seconds: praxis, performance, and peculiarities of ultrafast chiral liquid chromatography with superficially porous particles. Anal. Chem. 87, 9137−9148.
Pesek, J.J., Matyska, M.T., Fischer, S.M., Sana, T.R., 2008. Analysis of hydrophilic metabolites by high-performance liquid chromatography−mass spectrometry using a silica hydride-based stationary phase. J. Chromatogr. A 1204, 48−55.
Pesek, J.J., Matyska, M.T., Yu, R.J., 2002. Synthesis and characterization of endcapped C18 stationary phases using a silica hydride intermediate. J. Chromatogr. A 947, 195−203.
Poppe, H., 1997. Some reflections on speed and efficiency of modern chromatographic methods. J. Chromatogr. A 778, 3−21.
Przybyciel, M., 2005. Fluorinated HPLC phases − looking beyond C18 for reversed phase HPLC. LCGC N. Am. 23, 554−565.
Rauh, M., 2012. LC-MS/MS for protein and peptide quantification in clinical chemistry. J. Chromatogr. B Anal. Technol. Biomed. Life Sci. 883−884, 59−67.
Regalado, E.L., Zhuang, P., Chen, Y., Makarov, A.A., Schafer, W.A., McGachy, N., Welch, C.J., 2014. Chromatographic resolution of closely related species in pharmaceutical chemistry: dehalogenation impurities and mixtures of halogen isomers. Anal. Chem. 86, 805−813.
Schuster, S.A., Wagner, B.M., Boyes, B.E., Kirkland, J.J., 2013. Optimized superficially porous particles for protein separations. J. Chromatogr. A 1315, 118−126.
Snyder, L.R., Dolan, J.W., Carr, P.W., 2004. The hydrophobic-subtraction model of reversed-phase column selectivity. J. Chromatogr. A 1060, 77−116.
Snyder, L.R., Dolan, J.W., Carr, P.W., 2007. A new look at the selectivity of RPC columns. Anal. Chem. 79, 3255−3262.
Song, H., Vanderheyden, Y., Adams, E., Desmet, G., Cabooter, D., 2016. Extensive database of liquid phase diffusion coefficients of some frequently used test molecules in reversed-phase liquid chromatography and hydrophilic interaction liquid chromatography. J. Chromatogr. A 1455, 102−112.
Stöber, W., Fink, A., Bohn, E., 1968. Controlled growth of monodisperse silica spheres in the micron size range. J. Colloid. Interface. Sci. 26, 62−69.
Stoll, D.R., Danforth, J., Zhang, K., Beck, A., 2016. Characterization of therapeutic antibodies and related products by two-dimensional liquid chromatography coupled with UV absorbance and mass spectrometric detection. J. Chromatogr. B 1032, 51−60.
Subirats, X., Bosch, E., Roses, M., 2009. Buffer considerations for LC and LC-MS. LCGC N. Am. 27, 1000−1004.
Sun, P., Armstrong, D.W., 2010. Effective enantiomeric separations of racemic primary amines by the isopropyl carbamate-cyclofructan6 chiral stationary phase. J. Chromatogr. A 1217, 4904−4918.

Sun, P., Wang, C., Breitbach, Z.S., Zhang, Y., Armstrong, D.W., 2009. Development of new HPLC chiral stationary phases based on native and derivatized cyclofructans. Anal. Chem. 81, 10215−10226.

Swartz, M.E., Murphy, B., 2005. New frontiers in chromatography. Am. Lab. 37, 22−27.

Tanaka, N., McCalley, D.V., 2016. Core-shell, ultrasmall particles, monoliths, and other support materials in high-performance liquid chromatography. Anal. Chem. 88, 279−298.

Tang, D.Q., Zou, L., Yin, X.X., Ong, C.N., 2016. HILIC-MS for metabolomics: an attractive and complementary approach to RPLC-MS. Mass Spectrom. Rev. 35, 574−600.

Unger, K.K., 1979. Chapter 2 pore structure of silica. In: Unger, K.K. (Ed.), Journal of Chromatography Library. Elsevier, pp. 15−55.

Vaast, A., Broeckhoven, K., Dolman, S., Desmet, G., Eeltink, S., 2012. Comparison of the gradient kinetic performance of silica monolithic capillary columns with columns packed with 3 μm porous and 2.7 μm fused-core silica particles. J. Chromatogr. A 1228, 270−275.

van Deemter, J.J., Zuiderweg, F.J., Klinkenberg, A., 1956. Longitudinal diffusion and resistance to mass transfer nonideality in chromatography. Chem. Eng. Sci. 5, 271−289.

Vanderheyden, Y., Cabooter, D., Desmet, G., Broeckhoven, K., 2013. Isocratic and gradient impedance plot analysis and comparison of some recently introduced large size core-shell and fully porous particles. J. Chromatogr. A 1312, 80−86.

Wagner, B.M., Schuster, S.A., Boyes, B.E., Kirkland, J.J., 2012. Superficially porous silica particles with wide pores for biomacromolecular separations. J. Chromatogr. A 1264, 22−30.

Wang, X., Barber, W.E., Carr, P.W., 2006a. A practical approach to maximizing peak capacity by using long columns packed with pellicular stationary phases for proteomic research. J. Chromatogr. A 1107, 139−151.

Wang, X., Barber, W.E., Long, W.J., 2012. Applications of superficially porous particles: high speed, high efficiency or both? J. Chromatogr. A 1228, 72−88.

Wang, X., Stoll, D.R., Schellinger, A.P., Carr, P.W., 2006b. Peak capacity optimization of peptide separations in reversed-phase gradient elution chromatography: fixed column format. Anal. Chem. 78, 3406−3416.

Waters, 2004. UPLC: New Boundaries for the Chromatography Laboratory. White Paper 720000819EN.

Wei, T.-C., Mack, A., Chen, W., Liu, J., Dittmann, M., Wang, X., Barber, W.E., 2016. Synthesis, characterization, and evaluation of a superficially porous particle with unique, elongated pore channels normal to the surface. J. Chromatogr. A 1440, 55−65.

West, C., 2014. Enantioselective separations with supercritical fluids − review. Curr. Anal. Chem. 10, 99−120.

West, C., Lesellier, E., 2008. A unified classification of stationary phases for packed column supercritical fluid chromatography. J. Chromatogr. A 1191, 21−39.

Wiest, L.A., Jensen, D.S., Hung, C.-H., Olsen, R.E., Davis, R.C., Vail, M.A., Dadson, A.E., Nesterenko, P.N., Linford, M.R., 2011. Pellicular particles with spherical carbon cores and porous nanodiamond/polymer shells for reversed-phase HPLC. Anal. Chem. 83, 5488−5501.

Wilson, N.S., Gilroy, J., Dolan, J.W., Snyder, L.R., 2004. Column selectivity in reversed-phase liquid chromatography VI. Columns with embedded or end-capping polar groups. J. Chromatogr. A 1026, 91−100.

Wu, N., Lippert, J.A., Lee, M.L., 2001. Practical aspects of ultrahigh pressure capillary liquid chromatography. J. Chromatogr. A 911, 1−12.

Zhang, Y., Carr, P.W., 2009. A visual approach to stationary phase selectivity classification based on the Snyder-Dolan Hydrophobic-Subtraction Model. J. Chromatogr. A 1216, 6685−6694.

This page intentionally left blank

CHAPTER

7

INTRODUCTION TO TWO-DIMENSIONAL LIQUID CHROMATOGRAPHY—THEORY AND PRACTICE

Dwight R. Stoll
Gustavus Adolphus College, St. Peter, MN, United States

1. TWO-DIMENSIONAL SEPARATIONS: CORE CONCEPTS

1.1 VALUE OF A SECOND DIMENSION OF SEPARATION

Our interest in liquid chromatography carried out in two dimensions is motivated by the occasions when one-dimensional (1D) separations do not allow us to achieve our separation goals, or at least not in an efficient way (Snyder et al., 1981). The reasons for failure of 1D separations fall into two broad categories: (1) cases where the sample at hand is very heterogeneous, containing hundreds, thousands, or even tens of thousands of compounds; (2) cases where the sample contains one or more pairs or groups of compounds that are chemically homogeneous and therefore difficult to resolve. The simplest view of the benefit of the added second dimension (^{2}D) separation is shown in Fig. 7.1. The idea here is

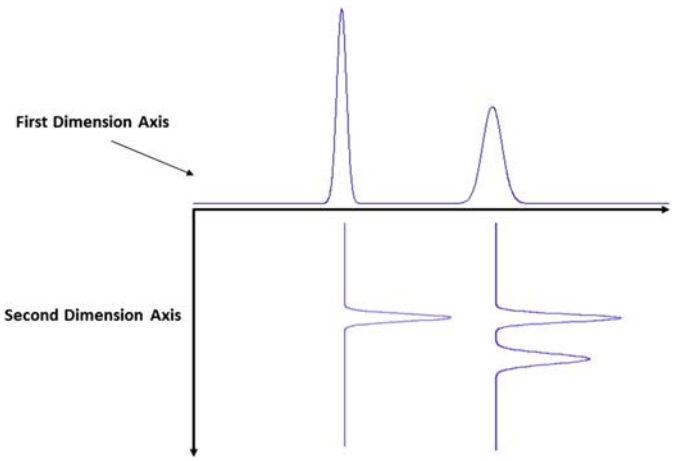

FIGURE 7.1

Simple view of the benefit of a second dimension of separation. The idea is that compounds not separated by the first dimension (^{1}D) column are transferred as mixtures to the second dimension (^{2}D) column for further separation.

Handbook of Advanced Chromatography/Mass Spectrometry Techniques. http://dx.doi.org/10.1016/B978-0-12-811732-3.00007-8

that compounds not separated by the first dimension (^{1}D) column will be transferred as a mixture to the second dimension and separated there prior to detection at the outlet of the ^{2}D column.

1.2 CONCEPT OF PEAK CAPACITY

Historically, the benefit of the added ^{2}D separation has been quantified using the concept of peak capacity, especially in the case of LC × LC separations where the ^{2}D is employed during the entire ^{1}D separation. The distinctions between different types of two-dimensional liquid chromatography (2D-LC) separations and different ways of measuring 2D separation performance are discussed in detail in Sections 5 and 6. Fig. 7.2 illustrates one way to view the concept of peak capacity in 1D and 2D separations. The idea in the case of a 1D separation is that each bin is equivalent to one unit of peak capacity and that this bin is wide enough to accommodate exactly one chromatographic peak, where the peak width is measured at the 4σ level (Giddings, 1967). It is important to note that the peak capacity is a theoretical maximum number of components that can be resolved. In practice the number of components that can be resolved in real samples is usually much less than the peak capacity because elution times of real components are disordered (Davis and Giddings, 1983). This issue is discussed briefly in Section 1.2. In the case where gradient elution LC is used, such that the widths of peaks are nominally the same throughout the chromatogram, the 1D peak capacity ($n_{c,1D}$) is simply the ratio of the size of the separation space to the average peak width (w_{avg}), as shown in Eq. (7.1). In the simplest case, the size of the separation space can be taken as the gradient time (t_g); however, for more accurate estimates factors including the column void and reequilibration times and the actual elution window of sample components should be considered (Wang et al., 2006).

$$n_{c,1D} = \frac{t_g}{w_{avg}} \tag{7.1}$$

As shown in Fig. 7.2, what draws us to 2D separations is that the peak capacity is expanded from a 1D array of bins to a 2D array of bins. This means that the peak capacity of the 2D separation is not the

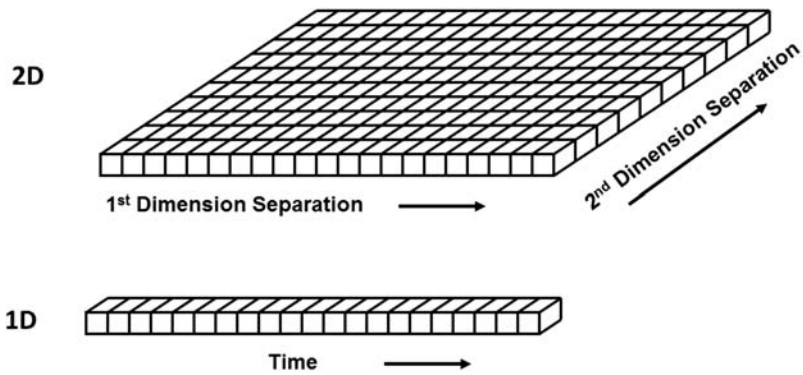

FIGURE 7.2

Illustration of the concept of peak capacity in one-dimensional and two-dimensional separations.

Adapted from Giddings, J.C., 1987. Concepts and comparisons in multidimensional separation. HRC CC J. High Resolut. Chromatogr. Chromatogr. Commun. 10, 319–323. http://dx.doi.org/10.1002/jhrc.1240100517.

sum of the peak capacities of the two 1D separations (i.e., the ^{1}D and ^{2}D peak capacities, ^1n_c and ^2n_c) that contribute to the 2D separation, but the product of them (Giddings, 1987; Karger et al., 1973). We quantify this relationship using what we refer to here at the product rule, shown in Eq. (7.2).

$$n_{c,2D} = {}^1n_c \times {}^2n_c \tag{7.2}$$

It is critically important to recognize that the product rule provides an estimate of the *maximum number* of compounds that can be resolved with a 2D-LC method. In real separations, the actual numbers of peaks that are resolved are much lower than this for a few reasons. First, as is the case in 1D separations, the distributions of compound elution times are usually not highly ordered, leading to some regions of unused separation space, whereas other regions are overcrowded. Second, it is generally more difficult to effectively use all of the available separation space in 2D separations than in 1D ones. In other words, spreading peaks across the bins of a 1D array is easier than spreading them across a 2D array of bins, which effectively reduces the amount of usable 2D peak capacity. This issue is discussed in more detail in Sections 5.1.2 and 7.4. Finally, in the process of transferring fractions of ^{1}D effluent to the ^{2}D column for further separation, there can be remixing of sample components that had been already separated by the ^{1}D column. This too effectively results in a loss of peak capacity and thus detracts from the potential indicated by Eq. (7.2). This issue is discussed in more detail in Section 5.2. Consideration of these practical details is important for developing high-performing 2D-LC methods and fair assessment of their performance.

Peak capacity is a very convenient metric for assessing the performance of 2D-LC separations carried out in the comprehensive mode. However, as discussed in Section 6.1, probably less than half of all 2D-LC in practice is done in the comprehensive mode. For other modes of 2D separation, other metrics of performance are more appropriate. Nevertheless, the fundamental concepts that come together in evaluating peak capacity—namely the complementarity of separation mechanisms and undersampling—are still critically important to noncomprehensive 2D separations, even if they are more difficult to quantify in those cases.

1.3 INTRODUCTION TO STATISTICAL OVERLAP THEORY FOR CHROMATOGRAPHY

Given that our interest in 2D separations is largely predicated on the limitations of 1D separations, it is useful to have an appreciation for these limitations in quantitative terms. In the preceding section, I alluded to the fact that peaks in real chromatograms tend not to be highly ordered. A practically important consequence of this is that the number of peaks we observe is less—sometimes much less—than the estimated peak capacity of the separation. A very useful framework for thinking about these issues is the so-called *statistical overlap theory* (SOT), which was developed by Davis and Giddings (1983) for 1D separations, and subsequently extended to 2D separations (Davis, 1991). The rate at which we can produce peak capacity using one-dimensional liquid chromatography (1D-LC) is discussed in more detail in Section 5.3. Here, it is useful to know that for small nonpeptide molecules, we can achieve peak capacities of about 150, 250, and 350 in 1D analysis times of 5, 20, and 60 min. SOT enables us to answer a variety of questions about how this peak capacity can be used to work toward particular separation goals. For example, for a given peak capacity one can estimate what fraction of components in a sample would be observed in a chromatogram as pure, single-component peaks, or as peaks that are multiplets (i.e., a peak that contains multiple, coeluting compounds). For practical problems, perhaps the most instructive question is—what is the likelihood of

chromatographically resolving *all* of the components of a particular sample, given the peak capacity of a particular separation method? We can answer this question using the principles of SOT and Eq. (7.3):

$$s = m \times \exp\left(\frac{-2m}{n_c}\right) \tag{7.3}$$

where s is the number of observed peaks that are singlets (i.e., pure peaks with no coelution), m is the number of components in the sample, and n_c is the peak capacity of the method. Fig. 7.3 shows the percentage of components in a sample that are resolved as single-component peaks for several practically relevant combinations of sample complexity and available peak capacity. In the context of a discussion about 2D separations, the most important observation from this figure is just how unlikely complete resolution (i.e., 100% of peaks are singlets) is for samples of even moderate complexity with the peak capacities provided by the best available 1D chromatography in reasonable analysis times.

Resolving more than 90% of the compounds in a 20-component sample is only achievable, from a probabilistic point of view, in a reasonable analysis time using 2D-LC.

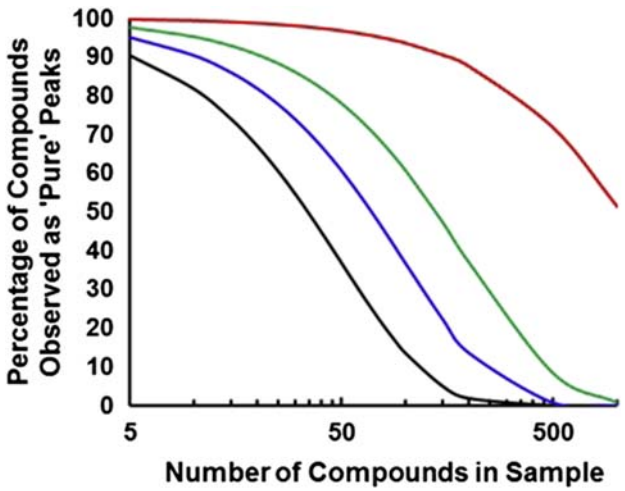

FIGURE 7.3

Percentage of sample constituents that are resolvable as chromatographically distinct peaks ("singlets," with a minimum resolution of 1.0) as a function of the number of compounds in a sample and different separation peak capacities. Effective peak capacities of **100** and **200** (dark gray in print versions) are easily achievable within 15 min using modern particle and instrument technologies. A peak capacity of **400** (light gray in print versions) is more difficult to reach for small molecules, but can be reached within an hour for peptides. An *effective peak capacity* of **3000** (gray in print versions) is not accessible by one-dimensional liquid chromatography in a practically reasonable time, but can be achieved by two-dimensional liquid chromatography in 1−2 h. Singlet peak numbers were calculated assuming the same concentrations for all components and using Eq. (7.3) from Davis and Giddings.

2. SCOPE OF THIS CHAPTER

In this chapter, I have aimed to provide prospective and current users of 2D-LC with a resource that is rich with practical guidance for developing effective, high-performing 2D-LC methods, and informed by guiding theoretical principles. As the field of 2D-LC develops, research in some aspects matures more quickly than others. I have touched on the more mature aspects only lightly, providing more room for discussion of those areas that are very active right now and likely will be for the foreseeable future. The chapter is not intended as a comprehensive review, thus the literature is not cited exhaustively in all areas. I have not dedicated too much space to the most basic operating principles of 2D-LC—the first diagram of a complete 2D-LC instrument is shown in Fig. 7.26. Readers looking to pick up some of these more basic details are referred to the review of Malerod et al. (2010), which gives a very concise but effective overview. As for specific applications, this chapter only provides an overview of the types of 2D-LC methods that have been implemented in such fields as pharmaceutical and food analysis (see Section 10), with occasional examples being used to illustrate important principles from theory and/or practice.

Importantly, I have chosen to focus the chapter nearly entirely on "online" 2D-LC separations—that is, cases where the entire 2D-LC separation is executed in a single contained flow path, without collecting fractions of ^{1}D effluent into vials or plates for storage prior to ^{2}D separation. While there undoubtedly is a place for off-line 2D-LC separations, commercial instrumentation and current user preference are tending strongly toward online operation for most 2D-LC work. Readers interested in off-line 2D-LC separations are referred to review articles that treat this subject in detail (Guiochon et al., 2008).

3. NOMENCLATURE

In this chapter, I have generally used the nomenclature suggested by Marriott and Schoenmakers for 2D separations (Marriott et al., 2012; Schoenmakers et al., 2003). Particularly important in this scheme is the distinction between ^{1}D and 1D and ^{2}D and 2D. The abbreviations **^{1}D** and **^{2}D** are used to refer to components of the first and second dimensions of a 2D-LC system, respectively. So, we might refer to a ^{1}D column or a ^{2}D flow rate. These would be the column used in the first dimension, and the flow rate used in the second dimension. On the other hand, the use of **1D** and **2D** is reserved for situations where we want to refer to the entire system as being either one- or two-dimensional. For example, we may refer to the *peak capacity of a 1D separation*, or a *2D separation of natural products*.

4. BRIEF HISTORY AND DEVELOPMENTAL MILESTONES

As we consider the state of the art of 2D-LC, and where the technology may develop in the future, it is useful to have a sense for how the technique has developed over the years up to this point. Figs. 7.4 and 7.5 show some of the characteristics of the three stages of development over the past 35 years, and some of the milestones that have been especially important along the way.

The first era, from the late 1970s to about 2000, was dominated by heartcutting applications, with the exception of comprehensive work in the areas of proteomics and polymer analysis. In this period most instruments were "home-made," or highly specialized commercial systems, and the majority of the literature was focused on applications of 2D-LC rather than fundamental studies.

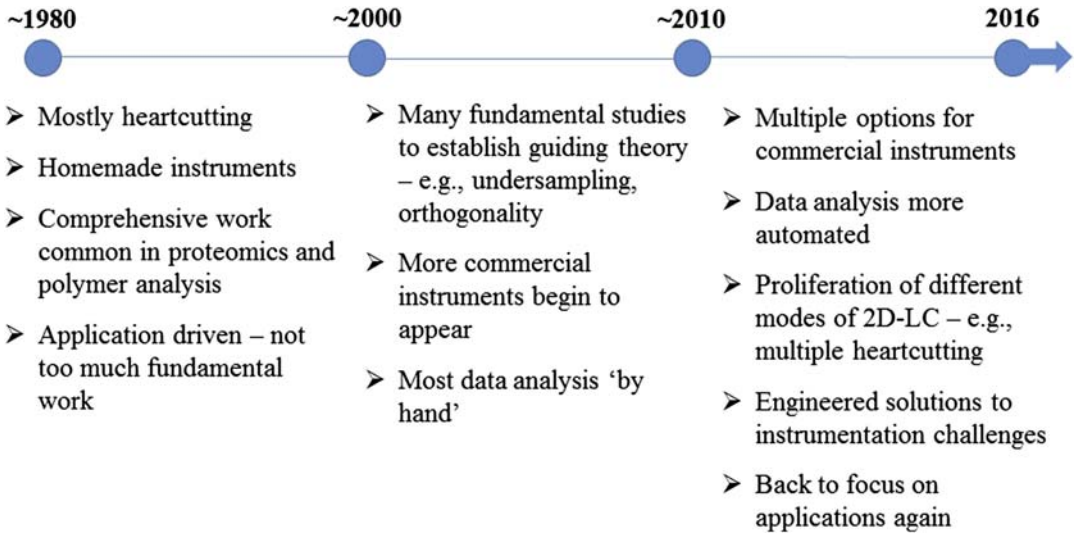

FIGURE 7.4

Some characteristics of the different eras of development of two-dimensional liquid chromatography (2D-LC).

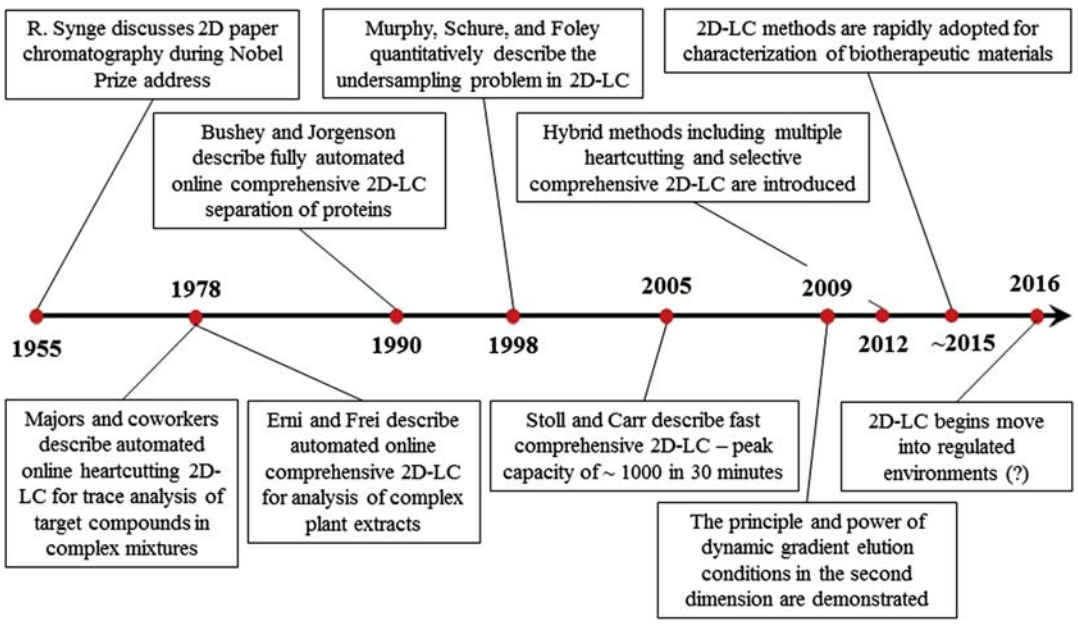

FIGURE 7.5

Some key milestones in the development of two-dimensional liquid chromatography (2D-LC). References for these events by year are: 1955 (Synge, 1952), 1978 (Apffel et al., 1981; Erni and Frei, 1978), 1990 (Bushey and Jorgenson, 1990), 1998 (Murphy et al., 1998), 2005 (Stoll and Carr, 2005), 2009 (Bedani et al., 2009; Jandera et al., 2010), 2012 (Groskreutz et al., 2012a; Zhang et al., 2013a), 2015 (Stoll et al., 2016), and 2016 (Largy et al., 2016).

The decade from about 2000 to 2010 was a very important period. In this era, several research groups engaged in fundamental studies that led to the principles (see Section 5) we now use to guide method development and assess the performance of the resulting 2D-LC methods. As it became clear that 2D-LC would be competitive with 1D-LC, even at analysis times typical of high-performance liquid chromatography (HPLC) (e.g., 15 min), instrument manufacturers began making significant investments in the development of dedicated instrumentation for 2D-LC.

Users engaging 2D-LC technology now for the first time will experience a landscape that is very different from what we observed as little as 5 years ago. In the current era, we find that several mainstream instrument vendors now offer both hardware and software that have been developed for 2D-LC applications. In some cases, they have addressed engineering challenges that are unique to 2D-LC to produce hardware that is more robust compared to the repurposed components from 1D-LC instruments that we used in past construction of home-made instruments. Now that users can simply buy a ready-made 2D-LC instrument, we are seeing the focus of research shift back to applications. Very importantly, we are seeing a proliferation of what I call "hybrid modes" of 2D-LC that are intermediate between the extreme implementations of single heartcutting and fully comprehensive 2D separation. These are discussed in detail in Section 6.1 and include approaches such as *multiple heartcutting* and *selective comprehensive* (sLC × LC) 2D separations. Ultimately, these hybrid modes provide users tremendous operational flexibility to use the power of 2D separation to address the needs of their application in the most effective way. Indeed, this is an exciting time for 2D-LC.

Fig. 7.5 is a timeline that lists some of the studies that have had the most impact on the development of 2D-LC and its adoption by users in a variety of fields. The principle of 2D separation was initially demonstrated over 70 years ago using paper chromatography for the separation of amino acids by Consden et al. (1944). The performance potential of 2D separation was highlighted again nearly 10 years later by Synge (1952) in his address on his acceptance of the Nobel Prize. However, the landmark publications demonstrating the feasibility of 2D separation in liquid chromatography came around 1980 with a pair of papers—one by Apffel et al. (1981) and one by Erni and Frei (1978). These proof-of-concept papers, along with several influential papers from this period on the theory of 2D separation (Giddings, 1987, 1984; Guiochon et al., 1983; Snyder et al., 1981) undoubtedly captured the imagination of a generation of chromatographers. The demonstration of *heartcutting* 2D-LC (LC−LC) by Majors et al. led to the development of thousands of methods for quantitation of target compounds in complex mixtures, sometimes at the trace level. This type of method has come to be known by a number of different names, such as *column switching*, and is still in common use today. The extreme opposite of LC−LC is the so-called *comprehensive* mode of 2D separation (LC × LC), where all of the material eluting from the ^{1}D column is subjected to further separation using the ^{2}D column. In this way, we gain a more comprehensive view of what the sample contains, and this is what was demonstrated by Erni and Frei through their LC × LC separation of a plant extract. Although some will assert that their initial work does not satisfy the modern definition of *comprehensive*, the value of this early proof-of-concept was that it showed people what was possible in the analysis of complex materials. This was followed just a decade later by the landmark paper of Bushey and Jorgenson, who demonstrated an LC × LC separation of intact proteins in an analysis time of 6 h.

One of the most cited fundamental papers in the 2D-LC literature is from Murphy et al. (1998), who discussed the significance of the rate at which fractions of ^{1}D effluent are transferred to a ^{2}D column for further separation. In LC × LC in particular, sampling the ^{1}D separation at a rate that is fast enough to avoid remixing sample components that had already been separated by the ^{1}D column is very

difficult. This results in a situation that has become known in the literature as *undersampling*, and in their landmark paper Murphy et al. quantified this effect for the first time. The influence of this work on the development of 2D-LC cannot be overstated; it has led several groups to study ways to mitigate the effects of undersampling by developing high speed ^{2}D separations, and other approaches such as sLC × LC. A detailed discussion of the undersampling problem is provided in Section 5.2.

In 2005 we began describing LC × LC separations with very fast ^{2}D gradient elution separations, on the order of 20 s, to mitigate the undersampling problem (Stoll et al., 2006; Stoll and Carr, 2005). Back then, this was difficult because of the large gradient delay volumes associated with high-pressure pumping systems. These delay volumes have dropped dramatically with the current generation of pumping systems, such that these fast ^{2}D separations are becoming common (Gargano et al., 2016; Vanhoenacker et al., 2015). An unexpected, but very important outcome of this period of our work was the finding that the performance of LC × LC, as measured by peak capacity, begins to exceed that of conventional 1D-LC at analysis times around 10 min. This means that 2D-LC has the potential to displace 1D-LC not only at long analysis times, but also at intermediate times that are associated with typical chromatography methods.

Before 2009, most work in 2D-LC involved separations where the ^{2}D elution conditions were fixed throughout the 2D analysis. That is, even if gradient elution was used in the ^{2}D, a particular set of elution conditions was used repeatedly through the analysis. Work by Bedani et al. (2009) and the Jandera group (Jandera et al., 2010) first showed that dynamically adjusting ^{2}D gradient elution conditions during the 2D analysis is feasible. They then went on to discuss the value of this capability, as it enables more complete usage of the 2D separation space. These concepts and capabilities have fundamentally changed the way we approach the optimization of 2D-LC methods. Some of the practical details are discussed in more detail in Section 7.4.

Informed by the challenges associated with undersampling and motivated by the need to develop 2D separation strategies for samples of intermediate complexity, hybrid modes of 2D separation began to appear around 2012, and are rapidly being adopted in a variety of industries. Specifically, multiple heartcutting (mLC−LC) (Zhang et al., 2013a) and selective comprehensive (sLC × LC) (Groskreutz et al., 2012a) are approaches that maximize the benefits of the more extreme implementations of LC−LC and LC × LC, while minimizing their weaknesses. Introduction of these alternative modes of 2D separation has resulted in a shift in mindset that encourages users to be open-minded and select the mode of operation that is most suitable for their analytical problem. The details associated with different modes of implementation are discussed in Section 6.1.

Finally, one of the areas of fastest adoption of 2D-LC is currently in the biopharmaceutical industry. The complexity of the samples (e.g., peptides, large proteins, drug formulations) encountered in this space demands high-resolution separation techniques. Importantly, the properties of the molecules and samples also lend themselves nicely to 2D separation in many cases. For example, antibody-based drugs in a formulation can vary significantly both in their size (because of aggregation) and charge (because of amino-acid sequence differences), thus separation by size-exclusion (SEC) in one dimension and ion-exchange (IEX) in a second dimension could provide a very effective 2D separation of these molecules. We are currently seeing development of 2D-LC methods for these applications that span the full range of implementations ranging from LC−LC to LC × LC; a recent review article summarized this work as of 2015 (Stoll et al., 2016). Perhaps most important to the future of 2D-LC is that we are now seeing the movement of 2D-LC into regulated environments as

quality assurance and quality control methods (Largy et al., 2016). If this trend continues, it will cement the role of 2D-LC as an important, mainstream technique for the foreseeable future.

5. PRIMARY THEORETICAL GUIDING PRINCIPLES

Readers interested in quickly assimilating the essential guiding principles in 2D-LC are encouraged to read the excellent, succinct review of Bedani et al. (2012). In this section, we first quickly review the core concepts that underpin method development decisions concerning choice of separation modes and stationary phases, and the rate at which the ^{1}D separation is sampled. We then provide updates from the literature on these topics from the last 5 years or so, and go on to discuss ideas that inform decisions about whether to even do 2D-LC separations, or just stick with conventional 1D-LC. In reading the last section in particular, it is important to not lose sight of the metrics of separation that are most important for you and your applications. Just because certain aspects of 2D chromatograms are easy to measure—such as peak capacity and coverage of the separation space—they may not be as important as other metrics, such as detection sensitivity or resolution of particular sets of compounds in a mixture.

5.1 COMPLEMENTARITY OF RETENTION MECHANISMS

5.1.1 Estimation of Separation Space Usage

One of the essential concepts in any 2D separation is that the separation modes or mechanisms used in the two dimensions must be different enough that there is a reasonable chance that two compounds coeluting will be separated on the second, complementary column (Giddings, 1987; Karger et al., 1973). This point is frequently made graphically using something like that shown in Fig. 7.6. Panel A shows the best case scenario, where there is no evident correlation between retention on the first column with retention on the second column. In this case there is a very good chance that two compounds coeluting on the first column will be separated on the second column, provided the separation efficiency of the second column is high enough. Panel B shows the worst-case scenario, where

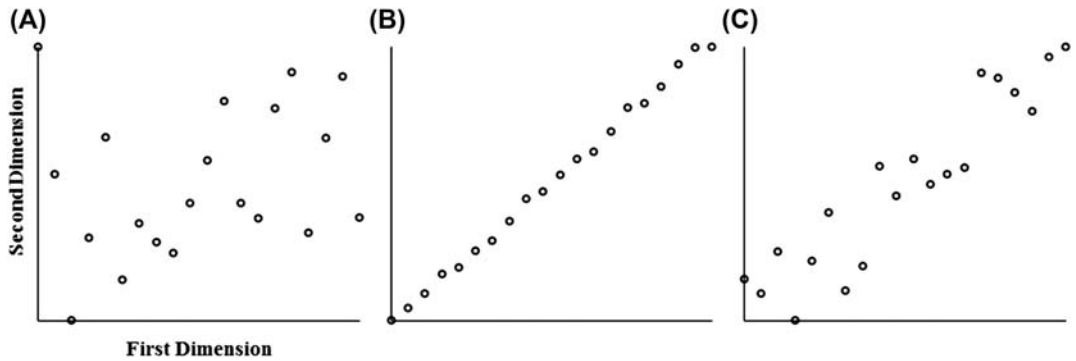

FIGURE 7.6

Illustration of the complementarity of retention mechanisms in 2D separations. (A) Example of peak pattern obtained with highly complementary ^{1}D and ^{2}D separations; (B) peak pattern obtained with separations that are not complementary; and (C) example of peak pattern obtained with separations that are somewhat complementary.

retention on the two columns is very highly correlated. In this case 2D separations are usually a waste of time, and better results can be obtained with highly optimized 1D separations. One notable exception to this exists when closely eluting peaks vary dramatically in their concentration in the sample. Readers interested in this concept are referred to the work of Venkatramani et al. (2014), who have demonstrated the point effectively, using samples of interest to the pharmaceutical industry. Panel C reflects the situation we face in 2D-LC analyses of real samples. In these cases, there often are some areas of the chromatogram where there is a high density of peaks, whereas other areas are sparsely occupied.

If the goal in 2D separations is to choose separation modes and stationary phases that are highly complementary, then the challenge we face is evaluating this degree of complementarity using data from chromatograms like that shown in Panel C. Early in the development of this aspect of the 2D-LC literature the term "orthogonality" was used to describe the extent to which two separation modes were complementary. Over the years many methods have been proposed and evaluated for assessing orthogonality/complementarity, ranging from very simple yet intuitive methods to much more sophisticated mathematically oriented methods. The principles of these different approaches and their advantages and disadvantages have been discussed at length elsewhere and these details are not repeated here. Readers interested in this topic are referred to a number of reviews and other articles (Camenzuli and Schoenmakers, 2014; Carr et al., 2012; Gilar et al., 2012; Schure and Davis, 2015). Figs. 7.7 and 7.8 illustrate two of the more intuitive yet effective methods. Schure and Davis (2015) have suggested that optimization of 2D-LC separations should be guided using information from both of these methods. Fig. 7.7 shows the implementation of a so-called "box-counting" method, which was initially described by Gilar et al. (2005) and adapted by Davis et al. (2008a). In this approach the separation space is divided into a number of discrete boxes, and the fraction of the boxes containing peaks is calculated relative to the total number of boxes in the space. The results obtained from this type of approach are sensitive to the box dimensions (Rutan et al., 2011, p. 267), thus this should be considered carefully.

Fig. 7.8 illustrates the implementation of convex hulls as a way to estimate the fraction of 2D separation space that is used for the analysis of a particular sample. In simple terms, this amounts drawing a polygon around the peak pattern observed, where each vertex in the polygon is centered on a chromatographic peak. Because there is no decision to be made about box dimensions, this approach is even more straightforward than the box-counting methods.

Both the box-counting and convex-hull methods are prone to overestimation of the effectiveness of the separation space usage in cases where there are a few outlying peaks surrounding a small space occupied by a much larger number of peaks. In other words, these methods are insensitive to the distribution of peaks across the space that they occupy. Other methods, such as the so-called asterisk equations developed by Camenzuli and Schoenmakers (2014), more effectively address the issue of peak distribution, but are a bit less intuitive.

5.1.2 Correction of Peak Capacities for Incomplete Usage of Separation Space

Both of the methods discussed above and illustrated in Figs. 7.7 and 7.8 enable estimation of the fraction of the 2D separation space that is occupied by peaks in the analysis of real samples. Obviously, maximizing this fractional coverage (f_{cov}) of the separation space is an important goal in method development. Equally important is the idea that this f_{cov} value can be used to make a correction to the

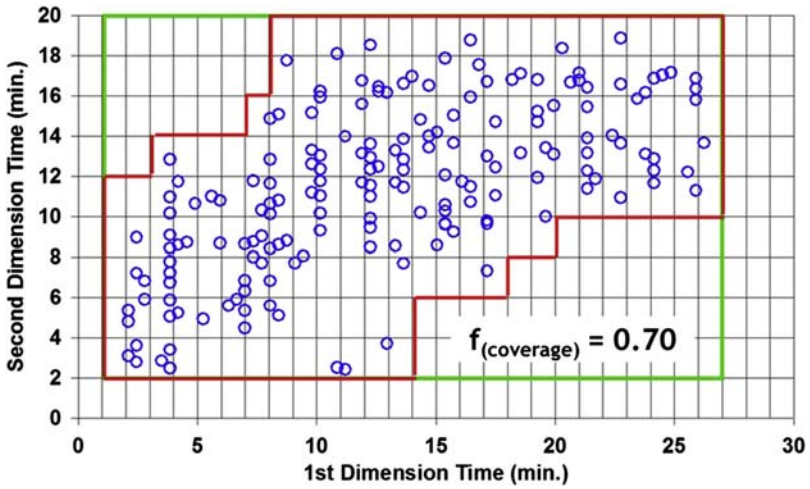

FIGURE 7.7

Illustration of a box-counting method, which counts the fraction of bins in a two-dimensional separation bed that is occupied by peaks. This fraction enables correction of the total peak capacity for incomplete usage of the separation space. *Circles* represent coordinates of observed peaks in an experimental LC × LC separation. The red (gray line in print versions) line defines the perimeter around the bins that are considered to be occupied. *LC*, liquid chromatography.

Reprinted with permission from Davis, J.M., Stoll, D.R., Carr, P.W., 2008a. Dependence of effective peak capacity in comprehensive two-dimensional separations on the distribution of peak capacity between the two dimensions. Anal. Chem. 80, 8122–8134. http://dx.doi.org/10.1021/ac800933z. Copyright 2008, American Chemical Society.

2D peak capacity estimated using the product rule (see Eq. 7.2) (Liu et al., 1995; Stoll et al., 2008). This is done by simply multiplying the 1D and 2D peak capacities by the f_{cov} value as in Eq. (7.4).

$$n^*_{c,2\text{D}} = {}^1n_c \times {}^2n_c \times f_{\text{cov}} \tag{7.4}$$

Given that $n^*_{c,2\text{D}}$ is directly proportional to f_{cov}, judicious choice of complementary ^{1}D and ^{2}D separations, along with optimization of elution conditions, can be a powerful way of increasing the practically useful peak capacity.

5.1.3 Combinations of Modes

There are many ways that one can imagine combining two complementary separations in a 2D separation scheme; Giddings (1984) discussed the scope of these thought experiments in the broadest terms. However, many of the conceivable combinations are not at all practical, for example, due to excessive dilution of the analyte (Schure, 1999) or very low separation efficiency in one or both of the separation steps. To help guide method development, we can score the commonly used and discussed combinations of modes using several attributes that are important in practice. Table 7.1 is an attempt at such scoring. It is important to recognize that the scores represent generalizations—indeed there are some niche applications where the combination of IEX and SEC may be very important (e.g., in

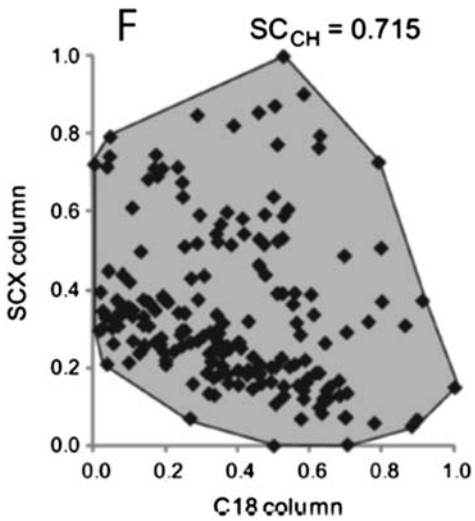

FIGURE 7.8

Illustration of the use of convex hulls to estimate the fraction of separation space occupied by peaks.

Reprinted with permission from Gilar, M., Fridrich, J., Schure, M.R., Jaworski, A., 2012. Comparison of orthogonality estimation methods for the two-dimensional separations of peptides. Anal. Chem. 84, 8722–8732. http://dx.doi.org/10.1021/ac3020214. Copyright 2012, American Chemical Society.

determination of the molecular weights and charge-state distributions of a protein mixture). To commit to a combination with a low score in developing a new method, there should be a compelling reason to choose that combination that overcomes other poor attributes of the combination. One trend that emerges from this analysis is that pairing two reversed-phase (RP) separations is attractive for a variety of reasons. This may seem counterintuitive because historically RP phases have been perceived as

Table 7.1 Comparison of Different Possible Combinations of Liquid Chromatography Separation Modes

Modes[a]	IEX × RP	SEC × RP	NP × RP	RP × RP	HILIC × RP	HILIC × HILIC	AC × RP	SEC × NP	SEC × IEX
Orthogonality	++	++	++	+	+	−	++	+	+
Peak capacity	+	+	+	++	+	+	−	−	—
Peak capacity/time	−	—	+	++	+	+	−	—	—
Solvent compatibility	+	+	—	++	+	++	+	+	+
Applicability	+	+	−	++	+	−	+	−	−
Score	4	3	1	**9**	5	2	2	−2	−3

[a]AC, *argentation;* HILIC, *hydrophilic interaction liquid chromatography;* IEX, *ion-exchange;* NP, *normal phase;* RP, *reversed-phase;* SEC, *size-exclusion.*

having similar selectivity. Indeed, choosing two RP phases that are different enough to be useful in a 2D separation is an important consideration—this is discussed in more detail in Section 7.2. Nevertheless, there are several other attributes of RP separations that make the RP × RP combination very attractive, including high efficiency, miscibility of mobile phases used in the two separations, compatibility with mass spectrometric (MS) detection, and compatibility with large biomolecules (e.g., proteins).

This has led us and others to focus on the use of RP × RP separations to address a variety of separation problems ranging from the analysis of biological extracts (Stoll et al., 2007) to peptide separations (Sarrut et al., 2015; Vanhoenacker et al., 2015) and analysis of environmental contaminants (Simpkins et al., 2010). Readers interested in practical details associated with these types of separations are referred to the review of Li and Schmitz that is focused on this topic (Li et al., 2014b).

5.1.4 Separation Modes Should Be Chosen Carefully

In this Section 5.1 we have emphasized the importance of choosing ^{1}D and ^{2}D separation modes that complement each other in terms of selectivity. However, we must also be careful not to sacrifice other measures of 2D separation performance in the name of obtaining high fractional coverage. Fig. 7.9 from the work of the Heinisch group clearly makes this point by way of example LC × LC separations of peptides (D'Attoma and Heinisch, 2013). Coupling RP–LC and hydrophilic interaction liquid chromatography (HILIC) separations together for 2D-LC is attractive from the point of view of selectivity because their separation mechanisms are known to be very different (Separation mechanisms in hydrophilic interaction chromatography, 2013). However, in the case of these peptide separations, it is evident that the ^{2}D peaks are much wider when HILIC is used in the second dimension compared to reversed-phase liquid chromatography (RP-LC). The authors offer possible explanations

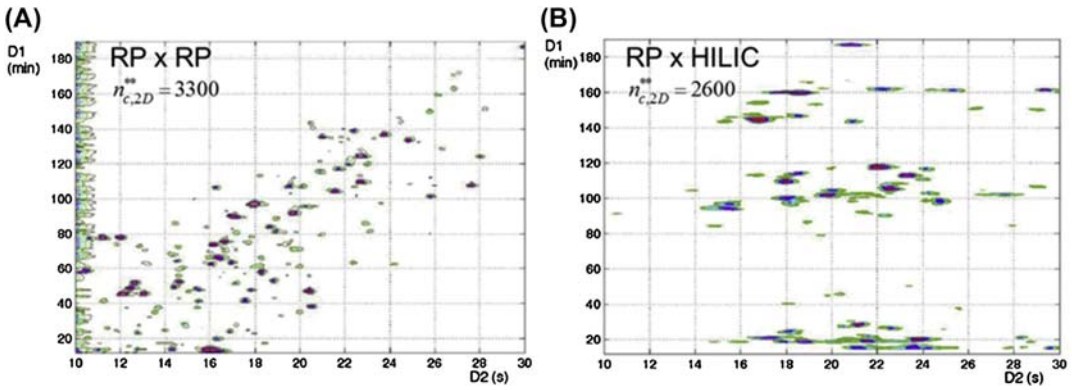

FIGURE 7.9

Comparison of LC × LC separations of peptides using RP–LC in the first dimension and either RP–LC (A) or HILIC (B) separation in the second dimension. In spite of the higher fractional coverage in the RP × HILIC case, the effective 2D peak capacity is lower because of the low peak capacity of the HILIC ^{2}D separation. *HILIC*, hydrophilic interaction liquid chromatography; *LC*, liquid chromatography; *RP*, reversed-phase.

Reprinted with permission from D'Attoma, A., Heinisch, S., 2013. On-line comprehensive two dimensional separations of charged compounds using reversed-phase high performance liquid chromatography and hydrophilic interaction chromatography. Part II: application to the separation of peptides. J. Chromatogr. A 1306, 27–36. http://dx.doi.org/10.1016/j.chroma.2013.07.048. Copyright 2013, Elsevier.

for the wider peaks, but the cause is irrelevant to the main point here. Specifically, the advantage of the increased orthogonality offered by the HILIC separation is outweighed by the disadvantage of its poorer peak width, resulting in a lower effective 2D peak capacity for the RP × HILIC separation compared to the RP × RP separation.

5.2 THE CONCEPT OF UNDERSAMPLING

In 1998, Murphy et al. pointed out in their seminal paper that the rate at which fractions of ^{1}D effluent are transferred to the ^{2}D column for further separation, relative to the native ^{1}D peak width, has an impact on the effective peak capacity of the ^{1}D separation. The development of our understanding of this issue between then and now has been discussed extensively elsewhere (Carr et al., 2012; Davis et al., 2008b; Horie et al., 2007; Seeley, 2002) and is not repeated here. In the extreme case where the time period over which a single fraction of ^{1}D effluent collected is large relative to the native widths of ^{1}D peaks, there is remixing of the ^{1}D peaks collected in that time interval as they are transferred to the ^{2}D column for further separation. In other words, this part of the ^{1}D separation is "undone," which is obviously counterproductive. Fig. 7.10 illustrates this point graphically. In cases where the ^{2}D separation does not contribute significantly to the total 2D resolution, using a sampling time (t_s) that is large relative to the native ^{1}D peak width results in serious loss of resolution.

Another perspective on this issue is shown in Fig. 7.11, which shows reconstructions of the ^{1}D separation after sampling at different rates. This makes it clear that the loss in 2D resolution originates from loss of resolution at the ^{1}D stage of the separation.

Using simulations (Davis et al., 2008b) we developed an empirical relationship that helps us understand the magnitude of the loss of ^{1}D peak capacity as the sampling time is increased. Eq. (7.5) gives an expression for $\langle\beta\rangle$, which is the average ratio of ^{1}D peak widths after and before sampling, as a function of the sampling time (t_s) and the native ^{1}D peak width ($^1\sigma$). This $\langle\beta\rangle$ value can then be used to make a correction to the ^{1}D peak capacity that quantitatively accounts for the remixing of ^{1}D peaks, as in Eq. (7.6).

$$\langle\beta\rangle = \sqrt{1 + 0.21\left(\frac{t_s}{{}^1\sigma}\right)^2} \tag{7.5}$$

$${}^1n_{c,corrected} = \frac{{}^1n_c}{\langle\beta\rangle} \tag{7.6}$$

With the illustrations in Figs. 7.10 and 7.11 and Eq. (7.5) in mind, it is tempting to come to the conclusion that one should use as small a sampling time as possible to minimize the effect of undersampling on the ^{1}D and thus the 2D peak capacity. However, the problem with this in the extreme is that very short sampling times require very short ^{2}D separation times, and thus low ^{2}D peak capacities. This is most evident in LC × LC separations where the sampling time and ^{2}D analysis time are very tightly coupled. Hybrid modes of 2D separation such as sLC × LC relax this linkage to a large degree, as discussed in Section 6.1.

The opposing effects of sampling time (and its connection to ^{2}D analysis time) on effective ^{1}D peak capacity and ^{2}D peak capacity lead to an optimum sampling time as shown in Fig. 7.12. While these results are based on theory, the optimum ^{2}D analysis time of about 10−20 s predicted from this type of calculation has been confirmed by experimental LC × LC separations (Huang et al., 2011). It is important to keep these trends in mind in the process of method development and selection of instrument hardware for 2D-LC.

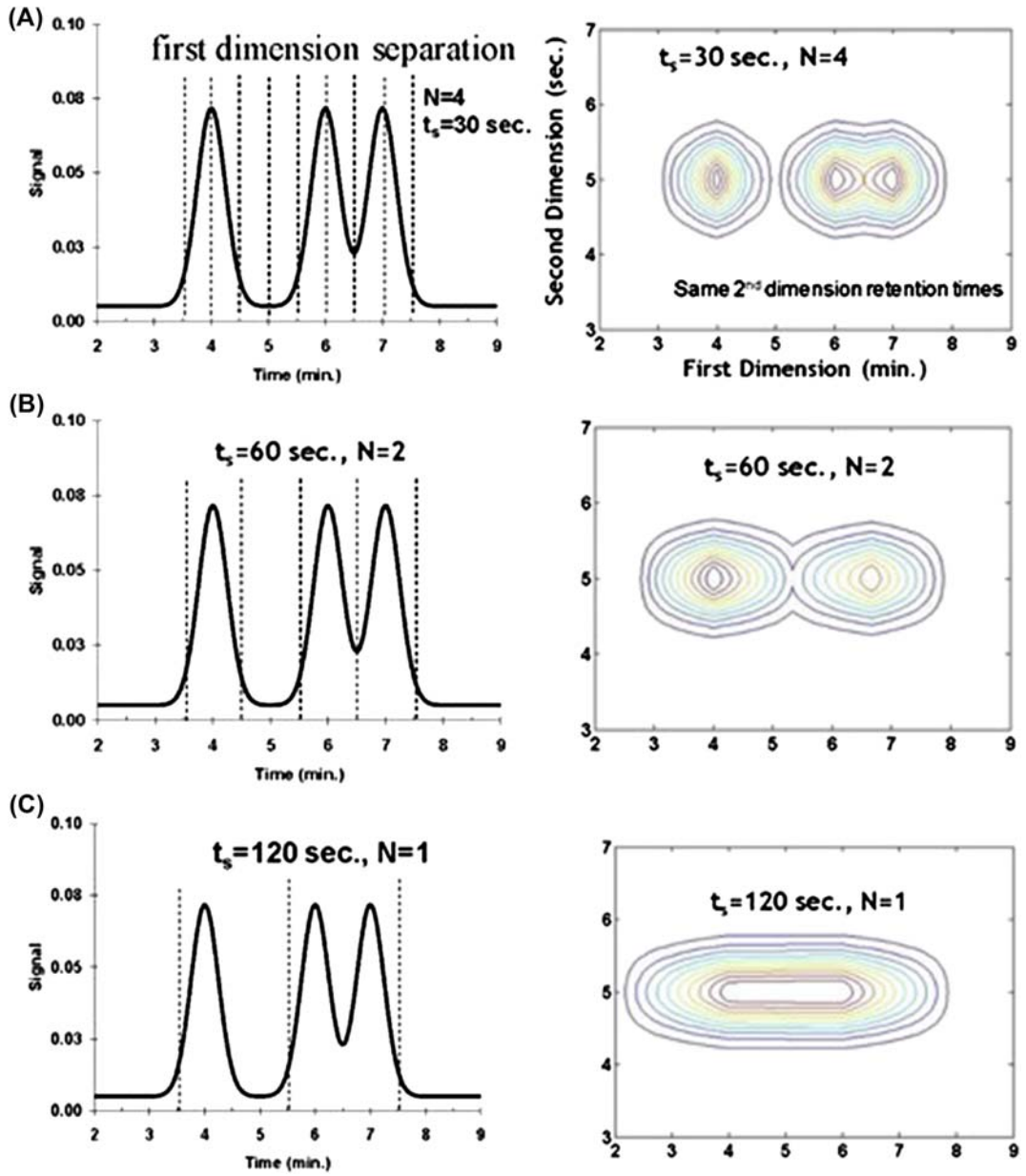

FIGURE 7.10

Effect of sampling time (rate) on resulting LC × LC contour plot. Panel (A) sampling at the Murphy–Schure–Foley recommendation of $t_s = 2\ ^1\sigma$; N = 4 samples/8 $^1\sigma$. As the sampling time is increased there is more remixing of ^{1}D peaks, and resolution in the two-dimensional chromatogram is lost; panel (B) sampling at N = 2; and panel (C) sampling at N = 1.

Reprinted with permission from Carr, P.W., Davis, J.M., Rutan, S.C., Stoll, D.R., 2012. Principles of online comprehensive multidimensional liquid chromatography. In: Gruska, E., Grinberg, N. (Eds.), Advances in Chromatography. CRC Press, Boca Raton, FL.

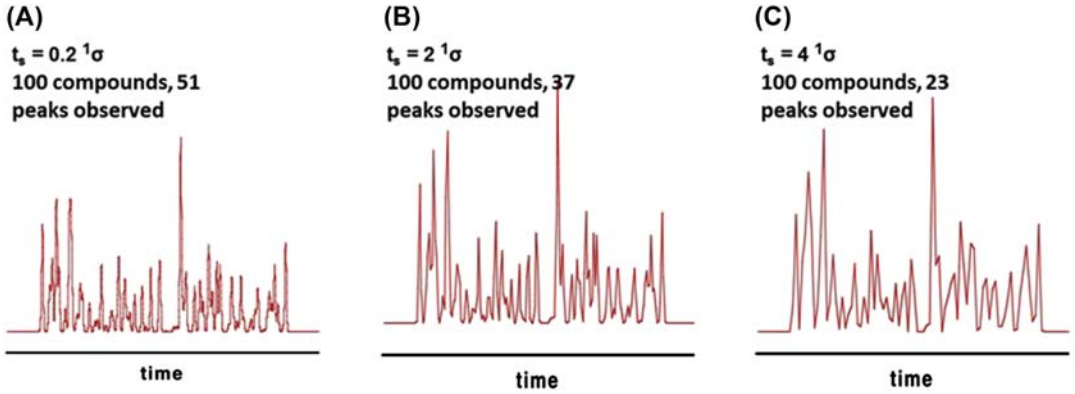

FIGURE 7.11

Effect of undersampling on effective one-dimensional (1D) peak capacity. Reconstructed 1D chromatograms for a hypothetical sample containing 100 randomly spaced compounds show that sampling at a rate of 5 samples per $^1\sigma$ ($t_s = 0.2\ ^1\sigma$) yields a separation with 51 peaks. Increasing the sampling time to 2 $^1\sigma$ (Panel B) or 4 $^1\sigma$ (Panel C) yields 37 or 23 peaks, respectively.

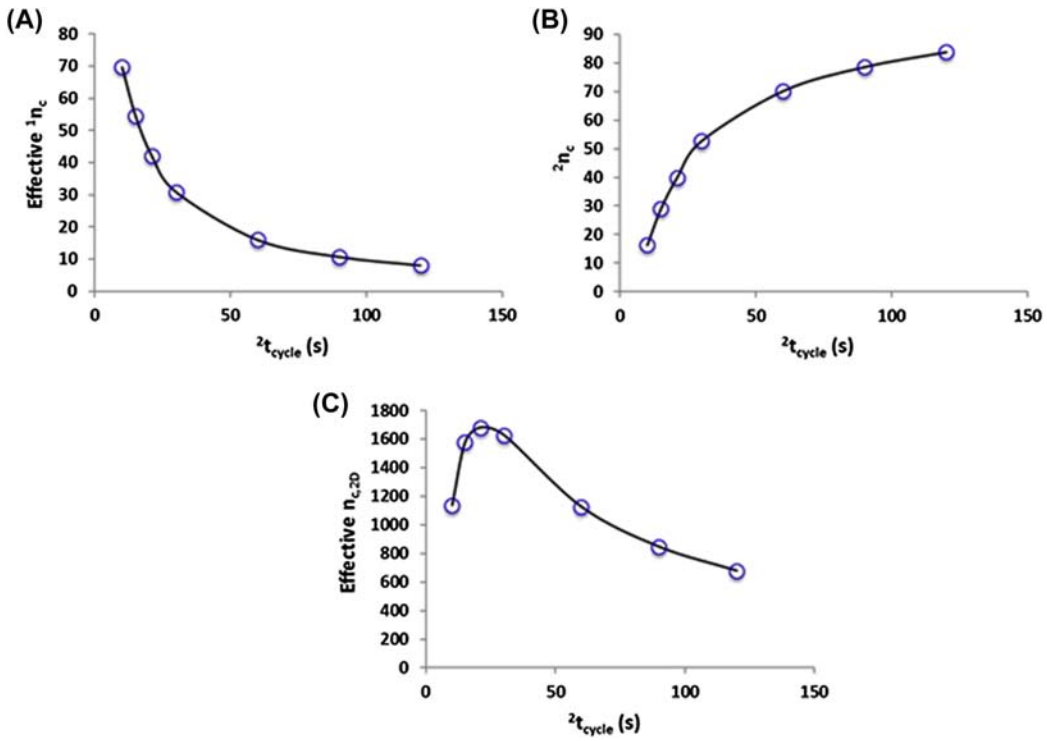

FIGURE 7.12

Illustration of the dependence of effective two-dimensional (2D) peak capacity ($n_{c,2D}$) on second dimension (^{2}D) analysis time ($^2t_{cycle}$). Calculations were made as follows: the native first dimension (^{1}D) analysis time and peak capacity (i.e., without undersampling) were assumed to be 30 and 100 min, respectively, and the effective ^{1}D peak capacity (A) was calculated using Eq. (7.5); the dependence of ^{2}D peak capacity (B) on ^{2}D cycle time is the same as that reported previously (Davis and Stoll, 2014); finally, the effective 2D peak capacity (C) is calculated as the product of the effective ^{1}D peak capacity and the ^{2}D peak capacity at each value of $^2t_{cycle}$.

Adapted from Bedani, F., Schoenmakers, P.J., Janssen, H-G., 2012. Theories to support method development in comprehensive two-dimensional liquid chromatography – a review. J. Sep. Sci. 35, 1697–1711. http://dx.doi.org/10.1002/jssc.201200070.

5.3 DECIDING WHETHER TO DO ONE- OR TWO-DIMENSIONAL LIQUID CHROMATOGRAPHY

Although it is certainly true that the barriers new users of 2D-LC face are much lower than they were a decade ago, the decision to develop and implement a 2D-LC method is still not a trivial one. Moving from 1D- to 2D-LC requires a significant financial commitment to acquire and maintain a 2D-LC instrument, and users of the instrument must be trained and acquire practical experience with the methodology. Given these commitments, one should be convinced that the performance of 2D-LC will very likely be superior to 1D-LC for the application at hand. And, "performance" and "success" can be measured in very different ways depending on where the method will be deployed, for what purpose, under certain financial and time constraints, and so on. There is no question that in cases where the sample of interest is very complex, the goal is to learn as much about the sample as possible, and long analysis times are not prohibitive, 2D-LC will yield results superior to those from 1D-LC. But, on the continuum of all LC applications, this type of scenario is not very common. Rather, there are many more situations in the "middle ground" where sample complexity challenges the capabilities of 1D-LC, but analysis time is still a concern, and minimizing it is a primary method development goal. On the other end of the continuum, where the sample is simple (e.g., one to five compounds) and very fast analysis is particularly important, 1D-LC is king—with current technology it is difficult to imagine this changing in the foreseeable future. This then sets up the key question—how does one decide whether to do 1D- or 2D-LC?

The literature on this topic contains a blend of experimental and theoretical studies. The two performance metrics that have been used to guide discussion are peak capacity and time to resolve n compounds. The concept of peak capacity is most useful for comprehensive separations and situations where a primary goal of the method is to simply separate as many compounds as possible without regard for the resolution of specific pairs of compounds (e.g., in proteomics). On the other hand, for less complex samples a common method development goal is to arrive at a method that resolves all of the compounds in a sample (or a specific subset of compounds) in the shortest possible time. This is what we refer to here as "time to resolve n compounds."

5.3.1 Comparison of One- and Two-Dimensional Liquid Chromatography in Terms of Peak Capacity

High-performance liquid chromatography (HPLC) theory predicts that the chromatographic efficiency (i.e., plate number) of columns used for 1D-LC increases with the ½ power of analysis time (Carr et al., 2009). Taken together with the fact that peak capacity in 1D-LC in gradient elution mode also depends on the ½ power of the plate number (Giddings, 1967), this means that peak capacity in 1D-LC increases with the ¼ power of analysis time. This is a very weak dependence. It means that to double the peak capacity in 1D-LC we must increase the analysis time 16-fold. Using typical chromatographic parameters yields plots like those shown in Fig. 7.13 where we have peak capacity as a function of analysis time. We see that even when allowing for high-pressure operation up to 1000 bar, the peak capacities we can expect in 1 h of analysis time are only on the order of 350 and 600 for small nonpeptide molecules (e.g., benzene) and peptides, respectively.

The product rule (Eq. 7.2) teaches us that if we take an existing 1D-LC separation with a peak capacity of 200 and add a ^{2}D of separation, even if the peak capacity of that ^{2}D is only 15, we will increase the peak capacity to 3000. This, of course, assumes that we properly optimize the system to

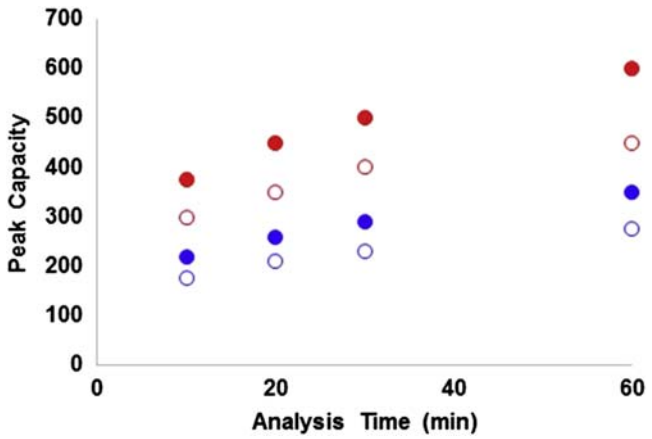

FIGURE 7.13

Peak capacity as a function of analysis time for one-dimensional liquid chromatography with different pressure limitations and for different analyte types. Blue (dark gray in print versions) circles are for small nonpeptide molecules with $d(\ln k)/d(\phi) = 8$, and red (light gray in print versions) circles are for peptide molecules with $d(\ln k)/d(\phi) = 25$. *Open circles* are for a pressure limit of 400 bar, and *filled circles* are for 1000 bar. Plate numbers are first estimated for dead times that are 10% of the analysis time assuming three-parameter optimization at 40°C (Carr et al., 2009), and then gradient peak capacity is calculated from these plate numbers using the approach prescribed by Neue (2005).

avoid serious degradation of the ^{1}D performance due to undersampling. But, this is stunning potential—increasing the peak capacity of 1D-LC by a factor of 15 would require an increase in analysis time by a factor of 15 to the fourth power.

If 1D-LC is clearly superior at very short analysis times, and 2D-LC is superior beyond an analysis time of 1 h, then there must be a region of analysis time in between where the performances of the two techniques cross over. The determination of this crossover time has been studied from both theoretical (Potts and Carr, 2013) and experimental points of view (Huang et al., 2011; Stoll et al., 2008). Fig. 7.14 shows results from the experimental work of Huang et al. who studied the effect of the ^{2}D cycle time on the effective peak capacities of LC × LC separations of plant extracts, and compared those to peak capacities for 1D-LC analyses of the same samples at comparable analysis times. More important than peak capacities are the numbers of peaks observed in real separations—these are plotted in Fig. 7.14. We see that at the shortest total analysis time of 6 min, the 1D-LC method outperforms the 2D one, no matter the ^{2}D cycle time. However, starting at an analysis time of 12 min, the 2D method outperforms the 1D one, provided optimal ^{2}D cycle times in the range of 12–20 s are used. LC × LC methods with shorter or longer ^{2}D cycle times of 6 or 40 s yield results that are inferior to those from the 1D method at that time. At the longest analysis time in the study of about 50 min, the LC × LC method yields threefold more peaks compared to the 1D method.

The essential message from this and related studies is that the performance crossover happens at relatively short times—10 min, rather than something longer like 100 min. This means that LC × LC should be considered as a viable option to either achieve increased resolving power compared to 1D-LC

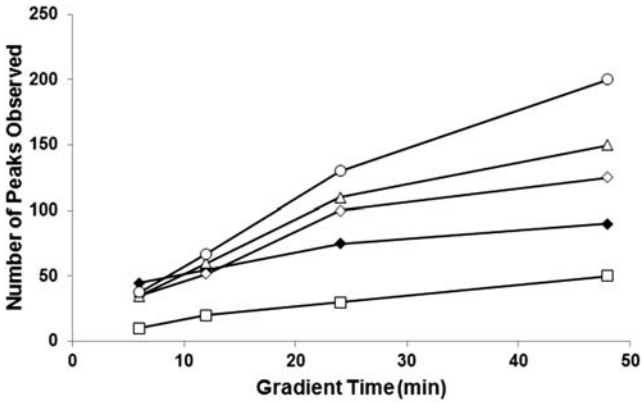

FIGURE 7.14

Numbers of peaks observed in separations of plant extracts. For LC × LC separations, the ^{2}D cycle time was varied to demonstrate the optimum cycle time—^{2}D cycle times are: 40 (*open diamonds*), 21, (*open circles*), 12 (*open triangles*), and 6 (*open squares*) sec. At analysis times of about 10 min, the two-dimensional liquid chromatography method outperforms the one-dimensional liquid chromatography method (*filled diamonds*) and remains superior at all longer times.

Reprinted with permission from Huang, Y., Gu, H., Filgueira, M., Carr, P.W., 2011. An experimental study of sampling time effects on the resolving power of on-line two-dimensional high performance liquid chromatography. J. Chromatogr. A 1218, 2984–2994. http://dx.doi.org/10.1016/j.chroma.2011.03.032. Copyright 2011, Elsevier.

at a given analysis time or perhaps reduce the analysis time of an existing method, even for analyses in the range of 10–60 min. The theoretical study of Potts and Carr (2013) suggests that highly optimized LC × LC methods may even be competitive with 1D-LC at analysis times as short as 3 min.

5.3.2 Time to Resolve n Compounds

As discussed in the preceding section, typically the goal of LC × LC is to maximize the effective peak capacity of the separation. For samples of moderate to low complexity, peak capacity may not be the most relevant performance metric, especially if we are concerned with the resolution of two or several neighboring peaks. In these cases, defining and measuring success can be highly variable, and is often dependent on the sample at hand. In our work simulating such scenarios, an important metric of performance that we have settled on is the *time to reach a specified probability of resolving all of the compounds in a particular mixture* (Davis and Stoll, 2014). Using this metric enables us to fairly compare different separation methodologies including 1D-LC and LC × LC, but also others such as multiple heartcutting, selective comprehensive, and stop-and-go 2D-LC. Fig. 7.15 shows the analysis time required to reach a 50% probability of resolving all of the components in a mixture as a function of the number of sample components, for different LC techniques. We see that even with a peak capacity of about 200 for 1D-LC at an analysis time of 20 min, we cannot expect more than 50% probability of resolving all components in the mixture if there are more than 10 components in the sample. In the same analysis time, moving (see horizontal blue arrow) to LC × LC provides 50%

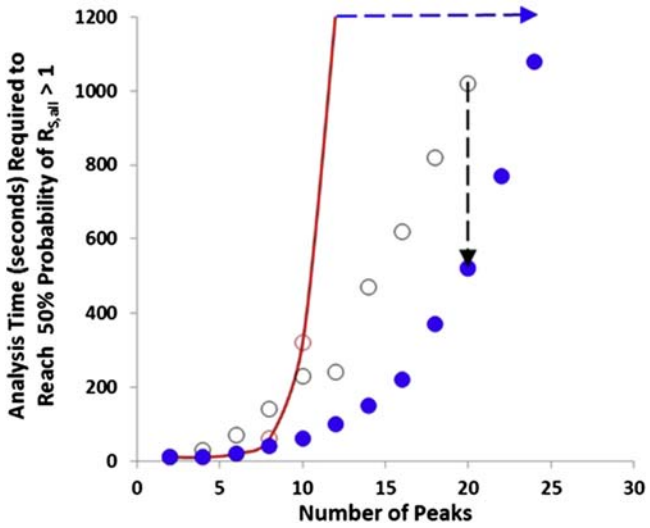

FIGURE 7.15

Time required to reach 50% probability of resolving all of the components in a mixture for different liquid chromatography (LC) techniques: one-dimensional liquid chromatography [○ (light gray in print versions)], LC × LC (○), sLC × LC [● (dark gray in print versions)]. The red (gray in print versions) line is an interpolation between the times for 10 and 12 sample components. *sLC* × *LC*, selective comprehensive two-dimensional liquid chromatography.

Adapted from Davis, J.M., Stoll, D.R., 2014. Likelihood of total resolution in liquid chromatography: evaluation of one-dimensional, comprehensive two-dimensional, and selective comprehensive two-dimensional liquid chromatography. J. Chromatogr. A 1360, 128–142. http://dx.doi.org/10.1016/j.chroma.2014.07.066.

probability of success for about 20 compounds, and with sLC × LC about 25 compounds. The other way to interpret these results is to ask the question—how much can analysis time be reduced for a given separation goal by changing techniques? One answer to this question is illustrated by the vertical black arrow, which shows that for a 20-component mixture, moving from LC × LC to sLC × LC enables a 50% reduction in analysis time.

6. IMPORTANT PRACTICAL DETAILS ASSOCIATED WITH IMPLEMENTATION

In this section we will discuss some of the most practically important details associated with setting up a 2D-LC system and implementing methods for the analysis of real samples. At the writing of this chapter 2D-LC is still a rapidly evolving technique and our community still has a lot to learn and discover about how to best implement 2D-LC methods; however, we have learned a lot in the last decade or so, especially with commercially available instrumentation. What follows is a major fraction of the distillate of those experiences.

6.1 CONCEPTS FOR DIFFERENT MODES OF TWO-DIMENSIONAL LIQUID CHROMATOGRAPHY SEPARATION

The first online 2D-LC separations were demonstrated in the 1970s and were focused on what we now refer to as "heartcutting" methods (Apffel et al., 1981), for which we use the symbol LC−LC. In this mode of 2D-LC, most of the components of a sample are neglected as they elute from the ^{1}D column, and a select portion of ^{1}D effluent containing analytes of interest are transferred to a ^{2}D column for further separation. As pointed out by Snyder et al. in their early description of "boxcar chromatography," the main reason for doing analysis by LC−LC over conventional 1D-LC is the potential for significant savings in analysis time (e.g., tenfold or more). Indeed, LC−LC has been incredibly effective for analysis of one or a few compounds in complex mixtures ranging from milk to plasma and environmental samples (Cassiano et al., 2012). Recently, we demonstrated that the concept can be extended to three dimensions, still with automated equipment, albeit at the cost of increases in the complexity of the instrumentation and method development (Simpkins et al., 2010). However, the fact that LC−LC methods ignore most of the content of the sample being analyzed limits them to a relatively small portion of the application space addressable by LC. Given this, and the fact that LC−LC concepts have been worked out in detail for decades, in this chapter we focus on modes of 2D-LC that are capable of addressing a larger fraction of the sample being analyzed. From the early 1980s until about 2010 the complement to LC−LC was comprehensive 2D-LC (LC × LC), which as the name suggests is capable of addressing the components of a sample in a more comprehensive way. In the past 5 years or so there has been significant development of, and interest in, modes of 2D-LC that are intermediate between LC−LC and LC × LC. These include multiple heartcutting (mLC-LC) (Zhang et al., 2013a), stop-flow (Bedani et al., 2006), and selective comprehensive (sLC × LC) (Groskreutz et al., 2012a) 2D-LC. We now have at our disposal a variety of modes of 2D-LC that span a continuum running from LC−LC at one extreme to LC × LC at the other. The trade-off for increased information resulting from analysis by 2D-LC is complexity of the instrumentation, method development, and data analysis associated with a particular mode of 2D-LC.

Fig. 7.16 shows conceptually how the LC−LC, LC × LC, and sLC × LC, modes of 2D-LC separation compare to each other. These have also been discussed extensively in a recent review article (Stoll and Carr, 2016). Fig. 7.17 shows examples of the valve interfaces that can be used for these approaches. Either of the configurations shown in Fig. 7.17 can be used for simple single heartcutting (LC−LC). A variety of other valve interfaces have been described in the literature, particularly for LC × LC. The biggest single collection of descriptions of interfaces that have been used appears in a book chapter by Francois et al. (2011).

The primary advantage of the mLC−LC approach is that it is tremendously flexible. Provided the interface is equipped with enough loops and there is adequate spacing between target peaks in the ^{1}D separation, one can easily target 10 ^{1}D peaks, and one can imagine targeting many more. The primary disadvantage, however, is that a single fraction of each targeted ^{1}D peak is transferred to the ^{2}D for further separation. This disadvantage manifests itself in two very different ways. First, in cases where the fraction volume is small relative to the peak volume, the quantity of analyte transferred from the target ^{1}D peak to the ^{2}D column will be very sensitive to exactly where on the peak a cut is made, and therefore very sensitive to ^{1}D retention time stability in successive analyses, which can severely

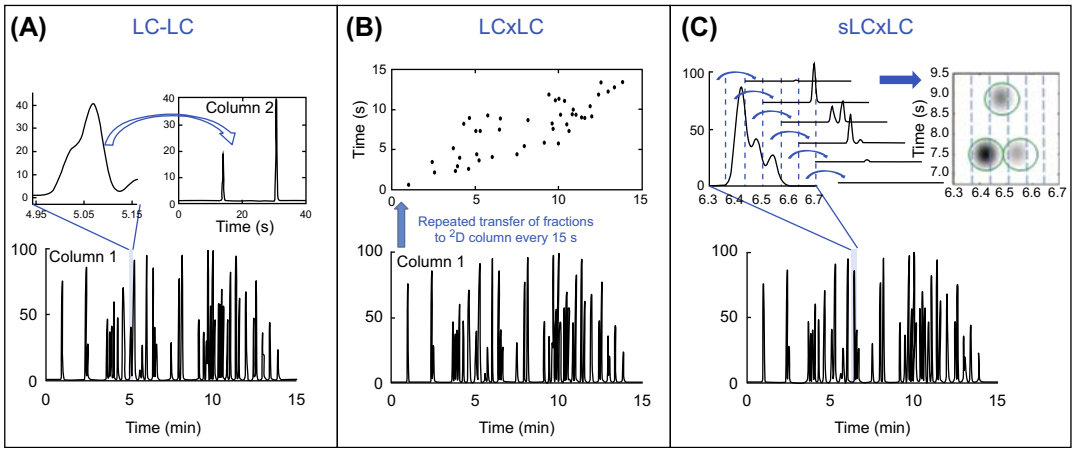

FIGURE 7.16

Conceptual comparison of LC−LC, LC × LC, and sLC × LC modes of two-dimensional liquid chromatography (2D-LC) separation. Panel A shows the case of LC−LC (heartcutting 2D-LC) where, in this case, only a single fraction is injected into the 2D column. Note that in multiple heartcutting (mLC−LC, not shown) more than one region of the first dimension (^{1}D) effluent would be injected onto the second dimension (^{2}D) column. Panel B shows the case of LC × LC (comprehensive 2D-LC) where the entire ^{1}D effluent is sequentially injected. Panel C shows the case of sLC × LC (selective comprehensive 2D-LC) where selected segments of the ^{1}D effluent are injected comprehensively on to the ^{2}D column.

Reprinted with permission from Stoll, D., Carr, P., 2016. Two-dimensional liquid chromatography: a state-of-the-art tutorial. Anal. Chem. (submitted for publication). http://dx.doi.org/10.1021/acs.analchem.6b03506. Copyright 2016, American Chemical Society.

degrade quantitative precision (Pursch and Buckenmaier, 2015). Second, mitigating the sensitivity to retention time stability is possible by making the fraction volume large relative to the peak volume; however, this inevitably results in mixing analytes from the target peak with neighboring ^{1}D peaks prior to transfer to the ^{2}D column. In other words, the target ^{1}D peak is severely undersampled in this case, defeating the progress made toward resolution by the ^{1}D column. These consequences are shown graphically in Fig. 7.18.

Recognizing the limitations of mLC−LC motivated us to develop sLC × LC. The principal difference between mLC−LC and sLC × LC is that in the case of sLC × LC multiple fractions of each target ^{1}D peak or region are transferred to the ^{2}D column in a comprehensive way—this is shown graphically in Fig. 7.16. This effectively solves the problems associated with shifting ^{1}D retention times making quantitation more robust (Pursch and Buckenmaier, 2015). This also avoids undersampling ^{1}D peaks, which is valuable in cases where the contribution of the ^{1}D separation to the overall resolution of the compounds of interest is important.

Stop-flow 2D-LC is an interesting concept that has received relatively little attention; interested readers are referred to a few papers in the literature on this topic for more detail (Bedani et al., 2006; Guiochon et al., 2008; Hou et al., 2015; Kalili and de Villiers, 2013a,b).

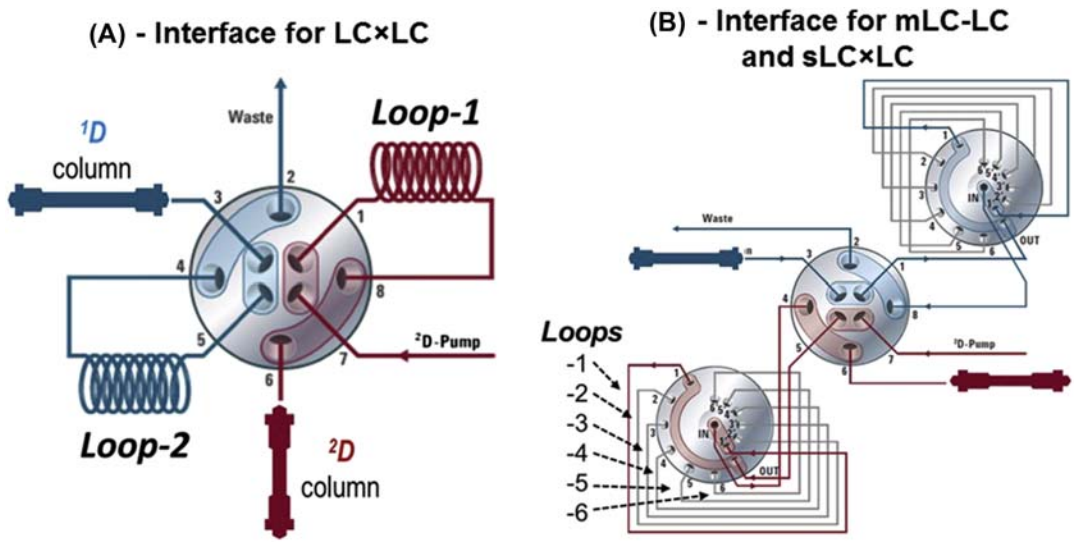

FIGURE 7.17

Example valve interfaces used for mLC−LC, sLC × LC, and LC × LC separations. Either configuration can also be used for simple single heartcut operation (LC−LC). *[1]D*, first dimension; *[2]D*, second dimension; *LC*, liquid chromatography.

Graphics courtesy of Agilent Technologies.

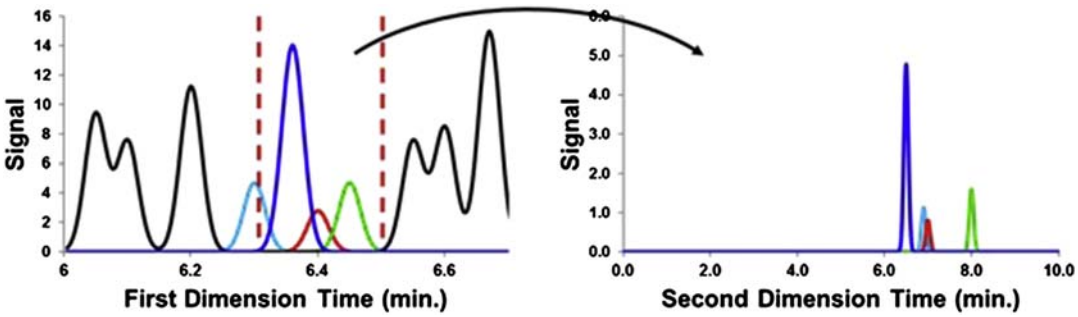

FIGURE 7.18

Consequence of using a large sampling window [indicated by the red (dark gray in print versions) *dashed vertical lines*] in the case of single heartcut operation of two-dimensional liquid chromatography. Sample components that had been separated from the target compound (*red peak* (dark gray in print versions)) by the [1]D column are remixed and some are not reseparated (the *teal peak* (gray in print versions) here) from the target analyte by the [2]D column.

6.2 IMPORTANT CHARACTERISTICS OF INSTRUMENT COMPONENTS

The operation of instruments assembled for 2D-LC places demands on the individual instrument components that are unique to 2D-LC and not normally encountered in the operation of a chromatograph for conventional 1D-LC. Thus, it is important to examine some of these challenges so that the user can make informed decisions when choosing which instrument components to use in their 2D-LC work. In the early days of the development of 2D-LC most instruments were "home-built" using components repurposed from existing 1D-LC instruments. Now, with the involvement of several major instrument manufacturers designing instrument components with 2D-LC in mind, we have a better understanding of some of the critical components and more options when assembling an instrument for 2D-LC.

6.2.1 The Sampling Interface

We refer to the valve and associated components that are used to transfer fractions of ^{1}D effluent to the ^{2}D column for further separation as the *sampling interface*, or simply *the interface*. This is without a doubt the most critical component of a 2D-LC system, as it ties the two separation dimensions together. The characteristics of the interface influence most aspects of the performance of a 2D-LC method including quantitation, retention repeatability, column stability, and detection sensitivity. Quantitation is discussed in Section 9.3, and detection sensitivity is discussed in Sections 6.2.3 and 8.4. Here, we discuss the topics of retention repeatability and column stability as they relate to the characteristics of the interface. As discussed in Section 6.1, many different valve types and configurations have been used as the interface for 2D-LC. In the following two sections we compare the characteristics of two particular valve types, as examples of the kinds of differences users can expect to see that depend on their choice of instrument components.

6.2.1.1 Effect of Interface Characteristics on Retention Repeatability

Fig. 7.19 shows the flow paths through two different valve designs in common use today. The difference between them that we highlight here is that the flow paths through the valves are asymmetric in

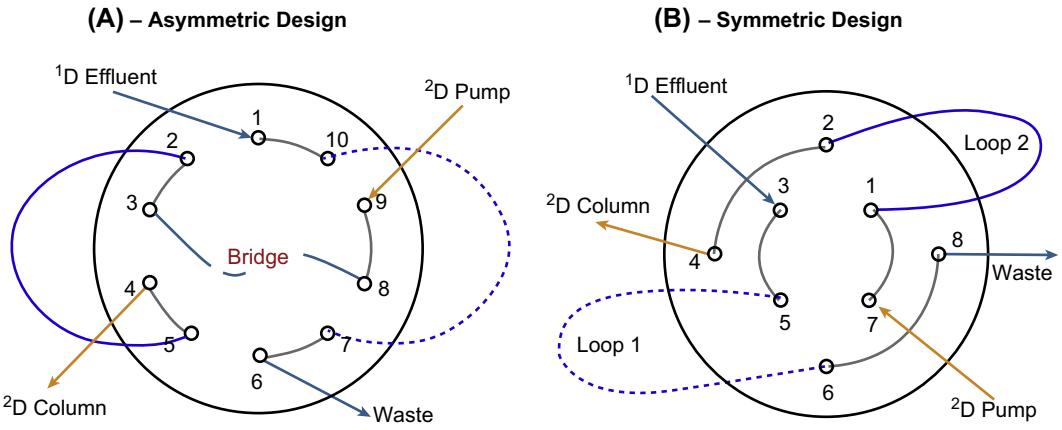

FIGURE 7.19

Flow paths through two different valve designs in common use. The valve shown in Panel A has an asymmetric design, whereas the valve shown in Panel B has a symmetric design. *^{1}D*, first dimension; *^{2}D*, second dimension.

Table 7.2 Delay of First Dimension Effluent Fraction Arrival Times as a Function of Crossover Connector Dimensions and Second Dimension (^{2}D) Flow Rate

^{2}D Flow Rate (mL/min)	Bridge Connector Volume (μL)	Retention Shift (min/s)
3.0	1.3[a]	0.00043/0.026
2.0	1.3	0.00065/0.039
1.0	1.3	0.0013/0.078

[a] *Volume of a 100 mm × 120 μm i.d. piece of connecting tubing.*

one case (Panel A) and symmetric in the other (Panel B). When the valve in Panel A is in Position 1 the path traveled by a fraction of ^{1}D effluent toward the ^{2}D column is slightly longer than when it is in Position 2 because the bridge connector between ports 3 and 8 is positioned between the sample loop and the ^{2}D column rather than between the sample loop and the ^{2}D pump. This slight difference in the arrival of the ^{1}D effluent fraction at the ^{2}D column inlet directly translates to a difference in the perceived retention times of analytes eluting from the ^{2}D column. Whether or not this difference is practically significant depends on a number of factors, including the dimensions of the bridge connector, the flow rate, and the dimension of the ^{2}D column. Table 7.2 shows the delay times for different combinations of bridge connector dimensions and flow rates. Whether this delay time will be observable as a retention time shift depends on the magnitude of the shift relative to the ^{2}D peak width and retention time precision when the valve asymmetry is not a factor.

Fig. 7.20 shows experimental results obtained using two 2D-LC systems differing only in the interface valve used. The goal of this experiment was to show the impact of the bridge connector on the

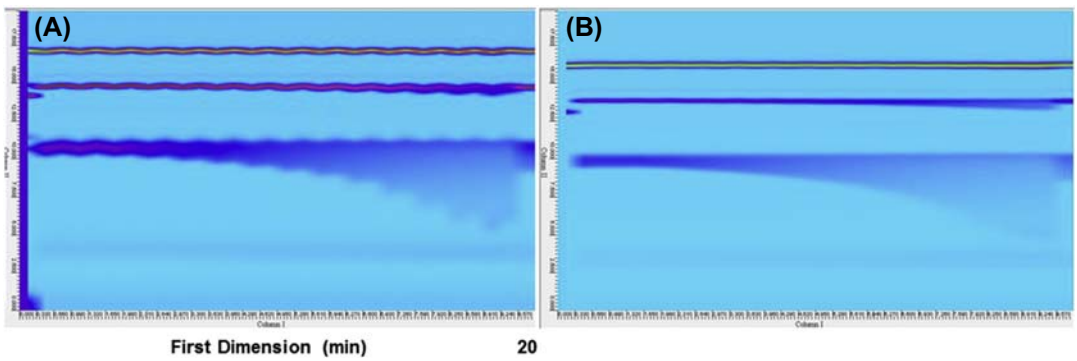

FIGURE 7.20

Pseudo two-dimensional liquid chromatography (2D-LC) chromatograms obtained from two nominally identical 2D-LC systems differing only in the type of valve used in the interface. A three-component analyte mixture was infused directly into the valve, resulting in repeated injection of the sample every 20 s throughout the analysis. The result in Panel A involved an asymmetric interface valve, whereas the result in Panel B involved a symmetric valve.

^{2}D retention time repeatability. In this case a simple mixture of three neutral analytes was infused directly into the valve interface with a syringe pump, and ^{2}D separations of the sample were completed by gradient elution in 20-s cycles. In this way the analytes appear in these images as streaks rather than spots because they are repeatedly injected into the ^{2}D column every 20 s. In comparing Panels A and B we see that the retention time repeatability is much better in the case of Panel B, which involves the symmetric valve design. We attribute this difference to the difference in valve designs.

In 2D-LC separations of real samples, often the composition of the sample is not fully known. So, the problem with ^{2}D retention times that vary depending on which loop they are injected from is as follows. For two peaks that appear in consecutive ^{2}D separations and have slightly different ^{2}D retention times, it is difficult to know with certainty if the difference in retention is due to the valve or a difference in chemical identity. In other words, are we actually seeing the same compound twice with the difference in retention time because of the valve design, or are we actually seeing two different compounds? The ability to use a symmetric valve design simply and effectively removes this source of uncertainty from the analysis of the chromatographic data.

6.2.1.2 Effect of Interface Characteristics on Second Dimension Column Stability

The design and operation of the interface valve can also have a significant impact on the behavior of instrument components connected to the valve. In this section we discuss one way that the valve design can impact the stability of ^{2}D columns. In a recent study in my laboratory (Talus et al., 2015) we evaluated the stability of ^{2}D columns operated in two 2D-LC systems varying only in the type of interface valve used. The two valve designs were the same as those shown in Fig. 7.19. Fig. 7.21 shows

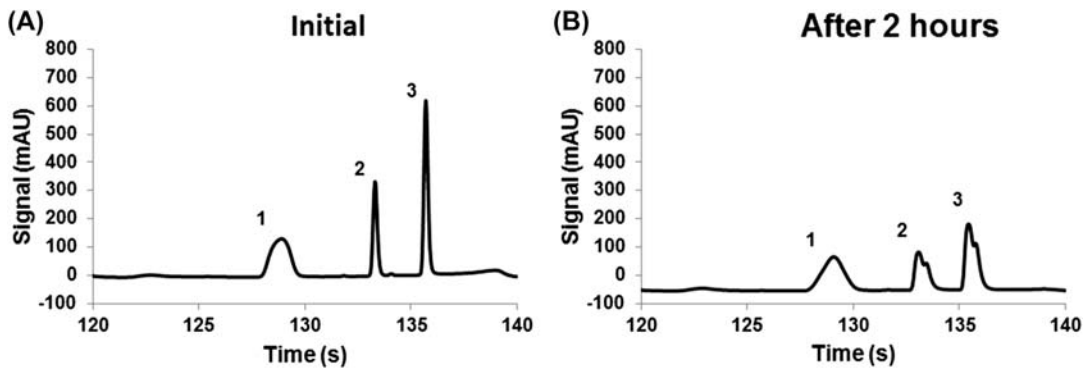

FIGURE 7.21

Second dimension (^{2}D) chromatograms showing the change in peak shape observed for the ^{2}D column after 2 h of continuous LC × LC operation (360 cycles) using an electrically actuated 10-port/2-position valve in the interface. The sample injection occurred at 120 s relative to the start of the LC × LC separation (2.0−2.33 min). Panel A shows the initial performance of the column during the very first LC × LC separation, and Panel B shows the performance of the same column after 2 h of use. The probe compounds are (1) nitropropane, (2) nitropentane, and (3) dipropyl phthalate. All of the ^{2}D columns used in this work were 30 mm × 2.1 mm i.d., packed with sub-three micron particles with a C18 stationary phase.

Reprinted with permission from Talus, E.S., Witt, K.E., Stoll, D.R., 2015. Effect of pressure pulses at the interface valve on the stability of second dimension columns in online comprehensive two-dimensional liquid chromatography. J. Chromatogr. A 1378, 50–57. http://dx.doi.org/10.1016/j.chroma.2014.12.019. Copyright 2015, Elsevier.

representative chromatograms for the three-component mixture used to evaluate the performance of the ^{2}D columns during many hours of continuous operation of the 2D-LC systems. Each ^{2}D separation cycle was 20 s, thus for every hour of operation of system 180 injections were made into the ^{2}D column. In this case the chromatogram in Panel A shows the initial performance of the column, and the chromatogram in Panel B shows the performance of the same column after 2 h of continuous operation of the system where the valve in use was the one shown in Fig. 7.19A.

It is clear from this result that after just 2 h of operation the performance of the ^{2}D column was severely compromised. To summarize the results of many stability tests of this type, we plotted the percent increase in peak width and the change in peak symmetry factor, as shown in Fig. 7.22. Significant changes in peak width and shape begin after just an hour of operation and within about 2 h the performance is severely compromised.

To understand the cause of these column failures we measured pressures in the system at several points in and around the interface valves, as shown in Panels A and B of Fig. 7.23. Panels C and D of the same figure show the pressure traces recorded as a function of time during a switch from Position 1 to

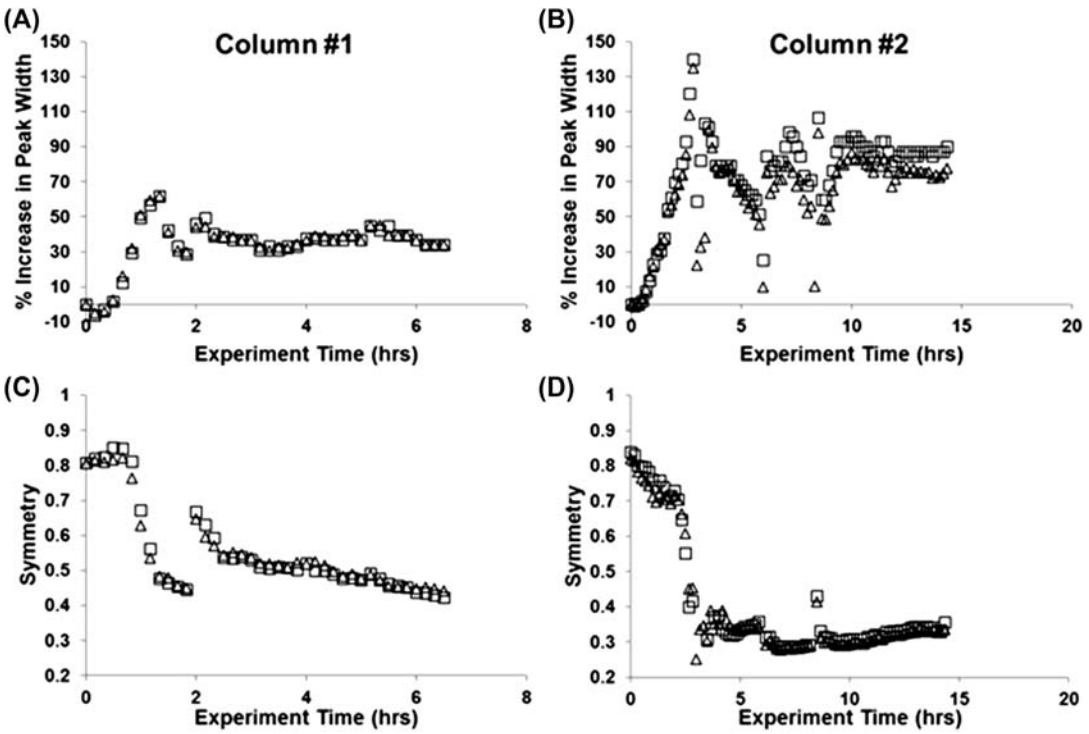

FIGURE 7.22

Changes in peak width (A, B) and symmetry (C, D) for the probe compound nitropentane using two nominally identical columns prepared with sub-three micron superficially porous particles and C18 bonded phase, and the 10-port/2-position valve design shown in Fig. 7.19A. Evidence of column failure appears after just an hour of two-dimensional liquid chromatography operation.

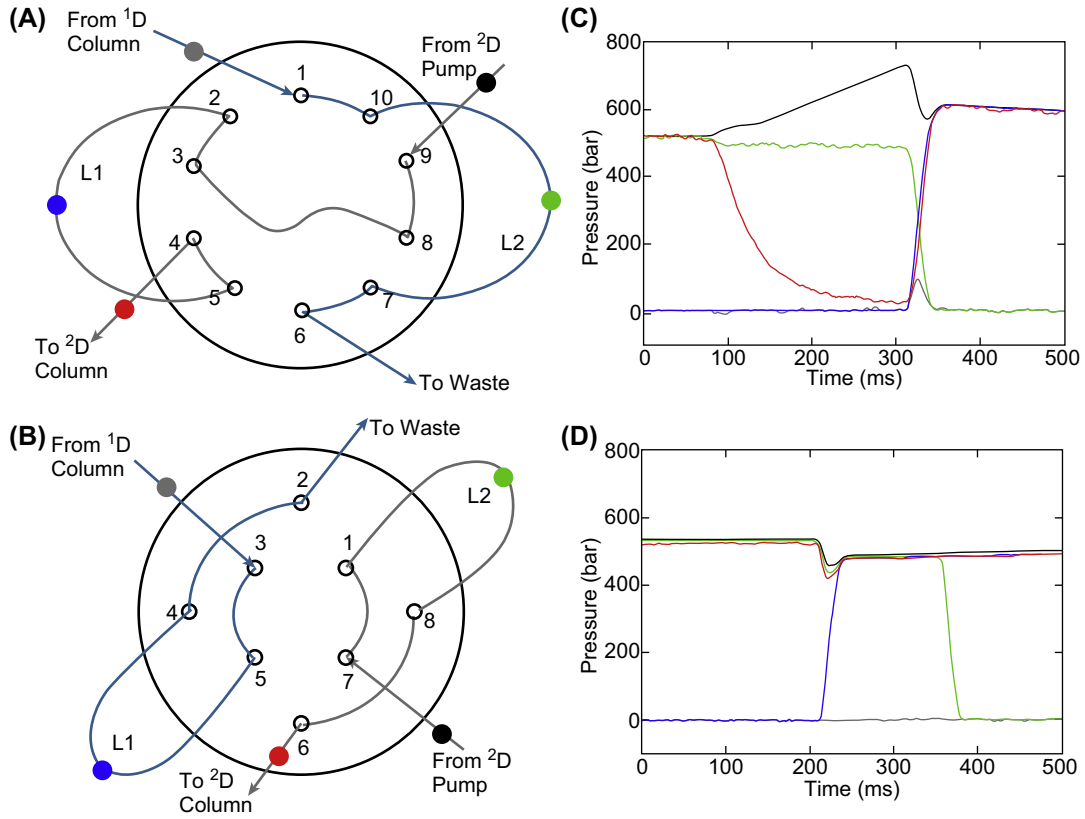

FIGURE 7.23

Locations of pressure sensors and resulting pressure traces recorded during the switch from Position 1 to Position 2 of these valves. The traces in (C) are for the valve shown in Panel A, and the traces in (D) are for the valve shown in Panel B. The colors of the traces correspond to the locations of the sensors indicated with the same colors. *^1D*, first dimension; *^2D*, second dimension.

Position 2 for these valves. Although we can rationalize the shapes of all of these pressure traces, we believe the red traces are the most important to ^{2}D column stability. In Panel C we see that with the 10-port/2-position valve the red trace drops from about 500 bar to nearly zero during the valve switch, and then quickly rebounds to 500 bar at the end of the switch. This red trace shows the pressure measured between the interface valve and the ^{2}D column inlet, meaning that in this case the column itself experiences these dramatic pressure fluctuations every time a fraction of ^{1}D effluent is injected into the ^{2}D column. Panel D shows the same pressure traces collected using the 8-port/2-position valve. We see that the red trace dips by about 15% during the switch, but most of the large change in pressure during the switch is mitigated by the difference in valve design. It is important to note that during normal operation of commercial 2D-LC systems, the pressure changes between the interface valve and column are not apparent to the user because there is no pressure sensor installed at that point. It is typical to have a single

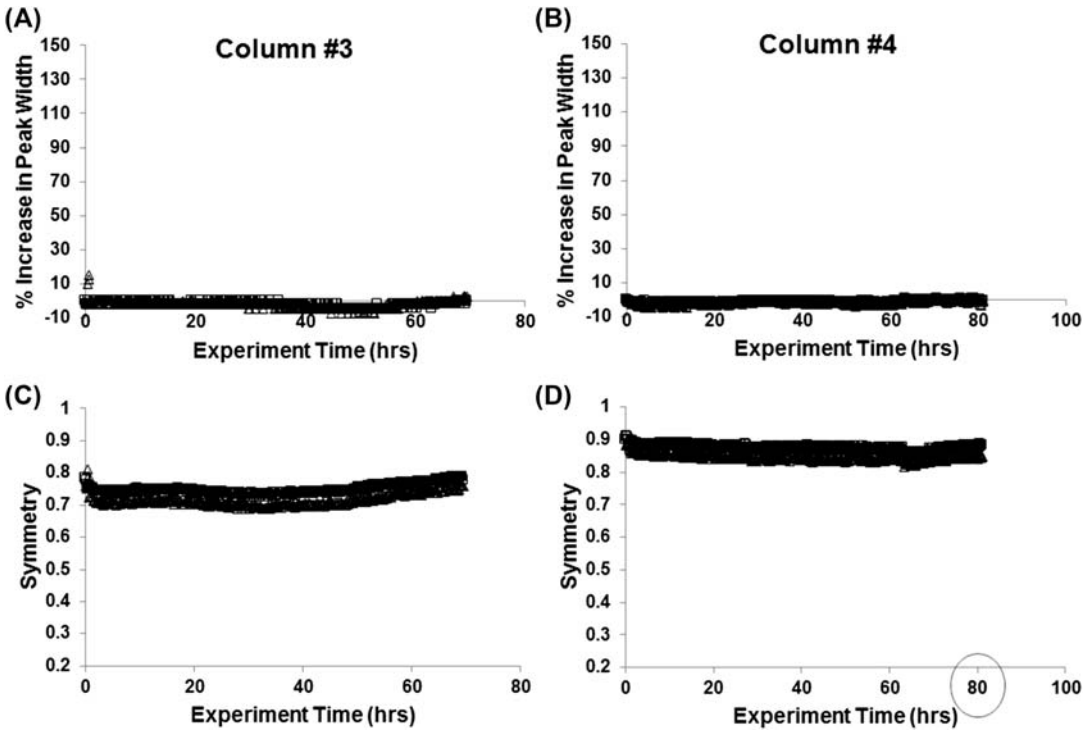

FIGURE 7.24

Changes in peak width (A, B) and symmetry (C, D) for the probe compound nitropentane using two nominally identical columns prepared with sub-three micron superficially porous particles and C18 bonded phase, and the 8-port/2-position valve design shown in Fig. 7.19B. The columns are stable under continuous operation for at least several days.

pressure sensor in the system, which is typically mounted onboard the pumping system. In this case, the pressure profile observed in everyday use would be the same as the black traces in Fig. 7.23.

Most importantly, we observe that ^{2}D columns are much more stable when the pressure changes between the interface valve and ^{2}D column are reduced. Fig. 7.24 shows the changes in peak width and symmetry observed for ^{2}D columns when the 8-port/2-position valve was used. We see that columns are very stable for at least several days.

In our view, the results of this study are very important to advancing both our knowledge of how the characteristics of the interface affect the performance and robustness of 2D-LC instruments, and our ability to use 2D-LC methods more effectively in situations where the robustness and reliability of the method is very important.

6.2.2 Pumping Systems

Next to the valve interface connecting the two dimensions in a 2D-LC system, the characteristics of the pumping system used in the second dimension have the biggest influence on the overall performance

and flexibility of 2D-LC separations. As discussed in Section 5, separation speed is a particularly desirable asset in the second dimension of 2D-LC systems. Setting aside decisions about column dimensions and particle size (discussed in Section 7), and particularly when gradient elution conditions are used in the second dimension, the gradient delay volume of the ^{2}D pumping system is of paramount importance. The reason for this is straightforward, but users who are unfamiliar with the mechanics of gradient elution and the way different pumping systems work are strongly encouraged to study these concepts carefully (e.g., see Snyder et al. (2010a)). All pumping systems that are capable of gradient elution are characterized by a finite gradient delay volume (V_d), which is the volume of solvent that must be displaced from the pump outlet before a change in solvent composition is actually delivered to the analytical column it is connected to. The delay time (t_d) associated with the arrival of a change in solvent composition at the column inlet is related to V_d through the flow rate (F):

$$t_d = \frac{V_d}{F} \tag{7.7}$$

In the context of the 2D separations, what is even more important than the delay time itself is what we call the flush-out time (t_{flush}). This is the time required for "strong solvent" (e.g., acetonitrile (ACN) or MeOH in the case of RP-LC) to be flushed from the pumping system and connections at the end of a gradient elution to begin delivering the initial solvent used in the gradient for the subsequent analysis. In our work we have taken $2 \times t_d$ as a reasonable estimate of t_{flush} (Schellinger et al., 2005). Table 7.3 shows the gradient delay times for different combinations of delay volume and flow rate. Also shown is the fraction of ^{1}D analysis or ^{2}D analysis times that remains after accounting for the loss of productivity during the flush-out time.

One of the principal conclusions that emerge from these numbers is that it is effectively impossible to do fast ^{2}D separations using older pumping systems with gradient delay volumes on the order of 1 mL. Choosing a modern pump with a low gradient delay volume on the order of 100 µL or less should be one of the highest priorities in assembling an instrument for 2D-LC. If this cannot be done, and very long ^{2}D separations are used in the case of LC × LC, ^{1}D peaks will be severely undersampled leading to much lower 2D separation performance than we expect. The noncomprehensive modes of 2D-LC are much more forgiving in this regard because there is generally more time available for each ^{2}D separation. Other possible solutions exist for increasing the throughput of the ^{2}D, such as using multiple ^{2}D pumps/columns in parallel (Fairchild et al., 2009a; Francois et al., 2008;

Table 7.3 Gradient Delay Times for Different Combinations of Delay Volume and Flow Rate

Gradient Delay Volume (V_d, mL)	Flow Rate (mL/min)	Gradient Delay Time (t_d)	Analysis Time	Fraction of Analysis Available for Separation (%)
1.0	0.25	4 min	30 min	74
1.0	3.0	20 s	40 s	0
0.1	0.25	24 s	30 min	97
0.1	3.0	2 s	30 s	88

The first two rows are typical of legacy high-performance liquid chromatography pumps. The first and third rows correspond to typical ^{1}D conditions, whereas the second and fourth rows correspond to typical ^{2}D conditions.

Venkatramani and Patel, 2006), but from a practical point of view these are much less desirable than simply choosing a high-performing pump from the start.

6.3 OPTIMIZING FOR DETECTION SENSITIVITY

Historically, the performance of 2D-LC methods has been most commonly assessed using the metrics of peak capacity and the degree of usage of the separation space. With a few exceptions (Gargano et al., 2016; Sarrut et al., 2015; Schure, 1999; Stoll et al., 2014; Vivó-Truyols et al., 2010), detection sensitivity (i.e., detection limits) has typically been overlooked as an important performance attribute. However, with the adoption of 2D-LC by more application-driven users, detection sensitivity is being identified as an increasingly important issue.

The fundamental problem is that under most circumstances the samples we inject into columns used in 2D-LC, whether they are used in the first or second dimension, become dispersed inside the column as they migrate from the inlet to the outlet of the column. So, whatever detection sensitivity we have at the outlet of the ^{1}D column [whether in terms of mass(t) or concentration(t)], we will have less sensitivity at the outlet of the ^{2}D column because the analytes of interest are spread out over a larger eluent volume. Fortunately, we have some ability to mitigate this effect by choosing conditions that promote "compression" or "focusing" of the analyte zone between elution from the ^{1}D column and the inlet of the ^{2}D column. At the writing of this chapter there is no single approach that completely solves this problem in 2D-LC for all applications. In the past 10 years or so, a number of approaches have been proposed, and some developed and commercialized, each with its unique advantages and disadvantages. This is a broad and rapidly evolving area of research. Here, we briefly touch on the different approaches that have been described in the literature and provide some detail on an approach we have used extensively in my laboratory.

Fig. 7.25 shows the impact of the volume and composition of fractions of ^{1}D effluent on the performance of ^{2}D separations, in the context of a 2D-LC separation where RP-LC separations are used in both dimensions. Note that a short, narrow column is used in the second dimension, which is necessary for very fast ^{2}D separations. We see that when the injection volume (2 μL) is small relative to the column volume (60 μL), and the sample solvent is matched to the initial solvent used in the gradient elution program (50/50 ACN/water), we get peaks that are symmetrical, narrow, and tall (Panel A). When we simply inject more of the same sample, as we would do in the context of a 2D-LC separation, the early eluting peaks in particular begin to broaden significantly (Panel B). If we then mimic the worst-case scenario where the ^{1}D effluent contains a higher fraction of "strong solvent" (in this case ACN) than the initial solvent used in the ^{2}D separation, the peaks are severely broadened and distorted (Panel C). However, the ability to change the properties of the ^{1}D effluent fraction between the outlet of the ^{1}D column and the inlet of the ^{2}D column can be very powerful. Panel D shows that even if we use the same injection volume of 40 μL, if we are able to drop the ACN content from 50% to 30%, this produces very nice-looking peaks that are not very different from those in Panel A. In other words, adjustment of the sample composition allows us to inject a large fraction of ^{1}D effluent to improve sensitivity without compromising chromatographic resolution in the ^{2}D.

The idea of diluting the ^{1}D effluent with weak solvent prior to transfer of the mixture to the ^{2}D column has a long history (Oda et al., 1991). Readers interested in its development, and other approaches over time, are also referred to a recent review article of ours (Stoll and Carr, 2016). Here, I describe representative results from our own work that demonstrate the potential benefits of the

approach. To understand how these effects play out in 2D-LC separations of real samples, we have quantified the benefit of the ability to change the composition of the ^{1}D effluent fraction in the case of detecting trace-level components of a mixture produced by forcibly degrading an active pharmaceutical ingredient (Stoll et al., 2014). Fig. 7.25 shows that the effect of the sample solvent composition on the performance of the ^{2}D column can be minimized by injecting smaller volumes of ^{1}D effluent (Panel A), but of course this reduces detection sensitivity simply because fewer moles of the analytes are injected into the ^{2}D column. To study the interplay of these variables, we used an instrument set up like that shown in Fig. 7.26. The virtue of this particular configuration was that it allowed us to

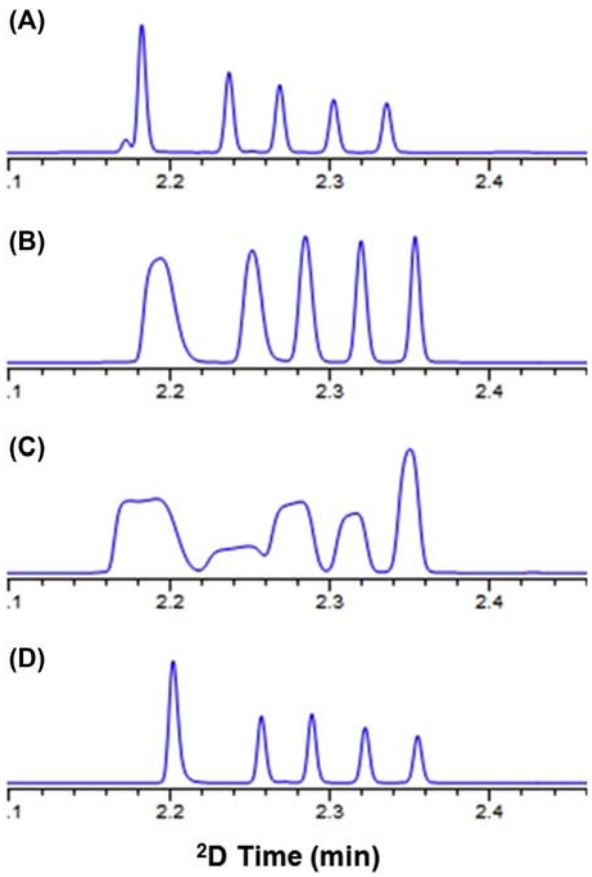

FIGURE 7.25

Effect of the volume and composition of fractions collected from the one-dimensional column and injected into the second dimension (^{2}D) column on performance of the ^{2}D separation. Conditions: 30 mm × 2.1 mm i.d. Zorbax SB-C18 column; 40°C; 2.5 mL/min; gradient elution from 50% to 90% ACN over 15 s; solutes are alkylphenone homologs. Chromatograms were obtained with: (A) 2 μL injection of sample in 50/50 ACN/water; (B) 40 μL injection of sample in 50/50 ACN/water; (C) 40 μL injection of sample in 70/30 ACN/water; and (D) 40 μL injection of sample in 30/70 ACN/water. ^{2}D, second dimension.

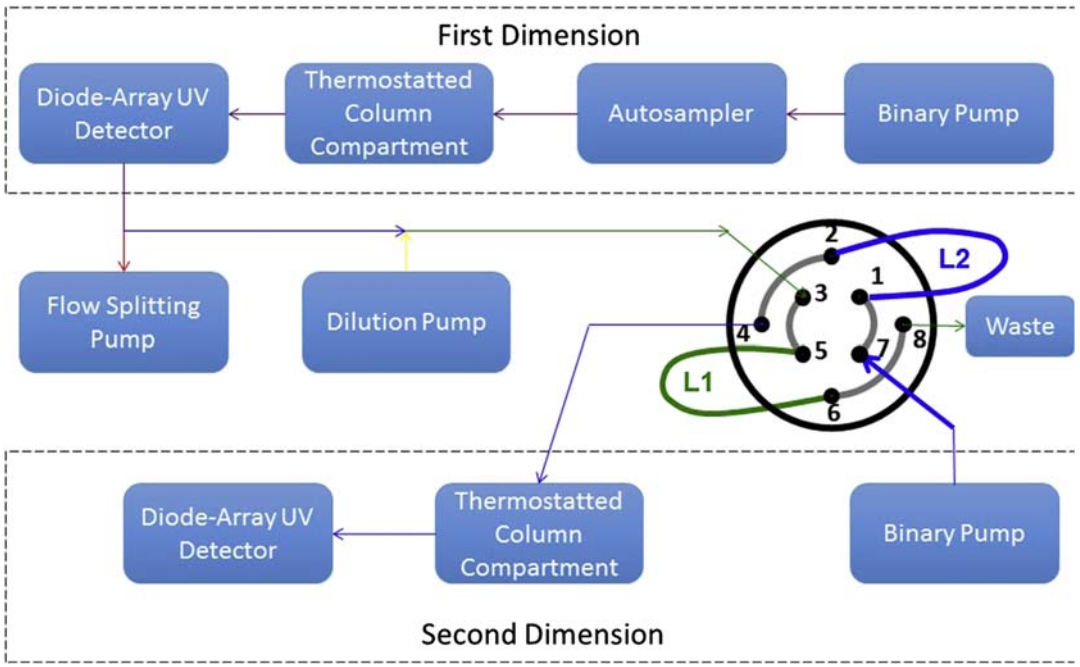

FIGURE 7.26

Instrument configuration used to study the effect of one-dimensional effluent fraction composition and volume on two-dimwnsional resolution and detection sensitivity.

Reprinted with permission of Springer from Stoll, D.R., Talus, E.S., Harmes, D.C., Zhang, K., 2014. Evaluation of detection sensitivity in comprehensive two-dimensional liquid chromatography separations of an active pharmaceutical ingredient and its degradants. Anal. Bioanal. Chem. 407, 265–277. http://dx.doi.org/10.1007/s00216-014-8036-9.

independently vary the volume and composition of the fraction of ^{1}D effluent injected into the ^{2}D column without changing the ^{1}D separation parameters.

Fig. 7.27 shows the impact of the interface conditions on the ability to both detect and resolve low-concentration degradants that coeluted with naproxen in the ^{1}D separation. Panel E shows the ^{1}D separation of naproxen and degradants produced on exposure to light, and Panels A–D show subsections of the resulting LC × LC chromatograms obtained using different interface conditions. In this case, the second dimension reveals the presence of a low-concentration degradant that coeluted with naproxen and was not visible in the ^{1}D chromatogram. Panels B–D all involve direct injection of ^{1}D effluent without any dilution but in decreasing volume. As we move from Panel B to Panel D we see that the widths of the ^{2}D peaks improve, but at the cost of detection sensitivity. In Panel A the ^{1}D effluent was diluted 1:1 with water before injection of the fraction into the ^{2}D column, and the injection volume was increased to 80 μL from 40 μL to accommodate the volume of the diluent. Even though the same volume of actual ^{1}D effluent was injected in both cases, we see that in Panel A the ^{2}D peaks are slightly taller and better resolved compared to Panel B. This is because of the focusing effect of the added water, resulting in narrower, taller, and better resolved peaks.

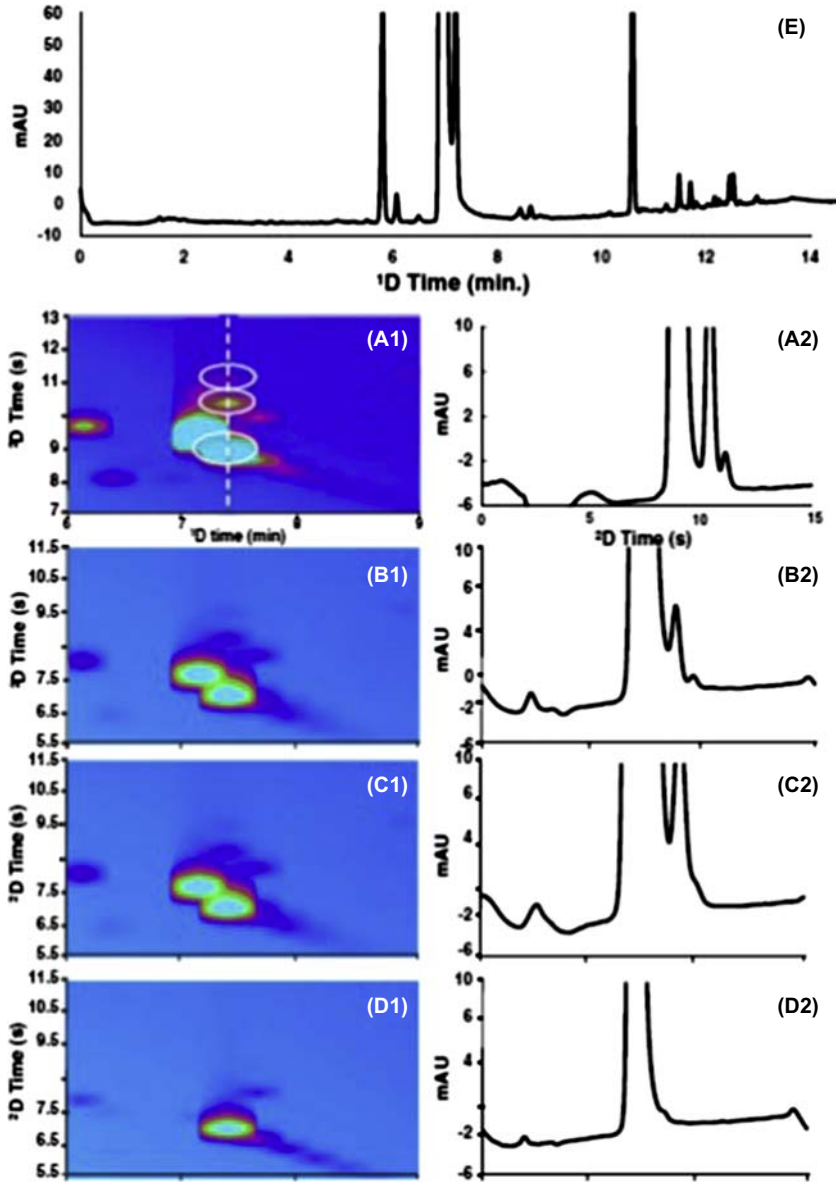

FIGURE 7.27

Effect of interface conditions on the ability to both resolve and detect trace-level degradants coeluting with the main peak (naproxen) in the first dimension of a high quality LC × LC separation of photodegraded naproxen. The one-dimensional (^{1}D) separation is shown in Panel E. Panels A1−D1 are subsections of LC × LC separations focused on the region where naproxen and neighboring peaks elute. Panels A2−D2 show the two-dimensional chromatograms observed at the position indicated by the *white dashed vertical line* in Panel A1. Interface conditions were: (A1/A2) 80 μL injection of ^{1}D effluent after 1:1 dilution with water; (B1/B2) 40 μL injection of undiluted ^{1}D effluent; (C1/C2) 20 μL injection of undiluted ^{1}D effluent; and (D1/D2) 7 μL injection of undiluted ^{1}D effluent.

Reprinted with permission of Springer from Stoll, D.R., Talus, E.S., Harmes, D.C., Zhang, K., 2014. Evaluation of detection sensitivity in comprehensive two-dimensional liquid chromatography separations of an active pharmaceutical ingredient and its degradants. Anal. Bioanal. Chem. 407, 265−277. http://dx.doi.org/10.1007/s00216-014-8036-9.

The examples and data discussed so far in this section are relevant to cases where RP-LC separations are used in both dimensions. Of course, not all 2D-LC applications rely on RP-LC in both dimensions; some combinations of separation modes suffer from the effects of the injected ^{1}D effluent on ^{2}D performance more than others. Fig. 7.28 makes the point that the strength of the ^{1}D effluent relative to the eluent used in the ^{2}D separation has a direct effect on detection sensitivity at the outlet of the ^{2}D column. In some cases, such as the combination of IEX separation, where eluents are primarily composed of aqueous solvents, and RP-LC, these solvent effects are minimal, and in fact fraction volumes that are several-fold larger than the ^{2}D column volume can be used, which translates to great sensitivity. One could argue that this is a major reason why 2D-LC separations of peptides involving IEX and RP-LC have been so successful. On the other hand, when coupling either HILIC or NP-LC separations in the first dimension to RP-LC in the second dimension, these solvent effects can be even more detrimental than they are in the case of coupling two RP-LC separations. This has led the 2D separations community to describe such combinations of separation modes as "incompatible" (Kivilompolo et al., 2011). In fact, 2D-LC separations involving such combinations of modes have been demonstrated (Dugo et al., 2004; François et al., 2006), but at great cost in terms of detection sensitivity. In these cases, the injected volume of ^{1}D effluent must be a small fraction of the ^{2}D column volume to avoid serious deterioration of the ^{2}D column performance.

In addition to the effect of the organic solvent/water composition of the ^{1}D effluent, the pH and concentration of buffering components of the ^{1}D effluent can also significantly impact the performance

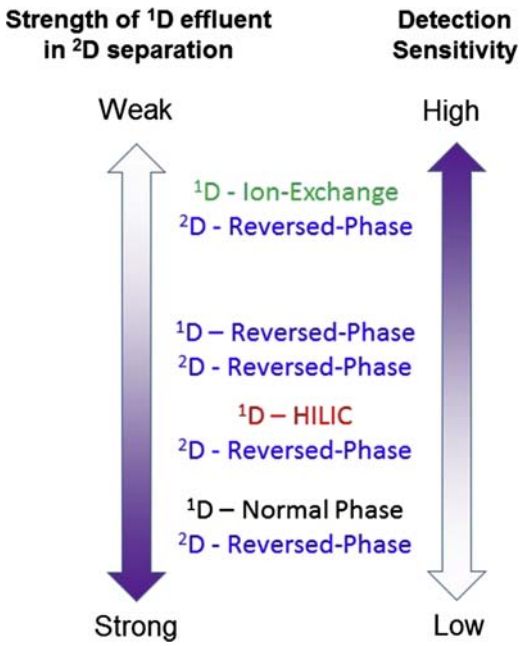

FIGURE 7.28

Effect of the solvent strength of the ^{1}D effluent in the ^{2}D separation mode on detection sensitivity at the outlet of the ^{2}D column. *HILIC*, hydrophilic interaction liquid chromatography.

of ^{2}D separations. In our study of buffer effects on 2D-LC separations of carboxylic acids using RP-LC in both dimensions, we found that these effects can actually be more serious than the effects of the organic solvent/water ratio, causing peak splitting in ^{2}D columns with injection volumes as low as 5 μL. On the other hand, the problem is more easily addressed in this case, because the ^{1}D effluent properties can be adjusted easily through the addition of a small amount of highly concentrated buffer solution. Readers interested in more details on this topic are referred to papers in the literature (Li et al., 2014a; Stoll et al., 2015).

In addition to the online dilution scheme described here, a variety of other approaches have been demonstrated. Ding et al. (2010) and Tian et al. (2006) have used interfaces that allow partial evaporation of the solvent in a fraction of ^{1}D effluent prior to injection into the ^{2}D column. Temperature modulation has been used to first focus analytes in a trapping cartridge mounted on the valve interface and maintained at low temperature, and then release those analytes into the ^{2}D by raising the temperature of the trapping cartridge (Sweeney and Shalliker, 2002; Verstraeten et al., 2011).

The concept of using a solid-phase adsorbent to focus and trap analytes in the interface between dimensions was demonstrated at least 25 years ago in a heartcutting application by Oda et al. (1991). This was also demonstrated in LC × LC applications with relatively slow ^{2}D separations (Cacciola et al., 2007, 2006; Holm et al., 2005; Li et al., 2011; Mihailova et al., 2008; Pepaj et al., 2006; Vonk et al., 2015; Wilson et al., 2007). More recently, however, such trapping functionality has been incorporated into LC × LC systems with faster ^{2}D cycle times, and in a system coupling LC and SFC in the first and second dimensions, respectively (Venkatramani et al., 2016). Figs. 7.29 and 7.30, from the work of Gargano et al. (2016), show an illustration of such a system involving traps in the interface, and comparison of LC × LC separations obtained for a surfactant mixture with either open loops or traps used in the interface. They refer to this approach as "active modulation." The use of the traps provides additional flexibility in method development (e.g., through use of higher flow rates in the ^{1}D), and can reduce the volume of sample injected in each ^{2}D cycle after the analytes have been focused in the trap.

This aspect of the development of 2D-LC is a very active area of research right now, and we can expect significant gains in the way of improvements these developments bring to the technique, including improvements in detection sensitivity, ease of use, and system robustness.

7. METHOD DEVELOPMENT

The topic of method development in 2D-LC could easily be expanded to fill an entire large chapter by itself, thus a detailed discussion of the topic is beyond the scope of this contribution. From the point of view of an analytical chemist, 2D-LC is a very powerful tool because of its flexibility—there are many variables that contribute to the outcome of a separation, and these can be adapted to a wide variety of analytical problems. However, from a user's point of view, the number of considerations can be overwhelming. The challenge, then, is to identify the most important decisions and focus on those first, leaving the other variables for further optimization later in the development process. In the last 10 years there have been several journal articles (Bedani et al., 2012, 2006; Fairchild et al., 2009b; Schoenmakers et al., 2006; Vivó-Truyols et al., 2010) and a book chapter (Murphy and Schure, 2008) describing method development strategies and protocols that can serve as guides to the method development process. Interested readers are encouraged to engage the details of these prior publications. However, some of them are becoming obsolete quickly because of advances in instrumentation

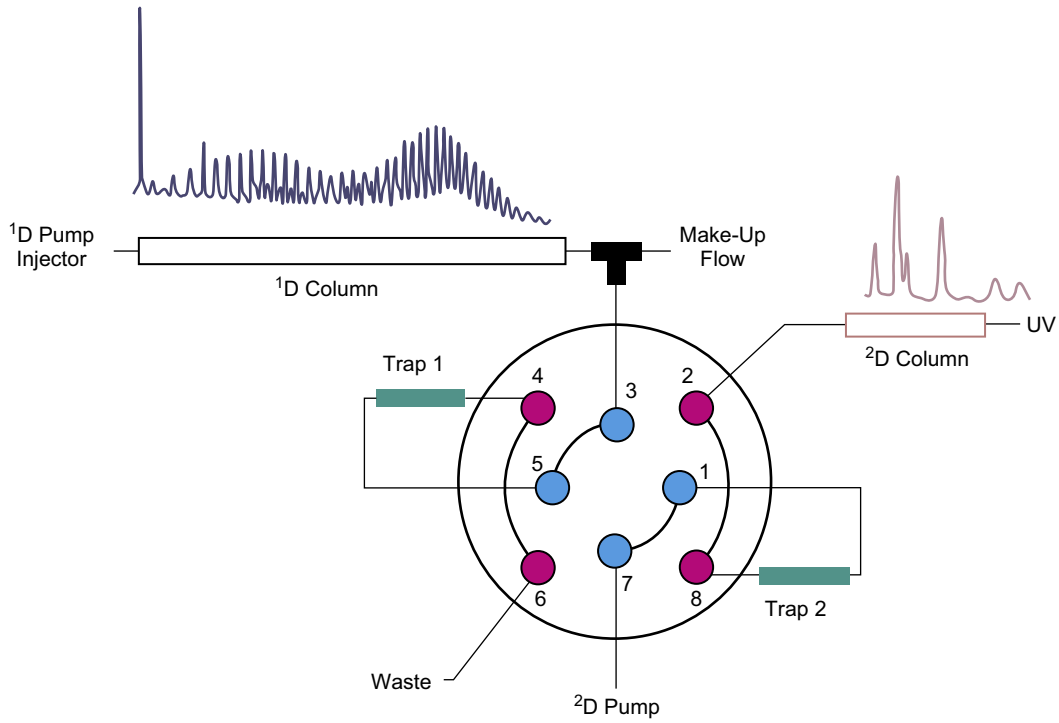

FIGURE 7.29

Illustration of a system for two-dimensional liquid chromatography capable of both online dilution between dimensions and the use of packed traps instead of open sample loops in the valve interface. *^{1}D*, first dimension; *^{2}D*, second dimension.

Reprinted with permission from Gargano, A.F.G., Duffin, M., Navarro, P., Schoenmakers, P.J., 2016. Reducing dilution and analysis time in online comprehensive two-dimensional liquid chromatography by active modulation. Anal. Chem. 88, 1785–1793. http://dx.doi.org/10.1021/acs.analchem.5b04051.

and development of new strategies for dealing with some of the long-standing challenges in method development (e.g., solvent "incompatiblity"). In the following sections, I briefly describe some of the major decisions that must be made early on in the development process, and then finish this subsection with a case study that illustrates this decision-making process with concrete details.

7.1 SELECTION OF TWO-DIMENSIONAL SEPARATION MODE

A decision that has to be made early on in the development process is which mode of 2D-LC separation will be used. As described in Section 6.1, this can range from simple heartcutting separations to more complex but more informative comprehensive separations. Readers are referred to Section 6.1 for a detailed discussion of the different modes, their strengths and weaknesses, and the types of applications they are typically used for. This initial decision will have a significant impact on subsequent decisions, especially concerning choice of column dimensions and operating conditions.

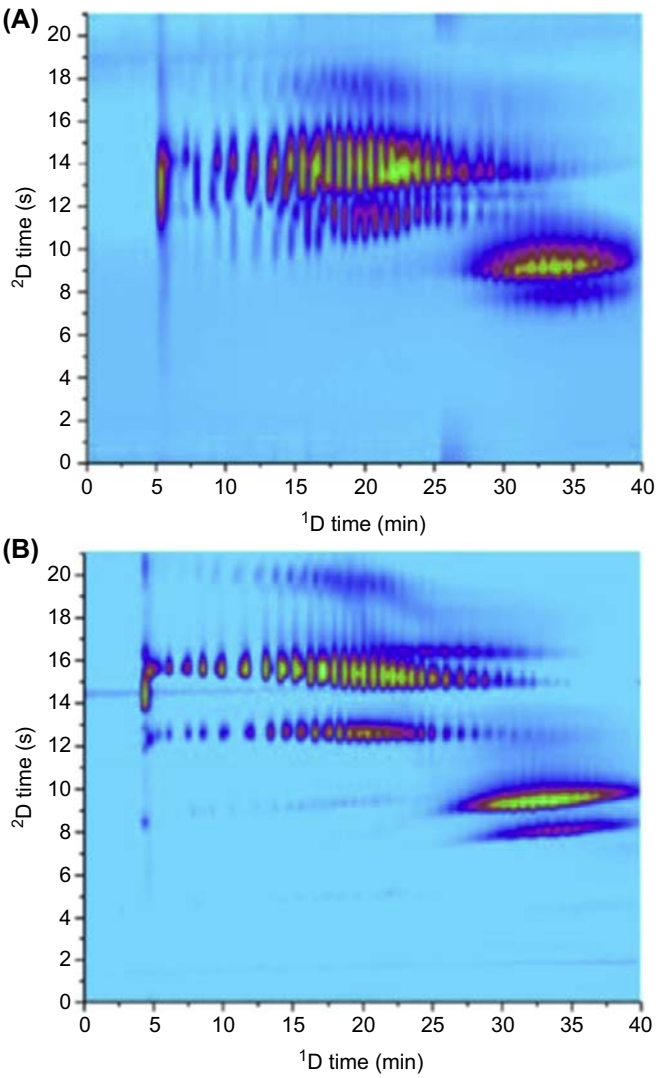

FIGURE 7.30

Comparison of chromatograms obtained from LC × LC separations of tristyrylphenol ethoxylate phosphate surfactants using an interface equipped with open loops (A) or packed traps (B). ^{1}D, first dimension; ^{2}D, second dimension.

Reprinted with permission from Gargano, A.F.G., Duffin, M., Navarro, P., Schoenmakers, P.J., 2016. Reducing dilution and analysis time in online comprehensive two-dimensional liquid chromatography by active modulation. Anal. Chem. 88, 1785–1793. http://dx.doi.org/10.1021/acs.analchem.5b04051.

7.2 SELECTION OF COMPLEMENTARY SEPARATIONS

In Section 5.1.3 I discussed some of the obvious possible combinations of separation modes and some of the potential disadvantages of these combinations. It is critically important at this stage of method development to understand the properties of the molecules in the sample at hand, and think about which separation mechanisms can be used most effectively to exploit the variation in two or more of the chemical characteristics of the analytes. For example, consider a 2D-LC separation of a surfactant sample where the molecules vary significantly in their charge or dipolarity (e.g., by end-group chemistry) and lipophilicity (e.g., by chain length). In a situation like this, it is chemically sensible to use an RP separation in one dimension, which will separate based on lipophilicity, and either IEX or HILIC in the other dimension, which will separate based on end-group charge or dipolarity.

As discussed in Section 5.1.3, and as we (Stoll et al., 2007) and others (Li et al., 2014b) have noted, doing 2D-LC with RP columns in both dimensions is attractive for several reasons. A challenge in this case, however, is selecting two RP columns that will be different enough to be useful together in the context of a 2D-LC method. When the analytes of interest are weak acids and/or bases, then simply changing the pH enough to change the ionization state of the analytes in the two dimensions can bring about a large selectivity change (Snyder et al., 2010b). This means that it is even conceivable to use the same RP column in both dimensions, but with eluents buffered at different pH values. This kind of scheme has been used very effectively for RP × RP separations of peptides (François et al., 2009; Gilar et al., 2005; Vanhoenacker et al., 2015).

In cases where changing the pH alone does not provide enough selectivity difference, significant differences in the stationary phase chemistry are required. The good news is that there are over 1000 commercially available RP phases to choose from today. However, this also presents a significant challenge because it is not feasible to screen them all experimentally, or even a significant fraction of them. Over the past two decades, several models of RP selectivity have been developed that can be leveraged to help identify phases that have complementary selectivities. These include procedures developed by the United States Pharmacopoeia, Katholieke Universiteit Leuven, and Euerby et al. (Snyder et al., 2012). In each case, selectivity data have been compiled for hundreds of phases. The largest single collection of freely available selectivity data has been compiled for the hydrophobic subtraction model (HSM), which was developed by Snyder et al. (2012). Interested readers are referred to their book chapter in *Advances in Chromatography* (Snyder et al., 2012), which contains a comprehensive description of the origins of the model, its strengths and weaknesses, and possible applications of the model and the database. At the time of this writing there are data for nearly 700 phases in the database (www.hplccolumns.org; PQRI Approach for Selecting Columns of Equivalent Selectivity). Briefly, the HSM approach enables a quantitative description of RP selectivity using Eq. (7.8)

$$\log\left(\frac{k_X}{k_{ref}}\right) = H\eta - S^*\sigma + A\beta + B\alpha + C\kappa \tag{7.8}$$

where k_X is the retention factor of any compound X, and k_{ref} is the retention factor of ethylbenzene. The parameters H, S^*, A, B, and C are parameters that are measures of stationary phase characteristics: hydrophobicity (H), steric hindrance (S^*), hydrogen bond acidity (A), hydrogen bond basicity (B), and cation-exchange capacity (C). The corresponding η, σ, β, α, and κ are the corresponding properties of the compound X: hydrophobicity (η), bulkiness (σ), hydrogen bond basicity (β), hydrogen bond acidity

(α), and cationic character (κ). With the H, S^*, A, B, and C values in hand for hundreds of phases, we can probe the data by asking about similarities or differences between phases. This can be done for any pair of columns using the so-called similarity factor (F_s):

$$F_s = \left([w_H(H_1 - H_2)]^2 + \left[w_{S^*}\left(S_1^* - S_2^*\right)\right]^2 + [w_A(A_1 - A_2)]^2 + [w_B(B_1 - B_2)]^2 + [w_C(C_1 - C_2)]^2 \right)^{1/2} \tag{7.9}$$

where the subscripts 1 and 2 on the column parameters indicate the columns being compared, and the terms w_i are weighting factors for each of the phase characteristics. Snyder et al. have asserted that two columns with $F_s < 3$ are similar enough to be practically "equivalent," and columns with $F_s > 50$ are different enough to be useful in applications where large selectivity differences are desired, such as 2D-LC. For the purpose of identifying pairs of phases with complementary characteristics, one can simply choose one column of the pair (Column A), and then calculate F_s for all possible pairs of columns involving Column A and identify those phases that produce the largest F_s values. This is tedious, however, which has led groups to establish more visual ways of exploring the HSM database (Græsbøll et al., 2014; Johnson et al., 2012; Zhang and Carr, 2009). One of these that is very intuitive involves plotting the column parameters in a pseudo-three-dimensional triangular selectivity space (Zhang and Carr, 2009). The parameters S^*, B, A, and C are first normalized to the parameter H. Then, any combination of three of the parameters (e.g., S^*/H, B/H, and C/H) can be plotted in a triangle. An example of such a plot is shown in Fig. 7.31. Each point in this space represents a single column. For phases that are very different, the distance between two points is a measure of how chemically different they are. The red, green, and yellow points provide an example of this. In this illustration, the Zorbax SB-C18 phase was chosen as the reference phase. The yellow point, which corresponds to a different Agilent C18 phase, is very close to the red point—indeed, the F_s value for this pair of phase is just 13. On the other hand, the red point for the Zorbax Bonus-RP phase is far away from the green point, and the F_s value for this pair of phases is 266. In this way, the selectivity triangles can be used to quickly identify pairs of phases that are likely to be different enough to be useful in 2D-LC separations.

7.3 SELECTION OF PARTICLE SIZES AND COLUMN DIMENSIONS

It is important to recognize that optimal combinations of column dimensions and particle sizes in the first and second dimensions of 2D systems are frequently specific to a given application. Challenges associated with specific groups of analytes and/or sample matrices and specific analytical goals (e.g., throughput, detection limits) can have a significant influence on these decisions. Nevertheless, it is useful to consider some general trends based on discussion of 2D-LC method development in the literature and our own practical experience.

7.3.1 First Dimension

Benefits and Challenges Associated with Narrow Columns (1.0−2.0 mm i.d.)

- Narrow ^{1}D columns allow one to work near the optimal velocity of these columns (i.e., in a van Deemter sense) without having to transfer very large volumes of ^{1}D effluent to the ^{2}D column.
- Using gradient elution with these columns requires the use of pumps with low gradient delay volumes (e.g., <200 μL), otherwise long gradient delay times will result in wasted analysis time (see Section 6.2.2 for more detail).

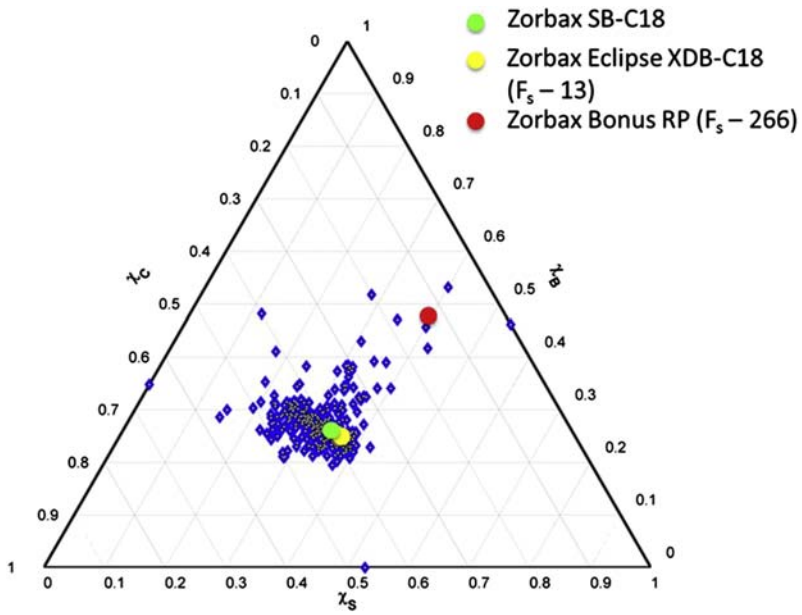

FIGURE 7.31

Selectivity classification of 632 reversed-phase columns using the S-B-C triangle with weighting factors inversely related to the range of each parameter (e.g., S/H), and normalized to the range of S^*. The coordinates of three specific phases are highlighted, along with the calculated F_s values for two of the phases in comparison to Zorbax SB-C18.

- Narrow ^{1}D columns will have lower loadability, in both volume and mass terms, compared to wider columns.

Benefits and Challenges Associated with Wide Columns (3.0−4.6 mm i.d.)

- Wide ^{1}D columns will have higher volume and mass loadability compared to narrow columns.
- Wide ^{1}D columns are more compatible with pumping systems having a large gradient delay volume.
- Use of flow rates corresponding to the optimal velocities for these columns results in very large fractions of ^{1}D effluent that must be transferred to the ^{2}D. This in turn leads to challenges related to the mismatch between solvents used in the two dimensions (see Section 6.3 for more detail).

7.3.2 Second Dimension

Benefits and Challenges Associated with Narrow Columns (1.0−2.0 mm i.d.)

- The primary potential benefit of using narrow ^{2}D columns is improved detection sensitivity (see Section 6.3 for details). Additional benefits may be derived from lower flow rates through these columns, including: less solvent cost and waste; and, ability to directly couple with mass spectrometry.

- Use of low flow rates and gradient elution conditions may lead to prohibitively long gradient delay and flush-out times—this is especially the case with 1 mm i.d. columns.
- These columns will be more sensitive to mismatch between the solvents used in the first and second dimensions because of their small dead volumes.

Benefits and Challenges Associated with Wide Columns (3.0−4.6 mm i.d.)

- Wide ^{2}D columns allow the use of high ^{2}D flow rates (e.g., >3 mL/min), which are helpful for achieving very fast ^{2}D cycle times. However, this leads to high solvent consumption and waste generation costs.
- Wide ^{2}D columns can mitigate the effects of mismatch between solvents used in the two dimensions; however, this comes at the cost of detection sensitivity.

In general, 2D-LC methods will involve ^{2}D separations that are much faster than the ^{1}D separation. With this in mind, it is generally true that smaller particles are more necessary in the second dimension than in the first dimension (Carr et al., 2009; Desmet et al., 2015; Matula and Carr, 2015). Many studies published in the past 5 years have involved ^{2}D columns with particles in the sub-two- to sub-three-micron diameter range. For LC × LC separations in particular, the first dimension need not be rigorously optimized because the effective performance of the ^{1}D separation will be dominated by the effects of undersampling in most cases (Li et al., 2009). In cases where the ^{1}D separation can be sampled very rapidly [e.g., one sample per second, as in sLC × LC (Groskreutz et al., 2012a)] or where information from the ^{1}D chromatogram obtained prior to sampling is used [e.g., as in 2D-assisted liquid chromatography (2DALC) (Cook et al., 2015)], the importance of optimizing the ^{1}D separation is elevated significantly.

7.4 SELECTION OF OPERATING CONDITIONS

I suggest the following steps to make decisions about operating conditions in the method development process. As with the preceding section, these are general guidelines, and specific applications may demand a different approach.

1. Choose the mode of 2D separation that will be used (i.e., LC−LC, LC × LC, etc.—see Section 6.1). This will have a significant impact on the following steps, primarily because different modes of 2D separation demand different levels of speed in the ^{2}D separation.
2. Determine the speed level needed in each ^{2}D separation. For LC × LC separations this should be in the range of 12−60 s. At the other extreme, ^{2}D separations for LC−LC may be 15 min or longer. For mLC−LC, sLC × LC and stop-and-go modes, cycle times for ^{2}D separations will be between these extremes. At this stage, think about whether isocratic or gradient elution conditions will be used in the ^{2}D. For LC × LC separations involving gradient elution in the second dimension, a ^{2}D pump with a low gradient delay volume is an absolute requirement.
3. Given the desired ^{2}D speed level, choose the ^{2}D column diameter and length and particle size. Detailed considerations are described in Section 7.3. For the fastest ^{2}D cycle times, narrow ^{2}D columns (2.1 or 1.0 mm i.d.) are required. With longer ^{2}D cycle times there is more flexibility. Larger diameters are less susceptible to peak broadening because of mismatch between the ^{1}D and ^{2}D eluents, but one must recognize that there is a trade-off with detection sensitivity here. For the fastest ^{2}D separations, short (2−5 cm) columns with small (sub-two- to sub-three-micron) particles should be used. For longer ^{2}D separations, longer lengths up to 15 cm will be

optimal; particle sizes in the 3 μm range are preferred. There is good guidance in the literature for choosing optimal length and particle size once the column diameter has been selected (Carr et al., 2009; Desmet et al., 2015).

4. Choose a reasonable sample loop size for the valve interface. This is the volume of ^{1}D effluent that will be injected into the ^{2}D column in each ^{2}D separation cycle. At this point one must decide if the ^{1}D effluent will be diluted (Stoll et al., 2014) or split (Filgueira et al., 2011) prior to entering the loop. Larger loop volumes are preferred for high detection sensitivity in the ^{2}D, but one has to be careful not to get into a volume overload situation because this will compromise resolution of the ^{2}D column. Currently, commonly used loop volumes are in the 10−100 μL range.
5. Choose the flow rate through the ^{1}D column. This is dictated by the sampling time (t_s) and the fraction volume that will be injected into the ^{2}D column. Two examples are useful here. Suppose we use a sampling time of 20 s, a loop volume of 40 μL, and there is no dilution or splitting of the ^{1}D effluent. In this case the ^{1}D flow rate must be 120 μL/min if we fill the loop 100%. In practice, we generally fill the interface loop 80%. If the ^{1}D effluent is diluted 1:1 with weak solvent prior to filling the loop, then the ^{1}D flow rate must be decreased to 60 μL/min.
6. Choose the diameter, length, and particle size for the ^{1}D column. Given the flow rates arrived at in the preceding step, it is clear that in most cases a 2.1 mm i.d. column is preferred. In cases where even lower flow rates are needed, one may consider using 1.0 mm i.d. columns. It is important to consider again the characteristics of the pumping system used in the first dimension, particularly if gradient elution will be used. If a pump with a large gradient delay volume cannot be avoided (e.g., >200 μL), one should consider using a higher ^{1}D flow rate and then split the effluent prior to transfer to the second dimension (Filgueira et al., 2011). As in Step 2, there is good guidance in the literature for choosing good combinations of column length and particle size, once the diameter has been chosen.
7. Finally, once the ^{1}D column diameter has been selected, the injection volume for the ^{1}D column can be set. Obviously larger injection volumes will generally lead to better detection limits, but one has to avoid mass and/or volume overload conditions.

Once one has made selections for the parameters outlined in the steps above, the 2D separation can be optimized according to the goals of the analysis, with a focus on performance metrics such as analysis time, detection limits, peak capacity, or resolution of specific pairs of peaks. One very powerful step in this optimization process is adjustment of elution conditions in the second dimension over the course of the 2D separation. In other words, the ^{2}D elution conditions used in the first 2 min of a 2D separation need not be the same as those used in the rest of the separation, and changing these dynamically can lead to significant improvements in one or more of the performance metrics mentioned here. The potential for this improvement is best illustrated by way of example. Fig. 7.32, adapted from the work of Li and Schmitz (Li and Schmitz, 2013), shows examples of the types of elution schemes that can be used in the second dimension, ranging from a consistent, repeating ^{2}D gradient (Panel A) to a so-called shifted gradient (Panel D) where the beginning and ending compositions used in each ^{2}D gradient are slightly different. Good examples of the impact of optimized ^{2}D elution conditions on usage of the available 2D separation space are shown in Fig. 7.33, from the work of the Jandera group (Jandera et al., 2015). Adopting dynamically adjusted ^{2}D elution conditions roughly doubles the fraction of the separation space that is actually used (compare Panels A and C). An additional benefit of using the so-called parallel gradients in Fig. 7.32C is that the

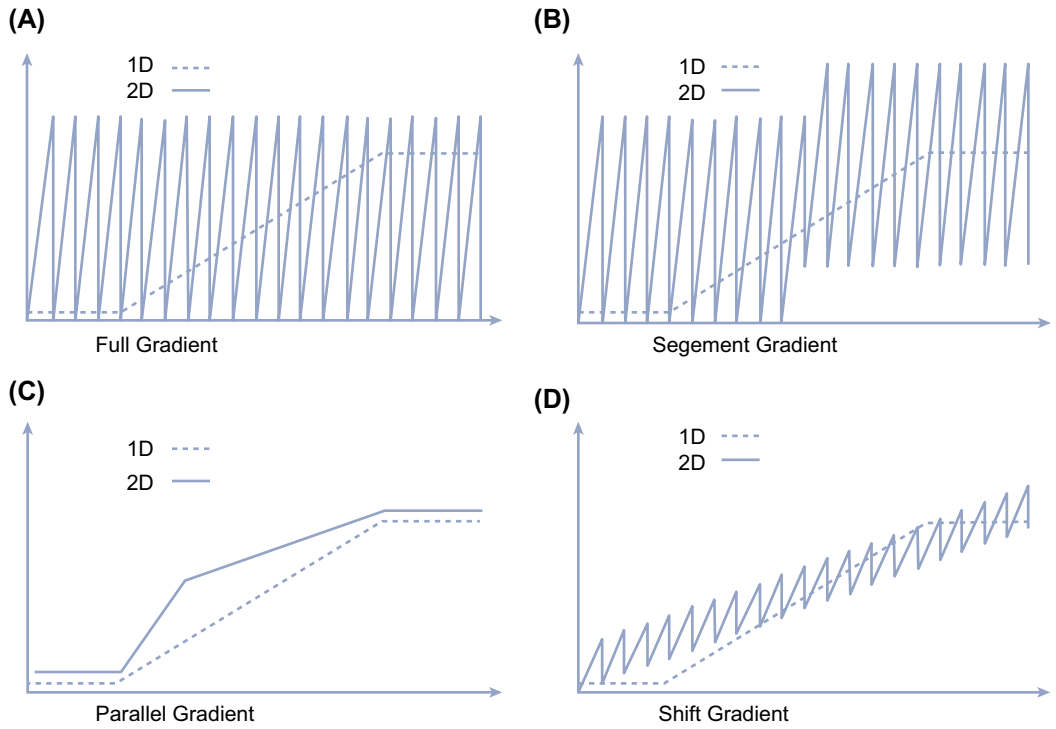

FIGURE 7.32

Examples of dynamic elution profiles that can be used in the second dimension of two-dimensional liquid chromatography systems. In each plot the *dashed trace* represents the eluent composition used in the first dimension, and the *solid trace* represents the eluent composition used in the second dimension.

Reprinted with permission of Springer from Li, D., Schmitz, O.J., 2013. Use of shift gradient in the second dimension to improve the separation space in comprehensive two-dimensional liquid chromatography. Anal. Bioanal. Chem. 405, 6511–6517. http://dx.doi.org/10.1007/s00216-013-7089-5.

use of isocratic conditions in each ^{2}D separation enables much faster sampling of the ^{1}D separation. On the other hand, this also results in wider ^{2}D peak widths because there is no compression of peak widths under isocratic conditions.

8. DETECTION

Many of the guidelines used for making decisions about detection in 1D chromatography apply in 2D-LC as well. However, there are some important characteristics of 2D-LC that change things a bit—in this section I will focus on those aspects that are different and deserve attention. In the case of coupling 2D-LC to MS detection in particular, interested readers are referred to the thorough review of Donato et al. (2012) that is focused on this topic.

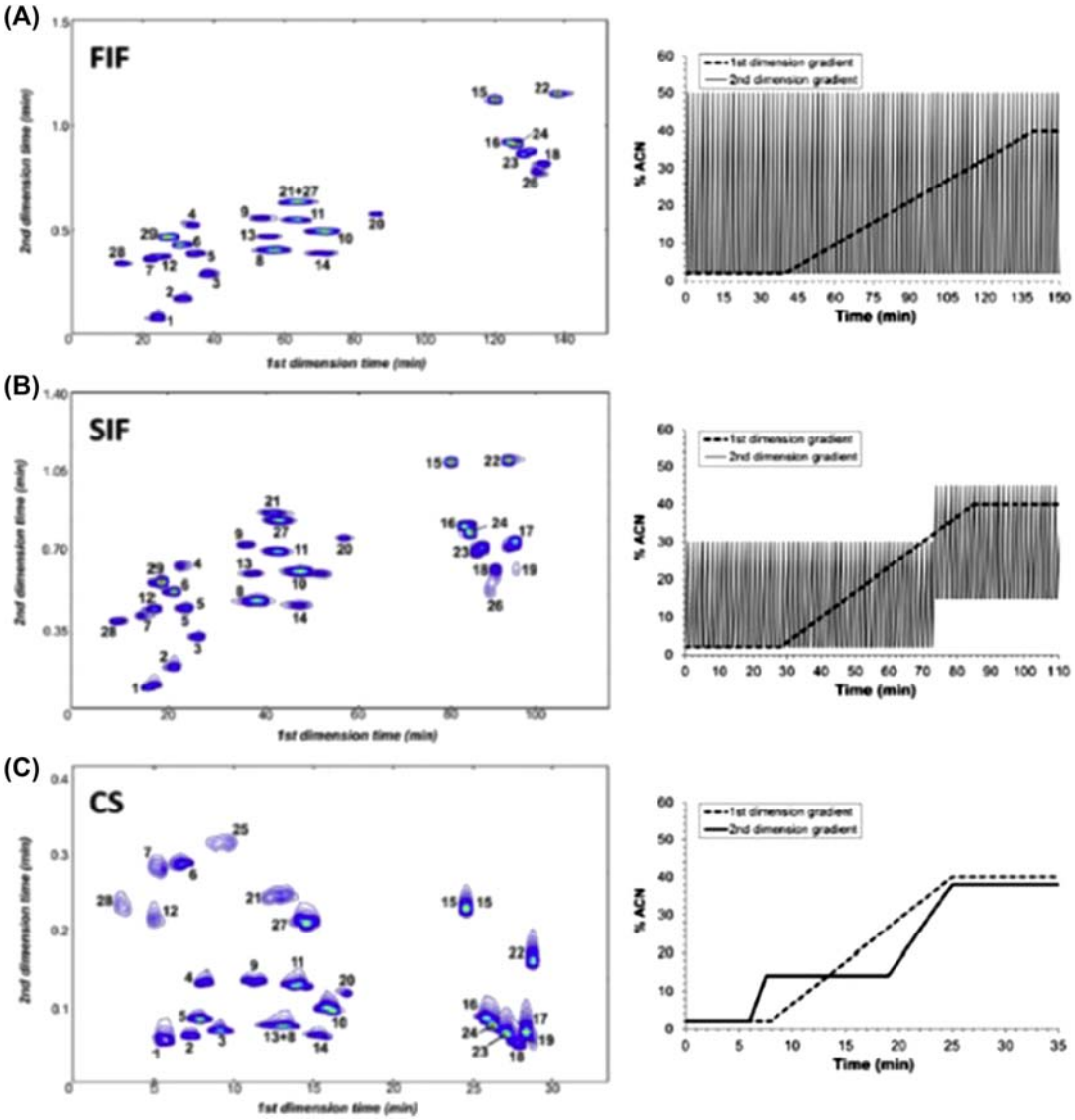

FIGURE 7.33

Examples of the effect of ^{2}D elution conditions on the utilization of the 2D separation space in LC × LC separations of phenolic acids and flavones. The separation in Panel (A) is obtained when the same ^{2}D gradient is used throughout the 2D separation. The separation in Panel (B) is obtained when the 2D separation is split into two segments, and different gradient elution programs are used in each segment. Finally, Panel (C) shows that the peaks can be further spread out by using isocratic conditions in the second dimension that are optimized over the course of the 2D analysis time to maximize use of the available separation space.

Reprinted with permission of Springer from Jandera, P., Hájek, T., Staňková, M., 2015. Monolithic and core–shell columns in comprehensive two-dimensional HPLC: a review. Anal. Bioanal. Chem. 407, 139–151. http://dx.doi.org/10.1007/s00216-014-8147-3.

8.1 ACQUISITION SPEED

As was discussed in Section 7.3, ^{2}D separations are generally much faster than ^{1}D ones in 2D-LC. This means that one need not be so concerned with acquisition speed for detectors employed between the ^{1}D column and the sampling interface. Indeed, slower acquisition is preferred at this point to allow smoothing of the signal to improve signal-to-noise ratios. In the second dimension, however, acquisition speed is often very important, especially in LC × LC work where peak widths less than 1 s are not uncommon. This is not a problem for state-of-the-art spectroscopic detectors (e.g., UV absorbance, fluorescence) that are capable of acquisition rates exceeding 100 Hz. Some types of mass analyzers are more suitable than others for MS detection with high acquisition rates. Time-of-flight and quadrupole-time-of-flight are especially well suited to fast separations, and this has been borne out in the recent literature describing coupling of 2D-LC and MS detection (Donato et al., 2012; Stoll et al., 2016).

8.2 EXTRA-COLUMN DISPERSION

Although dispersion in the tubing and connections between the ^{1}D column and the ^{1}D detector are important to the ^{1}D peak width, dispersion in the ^{1}D detection element itself (e.g., UV flow cell, MS ionization source) are usually not that important because relatively large fractions of the ^{1}D effluent are transferred to the ^{2}D column, which results in some amount of remixing of ^{1}D peaks anyway. Exceptions to this exist in the case of noncomprehensive 2D separations, where fractions of ^{1}D effluent can be very narrow in time (<5 s), and may be small in volume as well (e.g., <5 μL), depending on the conditions of the experiment. In these cases, one should carefully consider the contributions of flow-through detectors to the variance of the ^{1}D peaks as they travel to the sampling interface. Dispersion in the ^{2}D detector, on the other hand, can be much more detrimental to the resolving power of the 2D system. As we approach ^{2}D peak variances on the order of 10 μL^2 (Haidar Ahmad et al., 2015), it is becoming increasingly important to choose detection elements that are designed with low dispersion in mind.

8.3 BACKGROUND CHARACTERISTICS OF SECOND DIMENSION DETECTION

In comparison to typical conditions used in 1D-LC, several aspects of ^{2}D separations in 2D-LC are extreme. For example, it is common to have injection volumes of ^{1}D effluent that are a significant fraction of the ^{2}D column dead volume. It is usually the case that the composition of the ^{1}D effluent that is injected is significantly different from the ^{2}D eluent, with differences in organic solvent type, and buffer type and pH. Finally, when gradient elution is used, the gradients are usually quite fast in absolute time units (e.g., 10−60 s). These factors can lead to significant detector background disturbances (Stoll et al., 2014) and/or relatively steep baseline slopes in the case of gradient elution (Filgueira et al., 2012). These features of the detector background can, in turn, have a significant impact on signal-to-noise ratios at the ^{2}D detector and have negative effects on the implementation of peak detection (Filgueira et al., 2012) and chemometric data analysis tools (Bailey and Rutan, 2011).

8.4 DETECTION SENSITIVITY

As was discussed in Section 6.3, poor detection sensitivity at the ^{2}D column outlet has historically been a weakness of 2D-LC methods. This often results from a mismatch between the eluent compositions used in the two dimensions, which limits the volume of ^{1}D effluent that can be injected into the ^{2}D

column without compromising the performance of the ^{2}D separation. Aside from the strategies discussed in Section 6.3 to overcome these limitations, detection sensitivity can also be improved by increasing the signal-to-noise ratio at the point of detection following the ^{2}D separation. The most straightforward example of this is increasing the path length in a UV detector flow cell (Pursch and Buckenmaier, 2015). In principle, detection limit should improve in proportion to the increase in the detection path length. This is not strictly observed in practice with commercial instruments because an increase in path length is accompanied by an increase in cell volume, which in turn causes some peak dispersion and loss of peak height. The anticipated improvement also assumes that detector noise is independent of path length, which may not always be observed.

9. DATA ANALYSIS, SOFTWARE, AND QUANTITATION

Data handling and analysis is more complex in 2D-LC compared to 1D-LC. This presents both challenges that require the development of new analysis strategies and tools, and opportunities for the application of sophisticated chemometric methods that benefit from the high dimensionality of the data. As with instrumentation for 2D-LC, which a decade ago was largely "home-built" for most users, so too were many algorithms reported in the literature as "written in-house" for the analysis of data from 2D-LC experiments. Currently, there are good commercially available packages that provide functionalities for at least the most essential data processing and analysis steps in 2D-LC. A thorough discussion of these aspects is beyond the scope of this contribution. Readers interested in these topics are encouraged to study the review of Matos, Duarte, and Duarte (Matos et al., 2012). Unfortunately, our understanding of the fundamentals of quantitation and the development of software tools are not as advanced in 2D-LC as they are in 1D-LC—this is not surprising given the head start in 1D-LC of 30 years or so. But, the 2D-LC community is catching up quickly, and the future is promising in this area.

9.1 DATA STRUCTURES AND HANDLING

Fig. 7.34 shows one of the often-cited figures (Adahchour et al., 2006) that clearly illustrates how data from 2D-LC experiments are handled to produce 2D chromatograms.

In the absence of software dedicated to the analysis of 2D-LC data, these steps can be accomplished by first exporting raw data from the chromatography data system, and then manipulating those data using any of a number of programming and analysis packages such as MatLab or Mathematica. While this process is not onerous for spectroscopic data (e.g., UV absorbance, or fluorescence detection), it becomes practically untenable for high-resolution MS data because of the large volumes of data involved (e.g., >1 GB of data per analysis) and proprietary MS data file formats. Thus, the continued evolution of dedicated software for analysis of 2D-LC data is very important. From an analyst's point of view, it is far better to dedicate time to optimization of methods and data collection, than to development of software for data analysis.

9.2 DESIRABLE FEATURES OF SOFTWARE SUPPORTING TWO-DIMENSIONAL LIQUID CHROMATOGRAPHY

I have written this section to serve as a series of suggestions to new users considering getting involved in 2D-LC, either through shared equipment or a new equipment purchase. Following are several

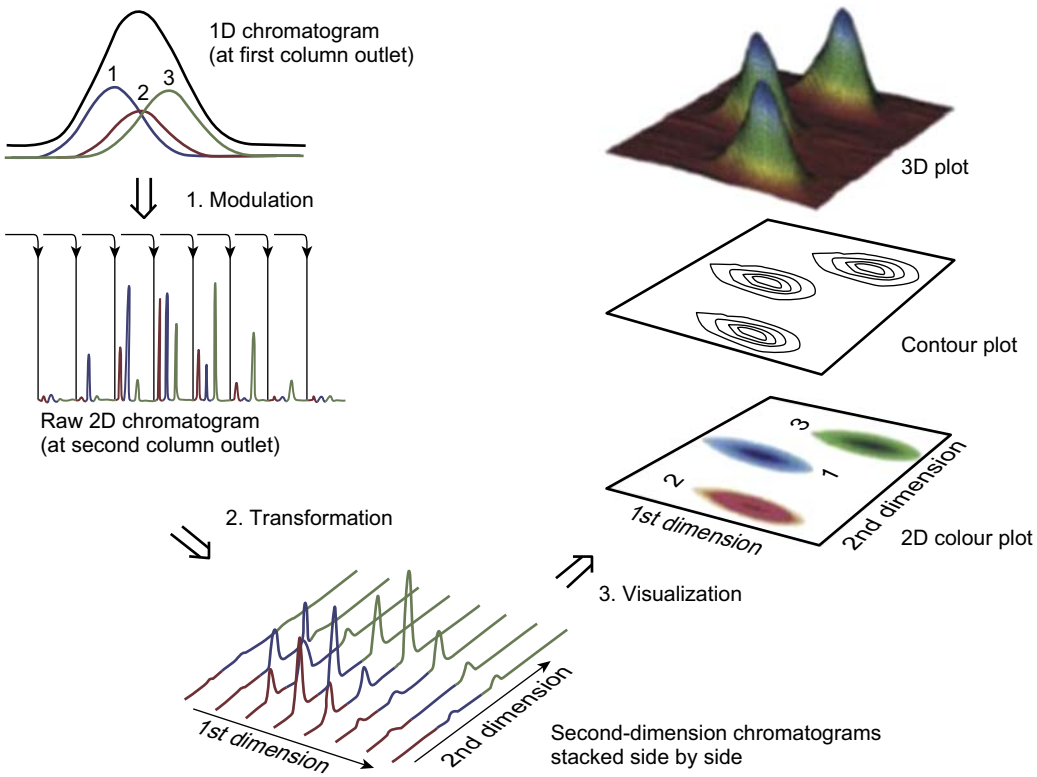

FIGURE 7.34

Illustration of the flow of information in a two-dimensional liquid chromatographyexperiment. The scenario shown here is precisely applicable to LC × LC, but can be extended to other implementations of 2D separation. (1) Peaks eluting from the ^{1}D column are sampled multiple times, which leads to the appearance of a particular compound in multiple ^{2}D chromatograms. (2) The data from these ^{2}D separations are then transformed into a 2D array of data where the two dimensions are ^{1}D and ^{2}D time. This array can then be visualized as a contour plot or a 2D topographic map, both of which can be colored in various ways to aid visualization.

Adapted with permission from Adahchour, M., Beens, J., Vreuls, R.J.J., Brinkman, U.A.T., 2006. Recent developments in comprehensive two-dimensional gas chromatography (GC×GC) – introduction and instrumental setup. TrAC Trends Anal. Chem. 25, 438–454. http://dx.doi.org/10.1016/j.trac.2006.03.002. Copyright 2006, Elsevier.

desirable features of software one might use for 2D-LC, not only for data analysis, but also for instrument control and data acquisition.

9.2.1 Instrument Control and Acquisition

As implementations of 2D-LC separations have become more creative and sophisticated, the need for dedicated software for instrument control and data acquisition has increased. For example, the concept of shifted gradients discussed in Section 7.4 is straightforward in principle, but is very tedious to

implement if gradient tables have to be entered on a line-by-line basis. Likewise, the concepts associated with the implementation of mLC–LC and sLC × LC discussed in Section 6.1 are straightforward, but leaving it to the user to keep track of all of the timed events (e.g., valve switches and gradient starts) is tedious and prone to error. Finally, software that "knows" which detector signals belong to which detector in the system facilitates efficient and effective use of all of the data that results from a single 2D-LC separation. Using software that is designed with these 2D-LC-specific operational features in mind again allows the user to focus more on the chromatography concepts and less on the actual implementation.

9.2.2 Data Processing—Peak Finding and Integration

The strategies used for peak finding and integration in 1D chromatography are not directly applicable to 2D-LC data. This has motivated a number of groups to develop and study alternatives that are more effective in the 2D case (Allen et al., 2012; Latha et al., 2011; Vivó-Truyols and Janssen, 2010). Peak finding is complicated by the fact that in 2D chromatograms we are interested in the evolution of the detector signal in two dimensions rather than a single dimension. Furthermore, the characteristics of the detector background (i.e., baseline) are different in the two dimensions (Filgueira et al., 2012), often more pronounced in the second dimension of 2D-LC compared to 1D-LC, and different enough from those in GC × GC that algorithms cannot be directly employed with LC × LC data. One of the most pronounced challenges, which is present in 1D chromatography but only in one dimension, is variability in ^{2}D retention time—both between 2D-LC analyses and between ^{2}D separations within a single 2D-LC analysis (Reichenbach et al., 2009). For compounds that are present in multiple fractions of ^{1}D effluent transferred to the ^{2}D and thus appear in multiple adjacent ^{2}D separations, this variability in ^{2}D retention time can make the assignment of multiple ^{2}D peaks to a single ^{1}D peak difficult. This is especially true in cases where unsupervised peak detection is used, and can lead to artificial peak splitting.

9.2.3 Advanced Processing—Application of Chemometric Methods

The higher dimensionality of data obtained from 2D-LC experiments compared to 1D-LC lends itself to processing using advanced chemometric methods. These methods enable extraction of chemically meaningful information by mathematical means that would remain obscured if we only relied on the physical separation of compounds as represented by 2D chromatograms (Stoll et al., 2007). The most powerful approaches involve the use of multichannel detectors along with two dimensions of chromatographic separation (e.g., multiple wavelength UV absorbance, or MS detection at multiple masses). So long as the UV or mass spectra of two overlapping chromatographic peaks are slightly different, they can be resolved by chemometric means even with chromatographic resolution in each dimension as little as 0.2 (Cook et al., 2015). This is remarkable considering that a resolution of about 1.5 is generally required for accurate quantitation in 1D-LC, and the fact that resolution is very expensive in terms of analysis time (see Section 5.3.1).

9.3 QUANTITATION

When comparing the quantitative performance of 2D-LC to that of 1D-LC it is convenient to use metrics such as accuracy and precision. 2D-LC has the potential to improve the accuracy of quantitative determinations, especially for complex samples that lead to crowded chromatograms.

When relatively nonselective detectors are used (e.g., UV absorbance), the potential for additional peak capacity and/or selectivity provided by a 2D separation compared to a 1D one simply reduces the degree of peak overlap in chromatograms. This reduces the likelihood that an interfering peak, whether known or unknown, will be overlapped with the peak for a target analyte that is being quantified, which would lead to an overestimation of the concentration of the target analyte (Bailey et al., 2012). On the other hand, even when highly selective detection is used (e.g., high-resolution MS or tandem MS) the potential for additional separation and/or selectivity provided by a 2D method can improve accuracy by reducing matrix effects (Donato et al., 2012; Groskreutz et al., 2012b; Pascoe et al., 2001). This is especially valuable in cases where isotope-labeled standards are either not available or prohibitively expensive, as the elimination of matrix effects enables achievement of good accuracy when using external standards for signal calibration (Simpkins et al., 2010).

The precision of quantitation in 2D-LC, however, is quite a different matter. Whereas in 1D-LC we are accustomed to percent relative standard deviations (%RSDs) for peak areas on the order of 1% or less for replicate injections, the data we see in the 2D-LC literature are generally not this precise, particularly for LC × LC separations. A quick survey of papers reporting peak area/volume precision reveals %RSDs in a range of about 1%−10% (Elsner et al., 2014; Mondello et al., 2008; Stevenson and Guiochon, 2013; Stoll et al., 2014, 2008; Vanhoenacker et al., 2015). In our own experimental work, we have measured the precision of peak areas obtained using detectors placed at the outlets of both the ^{1}D and ^{2}D columns in LC × LC systems to help understand the contributions of each part of the system to the total variance in peak area (Stoll et al., 2014, 2008). In a theoretical study of quantitative precision in LC × LC, Thekkudan et al. (2010) used simulations in an attempt to identify the factors that have the greatest influence on ^{2}D peak area variation. After considering factors including the modulation ratio (i.e., the number of samples of a ^{1}D peak that are transferred to the ^{2}D) and sampling phase (i.e., the time at which sampling a ^{1}D peak starts relative to its native centroid) they concluded that the poorer precision of peak areas observed in LC × LC experiments (4%−5%) compared to simulations (∼2%) may be due to imprecision in sampling the effluent from the ^{1}D column. The general observation that ^{2}D area is less precise than ^{1}D area, even in the same LC × LC system, in turn led us to test the idea that data from the ^{2}D detector could be used to inform the data analysis, but that quantitation would ultimately be based on data from the ^{1}D detector—we refer to this approach as (2DALC) (Cook et al., 2015).

Noncomprehensive 2D-LC separations present different challenges and opportunities relevant to quantitative performance. On one hand, simple heartcutting approaches require that a fraction of ^{1}D effluent much larger than the volume of the ^{1}D peak itself is transferred to the ^{2}D column to ensure that the peak is transferred quantitatively. If this is not done, then any shifts in ^{1}D retention of the peak will lead to significant variation in peak area measured at the ^{2}D detector. On the other hand, hybrid approaches such as sLC × LC effectively break several of the linkages between ^{1}D and ^{2}D parameters used in LC × LC separations, allowing more flexibility in the sampling process. For example, the ability to transfer a ^{1}D peak to the ^{2}D column as a series of small volumes enables quantitative transfer without the use of very large sample loop volumes. Initial reports of the quantitative precision of sLC × LC separations have been impressive—typically less than 1% RSD (Groskreutz et al., 2012a; Pursch and Buckenmaier, 2015).

10. FURTHER READING—SELECTED REVIEW ARTICLES

Much of this chapter is written with a general view of 2D-LC in mind. Of course, in every application area there are important details associated with the characteristics of analytes and sample matrices encountered, and typical analytical objectives that can significantly influence one or more of the aspects of the guidance discussed here (e.g., column selection). For this reason, readers interested in particular application areas are strongly encouraged to seek out review articles on the implementation of 2D-LC in these specific areas to increase their understanding of the nuances associated with the use of 2D-LC in these areas. Whereas 10 years ago most reviews on 2D-LC were more general in nature, currently several reviews are appearing that are more focused on the use of 2D-LC in specific areas. Table 7.4 provides a summary of a selection of these reviews, as well as some important general reviews.

Table 7.4 Summary of a Selection of Important Review Articles on Two-Dimensional Liquid Chromatography (2D-LC)

Application Area	Application Focus	Research Group	Year	References
General	Comprehensive review; focus on practical issues	Carr et al.	2007	Stoll et al. (2007)
General	Comprehensive review; focus on theoretical issues	Guiochon et al.	2008	Guiochon et al. (2008)
Proteomics	Comprehensive 2D-LC separations of peptides	Mondello et al.	2011	Donato et al. (2011)
Pharmaceutical analysis	Potential for 2D-LC in pharmaceutical analysis	Zhang et al.	2013	Zhang et al. (2013b)
Polymers	Characterization of synthetic polymers	Schoenmakers	2014	Schoenmakers and Aarnoutse (2014)
General	Separations with RP in both dimensions	Schmitz	2014	Li et al. (2014b)
Polymers	Characterization of polymers and biopolymers	Kilz and Radke	2015	Kilz and Radke (2015)
Bioanalysis	Overview of 2D-LC used for analysis of biological samples	Stoll	2015	Stoll (2015)
Traditional Chinese medicines (TCMs)	Characterization of TCMs	Li et al.	2016	Li et al. (2016)
Food analysis	Analysis of polyphenols in food	Mondello et al.	2016	Cacciola et al. (2016)
Pharmaceutical analysis	Characterization of biotherapeutic proteins	Stoll et al.	2016	Stoll et al. (2016)

11. FUTURE OUTLOOK

I believe that in the next 5 years we will see the most impactful gains in the following three areas.

1. Improvements in interfacing between the two dimensions of 2D-LC systems—The current challenges in this aspect of 2D-LC were described in considerable detail in Section 6. This is a very active research area in a number of research groups, and future developments will positively impact detection sensitivity, ease of use, the types of separation that can be coupled effectively, as well as the manner in which 2D-LC separations are carried out (e.g., mLC–LC vs. LC × LC).
2. Method development—A number of research groups are currently engaged in the development of strategies to improve the efficiency of method development for 2D-LC. Currently, a lot of experience is required to understand the interconnectivity between different variables encountered in the method development process. In addition to strategy, perhaps we will observe the emergence of software tools to simplify the process as well. I hope that the long sought after concept of "universal methods" develops in a way that is accessible to many users. That is, the development of a small number of powerful, but broadly applicable methods for 2D-LC, such that successful separations can be obtained with little method development.
3. Continuation of the rapid adoption of 2D-LC in the pharmaceutical industry—The most rapidly growing application area for 2D-LC is in the analysis of biopharmaceutical materials. Most of this effort is currently focused on the analysis of proteins, such as monoclonal antibodies. This is likely to expand to include analyses of therapeutic peptides in significant ways.

As we look further into the future, it will be interesting to see what comes of the resurgent interest in 3D-LC (Vonk et al., 2015). The potential for dramatically increased separation power is unquestionable. It remains to be seen whether or not the technological barriers to practical implementation of 3D-LC can be overcome in ways that are cost-effective.

ACKNOWLEDGMENTS

I want to thank Peter Carr, Claudia Seidl, and Gabriel Leme for helpful discussions during the writing of this contribution, Joe Davis for the contribution of Fig. 7.11, and Eli Larson for his careful review of the manuscript.

REFERENCES

Adahchour, M., Beens, J., Vreuls, R.J.J., Brinkman, U.A.T., 2006. Recent developments in comprehensive two-dimensional gas chromatography (GC × GC) – introduction and instrumental setup. TrAC Trends Anal. Chem. 25, 438–454. http://dx.doi.org/10.1016/j.trac.2006.03.002.

Allen, R.C., John, M.G., Rutan, S.C., Filgueira, M.R., Carr, P.W., 2012. Effect of background correction on peak detection and quantification in online comprehensive two-dimensional liquid chromatography using diode array detection. J. Chromatogr. A 1254, 51–61. http://dx.doi.org/10.1016/j.chroma.2012.07.034.

Apffel, J.A., Alfredson, T.V., Majors, R.E., 1981. Automated on-line multi-dimensional high-performance liquid chromatographic techniques for the clean-up and analysis of water-soluble samples. J. Chromatogr. A 206, 43–57. http://dx.doi.org/10.1016/S0021-9673(00)82604-7.

Bailey, H.P., Rutan, S.C., 2011. Factors that affect quantification of diode array data in comprehensive two-dimensional liquid chromatography using chemometric data analysis. J. Chromatogr. A 1218, 8411−8422.

Bailey, H.P., Rutan, S.C., Stoll, D.R., 2012. Chemometric analysis of targeted 3DLC-DAD data for accurate and precise quantification of phenytoin in wastewater samples. J. Sep. Sci. 35, 1837−1843. http://dx.doi.org/10.1002/jssc.201200053.

Bedani, F., Kok, W.T., Janssen, H.-G., 2009. Optimal gradient operation in comprehensive liquid chromatography × liquid chromatography systems with limited orthogonality. Anal. Chim. Acta 654, 77−84. http://dx.doi.org/10.1016/j.aca.2009.06.042.

Bedani, F., Kok, W.T., Janssen, H.-G., 2006. A theoretical basis for parameter selection and instrument design in comprehensive size-exclusion chromatography × liquid chromatography. J. Chromatogr. A 1133, 126−134. http://dx.doi.org/10.1016/j.chroma.2006.08.048.

Bedani, F., Schoenmakers, P.J., Janssen, H.-G., 2012. Theories to support method development in comprehensive two-dimensional liquid chromatography − a review. J. Sep. Sci. 35, 1697−1711. http://dx.doi.org/10.1002/jssc.201200070.

Bushey, M.M., Jorgenson, J.W., 1990. Automated instrumentation for comprehensive two-dimensional high-performance liquid chromatography of proteins. Anal. Chem. 62, 161−167. http://dx.doi.org/10.1021/ac00201a015.

Cacciola, F., Farnetti, S., Dugo, P., Marriott, P.J., Mondello, L., 2016. Comprehensive two-dimensional liquid chromatography for polyphenol analysis in foodstuffs. J. Sep. Sci. 40, 7−24. http://dx.doi.org/10.1002/jssc.201600704.

Cacciola, F., Jandera, P., Blahová, E., Mondello, L., 2006. Development of different comprehensive two dimensional systems for the separation of phenolic antioxidants. J. Sep. Sci. 29, 2500−2513. http://dx.doi.org/10.1002/jssc.200600213.

Cacciola, F., Jandera, P., Hajdu, Z., Cesla, P., Mondello, L., 2007. Comprehensive two-dimensional liquid chromatography with parallel gradients for separation of phenolic and flavone antioxidants. J. Chromatogr. A 1149, 73−87. http://dx.doi.org/10.1016/j.chroma.2007.01.119.

Camenzuli, M., Schoenmakers, P.J., 2014. A new measure of orthogonality for multi-dimensional chromatography. Anal. Chim. Acta 838, 93−101. http://dx.doi.org/10.1016/j.aca.2014.05.048.

Carr, P.W., Davis, J.M., Rutan, S.C., Stoll, D.R., 2012. Principles of online comprehensive multidimensional liquid chromatography. In: Gruska, E., Grinberg, N. (Eds.), Advances in Chromatography. CRC Press, Boca Raton, FL.

Carr, P.W., Wang, X., Stoll, D.R., 2009. Effect of pressure, particle size, and time on optimizing performance in liquid chromatography. Anal. Chem. 81, 5342−5353. http://dx.doi.org/10.1021/ac9001244.

Cassiano, N., Barreiro, J., Oliveira, R., Cass, Q., 2012. Direct bioanalytical sample injection with 2D LC−MS. Bioanalysis 4, 2737−2756. http://dx.doi.org/10.4155/bio.12.226.

Consden, R., Gordon, A.H., Martin, A.J.P., 1944. Qualitative analysis of proteins: a partition chromatographic method using paper. Biochem. J. 38, 224−232. http://dx.doi.org/10.1042/bj0380224.

Cook, D., Rutan, S.C., Stoll, D.R., Carr, P.W., 2015. 2D assisted liquid chromatography (2DALC) − a chemometric approach to improve accuracy and precision of quantitation in liquid chromatography using 2D separation, dual detectors, and multivariate curve resolution. Anal. Chim. Acta 859, 87−95. http://dx.doi.org/10.1016/j.aca.2014.12.009.

D'Attoma, A., Heinisch, S., 2013. On-line comprehensive two dimensional separations of charged compounds using reversed-phase high performance liquid chromatography and hydrophilic interaction chromatography. Part II: application to the separation of peptides. J. Chromatogr. A 1306, 27−36. http://dx.doi.org/10.1016/j.chroma.2013.07.048.

Davis, J.M., 1991. Statistical theory of spot overlap in two-dimensional separations. Anal. Chem. 63, 2141−2152. http://dx.doi.org/10.1021/ac00019a014.

Davis, J.M., Giddings, J.C., 1983. Statistical theory of component overlap in multicomponent chromatograms. Anal. Chem. 55, 418−424. http://dx.doi.org/10.1021/ac00254a003.

Davis, J.M., Stoll, D.R., 2014. Likelihood of total resolution in liquid chromatography: evaluation of one-dimensional, comprehensive two-dimensional, and selective comprehensive two-dimensional liquid chromatography. J. Chromatogr. A 1360, 128−142. http://dx.doi.org/10.1016/j.chroma.2014.07.066.

Davis, J.M., Stoll, D.R., Carr, P.W., 2008a. Dependence of effective peak capacity in comprehensive two-dimensional separations on the distribution of peak capacity between the two dimensions. Anal. Chem. 80, 8122−8134. http://dx.doi.org/10.1021/ac800933z.

Davis, J.M., Stoll, D.R., Carr, P.W., 2008b. Effect of first-dimension undersampling on effective peak capacity in comprehensive two-dimensional separations. Anal. Chem. 80, 461−473. http://dx.doi.org/10.1021/ac071504j.

Desmet, G., Cabooter, D., Broeckhoven, K., 2015. Graphical data representation methods to assess the quality of LC columns. Anal. Chem. 87, 8593−8602. http://dx.doi.org/10.1021/ac504473p.

Ding, K., Xu, Y., Wang, H., Duan, C., Guan, Y., 2010. A vacuum assisted dynamic evaporation interface for two-dimensional normal phase/reverse phase liquid chromatography. J. Chromatogr. A 1217, 5477−5483. http://dx.doi.org/10.1016/j.chroma.2010.06.053.

Donato, P., Cacciola, F., Mondello, L., Dugo, P., 2011. Comprehensive chromatographic separations in proteomics. J. Chromatogr. A 1218, 8777−8790. http://dx.doi.org/10.1016/j.chroma.2011.05.070.

Donato, P., Cacciola, F., Tranchida, P.Q., Dugo, P., Mondello, L., 2012. Mass spectrometry detection in comprehensive liquid chromatography: basic concepts, instrumental aspects, applications and trends. Mass Spectrom. Rev. 31, 523−559. http://dx.doi.org/10.1002/mas.20353.

Dugo, P., Favoino, O., Luppino, R., Dugo, G., Mondello, L., 2004. Comprehensive two-dimensional normal-phase (adsorption)−reversed-phase liquid chromatography. Anal. Chem. 76, 2525−2530. http://dx.doi.org/10.1021/ac0352981.

Elsner, V., Wulf, V., Wirtz, M., Schmitz, O.J., 2014. Reproducibility of retention time and peak area in comprehensive two-dimensional liquid chromatography. Anal. Bioanal. Chem. 407, 279−284. http://dx.doi.org/10.1007/s00216-014-8090-3.

Erni, F., Frei, R., 1978. Two-dimensional column liquid chromatographic technique for resolution of complex mixtures. J. Chromatogr. A 149, 561−569. http://dx.doi.org/10.1016/S0021-9673(00)81011-0.

Fairchild, J.N., Horváth, K., Guiochon, G., 2009a. Theoretical advantages and drawbacks of on-line, multidimensional liquid chromatography using multiple columns operated in parallel. J. Chromatogr. A 1216, 6210−6217. http://dx.doi.org/10.1016/j.chroma.2009.06.085.

Fairchild, J.N., Horváth, K., Guiochon, G., 2009b. Approaches to comprehensive multidimensional liquid chromatography systems. J. Chromatogr. A 1216, 1363−1371. http://dx.doi.org/10.1016/j.chroma.2008.12.073.

Filgueira, M.R., Castells, C.B., Carr, P.W., 2012. A simple, robust orthogonal background correction method for two-dimensional liquid chromatography. Anal. Chem. 84, 6747−6752. http://dx.doi.org/10.1021/ac301248h.

Filgueira, M.R., Huang, Y., Witt, K., Castells, C., Carr, P.W., 2011. Improving peak capacity in fast online comprehensive two-dimensional liquid chromatography with post-first-dimension flow splitting. Anal. Chem. 83, 9531−9539. http://dx.doi.org/10.1021/ac202317m.

François, I., Cabooter, D., Sandra, K., Lynen, F., Desmet, G., Sandra, P., 2009. Tryptic digest analysis by comprehensive reversed phase × two reversed phase liquid chromatography (RP-LC × 2RP-LC) at different pH's. J. Sep. Sci. 32, 1137−1144. http://dx.doi.org/10.1002/jssc.200800578.

François, I., de Villiers, A., Sandra, P., 2006. Considerations on the possibilities and limitations of comprehensive normal phase−reversed phase liquid chromatography (NPLC × RPLC). J. Sep. Sci. 29, 492−498. http://dx.doi.org/10.1002/jssc.200500451.

Francois, I., Devilliers, A., Tienpont, B., David, F., Sandra, P., 2008. Comprehensive two-dimensional liquid chromatography applying two parallel columns in the second dimension. J. Chromatogr. A 1178, 33−42. http://dx.doi.org/10.1016/j.chroma.2007.11.032.

Francois, I., Sandra, K., Sandra, P., 2011. Chapter 8: history, evolution, and optimization aspects of comprehensive two-dimensional liquid chromatography. In: Comprehensive Chromatography in Combination with Mass Spectrometry. Wiley, Hoboken, NJ, pp. 281−330.

Gargano, A.F.G., Duffin, M., Navarro, P., Schoenmakers, P.J., 2016. Reducing dilution and analysis time in online comprehensive two-dimensional liquid chromatography by active modulation. Anal. Chem. 88, 1785−1793. http://dx.doi.org/10.1021/acs.analchem.5b04051.

Giddings, J.C., 1987. Concepts and comparisons in multidimensional separation. HRC CC J. High Resolut. Chromatogr. Chromatogr. Commun. 10, 319−323. http://dx.doi.org/10.1002/jhrc.1240100517.

Giddings, J.C., 1984. Two-dimensional separations: concept and promise. Anal. Chem. 56, 1258A−1270A. http://dx.doi.org/10.1021/ac00276a003.

Giddings, J.C., 1967. Maximum number of components resolvable by gel filtration and other elution chromatographic methods. Anal. Chem. 39, 1027−1028. http://dx.doi.org/10.1021/ac60252a025.

Gilar, M., Fridrich, J., Schure, M.R., Jaworski, A., 2012. Comparison of orthogonality estimation methods for the two-dimensional separations of peptides. Anal. Chem. 84, 8722−8732. http://dx.doi.org/10.1021/ac3020214.

Gilar, M., Olivova, P., Daly, A.E., Gebler, J.C., 2005. Orthogonality of separation in two-dimensional liquid chromatography. Anal. Chem. 77, 6426−6434. http://dx.doi.org/10.1021/ac050923i.

Græsbøll, R., Nielsen, N.J., Christensen, J.H., 2014. Using the hydrophobic subtraction model to choose orthogonal columns for online comprehensive two-dimensional liquid chromatography. J. Chromatogr. A 1326, 39−46. http://dx.doi.org/10.1016/j.chroma.2013.12.034.

Groskreutz, S.R., Swenson, M.M., Secor, L.B., Stoll, D.R., 2012a. Selective comprehensive multi-dimensional separation for resolution enhancement in high performance liquid chromatography, Part I−principles and instrumentation. J. Chromatogr. A 1228, 31−40. http://dx.doi.org/10.1016/j.chroma.2011.06.035.

Groskreutz, S.R., Swenson, M.M., Secor, L.B., Stoll, D.R., 2012b. Selective comprehensive multi-dimensional separation for resolution enhancement in high performance liquid chromatography, Part II−applications. J. Chromatogr. A 1228, 41−50. http://dx.doi.org/10.1016/j.chroma.2011.06.038.

Guiochon, G., Beaver, L.A., Gonnord, M.F., Siouffi, A.M., Zakaria, M., 1983. Theoretical investigation of the potentialities of the use of a multidimensional column in chromatography. J. Chromatogr. A 255, 415−437. http://dx.doi.org/10.1016/S0021-9673(01)88298-4.

Guiochon, G., Marchetti, N., Mriziq, K., Shalliker, R., 2008. Implementations of two-dimensional liquid chromatography. J. Chromatogr. A 1189, 109−168. http://dx.doi.org/10.1016/j.chroma.2008.01.086.

Haidar Ahmad, I.A., Soliven, A., Allen, R.C., Filgueira, M., Carr, P.W., 2015. Comparison of core−shell particles and sub-2μm fully porous particles for use as ultrafast second dimension columns in two-dimensional liquid chromatography. J. Chromatogr. A 1386, 31−38. http://dx.doi.org/10.1016/j.chroma.2014.11.069.

Holm, A., Storbråten, E., Mihailova, A., Karaszewski, B., Lundanes, E., Greibrokk, T., 2005. Combined solid-phase extraction and 2D LC−MS for characterization of the neuropeptides in rat-brain tissue. Anal. Bioanal. Chem. 382, 751−759. http://dx.doi.org/10.1007/s00216-005-3146-z.

Horie, K., Kimura, H., Ikegami, T., Iwatsuka, A., Saad, N., Fiehn, O., Tanaka, N., 2007. Calculating optimal modulation periods to maximize the peak capacity in two-dimensional HPLC. Anal. Chem. 79, 3764−3770. http://dx.doi.org/10.1021/ac062002t.

Hou, X., Ma, J., He, X., Chen, L., Wang, S., He, L., 2015. A stop-flow two-dimensional liquid chromatography method for determination of food additives in yogurt. Anal. Methods 7, 2141−2148. http://dx.doi.org/10.1039/C4AY02855D.

hplccolumns.org (WWW Document), n.d. http://hplccolumns.org/index.php.

Huang, Y., Gu, H., Filgueira, M., Carr, P.W., 2011. An experimental study of sampling time effects on the resolving power of on-line two-dimensional high performance liquid chromatography. J. Chromatogr. A 1218, 2984−2994. http://dx.doi.org/10.1016/j.chroma.2011.03.032.

Jandera, P., Hájek, T., Česla, P., 2010. Comparison of various second-dimension gradient types in comprehensive two-dimensional liquid chromatography. J. Sep. Sci. 33, 1382–1397. http://dx.doi.org/10.1002/jssc.200900808.

Jandera, P., Hájek, T., Staňková, M., 2015. Monolithic and core–shell columns in comprehensive two-dimensional HPLC: a review. Anal. Bioanal. Chem. 407, 139–151. http://dx.doi.org/10.1007/s00216-014-8147-3.

Johnson, A.R., Johnson, C.M., Stoll, D.R., Vitha, M.F., 2012. Identifying orthogonal and similar reversed phase liquid chromatography stationary phases using the system selectivity cube and the hydrophobic subtraction model. J. Chromatogr. A 1249, 62–82. http://dx.doi.org/10.1016/j.chroma.2012.05.049.

Kalili, K.M., de Villiers, A., 2013a. Systematic optimisation and evaluation of on-line, off-line and stop-flow comprehensive hydrophilic interaction chromatography × reversed phase liquid chromatographic analysis of procyanidins. Part II: application to cocoa procyanidins. J. Chromatogr. A 1289, 69–79. http://dx.doi.org/10.1016/j.chroma.2013.03.009.

Kalili, K.M., de Villiers, A., 2013b. Systematic optimisation and evaluation of on-line, off-line and stop-flow comprehensive hydrophilic interaction chromatography × reversed phase liquid chromatographic analysis of procyanidins, Part I: theoretical considerations. J. Chromatogr. A 1289, 58–68. http://dx.doi.org/10.1016/j.chroma.2013.03.008.

Karger, B., Snyder, L., Horvath, C., 1973. Multistep separation schemes for complex samples. In: An Introduction to Separation Science. John Wiley & Sons, Inc., New York, NY, pp. 558–562.

Kilz, P., Radke, W., 2015. Application of two-dimensional chromatography to the characterization of macromolecules and biomacromolecules. Anal. Bioanal. Chem. 407, 193–215. http://dx.doi.org/10.1007/s00216-014-8266-x.

Kivilompolo, M., Pol, J., Hyotylainen, T., 2011. Comprehensive two-dimensional liquid chromatography (LC × LC): a review. LC-GC Eur. 24, 232, 234, 236, 238, 240–243.

Largy, E., Catrain, A., Van Vyncht, G., Delobel, A., 2016. 2D-LC–MS for the analysis of monoclonal antibodies and antibody–drug conjugates in a regulated environment. Curr. Trends Mass Spectrom. 14, 29–35.

Latha, I., Reichenbach, S.E., Tao, Q., 2011. Comparative analysis of peak-detection techniques for comprehensive two-dimensional chromatography. J. Chromatogr. A 1218, 6792–6798. http://dx.doi.org/10.1016/j.chroma.2011.07.052.

Li, D., Dück, R., Schmitz, O.J., 2014a. The advantage of mixed-mode separation in the first dimension of comprehensive two-dimensional liquid-chromatography. J. Chromatogr. A 1358, 128–135. http://dx.doi.org/10.1016/j.chroma.2014.06.086.

Li, D., Jakob, C., Schmitz, O.J., 2014b. Practical considerations in comprehensive two-dimensional liquid chromatography systems (LC × LC) with reversed-phases in both dimensions. Anal. Bioanal. Chem. 407, 153–167. http://dx.doi.org/10.1007/s00216-014-8179-8.

Li, D., Schmitz, O.J., 2013. Use of shift gradient in the second dimension to improve the separation space in comprehensive two-dimensional liquid chromatography. Anal. Bioanal. Chem. 405, 6511–6517. http://dx.doi.org/10.1007/s00216-013-7089-5.

Li, Q., Lynen, F., Wang, J., Li, H., Xu, G., Sandra, P., 2011. Comprehensive hydrophilic interaction and ion-pair reversed-phase liquid chromatography for analysis of di- to deca-oligonucleotides. J. Chromatogr. A 1255, 237–243. http://dx.doi.org/10.1016/j.chroma.2011.11.062.

Li, X., Stoll, D.R., Carr, P.W., 2009. Equation for peak capacity estimation in two-dimensional liquid chromatography. Anal. Chem. 81, 845–850. http://dx.doi.org/10.1021/ac801772u.

Li, Z., Chen, K., Guo, M., Tang, D., 2016. Two-dimensional liquid chromatography and its application in traditional Chinese medicine analysis and metabonomic investigation: liquid chromatography. J. Sep. Sci. 39, 21–37. http://dx.doi.org/10.1002/jssc.201500634.

Liu, Z., Patterson, D.G., Lee, M.L., 1995. Geometric approach to factor analysis for the estimation of orthogonality and practical peak capacity in comprehensive two-dimensional separations. Anal. Chem. 67, 3840–3845. http://dx.doi.org/10.1021/ac00117a004.

Malerod, H., Lundanes, E., Greibrokk, T., 2010. Recent advances in on-line multidimensional liquid chromatography. Anal. Methods 2, 110−122. http://dx.doi.org/10.1039/b9ay00194h.

Marriott, P.J., Schoenmakers, P.J., Wu, Z., 2012. Nomenclature and conventions in comprehensive multidimensional chromatography − an update. LC-GC Eur. 25, 266, 268, 270, 272−275.

Matos, J.T.V., Duarte, R.M.B.O., Duarte, A.C., 2012. Trends in data processing of comprehensive two-dimensional chromatography: state of the art. J. Chromatogr. B 910, 31−45. http://dx.doi.org/10.1016/j.jchromb.2012.06.039.

Matula, A.J., Carr, P.W., 2015. Separation speed and power in isocratic liquid chromatography: loss in performance of Poppe vs Knox-Saleem optimization. Anal. Chem. 87, 6578−6583. http://dx.doi.org/10.1021/acs.analchem.5b00329.

Mihailova, A., Malerød, H., Wilson, S.R., Karaszewski, B., Hauser, R., Lundanes, E., Greibrokk, T., 2008. Improving the resolution of neuropeptides in rat brain with on-line HILIC-RP compared to on-line SCX-RP. J. Sep. Sci. 31, 459−467. http://dx.doi.org/10.1002/jssc.200700257.

Mondello, L., Herrero, M., Kumm, T., Dugo, P., Cortes, H., Dugo, G., 2008. Quantification in comprehensive two-dimensional liquid chromatography. Anal. Chem. 80, 5418−5424. http://dx.doi.org/10.1021/ac800484y.

Murphy, R.E., Schure, M.R., 2008. Method development in multidimensional liquid chromatography. In: Schure, M., Cohen, S.A. (Eds.), Multidimensional Liquid Chromatography: Theory and Applications in Industrial Chemistry and the Life Sciences. Wiley-Interscience, Hoboken, N.J, pp. 127−145.

Murphy, R.E., Schure, M.R., Foley, J.P., 1998. Effect of sampling rate on resolution in comprehensive two-dimensional liquid chromatography. Anal. Chem. 70, 1585−1594. http://dx.doi.org/10.1021/ac971184b.

Neue, U., 2005. Theory of peak capacity in gradient elution. J. Chromatogr. A 1079, 153−161. http://dx.doi.org/10.1016/j.chroma.2005.03.008.

Oda, Y., Asakawa, N., Kajima, T., Yoshida, Y., Sato, T., 1991. On-line determination and resolution of verapamil enantiomers by high-performance liquid chromatography with column switching. J. Chromatogr. A 541, 411−418. http://dx.doi.org/10.1016/S0021-9673(01)96013-3.

Pascoe, R., Foley, J.P., Gusev, A.I., 2001. Reduction in matrix-related signal suppression effects in electrospray ionization mass spectrometry using on-line two-dimensional liquid chromatography. Anal. Chem. 73, 6014−6023. http://dx.doi.org/10.1021/ac0106694.

Pepaj, M., Holm, A., Fleckenstein, B., Lundanes, E., Greibrokk, T., 2006. Fractionation and separation of human salivary proteins by pH-gradient ion exchange and reversed phase chromatography coupled to mass spectrometry. J. Sep. Sci. 29, 519−528. http://dx.doi.org/10.1002/jssc.200500346.

Potts, L.W., Carr, P.W., 2013. Analysis of the temporal performance of one versus on-line comprehensive two-dimensional liquid chromatography. J. Chromatogr. A 1310, 37−44. http://dx.doi.org/10.1016/j.chroma.2013.07.102.

PQRI Approach for Selecting Columns of Equivalent Selectivity (WWW Document), n.d. USP. http://www.usp.org/usp-nf/compendial-tools/pqri-approach-column-equiv-tool.

Pursch, M., Buckenmaier, S., 2015. Loop-based multiple heart-cutting two-dimensional liquid chromatography for target analysis in complex matrices. Anal. Chem. 87, 5310−5317. http://dx.doi.org/10.1021/acs.analchem.5b00492.

Reichenbach, S.E., Carr, P.W., Stoll, D.R., Tao, Q., 2009. Smart templates for peak pattern matching with comprehensive two-dimensional liquid chromatography. J. Chromatogr. A 1216, 3458−3466. http://dx.doi.org/10.1016/j.chroma.2008.09.058.

Rutan, S.C., Davis, J.M., Carr, P.W., 2011. Fractional coverage metrics based on ecological home range for calculation of the effective peak capacity in comprehensive two-dimensional separations. J. Chromatogr. A 1255, 267−276. http://dx.doi.org/10.1016/j.chroma.2011.12.061.

Sarrut, M., D'Attoma, A., Heinisch, S., 2015. Optimization of conditions in on-line comprehensive two-dimensional reversed phase liquid chromatography. Experimental comparison with one-dimensional

reversed phase liquid chromatography for the separation of peptides. J. Chromatogr. A 1421, 48−59. http://dx.doi.org/10.1016/j.chroma.2015.08.052.

Schellinger, A., Stoll, D., Carr, P., 2005. High speed gradient elution reversed-phase liquid chromatography. J. Chromatogr. A 1064, 143−156. http://dx.doi.org/10.1016/j.chroma.2004.12.017.

Schoenmakers, P., Aarnoutse, P., 2014. Multi-dimensional separations of polymers. Anal. Chem. 86, 6172−6179. http://dx.doi.org/10.1021/ac301162b.

Schoenmakers, P.J., Marriott, P.J., Beens, J., 2003. Nomenclature and conventions in comprehensive multidimensional chromatography. LC-GC Eur. 16, 335−336, 338−339.

Schoenmakers, P.J., Vivó-Truyols, G., Decrop, W.M.C., 2006. A protocol for designing comprehensive two-dimensional liquid chromatography separation systems. J. Chromatogr. A 1120, 282−290. http://dx.doi.org/10.1016/j.chroma.2005.11.039.

Schure, M.R., 1999. Limit of detection, dilution factors, and technique compatibility in multidimensional separations utilizing chromatography, capillary electrophoresis, and field-flow fractionation. Anal. Chem. 71, 1645−1657. http://dx.doi.org/10.1021/ac981128q.

Schure, M.R., Davis, J.M., 2015. Orthogonal separations: comparison of orthogonality metrics by statistical analysis. J. Chromatogr. A 1414, 60−76. http://dx.doi.org/10.1016/j.chroma.2015.08.029.

Seeley, J., 2002. Theoretical study of incomplete sampling of the first dimension in comprehensive two-dimensional chromatography. J. Chromatogr. A 962, 21−27. http://dx.doi.org/10.1016/S0021-9673(02)00461-2.

Separation mechanisms in hydrophilic interaction chromatography. In: Hydrophilic Interaction Chromatography: A Guide for Practitioners, 2013. Wiley, pp. 1−38.

Simpkins, S.W., Bedard, J.W., Groskreutz, S.R., Swenson, M.M., Liskutin, T.E., Stoll, D.R., 2010. Targeted three-dimensional liquid chromatography: a versatile tool for quantitative trace analysis in complex matrices. J. Chromatogr. A 1217, 7648−7660. http://dx.doi.org/10.1016/j.chroma.2010.09.023.

Snyder, L.R., Dolan, J.W., Marchand, D.H., Carr, P.W., 2012. The hydrophobic-subtraction model of reversed-phase column selectivity. In: Advances in Chromatography. CRC Press, Boca Raton, pp. 297−376.

Snyder, L.R., Dolan, J.W., van der Wal, S., 1981. Boxcar chromatography. J. Chromatogr. A 203, 3−17. http://dx.doi.org/10.1016/S0021-9673(00)80277-0.

Snyder, L.R., Kirkland, J.J., Dolan, J.W., 2010a. Gradient elution. In: Introduction to Modern Liquid Chromatography. Wiley, Hoboken, N.J, pp. 430−434.

Snyder, L.R., Kirkland, J.J., Dolan, J.W., 2010b. Ionic samples: reversed-phase, ion-pair, and ion-exchange chromatography. In: Introduction to Modern Liquid Chromatography. Wiley, Hoboken, N.J, pp. 320−321.

Stevenson, P.G., Guiochon, G., 2013. Cumulative area of peaks in a multidimensional high performance liquid chromatogram. J. Chromatogr. A 1308, 79−85. http://dx.doi.org/10.1016/j.chroma.2013.07.067.

Stoll, D., Carr, P., 2016. Two-dimensional liquid chromatography: a state-of-the-art tutorial. Anal. Chem. 89, 519−531. http://dx.doi.org/10.1021/acs.analchem.6b03506.

Stoll, D., Cohen, J., Carr, P., 2006. Fast, comprehensive online two-dimensional high performance liquid chromatography through the use of high temperature ultra-fast gradient elution reversed-phase liquid chromatography. J. Chromatogr. A 1122, 123−137. http://dx.doi.org/10.1016/j.chroma.2006.04.058.

Stoll, D., Danforth, J., Zhang, K., Beck, A., 2016. Characterization of therapeutic antibodies and related products by two-dimensional liquid chromatography coupled with UV absorbance and mass spectrometric detection. J. Chromatogr. B 1032, 51−60. http://dx.doi.org/10.1016/j.jchromb.2016.05.029.

Stoll, D.R., 2015. Recent advances in 2D-LC for bioanalysis. Bioanalysis 7, 3125−3142. http://dx.doi.org/10.4155/bio.15.223.

Stoll, D.R., Carr, P.W., 2005. Fast, comprehensive two-dimensional HPLC separation of tryptic peptides based on high-temperature HPLC. J. Am. Chem. Soc. 127, 5034−5035. http://dx.doi.org/10.1021/ja050145b.

Stoll, D.R., Li, X., Wang, X., Carr, P.W., Porter, S.E.G., Rutan, S.C., 2007. Fast, comprehensive two-dimensional liquid chromatography. J. Chromatogr. A 1168, 3−43. http://dx.doi.org/10.1016/j.chroma.2007.08.054.

Stoll, D.R., O'Neill, K., Harmes, D.C., 2015. Effect of pH mismatch between the two dimensions of reversed-phase × reversed-phase two-dimensional separations on second dimension separation quality for ionogenic compounds − I. Carboxylic acids. J. Chromatogr. A 1383, 25−34. http://dx.doi.org/10.1016/j.chroma.2014.12.054.

Stoll, D.R., Talus, E.S., Harmes, D.C., Zhang, K., 2014. Evaluation of detection sensitivity in comprehensive two-dimensional liquid chromatography separations of an active pharmaceutical ingredient and its degradants. Anal. Bioanal. Chem. 407, 265−277. http://dx.doi.org/10.1007/s00216-014-8036-9.

Stoll, D.R., Wang, X., Carr, P.W., 2008. Comparison of the practical resolving power of one- and two-dimensional high-performance liquid chromatography analysis of metabolomic samples. Anal. Chem. 80, 268−278. http://dx.doi.org/10.1021/ac701676b.

Sweeney, A., Shalliker, R., 2002. Development of a two-dimensional liquid chromatography system with trapping and sample enrichment capabilities. J. Chromatogr. A 968, 41−52. http://dx.doi.org/10.1016/S0021-9673(02)00782-3.

Synge, R., 1952. Applications of Partition Chromatography. Nobel Lect.

Talus, E.S., Witt, K.E., Stoll, D.R., 2015. Effect of pressure pulses at the interface valve on the stability of second dimension columns in online comprehensive two-dimensional liquid chromatography. J. Chromatogr. A 1378, 50−57. http://dx.doi.org/10.1016/j.chroma.2014.12.019.

Thekkudan, D.F., Rutan, S.C., Carr, P.W., 2010. A study of the precision and accuracy of peak quantification in comprehensive two-dimensional liquid chromatography in time. J. Chromatogr. A 1217, 4313−4327. http://dx.doi.org/10.1016/j.chroma.2010.04.039.

Tian, H., Xu, J., Xu, Y., Guan, Y., 2006. Multidimensional liquid chromatography system with an innovative solvent evaporation interface. J. Chromatogr. A 1137, 42−48. http://dx.doi.org/10.1016/j.chroma.2006.10.005.

Vanhoenacker, G., Vandenheede, I., David, F., Sandra, P., Sandra, K., 2015. Comprehensive two-dimensional liquid chromatography of therapeutic monoclonal antibody digests. Anal. Bioanal. Chem. 407, 355−366. http://dx.doi.org/10.1007/s00216-014-8299-1.

Venkatramani, C.J., Al-Sayah, M., Li, G., Goel, M., Girotti, J., Zang, L., Wigman, L., Yehl, P., Chetwyn, N., 2016. Simultaneous achiral-chiral analysis of pharmaceutical compounds using two-dimensional reversed phase liquid chromatography-supercritical fluid chromatography. Talanta 148, 548−555. http://dx.doi.org/10.1016/j.talanta.2015.10.054.

Venkatramani, C.J., Girotti, J., Wigman, L., Chetwyn, N., 2014. Assessing stability-indicating methods for coelution by two-dimensional liquid chromatography with mass spectrometric detection: liquid chromatography. J. Sep. Sci. 37, 3214−3225. http://dx.doi.org/10.1002/jssc.201400590.

Venkatramani, C.J., Patel, A., 2006. Towards a comprehensive 2-D-LC−MS separation. J. Sep. Sci. 29, 510−518. http://dx.doi.org/10.1002/jssc.200500341.

Verstraeten, M., Pursch, M., Eckerle, P., Luong, J., Desmet, G., 2011. Thermal modulation for multidimensional liquid chromatography separations using low-thermal-mass liquid chromatography (LC). Anal. Chem. 83, 7053−7060. http://dx.doi.org/10.1021/ac201207t.

Vivó-Truyols, G., Janssen, H.-G., 2010. Probability of failure of the watershed algorithm for peak detection in comprehensive two-dimensional chromatography. J. Chromatogr. A 1217, 1375−1385. http://dx.doi.org/10.1016/j.chroma.2009.12.063.

Vivó-Truyols, G., van der Wal, S., Schoenmakers, P.J., 2010. Comprehensive study on the optimization of online two-dimensional liquid chromatographic systems considering losses in theoretical peak capacity in first- and second-dimensions: a Pareto-optimality approach. Anal. Chem. 82, 8525−8536. http://dx.doi.org/10.1021/ac101420f.

Vonk, R.J., Gargano, A.F.G., Davydova, E., Dekker, H.L., Eeltink, S., de Koning, L.J., Schoenmakers, P.J., 2015. Comprehensive two-dimensional liquid chromatography with stationary-phase-assisted modulation coupled to high-resolution mass spectrometry applied to proteome analysis of *Saccharomyces cerevisiae*. Anal. Chem. 87, 5387−5394. http://dx.doi.org/10.1021/acs.analchem.5b00708.

Wang, X., Stoll, D.R., Schellinger, A.P., Carr, P.W., 2006. Peak capacity optimization of peptide separations in reversed-phase gradient elution chromatography: fixed column format. Anal. Chem. 78, 3406−3416. http://dx.doi.org/10.1021/ac0600149.

Wilson, S.R., Jankowski, M., Pepaj, M., Mihailova, A., Boix, F., Vivo Truyols, G., Lundanes, E., Greibrokk, T., 2007. 2D LC separation and determination of bradykinin in rat muscle tissue dialysate with in-line SPE-HILIC-SPE-RP-MS. Chromatographia 66, 469−474. http://dx.doi.org/10.1365/s10337-007-0341-4.

Zhang, K., Li, Y., Tsang, M., Chetwyn, N.P., 2013a. Analysis of pharmaceutical impurities using multi-heartcutting 2D LC coupled with UV-charged aerosol MS detection: liquid Chromatography. J. Sep. Sci. 36, 2986−2992. http://dx.doi.org/10.1002/jssc.201300493.

Zhang, K., Wang, J., Tsang, M., Wigman, L., Chetwyn, N., 2013b. Two-dimensional HPLC in pharmaceutical analysis. Am. Pharm. Rev. 16, 39−44.

Zhang, Y., Carr, P.W., 2009. A visual approach to stationary phase selectivity classification based on the Snyder−Dolan Hydrophobic-Subtraction Model. J. Chromatogr. A 1216, 6685−6694. http://dx.doi.org/10.1016/j.chroma.2009.06.048.

CHAPTER

8

RECENT ADVANCES IN COMPREHENSIVE TWO-DIMENSIONAL LIQUID CHROMATOGRAPHY FOR THE ANALYSIS OF NATURAL PRODUCTS

Francesco Cacciola[1], Paola Donato[1], Luigi Mondello[1,2,3], Paola Dugo[1,2,3]

University of Messina, Messina, Italy[1]; *University Campus Bio-Medico of Rome, Rome, Italy*[2]; *Chromaleont SrL, Messina, Italy*[3]

1. INTRODUCTION

The analysis of real-world samples, e.g., biological, food, and environmental, poses a high demand for "conventional" one-dimensional liquid chromatography (1D-LC) methods enabling compound identification and quantification. However, a single column does not often have sufficient separation power for the baseline separation of all components in complex samples and the extent of peak overlap is enhanced as the number of compounds increases.

The development of comprehensive two-dimensional (2D) high-performance liquid chromatography (HPLC) (LC × LC) has been relatively slow until the last two decades, even though the advantages of the technique were already described in the late 1970s and early 1980s (Karger et al., 1973; Erni and Frei, 1978; Giddings, 1984). In the 1990s the application of LC × LC was limited to proteomic applications, and only afterward the utility of this technique in the separation of a variety of other complex mixtures has been demonstrated. The general motivation which lies ahead of this research area is linked to its potential for substantially more resolving (separating) power in comparison with the 1D-LC counterpart.

The most general set-up of an LC × LC system consists of two pumps, two columns, injector, interface, and detector. The interface is, in general, a high-pressure 2-position switching valve, and this device is often referred to as modulator or sampling device.

The suitability of any LC separation system for resolving complex samples can be expressed by theoretical peak capacity, n_c, which determines the maximum number of peaks that can be separated side by side, into the separation space at a desired degree of resolution e.g., $R_S = 1(n_c = t/w)$. The separation time can be specified as the retention time interval $\Delta t_R = t_{R,\,Z} - t_{R,\,1}$, between the first (1) and the last (z) sample peaks, while w can be estimated from the average bandwidth, w_{av}.

Handbook of Advanced Chromatography/Mass Spectrometry Techniques. http://dx.doi.org/10.1016/B978-0-12-811732-3.00008-X

LC × LC methods improve the likelihood for separation of a higher number of sample components because the peak capacity of an LC × LC separation is multiplicative of the product of the peak capacity values of the two single dimensions ($n_{2D} = n_{D1} \times n_{D2}$) (Karger et al., 1973; Giddings, 1984, 1987). The peak capacities of the two dimensions are shown as the number of adjacent Gaussian profiles that can be accommodated into the space along with the respective separation coordinates. The resolution is represented by rectangular boxes, which divide the separation plane. The total peak capacity, n_{2D}, is therefore approximately equal to the number of such boxes (Giddings, 1987).

In this regard, by careful selection of orthogonal separation systems both in the first (^{1}D) and the second dimension (^{2}D), the peak capacity of the overall systems can dramatically increase, making group separations of various samples often possible, so that various structurally related classes of compounds can be distinguished and located in different areas of the 2D retention plane, which helps in the interpretation of the LC × LC data.

Because of the tremendously higher separation power of LC × LC when compared with its 1D-LC counterpart, the technique has been employed in several fields, e.g., polymers, pharmaceuticals and biological mixtures, natural products, environmental and petrochemical samples, and has been the subject of various reviews (Liu and Lee, 2000; Evans and Jorgenson, 2004; Guttman et al., 2004; Stroink et al., 2005; Dixon et al., 2006; Jandera, 2006, 2012; Shalliker and Gray, 2006; Shellie and Haddad, 2006; Stoll et al., 2007; Dugo et al., 2008a,b; Guiochon et al., 2008; Pol and Hyotylainen, 2008; François et al., 2009a; Herrero et al., 2009; Sandra et al., 2009; Berek, 2010; Pierce et al. 2012; Donato et al., 2012; Bedani et al., 2012; Shi et al., 2014; Sarrut et al., 2014).

2. ADVANCES IN THEORY

In the last two decades, most theoretical work in LC × LC has been basically devoted to method optimization. In addition to the factors that affect resolution and performance in "conventional" 1D-LC methods, including retention, selectivity, and column efficiency, LC × LC methods imply many other factors. The most striking example of the dependence of the two dimensions on each other is related to the analysis speed in the ^{2}D. In this regard, many practitioners have recognized the effect of the sampling rate on the peak capacity of the overall LC × LC separations. In a former work, Murphy et al. (1998) investigated the effect of the sampling rate on the effective ^{1}D peak width and modeled a Gaussian peak as a histogram profile of the average concentration within every sampling period. The outcome of the research was that approximately three to four modulations per each ^{1}D peak (8σ), are needed to avoid serious loss of performance of the LC × LC system as a result of "undersampling" of ^{1}D peaks. However, this number is only valid when the sampling is "in-phase," which implies that the sampling should start exactly at the beginning of the peak. In experimental practice, this cannot be guaranteed so a minimum of four samplings is preferable. A few years later, Seeley, (2002) published another report on this topic investigating the sampling frequency for modulators with various duty cycles. On the one hand, when using an interface consisting of a 2-position/10- or 8-port switching valve provided with two storage loops, the primary effluent is collected throughout the entire sampling period and the duty cycle is equal to unity; on the other hand, when using devices, which do not integrally sample the ^{1}D effluent, the duty cycle is less than 1 as in the case of a 2-position/6-port switching valve equipped with only one sampling loop. Seeley defined the (average) peak broadening factor $\sigma*$ by introducing parameters such as sampling period τ_Z and sampling phase Φ. τ_Z is determined by the modulation period or sampling time t_s and $^1\sigma$ of the ^{1}D peak, whereas the latter

represents the way in which the primary peak is cut into aliquots. The sampling phase Φ is the time difference between the center of the sampling cycle nearest to the peak maximum and the peak maximum, divided by the sampling period. Peak broadening was less significant when the peak maximum was centered in one of the sampling periods and for low duty cycles. For systems with a duty cycle of 1, as is the case for most comprehensive separations, the peak broadening was practically independent of Φ. Basically, Seeley drew the same conclusions as Murphy extending his investigations to duty cycles less than 1. Afterward, Horie et al. (2007) nailed down that in general, modulation periods equal to 2.2−4 are sufficient to minimize "peak broadening." On the one hand, shorter modulation periods offer a higher number of cuts across the ^{1}D peaks, but the secondary column fails to provide sufficient separation power; on the other hand, longer sampling periods in combination with a longer ^{2}D column lead to a gain in resolution in the ^{2}D, but the overall resolution is in this case jeopardized because of the deleterious effect of the undersampling. In addition, they introduced a new parameter, e_M (Nobuo factor), which is defined as the ratio of the apparent peak capacity of the first column derived from $\sigma*$ to its actual peak capacity in the ^{1}D. A useful "protocol" for optimizing LC × LC separations based on proper sampling has been described by Schoenmakers et al. (2006): for such a scope, suitable chromatographic parameters, such as column dimensions, injection volumes, and flow rates, were taken into account. As a realistic example, the protocol was used to design specific LC × size exclusion chromatography (SEC) systems, starting with different diameters of the ^{1}D column, and the results achieved were close to best practices in this field. Great effort toward understanding the effect of undersampling has been devoted by Carr et al. In their reports, in contrast to all previous studies where the results were based on just a single pair of peaks, the investigation was extended to the overall chromatogram (Davis et al., 2008a,b; Li et al., 2009; Potts et al., 2010; Gu et al., 2011). They introduced an average ^{1}D broadening factor, β, as a function of the sampling time (t_s), and the standard deviation of the ^{1}D peaks prior to sampling ($^1\sigma$), which can be used together with the product rule for the calculation of the practical peak capacity (Davis et al., 2008a). For the determination of this factor, 2D statistical overlap theory along with the number of observed peaks in simulated LC × LC separations was used (Davis, 2005). In comparison with previous studies (Murphy et al., 1998; Seeley, 2002; Horie et al., 2007), in such a work the β values are 2%−35% larger; these differences are very significant from a practical perspective, given the large increase in analysis time required to increase effective peak capacity.

A very interesting work was reported by Potts et al. (2010) who examined the effects of the ^{1}D peak capacity and gradient time, and the ^{2}D cycle times on the overall peak capacity of the two-dimensional liquid chromatography (2D-LC) system; in addition, the effects of reequilibration time on undersampling as measured by the undersampling factor, and the influence of molecular type (peptide vs. small molecule) on peak capacity were studied. It was demonstrated that in fast LC × LC separations (less than 1 h), the ^{2}D was more important than the ^{1}D in determining overall peak capacity concluding that extreme measures to enhance the ^{1}D peak capacity are usually unwarranted. More recently, simulations of 1D-LC and LC × LC separations of simple to moderately complex mixtures with the goal of understanding the ranges of analysis times and sample complexities in which each of these separations provides the best performance as measured by the probability of completely resolving the sample mixture, were investigated (Davis and Stoll, 2014).

The benefits on the sampling rate of the ^{1}D effluent attained by the use of multiple ^{2}D columns have been shown by Fairchild et al. (2009). The most interesting result is the increased peak capacity of the LC × LC system, and the possibility of reducing the analysis time compared to an LC × LC system employing only a single ^{2}D column (Fairchild et al., 2009). The main drawback can be traced back to the strict requirements for the similarity of the multiple ^{2}D columns.

3. ADVANCES IN PRACTICE

The most significant development in the practice of LC × LC in recent years has been the introduction of ^{2}D small particles stationary phases with the aim to replace the monolithic types that have been used earlier for the same goal (Cacciola et al., 2006, 2007c; Dugo et al., 2008c; Kivilompolo and Hyotylainen, 2008; Krauze-Baranowska et al., 2014; Hájek et al., 2016). The use of monoliths was dictated by several reasons: in particular these columns allowed the use of high flow rates without loss of resolution because of the better mass transfer properties of a monolithic skeleton over particle-packed columns, thus reducing analysis time. Moreover, because of the higher permeability of these columns, successive cycles of gradient could be performed with very brief reequilibration times and significantly lower backpressures (Lubda et al., 2001). However, the possibility to use conventional particles-packed wide pore columns to obtain very fast ^{2}D gradient elution separation was also reported (Stoll et al., 2006, 2007).

In 2007, a new particle technology (Fused-Core)was developed to deliver hyperfast chromatographic separations, while avoiding the reliability issues often associated with fast HPLC (Way, 2007a,b). These HPLC columns consist of a 1.7 μm solid core with a 0.5 μm porous silica shell surrounding it (d.p. = 2.7 μm). The major benefit of these particles was therefore the smaller diffusion path, which reduced axial dispersion of solutes minimizing peak broadening. The unique performance of these particle columns, offering the advantages of higher efficiencies and rugged design, capable of high-pressure operation, was demonstrated in some studies (Gritti et al., 2007; Gritti and Guiochon, 2007; Marchetti et al., 2007; Cavazzini et al., 2007; Cunliffe and Maloney, 2007; Donato et al., 2009). Because of these attributes, these columns were chosen as ^{2}D of LC × LC systems, and several research groups (Mondello, Dugo, Jandera and Cifuentes) used them in natural products applications (Hajek et al., 2008; Dugo et al., 2008c, 2009a,b; Russo et al., 2011; Mondello et al., 2011; Cacciola et al., 2012; Leme et al., 2014; Jandera et al., 2010a; Jandera, 2012; Česla et al., 2009; Hájek and Jandera, 2012; Montero et al. 2013a,b, 2014, 2016a,b; Donato et al., 2016). In two of the abovementioned references (Dugo et al., 2008c; Hajek et al., 2008) the performance of a partially porous short column was compared with that of a monolithic column. The results obtained demonstrated the possibility to use partially porous columns in the ^{2}D of LC × LC systems to obtain fast analyses, using high flow rates, under repetitive gradient conditions with very brief reconditioning times. Also, Cacciola et al. (2012) investigated the potential of serially coupled ^{2}D C18 partially porous columns for ultrahigh pressure two-dimensional liquid chromatography (UHPLC) for carotenoid analysis.

Among recent developments, the introduction of sub-2 μm technology was considered a milestone in LC × UHPLC applications because it allowed ultrafast analysis and/or high-resolution separations. In this regard, remarkable efforts have been made to extend the pressure capability of the pumping systems to 1300 bar. In addition, compared to old generation HPLC instruments, the contribution of the system to band broadening was dramatically reduced by using short and narrow connecting tubes, low injected volumes, small UV-cell volumes, and fast acquisition rates (Kivilompolo et al., 2008; Kivilompolo and Hyotylainen, 2008; Cacciola et al., 2011; Hájek and Jandera, 2012, 2016; Krol-Kogus et al., 2014; Kalili and de Villiers, 2009, 2010; Beelders et al., 2015; Jandera et al., 2012, 2013; Kalili et al., 2013; Montero et al., 2014; Willemse et al., 2014, 2015; Scoparo et al., 2012).

Besides the selection of stationary phases, mobile phases also play a pivotal role in the development of LC × LC methods. The choice of either isocratic or gradient elution conditions in both dimensions is of utmost importance. In this regard, each mode has to be carefully chosen to suit specific case studies. An interesting approach has been proposed in a pioneering way by the group of Jandera et al. who have extensively contributed to the progress in this area. Gradients with matching profiles running in parallel in the two dimensions over the whole LC × LC separation time range were investigated. This approach allowed them to improve system orthogonality, suppressing bandwidth broadening and obtaining a more regular band distribution over the whole LC × LC retention plane for samples with partially correlated elution times in the two dimensions and increasing peak capacity in the different set-ups. In addition, it eliminated the necessity of ^{2}D column reequilibration after the independent gradient runs for each fraction (Cacciola et al., 2007c). In this work, two short trapping columns were employed in the 10-port switching valve sample transfer interface, in place of the two conventional loops. This contributed to attain significant suppression of the band broadening connected with the sample transfer between the two dimensions, as the sample compounds were less strongly retained on the ^{1}D column than on the trapping column, so that a narrow sample zone adsorbed on the top of the trapping column could be back-flushed to the ^{2}D column in a small volume of the mobile phase. The sample fraction modulation technique employed allowed using a longer monolithic column in the ^{2}D, resulting in narrower sample bands (spots) in an LC × LC chromatogram.

Another type of gradient profile (called segmented in fraction (SIF)) was more recently investigated and applied to antioxidant analysis, and it will be described in Section 5.3 (Leme et al. 2014). Nevertheless, such optimization strategies will likely be a very fruitful area of research as soon as they are implemented for the analysis of more sample types.

4. INSTRUMENTAL SET-UP AND DATA ANALYSIS

Nowadays commercial ready-to-use LC × LC systems are currently available from some manufacturers such as Agilent Technologies and Shimadzu, making the methodology much easier for practical uses, responding to the users' demands. All conventional LC detectors, such as photodiode array (PDA), mass spectrometry (MS), and evaporative light scattering (ELS) detectors can be used in LC × LC. Usually, a single detector is installed after the ^{2}D column, although an additional detector can be used to collect the ^{1}D data, with the ^{1}D separation monitored only during the optimization step. The high speed of the ^{2}D analysis requires a very fast detector acquisition rate to ensure the adequate sampling, which is critical for quantification purposes, otherwise loss in resolution, due to a low number of data points, may occur. As far as data analysis is concerned, a great amount of data are usually produced, and dedicated software for its elaboration is required. Usually, data are visualized in 2D plots or contour plots, where the retention times in the ^{1}D and the ^{2}D dimensions are plotted along the *x*- and *y*-axes, respectively, while the color of the spots is a measure for intensity. Most developments have been carried out for software applied to gas-chromatography-based instrumentation rather than LC-based systems. One of the main reasons for such a situation is related to the much more complicated background signals in LC × LC rather than those in GC × GC, at least for UV absorbance detection compared with flame ionization detection (Reichenbach et al., 2005; Amandor-Munoz and Marriott, 2008; Harynuk et al., 2008; Pierce et al., 2008; Adcock et al., 2009). In LC × LC,

quantification can be performed by combining the contribution of each individual ^{2}D "slice" of a ^{1}D chromatographic peak, or by using more advanced algorithms (Kivilompolo and Hyilompolo, 2007, 2008; Mondello et al., 2008; Dugo et al., 2009a; Russo et al., 2011; Cook et al., 2015; Beccaria et al., 2015; Donato et al., 2016). Advanced data analysis techniques, e.g., multivariate data analysis, can also be applied to LC × LC data, despite it being more complicated with respect to 1D-LC separations (Pierce and Mohler, 2012; Bailey and Rutan, 2013).

So far, two commercially available software packages, namely Chromsquare and GC Image LC × LC Edition Software specially designed for both visualization and quantification of 2D data, are available on the market. Additional work is deemed as essential in this field because of the increasing number of 2D applications that can be run by means of such a methodology for both qualitative and quantitative purposes.

5. LC × LC OF NATURAL PRODUCTS

The two most commonly used configurations of LC × LC systems for the analysis of natural products are represented by normal-phase LC combined with reversed-phase LC (NP × RP), and RP in both dimensions (RP × RP). On the one hand, for NP × RP separation of carotenoids, either silica or cyanopropyl (CN) stationary phases have been investigated (Dugo et al. 2006a, 2008d,e, 2009c; Cacciola et al., 2012, 2016a,b), whereas for triacylglycerol (TAG) separation, an Ag × RP combination turned out to be useful for this task (Mondello et al., 2005, 2011; Dugo et al., 2006b,c; Van der Klift et al., 2008; Holcapek et al., 2009; Yang et al., 2012; Hu et al., 2013; Wei et al., 2013, 2015; Costa et al., 2015; Beccaria et al., 2015). On the other hand, for RP × RP separation of phenolic antioxidants, the effect of several stationary phase chemistries (C8, C18, CN, Diol, F_5, NH_2, PEG, Phenyl, RP-Amide, and other laboratory-made stationary phases) on the separation selectivity and resolution has been investigated (Blahovà et al., 2006; Cacciola et al, 2006, 2007a,b,c, 2011; Kivilompolo and Hyilompolo, 2007, 2008; Pol et al., 2007, Pol and Hyotylainen, 2008; Dugo et al., 2008c, 2009a,b; Jandera et al., 2008a,b, 2012, 2013; Kivilompolo et al. 2008; Hájek et al., 2008, 2016; Česla et al., 2009; Jandera and Hájek, 2009; Kalili and de Villiers, 2009, 2010, 2013a,b; Zhou et al., 2009; Russo et al., 2011; Fu et al., 2012; Hájek and Jandera, 2012; Kalili et al. 2013, 2014; Montero et al., 2013a,b, 2014, 2016a,b; Krol-Kogus et al., 2014; Krauze-Baranowska et al., 2014; Leme et al., 2014; Tanaka et al., 2014; Willemse et al., 2014, 2015; Donato et al., 2016).

5.1 LC × LC OF CAROTENOIDS

Carotenoids are the most broadly distributed pigments in nature (Mendes-Pinto et al., 2005; Herrero et al., 2006). *Citrus* species, particularly orange, are commonly regarded as the most complex natural source of these compounds. Some of these compounds are reported to show different functional properties, such as antioxidant activity (Beutner et al., 2001; Leach et al., 1998), prevention of cancer (Nishino et al., 1999), cardiovascular diseases (Arab and Steck, 2000; Rao and Rao, 2007), and macular degeneration (Snodderly, 1995). Carotenoids are a very complex group of compounds based on a C40-tetraterpenoid skeleton and are usually classified into two main groups: hydrocarbon carotenoids, known as carotenes (e.g., β-carotene and lycopene), and oxygenated carotenoids, known as xanthophylls (e.g., β-cryptoxanthin and lutein). The elucidation of carotenoid patterns is particularly challenging because of the complex composition of carotenoids in natural matrices,

considering their great structural diversity and extreme instability. The first works were reported by Dugo et al. who investigated an NP-LC × RP-LC platform for the separation and identification of these compounds in intact and saponified *Citrus* samples (Dugo et al. 2006a, 2008d,e, 2009c). For identification purposes, PDA and atmospheric pressure chemical ionization mass spectrometry (APCI-MS) were employed, thanks to the complementary data of the two detection systems employed. In the earlier work, a microbore silica column in NP mode (^{1}D) and a monolithic C18 column in RP mode (^{2}D) were employed for the elucidation of the carotenoid pattern in saponified orange essential oil and juice samples (Dugo et al., 2006a,b,c). In the three subsequent studies, aiming to evaluate the native carotenoid composition of mandarin and red-orange essential oils, the ^{1}D microbore silica column was replaced with a CN column for the separation of free carotenoids and carotenoid esters (Dugo et al., 2008d,e, 2009c). The most recent works were carried out by Cacciola et al. for analysis of different food samples, namely red chili pepper (2012), overripe fruits (2016a), and *Pouteria sapote* (red mamey) (2016b). The set-up employed was the same as exploited in the former works but with the use of UHPLC conditions in the ^{2}D separations. In particular Cacciola et al. (2012) presented a comparison of a conventional NP-LC × RP-LC and a NP-LC × RP-UHPLC set-up. In the latter case, two columns of the same stationary phase (C18) were serially coupled with different gradient and modulation times (1.50 and 1.00 min). Despite the doubling of the stationary phase length, with respect to the "conventional" NP-LC × RP-LC set-up, the NP-LC × RP-UHPLC method with a 1.50 min modulation time (and gradient), greatly suffered from the reduced number of fractions transferred from the ^{1}D. On the other hand, among the two NP-LC × RP-UHPLC set-ups tested, the one at 1.00 min modulation time yielded the best results in terms of performance because of increased ^{1}D sampling.

A similar NP-LC × RP-UHPLC with modulation time of 1.00 min was employed for the carotenoid analysis of a red mamey saponified extract, and the 2D plot (wavelength 450 nm) is shown in Fig. 8.1. In total, 23 compounds belonging to 17 different carotenoid chemical classes were positively separated and identified.

5.2 LC × LC OF TRIACYLGLYCEROLS

Various lipidic matrixes such as donkey milk samples, plant oils, and marine organisms have been investigated using an LC × LC mode employing silver-ion chromatography (microbore Ag column) in the ^{1}D and nonaqueous RP-LC in the ^{2}D (C18 column) connected via a 10-port switching valve. In all cases, the use of APCI-MS greatly increased the potential for component identification, thanks to the absence of peak coelutions and to the restricted number of components that can be assigned to a spot located in a well-defined position of the 2D plane, making peak identification easier, even when commercial standards are not available.

Thorough elucidation of a rice oil TAG profile was reported by Mondello et al. (2005). A primary Ag microbore column operated under isocratic elution conditions was connected to a monolithic column and that operated under gradient elution conditions via a 10-port valve was equipped with two 20-μL loops. Because of the highest LC × LC resolving power and MS spectral information, 11 TAGs were positively identified, thus exploring a group of components that are of fundamental importance in food chemistry. A nice application to the analysis of TAGs in donkey milk, using a similar set-up, has been reported by Dugo et al. (2006b). With respect to the previous work, the main difference consisted in the use of gradient elution also in the ^{1}D, enabling the attainment of peaks with comparable widths

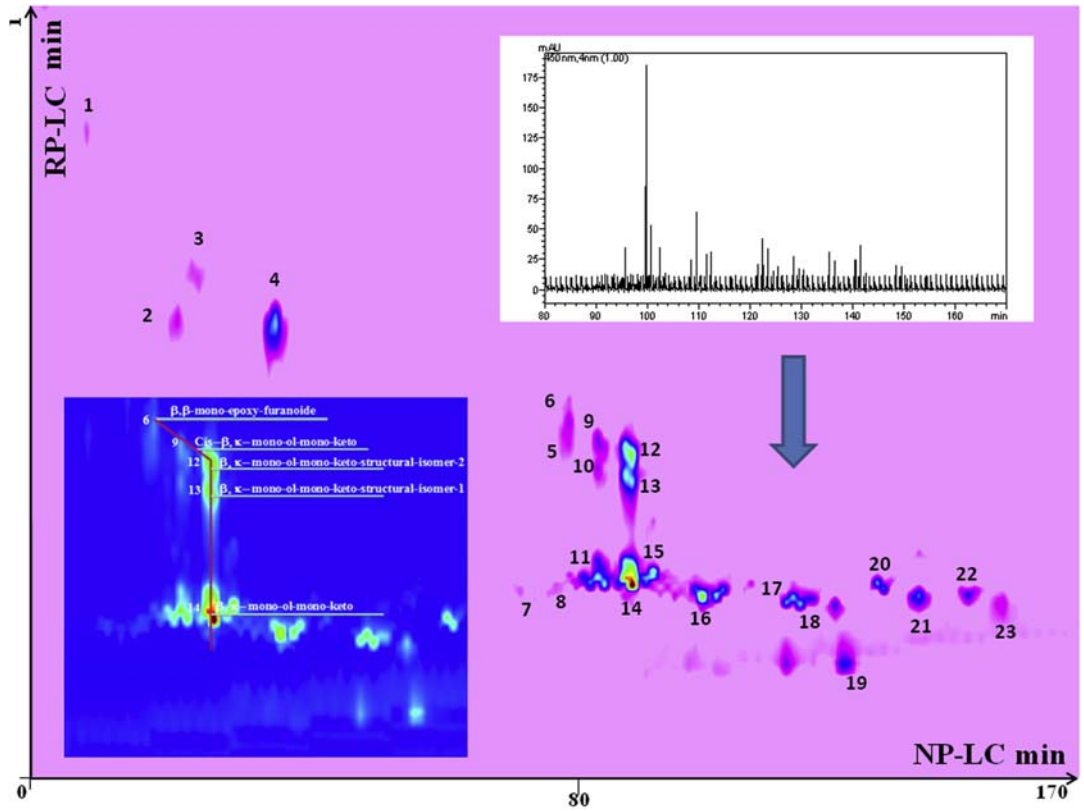

FIGURE 8.1

Contour plot (λ = 450 nm) of the NP-LC × UHP-RP-LC-PDA analysis of carotenoids in saponified red mamey. *NP-LC*, normal-phase liquid chromatography; *PDA*, photodiode array; *RP-LC*, reversed-phase liquid chromatography; *UHP*, ultrahigh pressure.

*Reprinted with Permission from Springer: Cacciola, F., Giuffrida, D., Utczas, M., Mangraviti, D., Dugo, P., Menchaca, D., Murillo, E., Mondello, L., 2016b. Application of comprehensive two-dimensional liquid chromatography for carotenoid analysis in red mamey (*Pouteria sapote*) fruit. Food Anal. Methods 9, 2335–2341.*

in a reasonable analytical time. By using this approach, nearly 60 TAGs were separated and identified revealing that the investigated system was an effective tool for characterization of the TAG fraction of such a complex matrix. The use of a gradient program in both LC dimensions was also applied to the analysis of different plant oils containing TAGs in a wide range of partition number (PN) (36–52) and DB numbers (1–9) such as linseed and soybean oils (Dugo et al., 2006c). In addition, the separation of some positional isomers was achieved. In all the cases, TAGs were separated under NP conditions in the ^{1}D and RP conditions in the ^{2}D. However, an interesting modification to the above described platforms was provided by Van der Klift et al. who clearly demonstrated that TAGs could be efficiently separated with a methanol-based solvent on an Ag-coated ion-exchanger medium, thus avoiding the

use of hexane (2008), allowing the detection of 44 TAGs in corn oil. Later, in 2011, the use of a partially porous C18 stationary phase was investigated in the ^{2}D of the LC × LC system in combination with ELS detection for the analysis of the TAG fraction in a *Borago officinalis* oil. Also, in the mobile phase employed in the ^{1}D separations acetonitrile was replaced by butyronitrile, which being less polar than acetonitrile, allowed to solve miscibility issues and the typical instability of mixtures of hexane/acetonitrile. A total of 78 different TAGs were identified throughout the LC × LC retention plane making the approach useful for identification purposes. Fig. 8.2 reports the silver ion × RPLC/APCI-MS for an analysis of an edible peanut oil investigated by Yang et al. (2012). Twenty-eight TAGs were identified based on the TAGs' retention behaviors on both columns and their APCI-MS fragments, labeled on the contour plot (Fig. 8.2A). It is easily understandable that the compounds aligned vertically or horizontally on the 2D contour plot would be coeluted if the conventional 1D analysis was performed. When applying the LC × LC separation system, the coeluted fractions were subjected to a ^{2}D, and then were well separated based on the individual PNs of the TAG species. As a result, five peaks which were almost baseline separated were obtained (Fig. 8.2B).

The potential of off-line LC × LC coupling of nonaqueous RP and silver-ion chromatography was successfully demonstrated in three different works (Holčapek et al., 2009; Beccaria et al., 2015; Costa et al., 2015). In all set-ups, the approach investigated provided the highest separation capacity of TAGs in complex natural samples of plant oils and marine fats resulting in the highest number of identified TAGs ever reported for studied samples. The only drawback of the approach is related to the long analysis time, making this method not useful for routine quality control of TAG mixtures of relatively low complexity.

A very recent approach for TAG analysis in edible oils has been reported by Wei et al. (2013, 2015): in such works novel mixed-mode single chromatographic columns were employed combining the features of traditional C8/C18 and silver-ion columns.

5.3 LC × LC OF POLYPHENOLIC ANTIOXIDANTS

Polyphenolic antioxidants represent a large family of naturally occurring compounds in fruits and vegetables, and in beverages originating from the plants used in production, such as barley, hop, and hop products used in the beer-brewing process. It has been demonstrated that some of them show strong antioxidant properties with beneficial, physiological, and anticarcinogenic properties for human health (Hertog et al., 1993; Tsuchiya et al., 1997; Dalluge et al., 1998). Because of higher peak capacity, selectivity, and resolution, LC × LC systems have been investigated for the separation of these compounds, taking the advantage of the different selectivity of various RP columns. According to literature data, various combinations of columns have been employed for the separation of polyphenolic antioxidants in vegetables, fruits, beer, and wine samples. Taking into consideration the chemical properties of polyphenols, for their separations RP-LC × RP-LC techniques were mostly employed because fully compatible solvents are employed. The main disadvantage of such a combination, when a common "full in fraction" is adopted (an equally generic and steep mobile-phase range in each repeated ^{2}D run), is the serious correlation of the two separation systems. The orthogonality of RP-LC × RP-LC systems can be improved through a critical selection of the mobile-phase composition (typically the organic modifier used because pH in the range used for flavonoid analysis has little effect on the selectivity), and especially the stationary phase chemistries used in both dimensions. In the case where gradient separation is performed in both dimensions, the ^{2}D

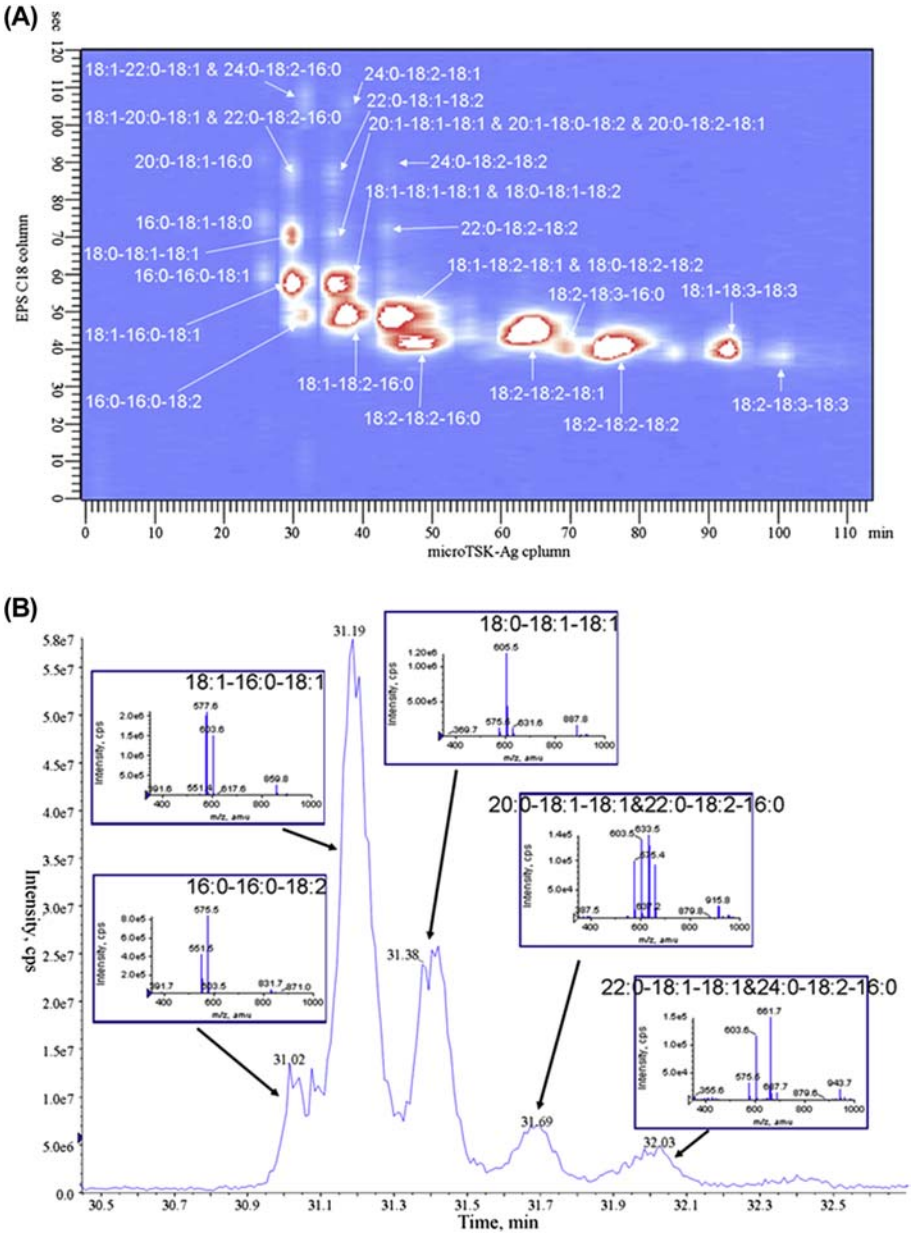

FIGURE 8.2

(A) Contour plot of comprehensive two-dimensional (2D) silver ion × RPLC separation of peanut oil. (B) A slice of expanded raw chromatogram of the comprehensive 2D liquid chromatography analysis of peanut oil. Triacylglycerols were denoted by the three fatty acids linked to the glycerol backbone, and their positions did not represent the stereochemical positions. *RPLC*, reversed-phase liquid chromatography.

Reprinted with Permission from Elsevier: Yang, Q., Shi, X., Gu, Q., Zhao, S., Zhao, Y., Shan, Y., Xu, G., 2012. On-line two dimensional liquid chromatography/mass spectrometry for the analysis of triacylglycerides in peanut oil and mouse tissue. J. Chromatogr. B 895–896, 48–55.

gradient can be varied throughout the ^{1}D separation to maximize the utilization of the RP-LC × RP-LC space (Česla et al., 2009; Jandera et al., 2010a,b; Hájek and Jandera, 2012; Leme et al., 2014; Donato et al., 2016): "continuously shifting" where only a single gradient spanning the whole ^{2}D separation time is adopted simultaneously to the ^{1}D gradient, and "SIF" where different gradient ranges in various segments of the ^{1}D separation are employed. Fig. 8.3 shows the RP-LC × RP-LC plots of a sugarcane leaf extract obtained by using the three different set-ups, using the optimized conditions for each dimension. In such an example, among the RP-LC × RP-LC strategies tested, the use of the SIF gradient (set-up 3B) was the most effective one, yielding the highest peak capacity, allowing the detection of 38 polyphenolic compounds, and among them 24 were positively identified in the sugarcane leaf extract analyzed by means of complementary data from PDA and MS detection and an in-house database.

More recently, a very promising column combination in LC × LC employs the use of hydrophilic interaction liquid chromatography (HILIC) and RP conditions in the ^{1}D and ^{2}D, respectively. The combination of HILIC and RP-LC promises higher orthogonality with respect to RP-LC × RP-LC, although hyphenation of the former modes is more complicated because of the relative elution strengths of the mobile phase used in each dimension. For such a reason, the employment of microflow rates in the ^{1}D is highly beneficial to minimize dilution and provide flow rates compatible with ^{2}D injection volumes (Kalili and de Villiers, 2009, 2010, 2013a,b; Beelders et al., 2015; Jandera et al., 2012, 2013; Kalili et al., 2013, 2014; Montero et al., 2013a,b, 2014, 2016a,b; Willemse et al., 2015; Hájek et al., 2016). As an example in Fig. 8.4, the contour plot obtained at 500 nm for the HILIC × RP-LC−UV−MS analysis of the 2013 Pinotage wine, is shown. Up to 94 anthocyanin-derived pigments were tentatively identified using accurate mass and fragmentation information obtained using quadrupole time-of-flight mass spectrometer. The structured elution order greatly improved the certainty in compound identification, holding promise for the detailed elucidation of the chemical alteration of anthocyanins during wine aging. In all applications the choice of RP-LC separations in the ^{2}D analysis lies in the compatibility with MS detection and the possibility to attain very fast separations (Dugo et al., 2008a; Tranchida et al., 2013), although HILIC was also employed for fast ^{2}D analysis prior to MS detection (Fu et al., 2012).

6. FUTURE PERSPECTIVES

Comprehensive 2D-LC has proven so far its viability as a powerful tool for separation of complex natural products samples. The possibility of taking advantage of commercial ready-to-use LC × LC systems from some manufacturers makes the methodology much easier for practical uses. The introduction into the market of partially porous particles and sub-2 μm stationary phases was a very exciting development. Surely progress in column technology will result in the commercialization of new types of columns with high efficiency, temperature stability, and permeability, enabling wider use of high-pressure and high-temperature fast ^{2}D operation. Also the number of applications involving the design of software capable to tune "smart" gradients for LC × LC is expected to grow in the following years. Finally, the development of more robust and flexible software for both qualitative and quantitative purposes will be worth considering for handling the complexity of resulting LC × LC data.

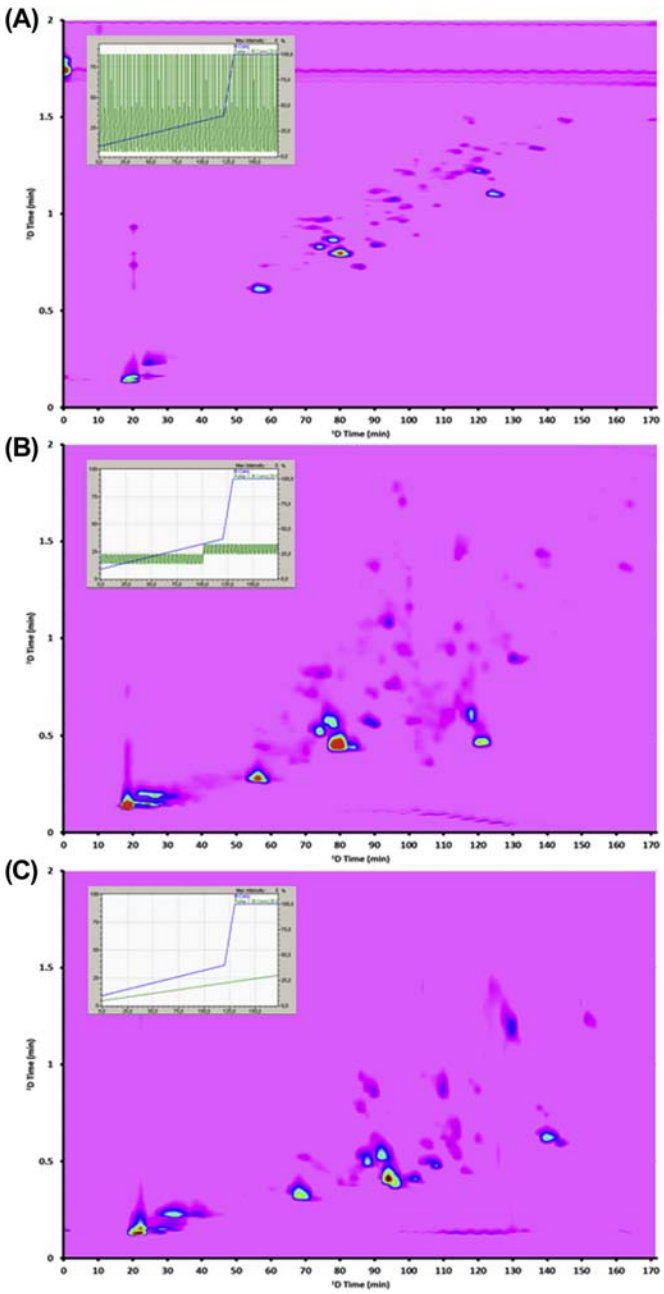

FIGURE 8.3

RP-LC × RP-LC contour plots of a sugarcane leaf extract by means of three different set-up, namely "full in fraction" (FIF, set-up 3A), "segmented in fraction" (SIF, set-up 3B), and "continuously shifting" (CS, set-up 3C) gradients. ^{1}D, first dimension; *RP-LC*, reversed-phase liquid chromatography.

*Reprinted with Permission from Springer: Leme, G.M., Cacciola, F., Donato, P., Cavalheiro, A.J., Dugo, P., Mondello, L., 2014. Continuous vs. segmented second-dimension system gradients for comprehensive two-dimensional liquid chromatography of sugarcane (*Saccharum *spp.). Anal. Bioanal. Chem. 406, 4315–4324.*

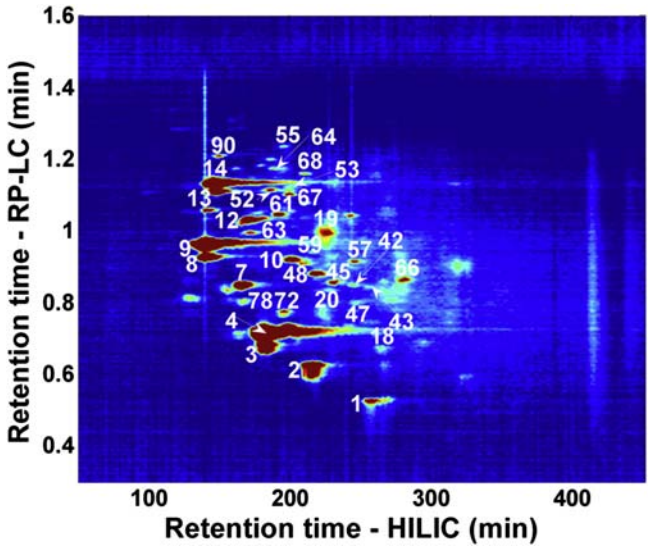

FIGURE 8.4

Contour plot for the online HILIC × RP-LC−UV-MS analysis of a 2013 Pinotage wine obtained at 500 nm. *HILIC*, hydrophilic interaction liquid chromatography; *MS*, mass spectrometry; *RP-LC*, reversed-phase liquid chromatography.

Reproduced with permission from ACS. Reprinted with Permission from Springer: Willemse, C.M., Stander, M.A., Vestner, J., Tredoux, A.G.J., de Villiers, A., 2015. Comprehensive two-dimensional hydrophilic interaction chromatography (HILIC) × reversed-phase liquid chromatography coupled to high-resolution mass spectrometry (RP-LC-UV-MS) analysis of anthocyanins and derived pigments in red wine. Anal. Chem. 87, 12006−12015.

REFERENCES

Adcock, J.L., Adams, M., Mitrevski, B.S., Marriott, P.J., 2009. Peak modeling approach to accurate assignment of first-dimension retention times in comprehensive two-dimensional chromatography. Anal. Chem. 81, 6797−6804.

Amador-Munoz, O., Marriot, P.J., 2008. Quantification in comprehensive two-dimensional gas chromatography and a model of quantification based on selected summed modulated peaks. J. Chromatogr. A 1184, 323−340.

Arab, L., Steck, S., 2000. Lycopene and cardiovascular disease. Am. J. Clin. Nutr. 71, 1691S−1695S.

Bailey, H.P., Rutan, S.C., 2013. Comparison of chemometric methods for the screening of comprehensive two-dimensional liquid chromatographic analysis of wine. Anal. Chim. Acta 770, 18−28.

Beccaria, M., Costa, R., Sullini, G., Grasso, E., Cacciola, F., Dugo, P., Mondello, L., 2015. Determination of the triacylglycerol fraction in fish oil by comprehensive liquid chromatography techniques with the support of gas chromatography and mass spectrometry data. Anal. Bioanal. Chem. 407, 5211−5225.

Bedani, F., Schoenmakers, P.J., Janssen, H.-G., 2012. Theories to support method development in comprehensive two-dimensional liquid chromatography − a review. J. Sep. Sci. 35, 1697−1711.

Berek, D., 2010. Two-dimensional liquid chromatography of synthetic polymers. Anal. Bioanal. Chem. 396, 421−441.

Beutner, S., Bloedorn, B., Frixel, S., Hernandez Blanco, I., Hoffman, T., Martin, H.-D., Mayer, B., Noack, P., Ruck, C., Schmidt, M., Schulke, I., Sell, S., Ernst, H., Haremza, S., Seybold, G., Sies, H., Stahl, W., Walsh, R., 2001. Quantitative assessment of antioxidant properties of natural colorants and phytochemicals: carotenoids, flavonoids, phenols and indigoids. The role of β-carotene in antioxidant functions. J. Sci. Food Agric. 81, 559−568.

Beelders, T., Kalili, K.M., Joubert, E., Beer, D., de Villiers, A., 2015. Comprehensive two-dimensional liquid chromatographic analysis of rooibos (*Aspalathus linearis*) phenolics. J. Sep. Sci. 35, 1808−1820.

Blahovà, E., Jandera, P., Cacciola, F., Mondello, L., 2006. Two-dimensional and serial column reversed-phase separation of phenolic antioxidants on octadecyl-, polyethyleneglycol-, and pentafluorophenylpropyl-silica columns. J. Sep. Sci. 29, 555−566.

Cacciola, F., Jandera, P., Blahovà, E., Mondello, L., 2006. Development of different comprehensive two-dimensional systems for the separation of phenolic antioxidants. J. Sep. Sci. 29, 2500−2513.

Cacciola, F., Jandera, P., Mondello, L., 2007a. Temperature effects on separation on zirconia columns: applications to one- and two-dimensional LC separations of phenolic antioxidants. J. Sep. Sci. 30, 462−474.

Cacciola, F., Jandera, P., Mondello, L., 2007b. Comparison of high-temperature gradient heart-cutting and comprehensive LC × LC systems for the separation of phenolic antioxidants. Chromatographia 66, 661−667.

Cacciola, F., Jandera, P., Hajdù, Z., Česla, P., Mondello, L., 2007c. Comprehensive two-dimensional liquid chromatography with parallel gradients for separation of phenolic and flavone antioxidants. J. Chromatogr. A 1149, 73−87.

Cacciola, F., Delmonte, P., Jaworska, K., Dugo, P., Mondello, L., Rader, J., 2011. Employing ultra high pressure liquid chromatography as the second dimension in a comprehensive two-dimensional system for analysis of *Stevia rebaudiana* extracts. J. Chromatogr. A 1218, 2012−2018.

Cacciola, F., Donato, P., Giuffrida, D., Torre, G., Dugo, P., Mondello, L., 2012. Ultra high pressure in the second dimension of a comprehensive two-dimensional liquid chromatographic system for carotenoid separation in chili red peppers. J. Chromatogr. A 1255, 244−251.

Cacciola, F., Giuffrida, D., Utczas, M., Mangraviti, D., Beccaria, M., Donato, P., Bonaccorsi, I., Dugo, P., Mondello, L., 2016a. Analysis of the carotenoid composition and stability in various overripe fruits by comprehensive two-dimensional liquid chromatography. LC-GC Eur. 5, 252−256.

Cacciola, F., Giuffrida, D., Utczas, M., Mangraviti, D., Dugo, P., Menchaca, D., Murillo, E., Mondello, L., 2016b. Application of comprehensive two-dimensional liquid chromatography for carotenoid analysis in red mamey (*Pouteria sapote*) fruit. Food Anal. Methods 9, 2335−2341.

Cavazzini, A., Gritti, F., Kaczmarski, K., Marchetti, N., Guiochon, G., 2007. Mass-transfer kinetics in a shell packing material for chromatography. Anal. Chem. 79, 5972−5979.

Česla, P., Hájek, T., Jandera, P., 2009. Optimization of two-dimensional gradient liquid chromatography separations. J. Chromatogr. A 1216, 3443−3457.

Cook, D.W., Rutan, S.C., Stoll, D.R., Carr, P.W., 2015. Two dimensional assisted liquid chromatography − a chemometric approach to improve accuracy and precision of quantitation in liquid chromatography using 2D separation, dual detectors, and multivariate curve resolution. Anal. Chim. Acta 859, 87−95.

Costa, R., Beccaria, M., Grasso, E., Albergamo, A., Oteri, M., Dugo, P., Fasulo, S., Mondello, L., 2015. Sample preparation techniques coupled to advanced chromatographic methods for marine organisms investigation. Anal. Chim. Acta 875, 41−53.

Cunliffe, J.M., Maloney, T.D., 2007. Fused-core particle technology as an alternative to sub-2-μm particles to achieve high separation efficiency with low backpressure. J. Sep. Sci. 30, 3104−3109.

Dalluge, J.J., Nelson, B.C., Brown Thomas, J., Sander, L.C., 1998. Selection of column and gradient elution system for the separation of catechins in green tea using high-performance liquid chromatography. J. Chromatogr. A 793, 265−274.

Davis, J.M., 2005. Statistical-overlap theory for elliptical zones of high aspect ratio in comprehensive two-dimensional separations. J. Sep. Sci. 28, 347−359.

Davis, J.M., Stoll, D.R., Carr, P.W., 2008a. Effect of first-dimension undersampling on effective peak capacity in comprehensive two-dimensional separations. Anal. Chem. 80, 461−473.

Davis, J.M., Stoll, D.R., Carr, P.W., 2008b. Dependence of effective peak capacity in comprehensive two-dimensional separations on the distribution of peak capacity between the two dimensions. Anal. Chem. 80, 8122−8134.

Davis, J.M., Stoll, D.R., 2014. Likelihood of total resolution in liquid chromatography: evaluation of one-dimensional, comprehensive two-dimensional, and selective comprehensive two-dimensional liquid chromatography. J. Chromatogr. A 1360, 128−142.

Dixon, S.P., Pitfield, I.D., Perrett, D., 2006. Comprehensive multi-dimensional liquid chromatographic separation in biomedical and pharmaceutical analysis: a review. Biomed. Chromatogr. 20, 508−529.

Donato, P., Dugo, P., Cacciola, F., Dugo, G., Mondello, L., 2009. High peak capacity separation of peptides through the serial connection of LC shell-packed columns. J. Sep. Sci. 32, 1129−1136.

Donato, P., Cacciola, F., Tranchida, P.Q., Dugo, P., Mondello, L., 2012. Mass spectrometry detection in comprehensive liquid chromatography: basic concepts, instrumental aspects, applications and trends. Mass Spectrom. Rev. 31, 523−559.

Donato, P., Rigano, F., Cacciola, F., Schure, M., Farnetti, S., Russo, M., Dugo, P., Mondello, L., 2016. Comprehensive two-dimensional liquid chromatography-tandem mass spectrometry for the simultaneous determination of wine polyphenols and target contaminants. J. Chromatogr. A 1458, 54−62.

Dugo, P., Škeřiková, V., Kumm, T., Trozzi, A., Jandera, P., Mondello, L., 2006a. Elucidation of carotenoid patterns in citrus products by means of comprehensive normal-phase and reversed-phase liquid chromatography. Anal. Chem. 78, 7743−7750.

Dugo, P., Kumm, T., Chiofalo, B., Cotroneo, A., Mondello, L., 2006b. Separation of triacylglycerols in a complex lipidic matrix by using comprehensive two dimensional liquid chromatography coupled with atmospheric pressure chemical ionization mass spectrometric detection. J. Sep. Sci. 29, 1146−1154.

Dugo, P., Kumm, T., Crupi, M.L., Cotroneo, A., Mondello, L., 2006c. Comprehensive two-dimensional liquid chromatography combined with mass spectrometric detection in the analyses of triacylglycerols in natural lipidic matrixes. J. Chromatogr. A 1112, 269−275.

Dugo, P., Cacciola, F., Kumm, T., Dugo, G., Mondello, L., 2008a. Comprehensive multidimensional liquid chromatography: theory and applications. J. Chromatogr. A 1184, 353−368.

Dugo, P., Kumm, T., Cacciola, F., Dugo, G., Mondello, L., 2008b. Multidimensional liquid chromatographic separations applied to the analysis of food samples. J. Liq. Chromatogr. Relat. Technol. 31, 1758−1807.

Dugo, P., Cacciola, F., Herrero, M., Donato, P., Mondello, L., 2008c. Use of partially porous column as second dimension in comprehensive two-dimensional system for analysis of polyphenolic antioxidants. J. Sep. Sci. 31, 3297−3308.

Dugo, P., Herrero, M., Kumm, T., Giuffrida, D., Dugo, G., Mondello, L., 2008d. Comprehensive normal-phase x reversed-phase liquid chromatography coupled to photodiode array and mass spectrometry detectors for the analysis of free carotenoids and carotenoid esters from mandarin. J. Chromatogr. A 1139, 196−206.

Dugo, P., Herrero, M., Giuffrida, D., Kumm, T., Dugo, G., Mondello, L., 2008e. Application of comprehensive two-dimensional liquid chromatography to elucidate the native carotenoid composition in red orange essential oil. J. Agric. Food Chem. 56, 3478−3485.

Dugo, P., Cacciola, F., Donato, P., Airado-Rodriguez, D., Herrero, M., Mondello, L., 2009a. Comprehensive two-dimensional liquid chromatography to quantify polyphenols in red wines. J. Chromatogr. A 1216, 7483−7487.

Dugo, P., Cacciola, F., Donato, P., Assis, R.A., Caramão, E.B., Mondello, L., 2009b. High efficiency liquid chromatography techniques coupled to mass spectrometry for the characterization of mate extracts. J. Chromatogr. A 1216, 7213−7221.

Dugo, P., Herrero, M., Giuffrida, D., Donato, P., Mondello, L., 2009c. Epoxycarotenoids esters analysis in intact orange juices using two-dimensional comprehensive liquid chromatography. J. Sep. Sci. 32, 973−980.

Erni, F., Frei, R.W., 1978. Two-dimensional column liquid chromatographic technique for resolution of complex mixture. J. Chromatogr. A 149, 561−569.

Evans, C.R., Jorgenson, J.W., 2004. Multidimensional LC-LC and LC-CE for high-resolution separations of biological molecules. Anal. Bioanal. Chem. 378, 1952−1961.

Fairchild, J.N., Horvath, K., Guiochon, G., 2009. Theoretical advantages and drawbacks of on-line, multidimensional liquid chromatography using multiple columns operated in parallel. J. Chromatogr. A 1216, 6210−6217.

François, I., Sandra, K., Sandra, P., 2009a. Comprehensive liquid chromatography: fundamental aspects and practical considerations-a review. Anal. Chim. Acta 641, 14−31.

Fu, Q., Guo, Z., Zhang, X., Liu, Y., Liang, X., 2012. Comprehensive characterization of *Stevia rebaudiana* using two-dimensional reversed-phase liquid chromatography/hydrophilic interaction liquid chromatography. J. Sep. Sci. 35, 1821−1827.

Giddings, J.C., 1984. Two-dimensional separations: concept and promise. Anal. Chem. 56, 1258A−1264A.

Giddings, J.C., 1987. Concepts and comparisons in multidimensional separation. J. High Resolut. Chromatogr. Chromatogr. Commun. 10, 319−323.

Gritti, F., Cavazzini, A., Marchetti, N., Guiochon, G., 2007. Comparison between the efficiencies of columns packed with fully and partially porous C_{18}-bonded silica materials. J. Chromatogr. A 1157, 289−303.

Gritti, F., Guiochon, G., 2007. Comparative study of the performance of columns packed with several new fine silica particles: would the external roughness of the particles affect column properties? J. Chromatogr. A 1166, 30−46.

Gu, H., Huang, Y., Carr, P.W., 2011. Peak capacity optimization in comprehensive two dimensional liquid chromatography: a practical approach. J. Chromatogr. A 1218, 64−73.

Guiochon, G., Marchetti, N., Mriziq, K., Shalliker, R.A., 2008. Implementations of two- dimensional liquid chromatography. J. Chromatogr. A 1189, 109−168.

Guttman, A., Varoglu, M., Khandurina, J., 2004. Multidimensional separations in the pharmaceutical arena. Drug Discov. Today 9, 136−144.

Hájek, T., Škeřiková, V., Česla, P., Vyňuchalová, K., Jandera, P., 2008. Multidimensional LC × LC analysis of phenolic and flavone natural antioxidants with UV-electrochemical coulometric and MS detection. J. Sep. Sci. 31, 3309−3328.

Hájek, T., Jandera, P., 2012. Columns and optimum gradient conditions for fast second-dimension separations in comprehensive two-dimensional liquid chromatography. J. Sep. Sci. 35, 1712−1722.

Hájek, T., Jandera, P., Staňková, M., Česla, P., 2016. Automated dual two-dimensional liquid chromatography approach for fast acquisition of three-dimensional data using combinations of zwitterionic polymethacrylate and silica-based monolithic columns. J. Chromatogr. A 1446, 91−102.

Harynuk, J.J., Kwong, A.H., Marriott, P.J., 2008. Modulation-induced error in comprehensive two-dimensional gas chromatographic separations. J. Chromatogr. A 1200, 17−27.

Herrero, M., Jaime, L., Martin-Alvarez, P.J., Cifuentes, A., Ibanez, E., 2006. Optimization of the extraction of antioxidants from *Dunaliella salina* microalga by pressurized liquids. J. Agric. Food Chem. 54, 5597−5603.

Herrero, M., Ibanez, E., Cifuentes, A., Bernal, J., 2009. Multidimensional chromatography in food analysis. J. Chromatogr. A 1216, 7110−7129.

Holčapek, M., Velinska, H., Lisa, M., Česla, P., 2009. Orthogonality of silver-ion and non-aqueous reversed-phase HPLC/MS in the analysis of complex natural mixtures of triacylglycerols. J. Sep. Sci. 32, 3672−3680.

Hertog, M.G.L., Hollman, P.C.H., Van de Putte, B., 1993. Content of potentially anticarcinogenic flavonoids of tea infusions, wines, and fruit juices. J. Agric. Food Chem. 41, 1242−1246.

Horie, K., Kimura, H., Ikegami, T., Iwatsuka, A., Saad, N., Fiehn, O., Tanaka, N., 2007. Calculating optimal modulation periods to maximize the peak capacity in two dimensional HPLC. Anal. Chem. 79, 3764−3770.

Hu, J., Wei, F., Dong, X.Y., Lv, X., Jiang, M.L., Li, G.M., Chen, H., 2013. Characterization and quantification of triacylglycerols in peanut oil by off-line comprehensive two-dimensional liquid chromatography coupled with atmospheric pressure chemical ionization mass spectrometry. J. Sep. Sci. 36, 288−300.

Jandera, P., 2006. Column selectivity for two-dimensional liquid chromatography. J. Sep. Sci. 29, 1763−1783.

Jandera, P., Česla, P., Hájek, T., Vohralik, G., Vyňuchalova, K., Fischer, J., 2008a. Optimization of separation in two-dimensional high-performance liquid chromatography by adjusting phase system selectivity and using programmed elution techniques. J. Chromatogr. A 1189, 207−220.

Jandera, P., Vynuchalova, K., Hájek, T., Česla, P., Vohralik, G., 2008b. Characterization of HPLC columns for two-dimensional LC × LC separations of phenolic acids and flavonoids. J. Chemom. 22, 203−207.

Jandera, P., Hájek, T., 2009. Utilization of dual retention mechanism on columns with bonded PEG and diol stationary phases for adjusting the separation selectivity of phenolic and flavone natural antioxidants. J. Sep. Sci. 32, 3603−3619.

Jandera, P., Hájek, T., Česla, P., 2010a. Comparison of various second-dimension gradient types in comprehensive two-dimensional liquid chromatography. J. Sep. Sci. 33, 1382−1397.

Jandera, P., Hájek, T., Škeřikova, V., Soukup, J., 2010b. Dual hydrophilic interaction-RP retention mechanism on polar columns: structural correlations and implementation for 2-D separations on a single column. J. Sep. Sci. 33, 841−852.

Jandera, P., 2012. Comprehensive two-dimensional liquid chromatography-practical impacts of theoretical considerations. a review. Cent. Eur. J. Chem. 10, 844−875.

Jandera, P., Hájek, T., Staňková, M., Vynuchalová, K., Česla, P., 2012. Optimization of comprehensive two-dimensional gradient chromatography coupling in-line hydrophilic interaction and reversed phase liquid chromatography. J. Chromatogr. A 1268, 91−101.

Jandera, P., Staňkova, M., Hájek, T., 2013. New zwitterionic polymethacrylate monolithic columns for one- and two-dimensional microliquid chromatography. J. Sep. Sci. 36, 2430−2440.

Karger, B.L., Snyder, L.R., Horvath, C., 1973. An Introduction to Separation Science. Wiley & Sons, New York.

Kalili, K.M., de Villiers, A., 2009. Off-line comprehensive 2-dimensional hydrophilic interaction × reversed phase liquid chromatography analysis of procyanidins. J. Chromatogr. A 1216, 6274−6284.

Kalili, K.M., de Villiers, A., 2010. Off-line comprehensive two-dimensional hydrophilic interaction x reversed phase liquid chromatographic analysis of green tea phenolics. J. Sep. Sci. 33, 853−863.

Kalili, K.M., de Villiers, A., 2013a. Systematic optimisation and evaluation of on-line, off-line and stop-flow comprehensive hydrophilic interaction chromatography × reversed phase liquid chromatographic analysis of procyanidins, part I: theoretical considerations. J. Chromatogr. A 1289, 58−68.

Kalili, K.M., de Villiers, A., 2013b. Systematic optimisation and evaluation of on-line, off-line and stop-flow comprehensive hydrophilic interaction chromatography × reversed phase liquid chromatographic analysis of procyanidins. part II: application to cocoa procyanidins. J. Chromatogr. A 1289, 69−79.

Kalili, K.M., Vestner, J., Stander, M.A., de Villiers, A., 2013. Toward unraveling grape tannin composition: application of online hydrophilic interaction chromatography × reversed-phase liquid chromatography-time-of-flight mass spectrometry for grape seed analysis. Anal. Chem. 85, 9107−9115.

Kalili, K.M., De Smet, S., van Hoeylandt, T., Lynen, F., de Villiers, A., 2014. Comprehensive two-dimensional liquid chromatography coupled to the ABTS radical scavenging assay: a powerful method for the analysis of phenolic antioxidants. Anal. Bioanal. Chem. 406, 4233−4242.

Kivilompolo, M., Hyötyläinen, T., 2007. Comprehensive two-dimensional liquid chromatography in analysis of *Lamiaceae* herbs: characterisation and quantification of antioxidant phenolic acids. J. Chromatogr. A 1145, 155−164.

Kivilompolo, M., Oburka, V., Hyotylainen, T., 2008. Comprehensive two-dimensional liquid chromatography in the analysis of antioxidant phenolic compounds in wines and juices. Anal. Bioanal. Chem. 391, 373−380.

Kivilompolo, M., Hyotylainen, T., 2008. Comparison of separation power of ultra performance liquid chromatography and comprehensive two-dimensional liquid chromatography in the separation of phenolic compounds in beverages. J. Sep. Sci. 31, 3466−3472.

Krauze-Baranowska, M., Glod, D., Kula, M., Majdan, M., Halasa, R., Matkowski, A., Kozlowska, W., Kawiak, A., 2014. Chemical composition and biological activity of *Rubus idaeus* shoots − a traditional herbal remedy of Eastern Europe. BMC Complement. Altern. Med. 14, 480−492.

Krol-Kogus, B., Glod, D., Krauze-Baranowska, M., Matlawska, I., 2014. Application of one- and two-dimensional high-performance liquid chromatography methodologies for the analysis of C-glycosylflavones from fenugreek seeds. J. Chromatogr. A 1367, 48−56.

Leach, G., Olivera, R., Morais, R., 1998. Production of a carotenoid-rich product by alginate entrapment and fluid-bed drying of *Dunaliella Salina*. J. Sci. Food Agric. 76, 298−302.

Leme, G.M., Cacciola, F., Donato, P., Cavalheiro, A.J., Dugo, P., Mondello, L., 2014. Continuous vs. segmented second-dimension system gradients for comprehensive two-dimensional liquid chromatography of sugarcane (*Saccharum* spp.). Anal. Bioanal. Chem. 406, 4315−4324.

Li, X., Stoll, D.R., Carr, P.W., 2009. Equation for peak capacity estimation in two-dimensional liquid chromatography. Anal. Chem. 81, 845−850.

Liu, Z., Lee, M.L., 2000. Comprehensive two-dimensional separations using microcolumns. J. Microcolumn Sep. 12, 241−254.

Lubda, D., Cabrera, K., Kraas, W., Shafer, C., Cunningham, D., 2001. New developments in the application of monolithic HPLC columns. LC-GC Eur. 14, 730−734.

Marchetti, N., Cavazzini, A., Gritti, F., Guiochon, G., 2007. Gradient elution separation and peak capacity of columns packed with porous shell particles. J. Chromatogr. A 1163, 203−211.

Mendes-Pinto, M.M., Silva Ferreira, A.C., Caris-Veyrat, C., Guedes de Pinto, P., 2005. Carotenoid, chlorophyll, and chlorophyll-derived compounds in grapes and port wines. J. Agric. Food Chem. 53, 10034−10041.

Mondello, L., Tranchida, P.Q., Stanek, V., Jandera, P., Dugo, G., Dugo, P., 2005. Silver-ion reversed-phase comprehensive two-dimensional liquid chromatography combined with mass spectrometric detection in lipidic food analysis. J. Chromatogr. A 1086, 91−98.

Mondello, L., Herrero, M., Kumm, T., Dugo, P., Cortes, H., Dugo, G., 2008. Quantification in comprehensive two-dimensional liquid chromatography. Anal. Chem. 80, 5418−5424.

Mondello, L., Beccaria, M., Donato, P., Cacciola, F., Dugo, G., Dugo, P., 2011. Comprehensive two-dimensional liquid chromatography with evaporative light-scattering detection for the analysis of triacylglycerols in *Borago officinalis*. J. Sep. Sci. 34, 688−692.

Montero, L., Herrero, M., Prodanov, M., Ibanez, E., Cifuentes, A., 2013a. Characterization of grape seed procyanidins by comprehensive two-dimensional hydrophilic interaction × reversed phase liquid chromatography coupled to diode array detection and tandem mass spectrometry. Anal. Bioanal. Chem. 405, 4627−4638.

Montero, L., Herrero, M., Ibanez, E., Cifuentes, A., 2013b. Profiling of phenolic compounds from different apple varieties using comprehensive two-dimensional liquid chromatography. J. Chromatogr. A 1313, 275−283.

Montero, L., Herrero, M., Ibanez, E., Cifuentes, A., 2014. Separation and characterization of phlorotannins from brown algae *Cystoseira abies-marina* by comprehensive two-dimensional liquid chromatography. Electrophoresis 35, 1644−1651.

Montero, L., Sánchez-Camargo, A.P., García-Canas, V., Tanniou, A., Stiger-Pouvreau, V., Russo, M., Rastrelli, L., Cifuentes, A., Herrero, M., Ibánez, E., 2016a. Anti-proliferative activity and chemical characterization by comprehensive two-dimensional liquid chromatography coupled to mass spectrometry of phlorotannins from the brown macroalga *Sargassum muticum* collected on North-Atlantic coasts. J. Chromatogr. A 1428, 115−125.

Montero, L., Ibanez, E., Russo, M., di Sanzo, R., Rastrelli, L., Piccinelli, A.L., Celano, R., Cifuentes, A., Herrero, M., 2016b. Metabolite profiling of licorice (*Glycyrrhiza glabra*) from different locations using

comprehensive two-dimensional liquid chromatography coupled to diode array and tandem mass spectrometry detection. Anal. Chim. Acta 913, 145−159.

Murphy, R.E., Schure, M.R., Foley, J.P., 1998. Effect of sampling rate on resolution in comprehensive two-dimensional liquid chromatography. Anal. Chem. 70, 1585−1594.

Nishino, H., Tokuda, H., Satomi, Y., Masuda, M., Bu, P., Onozuka, M., Yamaguchi, S., Okuda, Y., Takayasu, J., Tsuruta, J., Okuda, M., Ichiishi, E., Murakoshi, M., Kato, T., Misawa, N., Narisawa, T., Takasuka, N., Yano, M., 1999. Cancer prevention by carotenoids. Pure Appl. Chem. 71, 2273−2278.

Pierce, K.M., Hoggard, J.C., Mohler, R.E., Synovec, R.E., 2008. Recent advancements in comprehensive two-dimensional separations with chemometrics. J. Chromatogr. A 1184, 341−352.

Pierce, K.M., Kehimkar, B., Marney, L.C., Hoggard, J.C., Synovec, R.E., 2012. Review of chemometric analysis techniques for comprehensive two dimensional separations data. J. Chromatogr. A 1255, 3−11.

Pierce, K.M., Mohler, R.E., 2012. A review of chemometrics applied to comprehensive two-dimensional separations from 2008−2010. Sep. Purif. Rev. 41, 143−168.

Pol, J., Hohnova, B., Hyotylainen, T., 2007. Characterization of *Stevia Rebaudiana* by comprehensive two-dimensional liquid chromatography time-of-flight mass spectrometry. J. Chromatogr. A 1150, 85−92.

Pol, J., Hyotylainen, T., 2008. Comprehensive two-dimensional liquid chromatography coupled with mass spectrometry. Anal. Bioanal. Chem. 391, 21−31.

Potts, L.W., Stoll, D.W., Li, X., Carr, P.W., 2010. The impact of sampling time on peak capacity and analysis speed in on-line comprehensive two-dimensional liquid chromatography. J. Chromatogr. A 1217, 5700−5709.

Rao, A.V., Rao, L.G., 2007. Carotenoids and human health. Pharmacol. Res. 55, 207−216.

Reichenbach, S.E., Kottapalli, V., Ni, M., Visvanathan, A., 2005. Computer language for identifying chemicals with comprehensive two-dimensional gas chromatography and mass spectrometry. J. Chromatogr. A 1071, 263−269.

Russo, M., Cacciola, F., Bonaccorsi, I., Dugo, P., Mondello, L., 2011. Determination of flavanones in *Citrus* juices by means of one- and two-dimensional liquid chromatography. J. Sep. Sci. 34, 681−687.

Sandra, K., Moshir, M., D'hondt, F., Tuytten, R., Verleysen, K., Kas, K., François, I., Sandra, P., 2009. Highly efficient peptide separations in proteomics. Part 2: bi- and multidimensional liquid-based separation techniques. J. Chromatogr. B 877, 1019−1039.

Sarrut, M., Crétier, G., Heinisch, S., 2014. Theoretical and practical interest in UHPLC technology for 2D-LC. TrAC-Trends Anal. Chem. 63, 104−112.

Schoenmakers, P.J., Vivo-Truyols, G., Decrop, W.M.C., 2006. A protocol for designing comprehensive two-dimensional liquid chromatography separation systems. J. Chromatogr. A 1120, 282−290.

Scoparo, C.T., Souza, L.M., Dartora, N., Sassaki, G.L., Gorin, P.A.J., Lacomini, M., 2012. Analysis of *Camellia sinensis* green and black teas via ultra high performance liquid chromatography assisted by liquid−liquid partition and two-dimensional liquid chromatography (size exclusion × reversed phase). J. Chromatogr. A 1222, 29−37.

Seeley, J.V., 2002. Theoretical study of incomplete sampling of the first dimension in comprehensive two-dimensional chromatography. J. Chromatogr. A 962, 21−27.

Shalliker, R.A., Gray, M.J., 2006. Concepts and practice of multidimensional high-performance liquid chromatography. Adv. Chromatogr. 44, 177−236.

Shellie, R.A., Haddad, P.R., 2006. Comprehensive two-dimensional liquid chromatography. Anal. Bioanal. Chem. 386, 405−415.

Shi, X., Wang, S., Yang, Q., Lu, X., Xu, G., 2014. Comprehensive two-dimensional chromatography for analyzing complex samples: recent new advances. Anal. Methods 6, 7112−7123.

Snodderly, M.D., 1995. Evidence for protection against age-related macular degeneration by carotenoids and antioxidant vitamins. Am. J. Clin. Nutr. 62, S1448−S1461.

Stroink, T., Ortiz, M.C., Bult, A., Lingeman, H., de Jong, G.J., Underberg, W.J.M., 2005. On-line multidimensional liquid chromatography and capillary electrophoresis systems for peptides and proteins. J. Chromatogr. B 817, 49–66.

Stoll, D.R., Cohen, J.D., Carr, P.W., 2006. Fast, comprehensive online two-dimensional high performance liquid chromatography through the use of high temperature ultra-fast gradient elution reversed-phase liquid chromatography. J. Chromatogr. A 1122, 123–137.

Stoll, D.R., Li, X., Wang, X., Carr, P.W., Porter, S.E.G., Rutan, S.C., 2007. Fast comprehensive two-dimensional liquid chromatography. J. Chromatogr. A 1168, 3–43.

Tanaka, Y., Yanagida, A., Komeya, S., Kawana, M., Honma, D., Tagashira, M., Kanda, T., Shibusawa, Y., 2014. Comprehensive separation and structural analyses of polyphenols and related compounds from bracts of hops (*Humulus lupulus* L.). J. Agric. Food Chem. 62, 2198–2206.

Tranchida, P.Q., Donato, P., Cacciola, F., Beccaria, M., Dugo, P., Mondello, L., 2013. Potential of comprehensive chromatography in food analysis. TrAC-Trends Anal. Chem. 52, 186–205.

Tsuchiya, H., Sato, M., Kato, H., Okubo, T., Juneja, L.R., Kim, M., 1997. Simultaneous determination of catechins in human saliva by high performance liquid chromatography. J. Chromatogr. B 703, 253–258.

Van der Klift, E.J.C., Vivo-Truyols, G., Claassen, F.W., Van Holthoon, F.L., Van Beek, T.A., 2008. Comprehensive two-dimensional liquid chromatography with ultraviolet, evaporative light scattering and mass spectrometric detection of triacylglycerols in corn oil. J. Chromatogr. A 1178, 43–55.

Way, W., 2007a. Report. U.S.A. 25, 6–7.

Way, W.K., 2007b. Report. Eur. 28, 3–4.

Wei, F., Ji, S.-X., Hu, N., Lv, X., Dong, X.-Y., Feng, Y.-Q., Che, H., 2013. Online profiling of triacylglycerols in plant oils by two-dimensional liquid chromatography using a single column coupled with atmospheric chemical ionization mass spectrometry. J. Chromatogr. A 1312, 69–79.

Wei, F., Hu, N., Lv, X., Dong, X.-Y., Che, H., 2015. Quantitation of triacylglycerols in edible oils by off-line comprehensive two-dimensional liquid chromatography-atmospheric pressure chemical ionization mass spectrometry using a single column. J. Chromatogr. A 1404, 60–71.

Willemse, C.M., Stander, M.A., Tredoux, A.G.J., de Villiers, A., 2014. Comprehensive two-dimensional liquid chromatographic analysis of anthocyanins. J. Chromatogr. A 1359, 189–201.

Willemse, C.M., Stander, M.A., Vestner, J., Tredoux, A.G.J., de Villiers, A., 2015. Comprehensive two-dimensional hydrophilic interaction chromatography (HILIC) × reversed-phase liquid chromatography coupled to high-resolution mass spectrometry (RP-LC-UV-MS) analysis of anthocyanins and derived pigments in red wine. Anal. Chem. 87, 12006–12015.

Yang, Q., Shi, X., Gu, Q., Zhao, S., Zhao, Y., Shan, Y., Xu, G., 2012. On-line two dimensional liquid chromatography/mass spectrometry for the analysis of triacylglycerides in peanut oil and mouse tissue. J. Chromatogr. B 895–896, 48–55.

Zhou, D., Xu, Q., Xue, X., Zhang, F., Liang, X., 2009. Characterization of polymethoxylated flavones in *Fructus aurantii* by off-line two-dimensional liquid chromatography/electrospray ionization-ion trap mass spectrometry. J. Pharm. Biomed. Anal. 49, 207–213.

FURTHER READING

Huidobro, A.L., Pruim, P., Schoenmakers, P., Barbas, C., 2008. Ultra rapid liquid chromatography as second dimension in a comprehensive two-dimensional method for the screening of pharmaceutical samples in stability and stress studies. J. Chromatogr. A 1190, 182–190.

Ikegami, T., Hara, T., Kimura, H., Kobayashi, H., Hosoya, K., Cabrera, K., Tanaka, N., 2006. Two-dimensional reversed-phase liquid chromatography using two monolithic silica C18 columns and different mobile phase modifiers in the two dimensions. J. Chromatogr. A 1106, 112–117.

Jandera, P., 1989. Predictive calculation methods for optimization of gradient elution using binary and ternary solvent gradients. J. Chromatogr. A 485, 113−141.

Mondello, L., Donato, P., Cacciola, F., Fanali, C., Dugo, P., 2010. RP-LC × RP-LC analysis of a tryptic digest using a combination of totally porous and partially porous stationary phases. J. Sep. Sci. 33, 1454−1461.

Opiteck, G.J., Jorgenson, J.W., Anderegg, R.J., 1997. Two-dimensional SEC/RPLC coupled to mass spectrometry for the analysis of peptides. Anal. Chem. 69, 2283−2291.

Schoenmakers, P.J., 1986. Optimization of Chromatographic Selectivity, a Guide to Method Development. Elsevier, Amsterdam.

Stoll, D.R., Wang, X., Carr, P.W., 2008. Comparison of the practical resolving power of one- and two-dimensional high-performance liquid chromatography analysis of metabolomic samples. Anal. Chem. 80, 268−278.

Tanaka, N., Kimura, H., Tokuda, D., Hosoya, K., Ikegami, T., Ishizuka, N., Minakuchi, H., Nakanishi, K., Shintani, Y., Furuno, M., Cabrera, K., 2004. Simple and comprehensive two-dimensional reversed-phase HPLC using monolithic silica columns. Anal. Chem. 76, 1273−1281.

Toll, H., Oberacher, H., Swart, R., Huber, C.G., 2005. Separation, detection, and identification of peptides by ion-pair reversed-phase high-performance liquid chromatography-electrospray ionization mass spectrometry at high and low pH. J. Chromatogr. A 1079, 274−286.

This page intentionally left blank

CHAPTER

9 NANO-LIQUID CHROMATOGRAPHIC SEPARATIONS

Chiara Fanali[1], María Asensio-Ramos[2], Giovanni D'Orazio[3,4], Javier Hernández-Borges[3], Anna Rocco[4,†], Salvatore Fanali[4]

University Campus-Biomedico, Rome, Italy[1]; Volcanologic Institute of the Canary Islands (INVOLCAN), Puerto de la Cruz, Spain[2]; Universidad de la Laguna (ULL), La Laguna, Spain[3]; Italian National Council of Research, Monterotondo, Italy[4]

LIST OF ABBREVIATIONS

1D	First dimension
2D	Two dimensions/second dimension
Ac	Acetate
ACN	Acetonitrile
AETA	2-(Acryloyloxy)ethyltrimethylammonium methylsulfate
APCI	Atmospheric pressure chemical ionization
API	Atmospheric pressure ionization
APPI	Atmospheric pressure photoionization
BMA	Butyl methacrylate
CLC	Capillary liquid chromatography
CEC	Electrochromatography
CSP	Chiral stationary phase
CZE	Capillary zone electrophoresis
DAD	Diode array detector
DBDI	Ambient dielectric barrier discharge ionization
DEHP	Di(2-ethylhexyl)phthalate
DMB	1,2-Diamino-4,5-methylenediaoxy-benzene dihydrochloride
DVB	Divinyl benzene
DMMSA	Ammonium betaine
DNA	Deoxyribonucleic acid
EDMA	Ethylene dimethacrylate.
EI	Electron ionization source
EOF	Electroosmotic flow
ESI	Electrospray ionization
FMOC	9-Fluorenylmethoxycarbonyl chloride
FTICR	Fourier transform ion cyclotron resonance
GC	Gas chromatography
HAc	Acetic acid

[†]Deceased September 11, 2016.

Handbook of Advanced Chromatography/Mass Spectrometry Techniques. http://dx.doi.org/10.1016/B978-0-12-811732-3.00009-1

HDDMA	Hexanediol dimethacrylate
HFBA	Heptafluorobutyric acid
HFo	Formic acid
HILIC	Hydrophilic interaction chromatography
HP-β-CD	2-Hydroxypropyl)-β-cyclodextrin
HPLC	High-performance liquid chromatography
I.D.	Internal diameter
IMER	In-column immobilized enzymatic reactor
IT	Ion trap
IT-SPME	In-tube solid-phase microextraction
LC	Liquid chromatography
LIF	Laser-induced fluorescence detectors
L.-J.	Liquid-junction
LMA	Lauryl methacrylate
LOD	Limit of detection
LOQ	Limit of quantification
MAA	Methacrylic acid
MDA	3,4-Methylenedioxyamphetamine
MeOH	Methanol
MQD-co-HEMA-co-EDMA	*O*-9-[2-(methacryloyloxy)-ethylcarbamoyl]-10,11-dihydroquinidine-co-2-hydroxyethyl methacrylate-co-ethylene dimethacrylate
MIP	Molecularly imprinted polymer
MS	Mass spectrometry
Nano-LC	Nano-liquid chromatography
NMR	Nuclear magnetic resonance
NSAID	Nonsteroidal antiinflammatory drug
OT	Open tubular
PAGE	Polyacrylamide gel electrophoresis
PDMS	Polydimethylsiloxane
PEEK	Polyether ether ketone
PEG	Poly ethylene glycol
PGC	Porous graphitic carbon
PEGDA	Polyethylene glycol diacrylate
PETA	Pentaerythritol triacrylate
PFP-silane	3-(Pentafluorophenyl) propyldimethylchlorosilane
PLOT	Porous layer open tubular
PM	Particulate matter
PS	Polystyrene
Q	Quadrupole
QqQ	Triple quadrupole
Q-TOF	Quadrupole time-of-flight
RAM	Restricted-access media
RP	Reverse phase
SAX	Strong anion exchange
SCX	Strong cationic exchange

SDS	Sodium dodecyl sulphate
SEC	Size exclusion chromatography
SFC	Supercritical fluid chromatography
SP	Stationary phase
TAS	Total analysis system
TEA	Triethylamine
TFA	Trifluoroacetic acid
TMOS	Tetramethoxysilane
UHPLC	Ultra-high performance liquid chromatography
UV	Ultraviolet
WAX	Weak anion exchange
WCX	Weak cation exchange
WWTP	Wastewater treatment plant

1. INTRODUCTION

Nano-liquid chromatography (nano-LC), first introduced by Karlsson and Novotny in 1988, is a miniaturized liquid chromatographic technique where the separation of analytes takes place on a capillary column containing selected stationary phases (SPs). Even though a standard definition of nano-LC has not been accordingly fixed, this name is assigned to those techniques employing capillaries of internal diameter (I.D.) $\leq$ 100 μm and flow rates in the range 25−800 nL/min. In contrast, capillary liquid chromatography (CLC) makes use of 150−500 μm I.D. columns and flow rates in the range 1−20 μL/min.

In nano-LC, the relatively low flow rate represents an interesting advantage over conventional techniques, allowing the perfect coupling with mass spectrometry (MS). In addition, costs are reduced because of the limited use of mobile phases, and consequently, low waste makes this technique eco-friendly. In addition, peak dilution during the chromatographic run is reduced with an increase of mass sensitivity. Finally high efficiency, good resolution, and short analysis times are currently obtained (Karlsson and Novotny, 1988; Szumski and Buszewski, 2002; Hernández-Borges et al., 2007; Fanali et al., 2013a, 2015b).

Because of its features and advantages, nano-LC has been applied mainly in analytical chemistry for the analysis of a large number of compounds currently investigated in various fields such as proteomics, pharmaceutical, chiral, food and beverages, environmental, forensic and toxicology, etc.

The aim of this chapter is to illustrate the state of the art of nano-LC by reviewing fundamental principles, the instrumentation currently used, and its advantages over conventional high-performance liquid chromatography (HPLC). Specific selected applications of nano-LC are also reported and described. They cover not only the chromatographic separation of several compounds but also the validation of the method and quantitative aspects, both applied to the analysis of real samples of different origin. Although the use of microchips seems to be very promising, this technique will be only mentioned just to illustrate its potentiality in analytical chemistry.

2. MINIATURIZATION IN LIQUID CHROMATOGRAPHY

2.1 SOME THEORETICAL CONSIDERATIONS

2.1.1 Effect of Column Internal Diameter on Chromatographic Efficiency

In their study about the separation efficiency of packed columns with small inner diameters, Karlsson and Novotny (1988) evaluated packed columns in the I.D. range 44−265 μm. In this study the system variance $\left(\sigma^2_{\text{sys}}\right)$ can be described by the following equation:

$$\sigma^2_{\text{sys}} = \sigma^2_{\text{ext}} + \sigma^2_{\text{col}} \tag{9.1}$$

where σ^2_{ext} and σ^2_{col} are the external and column variances, respectively.

The external dispersion accounts for the broadening caused by the different parts of the liquid chromatography (LC) system with the exclusion of the column. To minimize σ^2_{ext}, the column was directly connected with the sample valve injection. In addition, the authors recorded several peaks in the same LC run moving the detector along the column. This approach was used to show the increase of peak width with column length having a constant external band broadening.

It has been reported that the extra-column variance should influence the decrease of column plate numbers not more than 10% (Yeung, 1985; Gluckman and Novotny, 1985).

Therefore there is a maximum extra-column variance acceptable as reported in the following equation:

$$\sigma^2_{\text{e(acc)}} \leq \sigma^2_{\text{col}} \times 0.10 \leq 0.10\ \frac{\pi^2 L^2 r^4 \varepsilon^2 (1+k)^2}{N} \tag{9.2}$$

where N is the number of theoretical plates, L the column length, k the retention factor, ε the column permeability, and r the column radius.

From this equation, it is evident that the most important parameter influencing the column variance is the radius of the column. Consequently, when using columns with very low I.D. there is a corresponding strong reduction of extra-column effect. This effect can be controlled selecting an appropriate design of the nano-LC system such as I.D. and length of connecting tubes, injection valve (type and volumes), detector (cell volume and electronic time constant), etc.

In nano-LC, cell volumes are on the order of a few nanoliters, whereas injected sample volumes are usually in the range 10−60 nL. However, when appropriate experimental conditions are selected, larger volumes can be injected utilizing the focusing effect to increase the sensitivity (D'Orazio et al., 2016b; Fanali et al., 2015a).

For plate-height evaluation, Karlsson and Novotny used the following equation:

$$u_s^2 M2_{\text{sys}} = M2_{\text{ext}} + HL \tag{9.3}$$

where $M2$ is the second central moment and u_s the migrating zone speed. Reporting $u_s^2 M2$ versus column length (mm) at different mobile phase flow rates, straight lines are obtained. The slopes of the lines give the plate-heights, whereas the intercepts offer data about external band broadening.

To study the influence of the column I.D., Karlsson and Novotny (1988) applied the equation studied by Kennedy and Knox (1972), based on reduced parameters h and υ:

$$h = A\upsilon^{0.33} + B/\upsilon + C\upsilon \tag{9.4}$$

B term slightly increased by decreasing the column I.D., whereas *A* and *C* were decreased by decreasing the column I.D. The lowest *h* values were obtained using the capillary column of 44 μm I.D. This work was the basis for modern capillary/nano-LC development.

2.1.2 Chromatographic Dilution

The driving force in LC is the movement of the mobile phase across the column. Analyzed compounds, even if injected as a narrow zone, are subjected to chromatographic dilution with a consequent zone broadening. Consequently, this effect must be minimized to avoid loss of efficiency.

The following equation about chromatographic dilution has been proposed (Vissers et al., 1997):

$$D = \frac{c_o}{c_{\max}} = \frac{\varepsilon \pi r^2 (1+k)\sqrt{2\pi LH}}{V_{inj}} \tag{9.5}$$

where c_o and $c_{\max}$ are the concentration of the sample at the injection and at the peak maximum, respectively; r and L are the column radius and length, respectively; H is the plate-height; ε the column porosity; and k the retention factor.

As can be observed in this equation, to have a low dilution, it is necessary to maximize the sample concentration at the peak maximum. This can be obtained either by injecting a high volume of sample and/or using a shorter column and/or a system with lower plate-height and lower porosity. Finally, the use of columns with low radius, because of the square root dependence, will give certainly the lowest chromatographic dilution. Therefore, injecting the same sample volume and using columns of different radius with SPs of the same characteristics, passing from an I.D. of 4.6 mm to ones of 300 μm or 75 μm, an increase in peak height of 235- and 3800-fold, respectively, can be calculated.

2.2 CAPILLARY COLUMNS

The choice of the appropriate chromatographic column, considering the length, the I.D., and the SP type, is fundamental for the success of any analytical separation undertaken. For a long time, in LC the geometry of the column was under investigation, especially to get better performance in terms of efficiency and to speedup analyses (Chen and Horvath, 1995; Poppe, 1997). The use of chromatographic columns with smaller and smaller I.D. aroused lively interest in the scientific community for several accessible advantages, such as easy coupling with MS, high efficiency, low consumption of reagents, and resultant low environmental pollution (Abian et al., 1999; Saito et al., 2004). This attention has even increased because recent studies on several *omics* branches of biology have been done on a large scale, as well as industrially (Svec, 2002; Mikulovic and Mechtler, 2006). As a result, miniaturized separation techniques, employing chromatographic columns with reduced I.D. (so-called capillary columns), i.e., CLC/nano-LC, capillary electrochromatography (CEC), have begun to be recognized worldwide as a valid alternative to classical and analytical techniques, specifically HPLC and GC (Fu et al., 2003; Gübitz and Schmid, 2008; Asensio-Ramos et al., 2009).

CEC, generally described as an hybrid technique exploiting advantages of both HPLC (i.e., selectivity) and capillary electrophoresis (i.e., high efficiency) (Fu et al., 2003), will be considered only in this section. In fact it makes use of the same capillary columns employed in CLC/nano-LC. The only exception is the requirement of particular properties of the SP, that in CEC has to assure an electroosmotic flow (EOF) (Svec, 2002). Theoretical considerations about this technique are out of the aim of this chapter, but they can be found in several reviews (Robson et al., 1997;

Rathore, 2002; Rocco et al., 2013a; D'Orazio et al., 2016a). However, procedures developed to obtain capillary columns in CEC can be adopted for CLC/nano-LC and vice versa, and for this reason it is possible to consider the parallel evolution of these miniaturized techniques, at least regarding the separation medium.

The I.D. of capillary columns is in the range of 100−500 μm for CLC, 10−100 μm for nano-LC (Vissers et al., 1997; Saito et al., 2004), and 10−350 μm for CEC (Eeltink et al., 2003). Usually columns consist of a fused silica capillary or a polyether ether ketone (PEEK) tube (Szumski and Buszewski, 2002; Cappiello et al., 1991). Fused silica capillaries are preferred owing to several benefits, including UV transparency, higher mechanical strength than polymeric materials (PEEK), and flexibility because of the polyimide coating (Szumski and Buszewski, 2002; Saito et al., 2004). In any case, some precautions have to be taken when working with these columns to preserve their performance and not to destroy them. For example, the presence of zones where the polyimide coating was removed (i.e., at detection window or frits) makes the capillary very fragile (Saito et al., 2004).

In CLC/nano-LC, as well as in CEC, three kinds of capillary columns can be employed: packed, monolithic, and open tubular ones. Each type will be discussed separately.

All mechanisms capable of selectively delaying the analytes and described elsewhere for LC (for instance, partition, adsorption, ion exchange, affinity chromatography) are exploited in CLC, nano-LC, and CEC, too. Furthermore, independently of the type of capillary column selected, the need for very small amount of stationary and mobile phase has made accessible the use of expensive materials (i.e., chiral stationary phases (CSPs) or additives) available on the market, to improve the selectivity of the chromatographic column (Rocco and Fanali, 2009). Nevertheless, the great majority of separations performed are based on reversed-phase (RP) mode (Hernández-Borges et al., 2007; Rocco et al., 2014; Fanali et al., 2015a).

Finally, the reduced dimensions of capillary columns make them particularly suitable for temperature studies (Saito et al., 2004).

2.2.1 Packed Capillary Columns

Packed capillary columns are widely used because of the considerable variety of particulate SPs existing from HPLC. These SPs allow the separation of analytes by partition, size exclusion, adsorption, affinity, and/or ion-exchange mechanisms and, arising from an exceedingly established technique such as HPLC, have well-defined packing parameters (regular particle and pore size, improved bonding chemistry) (Hernández-Borges et al., 2007; Svec, 2002). The selection of the packing material is done considering the nature of analytes (basic, acidic, or neutral compounds, chiral or achiral, with high or low molecular weight). SPs with a 3−5 μm particle diameter are mostly employed. More recently, particles of smaller size (1.1−1.8 μm), developed to obtain higher efficiency and selectivity, and specific for ultra-high performance liquid chromatography (UHPLC), have been also utilized in nano-LC and CEC (Robson et al., 1997; Blue and Jorgenson, 2015). In this last technique, the use of an EOF as the driving force avoids the occurrence of high back pressure, even when very small particles are employed (Svec, 2002).

Dwelling on CEC, it is worth noting that SPs have to guarantee specific interactions for the analytes and, at the same time, provide an EOF, which is indispensable as the driving force (Eeltink and Svec, 2007). Usually, SPs that are constituted by bonded silica material and residual silanol groups (Si−OH), ionisable at pH higher than 3, are good promoters for a high EOF. However, the same silanol groups are also responsible for peak tailing because of their strong adsorptive properties (Fanali et al., 2007).

The cost and the still low availability of commercial capillary columns force most researchers to prepare packed columns by themselves (Fanali et al., 2012a,b; Blue and Jorgenson, 2015; D'Orazio et al., 2016b). However, packing and retaining an SP in narrow-bore capillaries can be quite difficult and requires dedicated apparatuses, as well as a certain experience, to warrant a good stability and reproducibility between columns.

Different packing procedures are reported in literature. Among them the slurry packing is the most widespread, but also dry packing (Crescentini et al., 1988), packing with supercritical CO_2 (Malik et al., 1993), by gravity (Reynolds et al., 1998), and by electromigration of charged silica beads (Yan et al., 1995) were proposed as alternative to pumping the slurry suspension.

The slurry packing method is widely used because it has been introduced to prepare conventional HPLC columns, and therefore it is well known and largely described in literature (Svec, 2002). The term "slurry" refers to a suspension of the particulate SP in an appropriate solvent, which is placed in a reservoir and then introduced into the capillary column by a solvent delivery pump. During the filling, a temporary frit is positioned at the end of the capillary to retain the adsorbent. Usually a slurry solvent with low viscosity (i.e., acetone) is preferred for faster packing. Because of the fact that the slurry is a suspension, an ultrasonic bath or magnetic stirring can help to avoid agglomeration of particles in the reservoir, which can obstruct the packing (Colón et al., 2000).

Whatever the method of packing employed, retaining frits are required to keep the SP restricted into the capillary column. Functional frits have to resist the high pressure applied and, at the same time, allow the crossing of mobile phase and analytes through the column (Colón et al., 2000). Consequently frit fabrication represents a big challenge for the final performance of the column. Inlet and outlet frits are usually prepared in situ by sintering the packed material with a heated wire. Fig. 9.1 shows a scheme of the slurry-packing procedure of a capillary column.

As already mentioned, this procedure causes the removal of the polyimide coating at the frit zone and makes the column more fragile. Furthermore, a bad sinterization can compromise the flow through the column and change the properties of the packing material where the heating has been applied, generating a nonhomogeneous packing. This occurrence is particularly detrimental in CEC because it produces nonuniformity in the EOF, which can lead to bubble formation. Also the reproducibility of frits is problematic, and special attention has to be paid to the time and temperature of sintering. Furthermore, frit fabrication depends on column I.D., particle size, and type of packing material (Colón et al., 2000). Because of all these drawbacks, different solutions have been suggested to retain the SP, thereby avoiding the sintering of silica.

Externally and internally tapered columns have been proposed as well as columns with inlet, outlet, or both monolithic frits (Lord et al., 1997; Chen et al., 2000; Rocco and Fanali, 2008). Entrapment of particulate material by sintering and sol-gel technology (a hybrid between packed and monolithic columns) can also be mentioned as an alternative to frit formation (Colón et al., 2000).

After all, troubles in frit fabrication and the above-mentioned practical disadvantages related to packing procedures have led many researchers to consider monolithic media.

2.2.2 Monolithic Capillary Columns

Several aspects related to monolithic material make it attractive for the implementation of capillary columns complementary to packed ones. First of all, the generally simple in situ synthesis of monolithic beds, offered by the capillary format of the columns, does not require frits (Mistry et al., 2002; Maruška and Kornyšova, 2004). The continuous porous structure of monoliths, due to the

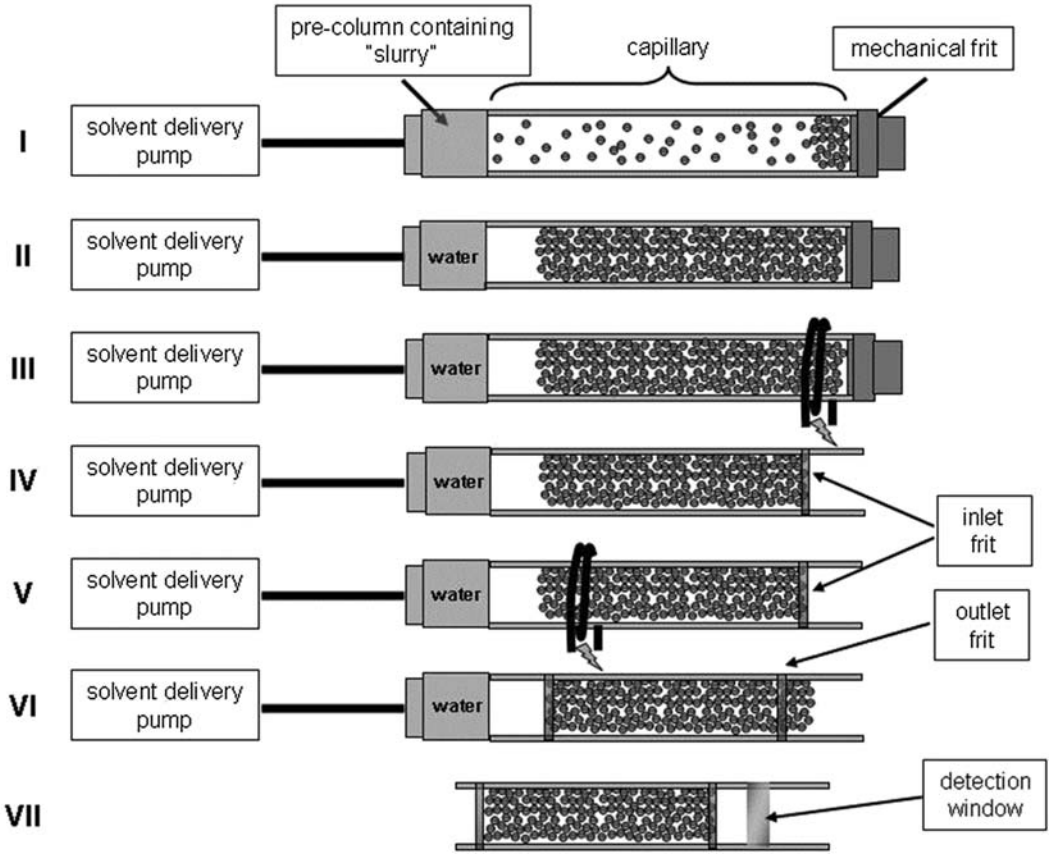

FIGURE 9.1

Scheme of the preparation of a capillary column using the "slurry" packing procedure. I: packing of the SP; II: flushing with water; III: inlet frit preparation with a heated wire; IV: outlet frit preparation; VI: removal of excess SP; VII: removal of the polyimide external layer for the detection window.

Reproduced from Fanali, C., Asensio-Ramos, M., Hernández-Borges, J., Rocco, A., Fanali, S., 2011. Nano-liquid chromatographic separations. In: Byrdwell, W.C., Holčapek, M. (Eds.), Extreme Chromatography: Faster, Hotter, Smaller. American Oil Chemists' Society (AOCS), Urbana, IL, USA, pp. 301–380.

presence of macropores and mesopores of different sizes, allows the use of high flow rates because of the lower backpressure generated, compared with that of packed columns (Tanaka et al., 2002). The wide availability of monomers permits one to obtain a separation medium with unique chromatographic properties.

Monolithic columns can be obtained by polymerization of organic monomers or by the sol-gel process, in the case of silica-based ones. In the first case, after an appropriate derivatization of the inner capillary wall for the anchoring of the polymer, the capillary is filled with a polymeric mixture and the radical polymerization can be accomplished thermally or photochemically (Maruška and

Kornyšova, 2004; Svec and Huber, 2006). The polymeric mixture is composed of functional monomers, a cross-linker, a porogenic agent, and an inert solvent; each of them can affect the porous structure of the monolithic material. Once the polymerization is complete, unreacted moieties are eliminated flushing the capillary column. Depending on the type of monomers, it is possible to distinguish water-soluble comonomers (acrylamide-based monoliths), where a salt is used as the porogen, and comonomers soluble in organic solvent (polystyrene- and methacrylate-based monoliths), where polymerization takes place in the presence of a porogen cosolvent (usually isopropanol) (Mistry et al., 2002; Svec, 2010). For each mixture, the proper initiator and accelerator must be present. When monolithic beds have to be employed in CEC, a charged monomer is included in the polymeric mixture to assure the EOF (Eeltink and Svec, 2007; Bragg and Shamsi, 2012). Even if characterized by an easy way of preparation, such kind of continuous bed presents low efficiency and poor reproducibility (Myers and Bartle, 2002).

Silica monolithic SPs are obtained by a more complicated procedure, but their properties are very attractive. Especially, they possess a well-defined pore size distribution of both macropores (few micrometers in size) and mesopores (few nanometers in size), which allows relatively high flow rates and high specific areas. Moreover, the thin skeleton reduces the mass transfer resistance, allowing to maintain high efficiencies at high flow rates (Tanaka et al., 2002; Chankvetadze et al., 2006). Their preparation (sol-gel process) is based on several steps and assures independent control of the size of the silica skeleton and through-pores (Tanaka et al., 2002): hydrolytic polymerization of an alkoxysilane (i.e., tetramethoxysilane) in an acidic medium; condensation of silica in the presence of poly(ethylene glycol) (PEG) as the porogen and phase separation between the silica/PEG system and water; separation of the resulting gel into solid- and liquid-rich domains that further react with each other to give the gel its final structure (syneresis); ageing and heat treatment, involved in tailoring mesopores; drying, to remove the liquid; and chemical modification. This last step is needed to give the surface features desired for chromatographic separation, and the functional groups can also be introduced directly by incorporation of functional monomers in the polymeric mixture (Wu et al., 2008).

Polymeric mixtures are appropriate for the preparation of molecularly imprinted monoliths, which have been used for several applications in the analytical field, such as SPs for solid-phase extraction and chromatography, sensors, etc. (Liu et al., 2005). The way to produce molecular imprinted SPs consists of the addition of a template (imprint) molecule in the polymeric mixture. Before starting polymerization, functional groups on the template interact with those on the monomer(s), and when the reaction begins, monomers result, arranged around the template. During the polymerization, the template, depending on its structure, can react, forming covalent bonds or giving rise to secondary interactions with other monomers (Tan and Remcho, 1998). If the imprinting is successful, after the removal of the imprint molecule, the polymer network will posses cavities having the shape, size, and functional groups complementary to those of the template. As a consequence, it will show a remarkable affinity toward the template (Simon et al., 2007). To increase the surface area, molecularly imprinted polymers (MIPs) can be grounded. However, these particles tend to have an extremely broad size and shape distribution (Tan and Remcho, 1998). Several approaches have been used to obtain molecularly imprinted particles with a controlled size and shape distribution. For example, suspension polymerization has been utilized to obtain monodispersed MIP particles. Submicron scale MIP particles have also been prepared by precipitation and emulsion polymerization. An improved methodology is miniemulsion polymerization, where the diffusion process in the continuous phase is

suppressed and a stable emulsion, of homogeneous size, is generated (Nilsson and Nilsson, 2006). When the aim of the research is the separation of a chiral compound, one of its enantiomers is used as template (Ou et al., 2007).

Monolithic material has also been employed to obtain restricted-access media (RAM). This type of support allows to the separation of analytes from complex matrices (i.e., human plasma) on-column, being characterized by a "bimodal surface topochemistry," where size exclusion chromatography (SEC) is combined with adsorption chromatography. SEC prevents the access of large biomolecules into the small pores of the RAM structure and consequently these undesired compounds elute from the column at the void volume. Molecules with a low molecular weight, instead, penetrate through active sites responsible of chromatographic retention (Jarmalavièienë et al., 2003).

2.2.3 Open Tubular Capillary Columns

Open tubular (OT) columns, where the SP is directly bonded or adsorbed to the inner wall of the capillary, usually have an I.D. between 10 and 60 μm. The adsorption of the SP, or modifier, can occur dynamically (weak interactions, the inner modifier is added to the mobile phase) or physically (modifier strongly adsorbed). Modifiers utilized for the preparation of adsorbed SPs can be grouped into: (1) cationic surfactants, (2) polymeric surfactants, and (3) charged polymers (Kapnissi-Christodoulou et al., 2003).

The layer of SP can also be fixed by covalent bonding and/or cross-linking. This approach offers a long capillary lifetime, but it usually requires a more complicated coating procedure.

OT columns are characterized by low convective dispersion, good efficiency, and high permeability. For this reason, conditioning of the columns is fast and their lengths can be increased without the occurrence of long analysis times.

OT capillaries can be used in gas chromatography (GC), supercritical fluid chromatography, and in open-tubular liquid chromatography, giving the possibility of a unified approach for separations, realized by employing a single column in all chromatographic modes (Wistuba and Schurig, 2000).

Longer columns can cause the poor selectivity typical of OT columns. In fact, they possess a very low phase ratio, and for best performance an I.D. ≤ 20 μm is recommended. However, this small I.D. aggravates the sensitivity when optical detection methods are employed (Schurig and Mayer, 2001).

Another drawback related to the low phase ratio is the low sample loading capacity of the column. As a result, column overloading can easily occur, causing peak asymmetry and decreasing efficiency. To enlarge the wall surface available for the "coating" with the SP and increase the phase ratio, the chemical etching of the inner wall has been proposed (Kapnissi-Christodoulou et al., 2003). The etching process increases the surface area of the capillary by a factor of up to 1000. This reaction is obtained by using a solution of ammonium hydrogen difluoride and is dependent on the time and temperature of exposure. Other chemical treatments and increasing the film thickness (porous layer OT, immobilized organic polymer) have been proposed for enhancing the phase ratio. However, reproducible creation of a thick SP coating on the inner walls of small-diameter columns is associated with considerable practical difficulties.

OT columns with dynamic nanoparticles as pseudostationary phases and sol-gel surface coatings have also been suggested (Dong et al., 2008).

2.3 NANOFLOW GENERATION

As previously mentioned, due to the reduced dimension of the capillary I.D. and use of small packed particles in nano-LC, it is necessary to reduce the mobile phase flow to levels of nL/min. If monolithic SPs are used, the flow rate can be increased to μL/min levels because they have higher permeability than packed columns.

Nowadays, different commercial devices that automatically generate a repeatable and constant delivery of solvents (also under gradient elution modes) are available from a number of manufacturers. Originally, commercialized instrumentation was based on the use of split-flow systems (the most common), which is also greatly applied in laboratory-made instrumentation because of its simplicity (Hernández-Borges et al., 2007; Sestak et al., 2015; Nazario et al., 2015). The device is assembled by connecting a micropump to a T-union with zero dead volume; the other two ends are connected to the packed capillary and to an empty tube of suitable length and I.D. The split ratio can be changed by modifying the length and the I.D. of the empty capillary (waste). The method is highly appropriate for obtaining nano/microflows in the isocratic mode but under laboratory-made instrumentation it frequently fails (especially in nano-LC) to achieve a reproducible gradient elution due to the change of the backpressure caused by the different viscosities of the mixed solvents. In addition, the mobile phase mixture is transferred into the column with a small delay. Current commercialized systems based on flow splitting normally use electronic flow-control devices to maintain a constant flow while the viscosity of the mobile phase changes (http://www.agilent.com). One of its main disadvantages is that solvent saving is not that high because it requires flow rates higher than those commonly used.

Several works have also proposed the use of conventional pumps with the aid of suitable switching valves with or without split flows (Takeuchi et al., 1987; Cappiello et al., 2003a; Ito et al., 2004).

This is the case of the work by Cappiello et al. (2003a) in which an electronically actuated, computer-controlled, multiposition HPLC valve was used. The valve had 14 ports and 6 loops, each loop containing a selected mixture of solvents of different strength. The electronic actuation allowed selecting which reservoir to be online with the column for a desired time, generating a specific mobile phase gradient. The lowest flow tested was 250 nL/min. This device was also used in a later work by the same group for the determination of nitro-polycyclic aromatic hydrocarbons, pesticides, and human hormones showing good precision, linearity, and sensitivity (Cappiello et al., 2003b).

Dedicated splitless miniaturized pumps (syringe or reciprocating pumps), on the contrary, have the advantage of low solvent consumption, but fewer are commercially available. An example is a commercialized nanopump (http://www.dionex.com), in which the continuous direct flow is delivered by four pistons (two per solvent channel). While one piston is refilled the other provides suitable flow delivery. After the refilling cycle, the refilled piston is pressurized and takes over the flow delivery. For this approach, suitable mobile phase degassing is even of higher importance.

2.4 INJECTION DEVICES

When working in nano-LC where the I.D. and the total volume of the columns are relatively low, the injected sample volume is one of the most important parameter to be carefully considered to avoid problems with sensitivity as well as with overloading related to low and high sample injection, respectively. Clearly the injected volume should be as low as possible to avoid band broadening.

However, a low sample volume will reduce the sensitivity. Therefore there must be a compromise allowing the highest efficiency with the best signal response.

The maximum volume that can be injected in a chromatographic system can be calculated utilizing the following equation proposed by Martin et al. (1975) for LC:

$$V_M = \theta \frac{\pi}{4} d_c \varepsilon \, (1 + k) \, \sqrt{LH} \tag{9.6}$$

This equation shows that the maximum cell volume depends on the diameter of the capillary (d_c) and also on its length (L) and plate height (H). Obviously, decreasing the column diameter requires a lower injected sample volume. Therefore, in nano-LC injection volumes in the range 10−100 nL are currently used, unless a focusing approach is done to increase the sensitivity. Commercial injection valves with fixed loops of 40, 60, and 100 nL are available from, e.g., Vici-Valco. For volumes lower than 20 nL, a split vent was inserted between the valve and the column (Chervet et al., 1996). Alternatively the sampling procedure can be controlled by regulating the injection time (Claessens et al., 1990; Fanali et al., 2010). This can also be done automatically, and it has been successfully applied to the autosamplers available with almost all commercial nano-LC instrumentation, where analytes can be injected with very high precision.

2.5 DETECTION SYSTEMS

As previously mentioned, although miniaturized techniques exhibit high mass sensitivity due to the reduction of the column I.D., concentration sensitivity is relatively low because the injected sample volume is limited. The detectors usually employed in electrodriven capillary and CLC/nano-LC techniques are the results of adaptation of those currently employed in conventional techniques. They include the UV, fluorescence, and conductivity ones. Good sensitivity can be obtained employing laser-induced fluorescence detectors where a laser source is used (Carlavilla et al., 2006).

To avoid dispersion problems during detection, the volume of the flow cell must be adapted to the size of the peak volumes eluting from the column. This is done employing a detector cell with the volume as low as possible. Best results are currently obtained with on-column detectors where the path length is the capillary I.D. Finally, data acquisition must be very fast to collect peak zones with low widths (1−2 s).

Absorption detectors, previously experimented on working with electrodriven techniques, have been widely used in CLC/nano-LC, achieving good results. Generally, in these devices the UV light is focused on the capillary cell to have the highest sensitivity. Recently, commercial detectors, UV diode array detectors, capable of offering very high sensitivity have become available. The use of extended path cells, well-known in conventional HPLC, has also been proposed for the applicability to miniaturized techniques. Applications employing bubble or zeta cells (Desiderio et al., 1999; Hampel, 2000) have been described in electrodriven techniques, whereas in CLC/nano-LC detectors' cell with extended path length are usually employed especially with commercial instrumentation.

2.6 IMPROVING SENSITIVITY IN NANO-LIQUID CHROMATOGRAPHY

Even if nano-LC is a very high mass sensitive chromatographic technique, the concentration detection limit is very questionable when compared with conventional HPLC where higher sample volumes are

currently injected (5−20 μL instead of 10−60 nL in nano-LC). In addition, in nano-LC the path length of the UV-detector cell is very low and usually corresponds to the I.D. of the capillary used (≤100 μm). Therefore, to increase the sensitivity when using the miniaturized technique, some approaches have been proposed to overcome the mentioned drawbacks, allowing analysts to applying nano-LC to real samples analysis. Among the different solutions proposed, the use of (1) sensitive and specific detectors, e.g., MS, (2) UV-detector cells with extended path length, (3) on-column focusing (Mills et al., 1997; Cappiello et al., 2002; Rocco et al., 2013b; Buonasera et al., 2009), and (4) pre- and/or 2D-column preconcentration are currently employed (Vissers et al., 1997).

On-column focusing is a quite simple approach that does not need special equipment. In fact, the sample is dissolved in a solvent mixture with poor elution capability toward analyzed compounds compared to the mobile phase. Consequently, a sample plug on the top of the column is formed even if a relatively high volume is injected. To show the feasibility of the on-column focusing by using nano-LC, some selected applications are reported here as an example. Cappiello et al. utilized a capillary column of 75 μm I.D. coupled with MS for trace level determination of organophosphorus pesticides. Even though only a few nanoliters of sample are currently injected in such systems to avoid overload, the authors injected about 500 nL, decreasing the limit of detection (LOD) by about 100-fold; the mobile phase was modified with water (Cappiello et al., 2002). To improve the sensitivity, on-column focusing was also studied for the chiral resolution of β-blockers such as atenolol, propranolol, oxprenolol, and metoprolol. The enantiomers were separated by nano-LC in a capillary column packed with silica modified with vancomycin. Racemic drugs were dissolved in only methanol (1500 nL injected), whereas the mobile phase used contained ammonium acetate pH 4.5/water/methanol (1:4:95, v/v/v). LOD and LOQ for the alprenolol enantiomers were 9 and 15.6 ng/mL, respectively. The method was validated and applied to the analysis of an extracted plasma sample (D'Orazio and Fanali, 2008).

2.7 HYPHENATION OF NANO-LIQUID CHROMATOGRAPHY WITH OTHER TECHNIQUES

Hyphenation of LC with other techniques is a fruitful, but challenging, topic for researchers on using the separation method alone. Hyphenation of miniaturized techniques with other ones offering, e.g., possibilities of (1) detailed characterization of analyte structures or (2) two-dimensional separation, is very important especially when complex matrices have to be investigated. Among these techniques, MS and nuclear magnetic resonance (NMR) are the most advanced tools recently studied. The hyphenation CLC−nano-LC and nano-LC−MS is currently performed and documented by several practical applications also reported in this chapter, whereas CLC or nano-LC coupled with NMR includes only a few reports.

2.7.1 CLC/Nano-LC−NMR

Wu et al. firstly reported the hyphenation of capillary zone electrophoresis (CZE) with NMR (Wu et al., 1994); later on, Albert's group demonstrated the possibility to couple CLC and CEC with NMR (Albert et al., 1996). The coupling of a commercial CLC instrumentation with NMR has been shown by Lacey et al. (2001), analyzing terpenoid compounds in a 320 μm I.D. capillary packed with 3 μm C_{18} particles. The detection was done by stopped-flow, achieving sensitivity sufficiently high for the detection of trace impurities (sub-nmol). Fig. 9.2 shows a scheme of CLC−NMR by using a

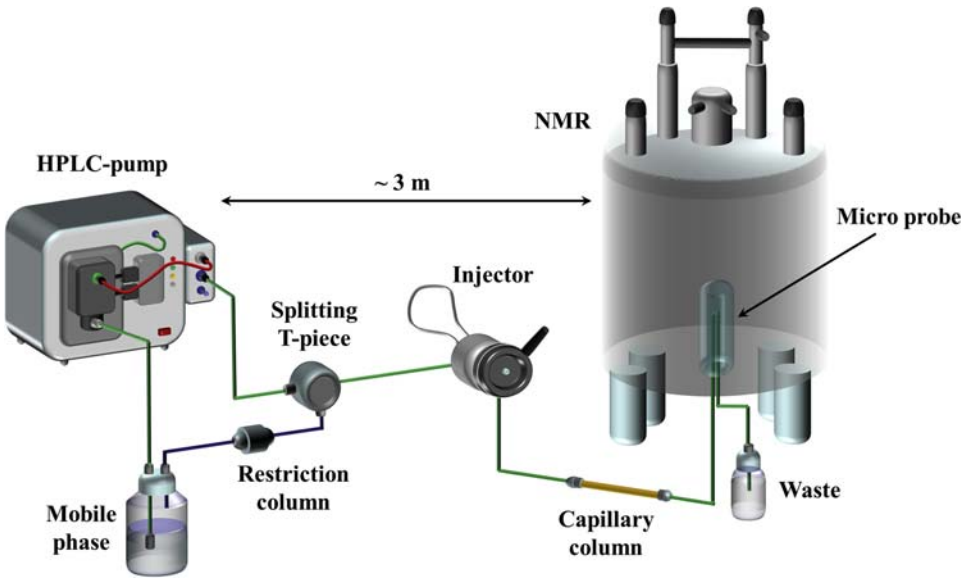

FIGURE 9.2

Scheme of capillary liquid chromatography coupled with nuclear magnetic resonance (NMR) through a continuous flow NMR probe. *HPLC*, high-performance liquid chromatography.

continuous flow NMR probe. In a recent review paper, Kuhnle et al. (2009) summarized the data available in literature dealing with hyphenation of microscale LC with NMR.

2.7.2 CLC/Nano-LC–Mass Spectrometry

Coupling LC with mass spectrometer has been done utilizing atmospheric pressure ionization sources, where the sample eluted by the mobile phase at atmospheric pressure is ionized and transferred into the MS. In LC, electrospray ionization and atmospheric pressure chemical ionization (ESI and APCI, respectively) are currently the most frequently used ionization techniques. The ESI source is the most applied with miniaturized chromatographic and electrodriven techniques (CZE and CEC), allowing mainly the analysis of compounds with charged or chargeable groups. This source type can be easily used for compounds with high molecular weight such as proteins, peptides, and other polymers because multiply charged ions are formed and detected. In addition, small ions are also often analyzed.

An APCI source is very useful, especially for the analysis of uncharged compounds and can be advantageously utilized in LC–MS. However, it presents some drawbacks in CLC or nano-LC mainly because of the reduced flow rate. The use of this source is rare with these techniques, although some studies document its applicability (Barefoot and Reiser, 1987; Hutton and Games, 1997; Östman et al., 2006; Kruve et al., 2011).

On the other hand, the use of an electron ionization source (EI) for nano-LC hyphenated with MS was reported by Cappiello et al. (2003b), who showed analysis of three different classes of compounds, namely nitro-polycyclic aromatic hydrocarbons, pesticides, and human hormones. Recently, the same EI detector type was coupled with nano-LC for the analysis of fatty acids in mussel (Rigano et al., 2016).

Because the relatively low flow rates used in CLC/nano-LC, nanospray ESI interfaces have to be used; they are commercially available and allow high sensitivity. The interface is quite simple and it can also be assembled in the laboratory. Fig. 9.3 shows a scheme of the 2D nano-LC system hyphenated with MS. The packed capillary column, joining directly the valve, is connected with the nanospray interface where a capillary tip emitter is positioned. The interface is moved carefully using an x, y, z manipulator and controlled with a camera to achieve the best ionization conditions. The distance between the MS orifice and the applied voltage, as well as the composition of the mobile phase, must be carefully controlled.

The capillary column and the tip are positioned into a union that can be of different materials, either stainless steel or PEEK polymer. With the metal union, the voltage is applied directly, whereas with the polymer, a wire is necessary for the connection with the MS power supply. The commercial interfaces can also employ metal or metal-coated tips. When using the latter, although good results can be obtained, some drawbacks can be expected, mainly related to the instability of the coating under the influence of the relatively high voltage applied (1.5−2.5 kV).

In our laboratory, capillary tips are currently prepared using fused silica capillaries of 25 or 50 μm I.D.; one end is worked with fine sandpaper to obtain the most appropriate shape (Fanali et al., 2007; D'Orazio et al., 2008).

The coupling of CEC with MS has also been demonstrated utilizing different ESI interfaces, e.g., sheathless (Warriner et al., 1998), coaxial sheath-flow (Desiderio and Fanali, 2000; Bragg et al., 2008), and liquid-junction (Lee et al., 1989; D'Orazio and Fanali, 2010). Among the interfaces used, the last one seems to be very promising because minimizing the drawbacks derived by the use of the high electric field applied, bubble formation, ion signal stability, and sensitivity.

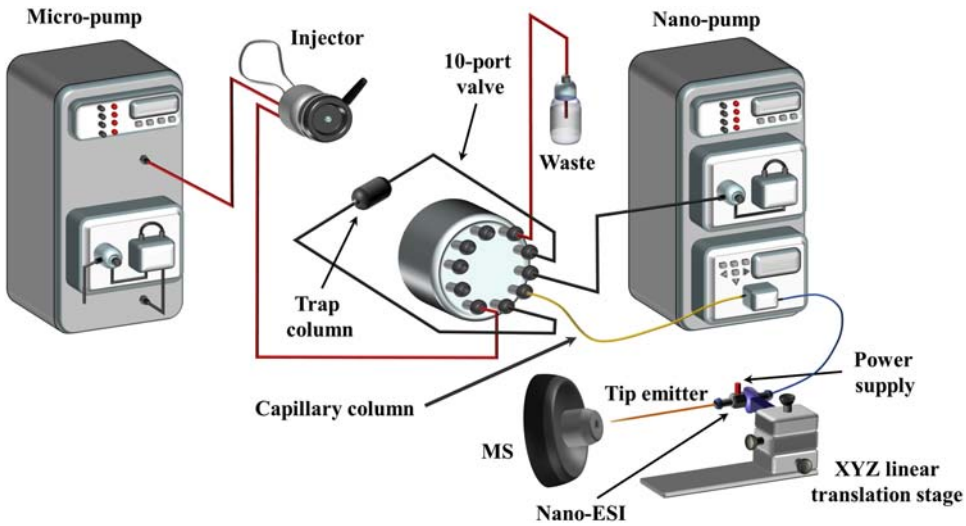

FIGURE 9.3

Schematic representation of a column-switching system coupled with mass spectrometry (MS). *ESI*, electrospray ionization.

3. APPLICATIONS

The application of an analytical technique over time clearly demonstrates its working potential and capacity. Following a previous review of the literature that we did in 2010 (Fanali et al., 2011a), we now present different applications of both techniques in proteomics, environmental, pharmaceutical, and food analysis, among others, from 2011 to 2016. The tables contain a selection of the published articles.

3.1 PROTEIN/PEPTIDE ANALYSIS

Proteomic/peptidomic research involves the analysis of proteins/peptides in cells, tissues, or biological fluids. Miniaturized chromatographic techniques, such as nano-LC and CLC, have found a great applicability in this field, much larger than that devoted to pharmaceutical, food, and environment analysis (Nazario et al., 2015), probably because the downscaling of the instrumentation leads to reduced injection volumes, an indispensable advantage when dealing with extracts of biological samples.

An enormous number of works have been published in the last decade in this field, establishing miniaturized techniques as very important approaches in proteomics/peptidomics. This section describes a selection of applications, outlining those with recent technological advances (see Table 9.1). Other articles dealing with the analysis of proteins or peptides in food matrices will be commented on in the food analysis section. In most cases, nano-LC or CLC has been used only as part of research work because in this type of study a good number of sample pretreatment steps (i.e., the extraction of proteins, digestion, cell fractionation, etc.) are necessary.

In the study of proteomics, the proteins can first be separated from the biological extract by gel electrophoresis or chromatography and then analyzed following two different strategies: *bottom-up* or *top-down* (Wehr, 2006). In the first case, proteins are frequently transformed to peptides by digestion with a specific enzyme (proteases such as trypsin, the most common) and then introduced into the analytical system. Peptide mass fingerprinting and tandem MS (MS/MS) are the two paths for new or known protein identification, followed by using the MASCOT peptide spectral library database (http://www.matrixscience.com/search_form_select.html).

In contrast, when intact protein molecular ions are introduced in the MS, the strategy is called *top-down* (Tran et al., 2011; Catherman et al., 2014). In this case, the use of an ESI source requires coupling with a highly accurate mass analyzer for unique identification, to locate and characterize posttranslational modifications.

Although the high-throughput *top-down* proteomic platforms provide routine identification of proteins, they are not so much employed for *bottom-up* analysis because it is generally less effective for protein identification. However, in *top-down* analysis, intact proteins, without the need of proteolysis, have been separated in 2D miniaturized LC systems with analytic columns employing an RP mechanism with pore sizes higher than 300 Å, precisely to host big molecular groups. Then they are identified by MS. The results obtained in this type of studies involve the deduction of protein masses, structures, and posttranslational modifications (Tipton et al., 2012; Cannon et al., 2014).

On the other hand, *bottom-up* analysis is much more usual. In this case, off-line procedures have usually been performed before the analytical separation. For instance, biological tissue lysis followed by digestion of the proteins has often been developed (Kocher et al., 2014; Delporte et al., 2015; Percy

Table 9.1 Nano-Liquid Chromatography Applications in Proteomic Analysis

Analytes	Matrix	Column	Detector	Mobile Phase	References
Top-down					
Proteins up to 78 kDa	Whole HeLa S3 lysate cells	1D: S.P.: polymer particles PS-DVB (5 μm, 1000 Å) (30 mm × 150 μm) 2D: S.P.: polymer particles PS-DVB (5 μm, 1000 Å) (100 mm × 75 μm)	FTICR-MS	1D: Isocratic (1 μL/min) ACN/water/HFo 2D: Gradient (400 nL/min) ACN/water/HFo	Tipton et al. (2012)
Proteins	*Escherichia coli* ribosomes	1D: S.P.: C_4 (5 μm, 300 Å) (−) 2D: S.P.: C_4 (5 μm, 300 Å) (40 cm × −)	MS (Orbitrap)	1D: Isocratic (−) ACN/water/HFo 2D: Gradient (300 nL/min) ACN/water/HFo	Cannon et al. (2014)
Bottom-up					
Peptides	Tryptic peptides mixture of HeLa cells	1D: S.P.: C_{18} (3 μm, 100 Å) (2 cm × 50 μm) 2D: S.P.: C_{18} (2 μm, 100 Å) (25 cm × 25 μm)	MS (Orbitrap)	1D: (−) 2D: Gradient (20 nL/min and 50 nL/min)	Kocher et al. (2014)
Proteins	Human synovial tissue	1D: S.P.: SCX (5 μm) (2.4 cm × 180 μm) 2D: S.P. C_{18} (5 μm) (15 cm × 100 μm)	MS (Orbitrap)	1D: Step gradient (20 μL/min) ACN/buffer 2D: Step gradient (500 nL/min) Water/ACN/HFo	Wang et al. (2012)

Continued

Table 9.1 Nano-Liquid Chromatography Applications in Proteomic Analysis—cont'd

Analytes	Matrix	Column	Detector	Mobile Phase	References
Peptides	Atheroma plaques proteins	*Nano-LC-chip* 1D: S.P.: C_{18} (5 μm, 180 Å) (−) 2D: S.P.: C_{18} (3 μm, 180 Å) (5 cm × 75 μm)	MS (Q-TOF)	Gradient (400 nL/min) Water/ACN/HFo	Delporte et al. (2015)
Peptides	Cardiovascular disease-related plasma proteins	*Nano-LC-chip* 1D: S.P.: C_{18} (5 μm, 300 Å) (−) 2D: S.P.: C_{18} (5 μm) (15 cm × 75 μm)	MS (QqQ)	Gradient (300 nL/min) Water/ACN/HFo	Percy et al. (2012)
Proteins	Human plasma/ serum	1D: (high pH) S.P.: C_{18} (3 μm) (50 cm × 200 μm) 2D: (low pH) S.P.: C_{18} (1.7 μm) (25 cm × 75 μm)	MS (QqQ)	1D: Gradient (300 nL/min to MS; 3.3 μL/min to 96-well plate) Water/ACN/buffer, pH 10 2D: Gradient (400 nL/min) Water/HFo/ACN	Shi et al. (2012)
Glycoproteins	Bovine ribonuclease B, bovine lactoferrin, bovine κ-casein, human IgG)	*Nano-LC-chip:* 1D: S.P.: PGC (0.9 cm × 75 μm) 2D: S.P.: PGC (15 cm × 75 μm)	MS (Q-TOF)	1D: Isocratic (4 μL/min) ACN/water/HFo 2D: Gradient (400 nL/min) ACN/water/HFo	Hua et al. (2012)
Proteins	Cell culture treated with spermine and spermidine	1D: S.P.: C_{18} (5 μm) (2 cm × 180 μm) 2D: S.P.: C_{18} (1.7 μm) (10 cm × 75 μm)	MS (Orbitrap)	1D: Isocratic (5 μL/min) Water/HFo 2D: Gradient (400 nL/min) Water/HFo/ACN	Su et al. (2015)

N-glycopeptides	Rat brain	*Off-line 2D system* 1D: S.P.: C_{18} (3 μm, 120 Å) (30 cm × 320 μm) 2D: S.P.: PGC (5 μm) (10 cm × 200 μm) or 2D: S.P.: C_{18} (3 μm, 120 Å) (30 cm × 75 μm)	MS (Orbitrap)	Gradient (250 nL/min) Water/HFo/ACN	Parker et al. (2013)
Peptides	Six different cell lines (DMS, MFM, HepG2, U2OS, 293T and yeast)	*Off-line 2D system* 1D: S.P.: C_{18} (5 μm) (25 cm × 4.6 mm) 2D: S.P.: C_{18} (3 μm, 90 Å) (14 cm × 75 μm)	MS (Q-Orbitrap)	1D: Gradient (0.7 mL/min) ACN/water/ammonia 2D: Gradient (300 nL/min) ACN/water/HFo	Wang et al. (2015)
Peptides	Rat liver sample, slow cycling cancer cells	1D: S.P.: BMA-EDMA monolithic (4.5 cm × 50 μm) 2D: S.P.: PLOT poly(PS-DVB) (800 cm × 10 μm)	MS (Orbitrap)	1D: Isocratic (500 nL/min) (−) 2D: Gradient (40 nL/min) ACN/water/HF	Rogeberg et al. (2013)
Peptides	Alzheimer's disease serum proteins	1D: S.P.: C_{18} (5 μm, 100 Å) 0.5 cm × 300 μm 2D: S.P.: C_{18} (3.5 μm, 300 Å) (15 cm × 75 μm)	MS (IT)	Gradient (200 nL/min) Water/ACN/HFo	Yang et al. (2012)
Peptides	*E. coli* whole cell lysate proteins	1D: S.P.: WAX/WCX mix-bed (5 μm) (15 cm × 150 μm) 2D: S.P.: C_{18} (5 μm, 200 Å) (15 cm × 75 μm)	MS (IT)	1D: Isocratic (1 μL/min) $AcNH_4$, pH 8.0 2D: Gradient (300 nL/min) ACN/water/HFo	Xia et al. (2012)

Continued

Table 9.1 Nano-Liquid Chromatography Applications in Proteomic Analysis—cont'd

Analytes	Matrix	Column	Detector	Mobile Phase	References
Peptides	Standard biotinylated proteins mixture (cytochrome c, lysozyme, myoglobin, β-lactoglobulin, bovine serum albumin)	*Online 3D nano-LC system* 1D: S.P.: trypsin immobilized monolithic enzyme reactor (21 cm × 100 μm) 2D: S.P.: monolithic affinity column with immobilized monomeric avidin (20 cm × 100 μm) 3D: Nano-LC-chip column S.P.: C_{18} (5 μm, 300 Å) (4.3 cm × 75 μm) *Online 2D nano-LC system* 1D: S.P.: monolithic affinity column with immobilized monomeric avidin (20 cm × 100 μm) 2D: S.P.: C_{18} (3 μm, 100 Å) (15 cm × 75 μm)	MS (Q-TOF and Orbitrap)	*Online 3D nano-LC system* 1D: Isocratic (300 nL/min) Water/buffer 2D: Gradient (500 nL/min) ACN/water/$AcNH_4$/HFo 3D: Gradient (300 nL/min) ACN/water/HFo *Online 2D nano-LC* 1D: Gradient (500 nL/min) ACN/water/$AcNH_4$ 2D: Gradient (300 nL/min) ACN/water/HFo	Sproß et al. (2013)

1D, *first dimension;* 2D, *two dimension;* ACN, *acetonitrile;* BMA, *butyl methacrylate;* DVB, *divinyl benzene;* EDMA, *ethylene dimethacrylate;* HFo, *formic acid;* MS, *mass spectrometry;* MS(IT), *mass spectrometry (ion trap);* PGC, *porous graphitic carbon;* PS, *polystyrene;* Q-TOF, *quadrupole time-of-flight;* WAX, *weak anion exchange;* WCX, *weak cation exchange.*

et al., 2012; Shi et al., 2012; Hua et al., 2012; Su et al., 2015; Parker et al., 2013; Wang et al., 2015) or 2D polyacrylamide gel electrophoresis (PAGE) followed by in-gel digestion (Rogeberg et al., 2013; Yang et al., 2012). Because this type of enzymatic digestion may require very long reaction times, a recent alternative is the employment of in-column immobilized enzymatic reactors for rapid digestion (seconds to minutes), coupled with a 2D analytical system (Xia et al., 2012; Sproß et al., 2013).

With respect to the analytical part of the methodology, an exhaustive review has been recently published about technological advances in nano-LC and CLC (Wilson et al., 2015). A great number of nano-LC and CLC columns for peptide separation are commercially available with different SPs. Most of them are packed with silica particles with C_{18} covalently linked. The analytical step can be addressed in different ways. For instance, Shi et al. (2012) proposed an off-line 2D system, including two C_{18}-silica packed capillary columns working at different pH, recovering the eluates from the first column in a 96-well plate. Also in an off-line approach, Parker et al. (2013) loaded the peptides onto a zwitterionic-HILIC−SPE cartridge, then enriched them in an RP-C_{18} packed capillary column, and finally, a fraction of the eluate was analyzed by nano-LC, either in a C_{18}-silica column or in a porous graphitic carbon column. Fig. 9.4 shows a scheme of the procedure. In another example, Wang et al. (2015) analyzed the fractions obtained from a conventional C_{18}-silica column with high-pH conditions, in a nano-LC system with a C_{18}-silica column.

On the other hand, online systems have also been employed. On two occasions, a 2D conventional salt step gradient was employed, combining an SCX column (Wang et al., 2012) or a WAX/WCX column (Xia et al., 2012) with a C18-silica column, but also online coupling of a BMA−EDMA monolithic column with a PLOT poly(PS-DVB) column has been described (Rogeberg et al., 2013).

Other applications have shown the potential of 2D systems, where the first dimension (1D) is a trap column packed with C_{18}-silica particles (Kocher et al., 2014; Percy et al., 2012; Su et al., 2015; Yang et al., 2012) or a monolithic affinity column with immobilized monomeric avidin as the trap column (Sproß et al., 2013). Furthermore, the use of an online 2D nano-LC-chip has been described on several occasions (Delporte et al., 2015; Hua et al., 2012).

3.2 ENVIRONMENTAL ANALYSIS

The introduction of contaminants into the environment can be truly harmful, particularly when the planet does not have any tools to process or neutralize harmful by-products of human activities. In the last decade, nano-LC and CLC have gained importance in environmental analysis, as can be seen in Table 9.2, which shows a selection of articles that deal with this issue.

Most of the articles regard the analysis of pesticides (Asensio-Ramos et al., 2011; Moliner-Martínez et al., 2011b; Gure et al., 2013; Otieno et al., 2013; Lerma-García et al., 2013; Berlioz-Barbier et al., 2014), but also other emerging pollutants have been determined with miniaturized techniques, such as perfluorinated compounds (Berlioz-Barbier et al., 2014; Onghena et al., 2012), phthalates (Jornet-Martínez et al., 2014; Muñoz-Ortuño et al., 2014), or hormones (Berlioz-Barbier et al., 2014; D'Orazio et al., 2016b; Kozlík et al., 2011), most of them in simple matrices (different types of waters). In a few other examples, pesticides (Otieno et al., 2013) and di-(2-ethylhexyl) phthalate (Muñoz-Ortuño et al., 2014) were determined in sediments, multiclass emerging pollutants in benthic invertebrates (Berlioz-Barbier et al., 2014), carbonyl compounds in wastewater filters, and biocides in industrial formulations (Prieto-Blanco et al., 2016). In general, 300−500 μm I.D. columns packed with 3−5 μm C_{18}-silica particles have been used, followed by UV or MS detection. Monolithic C_{18} columns

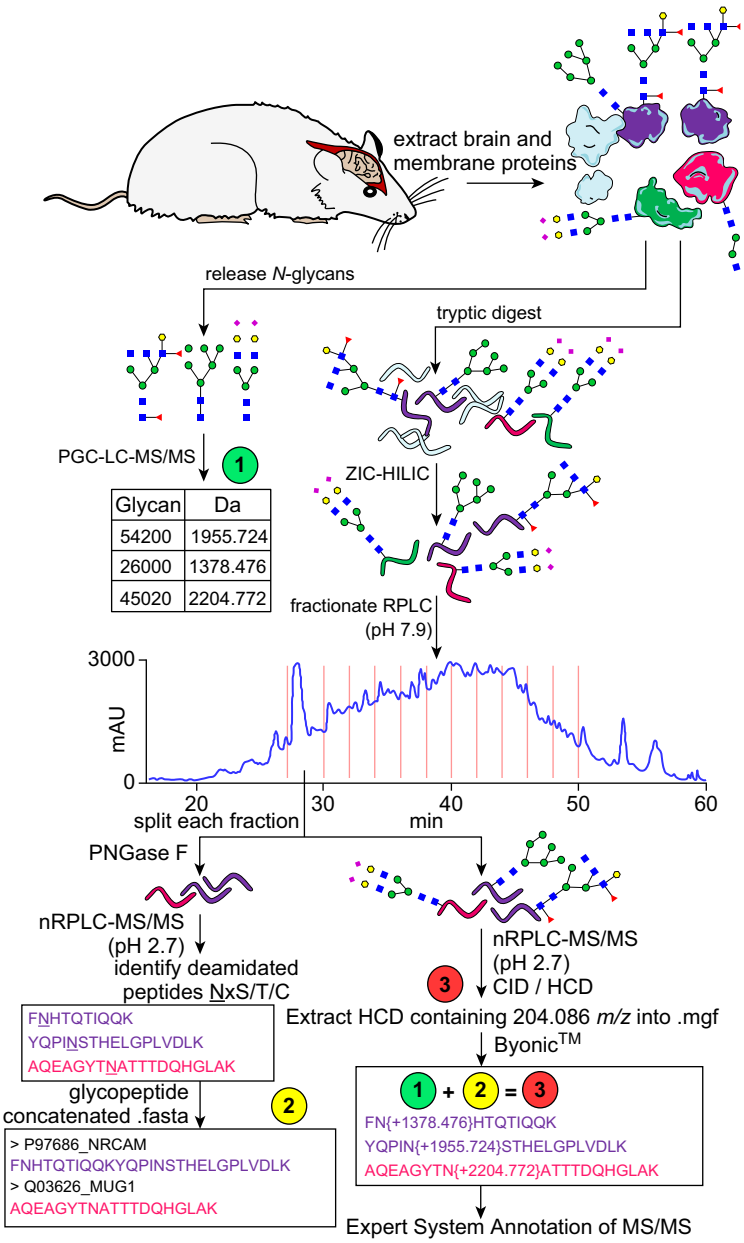

FIGURE 9.4

Scheme of a multidimensional approach utilizing a global *N*-glycome characterization followed by parallel analysis of deglycosylated and glycosylated peptides with orthogonal fractionation.

Reprinted from Parker, B.L., Thaysen-Andersen, M., Solis, N., Scott, N.E., Larsen, M.R., Graham, M.E., Packer, N.H., Cordwell, S.J., 2013. Site-specific glycan-peptide analysis for determination of N-glycoproteome heterogeneity. J. Proteome Res. 12, 5791–5800 with permission from ACS Publications.

Table 9.2 Nano-Liquid Chromatography and Capillary Liquid Chromatography Applications in Environmental Analysis

Analytes	Matrix	Column	Detector	Mobile Phase	References
Pesticides					
12 multiclass pesticides (carbaryl, fensulfothion, mecoprop, fenamiphos, haloxyfop, diclofop, fipronil, profenofos, fonofos, disulfoton, nitrofen, terbufos)	Milli-Q water	1D: S.P.: C_{18} (5 μm, 100 Å) (0.5 cm × 300 μm) 2D: S.P.: silica-phenyl phase (3 μm, 110 Å) (25 cm × 100 μm)	UV (200 nm)	Gradient (500 nL/min) ACN/water/HFo	Asensio-Ramos et al. (2011)
Eight multiclass pesticides (simazine, atrazine, terbutylazine, chlorfenvinphos, trifluralin, chlorpyrifos, diuron, isoproturon), DEHP	Wastewater	S.P.: C_{18} (3.5 μm, 80 Å) (15 cm × 500 μm) S.P.: monolithic C_{18} (15 cm × 200 μm)	UV (210–254 nm)	Isocratic (12 μL/min) ACN/water	Moliner-Martínez et al. (2011b)
Six sulfonylurea herbicides (triasulfuron, metsulfuron-methyl, chlorsulfuron, flazasulfuron, chlorimuronethyl, primisulfuron-methyl)	Bottled spring water, groundwater, river water	S.P.: C_{18} (5 μm, 100 Å) (15 cm × 300 μm)	UV (230 nm)	Gradient (15 μL/min) ACN/MeOH/water/HAc	Gure et al. (2013)
Three organochlorine pesticides (chlorpyrifos, carbofuran, diazinon)	Lake water, sediments	S.P.: C_{18} (3 μm, 100 Å) (15 cm × 300 μm)	UV (230, 246, 205 nm)	Gradient (4 μL/min) ACN/water	Otieno et al. (2013)
Five sulfonylurea herbicides (bensulfuronmethyl, metsulfuron-methyl, pyrazosulfuron-methyl, thifensulfuron-methyl, triasulfuron)	River water	S.P.: C_{18} (5 μm, 100 Å) (25 cm × 500 μm)	UV (230 nm)	Gradient (10 μL/min) ACN/water/HAc	Lerma-García et al. (2013)
Five triazines (terbutylazine, desethylterbutylazine, 2-hydroxyterbutylazine, atrazine, propazine)	Sea and transition waters	S.P.: monolithic C_{18} (15 cm × 200 μm)	UV (230 nm)	Gradient (5 μL/min) ACN/water	Moliner-Martínez et al. (2015)

Continued

Table 9.2 Nano-Liquid Chromatography and Capillary Liquid Chromatography Applications in Environmental Analysis—cont'd

Analytes	Matrix	Column	Detector	Mobile Phase	References
Other Organic Pollutants					
35 emerging pollutants (pharmaceuticals and their metabolites, pesticides, hormones, plasticizer, alkylphenols, perfluorinated compounds, UV filter)	Benthic invertebrates (*Potamopyrgus antipodarum*, *Gammarus fossarum*, *Chironomus riparius*)	1D: S.P.: C_{18} (5 μm, 100 Å) (0.5 cm × 300 μm) 2D: S.P.: C_{18} (3 μm, 100 Å) (15 cm × 75 μm)	MS (QqQ)	Gradient (300 nL/min) MeOH/ACN/water/HFo	Berlioz-Barbier et al. (2014)
18 perfluorinated compounds (perfluorobutanoic acid, perfluoropentanoic acid, perfluorohexanoic acid, pefluoroheptanoic acid, sodium pefluorohexanesulfonate, perfluorooctanoic acid, sodium perfluoroheptanesulfonate, perfluoro-7-methyloctanoic acid, perfluorononanoic acid, sodium perfluoroctanesulfonate, perfluorodecanoic acid, sodium perfluoro-7-methyloctanesulfonate, perfluoroundecanoic acid, sodium perfluordecanosulfonate, perfluorododecanoic acid, perfluorotridecanoic acid, perfluorotetradecanoic acid, perfluorohexadecanoic acid, perfluorooctadecanoic acid)	River water	S.P.: C_{18} (3.5 μm, 80 Å) (15 cm × 500 μm)	MS (Q)	Gradient (10 μL/min) MeOH/water/NH_4Fo	Onghena et al. (2012)
Four phthalates (di-(2-ethylhexyl) phthalate, (2-ethylhexyl) phthalate, diethyl phthalate, dibutyl phthalate)	Sea and transition waters, plastic tubing washing waters	S.P.: C_{18} monolith (15 cm × 200 μm)	UV (230 nm)	Isocratic (5 μL/min) ACN/water	Jornet-Martínez et al. (2014)

Di-(2-ethylhexyl) phthalate	Coastal sediments	S.P.: C_{18} (5 μm, 80 Å) (35 cm × 500 μm)	UV (230 nm)	Isocratic (10 μL/min) ACN/water	Muñoz-Ortuño et al. (2014)
11 estrogenic compounds (dienestrol, 17α-estradiol, 17β estradiol, estriol, estrone, 17α-ethinylestradiol, 2-methoxyestradiol, α-zearalanol, β-zearalanol, α-zearalenol), zearalenone)	Mineral water	S.P.: silica-phenyl phase (3 μm, 110 Å) (25 cm × 75 μm)	MS (IT)	Isocratic (100 nL/min) ACN/MeOH/water	D'Orazio et al. (2016b)
Five estrogens (estrone, 17α-estradiol, 17β-estradiol, 17α-ethynylestradiol, estriol)	River water from WWTP effluents	S.P.: C_{18} (5 μm, 80 Å) (15 cm × 500 μm)	MS (QqQ)	Gradient (18 μL/min) ACN/water/HFo	Kozlík et al. (2011)
12 carbonyl compounds (formaldehyde, acetaldehyde, propionaldehyde, butyraldehyde, crotonaldehyde, valeraldehyde, cyclohexanone, hexaldehyde, heptaldehyde, octylaldehyde, nonanaldehyde, decylaldehyde)	$PM_{2.5}$ and PM_{10} filters from wastewater plant, wastewater	S.P.: C_{18} (5 μm, 80 Å) (15 cm × 500 μm)	MS (Q)	Gradient (10 μL/min) ACN/water	Prieto-Blanco et al. (2013)
Acetylsalicylic acid, acetaminophen, diclofenac, ibuprofen	River water from WWTP effluents	S.P.: C_{18} (5 μm, 80 Å) (15 cm × 500 μm)	MS (Q)	Gradient (10 μL/min) ACN/water	Moliner-Martínez et al. (2011a)
Two biocides (C_{12}-BAK, C_{14}-BAK)	Industrial formulations	S.P.: C_{18} (5 μm, 70 Å) (35 cm × 500 μm)	UV (212 nm)	Isocratic (20 μL/min) ACN/water/$AcNH_4$, pH 4.5	Prieto-Blanco et al. (2016)
C_{12}-BAK	Treatment plant waters, wash water from a feed industry, coastal and transition waters, tap water	S.P.: polymer-coated RP-TiO_2 (5 μm) (10 cm × 100 μm)	UV (212, 270 nm)	Gradient (7−9 μL/min) ACN/water/Ac-buffer, pH 5	Prieto-Blanco et al. (2012)

Continued

Table 9.2 Nano-Liquid Chromatography and Capillary Liquid Chromatography Applications in Environmental Analysis—cont'd

Analytes	Matrix	Column	Detector	Mobile Phase	References
Inorganic or Organic Small Anions					
IO_3^-, BrO_3^-, NO_2^-, Br^-, NO_3^-	Public drinking water, seawater	S.P.: PEG monolith (10 cm × 320 μm)	UV (210 nm)	Isocratic (4 μL/min) Water/NaCl	Rahayu et al. (2015)
Cl^-, SO_4^{2-}, NO_3^-, F^-, methanesulfonate	Antarctic ice cores	S.P.: anion-exchange column (25 cm × 400 μm)	CD MS (Orbitrap)	Gradient (17 μL/min) Water/KOH	Rodriguez et al. (2015)
BrO_2^-, ClO_2^-, five holoacetic acids (monochloroacetic acid, dichloroacetic acid, trichloroacetic acid, monobromoacetic acid, dibromoacetic acid)	Tap water	1D: S.P.: hydroxide-selective anion-exchange (25 × 4 mm) Trap: S.P.: monolithic anion-exchange concentrator (8 cm × 750 μm) 2D: S.P.: hydroxide-selective anion-exchange (25 cm × 400 μm)	CD	1D: Gradient (1 mL/min) Water/KOH 2D: Gradient (10 μL/min) Water/KOH	Teh and Li (2015)

1D, *first dimension;* 2D, *two dimension;* ACN, *acetonitrile;* CD, *cyclodextrin;* HAc, *acetic acid;* MeOH, *methanol;* MS(Q), *mass spectrometry (quadrupole);* MS(IT), *mass spectrometry (ion trap);* WWTP, *wastewater treatment plan.*

(Moliner-Martínez et al., 2011b, 2015; Jornet-Martínez et al., 2014) or other SPs, such as phenyl-silica (D'Orazio et al., 2016b) or polymer-coated RP-TiO_2 (Prieto-Blanco et al., 2012), have been occasionally used. This last phase, based on a metal oxide, possesses lower hydrophobicity than those based on SiO_2, with titanol groups being much more basic than silanols. Also, in some of the works, a comparison between different SPs has been done; for example, Moliner-Martínez et al. (2011b) compared a 15 cm × 500 μm ID C_{18} particulate column with a 15 cm × 200 μm I.D. C_{18} monolithic column for the separation of organic contaminants, concluding that the monolith was clearly better (shorter analysis time, improved sensitivity, and superior selectivity).

To obtain better sensitivity by means of online strategies, different approaches have been used in this field. For instance, on two occasions a 2D commercial system has been employed to preconcentrate the analytes, injecting a high volume of sample onto a trap column (1D), from which they are later eluted onto the analytical column (second dimension (2D)) (Asensio-Ramos et al., 2011; Berlioz-Barbier et al., 2014). A simpler and cheaper solution, on-column focusing, was applied by D'Orazio et al. (2016b), who injected a high volume of sample diluted in a solvent with lower elution strength than that of the mobile phase directly on the analytical column, preconcentrating the analytes on the top of the column. However, the most popular method to preconcentrate the analytes online has been in-tube solid-phase microextraction (IT-SPME) (Moliner-Martínez et al., 2011b, 2015; Jornet-Martínez et al., 2014; Muñoz-Ortuño et al., 2014; Prieto-Blanco et al., 2012), normally carried out in a 40 cm piece of a 320 μm I.D. GC column coated with 5% diphenyl and 95% polydimethylsiloxane. The GC column is installed in the place of the sample loop.

Other environmental applications involve the determination of inorganic and organic small anions (Rahayu et al., 2015; Rodriguez et al., 2015; Teh and Li, 2015). Different SPs have been employed for this purpose, such as PEG monolith (Rahayu et al., 2015) or anion-exchange sorbents (Rodriguez et al., 2015; Teh and Li, 2015). An interesting example of these applications is the one by Teh and Li (2015), who developed a two-dimensional matrix elimination ion chromatographic method. A high capacity 4 mm I.D. column was used in the 1D to partially resolve the matrix from target analytes. Then, the target analytes, i.e., bromate, chlorite, and five haloacetic acids, were trapped in a monolithic anion-exchange concentrator (trap column) by using a 6-port valve, whereas the separated matrix was sent to waste. Finally, the analytes were eluted into a hydroxide-selective anion-exchange capillary column (2D) for separation.

3.3 PHARMACEUTICAL ANALYSIS

The pharmaceutical field involves not only the research and development of new active pharmaceutical molecules but also the quality control of pharmaceutical formulations, enantiomeric purity, pharmacokinetics studies in the clinical phase, and analysis of metabolites. In the pharmaceutical industry the analytical aspect is mostly carried out by conventional HPLC and affects the final cost of the commercial drug. In this respect, the introduction of LC miniaturized techniques (CLC and nano-LC) is competing with existing analytical methods to increase productivity, reduce analysis time, keep costs low, and follow the thinking "do more with less."

Table 9.3 shows some recent selected research works in which CLC and nano-LC have been employed, both for nonchiral (Flender et al., 2011; Zhao et al., 2011; D'Orazio and Fanali, 2013a; Meyer et al., 2016; D'Orazio et al., 2012b; Aturki et al., 2011; Aggarwal et al., 2014; Zheng et al., 2011) and chiral (Auditore et al., 2013; Fanali et al., 2012b; Rocchi et al., 2015; Gotti et al., 2012;

Table 9.3 Nano-Liquid Chromatography and Capillary Liquid Chromatography Applications in Pharmaceutical Analysis

Analytes	Matrix	Column	Detector	Mobile Phase	References
Nonchiral					
11 multiclass drugs (atenolol, caffeine, *n*-acetylprocainamide, propranolol, methoxyverapamil, imipramine, theophylline, bumetanide, aspartame, cortisone, reserpine)	Mice serum	S.P.: C_{18} (5 μm, 80 Å) (150 mm × 75 μm)	MS (Q-TOF)	Gradient (300 nL/min) ACN/water/HFo	Zhao et al. (2011)
Five basic drugs (terbutaline, nadolol, acebutolol, oxprenolol, alprenolol)	–	S.P.: 3 cm CSP-Teico (5 μm, 100 Å) and 25 cm C_{18} (4.2 μm, 100 Å) (28 cm × 100 μm)	UV (200 nm)	Isocratic (750 nL/min) MeOH/ACN/water/ NH_4Ac, pH 4.5	D'Orazio and Fanali (2013a)
Three Nitrobenzodiazepines (clonazolam, meclonazepam, nifoxipam) and metabolites	Human urine	S.P.: C_{18} (2 μm, 100 Å) (15 cm × 50 μm)	MS (Q-Orbitrap)	Gradient (300 nL/min) ACN/water/HFo	Meyer et al. (2016)
Eight steroids (triamcinolone, prednisolone, cortisone, dexamethasone, corticosterone, triamcinolone acetonide, 11-hydroxyprogesterone, cortisone 21-acetate), nine NSAIDs (indoprofen, ketoprofen, fenoprofen, flurbiprofen, ibuprofen, cicloprofen)	Pharmaceutical formulation (tablets)	S.P.: C_{18} hydrate (1.8 μm, 100 Å) (5 cm × 50 μm)	UV (200, 254 nm)	*Steroids*: Isocratic (380 nL/min) ACN/water/HFo *NSAIDs*: Isocratic (300 nL/min) ACN/water/HFo	D'Orazio et al. (2012b)
Seven sympathomimetic drugs (ephedrine hydrochloride, norephedrine, synephrine, epinephrine, norepinephrine hydrochloride (arterenol), norphenylephrine hydrochloride)	–	S.P: Cross-linked diol HILIC phase (5 μm, 195 Å) (25 cm × 100 μm)	UV (205 nm)	Isocratic (300 nL/min) ACN/water/NH_4Fo, pH 3	Aturki et al. (2011)
Four pharmaceuticals (paracetamol, ibuprofen, aspirin, indomethacin)	–	S.P.: PEGDA (15 cm × 150 μm)	UV (214 nm)	ACN/water/HFo, pH 2.5 (Gradient, 250 nL/min)	Aggarwal et al. (2014)

Acetaminophen, *p*-aminophenol, aspirin metabolites (salicylic acid, gentisic acid, salicyluric acid, 2,3-dihydroxybenzoic acid)	Human serum	S.P.: poly(PETA-co-DMMSA-co-AETA) monolithic column (35 cm × 50 μm)	AD	0.05 mL/min ACN/water/Tris, pH 8.5	Zheng et al. (2011)
11 pharmaceuticals or illicit drugs (bunitrolol, caffeine, cocaine, codeine, diazepam, doxepin, haloperidol, MDA, morphine, nicotine, zolpidem)	Human urine	S.P.: C_{18} (5 μm, 100 Å) (2 cm × 200 μm)	MS (Q-TOF)	Gradient (2 μL/min) ACN/water/HFBA	Schubert and Oberache (2011)
Ketamine and two metabolites (norketamine, dehydronorketamine)	Human hair	S.P.: C_{18} (3 μm, 100 Å) (10 cm × 20 μm)	MS (QqQ)	Gradient (150 nL/min) ACN/water/HFo	Parkin et al. (2013)
12 synthetic cannabinoids (JWH-018, JWH-019, JWH-073, JWH-081, JWH-122, JWH-200, JWH-203, JWH-210, JWH-250, AM-694, AM-2201, WIN-55,212-2), Δ^9-THC	Herbal mixtures	S.P.: C_{18} (4.2 μm, 100 Å) (25 cm × 100 μm)	UV (214 nm) MS (IT)	Isocratic (500 nL/min) ACN/MeOH/water/HFo	Merola et al. (2012)
14 drugs of abuse (cocaine, benzoylecgonine, cocaethylene, norcocaine, morphine, codeine, 6-acetylmorphine, phencyclidine, amphetamine, methamphetamine, MDMA, MDA, MDEA, methadone)	Human hair	*Nano-LC-chip* 1D: S.P.: C_{18} (5 μm) (2.5 cm × 500 nL) 2D: S.P.: C_{18} (5 μm, 80 Å) (15 cm × 75 μm)	MS (QqQ)	Gradient (400 nL/min) ACN/water/HFo	Zhu et al. (2012)
Chiral					
Amlodipine and two impurities	–	S.P.: CSP-silica based on cellulose tris(4-chloro-3-methylphenylcarbamate) (5 μm, 1000 Å) (30 cm × 100 μm)	UV (206 nm)	Isocratic (100 nL/min) ACN/water/NH_4-borate, pH 10	Auditore et al. (2013)
Racemic mixtures of temazepam, thalidomide, warfarin, etozoline	–	S.P.: CSP-silica based cellulose tris(4-chloro-3-methylphenylcarbanate) coated (10% w/w) (i) 3 μm native silica particles (ii) core-shell silica (2.8 μm) (25 cm × 75 μm)	UV (205 nm)	Isocratic (150 nL/min) ACN/water/NH_4Ac, pH 4.5	Fanal et al. (2012b)

Continued

Table 9.3 Nano-Liquid Chromatography and Capillary Liquid Chromatography Applications in Pharmaceutical Analysis—cont'd

Analytes	Matrix	Column	Detector	Mobile Phase	References
Racemic mixtures of eight NSAIDs (ibuprofen, indoprofen, ketoprofen, naproxen, carprofen, cicloprofen, flurbiprofen, suprofen), six β-blockers (alprenolol, metoprolol, oxprenolol, pindolol, propranolol, atenolol)	–	S.P.: CSP-diol silica-vancomycin (1.8 μm, 100 Å) (11 cm × 75 μm)	UV (200 nm)	*NSAIDs*: Isocratic (360 nL/min) ACN/water/NH_4Ac, pH 4.5 *β-blockers*: Isocratic (135 nL/min) MeOH/water/NH_4Ac, pH 4.5	Rocchi et al. (2015)
Racemic mixtures of four NSAIDs (ketoprofen, fenoprofen, flurbiprofen, suprofen)	Pharmaceutical formulation (tablets)	S.P.: Penicillin G acylase immobilized on epoxy derivatized monolithic silica column (7 cm × 100 μm)	UV (200 nm)	Isocratic (–) Na-phosphate, pH 7	Gotti et al. (2012)
Racemic mixtures of 50 multiclass pharmaceuticals (α- and β-blockers, antiinflammatory drugs, antifungal drugs, dopamine antagonists, norepinephrine-dopamine reuptake inhibitors, catecholamines, sedative hypnotics, diuretics, antihistaminics, anticancer drugs, antiarrhythmic drugs)	–	S.P.: Silica monolithic capillary β-CD–based CSPs (15/25 cm × 100 μm/150 μm)	UV (219–270 nm)	Isocratic (100–1000 nL/min) MeOH/ACN/TFA	Ghanem et al. (2015)
Racemic mixtures of 11 drugs (naproxen, ibuprofen, ketoprofen, suprofen, indoprofen, carprofen, nomifensine, praziquantel, metomidate, 5-methyl-5-phenyl-hydantoin, alprenolol)	–	S.P.: CSP-monolithic-hydroxypropyl-β-cyclodextrin (19 cm × 100 μm)	UV (205 nm)	Isocratic (200 nL/min) MeOH/water/TEA-Ac ACN/water/TEA-Ac	Rocco et al. (2012b)

Racemic mixtures of 50 multiclass pharmaceuticals (α- and β-blockers, antiinflammatory drugs, antifungal drugs, dopamine antagonists, norepinephrine-dopamine reuptake inhibitors, catecholamines, sedative hypnotics, diuretics, antihistaminics, anticancer)	–	S.P.: CSP-SWCNTs in polymer monolithic backbone (20 cm × 150 μm)	UV (219–270 nm)	Isocratic (300 nL/min) MeOH/ACN/water/TFA 2-propanol/MeOH *n*-hexane/2-propanol	Ahmed et al. (2014)
Racemic mixtures of eight NSAIDs (ibuprofen, ketoprofen, flurbiprofen, suprofen, indoprofen, cicloprofen, carprofen, naproxen)	–	S.P.: C_{18}-monolithic silica or C18 (3 μm, 110 Å) (10 cm × 100 μm)	UV (200 nm)	Isocratic (–) MeOH/water/HP-β-CD/NaAc, pH 3	Rocco et al. (2012a)

Ac, *acetate;* ACN, *acetonitrile;* CD, *cyclodextrin;* CSP, *choral stationary phase;* HFBA, *heptafluorobutyric acid;* HFo, *formic acid;* HILIC, *hydrophilic interaction chromatography;* MeOH, *methanol;* MS (QqQ), *mass spectrometry (triple quadrupole);* MS(IT), *mass spectrometry (ion trap);* NSAID, *nonsteroidal antiinflammatory drug;* PEGDA, *polyethylene glycol diacrylate;* SWCNTs, *single wall carbon nanotubes;* TEA, *triethylamine;* TFA, *trifluoroacetic acid.*

Ghanem et al., 2015; Rocco et al., 2012a,b; Ahmed et al., 2014) analysis of molecules of pharmaceutical interest in biological matrices, pharmaceutical formulations, and pure solvent (not a real application). In addition, the table also includes a selection of works in which molecules with pharmacological activity, defined as abuse or illicit drugs, have been analyzed (Schubert and Oberache, 2011; Parkin et al., 2013; Merola et al., 2012; Zhu et al., 2012).

In nonchiral analysis, chromatographic separation of compounds with a predominant hydrophobic component has been achieved by a RP mechanism (Flender et al., 2011; Zhao et al., 2011; D'Orazio and Fanali, 2013a; Meyer et al., 2016; D'Orazio et al., 2012b). Separation of NSAIDs (D'Orazio et al., 2012b), nitrobenzodiazepines (Meyer et al., 2016), β-blockers (Zhao et al., 2011; D'Orazio and Fanali, 2013a), and multiclass drugs (Zhao et al., 2011) were accomplished using columns packed with C_{18}-silica based SPs. Among these works, it is worth highlighting the application of the chip technology in the separation of 11 hydrophobic/basic compounds (Zhao et al., 2011). This work shows the advantages of the use of a commercially polyimide HPLC chip to obtain higher sensitivity (LOQs in the low pg/μL level), more suitable coupling with MS through a nanospray interface, and better peak shape, especially with basic compounds, by using a C_{18} end-capped stable bond SP. Fig. 9.5 shows two versions of the original HPLC chip, being different in the separation column length (4.3 and 15 cm, respectively) and in the enrichment column volume (40 and 500 nL, respectively).

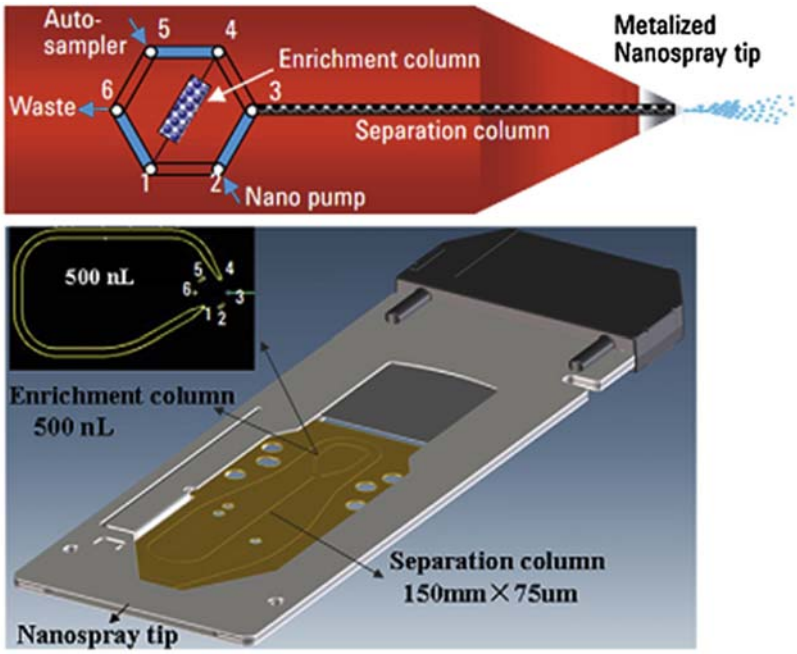

FIGURE 9.5

Schematic illustration of two versions of the original high-performance liquid chromatography chip.

Reprinted from Zhao, C., Wu, Z., Xue, G., Wang, J., Zhao, Y., Xu, Z., Lin, D., Herbert, G., Chang, Y., Cai, K., Xu, G., 2011. Ultra-high capacity liquid chromatography chip/quadrupole time-of-flight mass spectrometry for pharmaceutical analysis. J. Chromatogr. A 1218, 3669–3674 with permission from Elsevier.

Fast analyses were possible by choosing the appropriate SPs, as in the case of the separation of nitrobenzodiazepines (Meyer et al., 2016) or steroids/NSAIDs (D'Orazio et al., 2012b) using capillary columns packed with sub-2 μm C_{18}-silica particles. In the latter case, with 2 min of analysis time, the authors tested different I.D. short capillary columns, showing better chromatographic efficiency by reducing the I.D. from 100 to 50 μm. On other occasions, because of the poor selective power of the C_{18} phase toward polar pharmaceutical compounds, it has been replaced with SPs that promote strong electrostatic interactions, such as hydrophilic interaction/strong anion exchange (HI/SAX) (Zheng et al., 2011) or pure HILIC, such as cross-linked diol silica (Aturki et al., 2011).

Because of the small amount of real sample required for the analysis, CLC and nano-LC have also been employed for the analysis of illegal drugs. For instance, cocaine, codeine, diazepam, MDA, morphine, and nicotine, among others, were analyzed in human urine (Schubert and Oberache, 2011), as well as ketamine and its metabolites (Parkin et al., 2013), 14 drugs of abuse (Zhu et al., 2012) in hair samples, and synthetic cannabinoids in herbal mixtures (Merola et al., 2012).

Chiral analysis of pharmaceutical compounds is of great importance in the pharmaceutical industry because different enantiomers of the same drug may have unlike pharmacological activities and different pharmacokinetics and pharmacodynamics effects. Actually, it often happens that one isomer may produce the desired therapeutic activity, whereas the other may have no effect or even produce unwanted or irreversible consequences.

CLC and nano-LC have been employed in the analysis of drug enantiomeric purity, in particular to test new CSPs, requiring small amounts of CSP, achieving highest chromatographic efficiency, using more sustainable mobile phases, reducing the analysis time, and improving the compatibility with MS. The most popular chiral selectors are large molecular structures such as optically active proteins, peptides, and carbohydrates. In this respect, polysaccharides such as cellulose or amylose derivatized with phenyl-carbamate moieties and coated onto silica particles (Auditore et al., 2013; Fanali et al., 2012b), macrocyclic glycopeptides antibiotics such as vancomycin bonded on diol-silica (Rocchi et al., 2015) or proteins such as penicillin G acylase (Gotti et al., 2012) have been employed in the reviewed period. However, capillary columns have also been prepared by the continuous monolithic bed technology, by inserting a chiral selector as the functional monomer in the polymeric network, for instance, β-cyclodextrin derivatives (Ghanem et al., 2015; Rocco et al., 2012b) are trapped in the polymeric network, such as single wall carbon nanotubes (Ahmed et al., 2014). Although used minimally in LC because of the high workflows, chiral separation in nano-LC and CLC can be achieved using capillary columns with achiral SPs by adding chiral additives to the mobile phase (Rocco et al., 2012a).

3.4 FOOD ANALYSIS

Food analysis is focused in two key aspects: food quality and food safety. Table 9.4 summarizes a representative selection of nano-LC and CLC analytical methods focused on these applications.

Although human survival depends on food, the way it is produced has changed over time because of scientific and technological development. The study of endogenous molecules that characterize each food matrix constitutes crucial information to know its nutritional properties, its capacity as functional food, its quality level, and especially possible adulteration/frauds. Recent research trends have identified some food polyphenols as potential agents of health promotion for their ability to act as antioxidants and free-radical scavengers. A great percentage of articles deals with the analysis of this class of molecules in different food matrices such as fruit juices (Fanali et al., 2011b; Rocco et al.,

Table 9.4 Nano-Liquid Chromatography and Capillary Liquid Chromatography Applications in Food Analysis

Analytes	Matrix	Column	Detector	Mobile Phase	References
Food Quality					
14 anthocyanins (delphinidin-3-*O*-galactoside, delphinidin -3-*O*-glucoside, cyanidin-3-*O*-galactoside, delphindin-3-*O*-arabinoside, cyanidin-3 -*O*-glucoside, petunidin-3-*O*-galactoside, petunidin-3-*O*-glucoside, cyanidin -3-*O*-arabinoside, peonidin-3-*O*-galactoside, petunidin-3-*O*-arabinoside, peonidin -3-*O*-glucoside, malvidin-3-*O*-galactoside, malvidin-3-*O*-glucoside, malvidin -3-*O*-arabinoside)	Blueberry, raspberry, cherry and pomegranate juices	S.P.: C_{18} (4 μm, 100 Å) (25 cm × 100 μm)	MS (IT)	Gradient (400 nL/min) MeOH/water/HFo	Fanali et al. (2011b)
13 flavanoids (genistein *O*-hexoside I, genistein *O*-hexoside malonylated II, genistein *O*-hexoside II, genistein *O*-hexoside malonylated V, genistein, glycitein *O*-hexoside I, glycitein *O*-hexoside malonylated II, glycitein *O*-hexoside malonylated III, glycitein, kaempferol 7-*O*-rhamnosyl hexoside, kaempferol 7-Ohexoside, kaempferol 3-*O*-hexoside)	Soybean	HPLC Chip S.P.: C_{18} (5 μm, 80 Å) (15 cm × 75 μm)	MS (Q-TOF)	Gradient (300 nL/min) ACN/water/HFo	Chang et al. (2012)
47 phenolic compounds	Cranberry syrup	1D: S.P.: C_{18} (5 μm) (2 cm × 100 μm) 2D: S.P.: C_{18} (3 μm) (10.1 cm × 75 μm)	MS (TOF)	Gradient (300 nL/min) ACN/water/HFo	Contreras et al. (2015)

Seven flavanones (didymin, hesperetin, hesperidin, naringenin, naringin, neohesperidin, narirutin)	Freshly squeezed juice of orange, pink, white grapefruit	S.P.: C_{18} (1.8 μm) (10 cm × 75 μm)	UV (200 nm) MS (IT)	Step gradient (500 nL/min) ACN/water/HFo	Rocco et al. (2014)
11 polyphenols (gallic acid, protocatecuic acid, epigallocatechin, catechin, caffeic acid, epicatechin, epigallocatechin gallate, *p*-coumaric acid, epicatechin gallate, catechin gallate, *o*-coumaric acid), 3 methylxanthines (theobromine, theophylline, caffeine)	Green and black tea	S.P.: C_{18} (2.6 μm, 100 Å) (10 cm × 100 μm)	UV (200, 280 nm) MS (IT)	Step gradient (1200 nL/min) ACN/MeOH/water/HFo	Fanali et al. (2012a)
Six phenolic acids (gallic acid, protocatechuic acid, *p*-OH-benzoic acid, gentisic acid, vanillic acid, syringic acid), five hydroxycinnamic acids (caffeic acid, *p*-coumaric acid, ferulic acid, *o*-coumaric acid, cinnamic acid), four flavonoids (myricetin, naringenin, hesperetin, kaempferol)	Bee pollen	S.P.: C_{18} (2.6 μm, 100 Å) (10 cm × 100 μm)	UV (200 nm)	Step gradient (500 nL/min) ACN/water/HFo	Fanali et al. (2013b)
Polyphenolic profile	Red wine	S.P.: C_{18} (3.5 μm, 80 Å) (15 cm × 300 μm)	MS (IT)	Gradient (2 μL/min) EtOH/water/HFo	Hashim et al. (2013)
Five flavonoid aglycones (hesperetin, kaempferol, myricetin, naringenin, quercetin)	Dietary supplements	S.P.: hydride-based C_{18} (<2 μm) (10 cm × 75 μm)	UV (200 nm)	Isocratic (450 nL/min) ACN/MeOH/water/formic acid	Fanali et al. (2015a)
27 antioxidant peptides	Spanish dry-cured ham	1D: S.P.: C_{18} (5 μm) (0.5 cm × 100 μm) 2D: S.P.: C_{18} (5 μm, 100 Å) (15 cm × 75 μm)	MS (IT)	Gradient (250 nL/min) ACN/water/HFo	Escudero et al. (2013)
Peptide profile	Shrimp	S.P.: C_{18} (5 μm, 300 Å) (15 cm × 150 μm)	MS (IT)	Gradient (1.4−1.7 μL/min)	Ortea et al. (2011)

Continued

Table 9.4 Nano-Liquid Chromatography and Capillary Liquid Chromatography Applications in Food Analysis—cont'd

Analytes	Matrix	Column	Detector	Mobile Phase	References
VLIVP peptide	Soybean	S.P.: C_{18} (5 μm, 300 Å) (15 cm × 500 μm)	MS (IT)	ACN/water/HAc Gradient (20 μL/min) ACN/water/HAc	Puchalska et al. (2014)
Peptides	Olive pulp	1D: S.P.: C_{18} (5 μm) (1 cm × 300 μm) 2D: S.P.: C_{18} (5 μm 100 Å) (15 cm × 75 μm)	MS (Orbitrap)	Gradient (200 nL/min) ACN/water/HFo	Esteve et al. (2011)
Potential bioactive peptides	Soybean seeds, soy milk	1D: S.P.: C_{18} (5 μm, 100 Å) (0.5 cm × 300 μm 2D: S.P.: C_{18} (2.2 μm, 120 Å) (25 cm × 75 μm)	MS (Orbitrap)	1D: Isocratic (10 μL/min) Water/HFo/ACN 2D: Gradient (200 nL/min) Water/HFo/ACN	Capriotti et al. (2015)
Proteomic profile	Mechanically recovered chicken, hand de-boned chicken	1D: S.P: PS-DVB monolith (0.5 cm × 200 μm) 2D: S.P.: PS-DVB monolith (5 cm × 100 μm)	MS (Q-TOF)	1D: Isocratic (10 μL/min) Water/TFA 2D: Gradient (200 nL/min) Water/HFo/ACN	Surowiec et al. (2011)
Casein fraction profile	Bovine milk	S.P.: LMA-HDDMA monolith (27/50 cm × 250 μm)	UV (214 nm)	Gradient (10 μL/min) ACN/water/TFA	Pierri et al. (2013)
Lactoferrin *N*-glycan profile	Goat milk	S.P.: C_{18} (5 μm, 80 Å) (4.3 cm × 75 μm)	MSW (Q-TOF)	Gradient (300 nL/min) ACN/water/HFo	Parc et al. (2014)
Oligosaccharide profile	Human breast milk	S.P.: C_{18} (5 μm, 80 Å) (4.3 cm × 75 μm)	MS (TOF)	Gradient (300 nL/min) ACN/water/HFo	Totten et al. (2014)
78 oligosaccharides	Goat colostrum		MS (Q-TOF)	Gradient (300 nL)	

		S.P.: graphitized carbon (15 cm × 75 μm)		ACN/water/HFo	Martín-Ortiz et al. (2016)
12 sialic acids (Neu5Gc, Neu5Ac, Neu5GcS, Neu5Gc9Ac, Neu5AcS, Neu5-Gc7,9Ac_2, Neu5,9Ac_2, Neu5-Gc8Ac, Neu5-Gc7Ac, Neu5,7Ac_2, Neu5-Gc8,9Ac_2, Neu5,8Ac_2)	Egg jelly coat	S.P.: C_{18} (5 μm, 80 Å) (15 cm × 500 μm)	MS (IT)	Isocratic (20 μL/min) MeOH/ACN/water	Yeşilyurt et al. (2015)
Serotonin, 5-hydroxytryptophan, L-tryptophan	Chocolate	S.P.: C_{18} (5 μm, 80 Å) (15 cm × 500 μm)	MS (QqQ)	Gradient (20 μL/min) ACN/water/NH_4Fo	Guillén-Casla et al. (2012)
Caffeine	Tea, coffee, cocoa	S.P.: hexyl methacrylate monolith (15 cm × 530 μm)	UV (274 nm)	Isocratic (41 μL/min) ACN/water	Al-Othman et al. (2012)
Food Safety					
Seven quinolone antibiotics (ciprofloxacin, danofloxacin, oxolinic acid, flumequine, difloxacin, enrofloxacin, sarafloxacin)	Milk	S.P.: C_{18} (5 μm, 100 Å) (15 cm × 300 μm)	LIF	Gradient (15 μL/min) ACN/water/citric acid-NH_4OH buffer, pH 4.75	Lombardo-Agüí et al. (2011)
Six fluoroquinolone antibiotics (ofloxacin, flumeqine, ciprofloxacin, enrofloxacin, sarafloxacin, difloxacin)	Bovine milk	S.P.: C_{18} (5 μm, 80 Å) (15 cm × 500 μm)	UV (250 nm) MS (QqQ)	Gradient (20 μL/min) ACN/water/NH_4Fo, pH 3.7	Ruiz-Viceo et al. (2012)
18 sulfonamide antibiotics (sulfabenzamide, sulfachloropyridazine, sulfadiazine, sulfadimethoxine, sulfadoxin, sulfaguanidine, sulfamerazine, sulfameter, sulfamethazine, sulfamethizole, sulfamethoxazole, sulfamonomethoxine, sulfanilamide, sulfapyridine, sulfaquinoxaline, sulfisoxazole, sulfathiazole, sulfisomidine)	Bovine milk	S.P.: C_{18} core-shell (2.6 μm, 100 Å) (25 cm × 100 μm)	MS (IT)	Gradient (190 nL/min) ACN/water/HFo	D'Orazio et al. (2012a)
Eight cephalosporins (cephoperazone, cefquinome, cephalexin, cephapirin,	Spring and river water, beef and pork muscle	S.P.: C_{18} (3 μm, 100 Å) (15 cm × 300 μm)	UV (250 nm)	Gradient (20 μL/min) ACN/MeOH/water/HFo	Quesada-Molina et al. (2013)

Continued

Table 9.4 Nano-Liquid Chromatography and Capillary Liquid Chromatography Applications in Food Analysis—cont'd

Analytes	Matrix	Column	Detector	Mobile Phase	References
cephaloniun, cephamandole, cephazolin and cephadroxile)					
Three amphenicol antibiotics (chloramphenicol, thiamphenicol, florfenicol)	Milk, honey	S.P.: poly-LMA-MAA-EDMA monolith (15 cm × 250 μm)	MS (QqQ)	Gradient (4 μL/min) ACN/MeOH/water	Liu et al. (2016)
Fluoxetine, carbamazepine	Molluscs (*Potamopyrgus antipodarum, Valvata piscinalis)*	1D: S.P.: C_{18} (5 μm, 300 Å) (0.5 cm × 300 μm) 2D: S.P.: C_{18} (3 μm, 100 Å) (15 cm × 75 μm)	MS (QqQ)	Gradient (300 nL/min) ACN/water/HFo	Berlioz-Barbier et al. (2015)
18 multiclass pesticides (simazine, metolcarb, dichlorvos, propoxur, carbofuran, bendiocarb, atrazine, metalaxyl, isoproturon, ethiofencarb, isoprocarb, propham, terbuthylazine, metolachlor, malathion, phoxim, imidacloprid, 2,4,5-trichlorophenoxyacetic acid)	Apple, apple puree baby food	S.P.: C_{18} (3 μm, 120 Å) (15 cm × 75 μm)	MS (IT and Orbitrap)	Gradient (800 nL/min) ACN/water/HFo	Mirabelli et al. (2016)
Seven multiclass pesticides (oxamyl, methomyl, aldicarb, carbofuran, pirimicarb, methiocarb, ditalimfos)	Tomato	S.P.: C_{18} (3 μm, 100 Å) (5 cm × 300 μm)	MS (QqQ)	Gradient (5 μL/min) MeOH/water	Kruve et al. (2011)
Five carbamate pesticides (carbofuran, carbaryl, methiocarb, promecarb, benthiocarb)	Cucumber	S.P.: C_{18} (5 μm, 100 Å) (15 cm × 500 μm)	UV (210 nm)	Gradient (10 μL/min) ACN/water	Moreno-González et al. (2011)
Four sulfonylurea herbicides (flazasulfuron, prosulfuron, primisulfuron-methyl, triflusulfuron-methyl)	Wine	S.P.: C_{18} (5 μm, 100 Å) (15 cm × 300 μm)	UV (230 nm)	Gradient (10 μL/min) ACN/water/HAc	Gure et al. (2015)
Nine sulfonylurea herbicides (chlorosulfuron, foramsulfuron,		S.P.: C_{18} (5 μm, 100 Å) (15 cm × 300 μm)	UV (230 nm)	Gradient (10 μL/min)	Gure et al. (2014)

nicosulfuron, oxasulfuron, primisulfuron-methyl, prosulfuron, triasulfuron, triflusulfuron-methyl, flazasulfuron)	River water, groundwater, banana juice			ACN/water/HAc	
Ochratoxin A	Wine	S.P.: C_{18} (5 μm, 100 Å) (15 cm × 500 μm)	LIF (325 nm)	Isocratic (14 μL/min) MeOH/water/HAc/SDS	Arroyo-Manzanares et al. (2011)
Ochratoxin B	Wine	S.P.: C_{18} (5 μm, 100 Å) (15 cm × 500 μm)	LIF (325 nm)	Isocratic (14 μL/min) Water/MeOH/HAc/SDS	Arroyo-Manzanares et al. (2012)
Four ochratoxins (ochratoxin A, ochratoxin B, ochratoxin C, ochratoxin α, ochratoxin β)	Wheat, cereal	1D: S.P.: C_8 (5 μm) (2 cm × 180 μm) 2D: S.P.: C_{18} (1.7 μm, 130 Å) (10 cm × 75 μm)	MS (Q-TOF)	Gradient (500 nL/min) MeOH/water/HAc	Aqai et al. (2011)
Four aflatoxins (aflatoxin B1, aflatoxin B2, aflatoxin G1, aflatoxin G2)	Peanut, peanut butter	HPLC chip: 1D: enrichment column (500 nL) 2D: S.P.: C_8 (5 μm, 300 Å) (15 cm × 75 μm)	MS (QqQ)	Gradient (300 nL/min) MeOH/water/NH_4Ac	Liu et al. (2013)
Di(2-ethylhexyl) phthalate	Mussel, wastewaters	S.P.: C_{18} (3.5 μm, 80 Å) (15 cm × 500 μm)	UV (230 nm)	Isocratic (12 μL/min) ACN/water	Muñoz-Ortuño et al. (2012)

1D, *first dimension;* 2D, *two dimension;* ACN, *acetonitrile;* HAc, *acetic acid;* HDDMA, *hexanediol dimethylcrylate;* HPLC, *high-performance liquid chromatography;* LIF, *laser-induced flourescence detectors;* LMA, *laurylmrthacrylate;* MAA, *methacrylic acid;* MeOH, *methanol;* MS (IT), *mass spectrometry (ion trap);* MS (QqQ), *mass spectrometry (triple quadrupole);* MS (TOF), *mass spectrometry (time-of-flight);* PS–DVB, *polystyrene–divinyl benzene;* SDS, *sodium dodecyl sulphate.*

2014), soybean (Chang et al., 2012), tea (Fanali et al., 2012a), honey bee pollen (Fanali et al., 2013b), red wine (Hashim et al., 2013), cranberry syrup (Contreras et al., 2015), and dietary supplements (Fanali et al., 2015a). The analysis of anthocyanins in commercial red fruit juices was assessed by nano-LC by Fanali et al. (2011b). Although strong acid conditions (5%, v/v HFo) were used, the 100 μm I.D. capillary column packed with bidentade C_{18}-silica showed, as reported in Fig. 9.6, a nice and stable chromatographic profile.

The analysis of peptides and proteins in different foods opens new possibilities to identify their origins, and it can also be the base of new nutrigenomic studies. In this respect, several works along this interesting research line investigated the potential nutraceutical aspect. For instance, Escudero et al. (2013) used a 2D nano-LC−MS system to identify several peptides in dry-cured ham with powerful antioxidant properties, whereas Puchalska et al. (2014) did a simple digestion of soybean proteins for quantification of the highly antihypertensive peptide VLIVP in different soybean varieties. After trypsin−protein digestion and nano-LC−MS/MS, the peptide profile was applied for seafood product authentication (Ortea et al., 2011) or for the characterization of olive pulp proteins (Esteve et al., 2011). Also in this field, a 2D-enrichment online nano-LC−MS system was used for the determination of bioactive peptides produced during in vitro gastrointestinal digestion of soybean seeds and soy milk, undertaking a food-biotransformation study (Capriotti et al., 2015). Another interesting proteomic approach was the study of Surowiec et al. (2011), who developed an off-gel electrophoresis method followed by sodium dodecyl sulphate−PAGE−nano-LC−MS/MS, to find potential markers for the detection of chicken mechanically recovered meat or hand-deboned meat; or that developed by Pierri et al. (2013) to analyze the casein fraction profile in bovine milk for studying its time-dependent degradation in commercial products. Furthermore, milk matrices have also been subjected to different profile studies, such as a lactoferrin *N*-glycan profile in goat, bovine, and human milk (Parc et al., 2014), and oligosaccharide profiles of breast milk (Totten et al., 2014) and goat colostrum (Martín-Ortiz et al., 2016) by nano-LC-Chip−Q-TOF-MS.

CLC has also been applied in the determination of molecules that participate in numerous biological activities, such as the terminal sugar of carbohydrate chains like sialic acids in the egg jelly coat

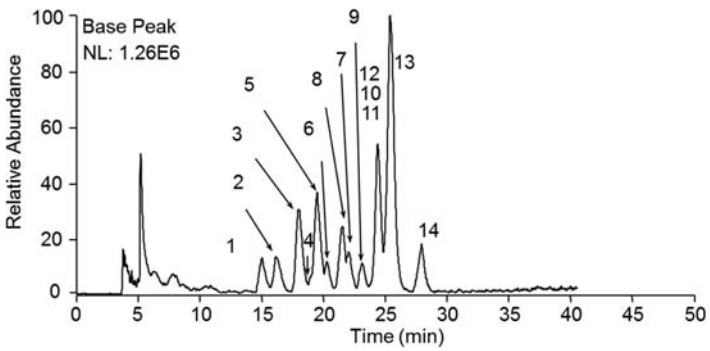

FIGURE 9.6

Nano-liquid chromatography−electrospray ionization mass spectrometry base peak chromatogram of the anthocyanin content of a commercial blueberry juice.

Reprinted from Fanali, C., Dugo, L., D'Orazio, G., Lirangi, M., Dachà, M., Dugo, P., Mondello, L., 2011b. Analysis of anthocyanins in commercial fruit juices by using nano-liquid chromatography-electrospray-mass spectrometry and high-performance liquid chromatography with UV-vis detector. J. Sep. Sci. 34, 150–159 with permission from Wiley-VCH.

of the sea urchin (Yeşilyurt et al., 2015), serotonin, 5-hydroxytryptophan, and L-tryptophan in chocolate (Guillén-Casla et al., 2012), or caffeine in tea, coffee, and cocoa (Al-Othman et al., 2012).

Food safety is arousing greater human concern because of the worldwide increased need for food production. Food products reach the consumer through human handling and action, which can introduce the presence of exogenous molecules that could endanger human health or impair the food quality. The second part of Table 9.4 describes selected recent research works in nano-LC and CLC regarding the determination of harmful compounds in food matrices such as antibiotics (Lombardo-Agüí et al., 2011; Ruiz-Viceo et al., 2012; D'Orazio et al., 2012a; Quesada-Molina et al., 2013; Liu et al., 2016), drugs (Berlioz-Barbier et al., 2015), pesticides (Mirabelli et al., 2016; Kruve et al., 2011; Moreno-González et al., 2011; Gure et al., 2014, 2015), mycotoxins (Arroyo-Manzanares et al., 2011, 2012; Aqai et al., 2011; Liu et al., 2013), and phthalates (Muñoz-Ortuño et al., 2012).

Two exciting applications regarding the determination of pesticides in food matrices both employed lab-made interfaces to couple nano-LC/CLC with MS. Mirabelli et al. (2016) published their results obtained by using an ambient dielectric barrier discharge ionization−based source, whereas Kruve et al. (2011) described a microfabricated heated nebulizer chip for atmospheric pressure photoionization combined with a 300 μm I.D. capillary column.

3.5 MISCELLANEOUS

This section shows some recent applications of nano-LC and CLC, reported in Table 9.5, which could not be included in the previous sections, either because they do not strictly fit in the commented fields or because they have not been employed for real sample analysis.

CLC has been applied for the analysis of emerging contaminants because of the rising concern about human health. Among them, phthalates and parabens are present in a wide range of daily products such as foods, cosmetics, and pharmaceutical formulations. In this respect, different methodologies have been described for their determination in biological matrices such as human urine (Jornet-Martínez et al., 2015; Carrasco-Correa et al., 2015) or serum (Carrasco-Correa et al., 2015). To better understand dialkyl phthalate human metabolism in human urine, the CLC system was improved with an online preconcentration/clean-up procedure. The sample enrichment was performed by IT-SPME, substituting the stainless steel conventional injection loop with a capillary column (Jornet-Martínez et al., 2015).

Inorganic anions have also been determined by CLC in biological samples. In this respect, Linda et al. (2013) described the baseline separation of six inorganic anions in water and human saliva by means of tosylated-poly(ethylene oxide) bonded to aminopropylsilica packing material.

Regarding chiral analysis, polysaccharides-based CSPs have been widely applied not only in the pharmaceutical field but also for the separation of other classes of compounds (Pérez-Fernández et al., 2012; Vega et al., 2011; Ciogli et al., 2014; Zhang et al., 2015). In recent applications, the use of cellulose derivatives in a CSP was evaluated for the chiral separation of a group of multiclass pesticides (Pérez-Fernández et al., 2012) and 9-fluorenylmethoxycarbonyl chloride-amino acid derivatives, demonstrating a high chiral recognition power (Vega et al., 2011).

On other occasions, some technological developments have been introduced. This is the case of a work in which the introduction of a novel nanospray interface was described. Defined as a nano-liquid junction, it has been principally developed for coupling the CEC−MS, but it has also been applied for the separation and determination of a mixture of organophosphorus pesticides by nano-LC−MS

Table 9.5 Nano-Liquid Chromatography and Capillary Liquid Chromatography Applications in Miscellaneous Analyses

Analytes	Matrix	Column	Detector	Mobile Phase	References
Six organophosphorus pesticides (methamidophos, fensulfothion, fenamiphos, isophenphos, profenofos, sulprophos)	–	S.P.: C_{18} (5 μm, 100 Å) (34 cm × 100 μm)	MS (IT)	Isocratic (160 nL/min) ACN/water	D'Orazio and Fanali (2013b)
Limonene racemate, linalool, citral	Shower gel, perfume, hand cream	S.P.: C_{18} (2.2 μm, 120 Å) (10 cm × 75 μm) S.P: PFP-silane (2.5 μm) (20 cm × 75 μm)	MS (QqQ)	Gradient (400 nL/min) ACN/water	Famiglini et al. (2014)
Four tocopherols (DL-α-tocopherol, rac-β-tocopherol, γ-tocopherol, α-tocopherol and α-tocopherol acetate, and α-, β-, γ-tocotrienol	Cosmetic products: body creams, facial creams, makeup, shampoos	S.P.: C_{18} (5 μm, 80 Å) (15 cm × 500 μm)	UV (292 nm)	Isocratic (20 μL/min) MeOH/water	Viñas et al. (2014)
Four parabens (methylparaben, ethylparaben, propylparaben, butylparaben)	Human urine and serum	S.P.: BMA-EDMA (15 cm × 250 μm)	UV (254 nm) MS (QqQ)	Gradient (2 μL/min) ACN/water	Carrasco-Correa et al. (2015)
Four phthalates (di(2-ethylhexyl) phthalate, diethyl phthalate, dibutyl phthalate, mono-ethylhexyl phthalate)	Human urine	S.P.: C_{18} (3.5 μm, 80 Å) (15 cm × 500 μm)	UV (230 nm)	Gradient (10 μL/min) ACN/water	Jornet-Martínez et al. (2015)
Six inorganic anions (IO_3^-, BrO_3^-, Br^-, NO_3^-, I^-, CNS^-)	Tap water, saliva	S.P.: tosylated poly(ethylene oxide) bonded aminopropylsilica (NH_2-60) (5 μm, 60 Å) (10 cm × 320 μm)	UV (210 nm)	Isocratic (3 μL/min) Water/NaCl	Linda et al. (2013)
Racemic mixtures of 16 pesticides (resmethrin, diniconazole, fenpropathrin, λ-cyhalothrin, β-cyfluthrin, cis-bifenthrin, metalaxyl, benalaxyl, hexaconazole, myclobutanil, tebuconazole, dichlorprop, mecoprop, α-cypermethrin, flutriafol, uniconazole)	–	S.P.: CSP-silica-based 25% (w/w) coated with cellulose phenyl carbamate derivatives (5 μm, 1000 Å) (24 cm × 100 μm)	UV (210 nm)	Isocratic (12 bar) ACN/water/NH_4Ac, pH 2.5	Pérez-Fernández et al. (2012)

Racemic mixture of 17 amino acids (threonine, asparagine, glutamine, cysteine, proline, isoleucine, leucine, allo-isoleucine, methionine, phenylalanine, valine, pipecolinic acid, pyroglutamic acid, lysine, citrulline, ornithine, hystidine)	–	S.P.: CSP-phenylcarbamate derivative silica-based (25% w/w, 5 μm, 1000 Å) (24 cm × 100 μm)	UV (210, 260 nm)	Isocratic (12 bar) Buffer/water/ACN	Vega et al. (2011)
Racemic mixtures of seven multiclass compounds (acenaphthenol, benzoin, fenvalerate, naproxen, praziquatel, trans-Stilbene oxide, warfarin)	–	S.P.: silica, SS-Whelk-O1−2.5-CSP (18/ 25 cm × 75 μm; 2.5 μm, 120 Å)	UV (214 nm) MS (Orbitrap)	Isocratic (300 nL/min) *n*-hexane/CH_2Cl_2/MeOH; Water/ACN/TFA; MeOH/NH_4Ac	Ciogli et al. (2014)
Seven phenoxy acid herbicides (dichlorprop, 2-(4-chlorophenoxy)propionic acid, 2-(3-chlorophenoxy)propionic acid, mecoprop, fenoprop, 2-phenoxypropionic acid, fenoxaprop	Herbicide formulation (mecoprop)	S.P.: poly MQD-co-HEMA-co-EDMA (20 cm × 100 μm)	UV (210 nm)	Isocratric (20 μL/min) ACN/water/NH_4Ac, pH 5.3	Zhang et al. (2015)
Caffeine, eight steroids (testosterone, methyltestosterone, testosterone acetate, nandrolone propionate, boldenone, estradiol, testosterone propionate, dehydromethyltestosterone)	–	S.P.: C_{18} (3 μm, 100 Å) (25 cm × 75 μm)	MS (Q)	Gradient (200 nL/min) ACN/water	Flender et al. (2011)

ACN, *acetonitrile;* BMA−EDMA, *butyl methacrylate−ethylene dimethacrylate;* CSP, *chiral stationary phase;* MA (IT), *mass spectrometry (ion trap);* MeOH, *methanol;* MQD-co-HEMA-co-EDMA, *O-9-[2-(methacryloyloxy)-ethylcarbamoyl]-10,11-dihydroquinidine-co-2-hydroxyethyl methacrylate-co-ethylene dimethacrylate;* MS (Q), *mass spectrometry (quadrupole);* MS (QqQ), *mass spectrometry (triple quadrupole).*

(D'Orazio and Fanali, 2013b). Another interesting alternative for coupling nano-LC to MS is the one proposed by Cappiello et al. (Famiglini et al., 2014) for the identification of neutral or hardly ionisable molecules by using a direct-EI MS interface. In this regard, three widely used compounds in personal care products were separated and determined in water- and oil-based real samples (perfume, shower gel and hand cream).

4. CONCLUSIONS AND FUTURE TRENDS

Miniaturization in analytical chemistry has been developed in the last decade to offer reliable separation methods capable to analyze the different compounds in a large number of samples present in various complex matrices. Theoretical principles, technological solutions, method validation, and several applications have been developed for the nanoscale separation techniques, including both electrodriven and chromatographic ones. Both tools offer several advantages over the conventional approaches. Among these, high separation efficiency, high resolution, short analysis time, easy coupling with MS, and use of minute volumes of both samples and mobile phases are the most attractive benefits for those working in the analytical field. In this chapter, the current state of the art of nano-LC has been reviewed focusing on (1) the general theoretical principles documenting the advantages in using this technique, (2) problems related to the instrumentation to be used, and (3) selected applications in different fields such as proteomic, environmental, and agrochemical.

Although the literature offers a valuable number of applications in various fields and commercial instrumentation being available, it cannot be concluded for certain that nano-LC is mature enough to be used routinely. In fact, some drawbacks, mainly related to sensitivity, must be carefully considered. This is mainly due to the use of low volumes of samples injected (nL). However, sample preconcentration, on-column focusing, or 2D separation is currently the proposed approach for increasing sensitivity.

Future development of nano-LC includes the realization of new SPs, the employment of those proposed for UHPLC with particles diameter <2 μm and new interfaces for coupling with other tools such as MS or NMR. The development of microdevices is another important research field for separation science, arising from the "lab-on-a-chip" concept, and valuable results have already been obtained. Microdevices offer the possibility to analyze even more minute amounts of samples, to further reduce analysis time, to integrate both sample pretreatment and analytical separation in the same instrument (μ-total analysis system, μ-TAS), and to achieve low LODs. Moreover, high throughput multichannel analysis devices for parallel experiments can be implemented and successfully applied for, i.e., peptide mapping, DNA hybridization analysis, and polymerase chain reaction analysis.

Many microdevices have been developed for electrophoretic techniques, and downsizing the chromatographic system has faced several technical challenges, such as the integration of on-chip of injectors, adaptation of mechanical valves, and the introduction of the SP into narrow channels.

Concerning the last drawback, the use of monolithic material, characterized by the advantageous in situ polymerization and high permeability, has given a new chance for an easier implementation of chromatographic microdevices. Further advances in microfabrication technique can lead to a wider number of commercialized microfluidic-LC chips and offer new separation solutions for application fields where extremely small quantities of sample are available and fast analyses are required.

REFERENCES

Abian, J., Oosterkamp, A.J., Gelpi, E., 1999. Comparison of conventional, narrow-bore and capillary liquid chromatography/mass spectrometry for electrospray ionization mass spectrometry: practical considerations. J. Mass Spectrom. 34, 244−254.

Aggarwal, P., Lawson, J.S., Tolley, H.D., Lee, M.L., 2014. High efficiency polyethylene glycol diacrylate monoliths for reversed-phase capillary liquid chromatography of small molecules. J. Chromatogr. A 1364, 96−106.

Ahmed, M., Yajadda, M.M., Han, Z.J., Su, D., Wang, G., Ostrikov, K.K., Ghanem, A., 2014. Single-walled carbon nanotube-based polymer monoliths for the enantioselective nano-liquid chromatographic separation of racemic pharmaceuticals. J. Chromatogr. A 1360, 100−109.

Al-Othman, Z.A., Aqel, A., Alharbi, M.K.E., Badjah-Hadj-Ahmed, A.Y., Al-Warthan, A.A., 2012. Fast chromatographic determination of caffeine in food using a capillary hexyl methacrylate monolithic column. Food Chem. 132, 2217−2223.

Albert, K., Schlotterbeck, G., Tseng, L.-H., Braumann, U., 1996. Application of on-line capillary high-performance liquid chromatography-nuclear magnetic resonance spectrometry coupling for the analysis of vitamin A derivatives. J. Chromatogr. A 750, 303−309.

Aqai, P., Peters, J., Gerssen, A., Haasnoot, W., Nielen, M.W., 2011. Immunomagnetic microbeads for screening with flow cytometry and identification with nano-liquid chromatography mass spectrometry of ochratoxins in wheat and cereal. Anal. Bioanal. Chem. 400, 3085−3096.

Arroyo-Manzanares, N., García-Campaña, A.M., Gámiz-Gracia, L., 2011. Comparison of different sample treatments for the analysis of ochratoxin A in wine by capillary HPLC with laser-induced fluorescence detection. Anal. Bioanal. Chem. 401, 2987−2994.

Arroyo-Manzanares, N., Gámiz-Gracia, L., García-Campaña, A.M., 2012. Determination of ochratoxin A in wines by capillary liquid chromatography with laser induced fluorescence detection using dispersive liquid−liquid microextraction. Food Chem. 135, 368−372.

Asensio-Ramos, M., Hernández-Borges, J., Rocco, A., Fanali, S., 2009. Food analysis: a continuous challenge for miniaturized separation techniques. J. Sep. Sci. 32, 3764−3800.

Asensio-Ramos, M., D'Orazio, G., Hernández-Borges, J., Rocco, A., Fanali, S., 2011. Multi-walled carbon nanotubes-dispersive solid-phase extraction combined with nano-liquid chromatography for the analysis of pesticides in water sample. Anal. Bioanal. Chem. 400, 1113−1123.

Aturki, Z., D'Orazio, G., Rocco, A., Si-Ahmed, K., Fanali, S., 2011. Investigation of polar stationary phases for the separation of sympathomimetic drugs with nano-liquid chromatography in hydrophilic interaction liquid chromatography mode. Anal. Chim. Acta 685, 103−110.

Auditore, R., Santagati, N.A., Aturki, Z., Fanali, S., 2013. Enantiomeric separation of amlodipine and its two chiral impurities by nanoliquid chromatography and capillary electrochromatography using a chiral stationary phase based on cellulose tris(4-chloro-3-methylphenylcarbamate). Electrophoresis 34, 2593−2600.

Barefoot, A.C., Reiser, R.W., 1987. Packed capillary liquid chromatography-mass spectrometry using both direct-coupling and moving-belt interface. J. Chromatogr. A 398, 221−226.

Berlioz-Barbier, J.A., Buleté, A., Faburé, J., Garric, J., Cren-Olivé, C., Vulliet, E., 2014. Multi-residue analysis of emerging pollutants in benthic invertebrates by modified micro-quick-easy-cheap-efficient-rugged-safe extraction and nanoliquid chromatography-nanospray-tandem mass spectrometry analysis. J. Chromatogr. A 1367, 16−32.

Berlioz-Barbier, A., Baudot, R., Wiest, L., Gust, M., Garric, J., Cren-Olivé, C., Buleté, A., 2015. Micro-QuEChERS-nanoliquid chromatography-nanospray-tandem mass spectrometry for the detection and quantification of trace pharmaceuticals in benthic invertebrates. Talanta 132, 796−802.

Blue, L.E., Jorgenson, J.W., 2015. 1.1 μm superficially porous particles for liquid chromatography: part II: column packing and chromatographic performance. J. Chromatogr. A 1380, 71−80.

Bragg, W., Shamsi, S.A., 2012. A novel positively charged achiral co-monomer for β-cyclodextrin monolithic stationary phase: improved chiral separation of acidic compounds using capillary electrochromatography coupled to mass spectrometry. J. Chromatogr. A 1267, 144−155.

Bragg, W., Norton, D., Shamsi, S.A., 2008. Optimized separation of β-blockers with multiple chiral centers using capillary electrochromatography-mass spectrometry. J. Chromatogr. B 875, 304−316.

Buonasera, K., D'Orazio, G., Fanali, S., Dugo, P., Mondello, L., 2009. Separation of organophosphorous pesticides by using nano-liquid chromatography. J. Chromatogr. A 1216, 3970−3976.

Cannon, J.R., Cammarata, M.B., Robotham, S.A., Cotham, C.V., Shaw, J.B., Fellers, R.T., Early, B.P., Thomas, P.M., Kelleher, N.L., Brodbelt, J.S., 2014. Ultraviolet photodissociation for characterization of whole proteins on a chromatographic time scale. Anal. Chem. 86, 2185−2192.

Cappiello, A., Palma, P., Mangani, F., 1991. New materials and packing techniques for micro-HPLC packed capillary columns. Chromatographia 32, 389−391.

Cappiello, A., Famiglini, G., Palma, P., Mangani, F., 2002. Trace level determination of organophosphorus pesticides in water with the new direct-electron ionization LC/MS interface. Anal. Chem. 74, 3547−3554.

Cappiello, A., Famiglini, G., Fiorucci, C., Mangani, F., Palma, P., Siviero, A., 2003a. Variable-gradient generator for micro- and nano-HPLC. Anal. Chem. 75, 1173−1179.

Cappiello, A., Famiglini, G., Mangani, F., Palma, P., Siviero, A., 2003b. Nano-high-performance liquid chromatography-electron ionization mass spectrometry approach for environmental analysis. Anal. Chim. Acta 493, 125−136.

Capriotti, A.L., Caruso, G., Cavaliere, C., Samperi, R., Ventura, S., Chiozzi, R.Z., Lagana, A., 2015. Identification of potential bioactive peptides generated by simulated gastrointestinal digestion of soybean seeds and soy milk proteins. J. Food Comp. Anal. 44, 205−213.

Carlavilla, D., Moreno-Arribas, M.V., Fanali, S., Cifuentes, A., 2006. Chiral MEKC-LIF of amino acids in foods: analysis of vinegars. Electrophoresis 27, 2551−2557.

Carrasco-Correa, E.J., Vela-Soria, F., Ballesteros, O., Ramis-Ramos, G., Herrero-Martínez, J.M., 2015. Sensitive determination of parabens in human urine and serum using methacrylate monoliths and reversed-phase capillary liquid chromatography-mass spectrometry. J. Chromatogr. A 1379, 65−73.

Catherman, A.D., Skinner, O.S., Kelleher, N.L., 2014. Top Down proteomics: facts and perspectives. Biochem. Biophys. Res. Commun. 445, 683−693.

Chang, Y., Zhao, C., Wu, Z., Zhou, J., Zhao, S., Lu, X., Xu, G., 2012. Chip-based nanoflow high performance liquid chromatography coupled to mass spectrometry for profiling of soybean flavonoids. Electrophoresis 33, 2399−2406.

Chankvetadze, B., Yamamoto, C., Kamigaito, M., Tanaka, N., Nakanishi, K., Okamoto, Y., 2006. High-performance liquid chromatographic enantioseparations on capillary columns containing monolithic silica modified with amylose tris(3,5- dimethylphenylcarbamate). J. Chromatogr. A 1110, 46−52.

Chen, H., Horvath, C., 1995. High-speed high performance liquid chromatography of peptides and proteins. J. Chromatogr. A 705, 3−20.

Chen, J.R., Dulay, M.T., Zare, R.N., Svec, F., Peters, E., 2000. Macroporous photopolymer frits for capillary electrochromatography. Anal. Chem. 72, 1224−1227.

Chervet, J.P., Ursem, M., Salzmann, J.P., 1996. Instrumental requirements for nanoscale liquid chromatography. Anal. Chem. 68, 1507−1512.

Ciogli, A., Pierri, G., Kotoni, D., Cavazzini, A., Botta, L., Villani, C., Kocergin, J., Gasparrini, F., 2014. Toward enantioselective nano ultrahigh-performance liquid chromatography with Whelk-O1 chiral stationary phase. Electrophoresis 35, 2819−2823.

Claessens, H.A., Burcinova, A., Cramers, C.A., Mussche, P., van Tilburg, C.C.E., 1990. Evaluation of injection systems for open tubular liquid chromatography. J. Microcol. Sep. 2, 132−137.

Colón, L.A., Maloney, T.D., Fermier, A.M., 2000. Packing columns for capillary electrochromatography. J. Chromatogr. A 887, 43−53.

Contreras, M., Arráez-Román, D., Fernández-Gutiérrez, A., Segura-Carretero, A., 2015. Nano-liquid chromatography coupled to time-of-flight mass spectrometry for phenolic profiling: a case study in cranberry syrups. Talanta 132, 929−938.

Crescentini, G., Bruner, F., Mangani, F., Yafeng, G., 1988. Preparation and evaluation of dry-packed capillary columns for high-performance liquid chromatography. Anal. Chem. 60, 1659−1662.

D'Orazio, G., Fanali, S., 2008. Enantiomeric separation by using nano-liquid chromatography with on-column focusing. J. Sep. Sci. 31, 2567−2571.

D'Orazio, G., Fanali, S., 2010. Coupling capillary electrochromatography with mass spectrometry by using a liquid-junction nano-spray interface. J. Chromatogr. A 1217, 4079−4086.

D'Orazio, G., Fanali, S., 2013a. Combination of two different stationary phases for on-line pre-concentration and separation of basic drugs by using nano-liquid chromatography. J. Chromatogr. A 1285, 118−123.

D'Orazio, G., Fanali, S., 2013b. Pressurized nano-liquid-junction interface for coupling capillary electrochromatography and nano-liquid chromatography with mass spectrometry. J. Chromatogr. A 1317, 67−76.

D'Orazio, G., Cifuentes, A., Fanali, S., 2008. Chiral nano-liquid chromatography-mass spectrometry applied to amino acids analysis for orange juice profiling. Food Chem. 108, 1114−1121.

D'Orazio, G., Rocchi, S., Fanali, S., 2012a. Nano-liquid chromatography coupled with mass spectrometry: separation of sulfonamides employing non-porous core-shell particles. J. Chromatogr. A 1255, 277−285.

D'Orazio, G., Rocco, A., Fanali, S., 2012b. Fast-liquid chromatography using columns of different internal diameters packed with sub-2 μm silica particles. J. Chromatogr. A 1228, 213−220.

D'Orazio, G., Asensio-Ramos, M., Fanali, C., Hernández-Borges, J., Fanali, S., 2016a. Capillary electrochromatography in food analysis. TrAC Trends Anal. Chem. 82, 250−267.

D'Orazio, G., Hernández-Borges, J., Asensio-Ramos, M., Rodríguez-Delgado, M.A., Fanali, S., 2016b. Capillary electrochromatography and nano-liquid chromatography coupled to nano-electrospray ionization interface for the separation and identification of estrogenic compounds. Electrophoresis 37, 356−362.

Delporte, C., Noyon, C., Raynal, P., Dufoura, D., Nève, J., Abts, F., Haex, M., Boudjelti, K.Z., Antwerpen, P.V., 2015. Application to atheroma plaque proteomics using nano-chip liquid chromatography and mass spectrometry. J. Chromatogr. A 1385, 116−123.

Desiderio, C., Fanali, S., 2000. Capillary electrochromatography and capillary electrochromatography-electrospray mass spectrometry for the separation of non-steroidal anti-inflammatory drugs. J. Chromatogr. A 895, 123−132.

Desiderio, C., Rudaz, S., Raggi, M.A., Fanali, S., 1999. Enantiomeric separation of fluoxetine and norfluoxetine in plasma and serum samples with high detection sensitivity capillary electrophoresis. Electrophoresis 20, 3432−3438.

Dong, X., Wu, R., Dong, J., Wu, M., Zhu, Y., Zou, H., 2008. A mesoporous silica nanoparticles immobilized open-tubular capillary column with a coating of cellulose tris(3,5-dimethylphenyl-carbamate) for enantioseparation in CEC. Electrophoresis 29, 3933−3940.

Eeltink, S., Svec, F., 2007. Recent advances in the control of morphology and surface chemistry of porous polymer-based monolithic stationary phases and their application in CEC. Electrophoresis 28, 137−147.

Eeltink, S., Rozing, G.P., Kok, W.T., 2003. Recent applications in capillary electrochromatography. Electrophoresis 24, 3935−3961.

Escudero, E., Mora, L., Fraser, P.D., Aristoy, M.C., Toldrá, F., 2013. Identification of novel antioxidant peptides generated in Spanish dry-cured ham. Food Chem. 138, 1282−1288.

Esteve, C., Cañas, B., Moreno-Gordaliza, E., Río, C.D., García, M.C., Marina, M.L., 2011. Identification of olive (*Olea europaea*) pulp proteins by matrix-assisted laser desorption/ionization time-of-flight mass spectrometry and nano-liquid chromatography tandem mass spectrometry. J. Agric. Food Chem. 59, 12093−12101.

Famiglini, G., Termopoli, V., Palma, P., Capriotti, F., Cappiello, A., 2014. Rapid LC-MS method for the detection of common fragrances in personal care products without sample preparation. Electrophoresis 35, 1339−1345.

Fanali, S., Aturki, Z., D'Orazio, G., Rocco, A., 2007. Separation of basic compounds of pharmaceutical interest by using nano-liquid chromatography coupled with mass spectrometry. J. Chromatogr. A 1150, 252−258.

Fanali, S., D'Orazio, G., Lomsadze, K., Samakashvili, S., Chankvetadze, B., 2010. Enantioseparations on amylose tris(5-chloro-2-methylphenylcarbamate) in nano liquid chromatography and capillary electrochromatography. J. Chromatogr. A 1217, 1166−1174.

Fanali, C., Asensio-Ramos, M., Hernández-Borges, J., Rocco, A., Fanali, S., 2011a. Nano-liquid chromatographic separations. In: Byrdwell, W.C., Holčapek, M. (Eds.), Extreme Chromatography: Faster, Hotter, Smaller. American Oil Chemists' Society (AOCS), Urbana, IL, USA, pp. 301−380.

Fanali, C., Dugo, L., D'Orazio, G., Lirangi, M., Dachà, M., Dugo, P., Mondello, L., 2011b. Analysis of anthocyanins in commercial fruit juices by using nano-liquid chromatography-electrospray-mass spectrometry and high-performance liquid chromatography with UV-vis detector. J. Sep. Sci. 34, 150−159.

Fanali, C., Rocco, A., Aturki, Z., Mondello, L., Fanali, S., 2012a. Analysis of polyphenols and methylxantines in tea samples by means of nano-liquid chromatography utilizing capillary columns packed with core-shell particles. J. Chromatogr. A 1234, 38−44.

Fanali, S., D'Orazio, G., Farkas, T., Chankvetadze, B., 2012b. Comparative performance of capillary columns made with totally porous and core-shell particles coated with a polysaccharide-based chiral selector in nano-liquid chromatography and capillary electrochromatography. J. Chromatogr. A 1269, 136−142.

Fanali, C., Dugo, L., Dugo, P., Mondello, L., 2013a. Capillary-liquid chromatography (CLC) and nano-LC in food analysis. TrAC Trends Anal. Chem. 52, 226−238.

Fanali, C., Dugo, L., Rocco, A., 2013b. Nano-liquid chromatography in nutraceutical analysis: determination of polyphenols in bee pollen. J. Chromatogr. A 1313, 270−274.

Fanali, C., Rocco, A., D'Orazio, G., Dugo, L., Mondello, L., Aturki, Z., 2015a. Determination of key flavonoid aglycones by means of nano-LC for the analysis of dietary supplements and food matrices. Electrophoresis 36, 1073−1081.

Fanali, S., Aturki, Z., Rocco, A., 2015b. Forensic drugs analysis: a review of miniaturized separation techniques. LC-GC Eur. 28.

Flender, C., Wolf, C., Leonhard, P., Karas, M., 2011. Nano-liquid chromatography-direct electron ionization mass spectrometry: improving performance by a new ion source adapter. J. Mass Spectrom. 46, 1004−1010.

Fu, H., Huang, X., Jin, W., Zou, H., 2003. The separation of biomolecules using capillary electrochromatography. Curr. Opin. Biotechnol. 14, 96−100.

Ghanem, A., Ahmed, M., Ishii, H., Ikegami, T., 2015. Immobilized β-cyclodextrin-based silica vs polymer monoliths for chiral nano liquid chromatographic separation of racemates. Talanta 132, 301−314.

Gluckman, J.C., Novotny, M.V., 1985. Microcolumn separations. In: Novotny, M.V., Ishi, D. (Eds.), J. Chromatogr. Library, vol. 30. Elsevier, Amsterdam, pp. 57−72.

Gotti, R., Fiori, J., Calleri, E., Temporini, C., Lubda, D., Massolini, G., 2012. Chiral capillary liquid chromatography based on penicillin G acylase immobilized on monolithic epoxy silica column. J. Chromatogr. A 1234, 45−49.

Gübitz, G., Schmid, M.G., 2008. Chiral separation by capillary electromigration techniques. J. Chromatogr. A 1204, 140−156.

Guillén-Casla, V., Rosales-Conrado, N., León-González, M.E., Pérez-Arribas, L.V., Polo-Díez, L.M., 2012. Determination of serotonin and its precursors in chocolate samples by capillary liquid chromatography with mass spectrometry detection. J. Chromatogr. A 1232, 158−165.

Gure, A., Lara, F.J., Megersa, N., García-Campaña, A.M., Olmo-Iruela, M.d, 2013. Hollow-fiber liquid-phase microextraction combined with capillary HPLC for the selective determination of six sulfonylurea herbicides in environmental waters. J. Sep. Sci. 36, 3395−3401.

Gure, A., Lara, F.J., Moreno-González, D., Megersa, N., Olmo-Iruela, M.d., García-Campaña, A.M., 2014. Salting-out assisted liquid-liquid extraction combined with capillary HPLC for the determination of sulfonylurea herbicides in environmental water and banana juice samples. Talanta 127, 51−58.

Gure, A., Lara, F.J., García-Campaña, A.M., Megersa, N., Olmo-Iruela, M.d, 2015. Vortex-assisted ionic liquid dispersive liquid-liquid microextraction for the determination of sulfonylurea herbicides in wine samples by capillary high-performance liquid chromatography. Food Chem. 170, 348−353.

Hampel, G., 2000. Strategies to improve the sensitivity in capillary electrophoresis for the analysis of drugs in biological fluids. Electrophoresis 21, 691−698.

Hashim, S.N., Schwarz, L.J., Boysen, R.I., Yang, Y., Danylec, B., Hearn, M.T., 2013. Rapid solid-phase extraction and analysis of resveratrol and other polyphenols in red wine. J. Chromatogr. A 1313, 284−290.

Hernández-Borges, J., Aturki, Z., Rocco, A., Fanali, S., 2007. Recent applications in nano-liquid chromatography. J. Sep. Sci. 30, 1589−1610.

Hua, S., Nwosu, C.C., Strum, J.S., Seipert, R.R., An, H.J., Zivkovic, A.M., German, J.B., Lebrilla, C.B., 2012. Site-specific protein glycosylation analysis with glycan isomer differentiation. Anal. Bioanal. Chem. 403, 1291−1302.

Hutton, K.A., Games, D.E., 1997. The analysis of β-blockers by capillary liquid chromatography/atmospheric pressure chemical ionization mass spectrometry. Rapid Commun. Mass Spectrom. 11, 735−744.

Ito, S., Yoshioka, S., Ogata, I., Takeda, A., Yamashita, E., Deguchi, K., 2004. Nanoflow gradient generator for capillary high-performance liquid chromatography−nanoelectrospray mass spectrometry. J. Chromatogr. A 1051, 19−23.

Jarmalavièienë, R., Kornyšova, O., Westerlund, D., Maruška, A., 2003. Non-particulate (continuous bed or monolithic) restricted-access reversed-phase media for sample clean-up and separation by capillary-format liquid chromatography. Anal. Bioanal. Chem. 377, 902−908.

Jornet-Martínez, N., Muñoz-Ortuño, M., Moliner-Martínez, Y., Herráez-Hernández, R., Campíns-Falcó, P., 2014. On-line in-tube solid phase microextraction-capillary liquid chromatography method for monitoring degradation products of di-(2-ethylhexyl) phthalate in waters. J. Chromatogr. A 1347, 157−160.

Jornet-Martínez, N., Antón-Soriano, C., Campíns-Falcó, P., 2015. Estimation of the presence of unmetabolized dialkyl phthalates in untreated human urine by an on-line miniaturized reliable method. Sci. Total Environ. 532, 239−244.

Kapnissi-Christodoulou, C.P., Zhu, X., Warner, I.M., 2003. Analytical separations in open-tubular capillary electrochromatography. Electrophoresis 24, 3917−3934.

Karlsson, K.E., Novotny, M., 1988. Separation efficiency of slurry-packed liquid chromatography microcolumns with very small inner diameters. Anal. Chem. 60, 1662−1665.

Kennedy, G.J., Knox, J.H., 1972. The performance of packings in high performance liquid chromatography (HPLC) I. Porous and surface layered supports. J. Chromatogr. Sci. 10, 549−556.

Kocher, T., Pichler, P., Pra, M.D., Rieux, L., Swart, R., Mechtler, K., 2014. Development and performance evaluation of an ultralow flow nanoliquid chromatography-tandem mass spectrometry set-up. Proteomics 14, 1999−2007.

Kozlík, P., Bosáková, Z., Tesařová, E., Coufal, P., Cabala, R., 2011. Development of a solid-phase extraction with capillary liquid chromatography tandem mass spectrometry for analysis of estrogens in environmental water samples. J. Chromatogr. A 1218, 2127−2132.

Kruve, A., Haapala, M., Saarela, V., Franssila, S., Kostiainen, R., Kotiaho, T., Ketola, R.A., 2011. Feasibility of capillary liquid chromatography-microchip-atmospheric pressure photoionization-mass spectrometry for pesticide analysis in tomato. Anal. Chim. Acta 696, 77−83.

Kuhnle, M., Holtin, K., Albert, K., 2009. Capillary NMR detection in separation science. J. Sep. Sci. 32, 719−726.
Lacey, M.E., Tan, Z.J., Webb, A.G., Sweedler, J.V., 2001. Union of capillary high-performance liquid chromatography and microcoil nuclear magnetic resonance spectroscopy applied to the separation and identification of terpenoids. J. Chromatogr. A 922, 139−149.
Lee, E.D., Muck, W., Henion, J.D., Convey, T.R., 1989. Liquid junction coupling for capillary zone electrophoresis/ion-spray mass spectrometry. Biomed. Environ. Mass Spectrom. 18, 844−850.
Lerma-García, M.J., Simó-Alfonso, E.F., Zougagh, M., Ríos, A., 2013. Use of gold nanoparticle-coated sorbent materials for the selective preconcentration of sulfonylurea herbicides in water samples and determination by capillary liquid chromatography. Talanta 105, 372−378.
Linda, R., Lim, L.W., Takeuchi, T., 2013. Poly(ethylene oxide)-bonded stationary phase for separation of inorganic anions in capillary ion chromatography. J. Chromatogr. A 1294, 117−121.
Liu, H., Row, K.H., Yang, G., 2005. Monolithic molecularly imprinted columns for chromatographic separation. Chromatographia 61, 429−432.
Liu, H.Y., Lin, S.L., Chan, S.A., Lin, T.Y., Fuh, M.R., 2013. Microfluidic chip-based nano-liquid chromatography tandem mass spectrometry for quantification of aflatoxins in peanut products. Talanta 113, 76−81.
Liu, H.Y., Lin, S.L., Fuh, M.R., 2016. Determination of chloramphenicol, thiamphenicol and florfenicol in milk and honey using modified QuEChERS extraction coupled with polymeric monolith-based capillary liquid chromatography tandem mass spectrometry. Talanta 150, 233−239.
Lombardo-Agüí, M., Gámiz-Gracia, L., Cruces-Blanco, C., García-Campaña, A.M., 2011. Comparison of different sample treatments for the analysis of quinolones in milk by capillary-liquid chromatography with laser induced fluorescence detection. J. Chromatogr. A 1218, 4966−4971.
Lord, G.A., Gordon, D.B., Myers, P., King, B.W., 1997. Tapers and restrictors for capillary electrochromatography and capillary electrochromatography mass spectrometry. J. Chromatogr. A 768, 9−16.
Malik, A., Li, W., Lee, M.L., 1993. Preparation of long packed capillary columns using carbon dioxide slurries. J. Microcol. Sep. 5, 361−369.
Martín-Ortiz, A., Salcedo, J., Barile, D., Bunyatratchata, A., Moreno, F., Martin-García, I., Clemente, A., Sanz, M.L., Matute, A.I.R., 2016. Characterization of goat colostrum oligosaccharides by nano-liquid chromatography on chip quadrupole time-of-flight mass spectrometry and hydrophilic interaction liquid chromatography-quadrupole mass spectrometry. J. Chromatogr. A 1428, 143−153.
Martin, M., Eon, C., Guiochon, G., 1975. Study of the pertinency of pressure in liquid chromatography II. Problems in equipment design. J. Chromatogr. A 108, 229−241.
Maruška, A., Kornyšova, O., 2004. Continuous beds (monoliths): stationary phases for liquid chromatography formed using the hydrophobic interaction-based phase separation mechanism. J. Biochem. Biophys. Methods 59, 1−48.
Merola, G., Aturki, Z., D'Orazio, G., Gottardo, R., Macchia, T., Tagliaro, F., Fanali, S., 2012. Analysis of synthetic cannabinoids in herbal blends by means of nano-liquid chromatography. J. Pharm. Biomed. Anal. 71, 45−53.
Meyer, M.R., Bergstrand, M.P., Helander, A., Beck, O., 2016. Identification of main human urinary metabolites of the designer nitrobenzodiazepines clonazolam, meclonazepam, and nifoxipam by nano-liquid chromatography-high-resolution mass spectrometry for drug testing purposes. Anal. Bioanal. Chem. 408, 3571−3591.
Mikulovic, G., Mechtler, K., 2006. HPLC techniques for proteomics analysis-a short overview of latest developments. Brief. Funct. Genomic Proteomic 5, 249−260.
Mills, M.J., Maltas, J., Lough, W.J., 1997. Assessment of injection volume limits when using on-column focusing with microbore liquid chromatography. J. Chromatogr. A 759, 1−11.
Mirabelli, M.F., Wolf, J.C., Zenobi, R., 2016. Pesticide analysis at ppt concentration levels: coupling nano-liquid chromatography with dielectric barrier discharge ionization-mass spectrometry. Anal. Bioanal. Chem. 408, 3425−3434.

Mistry, K., Krull, I., Grinberg, N., 2002. Capillary electrochromatography: an alternative to HPLC and CE. J. Sep. Sci. 25, 935−958.

Moliner-Martínez, Y., Ribera, A., Coronado, E., Campíns-Falcó, P., 2011a. Preconcentration of emerging contaminants in environmental water samples by using silica supported Fe_3O_4 magnetic nanoparticles for improving mass detection in capillary liquid chromatography. J. Chromatogr. A 1218, 2276−2283.

Moliner-Martínez, Y., Molins-Legua, C., Verdú-Andrés, J., Herráez-Hernández, R., Campíns-Falcó, P., 2011b. Advantages of monolithic over particulate columns for multiresidue analysis of organic pollutants by in-tube solid-phase microextraction coupled to capillary liquid chromatography. J. Chromatogr. A 1218, 6256−6262.

Moliner-Martínez, Y., Serra-Mora, P., Verdú-Andrés, J., Herráez-Hernández, R., Campíns-Falcó, P., 2015. Analysis of polar triazines and degradation products in waters by in-tube solid-phase microextraction and capillary chromatography: an environmentally friendly method. Anal. Bioanal. Chem. 407, 1485−1497.

Moreno-González, D., Huertas-Pérez, J.F., Gámiz-Gracia, L., García-Campaña, A.M., 2011. Determination of carbamates at trace levels in water and cucumber by capillary liquid chromatography. Int. J. Environ. Anal. Chem. 91, 1329−1340.

Muñoz-Ortuño, M., Moliner-Martínez, Y., Cogollos-Costa, S., Herráez-Hernández, R., Campíns-Falcó, P., 2012. A miniaturized method for estimating di(2-ethylhexyl) phthalate in bivalves as bioindicators. J. Chromatogr. A 1260, 169−173.

Muñoz-Ortuño, M., Argente-García, A., Moliner-Martínez, Y., Verdú-Andrés, J., Herráez-Hernández, R., Picher, M.T., Campíns-Falcó, P., 2014. A cost-effective method for estimating di(2-ethylhexyl)phthalate in coastal sediments. J. Chromatogr. A 1324, 57−62.

Myers, P., Bartle, K., 2002. Miniaturization in LC−MS. LC-GC Eur. 2, 2−5.

Nazario, C.E.D., Silva, M.R., Franco, M.S., Lancas, F.M., 2015. Evolution in miniaturized column liquid chromatography instrumentation and applications: an overview. J. Chromatogr. A 1421, 18−37.

Nilsson, C., Nilsson, S., 2006. Nanoparticle-based pseudostationary phases in capillary electrochromatography. Electrophoresis 27, 76−83.

Onghena, M., Moliner-Martinez, Y., Picó, Y., Campíns-Falcó, P., Barceló, D., 2012. Analysis of 18 perfluorinated compounds in river waters: comparison of high performance liquid chromatography-tandem mass spectrometry, ultra-high-performance liquid chromatography-tandem mass spectrometry and capillary liquid chromatography-mass spectrometry. J. Chromatogr. A 1244, 88−97.

Ortea, I., Cañas, B., Gallardo, J.M., 2011. Selected tandem mass spectrometry ion monitoring for the fast identification of seafood species. J. Chromatogr. A 1218, 4445−4451.

Östman, P., Jäntti, S., Ketola, R.A., Franssila, S., Kotiaho, T., Kostiainen, R., 2006. Capillary liquid chromatography−microchip atmospheric pressure chemical ionization−mass spectrometry. Lab Chip 6, 948−953.

Otieno, P.O., Owuor, P.O., Lalah, J.O., Pfister, G., Schramm, K.W., 2013. Impacts of climate-induced changes on the distribution of pesticides residues in water and sediment of Lake Naivasha. Kenya Environ. Monit. Assess 185, 2723−2733.

Ou, J., Li, X., Feng, S., Dong, J., Dong, X., Komg, L., Ye, M., Zou, H., 2007. Preparation and evaluation of a molecularly imprinted polymer derivatized silica monolithic column for capillary electrochromatography and capillary liquid chromatography. Anal. Chem. 79, 639−646.

Parc, A.L., Dallas, D.C., Duaut, S., Leonil, J., Martin, P., Barile, D., 2014. Characterization of goat milk lactoferrin *N*-glycans and comparison with the *N*-glycomes of human and bovine milk. Electrophoresis 35, 1560−1570.

Parker, B.L., Thaysen-Andersen, M., Solis, N., Scott, N.E., Larsen, M.R., Graham, M.E., Packer, N.H., Cordwell, S.J., 2013. Site-specific glycan-peptide analysis for determination of *N*-glycoproteome heterogeneity. J. Proteome Res. 12, 5791−5800.

Parkin, M.C., Longmoore, A.M., Turfus, S.C., Braithwaite, R.A., Cowan, D.A., Elliott, S., Kicman, A.T., 2013. Detection of ketamine and its metabolites in human hair using an integrated nanoflow liquid chromatography column and electrospray emitter fritted with a single porous 10 μm bead. J. Chromatogr. A 1277, 1−6.

Percy, A.J., Chambers, A.G., Yang, J., Domanski, D., Borchers, C.H., 2012. Comparison of standard- and nano-flow liquid chromatography platforms for MRM-based quantitation of putative plasma biomarker proteins. Anal. Bioanal. Chem. 404, 1089−1101.

Pérez-Fernández, V., Dominguez-Vega, E., Chankvetadze, B., Crego, A.L., García, M.Á., Marina, M.L., 2012. Evaluation of new cellulose-based chiral stationary phases Sepapak-2 and Sepapak-4 for the enantiomeric separation of pesticides by nano liquid chromatography and capillary electrochromatography. J. Chromatogr. A 1234, 22−31.

Pierri, G., Kotoni, D., Simone, P., Villani, C., Pepe, G., Campiglia, P., Dugo, P., Gasparrini, F., 2013. Analysis of bovine milk caseins on organic monolithic columns: an integrated capillary liquid chromatography-high resolution mass spectrometry approach for the study of time-dependent casein degradation. J. Chromatogr. A 1313, 259−269.

Poppe, H., 1997. Some reflections on speed and efficiency of modern chromatographic methods. J. Chromatogr. A 778, 3−21.

Prieto-Blanco, M.C., Argente-García, A., Campíns-Falcó, P., 2016. A capillary liquid chromatography method for benzalkonium chloride determination as a component or contaminant in mixtures of biocides. J. Chromatogr. A 1431, 176−183.

Prieto-Blanco, M.C., Moliner-Martínez, Y., López-Mahía, P., Campíns-Falcó, P., 2012. Ion-pair in-tube solid-phase microextraction and capillary liquid chromatography using a titania-based column: application to the specific lauralkonium chloride determination in water. J. Chromatogr. A 1248, 55−59.

Prieto-Blanco, M.C., Moliner-Martínez, Y., López-Mahía, P., Campíns-Falcó, P., 2013. Determination of carbonyl compounds in particulate matter PM2.5 by in-tube solid-phase microextraction coupled to capillary liquid chromatography/mass spectrometry. Talanta 115, 876−880.

Puchalska, P., García, M., Marina, M.L., 2014. Development of a capillary high performance liquid chromatography-ion trap-mass spectrometry method for the determination of VLIVP antihypertensive peptide in soybean crops. J. Chromatogr. A 1338, 85−91.

Quesada-Molina, C., García-Campaña, A.M., Olmo-Iruela, M.d, 2013. Ion-paired extraction of cephalosporins in acetone prior to their analysis by capillary liquid chromatography in environmental water and meat samples. Talanta 115, 943−949.

Rahayu, A., Lim, L.W., Takeuchi, T., 2015. Polymer monolithic methacrylate base modified with tosylated-polyethylene glycol monomethyl ether as a stationary phase for capillary liquid chromatography. Talanta 134, 232−238.

Rathore, A.S., 2002. Theory of electroosmotic flow, retention and separation efficiency in capillary electrochromatography. Electrophoresis 23, 3827−3845.

Reynolds, K.J., Maloney, T.D., Fermier, A.M., Colon, L.A., 1998. Capillary electrochromatography in columns packed by gravity - preliminary study. Analyst 123, 1493−1495.

Rigano, F., Albergamo, A., Sciarrone, D., Beccaria, M., Purcaro, G., Mondello, L., 2016. Nano liquid chromatography directly coupled to electron ionization mass spectrometry for free fatty acid elucidation in mussel. Anal. Chem. 88, 4021−4028.

Robson, M.M., Cikalo, M.G., Myers, P., Euerby, M.R., Bartle, K.D., 1997. Capillary electrochromatography - a review. J. Microcol. Sep. 9, 357−372.

Rocchi, S., Rocco, A., Pesek, J.J., Matyska, M.T., Capitani, D., Fanali, S., 2015. Enantiomers separation by nano-liquid chromatography: use of a novel sub-2 μm vancomycin silica hydride stationary phase. J. Chromatogr. A 1381, 149−159.

Rocco, A., Fanali, S., 2008. Capillary electrochromatography without external pressure assistance. Use of packed columns with a monolithic inlet frit. J. Chromatogr. A 1191, 263−267.

Rocco, A., Fanali, S., 2009. Enantiomeric separation of acidic compounds by nano-liquid chromatography with methylated-beta-cyclodextrin as a mobile phase additive. J. Sep. Sci. 32, 1696−1703.

Rocco, A., Maruška, A., Fanali, S., 2012a. Cyclodextrins as a chiral mobile phase additive in nano-liquid chromatography: comparison of reversed-phase silica monolithic and particulate capillary columns. Anal. Bioanal. Chem. 402, 2935−2943.

Rocco, A., Maruška, A., Fanali, S., 2012b. Enantioseparation of drugs by means of continuous bed (monolithic) columns in nano-liquid chromatography. Chemija 23.

Rocco, A., D'Orazio, G., Aturki, Z., Fanali, S., 2013a. Capillary electrochromatography: a look at its features and potential in separation science. In: Fanali, S., Haddad, P.R., Poole, C.F., Schoenmakers, P., Lloyd, D. (Eds.), Liquid Chromatography: Fundamental and Instrumentation. Elsevier BV, Amsterdam, pp. 469−492.

Rocco, A., Maruška, A., Fanali, S., 2013b. Enantiomeric separations by means of nano-LC. J. Sep. Sci. 30, 421−444.

Rocco, A., Fanali, C., Dugo, L., Mondello, L., 2014. A nano-LC/UV method for the analysis of principal phenolic compounds in commercial citrus juices and evaluation of antioxidant potential. Electrophoresis 35, 1701−1708.

Rodriguez, E.S., Poynter, S., Curran, M., Haddad, P.R., Shellie, R.A., Nesterenko, P.N., Paull, B., 2015. Capillary ion chromatography with on-column focusing for ultra-trace analysis of methanesulfonate and inorganic anions in limited volume Antarctic ice core samples. J. Chromatogr. A 1409, 182−188.

Rogeberg, M., Vehus, T., Grutle, L., Greibrokk, T., Wilson, S.R., Lundanes, E., 2013. Separation optimization of long porous-layer open-tubular columns for nano-LC−MS of limited proteomic samples. J. Sep. Sci. 36, 2838−2847.

Ruiz-Viceo, J.A., Rosales-Conrado, N., Guillén-Casla, V., Pérez-Arribas, L.V., León-González, M.E., Polo-Díez, L.M., 2012. Fluoroquinolone antibiotic determination in bovine milk using capillary liquid chromatography with diode array and mass spectrometry detection. J. Food Comp. Anal. 28, 99−106.

Saito, Y., Jinno, K., Greibrokk, T., 2004. Capillary columns in liquid chromatography: between conventional columns and microchips. J. Sep. Sci. 27, 1379−1390.

Schubert, B., Oberache, H., 2011. Impact of solvent conditions on separation and detection of basic drugs by micro liquid chromatography-mass spectrometry under overloading conditions. J. Chromatogr. A 1218, 3413−3422.

Schurig, V., Mayer, S., 2001. Separation of enantiomers by open capillary electrochromatography on polysiloxane-bonded permethyl-beta-cyclodextrin. J. Biochem. Biophys. Methods 48, 117−141.

Sestak, J., Moravcova, D., Kahle, V., 2015. Instrument platform for nano liquid chromatography. J. Chromatogr. A 1421, 2−17.

Shi, T., Fillmore, T.L., Sun, X., Zhao, R., Schepmoes, A.A., Hossain, M., Xie, F., Wu, S., Kim, J.S., Jones, N., Moore, R.J., Pasa-Tolić, L., Kagan, J., Rodland, K.D., Liu, T., Tang, K., Camp, D.G., Smith, R.D., Qian, W.J., 2012. Antibody-free, targeted mass-spectrometric approach for quantification of proteins at low picogram per milliliter levels in human plasma/serum. Proc. Natl. Acad. Sci. U.S.A 109, 15395−15400.

Simon, R., Collins, M.E., Spivak, D.A., 2007. Shape selectivity versus functional group pre-organization in molecularly imprinted polymer. Anal. Chim. Acta 591, 7−16.

Sproß, J., Brauch, S., Mandel, F., Wagner, M., Buckenmaier, S., Westermann, B., Sinz, A., 2013. Multidimensional nano-HPLC coupled with tandem mass spectrometry for analyzing biotinylated proteins. Anal. Bioanal. Chem. 405, 2163−2173.

Su, H.-H., Chuang, L.-Y., Tseng, W.-L., Lu, C.-Y., 2015. Micro-scale strategy to detect spermine and spermidine by MALDI−TOF MS in foods and identification of apoptosis-related proteins by nano-flow UPLC−MS/MS after treatment with spermine and spermidine. J. Chromatogr. B 978, 131−137.

Surowiec, I., Koistinen, K.M., Fraser, P.D., Bramley, P.M., 2011. Proteomic approach for the detection of chicken mechanically recovered meat. Meat Sci. 89, 233−237.

Svec, F., 2002. Capillary electrochromatography: a rapidly emerging separation method. In: Shepers, T., Freitag, R. (Eds.), Advances in Biochemical Engineering/Biotechnology: Modern Advances in Chromatograph. Springer-Verlag, Berlin Heidelberg, pp. 1−47.

Svec, F., 2010. Porous polymer monoliths: amazingly wide variety of techniques enabling their preparation. J. Chromatogr. A 1217, 902−924.

Svec, F., Huber, C.G., 2006. Monolithic materials: promises, challenges, achievements. Anal. Chem. 78, 2100−2107.

Szumski, M., Buszewski, B., 2002. State of the art in miniaturized separation techniques. Crit. Rev. Anal. Chem. 32, 1−46.

Takeuchi, T., Niwa, T., Ishii, D., 1987. Stepwise gradient elution using switching valves in micro high-performance liquid chromatography. J. Chromatogr. A 405, 117−124.

Tan, Z.J., Remcho, V.T., 1998. Bonded polymethacrylate stationary phases for open tubular liquid chromatographic and electrochromatographic separations. J. Microcol. Sep. 10, 99−105.

Tanaka, N., Kobayashi, H., Ishizuka, N., Minakuchi, H., Nakanishi, K., Hosoya, K., Ikegami, T., 2002. Monolithic silica columns for high-efficiency chromatographic separations. J. Chromatogr. A 965, 35−49.

Teh, H.B., Li, S.F.Y., 2015. Simultaneous determination of bromate, chlorite and haloacetic acids by two-dimensional matrix elimination ion chromatography with coupled conventional and capillary columns. J. Chromatogr. A 1383, 112−120.

Tipton, J.D., Tran, J.C., Catherman, A.D., Ahlf, D.R., Durbin, K.R., Lee, J.E., Kellie, J.F., Kelleher, N.L., Hendrickson, C.L., Marshall, A.G., 2012. Nano-LC FTICR tandem mass spectrometry for top-down proteomics: routine baseline unit mass resolution of whole cell lysate proteins up to 72 kDa. Anal. Chem. 84, 2111−2117.

Totten, S.M., Wu, L.D., Parker, E.A., Davis, J.C., Hua, S., Stroble, C., Ruhaak, L.R., Smilowitz, J.T., German, J.B., Lebrilla, C.B., 2014. Rapid-throughput glycomics applied to human milk oligosaccharide profiling for large human studies. Anal. Bioanal. Chem. 406, 7925−7935.

Tran, J.C., Zamdborg, L., Ahlf, D.R., Lee, J.E., Catherman, A.D., Durbin, K.R., Tipton, J.D., Vellaichamy, A., Kellie, J.F., Li, M., Wu, C., Sweet, S.M.M., Early, B.P., Siuti, N., LeDuc, R.D., Compton, P.D., Thomas, P.M., Kelleher, N.L., 2011. Mapping intact protein isoforms in discovery mode using top-down proteomics. Nature 480, 254−258.

Vega, E.D., Crego, A.L., Lomsadze, K., Chankvetadze, B., Marina, M.L., 2011. Enantiomeric separation of FMOC-amino acids by nano-LC and CEC using a new chiral stationary phase, cellulose tris(3-chloro-4-methylphenylcarbamate). Electrophoresis 32, 2700−2707.

Viñas, P., Pastor-Belda, M., Campillo, N., Bravo-Bravo, M., Hernández-Córdoba, M., 2014. Capillary liquid chromatography combined with pressurized liquid extraction and dispersive liquid-liquid microextraction for the determination of vitamin E in cosmetic products. J. Pharm. Biomed. Anal. 94, 173−179.

Vissers, J.P.C., Claessens, H.A., Cramers, C.A., 1997. Microcolumn liquid chromatography: instrumentation, detection and applications. J. Chromatogr. A 779, 1−28.

Wang, J.G., Xu, W.D., Zhai, W.T., Li, Y., Hu, J.W., Hu, B., Li, M., Zhang, L., Guo, W., Zhang, J.P., Wang, L.H., Jiao, B.H., 2012. Disorders in angiogenesis and redox pathways are main factors contributing to the progression of rheumatoid arthritis: a comparative proteomics study. Arthritis Rheum. 64, 993−1004.

Wang, H., Sunb, S., Zhangb, Y., Chena, S., Liub, P., Liu, B., 2015. An off-line high pH reversed-phase fractionation and nano-liquid chromatography−mass spectrometry method for global proteomic profiling of cell lines. J. Chromatogr. B 974, 90−95.

Warriner, R.N., Craze, A.S., Games, D.E., Lane, S.J., 1998. Capillary electrochromatography mass spectrometry - a comparison of the sensitivity of nanospray and microspray ionization techniques. Rapid Commun. Mass Spectrom. 12, 1143−1149.

Wehr, T., 2006. Top-down versus bottom-up approaches in proteomics. LC-GC N. Am. 24, 1004.
Wilson, S.R., Vehus, T., Berg, H.S., Lundanes, E., 2015. Nano-LC in proteomics: recent advances and approaches. Bioanalysis 7, 1799−1815.
Wistuba, D., Schurig, V., 2000. Enantiomer separation of chiral pharmaceuticals by capillary electrochromatography. J. Chromatogr. A 875, 255−276.
Wu, N., Peck, T.L., Webb, A.G., Magin, R.L., Sweedler, J.V., 1994. 1H-NMR spectroscopy on the nanoliter scale for static and on-line measurements. Anal. Chem. 66, 3849−3857.
Wu, R., Hu, L., Wang, F., Ye, M., Zou, H., 2008. Recent development of monolithic stationary phases with emphasis on microscale chromatographic separation. J. Chromatogr. A 1184, 369−392.
Xia, S., Tao, D., Yuan, H., Zhou, Y., Liang, Z., Zhang, L., Zhang, Y., 2012. Nano-flow multidimensional liquid chromatography platform integrated with combination of protein and peptide separation for proteome analysis. J. Sep. Sci. 35, 1764−1770.
Yan, C., Dadoo, R., Zhao, H., Zare, R.N., Rakestraw, D.J., 1995. Capillary electrochromatography - analysis of polycyclic aromatic hydrocarbons. Anal. Chem. 67, 2026−2029.
Yang, M.-H., Yang, Y.-H., Lu, C.-Y., Jong, S.-B., Chen, L.-J., Lin, Y.-F., Wu, S.-J., Chu, P.-Y., Chung, T.-W., Tyan, Y.-C., 2012. Activity-dependent neuroprotector homeobox protein: a candidate protein identified in serum as diagnostic biomarker for Alzheimer's disease. J. Proteomics 75, 3617−3629.
Yeşilyurt, B., Şahar, U., Deveci, R., 2015. Determination of the type and quantity of sialic acid in the egg jelly coat of the sea urchin *Paracentrotus lividus* using capillary LC-ESI-MS/MS. Mol. Reprod. Dev. 82, 115−122.
Yeung, E.S., 1985. Optical detectors for microcolumn liquid chromatography. In: Novotny, M.V., Ishi, D. (Eds.), Microcolumn Separations. Elsevier, Amsterdam, pp. 117−143.
Zhang, Q., Gil, V., Sánchez-López, E., García, M.Á., Jiang, Z., Marina, M.L., 2015. Evaluation of the potential of a quinidine-based monolithic column on the enantiomeric separation of herbicides by nano-liquid chromatography. Microchem. J. 123, 15−21.
Zhao, C., Wu, Z., Xue, G., Wang, J., Zhao, Y., Xu, Z., Lin, D., Herbert, G., Chang, Y., Cai, K., Xu, G., 2011. Ultra-high capacity liquid chromatography chip/quadrupole time-of-flight mass spectrometry for pharmaceutical analysis. J. Chromatogr. A 1218, 3669−3674.
Zheng, M., Wu, Y., Lu, L., Ding, K., Tang, F., Lin, Z., Wu, X., 2011. Simultaneous analysis of acetaminophen, *p*-aminophenol and aspirin metabolites by hydrophilic interaction and strong anion exchange capillary liquid chromatography coupled to amperometric detection. J. Sep. Sci. 34, 2072−2078.
Zhu, K.Y., Leung, K.W., Ting, A.K., Wong, Z.C., WY, N., Choi, R.C., Dong, T.T., Wang, T., Lau, D.T., Tsim, K.W., 2012. Microfluidic chip based nano liquid chromatography coupled to tandem mass spectrometry for the determination of abused drugs and metabolites in human hair. Anal. Bioanal. Chem. 402, 2805−2815.

This page intentionally left blank

CHAPTER

MULTIPLE PARALLEL MASS SPECTROMETRY FOR LIQUID CHROMATOGRAPHY

10

William C. Byrdwell
U.S. Department of Agriculture, Beltsville, MD, United States

1. INTRODUCTION

Liquid chromatography/mass spectrometry (LC−MS) has become one of the primary and most authoritative tools for analysis of most classes of molecules, including lipids. As high-resolution accurate-mass (HRAM) mass spectrometers become ever more affordable, their use is becoming more widespread and routine. When confronted with the dizzying array of options for available instruments, it can seem overwhelming to select the one best method for any analysis. One has options of whether to use a classic single quadrupole mass spectrometer or tandem sector quadrupole (TSQ) instrument, a time-of-flight mass detector, a classic ion-trap instrument (either a hyperbolic ion trap or linear ion trap), a HRAM Orbitrap instrument, or a magnetic sector mass analyzer, as well as hybrid instruments that incorporate combinations of these mass filters or others.

In addition to the type of mass filter, the type of ionization also plays a crucial role in any successful analytical strategy. Because this chapter is focused on MS coupled to LC, it focuses on the three most popular types of atmospheric pressure ionization (API) sources used to couple LC to MS. These are electrospray ionization (ESI), atmospheric pressure chemical ionization (APCI), and atmospheric pressure photoionization (APPI). Of course, there are numerous other ionization approaches that have been used for a wide range of applications, ranging from relatively recently developed ambient sampling techniques such as desorption ESI (Takáts et al., 2004) or direct analysis in real time (DART) (Cody et al., 2005) to well-established techniques such as matrix assisted laser desorption ionization. Atmospheric pressure, ambient, and desorption techniques have been reviewed extensively in recent years (Covey et al., 2009; Huang et al., 2011; Monge et al., 2013).

Our ongoing interest has been analysis of lipids, primarily triacylglycerols (TAGs), using high-performance liquid chromatography (HPLC) coupled to MS. We initially employed APCI-MS and ESI-MS for lipid analysis, but as APPI-MS became commercially available, this was incorporated into our analytical methodologies.

TAGs are composed of three fatty acyl chains (FAs) (often referred to in shorthand as fatty acids, even though this is not strictly accurate) attached to a three-carbon glycerol backbone, as shown in Fig. 10.1. Based on this, there are several traits that should be characterized by MS (or by LC or other techniques) for complete structural elucidation of TAG molecular species: (1) the length

Handbook of Advanced Chromatography/Mass Spectrometry Techniques. http://dx.doi.org/10.1016/B978-0-12-811732-3.00010-8

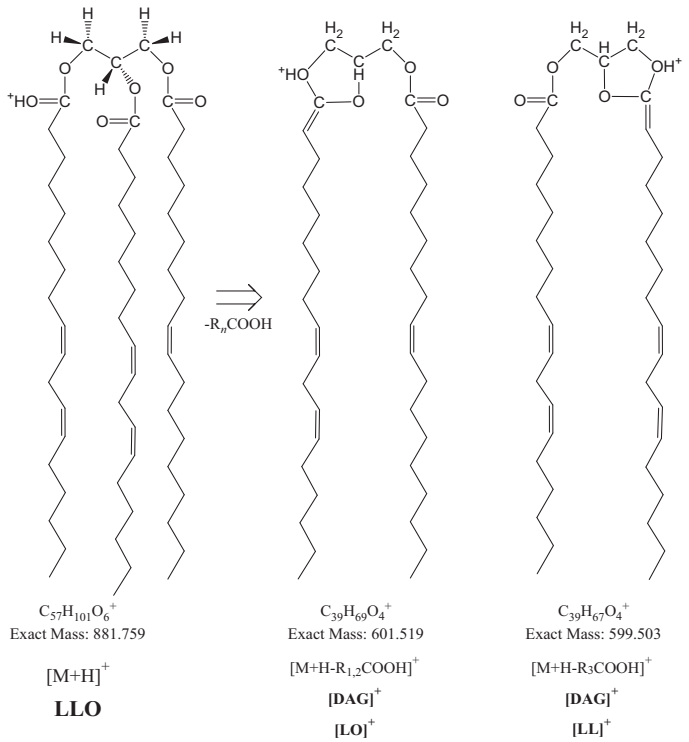

FIGURE 10.1

Structure of dilinoleoyl-oleoyl-glycerol (LLO) and diacylglycerol-like fragment ions, $[M + H{-}R_nCOOH]^+$, or $[DAG]^+$, formed from loss of a fatty acyl chain. Location of protons, H^+, is not limited to the positions shown as examples.

of the FA carbon chains; (2) the number of double bonds in the FAs (i.e., the degree of unsaturation); (3) the positions of the double bonds in the FAs (e.g., ω-3, ω-6); (4) the nature of double-bond isomers (*cis* vs. *trans*); (5) the positions of the FAs on the glycerol backbone (i.e., regioisomers); and (6) the chirality of the molecule (i.e., enantiomers). The positions of the FAs are specified using the stereospecific numbering (*sn*) system, referring to the three glycerol carbons at *sn*-1, *sn*-2, and *sn*-3. The carbon at the *sn*-2 position is a chiral carbon in many (i.e., nonsymmetric TAGs), giving rise to chirality of TAG molecular species. These characteristics also apply to glycerophospholipids, which have the same structures, except the *sn*-3 carbon is attached to a phosphate-containing head group instead of a FA.

The initial part of this chapter describes the characteristics of mass spectra obtained by the three API techniques used in our lab, and the structural information that can be obtained from each. The unique contributions to structural elucidation by each technique will be compared and contrasted. Then, the benefits of integrating different API techniques into a holistic analytical approach are described.

1.1 ATMOSPHERIC PRESSURE CHEMICAL IONIZATION MASS SPECTROMETRY

Because of our ongoing interest, we have reviewed the area of APCI-MS for TAG analysis multiple times in the past (Byrdwell, 1998a, 2001, 2003a, 2005b,c; Byrdwell and Neff, 1997). Řezanka and Sigler (2007) also reviewed APCI-MS for lipid analysis. Because this area has been so thoroughly covered previously, the history of HPLC−APCI-MS of TAGs will not be repeated here, but instead this chapter focuses on developments regarding the use of APCI-MS and ESI-MS, and later APPI-MS, used together in multiple parallel MS approaches (Byrdwell, 2005b, 2011b), and special considerations associated with coupling these techniques.

Ever since the first report of HPLC/APCI-MS for TAG analysis (Byrdwell and Emken, 1995), it has been shown that TAGs give simple mass spectra containing mostly the protonated molecule, $[M + H]^+$, and diacylglycerol-like fragment ions formed by loss of one FA, $[M + H - RCOOH]^+$, or simply $[DAG]^+$, exemplified in Fig. 10.2. The relative amounts of $[M + H]^+$ and $[DAG]^+$ ions correlate with the degree of unsaturation, such that polyunsaturated TAGs give a protonated molecule base peak and smaller $[DAG]^+$ fragments (as in Fig. 10.2A), but TAGs with few sites of unsaturation give a smaller $[M + H]^+$ and a $[DAG]^+$ base peak (as in Fig. 10.2B). Saturated TAGs give little or no $[M + H]^+$, which can be problematic for molecular weight identification.

1.1.1 Triacylglycerol Regioisomers

The TAG in Figs. 10.1 and 10.2A,C,E, dilinoleoyl-oleoyl-glycerol (LLO), has three possible structures. Specifically, it could be LLO, OLL, or LOL, depending on how the FAs are arranged on the glycerol backbone (i.e., regioisomers and enantiomers). Generically, such a TAG is referred to as AAB/BAA/ABA, where A and B are two different FAs arranged in different ways. Rather than continuously referring to these TAGs as AAB/BAA/ABA, Byrdwell introduced the nomenclature of referring to these as Type II TAGs because they have two FAs, give two $[DAG]^+$ fragments, and require two critical ratios to provide desired structural information and to reproduce the mass spectrum from these ratios (Byrdwell, 2005a, 2015a,b,c, 2016). Similarly, TAGs that have three different FAs, A, B, and C, have six isomers possible: ABC/CBA/BCA/ACB/CAB/BAC. For brevity and simplicity, these are referred to as Type III TAGs because they have three FAs, give three $[DAG]^+$ fragments, and require three critical ratios. Obviously, monoacid TAGs, AAA, have one FA, give one $[DAG]^+$, and are called Type I TAGs.

One of the most important structural traits that APCI-MS provides information about is the identity of the FA in the *sn*-2 position. This information is important for nutritional considerations because plants synthesize TAGs with structural specificity, with saturated FAs preferred at the *sn*-1 and *sn*-3 positions, and polyunsaturated FAs in the *sn*-2 position. In a complementary fashion, human digestive enzymes metabolize fats with regiospecificity, such that the FAs in the *sn*-1 and *sn*-3 positions are preferentially removed, meaning that the FA in the *sn*-2 is conserved on the glycerol backbone and incorporated into other lipids to a substantial extent. In November 1996, Mottram and Evershed published the first report using APCI-MS that indicated that loss of the FA in the *sn*-2 position in AAB/BAA/ABA TAGs was energetically less favorable than loss of the FAs from the *sn*-1 or *sn*-3 positions. Furthermore, they reported that the smallest $[DAG]^+$ fragment in mass spectra of ABC/CBA/BCA/ACB/CAB/BAC TAGs was formed by loss of the FA in the *sn*-2 position. Then, in December 1996, Laakso and Voutilainen also demonstrated that APCI-MS provides an indication of the position of the FA located in the *sn*-2 position. Using silver-ion chromatography coupled to APCI-MS, they showed

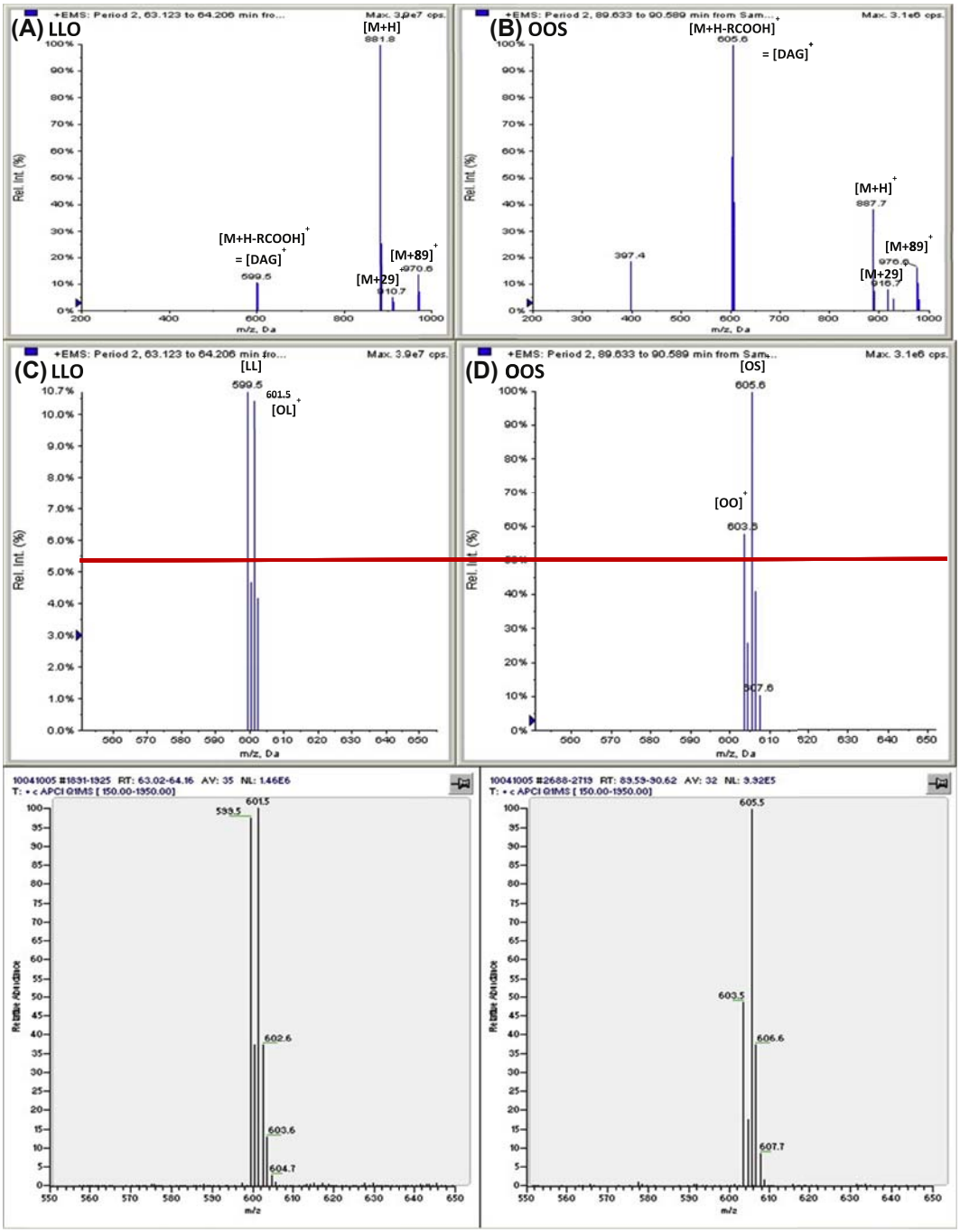

FIGURE 10.2

Atmospheric pressure chemical ionization (APCI) mass spectrometry (MS) spectra of triacylglycerols in rice bran oil from AB Sciex QTrap 4000 hybrid (A−D) and TSQ 7000 (E−F) mass spectrometers. Fatty acid abbreviations: $[DAG]^+$, diacylglycerol-like fragment; *L*, linoleic acid; $[M + 29]^+$, acetonitrile-derived adduct; $[M + 89]^+$, acetonitrile + dichloromethane-derived adduct; $[M + H]^+$, protonated molecule; *O*, oleic acid; *S*, stearic acid. *Red (gray in print versions) line* indicates statistically expected amount of $[AA]^+$ fragment compared with $[AB]^+$ fragment (=1/2) from AAB/BAA/ABA triacylglycerols. *TSQ*, tandem sector quadrupole.

that the $[M + H - RCOOH]^+$ fragment formed by loss of the FA in the *sn*-2 position (R_2COOH) was smaller than the same fragment formed when the FA was lost from the *sn*-1 or *sn*-3 positions. This trend provides a facile way to identify the FA in *sn*-2 position.

In addition to the factors discussed above that affect the relative abundances of ions in APCI-MS spectra, Manninen and Laakso (1997) reported that the proximity of the double bonds to the glycerol backbone also affects fragment formation. Specifically, they reported that: "The abundance of the $[M - 18{:}3n\text{-}3]^+$ ion was lower than that of $[M - 18{:}3n\text{-}6]^+$ ion, whereas the abundance of the $[M + H]^+$ ion was higher." This trend was reported using supercritical fluid (SFC) APCI-MS, whereas the trend was not evident in data from Ag-ion HPLC (Laakso, 1997; Laakso and Voutilainen, 1996).

In 2002, a review by Mondello et al. showed what appears to be the first published calibration curve for TAG regioisomer quantification by APCI-MS. They showed the amounts of OPO in beef tallow and lard, which was later reported in more detail (Dugo et al., 2006c). In 2003, Holčapek et al. reported calibration curve parameters for OOP/OPO and OPP/POP regioisomers, and shortly thereafter, Jakab et al. (2003) reported a detailed quantification of regioisomers of LLO/LOL by APCI-MS. The next year, Fauconnot et al. (2004) reported analysis of seven sets of regioisomers of AAB/ABA TAGs. All of these groups of researchers constructed linear calibration curves with good correlation coefficients from defined mixtures of regioisomer pairs of Type II TAGs (AAB/BAA/ABA) to allow quantification of regioisomers.

At this point, it is important to mention that if there were no discrimination during the fragmentation process, the abundance of the $[AB]^+$ fragment should theoretically always be twice that of the $[AA]^+$ fragment because there are two indistinguishable "A" FAs in AAB/BAA/ABA combined with one "B" FA. Thus, there are two ways to get $[AB]^+$, but only one way to get $[AA]^+$. Therefore, if the ratio of $[AA]^+/[AB]^+$ is constructed, it should always be ½ or 0.5. For example, the red lines in Fig. 10.2 show the statistically expected levels at which the $[AA]^+$ fragment is ½ of the abundance of the $[AB]^+$ fragment for LLO and OOS.

Based on the reports of Jakab et al. (2003) and Fauconnot et al. (2004), Byrdwell (2005a,d) showed that calibration lines could be simplified and constructed from only the $[AA]^+/[AB]^+$ from the two pure regioisomers. The $[AA]^+/[AB]^+$ was identified as one of three critical ratios and was applied with tabulated literature values of the ratio from pure regioisomers for quantification of TAG regioisomers. Tabulated values from a variety of authors obtained on a variety of instruments (Byrdwell, 2003a, 2005d) showed a couple of important points. First, the $[AA]^+/[AB]^+$ from a variety of instruments over a wide time span were similar, with the exception of a Micromass instrument with a ZSpray interface. Second, in general ABA TAGs gave $[AA]^+/[AB]^+$ less (often much less) than the statistically predicted value of 0.5, whereas AAB/BAA TAGs gave $[AA]^+/[AB]^+$ close to or greater than 0.5 (as in Fig. 10.2).

Leskinen et al. (2007) used linear calibration curves, similar to those first reported by the authors mentioned above, for quantification of regioisomers of four specific TAGs: LLO, LOO, POO, and PPO. In 2010, Holčapek et al. published the most thorough tabulation of ion abundances to date, comparing the results from five mass analyzers for a large set of TAG regioisomer molecular species (54 Type II TAGs and 30 Type III TAGs). Analysis of regioisomers of TAGs by a variety of means, including APCI-MS, has been discussed by Kalo (2013). Analysis of regioisomers of TAGs was also included in the review by Řezanka and Sigler (2014).

In this section, mention has only been made of identification of the FA in the *sn*-2 position. This is because all reports, until recently, have indicated that $[DAG]^+$ fragments obtained by APCI-MS do not

allow differentiation of the FAs in the *sn*-1 and *sn*-3 positions. Thus, all literature reports to date identify only the relative amount of ABA versus AAB/BAA for Type II TAGs and the identity of the FA in the *sn*-2 position of Type III TAGs. Recently, Byrdwell (2015c) recalculated the tabulated data of Holčapek et al. (2010) into critical ratios to identify trends in formation of $[M + H - R_1COOH]^+/[M + H - R_3COOH]^+$ fragments. The predominant influences that affect formation of the $[DAG]^+$, other than the one formed by loss of the *sn*-2 FA, are the degree of unsaturation and the grouping of FAs.

1.1.2 Triacylglycerol Enantiomers

APCI-MS mass spectra cannot differentiate FAs in the *sn*-1 and *sn*-3 positions, and thus do not provide sufficient information to differentiate TAG enantiomers (see Fig. 10.1). Therefore, they are typically separated using chiral column chromatography followed by MS. The separation is crucial to accurate identification of enantiomers. Although Iwasaki et al. (2001) used chiral HPLC for identification of TAG enantiomers using UV detection, it appears that the first application of chiral HPLC/APCI-MS was reported by Řezanka et al. (2012), who used preparative chromatography followed by chiral HPLC/APCI-MS for analysis of EPP/PPE and EEP/PEE in the diatom *Phaeodactylum tricornutum* (E = eicosapentaenoic acid, 20:5; P = palmitic acid, 16:0). That research group has followed their initial work with multiple reports of chiral LC/APCI-MS for enantiomer analysis, which are required reading for those entering that field of analysis. Lísa and Holčapek (2013) published a report describing the synthesis of a large number of TAG enantiomer standards and their analysis by chiral HPLC/APCI-MS. The method was then applied to analysis of TAG enantiomers in hazelnut oil and human plasma.

The primary problem with chiral HPLC separations of TAGs is that they tend to be very long chromatographic runs, often longer than 160 min. But again, because the chiral separation is critical to identification of enantiomers using APCI-MS, this is simply the cost of obtaining this structural information by LC−MS.

1.2 ELECTROSPRAY IONIZATION MASS SPECTROMETRY

In contrast to APCI-MS, Duffin et al. (1991) showed that using ESI-MS for analysis of TAGs produced predominantly or exclusively sodium or ammonium adducts (depending on the electrolyte used), with minimal fragmentation. This initial report also mentioned that the signal from ESI-MS depended on the polarity of the molecules, the carbon chain length, and the degree of unsaturation. Regarding polarity, monoacylglycerols (MAGs) gave more signal than diacylglycerols, which gave more signal than TAGs. Shorter and unsaturated TAGs gave more signal than longer and saturated TAGs. The molecular adduct ions formed from TAGs by ESI-MS, with little fragmentation, were shown to be well suited to act as the precursor ions for structural analysis by MS/MS.

Although that report used infusion, with no prior separation, it showed the utility of ESI-MS for TAG analysis, which has also been shown to be ideal for phospholipid (PL) analysis (Deeg et al., 1992; Han and Gross, 1994; Kerwin et al., 1994; Kim et al., 1994; Pulfer and Murphy, 2003; Smith et al., 1995; Stahl et al., 1991). Schuyl et al. (1998) used ESI-MS with argentation (silver ion) HPLC for analysis of TAGs, Sandra et al. (1997) coupled ESI-MS with capillary electrochromatography, and Hvattum (2001) appears to be the first to use ESI-MS coupled to nonaqueous reversed-phase (NARP) HPLC for TAG analysis. Another key contribution to the development of ESI-MS applied to TAGs was

the analysis of normal and deuterium-labeled TAGs (by infusion) using lithium adducts as precursors (Hsu and Turk, 1999). The authors provided good evidence, based on collisionally activated dissociation [CAD, now more often referred to a collision-induced dissociation, (see http://mass-spec.lsu.edu/msterms/index.php/CAD_vs._CID)], for the proposed fragmentation mechanism that is now generally assumed to be the *de facto* mechanism seen in ESI-MS/MS of TAGs. And because the exact same $[DAG]^+$ fragments are produced by APCI-MS as are produced by ESI-MS/MS, the mechanism is imputed to be the same, in the absence of an equally thorough treatment of deuterium-labeled TAGs by APCI-MS.

1.2.1 Triacylglycerol Regioisomers by Electrospray Ionization Mass Spectrometry

Hsu and Turk used ESI-MS/MS with infusion of lithium salts to identify not only the mechanism of fragmentation, mentioned above, but also to identify the FA in the *sn*-2 position. The most abundant fragments were formed by losses of acyl chains as fatty acids and also as lithium salts, $[M + Li - RCOOH]^+$ and $[M + Li - RCOOLi]^+$, respectively. These fragments formed by loss of the *sn*-2 FA were smaller than those fragments formed by loss of the *sn*-1 or *sn*-3 FAs. Additional fragments representing loss of two acyl chains, one as a fatty acid and one as an α,β unsaturated FA, $[M + Li - RCOOH - R'CH{=}CHCOH]^+$, to give MAG-like fragments, also allowed identification of the FA at the *sn*-2 position.

1.3 ATMOSPHERIC PRESSURE PHOTOIONIZATION MASS SPECTROMETRY

Robb et al. (2000) reported the first combination of APPI with LC−MS in 2000. Since then, there have been more than 450 publications reporting applications of APPI to analysis by LC−MS, SFC−MS, and other hyphenated techniques. Because APPI is the most recently developed of the three most popular API techniques, quite a few of these publications report comparisons to one or more of the API or other ionization methods. Even the first report by Robb et al. (2000) included a comparison of APPI and APCI. Many of these applications are discussed further below in the section on sequential API methodologies.

Only a subset of molecules have ionization potentials (IPs) below the energies provided by the krypton lamps used in commercially available APPI sources, which has two emission lines at 10.03 and 10.64 eV (Marchi et al., 2009; Robb and Blades, 2006; Short et al., 2007a). Therefore, only a subset of analytes can be directly ionized by the energy ($E = h\nu$) provided by the krypton lamp. Therefore, an easily ionizable component, called a dopant, is either included in the LC solvent system or is added postcolumn, such as via a tee (Table 10.1). Most common LC solvents (such as methanol (MeOH), water, acetonitrile (ACN), chloroform, and dichloromethane (DCM)) have IPs greater than the energy provided by the krypton lamp, so methods that employ these solvents require the use of a dopant. Greater details regarding the ionization process, and a list of IPs of LC solvents, dopants, and gases (e.g., N_2 commonly used as the APPI sheath gas) are provided in previous reports (Kauppila et al., 2002, 2004; Marchi et al., 2009).

Reviews of APPI-MS, including recent advances in this field, have been provided by, among others, Marotta et al. (2003), Raffaelli and Saba (2003), Tubaro et al. (2003), Syage et al. (Syage, 2004; Syage et al., 2004, 2008), Hanold et al. (2004), Robb and Blades (2005, 2006, 2008), Kauppila et al. (2005, 2014, 2017), Bos et al. (2006), Purcell et al. (2006), Song et al. (2007), and Marchi et al. (2009).

Table 10.1 Mechanisms of Ion Formation by Atmospheric Pressure Photoionization Mass Spectrometry (APPI-MS)

Direct APPI (No Dopant)	
$M + h\nu \rightarrow M^{\bullet+} + e^-$	Analyte molecule, M, has ionization potential (IP) below the energy ($E = h\nu$) provided by the krypton lamp, 10.0 and 10.6 eV. The analyte is ionized directly to a molecular ion, which is an odd-electron radical cation. Radical cation can abstract a hydrogen, H, from a solvent molecule to form $[M + H]^+$.
Dopant-Assisted APPI	
Step 1. $D + h\nu \rightarrow D^{\bullet+} + e^-$	Dopant (or LC solvent) with IP $\leq$ 10.0 or 10.6 eV is ionized to radical cation.
Step 2. $D^{\bullet+} + M \rightarrow [M + H]^+ + [D - H]^{\bullet}$	$D^{\bullet+}$ ionizes analyte M by proton transfer.
OR $D^{\bullet+} + M \rightarrow M^{\bullet+} + D$	$D^{\bullet+}$ ionizes analyte M by electron transfer.
Adapted from Syage, J.A., Evans, M.D., Hanold, K.A., 2000. Photoionization mass spectrometry. Am. Lab. 32, 24–29.	

Reviews on ionization techniques for MS, including APPI, include those by Karst (2002), Hayen and Karst (2003), Van Berkel (2003), Zweiner and Frimmel (2004), Balogh (2005), Feldman (2005), Jemal and Xia (2006), Ma et al. (2006), Donegan and Browning (2012), Himmelsbach (2012), Alagar Raja et al. (2014), and Awad et al. (2015).

Methods for analysis of specific classes of molecules using APPI-MS include reports describing analysis of: pharmaceutical samples and drugs and their metabolites (Cai et al., 2005, 2007a; Culzoni et al., 2014; Evans et al., 2002; Keski-Hynnilä et al., 2002; Lee, 2005; Lim and Lord, 2002; Ma et al., 2006; Narayanam et al., 2014; Wang et al., 2005), other biological samples (Jemal and Xia, 2006; Meyer et al., 2016) including neurotransmitters (Kauppila et al., 2006), steroids and hormones (Gouveia et al., 2013; Kalogera et al., 2013; Stolze et al., 2016; Yan et al., 2012; Zendjabil et al., 2016), napthalenes and other polyaromatic hydrocarbons (Cai et al., 2009, 2012; Diao et al., 2012; Itoh et al., 2006; Kauppila et al., 2002; Short et al., 2007a; Song et al., 2011; Straube et al., 2004; Vaikkinen et al., 2016), flavonoids (Rauha et al., 2001), lignins (Banoub et al., 2015), food samples and food contaminants (Sforza et al., 2006; Takino et al., 2004), mycotoxins (Zöllner and Mayer-Helm, 2006), and TAGs and other lipids (Cai et al., 2007b; Cai and Syage, 2006a,b; Gaudin et al., 2012; Kéki et al., 2008; Rivera et al., 2011).

1.4 MULTIPLE MASS SPECTROMETRY APPROACHES

The sections above describe the complementary types of data that are obtained by APCI-MS, ESI-MS, and APPI-MS. Almost as early as those API techniques were developed, researchers started comparing and contrasting the results obtained by the different techniques by sequential analyses obtained on different instruments or by changing the ionization source between analyses on one instrument. Also early in the development of API methods, new multimode ionization sources started to be reported,

which incorporated two or more API techniques into a single housing. Soon, multiple parallel techniques started to appear, in which multiple API techniques were used on different instruments simultaneously in parallel. Thus, there are three ways the popular API techniques are used together: (1) sequential, (2) multimode, and (3) parallel.

Sequential analyses using now common API techniques were reported as early as 1994, when Iwabuchi et al. (1994) reported a comparison of APCI-MS, ESI-MS, and thermospray MS. Now, there are hundreds of applications of combinations of API techniques. Because of the large number of reports, only a subset of those that directly compare API techniques are discussed here. There are more than 500 citations for the combination of APCI-MS and ESI-MS, over 130 citations for combinations of APCI-MS and APPI-MS, and around 150 citations for ESI-MS and APPI-MS at the time of this writing. Therefore, only reports that employed all three of the most popular API techniques are listed below.

1.4.1 Sequential Analyses by Electrospray Ionization, Atmospheric Pressure Chemical Ionization, and Atmospheric Pressure Photoionization

There have been a surprising number of reports comparing all three API techniques. These can be valuable for anyone undertaking analysis by any of these techniques because they often indicate what is the most sensitive and effective technique for a particular class of compounds. Among the classes of molecules or samples for which three API techniques have been compared head-to-head are these (by year): polyphenols (Parets et al., 2016), fungi (Cirigliano et al., 2016), petroleum (Huba et al., 2016), crude oil (Lababidi and Schrader, 2014), biofuels (Chiaberge et al., 2014), metalosalen catalysts (Słomińska et al., 2014), benzimidazoles (Martínez-Villalba et al., 2013), metabolites in plasma (Tian et al., 2013), estradiol (Keski-Rahkonen et al., 2013), drug metabolites (Louw et al., 2012), *Leishmania donovani* promastigotes (Imbert et al., 2012), fullerenes (Li et al., 2012), hormones (Vilaró et al., 2012), polyaromatic hydrocarbons (Ghislain et al., 2012), epoxides (Wu et al., 2011), environmental and wastewater sample analysis for personal care product components and pharmaceuticals by DART and API techniques (Beißmann et al., 2011), cycloartane derivatives (Cicek et al., 2011), carotenoids (Rivera et al., 2011), pharmaceuticals in wastewater (Garcia-Ac et al., 2011), illicit drugs in oral fluids (Wang et al., 2010), products of the Meerwein reaction with epoxides (Wu et al., 2010), lung cancer biomarkers (An et al., 2010), flame retardants (Mascolo et al., 2010), polar components by dielectric barrier discharge ionization and API techniques (Hayen et al., 2009), drugs and their impurities (Hommerson et al., 2009), dimers of 4-(methyl mercapto)-phenol (Wu et al., 2009), polymer additives (antioxidants, UV absorbers, and processing stabilizers) (Himmelsbach et al., 2009), estrogenic chemicals in wastewater (Lien et al., 2009), pentacyclic triterpenes (Rhourri-Frih et al., 2009), hydroperoxides from linalool and limonene (Nilsson et al., 2008), domoic acid (a neurotoxin) in shellfish (Pardo et al., 2007), polyaromatic hydrocarbons (Grosse and Letzel, 2007), plant melatonin, serotonin, and indole-3-acetic acid (Cao et al., 2006), fatty acids, MAGs, DAGs, and TAGs, (Cai and Syage, 2006b), drugs (Cai et al., 2005), pharmaceutical stereoisomers (Chen et al., 2005), dinitropyrene and aminonitropyrene (Straube et al., 2004), test compounds including polycyclic aromatic hydrocarbons, steroids, hormones, caffeine, and others (Syage et al., 2004), reserpine, nonpolar aromatics, vitamin D_3, and others (Hanold et al., 2004), and apomorphine, dobutamine, and entacapone metabolites in biological samples (Keski-Hynnilä et al., 2002).

1.4.2 Multimode Sources

Siegel et al. (1998) first reported a lab-built combination ESI/APCI source for analysis by infusion, and later followed that up using a commercially available ESI/APCI (referred to as ESCi) source for HPLC MS on a Micromass-Waters instrument (Siegel et al., 2002). This multimode source employed fast switching between modes. The data showed that the optimal flow rate were limited by ESI, which gave the highest signal at low flow rates (50−200 μL/min), whereas the APCI-MS signal increased up to 1.0 mL/min. The ESCi source was reported in detail by Gallagher et al. (2003).

In the same American Society for Mass Spectrometry (ASMS) session at the 2002 meeting, Castoro reported use of the Waters multimode source for analysis of a six-component mixture having a range of polarities using simultaneous ESI/APCI. In that same ASMS session, Kovarik et al. (2002) of MDS Sciex reported their version of a new commercially available ESI/APCI source that allowed operation in either simultaneous or switching modes.

In the same ASMS session in 2002, a commercially available multimode APPI/APCI source was introduced by a collaboration of Syagen Technology (now Morpho Detection), Thermo Finnigan (now ThermoScientific), and Agilent Technologies (Hanold et al., 2002). That source was described in detail by Syage et al. (2004). The source allowed operation in either mode separately or simultaneously. However, the krypton lamp is either turned on or off, and is not software switchable within analyses. This multimode ionization source is the one used on our ThermoScientific instruments, in contrast to the dedicated APPI source (Photospray) used in our previous reports that used the AB Sciex QTrap 4000 instrument.

Most recently, Syagen Technology introduced a multimode ESI/APPI source, referred to as an electrospray photoionization (ESPI) source (Short et al., 2007b; Short and Syage, 2008; Syage et al., 2004).

Having a single multimode source provides more value for an MS instrument investment, allowing more experiments to be performed on a single mass spectrometer. The value of having data from multiple API sources is demonstrated by the large number of reports of sequential API experiments described in the section above, which are only a subset of the many reports of sequential API techniques. Discussion of multiplexed ionization sources, in which multiple effluent streams enter an ionization source and are sequentially directed to a single mass analyzer, is not discussed here because there are many hundreds of reports employing this technology.

1.4.3 Simultaneous Parallel Liquid Chromatography Atmospheric Pressure Ionization Mass Spectrometry

With the utility of APCI-MS and ESI-MS for PL and TAG analysis firmly established in the early to mid 1990s, Byrdwell and Borchman (1997) used APCI-MS and ESI-MS sequentially for analysis of sphingolipids in the human eye lens. It was a natural next step to combine these instruments into a single analytical method. Shortly thereafter, Byrdwell (1998b) reported the first experiments using APCI-MS and ESI-MS together for simultaneous parallel detection coupled to HPLC. APCI-MS on a single-quadrupole instrument was used in parallel with ESI-MS and MS/MS on a TSQ instrument for identification of PL molecular species.

This “dual parallel MS” approach was then extended to TAGs and triacylglycerol oxidation products (Byrdwell and Neff, 2002). The intact ammonium adducts formed by ESI-MS combined with the structurally significant fragments formed by APCI-MS highlighted the complementary nature of these API sources.

Liu et al. (2002) demonstrated a parallel MS approach using ESI on both instruments, which takes advantage of the different scanning capabilities of ion trap versus TSQ mass analyzers. Although ion-trap instruments are ideal for MS^n, TSQ instruments allow precursor and neutral loss scanning experiments. The method was used for analysis of *in vitro* metabolism of ethinylestradiol in cryopreserved monkey and human hepatocytes.

Shortly thereafter, Byrdwell (2003b) reported the proof-of-concept report of a new and different configuration of instruments, in which two liquid chromatographs, one for normal-phase (NP)-HPLC and one for NARP-HPLC, were used in a column-switching arrangement with a different mass spectrometer attached to each HPLC. This arrangement was used for a total lipid analysis of polar and nonpolar lipids from a commercially available bovine brain extract. Polar lipids (e.g., phospholipids and glycosphingolipids) were analyzed by NP-HPLC with ESI-MS, MS/MS, and MS^3, and neutral lipids (e.g., ceramides, DAGs, TAGs) were analyzed by NARP-HPLC with ESI-MS and MS/MS. This gave rise to the nomenclature of LC*x*/MS*y* to refer to one or more HPLCs coupled to multiple mass spectrometers for simultaneous parallel analysis. The LC*x*/MS*y* applications up to 2005 were discussed in our previous book chapter on dual parallel MS for lipid analysis (Byrdwell, 2005b).

Byrdwell extended the original dual parallel MS approach (LC1/MS2), with APCI-MS and ESI-MS, to bovine brain and chicken egg yolk sphingolipids in commercially available samples (Byrdwell and Perry, 2006) and then bovine milk sphingolipid samples (Byrdwell and Perry, 2007).

LC2/MS2 analyses of bovine brain extract and a Bligh and Dyer (1959) extract of a fish filet were described in 2008 (Byrdwell, 2008). A review of multiple applications of LC1/MS2 and LC2/MS2 for analysis of TAGs, milk sphingolipids, and vitamin D by LC1/MS2 and the total lipid analysis of a bovine brain extract by LC2/MS2 were later reviewed (Byrdwell, 2010). Those reports were included in our earlier book chapter on multiple parallel MS techniques for lipid and vitamin D analysis (Byrdwell, 2011b).

Although it did not use HPLC−API-MS techniques, a recent report by Hejazi et al. (2014) deserves mention because it reported a dual parallel MS approach for gas chromatography (GC) using detection by two separate mass spectrometers with complementary hard and soft ionization sources. One was a single-quadrupole instrument operated in electron ionization (EI) mode, and the second was a time-of-flight instrument operated with a field ionization (FI) source. The FI-MS instrument produced protonated molecules, and the EI-MS instrument produced extensive fragmentation. This arrangement was applied to test compounds, fatty acid methyl esters (FAMEs), hydrocarbons, and yeast metabolites.

Parallel MS has now been raised to the next level by including a third mass spectrometer in a "triple parallel MS" arrangement, for LC1/MS3 (Byrdwell, 2011a). Instead of using all three different API techniques, this application used a new and sensitive instrument for APCI-MS of vitamin D in an oil-filled supplement combined with APCI-MS on an older, less-sensitive instrument for TAG analysis of the bulk excipient rice bran oil (RBO) combined with ESI-MS, MS/MS, and MS^3 of the RBO TAGs.

The LC1/MS*y* approach was extended even further in the first report of "quadruple parallel MS." In that report (Byrdwell, 2013b), high- and low-sensitivity APCI-MS were combined with ESI-MS and APPI-MS, for four mass spectrometers altogether, as shown below.

In an early review, we proposed the possibility of LC2/MS4 (Byrdwell, 2010) and later extrapolated to absurdity with the proposition of up to LC2/MS8 (Byrdwell, 2013a)! Although we have not yet reached that level of complexity, we do present here the first preliminary data demonstrating a new approach to comprehensive two-dimensional liquid chromatography (2D-LC) (LC × LC), in which

two mass spectrometers are used to monitor the first dimension, and two mass spectrometers monitor the second dimension in an LC2/MS4 (LC1/MS2 × LC1/MS2) configuration.

2. EXPERIMENTAL

Specific details for operating conditions for various instruments and detectors are presented in specific publications in the literature. Here, we present generic conditions and emphasize the special considerations that are unique to each API type.

2.1 THE WIRELESS COMMUNICATION CONTACT CLOSURE SYSTEM

Coupling liquid chromatographs to mass spectrometers is often done using contact closures or relays from the liquid chromatograph's autosampler to other detectors, to coordinate the start of the instruments involved in experiments. When multiple detectors are employed, it is convenient to have a contact closure distribution manifold, in which a single contact closure can be distributed to multiple detectors. Previously, we described the LC*x*/MS*y* switching panel that accomplished selectable contact closure distribution (Byrdwell, 2011b). That system has now been upgraded and made more robust by converting it to a wireless communication contact closure system (WCCCS), shown in Fig. 10.3 and

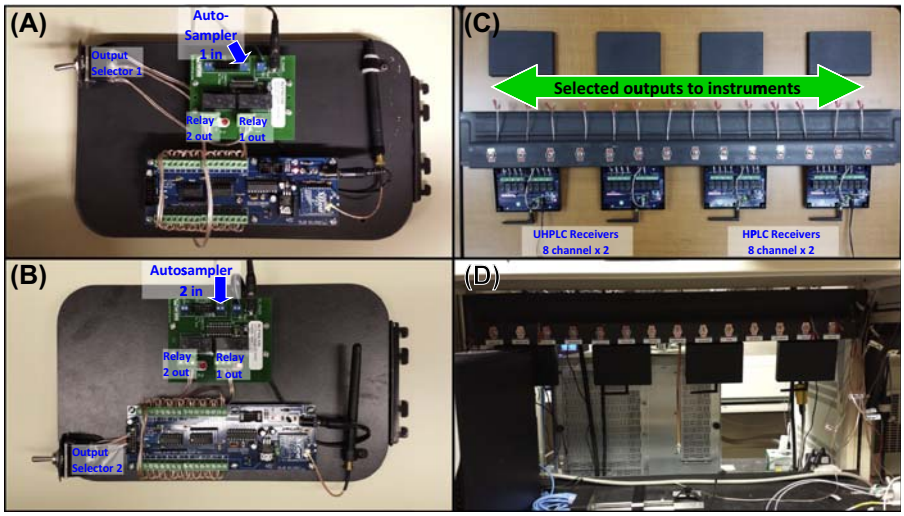

FIGURE 10.3

Wireless communication contact closure system (WCCCS). (A) Two-channel voltage-to-relay converter connected to 16-channel wireless sending unit #1 for high-performance liquid chromatography (HPLC) autosampler; (B) two-channel voltage-to-relay converter connected to wireless sending unit #2 for ultra-high performance liquid chromatography (UHPLC) autosampler; (C) wireless receiving modules attached to wire distribution trace with switches mounted—left two receiving modules for UHPLC, right two receiving modules for HPLC; (D) WCCCS receiving module and switching system installed and operational. Switches in UP position select contact closure from HPLC, in DOWN position select contact closure from UHPLC.

described in detail elsewhere (Byrdwell, 2014a). Using wireless communication eliminated the hard-wired connections between instruments, and kept electronic problems (such as failure of a board in a single syringe pump or detector) from propagating through the system. The red lights illuminated on the boards in Fig. 10.3C show test signals being received in a conference room down the hall from the sending units in the lab. The wireless signals have a range of a mile, which is far more than adequate for intralab communication.

The WCCCS provides maximum flexibility in setting up experiments. Mass spectrometers, other detectors, syringe pumps, and other devices can be selected to participate in experiments simply by flipping a switch to select or deselect the devices. For example, Fig. 10.4 shows a schematic diagram of the arrangement of instruments used for the first "quadruple parallel MS," or LC1/MS4, experiment recently reported (Byrdwell, 2015b,c). Since publication of that work, the TSQ 7000 mass spectrometer has been replaced with a TSQ Quantum Access Max mass spectrometer with an APPI source, and the QTrap 4000 mass spectrometer has been replaced with a Q Exactive HRAM Orbitrap instrument that is operated in ESI-MS^n mode. Using the WCCCS, new instruments are easily incorporated into the system by simply connecting the start signal inputs for the new instruments to the outputs of the WCCCS, shown in Fig. 10.3C and D.

Because we use both HPLC and ultra-high performance LC (UHPLC), we have two wireless sending boards; one connected to each LC autosampler. The two LCs and four mass spectrometers allow us to perform column-switching LC2/MS4 experiments (Byrdwell, 2013a).

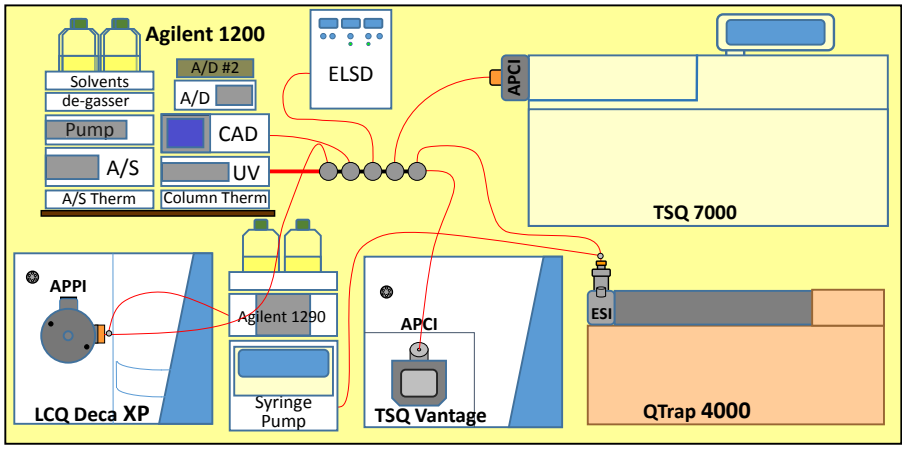

FIGURE 10.4

Arrangement of instruments for the first report of LC1/MS4, quadruple parallel mass spectrometry. Effluent after the UV detector (nondestructive) is split via Valco tees and fused-silica capillary tubing to go to various mass spectrometers and other detectors (ELSD and CAD). Electrolyte is supplied via syringe pump for electrospray ionization mass spectrometry and acetone dopant supplied via by an Agilent 1290 for APPI-MS. High- and low-sensitivity atmospheric pressure chemical ionization mass spectrometry used for vitamin D and triacylglycerols, respectively. *APPI*, atmospheric pressure photoionization; *CAD*, charged aerosol detector; *ELSD*, evaporative light scattering detector.

2.2 ATMOSPHERIC PRESSURE CHEMICAL IONIZATION MASS SPECTROMETRY

Although conditions should be optimized on each instrument, typical APCI-MS conditions for TAGs are as follows: vaporizer heater 400°C, capillary heater 265°C, sheath gas 25−40 arbitrary units (au), auxiliary gas 5−10 au, and corona current 4.0 μA. Signal is especially susceptible to the temperatures used, with a lower vaporizer temperature giving less signal and also less fragmentation.

APCI-MS is a very versatile ionization method that is effective for ionization of many classes of molecules. Very few classes of molecules do not respond well to APCI-MS. The main problems with APCI-MS stem from the "CI" part of the process, i.e., chemical ionization. First of all, APCI-MS typically produces more chemical background noise than other API techniques, especially ESI. The corona discharge formed at the tip of the APCI corona needle is more energetic than the voltage supplied by ESI and produces both more fragmentation and more by-product ions from the LC effluent solvent(s) and ambient components.

More problematic than overall noise, however, is the polymerization of some solvents on the tip of the APCI corona needle. Reactive solvents, such as ACN, may polymerize to form a black residue on the tip of the corona needle that greatly reduces sensitivity over the course of a long set of experiments. In our experience of using an ACN/DCM gradient for NARP-HPLC, sensitivity declines sharply after approximately three sequential runs of a long ACN/DCM gradient, or ~10−12 h of run time. Although adequate results are usually obtained despite formation of this residue, signal levels can be better maintained if a sequence of runs is paused periodically and the corona needle cleaned. The use of only MeOH, ethanol (EtOH), DCM, and other solvents minimizes or even eliminates formation of this residue. However, ACN has such beneficial effects on the chromatographic peak shapes and other elution characteristics that it is often worth enduring the residue formation to attain optimal chromatographic separation.

If the corona needle is cleaned daily, residue formation does not become problematic. But if the instrument is run around the clock for several days without pausing sequences to clean the needle, residue formation can cause a loss of sensitivity. Furthermore, formation of the ACN adduct seems to be source design and instrument dependent. In personal communications, Prof. Holčapek has indicated that residue formation is not a substantial problem on their APCI-MS instrument, noting that the corona needle is cleaned daily.

2.3 ATMOSPHERIC PRESSURE PHOTOIONIZATION MASS SPECTROMETRY

The APPI source is very similar to the APCI source, having an inlet fused-silica capillary that sprays (via sheath gas) down the center of a heated vaporizer. But ionization occurs from passing in front of a krypton lamp having emission energies of 10.0 and 10.6 eV, instead of a corona discharge needle (as in APCI). Because of these similarities, the operating conditions for our newer APPI source (on TSQ Quantum Access Max) and APCI source (on TSQ Vantage EMR) from the same manufacturer are very similar. For APPI-MS, we now typically use: vaporizer heater 400°C, capillary heater 265°C, sheath gas 25−40 arbitrary units (au), auxiliary gas 5−10 au.

There are two important differences between the experimental conditions for APPI and APCI. First, the best sensitivity is usually obtained by incorporating a dopant into the flow stream, which was well demonstrated by Syage and coworkers (Cai et al., 2007b). For our NARP-HPLC/APPI-MS applications, we use a syringe pump to provide acetone at 40−50 μL/min via a tee connected to the ion source inlet. The syringe pump is connected to the WCCCS to synchronize refilling the dopant pump between runs.

The second important difference between APPI and APCI is the fact that it is a noncontact source, meaning the effluent passes by the krypton lamp without touching it, or at least without accumulating a substantial residue on it. This completely overcomes the problem of residue formation on the APCI corona needle tip, making APPI a more robust ionization source for extended sequences of runs. This is one of the primary benefits that APPI has over APCI.

Thus, with all else being very similar, the APPI source has the great advantage of being able to operate for extended periods of time without fouling or needing cleaning, but usually requires the use of a dopant supplied by a secondary pump to obtain maximum sensitivity.

2.4 ELECTROSPRAY IONIZATION MASS SPECTROMETRY

The mechanism of ESI and practical considerations for implementing it has been thoroughly discussed over the last decades, such as in the excellent volume by Cole (1997). In most cases, HPLC/ESI-MS incorporates an electrolyte into the mobile phase to promote ionization. This electrolyte should be a volatile buffer to avoid clogging the inlet of the mass spectrometer. In cases of HPLC that does not include an aqueous component, such as NARP-HPLC, the electrolyte is routinely supplied postcolumn via a tee attached to the ESI inlet. In our applications to multiple parallel MS, we use ammonium formate supplied via a syringe pump at 20−50 μL/min. This dual piston syringe pump is connected to the WCCCS described above, to synchronize refilling of the pistons between runs. Because of the ACN/DCM solvent system used for NARP-HPLC of TAGs, we use an electrolyte that is 20% of 100 mM NH_4OCOH in ACN (or more recently in MeOH), to give 20 mM NH_4OCOH in ACN (or MeOH) 1:4, which is more miscible with the mobile phase than aqueous ammonium formate alone.

Because we routinely perform sequences of runs that run around the clock for up to multiple days, we have found that even 20 mM NH_4OCOH in ACN 1:4 can clog the ESI needle over an extended run time. Therefore, we plumb the electrolyte through the electronic switching valve on the front of the mass spectrometer, along with water supplied by an older LC pump, as shown in Fig. 10.5. Timed events included in MS methods cause water to wash the electronic valve, postcolumn tee, and ESI source from 0.5 min before the end of each run, through the injection process, then to ~5.5 min (equal to the dead time) into the next run. Each instrument has its own idiosyncrasies, and the Q Exactive ESI source is much more prone to clogging, even with the between-run washing implemented.

We prefer ammonium formate over lithium hydroxide (LiOH) as the electrolyte for two primary reasons. First, ESI-MS/MS with LiOH produces twice as many DAG-like fragments as ammonium adducts do. As shown by Hsu and Turk (1999), $[M + Li]^+$ precursors produce ions from loss of FAs as $[M + Li - RCOOH]^+$ and $[M + Li - RCOOLi]^+$. Thus, the overall population of ions is split into more fragments, requiring processing and treatment of more mass traces than those in data from ammonium adducts, which produce almost exclusively $[M + NH_4 - RCOONH_4]^+$ ions.

2.5 OTHER DETECTORS AND PUMPS

We always acquire data from an evaporative light scattering detector (ELSD) and corona CAD, as well as from a UV detector (both single-channel and spectra), in addition to the MS data. Although the ELSD and CAD are not as sensitive as any of the mass spectrometers we now use, they nevertheless provide a needed confirmatory tool. Because there are numerous issues that can cause a loss of peaks

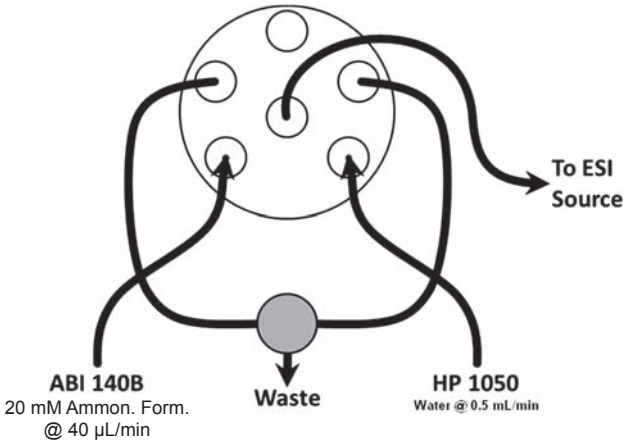

FIGURE 10.5

Plumbing diagram for electrospray ionization (ESI) source rinsing between runs using deionized water supplied by an HP 1050 pump. The outlet from the valve goes as an input to the perpendicular arm of a tee attached to the ESI source grounding nut. Ammonium formate supplied during runs, water supplied between runs.

by MS, such as failure of the dopant pump for APPI-MS or failure of the electrolyte pump or clogged needle for ESI-MS, it is very useful to have additional signals to monitor the presence of chromatographic peaks. The ELSD and CAD respond surprising differently to TAGs, which is their main application in our lab.

Recently, as we have expanded beyond vitamin D to other fat-soluble vitamins, especially tocopherols, we have added a fluorescence detector (FLD) after the UV detector. The FLD has a short flow path and is also nondestructive, so the full effluent before splitting flows through it, and does not negatively impact chromatographic parameters to a noticeable degree. Emission wavelengths for the various fat-soluble vitamins are summarized in the classic work of G.F.M. Ball (1988).

Thus, our experiments overall now routinely employ seven or eight detectors: (1) UV (full scan and single-channel); (2) fluorescence; (3) corona CAD; (4) ELSD; (5) APCI-MS on a TSQ Vantage EMR; (6) APPI-MS on a TSQ Quantum Access Max; (7) ESI-MS on a Q Exactive Orbitrap; and (8) secondary ESI-, APCI-, or APPI-MS^n on an LCQ Deca XP hyperbolic ion trap. Flow to these detectors is directed by a series of Valco tees, such as those described in detail previously (Byrdwell, 2011a). The amount of effluent going to each detector is dictated by the length and internal diameter of the fused-silica capillary tubing between the splitter and the detector. Generally, 2D detectors (CAD and ELSD) are less sensitive and so have a higher flow, e.g., 250 µL/min, to them, whereas mass spectrometers are more sensitive and use lower flow rates, around 100−150 µL/min.

UHPLC is popular nowadays, and we use a UHPLC instrument as the second dimension in column-switching and comprehensive 2D analyses. However, the higher flow rates typically used by HPLC are more amenable to splitting into multiple branches for flow to multiple detectors. Therefore, we use HPLC as the primary LC system for most of our multiple parallel MS experiments.

3. RESULTS

3.1 QUADRUPLE PARALLEL MASS SPECTROMETRY #1 (LC1/MS4)

The first report of one liquid chromatograph coupled to four mass spectrometers (LC1/MS4) using three different API sources by Byrdwell (2013b) utilized the arrangement of instruments pictured in Fig. 10.4 and showed chromatograms and spectra from olive oil and vitamin D. The normal method of quantification had to be modified to accommodate ESI charge saturation on the QTrap 4000. Also, an improvement to quantification was implemented by including the $1 \times {}^{13}C$ isotopic peaks in quantification of all molecules. Because TAGs differ by double bonds, which are two mass units, the total signal integrated area can be increased with no loss of specificity by including the first isotopic peak. This benefit is now routinely incorporated into our analytical methodologies.

Later, the QTrap 4000 was changed from ESI-MS to APPI-MS, and the LCQ Deca XP was changed from APPI-MS to ESI-MS because of the ESI charge saturation mentioned. That arrangement was used for the LC1/MS4 experiments used to prove the accuracy of the Updated Bottom Up Solution (UBUS) for APCI-MS of soybean oil (Byrdwell, 2015c), and all of the trends in critical ratios from APCI-MS of TAGs were explored in greater detail. In an accompanying publication, it was proved that the UBUS applies equally well to APPI-MS and ESI-MS of TAGs (Byrdwell, 2015b). Chromatograms and mass spectra of those samples, not previously shown, are given in Figs. 10.6–10.9. The quantification of TAGs from these samples was given in the two previous reports and showed that the response-factor-adjusted TAG compositions, and especially the resultant FA compositions, agreed well across the three API techniques, using the response factor approach of Byrdwell et al. (2001).

Because the TSQ Vantage EMR mass spectrometer (Fig. 10.6) did not suffer from signal saturation like the QTrap 5500 did, the second APCI-MS instrument (Fig. 10.9) used for LC1/MS4 experiments simply provided backup data and confirmation of molecular species identities. Similar to the LC1/MS3 reports, however, the TSQ 7000 was not as sensitive for vitamin D analysis, as seen by comparison of Figs. 10.6C–10.9B. Fig. 10.7 shows that APPI-MS mass spectra are very similar to APCI-MS spectra, and Fig. 10.7B shows that APPI-MS was similarly useful for quantification of vitamin D, with a good S/N. However, because the Photospray source was new, it produced a substantial amount of ions from a variety of phthalates (i.e., dibutyl-, dioctyl-, and nonyl, decyl-phthalates) commonly used as plasticizers. Many of the trends observed in the critical ratios for APCI-MS were observed for APPI-MS, but the range of values of $[MH]^+/\Sigma[DAG]^+$ was larger for APPI-MS (Byrdwell, 2015b).

3.2 QUADRUPLE PARALLEL MASS SPECTROMETRY #2 (LC1/MS4)

After the initial dilute-and-shoot (D&S) application of LC1/MS4, we expanded the range of samples to which the technique was applicable by applying it to dry powdered samples. These required a filtration step through a syringe-mounted filter, and the powders were not fully soluble, so the sample was extracted from the excipient powder, instead of being dissolved. Thus, the D&S procedure became an extract-filter-shoot (EFS) process. Because of this, we had to confirm complete extraction of the sample from the excipient by analyzing a similar standard reference material (SRM). For this purpose, we performed the EFS procedure on National Institute of Standards and Technology SRM 3280, a compressed powder vitamin supplement. The commercially available supplement we then used the EFS procedure on was a vitamin D_2 supplement having rice bran flour as the excipient powder. The

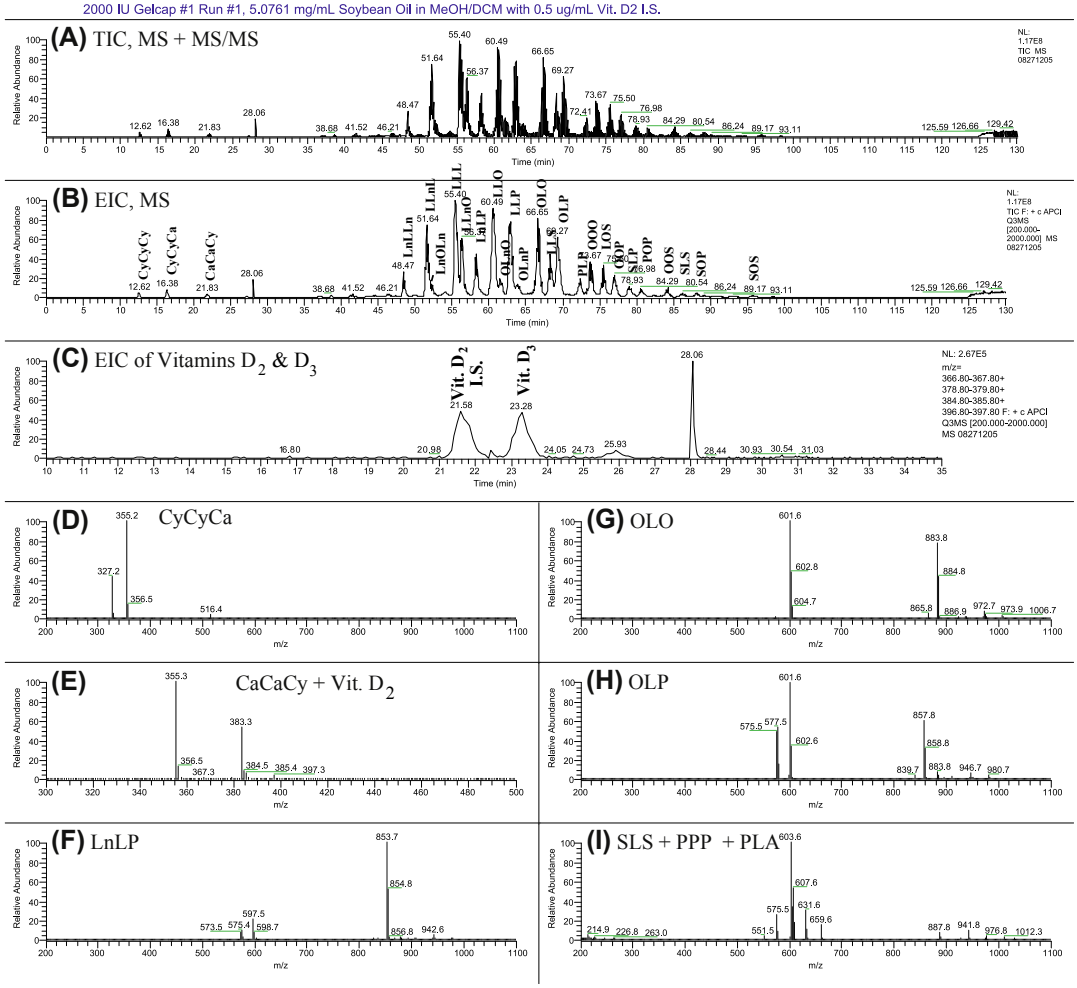

FIGURE 10.6

APCI-MS(/MS) of soybean oil in dietary supplement containing vitamin D_3 from fish oil, from TSQ Vantage EMR mass spectrometer. (A) Total ion current chromatogram (TIC); (B) extracted ion chromatogram (EIC) of full scans; (C) EIC of vitamins D_2 and D_3; (D) mass spectrum of CyCyCa; (E) CaCaCy and vitamin D_2 (internal standard); (F) LnLP; (G) OLO; (H) OLP; and (I) SLS + PPP + PLA. *A*, arachidic, 20:0; *Ca*, capric, 10:0; *Cy*, caprylic, 8:0; *L*, linoleic, 18:2; *Ln*, linolenic, 18:3; *O*, oleic, 18:1; *P*, palmitic, 16:0; *S*, stearic, 18:0. Labels are regiospecific at *sn*-2. *APCI-MS*, atmospheric pressure chemical ionization mass spectrometry; *TSQ*, tandem sector quadrupole.

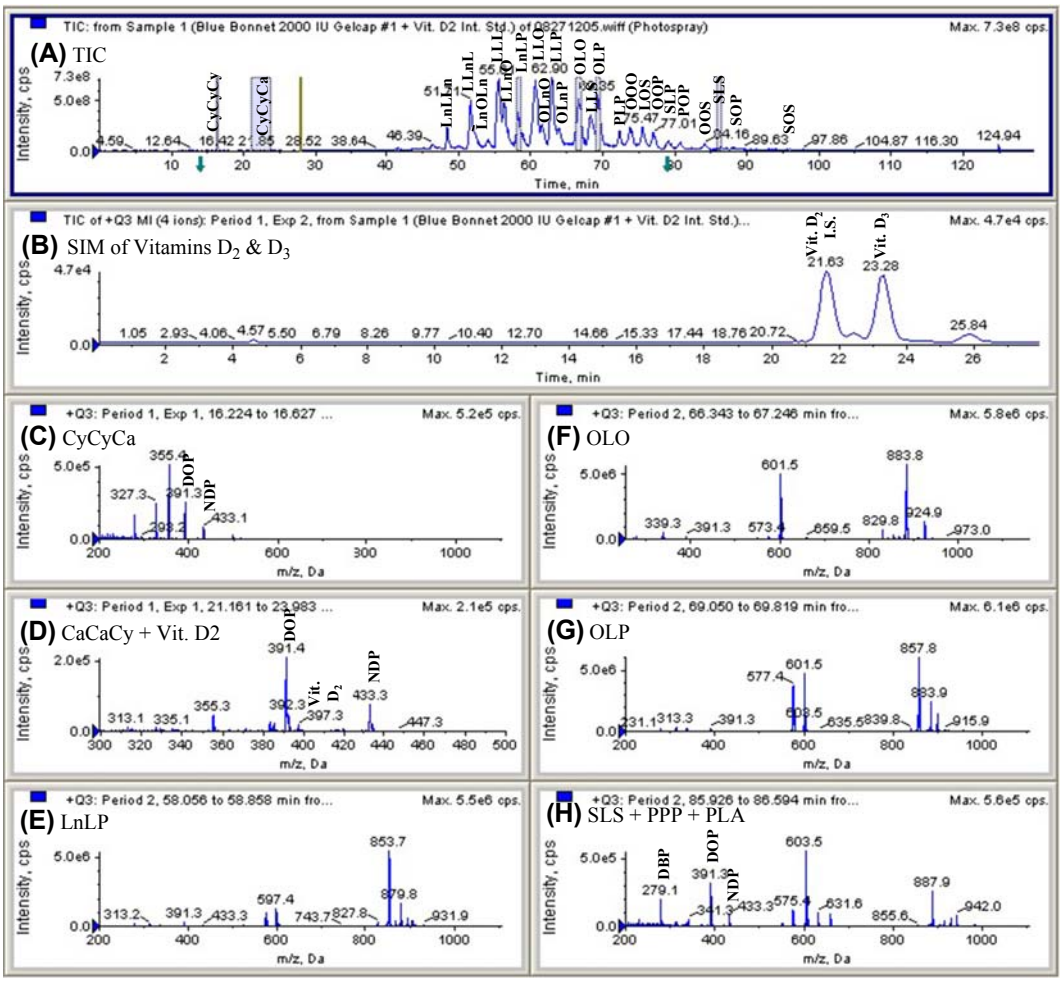

FIGURE 10.7

APPI-MS of soybean oil in dietary supplement containing vitamin D_3 from fish oil, on QTrap 4000 hybrid mass spectrometer. (A) Total ion current chromatogram (TIC); (B) selected ion monitoring (SIM) of vitamins D_2 and D_3; (C) mass spectrum of CyCyCa; (D) CaCaCy and vitamin D_2 (internal standard); (E) LnLP; (F) OLO; (G) OLP; and (H) SLS + PPP + PLA. *DBP*, dibutyl phthalate; *DOP*, dioctyl phthalate; *NDP*, nonyl, decyl phthalate; other abbreviations are given in Fig. 10.6. *APPI-MS*, atmospheric pressure photoionization mass spectrometry.

Phthalates from new Photospray source.

instrument arrangement in Fig. 10.4 was used for the EFS analysis. Figs. 10.10–10.12 show APCI, APPI, and ESI data from the EFS experiments.

Vitamin D was easily analyzed by APCI-MS, Fig. 10.10C, and results by several instrumental and calculation approaches were compared. Extracted ion chromatograms (EICs) of vitamin D ions from full scans, selected ion monitoring, and multiple reaction monitoring analyses were compared using

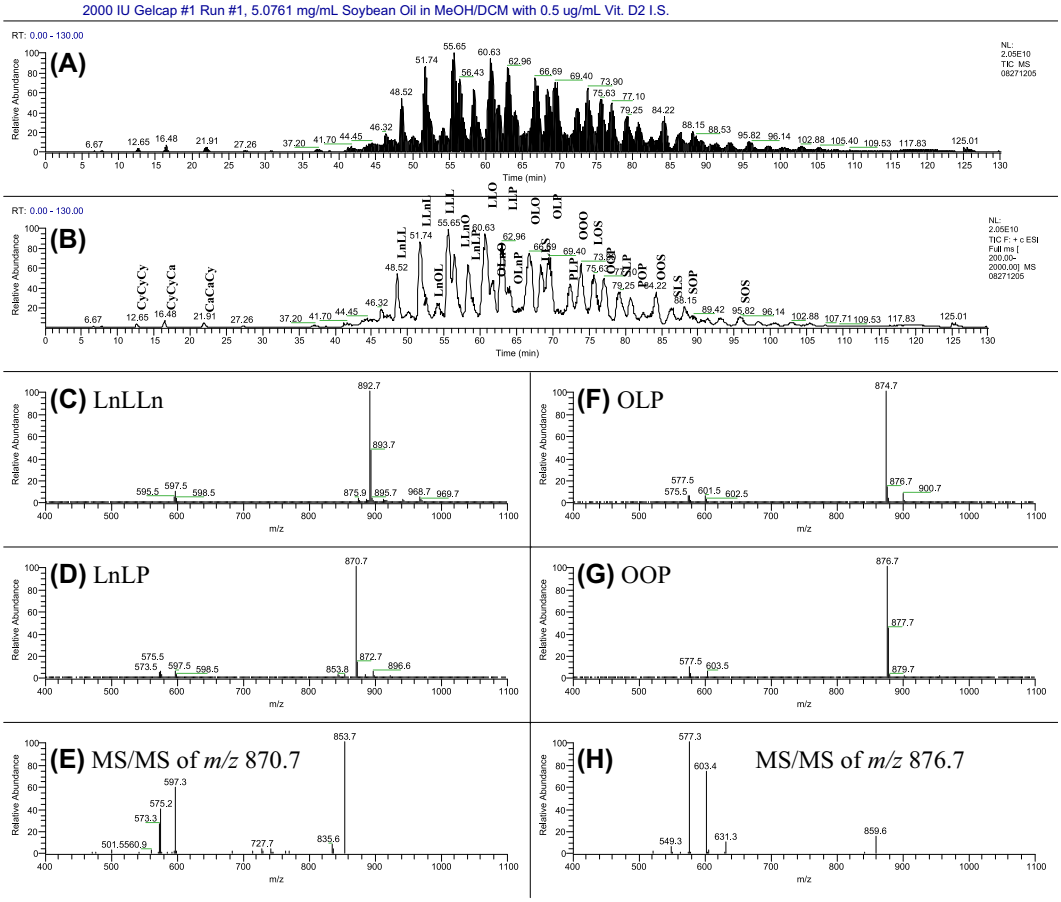

FIGURE 10.8

NARP-HPLC–ESI-MS of soybean-oil-based dietary supplement containing 2000 IU vitamin D_3 on LCQ Deca XP ion-trap mass spectrometer. Mass spectra show ammonium adducts, $[M + NH_4]^+$. (A) Total ion current chromatogram (TIC); (B) extracted ion chromatogram (EIC) of full scans; (C) LnLLn; (D) LnLP; (E) MS/MS spectrum of $[LnLP + NH_4]^+$ *m/z* 870.7; (F) OLP; (G) OOP; and (H) MS/MS spectrum of $[OOP + NH_4]^+$ *m/z* 876.7. Vitamin D_3 from distilled fish oil included three short-chain triacylglycerols (TAGs), CyCyCy, CyCyCa, and CaCaCy. TAGs labeled with most abundant regioisomer identified by APCI-MS. Fatty acid abbreviations are given in Fig. 10.6. *APCI-MS*, atmospheric pressure chemical ionization mass spectrometry; *ESI-MS*, electrospray ionization mass spectrometry; *NARP-HPLC*, nonaqueous reversed-phase high-performance liquid chromatography.

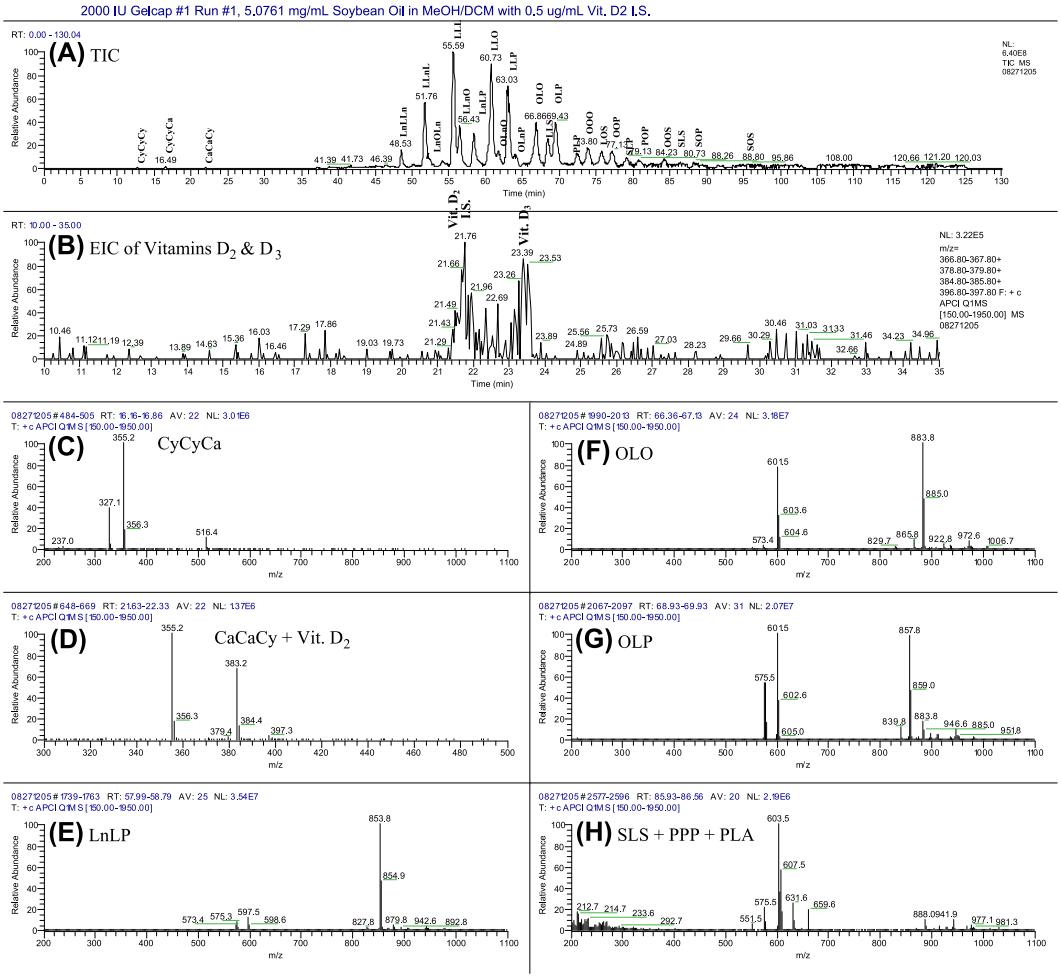

FIGURE 10.9

APCI-MS(/MS) of soybean oil in dietary supplement containing vitamin D_3 from fish oil. (A) Total ion current chromatogram (TIC); (B) EIC of vitamins D_2 and D_3; (C) mass spectrum of CyCyCa; (D) CaCaCy and vitamin D_2 (internal standard); (E) LnLP; (F) OLO; (G) OLP; and (H) SLS + PPP + PLA. Abbreviations are given in Fig. 10.6. *APCI-MS*, atmospheric pressure chemical ionization mass spectrometry; *EIC*, extracted ion chromatogram.

internal standard (IS) calibration curve, external standard calibration curve, and internal standard response factor approaches. As expected, the IS approaches produced results closest to the SRM's certified value. APCI-MS and APPI-MS gave surprisingly good chromatograms and mass spectra of the rice flour oil extracted from the excipient powder in the commercial supplement sample, as seen in the figures. However, only APCI-MS on the TSQ Vantage EMR instrument was sensitive enough for accurate quantification of vitamin D_2. APPI-MS on the LCQ Deca XP mass spectrometer (an older hyperbolic ion-trap instrument) was not sensitive enough for quantification, so no EIC for vitamin D is

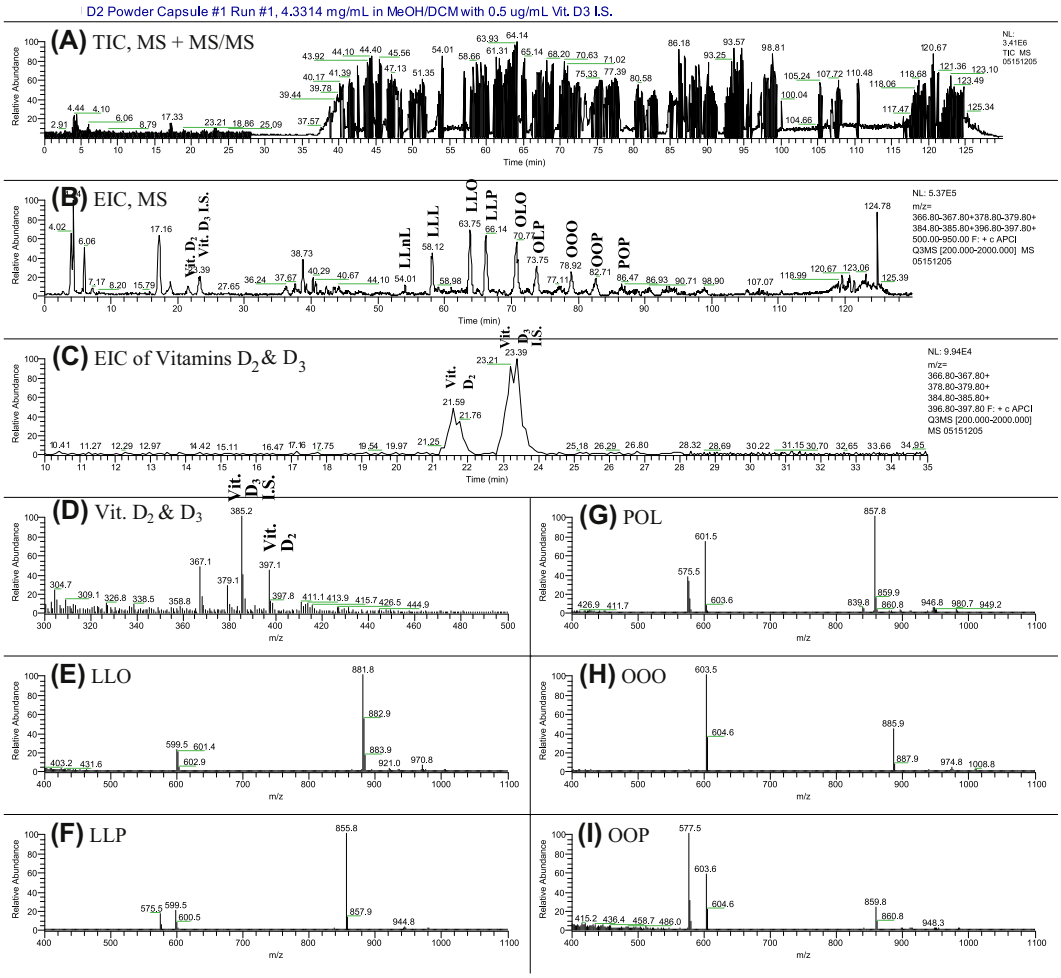

FIGURE 10.10

APCI-MS of rice flour oil from extract-filter-shoot analysis of vitamin D_2 powdered supplement, on TSQ Vantage EMR mass spectrometer. (A) TIC; (B) EIC of full scans from *m/z* 500−950 plus vitamin D; (C) EIC of vitamin D_2 and D_3 ions; (D) mass spectrum of vitamins D_2 and D_3; (E) LLO; (F) LLP; (G) POL; (H) OOO; and (I) OOP. Abbreviations are given in Fig. 10.6. Labels not regiospecific. *APCI-MS*, atmospheric pressure chemical ionization mass spectrometry; *EIC*, extracted ion chromatogram; *TIC*, total ion current chromatogram; *TSQ*, tandem sector quadrupole.

shown in Fig. 10.11. Another point to mention is that many people do not realize that the concentration of analyte affects the mass calibration on these TSQ instruments, causing a slight shift in masses compared to samples where TAGs are present at higher concentrations.

The powdered samples produced more background and did not give a good enough S/N for ESI-MS analysis of TAGs or vitamin D on the QTrap 4000 instrument, so only a total ion current

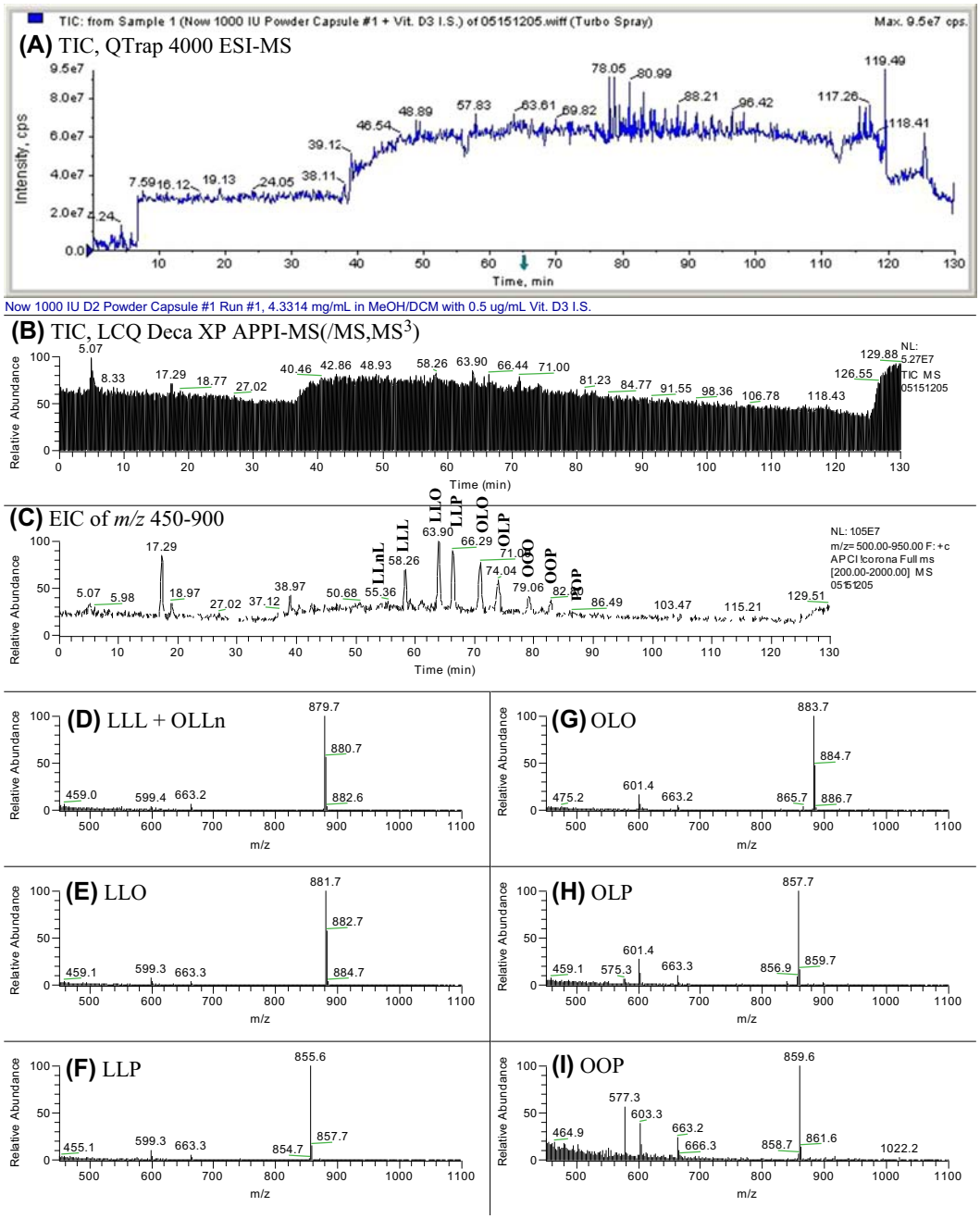

FIGURE 10.11

Electrospray ionization mass spectrometry (ESI-MS) on QTrap 4000 hybrid mass spectrometer and atmospheric pressure photoionization mass spectrometry (APPI-MS) on LCQ Deca XP ion-trap mass spectrometer data for rice flour oil from extract-filter-shoot experiment applied to vitamin D_2 dry powdered supplement. (A) Total ion current chromatogram (TIC) of ESI-MS on QTrap 4000; (B) TIC of APPI-MS on LCQ Deca XP; (C) extracted ion chromatogram (EIC) of *m/z* 500−950; (D) mass spectrum of LLL and OLLn; (E) LLO; (F) LLP; (G) OLO; (H) OLP; and (I) OOP. Abbreviations are given in Fig. 10.6. Labels not regiospecific.

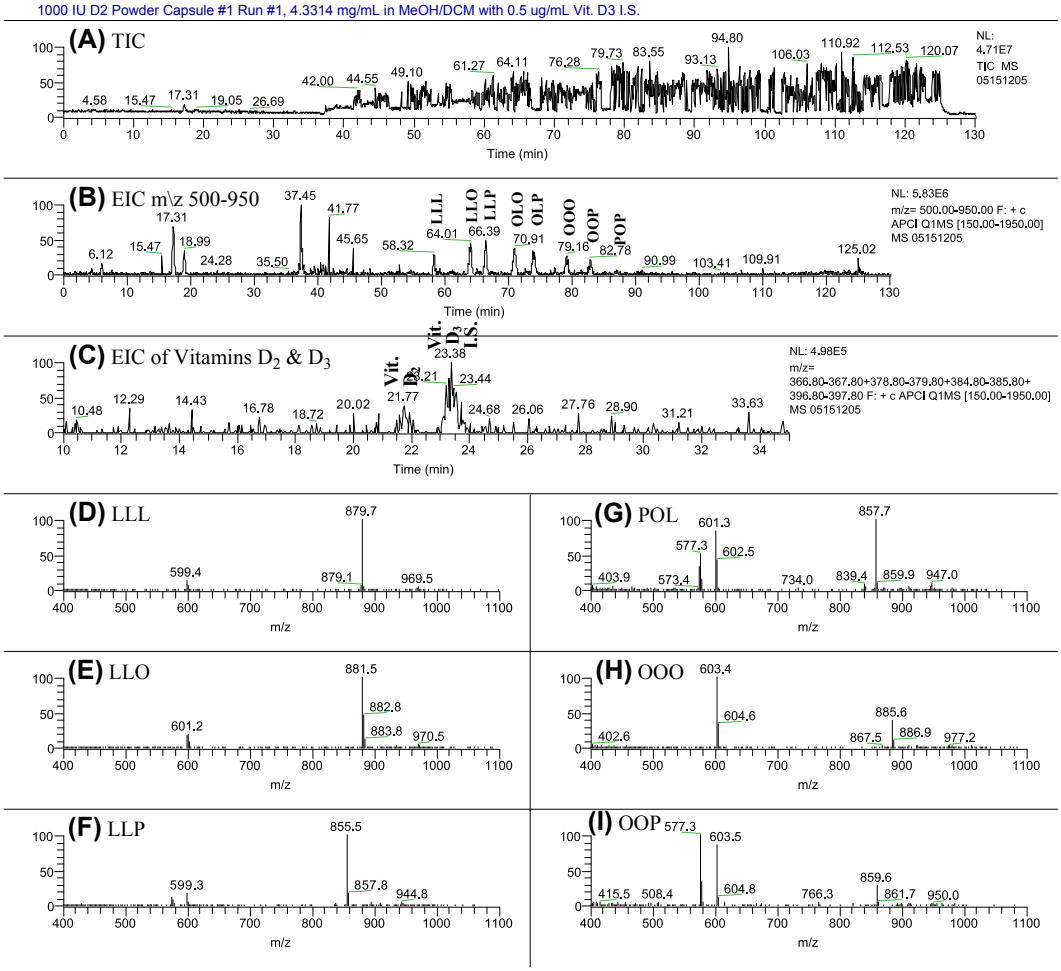

FIGURE 10.12

APCI-MS of rice flour oil from extract-filter-shoot analysis of vitamin D_2 powdered supplement, on TSQ 7000 mass spectrometer. (A) Total ion current chromatogram (TIC); (B) extracted ion chromatogram (EIC) of *m/z* 500-950; (C) EIC of vitamin D_2 and D_3 ions; (D) mass spectrum of LLL; (E) LLO; (F) LLP; (G) POL; (H) OOO; and (I) OOP. Abbreviations are given in Fig. 10.6. Labels not regiospecific. *APCI-MS*, atmospheric pressure chemical ionization mass spectrometry; *TSQ*, tandem sector quadrupole.

chromatogram (TIC) is shown for ESI-MS in Fig. 10.11A. This was especially evident in the UV chromatograms for SRM 3280 shown elsewhere (Byrdwell, 2014b), which clearly showed a large sloping background that rendered UV data unreliable for that sample. Furthermore, the mass spectra clearly showed an interfering species, tentatively identified as a vitamin E homolog, present at a much higher level, as discussed in that report. Those data clearly showed the danger of relying on UV data without confirmation of peak purity by MS. The problem with UV data was easily overcome by

quantification of vitamin D_2 using the APCI-MS data. Fig. 10.12 showed that APCI-MS on the TSQ 7000 mass spectrometer was also adequate for TAG quantification, although the S/N for vitamin D, Fig. 10.12C, was not as good as that on the newer APCI-MS instrument.

The data in these sections demonstrate not only the similarities between APCI-MS and APPI-MS and the complementary data obtained by ESI-MS but also that each instrument has its own peculiarities, sensitivity, tendency for the ion source to undergo charge saturation, and other factors. Therefore, it is beneficial to have as many API sources for each instrument available as possible, and these can be combined in a variety of configurations for different experiments that are applicable to different types of samples.

3.3 LC × LC WITH QUADRUPLE PARALLEL MASS SPECTROMETRY

Conventional comprehensive 2D-LC is done by having a short second-dimension chromatographic run, such that several ^{2}D runs can be accomplished over the width of a ^{1}D peak, to adequately reconstruct the peak profile. As Davis et al. (2008) discussed elsewhere, "undersampling" results when too few samples are taken across a peak (also see Chapter 7). Often, a low flow rate is used in the first dimension, so all of the effluent can be transferred, via a switching valve, to the second-dimension chromatograph. A low first-dimension flow rate also minimizes solvent incompatibility between the two dimensions and produces peaks that are broad enough to be effectively transferred to the second dimension (personal communication with L. Mondello).

For lipids, Mondello et al. (Dugoet al., 2006a,b; Mondello et al., 2005) and others (van der Klift et al., 2008; Yang et al., 2012) have pioneered the use of comprehensive LC × LC using Ag-ion chromatography, which does a partial separation into groups by degree of unsaturation, coupled to NARP-HPLC, which further separates into distinct peaks by equivalent carbon number (ECN), where the ECN = # carbons - 2 × # double bonds. Other combinations of stationary phases have also been applied to TAG analysis (Bang and Moon, 2013; Holčapek et al., 2015). Comprehensive LC × LC analysis of lipids has been reviewed elsewhere (Dugo et al., 2008; Guo and Lankmayr, 2010; Tranchida et al., 2007).

Instead of using an Ag-ion partial separation in the first dimension, we already had an NARP-HPLC separation that we liked for the first dimension, and just wanted to use Ag-ion UHPLC to "tease apart" a few remaining overlaps, and separate isomers. Two problems were immediately encountered. The first was that the full selection of columns available for HPLC is not yet available for UHPLC. Chiral columns and charge-exchange columns for UHPLC are available from only a few select manufacturers, and a Ag-ion UHPLC column is not yet commercially available. Thus, we made our own Ag-ion UHPLC column from a strong cation exchange column that we loaded with silver using an approach to be described elsewhere. The second problem was that our standard NARP-HPLC method utilized a substantial amount of ACN, which caused a lack of retention on the Ag-ion UHPLC column. Thus, we are working on development and optimization of a MeOH/EtOH/DCM gradient for NARP-HPLC that is compatible with the Ag-ion second dimension. The resolution is not quite as good as our standard MeOH/ACN/DCM method, so we are giving up a little resolution in the first dimension but getting good separation in the second dimension.

We bypassed the problem of undersampling by using two mass spectrometers, operated in APCI-MS and ESI-HRAM-MS modes, as well as UV, FLD, CAD, and ELSD to monitor the first dimension, coupled with two other mass spectrometers, operated in APPI-MS and ESI-MS modes, plus UV, for a comprehensive LC2/MS4, or LC1/MS2 × LC1/MS2, analysis, shown schematically in

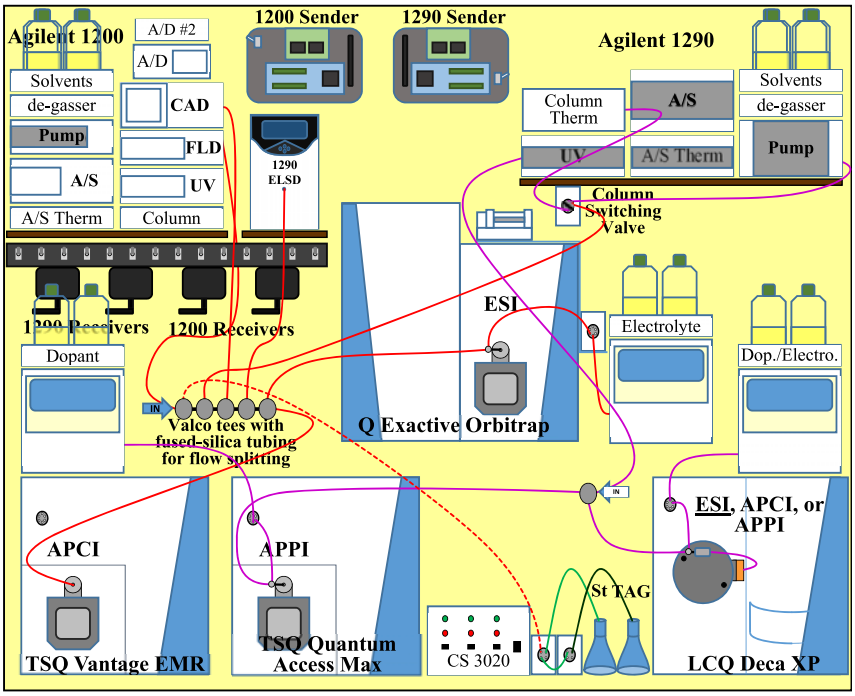

FIGURE 10.13

Schematic of arrangement of instruments for LC2/MS4 (LC1MS2 × LC1/MS2) experiments. Two mass spectrometers (APCI-MS and ESI-MS) monitor first dimension, along with a UV detector, fluorescence detector (FLD), corona charged aerosol detector (CAD), and an evaporative light scattering detector (ELSD). Two other mass spectrometers (APCI-MS or ESI-MS and APPI-MS) monitor second dimension, along with UV detector. Optional valves collect elution ranges for sterols (ST) and triacylglycerols (TAGs) to allow further analysis (e.g., FAME) by GC and/or GC-MS. All systems synchronized by wireless communication contact closure system. Additional HPLC pumps for deionized water wash of ESI probes between runs not shown. Connecting fused-silica capillary tubing not shown actual size; wiring from autosamplers (A/S) to wireless senders and from wireless receivers to instruments not shown. *APCI-MS*, atmospheric pressure chemical ionization mass spectrometry; *APPI-MS*, atmospheric pressure photoionization mass spectrometry; *ESI-MS*, electrospray ionization mass spectrometry.

Fig. 10.13. This is pursuant to the conjectured LC2/MS8 mentioned in jest in our earlier featured report (Byrdwell, 2013a). Because we don't have to reconstruct the first dimension only from a MS detector (or UV detector) at the end of the second dimension, we can use longer second-dimension runs that would cause undersampling in conventional 2D-LC analyses. Thus, we are using "slow" comprehensive 2D-LC compared with the normal "fast" 2D-LC that is conventionally done. Also, we use a higher flow rate in the first dimension, which is split to go to the multiple detectors and to the second-dimension chromatograph. The flow rate split to go to the second dimension is similar to flow rates often used for the first-dimension analysis on other systems.

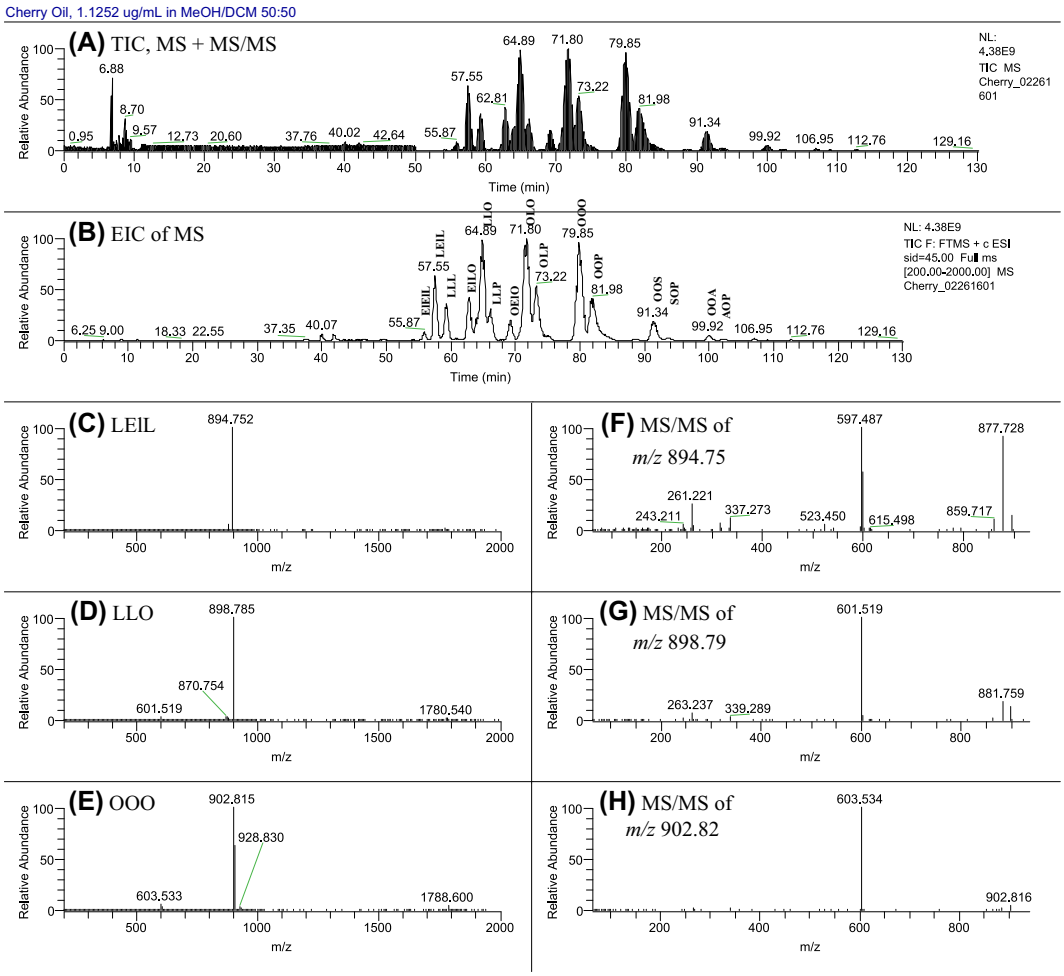

FIGURE 10.14

Analysis of cherry pit oil using ESI-HRAM-MS on Q Exactive orbitrap instrument as part of comprehensive LC1MS2 × LC1MS2 (LC2MS4) analysis. (A) Total ion current chromatogram (TIC); (B) extracted ion chromatogram (EIC) of full scans; (C) mass spectrum of LEIL showing $[M + NH_4]^+$ adduct; (D) LLO; (E) OOO; (F) MS/MS of $[M + NH_4]^+$ of LLEl at *m/z* 894.75; (G) MS/MS of $[LLO + NH_4]^+$ *m/z* 898.79; and (H) MS/MS of $[OOO + NH_4]^+$ *m/z* 902.815. Abbreviations are given in Fig. 10.6. *El*, eleostearic acyl chain, (9*Z*,11*E*,13*E*)18:3. *ESI*, electrospray ionization; *HRAM*, high-resolution accurate-mass; *MS*, mass spectrometry. Labels are regiospecific at *sn*-2.

Thanks to Dharma Kodali and Lucas Stolp for CPO sample.

Figs. 10.14 and 10.15 show the results from the APCI-MS(/MS) and ESI-HRAM-MS(/MS) instruments used to monitor the first-dimension NARP-HPLC, whereas Fig. 10.16 shows the raw (untransformed) data from the APPI-MS and ESI-MS(/MS) instruments used to monitor the second-dimension Ag-ion UHPLC. Fig. 10.17 shows the second-dimension APPI-MS data processed through

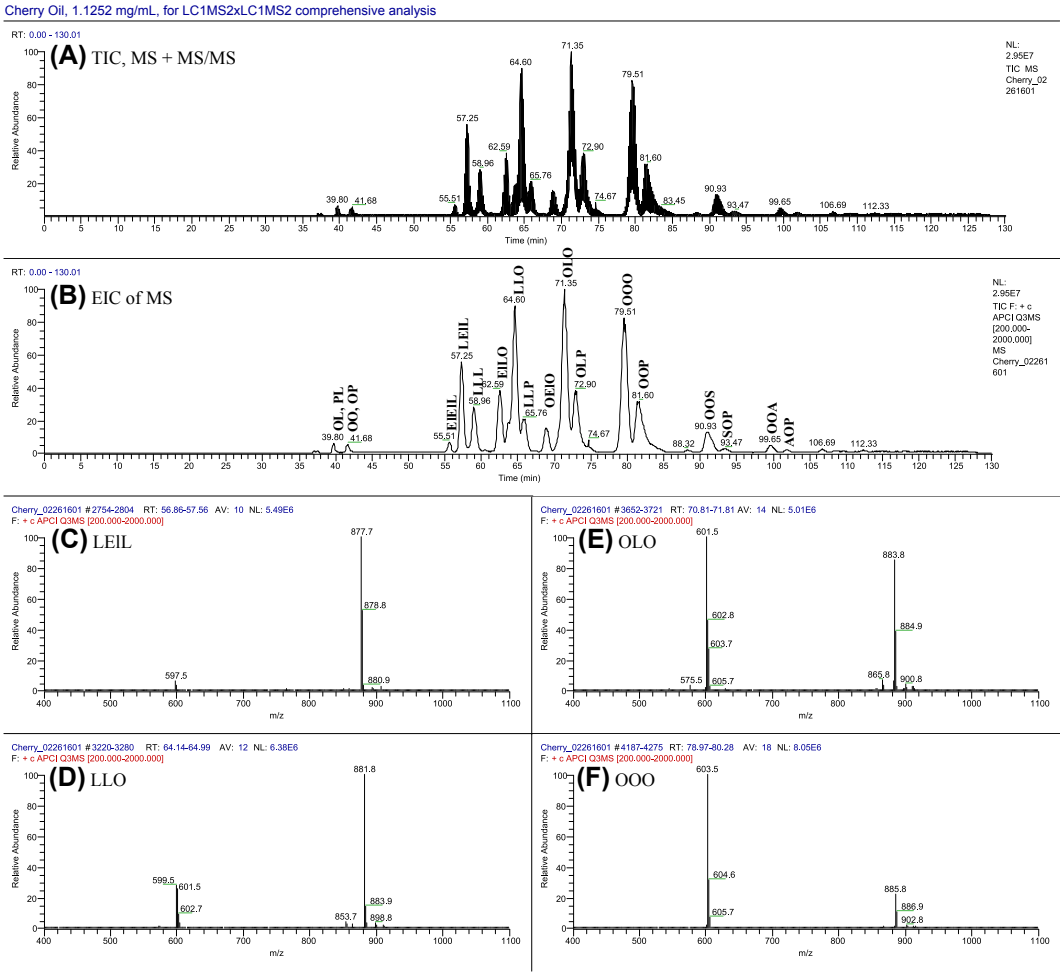

FIGURE 10.15

Analysis of cherry pit oil using APCI-MS on TSQ Vantage EMR instrument as part of comprehensive LC1MS2 × LC1MS2 (LC2MS4) analysis. (A) Total ion current chromatogram (TIC); (B) extracted ion chromatogram (EIC) of full scans; (C) mass spectrum of LEIL; (D) LLO; (E) OLO; and (F) OOO. Abbreviations are given in Fig. 10.6. *El*, eleostearic acyl chain, (9*Z*, 11*E*, 13*E*) 18:3. *APCI-MS*, atmospheric pressure chemical ionization mass spectrometry; *TSQ*, tandem sector quadrupole. Labels are regiospecific at *sn*-2.

Thanks to Dharma Kodali and Lucas Stolp for CPO sample.

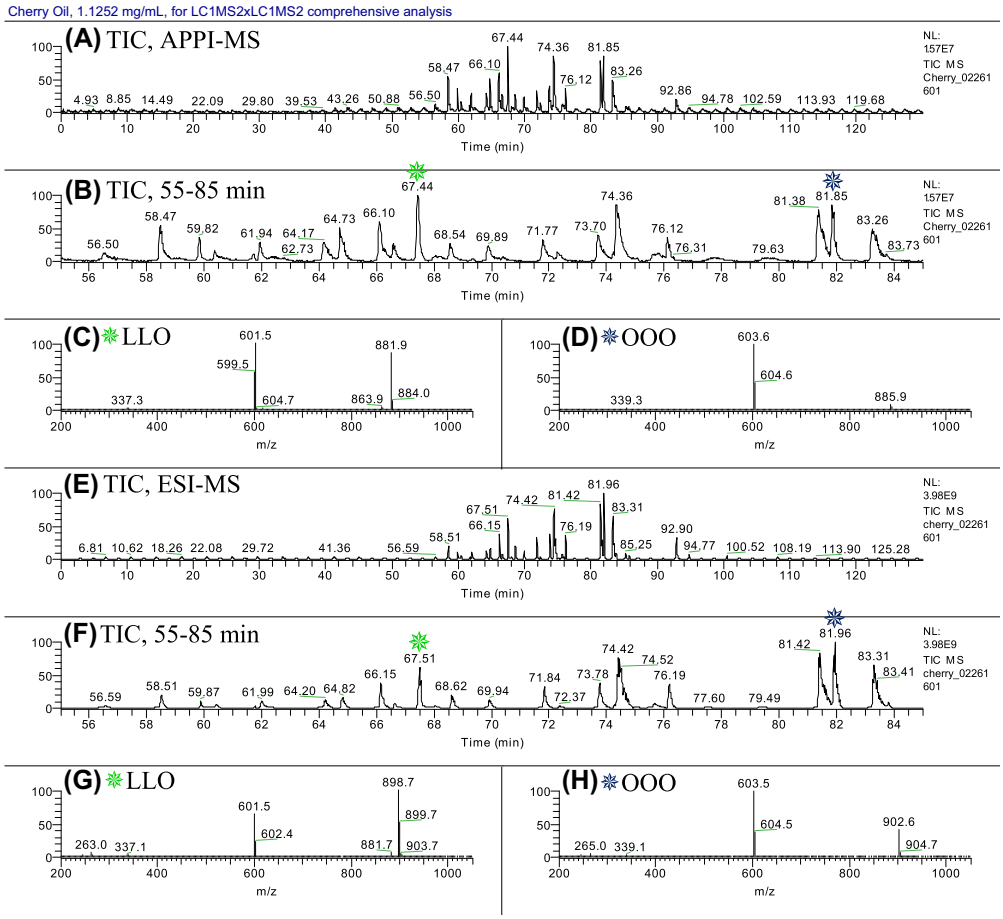

FIGURE 10.16

Second-dimension separation of cherry pit oil triacylglycerols by Ag-ion UHPLC detected using APPI-MS on TSQ Quantum Access Max mass spectrometer and ESI-MS on LCQ Deca XP (55 V up-front collision energy provided to cause nonspecific fragment formation). Modulation time 1.91 min. (A) TIC of APPI-MS; (B) APPI-MS TIC of 55−85 min; (C) APPI-MS mass spectrum of LLO at 67.44 min; (D) OOO at 81.85 min; (E) TIC of ESI-MS; (F) ESI-MS TIC 55−85 min; (G) ESI-MS mass spectrum of LLO at 67.51 min; and (H) OOO at 81.96 min. 55 V of up-front CID applied with ESI-MS for nonspecific fragmentation. *APPI-MS*, atmospheric pressure photoionization mass spectrometry; *ESI-MS*, electrospray ionization mass spectrometry; *TIC*, total ion current chromatogram; *TSQ*, tandem sector quadrupole; *UHPLC*, ultra-high performance liquid chromatography.

Thanks to Dharma Kodali and Lucas Stolp for CPO sample.

the GC Image, Inc. LC × LC software. The second-dimension runs had a modulation time of 1.91 min, constituting "slow" 2D-LC. The contour plot for the second mass spectrometer in the second dimension (ESI-MS on LCQ Deca XP) is not shown because of software irregularities regarding the modulation time setting that require further investigation.

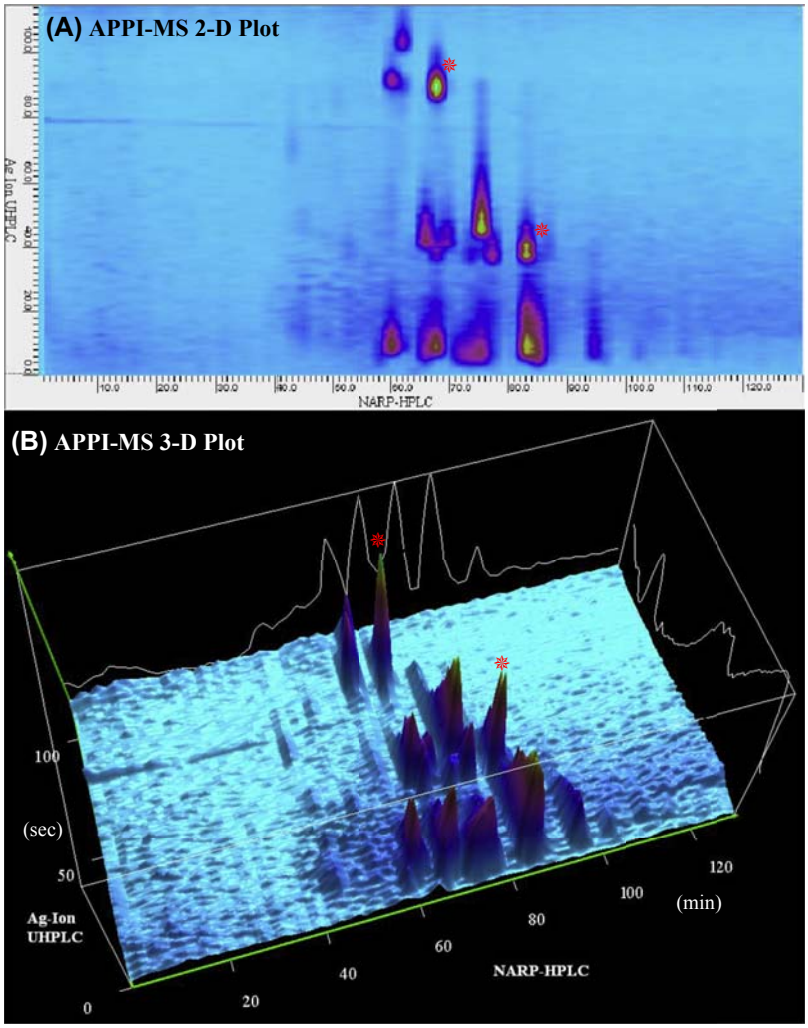

FIGURE 10.17

APPI-MS detection of cherry pit oil (CPO) triacylglycerols (TAGs) as part of comprehensive LC1MS2 × LC1MS2 experiment. Visualized using LC × LC software by GC Image, Inc. (A) Two-dimensional contour plot of CPO TAGs and (B) three-dimensional plot from the same MS detector. Peaks marked by ❋ correspond to the same peaks in Fig. 10.16. *APPI-MS*, atmospheric pressure photoionization mass spectrometry; *NARP-HPLC*, nonaqueous reversed-phase high-performance liquid chromatography; *UHPLC*, ultra-high performance liquid chromatography.

Thanks to Dharma Kodali and Lucas Stolp for CPO sample.

These data show the proof of concept of what is possible, but are method development runs that are not yet ready to fully report in the literature. A report describing the new Ag-ion column preparation technique, splitting procedure, and complete LC1/MS2 × LC1/MS2 results will be prepared shortly.

4. CONCLUSION

Because of the complementary nature of the most popular API techniques used for LC-MS, it has become recognized as highly desirable to obtain data from multiple techniques for the same samples. The body of literature describing sequential use of multiple techniques is burgeoning. However, very few authors are using the multiple parallel MS technique for LC analysis pioneered by Byrdwell. Some researchers believe that dedicating two or more instruments to a single analysis is impractical, but the parallel technique saves time, money, and resources, and eliminates run-to-run variability, compared with sequential analysis of the same sample using two different ionization sources.

It is not practical to go out and buy four new mass spectrometers to allow an LC2/MS4 analysis. However, it is practical to keep older instruments online as auxiliary detectors when new instruments are acquired during the natural process of upgrading and evolution of a lab. Thus, as more researchers overcome the preconceptions regarding multiple parallel MS, it is expected that others will join Byrdwell in reporting an expanding range of applications using LC*x*/MS*y*.

REFERENCES

Alagar Raja, M., Shailaja, V., David, B., Rao, K.N.V., Selva Kumar, D., 2014. Updated review on LC-MS. Res. J. Pharm. Biol. Chem. Sci. 5, 276–291.

An, Z., Chen, Y., Zhang, R., Song, Y., Sun, J., He, J., Bai, J., Dong, L., Zhan, Q., Abliz, Z., 2010. Integrated ionization approach for RRLC-MS/MS-based metabonomics: finding potential biomarkers for lung cancer. J. Proteome Res. 9, 4071–4081.

Awad, H., Khamis, M.M., El-Aneed, A., 2015. Mass spectrometry, review of the basics: ionization. Appl. Spectrosc. Rev. 50, 158–175.

Ball, G.F.M., 1988. Fat-Soluble Vitamin Assays in Food Analysis: A Comprehensive Review. Elsevier Science Publishing, New York.

Balogh, M.P., 2005. Emerging technologies in the MS arsenal. LC GC Eur. 18, 205–212.

Bang, D.Y., Moon, M.H., 2013. On-line two-dimensional capillary strong anion exchange/reversed phase liquid chromatography-tandem mass spectrometry for comprehensive lipid analysis. J. Chromatogr. A 1310, 82–90.

Banoub, J., Delmas Jr., G.H., Joly, N., Mackenzie, G., Cachet, N., Benjelloun-Mlayah, B., Delmas, M., 2015. A critique on the structural analysis of lignins and application of novel tandem mass spectrometric strategies to determine lignin sequencing. J. Mass Spectrom. 50, 5–48.

Beißmann, S., Buchberger, W., Hertsens, R., Klampfl, C.W., 2011. High-performance liquid chromatography coupled to direct analysis in real time mass spectrometry: investigations on gradient elution and influence of complex matrices on signal intensities. J. Chromatogr. A 1218, 5180–5186.

Bligh, E.G., Dyer, W.J., 1959. A rapid method of total lipid extraction and purification. Can. J. Biochem. Physiol. 37, 911–917.

Bos, S.J., van Leeuwen, S.M., Karst, U., 2006. From fundamentals to applications: recent developments in atmospheric pressure photoionization mass spectrometry. Anal. Bioanal. Chem. 384, 85–99.

Byrdwell, W.C., 1998a. APCI-MS for lipid analysis. INFORM Int. News Fats Oils Relat. Mater. 9, 986–997.

Byrdwell, W.C., 1998b. Dual parallel mass spectrometers for analysis of sphingolipid, glycerophospholipid and plasmalogen molecular species. Rapid Commun. Mass Spectrom. 12, 256−272.

Byrdwell, W.C., 2001. Atmospheric pressure chemical ionization mass spectrometry for analysis of lipids. Lipids 36, 327−346.

Byrdwell, W.C., 2003a. APCI-MS in lipid analysis. In: Adlof, R.O. (Ed.), Advances in Lipid Methodology − Five. P.J. Barnes & Associates, Bridgwater, England, pp. 171−253.

Byrdwell, W.C., 2003b. Dual parallel liquid chromatography/dual mass spectrometry (LC2/MS2) of bovine brain total lipid extract. J. Liq. Chromatogr. Relat. Technol. 26, 3147−3181.

Byrdwell, W.C., 2005a. The bottom up solution to the triacylglycerol lipidome using atmospheric pressure chemical ionization mass spectrometry. Lipids 40, 383−417.

Byrdwell, W.C., 2005b. Dual parallel liquid chromatography/mass spectrometry for lipid analysis. In: Byrdwell, W.C. (Ed.), Modern Methods for Lipid Analysis by Liquid Chromatography/Mass Spectrometry and Related Techniques. AOCS Press, Champaign, IL, pp. 510−576.

Byrdwell, W.C., 2005c. Liquid chromatography with electrospray ionization mass spectrometry for lipid analysis. In: Lin, J.T., McKeon, T.A. (Eds.), HPLC of Acyl Lipids. HNB Publishing, New York, NY, pp. 315−371.

Byrdwell, W.C., 2005d. Qualitative and quantitative analysis of triacylglycerols by atmospheric pressure ionization (APCI and ESI) mass spectrometry techniques. In: Byrdwell, W.C. (Ed.), Modern Methods for Lipid Analysis by Liquid Chromatography/Mass Spectrometry and Related Techniques. AOCS Press, Champaign, IL, pp. 298−412.

Byrdwell, W.C., 2008. Dual parallel liquid chromatography with dual mass spectrometry (LC2/MS2) for a total lipid analysis. Front. Biosci. 13, 100−120.

Byrdwell, W.C., 2010. Dual parallel mass spectrometry for lipid and vitamin D analysis. J. Chromatogr. A 1217, 3992−4003.

Byrdwell, W.C., 2011a. "Dilute-and-shoot" triple parallel mass spectrometry method for analysis of vitamin D and triacylglycerols in dietary supplements. Anal. Bioanal. Chem. 401, 3317−3334.

Byrdwell, W.C., 2011b. Multiple parallel mass spectrometry techniques for lipid and vitamin D analysis. In: Byrdwell, W.C., Holčapek, M. (Eds.), Extreme Chromatography: Faster, Hotter, Smaller. AOCS Press, Urbana, IL, pp. 255−299.

Byrdwell, W.C., 2013a. How many mass spectrometers are enough? Adventures in multiple parallel mass spectrometry. INFORM Int. News Fats Oils Relat. Mater. 24, 312−316.

Byrdwell, W.C., 2013b. Quadruple parallel mass spectrometry for analysis of vitamin D and triacylglycerols in a dietary supplement. J. Chromatogr. A 1320, 48−65.

Byrdwell, W.C., 2014a. Construction of a wireless communication contact closure system for liquid chromatography with multiple parallel mass spectrometers and other detectors. J. Lab. Autom. 19, 461−467.

Byrdwell, W.C., 2014b. Extract-filter-shoot liquid chromatography with mass spectrometry for the analysis of vitamin D2 in a powdered supplement capsule and standard reference material 3280. J. Sep. Sci. 37, 2095−2110.

Byrdwell, W.C., 2015a. Critical ratios for structural analysis of triacylglycerols using mass spectrometry. Lipid Technol. 27, 258−261.

Byrdwell, W.C., 2015b. The updated bottom up solution applied to atmospheric pressure photoionization and electrospray ionization mass spectrometry. JAOCS J. Am. Oil Chem. Soc. 92, 1533−1547.

Byrdwell, W.C., 2015c. The updated bottom up solution applied to mass spectrometry of soybean oil in a dietary supplement gelcap. Anal. Bioanal. Chem. 407, 5143−5160.

Byrdwell, W.C., 2016. The simulacrum system as a construct for mass spectrometry of triacylglycerols and others. Lipids 51, 211−227.

Byrdwell, C., Borchman, D., 1997. Liquid chromatography/mass-spectrometric characterization of sphingomyelin and dihydrosphingomyelin of human lens membranes. Ophthalmic Res. 29, 191−206.

Byrdwell, W.C., Emken, E.A., 1995. Analysis of triglycerides using atmospheric pressure chemical ionization mass spectrometry. Lipids 30, 173−175.

Byrdwell, W.C., Neff, W.E., 1997. Qualitative and quantitative analysis of triacylglycerols using atmospheric pressure chemical ionization mass spectrometry. In: McDonald, R.E., Magdi, M.M. (Eds.), New Techniques and Applications in Lipid Analysis. AOCS Press, Champaign, IL, pp. 45−80.

Byrdwell, W.C., Neff, W.E., 2002. Dual parallel electrospray ionization and atmospheric pressure chemical ionization mass spectrometry (MS), MS/MS and MS/MS/MS for the analysis of triacylglycerols and triacylglycerol oxidation products. Rapid Commun. Mass Spectrom. 16, 300−319.

Byrdwell, W.C., Perry, R.H., 2006. Liquid chromatography with dual parallel mass spectrometry and 31P nuclear magnetic resonance spectroscopy for analysis of sphingomyelin and dihydrosphingomyelin. I. Bovine brain and chicken egg yolk. J. Chromatogr. A 1133, 149−171.

Byrdwell, W.C., Perry, R.H., 2007. Liquid chromatography with dual parallel mass spectrometry and 31P nuclear magnetic resonance spectroscopy for analysis of sphingomyelin and dihydrosphingomyelin. II. Bovine milk sphingolipids. J. Chromatogr. A 1146, 164−185.

Byrdwell, W.C., Neff, W.E., List, G.R., 2001. Triacylglycerol analysis of potenial margarine base stocks by high-performance liquid chromatography with atmospheric pressure chemical ionization mass spectrometry and, flame ionization detection. J. Agric. Food Chem. 49, 446−457.

Cai, S.S., Syage, J.A., 2006a. Atmospheric pressure photoionization mass spectrometry for analysis of fatty acid and acylglycerol lipids. J. Chromatogr. A 1110, 15−26.

Cai, S.S., Syage, J.A., 2006b. Comparison of atmospheric pressure photoionization, atmospheric pressure chemical ionization, and electrospray ionization mass spectrometry for analysis of lipids. Anal. Chem. 78, 1191−1199.

Cai, Y., Kingery, D., McConnell, O., Bach Ii, A.C., 2005. Advantages of atmospheric pressure photoionization mass spectrometry in support of drug discovery. Rapid Commun. Mass Spectrom. 19, 1717−1724.

Cai, S.S., Hanold, K.A., Syage, J.A., 2007a. Comparison of atmospheric pressure photoionization and atmospheric pressure chemical ionization for normal-phase LC/MS chiral analysis of pharmaceuticals. Anal. Chem. 79, 2491−2498.

Cai, S.S., Short, L.C., Syage, J.A., Potvin, M., Curtis, J.M., 2007b. Liquid chromatography-atmospheric pressure photoionization-mass spectrometry analysis of triacylglycerol lipids-effects of mobile phases on sensitivity. J. Chromatogr. A 1173, 88−97.

Cai, S.S., Syage, J.A., Hanold, K.A., Balogh, M.P., 2009. Ultra performance liquid chromatography-atmospheric pressure photoionization-tandem mass spectrometry for high-sensitivity and high-throughput analysis of U.S. Environmental protection agency 16 priority pollutants polynuclear aromatic hydrocarbons. Anal. Chem. 81, 2123−2128.

Cai, S.S., Stevens, J., Syage, J.A., 2012. Ultra high performance liquid chromatography-atmospheric pressure photoionization-mass spectrometry for high-sensitivity analysis of US environmental protection agency sixteen priority pollutant polynuclear aromatic hydrocarbons in oysters. J. Chromatogr. A 1227, 138−144.

Cao, J., Murch, S.J., O'Brien, R., Saxena, P.K., 2006. Rapid method for accurate analysis of melatonin, serotonin and auxin in plant samples using liquid chromatography-tandem mass spectrometry. J. Chromatogr. A 1134, 333−337.

Chen, J., Korfmacher, W.A., Hsieh, Y., 2005. Chiral liquid chromatography-tandem mass spectrometric methods for stereoisomeric pharmaceutical determinations. J. Chromatogr. B Anal. Technol. Biomed. Life Sci. 820, 1−8.

Chiaberge, S., Leonardis, I., Fiorani, T., Cesti, P., Reale, S., Angelis, F.D., 2014. Bio-oil from waste: a comprehensive analytical study by soft-ionization FTICR mass spectrometry. Energy Fuels 28, 2019−2026.

Cicek, S.S., Aberham, A., Ganzera, M., Stuppner, H., 2011. Quantitative analysis of cycloartane glycosides in black cohosh rhizomes and dietary supplements by RRLC-ELSD and RRLC-QTOF-MS. Anal. Bioanal. Chem. 400, 2597−2605.

Cirigliano, A.M., Rodriguez, M.A., Gagliano, M.L., Bertinetti, B.V., Godeas, A.M., Cabrera, G.M., 2016. Liquid chromatography coupled to different atmospheric pressure ionization sources-quadrupole-time-of-flight mass spectrometry and post-column addition of metal salt solutions as a powerful tool for the metabolic profiling of *Fusarium oxysporum*. J. Chromatogr. A 1439, 97−111.

Cody, R.B., Laramée, J.A., Durst, H.D., 2005. Versatile new ion source for the analysis of materials in open air under ambient conditions. Anal. Chem. 77, 2297−2302.

Cole, R.B., 1997. Electrospray Ionization Mass Spectrometry: Fundamentals, Instrumentation, & Applications. John Wiley & Sons, Inc., New York.

Covey, T.R., Thomson, B.A., Schneider, B.B., 2009. Atmospheric pressure ion sources. Mass Spectrom. Rev. 28, 870−897.

Culzoni, M.J., Dwivedi, P., Green, M.D., Newton, P.N., Fernández, F.M., 2014. Ambient mass spectrometry technologies for the detection of falsified drugs. Med. Chem. Commun. 5, 9−19.

Davis, J.M., Stoll, D.R., Carr, P.W., 2008. Effect of first-dimension undersampling on effective peak capacity in comprehensive two-dimensional separations. Anal. Chem. 80, 461−473.

Deeg, M.A., Humphrey, D.R., Yang, S.H., Ferguson, T.R., Reinhold, V.N., Rosenberry, T.L., 1992. Glycan components in the glycoinositol phospholipid anchor of human erythrocyte acetylcholinesterase: novel fragments produced by trifluoroacetic acid. J. Biol. Chem. 267, 18573−18580.

Diao, R., Wang, W., Wang, N., Liu, Z., Dai, L., Tian, S., 2012. Molecular characterization of hydrotreated atmospheric residue derived from arabian heavy crude by GC FI/FD TOF MS and APPI-FTICR-MS. China Pet. Process. Petrochem. Technol. 14, 80−88.

Donegan, M., Browning, M., 2012. A review recent developments in sample ionization interfaces used in mass spectrometry. J. Liq. Chromatogr. Relat. Technol. 35, 2345−2363.

Duffin, K.L., Henion, J.D., Shieh, J.J., 1991. Electrospray and tandem mass spectrometric characterization of acylglycerol mixtures that are dissolved in nonpolar solvents. Anal. Chem. 63, 1781−1788.

Dugo, P., Kumm, T., Chiofalo, B., Cotroneo, A., Mondello, L., 2006a. Separation of triacylglycerols in a complex lipidic matrix by using comprehensive two-dimensional liquid chromatography coupled with atmospheric pressure chemical ionization mass spectrometric detection. J. Sep. Sci. 29, 1146−1154.

Dugo, P., Kumm, T., Crupi, M.L., Cotroneo, A., Mondello, L., 2006b. Comprehensive two-dimensional liquid chromatography combined with mass spectrometric detection in the analyses of triacylglycerols in natural lipidic matrixes. J. Chromatogr. A 1112, 269−275.

Dugo, P., Kumm, T., Fazio, A., Dugo, G., Mondello, L., 2006c. Determination of beef tallow in lard through a multidimensional off-line non-aqueous reversed phase-argentation LC method coupled to mass spectrometry. J. Sep. Sci. 29, 567−575.

Dugo, P., Cacciola, F., Kumm, T., Dugo, G., Mondello, L., 2008. Comprehensive multidimensional liquid chromatography: theory and applications. J. Chromatogr. A 1184, 353−368.

Evans, M.D., Nies, B.J., Esser, C.K., Syage, J.A., 2002. Direct injection photoionization MS − High-speed purity assessment of pharmaceutical samples. In: Proceedings of the 50th ASMS Conference on Mass Spectrometry and Allied Topics, pp. 787−788.

Fauconnot, L., Hau, J., Aeschlimann, J.M., Fay, L.B., Dionisi, F., 2004. Quantitative analysis of triacylglycerol regioisomers in fats and oils using reversed-phase high-performance liquid chromatography and atmospheric pressure chemical ionization mass spectrometry. Rapid Commun. Mass Spectrom. 18, 218−224.

Feldmann, J., 2005. What can the different current-detection methods offer for element speciation? TrAC Trends Anal. Chem. 24, 228−242.

Gallagher, R.T., Balogh, M.P., Davey, P., Jackson, M.R., Sinclair, I., Southern, L.J., 2003. Combined electrospray ionization-atmospheric pressure chemical ionization source for use in high-throughput LC-MS applications. Anal. Chem. 75, 973−977.

Garcia-Ac, A., Segura, P.A., Viglino, L., Gagnon, C., Sauvé, S., 2011. Comparison of APPI, APCI and ESI for the LC-MS/MS analysis of bezafibrate, cyclophosphamide, enalapril, methotrexate and orlistat in municipal wastewater. J. Mass Spectrom. 46, 383−390.

Gaudin, M., Imbert, L., Libong, D., Chaminade, P., Brunelle, A., Touboul, D., Laprévote, O., 2012. Atmospheric pressure photoionization as a powerful tool for large-scale lipidomic studies. J. Am. Soc. Mass Spectrom. 23, 869−879.

Ghislain, T., Faure, P., Michels, R., 2012. Detection and monitoring of PAH and oxy-PAHs by high resolution mass spectrometry: comparison of ESI, APCI and APPI source detection. J. Am. Soc. Mass Spectrom. 23, 530−536.

Gouveia, M.J., Brindley, P.J., Santos, L.L., Correia da Costa, J.M., Gomes, P., Vale, N., 2013. Mass spectrometry techniques in the survey of steroid metabolites as potential disease biomarkers: a review. Metab. Clin. Exp. 62, 1206−1217.

Grosse, S., Letzel, T., 2007. Liquid chromatography/atmospheric pressure ionization mass spectrometry with post-column liquid mixing for the efficient determination of partially oxidized polycyclic aromatic hydrocarbons. J. Chromatogr. A 1139, 75−83.

Guo, X., Lankmayr, E., 2010. Multidimensional approaches in LC and MS for phospholipid bioanalysis. Bioanalysis 2, 1109−1123.

Han, X., Gross, R.W., 1994. Electrospray ionization mass spectroscopic analysis of human erythrocyte plasma membrane phospholipids. Proc. Natl. Acad. Sci. U.S.A. 91, 10635−10639.

Hanold, K.A., Horner, J., Thakur, R., Miller, C., 2002. Dual APPI/APCI source for LC/MS. In: Proceedings of the 50th ASMS Conference on Mass Spectrometry and Allied Topics, pp. 31−32.

Hanold, K.A., Fischer, S.M., Cormia, P.H., Miller, C.E., Syage, J.A., 2004. Atmospheric pressure photoionization. 1. General properties for LC/MS. Anal. Chem. 76, 2842−2851.

Hayen, H., Karst, U., 2003. Strategies for the liquid chromatographic-mass spectrometric analysis of non-polar compounds. J. Chromatogr. A 1000, 549−565.

Hayen, H., Michels, A., Franzke, J., 2009. Dielectric barrier discharge ionization for liquid chromatography/mass spectrometry. Anal. Chem. 81, 10239−10245.

Hejazi, L., Guilhaus, M., Hibbert, D.B., Ebrahimi, D., 2014. Gas chromatography with parallel hard and soft ionization mass spectrometry. Rapid Commun. Mass Spectrom. 29, 91−99.

Himmelsbach, M., 2012. 10 years of MS instrumental developments − Impact on LC-MS/MS in clinical chemistry. J. Chromatogr. B Anal. Technol. Biomed. Life Sci. 883−884, 3−17.

Himmelsbach, M., Buchberger, W., Reingruber, E., 2009. Determination of polymer additives by liquid chromatography coupled with mass spectrometry. A comparison of atmospheric pressure photoionization (APPI), atmospheric pressure chemical ionization (APCI), and electrospray ionization (ESI). Polym. Degrad. Stab. 94, 1213−1219.

Holčapek, M., Jandera, P., Zderadička, P., Hrubá, L., 2003. Characterization of triacylglycerol and diacylglycerol composition of plant oils using high-performance liquid chromatography-atmospheric pressure chemical ionization mass spectrometry. J. Chromatogr. A 1010, 195−215.

Holčapek, M., Dvořáková, H., Lísa, M., Giron, A.J., Sandra, P., Cvačka, J., 2010. Regioisomeric analysis of triacylglycerols using silver-ion liquid chromatography-atmospheric pressure chemical ionization mass spectrometry: comparison of five different mass analyzers. J. Chromatogr. A 1217, 8186−8194.

Holčapek, M., Ovčačíková, M., Lísa, M., Cífková, E., Hájek, T., 2015. Continuous comprehensive two-dimensional liquid chromatography-electrospray ionization mass spectrometry of complex lipidomic samples. Anal. Bioanal. Chem. 407, 5033−5043.

Hommerson, P., Khan, A.M., Bristow, T., Harrison, M.W., Jong, G.J.D., Somsen, G.W., 2009. Drug impurity profiling by capillary electrophoresis/mass spectrometry using various ionization techniques. Rapid Commun. Mass Spectrom. 23, 2878−2884.

Hsu, F.F., Turk, J., 1999. Structural characterization of triacylglycerols as lithiated adducts by electrospray ionization mass spectrometry using low-energy collisionally activated dissociation on a triple stage quadrupole instrument. J. Am. Soc. Mass Spectrom. 10, 587–599.

Huang, M.Z., Cheng, S.C., Cho, Y.T., Shiea, J., 2011. Ambient ionization mass spectrometry: a tutorial. Anal. Chim. Acta 702, 1–15.

Huba, A.K., Huba, K., Gardinali, P.R., 2016. Understanding the atmospheric pressure ionization of petroleum components: the effects of size, structure, and presence of heteroatoms. Sci. Total Environ. 568, 1018–1025.

Hvattum, E., 2001. Analysis of triacylglycerols with non-aqueous reversed-phase liquid chromatography and positive ion electrospray tandem mass spectrometry. Rapid Commun. Mass Spectrom. 15, 187–190.

Imbert, L., Gaudin, M., Libong, D., Touboul, D., Abreu, S., Loiseau, P.M., Laprévote, O., Chaminade, P., 2012. Comparison of electrospray ionization, atmospheric pressure chemical ionization and atmospheric pressure photoionization for a lipidomic analysis of *Leishmania donovani*. J. Chromatogr. A 1242, 75–83.

Itoh, N., Aoyagi, Y., Yarita, T., 2006. Optimization of the dopant for the trace determination of polycyclic aromatic hydrocarbons by liquid chromatography/dopant-assisted atmospheric-pressure photoionization/mass spectrometry. J. Chromatogr. A 1131, 285–288.

Iwabuchi, H., Kitazawa, E., Kobayashi, N., Watanabe, H., Kanai, M., Nakamura, K.I., 1994. Studies on drug metabolism using liquid chromatography/mass spectrometry: comparison of three liquid chromatographic/mass spectrometric interfaces. Biol. Mass Spectrom 23, 540–546.

Iwasaki, Y., Yasui, M., Ishikawa, T., Irimescu, R., Hata, K., Yamane, T., 2001. Optical resolution of asymmetric triacylglycerols by chiral-phase high-performance liquid chromatography. J. Chromatogr. A 905, 111–118.

Jakab, A., Jablonkai, I., Forgács, E., 2003. Quantification of the ratio of positional isomer dilinoleoyl-oleoyl glycerols in vegetable oils. Rapid Commun. Mass Spectrom. 17, 2295–2302.

Jemal, M., Xia, Y.Q., 2006. LC-MS development strategies for quantitative bioanalysis. Curr. Drug Metab. 7, 491–502.

Kalo, P., 2013. Regiospecific analysis of triacylglycerols. Lipid Technol. 25, 230–234.

Kalogera, E., Pistos, C., Provatopoulou, X., Athanaselis, S., Spiliopoulou, C., Gounaris, A., 2013. Androgen glucuronides analysis by liquid chromatography tandem-mass spectrometry: could it raise new perspectives in the diagnostic field of hormone-dependent malignancies? J. Chromatogr. B Anal. Technol. Biomed. Life Sci. 940, 24–34.

Karst, U., 2002. Detection techniques for liquid chromatography. Anal. Bioanal. Chem. 372, 27–28.

Kauppila, T.J., Kuuranne, T., Meurer, E.C., Eberlin, M.N., Kotiaho, T., Kostiainen, R., 2002. Atmospheric pressure photoionization mass spectrometry. Ionization mechanism and the effect of solvent on the ionization of naphthalenes. Anal. Chem. 74, 5470–5479.

Kauppila, T.J., Kostiainen, R., Bruins, A.P., 2004. Anisole, a new dopant for atmospheric pressure photoionization mass spectrometry of low proton affinity, low ionization energy compounds. Rapid Commun. Mass Spectrom. 18, 808–815.

Kauppila, T.J., Bruins, A.P., Kostiainen, R., 2005. Effect of the solvent flow rate on the ionization efficiency in atmospheric pressure photoionization-mass spectrometry. J. Am. Soc. Mass Spectrom. 16, 1399–1407.

Kauppila, T.J., Nikkola, T., Ketola, R.A., Kostiainen, R., 2006. Atmospheric pressure photoionization-mass spectrometry and atmospheric pressure chemical ionization-mass spectrometry of neurotransmitters. J. Mass Spectrom. 41, 781–789.

Kauppila, T.J., Kersten, H., Benter, T., 2014. The ionization mechanisms in direct and dopant-assisted atmospheric pressure photoionization and atmospheric pressure laser ionization. J. Am. Soc. Mass Spectrom. 25, 1870–1881.

Kauppila, T.J., Syage, J.A., Benter, T., 2017. Recent developments in atmospheric pressure photoionization-mass spectrometry. Mass Spectrom. Rev. 36, 423–449.

Kéki, S., Nagy, L., Kuki, Á., Zsuga, M., 2008. A new method for mass spectrometry of polyethylene waxes: the chloride ion attachment technique by atmospheric pressure photoionization. Macromolecules 41, 3772−3774.

Kerwin, J.L., Tuininga, A.R., Ericsson, L.H., 1994. Identification of molecular species of glycerophospholipids and sphingomyelin using electrospray mass spectrometry. J. Lipid Res. 35, 1102−1114.

Keski-Hynnilä, H., Kurkela, M., Elovaara, E., Antonio, L., Magdalou, J., Luukkanen, L., Taskinen, J., Kostiainen, R., 2002. Comparison of electrospray, atmospheric pressure chemical ionization, and atmospheric pressure photoionization in the identification of apomorphine, dobutamine, and entacapone phase II metabolites in biological samples. Anal. Chem. 74, 3449−3457.

Keski-Rahkonen, P., Huhtinen, K., Desai, R., Tim Harwood, D., Handelsman, D.J., Poutanen, M., Auriola, S., 2013. LC-MS analysis of estradiol in human serum and endometrial tissue: comparison of electrospray ionization, atmospheric pressure chemical ionization and atmospheric pressure photoionization. J. Mass Spectrom. 48, 1050−1058.

Kim, H.Y., Wang, T.C.L., Ma, Y.C., 1994. Liquid chromatography/mass spectrometry of phospholipids using electrospray ionization. Anal. Chem. 66, 3977−3993.

Kovarik, P., LeBlanc, Y., Covey, T., 2002. A simultaneous electrospray and APCI ionization system. In: Proceedings of the 50th ASMS Conference on Mass Spectrometry and Allied Topics, pp. 29−30.

Laakso, P., 1997. Characterization of α- and γ-linolenic acid oils by reversed-phase high-performance liquid chromatography-atmospheric pressure chemical ionization mass spectrometry. JAOCS J. Am. Oil Chem. Soc. 74, 1291−1300.

Laakso, P., Voutilainen, P., 1996. Analysis of triacylglycerols by silver-ion high-performance liquid chromatography-atmospheric pressure chemical ionization mass spectrometry. Lipids 31, 1311−1322.

Lababidi, S., Schrader, W., 2014. Online normal-phase high-performance liquid chromatography/Fourier transform ion cyclotron resonance mass spectrometry: effects of different ionization methods on the characterization of highly complex crude oil mixtures. Rapid Commun. Mass Spectrom. 28, 1345−1352.

Lee, H., 2005. Pharmaceutical applications of liquid chromatography coupled with mass spectrometry (LC/MS). J. Liq. Chromatogr. Relat. Technol. 28, 1161−1202.

Leskinen, H., Suomela, J.P., Kallio, H., 2007. Quantification of triacylglycerol regioisomers in oils and fat using different mass spectrometric and liquid chromatographic methods. Rapid Commun. Mass Spectrom. 21, 2361−2373.

Li, L., Huhtala, S., Sillanpää, M., Sainio, P., 2012. Liquid chromatography-mass spectrometry for C60 fullerene analysis: optimisation and comparison of three ionisation techniques. Anal. Bioanal. Chem. 403, 1931−1938.

Lien, G.W., Chen, C.Y., Wang, G.S., 2009. Comparison of electrospray ionization, atmospheric pressure chemical ionization and atmospheric pressure photoionization for determining estrogenic chemicals in water by liquid chromatography tandem mass spectrometry with chemical derivatizations. J. Chromatogr. A 1216, 956−966.

Lim, C.K., Lord, G., 2002. Current developments in LC-MS for pharmaceutical analysis. Biol. Pharm. Bull. 25, 547−557.

Lísa, M., Holčapek, M., 2013. Characterization of triacylglycerol enantiomers using chiral HPLC/APCI-MS and synthesis of enantiomeric triacylglycerols. Anal. Chem. 85, 1852−1859.

Liu, D.Q., Xia, Y.Q., Bakhtiar, R., 2002. Use of a liquid chromatography/ion trap mass spectrometry/triple quadrupole mass spectrometry system for metabolite identification. Rapid Commun. Mass Spectrom. 16, 1330−1336.

Louw, S., Njoroge, M., Chigorimbo-Murefu, N., Chibale, K., 2012. Comparison of electrospray ionisation, atmospheric pressure chemical ionisation and atmospheric pressure photoionisation for the identification of metabolites from labile artemisinin-based anti-malarial drugs using a QTrap® mass spectrometer. Rapid Commun. Mass Spectrom. 26, 2431−2442.

Ma, S., Chowdhury, S.K., Alton, K.B., 2006. Application of mass spectrometry for metabolite identification. Curr. Drug Metab. 7, 503−523.

Manninen, P., Laakso, P., 1997. Capillary supercritical fluid chromatography − atmospheric pressure chemical ionization mass spectrometry of γ- and α-linolenic acid containing triacylglycerols in berry oils. Lipids 32, 825−831.

Marchi, I., Rudaz, S., Veuthey, J.L., 2009. Atmospheric pressure photoionization for coupling liquid-chromatography to mass spectrometry: a review. Talanta 78, 1−18.

Marotta, E., Seraglia, R., Fabris, F., Traldi, P., 2003. Atmospheric pressure photoionization mechanisms: 1. The case of acetonitrile. Int. J. Mass Spectrom. 228, 841−849.

Martínez-Villalba, A., Moyano, E., Galceran, M.T., 2013. Ultra-high performance liquid chromatography-atmospheric pressure chemical ionization-tandem mass spectrometry for the analysis of benzimidazole compounds in milk samples. J. Chromatogr. A 1313, 119−131.

Mascolo, G., Locaputo, V., Mininni, G., 2010. New perspective on the determination of flame retardants in sewage sludge by using ultrahigh pressure liquid chromatography-tandem mass spectrometry with different ion sources. J. Chromatogr. A 1217, 4601−4611.

Meyer, G.M., Maurer, H.H., Meyer, M.R., 2016. Multiple stage MS in analysis of plasma, serum, urine and in vitro samples relevant to clinical and forensic toxicology. Bioanalysis 8, 457−481.

Mondello, L.D., Dugo, G., Dugo, P., 2002. Recent applications in LC-MS: food and flavours. LC GC Eur. 2−8.

Mondello, L., Tranchida, P.Q., Staněk, V., Jandera, P., Dugo, G., Dugo, P., 2005. Silver-ion reversed-phase comprehensive two-dimensional liquid chromatography combined with mass spectrometric detection in lipidic food analysis. J. Chromatogr. A 1086, 91−98.

Monge, M.E., Harris, G.A., Dwivedi, P., Fernández, F.M., 2013. Mass spectrometry: recent advances in direct open air surface sampling/ionization. Chem. Rev. 113, 2269−2308.

Mottram, H.R., Evershed, R.P., 1996. Structure analysis of triacylglycerol positional isomers using atmospheric pressure chemical ionisation mass spectrometry. Tetrahedron Lett. 37, 8593−8596.

Narayanam, M., Handa, T., Sharma, P., Jhajra, S., Muthe, P.K., Dappili, P.K., Shah, R.P., Singh, S., 2014. Critical practical aspects in the application of liquid chromatography-mass spectrometric studies for the characterization of impurities and degradation products. J. Pharm. Biomed. Anal. 87, 191−217.

Nilsson, J., Carlberg, J., Abrahamsson, P., Hulthe, G., Persson, B.A., Karlberg, A.T., 2008. Evaluation of ionization techniques for mass spectrometric detection of contact allergenic hydroperoxides formed by autoxidation of fragrance terpenes. Rapid Commun. Mass Spectrom. 22, 3593−3598.

Pardo, O., Yusà, V., León, N., Pastor, A., 2007. Development of a pressurised liquid extraction and liquid chromatography with electrospray ionization-tandem mass spectrometry method for the determination of domoic acid in shellfish. J. Chromatogr. A 1154, 287−294.

Parets, L., Alechaga, É., Núñez, O., Saurina, J., Hernández-Cassou, S., Puignou, L., 2016. Ultrahigh pressure liquid chromatography-atmospheric pressure photoionization-tandem mass spectrometry for the determination of polyphenolic profiles in the characterization and classification of cranberry-based pharmaceutical preparations and natural extracts. Anal. Methods 8, 4363−4378.

Pulfer, M., Murphy, R.C., 2003. Electrospray mass spectrometry of phospholipids. Mass Spectrom. Rev. 22, 332−364.

Purcell, J.M., Hendrickson, C.L., Rodgers, R.P., Marshall, A.G., 2006. Atmospheric pressure photoionization fourier transform ion cyclotron resonance mass spectrometry for complex mixture analysis. Anal. Chem. 78, 5906−5912.

Raffaelli, A., Saba, A., 2003. Atmospheric pressure photoionization mass spectrometry. Mass Spectrom. Rev. 22, 318−331.

Rauha, J.P., Vuorela, H., Kostiainen, R., 2001. Effect of eluent on the ionization efficiency of flavonoids by ion spray, atmospheric pressure chemical ionization, and atmospheric pressure photoionization mass spectrometry. J. Mass Spectrom. 36, 1269−1280.

Řezanka, T., Sigler, K., 2007. The use of atmospheric pressure chemical ionization mass spectrometry with high performance liquid chromatography and other separation techniques for identification of triacylglycerols. Curr. Anal. Chem. 3, 252−271.

Řezanka, T., Sigler, K., 2014. Separation of enantiomeric triacylglycerols by chiral-phase HPLC. Lipids 49, 1251−1260.

Řezanka, T., Lukavský, J., Nedbalová, L., Kolouchová, I., Sigler, K., 2012. Effect of starvation on the distribution of positional isomers and enantiomers of triacylglycerol in the diatom *Phaeodactylum tricornutum*. Phytochemistry 80, 17−27.

Rhourri-Frih, B., Chaimbault, P., Claude, B., Lamy, C., André, P., Lafosse, M., 2009. Analysis of pentacyclic triterpenes by LC-MS. A comparative study between APCI and APPI. J. Mass Spectrom. 44, 71−80.

Rivera, S., Vilaró, F., Canela, R., 2011. Determination of carotenoids by liquid chromatography/mass spectrometry: effect of several dopants. Anal. Bioanal. Chem. 400, 1339−1346.

Robb, D.B., Blades, M.W., 2005. Effects of solvent flow, dopant flow, and lamp current on dopant-assisted atmospheric pressure photoionization (DA-APPI) for LC-MS. Ionization via proton transfer. J. Am. Soc. Mass Spectrom. 16, 1275−1290.

Robb, D.B., Blades, M.W., 2006. Factors affecting primary ionization in dopant-assisted atmospheric pressure photoionization (DA-APPI) for LC-MS. J. Am. Soc. Mass Spectrom. 17, 130−138.

Robb, D.B., Blades, M.W., 2008. State-of-the-art in atmospheric pressure photoionization for LC/MS. Anal. Chim. Acta 627, 34−49.

Robb, D.B., Covey, T.R., Bruins, A.P., 2000. Atmospheric pressure photoionization: an ionization method for liquid chromatography-mass spectrometry. Anal. Chem. 72, 3653−3659.

Sandra, P., Dermaux, A., Ferraz, V., Dittmann, M.M., Rozing, G., 1997. Analysis of triglycerides by capillary electrochromatography. J. Microcolumn Sep. 9, 409−419.

Schuyl, P.J.W., de Joode, T., Vasconcellos, M.A., Duchateau, G.S.M.J.E., 1998. Silver-phase high-performance liquid chromatography-electrospray mass spectrometry of triacylglycerols. J. Chromatogr. A 810, 53−61.

Sforza, S., Dall'Asta, C., Marchelli, R., 2006. Recent advances in mycotoxin determination in food and feed by hyphenated chromatographic techniques/mass spectrometry. Mass Spectrom. Rev. 25, 54−76.

Short, L.C., Syage, J.A., 2008. Electrospray photoionization (ESPI) liquid chromatography/mass spectrometry for the simultaneous analysis of cyclodextrin and pharmaceuticals and their binding interactions. Rapid Commun. Mass Spectrom. 22, 541−548.

Short, L.C., Cai, S.S., Syage, J.A., 2007a. APPI-MS: effects of mobile phases and VUV lamps on the detection of PAH compounds. J. Am. Soc. Mass Spectrom. 18, 589−599.

Short, L.C., Hanold, K.A., Cai, S.S., Syage, J.A., 2007b. Electrospray ionization/atmospheric pressure photoionization multimode source for low-flow liquid chromatography/mass spectrometric analysis. Rapid Commun. Mass Spectrom. 21, 1561−1566.

Siegel, M.M., Tabei, K., Lambert, F., Candela, L., Zoltan, B., 1998. Evaluation of a dual electrospray ionization/atmospheric pressure chemical ionization source at low flow rates ($\sim$50 μl/min) for the analysis of both highly and weakly polar compounds. J. Am. Soc. Mass Spectrom. 9, 1196−1203.

Siegel, M.M., Tabei, K., Huang, J., Balogh, M.P., Jackson, M.R., 2002. Approaches to a universal source for atmospheric pressure ionization (API): a combined ESI/APCI source using low carrier solvent flow rates. In: Proceedings of the 50th ASMS Conference on Mass Spectrometry and Allied Topics, pp. 27−28.

Smith, P.B.W., Snyder, A.P., Harden, C.S., 1995. Characterization of bacterial phospholipids by electrospray ionization tandem mass spectrometry. Anal. Chem. 67, 1824−1830.

Song, L., Wellman, A.D., Yao, H., Bartmess, J.E., 2007. Negative ion-atmospheric pressure photoionization: electron capture, dissociative electron capture, proton transfer, and anion attachment. J. Am. Soc. Mass Spectrom. 18, 1789−1798.

Song, L., Cho, D.S., Bhandari, D., Gibson, S.C., McNally, M.E., Hoffman, R.M., Cook, K.D., 2011. Liquid chromatography/dopant-assisted atmospheric pressure chemical ionization mass spectrometry for the analysis of non-polar compounds. Int. J. Mass Spectrom. 303, 173−180.

Stahl, N., Baldwin, M.A., Prusiner, S.B., 1991. Electrospray mass spectrometry of the glycosylinositol phospholipid of the scrapie prion protein. Cell Biol. Int. Rep. 15, 853−862.

Stolze, B.R., Gounden, V., Gu, J., Elliott, E.A., Masika, L.S., Abel, B.S., Merke, D.P., Skarulis, M.C., Soldin, S.J., 2016. An improved micro-method for the measurement of steroid profiles by APPI-LC−MS/MS and its use in assessing diurnal effects on steroid concentrations and optimizing the diagnosis and treatment of adrenal insufficiency and CAH. J. Steroid Biochem. Mol. Biol. 162, 110−116.

Straube, E.A., Dekant, W., Völkel, W., 2004. Comparison of electrospray ionization, atmospheric pressure chemical ionization, and atmospheric pressure photoionization for the analysis of dinitropyrene and aminonitropyrene LC-MS/MS. J. Am. Soc. Mass Spectrom. 15, 1853−1862.

Syage, J.A., 2004. Mechanism of $[M + H]^+$ formation in photoionization mass spectrometry. J. Am. Soc. Mass Spectrom. 15, 1521−1533.

Syage, J.A., Evans, M.D., Hanold, K.A., 2000. Photoionization mass spectrometry. Am. Lab. 32, 24−29.

Syage, J.A., Hanold, K.A., Lynn, T.C., Horner, J.A., Thakur, R.A., 2004. Atmospheric pressure photoionization: II. Dual source ionization. J. Chromatogr. A 1050, 137−149.

Syage, J.A., Short, L.C., Cai, S.S., 2008. Atmospheric pressure photoionization − The second source for LC-MS? LC GC N. Am. 26, 286−296.

Słomińska, B., Chaładaj, W., Danikiewicz, W., 2014. Assessment of the various ionization methods in the analysis of metal salen complexes by mass spectrometry. J. Mass Spectrom. 49, 392−399.

Takáts, Z., Wiseman, J.M., Gologan, B., Cooks, R.G., 2004. Mass spectrometry sampling under ambient conditions with desorption electrospray ionization. Science 306, 471−473.

Takino, M., Tanaka, T., Yamaguchi, K., Nakahara, T., 2004. Atmospheric pressure photo-ionization liquid chromatography/mass spectrometric determination of aflatoxins in food. Food Addit. Contam. 21, 76−84.

Tian, H., Bai, J., An, Z., Chen, Y., Zhang, R., He, J., Bi, X., Song, Y., Abliz, Z., 2013. Plasma metabolome analysis by integrated ionization rapid-resolution liquid chromatography/tandem mass spectrometry. Rapid Commun. Mass Spectrom. 27, 2071−2080.

Tranchida, P.Q., Donato, P., Dugo, G., Mondello, L., Dugo, P., 2007. Comprehensive chromatographic methods for the analysis of lipids. TrAC Trends Anal. Chem. 26, 191−205.

Tubaro, M., Marotta, E., Seraglia, R., Traldi, P., 2003. Atmospheric pressure photoionization mechanisms. 2. The case of benzene and toluene. Rapid Commun. Mass Spectrom. 17, 2423−2429.

Vaikkinen, A., Kauppila, T.J., Kostiainen, R., 2016. Charge exchange reaction in dopant-assisted atmospheric pressure chemical ionization and atmospheric pressure photoionization. J. Am. Soc. Mass Spectrom. 27, 1291−1300.

Van Berkel, G.J., 2003. An overview of some recent developments in ionization methods for mass spectrometry. Eur. J. Mass Spectrom. 9, 539−562.

van der Klift, E.J.C., Vivó-Truyols, G., Claassen, F.W., van Holthoon, F.L., van Beek, T.A., 2008. Comprehensive two-dimensional liquid chromatography with ultraviolet, evaporative light scattering and mass spectrometric detection of triacylglycerols in corn oil. J. Chromatogr. A 1178, 43−55.

Vilaró, F., Pérez-Hedo, M., Eras, J., Canela, R., Eizaguirre, M., 2012. UHPLC-MS analysis of juvenile hormone II in mediterranean corn borer (*Sesamia nonagrioides*) hemolymph using various ionization techniques. J. Agric. Food Chem. 60, 3020−3025.

Wang, G., Hsieh, Y., Korfmacher, W.A., 2005. Comparison of atmospheric pressure chemical ionization, electrospray ionization, and atmospheric pressure photoionization for the determination of cyclosporin A in rat plasma. Anal. Chem. 77, 541−548.

Wang, I.T., Feng, Y.T., Chen, C.Y., 2010. Determination of 17 illicit drugs in oral fluid using isotope dilution ultra-high performance liquid chromatography/tandem mass spectrometry with three atmospheric pressure ionizations. J. Chromatogr. B Anal. Technol. Biomed. Life Sci. 878, 3095−3105.

Wu, L., Eberlin, M.N., Corilo, Y.E., Liu, D.Q., Yin, H., 2009. Dimerization of ionized 4-(methyl mercapto)-phenol during ESI, APCI and APPI mass spectrometry. J. Mass Spectrom. 44, 1389−1394.

Wu, L., Liu, D.Q., Kord, A.S., 2010. Gas-phase meerwein reaction of epoxides with protonated acetonitrile generated by atmospheric pressure ionizations. J. Am. Soc. Mass Spectrom. 21, 1802−1813.

Wu, L., Liu, D.Q., Vogt, F.G., Kord, A.S., 2011. Gas-phase derivatization via the meerwein reaction for selective and sensitive LC-MS analysis of epoxides in active pharmaceutical ingredients. J. Pharm. Biomed. Anal. 56, 1106−1111.

Yan, Z., Cheng, C., Liu, S., 2012. Applications of Mass Spectrometry in Analyses of Steroid Hormones, LC-MS in Drug Bioanalysis. Springer, US, pp. 251−286.

Yang, Q., Shi, X., Gu, Q., Zhao, S., Shan, Y., Xu, G., 2012. On-line two dimensional liquid chromatography/mass spectrometry for the analysis of triacylglycerides in peanut oil and mouse tissue. J. Chromatogr. B Anal. Technol. Biomed. Life Sci. 895−896, 48−55.

Zendjabil, M., Chellouai, Z., Abbou, O., 2016. Role of mass spectrometry in steroid assays. Ann. Endocrinol. 77, 43−48.

Zöllner, P., Mayer-Helm, B., 2006. Trace mycotoxin analysis in complex biological and food matrices by liquid chromatography-atmospheric pressure ionisation mass spectrometry. J. Chromatogr. A 1136, 123−169.

Zwiener, C., Frimmel, F.H., 2004. LC-MS analysis in the aquatic environment and in water treatment − A critical review: Part I: instrumentation and general aspects of analysis and detection. Anal. Bioanal. Chem. 378, 851−861.

This page intentionally left blank

CHAPTER

11

COMPREHENSIVE GAS CHROMATOGRAPHY METHODOLOGIES FOR THE ANALYSIS OF LIPIDS

Giorgia Purcaro[1], Peter Q. Tranchida[2], Luigi Mondello[1,2]
Chromaleont SrL, Messina, Italy[1]; *University of Messina, Messina, Italy*[2]

1. INTRODUCTION

One of the main challenges of separation scientists, in general, is to unravel the chemical profiles of complex, naturally occurring samples. Among the analytical techniques, gas chromatography (GC) is one of the most widely employed for such a purpose. GC was invented ~60 years ago, and since then a considerable degree of progress has been made (James and Martin, 1952). The introduction of comprehensive two-dimensional GC (GC × GC) in 1991 by Liu and Phillips represents one of the most important steps toward the increase of separation power.

In GC × GC experiments, the separation process is carried out on two columns of different selectivity. An interface, defined as the modulator, is located between the two capillaries, and generates a separation peak capacity, which is roughly equal to the product of the two peak capacities (peak capacity can be defined as "the number of peaks that can be potentially located in the one or two dimensional space, with a specific resolution value") in each dimension. Comprehensive GC can be considered as an extension of conventional heartcut multidimensional GC, which involves the separation of specific fractions on two different columns with similar lengths. A comprehensive GC separation is obtained when all the components from the first dimension (1D), usually a conventional column (e.g., 25−30 m × 0.25 mm ID × 0.25 μm), are reanalyzed on the second dimension (2D), commonly a short microbore capillary segment (e.g., 1−2 m × 0.10 mm ID × 0.10 μm). 2D analyses are carried out in a rapid manner, with a duration equal to what is defined as the modulation period (typically in the 4−8 s range).

In this chapter, GC × GC fundamentals will be discussed, along with the main applications in the lipid analysis field.

2. INSTRUMENTATION AND FUNDAMENTAL OPERATIONAL PARAMETERS

As aforementioned, a GC × GC separation is carried out on two columns of different selectivity. The eluate coming from the first column is fractionated and reinjected, through the modulator, onto the

Handbook of Advanced Chromatography/Mass Spectrometry Techniques. http://dx.doi.org/10.1016/B978-0-12-811732-3.00011-X

second capillary column. The two columns can be mounted in a single oven, or in two different ones, the latter option providing a higher degree of flexibility during method optimization. Because the separation on the second column is a very fast GC one, ideally it should last a modulation period (to abide the requirement for a comprehensive analysis). Dedicated detectors, with high acquisition rates, negligible internal volumes, and rapid rise times, are required to accurately reconstruct the narrow chromatography bands generated.

The entire GC × GC process requires data elaboration and visualization. Although basic information on the chromatographic performance can be deducted by expert operators from the modulated raw signal, a transformation process is necessary to visualize and elaborate the results. Dedicated software packages stack 2D chromatograms side-by-side and, considering the modulation time, derive the 1D and 2D retention times for each peak. Peak areas are attained by summing the areas relative to each modulated peak, whereas signal intensity is considered as the height of the tallest modulated peaks and can be visualized in a different way: (1) by the means of colors (color plot), (2) by contour lines (contour plot), or (3) by a 3D plot.

2.1 MODULATORS

The modulator, which is the heart of the GC × GC system, enables the isolation, reconcentration, and reinjection of chromatography bands from a primary to a secondary column, in a continuous and sequential manner. Ideally, the separation on the 2D must end before the following reinjection. The time required to complete a single cycle of events is called the modulation period (P_M). The latter parameter is very important because it must be sufficiently low to maintain the resolution achieved on the primary column but high enough to avoid a loss of sensitivity and to enable the complete elution of the compounds from the second column before the following injection, thus avoiding wrap-around. However, the occurence of wrap-around can be a problem only in specific analytical situations (e.g., in the case of structured chromatograms or if coelutions arise with constituents of the latter fraction). In 1998, Murphy et al. studied the effects of the modulation period, concluding that 1D resolution can be preserved only if every eluting peak is sampled at least three or four times, in the case of in-phase and out-of-phase sampling, respectively. Therefore, in most GC × GC experiments the operational conditions enable the attainment of 15−20 s 1D peak widths and the application of 4−6-s modulation periods.

The different types of modulators that have been developed can be divided into three main classes: (1) heat-based, (2) cryogenic, and (3) flow. The following discussion can be considered as a brief overview, rather than an exhaustive review of all the modulators developed, which are described in more detail by Tranchida et al. (2011a).

2.1.1 Heat-Based Modulators

The very first modulator (Liu and Phillips, 1991) consisted of a 15 cm segment of thick-film capillary column, divided equally into two stages, painted with an electrically conductive film and looped outside the oven, under room temperature conditions. The primary column eluate was focused by the thick stationary-phase film in the first part of the capillary segment; then, the analyte band was remobilized by the application of 20 ms electrical pulse directed to the first segment of the modulator. After the electrical pulse terminated, the segment cooled down to the initial trapping temperature, and the electrical pulse was applied to the second segment of the modulator, with a 100 ms delay between stages. The second pulse launched the entrapped analytes onto the second

column. The described procedure prevented breakthrough of analytes in the modulator. Although the results obtained with the primordial modulator were outstanding (Liu and Phillips, 1994; Phillips and Xu, 1995; Venkatramani and Phillips, 1993), the device was also characterized by low run-to-run repeatability and by excessive fragility.

The first commercial modulator, also developed by Philips (Phillips and Ledford, 1996; Phillips et al., 1999), was the rotating thermal modulator, better known as "sweeper". It consisted of a moving metallic slotted heater, with a gap to allow the capillary column to pass through. The two columns were connected by using an accumulation section, an intermediate thicker film column, which retarded the travel of solutes through this section, and a short section of an uncoated column (called a pigtail), which then delivered the analytes to the second column. The analytes were retained in the accumulation segment, until the rotating sweeper (at about 100°C above the oven temperature) forced them forward in a focused band.

In spite of the several applications carried out with this kind of modulator (Beens et al., 1998a,b; Frysinger and Gaines, 1999; Frysinger et al., 1999; Phillips et al., 1999), it was abandoned because of a series of disadvantages: the correct alignment of all the modulator parts, to avoid contact with the moving heater, was a critical issue; the system was not suitable for highly volatile compounds, and the maximum oven temperature had to be limited to 100°C below the maximum operating temperature of the modulator stationary phase, thus restricting the range of applications.

Several other thermal modulators were developed, based on the first experiment carried out by Liu and Phillips (1991), although the main disadvantage was the limited thermal stability of the sorbent, restricting the use to highly volatile compounds (Harynuk and Górecki, 2002; Goldstein et al., 2008; Górecki et al., 2009).

2.1.2 Cryogenic Modulators

The first cryogenic modulator was developed by Kinghorn and Marriott (1998). The longitudinally modulated cryogenic system (LMCS) consisted of a small CO_2 cryogenic trap, characterized by a hollow-sleeve configuration, which oscillated across a segment of column located at the head of the 2D. The primary column eluate was trapped and focused by the liquid CO_2-cooled trap; then the trap was moved along the capillary column, exposing the previously cooled spot to the GC oven, and thus ejecting the entrapped compounds, in a narrow band, onto the second column (Kinghorn and Marriott, 1999). Analyte desorption occurred by moving the trap to the downstream position, to avoid breakthrough. Compared to heat-based modulators, the LMCS entrapped highly volatile compounds (although limited to the C_4–C_6 alkanes range), and the final oven temperature was related to the specific columns employed. The LMCS operating temperature is an important optimization parameter. A temperature of *circa* 100°C lower than the GC elution temperature is generally sufficient for effective entrapment of most compounds. However, excessively low temperatures can retard analyte release (especially for high molecular weight (MW) compounds), whereas intense cooling (−120/−140°C) is required for entrapment of highly volatile compounds (i.e., C_4–C_6 alkanes). The main disadvantage of the LMCS modulator is the "wear and tear" caused by the continuous movement.

Shortly after the introduction of the first cryogenic modulator, several other approaches were developed with the aim of avoiding moving instrumental parts. In 2000, Ledford presented a dual-stage modulator, formed by two cold jets and two hot jets; hence, the name quad-jet modulator. The quad-jet modulator has been used both with CO_2 or liquid nitrogen; the version commercialized by LECO Corporation uses the latter.

In 2001, Beens et al. simplified the quad-jet configuration by removing the hot jets. The remobilization of the entrapped compounds was achieved by exploiting the heated oven air. The "Beens" version has been commercialized by Thermo Scientific.

The most successful simplification of the original quad-jet modulator was developed by Ledford et al. (2002). The simple introduction of a delay loop enabled the performance of dual-stage modulation with a single cold jet that cooled two different segments of the trapping capillary, and a hot jet, positioned perpendicularly, that assured effective removal of the entrapped compounds. The main drawback of this modulator is the high consumption of liquid nitrogen. The loop-type modulator is commercialized by Zoex Corporation.

Other dual-stage modulators have been proposed but all remain at a research stage (Kallio et al., 2003a, 2008; Hyötyläinen et al., 2002).

2.1.3 Flow Modulators

Considering the high costs of cryogenic fluids, it comes as a natural consequence that the development of flow (or pneumatic) modulators is, in general, desirable. The first attempt in this direction was made by Bruckner et al. in 1998, who used four ports (out of six) of a diaphragm valve. The primary column flow was directed to a waste line for most of the modulation period; afterward, the valve was rapidly switched for a brief period, directing the effluent to the second column, pushed by a relatively high auxiliary flow (15 mL/min). Consequently, differential flows were used in the first and second column. Because the valve was located between the two dimensions, such flow modulation (FM) devices can be defined as "in-line" ones. Even though interesting results were obtained, a series of drawbacks limited the applicability of the valve system, namely the loss in sensitivity, due to the low duty cycle and the temperature constraints because the diaphragm valve (maximum operational temperature 175°C) was located inside the GC oven. In other research, the problem related to the temperature limitation was, in part, circumvented by positioning the sensitive portion of the valve outside of the oven; additionally, duty cycles were increased greatly (Seeley et al., 2000; Sinha et al., 2003; Mohler et al., 2006). Nowadays, the thermal stability of diaphragm valves has been greatly improved, with FM operation possible at temperatures of up to 325°C (Freye et al., 2015).

In 2004, Bueno and Seeley developed a differential-flow system, with no diaphragm valve. The system was composed of two sample loops connected through four T-unions. The direction of the primary column flow, which entered the modulator, was controlled by an auxiliary flow, regulated by a three-port solenoid valve located outside the oven. When the D^1 flow was directed to one loop (fill mode), the content of the other was released (flush mode) onto the second column. At the end of the "fill" (or "flush") period, the solenoid valve was activated, leading to an inversion of the flow directions (e.g., the loop previously flushed passes to the "fill" state). With such a configuration, a 100% duty cycle was attained because all the primary column effluent was flushed onto the second column, and there were no temperature limitations. Because the valve was not located between the two dimensions, such FM systems can be defined as "out-of-line" ones.

Seeley et al. (2006) modified the previous FM device, and developed a simpler out-of-line modulator, consisting of a single fill/flush loop constructed by using a 15 cm × 0.45 mm ID segment of deactivated fused silica. The loop was bridged between two micro T-unions, an upstream and downstream one, with the former connected to the first column and the latter linked to the second. Both unions were connected to an auxiliary flow source by using two fused-silica branches. When the FM was in the "fill" (or accumulation) mode, the auxiliary flow (20 mL/min) was directed to the

downstream union, and the 1D effluent (about 1 mL/min) flowed through the loop. It is noteworthy that the accumulation time (1400 ms) was less than the time necessary for the effluent to reach the downstream union (about 1500 ms). When the solenoid valve was activated for a brief period (100 ms), the auxiliary flow emptied the content of the loop onto the 2D (flush or reinjection mode), whereas the flow in the first column was temporarily interrupted.

Following such an FM model, other devices have been developed, i.e., one in the form of a metallic plate, with an internal accumulation chamber (Quimby et al., 2007), and another composed of a 7-port wafer chip, with an external loop (Tranchida et al., 2011a,b). The latter device presented two ports linked to the two outlets of the solenoid valve, two ports connected to the first and second columns, and two ports bridged with a 40-μL accumulation loop, whereas the seventh port was linked to a manually regulated split valve and worked as a waste line. Obviously, if required, a second detector could be used instead of the split valve. The presence of a waste line enabled the regulation of gas flows through the second column, thus avoiding one of the main disadvantages of FM, namely the generation of excessively high gas flows, leading to obvious difficulties when using mass spectrometry (MS). In rather recent research, FM experiments were carried out at greatly reduced gas flows (6−8 mL/min) compared to previous work (Tranchida et al., 2014b). The approach proposed was both simple and effective: a reinjection period of 100 ms, with a flow of 24 mL/min, which is equivalent to one of 400 ms, with a flow of 6 mL/min. It was reported that the duration of the reinjection process must not be too long; otherwise the D^1 stop-flow conditions will not be maintained. The main drawback of such an occurrence will be that the D^1 effluent will start filling the loop before the end of the reinjection process.

The FM systems herein described are far from complete; however, an outlook on promising FM systems has been given, in particular on those based on the model proposed by Seeley et al. (2006). It can be anticipated that future interest will be directed to FM systems characterized by a 100% duty cycle, the non-necessity of high gas flows, and with satisfactory thermal stability. In general, apart from the low expense requirements, FM is a good choice when very volatile ($\leq$C4) or high MW ($\geq$C30) analytes are subjected to analysis. On the other hand, the lack of compound reconcentration and a complex optimization process are the main disadvantages.

2.2 COMPREHENSIVE TWO-DIMENSIONAL GAS CHROMATOGRAPHY METHOD OPTIMIZATION

Although the hardware configuration is quite straightforward, method optimization can be a cumbersome issue, and a factor inhibiting the widespread employment of GC × GC. Indeed, solid knowledge of chromatographic basic theory and experience in different branches of the GC field, such as conventional, classical multidimensional, fast microbore column, and high-speed megabore column low-pressure GC, are of great help for rapid and effective GC × GC optimization. The main parameters to be considered are: modulation parameters (temperature and period), stationary phase chemistry, capillary column dimensions, gas flow, temperature program(s), outlet pressure conditions, and the detector settings.

2.2.1 Modulation Parameters

As briefly described previously, modulation parameters are very important and must be carefully addressed in relation to each specific application and type of modulator. The most common types of modulation systems will be herein discussed, namely cryogenic and flow.

In general, 1D peaks must be sampled three to four times to preserve resolution (Murphy et al., 1998); if a D^1 peak is sampled excessively, then a reduction in sensitivity will inevitably occur. Regarding cryogenic systems, important parameters are the entrapment and the releasing temperatures and periods, all issues tightly linked to the specific modulator. It is generally accepted that a temperature of 100°C lower than that of the GC oven is sufficient for the effective focusing of most compounds; a greater temperature difference is required for very volatile analytes (e.g., ≤C4), with liquid N_2 often used for such a scope (if not, breakthrough will occur). On the contrary, a more restricted temperature difference is applied in the analysis of high MW (e.g., ≥C30) compounds, which is necessary to avoid excessive intramodulator retention.

Regarding the release (reinjection) process, a distinction is necessary between hot gas and oven-temperature remobilization. In the latter case, the entrapment temperature has to be carefully tuned to avoid a delay in analyte release, particularly for high MW compounds. The reinjection process can be accelerated by entrapping on a segment of uncoated column and/or extending the release time.

A study focused on the thermal requirements of the loop-type modulator has been reported (Gaines and Frysinger, 2004). It was observed that a difference of maximum 120−140°C between the entrapment and 1D elution temperatures is ideal in most applications. A greater temperature difference will cause peak tailing because of a nonsatisfactory reinjection process. The hot-jet temperature should be at least 40°C higher than the temperature of primary column elution; the duration of the reinjection step should be a compromise: it is necessary to both reduce analyte k values below a specific level and to avoid breakthrough. The authors advised a duration of 300 ms for the reinjection stage. Although not mentioned by the authors, the length of the delay loop is a further important aspect; indeed, if the loop is too long, then analytes are not sufficiently refocused at the second cold segment or, even worse, can cause alternate "misses" in 2D analysis. On the other hand, if the loop is too short then breakthrough can occur during hot-jet operation.

Method optimization using a differential flow modulator, based on the model proposed by Seeley et al. (2006), is even more challenging than cryogenically modulated GC × GC. Three pressure values must be addressed, namely, the inlet, outlet, and modulator pressures. The accumulation and reinjection periods have to be carefully tuned, as well as the 1D and 2D flows. In fact, the accumulation time is highly dependent on the 1D gas flow and the collection loop volume, where overfilling (or breakthrough) must be avoided during the collection step. The reinjection process must enable efficient flushing of the accumulation loop; important reinjection parameters are its duration and the 2D gas flow. For the processes of accumulation and reinjection, it is more convenient to consider loop length (rather than volume) and intraloop gas linear velocities during the two stages (Tranchida et al., 2014b).

2.2.2 Stationary-Phase Combinations

The main aim of GC × GC method development is to maximize the amount of exploitable separation space, which is mainly achieved by choosing a proper stationary-phase combination. The separation mechanisms of the two columns must be different to obtain a so-called "orthogonal" separation. Theoretically, considering two completely independent column selectivities and a fully optimized separation, the peak capacity of a GC × GC system should be equal to the product of the peak capacity value relative to each column. However, such a result is an excessive estimation because both of the aforementioned conditions are never fully achieved. Indeed, entirely dissimilar separation mechanisms do not exist because analyte vapor pressures play a major role in all GC separation processes; furthermore, GC × GC optimization is the result of a compromise between the best conditions for each dimension.

The selection of the column set is related to the primary objectives of a specific application. The most popular and orthogonal combination employs a nonpolar column (e.g., 100% dimethylpolysiloxane or 5% diphenyl + 95% dimethylpolysiloxane) as the 1D and a polar one (e.g., 100% polyethylene glycol or 50% diphenyl + 50% dimethylpolysiloxane) in the 2D. In such a case, the primary column elution order occurs according to increasing boiling points, whereas the secondary column separation is dependent on specific polarity-based interactions (H-bond, dipole−dipole, dispersion forces, etc.). Because separation occurs in the two dimensions according to specific interactions, chemically similar compounds can form bidimensional patterns, which are a very useful tool for peak identification. Using an orthogonal set, the nonpolar compounds are located in the lower parts of the 2D chromatogram, whereas the more polar compounds are more retained in the 2D, and thus are present in the upper part of the contour plot. The GC × GC analysis of fatty acid methyl esters (FAMEs) is a perfect example to illustrate group-type order: Fig. 11.1 shows a complex human plasma fatty acid (FA) profile. Homologous compounds are situated in a grid, according to their chemical characteristics; in particular, saturated FAMEs are in the lower part of the 2D chromatogram, while an increase in the number of double bonds (DBs) in the FA chain intensifies retention in the 2D. FAMEs are also separated according to the DB position. Compounds with the DB in the same ω position are aligned in parallel diagonal lines, with the higher ω positions eluting before the lower ones (ω6 FAMEs elute before ω3 ones).

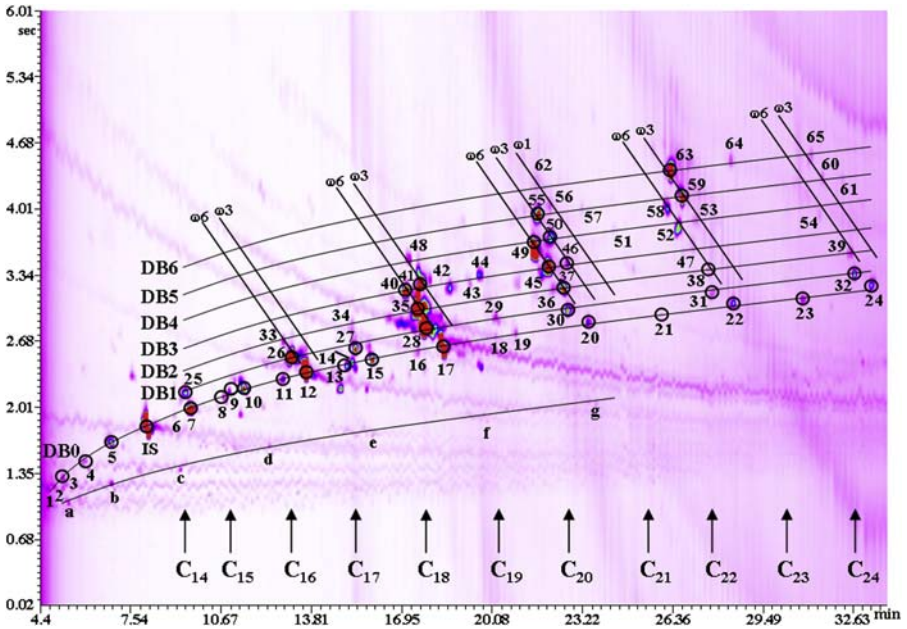

FIGURE 11.1

GC × GC analysis of human plasma fatty acids. For peak identification refer to Tranchida et al. (2008b). *GC*, gas chromatography.

Often, a so-called "reversed" set (polar × nonpolar) can better satisfy the aims of a specific research project. Adahchour et al. (2004) studied and compared orthogonal and nonorthogonal sets for two different complex matrices, namely diesel oil and food flavors. For the former sample type, a completely reversed ordered structure was obtained, with the different classes (alkanes, monoaromatics, diaromatics, etc.) grouped tightly together, giving an advantage when group-type determination is required. When food flavor samples were analyzed, the nonorthogonal approach improved the peak shape of polar compounds, such as aliphatic acids and alcohols, which also improved the ordered structure of the chromatogram. Consequently, the conventional and reversed set must both be considered for the determination of target and unknown compounds in complex matrices.

2.2.3 Carrier-Gas Linear Velocities

The most popular (cryogenic) GC × GC column combination comprises a 30 m × 0.25 mm ID capillary in the low-polarity 1D, and a 1−1.5 m × 0.1 mm ID polar one in the second. Consequently, an inlet pressure value will produce a column flow, which in turn will generate a different linear velocity in each dimension. More specifically, using such a configuration, optimum gas linear velocities cannot be attained in both columns.

Commonly, cryogenically modulated GC × GC experiment gas velocities are close to ideal in the first column (usually slightly slower) and far from ideal (usually much higher) in the second (Shellie et al., 2004; Beens et al., 2005; Tranchida et al., 2007a). Nonoptimum chromatography conditions lead to a loss in overall efficiency. There are different ways to circumvent such a drawback: (1) a wider-bore ID second column (0.15−0.25 mm ID) could be used, generating lower linear velocities, even though this would cause a loss in resolving power; (2) a reduction of the inlet pressure would generate decreased linear velocities, both in the 1D and 2D. Such a solution would have a negative impact on 1D resolution because analytes will elute at higher temperatures, reducing the benefits of the decreased linear velocity in the 2D; and (3) a longer second column would reduce linear velocities; however, the occurrence of wrap-around would increase, requiring extended modulation periods, causing losses in 1D resolution. As can be seen, all three options present both advantages and disadvantages. A further solution to the "gas-velocity" problem was reported by the inventor of GC × GC (et al.), in initial publications (Liu and Phillips, 1991; Venkatramani and Phillips, 1993): specifically, a splitter was used to divert part of the secondary column flow to waste. Such an analytical option was discarded in later papers; however, in 2007 Tranchida et al. described a method defined as split-flow GC × GC (Tranchida et al., 2007a). In the latter experiments, about 30% of the primary column flow was diverted to waste, by connecting the two analytical columns to a short splitter. The splitter was then linked to a manually operated needle valve (located on top of the GC oven), to split the effluent deriving from the primary column and, hence, regulating gas flows in both dimensions. In an initial experiment, fish oil FAMEs were analyzed with the split valve closed; that is, using conventional GC × GC. A H_2 inlet pressure of 194.9 kPa was applied, generating a linear velocity of about 35 and 333 cm/s in the 1D and 2D, respectively. A highly organized chromatogram was obtained under such conditions, though a large amount of two-dimensional space remained unoccupied. Under split-flow conditions, gas velocities were 35 and 213 cm/s in the first and second columns, respectively. The chromatographic improvement was evident: occupation of the 2D space underwent an increase of over 70% (from 22% to 38.4% of the occupied space), whereas resolution was enhanced by more than 50% for many FAMEs (Fig. 11.2). It must be added that 2D overloading is also avoided by using a split-flow configuration. On the other hand, there is an inevitable loss in sensitivity.

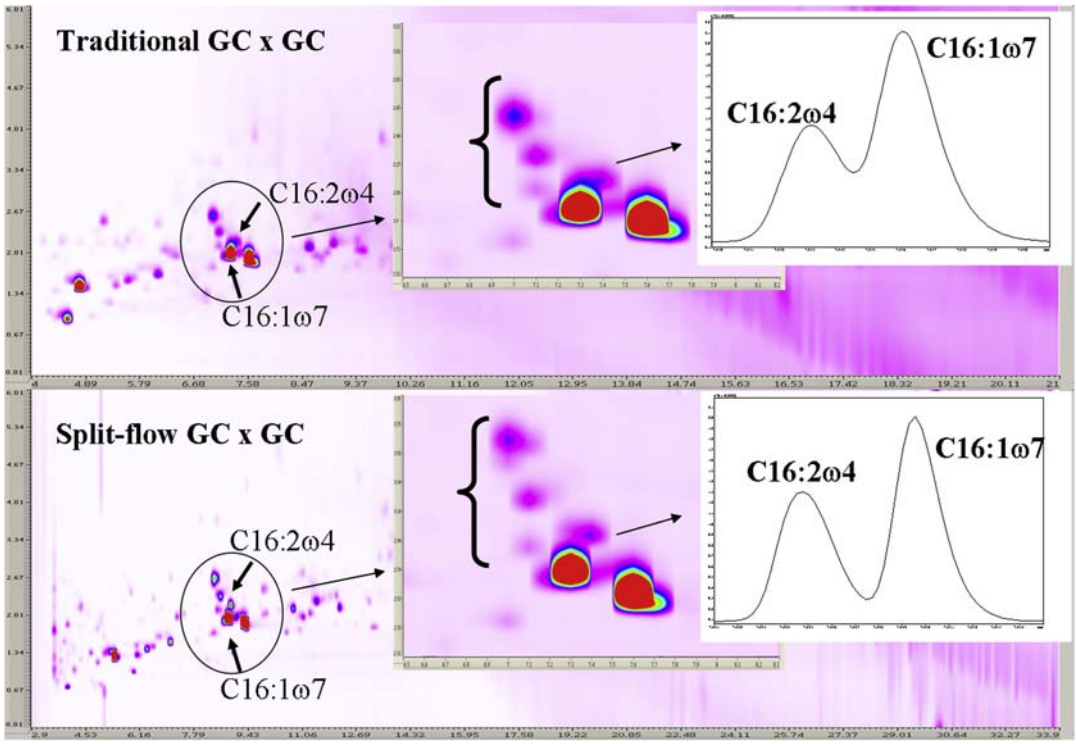

FIGURE 11.2

Comparison of the second-dimension resolution between a traditional and a split-flow GC × GC system, in cod liver fatty acid methyl esters analysis; expansion of the C16 group. *GC*, gas chromatography.

Reproduced with permission from Purcaro, G., Tranchida, P.Q., Mondello, L., 2011. Comprehensive 2D GC methodologies for the analysis of lipids. In: Byrdwell, W.C., Holčapek, M. (Eds.), Extreme Chromatography – Faster, Hotter, Smaller. AOCS Press, Urbana, IL, pp. 381–430.

Regarding differential FM, as mentioned previously, inlet, outlet, and modulator pressures must be addressed during method optimization. In the first instance, one could think that the 1D and 2D gas flows can be decoupled because of the possibility to regulate the modulator pressure. Even though such a conclusion is true to a certain point, it is also true that the accumulation gas flow can be considered equal to that of the first column, whereas the reinjection flow is equal to that of the second column. Consequently, there is a rather complex interplay between the FM parameters and gas velocities in each dimension (Tranchida et al., 2014b).

2.3 DETECTORS

If, in general, the performance of a detector must be carefully evaluated, it must be more so in the field of GC × GC. In fact, the enhanced separation power produced by the two analytical columns can be impaired by detection-derived band enlargement.

As seen previously, modulated peaks are characterized by widths generally in the 100−600 ms range (even less in some applications), and hence the detectors used must be characterized by: (1) very low internal volumes; (2) rapid rise times; and (3) fast acquisition rates for reliable peak reconstruction. The minimum number of data points per peak necessary for correct reconstruction (and quantification) has been widely discussed in the literature, and a variety of opinions exist. For instance, Hinshaw stated that 10 data points across the width at half height are required (Hinshaw, 2003), whereas Dyson concluded that at least 15−20 data points per peak are needed (Dyson, 1999). Adahchour et al. (2005a) were less restrictive, concluding that seven data points per peak were sufficient.

The most commonly used detector in GC × GC has been the flame ionization detector, which is characterized by all the features previously mentioned. The flame ionization detector (FID) is a universal detector, with a response proportional to the carbon content, thus suitable for most quantitative applications. For instance, the FID is highly suitable for petrochemical applications (Phillips and Xu, 1995) because such samples are formed of thousands of compounds belonging to specific chemical groups, and for the majority of which pure standards are lacking. The FID can be used to pinpoint a group-type pattern (e.g., monoaromatics, diaromatics, etc.), and then quantification can be easily performed if representative standard compounds are available. Biedermann and Grob (2009) used GC × GC-FID and group-type pattern formation, for the quantification of mineral oil constituents contained in a contaminated sunflower oil. GC × GC-FID has been used in several other application fields, such as environmental (Reddy et al., 2002; Frysinger et al., 2003) and food (Tranchida et al., 2008a; Vlaeminck et al., 2007).

The electron capture detector (ECD) offers high sensitivity and selectivity for organic molecules containing electronegative functional groups (halogens, phosphorous, and nitro groups). The main concern in the use of the ECD for GC × GC has been related to a rather high internal volume. Kristenson et al. (2003) evaluated and compared the performance of six modulator types (sweeper, LMCS, quad-jet, dual-jet CO_2, semirotating cryo, loop) coupled with three commercially available ECDs. The detectors were characterized by different internal volumes, namely 150, 450, and 1500 μL. It was demonstrated that peak broadening was greatly limited by adjusting the make-up flow in an adequate manner.

The nitrogen−phosphorous detector (NPD) is structurally similar to the FID, except for a ceramic bead above the jet containing an alkali metal salt, which catalyzes the electron transfer to N and P compounds, forming negative ions in a flameless gaseous environment. Ions are then directed to a collector electrode. NPD temperature and gas flow modification can reduce the peak tailing that often occurs because of the temporary adsorption of decomposition products on the ceramic bead (Poole, 2003). GC × GC-NPD has been used for pesticide analysis (Khummueng et al., 2006) and for heavy gas oil samples (von Muehlen et al., 2007).

The sulfur chemiluminescence (SCD) and nitrogen chemiluminescence (NCD) detectors are S-and N-compound selective detectors. Oxidation and combustion, under H_2-rich conditions, generate the corresponding oxide compound, which reacts with O_3 to form an electronically excited dioxide derivative. The latter generates light energy when returning back to the ground state: SO_2 in the blue region of the spectrum, and NO_2 in the red and infrared region. Blomberg et al. (2004) analyzed dibenzothiophene using SCD and FID in a parallel mode. It was found that the electronics, rather than the dead volumes, caused band broadening. Once the problem was circumvented, by using a modified electrometer, S compounds were analyzed in a series of petrochemical products. The NCD has been employed to characterize N-compounds in a diesel sample, in particular carbazoles and indoles (Wang et al., 2004).

The atomic emission detector (AED) is a multielement system, with the possibility to measure up to 23 elements. The GC column ends into a microwave-induced He plasma chamber where all the elements contained in a sample are atomized and excited. Characteristic atomic emission spectra pass through a diffraction grating and are detected by a photodiode array system. van Stee et al. (2003) used an AED, characterized by a rather limited acquisition frequency (10 Hz), for the GC × GC analysis of pesticides. With the aim of obtaining quantitative data and considering the low AED sampling rate, the authors induced band broadening by connecting a 0.7 m × 0.25 mm ID uncoated column to the end of the 0.6 m × 0.10 mm ID polar 2D.

The discharge helium ionization detector is a system with a universal and sensitive response, which can be used for analytes with little or no response to the FID, and present in too low concentrations for thermal conductivity systems. Compounds eluting from the column are subjected to ionization in a secondary region by high-energy photons generated in a nearby He discharge chamber. The separation of the discharge zone from the secondary ionization location, along with the use of a counter-current flow of helium, guarantees that only pure He passes through the discharge chamber, limiting the possibility of contamination (Poole, 2015). Winniford et al. (2006) carried out cryogenic GC × GC using a miniaturized pulsed discharge detector (acquisition frequency 100 Hz). Mixtures of alkanes and aromatic compounds were used to evaluate the detector performance. It was found that extra-column band broadening was 20% (±5%) more compared to an FID, while sensitivity was similar. Franchina et al. (2015) performed FM GC × GC applications with a newly introduced helium ionization detector, defined as a barrier discharge ionization detector (BID). The authors found that, compared to the FID, the BID was characterized by a more limited dynamic range and increased sensitivity (especially for the aromatics).

An independent discussion must be made on MS, which is in its own right a distinct analytical dimension. The hyphenation of MS with a GC × GC system was first made by Frysinger and Gaines (1999), 8 years after the invention of the 2D GC technique (Liu and Phillips, 1991). A single quadrupole MS (qMS), with a limited spectral production frequency (2.43 scan/s), was used. To circumvent such a disadvantage, the 2D peaks were intentionally broadened to a minimum 1 s baseline width, by using a thick 2D stationary phase and by slowing the heating rate down to 0.5°C/min; under such conditions, less than three spectra per peak were obtained. It was concluded that time-of-flight (TOF) MS would be the ideal solution to satisfy GC × GC requirements.

A short period thereafter, van Deursen et al. (2000) described the first GC × GC−TOF MS application, focused again on petrochemical analysis (kerosene). The TOF MS (low resolution (LR)) process generates a complete spectrum from every ion packet exiting the ion source; LR-TOF MS systems can operate in a very fast manner (e.g., 500 spectra/s), potentially generating huge amounts of data. The acquisition of complete spectra and the absence of peak skewing enable the exploitation of deconvolution, a useful tool to unravel peak overlapping. The factors to be considered during optimization of a TOF MS method are: (1) data points per peak, which have to be sufficient not only for reliable peak reconstruction but also for deconvolution; (2) sensitivity, which decreases with an increase of the spectral production rate; and (3) data file size. Consequently, an acquisition rate of 50 Hz is a frequent compromise in GC × GC−TOF MS experiments.

Although TOF MS systems fully satisfy GC × GC requirements, efforts have been made to use qMS, by carefully tuning the qMS parameters in relation to the specific GC × GC application. Moreover, considerable evolution has been made regarding scanning velocity.

In a quadrupole analyzer, the scanning frequency (Hz) is defined by dividing 1000 by the scan time (ms) plus the interscan delay (ms) (Eq. 11.1), where the scan time depends on the mass range (set by the operator) and q scan speed (instrument parameter) (Eq. 11.2). The interscan delay is defined as the time required to reset the initial q voltage, prior to the next scan.

$$\text{Data acquisition rate (Hz)} = \frac{1000}{\text{scan time (ms)} + \text{inter-scan delay (ms)}} \tag{11.1}$$

$$\text{Scan time (s)} = \frac{\text{Mass range scanned } (m/z)}{\text{Scan speed } (m/z) \text{ per second}} \tag{11.2}$$

Several authors tried to push the performance of qMS devices by playing with the mass range; for example, Shellie et al. (2003) attained 20 scan/s using a 4000 *m/z* per second qMS scan speed and by reducing the mass range, in ginseng applications. Cordero et al. (2007) used a qMS system with a high scan speed (11,111 *m/z* per second) in allergen analysis; however, it was found necessary to reduce the mass range (40−240 *m/z*) to achieve 18.52 scan/s because of the rather high interscan delay (30 ms). Mondello et al. (2005) analyzed a commercial perfume using GC × GC in combination with a rapid-scanning qMS (10,000 *m/z* per second). Because of the relatively low interscan delay (calculated to be 14 ms), an acquisition frequency of 20 Hz was achieved using a "normal GC" mass range (40−400 *m/z*).

Considering its operational limitations, qMS instruments have often been considered suitable only for qualitative purposes. The single ion monitoring (SIM) mode has been used to meet the requirements for quantitative analysis because higher acquisition rates can be attained. However, full-scan information is lost in the SIM mode.

The performance of a very rapid qMS system, with a 20,000 *m/z* per second scan speed and a brief interscan delay (5 ms), has been reported (Purcaro et al., 2010a). The reliable GC × GC−qMS quantification of perfume allergens was reported; an average of more than 15 data points per peak were obtained, by using a 50 Hz acquisition rate and a 40−340 *m/z* mass range.

The combination of GC with high-resolution (HR) TOF MS generates a powerful analytical method, due more to the second analytical dimension. In fact, HR-TOF MS generates sensitive full-spectrum information characterized by both high mass resolution and accuracy. The presence of a molecular ion in the spectrum is most desirable because it can give a good idea of the molecular formula. Additionally, the use of extracted ion chromatograms with narrow mass windows is a highly selective procedure, used in targeted analysis because it reduces or eliminates chemical noise and matrix interferences (Hernández et al., 2011). GC−HR-TOF MS can be used for (pre) targeted and untargeted applications; in addition, the full-spectrum data can be investigated at a later stage to look for previously unsearched analytes (posttargeted analysis).

GC × GC has been rarely combined with HR-TOF MS; for instance, Ochiai et al. (2011) used GC × GC−HR-TOF MS to analyze (pretargeted) organochlorine pesticides and untargeted solutes in river water. Sample preparation was carried out through stir-bar sorptive extraction, an approach that contributed toward excellent limits of detection (in the 10−44 pg/L range). The HR-TOF MS system generated 25 spectra/s using a 45−500 *m/z* range. When using a wider extracted mass window, a series of interferences is present in the chromatogram. On the other hand, the application of a 0.05 *m/z* window had a stunning effect on selectivity, eliminating not only all the matrix interferences but also the need for a HR-GC separation.

Triple quadrupole (QqQ) MS devices are highly selective and sensitive instruments, very often used in GC-based pretargeted experiments. Multiple reaction monitoring (MRM) is the most common tandem MS (MS/MS) mode: the first and third quadrupoles (Q1 and Q3) are operated in the SIM mode, whereas collision-induced dissociation reactions occur in a middle cell. Usually, two or three product ions are used, one as a quantifier and the other(s) as qualifier(s); product ions can derive from the same or different precursor ions.

The first GC × GC−QqQ MS experiment was reported in 2008, in an FM pretargeted application (Poliak et al., 2008). Analyte fragmentation was achieved through supersonic molecular beam (SMB) electron ionization (EI), an approach defined as "cold EI" because it generates intense molecular ion peaks. Additionally, the SMB interface had no problem in handling the high FM gas flows. Mass spectral quality increased considerably (94% hit) when GC × GC-SMB MS was used. As was to be expected, diazinon was completely free from matrix interferences when using GC × GC-SMB−MS/MS: Q1 isolated an ion with an *m/z* of 304, whereas Q3 transmitted a product ion with an *m/z* of 179.

In recent research, a vacuum ultraviolet (VUV) detector, with the capability to monitor absorption spectra in the 125−240 nm wavelength range, has been employed in cryogenic GC × GC applications (Gröger et al., 2016). In general, the VUV detector can discriminate between isomeric compounds (i.e., cis−trans isomers) or structurally related isobars; consequently, VUV information is complementary to that of MS. In the preliminary GC × GC study, the VUV system used was characterized by an 80 μL flow cell, operated at a spectral production frequency of 50 Hz, and was found to not have a negative effect on peak shape and chromatographic resolution. The promising GC × GC-VUV results obtained laid the path for further studies using this powerful detector.

3. APPLICATIONS

GC × GC techniques have been applied successfully in many application areas, such as petrochemical, biological and biota samples, environmental and food contamination, and to unravel the complexity of foods and fragrances, in particular coupled to an MS detector.

The number of applications has been continuously increasing during the last 25 years, and several GC × GC reviews have been published. For more thorough information, a series of reviews can be consulted (Adahchour et al., 2006a,b,c, 2008; Tranchida et al., 2004, 2007b, 2015, 2016; Cortes et al., 2009; Nizio et al., 2012; Shi et al., 2014; Cordero et al., 2015; Sampat et al., 2016). The focus of this chapter will be devoted to the penetration of GC × GC into the lipid analysis field.

3.1 LIPIDS ANALYSIS

Lipids are a large class of organic compounds essential for the structure and function of living cells. Their main biological functions are energy storage, structural components of cell membranes, and important signaling molecules. Lipids, as fats and oils, provide an important part of the human dietary intake, both as natural constituents of foods and as ingredients. They are an important source of vitamins and they greatly affect the physical structure of foods and the solubility of taste and aroma constituents (Christie, 2003; Gurr et al., 2002). Lipids comprise a broad range of structures, characterized by nonpolar and hydrophobic skeletons, but some of them contain a polar or hydrophilic group, giving them an amphiphilic character. A general classification divides lipids into saponifiable and

nonsaponifiable fractions. The saponifiable compounds are FAs derivatives, mainly acylglycerols (tri-, di-, and monoacylglycerols), phospholipids, glycolipids, waxes, and sterol esters. The nonsaponifiable constituents include mainly free FAs, isoprenoid lipids (steroids, carotenoids, monoterpenes), and tocopherols.

Comprehensive 2D GC is certainly a valuable tool for lipid analysis, considering the complexity of many samples, and the high importance of thoroughly investigating fat and oil profiles. GC × GC applications on the main classes of lipids are summarized in Table 11.1 and will be hereafter discussed. It is rather evident that most of the applications were initially focused on the investigation of FAs, whereas more recently the attention has moved to considering other classes of lipids in more detail, individually or in a more "−omics" approach (e.g., minor components), and to define the volatile blueprint of high value lipid products, such as extra-virgin olive oil (EVO) for quality assessment.

3.1.1 Fatty Acid Analysis

To characterize the FA profile of any sample, it is usually necessary to preseparate a specific lipid class, and then transform the FAs into less polar and more volatile analytes, mainly methyl esters (FAMEs). To fully separate such a variety of compounds and geometrical and conjugated FA isomers, rather long (up until 100 m) and high-polarity columns are required, such as the bis-cyanopropyl polysiloxane phase (Christie, 2003) or the novel ionic-liquid (IL) phase (Ragonese et al., 2009). Furthermore, although the use of the MS detector with the support of linear retention indices (LRI) has proven useful for peak identification, the confirmation of FA identity can still be a cumbersome task because of the very similar mass spectra of the isomers. GC × GC has been used extensively not only to unravel particularly complex samples but also to highlight an unsuspected complexity of some of these FAME profiles. In fact, the formation of rationalized chemical patterns of compounds over the chromatographic plane, on the basis of the number of carbons and DB, is of great value for the assignment of FA "unknowns". Furthermore, the increase of analytical sensitivity has revealed the presence of minor components, such as odd carbon-number FAs. The advantages obtained using GC × GC in FAME analysis are undoubted.

The first FA investigation in the GC × GC field was carried out in 2001 by de Geus et al., using a thermal sweeper (5 s modulation period), a 9.0 m × 0.2 mm ID × 0.33 μm HP-1 (dimethylpolysiloxane) column in the 1D, and a 0.30 m × 0.1 mm ID × 0.2 μm CP-WAX-52 (polyethylene glycol) as the second column. The FA profiles of several vegetable and fish oil samples were visualized using an FID detector.

Marriott et al. (Western et al., 2002) confirmed the advantages of GC × GC in FA analysis by employing a cryogenic modulator, namely the LMCS and testing two sets of columns: BPX5 (5% phenyl-equivalent polysilphenylene phase) × BP20 (polyethylene glycol phase) and BP1 (100% polydimethylsiloxane) × BPX70 (cyanopropyl polysilphenylene equivalent to 70% cyanopropyl siloxane). With the latter set about 70 peaks were separated, of these 49 peaks were identified by exploiting group-pattern formation. Harynuk et al. (2006) studied what they called "sample dimensionality" in the case of FAMEs. It is noteworthy that, in the case of FAMEs analysis, the universally accepted Kovats' LRI is often replaced by analogous parameters known as equivalent chain length (ECL) and fractional chain length (FCL). The former is calculated by plotting the logarithms of the retention times of a homologous series of straight-chain saturated FAMEs versus the number of carbon atoms in the aliphatic chain. The FCL is simply the fractional increment in the ECL value, which is dependent on the number and positions of DB and the presence of substituent groups (methyl branches,

Table 11.1 GC × GC Applications in the Lipidic Field

Compounds	Detector	1D Column	2D Column	Observation	Reference
FAMEs in edible oils	FID	HP-1 9 m × 0.2 mm ID × 0.33 μm	CP-Wax 52 0.3 m × 0.1 mm ID × 0.2 μm	First FAMEs separation in GC × GC.	de Geus et al. (2001)
FAMEs in natural fats and oils	FID	BPX-5MS 30 m × 0.25 mm ID × 0.25 μm Supelcowax-10 30 m × 0.25 mm ID × 0.25 μm	Supelcowax-10 1 m × 0.1 mm ID × 0.1 μm SPB-5 1 m × 0.1 mm ID × 0.1 μm	Use of orthogonal and nonorthogonal set.	Mondello et al. (2003)
FAMEs in olive oils	FID	CPSil 8 10 m × 0.25 mm ID × 0.25 μm BP20 wax 25 m × 0.32 mm ID × 0.25 μm	BP20 wax 1 m × 0.1 mm ID × 0.1 μm BPX35 1 m × 0.1 mm ID × 0.1 μm	Twin-GC × GC split into orthogonl and nonorthogonal sets.	Adahchour et al. (2005b)
FAMEs in olive oil	FID	SP-2560 100 m × 0.25 mm ID × 0.20 μm	Equity-1 0.9 m × 0.1 mm ID × 0.1 μm	Identification of odd-C number FAMEs.	Tranchida et al. (2008a)
FAMEs in milk	FID	CP 7420 100 m × 0.25 mm ID × 0.25 μm CP 7420 100 m × 0.25 mm ID × 0.25 μm HP-1 30 m × 0.25 mm ID × 0.25 μm HP-1 30 m × 0.25 mm ID × 0.25 μm	HP-5MS 1.5 m × 0.1 mm ID × 0.1 μm HP-1 1 m × 0.1 mm ID × 0.1 μm cyano col 1 m × 0.1 mm ID × 0.1 μm DB-Wax 1 m × 0.1 mm ID × 0.1 μm	Four different sets were studied.	Hyötyläinen et al. (2004)
FAMEs in milk	FID	BPX-5MS 30 m × 0.25 mm ID × 0.25 μm BPX-80 30 m × 0.25 mm ID × 0.25 μm	BP-20 0.85 m × 0.1 mm ID × 0.2 μm BP-35 0.25 m × 0.1 mm ID × 0.1 μm	Identified 27 FAMEs.	Vlaeminck et al. (2007)

Continued

Table 11.1 GC × GC Applications in the Lipidic Field—cont'd

Compounds	Detector	1D Column	2D Column	Observation	Reference
FAMEs in animal fat	TOF-MS	SLB-5MS 10 m × 0.1 mm ID × 0.1 μm	DB-Wax 0.5 m × 0.1 mm ID × 0.1 μm	Fast separation.	Chin et al. (2009)
FAMEs in bovine fats and milk	FID	SLB-IL100 60 m × 0.2 mm ID × 0.2 μm	BPX-50 3 m × 0.1 mm ID × 0.1 μm	Study of the cis/trans separation on five different sets.	Villegas et al. (2010)
FAMEs in animal fats	TOF-MS	DB-5 ms 30 m × 0.25 mm ID × 0.25 μm	DB-Wax 1 m × 0.1 mm ID × 0.1 μm	Identified 51 FAMEs.	Indrasti et al. (2010b)
FAMEs in menhaden oil and human cells	FID	SLB-111 200 m × 0.25 mm ID × 0.2 μm	SLB-111 2.5 m × 0.10 mm ID × 0.08 μm	A palladium-coated capillary between the 1D and 2D column reduced the unsaturated FAMEs.	Delmonte et al. (2013)
FAMEs in menhaden oil	FID	SLB-111 100 m × 0.25 mm ID × 0.2 μm	SLB-111 2 m × 0.10 mm ID × 0.08 μm	A palladium-coated capillary between the 1D and 2D column reduced the unsaturated FAMEs.	Delmonte et al. (2014)
FAMEs in anchovy's brain and vegetable oil	qMS	ZB-5 30 m × 0.25 mm ID × 0.25 μm	ZB-50 1 m × 0.1 mm ID × 0.1 μm		Lucci et al. (2009)
FAMEs in cod liver oil	FID	BPX5 30 m × 0.25 mm ID × 0.25 μm	BP20 0.8 m × 0.1 mm ID × 0.1 μm	Study of sample dimensionality.	Harynuk et al. (2006)
FAMEs in cod liver oil	FID	Equity-5 30 m × 0.25 mm ID × 0.25 μm	Supelcowax-10 1 m × 0.25 mm ID × 0.25 μm	GC × GC separation used to support peak identification in fast GC.	Mondello et al. (2006)
FAMEs in cod liver oil	FID	Equity-5 30 m × 0.25 mm ID × 0.25 μm	Supelcowax-10 1 m × 0.25 mm ID × 0.25 μm	First use of the split-flow system.	Tranchida et al. (2007a)
FAMEs in marine oil	FID	BPX-5 30 m × 0.25 mm ID × 0.25 μm BP 1 25 m × 0.22 mm ID × 0.2 μm	BP 20 0.8 m × 0.1 mm ID × 0.1 μm BPX 70 1 m × 0.1 mm ID × 0.2 μm	Study of isomers separation in two sets of column.	Western et al. (2002)

FAMEs in human plasma	FID	Equity-1 30 m × 0.25 mm ID × 0.25 μm	Supelcowax-10 0.95 m × 0.1 mm ID × 0.1 μm	Identified 65 FAMEs.	Tranchida et al. (2008b)
FAMEs of glycerophospholipids from human buccal mucosal cells	FID	HP-5 30 m × 0.25 mm ID × 0.25 μm	polar (not specified) 1 m × 0.1 mm ID × 0.1 μm		Bogusz et al. (2012)
FAMEs in biota	TOF-MS	HP-5MS 30 m × 0.25 mm ID × 0.25 μm	BPX 50 1 m × 0.1 mm ID × 0.1 μm	Direct-thermal-desorption (DTD) interface was employed to inject whole cell suspension.	Akoto et al. (2008)
FAMEs in benthic diatoms	FID	DB-1MS 10 m × 0.1 mm ID × 0.1 μm	SLB-IL 82/SLB-IL 100/HP-88 4 m × 0.25 mm ID × 0.2 μm	Used a commercial flow modulator.	Gu et al. (2011)
Bacteria FAs (BAMEs)	FID	HP-5MS 30 m × 0.25 mm ID × 0.25 μm	BPX 70 1 m × 0.1 mm ID × 0.1 μm	The method was compared to a reference one for taxonomic identification (Sherlock MIDI).	David et al. (2008)
Bacteria FAs (BAMEs)	FID, qMS	HP-5MS 30 m × 0.25 mm ID × 0.25 μm	BPX 70 4 m × 0.25 mm ID × 0.25 μm	A first commercialized flow modulator was employed. After the second dimension separation the flow was split between an FID and an MS detector.	Gu et al. (2010)
Bacteria FAs (BAMEs)	qMS	SLB-5MS 11.4 m × 0.1 mm ID × 0.1 μm	Supelcowax-10 1 m × 0.05 mm ID × 0.05 μm	Two dedicated libraries were built, namely a GC × GC BAMEs library and Bacteria library.	Purcaro et al. (2010b)

Continued

Table 11.1 GC × GC Applications in the Lipidic Field—cont'd

Compounds	Detector	1D Column	2D Column	Observation	Reference
FAMEs in biodisel	FID, TOF-MS	Solgel Wax 30 m × 0.25 mm ID × 0.25 µm	DB1 1 m × 0.1 mm ID × 0.1 µm	Several type of first and second dimension stationary phases were compared to maximize the FAs and alkanes resolution.	Adam et al. (2008)
FAMEs in biodiesel	FID	BPX-5 15 m × 0.25 mm ID × 0.25 µm	BP 20 1 m × 0.1 mm ID × 0.1 µm	Useful method to differentiate the origin and type of biodiesel.	Tiyapongpattana et al. (2008)
Mono- and diglyceride in fats and oils	TOF-MS	DB17ht 6 m × 0.1 mm ID × 0.1 µm	SLB-5MS 0.6 m × 0.1 mm ID × 0.1 µm	Regioisomers separation.	Indrasti et al. (2010a)
TAGs edible oils and fats	FID	CP-Wax 30 m × 0.25 mm ID × 0.25 µm	VF-23 3 m × 0.1 mm ID × 0.1 µm	TAGs previously separated in AgLC and derivatized to FAMEs prior GCxGC analysis.	de Koning et al. (2006)
Waxs in lanolin	TOF-MS	XTI-5 10 m × 0.25 mm ID × 0.25 µm	BPX-50 1 m × 0.1 mm ID × 0.1 µm	Five different sets were tested.	Jover et al. (2005)
Wax in edible oils	FID	PS-255 20 m × 0.25 mm ID × 0.12 µm	SOP-50 1.5 m × 0.15 mm ID × 0.075 µm	Use of an LC preseparation.	Biedermann et al. (2008)
Sterols in lip mussels and cow faecal mixtures	FID	BPX-5 30 m × 0.25 mm ID × 0.25 µm	BP 50 2 m × 0.1 mm ID × 0.1 µm	Separation of critical couples.	Truong et al. (2003)
Unsaponifable in vegetable oils	FID/MS	SLB-5MS 30 m × 0.25 mm ID × 0.25 µm	Rxi-17Sil MS 2 m × 0.25 mm ID × 0.25 µm		Tranchida et al. (2013a)
Unsaponifable in milk and butter	FID/MS	SLB-5MS 30 m × 0.25 mm ID × 0.25 µm	Rxi-17Sil MS 2 m × 0.25 mm ID × 0.25 µm		Tranchida et al. (2013b)
Unsaponifable in plasma	FID/MS	SLB-5MS 30 m × 0.25 mm ID × 0.25 µm	Rxi-17Sil MS 2 m × 0.25 mm ID × 0.25 µm		Salivo et al. (2015)

FAMEs and unsaponifable in lemon seed	QqQ-MS	SLB-5MS 20 m × 0.18 mm ID × 0.18 μm	SPB-50 10 m × 0.32 mm ID × 0.20 μm	A flow modulator was used.	Tranchida et al. (2014a)
Minor components in vegetabl oils	FID/MS	Rxi-5Sil MS 8 m × 0.25 mm ID × 0.25 μm	Rxi-17Sil MS 1.5 m × 0.15 mm ID × 0.15 μm	Validation of quantity results for waxes and alkyl fatty acids.	Purcaro et al. (2015)
Minor components in vegetabl oils	FID/MS	Rxi-5Sil MS 8 m × 0.25 mm ID × 0.25 μm	Rxi-17Sil MS 1.5 m × 0.15 mm ID × 0.15 μm		Purcaro et al. (2016)
POPs in human plasma	TOF-MS	DB-1MS 30 m × 0.25 mm ID × 0.25 μm	BPX-50 1.5 m × 0.1 mm ID × 0.1 μm	Identify 18 POPs; the method was fully validate for 10 compounds.	Menéndez-Carreño et al. (2012)
Steroids (standards)	IRMS	DB-5 ms 30 m × 0.25 mm ID × 0.25 μm	DB-17 1 m × 0.1 mm ID × 0.1 μm	Optimization of the IRMS coupling.	Tobias et al. (2008)
Steroids in urine	FID, TOF-MS	BPX-5 30 m × 0.25 mm ID × 0.25 μm BPX-50 30 m × 0.25 mm ID × 0.25 μm	BPX 50 1 m × 0.1 mm ID × 0.1 μm BPX 5 1 m × 0.1 mm ID × 0.1 μm	Highlighted the necessity of dedicated TOF-MS library.	Mitrevski et al. (2008)
Steroids in urine	FID	BPX-5 18 m × 0.18 mm ID	BPX 50 1 m × 0.1 mm ID	Stationary phase thickness not reported.	Mitrevski et al. (2007)
Steroids in urine	FID, TOF-MS	BPX-5 30 m × 0.25 mm ID × 0.25 μm	BPX 50 1 m × 0.1 mm ID × 0.2 μm	Six anabolic agents listed by World Anti-Doping Agency (WADA) were investigated.	Mitrevski et al. (2010)
Steroid in urine	TOF-MS	HP-1 17 m × 0.2 mm ID × 0.11 μm	OV-1701 1 m × 0.1 mm ID × 0.1 μm	Method validated for five steroid-doping compounds.	Silva et al. (2009)
Steroids in nutritional supplements	TOF-MS	DB-5 ms 30 m × 0.25 mm ID × 0.25 μm	BPX-50 2 m × 0.1 mm ID × 0.1 μm	Twenty-five steroids were analyzed.	Stepan et al. (2008)
Volatile of olive oils	TOF-MS	BPX-5 30 m × 0.25 mm ID × 0.25 μm	BPX-20 1.5 m × 0.1 mm ID × 0.1 μm	Data handling performed using image analysis.	Vaz-Freire et al. (2009)

Continued

Table 11.1 GC × GC Applications in the Lipidic Field—cont'd

Compounds	Detector	1D Column	2D Column	Observation	Reference
Volatile of olive oils	TOF-MS	DB-5 25 m × 0.2 mm ID × 0.33 μm	Supelcowax-10 1.2 m × 0.1 mm ID × 0.1 μm	Data reduction performed by evaluating the GC–O analysis results.	Peres et al. (2013)
Volatile of olive oils	TOF-MS	DB-5 25 m × 0.2 mm ID × 0.33 μm	Supelcowax-10 1.2 m × 0.1 mm ID × 0.1 μm	Data handling performed on monodimensional GC. GC × GC used only for identification purposes.	Cajka et al. (2010)
Volatile of olive oils	qMS	Rxi-5MS 30 m × 0.25 mm ID × 0.25 μm Solgel Wax 30 m × 0.25 mm ID × 0.25 μm	Supelcowax-10 1.2 m × 0.1 mm ID × 0.1 μm OV1701 1 m × 0.1 mm ID × 0.1 μm	Two different GC × GC system, equipped with different column set, were used, obtaining consistent information.	Purcaro et al. (2014)
Volatile of seed oil	TOF-MS	DB-5 60 m × 0.25 mm ID × 0.1 μm	Rxi-17Sil 2 m × 0.15 mm ID × 0.15 μm		Hu et al. (2014)

1D, *first dimension;* 2D, *second dimension;* FAs, *fatty acids;* FAMEs, *fatty acid methyl esters;* FID, *flame ionization detector;* GC, *gas chromatography;* GC–O, *GC–olfactometry;* IRMS, *isotope ratio mass spectrometry;* LC, *liquid chromatography;* MS, *mass spectrometry;* POPs, *phytosterol oxidation products;* TAG, *triacylglycerols;* TOF, *time-of-flight;* QqQ, *triple quadrupole.*

ring system, and oxygenated moieties). In GC × GC separations, group pattern formation has usually been discussed in terms of primary and secondary retention times (^1t_R and ^2t_R), though using such parameters the relationship is strictly limited to the given instrumental set-up. Therefore, the authors explored the relationship between "sample dimensionality" and "separation dimensionality". Dimensionality is defined by Giddings as "the number of independent variables that must be specified to identify the components of the sample" (Giddings, 1995), thus "sample dimensionality" comprises chemical characteristics, such as carbon chain length, number of DB, branch position, functional groups, etc. On the other hand, "separation dimensionality" is the number of different, isolated separation mechanisms to which the sample is subjected. To achieve a better understanding of the FAMEs analyzed, the plot of ^1t_R versus ^2t_R was compared with several other plots using basic chemical information, such as ^2k versus the chain length, ^2t_R versus chain length, and FCL versus the number of DB. Such information can be used to predict the separation of a known sample in the 2D space and to extract basic chemical information of "unknowns" from the GC × GC chromatogram.

The performances of four column combinations were studied in the analysis of milk FAs, to maximize FAME resolution (Hyötyläinen et al., 2004). A very long (100 m) cyano column (CP7420), coupled with two different nonpolar columns (HP-1 and HP-5), was compared to a traditional 30 m nonpolar column (HP-1) coupled with a 1 m × 0.1 mm ID × 0.1 μm cyano capillary and with a 0.35 m × 0.05 mm ID × 0.1 μm DB-Wax column. The latter column combination resulted in the best choice, even if the high backpressure caused by the microbore column enabled the use of only a short segment. Villegas et al. (2010) tested five different sets of columns to optimize the resolution of *cis*/*trans* C_{18} isomers, to quantify *trans*-vaccenic acid in bovine fat without any interference. The best results were obtained using an SLB-IL 100 column (60 m × 0.2 mm × 0.2 μm) as the 1D and a medium polarity column in the 2D (BPX-50 3 m × 0.1 mm × 0.1 μm).

Indrasti et al. (2010b) used a GC × GC system, coupled with a TOF-MS detector, to study the FAME profile of lard in comparison with goat, chicken, and cattle fat; the objective of the investigation was to evaluate the possibilities to determine lard adulteration. It is worth noting that the FAME composition was statistically different ($P < .05$) among the various species of animals. In total, 51 components were identified, and in particular the authors concluded that three FAs can be used as markers for lard, namely $C_{18:3n3t}$, $C_{20:3n3t}$, and $C_{20:2n6}$.

Mondello et al. (2003) applied GC × GC-FID to the analysis of vegetable and fish oils, using both nonpolar × polar and polar × nonpolar column combinations; and they thoroughly studied FA-class pattern formation. The 2D position of each series of homologous compounds was mathematically described by logarithmic curves. Identification was also supported by using GC−MS and LRI data.

A nonorthogonal set with a long polar column in the 1D (100 m) was employed by Tranchida et al. (2008a) to optimize the separation of critical isomer couples in olive and hazelnut oils. Thanks to the increased sensitivity, several odd C-number FAMEs were detected for the first time in such samples; furthermore, a series of FAMEs was identified only in hazelnut oil, in particular $C_{16:1\omega5}$ was detected at relatively high concentrations (0.007%), enabling the detection of the fraudulent addition of 5% of hazelnut oil into olive oil.

It has been previously discussed that both orthogonal and nonorthogonal column sets can be useful to unravel the profiles of complex samples. In 2005, Adahchour et al. (2005b) analyzed olive oil FAMEs by combining two methods in one system by using a column-entrance-split, which diverted the sample (50:50) onto two distinct sets; therefore, all the desired information was obtained in the time of a single run. Retention time repeatability was evaluated using both configurations, injecting a standard

mixture five consecutive times. Values lower than 0.3% and 1.7% were obtained on the first and second columns, respectively. One drawback of the reverse set was the lower thermal stability of the wax phase, which generated bands of modulated bleed material.

FAs are usually bonded to glycerol, forming triacylglycerols (TAGs), the main constituents of fats and oils (up to 98%). TAGs are high boiling point compounds, and therefore are usually analyzed intact by means of high-performance liquid chromatography, or by GC equipped with high-temperature stable columns. An on-line three-step approach was proposed to characterize TAG profiles: after a silver-phase LC separation, online transmethylation of the TAGs was performed prior to GC × GC analysis (de Koning et al., 2006). A CP-Wax column was used as the 1D, to separate FAMEs according to chain length and the number and positions of the DB, whereas a VF-23 ms capillary column was employed as the 2D, for improved *cis*/*trans* isomer isolation. Method optimization was carried out with a relatively simple sample of hydrogenated vegetable oil, with a total analysis time of 2 h.

A very interesting approach was presented by Delmonte et al. (2013, 2014). The issue was faced from a different viewpoint; in fact the same stationary phase was employed in the 1D and 2D, while the chemical nature of the analyzed compounds was altered. A capillary tube catalyzer (in this specific case Pd) was located at the exit of the first column before entering the modulator, and H_2 was used as the carrier gas. Under these conditions, unsaturated FAMEs are reduced to their fully saturated analogues, thus decreasing dimensionality of the sample solely to their unique alkyl chain structures. A well-ordered 2D plot was thus obtained, where the FAMEs within the same carbon number group are aligned along parallel horizontal lines, with increasing chain lengths moving toward the upper part of the chromatogram. However, the identification was only partially supported by the rationalized chemical patterns, whereas additional support was required from available literature, GC−MS analysis, fractionation using silver-ion chromatography, and separation of reference materials. The proposed method was applied to the analysis of FAMEs in different samples, such as menhaden oil (Fig. 11.3) and human colon adenocarcinoma cells.

Although the investigation of FAs profile is of high interest in biological samples (e.g., plasma and other fluids) since it can be related to a series of diseases (e.g., hypertension, diabetes, coronary heart disease, inflammatory and autoimmune disorders, and cancer), few works have been published on this topic. Tranchida et al. (2008b) identified 65 compounds in human plasma using pure standard compounds according to specific positions in highly structured chromatograms (Fig. 11.1). Bogusz et al. (2012) investigated the FA profile of the glycerophospholipid fraction from a buccal swab, after a base-catalyzed derivatization and a solid-phase microextraction (SPME) preconcentration.

The FA profile is important to classify living organisms, such as microalgae, meiofauna species, and microorganisms. Akoto et al. (2008) used a GC × GC−TOF MS system, equipped with a direct thermal desorption injection interface, for the analysis of whole/intact phytoplankton and zooplankton samples, by simultaneously performing a thermally assisted hydrolysis and methylation. Thanks to the increased sensitivity and to the improved separation, the authors found a series of FAs never mentioned before in several types of microalgae and plankton. Gu et al. (2011) studied the FAME profiles of two types of benthic diatoms, namely *Cylindrotheca closterium* and *Sillago robusta* by using GC × GC equipped with a flow modulator. A nonpolar DB-1MS column (10 m × 0.1 mm × 0.1 μm) was used in the 1D; while the separation performance of different 2D stationary phases (4 m × 0.25 mm × 0.2 μm) were compared. In particular, the authors compared two IL columns (SLB-IL 82 and SLB-IL 100) and a bis(cyanopropyl)silicone stationary phase (HP-88), obtaining very comparable results.

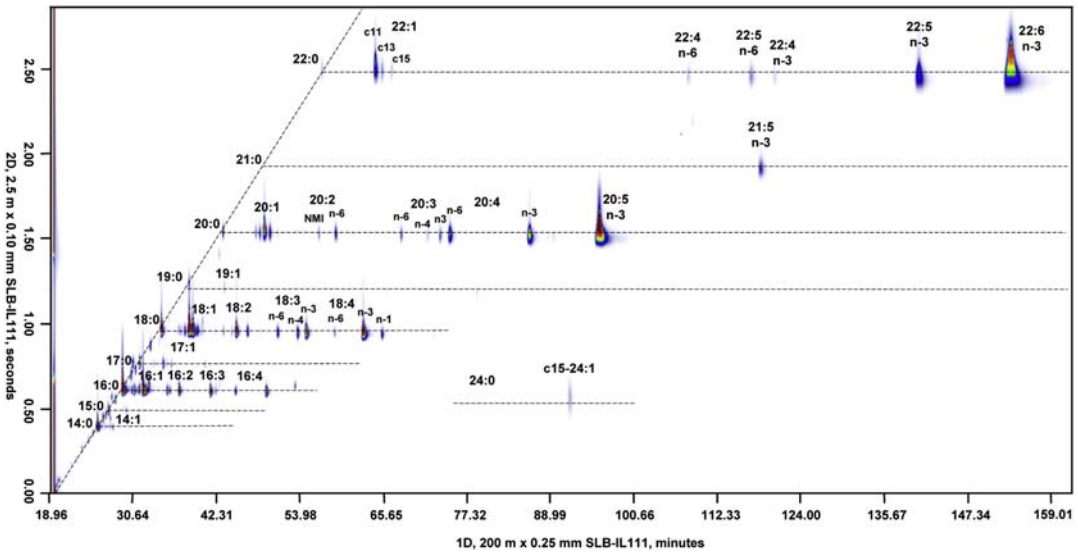

FIGURE 11.3

Two-dimensional chromatogram of menhaden fish oil sample obtained using GC-online hydrogenation × GC-FID. *FID*, flame ionization detector; *GC*, gas chromatography.

Reproduced with permission from Delmonte, P., Fardin-Kia, A.R., Rader, J.I., 2013. Separation of fatty acid methyl esters by GC-online hydrogenation × GC. Anal. Chem. 85, 1517–1524.

The use of FA profiles in the taxonomic classification of microorganisms has been described since 1963 (Abel et al., 1963). The FA composition is markedly affected, both in qualitative and quantitative terms, by the nature of the medium, growth conditions, and age of the culture when harvested. Bacterial lipids are characterized by uncommon FAs, such as odd-chain, branched-chain (mainly iso- and anteiso-), cyclopropane, and hydroxyl FAs, as well as positional isomers of unsaturated FAs. Therefore, the structured chromatograms obtained through GC × GC analysis are very useful to elucidate the composition of such sample types. David et al. (2008) compared the data obtained from the well-established Sherlock MIDI analysis method (M. Sasser, MIDI Technical Note 101, 1990, www.midi-inc.com) with that derived by using loop-modulated GC × GC-FID. Two parameters were exploited for peak assignment, namely ECL in the 1D and relative polarity in the 2D. The latter was calculated as the ratio between retention time of the solute over the average retention times of preceding and proceeding saturated linear methyl esters. The same group (Gu et al., 2010) compared the separations obtained for the same bacteria FA sample, using a cryogenic modulator and a flow modulator. Furthermore, a flow-modulated method was optimized using parallel detection. A Y-splitter was located at the end of the second column, diverting the flow between a 1.2 m × 0.25 mm ID uncoated tube connected to an FID and a 0.5 m × 0.1 mm ID capillary linked to a qMS detector. Using such an instrumental configuration, the MS can be used to identify unknown compounds and the FID for quantification purposes.

Purcaro et al. (2010b) used fast one-step sample preparation for extraction and methylation of bacteria FAs, requiring 2 min, and a relatively rapid split-flow twin-oven comprehensive 2D GC–qMS

separation (25 min). The authors used the linear retention index approach as support to unambiguously identify each compound. Dedicated MS libraries, created using both comprehensive and monodimensional GC systems, were employed. The library LRIs, calculated under monodimensional GC conditions, were comparable to the LRI values obtained using the 2D GC system equipped with the same nonpolar column (SLB-5 ms) in the 1D. Furthermore, the authors proposed a so-called "Bacteria Library," containing single averaged spectra relative to specific bacterium samples, comprising all the methyl esters in the retention time range and then subtracting the compressed chemical noise at three points across the chromatogram. The data derived can be considered as a sample fingerprint, comparable to a direct MS injection. The idea of the authors was to first give a name to the bacteria analyzed, and then investigate the FA profile.

Finally, GC × GC has also proven to be effective in the characterization of the FA profiles of biodiesel, where it is important for both quality control and forensic reasons. Usually, biodiesel is mixed with conventional diesel, and these blends are designed as BX fuels (where X is the percentage of pure biodiesel). The unraveling of such mixtures is a challenging task. Several stationary phases were investigated by Adam et al. (2008) to maximize the resolution of three different series of homologs (alkanes, FAMEs, and n-alkylaromatic compounds) in both the 1D and 2D. Six types of columns of the same dimension (30 m × 0.25 mm × 0.25 μm) were tested as the 1D, namely SPB 5, DB 1701, UB Wax, Solgel Wax, BPX 50, and BPX 90. Poor resolution between alkanes and FAMEs, as well as between FAMEs with different double bond numbers, was obtained using an apolar phase (DB-1). Solgel Wax and UB Wax showed the best performance, with the former the prime choice because of the maximum operating temperature (300°C vs. 260°C). Five different stationary phases were evaluated in the 2D (1 m × 0.1 mm × 0.1 μm), namely DB 1, DB 1701, BPX 50, BPX 70, and BPX 90. Obviously, poor resolution results were reported using either the BPX 70 or BPX 90 column because the combination with the Solgel Wax was excessively correlated. The best separation between FAs and aromatics was obtained, as expected, by coupling a secondary nonpolar column (DB-1). The optimized set was employed to analyze two blends of commercial petroleum diesel, with transesterified coprah oil and rapeseed oil; an MS detector was employed for identification, whereas an FID was exploited for quantification purposes. The quantitative results obtained were in good agreement with the reference European method (European Standard EN 14331: Liquid petroleum products, separation and characterization of FAMEs from middle distillates, 1 April 2004), except for minor components, where slight differences were highlighted. It was the authors' opinion that such inconsistency was caused by the increased sensitivity and resolution obtained by using GC × GC, compared with monodimensional GC.

3.1.2 Other Lipid Compounds

Fewer applications, compared to FA analysis, have been carried out on other lipid components, although their exploration has increased in recent years. The analysis of TAGs directly by GC is rather cumbersome because of their high boiling points. Their investigation by GC × GC is even more complicated because the elution occurs at even higher temperature, and optimization of the modulation conditions can be tricky. Rather high temperature or longer time is necessary to remobilize them after cryofocalization at the modulator, not considering that some compounds are thermolabile. The diffusion of the flow modulator can probably enlarge the fields of application also to these compounds. So far, the only application related to TAGs in GC × GC involves an online transesterification after a preseparation in an LC column, for a GC × GC characterization of the derived FAMEs (as described

previously) (de Koning et al., 2006). Alternatively, many minor components can be much more easily analyzed, not only by GC but also by GC × GC, after derivatization to trimethylsilyl ethers (TMS) to improve volatility. Among these compounds, the main classes are mono- and diacylglycerols (MGs and DGs), sterols, and waxes. MGs and DGs, important intermediates in the biosynthesis of TAGs, but also widely used as emulsifiers in numerous products, are usually analyzed by monodimensional GC (e.g., using the IUPAC-AOAC standard method). However, several coelutions between saturated and unsaturated compounds occur, thus the support of a properly configured GC × GC system was investigated (Indrasti et al., 2010a). A short high-temperature resistant column (DB17ht 6 m × 0.10 mm × 0.1 μm) and a short capillary fragment of an SLB-5 MS column (60 cm × 0.10 mm × 0.1 μm) were used in the 1D and 2D, respectively. Despite the poor orthogonality, a useful structured chromatogram was obtained. Compounds were separated according to the number of carbon atoms and DB, with MGs eluted earlier than DGs. Regioisomers were also resolved, with the 1,2-DGs eluted prior to 1,3-DGs.

Promising results have been obtained using GC × GC to investigate steroids, sterols, phytosterol oxidation products (POPs), and other minor lipid compounds. These compounds are of interest in many fields of application; therefore, depending on the final purpose, many different sample preparation and derivatization approaches (when needed) can be exploited.

Several GC × GC−TOF MS works have been focused on the study of steroids in urine for antidoping purposes (Mitrevski et al., 2007, 2008, 2010; Silva et al., 2009). In particular, Mitrevski et al. (2008) derivatized urine samples by using N,O-bis(trimethylsilyl)trifluoroacetamide (BSTFA), prior to injection into a GC × GC system equipped both with FID and TOF MS detectors. The TOF MS mass spectra obtained were searched against a commercial quadrupole-based MS database (NIST05) and a laboratory-made TOF MS database. Although the mass spectra appeared very similar, the 19 standard sterols evaluated were positively identified, with an average match quality of 950, when the laboratory-made database was employed; on the other hand, only four sterols were positively identified, setting a match threshold of 800, using the NIST05 library. It can be concluded that dedicated MS libraries would be needed when using TOF MS detection.

Stepan et al. (2008) optimized a GC × GC−TOF MS method for the analysis of 25 anabolic steroids contained in nutritional supplements. Ethyl acetate, employed as extraction solvent, did not eliminate several interfering compounds, namely FAs (palmitic acid, stearic acid), saccharide-related compounds (1,6-anhydro-D-glucopyranose, 1,6-anhydro-D-galactofuranose), and aromatic compounds (vanillin, 4-hydroxy-2-methoxycinnamaldehyde). Such compounds may pose a problem for the chromatographic performance, by deposition in the injection liner and in the first part of the capillary column; therefore, a dispersive solid-phase extraction was performed as a clean-up step, by using primary secondary amine (PSA) as a sorbent. The validated method showed good results, except for the steroid oxymetholone, which because of the particular chemical structure, interacted more strongly with PSA (through hydrogen bonding), causing low recovery.

Tobias et al. (2008) coupled a GC × GC system with an isotope ratio MS (IRMS) system for the measurement of steroid $^{13}C/^{12}C$ ratios. In carbon-13 IRMS analyses, all the organic compounds are transformed into CO_2, isotopic abundance measurements are achieved, and thus fragmentation profiles are not generated. The main problem in the GC × GC and IRMS system is excessive band broadening caused by the combustion chamber (about 1 s) and a slow detector response (again, about 1 s). Therefore, the instrument was carefully modified, in terms of the solvent-elimination process, combustion reactor, transfer lines, water trap, and the open split. The description of such modifications is

out of the aim of this chapter; however, band broadening was greatly reduced. The final acquisition frequency of the IRMS was 25 Hz.

GC × GC followed by FID was first applied to the analysis of sterols to analyze their content in environmental water samples (Truong et al., 2003); the ratio between faecal sterols and their hydrogenated products (stanols) is a marker of faecal pollution. Slightly polar and moderately polar thermally stable columns were employed because of the low volatility of the analytes of interest. The entire unsaponifiable fraction of different samples, such as plasma, vegetable oils, and milk were later investigated by cryogenic modulator GC × GC with dual qMS and FID detection, allowing them to perform both qualitative and quantitative analysis in a single chromatographic run (Tranchida et al., 2013a,b; Salivo et al., 2015). The entire unsaponifiable fraction was subjected to derivatization, using BSTFA−1% trimethylchlorosilane (TMCS) [BSTFA−1% TMCS], avoiding the tedious thin-layer chromatography purification step to isolate sterols. Thanks to the high separation power obtained using GC × GC, no coelution occurred between sterols and other lipid classes. In fact, unsaponifiable constituents are nicely spread out on the 2D plane, using an apolar × medium polar set (1D column: SLB-5MS 30 m × 0.25 mm ID × 0.25 μm; 2D column: Rxi-17Sil MS 2 m × 0.25 mm ID × 0.25 μm), with each chemical class located in a specific position.

The same authors translated the proposed method to a GC × GC system equipped with a flow modulator and a QqQ MS detector to investigate the unsaponifiable fraction of a lemon seed extract. Column sizes were properly selected to maximize the separation performance of the flow modulator system, namely an SLB-5 ms 20 m × 0.18 mm ID × 0.18 μm as the 1D and a SPB-50 capillary segment 10 m × 0.32 mm ID × 0.20 μm as the 2D. A simultaneous scan/MRM acquisition mode was used, thus the compounds were identified in scan mode, whereas cholesterol was quantified using MRM data (Tranchida et al., 2014a).

Menéndez-Carreño et al. (2012) performed a silica solid-phase extraction purification and preconcentration step, after cold saponification, to isolate POPs from less polar and more abundant compounds, such as the corresponding sterols. Although many interfering compounds were still present, the target analytes were well resolved because of the gained separation power using GC × GC−TOF MS, which resulted in a superior separation compared to monodimensional GC−HR-TOF MS.

Jover et al. (2005) analyzed lanolin, the wool wax secreted by the sebaceous glands of sheep, by GC × GC−TOF MS without prefractionation from the other various classes of lipids. Various derivatization processes (methylation, silylation, and methylation/silylation) and column combinations were tested. Although the double derivatization process (methylation for acidic groups and silylation for alcoholic groups) was the most time-consuming, it also proved to be the most effective in reducing peak tailing. In fact, the 2D separation was maximized when the polarities of both acidic and alcoholic groups were reduced. A well-structured chromatogram was obtained, highlighted by extracting ions (Fig. 11.4); a series of horizontal analyte bands was observed, formed by compounds of the same chemical class, namely FAs, fatty alcohols, hydroxyl acids, and diols. Despite the large number of compounds reported by the TOF MS software, only 30 compounds were identified with an acceptable spectral similarity (over 800 on a similarity scale varying in the 0−999 range). According to the authors, such a poor result was due to a rather incomplete MS library, especially in the high MW range, and to poor-quality mass spectra, characterized by a considerable reduction of the high MW ion intensity.

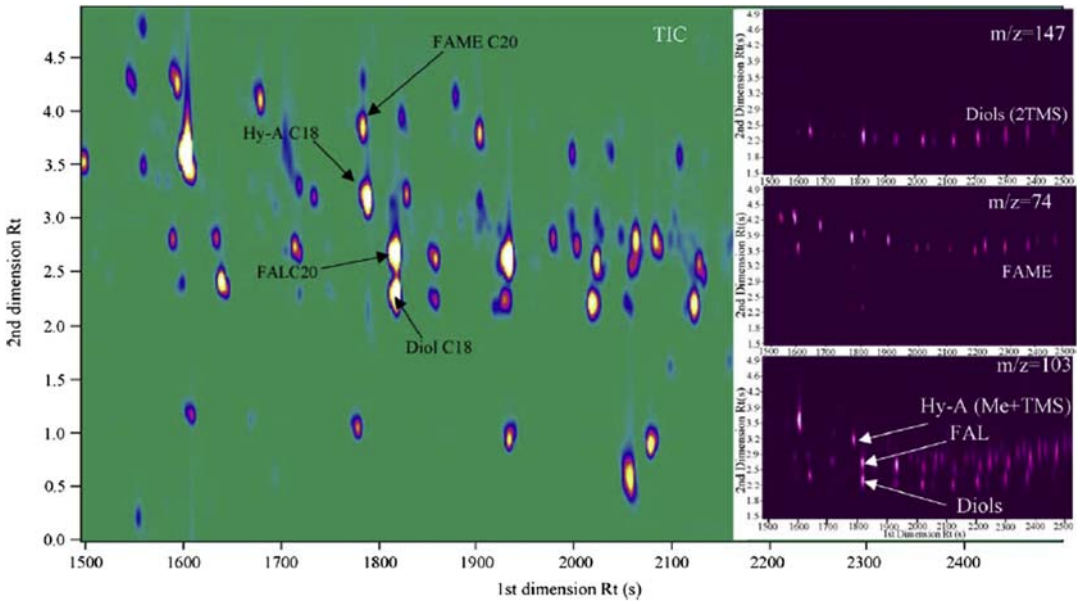

FIGURE 11.4

GC × GC—time-of-flight mass spectrometry total ion current (TIC)-chromatogram of a methylated and silylated lanolin sample (on the left). Inserted windows of extracted ions (*m/z* 74, 103, 147). *FAL*, fatty alcohol; *FAME*, fatty acid methyl ester; *Hy-A*, hydroxyl acids; *ME*, methyl derivative; *TMS*, trimethylsilyl derivative.

Reproduced with permission from Jover, E., Adahchour, M., Bayona, J.M., Vreuls, R.J.J., Brinkman, U.A.T., 2005. Characterization of lipids in complex samples using comprehensive two-dimensional gas chromatography with time-of-flight mass spectrometry. J. Chromatogr. A 1086, 2–11.

Biedermann et al. (2008) investigated the wax ester fraction of various plant oils, by using LC—GC—MS and LC—GC × GC-FID. The normal-phase LC step achieved preseparation of the TAGs, before transferring the wax fraction to the GC system through an on-column interface, by using the concurrent eluent evaporation technique. The LC fraction of interest was collected on a laboratory-coated precolumn (OV-1701-OH, 40 cm × 0.53 mm ID × 0.03 μm film thickness) connected to a vapor exit. Then, the precolumn was dismounted and attached to the inlet of the first column in the GC × GC instrument, where the analysis was performed. The authors highlighted a certain degree of degradation due to thermal stress, in particular of diterpene esters. Such an effect was aggravated by using GC × GC because the flow resistance generated by the second microbore column retarded elution from the first column, thus increasing the elution temperatures. Compound losses were held to a moderate level by using a high flow rate (2 mL/min), using hydrogen as the carrier gas, shortening columns, and carefully selecting the geometry and film thicknesses of the stationary phases.

These classes of compounds were comprehensively investigated by Purcaro et al. (2015, 2016). The official International Olive Council method for FA alkyl esters and waxes was slightly modified by introducing a derivatization step directly on the oil prior to silica column purification; thus free sterols, alcohols, and other polar minor compounds can be eluted as TMS-ether moieties in the same fraction

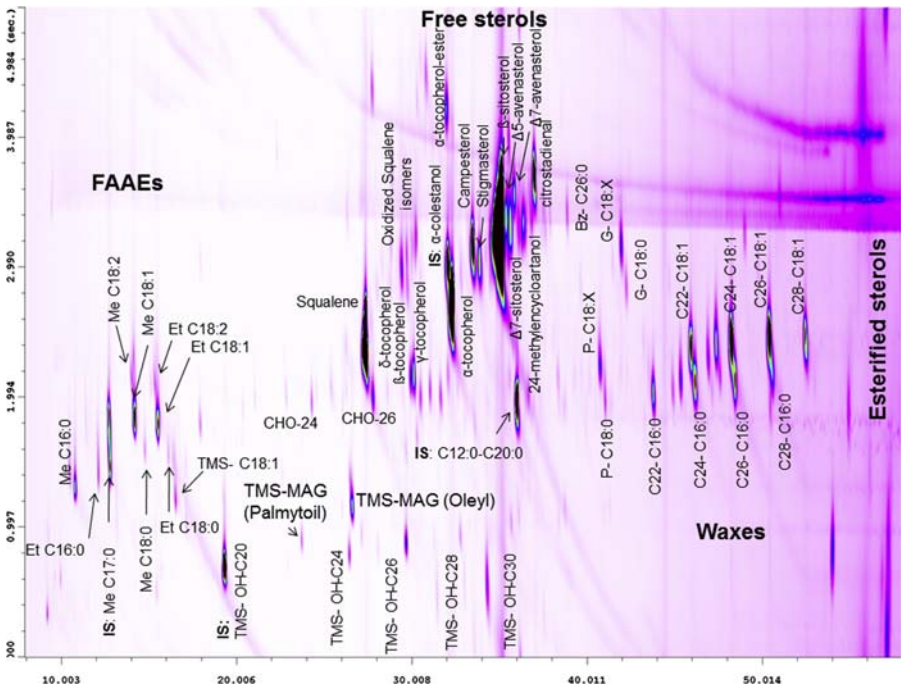

FIGURE 11.5

GC × GC chromatogram of minor components of an extra-virgin olive oil. *FAAEs*, fatty acid alkyl esters; *GC*, gas chromatography; *MAG*, monoacylglycerol.

Reproduced with permission from Purcaro, G., Barp, L., Beccaria, M., Conte, L., 2015. Fingerprinting of vegetable oil minor components by multidimensional comprehensive gas chromatography with dual detection. Anal. Bioanal. Chem. 407 (1), 309–319.

as FA alkyl esters and waxes. The optimization of the chromatographic conditions was rather complicated because several compromises were necessary to locate such different chemical classes in the 2D space, maintaining the chromatographic structure, avoiding wrap-around, and assuring the elution of high boiling compounds in a reasonable time. Although a short 1D column was used (8 m × 0.25 mm ID), an oven offset of +25°C was necessary to avoid extensive wrap-around; thus the structure for esterified sterols was lost because they eluted in the isothermal part of the chromatogram (Fig. 11.5). Such a method was used to investigate several different vegetable oils, but in particular virgin olive oil (VO) and its mixture with extraneous oils (such as hazelnut, sunflower, and palm oil). The reliability of the quantitative data regarding FA alkyl esters and waxes was verified to comply with the legal requirement of the European legislation for these classes of compounds. At the same time, it was pointed out that useful diagnostic information can be extrapolated from the free sterols zone of the chromatogram for facing authentication issues.

3.1.3 Volatiles of Oils and Fats

GC × GC expresses its full separation potential in untargeted analysis (in both qualitative profiling and fingerprinting research) of complex samples, such as food volatiles. It is important to highlight

that GC × GC data processing for general qualitative profiling does not differ from conventional GC−MS (mass spectra similarity matching, use of LRI, etc.), whereas advanced software tools and chemometric elaboration are required to extract information in GC × GC fingerprinting investigations, which have mainly been applied in the field of volatiles analysis. The diagnostic features extrapolated can be used, in principle, to define food authenticity, origin, quality, and safety. The information obtained after data handling can be exploited for comparative pattern analysis, for example, for sample identification (within a set of samples), or for correlation between a chemical profile and a sensorial quality. The latter application is particularly important in the VO field. In fact, both chemical and sensory assessments are officially required to classify an oil into three categories, namely EVO, virgin, and *lampante* olive oil (EU Regulation, 2013). Specifically, the presence (or absence) and intensities of specific defects and of the "fruity" perception are evaluated through well-standardized protocols involving both smelling and tasting. However, many variables affect the flavor and off-flavors of olive oils, including cultivar, geographical origin, fruit ripeness, processing practices, and storage conditions. Despite the fact that extensive knowledge on the volatile composition of olive oil has been accumulated, a robust correlation between chemical features and sensory evaluation has not been achieved yet. This is probably mainly due to the complexity of sensory perception, the fuzziness of the semantics of some descriptors, and the necessity to improve analytical selectivity and resolution along with the preconcentration procedure (Aparicio et al., 2012). From this perspective, the application of GC × GC seems to be the right tool to support analytical fingerprint characterization, as proposed by several authors. However, the main problem is to handle the huge amount of information obtained by GC × GC, for which reliable data handling tools are necessary. Hu et al. (2014) analyzed by GC × GC−TOF MS the volatile fraction of 94 vegetable oils divided into four types, namely soybean (18), peanuts (25), rapeseed (24), and sunflower (27). A "conventional" identification of the 2D plots was carried out, collecting a total of 114 compounds. The obtained dataset was subjected to further statistical elaboration (principal component analysis (PCA) and cluster discriminant analysis) obtaining a well-explained discrimination. It is evident that the identification of all the samples is rather long and tedious, and cannot be used for more complex samples and for large-scale studies. Peres et al. (2013) reduced the information obtained by SPME-GC × GC−TOF MS analyses of two Portugal varieties by performing a GC−olfactometry screening of the same samples. Fifteen odor active compounds were identified, based on their concentrations and odor thresholds, and information relative only to these analytes were extrapolated from the 2D analyses performed. Vaz-Freire et al. (2009) applied SPME followed by GC × GC−TOF MS to discriminate between two different olive oil extraction technologies in three Portugese varieties. The 2D plots were transformed into jpeg format images, divided into quadrants (12 equal-sized for each chromatogram) and then evaluated by using open-source imaging software (ImageJ), obtaining a mapping value for each quadrant related to the pixel-based quantification. Performing PCA, it was possible to determine which quadrant accounted for the highest discrimination, thus allowing a significant reduction in peaks to be considered for further identification and quantification. Purcaro et al. (2014) evaluated whether information obtained by HS-SPME-GC × GC−MS, coupled with advanced data elaboration tools, can be a valuable and more informative analytical approach for a blueprint definition of the volatile fraction of olive oil through an iterative process based on sensory-active volatiles (Fig. 11.6).

Nineteen samples, including EVO, VO, and *lampante* oils, as previously evaluated by a panel test were considered. The 2D plots obtained from two laboratories using different sets of columns, namely

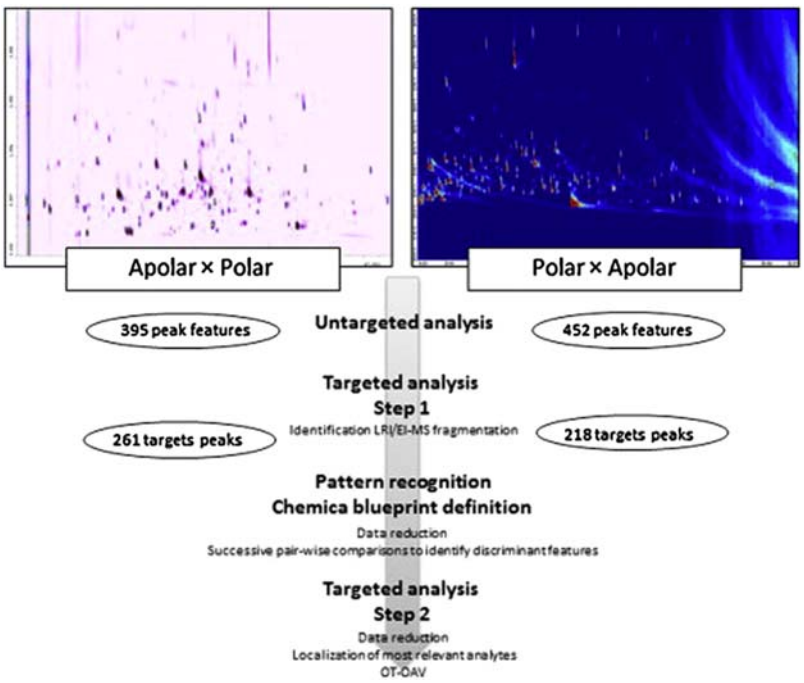

FIGURE 11.6

Scheme of the sequential process applied in the blueprint characterization of virgin olive oils by GC × GC. *GC*, gas chromatography.

Reproduced with permission from Purcaro, G., Cordero, C., Bicchi, C., Conte, L.S., 2014. Toward a definition of blueprint of virgin olive oil by comprehensive two-dimensional gas chromatography. J. Chromatogr. A 1334, 101–111.

apolar × polar and polar × apolar, were elaborated using *Comprehensive Template Matching* fingerprinting (CTMF) (Cordero et al., 2010).

This data handling approach offers the possibility to fully exploit the data matrix generated by GC × GC–MS, by extending correspondences not only to 1D and 2D retention but also to the similarities within the MS fragmentation patterns. The peak features present in all the samples analyzed were collected in a cumulative template, and used to align 2D peaks across sample chromatograms. A total of 395 and 452 untargeted peak features were provided by the apolar × polar and polar × apolar sets, respectively. This information was elaborated by PCA, but a clear discrimination was obtained only for *lamapante* oil, whereas EVO and VO were not clustered separately. Therefore, the 2D patterns were submitted to pairwise comparisons to reveal peculiar quali-quantitative distributions of informative chemicals to be correlated with the sensory data. The analytes selected were normalized by their specific odor threshold values and the data obtained were further elaborated by performing a partial least square discriminant analysis, obtaining a well-explained discrimination (71.28%) of the EVOs from the defective oils.

4. FINAL REMARKS

1. Comprehensive two-dimensional GC, especially if combined with MS, appears to be a perfect technique for the analysis of volatile and semivolatile lipid molecules. In fact, any lipid analyst would be glad of the heightened selectivity (three separation dimensions, related to volatility, polarity, and mass), increased peak capacity and sensitivity, as well as enhanced speed, generated by the 2D approach. In recent years, great effort has been devoted to developing advanced tools to handle the huge amount of information generated by GC × GC, thus simplifying and smartening data elaboration. The technique is now certainly ready to be used for large-scale studies involving high numbers of samples and to exploit it to obtain multilevel information.
2. It is noteworthy that evolution in the MS field, which has been largely observed in recent years, will probably reduce the necessity to increase separation quality, thus slowing down further expansion of the GC × GC technique.

REFERENCES

Abel, K., De Schmertzing, H., Peterson, J.I., 1963. Classification of microorganisms by analysis of chemical composition. I. Feasibility of gas-chromatography. J. Bacteriol. 85, 1039−1044.

Adahchour, M., Beens, J., Vreuls, R.J.J., Batenburg, A.M., Brinkman, U.A.T., 2004. Comprehensive two-dimensional gas chromatography of complex samples by using a "reversed-type" column combination: application to food analysis. J. Chromatogr. A 1054, 47−55.

Adahchour, M., Brandt, M., Baier, H.-U., Vreuls, R.J.J., Batenburg, A.M., Brinkman, U.A.T., 2005a. Comprehensive two-dimensional gas chromatography coupled to a rapid-scanning quadrupole mass spectrometer: principles and applications. J. Chromatogr. A 1067, 245−254.

Adahchour, M., Jover, E., Beens, J., Vreuls, R.J.J., Brinkman, U.A.T., 2005b. Twin comprehensive two-dimensional gas chromatographic system: concept and applications. J. Chromatogr. A 1086 (1−2), 128−134.

Adahchour, M., Beens, J., Vreuls, R.J.J., Brinkman, U.A.T., 2006a. Recent developments in comprehensive twodimensional gas chromatography (GC × GC) I. Introduction and instrumental set-up. TrAC Trends Anal. Chem. 25 (5), 438−454.

Adahchour, M., Beens, J., Vreuls, R.J.J., Brinkman, U.A.T., 2006b. Recent developments in comprehensive two-dimensional gas chromatography (GC × GC) III. Applications for petrochemicals and organohalogens. TrAC Trends Anal. Chem. 25 (7), 726−741.

Adahchour, M., Beens, J., Vreuls, R.J.J., Brinkman, U.A.T., 2006c. Recent developments in comprehensive two-dimensional gas chromatography (GC × GC) IV. Further applications, conclusions and perspectives. TrAC Trends Anal. Chem. 25 (8), 821−840.

Adahchour, M., Beens, J., Brinkman, U.A.T., 2008. Recent developments in the application of comprehensive two-dimensional gas chromatography. J. Chromatogr. A 1186 (1−2), 67−108.

Adam, F., Bertoncini, F., Coupard, V., Charon, N., Thiébaut, D., Espinat, D., Hennion, M.-C., 2008. Using comprehensive two-dimensional gas chromatography for the analysis of oxygenates in middle distillates. I. Determination of the nature of biodiesels blend in diesel fuel. J. Chromatogr. A 1186 (1−2), 236−244.

Akoto, L., Stellaard, F., Irth, H., Vreuls, R.J.J., Pel, R., 2008. Improved fatty acid detection in micro-algae and acquatic meiofauna species using a direct thermal desorption interface combined with comprehensive gas chromatography-time-of-flight mass spectrometry. J. Chromatogr. A 1186, 254−261.

Aparicio, R., Morales, M.T., García-González, D.L., 2012. Towards new analyses of aroma and volatiles to understand sensory perception of olive oil. Eur. J. Lipid Sci. Technol. 114, 1114−1125.

Beens, J., Boelens, H., Tijssen, R., Blomberg, J., 1998a. Simple, non-moving modulation interface for comprehensive two-dimensional gas chromatography. J. High Resolut. Chromatogr. 21 (1), 47−54.

Beens, J., Tijssen, R., Blomberg, J., 1998b. Comprehensive two-dimensional gas chromatography (GC × GC) as a diagnostic tool. J. High Resolut. Chromatogr. 21 (1), 63−64.

Beens, J., Adahchour, M., Vreuls, R.J.J., van Altena, K., Brinkman, U.A.T., 2001. Simple, non-moving modulation interface for comprehensive two-dimensional gas chromatography. J. Chromatogr. A 919 (1), 127−132.

Beens, J., Janssen, H.-G., Adahchour, M., Brinkman, U.A.T., 2005. Flow regime at ambient outlet pressure and its influence in comprehensive two-dimensional gas chromatography. J. Chromatogr. A 1086, 141−150.

Biedermann, M., Grob, K., 2009. Comprehensive two dimensional GC after HPLC preseparation for the characterization of aromatic hydrocarbons of mineral oil origin in contaminated sunflower oil. J. Sep. Sci. 32, 3726−3737.

Biedermann, M., Hasse-Aschoff, P., Grob, K., 2008. Wax ester fraction of edible oils: analysis by on-line LC-GC-MS and GC × GC-FID. Eur. J. Lipid Sci. Technol. 110, 1084−1094.

Blomberg, J., Riemersma, T., van Zuijlen, M., Chaabani, H., 2004. Comprehensive two-dimensional gas chromatography coupled with fast sulphur-chemiluminescence detection: implications of detector electronics. J. Chromatogr. A 1050, 77−84.

Bogusz Jr., S., Hantao, L.W., Braga, S.C.G.N., De Matos França, V.D.C.R., Da Costa, M.F., Hamer, R.D., Ventura, D.F., Augusto, F., 2012. Solid-phase microextraction combined with comprehensive two-dimensional gas chromatography for fatty acid profiling of cell wall phospholipids. J. Sep. Sci. 35 (18), 2438−2444.

Bruckner, C.A., Prazen, B.J., Synovec, R.E., 1998. Comprehensive two-dimensional high-speed gas chromatography with chemometric analysis. Anal. Chem. 70 (14), 2796−2804.

Bueno, P.A., Seeley, J.V., 2004. Flow-switching device for comprehensive two-dimensional gas chromatography. J. Chromatogr. A 1027, 3−10.

Cajka, T., Riddellova, K., Klimankova, E., Cerna, M., Pudil, F., Hajslova, J., 2010. Traceability of olive oil based on volatiles pattern and multivariate analysis. Food Chem. 121 (1), 282−289.

Chin, S.-T., Che Man, Y.B., Tan, C.P., Hashim, D.M., 2009. Rapid profiling of animal-derived fatty acids using fast GC × GC coupled to time-of-flight mass spectrometry. J. Am. Oil. Chem. Soc. 86 (10), 949−958.

Christie, W.W., 2003. Lipid Analysis. The oily press, Bridgwater, England.

Cordero, C., Bicchi, C., Joulain, D., Rubiolo, P., 2007. Identification, quantitation and method validation for the analysis of suspected allergens in fragrances by comprehensive two-dimensional gas chromatography coupled with quadrupole mass spectrometry and with flame ionization detection. J. Chromatogr. A 1150, 37−49.

Cordero, C., Liberto, E., Bicchi, C., Rubiolo, P., Reichenbach, S.E., Tian, X., Tao, Q., 2010. Targeted and non-targeted approaches for complex natural sample profiling by GC × GC-qMS. J. Chromatogr. Sci. 48, 251−261.

Cordero, C., Kiefl, J., Schieberle, P., Reichenbach, S.E., Bicchi, C., 2015. Comprehensive two-dimensional gas chromatography and food sensory properties: potential and challenges. Anal. Bioanal. Chem. 407 (1), 169−191.

Cortes, H.J., Winniford, B., Luong, J., Pursch, M., 2009. Comprehensive two dimensional chromatography review. J. Sep. Sci. 32, 883−904.

David, F., Tienpont, B., Sandra, P., 2008. Chemotaxonomy of bacteria by comprehensive GC and GC-MS in electron impact and chemical ionisation mode. J. Sep. Sci. 31, 3395−3403.

de Geus, H.-J., Aidos, I., de Boer, J., Luten, J.B., Brinkman, U.A.T., 2001. Characterisation of fatty acids in biological oil samples using comprehensive multidimensional gas chromatography. J. Chromatogr. A 910, 95−103.

de Koning, S., Janssen, H.-G., Brinkman, U.A.T., 2006. Characterization of triacylglycerides from edible oils and fats using a single and multidimensional techniques. LC-GC Eur. 19 (11), 590−600.

Delmonte, P., Fardin-Kia, A.R., Rader, J.I., 2013. Separation of fatty acid methyl esters by GC-online hydrogenation × GC. Anal. Chem. 85, 1517−1524.

Delmonte, P., Kramer, J.K.G., Hayward, D.G., Mossoba, M.M., 2014. Comprehensive two dimensional gas chromatographic separation of fatty acids methyl esters with online reduction. Lipid Technol. 26, 11−12.

Dyson, N., 1999. Peak distortion, data sampling errors and the integrator in the measurement of very narrow chromatographic peaks. J. Chromatogr. A 842, 321−340.

European Union (EU) Regulation, 2013. EU Reg. n. 1348/2013. Off. J. Eur. Commun. L338, 31.

Franchina, A.F., Maimone, M., Sciarrone, D., Purcaro, G., Tranchida, P.Q., Mondello, L., 2015. Evaluation of a novel helium ionization detector within the context of (low-)flow modulation comprehensive two-dimensional gas chromatography. J. Chromatogr. A 1402, 102−109.

Freye, C.E., Mu, L., Synovec, R.E., 2015. High temperature diaphragm valve-based comprehensive two-dimensional gas chromatography. J. Chromatogr. A 1424, 127−133.

Frysinger, G.S., Gaines, R.B., 1999. Comprehensive two-dimensional gas chromatography with mass spectrometric detection (GC × GC/MS) applied to the analysis of petroleum. J. High Resolut. Chromatogr. 22 (5), 251−255.

Frysinger, G.S., Gaines, R.B., Ledford, E.B., 1999. Quantitative determination of BTEX and total aromatic compounds in gasoline by comprehensive two-dimensional gas chromatography (GC × GC). J. High Resolut. Chromatogr. 22 (4), 195−200.

Frysinger, G.S., Gaines, R.B., Xu, L., Reddy, C.M., 2003. Resolving the unresolved complex mixture in petroleum-contaminated sediments. Environ. Sci. Technol. 37, 1653−1662.

Gaines, R.B., Frysinger, G.S., 2004. Temperature requirements for thermal modulation in comprehensive two dimensional gas chromatography. J. Sep. Sci. 27, 380−388.

Giddings, J.C., 1995. Sample dimensionality: a predictor of order-disorder in component peak distribution in multidimensional separation. J. Chromatogr. A 703, 3−15.

Goldstein, A.H., Worton, D.R., Williams, B.J., Hering, S.V., Kreisberg, N.M., Panic, O., Górecki, T., 2008. Thermal desorption comprehensive two-dimensional gas chromatography for in-situ measurements of organic aerosols. J. Chromatogr. A 1186 (1−2), 340−347.

Górecki, T., Goldstein, A.H., Kreisberg, N.M., Hering, S.V., Teng, A.P., Worton, D.R., Mcneish, C., 2009. Abstracts. In: International Network of Environmental Forensics Conference, August 31−September 2, Calgary (AB), p. 30.

Gröger, T., Gruber, B., Harrison, D., Saraji-Bozorgzad, M., Mthembu, M., Sutherland, A., Zimmermann, R., 2016. A vacuum ultraviolet absorption array spectrometer as a selective detector for comprehensive two-dimensional gas chromatography: concept and first results. Anal. Chem. 88, 3031−3039.

Gu, Q., David, F., Lynen, F., Rumpel, K., Xu, G., De Vos, P., Sandra, P., 2010. Analysis of bacteria fatty acids by flow modulated comprehensive two-dimensional gas chromatography with parallel flame ionization detector/mass spectrometry. J. Chromatogr. A 1217, 4448−4453.

Gu, Q., David, F., Lynen, F., Vanormelingen, P., Vyverman, W., Rumpel, K., Xu, G., Sandra, P., 2011. Evaluation of ionic liquid stationary phases for one dimensional gas chromatography-mass spectrometry and comprehensive two dimensional gas chromatographic analyses of fatty acids in marine biota. J. Chromatogr. A 1218 (20), 3056−3063.

Gurr, M.I., Harwood, J.L., Frayn, K.N., 2002. In: Lipid Biochemistry. W.H. Freeman Publishers, New York, USA.

Harynuk, J., Górecki, T., 2002. Design considerations for a GC × GC system. J. Sep. Sci. 25 (5/6), 304−310.

Harynuk, J., Vlaeminck, B., Zaher, P., Marriott, P.J., 2006. Projection of multidimensional GC data into alternative dimensions- exploiting sample dimensionality and structured retention patterns. Anal. Bioanal. Chem. 386 (3), 602−613.

Hernández, F., Portolés, T., Pitarch, E., López, F.J., 2011. Gas chromatography coupled to high-resolution time-of-flight mass spectrometry to analyse trace-level organic compounds in the environment, food safety and toxicology. TrAC Trends Anal. Chem. 30, 388−400.

Hinshaw, J.V., 2003. Handling fast peaks. LC-GC N.Am. 21, 268−272.

Hu, W., Zhang, L., Li, P., Wang, X., Zhang, Q., Xu, B., Sun, X., Ma, F., Ding, X., 2014. Characterization of volatile components in four vegetable oils by headspace two-dimensional comprehensive chromatography time-of-flight mass spectrometry. Talanta 129, 629−635.

Hyötyläinen, T., Kallio, M., Hartonen, K., Jussila, M., Palonen, S., Riekkola, M., 2002. Modulator design for comprehensive two-dimensional gas chromatography: quantitative analysis of polyaromatic hydrocarbons and polychlorinated biphenyls. Anal. Chem. 74 (17), 4441−4446.

Hyötyläinen, T., Kallio, M., Lehtonen, M., Lintonene, S., Peräjoki, P., Jussila, M., Riekkola, M.-L., 2004. Comprehensive two-dimensional gas chromatography in the analysis of dietary fatty acids. J. Sep. Sci. 27, 459−467.

Indrasti, D., Che Man, Y.B., Chin, S.T., Mustafa, S., Mat Hashim, D., Abdul Manaf, M., 2010a. Regiospecific analysis of mono- and diglycerides in glycerolysis products by GC × GC-TOF-MS. J. Am. Oil Chem. Soc. 87, 1255−1262.

Indrasti, D., Che Man, Y.B., Mustafa, S., Hashim, D.M., 2010b. Lard detection based on fatty acids profile using comprehensive gas chromatography hyphenated with time-of-flight mass spectrometry. Food Chem. 122 (4), 1273−1277.

James, A.T., Martin, A.J.P., 1952. Gas-liquid partition chromatography: the separation and micro-estimation of volatile fatty acids from formic acid to dodecanoic acid. Biochem. J. 50, 679−690.

Jover, E., Adahchour, M., Bayona, J.M., Vreuls, R.J.J., Brinkman, U.A.T., 2005. Characterization of lipids in complex samples using comprehensive two-dimensional gas chromatography with time-of-flight mass spectrometry. J. Chromatogr. A 1086, 2−11.

Kallio, M., Hyötyläinen, T., Jussila, M., Hartonen, K., Palonen, S., Shimmo, M., Riekkola, M.-L., 2003a. Semi-rotating cryogenic modulator for comprehensive two-dimensional gas chromatography. Anal. Bioanal. Chem. 375 (6), 725−731.

Kallio, M., Jussila, M., Raimi, P., Hyötyläinen, T., 2008. Modified semi-rotating cryogenic modulator for comprehensive two-dimensional gas chromatography. Anal. Bioanal. Chem. 391 (6), 2357−2363.

Khummueng, W., Trenerry, C., Rose, G., Marriott, P.J., 2006. Application of comprehensive two-dimensional gas chromatography with nitrogen-selective detection for the analysis of fungicide residues in vegetable samples. J. Chromatogr. A 1131, 203−214.

Kinghorn, R.M., Marriott, P.J., 1998. Comprehensive two-dimensional gas chromatography using a modulating cryogenic trap. J. High Resolut. Chromatogr. 21 (11), 620−622.

Kinghorn, R.M., Marriott, P.J., 1999. High speed cryogenic modulation − a technology enabling comprehensive multidimensional gas chromatography. J. High Resolut. Chromatogr. 22 (4), 235−238.

Kristenson, E.M., Korytár, P., Danielsson, C., Kallio, M., Brandt, M., Mäkelä, J., Vreuls, R.J.J., Beens, J., Brinkman, U.A.T., 2003. Evaluation of modulators and electron-capture detectors for comprehensive two-dimensional GC of halogenated organic compounds. J. Chromatogr. A 1019, 65−77.

Ledford, E.B., 2000. Presented at the 23rd Symposium on Capillary Gas Chromatography (Riva del Garda).

Ledford, E.B., Billesbach, C., Termaat, J., 2002. Pittcon, March 17−22, New Orleans, LA. Contribution #2262P.

Liu, Z., Phillips, J.B., 1991. Comprehensive two-dimensional gas chromatography using an on-column thermal modulator interface. J. Chromatogr. Sci. 29 (6), 227−231.

Liu, Z., Phillips, J.B., 1994. Sensitivity and detection limit enhancement of gas chromatography detection by thermal modulation. J. Microcolumn Sep. 6 (3), 229−235.

Lucci, P., Pacetti, D., Boselli, E., Frega, N.G., 2009. Comprehensive multidimensional gas chromatography in the analysis of food lipids. Prog. Nutr. 11 (3), 143−148.

Menéndez-Carreño, M., Steenbergen, H., Janssen, H.-G., 2012. Development and validation of a comprehensive two-dimensional gas chromatography-mass spectrometry method for the analysis of phytosterol oxidation products in human plasma. Anal. Bioanal. Chem. 402 (6), 2023−2032.

Mitrevski, B.S., Brenna, J.T., Zhang, Y., Marriott, P.J., 2007. A new paradigm in drugs analysis: comprehensive two-dimensional gas chromatography for steroid analysis. Chem. Aust. 74, 3−5.

Mitrevski, B.S., Brenna, J.T., Zhang, Y., Marriott, P.J., 2008. Application of comprehensive two-dimensional gas chromatography to sterols analysis. J. Chromatogr. A 1214 (1−2), 134−142.

Mitrevski, B.S., Wilairat, P., Marriott, P.J., 2010. Comprehensive two-dimensional gas chromatography improves separation and identification of anabolic agents in doping control. J. Chromatogr. A 1217 (1), 127−135.

Mohler, R.E., Prazen, B.J., Synovec, R.E., 2006. Total-transfer, valve-based comprehensive two-dimensional gas chromatography. Anal. Chim. Acta 555 (1), 68−74.

Mondello, L., Casilli, A., Tranchida, P.Q., Dugo, P., Dugo, G., 2003. Detailed analysis and group-type separation of natural fats and oils using comprehensive two-dimensional gas chromatography. J. Chromatogr. A 1019, 187−196.

Mondello, L., Casilli, A., Tranchida, P.Q., Dugo, G., Dugo, P., 2005. Comprehensive two-dimensional gas chromatography in combination with rapid scanning quadrupole mass spectrometry in perfume analysis. J. Chromatogr. A 1067, 235−243.

Mondello, L., Tranchida, P.Q., Dugo, P., Dugo, G., 2006. Rapid, micro-scale preparation and very fast gas chromatographic separation of cod liver oil fatty acid methyl ester. J. Pharm. Bio. Anal. 41, 1566−1570.

Murphy, R.E., Schure, M.R., Foley, J.P., 1998. Effect of sampling rate on resolution in comprehensive two-dimensional liquid chromatography. Anal. Chem. 70 (8), 1585−1594.

Nizio, K.D., McGinitie, T.M., Harynuk, J.J., 2012. Comprehensive multidimensional separations for the analysis of petroleum. J. Chromatogr. A 1255, 12−23.

Ochiai, N., Ieda, T., Sasamoto, K., Takazawa, Y., Hashimoto, S., Fushimi, A., Tanabe, K., 2011. Stir bar sorptive extraction and comprehensive two-dimensional gas chromatography coupled to high-resolution time-of-flight mass spectrometry for ultra-trace analysis of organochlorine pesticides in river water. J. Chromatogr. A 1218, 6851−6860.

Peres, F., Jeleń, H.H., Majcher, M.M., Arraias, M., Martins, L.L., Ferreira-Dias, S., 2013. Characterization of aroma compounds in Portuguese extra virgin olive oils from Galega Vulgar and Cobrançosa cultivars using GC-O and GC × GC-TOF MS. Food Res. Int. 54 (2), 1979−1986.

Phillips, J.B., Xu, J., 1995. Comprehensive multi-dimensional gas chromatography. J. Chromatogr. A 703 (1−2), 327−334.

Phillips, J.B., Gaines, R.B., Blomberg, J., van der Wielen, F.W.M., Dimandja, J., Green, V., Granger, J., Patterson, D., Racovalis, L., De Geus, H., de Boer, J., Haglund, P., Lipsky, J., Sinha, V., Ledford, E.B., 1999. A robust thermal modulator for comprehensive two-dimensional gas chromatography. J. High Resolut. Chromatogr. 22 (1), 3−10.

Phillips, J.B., Ledford, E.B., 1996. Thermal modulation: a chemical instrumentation component of potential value in improving portability. Field Anal. Chem. Technol. 1 (1), 23−29.

Poliak, M., Fialkov, A.B., Amirav, A., 2008. Pulsed flow modulation two-dimensional comprehensive gas chromatography-tandem mass spectrometry with supersonic molecular beams. J. Chromatogr. A 1210, 108−114.

Poole, C.F., 2003. The Essence of Chromatography. Elsevier, Amsterdam, pp. 66−67.

Poole, C.F., 2015. Ionization-based detectors for gas chromatography. J. Chromatogr. A 1421, 137−153.

Purcaro, G., Tranchida, P.Q., Ragonese, C., Conte, L.S., Dugo, P., Dugo, G., Mondello, L., 2010a. Evaluation of a novel rapid-scanning quadrupole mass spectrometer in an apolar × ionic-liquid comprehensive two-dimensional gas chromatography system. Anal. Chem. 82, 8583−8590.

Purcaro, G., Tranchida, P.Q., Dugo, P., La Camera, E., Bisignano, G., Conte, L., Mondello, L., 2010b. Characterization of bacterial lipid profiles by using rapid sample preparation and fast comprehensive two-dimensional gas chromatography in combination with mass spectrometry. J. Sep. Sci. 33, 2334−2340.

Purcaro, G., Cordero, C., Bicchi, C., Conte, L.S., 2014. Toward a definition of blueprint of virgin olive oil by comprehensive two-dimensional gas chromatography. J. Chromatogr. A 1334, 101−111.

Purcaro, G., Barp, L., Beccaria, M., Conte, L., 2015. Fingerprinting of vegetable oil minor components by multidimensional comprehensive gas chromatography with dual detection. Anal. Bioanal. Chem. 407 (1), 309−319.

Purcaro, G., Barp, L., Beccaria, M., Conte, L., 2016. Characterization of minor components in vegetable oil by multidimensional comprehensive gas chromatography. Food Chem. 212, 730−738.

Quimby, B., McCurry, J., Norman, W., April 2007. Chromatography: Reinvigorating a Mature Analytical Discipline. LC GC The Peak, pp. 7−15.

Ragonese, C., Tranchida, P.Q., Dugo, P., Dugo, G., Sidisky, L.M., Robillard, M.W., Mondello, L., 2009. Evaluation of use of a dicationic liquid stationary phase in the fast and conventional gas chromatographic analysis of health-hazardous C-18 cis/trans fatty acids. Anal. Chem. 81 (13), 5561−5568.

Reddy, C.M., Eglinton, T.I., Hounshell, A., White, H.K., Xu, L., Gaines, R.B., Frysinger, G.S., 2002. The West Falmouth oil spill after thirty years: the persistence of petroleum hydrocarbons in marsh sediments. Environ. Sci. Technol. 36, 4754−4760.

Salivo, S., Beccaria, M., Sullini, G., Tranchida, P.Q., Dugo, P., Mondello, L., 2015. Analysis of human plasma lipids by using comprehensive two-dimensional gas chromatography with dual detection and with the support of high-resolution time-of-flight mass spectrometry for structural elucidation. J. Sep. Sci. 38 (2), 267−275.

Sampat, A., Lopatka, M., Sjerps, M., Vivo-Truyols, G., Schoenmakers, P., van Asten, A., 2016. Forensic potential of comprehensive two-dimensional gas chromatography. TrAC Trends Anal. Chem. 80, 345−363.

Seeley, J.V., Kramp, F., Hicks, C.J., 2000. Comprehensive two-dimensional gas chromatography via differential flow modulation. Anal. Chem. 72, 4346−4352.

Seeley, J.V., Micyus, N.J., McCurry, J.D., Seeley, S.K., 2006. Comprehensive two-dimensional gas chromatography with a simple fluidic modulator. Am. Lab. 38, 24−26.

Shellie, R.A., Marriott, P.J., Huie, C.W., 2003. Comprehensive two-dimensional gas chromatography (GC × GC) and GC × GC- quadrupole MS analysis of Asian and American ginseng. J. Sep. Sci. 26, 1185−1192.

Shellie, R., Marriott, P., Morrison, P., Mondello, L., 2004. Effects of pressure drop on absolute retention matching in comprehensive two-dimensional gas chromatography. J. Sep. Sci. 27, 504−512.

Shi, X., Wang, S., Yang, Q., Lu, X., Xu, G., 2014. Comprehensive two-dimensional chromatography for analyzing complex samples: recent new advances. Anal. Methods 6 (18), 7112−7123.

Silva, A.I., Pereira, H.M.G., Casilli, A., Conceicao, F.C., Neto, F.R.A., 2009. Analytical challenges in doping control: comprehensive two-dimensional gas chromatography with time of flight mass spectrometry, a promising option. J. Chromatogr. A 1216, 2913−2922.

Sinha, A.E., Johnson, K.J., Prazen, B.J., Lucas, S.V., Fraga, C.G., Synovec, R.E., 2003. Comprehensive two-dimensional gas chromatography of volatile and semi-volatile components using a diaphragm valve-based instrument. J. Chromatogr. A 983, 195−204.

Stepan, R., Cuhra, P., Barsova, S., 2008. Comprehensive two-dimensional gas chromatography with time-of-flight mass spectrometric detection for the determination of anabolic steroids and related compounds in nutritional supplements. Food Add. Contam. - Part A 25 (5), 557−565.

Tiyapongpattana, W., Wilairat, P., Marriott, P.J., 2008. Characterization of biodiesel and biodiesel blends using comprehensive two-dimensional gas chromatography. J. Sep. Sci. 31, 2640−2649.

Tobias, H.J., Sacks, G.L., Zhang, Y., Brenna, J.T., 2008. Comprehensive two-dimensional gas chromatography combustion isotope ratio mass spectrometry. Anal. Chem. 80, 8613−8621.

Tranchida, P.Q., Dugo, P., Dugo, G., Mondello, L., 2004. Comprehensive two-dimensional chromatography in food analysis. J. Chromatogr. A 1054 (1−2), 3−16.

Tranchida, P.Q., Casilli, A., Dugo, P., Dugo, G., Mondello, L., 2007a. Generation of improved gas linear velocities in a comprehensive two-dimensional gas chromatography system. Anal. Chem. 79, 2266−2275.

Tranchida, P.Q., Donato, P., Dugo, P., Dugo, G., Mondello, L., 2007b. Comprehensive chromatographic methods for the analysis of lipids. TrAC Trends Anal. Chem. 26, 191−205.

Tranchida, P.Q., Giannino, A., Mondello, M., Sciarrone, D., Dugo, P., Dugo, G., Mondello, M., 2008a. Elucidation of fatty acid profiles in vegetable oils exploiting group-type patterning and enhanced sensitivity of comprehensive two-dimensional gas chromatography. J. Sep. Sci. 31, 1797−1802.

Tranchida, P.Q., Costa, R., Donato, P., Sciarrone, D., Ragonese, D., Dugo, P., Dugo, G., Mondello, L., 2008b. Acquisition of deeper knowledge on the human plasma fatty acid profile exploiting comprehensive 2-D GC. J. Sep. Sci. 31, 3347−3351.

Tranchida, P.Q., Purcaro, G., Dugo, P., Mondello, L., 2011a. The modulators for comprehensive two-dimensional gas chromatography: a review. TrAC Trends Anal. Chem. 30 (9), 1437−1461.

Tranchida, P.Q., Purcaro, G., Visco, A., Conte, L., Dugo, P., Dawes, P., Mondello, L., 2011b. A flexible loop-type flow modulator for comprehensive two-dimensional gas chromatography. J. Chromatogr. A 1218, 3140−3145.

Tranchida, P.Q., Salivo, S., Franchina, F.A., Bonaccorsi, I., Dugo, P., Mondello, L., 2013a. Qualitative and quantitative analysis of the unsaponifiable fraction of vegetable oils by using comprehensive 2D GC with dual MS/FID detection. Anal. Bioanal. Chem. 405 (13), 4655−4663.

Tranchida, P.Q., Salivo, S., Bonaccorsi, I., Rotondo, A., Dugo, P., Mondello, L., 2013b. Analysis of the unsaponifiable fraction of lipids belonging to various milk-types by using comprehensive two-dimensional gas chromatography with dual mass spectrometry/flame ionization detection and with the support of high resolution time-of-flight mass spectrometry for structural elucidation. J. Chromatogr. A 1313, 194−201.

Tranchida, P.Q., Franchina, F.A., Salivo, S., Russo, M., Dugo, P., Mondello, L., 2014a. Flow-modulated comprehensive 2D gas chromatography−triple quadrupole MS elucidation of the fatty acids and unsaponifiable constituents of oil derived from lemon seeds, a food-industry waste product. LC-GC N. Am. 32, 24−29.

Tranchida, P.Q., Franchina, F.A., Dugo, P., Mondello, L., 2014b. Use of greatly-reduced gas flows in flow-modulated comprehensive two-dimensional gas chromatography-mass spectrometry. J. Chromatogr. A 1359, 271−276.

Tranchida, P.Q., Maimone, M., Purcaro, G., Dugo, P., Mondello, L., 2015. The penetration of green sample-preparation techniques in the field of comprehensive two-dimensional gas chromatography. TrAC Trends Anal. Chem. 71, 74−84.

Tranchida, P.Q., Purcaro, G., Maimone, M., Mondello, L., 2016. Impact of comprehensive two-dimensional gas chromatography-mass spectrometry on food analysis. J. Sep. Sci. 39, 149−161.

Truong, T.T., Marriott, P.J., Porter, N.A., Leeming, R., 2003. Application of comprehensive two-dimensional gas chromatography to the quantification of overlapping faecal sterols. J. Chromatogr. A 1019, 197−210.

van Deursen, M., Beens, J., Reijenga, J., Lipman, P., Cramers, C., Blomberg, J., 2000. Group-type identification of oil samples using comprehensive two-dimensional gas chromatography coupled to a time-of-flight mass spectrometer (GC × GC-TOF). J. High Resolut. Chromatogr. 23, 507−510.

van Stee, L.L.P., Beens, J., Vreuls, R.J.J., Brinkman, U.A.T., 2003. Comprehensive two-dimensional gas chromatography with atomic emission detection and correlation with mass spectrometric detection: principles and application in petrochemical analysis. J. Chromatogr. A 1019, 89−99.

Vaz-Freire, L.T., da Silva, M.D.R.G., Freitas, A.M.C., 2009. Comprehensive two-dimensional gas chromatography for fingerprint pattern recognition in olive oils produced by two different techniques in Portuguese olive varieties Galega Vulgar, Cobrançosa e Carrasquenha. Anal. Chim. Acta 633, 263−270.

Venkatramani, C.J., Phillips, J.B., 1993. Comprehensive two-dimensional gas chromatography applied to the analysis of complex mixtures. J. Microcolumn Sep. 5 (6), 511−516.

Villegas, C., Zhao, Y., Curtis, J.M., 2010. Two methods for the separation of monounsaturated octadecenoic acid isomers. J. Chromatogr. A 1217, 775−784.

Vlaeminck, B., Harynuk, J., Fievez, V., Marriott, P.J., 2007. Comprehensive two-dimensional gas chromatography for the separation of fatty acids in milk. Eur. J. Lipid Sci. Technol. 109, 757−766.

von Muehlen, C., de Oliveira, E.C., Morrison, P.D., Zini, C.A., Caramao, E.B., Marriott, P.J., 2007. Qualitative and quantitative study of nitrogen-containing compounds in heavy gas oil using comprehensive two-dimensional gas chromatography with nitrogen phosphorus detection. J. Sep. Sci. 30, 3223−3232.

Wang, F.C.Y., Robbins, W.K., Greaney, M.A., 2004. Speciation of nitrogen-containing compounds in diesel fuel by comprehensive two-dimensional gas chromatography. J. Sep. Sci. 27, 468−472.

Western, R.J., Lau, S.S.G., Marriott, P.J., Nichols, P.D., 2002. Positional and geometrical isomer separation of FAME by comprehensive 2-D GC. Lipids 37 (7), 715−724.

Winniford, B.L., Sun, K., Griffith, J.F., Luong, J.C., 2006. Universal and discriminative detection using a miniaturized pulsed discharge detector in comprehensive two-dimensional GC. J. Sep. Sci. 29, 2664−2670.

CHAPTER

12 ULTRA-HIGH PERFORMANCE SUPERCRITICAL FLUID CHROMATOGRAPHY—MASS SPECTROMETRY

Lucie Nováková, Kateřina Plachká, Pavel Jakubec
Charles University, Hradec Králové, Czech Republic

1. INTRODUCTION

Supercritical fluid chromatography (SFC) is a separation technique that uses instrumentation similar to high performance liquid chromatography (HPLC) and a dense compressed gas, almost always carbon dioxide (CO_2), as a mobile phase. SFC has long been overshadowed by other chromatographic methods, both HPLC and gas chromatography (GC). Although the advantages of the SFC mobile phase in chromatographic separations are indisputable and will be discussed in detail in Section 1.1, the technique itself has experienced a period of rediscovery only recently, with the introduction of advanced SFC instrumental platforms, new stationary phases, and a different view of the technique itself. Although an old view of SFC was limited to strictly supercritical conditions using only pure CO_2 as a mobile phase, which substantially limited the range of compounds that could be analyzed, a modern view of SFC is now represented by CO_2-based mobile phases with the addition of organic modifiers, which remarkably extended the range of applications and the versatility of method development. The addition of an organic modifier of course results in a mobile phase that is not in the supercritical state, usually meaning that the pressure is above the critical pressure, but the temperature is below the critical temperature. However, there is a continuity of physicochemical properties between the supercritical and subcritical state (details given in Section 1.1). Therefore, it is now widely accepted that SFC is used as the name of the technique, bearing in mind that the separations are not always strictly supercritical (Tarafder, 2016; Desfontaine et al., 2015; Nováková et al., 2014).

During the development of SFC over the years, the technique was given many other names, such as: high temperature—high pressure chromatography; dense GC; high pressure gas chromatography (HPGC); solvating gas chromatography; subcritical fluid chromatography; near critical chromatography; convergence chromatography; enhanced fluidity chromatography; HPLC with enhanced fluidity or sometimes even unified chromatography (Lesellier and West, 2015; Guiochon and Tarafder, 2011; Taylor, 2009). In the most modern interpretations, the name could also be translated as separations facilitated by carbon dioxide. Despite this diversity in terminology, the name SFC is the one most widely accepted by the chromatographic community. It is actually interpreted as a definition

Handbook of Advanced Chromatography/Mass Spectrometry Techniques. http://dx.doi.org/10.1016/B978-0-12-811732-3.00012-1

of a technique, chromatography with CO_2 in the mobile phase, rather than a definition of a fluid state (Lesellier and West, 2015). Indeed, as also suggested by Berger (2015a), SFC should be used as a single acronym that includes all the above stated other names. Similar to ultra-high performance liquid chromatography (UHPLC), the highly efficient and faster variant of SFC taking advantage of sub-2 μm particles and dedicated instrumentation is designated as ultra-high performance supercritical fluid chromatography (UHPSFC) (Desfontaine et al., 2015; Nováková et al., 2014).

1.1 SUPERCRITICAL FLUIDS

A supercritical fluid is a state of a fluid that is reached at a temperature and pressure higher than its critical temperature (T_c) and critical pressure (P_c). The most common definition of the supercritical state is based on a P−T diagram showing the vapor−liquid phase equilibrium behavior of the compound. This diagram is shown in Fig. 12.1 for CO_2. At the critical point, the densities of the gas and the liquid become equal and a single fluid, the supercritical fluid, exists under higher pressures, at higher temperatures. The supercritical region corresponds to conditions above the critical pressure and temperature, whereas the conditions below the critical values are designated as subcritical. Furthermore, there are many intermediate states, such as a high-density liquid, high-temperature gas, etc. A wide range of states with intermediate densities (from gas-like to liquid-like density) can thus be reached without the formation of an interface and may be changed by adjusting the temperature and/or the pressure (Guiochon and Tarafder, 2011).

The low viscosity of CO_2 permits the operation of HPLC columns with fine particles at high velocities with low or moderate inlet pressures. Consequently, longer columns and finer particles may be used. High solute diffusion coefficients in supercritical fluids require operation at high velocities,

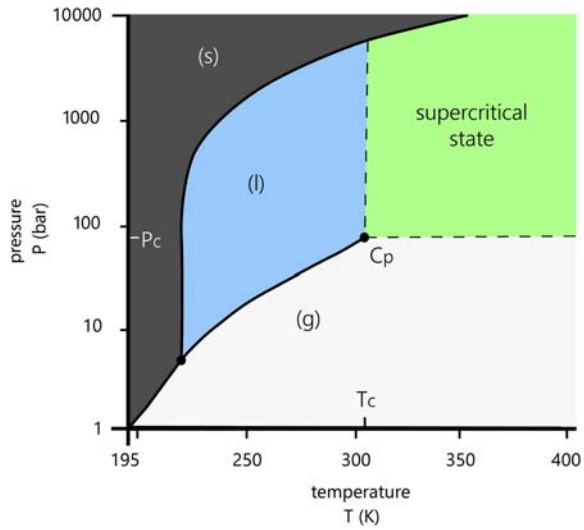

FIGURE 12.1

Phase diagram of carbon dioxide. Solid (s), liquid (l), and gas state (g). C_p, critical point; P_c, critical pressure; T_c, critical temperature.

which provide the method with inherent chromatographic advantages, especially high speed and high separation efficiency, which is maintained at high mobile phase velocities. Column equilibration is also faster, allowing for short cycle times in gradient analysis. The backpressures generated are lower compared to liquid phases, while providing the solvating power similar to that of a liquid, allowing for good solubility and fast transport of the analytes (Guiochon and Tarafder, 2011).

The first use of fluids in the supercritical state in a chromatographic separation was reported by Klesper et al. in 1962, as HPGC. Thermally labile porphyrin mixtures were separated on a polyethylene glycol stationary phase with two mobile phase gases, dichlorodifluoromethane at 112°C and monochlorodifluoromethane at 96°C, at elevated pressures of 70−98 bar. Several fluids were examined as supercritical mobile phases in later studies. However, CO_2 has become the fluid of choice for SFC because of the lack of viable alternatives and many advantages, including low viscosity and surface tension, easy to achieve critical point (74 bar and 31°C, Fig. 12.1; Table 12.1), low cost, the nonflammability, the safety, the availability with adequate purity, the nontoxicity, the inertness toward most compounds, the miscibility to a large variety of organic solvents, and the weak UV absorbance at low wavelengths (Lesellier and West, 2015; Smith, 1999; Berger, 1997). The first use of CO_2 as a supercritical mobile phase in SFC was reported by Sie et al. in 1966.

Although many different fluids (Table 12.1), such as light hydrocarbons (Huetz and Klesper, 1992; Lochmuller and Mink, 1990; Leyendecker et al., 1987; Wright et al., 1985; Novotny et al., 1971),

Table 12.1 An Overview of Supercritical Fluids Tested as Mobile Phases in Supercritical Fluid Chromatography and Critical Parameters of These Fluids

Fluid	MW (g/mol)	T_c (°C)	P_c (bar)
Carbon dioxide	44.01	31.3	73.7
Argon	39.95	−122.5	48.6
Xenon	131.29	16.6	57.6
Ethane	30.07	32.2	48.7
Nitrous oxide	44.01	36.5	72.5
Chlorodifluoromethane	86.47	96.2	49.9
Propane	44.09	96.7	42.5
Dichlorodifluoromethane	120.91	111.9	41.4
Ammonia	17.03	132.2	113.3
Dimethyl ether	46.07	127.2	53.4
Sulfur dioxide	64.06	157.5	78.8
Diethyl ether	74.12	192.7	35.6
Pentane	72.15	196.7	33.6
Isopropanol	60.10	235.3	47.0
Methanol	32.04	240.5	78.9
Water	18.02	373.9	220.6

MW, *molecular weight;* P_c, *critical pressure;* T_c, *critical temperature.*

xenon (Raynor et al., 1991), argon (Thurbide and Cooke, 2003), nitrous oxide (Wright et al., 1985), sulfur dioxide (Leren et al., 1991), chlorofluorocarbons (Berger and Deye, 1991b; Klesper et al., 1962), ammonia (Lauer et al., 1983), and others (Leyendecker et al., 1984) have been tested, no viable alternative has been discovered (Berger, 1997). Many of these fluids presented several drawbacks, such as safety issues, hardware damage, unsuitability for thermolabile compound analysis, and environmental pollution. Although ammonia may represent an interesting variant for more polar compounds, its use produced irreproducible results and has not been accepted because of important safety risks (Raynie et al., 1993; Lauer et al., 1983; Giddings et al., 1968). Sulfur dioxide offers solvent polarity, but it is too corrosive and difficult to obtain in a pure form (Leren et al., 1991). Nitrous oxide has been tested in many SFC studies, it exhibits similar solvent strength as CO_2, but it is a strong oxidizing agent and should not be mixed with organic solvents (Berger, 1997; Wright et al., 1985). An important limitation is also that it may be difficult to achieve the critical point, such as in the cases of water, methanol, isopropanol, and argon (Table 12.1).

The solvating power of a supercritical fluid mobile phase depends on the density of the fluid. Therefore, density is often considered as the most influential feature for SFC, especially when using pure CO_2 as a mobile phase (Lesellier and West, 2015). In a neat CO_2 mobile phase, the pressure (density) gradient is used to promote the elution of the analytes. However, with the variations of pressure and/or temperature the solvent polarity of CO_2 does not change very much. CO_2 displays highly lipophilic properties, similar to those of hexane or heptane, which limits the applicability of the neat CO_2 to the analysis of lipophilic compounds and makes it unsuitable for working with polar analytes. Therefore, in modern SFC, addition of a polar modifier to CO_2, using isocratic or gradient elution, is a more common and successful option. An important benefit of the modern SFC approach is the miscibility of CO_2 with organic modifiers of a wide range of polarities over a broad range of pressures and temperatures. This property made SFC a very versatile technique, enabling separation of a very wide range of compounds with only one system, taking advantage of combinations of CO_2-based mobile phases and both polar and nonpolar stationary phases (Tarafder, 2016).

It should be mentioned here that, with the addition of an organic modifier, both T_c and P_c are rapidly increased. Indeed, at 30% of an organic modifier the critical values are increased substantially, resulting in $T_c = 135°C$ and $P_c = 168$ bar, instead of the critical values shown for neat CO_2 in Table 12.1. Consequently, under commonly used SFC conditions, such as 100−150 bar and 40°C, the mobile phase is not any more in the supercritical state. Under such conditions, the solvating power or retention can hardly be controlled by changing the pressure because the temperature and pressure are below the critical values of the binary mixture fluid, and thus the density does not change much with the pressure (Saito, 2013). This mixture is thus a simple mixture of a liquefied CO_2 gas and an organic modifier, which may also be called a subcritical fluid, when it is a little under the critical values. However, due to the continuity between the properties of supercritical and subcritical fluids, all the advantages for chromatographic separations remain. Therefore, the defined state of the fluid is generally irrelevant. Subcritical mobile phases still possess lower viscosity than those of a liquid and a high diffusivity. Indeed, viscosity, diffusion coefficients, density, and solvent strength are nearly identical for just supercritical or just subcritical fluids with the same composition. Phase separation almost never occurs if the pressure remains high enough (Saito, 2013; Maftouh et al., 2005; Berger, 1997). The physical characteristics of CO_2, and the binary mixtures with organic modifiers, are addressed in more detail in recently published papers (Lesellier and West, 2015; Guiochon and Tarafder, 2011).

1.2 HISTORY OF SUPERCRITICAL FLUID CHROMATOGRAPHY

Despite interesting properties of supercritical fluids for chromatographic separations and new possible selectivity, SFC raised little interest in the early times since its first description (Klesper et al., 1962). There are several reasons for this fact. First, at that time GC was already a well-established method and its instrumentation was commercially available. Second, with the introduction of liquid chromatography (LC), most of the effort was put in its development whereas SFC was neglected (Saito, 2013). Only few research groups focused on the development of SFC instrumentation and explored its capabilities at that time (Hartmann and Klesper, 1977; Jentoft and Gouw, 1970; Giddings et al., 1969; Karayannis et al., 1968; Sie et al., 1966).

In the 1980s, Novotny and Lee (Peaden and Lee, 1983; Peaden et al., 1982; Springston and Novotny, 1981; Novotny et al., 1981) introduced the new concept of open tubular capillary column SFC (cSFC). A typical capillary column was a fused silica capillary coated with a polymer, such as dimethyl polysiloxane stationary phase. This cSFC was patented in 1986 and marketed by Lee Scientific because of large expectations of high efficiency at the low flow-rates facilitating interfacing SFC with MS and other detectors. This type of SFC instrument is sometimes designated as a GC-like system. The pressure as the most important operating parameter in cSFC could only be varied by changing the flow velocity because of the limitation of the constant restrictor. Because of this issue, method development was strongly limited and did not allow working at optimized conditions for both parameters. Moreover, the use of the standard flame ionization detector (FID) was allowed only when a CO_2 mobile phase without any organic modifier was employed (Saito, 2013; Arpino and Hass, 1995). Anyway, back then it was widely believed that density was the primary control variable in SFC and that changing the mobile phase density had the biggest effect on retention. This presumption was a result of mistakes made in Giddings' measurements of CO_2 density (Giddings et al., 1968), which was compared to isopropanol. Consequently, eluotropic effects corresponding to the gradient from pure hexane to pure isopropanol could be reached only through density programming. The effect of methanol concentration on retention at constant density, demonstrating the dramatic increase in the eluotropic strength due to the modifier presence, was confirmed later. In cSFC, there were also few attempts to use premixed CO_2 with an organic solvent in the cylinder to increase the mobile phase polarity using UV detection. However, the modifier content could not be changed and gradient elution was impossible, which prevented this approach from being accepted in practical laboratories. cSFC provided a large number of theoretical plates with a minimal column pressure drop, but the incorporation of an organic modifier, UV detection, variable restrictors, and a simple injection technique were either not straightforward or not experimentally possible. These experimental difficulties and the need for a broader range of stationary phases, especially those that are chiral, meant that the use of cSFC was strongly diminished in the early 1990s (Saito, 2013; Combs et al., 1997).

Although cSFC was a GC-like instrument, packed-column SFC (pSFC) was based on HPLC instrumentation, sometimes designated as an LC-like system. The development of pSFC took a direction that was independent of that of cSFC. pSFC was employed in very early research work, then it became less popular because of the marketing strategy of cSFC, but in the end it regained its popularity when packed columns were found to have a wider application range than open tubular capillary columns. The first commercial pSFC was introduced by Hewlett Packard in 1981 as a modification of an HPLC system with independent flow, composition, pressure, and temperature controls (Gere et al., 1982). Unlike cSFC, pSFC enabled researchers to add more organic modifier to the supercritical fluid, and thereby to increase its polarity and widen the range of analyzable compounds (Crowther and

Henion, 1985). pSFC offered the ability to analyze polar compounds with improved selectivity and shorter analysis time (Schwartz, 1987; Schoenmakers and Uunk, 1987). In a modern SFC system, the most important device is a backpressure regulator (BPR), which allows for pressure control independent of the mobile phase flow-rate, and it has become the standard device in pSFC. However, the interest in SFC was still quite low compared to the well-established separation techniques of GC and HPLC. The reason for this lower popularity may be attributed to the poor quantitative performance of old SFC platforms, a lack of reproducibility and robustness of the analytical instrumentation, and also to a limited knowledge of SFC principles, constraints, and method development rules because most practical users of chromatographic equipment were trained only in HPLC. In some applications, lower sensitivity of UV detection in SFC compared with HPLC might have also played a significant role.

Important advances in the development of SFC instrumentation have been reported in the past few years and will be discussed in detail in Section 2. This new generation of instruments, with a novel BPR design, higher upper pressure limit, and reduced void volumes, demonstrates improved performance and provides the robustness and reliability comparable with HPLC or UHPLC platforms. The modern SFC platforms are fully compatible with the most modern stationary phases based on sub-2 μm fully porous and sub-3 μm core−shell particles, and may be designated as UHPSFC, analogous to UHPLC in liquid phase separations (Desfontaine et al., 2015; Nováková et al., 2014). Several periods of rediscovery and decline of interest in SFC have been observed in the 1980s and 1990s, as

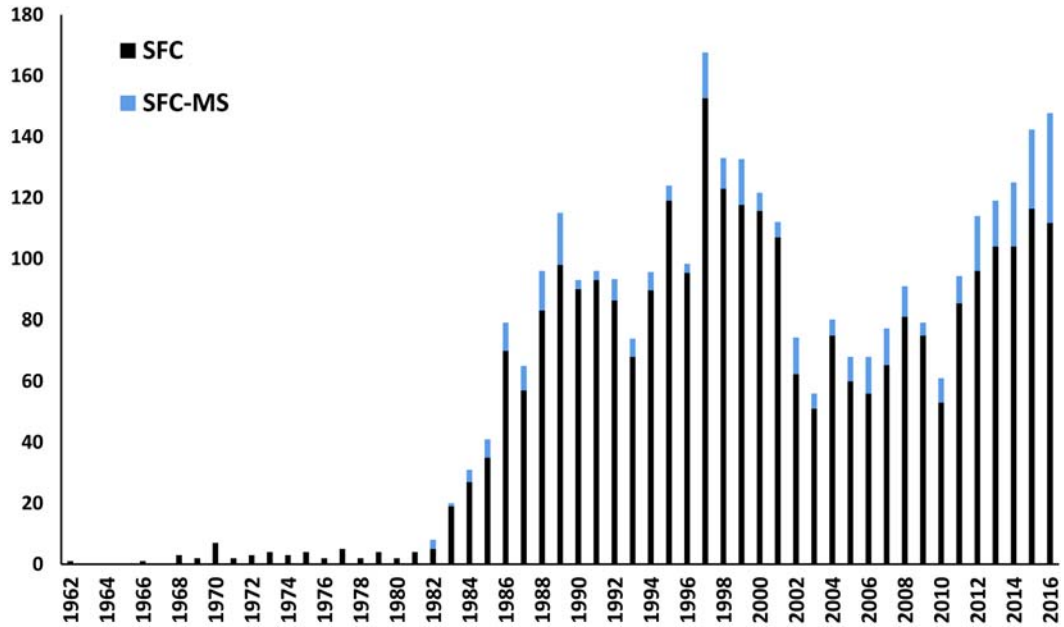

FIGURE 12.2

The number of scientific papers published with the focus on supercritical fluid chromatography (SFC) within the time period 1962−2016. The search was made using the Scifinder database, the keywords "SFC" and "SFC−mass spectrometry (MS)," and all their respective synonyms discussed in Section 1, with the filtration of duplicate results.

The bibliography search was made in November 2016.

shown in Fig. 12.2. The first one is attributed to the introduction of cSFC in the 1980s; the second one is related to regained interest in pSFC in the 1990s, whereas the most recent growth of interest in SFC is in good agreement with the introduction of modern UHPSFC platforms in 2012. This is especially true for applications using the hyphenated techniques of SFC and mass spectrometry (MS). An important increase of scientific reports related to SFC−MS has become stable since 2012.

1.3 SEPARATION EFFICIENCY IN SUPERCRITICAL FLUID CHROMATOGRAPHY AND ULTRA-HIGH PERFORMANCE SUPERCRITICAL FLUID CHROMATOGRAPHY

The kinetic performance in chromatography may be described using the van Deemter equation (Eq. 12.1), where u is the linear velocity of the mobile phase, and A, B, and C are constants related to eddy diffusion (A), longitudinal diffusion (B), and mass transfer in the mobile and stationary phases (C), d_p is the particle diameter of the column packing material, D_M is the analyte diffusion coefficient, λ is the structure factor of the packing material, γ is a constant termed tortuosity or obstruction factor, and k is the retention factor for an analyte (Van Deemter et al., 1956):

$$H = A + \frac{B}{u} + Cu = 2\lambda d_p + \frac{2\gamma D_M}{u} + \frac{f(k) d_p^2 u}{D_M} \tag{12.1}$$

One of the main features of an SFC mobile phase is low viscosity, which results in fast diffusion and improves the overall kinetic performance of the separation. Indeed, diffusion coefficients of the analytes in pure CO_2 are typically about 10−15 times higher than those in water or aqueous mixtures. As shown in Eq. (12.1), smaller particles can further significantly increase the efficiency and speed of analysis. Although columns packed with sub-2 μm particles have become widely employed in UHPLC for more than 10 years, their use in SFC started substantially later. The use of sub-2 μm particles in HPLC often requires pumps capable of pressure greater than 1000 bar. In SFC, the viscosity of CO_2/modifier mixtures is dramatically lower, which is why the generated pressure drops are much lower than in HPLC, even at higher flow-rates (Berger, 2015b). However, the use of sub-2 μm particles in SFC became common in only since 2012, when new instrumental platforms were introduced, resulting in the advanced direction of SFC designated as UHPSFC. Only few reports have focused on SFC using sub-2 μm particles before this date (Berger, 2010).

Separation efficiency between UHPLC and UHPSFC was compared in detail in a recent study using columns packed with 5 and 3.5 μm particles versus those packed with sub-2 μm particles of 1.7 μm size (Grand-Guillaume Perrenoud et al., 2012). As shown in Fig. 12.3A, conventional HPLC was the least powerful strategy (blue dotted curve), able to achieve an H_{min} (minimum height equivalent to a theoretical plate) value of only 8.4 μm at a low optimal linear velocity. Because of the important reduction in viscosity in SFC, the diffusion coefficients are improved, which result in an increase of the optimal linear velocity (purple squares). The value of H_{min} corresponded to 7.9 μm. Fig. 12.3A also clearly shows that both the B-term and the C-term are more favorable for SFC. An increase in optimal linear velocity between HPLC and SFC conditions corresponded to a factor of four. Because of the decrease of particle size under UHPLC conditions using 1.7 μm particles, the H_{min} was significantly reduced down to 3.8 μm. However, the van Deemter curve was the most interesting for UHPSFC, providing the advantages of both UHPLC and SFC, i.e., high efficiency, improved diffusion coefficients, speed of analysis, and a substantially reduced C-term of the van Deemter curve. The value of H_{min} was 4.7 μm, which was higher than that for UHPLC but remained acceptable and was achieved at about four times higher optimal linear velocity.

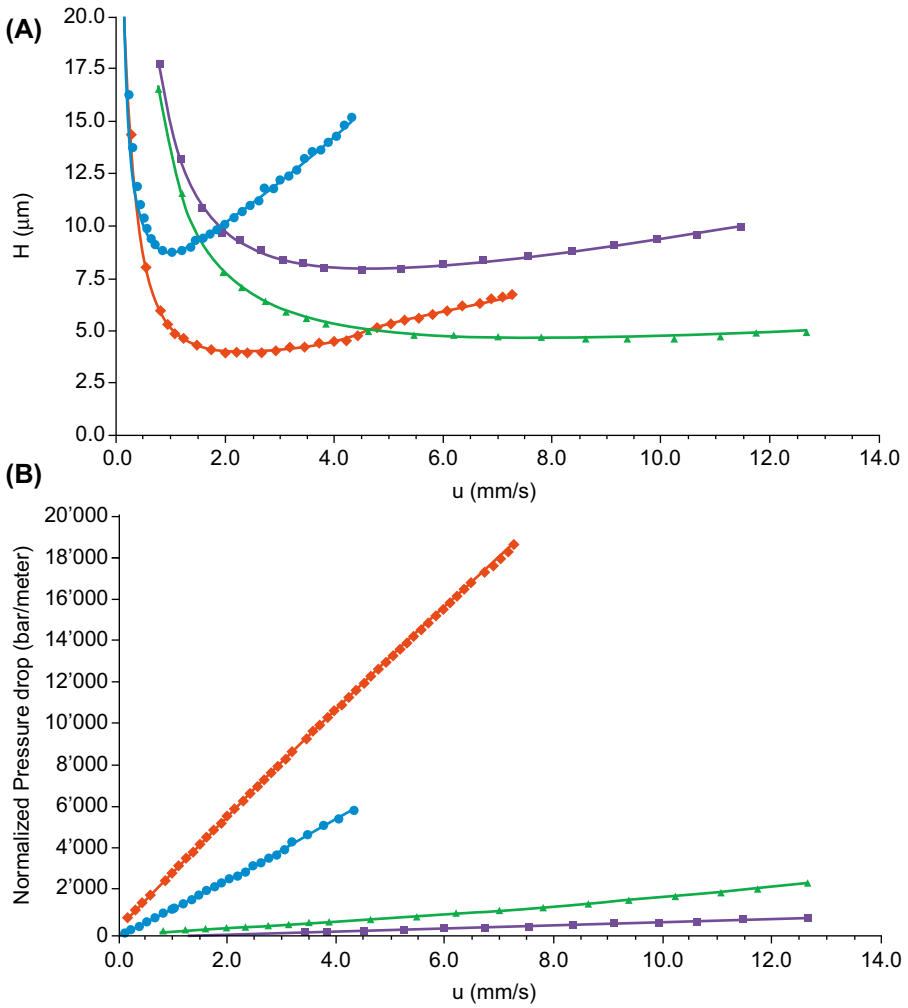

FIGURE 12.3

Kinetic performance and normalized generated pressure drop as a function of linear velocity for 1.7 and 3.5 µm particles in ultra-high performance liquid chromatography (UHPLC) and ultra-high performance supercritical fluid chromatography (UHPSFC). (A) van Deemter curves for high performance liquid chromatography with 3.5 µm particles (*blue dots* (dark gray in print versions)), UHPLC with 1.7 µm particles (*red diamonds* (gray in print versions)), supercritical fluid chromatography with 3.5 µm particles (*purple squares* (black in print versions)), and UHPSFC with 1.7 µm particles (*green triangles* (light gray in print versions)). (B) Corresponding generated column pressure drops normalized to a 1 m column.

Reproduced from Grand-Guillaume Perrenoud, A., Veuthey, J.-L., Guillaume, D., 2012. Comparison of ultra-high performance supercritical fluid chromatography and ultra-high performance liquid chromatography for analysis of pharmaceutical compounds. J. Chromatogr. A 1266, 158–167 with permission. Also see this reference for details of experimental measurements.

The comparison of system pressures reported as a value of pressure drop per meter is shown in the Fig. 12.3B. The highest pressure drop was observed for UHPLC with 1.7 μm particles, although only a 50 mm long column was employed, whereas the lowest values were observed for UHPSFC with 1.7 μm particles and SFC with 3.5 μm particles. Such low pressure drops are very important for the practical use of SFC for two reasons. First, additional backpressure of 120−150 bar must be added to the system via a BPR. Secondly, when using a high proportion of an organic modifier or gradient elution up to 40%−50% of an organic modifier, the upper limit of the UHPSFC instrument might be quickly attained at high flow-rates. An upper pressure limit of 400 bar was found to be insufficient for ultrafast analysis when using high flow-rates (>2 mL/min), sub-2 μm particles, and a higher proportion of an organic modifier (Grand-Guillaume Perrenoud et al., 2012).

Other authors have also shown similar results for the minimum plate heights in both HPLC and SFC modes, except under supercritical conditions, where about 30% larger H_{min} were observed compared to other conditions (Lambert and Felinger, 2015; Delahaye et al., 2012, 2013). For core−shell columns, reduced plate heights of 1.67 μm were found in an SFC system (Berger, 2011). When using a modified commercial system to create a low-dispersion version, reduced plate heights lower than 2 μm were observed for the first time during a chiral separation on sub-2 μm particles in SFC (Berger, 2016). The optimum flow-rate varied substantially with the proportion of organic modifier.

2. SUPERCRITICAL FLUID CHROMATOGRAPHY AND ULTRA-HIGH PERFORMANCE SUPERCRITICAL FLUID CHROMATOGRAPHY INSTRUMENTATION

Modern SFC instruments are very similar to HPLC instrumentation and use much of the same hardware with important modifications. The typical components of an SFC system involve a solvent degasser, modifier pump, CO_2 pump, autosampler, column oven, detector(s), and BPR, as shown in Fig. 12.4.

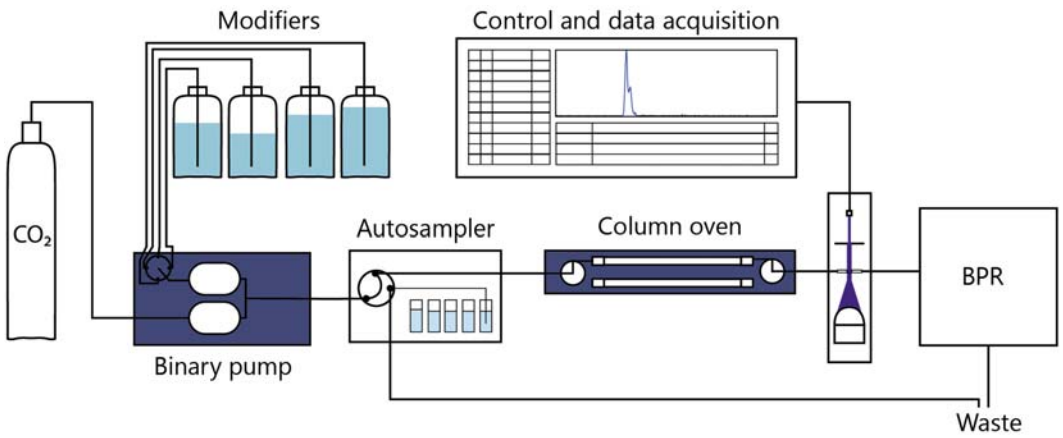

FIGURE 12.4

Schematic of supercritical fluid chromatography instrumentation.

The main hardware differences between SFC and HPLC stem from the use of a compressed gas as the main component of the mobile phase. The most important modifications of SFC compared with HPLC include the presence of a BPR and a different design of the CO_2 pump. Further modifications are needed in the autosampler and detector modules. The software to control an SFC instrument is also identical to that used in HPLC, except an additional control variable, column outlet pressure, is used (Berger, 2015a; Lesellier and West, 2015; Saito, 2013; Guiochon and Tarafder, 2011).

2.1 GENERAL FEATURES OF SUPERCRITICAL FLUID CHROMATOGRAPHY INSTRUMENTATION

2.1.1 Supercritical Fluid Chromatography Pumps

In SFC, binary pumps are necessary for pumping the CO_2 and an organic modifier because of the very different natures of the two components. While CO_2 is usually supplied from steel cylinders containing liquefied CO_2 with a gaseous headspace, the modifier is a liquid at laboratory conditions. Consequently, this mismatch in pressures definitely requires separate pumps. To ensure precise metering of the mobile phase and to decrease the compression ratio, the CO_2 is needed to be in the liquid state. This can be obtained via chilling of the pump heads down to a temperature that is usually around 2−5°C, which is ensured by Peltier modules or by a combination of Peltier-glycol circulation. It is useful to note that modern SFC systems have powerful chillers that liquefy the vapor phase from the CO_2 cylinder. Consequently, an eductor or dip tube, extending from the valve to just above the bottom of the cylinder, is not needed any more. By using the vapor phase and not the liquefied phase, the fluid is actually distilled just before use, leaving any eventual nonvolatile contaminants behind in the cylinder (Berger, 2015b).

The CO_2 compression is critical for flow uniformity because of thermal exchanges that may be either isothermal or adiabatic. At a given flow, the density changes with pressure, thus the mass transferred by one stroke differs. The pumps uniformly deliver flow based on volumetric displacement per unit time. If such changes in density are not taken into account, the actual composition of the fluid changes as a function of the column head pressure. During an isothermal process, at lower flow-rates, the compressibility of CO_2 at 50 bar is nearly 27× higher than that of water. Higher flow-rates favor adiabatic compression, where the compressibility of CO_2 at 50 bar is 9× higher than that of water. Using higher flow-rates is preferred because of better robustness and less-demanding requirements for the compressibility compensation. The distinction between fluid compression and fluid delivery is important for a stable flow-rate independent of compression (Berger, 2015a; Enmark et al., 2015).

A typical SFC pump is composed of a CO_2 inlet, motors, pistons, pump head chillers, and a mixer. Dual piston pumps, where one piston is delivering, whereas the other one is refilling, are necessary for uniformity of the mobile phase flow. Various piston pump designs, such as cam driven piston, ball screws ganged in series, and multiple independent pistons, have been developed for SFC. The best pump versatility and flow uniformity come from the design where each piston has its own motor, achieving more stable flow characteristics due to the separation of delivery and compression phases. Interestingly, this approach has been known since 1982 and was originally used for photographic film production. It is now the most widely used pump design in modern UHPLC and UHPSFC instrumentation. Another approach to ensure uniform flow in SFC is using a precompression booster pump,

which compresses the CO_2 only a few bar below the column head pressure, whereas the second main pump only meters the flow (Berger, 2015a,b).

2.1.2 Autosamplers in Supercritical Fluid Chromatography

The main differences between HPLC and SFC autosamplers are related to the nature of the mobile phase, which prevents use of some common HPLC setups, such as a flow-through needle autosampler design. In SFC, the highly compressed mobile phase fills the autosampler parts including the syringe, tubing, and needle when the valve is in the inject position. When the loop is switched back to the load position, the remaining compressed mobile phase expands to the waste. The expansion is accompanied by a 500 times increase in the volume. However, such an empty syringe cannot aspirate liquid samples. Therefore, a separate low pressure pump is required to flush the system between injections and to fill the syringe and needle with the wash solvent (Lesellier and West, 2015; Berger, 2015a).

2.1.3 Column Oven

The density of SFC mobile phases varies depending on temperature and pressure. Consequently, it is necessary to use thorough temperature regulation and control. Besides, temperature is an important parameter for fine-tuning selectivity in SFC separations (see Section 3.3 for details). A column oven is therefore a typical component of an SFC system, enabling cooling or heating, mostly in the temperature range from 20 to 90°C. However, some column ovens have a limited capability of cooling, which may be restrictive for some applications (Lesellier and West, 2015; Berger, 2015a).

2.1.4 Backpressure Regulator

Regulating the backpressure is the most crucial task in SFC systems because of the important impact of pressure changes on the robustness and refractive index (RI) of the mobile phase, which in turn affects UV−VIS detector noise. Although pressure is a secondary control variable and has only a small influence on retention and selectivity in modern SFC (see Section 3.3 for details), the resulting variations of retention times are undesirable. Mechanical regulators and fixed restrictors used in early SFC designs usually were not capable of regulating pressure sufficiently and resulted in differences from the set values and fluctuations. The challenge in BPR development laid in the material properties and technical issues related to the expansion of the mobile phase between the orifice and flow regulator. The best automatic BPR available can withhold pressure with fluctuations of ±0.05 bar. Such stable pressure yields almost no change in RI, providing a clean smooth baseline in UV detection. The modern automatic BPRs can have different designs, either single or two stage ones. The two stage systems have dynamic and static parts. The latter regulates the pressure up to 1500 psi, whereas the active BPR part takes over above this pressure. The modern automatic BPRs have dead volumes of 10−40 μL. The design is based on a linear actuator compressing a spring pushing a pin regulating flow through the chamber, and an upstream pressure sensor with electronic feedback for control of the actuator motor (Berger, 2015a; Desfontaine et al., 2015; Berger et al., 2013; Berger and Berger, 2011).

2.1.5 UV Detection

Sensitivity of UV detection in SFC was the most important challenge limiting its long-term use for trace compound analysis or in regulated environments. Baseline noise depends on the RI of the mobile

phase, which is not influenced by the UV detector design. The RI, just like mobile phase density, is strongly dependent on the temperature and pressure. The RI of CO_2 varies from 1.06 to 1.24 under commonly employed SFC conditions, whereas those for HPLC solvents belong to the much narrower range of 1.33−1.39. Consequently, the changes in RI caused by changes in temperature, pressure, or mobile phase composition can result in baseline shifts or increased baseline noise. Another factor that produces changes in RI is the temperature difference of the mobile phase and the detector flow cell. There are two approaches to prevent this problem. First, the temperature of the mobile phase is adjusted to match the temperature of the detector flow cell. Second, the flow cell is insulated from the optical system (Berger, 2014, 2015a,b).

The UV detectors in SFC are of the same design as in UHPLC, with the only difference being in the design of the flow cell. In SFC, the flow cell must withstand high pressures reaching the maximum that the BPR can deliver. Flow cell windows can be made of 6 mm thick polymers that do not absorb from as low as 190 nm. The shape of the flow cell can be either cylindrical or conical because of a lower RI of the SFC mobile phases because light bending occurs on a much lower scale compared to LC (Berger, 2015a; Berger and Berger, 2011).

2.1.6 Evaporative Light Scattering Detector and Charged Aerosol Detector

These detectors are often referred to as universal detectors because the response is chemical structure independent. Principally, they are based on nebulization and subsequent particle detection. The depressurization of a dense fluid mobile phase provides better conditions for the aerosol formation process and evaporation than in HPLC, providing these detectors the potential to work better in SFC than in HPLC. However, the nebulization chamber must be heated to prevent condensation and ice formation, due to the cooling effect of the depressurized mobile phase. In evaporative light scattering detector (ELSD), the detector is composed of a nebulization chamber, drift evaporation tube, and detector cell, where the stream of particles causes deflection of laser light for detection. The hyphenation to the ELSD is after the BPR. The size of particles and the given response depends on the type of analyte, mobile phase composition, temperature, surface tension, difference between the mobile phase and nebulizing gas, flow-rate, injection volume, and concentration. The ELSD coupled with SFC generally provides better sensitivity than HPLC but cannot be used for the analysis of volatile compounds (Lecoeur et al., 2014; Lesellier et al., 2012a,b).

In a CAD, the particles created by nebulization are detected because of a positively charged stream, producing charged particles that are collected in the collector and measured by a sensitive electrometer. There are two approaches for coupling between the SFC system and a CAD, the pre-BPR and post-BPR. The post-BPR detector's nebulization process occurs directly after the BPR and in the transfer line. In this set up, a lower percentage of organic modifier resulted in higher response (Brunelli et al., 2007). Pre-BPR coupling nebulization happens in the nebulization chamber, and a higher percentage of organic modifier was found to be more convenient for the best sensitivity (Bu et al., 2016; Swartz et al., 2009).

For both CAD and ELSD detectors, it is often recommended to add a make-up solvent after depressurization to avoid analyte precipitation or segmented flow due to the presence of separated phases in the transfer line, when using mobile phases containing only low concentrations of organic modifier. To obtain a uniform response in gradient elution, it is beneficial to use gradient compensation, similar to what is sometimes employed in HPLC (Bu et al., 2016; Brunelli et al., 2007).

2.2 ULTRA-HIGH PERFORMANCE SUPERCRITICAL FLUID CHROMATOGRAPHY INSTRUMENTATION

The major drawbacks of old SFC platforms precluded the use of SFC as a robust and reliable technique. The most important one was caused by changes in the mobile phase density because of poor stability of the backpressure, resulting in strong baseline noise and retention time shifts. Consequently, system sensitivity and repeatability did not achieve the standard quality of robust HPLC systems. Modern analytical SFC platforms benefit from technological advances in the pumping systems and backpressure regulation, allowing for better control of the mobile phase compressibility (Grand-Guillaume Perrenoud et al., 2014a). The design of new instruments is based on the pinnacle of UHPLC instrumentation, enabling SFC to become a modern, robust, high efficiency, analytical method. Reduced void volumes and higher upper pressure limits allow better compatibility with the most recent stationary phases, such as sub-2 μm fully porous and sub-3 μm core−shell particles. An important advantage is a comparable efficiency at much lower pressure, as discussed in detail in Section 1.3 (Desfontaine et al., 2015). Currently, two commercially available systems are providing UHPSFC capabilities. Although the Waters Acquity UPC^2 is a holistic system designed specifically for UHPSFC operation, the Agilent 1260 Infinity is a hybrid UHPLC/UHPSFC system. Using switching valves and two different pumps for each mode, the system can be easily modified, but an adequate rinsing is mandatory when switching between the two modes. A comparison of the main features of both UHPSFC systems is shown in Table 12.2.

The system dwell volumes for both instruments are quite large compared with a typical UHPLC system of <100 μL, but this is easily explained by the need for a larger mixing chamber to produce higher flow-rates than in UHPLC. However, such dwell volume is not a critical feature of the modern UHPSFC systems because higher optimal linear velocities allow for reduction of the isocratic hold time (Nováková et al., 2014). The UHPSFC system variance was found to be lower than 85 μL^2 at typical UHPSFC conditions (flow-rate 2 mL/min), which is also much higher than on UHPLC systems (2−20 μL^2) (Fekete et al., 2014; Grand-Guillarme Perrenoud et al., 2013). This difference is mostly related to the tubing dimensions and the UV detection cell volume. The contribution of the system variance to band broadening is very important for column dimensions selection. As a rule of thumb, extra-column variance should represent, at maximum, 10% of the total system variance to maintain a negligible contribution of the system to band broadening (Fekete et al., 2014). Consequently, columns

Table 12.2 A Comparison of the Main Features of the Two Commercially Available Ultra-high Performance Supercritical Fluid Chromatography Systems

System Name	Introduction to Market	Pressure Limit (bar)	Maximum Flow-Rate (mL/min)	Maximum No. Columns	Extra-Column Variance (μL^2)	Dwell Volume (μL)	UV Cell Volume (μL)	UV Cell Length (mm)
Waters acquity UPC^2	2012	414	4	8	83	440	8	10
Agilent 1260 Infinity	2012	600	5	6	81	700	1.7	6

of 50 mm × 2.1 mm, 1.7 μm are not recommended for UHPSFC systems because the efficiency loss may be up to 45%. The best suitable column I.D. for the current UHPSFC is 4.6 mm. However, flow-rates that should be used on 4.6 mm I.D. columns in UHPSFC may be beyond the system limits and would result in large solvent consumption. Therefore, columns of 100 mm × 3.0 mm are considered the best compromise for UHPSFC systems, with the efficiency loss up to 9% (Grand-Guillarme Perrenoud et al., 2013).

3. OPERATING PARAMETERS IN SUPERCRITICAL FLUID CHROMATOGRAPHY

3.1 MOBILE PHASE

One of the most significant changes in SFC, since the time of its introduction until modern times, has been in the mobile phase selection and composition. Initially, the supercritical state of the mobile phase was responsible for the technique's name. However, with the evolution of the technique this name is currently irrelevant (Tarafder, 2016), see also Section 1.1. Today, SFC is performed using CO_2 as a main component of the mobile phase. To prompt the elution and shorten the analysis time of polar and/or ionizable compounds, the addition of a small amount of a more polar organic modifier (cosolvent) is often needed (Tarafder, 2016; Desfontaine et al., 2015; Nováková et al., 2014). The role of the organic modifier in SFC involves several functions (Tarafder, 2016; Poole, 2012; Berger, 1997; Strubinger et al., 1991):

- modifying the polarity, hence the solvating power of the mobile phase
- modifying stationary phase characteristics through sorption
- blocking active sites on the stationary phase
- altering the density of the mobile phase
- altering the phase ratio due to the sorption of organic modifier
- solvating polar compounds in the mobile phase leading to cluster formation
- improvement of analyte solubility to avoid sample precipitation at the column inlet

The combination of these factors can change retention in an unpredictable manner, whereas some of these factors result in a change in stationary phase properties with a strong dependence on mobile phase composition, column temperature, and density drop along the column. For the conditions in pSFC, significant amounts of both CO_2 and an organic modifier are adsorbed by silica and chemically bonded stationary phases and function as components of the stationary phase (Poole, 2012). Typical organic modifiers most commonly employed in SFC include not only alcohols, namely methanol, ethanol, and isopropanol but also other solvents, such as acetonitrile or some less polar solvents may be used. Methanol is usually a modifier of first choice because of high eluotropic strength leading to higher separation efficiency compared with other alcohols, low viscosity, high polarity, low UV cutoff (about 205 nm), and lower surface tension favoring ionization in SFC−MS coupling (Brunelli et al., 2008a; Zou et al., 2000). The miscibility of CO_2 with methanol and other organic solvents of very different polarity over a broad range of pressures and temperatures is an inherent advantage of SFC mobile phases and makes the technique highly versatile (Tarafder, 2016; Desfontaine et al., 2015; Nováková et al., 2014). The organic modifier is chosen during method optimization (West and

Lesellier, 2013) based on its eluent strength and resultant separation selectivity, efficiency, and peak shape. As a result of the choice of modifier, several characteristics, such as dielectric constant, hydrogen-bond capabilities, mass transfer, and solvent viscosity may be altered. Free silanols at the surface of the stationary phases may be responsible for undesirable peak shapes for analytes of the hydrogen-bond donor type, when using hydrogen-bond acceptor types of organic modifiers (alcohols, dioxane, tetrahydrofuran, or acetonitrile), while those with hydrogen-bond donor capacity, such as alcohols, should minimize this effect. As silanols also possess hydrogen-bond donor character, modifiers with hydrogen-bond acceptor properties will provide advantages in their compensation. Thus, alcohols seem to be the most universal organic modifiers, also providing a higher solvating power than, for example, acetonitrile (Desfontaine et al., 2015; Nováková et al., 2014; Brunelli et al., 2008a; Blackwell et al., 1997; Cantrell et al., 1996). Acetonitrile may be an interesting modifier because of its unique selectivity. However, its performance in SFC was found to be substantially worse compared to alcohols, resulting in low efficiency and poor peak symmetry, probably because of low coverage of free silanols (Zou et al., 2000). An interesting solution to obtain different selectivity without sacrificing the performance and peak shapes was observed when using a mixture of methanol and acetonitrile as the organic modifier (Brunelli et al., 2008b).

Examples of different selectivities obtained with various single organic modifiers and modifier blends are shown in Fig. 12.5. Notably, an advantage of the combination of an alcohol and acetonitrile

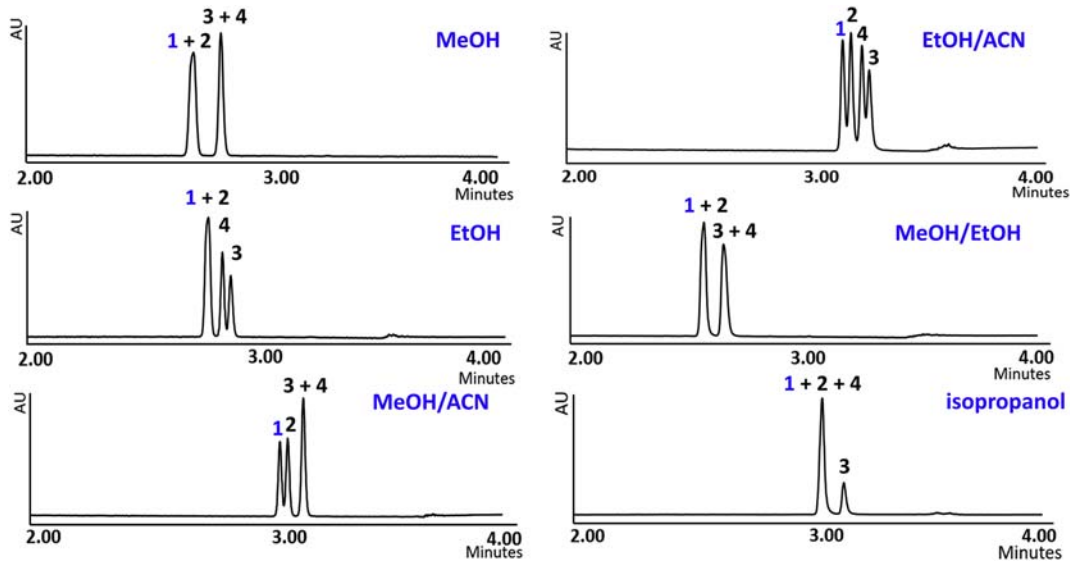

FIGURE 12.5

The influence of organic modifier type on ultra-high performance supercritical fluid chromatography (UHPSFC) separations. Chromatograms show separations of the active pharmaceutical ingredient (API) ticagrelor [blue (gray in print versions) 1] and its three impurities (2, 3, 4) on a Torus Diol column (100 mm × 3.0 mm, 1.7 μm), with gradient elution 5%−40% of organic modifier in 3 min, flow-rate 1.5 mL/min, temperature 40°C, backpressure regulator 2000 psi, UV detection at 225 nm. *ACN*, acetonitrile; *EtOH*, ethanol; *MeOH*, methanol.

in one modifier is also shown in this case. To compare mobile phase elution strength, various approaches may be used, such as Snyder's P'elution strength scale (Snyder, 1974), the Hildebrand solvent strength scale for silica (Snyder, 1968), or the use of solvatochromic dyes, for example Nile red (Deye et al., 1990).

With addition of an organic modifier, the main parameter ruling retention is the modifier percentage, and retention changes can be described by a nonlinear relationship (Eq. 12.2; Lesellier and West, 2015):

$$\ln k = a(\%)^2 - b(\%) + c \tag{12.2}$$

The most significant changes in retention are usually observed between 0% and 2% of an organic modifier, probably because of the adsorption of the modifier on the "active sites" of the stationary phase. The retention usually decreases with increasing amount of an organic modifier, with a generally stronger decrease up to 10%. However, at high modifier concentration the retention may eventually be increased again in some cases, such as in the case when nonpolar analytes are analyzed on a C18-bonded stationary phase with a modifier having a high dielectric constant (Lesellier and West, 2015). In modern SFC, a gradient elution starting from 2% to 5% of organic modifier up to 40%−50% organic modifier is currently favored.

Some analytes, especially strong acids and bases and also amphoteric compounds, do not elute or elute with poor peak shapes when using binary mixtures of CO_2/organic modifier. In such cases, the addition of a small amount of a highly polar additive is necessary to improve the peak shapes and to promote the elution. The additive is dissolved in an organic modifier at a concentration between 0.05% and 2%. The concentration of additives in the mobile phase depends on the nature of the analytes and stationary phase and should be optimized during method development. Although the mode of action is not always clearly elucidated for additives, they are supposed to act via several different mechanisms, as was discussed in detail in recently published papers (Tarafder, 2016; Lesellier and West, 2015; West, 2013; Poole, 2012; Wen and Olesik, 2000):

- changing the acidity of the mobile phase, the ionization state of ionizable analytes, and ionizable functional groups of the stationary phase
- enhancement of solvating power of the mobile phase
- modification of the stationary phase surface properties by covering the active sites, changing polarity, etc., resulting in creation or cancellation of an interaction
- clustering around the analytes resulting in enhanced local solvent strength
- ionization suppression or ion-pairing with charged analytes

Although the reaction between CO_2 and an alcohol modifier results in the formation of methylcarbonic acid, which can actually work as an acidic additive creating a mobile phase pH around 4−5, the effect of stronger acids has been found beneficial (West, 2013; Dijkstra et al., 2007; Wen and Olesik, 2000). Generally, acidic additives such as formic acid, acetic acid, citric acid, or trifluoroacetic acid (TFA) improve the analysis and peak shapes of organic acids, whereas basic additives such as isopropylamine (IPA), diethylamine (DEA), or trimethylamine are beneficial for the analysis of bases (Sen et al., 2016; Berger, 2015b; Desfontaine et al., 2015; Nováková et al., 2014; Berger and Wilson, 1995; Berger and Deye, 1991a). However, sometimes the opposite may be true, probably as a result of ion-pair−like behavior. In light of these findings, it is also possible to use a mixture of acidic and basic additives within modifiers for simultaneous analysis of acids and

bases. This approach is popular especially in chiral separations using, for example, a combination of TFA/DEA (Nováková and Douša, 2017) or TFA/IPA (De Klerck et al., 2012a). It is important to note that these agents (organic amines and TFA) are MS unfriendly, due to serious ion suppression effects, and their presence may consequently result in long-term MS contamination.

In recent studies, the use of volatile additives (ammonium hydroxide, ammonium formate, ammonium acetate) is clearly preferred because of compatibility with MS detection (Desfontaine et al., 2016; Nováková et al., 2015a,b, 2016; Lemasson et al., 2015a; Grand-Guillaume Perrenoud et al., 2012; Zheng et al., 2005; Pinkston et al., 2004). Examples of various influences of additives are shown in Fig. 12.6. Two compounds were not eluted with organic modifier without any additive (Fig. 12.6A) for both mixtures, but addition of either ammonium acetate or formate enabled the elution of all mixture components. In some cases, ammonium formate was more convenient, providing adequate separation selectivity (Fig. 12.6B, BEH, bridged ethyl hybrid column), while ammonium acetate was more successful in the second case study (Fig. 12.6C, charged surface hybrid pentafluorphenyl column).

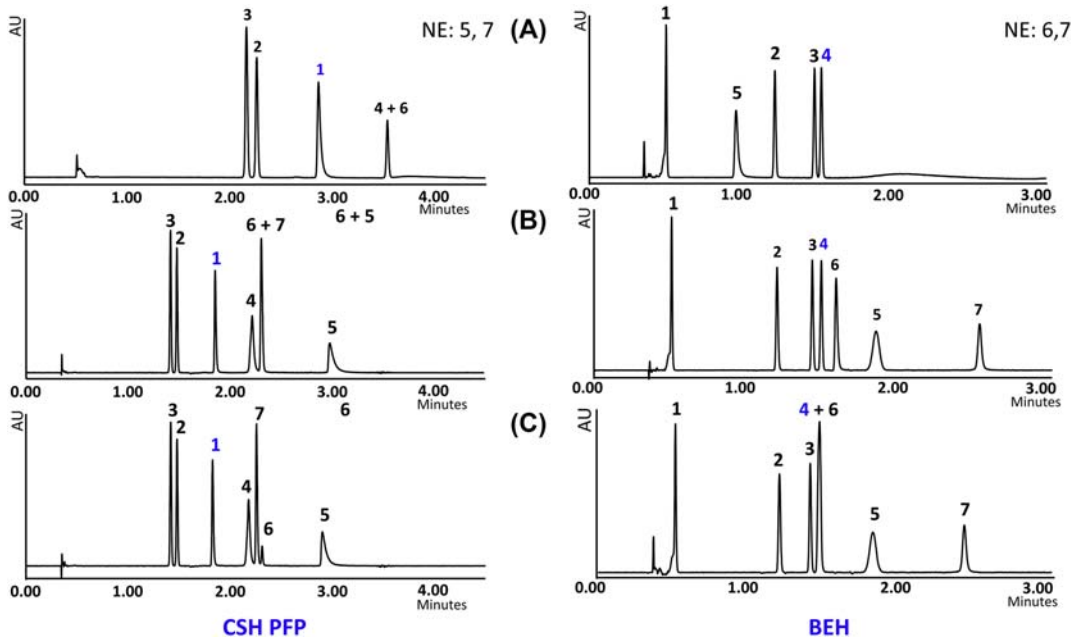

FIGURE 12.6

Comparison of analysis with and without additives in a ultra-high performance supercritical fluid chromatography method for the separation of vardenafil (API, peak 1) and its six impurities on a charged surface hybrid pentaflurophenyl (CSH PFP) column and for the separation of agomelatine (API, peak 4) and its six impurities on a bridged ethyl hybrid (BEH) column. Gradient elution of 5%−40% was performed with methanol as an organic modifier (A), with methanol + 10 mM ammonium formate (B), and with methanol + 10 mM ammonium acetate (C) in 3 min, flow-rate 1.5 mL/min, temperature 40°C, backpressure regulator 2000 psi, UV detection at 225 nm. *NE*, not eluted.

Despite positive effects on retention, selectivity, and peak shapes, the use of additives should be associated with some precautions (Lesellier and West, 2015; Berger, 2015b). With the introduction of an additive in the mobile phase, it will first adsorb at the surface of the stationary phase. Care should be taken to wait long enough for the additive concentration to equilibrate. Once the stationary phase is saturated, the additive will elute from the column resulting in increased baseline noise when using UV detection. In SFC, this baseline shift cannot be compensated by the addition of the same additive to the CO_2 component, therefore the stationary phases that do not require additive may be beneficial in SFC-UV (Alexander et al., 2012). Finally, the removal of the additive after use is not ensured because strong interactions between the additive and stationary phase may occur. As a result, the beneficial effect of an additive remains and may persist even when returning to additive-free mobile phases. It is also important to keep in mind to wash the column properly before storage because it should never be stored without careful washout of an additive. A rinsing step using 40% modifier in CO_2 for greater than 10 column volumes should be a basic minimum washing step (Lesellier and West, 2015; Berger, 2015b).

Another current trend consists of employing water as an additive in the SFC mobile phase to improve the peak shapes of polar analytes and to improve their elution. Moreover, water does not have some of the negative characteristics of organic modifiers, such as UV absorbance. Although water is not fully soluble in CO_2, it can be mixed into a CO_2/methanol mobile phase up to 10%. Water is more polar and possesses twice the hydrogen bonding capability of methanol. Because of contact with CO_2, it becomes acidic through the formation and dissociation of carbonic acid. Furthermore, beneficial effects of water addition to an SFC mobile phase on MS response have been noted in positive-ion eletrospray ionization (ESI) (Nováková et al., 2015a, 2016; Berger, 2015b; Taylor, 2012; Ashraf-Khorassani and Taylor, 2010; Wang et al., 1995).

3.2 STATIONARY PHASE

SFC enables both chiral and achiral separations. Different chromatographic modes (normal phase (NP)-HPLC, reversed phase (RP)-HPLC, hydrophilic interaction chromatography (HILIC), ion-exchange chromatography, and others) are needed in LC. However, in SFC, a wide range of compounds of different polarities may be analyzed using the same CO_2-based mobile phase in combination with various stationary phases, polar, and nonpolar (Tarafder, 2016; Lesellier and West, 2015; Lesellier, 2009). The dominant column technology for both HPLC and SFC remains porous silica particles with siloxane-bonded surface modifications. Basically, most HPLC stationary phases may be also employed in SFC, but columns optimized for RP-HPLC may not be optimal for SFC (Poole, 2012). So far, only a few stationary phases have been designed specifically for SFC. The first SFC-dedicated achiral column was introduced by Princeton Chromatography in 2001, with a 2-ethylpyridine stationary phase bonded on totally porous silica particles (Berger and Berger, 2010). This stationary phase was aimed to reduce peak tailing of basic compounds in SFC without the need for additives and to provide alternate selectivity. The introduction of this phase initiated a fairly consistent, progressive development of a number of phases by Princeton and other manufacturers (ES Industries, Phenomenex, Waters, etc.). Further SFC-dedicated stationary phases were developed: 4-ethylpyridine, pyridine amide, propylacetamide, amino phenyl, pyridyl amide, morpholine, benzamide, and some others (Tarafder, 2016; Poole, 2012). New SFC-dedicated chemistries were recently introduced by Waters Corporation as Torus columns (2-picolylamine, diol, DEA, and 1-amino-anthracene). SFC has wide method development possibilities, but the choice of the right column can be

rather difficult (Desfontaine et al., 2015). When using nonpolar stationary phases (from C5- to C18-bonded silica, phenylhexyl, etc.), hydrophobic compounds are most retained, and retention patterns are comparable to RP-HPLC with an organic-rich mobile phase (West and Lesellier, 2006a). Using polar stationary phases (bare silica, silica bonded with aminopropyl, propanediol, etc.), the polar analytes are more retained, and the retention model is similar to NP-HPLC (West and Lesellier, 2006b). The use of a stationary phase with mixed polarity results in a unique retention pattern that is neither of the RP- nor NP type. C18-bonded silica with polar endcapping or polar embedded groups, or silica with aromatic ligands (phenylpropyl, pentafluorophenylpropyl, etc.), belong among such stationary phases (Lesellier and West, 2015). For these stationary phases, a classification system was developed with a solvation parameter model (linear solvation energy relationship (LSER)) that uses five descriptors (charge transfer, dipole−dipole, hydrogen-bond acceptor and donor, and dispersion) related to the interactions of the analyte with the chromatographic system. In the resulting diagram, nonpolar and polar stationary phases can be found in opposite areas, and phases with mixed-mode behavior are located in between (aromatic phases at the top and the polar embedded or end-capped at the bottom) (Galea et al., 2015b; Khater et al., 2013; Lesellier, 2009). Although in early SFC reports mostly 5 μm fully porous particle packed column were employed, recently there is a growing trend in use of sub-2 μm fully porous particles and sub-3 μm core−shell particles (Nováková et al., 2015a,b; Grand-Guillaume Perrenoud et al., 2012, 2014b; Delahaye et al., 2013; Lesellier et al., 2014; Berger, 2011).

SFC stationary phases are predominantly silica-based, and the silica surface plays a key role in retention and selectivity. Therefore, most of the SFC columns are not endcapped. However, highly reactive residual silanols on the surface may suffer transformations during a column's lifetime. A thin layer of organic modifier exists on the surface of the stationary phase (Taylor and Ashraf-Khorassani, 2010; Strubinger et al., 1991), which can lead to silyl ether formation because of slow condensation between alcohols and residual silanols (Fairchild et al., 2015). This can affect reproducibility, due to loss of retention over time. To limit this unwanted effect, it is advised to use a small percentage of water in the mobile phase and to store the column in pure CO_2. A regeneration procedure is proposed to reverse this phenomenon (Fairchild et al., 2015).

Chiral stationary phases used in SFC are the same as in HPLC. SFC-dedicated chiral stationary phases have not been developed, but some manufacturers use different packing procedures and column dimensions for SFC applications. Most chiral separations, both in HPLC and SFC, are currently performed on polysaccharide-based stationary phases including a large variety of derivatives of amylose and cellulose (Nováková and Douša, 2017; Kalíková et al., 2014; West, 2014; De Klerck et al., 2012a,b; Maftouh et al., 2005).

3.3 BACKPRESSURE AND TEMPERATURE

In a pure CO_2 mobile phase, density is the key factor to control the mobile phase strength and consequently retention and selectivity. The mobile phase density depends on system pressure, temperature, and also on mobile phase composition. Both methanol concentration and increasing pressure can increase the density. However, it was confirmed that there is a small density effect once the modifier is added, whereas the modifier concentration produces most of the retention change when using CO_2/modifier binary mixture mobile phases (Berger and Deye, 1990). Based on this observation, the most influential parameters in modern SFC involve the stationary and the mobile phases. Therefore, these should make the starting point of method development, whereas the

pressure and the temperature should be considered as secondary parameters, for fine tuning of the method. The density of CO_2 changes over a wide range with changes in temperature and pressure, with most of the changes in a narrow range between 70 and 110 bar (Berger, 2015b; Nováková et al., 2014).

The influence of pressure and temperature on retention in SFC is very different from that in HPLC. The effect of temperature in SFC is more complex because it is a combination of several factors including vapor pressure of the solute, density of the mobile phase, solubility parameters of both the analyte and the supercritical fluid, affinity of the analyte for the stationary phase, and the properties of the analyte (Lou et al., 1997). Usually, the retention first increases with an increase of temperature and after reaching a maximum, the retention decreases at very high temperatures (Zou et al., 2000; Fig. 12.7A). Such high temperatures will usually not be achieved in experiments with LC-like SFC

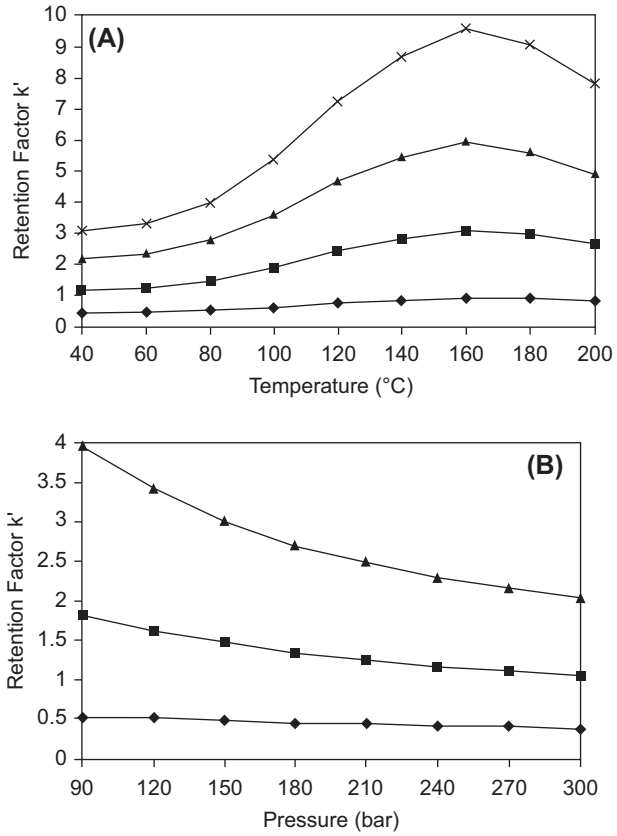

FIGURE 12.7

Plots of analyte retention versus temperature (A) and pressure (B) on a C18 stationary phase, at 2 mL/min with CO_2/methanol (95:5) at 210 bar (A) and CO_2/methanol (97:3) at 40°C (B).

Reproduced from Zou, W., Dorsey, J.G., Chester, T.L., 2000. Modifier effects on column efficiency in packed-column supercritical fluid chromatography. Anal. Chem. 72, 3620–3626 with permission. Also see the reference for further details of experimental measurements.

instruments because column oven maximum temperatures are typically up to 90°C. Although temperature has only a small effect on retention, it can have a surprisingly significant effect on the selectivity (Berger, 2015b).

On the other hand, the effect of pressure is straightforward. When using pure CO_2 mobile phase, an increase in pressure induces higher fluid density, which results in lower retention factors (Lou et al., 1997). Because of compressibility of this mobile phase, the variation of density can be large and leads to important retention shifts. Therefore, pressure gradients may be used for elution. On the other hand, with the introduction of an organic modifier, the compressibility of the fluid decreases as a function of increasing modifier concentration, and variation of the pressure will have very limited impact on the density and retention. This way, the peaks in gradient elution eluted at a low-modifier concentration might be affected by a change in pressure more significantly than those eluted with a high concentration of an organic modifier (Brunelli et al., 2008a). Anyway, a decrease of retention will be observed with an increase of pressure, as shown in Fig. 12.7B. Pressure is definitely only a fine-tuning parameter and the secondary control variable after temperature because its impact on either retention or selectivity is very little (Berger, 2015b). However, its precise control is crucial for retention time stability.

For practical experiments, it is important to be aware of three issues. First, the pressure gradients in the column can also generate density and velocity gradients, resulting in loss of efficiency and band broadening. When the pressure decreases linearly along the column, CO_2 undergoes decompression cooling and can impact the temperature inside the column. The efficiency loss can be limited at high temperatures in the presence of a significant amount of modifier or when the pressure gradient is compensated by a temperature gradient (Bouigeon et al., 1996). Second, the introduction of sub-2 μm particles and their use in SFC may induce the phenomenon of frictional heating, similar to UHPLC (Nováková et al., 2011). The two effects, decompression cooling and frictional heating, coexist in the column and, depending on the mobile phase composition, the pressure and the temperature, one of them will prevail, resulting in either a decrease or an increase of the temperature in different regions of the column. The third issue is a possible phase separation, which would also lead to peak shape degradation. The knowledge of all these thermodynamic phenomena allows analysts to avoid operating an SFC system under conditions that cause poor separation. A reasonable compromise for SFC operation appears to be working conditions at 40°C and 150 bar. The above stated is also very important for the transfer of an SFC method between different analytical conditions. Changing column dimensions or particle sizes (e.g., transfer of an analytical SFC method to the preparative scale) will result in system pressure and mobile phase density changes, which can lead to notable changes in retention and selectivity. To prevent such phenomena, the density between the two systems should be kept as close as possible (Desfontaine et al., 2015).

3.4 FLOW-RATE

While in HPLC a change in flow-rate has a small effect on selectivity and may only influence the resolution via shortening the retention, the situation is more complicated in SFC. Indeed, increasing the flow-rate also increases the pressure drop in the column and system. Because the BPR keeps the system outlet pressure constant, an increase in pump pressure is observed. Higher pressure induces an increase in density resulting in a decrease of retention beyond that expected only because of the higher flow-rate. Although the effect can be mild in some cases, SFC operators should be aware of this behavior (Berger, 2015b).

Knowledge of this background is also important for the measurement of van Deemter curves in SFC. Because the *k* values influence the shape of the van Deemter curve in the B- and C-terms, their reliability may be questionable. Therefore, the conditions for the measurement should be selected wisely. The comparison of van Deemter curves for SFC, UHPSFC, and HPLC methods is shown in Fig. 12.3 and is discussed in detail in Section 1.3. Compared with UHPLC, the optimum linear velocity in SFC is shifted toward higher values by about a factor of 3−5. The optimum linear velocities were found to be about 4.5 and 10 mm/s in SFC and UHPSFC, respectively. The latter value corresponds to 2.6 mL/min for a 3.0 mm I.D. column packed with 1.7 μm particles (Grand-Guillaume Perrenoud et al., 2012).

3.5 INJECTION SOLVENT

Sample diluent solvent may cause a significant peak distortion and affects the efficiency of the chromatographic separation if not selected correctly. In LC methods, the sample is usually diluted in the same solvent that is used as the mobile phase or in a solvent with weaker elution strength. The dilution solvent is of equal importance in SFC, but the rule of similarity with the mobile phase is not practically feasible because the mobile phase is composed of a large proportion of CO_2 in a fluid state. Therefore, samples are often diluted in the pure modifier, such as methanol, which has a significantly higher elution strength, resulting in serious distortions of the peak profiles (Enmark et al., 2015; Fairchild et al., 2013). Nevertheless, if the injection volume is decreased, the peak distortion could be substantially reduced (Fairchild et al., 2013; Nováková et al., 2014).

Nonpolar solvents, such as hexane and heptane, have polarities closer to CO_2 and are considered as better solvent options in SFC (Fairchild et al., 2013). Their use is related to several challenges, including limited dissolving power for polar and ionizable compounds, and high volatility resulting in fast evaporation, sample preconcentration, and issues when precise quantitation is required (Fairchild et al., 2013). To preserve acceptable peak shapes and to improve sample solubility, the mixing of nonpolar solvents with more polar ones may be used. A compromise should be found between the sample solubility, the peak shape, the sample stability, the solvent volatility, and the compound retention. Using small injection volumes (0.1%−0.5% of the column volume) may mitigate the peak distortion, but sensitivity will also be affected (Nováková et al., 2014; Fairchild et al., 2013). The less retained compounds are always the most distorted. The injection solvent interacts with the analyte as well as with the stationary phase. Therefore, the same sample diluent may behave differently on a polar versus a nonpolar stationary phase. On a polar stationary phase, such as bare silica, the injection solvent minimizes interactions with free silanols. Thus, the diluent's dielectric constant, dipole moment, hydrogen bonding, and eluent strength are highly correlated to poor efficiency. Contrarily, injection solvents with higher dielectric constants and dipole moments are suitable for separations on nonpolar stationary phases, such as a C18 column (Abrahamsson and Sandahl, 2013).

For analysis of pharmaceuticals, acetonitrile and tetrahydrofuran, both aprotic solvents with no H-bond donor capability, provide acceptable peak shapes and solubility (Nováková et al., 2014). Moreover, acetonitrile is not retained and does not interfere with analytes. Other commonly used solvents, dimethylsulfoxide and dimethylformamide, are inconvenient in SFC because of distorted peaks observed even at low injection volumes, important absorption in the UV region, and retention on polar columns resulting in interfering peaks (Abrahamsson and Sandahl, 2013; Fairchild et al., 2013).

As shown by De Pauw et al., the optimal sample solvent composition varies, depending on the solubility and retention properties of sample. After optimization (decreased injection volume, minimized extra-column volumes), nearly the same performance was obtained for 20%–40% water/acetonitrile mixtures and ethanol/isopropanol/hexane (5:10:85) sample solvents (De Pauw et al., 2015).

A simple dilute and shoot approach used for analysis of urine samples may be seen as unfeasible in SFC because water is often employed as the dilution solvent in HPLC methods. When using organic solvents for dilution, the precipitation of salts from urine must be taken into account. Although water seems to be an inappropriate solvent for SFC because of its completely different properties compared with the SFC mobile phase, it was demonstrated that injection of a sample in water was feasible for most compounds out of 110 tested doping agents, when using low injection volumes and low sample concentrations. Mixtures of water and organic solvents have been proven to be a good compromise (Nováková et al., 2015a).

4. INTERFACING SUPERCRITICAL FLUID CHROMATOGRAPHY AND MASS SPECTROMETRY

4.1 ION SOURCES AND INTERFACES IN SUPERCRITICAL FLUID CHROMATOGRAPHY–MASS SPECTROMETRY

Interfacing SFC to MS is of special interest because of the high degree of sensitivity and selectivity of MS. A lot of research on the development of easy to use and efficient interfaces has been reported. The early SFC–MS ionization sources followed the evolution of the ionization sources in LC–MS and GC–MS. An ideal SFC–MS interface should meet the following requirements (Combs et al., 1997; Arpino and Haas, 1995):

- chromatographic integrity should be maintained
- a range of ionization methods should be possible
- high sensitivity
- no thermal gradients of analyte
- compatibility with different fluids under pressure programming and with modifiers
- reliability and low maintenance
- a minimal dead volume
- sufficient heating of the restrictor tip to compensate for the adiabatic cooling of the rapidly expanding fluid
- postcolumn pressure control

At first sight, it might seem to be relatively easier to achieve SFC–MS coupling compared with HPLC–MS. The SFC mobile phase contains a high proportion of volatile CO_2, which should enhance the evaporation step during the ionization process. However, the compressibility and phase behavior in SFC make this interfacing challenging. Because of the density drop, the solvating power of the mobile phase can decrease to a point where analytes may precipitate. Such an effect results in loss of chromatographic performance, degraded peak shapes, deteriorated mass transfer, and decreased detector response and stability. The analyte molecules may also stick to the walls of the capillary because of a decrease of solubility, resulting in carryover effects. Therefore, thorough optimization of the interfacing device was needed. Many different approaches have

been tested for interfacing SFC and MS, including direct fluid introduction, the moving belt interface, the thermospray interface, the particle beam interface, plasma ion sources, such as microwave-induced plasma and inductively coupled plasma, and finally atmospheric pressure ionization sources, namely ESI and atmospheric pressure chemical ionization (APCI). Table 12.3 shows an overview of benefits and drawbacks of individual interfaces (Pinkston, 2005; Combs et al.,

Table 12.3 An Overview of Benefits and Drawbacks of Supercritical Fluid Chromatography–Mass Spectrometry Interfaces

Interface	Benefits	Drawbacks
DFI	Simple, rugged	Low flow-rates needed
	No additional hardware needed	Need to split the column effluent
	Library-searchable spectra	Reduced sensitivity
Moving belt	Mobile phase is eliminated prior to MS	Poor sensitivity
	Flow-rate and mobile phase composition can be altered	Sample carryover
	Electron ionization (EI) or chemical ionization (CI) spectra	Nonvolatile and polar compounds cannot be analyzed due to poor desorption from the belt
Thermospray	EI and CI ionization and spectra	Constant flow-rate source
	High flow-rates possible	No density programming
	Additional reagent gases possible	Low sensitivity
		The intensities of mass fragments are not always indicative
		Thermal degradation is very possible
Particle beam	Mobile phase is eliminated prior to MS	Volatile and highly nonvolatile analytes are problematic
	Wide range of conditions to be used	Lack of sensitivity
	EI and CI ionization and spectra with little spectral interference	
ESI	Versatile chromatographic conditions may be employed (flow, composition)	Non-polar analytes are less easily ionized
	Ionization of macromolecules	Insufficient heating of the restrictor and transfer lines results in peak deformation
	Multiply charged ions	
	Simple spectra	
APCI	Versatile chromatographic conditions may be employed (flow, composition)	Very polar analytes are not ionized
	Simple spectra	Insufficient heating of the restrictor and transfer lines results in peak deformation

APCI, *atmospheric pressure chemical ionization;* DFI, *direct fluid introduction;* ESI, *eletrospray ionization;* MS, *mass spectrometry.*

1997; Arpino and Haas, 1995). Because of limited sensitivity and other constraints of most of the mentioned interfaces, API techniques are currently the most interesting option in both HPLC–MS and SFC–MS.

The first attempts to interface SFC to MS were made in the 1980s, in cSFC using a direct introduction method that required only minor modifications of the instrumentation and enabled electron ionization (EI) and chemical ionization (CI) (Arpino and Haas, 1995; Arpino and Cousin, 1987). The low flow-rate and instantly evaporating nature of the pure CO_2 mobile phase in cSFC facilitated this interfacing. However, with the development of pSFC using an organic modifier as a mobile phase component, atmospheric pressure ionization techniques have become the interfaces of choice, similar to HPLC–MS (Pinkston, 2005; Arpino and Haas, 1995). Although ESI requires droplet formation to occur in the liquid phase, APCI is a gas-phase ionization process. One of the first uses of APCI for SFC–MS hyphenation was described by Huang et al. (1990), whereas it was slightly later for ESI (Sadoun et al., 1993). No ionization method is universally applicable, thus APCI is convenient especially for low molecular weight, thermally stable, and less polar molecules, whereas ESI favors ionization of more polar, medium to high-molecular-weight-compounds.

4.2 INTERFACING ATMOSPHERIC PRESSURE IONIZATION TECHNIQUES WITH SUPERCRITICAL FLUID CHROMATOGRAPHY

Interfacing atmospheric pressure ionization sources may be implemented using various different approaches (Pinkston, 2005):

1. pre-BPR flow splitting
2. total flow introduction–pressure-regulating fluid interface
3. total flow introduction with mechanical BPR
4. total flow introduction with passive BPR

Pre-BPR splitting is straightforward and allows full control of the postcolumn pressure via software. It provides good chromatographic fidelity when the dimensions of the transfer line are selected wisely to prevent the precipitation of the analytes. One of the drawbacks of this approach is lower response of mass sensitive ionization methods, such as APCI, due to limited fraction of the effluent directed to the mass spectrometer. The split ratio may also vary with the mobile phase pressure and with any changes in the restriction or transfer lines (Pinkston, 2005).

Because of the needs for a wider dynamic range and better sensitivity, various total-flow introduction interfaces have been investigated. The details are discussed by Pinkston (2005) and only a brief summary will be presented here. A pressure regulating fluid interface uses a zero-dead-volume chromatographic tee to mix the chromatographic eluent with a low flow of miscible fluid from a pump operated under pressure control. The benefits of this approach include active pressure control nearly

to the outlet of the interface, excellent chromatographic fidelity, very low dead volume, minimal extra-column band broadening, sample delivery without any splitting, allowing for a lower limit of detection and wider dynamic range for mass sensitive sources, and finally, addition of a pressure regulating fluid. An important drawback of this interface is the downstream pressure control by an independent pump instead of system software, which is less user-friendly and requires occasional manual interventions. The dimensions of the transfer line influence the range of compatible flow-rates and finally, an additional pump for the pressure-regulating liquid is necessary (Pinkston, 2005; Chester and Pinkston, 1998).

Total flow introduction with a mechanical BPR should compensate for some complications of the previous interface but represents a great challenge in terms of large dead volume components. The pressure transducer has a relatively large internal volume, but it is required for proper feedback control of the downstream pressure. The main benefit is full control of the downstream pressure by the system software. The chromatographic fidelity is good if the dead volumes are minimized and the conditions are properly setup to prevent phase separation or analyte precipitation. The simplest method among total flow introduction approaches is the one using a passive BPR. The column is coupled directly to the mass spectrometer's ion source. Because of only passive downstream pressure control, this interface works well only under a specified combination of conditions, which are close to a liquid-like mobile phase. To sum up, under liquid-like conditions BPR control may not be required, but under less liquid-like conditions, the postcolumn pressure must be controlled using some of the discussed variants (Pinkston, 2005).

Recently, further extensive study focused on optimization of UHPSFC−MS hyphenation was performed (Grand-Guillaume Perrenoud et al., 2014a). Two interface geometries and configurations using pre-BPR splitting, either with or without the use of a sheath pump, were compared. The influence on chromatographic performance, on the MS detection sensitivity, and on user-friendliness was evaluated. The pre-BPR splitting interface with a make-up pump was evaluated as a more interesting variant because of good flexibility in terms of applicable chromatographic conditions, extended robustness, slightly better efficiency, improved detection sensitivity attributed to the additional methanol coming from the sheath pump, and ease of use. The presence of a make-up solvent also helps to avoid analyte precipitation inherent to CO_2 decompression. A small loss of separation efficiency was observed (25%) compared to a UV detection configuration, which was attributed to the postsplitter CO_2 decompression phenomenon.

Moreover, all the parameters (mobile phase flow-rate, mobile phase composition, make-up solvent flow-rate, back-pressure, and the split ratio) that influence the amount of methanol directed to the MS detector were also finely optimized using both an experimental approach and subsequent computer simulation, as shown in Fig. 12.8. This interface was well suited for the concentration-sensitive ionization techniques, such as ESI, to minimize the changes in sensitivity due to splitting. Indeed, the detection sensitivity could be affected by addition of the makeup fluid, introducing a dilution factor of only 1.1−1.5 under typical SFC conditions, which is not significant.

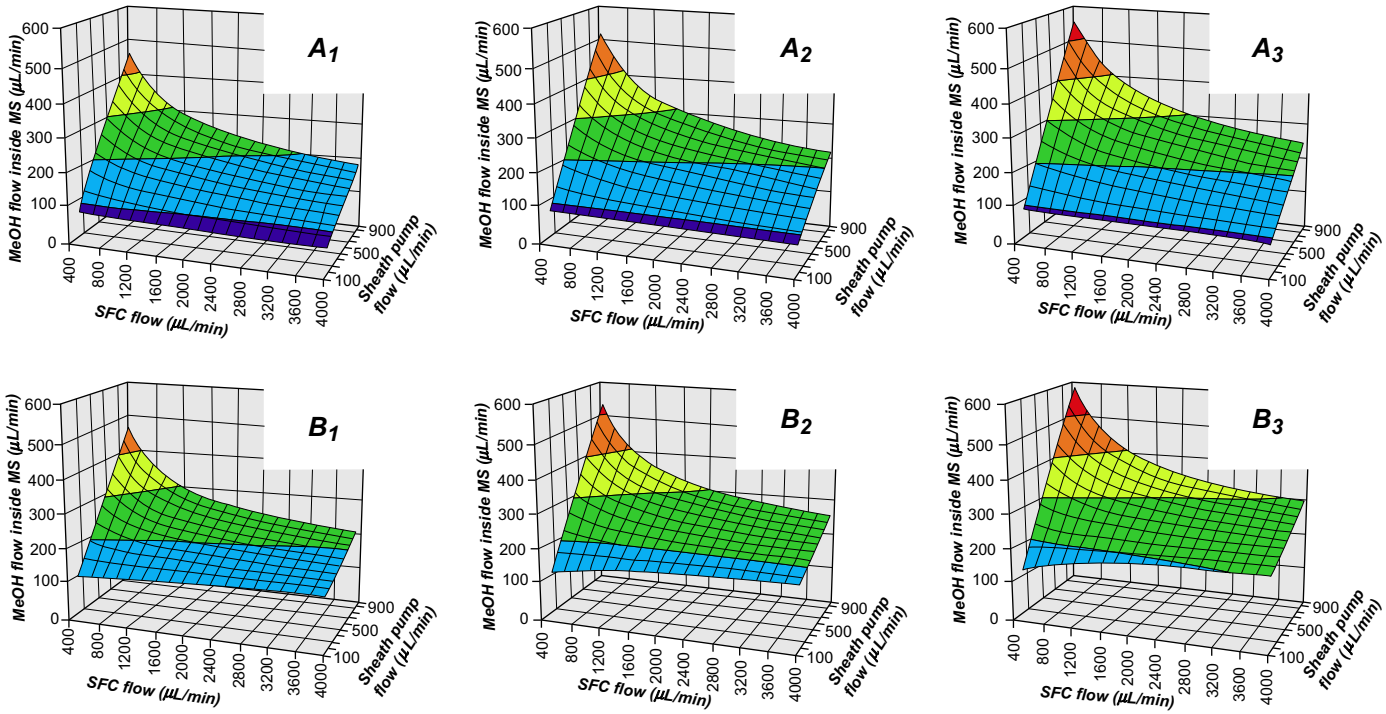

FIGURE 12.8

Model of total MeOH amount entering the eletrospray ionization probe using a prebackpressure regulator splitter with the sheath pump interface as a function of the ultra-high performance supercritical fluid chromatography mobile phase flow-rate (*x*-axis) and sheath pump flow-rate (*y*-axis) for two different mobile phase CO_2/methanol compositions. (A) composition 95:5, (B) 80:20 and three different fixed back-pressures: 120 bar (A_1, B_1), 150 bar (A_2, B_2), and 180 bar (A_3, B_3). *MeOH*, methanol; *MS*, mass spectrometry; *SFC*, supercritical fluid chromatography.

Adapted from Grand-Guillaume Perrenoud, A., Veuthey, J.-L., Guillaume, D., 2014a. Coupling state-of-the-art supercritical fluid chromatography and mass spectrometry: from hyphenation interface optimization to high-sensitivity analysis of pharmaceutical compounds. J. Chromatogr. A 1339, 174–184 with permission.

4.3 SUPERCRITICAL FLUID CHROMATOGRAPHY—MASS SPECTROMETRY CONDITIONS

The mobile phase composition and the ion source set-up might alter ionization efficiency in SFC—MS, and thus method sensitivity, similar to HPLC—MS. ESI ion source settings for both UHPLC—MS and UHPSFC—MS have been compared in two recent studies (Nováková et al., 2015a; Grand-Guillaume Perrenoud et al., 2014a). The results were quite similar for both techniques indicating high-desolvation temperatures, high gas flows, and low capillary voltages to be the most important for method sensitivity. Similarly, the same results for APCI source settings were found in both LC—MS and SFC—MS configurations (Pinkston et al., 2006). Beause SFC—MS coupling has recently gained great popularity, many studies focus on detailed optimization of the individual parameters of SFC—MS, including ion source set-up, mobile phase composition, make-up solvent composition, temperature, and BPR pressure (Pilařová et al., 2016; Yuan et al., 2016; Nováková et al., 2015a). As a result of the evaluation of mobile phase composition, methanol with an addition of 10 mM of ammonium formate and a small percentage of water (1%—5%) was found to be the most generic, providing both good overall MS sensitivity and chromatographic performance (Nováková et al., 2015a, 2016; Liu et al., 2015; Spaggiari et al., 2014; Taguchi et al., 2014). In some studies, advantage was taken of the benefits of SFC-dedicated stationary phases (BEH 2-EP or Torus chemistries), and thus no additives were used for the analyses (Yuan et al., 2016). Volatile additives, such as ammonium acetate, ammonium formate, and ammonia were generally also recommended in other studies (Yang et al., 2016; Grand-Guillaume Perrenoud et al., 2012; Hamman et al., 2011). In most studies, a positive effect of an additive on MS sensitivity has been noted (Nováková et al., 2015a,b, 2016; Pilařová et al., 2016; Wolrab et al., 2016; Bamba et al., 2008).

A comparison of ESI-MS response when using methanol alone as a pure organic modifier and methanol with different additives including 2% water, 10 mM ammonium acetate, 10 mM ammonium formate, and 10 mM ammonium formate with 2% water is shown in Fig. 12.9 for a group of selected doping agents. This comparison reveals that both volatile buffers, ammonium acetate and formate, provided about the same MS response, therefore the latter was used as a scaling value of 100%. The MS response showed a notable increase compared with pure methanol or methanol with 2% water. On the other hand, a further increase in MS response was obtained when 2% water was added to 10 mM ammonium formate in methanol.

Several studies focused on the comparison of sensitivity between UHPSFC—MS and UHPLC—MS techniques. In some papers, improved sensitivity was observed for the UHPSFC—MS configuration compared with UHPLC—MS (Nováková et al., 2015a; Grand-Guillaume Perrenoud et al., 2014a). However, results indicating similar sensitivity or the opposite case, i.e., lower sensitivity for SFC—MS compared with LC—MS, have been also described (Desfontaine et al., 2016; Lemasson et al., 2016; Nováková et al., 2015b; Spaggiari et al., 2014). Therefore, it may be concluded that the sensitivity of resulting SFC—MS methods is strongly dependent on the mass analyzer type and on the type of analyte. The two techniques may also be complementary in terms of sensitivity, as well as chromatographic separation selectivity.

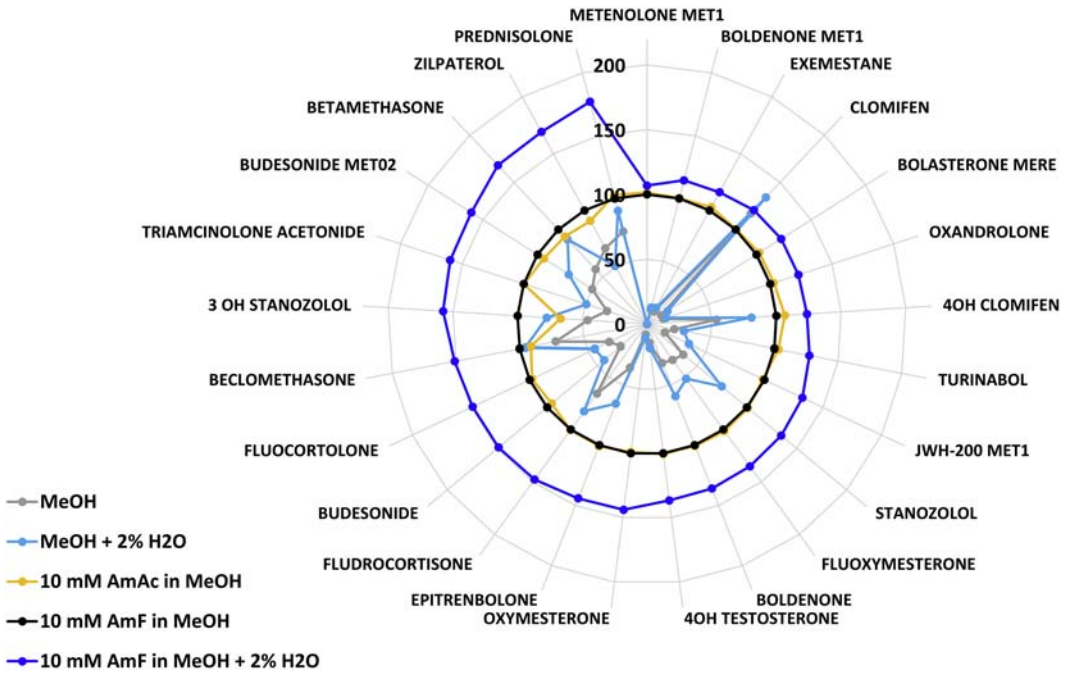

FIGURE 12.9

Influence of additives on eletrospray ionization-mass spectrometry response.

Unpublished figure created using data obtained in Nováková, L., Desfontaine, V., Ponzetto, F., Nicoli, R., Saugy, M., Veuthey, J.-L., Guillaume, D., 2016. Fast and sensitive supercritical fluid chromatography – tandem mass spectrometry multi-class screening method for the determination of doping agents in urine. Anal. Chim. Acta. 915, 102–110. See this reference for further details of experimental measurements.

5. APPLICATIONS OF SUPERCRITICAL FLUID CHROMATOGRAPHY

In the early days of SFC, most applications involved the separation of relatively nonpolar compounds, such as silicone oils, surfactants, waxes, or lipids using pure CO_2 as a mobile phase and pressure programming to enable sample elution. The scope of current applications is much wider. Various CO_2/modifier mobile phase combinations cover nearly the same scope of applications as HPLC in all its various modes, including RP-HPLC, NP-HPLC, HILIC, and also partially, ion-pair and ion-exchange chromatography. The applicability of SFC decreases with an increase in polarity, such as in the case of ionic compounds, polypeptides, proteins, etc.

Because of the well-established positions of HPLC and GC in routine laboratories, SFC is now competing for its space to become a complementary technique. The distribution of the involvement of SFC in selected application fields is shown in Fig. 12.10. However, it is remarkable that most of the

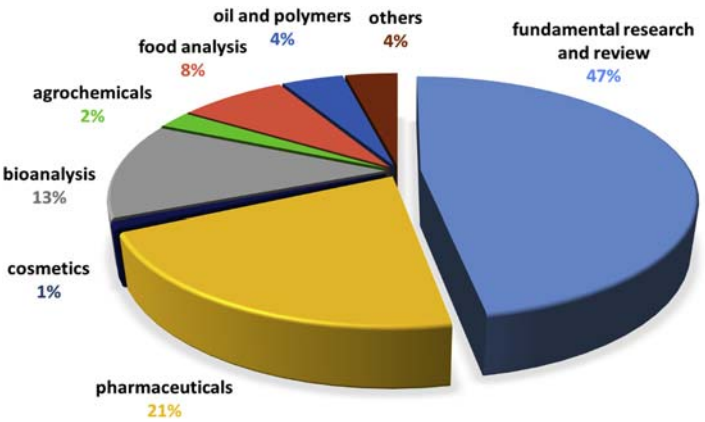

FIGURE 12.10

The involvement of supercritical fluid chromatography (SFC) technology in various application and research fields. The search was made using the Scifinder database using the keyword "SFC" with filtration of duplicate results. November 2016.

papers published with the focus on SFC are represented by fundamental research and review papers so far (47% of all papers). Major applications of SFC include pharmaceutical analysis (21%), especially chiral analysis and preparative SFC, and bioanalysis (13%, therapeutic drug monitoring, forensic analysis, lipidomics, etc.). Less common applications involve agrochemicals analysis, food analysis, and the analysis of oils and polymers. Other applications were only minor and their variability was too extensive; therefore they are not displayed individually in the graphical presentation and are rather classified as the group "others." In Fig. 12.10 we have not distinguished between SFC and UHPSFC applications.

5.1 PREDOMINANT SUPERCRITICAL FLUID CHROMATOGRAPHY APPLICATIONS

The main applications of SFC over the last 15 years have definitely been for chiral analysis and preparative separations in the pharmaceutical industry (Desfontaine et al., 2015; Ren-Qi et al., 2012), which corresponds to 21% of all published works, as shown in Fig. 12.10. Moreover, it is important to keep in mind that the number of published works on SFC in pharmaceutical analysis does not have to be representative of its real use in the pharmaceutical industry because there are a lot of pharmaceutical companies that are using SFC routinely without publishing their work. SFC with UV detection is the method of choice in this field. Of course, SFC−MS may also be employed. However, UV detection is strongly preferred for routine quality control (QC) analyses because of lower cost, user-friendliness, and straightforward method validation, compared with MS detection. Among drugs, many compounds are chiral and the two enantiomers may have different pharmacological effects, ranging from nonactivity to harmful effects (Zhang et al., 2005; Patel and Hutt, 2004). As a consequence of the severe affair with thalidomide, the Food and Drug Administration (FDA) now requires biological testing of each enantiomer. Pure enantiomer drugs are usually prepared by stereospecific synthesis. The enantiomeric purity has to be evaluated for the final product, as well as for the intermediate products of this synthesis. In many leading pharmaceutical companies, SFC has already became the first choice for chiral separations (Desfontaine et al., 2015;

Płotka et al., 2014; Zhao et al., 2003). Consequently, several research groups focus on the development of high throughput chiral screening strategies (Nováková and Douša, 2017; West, 2014; De Klerck et al., 2012a,b; Maftouh et al., 2005; White, 2005). Preparative SFC is used for purification in both achiral and chiral environments and is equally widely used in the pharmaceutical industry, due to several advantages relative to LC: (1) increased flow-rates allowing higher productivities and reduced time required to generate pure compounds, (2) the majority of the mobile phase being CO_2 makes the method more environmentally friendly and cost-effective, and finally, (3) CO_2 is easily removed postchromatography by decreasing the pressure, allowing them to obtain a highly concentrated product in the modifier, which is followed by easy removal (Speybrouck and Lipka, 2016; Miller, 2012; White, 2005).

Although the use of SFC in chiral analysis and purification is well established, the implementation of SFC in regulated pharmaceutical laboratories that are focused on QC has been much slower. Such laboratories require both analytical instrumentation and the method to be robust and capable to meet rigorous criteria for the method validation (method accuracy, precision, sensitivity, linearity, dynamic range, and robustness) requested by regulatory authorities, such as the ICH (International Conference on Harmonization of technical requirements for registration of pharmaceuticals for human use), FDA, or EMA (European Medicines Agency). As discussed in Section 2.2, this was not possible with the old SFC platforms. Therefore, the first methods for impurity profiling were reported only in 2000 and 2001, with the focus on evaluation of impurity concentrations relative to the API, provided that the criterion of sensitivity was met (Roston et al., 2001; Gyllenhaal and Karlsson, 2000), but full validation was still missing. The studies focused on all aspects of impurity profiling, including quantitative aspects, and full method validations were published only recently (Plachká et al., 2016; Li et al., 2015; Wang et al., 2011). All these studies have shown that SFC is a viable option for impurity profiling in pharmaceutical quality control, but the adoption of SFC for routine use in this QC task will require substantially more time. Nevertheless, due to the different separation mechanism, SFC can bring an orthogonality, which is very important to minimize the possibility that some impurity peaks remain unnoticed under the peak of the API or another impurity (Plachká et al., 2016; Wang et al., 2011) and to allow SFC to become a complementary technique to HPLC. Several fundamentally based studies used artificial mixtures or large sets of pharmaceuticals to determine initial SFC screening conditions (Dispas et al., 2016; Galea et al., 2015a; Lemasson et al., 2015a,b). Although these methods dealt only with method development and not with quantitative aspects of impurity profiling, they are a very useful base for further research in this field.

Besides the predominant applications, SFC is currently also used for moderate-to-minor interest applications, including cosmetic product analysis (Lesellier et al., 2015; Khater and West, 2015), use in the petrochemical industry (Thiébaut, 2012), polymer analysis (Takahashi, 2013), surfactant analysis (Takahashi et al., 2013), pesticide analysis (Pan et al., 2016; Ishibashi et al., 2012), and food analysis (Bernal et al., 2013).

5.2 APPLICATIONS OF SUPERCRITICAL FLUID CHROMATOGRAPHY—MASS SPECTROMETRY

There are substantially fewer SFC—MS methods than SFC methods with other, mostly UV, detection types, as was already discussed in Section 1.2 and shown in Fig. 12.2. On average, SFC—MS methods made up only about 10% of all SFC methods. This abundance has increased since 2002 and approached 20% with no decline since 2012.

Most SFC−MS applications were developed for bioanalysis. These include several different fields of interest, especially lipid analysis, toxicology, doping analysis, therapeutic drug monitoring, and analysis of biomarkers. Biological fluids are very complex samples containing the target analytes at very low concentrations, whereas interfering compounds are abundant. Consequently, important method development challenges, in terms of method sensitivity and selectivity, are inherent to bioanalytical procedures. Chromatographic techniques coupled to MS are the methods of choice (Nováková, 2013). However, SFC−MS is still much less widely utilized compared with HPLC-MS, although a significant increase in the number of published papers has occurred very recently (Desfontaine et al., 2015). The main purposes to employ SFC in bioanalysis were: (1) to analyze groups of compounds that are challenging in RP-HPLC, such as antibiotics (Yuan et al., 2016; Eom et al., 2016), lipids, and fat-soluble vitamins (Pilařová et al., 2016; Jumaah et al., 2016; Taguchi et al., 2014), (2) to develop enantioselective methods for the quantification of drugs and their chiral metabolites (Yang et al., 2016), and finally, (3) to obtain different selectivity for the analysis of metabolites (Sen et al., 2016; Spaggiari et al., 2014). Chromatograms exemplifying the benefits of UHPSFC−MS in analysis of structural isomers of vitamin E in human serum are shown in Fig. 12.11.

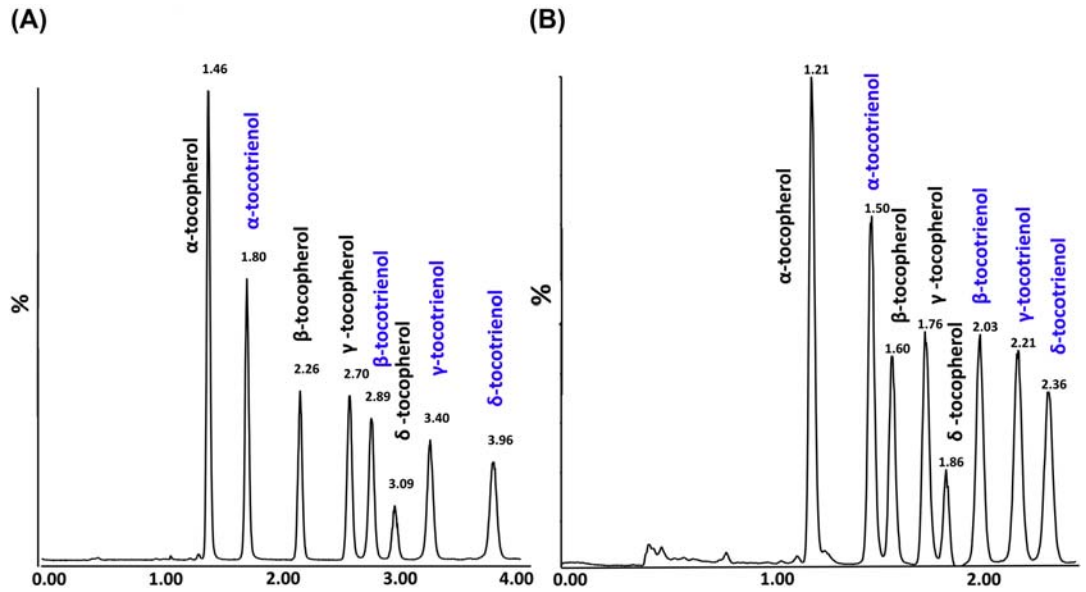

FIGURE 12.11

Ultra-high performance supercritical fluid chromatography−mass spectrometry chromatograms of the separation of eight isomers of vitamin E. (A) High-resolution method. (B) High-speed method.

Reproduced from Pilařová, V., Gottvald, T., Svoboda, P., Novák, O., Benešová, K., Běláková, S., Nováková, L., 2016. Development and optimization of ultra-high performance supercritical fluid chromatography mass spectrometry method for high-throughput determination of tocopherols and tocotrienols in human serum. Anal. Chim. Acta 934, 252–265 with permission. Also see this reference for the details of the experimental study.

UHPSFC enabled fast analysis and baseline separation of all isomers, although they are structurally very closely related. MS detection using a single quadrupole analyzer provided sufficient sensitivity for routine analysis of biological samples at a reasonable analysis cost.

Because SFC−MS is quite a new approach in bioanalysis, many studies focus on detailed optimization of the individual parameters of SFC−MS, including ion source set-up, mobile phase composition, make-up solvent composition, temperature, and BPR pressure (Jumaah et al., 2016; Pilařová et al., 2016; Sen et al., 2016; Yuan et al., 2016; Yang et al., 2016; Spaggiari et al., 2014). Matrix effects are an important obstacle of HPLC−MS and their determination is now obligatory in bioanalytical methods. They have been extensively studied in LC−MS, but reports in SFC−MS are quite rare so far. Recently, a few studies have focused on the systematic evaluation of matrix effects and a comparison among UHPSFC−tandem mass spectrometry (MS/MS), UHPLC−MS/MS, and GC−MS/MS (Desfontaine et al., 2016; Nováková et al., 2015b). Urine samples were evaluated with the aim to develop doping screening methods using simple dilute and shoot sample pretreatment and supported liquid extraction. The results revealed a generally lower incidence of matrix effects in the case of UHPSFC−MS/MS compared with UHPLC−MS/MS (Desfontaine et al., 2016; Nováková et al., 2015b) and the occurrence of serious matrix effects in the case of GC−MS/MS (Desfontaine et al., 2016). The applicability of UHPSFC−MS/MS in doping screening analysis has been proven, provided that orthogonal selectivity to UHPLC−MS/MS and very fast analytical runs were obtained, and the desired sensitivity for most analytes was achieved (Desfontaine et al., 2016; Nováková et al., 2015b, 2016).

SFC has demonstrated remarkable success, especially in lipid analysis. Although the state-of-the-art UHPLC−MS techniques cannot separate isomeric lipids with adequate resolution, SFC−MS can yield a wider spectrum of separations with one mobile phase and mostly no need for derivatization. Using SFC−MS, tens of isomers can be separated in a single run, allowing not only the fingerprint screening of samples but also the detailed profiling of individual components. Lipid extracts can be separated into their respective classes, and subsequently individual lipid species can be identified using high-resolution MS (HRMS) or MS/MS spectra. SFC−MS offers higher throughput than LC−MS (Laboureur et al., 2015; Lísa and Holčapek, 2015; Bamba et al., 2008).

An impressive speed of separation for this group of compounds is shown in Fig. 12.12. To further increase the throughput by reducing the sample preparation time, the use of an on-line supercritical fluid extraction−SFC method is advised, which also favors the extraction of lipophilic compounds (Uchikata et al., 2012). A make-up fluid for UHPSFC effluent is required for assuring good ionization efficiency of lipids (Yamada et al., 2013). Many of the SFC−MS analytical approaches from bioanalysis are also applied in food analysis for the determination of various groups of lipids and fat-soluble vitamins (Gee et al., 2016; Mejean et al., 2015; Bernal et al., 2013).

UHPSFC−MS has also been shown to be applicable for the analysis of natural compounds in various plant extracts, although the reports are quite few for the moment. One hundred and twenty compounds were screened on 15 different stationary phases. Among them, three phases, diol, non-endcapped C18, and 2-ethylpyridine, were determined to be of particular interest (Grand-Guillaume Perrenoud et al., 2016). The analysis of both polar and nonpolar plant extracts gave evidence that UHPSFC−HRMS could be applied for the metabolite profiling of natural complex matrices (Duval et al., 2016; Grand-Guillaume Perrenoud et al., 2016).

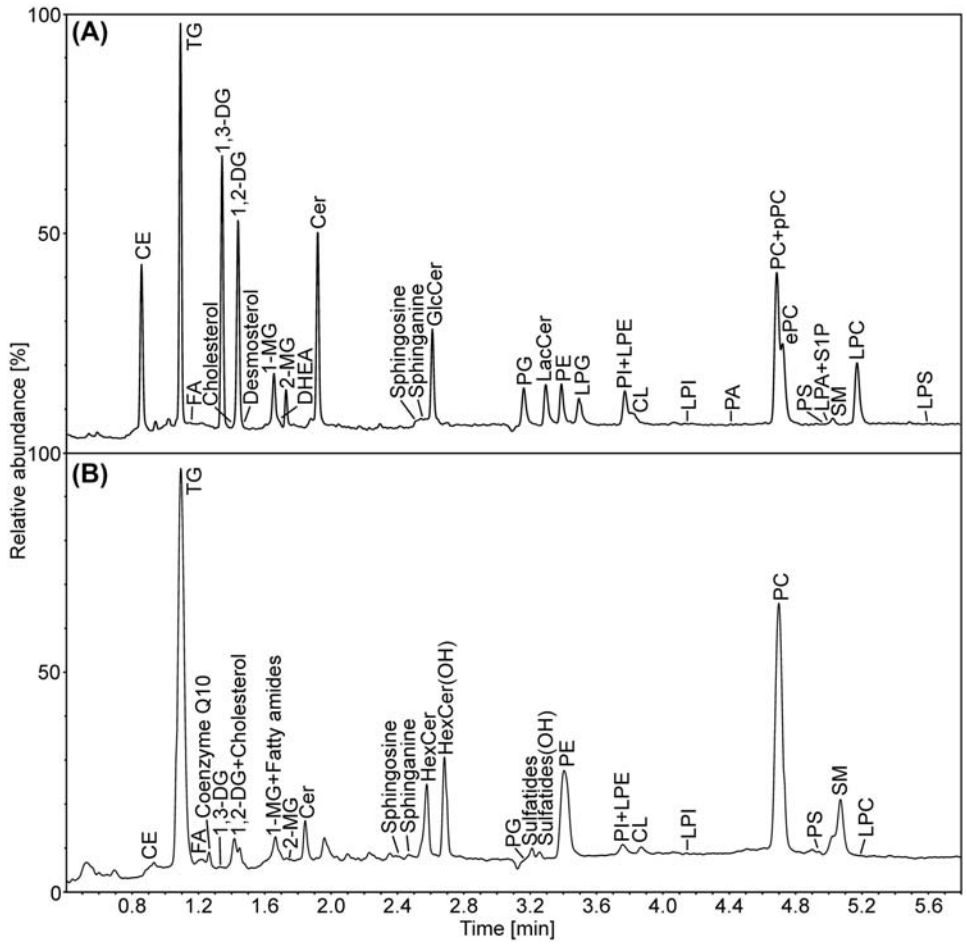

FIGURE 12.12

Positive-ion ultra-high performance supercritical fluid chromatography/eletrospray ionization mass spectrometry chromatograms of a mixture of lipid class standards (A) and a total lipid extract of porcine brain (B).

Reprinted from Lísa, M., Holčapek, M., 2015. High-throughput and comprehensive lipidomic analysis using ultrahigh-performance supercritical fluid chromatography–mass spectrometry. Anal. Chem. 87, 7187–7195 with permission. Also see this reference for the details of the experimental study and for the explanation of individual abbreviations.

6. CONCLUSIONS

The development of SFC techniques has experienced light and dark periods. Because of the well-established techniques HPLC and GC, it remained a neglected tool in separation science for a long time and it struggled to find its stable position among them. Taking advantage of sub-2 μm particles and advanced UHPSFC instrumentation, a new dimension in separation speed could now be achieved

for both chiral and achiral separations. Currently, UHPSFC is a very interesting complementary technique to HPLC and GC, which brings multiple benefits. These include fast analysis, high separation efficiency, versatility of applications and method development, lower pressure drops, orthogonality to RP-HPLC separations, ability to separate chiral and other isomers, lower operating costs, and finally, environmental friendliness. Coupling of UHPSFC and MS has been facilitated because of important developments in the atmospheric pressure ionization techniques, ESI and APCI. The enhanced sensitivity and selectivity of UHPSFC−MS is favored in the analysis of complex matrices, such as biological materials, foods, and natural products.

REFERENCES

Abrahamsson, V., Sandahl, M., 2013. Impact of injection solvents on supercritical fluid chromatography. J. Chromatogr. A 1306, 80−88.

Alexander, A.J., Hooker, T.F., Tomasella, F.P., 2012. Evaluation of mobile phase gradient supercritical fluid chromatography for impurity profiling of pharmaceutical compounds. J. Pharm. Biomed. Anal. 70, 77−86.

Arpino, P.J., Cousin, J., 1987. Supercritical fluid chromatography-mass spectrometry coupling. TrAC Trends Anal. Chem. 6, 69−73.

Arpino, P.J., Haas, P., 1995. Recent developments in supercritical fluid chromatography-mass spectrometry coupling. J. Chromatogr. A 703, 479−488.

Ashraf-Khorassani, M., Taylor, L.T., 2010. Subcritical fluid chromatography of water soluble nucleobases on various polar stationary phases facilitated with alcohol-modified CO_2 and water as the polar additive. J. Sep. Sci. 33, 1682−1691.

Bamba, T., Shimonishi, N., Matsubara, A., Hirata, K., Nakazawa, Y., Kobayashi, A., Fukusaki, E., 2008. High throughput and exhaustive analysis of diverse lipids by using supercritical fluid chromatography-mass spectrometry for metabolomics. J. Biosci. Bioeng. 105, 460−469.

Berger, T.A., 1997. Separation of polar solutes by packed column supercritical fluid chromatography. J. Chromatogr. A 785, 3−33.

Berger, T.A., 2010. Demonstration of high speed with low pressure drops using 1.8 μm particles in SFC. Chromatographia 72, 597−602.

Berger, T.A., 2011. Characterization of a 2.6 μm Kinetex porous shell hydrophilic interaction liquid chromatography column in supercritical fluid chromatography with a comparison to 3 μm totally porous silica. J. Chromatogr. A 1218, 4559−4568.

Berger, T.A., 2014. Minimizing ultraviolet noise due to mis-matches between detector flow cell and post column mobile phase temperatures in supercritical fluid chromatography: effect of flow cell design. J. Chromatogr. A 1364, 249−260.

Berger, T.A., 2015a. Instrumentation for analytical scale supercritical fluid chromatography. J. Chromatogr. A 1421, 171−183.

Berger, T.A., 2015b. Supercritical Fluid Chromatography. Primer. Document #5991−5509EN. Agilent Technologies, Inc., USA.

Berger, T.A., 2016. Kinetic performance of a 50 mm long 1.8 μm chiral column in supercritical fluid chromatography. J. Chromatogr. A 1459, 136−144.

Berger, T.A., Berger, B.K., 2010. A review of column developments for supercritical fluid chromatography. LC GC N.Am. 28, 344−357.

Berger, T.A., Berger, B.K., 2011. Minimizing UV noise in supercritical fluid chromatography: I. Improving back pressure regulator pressure noise. J. Chromatogr. A 1218, 2320−2326.

Berger, T.A., Deye, J.F., 1990. Composition and density effects using methanol/carbon dioxide in packed column supercritical fluid chromatography. Anal. Chem. 62, 1181−1185.

Berger, T.A., Deye, J.F., 1991a. Effect of basic additives on peak shapes of strong bases separated by packed-column supercritical fluid chromatography. J. Chromatogr. Sci. 29, 310−317.

Berger, T.A., Deye, J.F., 1991b. Supercritical fluid chromatographic retention of anilines with pure and modified fluids on standard and deactivated columns. J. Chromatogr. Sci. 29, 390−395.

Berger, T.A., Wilson, W.H., 1995. Separation of basic drugs by packed-column supercritical fluid chromatography. 3. Stimulants. J. Pharm. Sci. 84, 489−492.

Berger, T.A., Colgate, S., Casale, M., 2013. Low Noise Back Pressure Regulator for Supercritical Fluid Chromatography. Patent US8419936 B2.

Bernal, J.L., Martín, N.T., Toribio, L., 2013. Supercritical fluid chromatography in food analysis. J. Chromatogr. A 1313, 24−36.

Blackwell, J.A., Stringham, R.W., Weckwerth, J.D., 1997. Effect of mobile phase additives in packed-column subcritical and supercritical fluid chromatography. Anal. Chem. 69, 409−415.

Bouigeon, C., Thiébaut, D., Caude, M., 1996. Long packed column supercritical fluid chromatography: influence of pressure drop on apparent efficiency. Anal. Chem. 68, 3622−3630.

Brunelli, C., Gorecki, T., Zhao, Y., Sandra, P., 2007. Corona-charged aerosol detection in supercritical fluid chromatography for pharmaceutical analysis. Anal. Chem. 79, 2472−2482.

Brunelli, C., Zhao, Y., Brown, M.-H., Sandra, P., 2008a. Development of a supercritical fluid chromatography high-resolution separation method suitable for pharmaceuticals using cyanopropyl silica. J. Chromatogr. A 1185, 263−272.

Brunelli, C., Zhao, Y., Brown, M.-H., Sandra, P., 2008b. Pharmaceutical analysis by supercritical fluid chromatography: optimization of the mobile phase composition on a 2-ethylpyridine column. J. Sep. Sci. 31, 1299−1306.

Bu, X., Regalado, E.L., Cuff, J., Gong, X., 2016. Chiral analysis of poor UV absorbing pharmaceuticals by supercritical fluid chromatography-charged aerosol detection. J. Supercrit. Fluids 116, 20−25.

Cantrell, G.O., Stringham, R.W., Blackwell, J.A., Weckwerth, J.D., Carr, P.W., 1996. Effect of various modifiers on selectivity in packed-column subcritical and supercritical fluid chromatography. Anal. Chem. 68, 3645−3650.

Chester, T.L., Pinkston, J.D., 1998. Pressure-regulating fluid interface and phase behaviour considerations in the coupling of packed-column supercritical fluid chromatography with low-pressure detectors. J. Chromatogr. A 807, 265−273.

Combs, M.T., Ashraf-Khorassani, M., Taylor, L.T., 1997. Packed column supercritical fluid chromatography-mass spectroscopy: a review. J. Chromatogr. A 785, 85−100.

Crowther, J.B., Henion, J.D., 1985. Supercritical fluid chromatography of polar drugs using small-particle packed columns with mass spectrometric detection. Anal. Chem. 57, 2711−2716.

De Klerck, K., Mangelings, D., Click, D., De Boever, F., Vander Heyden, Y., 2012a. Combined use of isopropylamine and trifluoroacetic acid in methanol-containing mobile phases for chiral supercritical fluid chromatography. J. Chromatogr. A 1234, 72−79.

De Klerck, K., Mangelings, D., Vander Heyden, Y., 2012b. Supercritical fluid chromatography for the enantioseparation of pharmaceuticals. J. Pharm. Biomed. Anal. 69, 77−92.

De Pauw, R., Shoykhet, K., Desmet, G., Broeckhoven, K., 2015. Understanding and diminishing the extra-column band broadening effects in supercritical fluid chromatography. J. Chromatogr. A 1403, 132−137.

Delahaye, S., Broeckhoven, K., Desmet, G., Lynen, F., 2012. Design and evaluation of various methods for the construction of kinetic performance limit plots for supercritical fluid chromatography. J. Chromatogr. A 1258, 152−160.

Delahaye, S., Broeckhoven, K., Desmet, G., Lynen, F., 2013. Application of the isopycnic kinetic plot method for elucidating the potential of sub-2-μm and core-shell particles in SFC. Talanta 116, 1105−1112.

Desfontaine, V., Guillaume, D., Francotte, E., Nováková, L., 2015. Supercritical fluid chromatography in pharmaceutical analysis. J. Pharm. Biomed. Anal. 113, 56−71.

Desfontaine, V., Nováková, L., Ponzatto, F., Nicoli, R., Saugy, M., Veuthey, J.-L., Guillaume, D., 2016. Liquid chromatography and supercritical fluid chromatography as alternative techniques to gas chromatography for the rapid screening of anabolic agents in urine. J. Chromatogr. A 1451, 145−155.

Deye, J.F., Berger, T.A., Anderson, A.G., 1990. Nile red as a solvatochromic dye for measuring solvent strength in normal liquids and mixtures of normal liquids with supercritical and near critical fluids. Anal. Chem. 62, 615−622.

Dijkstra, Z.J., Doornbos, A.R., Weyten, H., Ernsting, J.M., Elsevier, C.J., Keurentjes, J.T.F., 2007. Formation of carbamic acid in organic solvent and in supercritical carbon dioxide. J. Supercrit. Fluids 41, 109−114.

Dispas, A., Lebrun, P., Sacré, P.Y., Hubert, P., 2016. Screening study of SFC critical method parameters for the determination of pharmaceutical compounds. J. Pharm. Biomed. Anal. 125, 339−354.

Duval, J., Colas, C., Pecher, V., Poujol, M., Tranchant, J.-L., Lesellier, E., 2016. Contribution of supercritical fluid chromatography coupled to high resolution mass spectrometry and UV detections for the analysis of a complex vegetable oil − application for characterization of a *Kniphofia uvaria* extract. C. R. Chim. 19, 1113−1123.

Enmark, M., Asberg, D., Shalliker, A., Samuelsson, J., Fornstedt, T., 2015. A closer study of peak distortions in supercritical fluid chromatography as generated by the injection. J. Chromatogr. A 1400, 131−139.

Eom, H.Y., Kang, M., Kang, S.W., Kim, U., Suh, J.H., Kim, J., Cho, H.-D., Yang, D.-H., Han, S.B., 2016. Rapid chiral separation of racemic cetirizine in human plasma using subcritical fluid chromatography-tandem mass spectrometry. J. Pharm. Biomed. Anal. 117, 380−389.

Fairchild, J.N., Hill, J.F., Iraneta, P.C., 2013. Influence of sample solvent composition for SFC separations. LC GC N. Am. 31, 326−333.

Fairchild, J.N., Brousmiche, D.W., Hill, J.F., Morris, M.F., Boissel, C.A., Wyndham, K.D., 2015. Chromatographic evidence of silyl ether formation (SEF) in supercritical fluid chromatography. Anal. Chem. 87, 1735−1742.

Fekete, S., Kohler, I., Rudaz, S., Guillaume, D., 2014. Importance of instrumentation for fast liquid chromatography in pharmaceutical analysis. J. Pharm. Biomed. Anal. 87, 105−119.

Galea, C., Mangelings, D., Vander Heyden, Y., 2015a. Method development for impurity profiling in SFC: the selection of a dissimilar set of stationary phases. J. Pharm. Biomed. Anal. 111, 333−343.

Galea, C., Mangelings, D., Vander Heyden, Y., 2015b. Characterization and classification of stationary phases in HPLC and SFC − a review. Anal. Chim. Acta 886, 1−15.

Gee, P.T., Liew, C.Y., Thong, M.C., Gay, M.C.L., 2016. Vitamin E analysis by ultra-performance convergence chromatography and structural elucidation of novel α-tocodienol by high-resolution mass spectrometry. Food Chem. 196, 367−373.

Gere, D.R., Board, R., McManigill, D., 1982. Supercritical fluid chromatography with small particle diameter packed columns. Anal. Chem. 54, 736−740.

Giddings, J.C., Myers, M.N., McLaren, L.M., Keller, R.A., 1968. High pressure gas chromatography of nonvolatile species. Science 162, 67−73.

Giddings, J.C., Myers, M.N., King, J.W., 1969. Dense gas chromatography at pressures to 2000 atmospheres. J. Chromatogr. Sci. 7, 276−283.

Grand-Guillarme Perrenoud, A., Guillaume, D., Boccard, J., Veuthey, J.-L., Barron, D., Moco, S., 2016. Ultra-high performance supercritical fluid chromatography coupled with quadrupole-time-of-flight mass spectrometry as a performing tool for bioactive analysis. J. Chromatogr. A 1450, 101−111.

Grand-Guillaume Perrenoud, A., Veuthey, J.-L., Guillaume, D., 2012. Comparison of ultra-high performance supercritical fluid chromatography and ultra-high performance liquid chromatography for analysis of pharmaceutical compounds. J. Chromatogr. A 1266, 158−167.

Grand-Guillaume Perrenoud, A., Hamman, C., Goel, M., Veuthey, J.-L., Guillaume, D., Fekete, S., 2013. Maximizing kinetic performance in supercritical fluid chromatography using state-of-the-art instruments. J. Chromatogr. A 1314, 288−297.

Grand-Guillaume Perrenoud, A., Veuthey, J.-L., Guillaume, D., 2014a. Coupling state-of-the-art supercritical fluid chromatography and mass spectrometry: from hyphenation interface optimization to high-sensitivity analysis of pharmaceutical compounds. J. Chromatogr. A 1339, 174−184.

Grand-Guillaume Perrenoud, A., Farrell, W.P., Aurigemma, C.M., Aurigemma, N.C., Fekete, S., Guillaume, D., 2014b. Evaluation of stationary phases packed with superficially porous particles for the analysis of pharmaceutical compounds using supercritical fluid chromatography. J. Chromatogr. A 1360, 275−287.

Guiochon, G., Tarafder, A., 2011. Fundamental challenges and opportunities for preparative supercritical fluid chromatography. J. Chromatogr. A 1218, 1037−1114.

Gyllenhaal, O., Karlsson, A., 2000. Packed-column supercritical fluid chromatography for the analysis of isosorbide-5-mononitrate and related compounds in bulk substance and tablets. J. Biochem. Biophys. Methods 43, 135−146.

Hamman, C., Schmidt Jr., D.E., Wong, M., Hayes, M., 2011. The use of ammonium hydroxide as an additive in supercritical fluid chromatography for achiral and chiral separations and purifications of small, basic medicinal molecules. J. Chromatogr. A 1218, 7886−7894.

Hartmann, W., Klesper, E., 1977. Preparative supercritical fluid chromatography of styrene oligomers. J. Polym. Sci. Polym. Lett. Ed. 15, 713−719.

Huang, E., Henion, J., Covey, T.R., 1990. Packed-column supercritical fluid chromatography-mass spectrometry and supercritical fluid chromatography-tandem mass spectrometry with ionization at atmospheric pressure. J. Chromatogr. A 511, 257−270.

Huetz, A., Klesper, E., 1992. Efficiency in supercritical fluid chromatography as a function of linear velocity, pressure/density, temperature and diffusion coefficient employing *n*-pentane as the eluent. J. Chromatogr. A 607, 79−89.

Ishibashi, M., Ando, T., Sakai, M., Matsubara, A., Uchikata, T., Fukusaki, E., Bamba, T., 2012. High-throughput simultaneous analysis of pesticides by supercritical fluid chromatography/tandem mass spectrometry. J. Chromatogr. A 1266, 143−148.

Jentoft, R.E., Gouw, T.H., 1970. Pressure-programmed supercritical fluid chromatography of wide molecular weight range mixtures. J. Chromatogr. Sci. 8, 138−142.

Jumaah, F., Larsson, S., Essén, S., Cunico, L.P., Holm, C., Turner, C., Sandahl, M., 2016. A rapid method for the separation of vitamin D and its metabolites by ultra-high performance supercritical fluid chromatography-mass spectrometry. J. Chromatogr. A 1440, 191−200.

Kalíková, K., Šlechtová, T., Vozka, J., Tesařová, E., 2014. Supercritical fluid chromatography as a tool for enantioselective separation; a review. Anal. Chim. Acta 821, 1−33.

Karayannis, N.K., Corwin, A.H., Baker, E.W., Klesper, E., Walter, J.A., 1968. Apparatus and materials for hyperpressure gas chromatography of nonvolatile compounds. Anal. Chem. 40, 1736−1739.

Khater, S., West, C., 2015. Development and validation of a supercritical fluid chromatography method for the direct determination of enantiomeric purity of provitamin B5 in cosmetic formulations with mass spectrometric detection. J. Pharm. Biomed. Anal. 102, 321−325.

Khater, S., West, C., Lesellier, E., 2013. Characterization of five chemistries and three particle sizes of stationary phases used in supercritical fluid chromatography. J. Chromatogr. A 1319, 148−159.

Klesper, E., Corwin, A.H., Turner, D.A., 1962. High pressure gas chromatography above critical temperatures. J. Org. Chem. 27, 700−701.

Laboureur, L., Ollero, M., Toubout, D., Astarita, G., 2015. Lipidomics by supercritical fluid chromatography. Int. J. Mol. Sci. 16, 13868−13884.

Lambert, N., Felinger, A., 2015. Performance of the same column in supercritical fluid chromatography and in liquid chromatography. J. Chromatogr. A 1409, 234−240.

Lauer, H.H., McManigil, D., Board, R.D., 1983. Mobile-phase transport properties of liquefied gases in near critical and supercritical fluid chromatography. Anal. Chem. 55, 1370−1375.

Lecoeur, M., Simon, N., Sautou, V., Decaudin, B., Vaccher, C., 2014. A chemometric approach to elucidate the parameter impact in the hyphenation of evaporative light scattering detector to supercritical fluid chromatography. J. Chromatogr. A 1333, 124−133.

Lemasson, E., Bertin, S., Henning, P., Boiteux, H., Lesellier, E., West, C., 2015a. Development of an achiral supercritical fluid chromatography method with ultraviolet absorbance and mass spectrometric detection for impurity profiling of drug candidates: Part I: optimization of mobile phase composition. J. Chromatogr. A 1408, 217−226.

Lemasson, E., Bertin, S., Henning, P., Boiteux, H., Lesellier, E., West, C., 2015b. Development of an achiral supercritical fluid chromatography method with ultraviolet absorbance and mass spectrometric detection for impurity profiling of drug candidates: Part II: selection of an orthogonal set of stationary phases. J. Chromatogr. A 1408, 227−235.

Lemasson, E., Bertin, S., Henning, P., Lesellier, E., West, C., 2016. Comparison of ultra-high performance methods in liquid and supercritical fluid chromatography coupled to electrospray ionization − mass spectrometry for impurity profiling of drug candidates. J. Chromatogr. A 1472, 117−128.

Leren, E., Landmark, K.E., Greibrokk, T., 1991. Sulphur dioxide as a mobile phase in supercritical fluid chromatography. Chromatographia 31, 535−538.

Lesellier, E., 2009. Retention mechanisms in super/subcritical fluid chromatography on packed columns. J. Chromatogr. A 1216, 1881−1890.

Lesellier, E., West, C., 2015. The many faces of packed column supercritical fluid chromatography − a critical review. J. Chromatogr. A 1382, 2−46.

Lesellier, E., Valarché, A., West, C., Dreux, M., 2012a. Effects of selected parameters on the response of the evaporative light scattering detector in supercritical fluid chromatography. J. Chromatogr. A 1250, 220−226.

Lesellier, E., Bizet, T., Valarché, A., West, C., Dreux, M., 2012b. Coupling supercritical fluid chromatography with evaporating light scattering detection: a study of the relevant parameters ruling response. LC GC N. Am. 30, 240−249.

Lesellier, E., Latos, A., Lopes de Oliveira, A., 2014. Ultra high efficiency/low pressure supercritical fluid chromatography with superficially porous particles for triglyceride separation. J. Chromatogr. A 1327, 141−148.

Lesellier, E., Mith, D., Dubrulle, I., 2015. Method developments approaches in supercritical fluid chromatography applied to the analysis of cosmetics. J. Chromatogr. A 1423, 158−168.

Leyendecker, D., Schmitz, F.P., Klesper, E., 1984. Chromatography with sub- and supercritical eluents: the influence of temperature, pressure and flow-rate on the behaviour of dimethyl and diethyl ether. J. Chromatogr. A 315, 19−30.

Leyendecker, D., Leyendecker, D., Lorenschat, B., Schmitz, F.P., Klesper, E., 1987. Influence of density on the chromatographic behaviour of lower alkanes as mobile phases in supercritical fluid chromatography. J. Chromatogr. A 398, 89−103.

Li, W., Wang, J., Yan, Z.Y., 2015. Development of a sensitive and rapid method for rifampicin impurity analysis using supercritical fluid chromatography. J. Pharm. Biomed. Anal. 114, 341−347.

Lísa, M., Holčapek, M., 2015. High-throughput and comprehensive lipidomic analysis using ultrahigh-performance supercritical fluid chromatography−mass spectrometry. Anal. Chem. 87, 7187−7195.

Liu, X.-G., Qi, L.-W., Fan, Z.-Y., Dong, X., Guo, R.-Z., Lou, F.-C., Fanali, S., Li, P., Yang, H., 2015. Accurate analysis of ginkgolides and their hydrolyzed metabolites by analytical supercritical fluid chromatography hybrid tandem mass spectrometry. J. Chromatogr. A 1388, 251−258.

Lochmuller, C.H., Mink, L.P., 1990. Comparison of supercritical carbon dioxide and supercritical propane as mobile phases in supercritical fluid chromatography. J. Chromatogr. 505, 119−137.

Lou, X., Janssen, H.-G., Cramers, C.A., 1997. Temperature and pressure effects on solubility in supercritical carbon dioxide and retention in supercritical fluid chromatography. J. Chromatogr. A 785, 57−64.

Maftouh, M., Granier-Loyaux, C., Chavana, E., Marini, J., Pradines, A., Heyden, Y.V., 2005. Screening approach for chiral separation of pharmaceuticals. J. Chromatogr. A 1088, 67−81.

Mejean, M., Brunelle, A., Touboul, D., 2015. Quantification of tocopherols and tocotrienols in soybean oil by supercritical-fluid chromatography coupled to high-resolution mass spectrometry. Anal. Bioanal. Chem. 407, 5133−5142.

Miller, L., 2012. Preparative enantioseparations using supercritical fluid chromatography. J. Chromatogr. A 1250, 250−255.

Nováková, L., 2013. Challenges in the development of bioanalytical liquid chromatography-mass spectrometry method with emphasis on fast analysis. J. Chromatogr. A 1292, 25−37.

Nováková, L., Douša, M., 2017. General screening and optimization strategy for fast chiral separations in modern supercritical fluid chromatography. Anal. Chim. Acta 950, 199−210.

Nováková, L., Veuthey, J.-L., Guillaume, D., 2011. Practical method transfer from high performance liquid chromatography to ultra-high performance liquid chromatography: the importance of frictional heating. J. Chromatogr. A 1218, 7971−7981.

Nováková, L., Grand-Guillaume Perrenoud, A., Francois, I., West, C., Lesellier, E., Guillaume, D., 2014. Modern analytical supercritical fluid chromatography using columns packed with sub-2 μm particles: a tutorial. Anal. Chim. Acta 824, 18−35.

Nováková, L., Grand-Guillaume Perrenoud, A., Nicoli, R., Saugy, M., Veuthey, J.-L., Guillaume, D., 2015a. Ultra high performance supercritical fluid chromatography coupled with tandem mass spectrometry for screening of doping agents: I: investigation of mobile phase and MS conditions. Anal. Chim. Acta 853, 637−646.

Nováková, L., Grand-Guillaume Perrenoud, A., Nicoli, R., Saugy, M., Veuthey, J.-L., Guillaume, D., 2015b. Ultra high performance supercritical fluid chromatography coupled with tandem mass spectrometry for screening of doping agents: II: analysis of biological samples. Anal. Chim. Acta 853, 647−659.

Nováková, L., Desfontaine, V., Ponzetto, F., Nicoli, R., Saugy, M., Veuthey, J.-L., Guillaume, D., 2016. Fast and sensitive supercritical fluid chromatography − tandem mass spectrometry multi-class screening method for the determination of doping agents in urine. Anal. Chim. Acta 915, 102−110.

Novotny, M., Bertsch, W., Zlatkis, A., 1971. Temperature and pressure affects in supercritical-fluid chromatography. J. Chromatogr. A 61, 17−28.

Novotny, M., Springston, S.R., Peaden, P.A., Fjeldsted, J.C., Lee, M.L., 1981. Capillary supercritical fluid chromatography. Anal. Chem. 53, 407A−414A.

Pan, X., Dong, F., Xu, J., Liu, X., Chen, Z., Zheng, Y., 2016. Stereoselective analysis of novel chiral fungicide pyrisoxazole in cucumber, tomato and soil under different application methods with supercritical fluid chromatography/tandem mass spectrometry. J. Hazard. Mater. 311, 115−124.

Patel, B.K., Hutt, A.J., 2004. Stereoselectivity in drug action and disposition: an overview. In: Reddy, I.K., Mehvar, R. (Eds.), Chirality in Drug Design and Development. Marcel Dekker Inc., New York, pp. 139−187.

Peaden, P.A., Lee, M.L., 1983. Theoretical treatment of resolving power in open tubular column supercritical fluid chromatography. J. Chromatogr. A 259, 1−16.

Peaden, P.A., Fjeldsted, J.C., Lee, M.L., Springston, S.R., Novotny, M., 1982. Instrumental aspects of capillary supercritical fluid chromatography. Anal. Chem. 54, 1090−1093.

Pilařová, V., Gottvald, T., Svoboda, P., Novák, O., Benešová, K., Běláková, S., Nováková, L., 2016. Development and optimization of ultra-high performance supercritical fluid chromatography mass spectrometry method for high-throughput determination of tocopherols and tocotrienols in human serum. Anal. Chim. Acta 934, 252−265.

Pinkston, J.D., 2005. Advantages and drawbacks of popular supercritical fluid chromatography interfacing approaches-A user's perspective. Eur. J. Mass. Spectrom. 11, 189−197.

Pinkston, J.D., Stanton, D.T., Wem, D., 2004. Elution and preliminary structure-retention modeling of polar and ionic substances in supercritical fluid chromatography using volatile ammonium salts as mobile phase additives. J. Sep. Sci. 27, 115−123.

Pinkston, J.D., Weng, D., Morand, K.L., Tirey, D.A., Stanton, D.T., 2006. Comparison of LC/MS and SFC/MS for screening of a large and diverse library of pharmaceutically relevant compounds. Anal. Chem. 78, 7467−7472.

Plachká, K., Chrenková, L., Douša, M., Nováková, L., 2016. Development, validation and comparison of UHPSFC and UHPLC methods for the determination of agomelatine and its impurities. J. Pharm. Biomed. Anal. 125, 376−384.

Poole, C.F., 2012. Stationary phases for packed-column supercritical fluid chromatography. J. Chromatogr. A 1250, 157−171.

Płotka, J.M., Biziuk, M., Morrison, C., Namieśnik, J., 2014. Pharmaceutical and forensic applications of chiral supercritical fluid chromatography. TrAC Trends Anal. Chem. 56, 74−89.

Raynie, D.E., Payne, K.M., Markides, K.E., Lee, M.L., 1993. Evaluation of microbore and packed capillary column chromatography with an ethylvinylbenzene-divinylbenzene polymeric packing material and supercritical ammonia as the mobile phase. J. Chromatogr. A 638, 75−83.

Raynor, M.W., Shilstone, G.F., Clifford, A.A., Bartle, K.D., 1991. Xenon as a mobile phase in supercritical fluid chromatography. J. Microcolumn Sep. 3, 337−347.

Ren-Qi, W., Teng-Teng, O., Siu-Choon, N., Weihua, T., 2012. Recent advances in pharmaceutical separations with supercritical fluid chromatography using chiral stationary phases. TrAC Trends Anal. Chem. 37, 83−100.

Roston, D.A., Ahmed, S., Williams, D., Catalano, T., 2001. Comparison of drug substance impurity profiles generated with extended length columns during packed-column SFC. J. Pharm. Biomed. Anal. 26, 339−355.

Sadoun, F., Virelizier, H., Arpino, P.J., 1993. Packed-column supercritical fluid chromatography coupled with electrospray ionization mass spectrometry. J. Chromatogr. A 647, 351−359.

Saito, M., 2013. History of supercritical fluid chromatography: instrumental development. J. Biosci. Bioeng. 115, 590−599.

Schoenmakers, P.J., Uunk, L.G.M., 1987. Effects of the column pressure drop in packed-column supercritical-fluid chromatography. Chromatographia 24, 51−57.

Schwartz, H.E., 1987. Columns for supercritical fluid chromatography: packed vs capillary. LC GC 5, 14−22.

Sen, A., Knappy, C., Lewis, M.R., Plumb, R.S., Wilson, I.D., Nicholson, J.K., Smith, N.W., 2016. Analysis of polar urine metabolites for metabolic phenotyping using supercritical fluid chromatography and mass spectrometry. J. Chromatogr. A 1449, 141−155.

Sie, S.T., Beersum, W.V., Rjinders, G., 1966. High-pressure gas chromatography and chromatography with supercritical fluids. I. The effect of pressure on partition coefficients in gas-liquid chromatography with carbon dioxide as a carrier gas. J. Sep. Sci. 1, 459−490.

Smith, R.M., 1999. Supercritical fluids in separation science−the dreams, the reality and the future. J. Chromatogr. A 856, 83−115.

Snyder, L.R., 1968. Principles of Adsorption Chromatography: Separation of Nonionic Organic Compounds. Dekker, New York (Chapter 8).

Snyder, L.R., 1974. Classification of the solvent properties of common liquids. J. Chromatogr. A 92, 223−230.

Spaggiari, D., Mehl, F., Desfontaine, V., Grand-Guillaume Perrenoud, A., Fekete, S., Rudaz, S., Guillaume, D., 2014. Comparison of liquid chromatography and supercritical fluid chromatography coupled to compact single quadrupole mass spectrometer for targeted in vitro metabolism assay. J. Chromatogr. A 1371, 244−256.

Speybrouck, D., Lipka, E., 2016. Preparative supercritical fluid chromatography: a powerful tool for chiral separations. J. Chromatogr. A 1467, 33−55.

Springston, S.R., Novotny, M., 1981. Kinetic optimization of capillary supercritical fluid chromatography using carbon dioxide as the mobile phase. Chromatographia 14, 679−684.
Strubinger, J.R., Song, H., Parcher, J.F., 1991. High-pressure phase distribution isotherm for supercritical fluid chromatography systems 2. Binary isotherms of carbon dioxide and methanol. Anal. Chem. 63, 104−108.
Swartz, M., Emanuele, M., Hartley, D., Awad, A., 2009. Charged aerosol detection in pharmaceutical analysis: an overview. LC GC 27, 40−48 (special issue).
Taguchi, K., Fukusaki, E., Bamba, T., 2014. Simultaneous analysis of water- and fat- soluble vitamins by a novel single chromatography technique unifying supercritical fluid chromatography and liquid chromatography. J. Chromatogr. A 1362, 270−277.
Takahashi, K., 2013. Polymer analysis by supercritical fluid chromatography. J. Biosci. Bioeng. 116, 133−140.
Takahashi, K., Takahashi, R., Horikawa, Y., Matsuyama, S., Kinugasa, S., Ehara, K., 2013. Optimization of experimental parameters for separation of nonionic surfactants by supercritical fluid chromatography. J. Supercrit. Fluids 82, 256−262.
Tarafder, A., 2016. Metamorphosis of supercritical fluid chromatography to SFC: an overview. TrAC Trends Anal. Chem. 81, 3−10.
Taylor, L.T., 2009. Supercritical fluid chromatography for the 21st century. J. Supercrit. Fluids 47, 566−573.
Taylor, L.T., 2012. Packed column supercritical fluid chromatography of hydrophilic analytes via water-rich modifiers. J. Chromatogr. A 1250, 196−204.
Taylor, L.T., Ashraf-Khorassani, M., 2010. Bare silica has a future in supercritical fluid chromatography. LC GC N. Am. 28, 810−816.
Thiébaut, D., 2012. Separations of petroleum products involving supercritical fluid chromatography. J. Chromatogr. A 1252, 177−188.
Thurbide, K.B., Cooke, B.W., 2003. Supercritical argon as a mobile phase for the flame photometric detection of sulphur. Can. J. Chem. 81, 1051−1056.
Uchikata, T., Matsubara, A., Fukusaki, E., Bamba, T., 2012. High-throughput phospholipid profiling system based on supercritical fluid extraction−supercritical fluid chromatography/mass spectrometry for dried plasma spot analysis. J. Chromatogr. A 1250, 69−75.
Van Deemter, J.J., Zuidewerd, F.J., Kligeberg, A., 1956. Longitudinal diffusion and resistance to mass transfer as causes of nonideality in chromatography. Chem. Eng. Sci. 5, 271−289.
Wang, S., Elshani, S., Wai, C.M., 1995. Selective extraction of mercury with ionizable crown ethers in supercritical carbon dioxide. Anal. Chem. 67, 919−923.
Wang, Z., Zhang, H., Liu, O., Donovan, B., 2011. Development of an orthogonal method for mometasone furoate impurity analysis using supercritical fluid chromatography. J. Chromatogr. A 1218, 2311−2319.
Wen, D., Olesik, S.V., 2000. Characterization of pH in liquid mixtures of methanol/H_2O/CO_2. Anal. Chem. 72, 109−114.
West, C., 2013. How good is SFC for polar analytes? Chromatogr. Today 6, 22−27.
West, C., 2014. Enantioselective separations with supercritical fluids-Review. Curr. Anal. Chem. 10, 99−120.
West, C., Lesellier, E., 2006a. Characterisation of stationary phases in subcritical fluid chromatography with the solvation parameter model: I. Alkylsiloxane-bonded stationary phases. J. Chromatogr. A 1110, 181−190.
West, C., Lesellier, E., 2006b. Characterisation of stationary phases in subcritical fluid chromatography with the solvation parameter model: III. Polar stationary phases. J. Chromatogr. A 1110, 200−213.
West, C., Lesellier, E., 2013. Effects of mobile phase composition on retention and selectivity in achiral supercritical fluid chromatography. J. Chromatogr. A 1302, 152−162.
White, C., 2005. Integration of supercritical fluid chromatography into drug discovery as a routine support tool Part I. Fast chiral screening and purification. J. Chromatogr. A 1074, 163−173.

Wolrab, D., Fruhauf, P., Gerner, C., 2016. Quantification of the neurotransmitters melatonin and *N*-acetylserotonin in human serum by supercritical fluid chromatography coupled with tandem mass spectrometry. Anal. Chim. Acta 937, 168−174.

Wright, B.W., Kalinoski, H.T., Smith, R.D., 1985. Investigation of retention and selectivity effects using various mobile phases in capillary supercritical fluid chromatography. Anal. Chem. 57, 2823−2829.

Yamada, T., Uchikata, T., Sakamoto, S., Yokoi, Y., Nishiumi, S., Yoshida, M., Fukusaki, E., Bamba, T., 2013. Supercritical fluid chromatography/orbitrap mass spectrometry based lipidomics platform coupled with automated lipid identification software for accurate lipid profiling. J. Chromatogr. A 1301, 237−242.

Yang, Z., Sun, L., Liang, C., Xu, Y., Cao, J., Yang, Y., Gu, J., 2016. Simultaneous quantitation of the diastereoisomers of scholarisine and 19-epischolarisine, vallesamine, and picrinine in rat plasma by supercritical fluid chromatography with tandem mass spectrometry and its application to a pharmacokinetic study. J. Sep. Sci. 39, 2652−2660.

Yuan, Z., Wei-, E.Z., Shao-Hui, L., Zhi-Qin, R., Wei-Qing, L., Yu, Z., Xue-Song, F., Wen-Jie, W., Feng, Z., 2016. A simple, accurate, time-saving and green method for the determination of 15 sulfonamides and metabolites in serum samples by ultra-high performance supercritical fluid chromatography,. J. Chromatogr. A 1432, 132−139.

Zhang, Y., Wu, D.R., Wang-Iverson, D.B., Tymiak, A.A., 2005. Enantioselective chromatography in drug discovery. Drug Discov. Today 10, 571−577.

Zhao, Y., Woo, G., Thomas, S., Semin, D., Sandra, P., 2003. Rapid method development for chiral separation in drug discovery using sample pooling and supercritical fluid chromatography-mass spectrometry. J. Chromatogr. A 1003, 157−166.

Zheng, J., Taylor, L.T., Pinkston, J.D., Mangels, M.L., 2005. Effect of ionic additives on the elution of sodium aryl sulfonates in supercritical fluid chromatography. J. Chromatogr. A 1082, 220−229.

Zou, W., Dorsey, J.G., Chester, T.L., 2000. Modifier effects on column efficiency in packed-column supercritical fluid chromatography. Anal. Chem. 72, 3620−3626.

This page intentionally left blank

Index

'*Note*: Page numbers followed by "f" indicate figures, "t" indicate tables.'

C

D

E

F

G

H

M

N

O

P

Q

R

S

T

U

V

W

X

Z

Handbook of Advanced Chromatography/ Mass Spectrometry Techniques

Edited by
Michal Holčapek
Department of Analytical Chemistry, Faculty of Chemical Technology, University of Pardubice, Pardubice, Czech Republic

Wm. Craig Byrdwell
Food Composition and Methods Development Lab, USDA, ARS, Beltsville Human Nutrition Research Center, Beltsville, Maryland, USA.

Handbook of Advanced Chromatography/Mass Spectrometry Techniques is a compendium of new and advanced analytical techniques that have been developed in recent years for analysis of all types of molecules in a variety of complex matrices, from foods to fuel to pharmaceuticals and more. Focusing on areas that are becoming widely used or growing rapidly, this is a comprehensive volume that describes both theoretical and practical aspects of advanced methods for analysis. Written by authors who have published the foundational works in the field, the chapters have an emphasis on lipids but reach a broader audience by including advanced analytical techniques applied to a variety of fields.

Handbook of Advanced Chromatography/Mass Spectrometry Techniques is the ideal reference not only for those just entering the analytical fields covered but also for those experienced analysts who want a combination of an overview of the techniques plus specific and pragmatic details not often covered in journal reports. The authors provide, in one source, a synthesis of knowledge that is scattered across a multitude of literature articles. The combination of pragmatic hints and tips with theoretical concepts and demonstrated applications provides both breadth and depth to produce a valuable and enduring reference manual. It is well suited for advanced analytical instrumentation students as well as for analysts seeking additional knowledge or a deeper understanding of familiar techniques.

Key Features

- Includes UHPLC, HILIC, nano liquid chromatographic separations, two-dimensional LC-MS (LCxLC), multiple parallel MS, 2D-GC (GCxGC) methodologies for lipids analysis, and more.
- Contains both practical and theoretical knowledge, providing core understanding for implementing modern chromatographic and mass spectrometric techniques.
- Presents chapters on the most popular and fastest-growing new techniques being implemented in diverse areas of research.

Related Titles

Lindon et al., *Encyclopedia of Spectroscopy and Spectrometry*, Third Edition, 9780128032244
www.elsevier.com/books/encyclopedia-of-spectroscopy-and-spectrometry/lindon, Second Edition, 9780128032244
Sparkman et al., *Gas Chromatography and Mass Spectrometry: A Practical Guide*, Second Edition, 9780123736284
Riekkola, *Liquid Chromatography*, 9780128053935
Fanali, et al., *Liquid Chromatography: Fundamentals and Instrumentation*, Second Edition, 9780128053935
Ferrer, *Advanced Techniques in Gas Chromatography-Mass Spectrometry (GC-MS-MS and GC-TOF-MS) for Environmental Chemistry, Volume 61*, 9780444626233

ANALYTICAL CHEMISTRY/
LIPID RESEARCH

ISBN 978-0-12-811732-3

AOCS PRESS
ELSEVIER
ACADEMIC PRESS
An imprint of Elsevier
elsevier.com/books-and-journals